GEOLOGICAL DEVELOPMENT OF AND NATURE OF FRACTURES IN THE SHEETED DYKE COMPLEX OF THE SPILIA-POLITIKO AREA, TROODOS OPHIOLITE, CYPRUS: IMPLICATIONS FOR PERMEABILITY IN OCEANIC CRUST

NEWFOUNDLAND STUDIES

TAL ~ 10 PAGES ONLY
MAY BE XEROXED

(Without Author's Permission)

DAVID VAN EVERDINGEN

National Library of Canada
Acquisitions and Bibliographic Services Branch
395 Wellington Street
Ottawa, Ontario
K1A 0N4

Bibliothèque nationale du Canada
Direction des acquisitions et des services bibliographiques
395, rue Wellington
Ottawa (Ontario)
K1A 0N4

NOTICE

The quality of this microform is heavily dependent upon the quality of the original thesis submitted for microfilming. Every effort has been made to ensure the highest quality of reproduction possible.

If pages are missing, contact the university which granted the degree.

Some pages may have indistinct print especially if the original pages were typed with a poor typewriter ribbon or if the university sent us an inferior photocopy.

Reproduction in full or in part of this microform is governed by the Canadian Copyright Act, R.S.C. 1970, c. C-30, and subsequent amendments.

AVIS

La qualité de cette microforme dépend grandement de la qualité de la thèse soumise au microfilmage. Nous avons tout fait pour assurer une qualité supérieure de reproduction.

S'il manque des pages, veuillez communiquer avec l'université qui a conféré le grade.

La qualité d'impression de certaines pages peut laisser à désirer, surtout si les pages originales ont été dactylographiées à l'aide d'un ruban usé ou si l'université nous a fait parvenir une photocopie de qualité inférieure.

La reproduction, même partielle, de cette microforme est soumise à la Loi canadienne sur le droit d'auteur, SRC 1970, c. C-30, et ses amendements subséquents.

Canada

Geological Development of and Nature of Fractures in the Sheeted Dyke Complex of the Spilia-Politiko Area, Troodos Ophiolite, Cyprus: Implications for Permeability in Oceanic Crust

By

©David van Everdingen, B.Sc., M.Sc.

A thesis submitted to the School of Graduate Studies
in partial fulfillment of the
requirements for the degree of
Doctor of Philosophy

Department of Earth Sciences
Memorial University of Newfoundland

1993

St. John's Newfoundland

National Library of Canada
Acquisitions and Bibliographic Services Branch
395 Wellington Street
Ottawa, Ontario
K1A 0N4

Bibliothèque nationale du Canada
Direction des acquisitions et des services bibliographiques
395, rue Wellington
Ottawa (Ontario)
K1A 0N4

Your file Votre référence

Our file Notre référence

The author has granted an irrevocable non-exclusive licence allowing the National Library of Canada to reproduce, loan, distribute or sell copies of his/her thesis by any means and in any form or format, making this thesis available to interested persons.

L'auteur a accordé une licence irrévocable et non exclusive permettant à la Bibliothèque nationale du Canada de reproduire, prêter, distribuer ou vendre des copies de sa thèse de quelque manière et sous quelque forme que ce soit pour mettre des exemplaires de cette thèse à la disposition des personnes intéressées.

The author retains ownership of the copyright in his/her thesis. Neither the thesis nor substantial extracts from it may be printed or otherwise reproduced without his/her permission.

L'auteur conserve la propriété du droit d'auteur qui protège sa thèse. Ni la thèse ni des extraits substantiels de celle-ci ne doivent être imprimés ou autrement reproduits sans son autorisation.

ISBN 0-315-91597-8

Canada

Frontispiece

Rule 31. Each successive fracture episode is the very first to break an area. This assumption of eternal crustal virginity assures mechanical isotropy of an area and does not confuse readers with such complicated concepts as tectonic heredity and pre-existing influences on fracture directions.

From: Wise, R.; 1982; Linemanship and the Practice of Linear Geo-art; Geological Society of America Bulletin v93, p888.

For the field geologist, eroded dykes may be viewed as full scale tests of the fracture strength of the Earths crust.

From: Pollard, D.D.; 1987; Elementary Fracture Mechanics Applied to the Structural Interpretation of Dykes; in Halls, H.C. and Fahrig, W.F. (eds.); Mafic Dyke Swarms; Geological Association of Canada Special Paper 34, p6.

ABSTRACT

The presence of hydrothermal vents on the seafloor at present-day spreading centres, and the lower than expected conductive heat flow values at ridge crests requires the convective circulation of fluids in oceanic crust. The fractured nature of oceanic crustal rocks further suggests that fractures rather than the rock matrix control the fluid circulation and hydrothermal alteration. Study of the nature and role of these fractures in the sub-surface below the modern seafloor is at present done only through one-dimensional boreholes and seismic refraction studies. These fracture networks are better described through analogues such as the ancient obducted oceanic crust of the Troodos ophiolite, Cyprus, which provide a three-dimensional, well-exposed cross-section through the oceanic crust.

The Spilia-Politiko area, Cyprus, was chosen to investigate the characteristics of fractures in the sheeted dyke complex of the Troodos ophiolite. Sheeted dykes in the study area were intruded along a fast spreading, ridge in the Tethys Sea approximately 90 Ma. A jump of the spreading axis from the Solea graben to the Spilia-Politiko area, a second ridge jump further to the east, and movement along the South Troodos Transform Fault have contributed to the formation of five, partly fault-bounded, dyke domains which are defined by their strike orientations. The chemistry of the dykes and the distribution of hydrothermal alteration zones are indicative of multiple, small, transient magma chambers. A later phase of amagmatic extension, post-dating hydrothermal alteration, resulted in the formation of the Mitsero graben structure through a roughly 12% extension of the crust.

Fracture characteristic data for roughly 3200 fractures were systematically collected at 41 locations in the different dyke domains and throughout a vertical section of the Troodos crust, using a scanline mapping method. The mapped characteristics included fracture type, orientation, aperture, length, termination mode, and mineral filling. Fractures within the sheeted dyke complex of the Spilia-Politiko area are sub-divided into two distinct sets: (1) fractures parallel to dyke margins; and (2) those related to columnar jointing. The dyke-parallel fractures tend to exhibit longer trace lengths and larger apertures than those related to columnar jointing. In addition, the dyke-parallel fractures tend to contain epidote whereas the columnar joints were filled by calcite which formed at a later time. Both fracture types formed as the result of contraction during cooling of the dykes, such that fracture orientations are related to the paleo-orientation of the dykes. Other fracture characteristics, such as trace length, aperture, and mineral filling, are generally consistent across the different dyke domains suggesting that the tectonic and hydrothermal processes during the period immediately following dyke emplacement were homogeneous. Fracture aperture and trace length decrease with paleo-depth through the sheeted dyke complex, whereas the occurrence of hydrothermal minerals increases with depth.

Paleo-permeability of the sheeted dyke complex, numerically modelled on the basis of fracture radius, aperture, orientation, and density data from the study area, ranges from 10^{-8} to $10^{-12}m^2$. An observed decrease in the calculated paleo-permeability with depth corroborates studies of modern ocean crustal permeability as reported from Deep Sea Drilling Project borehole packer tests. Areas of intense hydrothermal alteration are more fractured than unaltered dykes, therefore their calculated permeabilities are higher, but only by 6%. The intensely altered zones are 50-100 metres wide and contain fluid inclusion and mineralogical evidence for the passage of hot, *circa* 350°C, seawater-salinity fluids. They are considered to be the up-flow portions of hydrothermal circulation cells which resulted in the formation of epidosite bodies. Preferential fracturing along the dyke margins favours vertical permeability, which facilitates vertical hydrothermal convection driven by heat from the small magma chambers. In the study area, the distribution of epidosite bodies suggests that the hydrothermal cells have a mean cross-strike spacing of 5.3 kilometres. Restriction of hydrothermal alteration to well defined zones higher in the sheeted dyke section and an increase in the occurrence of hydrothermal mineral precipitation with depth implies focussing of hydrothermal up-flow higher in the section. Because the amount of fracturing in the diabase does not vary significantly from that of well-defined epidosite zones it is concluded that the location of hydrothermal circulation cells is controlled by the position of the heat source.

Study of the variation in dyke orientations provides a useful basis for establishing a tectonic framework for sheeted dyke complexes. The study of fractures, alteration and permeability in ophiolites within such a tectonic framework provides valuable information about the fracture characteristics and permeability structure of the upper oceanic crust. The permeabilities calculated for the study area give an indication of the magnitude of permeability in oceanic crust at a spreading axis during hydrothermal circulation, whereas sub-sea boreholes (e.g. DSDP hole 504B), with present technology, can only provide information on permeability at off-axis locations and may not be as useful for estimating permeabilities in active hydrothermal systems.

ACKNOWLEDGMENTS

It gives me great pleasure to thank Peter Cawood, Mark Wilson and Garry Quinlan for their guidance and discussions. The thesis also benefitted from discussions with Tom Calon.

This project would not have been completed without the technical support, at Memorial University of Newfoundland, of Gert Andrews (major element analyses), Daryl Clarke (XRF analyses and discussions about seemingly unsolvable computer programming and hardware problems), and the boys in the lapidary workshop, Gerry Ford, Foster Thornhill, Rick Soper, and Lloyd Warford. Many thanks also go to Pat Browne, who untangled administrative knots with the greatest of ease.

I am very grateful to William Dershowitz (Golder Associates, Inc.) who graciously allowed me the use of his fracture and flow modelling programs and to Glori Lee (Golder Associates, Inc.) for her technical support. Bill Bruce (Canada Centre for Remote Sensing), is thanked for access to satellite imagery of Cyprus, as is Peter Davenport (Newfoundland Department of Mines), for use of their image analysis system. I thank George Maliotis (Hellenic Mining Co.) for useful discussions, accommodation in Mitsero, and for sample shipping. The help of John Malpas (Memorial University) and Costas Xenophontos (Geological Survey Department of Cyprus), in introducing me to Cyprus, is greatly appreciated.

Funding for this project came from a Presidents Natural Sciences and Engineering Research Council award to John Gale, John Welhan and Tom Calon, and from George Jenner for sample shipping costs. Funding to support myself during the course of this project came from a Natural Sciences and Engineering Research Council post-graduate scholarship as well as from a Memorial University of Newfoundland graduate fellowship and from NSERC operating grants to Peter Cawood and Mark Wilson. Extra funding resulted from furniture installation in local banks.

The discussions and useful comments of Günter Suhr, Stephen Edwards and Scott Schillereff were greatly appreciated. They, Karen Hudson, Wendy Millar-Diaz, Jeroen van Gool, Gee-Woong Sung, Adnan Aydin, Mike Basha and Jim and Jackie Turner made my stay in St. John's memorable.

Lastly my thanks go to Sarah Percy, without whose support in the darker times of this project, this thesis would never have been completed. For that I will always be in her debt.

This thesis is dedicated to my mother and father whose support, both moral and emotional, I hope someday to be able to repay.

TABLE OF CONTENTS

ABSTRACT ii
ACKNOWLEDGEMENTS v
TABLE OF CONTENTS vi
LIST OF TABLES x
LIST OF FIGURES xiii
LIST OF PLATES xx
1. INTRODUCTION 1
1.1 BACKGROUND 1
1.2 STATEMENT OF THE PROBLEM 4
1.3 PREVIOUS WORK 4
1.4 PURPOSE AND SCOPE 5
2. GEOLOGIC AND STRUCTURAL FRAMEWORK OF THE STUDY AREA 11
2.1 INTRODUCTION 11
2.2 GEOLOGICAL SETTING OF THE TROODOS OPHIOLITE 11
2.2.1 Origin 13
2.2.2 Obduction and Emplacement 13
2.2.3 Plutonic Complex 15
2.2.4 Sheeted Dyke Complex and Basal Group 15
2.2.5 Pillow Lavas 19
2.2.6 Circum Troodos Sedimentary Sequence 20
2.2.7 South Troodos Transform Fault 20
2.2.8 Mineralization 21
2.3 STRUCTURAL GEOLOGY 22
2.3.1 Large Scale Features 25
2.3.2 Dyke Relations 32
2.3.2.1 *Basis For Dyke Domains* 33
2.3.2.2 *Geological Significance of Dyke Domains* 42
2.3.2.3 *Dyke Geochemistry* 48
2.3.3 Rotational Axis for Extensional Deformation 49
2.3.4 Fault Geometry 54
2.4 SUMMARY AND CONCLUSIONS 63
3. FRACTURE CHARACTERISTICS IN THE STUDY AREA 67
3.1 INTRODUCTION 67
3.2 SCANLINE METHODOLOGY 68
3.3 EVALUATION OF FRACTURE DATA 73
3.3.1 Sources of Bias 73
3.3.1.1 *Scanline Versus Area Mapping* 74
3.3.1.2 *Orientation Bias* 74

3.3.1.3 *Trace Length Bias* 76
3.3.2 Fracture Aperture 77
3.3.3 Fracture Orientation 82
3.3.4 Fracture Filling Minerals: Type and Distribution 97
3.3.5 Fracture Termination Mode 111
3.3.6 Fracture Trace Length 119
3.3.6.1 *Mineral Filling by Trace Length* 125
3.3.7 Fracture Frequency 127
3.4 SUMMARY 130
4. APPLICATION OF FRACTURE CHARACTERISTICS TO ROCK PROPERTIES 132
4.1 INTRODUCTION 132
4.2 RELATIVE AGES OF FRACTURES 133
4.3 PALEO-PERMEABILITY 135
4.3.1 Parallel-Plate Method 138
4.3.2 Bianchi and Snow Method 142
4.3.3 Discrete-Fracture Geometric Modelling 150
4.3.3.1 *Fracture Intensity* 154
4.3.3.2 *Fracture Shape and Size* 158
4.3.3.3 *Method of Permeability Determination* 163
4.3.3.4 *Paleo-Permeability* 171
4.3.3.4.1 On-Axis Permeability 172
4.3.3.4.2 Off-Axis Permeability 172
4.3.3.4.3 Effects of Variation in Fracture Density and Fracture Aperture 178
4.3.3.5 *Comparison of the Methods of Permeability Determination* 181
4.4 STRESS CONSIDERATIONS 184
4.5 SUMMARY 187
5. NATURE AND DEVELOPMENT OF THE SHEETED DYKE COMPLEX 188
5.1 INTRODUCTION 188
5.2 THE TROODOS OPHIOLITE AS AN OCEANIC ANALOGUE . . . 191
5.3 NATURE AND DEVELOPMENT OF THE SHEETED DYKE COMPLEX 193
5.3.1 Magma Chamber Model 194
5.3.2 Formation of the Sheeted Dyke Complex 195
5.3.3 Graben Formation 204
5.3.4 Significance of the Spilia-Politiko Area Dyke Domains 209
5.3.5 Hydrothermal Circulation 216
5.3.5.1 *Hydrothermal Fluid Properties* 229

5.3.5.2 *Interpretation of Fluid Inclusion Data* 232
5.4 REGIONAL TECTONIC SETTING FOR THE TROODOS OPHIOLITE 235
6. FRACTURE AND PERMEABILITY CHARACTERISTICS OF THE SHEETED DYKE COMPLEX: IMPLICATIONS 241

6.1 INTRODUCTION 241
6.2 FRACTURE CHARACTERISTICS 241
6.3 PERMEABILITY 245
6.4 PERMEABILITY COMPARISON AND IMPLICATIONS FOR OCEANIC CRUST 251
6.4.1 *Parallel Plate Method Results* 252
6.4.2 *Matrix Addition Method Results* 255
6.4.3 *Stochastic Method Results* 255
6.5 CONCLUSIONS 257
6.6 RECOMMENDATIONS 261
REFERENCES 264
APPENDICES 286
A. METHODOLOGY AND DATA PRESENTATION 287
A.1 FRACTURE MEASUREMENTS AND SCANLINE PHOTOGRAPHS 287
A.2 SAMPLES COLLECTED 331
A.3 FRACTURE CHARACTERISTICS 341
A.3.1 Plots of All Scanline Data 342
A.3.2 Fracture Filling Minerals vs. Orientation 347
A.3.3 Fracture Filling Minerals vs. Trace Length 355
A.3.4 Trace Length vs. Orientation 360
A.3.5 Fracture Type vs. Orientation 365
A.3.6 Termination Style vs. Orientation 376
A.3.7 Trace Length vs Censoring and Termination 375
A.3.7.1 Histograms by Scanline 375
A.3.7.2 Histograms by Domain 384
A.3.8 Fracture Spacing and Frequency 390
A.3.8.1 Fracture Frequency 390
A.3.8.2 Fracture Spacing 412
A.3.9 Orientation Cluster Analysis 418
A.3.10 Termination Mode Ratios vs. Mineral Filling Presence . . . 425
A.4 BLIND ZONE STEREOGRAPHIC PROJECTIONS 427
A.5 SLICKENSIDE LINEATIONS 433
A.6 FRACTURE AREA MAPPING 440
A.7 PERMEABILITY CALCULATIONS 449
A.7.1 PARALLEL PLATE METHOD 453
A.7.2 BIANCHI AND SNOW (1969) METHOD 456

A.8 TRACE LENGTH SIMULATION 486
B. DYKE DATA 493
B.1 DYKE ORIENTATION DATA 494
B.2 DYKE GEOCHEMISTRY 505
C. ISOTOPE AND FLUID INCLUSION DATA 512
C.1 STABLE ISOTOPE ANALYSES OF CALCITE 513
C.2 FLUID INCLUSION ANALYSES 516

C.2.1 Methodology 516
C.2.2 Fluid Inclusion Types and Results 516
C.2.2.1 *Fluid Temperatures* 517
C.2.2.2 *Fluid Composition* 517
C.2.2.3 *Estimated Pressures* 518
D. PROGRAM DESCRIPTIONS AND LISTINGS 538
D.1 PROGRAM DESCRIPTIONS 539
d.2 PROGRAM LISTINGS 546

LIST OF TABLES

2.1 Comparison of characteristics between the Mitsero and Solea grabens 23

2.2 Fault type in the Spilia-Politiko area 56

3.1 Field relations of the scanlines 72

3.2 Fracture aperture versus dyke orientation and mineral filling 80

3.3 Orientation distributions for the scanlines and dyke domains 88

3.4 Cluster/girdle distributions of the scanline fracture data 89

3.5 Fracture mineral filling by dyke domain 100

3.6 Number of fractures containing no minerals as a percentage of all fractures . 110

3.7 Fracture termination mode by dyke domain 113

3.8 Trace length versus termination modes for the complete scanline data set . . 116

3.9 Mineral filling versus termination modes for the complete scanline data set . 117

3.10 Termination mode statistics by scanline using mineral filled fractures 118

3.11 Fracture trace length statistics 122

3.12 Average mineral filling versus trace length statistics 126

3.13 Fracture frequency by scanline 128

4.1 Average permeability magnitudes by area and fracture mineral filling - parallel plate method 140

4.2 Average permeability magnitudes and orientations - Bianchi and Snow method 144

4.3 Average permeability magnitudes by area and fracture mineral filling - Bianchi and Snow method 148

4.4 Effect of fault size on permeability 149

4.5 Joint system models 151

4.6 Fracture intensity by rock volume 159

4.7 Fracture radius determination by trace length sampling 162

4.8 Fracture model data set 165-168

4.9 Permeability modelling results 174

4.10 Permeability calculations using calcite-filled fractures 177

4.11 Sensitivity analysis results 179

4.12 Comparison of calculated permeabilities 182

5.1 Sheeted Dyke Complex Properties 189-190

5.2 Comparison of slow versus fast spreading rates at spreading centres 192

A.1.2 Universal Transverse Mercator coordinates dyke domain number of fracture scanline surveys. 288

A.1.3 Format used for scanline data. 289

A.1.4 Scanline fracture measurements 295

A.1.5 Tabulated fracture characteristics for the Spilia-Politiko area by scanline . 320

A.3.3.1 Mineral filling versus trace length statistics 356

A.3.3.2 Mineral filling versus trace length for complete scanline data set 359

A.3.8.1 Dyke-parallel fracture statistics 416

A.3.8.2 Spacing as a function of trace length truncation by scanline 417

A.3.10.1 Termination mode versus presence of mineral filling by scanline. . . . 426

A.5.1 Slickenside lineations and accompanying plane orientations listed by scanline or area. 434

A.6.1 Scanline versus area map: tabulated properties of fractures. 447

A.7.1 Fracture permeability magnitudes calculated for each scanline on the basis of the parallel plate method 454

A.7.2 Fracture permeability magnitudes and directions for all scanline areas by mineral filling, calculated based on the Bianchi and Snow method 457

A.7.3 Fracture permeability magnitude and anisotropy based on results from the Bianchi and Snow method 474

B.1.1 Eigen analysis of the dyke domain orientation data for the Spilia Politiko area, Troodos Ophiolite, Cyprus. 495

B.1.2 Fisher analysis of the dyke domain orientation data for the Spilia Politiko area, Troodos Ophiolite, Cyprus. 495

B.1.3 Dyke orientation data compilation for the Spilia-Politiko area, Troodos Ophiolite, Cyprus 496

B.3.1 Whole rock geochemical analyses 510

C.2.1 Compiled fluid inclusion results 521

C.2.2 Fluid inclusion sample descriptions. 522

C.2.3 Fluid inclusion temperature and salinity data 523

C.2.4 Pressure correction of fluid inclusion homogenization temperatures . . 535-537

LIST OF FIGURES

1.1 Lithologic layering in oceanic crust 2

1.2 Internal structure of the sheeted dyke sequence in the Troodos Ophiolite, Cyprus 6

2.1 Geological map of the Spilia - Politiko area, Cyprus. 12

2.2 Flow chart of data and programs used in Chapter 2 26

2.3A Landsat Multi-Spectral Scan image of the Troodos Ophiolite 27

2.3B Lineaments interpreted from Landsat Thematic Mapper images in the Troodos Ophiolite 29

2.4 Landsat lineament analysis in the Troodos Ophiolite, Cyprus 30

2.5 Dyke orientation data in the Spilia-Politiko area, Cyprus 34

2.6 Estimated strike of dykes in the Spilia - Politiko area, Cyprus 36

2.7 Estimated dyke dip, Spilia - Politiko area, Cyprus 37

2.8 Dyke domains and dyke orientations, Spilia - Politiko area, Cyprus. 39

2.9 Stereographic projection of the dyke domain mean orientations 40

2.10 Dyke domains referenced to the geology of the Spilia - Politiko area. 41

2.11 Domain boundaries and lineaments in the Spilia-Politiko area, Cyprus 43

2.12 Contoured angle of intersection between dykes at adjacent nodes, Spilia - Politiko area, Cyprus 45

2.13 Contoured dyke dips, Spilia - Politiko area, Cyprus 47

2.14 Rotation of dyke domain mean orientations, Mitsero graben 51

2.15 Relation between fault rotation and amount of extension 53

2.16 Slickenside Orientation map, Spilia-Politiko area, Cyprus. 55

2.17 Fault types in the Spilia - Politiko area 57

2.18 Schematic diagram to provide an explanation for formation of north-south oriented strike-slip faults 60

2.19 Faults and Mineralization 61

2.20 Domain boundaries and faults in the Spilia-Politiko area, Cyprus. 62

2.21 Schematic cross-section of the Spilia-Politiko area 64

3.1 Flow chart of data and programs used in Chapter 3 69

3.2 Scanline location map, Spilia - Politiko area, Cyprus. 70

3.3 Fracture aperture histograms, Spilia-Politiko area, Cyprus 79

3.4 Dyke orientations by scanline 84

3.5 Spatial distribution of fracture data in domain 6 (by scanline) 86

3.6 Cluster/Girdle relationships for domain 6, central domain 4, Alona, and scanlines 1204, 0213, 1305, 1211, and 1124 87

3.7 Schematic diagram to illustrate internal columnar jointing in dykes 91

3.8 Fracture sets by scanline 92

3.9 Rotated fractures by scanline 94

3.10 Comparison of fracture orientations within subdomains 2A and 2B 96

3.11 Fracture frequency map, Spilia - Politiko area, Cyprus 99

3.12 Variation with depth of various fracture properties 101

3.13 Epidote frequency map, Spilia-Politiko area, Cyprus 103

3.14 Zeolite frequency map, Spilia-Politiko area, Cyprus. 104

3.15 Calcite frequency map, Spilia-Politiko area, Cyprus 105

3.16 Calcite vein orientations by domain 106

3.17 Alona section dykes and gabbros 108

3.18 Orientations of unfilled fractures by domain 109

3.19 Unfilled fracture frequency map, Spilia-Politiko area, Cyprus. 112

3.20 Termination mode ratio map, Spilia-Politiko area, Cyprus 115

3.21 Trace length histograms by set and level of censoring 120

3.22 Lineament and fracture trace length distributions 124

3.23 Dyke frequency map, Spilia-Politiko area, Cyprus 129

4.1 Flow chart of data and programs used in Chapter 4 134

4.2 Permeability anisotropy definition 146

4.3 Schematic showing the process for determination of the fracture area per unit volume measure from the scanline fracture data 157

4.4 Boundary conditions applied to the fracture networks 169

4.5 Permeability variation in the Spilia-Politiko area, Cyprus 173

5.1 Magma chamber model 196

5.2 Dyke emplacement (A) away from and (B) near a transform fault 199

5.3 Dyke emplacement at a ridge axis far from a transform fault 201

5.4A Dyke characteristics near ridge-transform intersections, using a sinistrally offset transform exhibiting dextral shear 202

5.4B Dyke orientation upon injection at a ridge-transform intersection 202

5.5 On- and off-axis graben formation 206

5.6 Schematic of dyke orientation resulting from a ridge jump along a sinistrally

offset, dextrally slipping transform fault 211

5.7 Troodos dyke domain formation history 214

5.8 Schematic diagram of hypothetical hydrothermal circulation at a spreading centre 217

5.9 Epidosite occurrence map, Spilia-Politiko area, Cyprus 219

5.10 Contour map of the number of mine, gossan and mineral occurrences in the Spilia-Politiko area, Cyprus 224

5.11 Hydrothermal fluid circulation 227-228

5.12 Fluid inclusion homogenization temperature versus salinity data from the Spilia-Politiko area, Troodos Ophiolite, Cyprus 231

5.13 Tectonic setting of the Troodos ophiolite 236-237

5.14 Ophiolite uplift shown in a North-South section 240

6.1 Early fracture formation in sheeted dykes 242

6.2 Principal permeability directions in Layer 2B oceanic crust 247

6.3 Bulk permeabilities of oceanic crust 253

A.1.1 Coding convention used for fracture scanline mapping. 291

A.1.2 Example of fracture sampling using the fracture scanline mapping method 292

A.1.3 Scanline survey location map, Spilia-Politiko area, Cyprus. 293

A.1.4 Scanline location map 293

A.1.5 Scanline Location With Depth 294

A.2.1.1 Sample location map 340

A.3.1.1 Stereographic projections of all fracture data by scanline. 343

A.3.1.2 Stereographic projections of all fracture data by domain. 346

A.3.2.1 Stereographic projection symbol explanation 348

A.3.2.2 Stereographic projections of fracture data by scanline and mineral filling. 349

A.3.2.3 Stereographic projections of fracture data by domain and mineral filling. 352

A.3.3.1 Box plots of fracture mineral filling versus trace length by domain . . . 357

A.3.4.1 Stereographic projections of fracture data of trace length by scanline. . 361

A.3.4.2 Stereographic projections of fracture data of trace length by domain. . . 364

A.3.5.1 Stereographic projections of fracture data of fracture type by scanline. . 366

A.3.5.2 Stereographic projections of fracture data of fracture type by domain. . 369

A.3.6.1 Stereographic projections of fracture data of termination mode by scanline 371

A.3.6.2 Stereographic projections of fracture data of termination mode by domain. 374

A.3.7.1 Trace length histograms by scanline and orientation set 376

A.3.7.2 Stacked bar graphs of trace length versus censoring style and termination mode all scanline data and by domain (Area) 385

A.3.8.1 Fracture frequency as a function of scanline distance by scanline 391

A.3.8.2.1 Dyke-parallel fracture spacing as a function of trace length distribution 414

A.3.8.2.2 Quantile plots for exponential and log-normal models fitted to the spacing distributions of dyke-parallel fractures 415

A.3.9.1 Lower hemisphere equal area stereographic projections of data subsets from individual scanlines extracted by CLUSTRAN 419

A.3.9.2 Lower hemisphere equal area stereographic projections of data subsets from individual scanlines on the basis of contoured data 422

A.4.1 Stereographic projections of blind zone areas for each scanline 428

A.5.1 Lower hemisphere, equal area stereographic projections of slickenside

lineations on fault surfaces. 437

A.6.1 Map of fracture location in the 1137 scanline area collected using the area mapping technique 441

A.6.2 Map of fracture locations in the 1137 scanline area collected using the scanline mapping technique 442

A.6.1 Map of fracture location in the 1305 scanline area collected using the area mapping technique 443

A.6.2 Map of fracture locations in the 1305 scanline area collected using the scanline mapping technique 444

A.6.3 Stereographic projections of fracture orientations in the 1137 and 1305 scanline areas 445

A.6.4 Trace length histograms for scanline area 1137 and 1305 on the basis of area or scanline mapping 446

A.6.4 Effect of Terzaghi correction at scanline location 1137 448

A.7.1 Principal permeability directions - stereographic projections for all and dyke parallel fractures by scanline 463

A.7.2 Prinicpal permeability directions - stereographic projections by area 480

A.8.1 Fracture trace length simulation 489

A.8.2 Fracture trace length simulation histograms 490

B.1.1 Dyke Orientation data (raw) for the Spilia-Politiko area, Cyprus with superimposed faults compiled from the Geological Survey Department of Cyprus Memoirs 503

B.1.2 Dyke Orientation data (raw) for the Spilia-Politiko area, Cyprus with superimposed lineaments interpreted from Landsat Thematic Mapper images 504

B.3.1 Location map of scanlines and dyke sections in the Spilia-Politiko area, Cyprus 506

B.3.2 Graph of Log Zr versus Log (Zr/Y) 507

B.3.3 Graph of Log Cr versus Log Ti 507

B.3.4 Plot of Log (Nb/Y) versus Log (Zr/TiO_2) 508

B.3.5 Plot of Zr versus Ti. 508

B.3.6 Mg# versus Sr/Y plot 509

B.3.7 Plot of Zr/Y versus Ti/Y 509

C.1.1 Carbon and oxygen isotope analyses of calcite and calcite sample location map, Spilia-Politiko area, Cyprus 515

C.2.1 Location map of the fluid inclusion sections in the Spilia-Politiko area, Cyprus 520

C.2.2 Fluid inclusion microscope light source temperature effects 529

C.2.3 Homogenization temperature versus pressure of the fluid inclusion data . . 530

C.2.4 Histogram of fluid inclusion homogenization temperatures by rock type . . 531

C.2.5 Histograms of fluid inclusion homogenization temperatures by sample. 532-534

LIST OF PLATES

2.1 Thin section of chilled margin between light coarser dyke and dark fine dyke with glassy matrix in plane polarized light (Sample O/C-6). 17

2.2 Outcrop (near scanline section 1107) showing dyke cross cutting relationships. Late unaltered dyke cutting earlier epidosite dykes 18

3.1A Thin section in plane polarized light showing fracture filling minerals including quartz and epidote 81

3.1B Same section as Plate 3.3A but under cross polarized light. 81

1. INTRODUCTION

1.1 BACKGROUND

Oceanic lithosphere is composed of four layers, which from top to bottom are: Layer 1, marine sediments; Layer 2, extrusive and intrusive igneous rocks; Layer 3, intrusive igneous rocks; and Layer 4, upper mantle (Cann, 1974) (Figure 1.1). The Layer 2 rocks are further subdivided into Layer 2A, extrusive volcanic pillow and flow lavas, and Layer 2B, intrusive diabasic dykes (Cann, 1974). Formation of this oceanic lithosphere at accreting tectonic plate boundaries, through the injection and cooling of magma, transfers heat from the mantle to the seafloor.

Conductive heat flow values measured near mid-ocean ridges are lower than those predicted from conductive heat-flow models (Lister, 1972; Williams et al., 1974; McKenzie and Sclater, 1969; Sclater and Francheteau, 1970; Parker and Oldenburg, 1973). To explain the lower than expected values, hydrothermal convection was postulated as a means to remove heat from the oceanic crust (Hyndman et al., 1976; Lewis, 1983). The discovery of the black-smoker hot springs, venting fluids with temperatures up to 350°C, at the seafloor on the East Pacific Rise (Weiss et al., 1977; RISE Project Group, 1980), confirmed the importance of hydrothermal convection in modifying the thermal structure of the oceanic crust.

The significance of hydrothermal circulation in the oceanic crust goes beyond its effects on heat-flow characteristics. Hydrothermal circulation through oceanic crust has clearly played a role of both economic importance (in the formation of metal-sulfide deposits) and environmental significance (in the evolution of the hydrosphere). A direct consequence of the circulation of seawater through the oceanic crust is

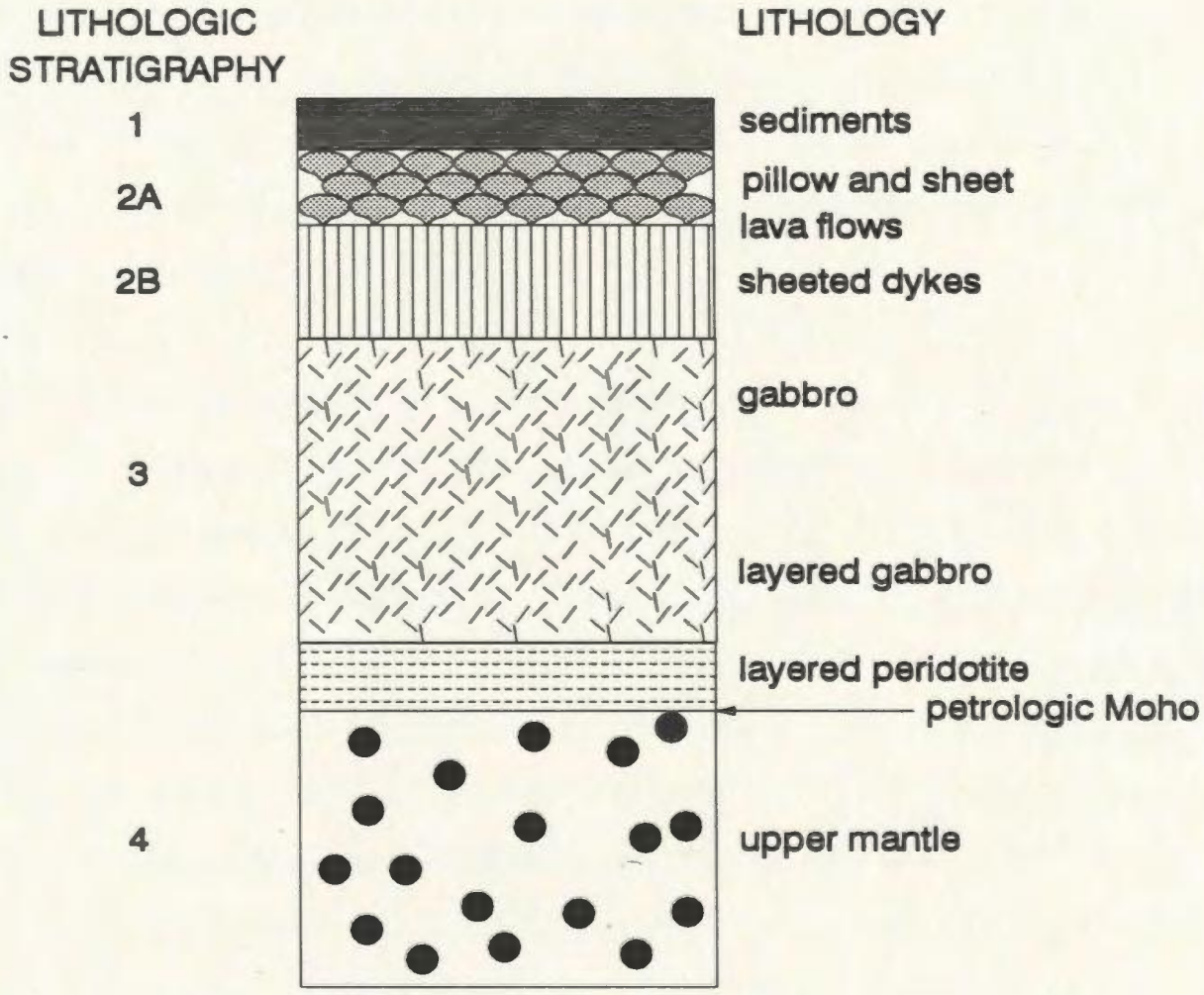

FIGURE 1.1 LITHOLOGIC LAYERING IN OCEANIC CRUST (AFTER CANN, 1974 AND KENNETT, 1982).

chemical exchange between the rocks and the circulating fluid. The fluid flux is of sufficient quantity that it buffers the major element composition of the oceans (Von Damm, 1990), and their isotopic composition, such as $\delta^{18}O$ (Gregory and Taylor, 1981) and $^{87}Sr/^{86}Sr$ (Holser, 1984; Veizer, 1988).

Fluid circulation in the oceanic crust, driven by thermally induced buoyancy effects, includes seawater recharge into the extrusive volcanic rocks (Layer 2A) and fluid movement into, and through, the sheeted dykes (Layer 2B), toward the top of the magma chamber heat source. The sheeted dykes (Layer 2B) are assumed to play a major role in constraining fluid flow characteristics, because a large portion of the flow path lies within them.

The effective bulk permeability of a rock mass will control the flow of fluids through the rock. The *in situ* bulk permeability of Layer 2A (extrusive volcanic rocks) has been measured in Deep Sea Drilling Project (DSDP) drill hole 504B as 4×10^{-14} m^2, whereas that for Layer 2B ranged between 4×10^{-17} and 5×10^{-18} m^2 (Becker, 1989). In contrast, experimentally determined permeabilities of unfractured basalt, diabase, and gabbro are much lower than those of the fractured equivalents, at 9.9×10^{-17} m^2 (De Wiest, 1966), 8.4×10^{-22} m^2 (Ohle, 1951), and 8×10^{-24} m^2 (Trimmer et al., 1980), respectively. Thus fluid flow through the rock matrix is not a likely mechanism for the movement of fluids through the oceanic crust. The large difference between the *in situ* bulk permeability of Layer 2 and that of unfractured igneous rocks implies the presence of a large-scale interconnected fracture system within Layer 2.

1.2 STATEMENT OF PROBLEM

Early efforts to numerically model hydrothermal flow systems in oceanic lithosphere treated the rock mass as an equivalent porous medium (e.g. Fehn et al., 1983), using hydraulic properties and equations that assumed that the fluid flowed through the rock matrix. Although the porous-medium modelling approach may be valid and necessary for the very large scale (> 10 kilometres), it does not incorporate the presence of fracture systems through which the bulk of the fluid flow is likely to take place (MacDonald, 1983). Fractures have flow and transport properties that are very different from those of the rock matrix. Both theoretical and experimental studies of fluid flow in fractured rocks have shown that the flow through the fractures is volumetrically more important than the flow through the rock matrix for low permeability rocks (Romm, 1966; Snow, 1969).

Understanding the role that fractures play during the development of oceanic crust is essential in the explanation of the nature of hydrothermal fluid circulation. The geometry of fracture systems (including orientation, location and size of fractures, and their degree of interconnection) is likely to be one of the major factors determining the direction and volume of hydrothermal fluid flow in oceanic lithosphere.

1.3 PREVIOUS WORK

Studies of fracture systems in modern oceanic crust are limited to a few DSDP and Ocean Drilling Program (ODP) drill holes (e.g. DSDP hole 504B off the Costa Rica rift). The oldest fractures measured in such studies are related to cooling stresses (Adamson, 1985; Simmons and Richter, 1976). In DSDP hole 504B, fractures with

varying orientations and inconsistent cross-cutting relations, but containing the same mineral filling, suggest that pressure conditions strongly control fracture geometries (Agar, 1990). This also shows that pore fluid pressures were higher than lithostatic pressure (Agar, 1990).

Data obtained through indirect marine geophysical sensing methods (sonar, heat flow, electromagnetic, etc.) do not allow accurate definition of the fracture geometry at depth in the oceanic crust (Lewis, 1983). Wilkens et al. (1991) showed that a better understanding of ocean crustal evolution requires that more refraction seismic measurements be made, and that the links between the pore structure of oceanic crustal rocks and velocity-porosity relationships be examined in greater detail.

Systematic (lateral and vertical) investigations of fracture characteristics in oceanic lithosphere can more easily be made in ophiolites which are regarded as remnants of oceanic lithosphere now residing on land (Church and Stevens, 1971; Anonymous, 1972; Church, 1972). So far, systematic studies of fracture systems have generally been restricted to granitic massifs (e.g. Stripa mine, Sweden, Rouleau, 1984; Fanay-Augeres mine, France, Long and Billaux, 1987), and sedimentary rocks (e.g. Lannon quarry, Wisconsin, Lapointe and Hudson, 1985). They have further been restricted to the study of present-day engineering and hydraulic properties of the fractured rocks, ignoring the processes which led to the current rock properties.

1.4 PURPOSE AND SCOPE

The nature of hydrothermal fluid circulation in the sheeted dyke portion of the oceanic crust is not well known and little studied. The purpose of this study is to investigate the physical aspects of fracture systems that controlled hydrothermal circulation in the

FIGURE 1.2 INTERNAL STRUCTURE OF THE SHEETED DYKE SEQUENCE IN THE TROODOS OPHIOLITE, CYPRUS (AFTER MOORES ET AL, 1990). THE SHEETED DYKES ARE IN THE UNPATTERNED AREAS OF ENLARGED MAP. INSET MAP SHOWS LOCATION OF THE TROODOS OPHIOLITE.

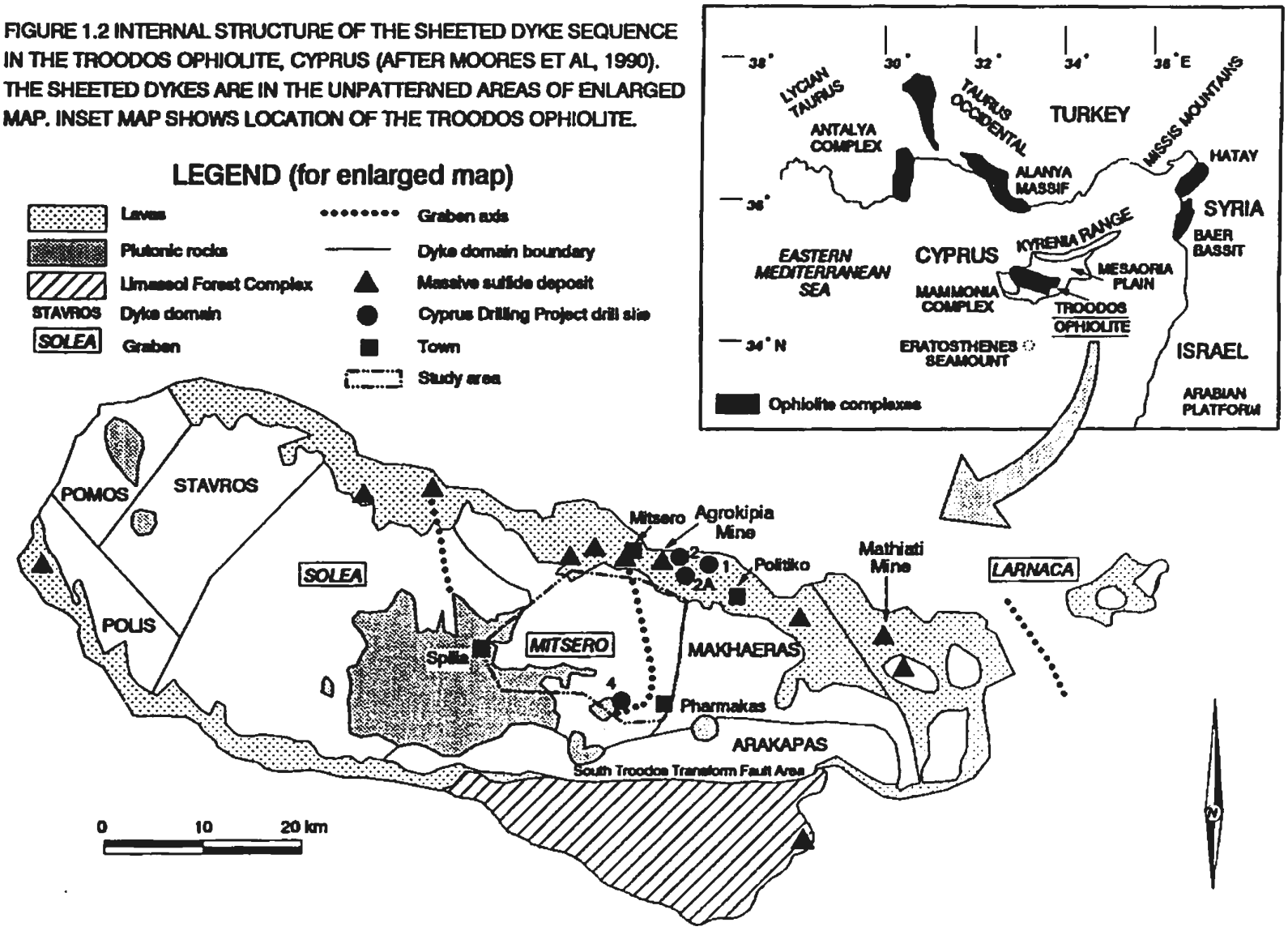

sheeted dyke complex of a well exposed ophiolite, and to use this as an analogue of the oceanic crust, to describe the development of Layer 2B of the oceanic crust and the circulation of hydrothermal fluids through Layer 2B.

The Troodos ophiolite, located on the island of Cyprus in the Eastern Mediterranean Sea (Figure 1.2), is one of the best documented ophiolite complexes in the world (e.g. Panayioutou, 1979; Malpas et al., 1990), and it was therefore selected for this study. Outcrop exposures provide a relatively complete cross-section through this upper oceanic lithosphere analogue. In particular the sheeted dyke sequence, layer 2B, is extremely well exposed and little deformed, providing ideal vertical and lateral sections through the dykes and their upper and lower contacts.

Earlier studies of fracture systems in the Troodos ophiolite have been restricted to: 1) the mapping of faults (e.g. Bear, 1960; Carr and Bear, 1960; Varga, 1991); 2) descriptions of veins at isolated points, in the context of establishing the original fluid properties and the extent of hydrothermal alteration, through fluid-inclusion studies (e.g. Spooner and Bray, 1977; Richardson et al., 1987; Kelley et al., 1992) and stable-isotope studies (Heaton and Sheppard, 1977; Schiffman et al., 1987); and 3) two-dimensional theoretical modelling of hydrothermal fluid circulation in a ridge-parallel fault at a spreading centre (Strens and Cann, 1986). Structural studies (e.g. Varga and Moores, 1985; Ramsden, 1987; Varga, 1991) outlined the structural setting of the Sheeted Dyke Complex, in which the development of Layer 2B can be studied.

The principal objectives of this thesis are:

1) to use dyke orientation data and other structural observations to describe the geological development of a carefully selected study area; this will include the

delineation of dyke domains in the study area, through analysis of dyke orientations;

2) to characterize fracture geometry in the study area, and to describe the statistics of the fracture data;

3) to determine whether differences in fracture characteristics are related to stratigraphic position in Layer 2B, or to position in different dyke domains;

4) to estimate the permeability characteristics of the sheeted dyke section during the early stages of its formation, using the fracture characteristics established through objectives 2 and 3 above;

5) to integrate the geological and fracture-geometry databases into a self-consistent model for the development of Layer 2B oceanic crust in the study area and, by implication, elsewhere.

The field area chosen for this study of the Troodos ophiolite lies in the area between Spilia to the west, Politiko to the east, Mitsero to the north, and Pharmakas to the south (Figure 1.2). The field area, which covers roughly 280 square kilometres, will be referred to as the Spilia-Politiko area. It lies within the structure identified as the Mitsero graben (Moores et al., 1990), formerly the Ayios Epiphanos graben (Varga and Moores, 1985). The Mitsero graben is bounded to the north by the sedimentary sequences of the Mesaoria Plain, and to the south by the Arakapas fault zone, now renamed the South Troodos Transform Fault, to include part of tne Limassol Forest Complex (MacLeod, 1990; MacLeod et al.,1990). To the west it is bounded by the Solea graben, and to the east by the Makhaeras dyke domain. The Mitsero graben

provides a cross-section through an ancient spreading centre (Chapter 2) which, in combination with the undeformed nature of the rock units, allows along-strike and across-strike interpretation of the fracture characteristics with respect to spreading centres. The map view of the field area provides an oblique section, tilted to the north, through the Mitsero graben structure, and it includes contrasting areas of greater and lesser intensities of hydrothermal alteration. Earlier structural and hydrothermal investigations carried out in an adjacent area to the West (Varga, 1991; Schiffman et al., 1990), provide a database for comparison.

Locations for measurements and sample collection were selected throughout the field area to enable determination of the variation of fracture properties throughout the Sheeted Dyke Complex and in immediately adjoining sections at the base of the pillow lavas and at the top of the underlying gabbros. The collection of fracture characteristic data requires fresh outcrops, because some of the fracture information will be lost during weathering of the exposed rocks. Numerous fresh outcrops were available for this study in the form of recent road cuts.

Fracture characteristics, including fracture orientation, trace length, censoring (fracture continuation beyond the visible outcrop edge), termination mode (fracture interaction with other fractures), surface roughness (fracture curvature and aperture variation), mineral infilling, average aperture, and rock type were determined by scanline survey (described further in Chapter 3) for 3221 fractures at 41 outcrop localities. The data were used to compute parameters describing the distribution of fracture characteristics. The parameters in turn were used to compare the fracture characteristics of different sites, and to estimate paleo-permeabilities at specific levels and locations in the ophiolite complex and, by analogy, in Layer 2B of the oceanic crust.

Almost 3300 dyke orientations, mostly at points in the Sheeted Dyke Complex, were compiled from field measurements made during this study (848), and from the literature (2428). The dyke orientation data, supplemented by published work on the structure and history of the field area, were used to place this study of fracture characteristics into a tectonic framework.

Samples of fracture filling minerals and rock matrix were collected from the field area. They were used for: 1) micro-thermometric studies of fluid inclusions to determine hydrothermal temperatures, salinities, and possible fluid sources; 2) stable-isotope analyses of calcite (for C and O), to estimate the temperature and timing of its formation; and 3) whole-rock geochemical analyses, utilizing X-ray fluorescence techniques, to determine whether chemical signatures would indicate contrasts within or between orientation-based dyke domains.

The extensive database generated by this study, particularly with respect to fracture characteristics and dyke orientations, required computer management and manipulation. Special programs were written for various tasks, including database management, compilation of data based on various parameters, and the calculation of derived properties such as orientation statistics and fracture permeability. The introductory sections of Chapters 2, 3, and 5 contain flow charts showing the programs used within each chapter, and the pathways followed during the data manipulation process. Appendix D presents the program listings, input requirements, output specifications, and a description of purpose for each of the programs written for this study.

2. GEOLOGIC AND STRUCTURAL FRAMEWORK OF THE STUDY AREA

2.1 INTRODUCTION

The purpose of this chapter is to use the orientations and geological relationships of the dykes in the Sheeted Dyke Complex and the Basal Group, of the Troodos ophiolite, to develop a framework within which to analyze the fracture geometry and characteristics (Chapter 3) of the Sheeted Dyke Complex. Specifically, this chapter undertakes: introduction of the geology of the study area; analysis of the large scale features within the Troodos ophiolite through use of remotely sensed data; delineation of dyke domains and graben structures within the Spilia-Politiko area, based on orientation of dykes and geometry of faults; and description of a structural framework for the field area. The basic geology of the field area, outlined in the following section, is presented on the map in Figure 2.1.

2.2 GEOLOGICAL SETTING OF THE TROODOS OPHIOLITE, CYPRUS

The Troodos ophiolite underlies 3200 km^2 or about one third of the island of Cyprus. It has a maximum elevation of about 2000 metres above sea level. The pseudo-stratigraphy of the Troodos massif consists of three parts: the Plutonic Complex at the base of the section; the overlying Sheeted Dyke Complex; and extrusive volcanic rocks capping the entire sequence (Wilson and Ingham, 1959) (Figure 1.2).

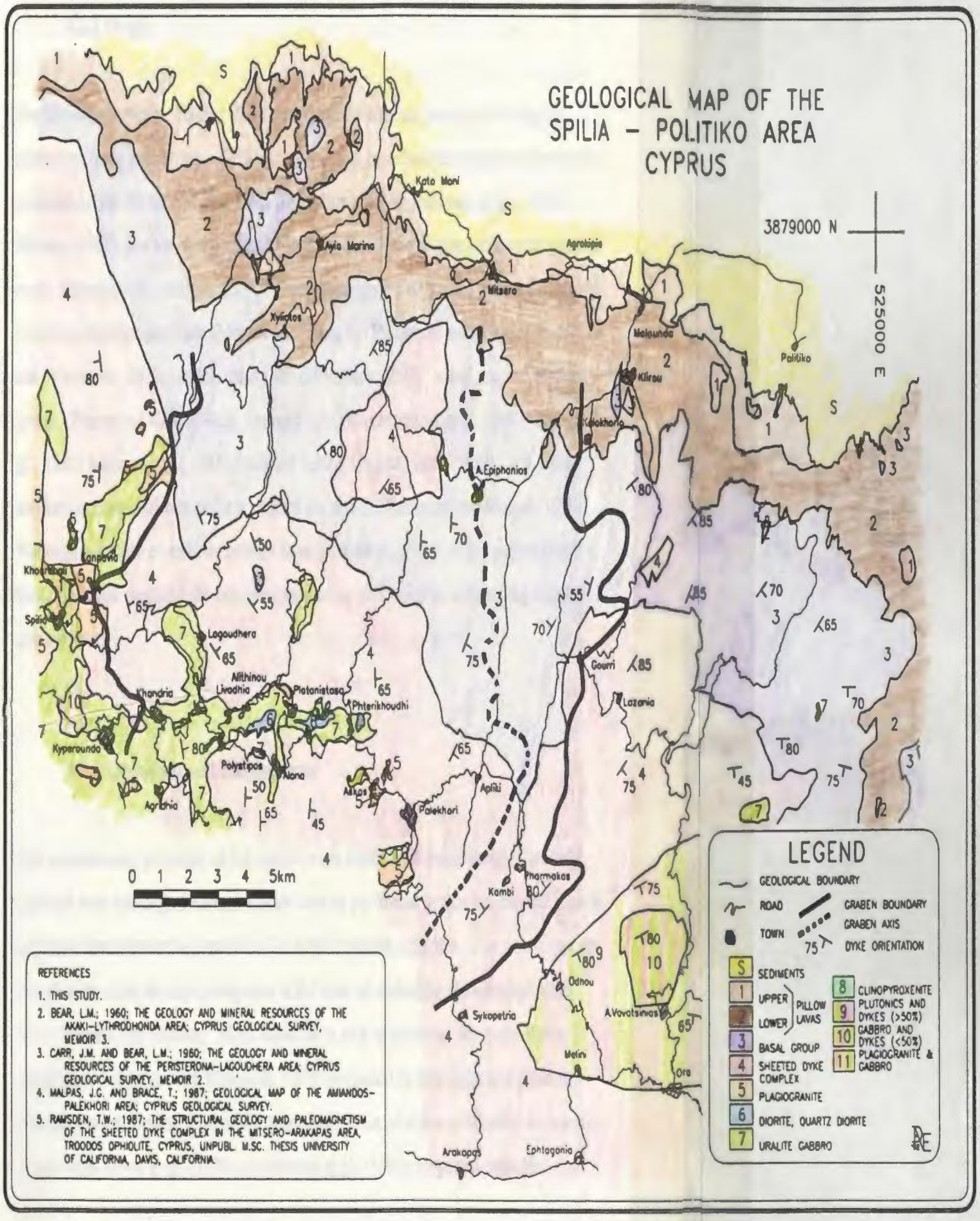

REFERENCES

1. THIS STUDY.
2. BEAR, L.M.; 1960; THE GEOLOGY AND MINERAL RESOURCES OF THE AKAKI–LYTHRODHONDA AREA; CYPRUS GEOLOGICAL SURVEY, MEMOIR 3.
3. CARR, J.M. AND BEAR, L.M.; 1960; THE GEOLOGY AND MINERAL RESOURCES OF THE PERISTERONA–LAGOUDHERA AREA; CYPRUS GEOLOGICAL SURVEY, MEMOIR 2.
4. MALPAS, J.G. AND BRACE, T.; 1987; GEOLOGICAL MAP OF THE AMIANDOS–PALEKHORI AREA; CYPRUS GEOLOGICAL SURVEY.
5. RAWSDEN, T.W.; 1987; THE STRUCTURAL GEOLOGY AND PALEOMAGNETISM OF THE SHEETED DYKE COMPLEX IN THE MITSERO–ARAKAPAS AREA, TROODOS OPHIOLITE, CYPRUS, UNPUBL. M.SC. THESIS UNIVERSITY OF CALIFORNIA, DAVIS, CALIFORNIA.

2.2.1 Origin

The Troodos ophiolite formed 92-90 Ma above an oblique, possibly NE-dipping, subduction zone (Robertson, 1990). Partial melting of a depleted mantle source is the accepted origin for the Troodos lavas (Greenbaum, 1972; Robinson et al., 1983). Bishopp (1952) was the first to suggest that the Troodos ophiolite represented oceanic crust. Subsequently, various oceanic settings were proposed for the Troodos ophiolite including major ocean basin (Moores and Vine, 1971), narrow ocean basin (Robertson and Woodcock, 1979), mature island arc (Miyashiro, 1973), island arc and seafloor setting (Pearce and Cann, 1973), immature arc (Rautenschlein et al., 1985; Thy et al., 1985; Moores et al., 1984), back-arc setting (Pearce, 1975, 1983), or a supra-subduction zone environment in a nascent arc setting (Robinson and Malpas, 1990). Although a variety of tectonic settings have been proposed, all authors agree that the well developed sheeted dyke complex requires its generation at a spreading centre environment.

2.2.2 Obduction and Emplacement

The emplacement processes of the ophiolite are a matter of controversy. Vertically oriented flow banding of mineral phases such as pyroxenes within the residual mantle sequence demonstrate the presence of a diapiric mantle structure. This shows that the complex lay close to a spreading axis at the time of obduction (Moores and Vine, 1971; Nicolas and Violette, 1982). Based on a lack of evidence for major thrust repetitions, Robertson and Woodcock (1979) suggested *in situ* uplift and rotation overlying north-dipping tectonically underthrust crust of either continental or oceanic origin. Biju-Duval et al. (1976) and Moores et al. (1984) supported ophiolite

emplacement from the north. On the basis of paleo-magnetic evidence, a 90° counterclockwise rotation of the whole ophiolite is believed to have taken place since its formation in the late Cretaceous to the early Eocene (Moores and Vine, 1971). This means that features presently trending north-south were originally east-west trending at the time of formation and thus would be related to oceanic or back-arc spreading along an east-west trending axis. Clube et al. (1985) stated that at least 60° of the rotation had been completed prior to the Lower Eocene; the remainder was completed by the end of the Lower Eocene. They suggested that an oblique subduction zone beneath the Troodos ophiolite could provide the necessary driving force for the tectonic rotation.

Regional gravity surveys indicate the presence of a high density (3.01 g/cm^3), 30 km thick slab beneath Cyprus overlying an up to 30-km-thick, lower density (2.7 g/cm^3) slab of possible continental crust which extends south to the Eratosthenes seamount (Figure 1.2) (Makris, 1983). A gravity low centred over Mt. Olympos, at the centre of the ophiolite (density = 2.55 g/cm^3) is interpreted as a narrow pipe-like serpentine diapir beneath Mt. Olympos (Makris, 1983).

Serpentinization of ultramafic rocks may have been, in part, responsible for the uplift of the ophiolite (Allen, 1975; Gass, 1979). Robertson (1977) estimated 4 kilometres of uplift for the ophiolite, which occurred in pulses. By Late Miocene the Troodos ophiolite was a low island. In the Pliocene (6-2Ma) the ophiolite was further uplifted relative to the Mesaoria Plain (Figure 1.2) which was subsiding as a half graben. Major uplift occurred during the Pleistocene (2 kilometres of the uplift occurred after the Pliocene (Robertson, 1977, 1990)). During the last 200,000 years, 20 metres of uplift have been documented (Poole et al., 1990). Most of the uplift is related to the convergence of Africa and Eurasia (McCallum and Robertson, 1990). Stream terraces

and incised valleys suggest that uplift processes are still active.

2.2.3 Plutonic Complex

The Plutonic Complex of the Troodos ophiolite (Wilson and Ingham, 1959) occurs at the centre of the massif (George, 1975). The Plutonic Complex comprises massive to foliated, tectonized harzburgite, dunite and minor lherzolite. Serpentinization of these rocks ranges from 40% to 100%.

A sequence of melagabbros, olivine gabbros, and pyroxene gabbros is interpreted as former magma chambers (Malpas et al., 1989a, 1989b). The primary texture and mineralogy of the gabbros are still preserved. Malpas et al. (1989a, 1989b), as well as Allen (1975) provide evidence for magma intrusions in multiple magma chambers. These intrusions are spatially and temporally variable; some are high-level intrusions in the dykes (Malpas et al., 1989b) and others are deep-seated, within the residual mantle (Malpas et al., 1987).

Discontinuous pods of plagiogranite (granophyre of Bear, 1960) composed mainly of feldspar and quartz, occur above the gabbros. In the Troodos ophiolite, the plagiogranites seem to be mainly associated with the gabbros and they are interpreted as capping magma chambers (Malpas, 1989, pers. comm.).

2.2.4 Sheeted Dyke Complex and Basal Group

The Sheeted Dyke Complex (Gass, 1979) is 1 to 1.2 kilometres thick. Both the top

and the bottom of the section show a rapid transition (over 100 metres) from 95% to 50% dykes. At the top, the Basal Group (Wilson and Ingham, 1959) is a transition zone upwards from sheeted dykes to extrusive volcanic rocks. Relations with the gabbros at the base of the sheeted complex are variable, i.e. gabbro intruding dyke; dyke cutting gabbro; and dyke originating in gabbro (Malpas et al. 1989a). These relationships reflect multiple magma emplacement events. The dykes are fine to medium grained and of basaltic to andesitic composition. They were affected by later sodium metasomatism, uralitization, chloritization, and epidotization. Mineral phases in the dykes include quartz, plagioclase, actinolite, chlorite, epidote with subordinate zeolite, prehnite, calcite, sphene, leucoxene, and iron oxides, hydroxides and sulfides. The dykes were subdivided by Bear (1960), on the basis of mineralogy, into four types: albite-diabase, quartz-diabase, epidote-diabase, and epidosite (epidote + quartz $\pm$ chlorite). Epidosites and their significance are discussed in Section 5.2.

In the study area, diabase dykes vary from fine (and glassy) to coarse grained (Plate 2.1), massive to highly fractured and from virtually unaltered diabases to highly altered epidosites. Plate 2.2 shows unaltered diabase dykes cutting altered epidosite dykes, indicating that alteration was probably contemporaneous with dyke formation. The bulk dyke mineralogy consists of quartz, plagioclase, hornblende, chlorite, and epidote; and minor amounts of sphene, rutile, and chlorite. For example, the coarse grained portion of sample O/C-6 (listing of samples in Appendix A.2) consists of 30% albitized plagioclase, 30% secondary quartz, 25% chlorite, 5% pyroxene, 5% ilmenite (associated with quartz and chlorite) and 5% epidote (associated with the quartz) whereas the fine grained portion consists of 80% glassy matrix with small laths of plagioclase, 10% quartz, 5% chlorite and 5% opaques. The quartz is anhedral to subhedral.

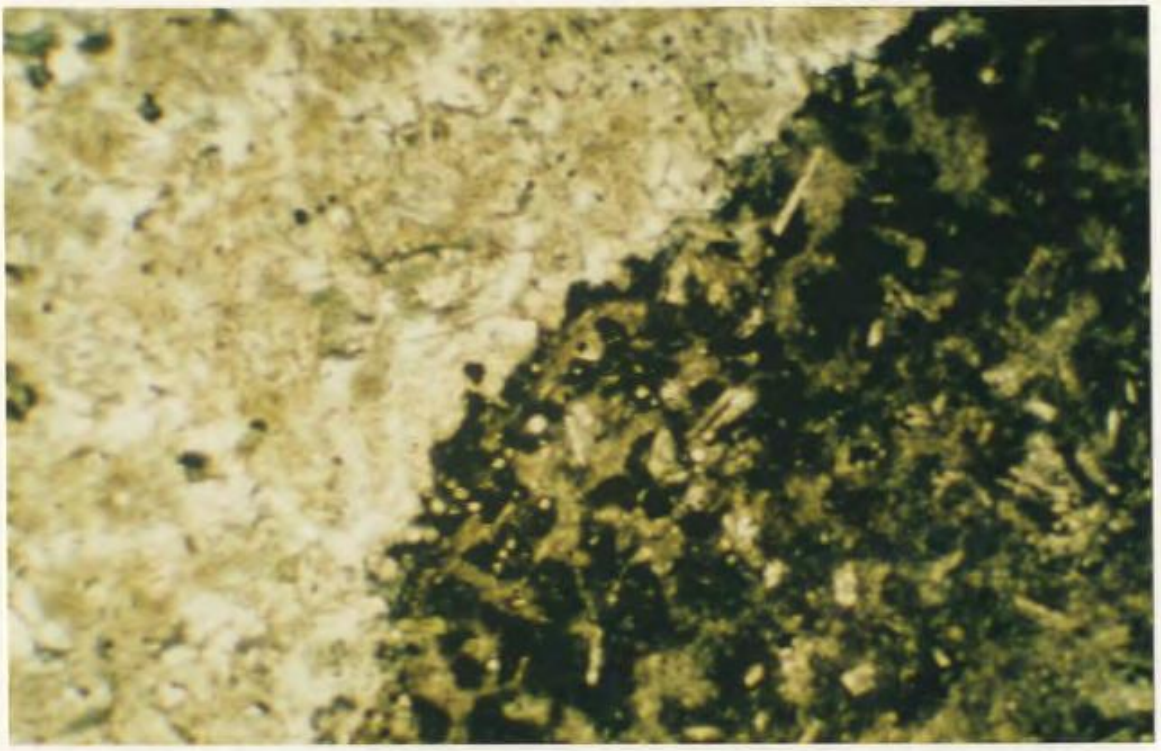

PLATE 2.1 Photomicrograph of chilled margin between light coarser dyke and dark fine dyke with glassy matrix in plane polarized light (Sample O/C-6). Field of view is 2.2 x 3.3 mm^2.



PLATE 2.2 Outcrop (near scanline section 1107) showing dyke cross cutting relationships. Late unaltered dyke cutting earlier epidosite dykes. Field notebook for scale.

On the basis of dyke orientations, the Sheeted Dyke Complex can be divided into five structural domains and three grabens (Verosub and Moores, 1981; Varga and Moores, 1985) (Figure 1.2). These domains include three graben structures, from west to east, the Solea, Mitsero and Larnaca grabens (Moores et al., 1990). These graben structures may be separated from each other by bounding listric normal faults which are thought to sole at depth near the dyke-gabbro interface (esp. Solea graben, Varga and Moores, 1985). The grabens are composed of fault bounded blocks of pillow lavas overlying sheeted dykes and sometimes gabbros and plagiogranites (Moores et al., 1990).

2.2.5 Pillow Lavas

Extrusive rocks of the Troodos ophiolite are 0.2 to 3 kilometres thick and are dominated by pillowed flows. Sheet flows, flow breccias, and hyaloclastites are also present. Common mineral phases include quartz, plagioclase, diopside, celadonite (formed at the expense of pyroxene), and glass. The lavas were initially divided into a Lower (axis) and an Upper (off-axis) sequence (Gass and Smewing, 1973; Smewing et al., 1975). Later geochemical work outlined two distinct geochemical suites referred to as 1) the arc tholeiite suite and 2) the high MgO - high SiO_2 suite (Robinson et al., 1983; Rautenschlein et al., 1985; Gillis, 1986). The rock types include basalt, andesite and dacite, and their low grade metamorphic equivalents (spilites and keratophyres).

The pillow lavas are variably altered, although fresh glass is locally preserved. The presence of fresh glass throughout the extrusive sequence indicates that the alteration, and thus fluid circulation, in the extrusive rocks was not pervasive and that the

alteration facies were not stratigraphically controlled (Robinson et al., 1983). The alteration appears to have been controlled by permeability variations, changes in lithology and proximity to intrusions (Gillis, 1983). Gillis (1983) considered this to be a reflection of variations in the hydrothermal recharge and discharge regimes in the oceanic crust.

2.2.6 Circum-Troodos Sedimentary Sequence

The pillow lavas are locally capped by manganiferous umbers, which represent exhalative rocks formed as a result of hydrothermal discharge at vents or fossil black smokers (Oudin and Constantinou, 1984). The umbers appear to have ponded in depressions on a seafloor comprising pillowed and massive flows (Robertson, 1977). To the north of the Mitsero graben are the overlying calcareous sedimentary rocks of Campanian to Oligocene age belonging to the Perapedhi, Kannaviou, Moni and Lefkara Formations (Bear, 1960, Robertson and Hudson, 1974).

2.2.7 South Troodos Transform Fault

The South Troodos Transform Fault (STTF; MacLeod, 1990) is a linear east-west trending zone to the south of the study area which consists of pillow lavas intercalated with clastic wedges, overlying intensely brecciated sheeted dykes (Simonian and Gass, 1978). Its exposed length is 35 kilometres and its width varies from 0.5 to 1.5 kilometres (Simonian and Gass, 1978). Simonian and Gass (1978) suggested two hypotheses to account for the swing in dyke orientation in the study area to the west as the STTF is approached from the north: 1) the dykes were injected into the crust in

a sigmoidal stress field formed between two spreading ridges; or 2) the dykes, originally injected in a north-south orientation (present coordinates), were rotated by continued movement on the fault. These two hypotheses imply opposite senses of motion and offset along the transform feature. The first, supported by Varga and Moores (1985) and Murton (1986) on the basis of comparison with the sonar surveys of oceanic fracture zones, implies sinistral slip along a dextrally offset transform fault, whereas the second, supported by Simonian and Gass (1978), Allerton and Vine (1987), Bonhommet et al. (1988), and MacLeod et al. (1990, 1992) on the basis of paleomagnetic data and similarity to Icelandic fracture zones, imply dextral slip along a sinistrally offset tranform fault.

2.2.8 Mineralization

Massive sulfide bodies within the extrusive sequence have been mined in five different mining districts. The massive sulfide tonnage varies from 50,000 to 18,000,000 tonnes with Cu grades ranging from 0.5% to 4.5%. The ore bodies occur throughout the Upper and Lower Pillow Lavas. Many of the deposits are overlain by a thin layer of ochre, an iron-rich sediment which may have been formed by the submarine weathering of the underlying sulfide ores (Robertson and Hudson, 1974; Herzig et al., 1990). Most of the larger orebodies appear to have filled depressions on the ancient seafloor. They are commonly zoned, with massive ore overlying sulfide and quartz ore which in turn overlies a stockwork of quartz and sulfide veins.

Minor sulfide mineralization is common in the sheeted dykes, generally in the form of pyrite-quartz associations which are not economic. The ore-forming fluids are thought to have been modified seawater fluids (Spooner, 1977; Spooner and Bray, 1977),

implying the existence of fluid-convecting cells driven by a heat source. Zones within the lower part of the Sheeted Dyke Complex contain 30-50% epidosite (epidote + quartz ± chlorite assemblages) in sheets and pipes up to 1 kilometre wide, which replace the diabase. These zones are regarded as the up-flow zones of the hydrothermal systems. Their location directly above the gabbros indicates that the heat source driving the systems was likely the underlying magma chamber (Richardson et al., 1987).

2.3 STRUCTURAL GEOLOGY

Verosub and Moores (1981), with further refinements by Moores et al. (1990) and Varga and Moores (1985, 1990), divided the Troodos ophiolite into five domains and three graben structures, based on the orientation of dykes within the Sheeted Dyke Complex (Figure 1.2). Moores et al. (1990) suggested that the Solea, Mitsero and Larnaca grabens are fossil axial valleys of former spreading centres. The characteristics of the Solea and Mitsero grabens are compared in Table 2.1 (the Larnaca graben was not included because of a lack of information). These grabens are constructed of fault-bounded blocks, which are assumed to have rotated along curved listric faults as a consequence of amagmatic extension (Varga and Moores, 1985). The Mitsero graben, the focus of this thesis, has been considered to have formed both in an on-axis position (Dilek et al., 1990; Moores et al., 1990; Varga and Moores, 1985) and, in an off-axis position Allerton and Vine (1991). This chapter, through an analysis of dyke orientations, large scale lineaments, and faults, will assess the validity of these two contrasting interpretations.

Table 2.1 Comparison Between Mitsero and Solea Graben Areas

Mitsero	Solea
■ smaller graben	■ larger graben
■ asymmetric	■ asymmetric
■ small dyke rotations (avg. 18°)	■ large rotations of dykes (avg. 40°-50°)
■ less amagmatic extension	■ greater amagmatic extension
■ southward swing in dyke orientation	■ dykes oriented north-south
■ axis curves to west	■ straight axis
■ tectonic extension	■ magmatic/tectonic extension > Mitsero
■ small isolated epidosites fault controlled	■ large epidosite area cross -cuts axis
■ many small ore deposits	■ 3 large ore deposits
■ west side more ore deposits than east side	■ west side more mineral deposits (less than Mitsero)
■ a few deposits on axis	■ 1 deposit centred on axis, others near
■ (possible detachment zone)	■ detachment at Kakopetria
■ temperatures 300° to 350°C	■ temperatures 300° to 350°C
■ thicker sediment cover	■ thinner sediment cover
■ U.P.L thin	■ U.P.L. thicker
■ L.P.L. thick	■ L.P.L. very thin
■ thick Basal Group	■ thin Basal Group
■ thicker crust	■ thinner crust
■ possible off-axis formation	■ possible fossil ridge

The Spilia-Politiko field area encompasses the Mitsero graben structure and western portion of the Makhaeras domain. This area can be sub-divided into domains, on the basis of dyke orientations. These dyke domains are useful in establishing the sequence of events leading to the formation of the Mitsero graben.

The Mitsero graben is an asymmetric structure; its western portion is 12 kilometres wide compared with a width of only 4 kilometres for the eastern portion (cf. Varga and Moores, 1985). The graben has a minimum length of 8 kilometres parallel to the north-striking axis. Its full extent parallel to dyke strike is obscured by the northerly dip of the ophiolite units beneath the sediments of the Mesaoria Plain. The axis of the graben is defined by an area of steeply dipping dykes with large variations in strike. East of the graben axis, dykes dip steeply to the west whereas to the west of the axis the dyke dips are shallower and to the east. The graben axis coincides with a 500 metre wide breccia zone described by Ramsden (1987), in which the dykes are extensively shattered. The axis trends south from Mitsero village. As it nears the South Troodos Transform Fault south of Apliki, the axis curves to the west, suggesting that the graben and the fault interacted.

Discrete features at different scales, such as large scale lineaments, faults and dykes, aid in developing a tectonic framework for the field area. Previously published work on the interpretation of remotely sensed images of the Troodos Ophiolite has been restricted to attempts to delineate domains within the entire complex (e.g. Moores et al., 1990).

The delineation of dyke subdomains within the study area required the manipulation of a large amount of dyke orientation data; this was accomplished through the use of the several programs written during the course of this study (refer to flow chart

Figure 2.2; Appendix D). These subdomains lie within the Spilia-Politiko area and are distinct from the domains delineated by Varga an Moores (1985, 1990). Further references to domains, unless otherwise stated, refer to the subdomains within the Spilia-Politiko area.

The description of the structural geology of the study area is based largely on the relationships and orientations of dykes and faulting. Domains were recognized on the basis of different dyke orientations. These dykes were later rotated as a result of the formation of the Mitsero graben. The Troodos ophiolite is cut by major lineaments which are thought to be faults which developed during the formation of the ophiolite and during its uplift.

2.3.1 Large Scale Features

Large scale lineaments in the Troodos Ophiolite are visible on Landsat Thematic Mapper and Multi Spectral Scanner (Figure 2.3A) images. Using various combinations of four wavelength bands (2 visible and 2 near infrared), a lineament map was constructed (Figure 2.3B). These lineaments are thought to represent the surface exposures of fault traces because many of them coincide with faults mapped by the Cyprus Geological Survey Department (Bear, 1960), and with known fault traces in north-south trending valleys.

The extreme relief of the Troodos ophiolite, in the form of north-north-east to south-south-west trending valleys, adds a bias to the lineament analysis. Whereas many valleys may be fault controlled, in which case their lineaments are important to this study, it was not possible to exclude purely erosional topographic control for

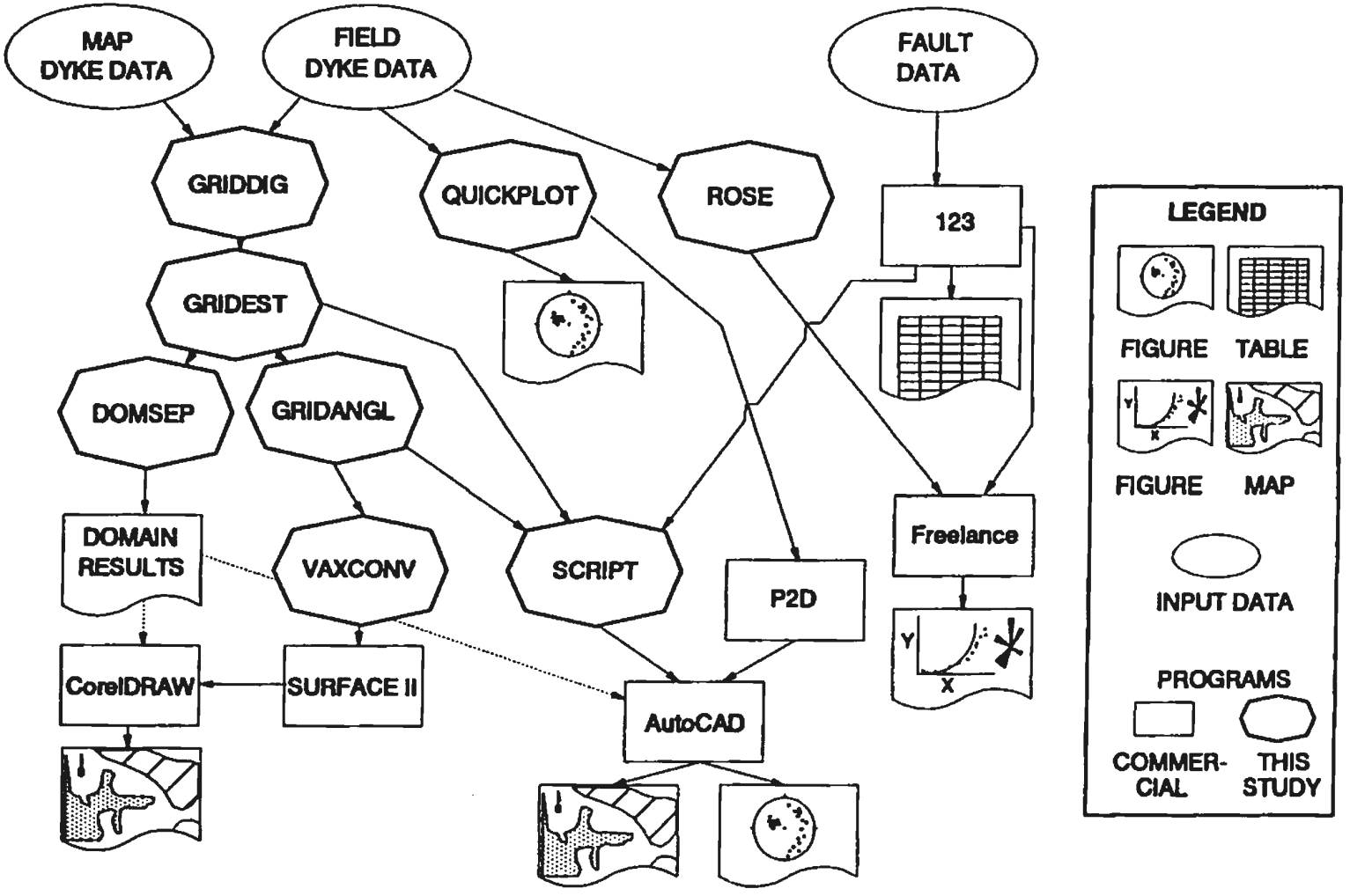

FIGURE 2.2 FLOWCHART OF DATA AND PROGRAMS USED IN CHAPTER 2. COMMERCIAL PROGRAMS INCLUDE: 123 - SPREADSHEET; AutoCAD,FreeLance AND CorelDRAW - GRAPHICS; P2D - PIC TO DXF CONVERSION AND SURFACE II - CONTOURING AND PLOTTING.

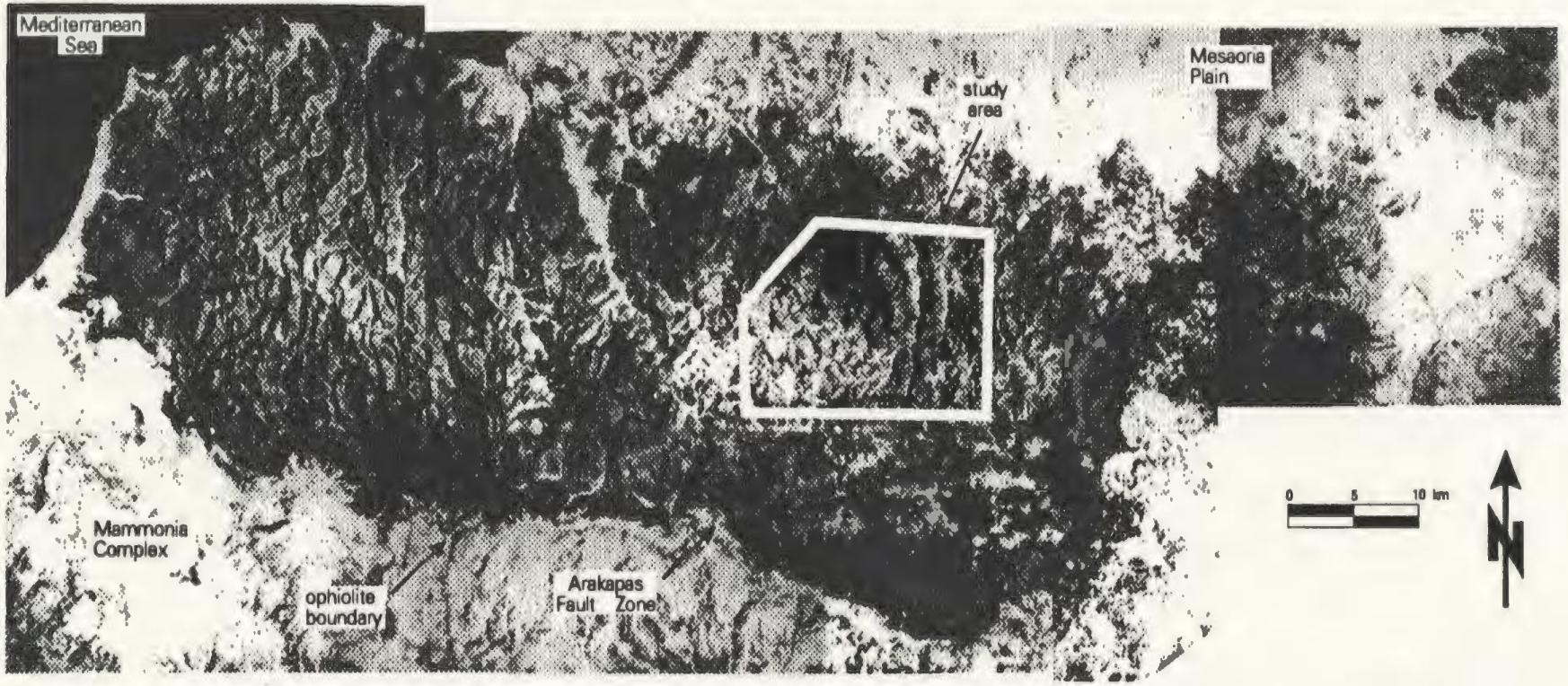

FIGURE 2.3A LANDSAT MULTI-SPECTRAL SCAN IMAGE OF THE TROODOS OPHIOLITE SHOWING THE LOCATION OF THE STUDY AREA OUTLINED IN WHITE

many of the lineaments. North-south lineaments were thus not included in the lineament map unless they included several valleys. As a result some of the shorter north-south trending lineaments may not have been noted.

The distribution of orientations of lineaments which lie entirely within the boundaries of the ophiolite is similar to the distribution of orientations for the complete lineament set (Figure 2.3B). On the basis of their orientation, the lineament data can be subdivided into four sets (Figure 2.4). Set 1 consists of roughly east-west (70°-110°) trending lineaments within the ophiolite boundaries that also cut the younger sediments of the allochthonous Mammonia complex to the south, implying that the lineaments formed during syn- to post-uplift fracturing caused by the updoming/emplacement of the ophiolite. Set 2 are north-south (350°-010°) trending lineaments that generally do not cut the sediments, stopping abruptly at the ophiolite/sediment boundary, indicating these lineaments may have developed during formation of the ophiolite in the oceanic lithosphere beneath the seafloor. These lineaments trend parallel to the paleo-spreading ridge as defined by Varga and Moores (1990). Set 3 comprises NNW-SSE (150°) trending lineaments which cut the ophiolite/sediment boundary indicating a late origin post-dating sediment deposition. A fourth set of lineaments with curved trajectories lies just east of the centre of the ophiolite. These are confined within the ophiolite boundaries. These lineaments were the basis for the definition of the Mitsero graben axis by Moores et al. (1990) and Varga and Moores (1985). The lineaments greater than 6 kilometres long are more uniformly distributed with respect to their orientation than the short lineaments (Figure 2.4). The longer set of lineaments shows a weak maximum at the same azimuths as the shorter lineaments.

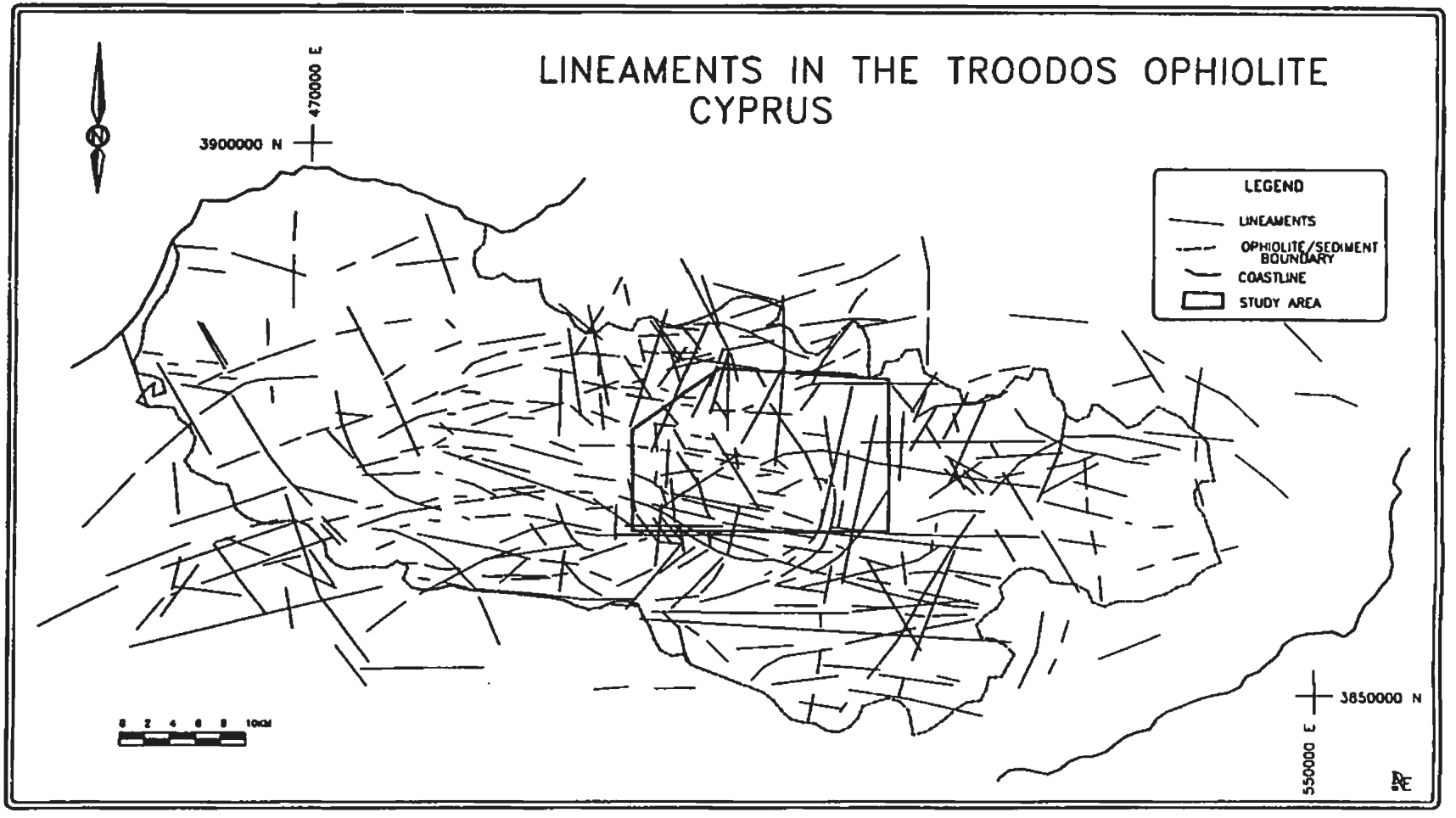

FIGURE 2.38 LINEAMENTS INTERPRETED FORM LANDSAT THEMATIC MAPPER IMAGES OF THE TROODOS OPHIOLITE, CYPRUS. FOUR WAVELENGTHS OF LIGHT, TWO VISIBLE AND TWO INFRARED WERE USED TO CREATE FALSE COLOUR COMPOSITE PLOTS USING COMBINATIONS OF TWO OF THE WAVELENGTHS. THE LINEAMENT INTERPRETATIONS WERE COMPILED FROM FOUR COMPOSITE PLOTS FOR THIS FIGURE.

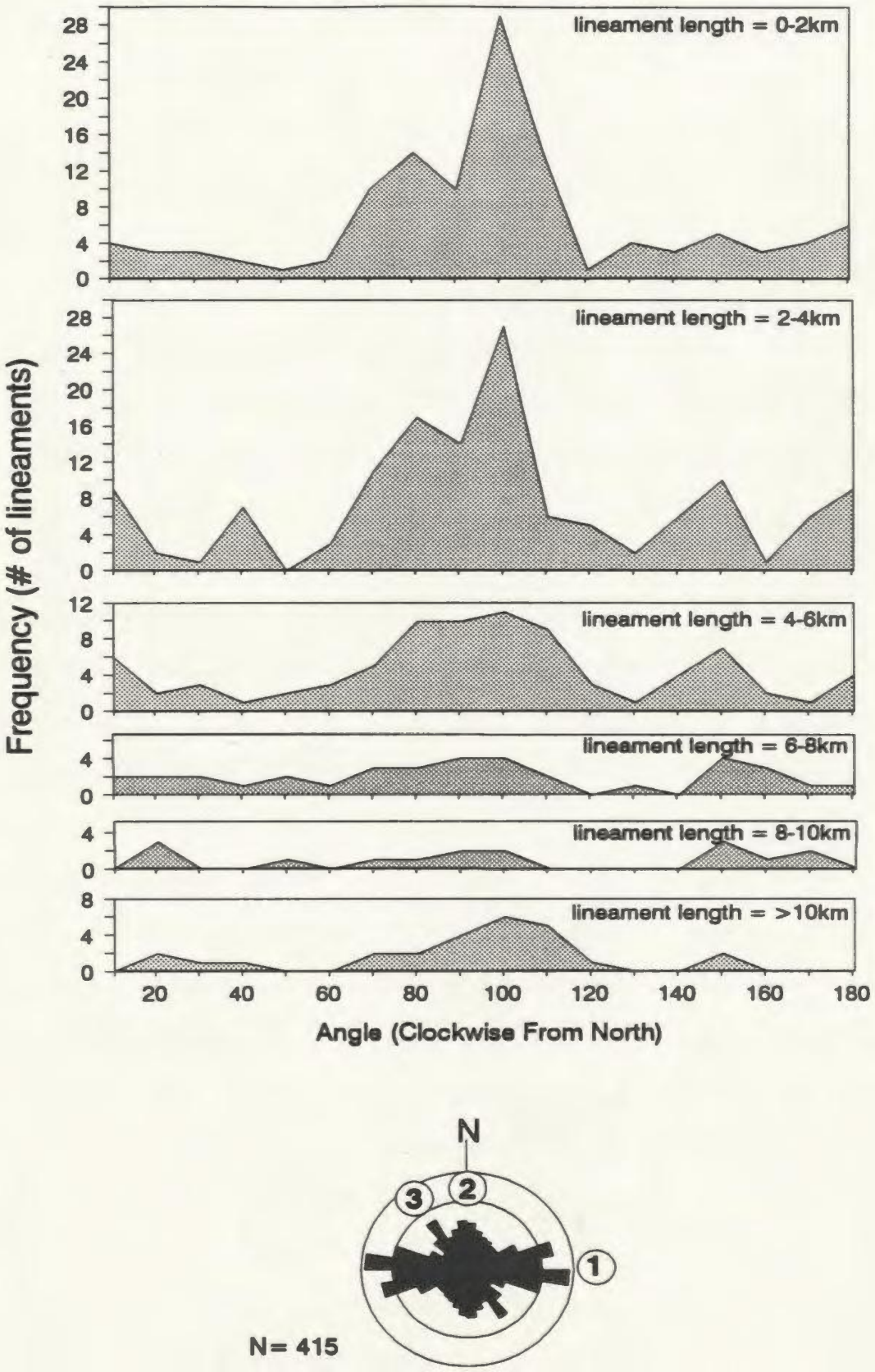

FIGURE 2.4 LANDSAT LINEAMENT ANALYSIS FOR THE TROODOS OPHIOLITE, CYPRUS. FREQUENCY PLOTS OF LINEAMENTS BY ORIENTATION AND LENGTH. ROSE DIAGRAM OF THE DISTRIBUTION OF ALL LINEAMENT ORIENTATIONS. NUMBERS IN CIRCLES ARE LINEAMENT SET NUMBERS (SEE TEXT FOR DISCUSSION).

The two lineament data sets (#2 and #4) related to the formation of the oceanic crust, form a pattern similar to the fracture pattern found in clay model doming experiments by Withjack and Scheiner (1982). These showed that dome-flanking fractures develop primarily as normal faults. A north-south directed compressional event during up-doming would result in a north-south oriented lineament pattern, whereas a north-south directed tensional event would result in east-west directed lineaments. In the case of the Troodos Complex, the majority of lineaments are oriented in an east-west direction (Figure 2.4). Comparison with the clay modelling experiments performed by Withjack and Scheiner (1982), indicates that the pattern of lineaments in the Troodos Complex may have formed in an environment of either solely up-doming or one of updoming combined with extension, with the maximum horizontal tensional stress oriented in an north-south direction (present coordinates). Due to the 90° rotation of the ophiolite, this translates to a north-south oriented maximum horizontal compressive stress while the ophiolite was still part of the seafloor. Varga's (1991) work on fault motion in the Solea graben documents a north-south compressional event postdating the hydrothermal events. Compressional events result in more north-south oriented lineaments unless the rate of compression was much smaller than the rate of uplift (Withjack and Scheiner, 1982). The roughly north-south directed set 2 lineaments, which lie entirely within the boundaries of the ophiolite, could have formed as a result of the compressional event which Varga (1991) postulated was uplift related. Since these lineaments do not extend beyond the boundary of the igneous rocks into the sediments, they likely formed while the ophiolite was still part of the oceanic crust before substantial sedimentation had taken place, although the uplift may have been part of the ridge process (Malpas, pers.comm., 1989) or ophiolite emplacement process (Gass, 1979; Robertson, 1990). Sets 1 and 3 are likely primarily related to the uplift and emplacement of the ophiolite, whereas sets 2 and 4 may have formed while the Troodos ocean crust was still forming.

2.3.2 Dyke Relations

Much information concerning the characteristics of sheeted dykes in ophiolitic terranes, comes from studies done in the Troodos ophiolite (e.g. Cann, 1974; Kidd and Cann, 1974), the Bay of Islands ophiolite, Newfoundland (e.g. Rosencrantz, 1980, 1982) and the Semail ophiolite, Oman (MacLeod et al., 1992).

Dip directions of dykes with respect to the spreading axis can be predicted from two models: (1) a variable subsidence model in which dykes dip away from the axis, their rotation caused by loading of lensoid volcanic piles (Cann, 1974, Rosencrantz, 1980, seen in the Bay of Islands Ophiolite Complex, Newfoundland), and (2) a normal faulting model in which the dykes dip toward the spreading axis (seen in the Josephine ophiolite, California, U.S.A. (Harper, 1982; 1985) and in the Troodos Ophiolite, Cyprus (Verosub and Moores, 1981; Varga and Moores, 1985).

In the Sheeted Dyke Complex of the Troodos Ophiolite, three dyke domain boundary types have been distinguished (Moores et al., 1990): 1) graben boundaries defined by dykes dipping toward each other (the graben axis); 2) graben boundaries defined by dykes dipping away from each other (the graben edge); and 3) intrusive contacts. Dykes at the boundary of the Mitsero graben and the Makhaeras domain are steeply dipping and dip away from each other.

In the study area, the following outcrop-scale dyke injection relations were seen: dykes injected along dyke margins between two dykes; into the interior of a single dyke, effectively splitting it; or in a cross-cutting fashion where the later dyke is intruded at a different angle than the earlier dyke. In the field area where a dyke

cross-cuts another dyke, the younger dyke generally has the steeper dip. Dyke propagation is controlled by either pre-existing fractures in the crust or the orientation of the least compressive principal stress (Pollard, 1987). Alteration, where present in the dykes is limited to a hydrothermal mineral assemblage (epidote, quartz and chlorite). The hydrothermal alteration is patchy. In the most intensely altered outcrops, not more than 50% of the exposed dykes are altered to epidosite (quartz-epidote-chlorite assemblage). Unaltered dykes were seen to cut hydrothermally altered dykes indicating the hydrothermal alteration was preceded, as well as succeeded, by magmatic activity.

2.3.2.1 *Basis For Dyke Domains*

An analysis of dyke orientations in the Spilia-Politiko area was undertaken to distinguish among different dyke domains and then to create a tectonic model of the study area. Roughly 3300 dyke orientations were collected in the study area (848 by the author with the remainder taken from various published maps, Bear, 1960; Carr and Bear, 1960; Malpas and Brace, 1987; Ramsden, 1987; Figure 2.5).

To facilitate the interpretation of the variation in dyke orientations, dyke orientation was estimated at node points on a grid with a spacing of 500 metres, superimposed on a map of the field area. The density of data points was too low to allow estimation of dyke orientation values at a grid node spacing of less than 500 metres. The estimation method used to calculate dyke orientations at grid node points was a nearest neighbour, exponential distance method. This method proceeded by searching for data points within a specified radius of a node point (500 metres). A weight, exponentially dependent on the distance from the data point to the node point, was assigned to each

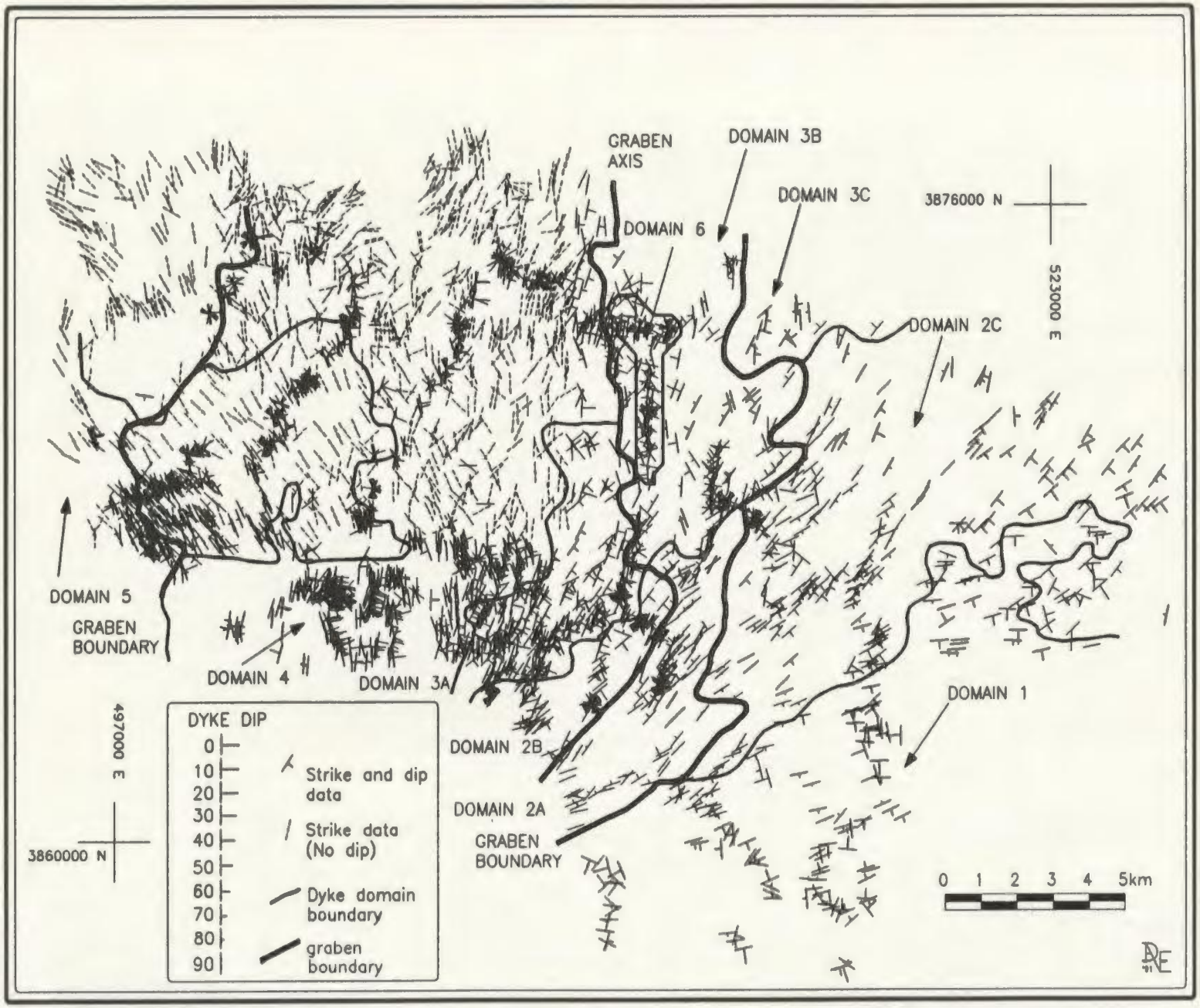

FIGURE 2.5 DYKE ORIENTATION DATA, SPILIA – POLITIKO AREA, CYPRUS. GRABEN AND DOMAIN BOUNDARIES BASED ON INFORMATION IN FIGURES 2.6 AND 2.7.

data point within the specified radius. These weights were then applied to the direction cosines of the orientation of the dyke at the data point. The normalized sum of these values was used to compute an orientation for each node point. A more complete description of the method is presented in Appendix D (program: GRIDEST).

In the field area there is a general trend in the strike of dykes from NW-SE in the west through NE-SW to E-W in the east (Figure 2.6). There are abrupt changes, on the scale of the 500 metre node spacings, in dyke strike at various locations in the area. These abrupt changes in the dyke strike were used to delineate five major dyke domains numbered 1 to 5 from east to west. From one domain to the next, the mean strike rotates counterclockwise by roughly 25°. In the eastern-most domain (#1), dyke strikes are roughly 070°, and progressively westward the mean strikes of dykes within domains are roughly 045° (#2), 026° (#3), 000° (#4) and 324° (#5) (Figure 2.6). Within the domains the dyke trends show no systematic changes in strike toward the domain edges. A sixth, smaller domain, showing a bimodal distribution of dyke orientations, at 018° and 113°, lies within domain 3, and is designated domain 6.

The gridded data were used to create a dip map of the Spilia-Politiko area (Figure 2.7). Less dip estimates than strike estimates (Figure 2.6) were made because about 30% of the literature dyke orientation data contained only strike information. There are several areas characterized by opposing dyke dip directions. Areas of near-vertical to vertical dyke dips generally coincide with areas where dyke dips change from east-dipping to west-dipping. In the south-west of the field area there are areas of near vertically dipping dykes which did not coincide with changes in dip direction (Figure 2.7); these lie in the Plutonic Complex.

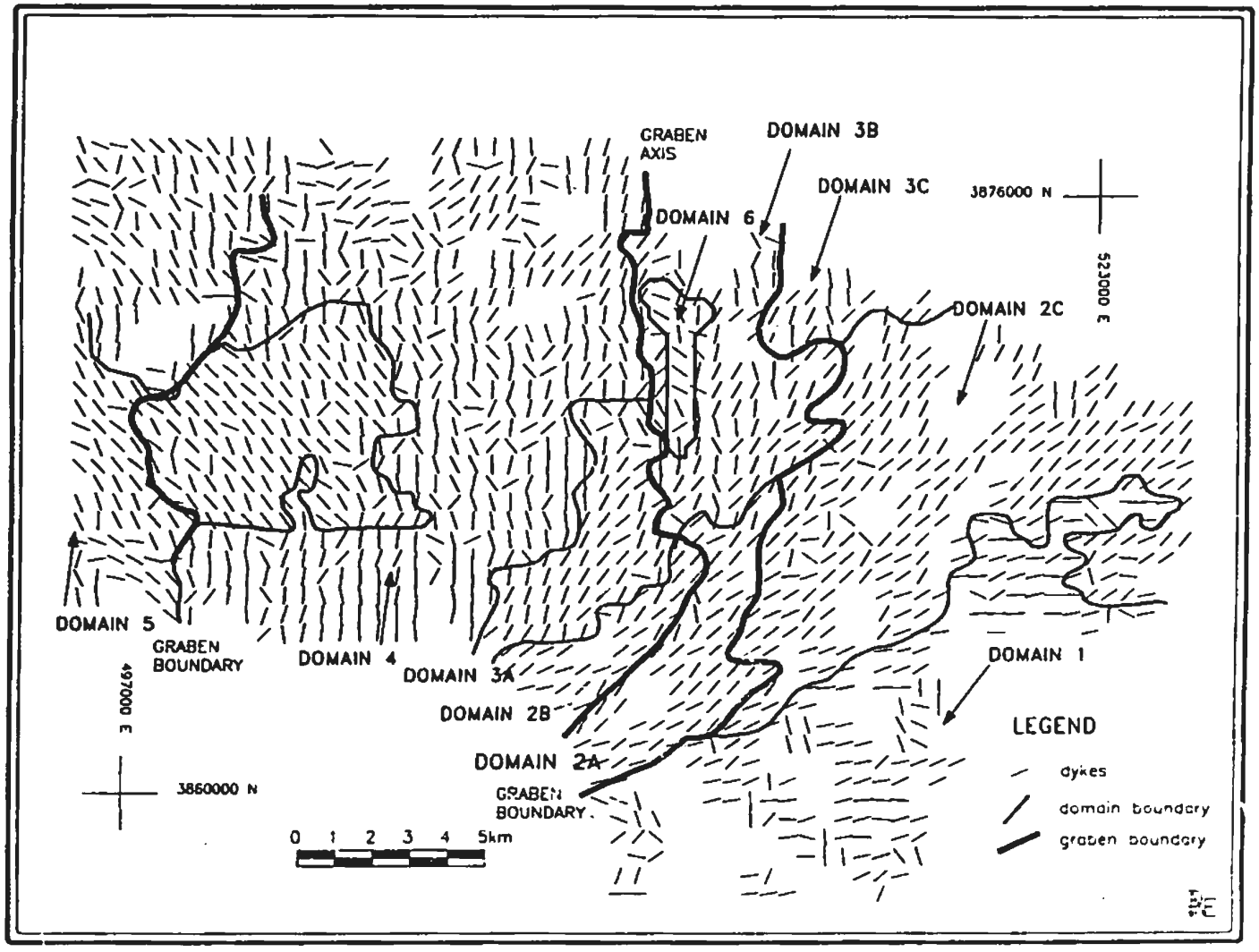

FIGURE 2.6 ESTIMATED STRIKE OF DYKES, SPILIA – POLITIKO AREA, CYPRUS

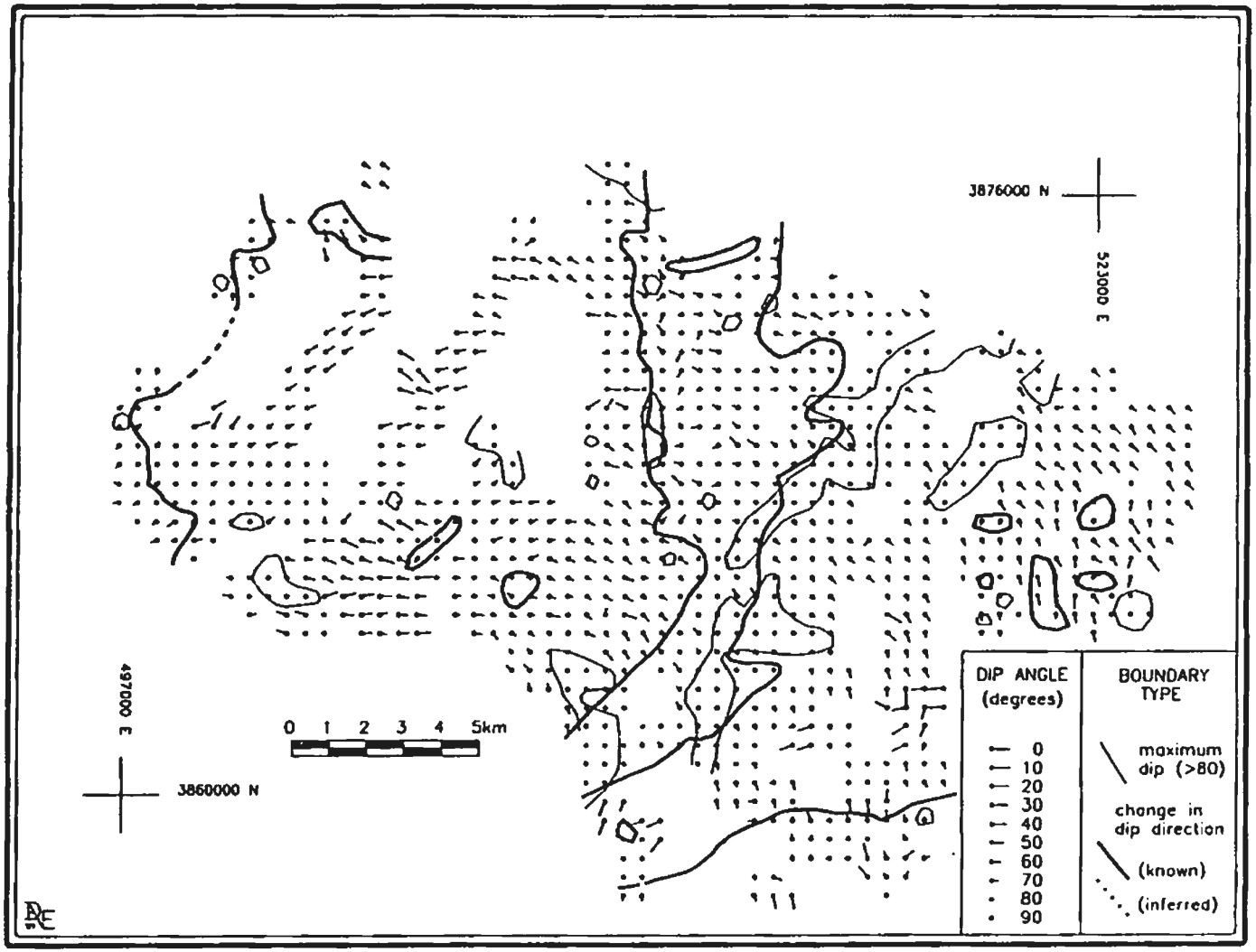

FIGURE 2.7 ESTIMATED DYKE DIP, SPILIA – POLITIKO AREA, CYPRUS.

The consistent dip of dykes toward the lineament, defined by Varga and Moores (1985) as the Mitsero graben axis, suggests that the subsidence model of Cann (1974) does not apply in this area and that the dyke rotations are consistent with the normal faulting model of Verosub and Moores (1971), assuming on-axis formation of the graben structure. Boundaries separating changes in dip direction, were in roughly the same positions as the graben boundaries and axis presented by Moores et al. (1990) for the Mitsero graben. The boundaries are thought to be more accurate than the Moores et al. (1990) boundaries which were based on LandSat-imagery-interpreted lineaments (compare figures 1.2 and 2.5).

The graben axis and eastern graben boundaries subdivide domains 2 and 3 into three sub-domains (labelled A, B, C on Figure 2.8). Domain 3C will not be dealt with further as the sparseness of the data within its bounds precludes useful interpretation; there were only 13 data points. Note that all stereographic projections in this study, are plots of poles to dyke planes on lower-hemisphere, equal-area projections. Although there is some overlap in the mean orientations of dykes between domains, none of the 95% level of confidence circles of the mean domain orientations of domains 1, 2A, 3A, 4, 5 and 6B overlap with each other, indicating that the mean orientation of each of these domains is distinct (Figure 2.9). The standard deviations of the dyke orientations are large enough that there is some overlap between the domains. Domain 2B and 2C confidence circles of the mean orientations overlap indicating they may be part of the same domain. The boundaries of the sub-domains within domains 2 and 3 coincide with boundaries established by Varga and Moores (1985) and Ramsden (1987), which delineate the axis and eastern boundary of the Mitsero graben (compare Figures 1.2 and 2.10). Domain 6 was subdivided into 6A and 6B on the basis of distinct populations of dyke orientations. The dykes of the two populations, 6A and 6B, are not spatially separated within domain 6. That the strike

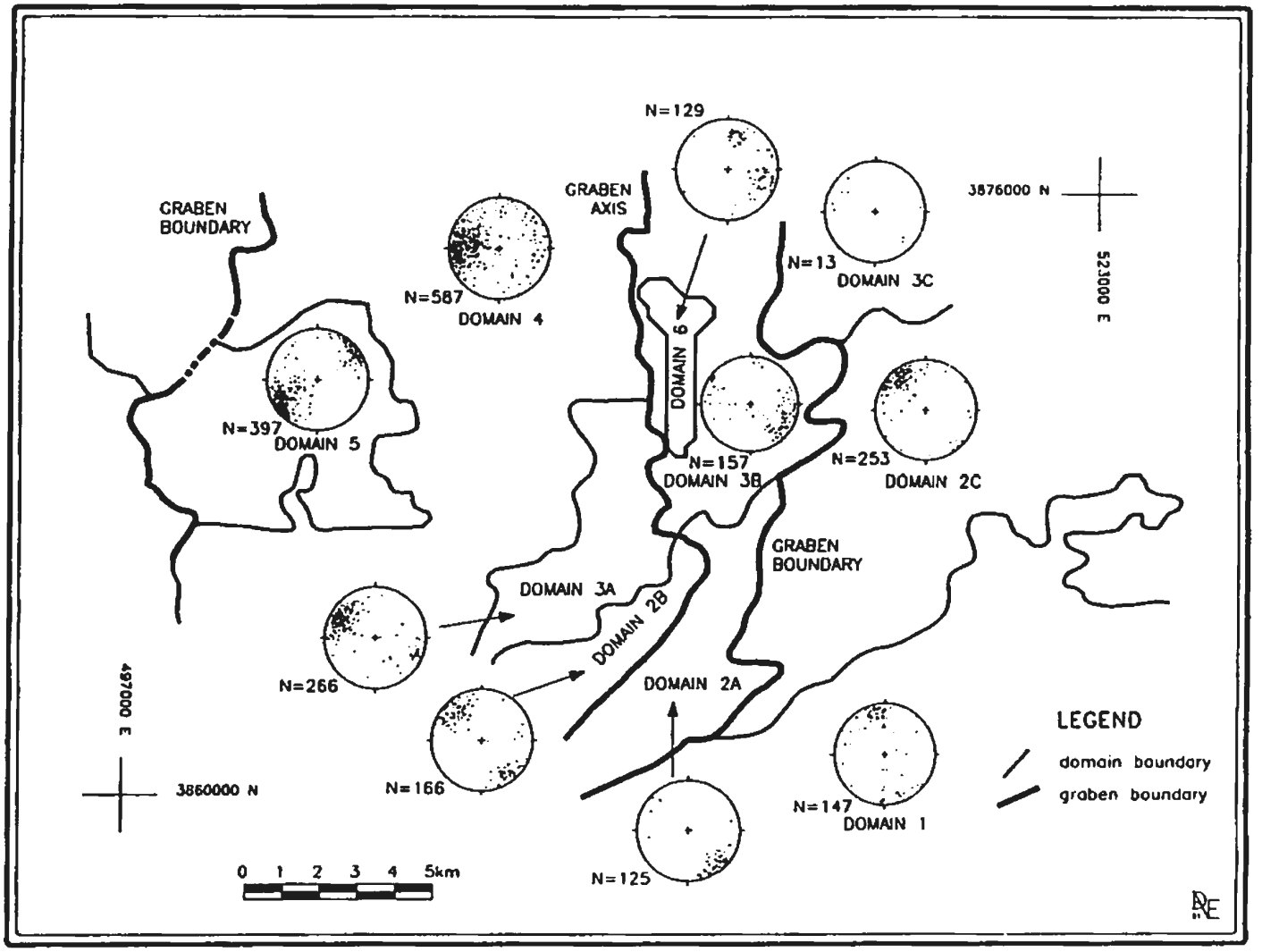

FIGURE 2.8 DYKE DOMAINS AND DYKE ORIENTATIONS, SPILIA – POLITIKO AREA, CYPRUS. DATA ARE POLES TO PLANES ON EQUAL AREA, LOWER HEMISPHERE PROJECTIONS.

Domain	N	Mean Az. Dip	95% Level (degrees)
1	147	164 80	14.0
2A	125	318 81	6.8
2B	166	137 82	14.2
2C	253	138 78	6.6
3A	266	116 71	5.9
3B	157	294 76	11.0
4	587	92 65	3.9
5	397	55 80	7.9
6A	66	288 65	8.0
6B	63	203 63	8.1

95% Level = cone of 95% confidence within which the mean is located, in degrees

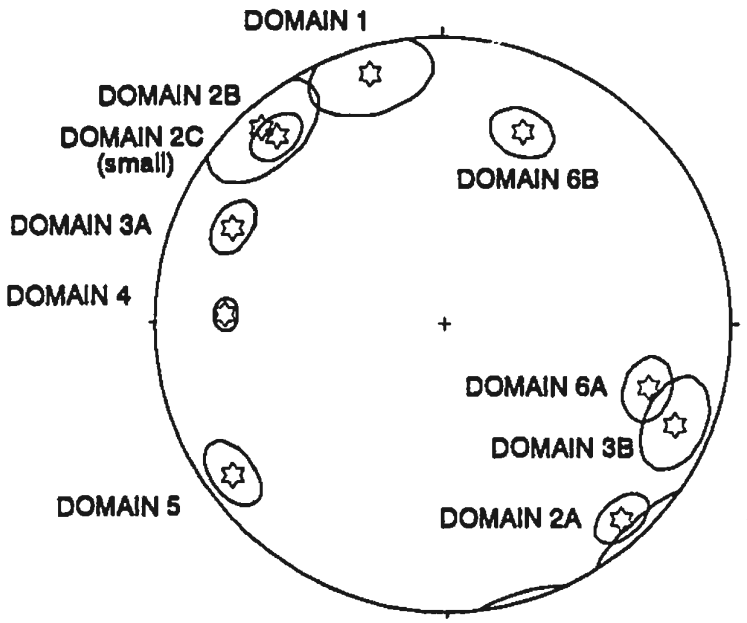

FIGURE 2.9 STEREOGRAPHIC PROJECTION OF THE DYKE DOMAIN MEAN DYKE ORIENTATIONS. STARS SHOW POLES TO MEAN DYKE ORIENTATION AND ELLIPSES ARE THE 95% LEVEL OF CONFIDENCE FOR THE LOCATION OF THE MEAN OF THE DATA SET (AFTER FISHER, 1956).

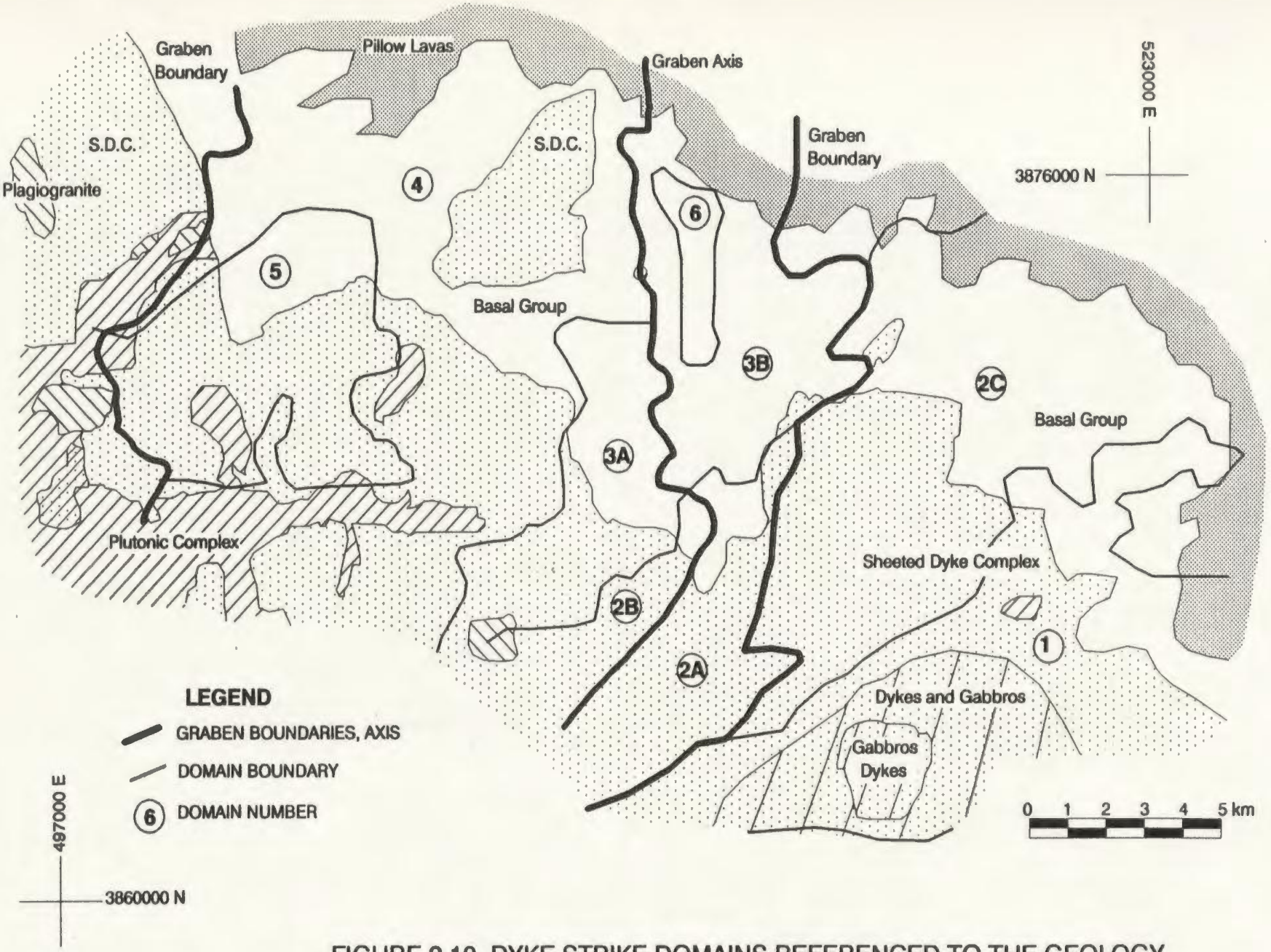

FIGURE 2.10 DYKE STRIKE DOMAINS REFERENCED TO THE GEOLOGY OF THE SPILIA-POLITIKO AREA, CYPRUS.

of dykes is continuous across the graben boundaries indicates the dyke strike orientations predate the graben formation. The formation of the graben structure affected only the dip direction of dykes.

2.3.2.2 *Geological Significance of Dyke Domains*

The bi-modal distribution of dyke orientations of domain 6 (subdivided into 6A and 6B), lies east of Ayios Epiphanios in sub-domain 3B. Domain 6A dykes have a similar mean orientation to domain 3B dykes. The domain 6B dykes may be later intrusions related to a small, possibly off-axis, gabbro body which intrudes the dykes of the Basal Group, near Ayios Epiphanios. The domain 6B dykes intruded the original dykes of sub-domain 3B, in the area of domain 6, almost at right angles to the original strike (85°) (see Figure 2.9 for orientations of the two sets of dykes in domain 6). A rotation in the stress field may have resulted in the intrusion of these dykes at a high angle to the existing dykes. Domain 6A dyke orientations, although overlapping with 3B, may also have an affinity to domain 4; they have very similar strikes, and equal but opposite dips. This may be explained in that the domains 3B and 6A lie on opposite sides of the graben axis from domain 4 but they may have been part of the same domain before the formation of the graben structure.

The graben axis, defined on the basis of dyke domain boundaries, closely corresponds to a major curved lineament (Figure 2.11). In several other cases there is a correspondence between lineaments and domain boundaries (e.g. portions of the boundaries of domains 2B, 3A, 3C and 5). This indicates that portions of the domain boundaries are controlled by the lineaments which may be fault traces. The magnitude of possible offsets or rotations along these lineaments is not known.

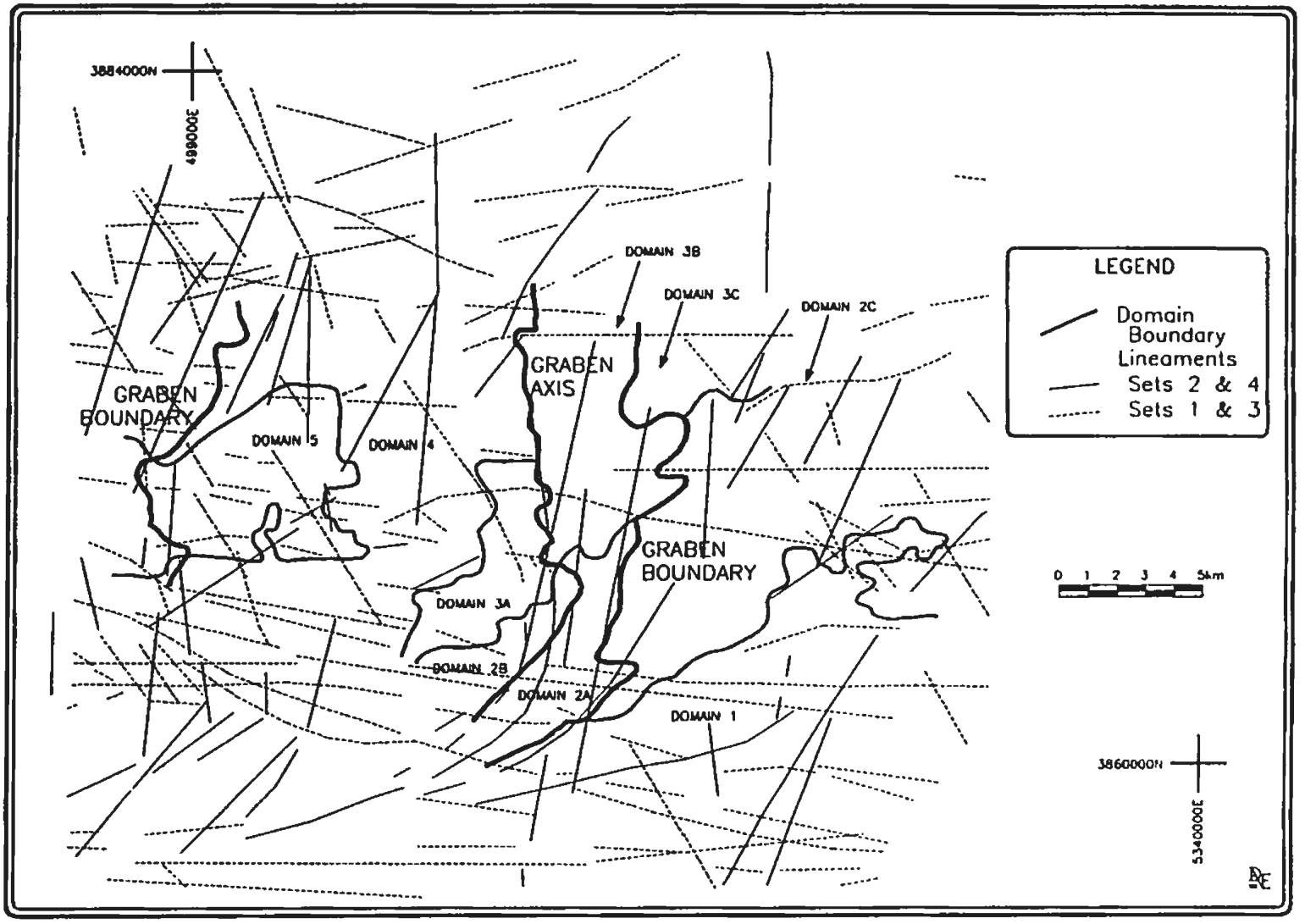

FIGURE 2.11 DOMAIN BOUNDARIES AND LINEAMENTS IN THE SPILIA – POLITIKO AREA, CYPRUS.

The domain boundaries do not appear to be influenced by the ophiolite stratigraphy (Figure 2.10). The map view of the area is an oblique section through the ophiolite, with deeper stratigraphic levels exposed to the south. Dykes, originally overlying gabbros, and now eroded, may have originally had strikes similar to the dykes presently exposed in the domain. Continuity of dyke strike with depth is exemplified by domain 4 (figure 2.6).

Comparison of the angle of intersection between estimated dyke orientations at adjacent nodes may indicate changes in the lithological properties of the rock. The orientation of dykes intruding, for example, into pillow lavas, may be different from those intruding into other sheeted dykes. This is because the structural fabric of the pillow lavas is different from that of the sheeted dykes. The magnitude of the acute angle of the intersection of poles to adjacent dykes (estimated) at grid nodes is contoured in Figure 2.12 (Appendix D explains the methodology used to produce this figure; program: GRIDANGL). This map shows that dyke orientations within the Sheeted Dyke Complex proper (excluding the Basal Group) are very consistent on a local scale; that is, there are few abrupt changes in dyke attitude within domain boundaries. However, changes in rock type, such as the transition zone from the Sheeted Dyke Complex to the Pillow Lavas (Basal Group), and the transition to the Plutonic Complex at the bottom, cause abrupt local changes in dyke orientation. The largest changes in orientation occur along the graben axis.

Within the Basal Group, changes in dyke orientation between adjacent grid nodes are greater than in the areas of 100% sheeted dykes. Differences between the lithological characteristics of the Basal Group (which has randomly located pillow screens among the dykes) and the Sheeted Dyke Complex (which has a well defined fabric) are a likely cause of this discrepancy. This suggests a possible history for the formation of

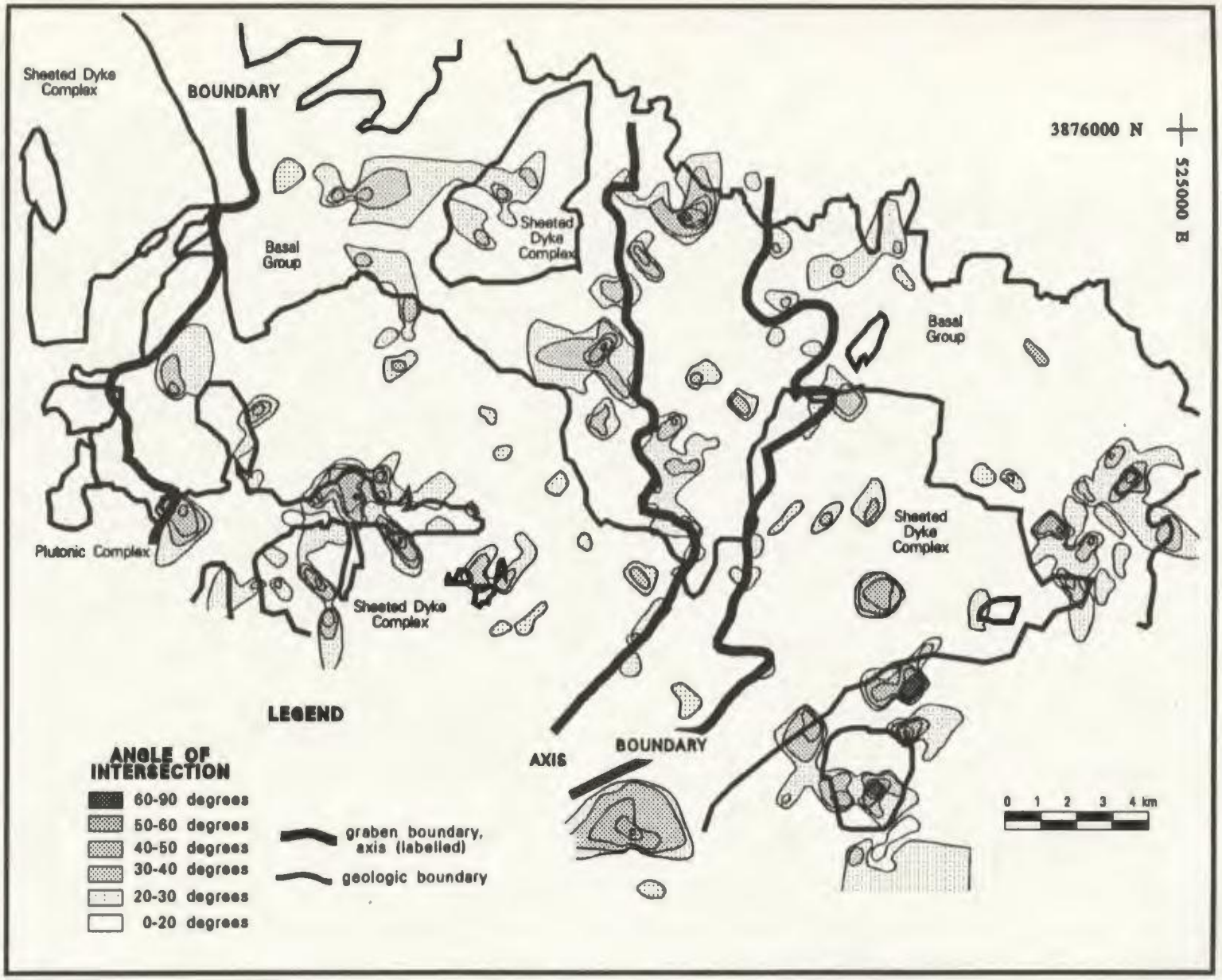

FIGURE 2.12 CONTOURED ANGLE OF INTERSECTION BETWEEN DYKES AT ADJACENT NODES, SPILIA-POLITIKO AREA, CYPRUS (SEE TEXT FOR FURTHER EXPLANATION).

the Basal Group as follows: initially the Basal Group was composed entirely of pillow lavas and flows. They were subsequently intruded by dykes as the sequence increased in thickness. Although presently the Basal Group contains nearly 100% dykes at its base, the first dykes intruded into pillow lavas and flow units rather than into earlier dykes. Later dykes intruded into these earlier dykes as well as into pillowed and flow lavas, which are now seen as discontinuous screens throughout the Basal Group.

The boundaries of the Mitsero graben are defined on the basis of spatial variations in the strike and dip of the dykes (Moores et al., 1990; Varga and Moores, 1985). The western boundary, separating the Mitsero graben and the neighbouring Solea graben is not abrupt; the relationships of dykes between the grabens may be intrusive rather than fault bounded (Moores et al., 1990). According to Varga and Moores (1985), the eastern boundary of the Mitsero graben with the Makhaeras domain is well-defined by an abrupt change in the azimuth and dip of the dykes. However, the present analysis shows that the dykes of the Makhaeras domain (which include the dykes of domains 1, 2C and 3C in this study) do not appear to overprint the dykes in the eastern portion of the Mitsero graben, since there is no change in the strike of the dykes. The change in dip direction of dykes, between the Mitsero graben and Makhaeras domain, seems to be purely a function of the rotation of the dyke blocks during the formation of the graben structure. This implies that the dykes of the Mitsero and Makhaeras domains formed contemporaneously and that the graben structure was superimposed on the dykes at a later time.

A contour map of the magnitude of dyke dip (irrespective of dip direction) (Figure 2.13) shows that dyke dips tend to be steeper east of the Mitsero graben axis than west of the axis. A band of dykes with shallow dips is in the western portion of the graben, near the Basal Group/Sheeted Dyke Complex transition. Gaps in the data

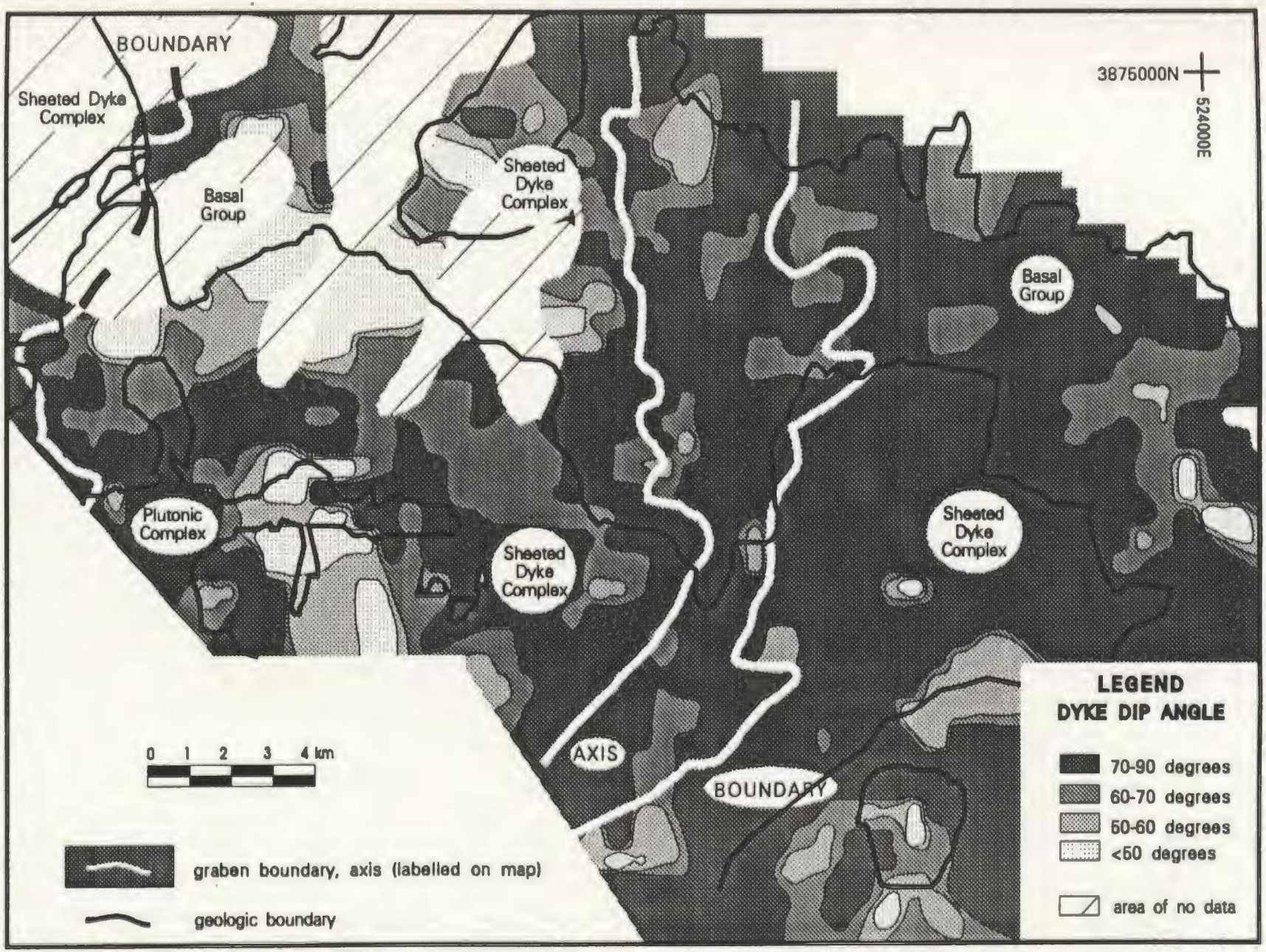

FIGURE 2.13 CONTOURED DYKE DIPS, SPILIA - POLITIKO AREA, CYPRUS.

coverage in this area make interpretation difficult. To the west of the Mitsero-Solea graben boundary dyke dips are again steep. Within the Makhaeras domain, dyke dips are very steep, shallowing only slightly in the eastern part of the domain. In the area of the Plutonic Complex there is a sequence of dykes with a shallow-steep-shallow-steep dipping pattern repeated from east to west forming an undulating pattern. This pattern may result from unequal rotations of fault bounded blocks in the area of the Plutonic Complex. Dyke trends in the Plutonic Complex show a larger scatter around a mean orientation than do those in the Sheeted Dyke Complex (Figure 2.12). This may be the result of the intrusion of dykes of various orientations from different plutonic centres.

The available dyke data were not appropriate to determine the relative age relations between the domains. However, a model of the geological development of the field area, based on data presented in this chapter, does enable prediction of temporal relations between the domains.

2.3.2.3 *Dyke Geochemistry*

To determine whether domains defined by the orientation of dykes were identifiable on the basis of the chemical signature of the dykes, 20 whole rock analyses were done on relatively fresh dyke samples, covering each dyke domain in the study area (see Appendix B.2 for analyses and sample locations). These were combined with 417 analyses from ten road-cut sections available in the literature (Baragar et al., 1989) (Refer to Appendix B.2 for the road section location map and discrimination plots). The geochemical data indicate that the majority of dykes from all domains plot as low-potassium tholeiites on a Ti versus Cr diagram (after Pearce, 1975), and within

the island-arc basalt field of a Zr versus Zr/Y diagram (after Pearce and Norry, 1979). Both depleted and undepleted suites are represented by the dykes in all domains (classified on the basis of lower levels of incompatible elements and $MgO > 5.5\%$, $TiO_2 < 0.85\%$ and $Cr > 40ppm$ in the depleted suite - Baragar et al., 1989). Cross-cutting relationships of the dykes indicate that the depleted or undepleted dykes have no consistent age relationship to one another (Baragar et al. 1989). This indicates that the two suites may be coeval. The dyke chemistry implies that there were at least two magma sources operating contemporaneously within each dyke domain. Although variations are present in the data, these variations are not consistent with dyke domain boundaries. Therefore the dyke chemistry is independent of the subdivision of the dykes into domains.

2.3.3 Rotational Axis For Extensional Deformation

It is assumed by most workers (e.g. Varga, 1991), that the dykes were originally injected vertically into the crust. This means that any tilting present in the dykes now is due to tectonic rotations that took place after their injection. The effects of rotation, uplift and emplacement of the ophiolite are superimposed on the original orientations of the dykes. Since a sheeted dyke sequence does not generally have any horizontal marker horizons, it is difficult to determine the amount of rotation the ophiolite complex has undergone during, for example, uplift. The only originally sub-horizontal surface present in the field area is the sediment-pillow lava boundary. The dykes, in the Mitsero graben, were rotated with respect to their original, vertical orientation as a result of graben formation. The amount of rotation is used to calculate the amount of extension in the study area.

Although the sediments on the northern flank of the ophiolite presently dip 10° to 20° to the north (Bear, 1960), they are thought to have been originally flat-lying. The sediments and the lavas, however were not necessarily laid down on a horizontal surface. Their tilting was caused by the updoming of the ophiolite during uplift and emplacement (Cleintaur et al., 1977). This rotation must be removed from the dyke orientation data before dealing with the graben formation event because the graben formation is thought to pre-date the final updoming of the ophiolite. Whereas the dip at the sediment-pillow lava boundary is roughly 15° to the north (Cleintaur et al., 1977), the dome shape of the ophiolite dictates a 0° dip along the highest part of the dome. The dip variation across the dome is not expected to change consistently; however there is insufficient information to constrain the variation from north to south.

The poles of the mean orientations of each of the dyke domains and sub-domains lie on great circles; one for the west-dipping dykes on the eastern side of the Mitsero graben and one for the east-dipping dykes on the western side (Figure 2.14). The mean values for sub-domains 6A and 6B were not included in this manipulation because they are anomalous in that a best-fit-circle including these data requires much greater rotations than otherwise necessary to bring the dykes to a vertical position. As discussed before, the dykes from domain 6 may have been intruded at a later time, possibly after the formation of the graben. The pole to the great circle, for the western side of the Mitsero graben, lies at 098°/71° and that to the eastern great circle lies at 260°/73° (Figure 2.14). The mean effects of the ophiolite updoming can be removed from the dyke orientations through a 3° clockwise rotation (viewed from above), of the intersection (000°/3°) between the great circles, about a horizontal axis trending toward 090°. It was assumed that the graben blocks were originally rotated about a horizontal axis. Thus this axis, the intersection between the two great circles,

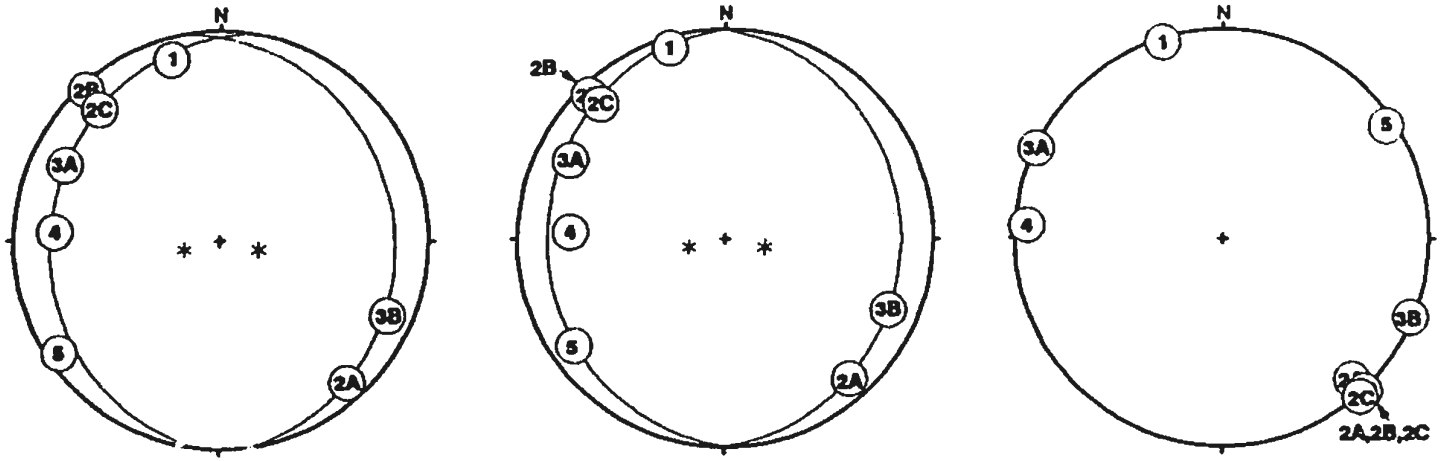

FIGURE 2.14 ROTATION OF DYKE DOMAIN MEAN ORIENTATIONS IN THE SPILIA-POLITIKO AREA, TO REMOVE THE EFFECTS OF UP-DOMING AND GRABEN FORMATION. DATA ARE POLES TO PLANES PLOTTED ON EQUAL AREA LOWER HEMISPHERE PROJECTIONS. NUMBERS IN CIRCLES ARE DOMAIN NUMBERS PLOTTED AT MEAN DOMAIN ORIENTATION.

must be brought back to the horizontal. The 3° rotation puts the great circle intersection into a horizontal position.

The mean orientations of the various dyke domains, after completing the above rotation, now lie on two great circles which intersect at 000°/0° (dip-azimuth/dip). The dyke data belonging to the west and east graben halves can be rotated 19° and -16°, respectively, about a horizontal axis trending 000°, so that the best-fitting great circles become horizontal (positive rotations are clockwise looking down the axis, that is, toward 000°)(Figure 2.14). This places the dykes approximately into their pre-graben, sub-vertical orientation. Only the dykes within domain 4 are oriented parallel to the rotation axis.

The amount of extension that has taken place, as a result of the formation of the Mitsero graben, depends on the original dip of the dykes and the original dip of the fault along which the dyke rotation took place (Figure 2.15A) (Norrell and Harper, 1988). This method of calculating graben extension assumes the faults were planar and that their surfaces rotated with continued deformation, keeping the angle between the dyke and fault constant (Axen, 1988). To enable dyke rotations to take place, fault slip surfaces must either be curved or the fault planes themselves must rotate (Jackson and White, 1989). The dips of dip-slip faults (Section 2.3.4 and Appendix A.5) and the dips of associated dykes indicate a variation in the amount of extension from 0% to 31% with an average extension of 12% (Figure 2.15B). The greatest amount of extension is in the central portion of the west half of the graben (domain 4), where dyke dips are the shallowest (Figure 2.13). The amount of extension is least near the graben boundaries and near the graben axis. The dyke orientations near the graben axis may have been affected by the large amount of brecciation in the graben shear zone.

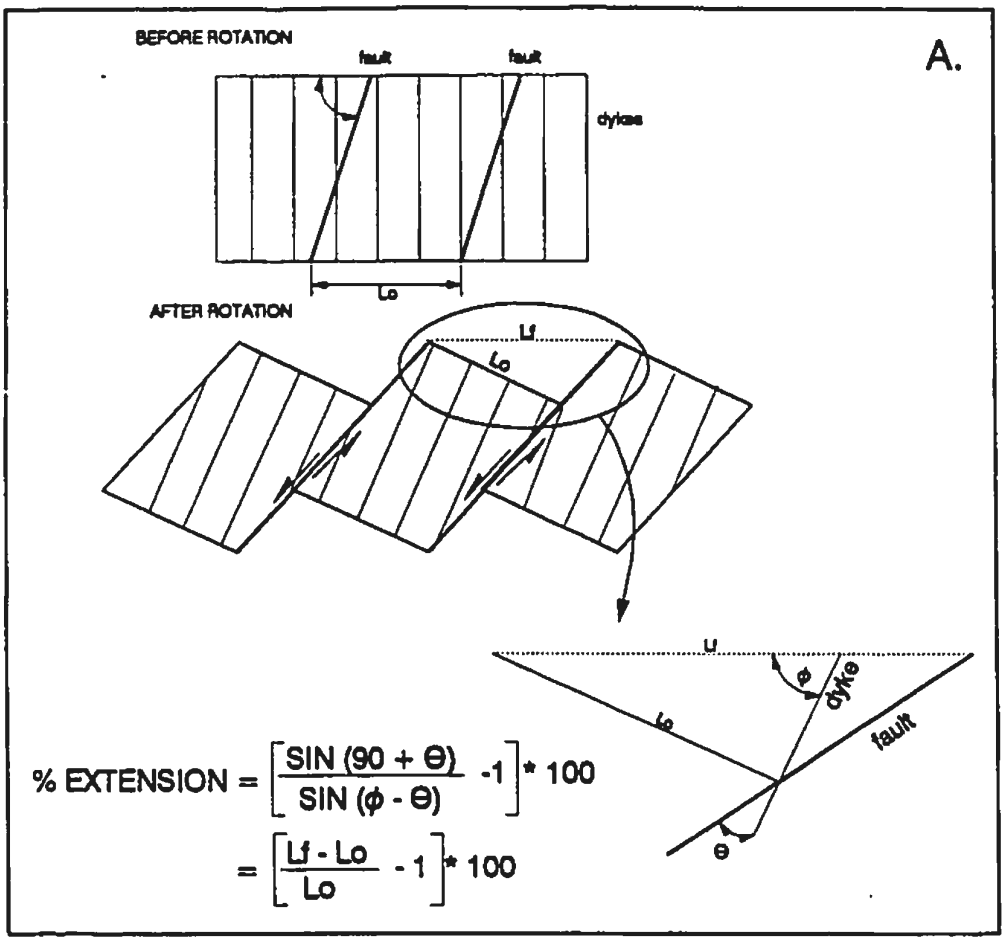

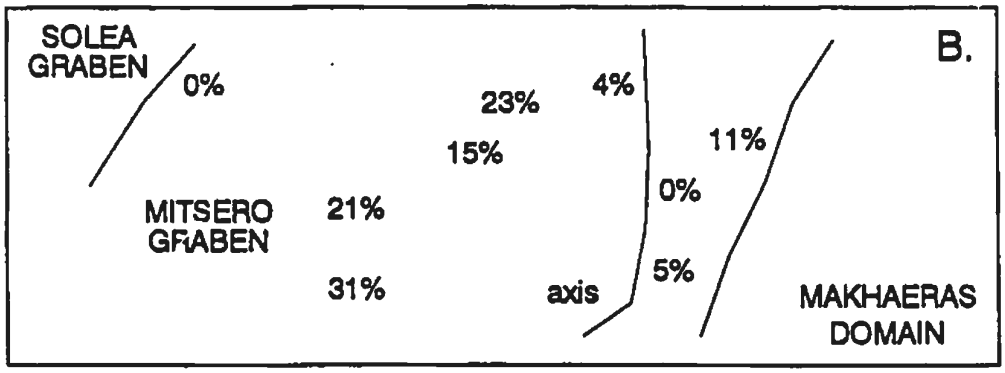

FIGURE 2.15 RELATION BETWEEN FAULT ROTATION AND AMOUNT OF EXTENSION. A) ϕ IS FINAL DYKE DIP, Θ IS THE COMPLEMENT OF THE ANGLE BETWEEN THE FAULT AND THE DYKE PLANE. Θ IS ALSO THE COMPLEMENT TO THE ORIGINAL FAULT DIP ASSUMING ORIGINALLY VERTICAL DYKES (AFTER AXEN, 1988; NORRELL AND HARPER, 1986). DOTTED LINE IS PALEO-HORIZONTAL SURFACE, SOLID LINES ARE FAULTS. B) AMOUNTS OF EXTENSION IN THE MITSERO GRABEN.

2.3.4 Fault Geometry

The majority of the 136 faults examined in the study area, for which a sense of motion could be established, are strike-slip or normal faults, whereas only three showed reverse motion. At the outcrop-scale, less than one metre of motion was indicated. Faults generally dip less steeply than the dykes they cut. In the field, fault traces tend to follow the dyke margins for several metres and then abruptly cut across a dyke to follow the next dyke margin. Slickenside striations, on fault plane surfaces, were measured at 50 locations for a total of 136 data points (Figure 2.16, see Appendix A.5 for plots).

Slickensides occur on both uncoated and mineral coated fracture surfaces, although cross-cutting relations between the two variations were not seen. The slickensides formed on various mineral surfaces; including, epidote, hematite, pyrite and calcite. The direction of motion along faults, on the basis of slickenside striations, was in general difficult to determine unless there was a marker (e.g. offset dyke) available. Slickenside lineations indicate motion along faults ranging from dip-slip to strike-slip. Fault types in the field area (Table 2.2 and Figure 2.17) indicate a predominance of strike-slip faults. On the basis of fault orientations it is believed the north-south trending dip-slip faults are related to block rotation during graben formation. East-west strike-slip faults may be transfer faults; these were noted by Hurst et al. (1988) in the eastern part of the Solea graben. Some of the faults may be related to the resolution of space problems arising during fault block rotations; the data are not detailed enough to resolve this.

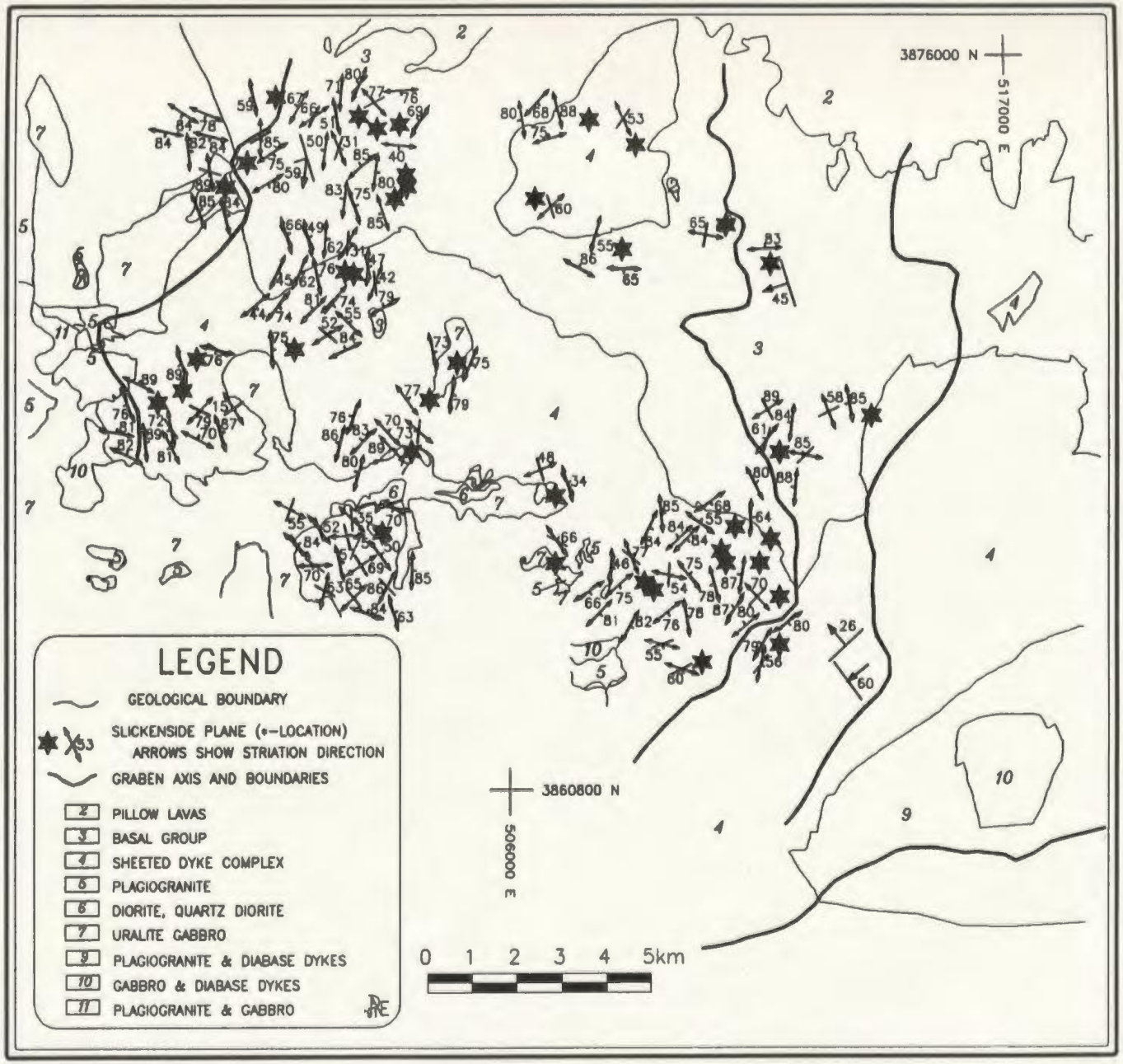

FIGURE 2.16 SLICKENSIDE ORIENTATION MAP, SPILIA–POLITIKO AREA, CYPRUS.

TABLE 2.2 FAULT TYPE IN THE SPILIA - POLITIKO AREA

LOCATION	TYPE	DIP SLIP	OBLIQUE SLIP DIP	OBLIQUE SLIP STRIKE	OBLIQUE SLIP STRIKE SLIP
NORTH-WEST		3	2	4	18
	E-W	2	2	1	8
	N-S	1	-	3	10
CENTRAL WEST		2	-	13	17
	E-W	2	-	6	5
	N-S	-	-	7	12
SOUTH-WEST		10	8	10	12
	E-W	4	5	2	3
	N-S	6	3	8	9

GRABEN AXIS

LOCATION	TYPE	DIP SLIP	OBLIQUE SLIP DIP	OBLIQUE SLIP STRIKE	OBLIQUE SLIP STRIKE SLIP
NORTH-EAST		1	-	-	1
	E-W	1	-	-	1
	N-S	-	-	-	-
CENTRAL EAST		4	-	3	6
	E-W	3	-	-	1
	N-S	1	-	3	5
SOUTH-EAST		1	5	5	11
	E-W	-	5	4	7
	N-S	1	-	1	4

TOTALS:

DIP SLIP =	21
OBLIQUE DIP SLIP =	15
OBLIQUE STRIKE SLIP	35
STRIKE SLIP =	65
	136

NOTE: E-W and N-S refer to fault strike

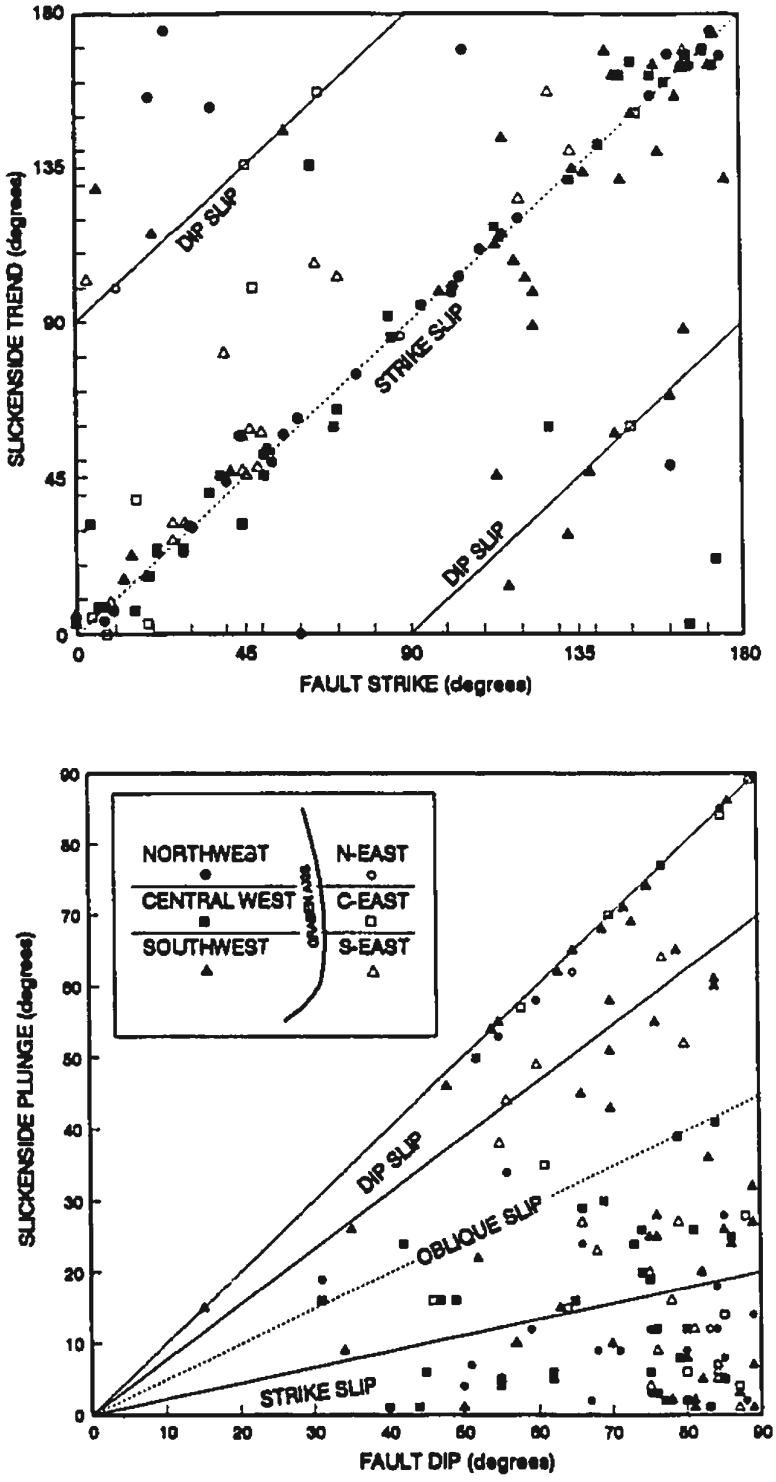

FIGURE 2.17 FAULT TYPES IN THE SPILIA - POLITIKO AREA

Since many of the fault data may pertain to motions after the formation of the graben there is little sense in rotating the faults using the graben rotation axes (discussed in Section 2.3.3). The fact that this rotation does not simplify the interpretation of the slickenside data implies that motion along these fault planes may have been syn- to post-graben formation.

Several major faults, roughly parallel to the north-south dyke strike, cut the rocks in the vicinity of the graben axis. These faults trend 170° from Kalokhorio, in the north, to Gourri and Pharmakas in the south, and 190° from Ayios Epiphanios south to Apliki and Palekhori (Bear, 1960), forming the eastern graben boundary and the graben axis, respectively (see Figure 2.1 for village locations). It was not possible to establish a sense of motion for these faults.

Of the 136 faults measured in the field area, 13 strike 90° to the graben axis trend and 35 faults had dips too steep to enable unambiguous assignment of dip direction with respect to the graben axis. The remaining faults trend sub-parallel to the graben axis. Axis-parallel faults dipping away from the graben axis (63) dominate over axis-parallel faults dipping toward the Mitsero graben axis (25). The dominance of outward-dipping faults implies the spreading rate may have been fast, since inward-dipping faults dominate over outward-dipping faults at slow spreading axes (Lonsdale, 1977).

In the north, west of Ayios Epiphanios, both strike- and dip-slip fault movement was E-W directed. In the south, near Apliki, the fault movement ranges from N-S on N-S trending faults to NE-SW on NE-SW trending faults. Ramsden (1987) reported similar findings in the area of the Mitsero graben axis. To the west, near Xyliatos, fault movements are N-S on N-S trending faults becoming more NE-SW on generally

NE-SW trending faults, to the south.

Between Spilia and Lagoudhera the slickenside striations indicate strike-slip movement on WNW-ESE trending faults. South of the Plutonic Complex, near Alona, the slickenside striations are more chaotic and give no consistent axis of motion. West of Xyliatos, across the Solea graben boundary, the slickenside lineations on fault planes indicate that the major component of fault motion was strike-slip E-W to NW-SE. East-west trending dip-slip faults, west of Ayios Epiphanios, lie at shallow crustal depths and may be related to the graben formation. The north-south to NE-SW trending strike-slip faults in the south of the field area may be related to deflection of dykes by movement along the South Troodos Transform Fault (Figure 2.18).

Epidote vein filling material, related to the circulation of hydrothermal fluids (Section 5.2 and 5.4), is found along some faults. Hydrothermal circulation and alteration is contemporaneous with the formation of the Troodos ocean crust (Chapter 3 and 5), suggesting these faults existed while the Troodos ocean crust was still forming. The mean orientation of these epidote coated fault surfaces (Figure 2.19) is roughly 096°/72° (dip-direction/dip), roughly parallel to local dyke strike. The changes in the fault orientation from area to area generally parallel changes in dyke orientations from area to area (compare Figures 2.20 and 2.6).

Rotation of dykes may be accomplished by either simple domino-style block rotations or rotations along curved fault planes. In the Solea Graben area, work by Varga (1991) has demonstrated that planar faults link to form listric geometries. Given the proximity of the two graben structures, the deformational style in the Mitsero graben may be similar. Faults in the field area, taken from existing Cyprus Geological Survey maps (Bear, 1960; Carr and Bear, 1960), show a radial pattern converging to

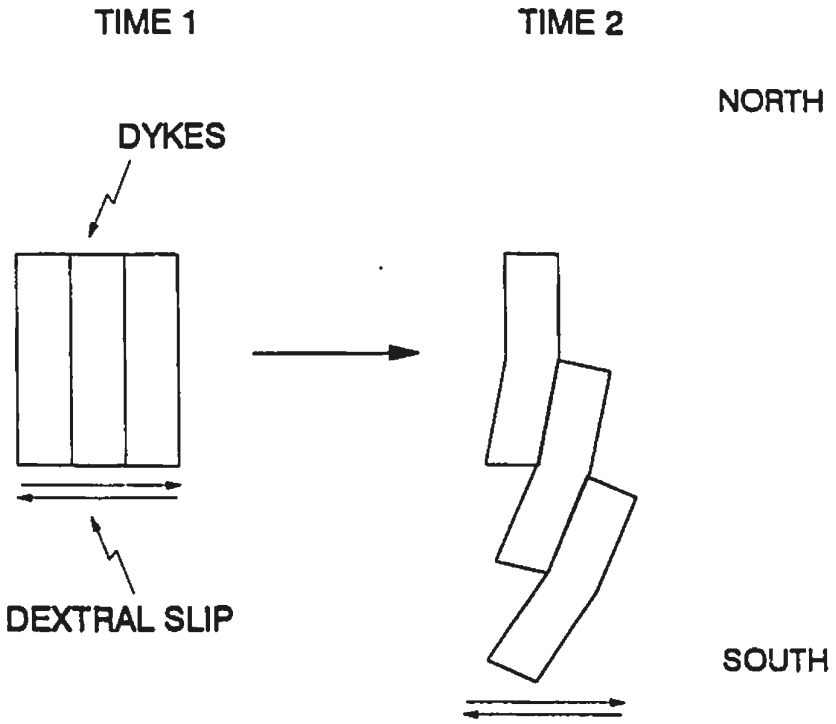

FIGURE 2.18 SCHEMATIC DIAGRAM TO PROVIDE EXPLANATION FOR FORMATION OF NORTH-SOUTH ORIENTED STRIKE-SLIP FAULTS (PLAN-VIEW).

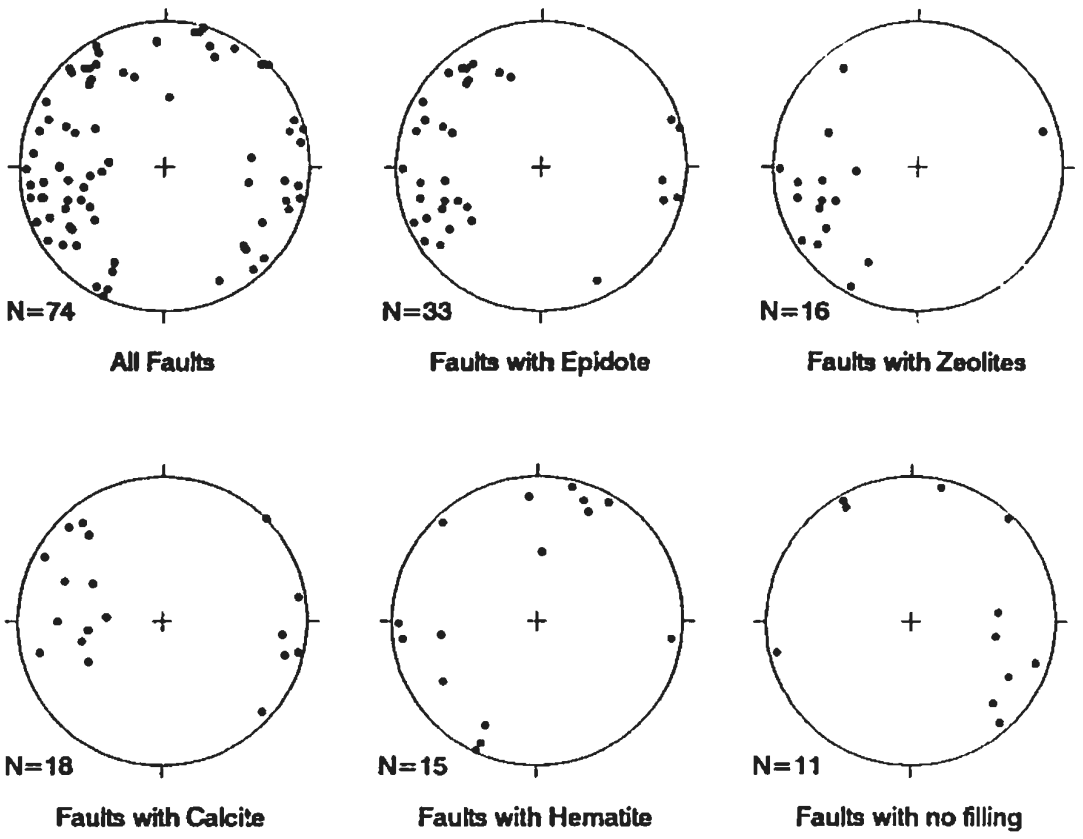

Note: some faults contain moro than one mineral filling.

FIGURE 2.19 FAULTS AND MINERALIZATION

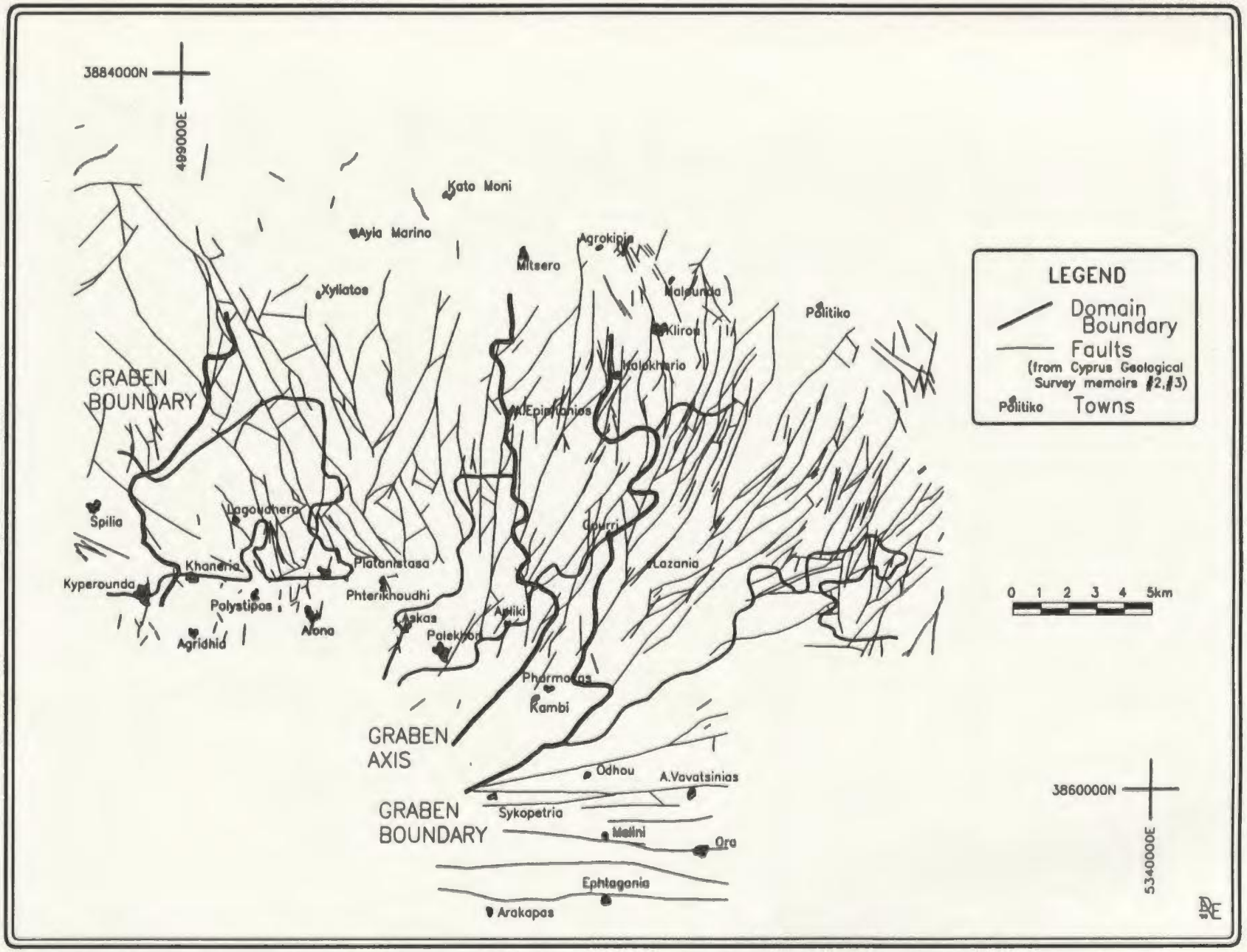

FIGURE 2.20 DOMAIN BOUNDARIES AND FAULTS IN THE SPILIA – POLITIKO AREA, CYPRUS.

the south and striking NW-SE in the west and NE-SW in the east (Figure 2.20). Fault trajectories, for listric-normal faults, in the map view of the oblique section through the ophiolite (down-section being to the south) should curve toward the graben axis. The intersection point of these faults (by extending their trajectories) indicates a possible zone of detachment along an east-west line just south of Palekhori.

A sub-horizontal fault possibly indicative of low-angle detachment faulting, like those near the base of the Sheeted Dyke Complex in the Solea graben (Moores et al., 1990; Varga and Moores, 1985), was seen only near Platanistasa in the Mitsero graben; this may be due to lack of sufficient exposure at depth, near the Sheeted Dyke - Plutonic Complex contact. A possible detachment zone is inferred by Moores et al. (1990) from the Cyprus Crustal Drilling Project Hole CY-4 near Palekhori (labelled as '4' on Figure 1.2). A highly altered interval between a depth of 700 to 850 metres, at the base of the sheeted dyke sequence, is a transition from faulted and altered dykes above 700m to relatively unaltered dykes and gabbros below 850m. Such a detachment zone would lie within the Plutonic Complex; this is shown on a schematic cross-section of the Spilia-Politiko area (Figure 2.21).

2.4 SUMMARY AND CONLCUSIONS

In summary, the following is concluded from the dyke and fault data in the Spilia-Politiko area:

1) The Mitsero graben is roughly 16 kilometres wide (12 kilometres to the west of the graben axis and 4 to the east). The axis of the graben is a curved lineament trending south from Ayios Epiphanios.

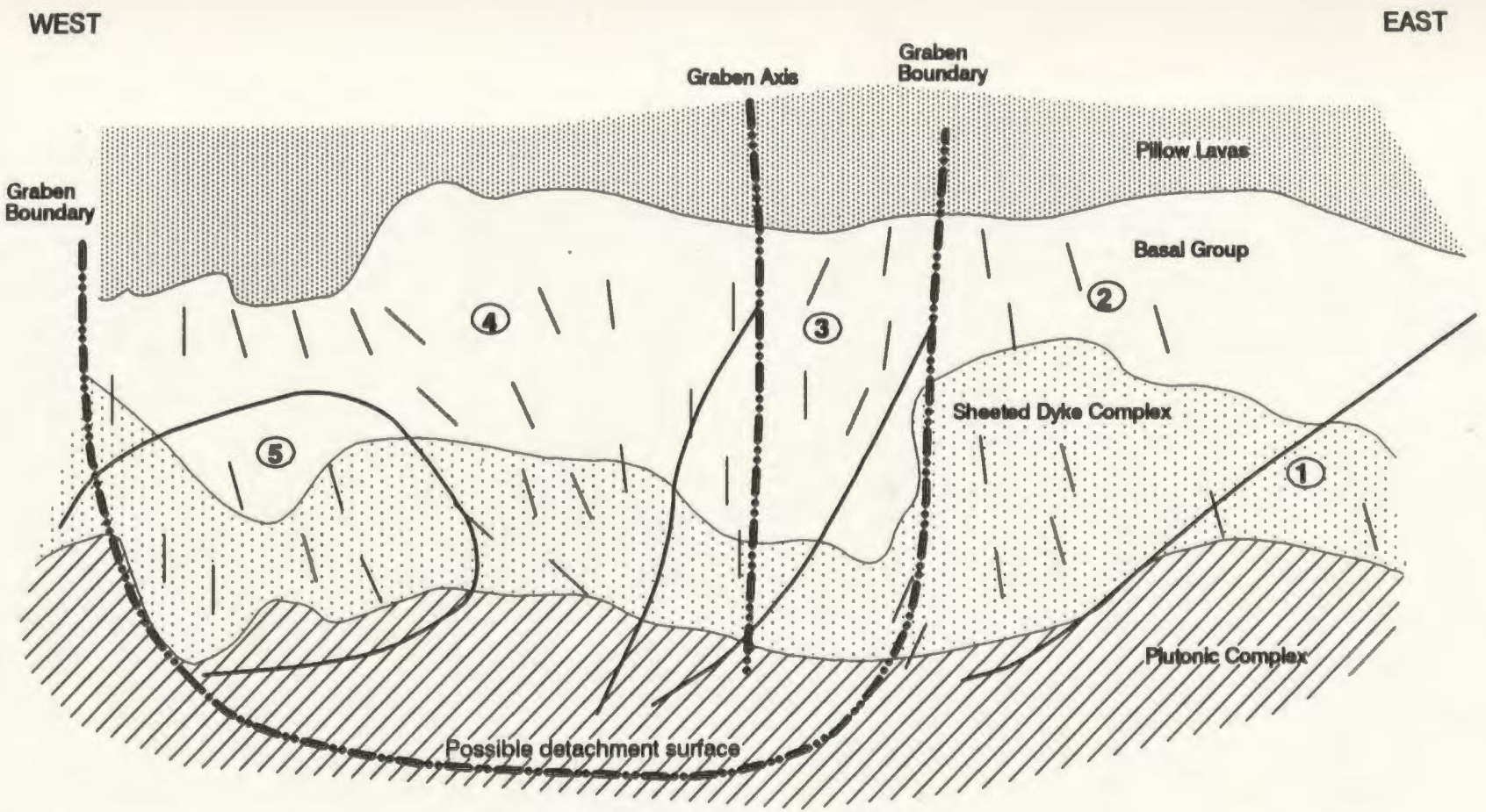

LEGEND

- GRABEN BOUNDARIES, AXIS
- DOMAIN BOUNDARY
- ⑤ DOMAIN NUMBER
- DYKE DIP

FIGURE 2.21 SCHEMATIC EAST-WEST CROSS-SECTION OF THE SPILIA-POLITIKO AREA SHOWING THE RELATIVE POSITION OF MAJOR FAULTS AND DYKE DOMAINS. DYKES DIPS BASED ON FIGURE 2.7.

2) Five major dyke domains have been delineated on the basis of dyke orientations in the Sheeted Dyke Complex. The domain boundaries are defined by abrupt, but regular, changes in dyke orientation from one domain to the next. This suggests that periods of magmatism with multiple intrusions are punctuated by periods of tectonic extension.

3) Dyke orientations are more variable near the boundaries of the sheeted dykes with the pillowed lavas and the gabbros. The systematic variation in dyke dip supports the presence of an asymmetric graben structure. Rotation of dykes was along an axis parallel to the graben axis.

4) Major and trace element geochemistry of the dykes neither supports nor refutes the existence of the dyke domains. The geochemical patterns are indicative of a multiple intrusive environment from at least two sources.

5) Lineaments, representing fault traces, match the dyke domain boundaries in various locations. Cross-cutting relations suggests two sets of lineaments formed during the formation of the graben while the remaining two lineament sets formed during the uplift and emplacement of the ophiolite.

6) Faulting appears to have been concurrent with hydrothermal alteration, implying faults were present at the earliest stages of the formation of the Sheeted Dyke Complex. In the north, E-W dip-slip slickensides on faults may be related to graben formation, whereas in the south, strike-slip slickensides indicate interaction with the transform fault. Major faults bound the graben structure to the east, as well as delineating the graben axis. To the west the boundary may be fault bounded, although this is not clear.

7) As stated in the introduction to this chapter, Dilek et al. (1990) implied the Mitsero graben formed at the spreading ridge axis, whereas Allerton and Vine (1987) suggested that the graben formed formed in an off-axis position after a ridge jump caused abandonment of the spreading axis. If the former was the case, then evidence, in the form of intrusive cross-cutting dyke relations, should be seen at the graben margins. Such relations were noted at the western margin of the Solea graben (MacLeod et al., 1992, quoting E.M. Moores, 1987) and at the western margin of the Larnaca graben (Allerton, 1989). These relationships were not seen, during this study, at the Mitsero graben boundaries, arguing against an on-axis formation of the graben structure.

3. FRACTURE CHARACTERISTICS IN THE STUDY AREA

3.1 INTRODUCTION

Fractures within the sheeted dykes and along their margins form conduits for hydrothermal fluid circulation and therefore control the distribution of the fluids. Thus, knowledge of fracture characteristics is essential for inferring variations in the permeability and hence fluid distribution in the oceanic crust.

In previous studies of the Troodos ophiolite, fracture characteristics have not been measured in a comprehensive fashion, because these studies were interested in the chemical rather than the physical interaction of the fluid and the rock (e.g. Gillis, 1986; Richardson et al., 1987; Baragar et al., 1989). Thus, it has in the past, not been possible to compare fracture characteristics from one area of the ophiolite to another in a rigourous manner. The purpose of this chapter is to present a detailed evaluation of fracture characteristics and their variability in the Sheeted Dyke Complex in the Mitsero graben. This evaluation is important in establishing the nature and development of Layer 2B oceanic crust in terms of its permeability and hydrothermal circulation characteristics.

Fracture geometry is controlled by the host rock lithology, pre-existing planes of weakness and the externally applied stress field. In the study area, fracture characteristics were measured in a variety of rock types including pillow basalts, diabase dykes, epidosites, plagiogranites, and gabbros. The majority of fracture measurements in the study area were taken from the diabase dykes and epidosites of the Sheeted Dyke Complex and the Basal Group, because these areas are thought to be analogous to Layer 2 of the oceanic crust.

Fracture geometry was mapped using scanline methods described below (after Piteau, 1970; Hudson and Priest, 1979; LaPointe and Hudson, 1985). The fracture data collected for this study are used for the following: 1) to group fractures into sets based on their orientations; 2) to assess fracture aperture variation; 3) to assess the spatial and temporal variation of mineral filling with respect to fracture sets; 4) to evaluate the significance of fracture interaction with other fractures (termination mode); 5) to determine fracture trace length distributions and the relationships between fracture trace length and fracture type and mineral infilling; and 6) to determine the fracture frequency within the mapped areas. The determination of the trace length distribution and the fracture frequency were undertaken as part of the process of the permeability estimation. The results of these analyses are summarized at the end of this chapter.

The manipulation of the large amount of fracture data (3221 fractures) was facilitated by the use of a series of computer programs written for this study. Figure 3.1 shows a schematic of the use of these programs. Program listings and descriptions are in Appendix D.

3.2 SCANLINE METHODOLOGY

In general, the scanline method entails mapping characteristics of fractures which intersect a line or measuring tape laid out on a rock outcrop surface. Scanline lengths varied from 18 metres (site: 1305) to 85 metres (site: 0122); the majority had lengths of 30 metres. Figure 3.2 shows scanline mapping locations in the study area. In this study, 41 rock outcrops were mapped throughout the field area. The scanline numbering system is described in Appendix A. A total of 3221 fractures was

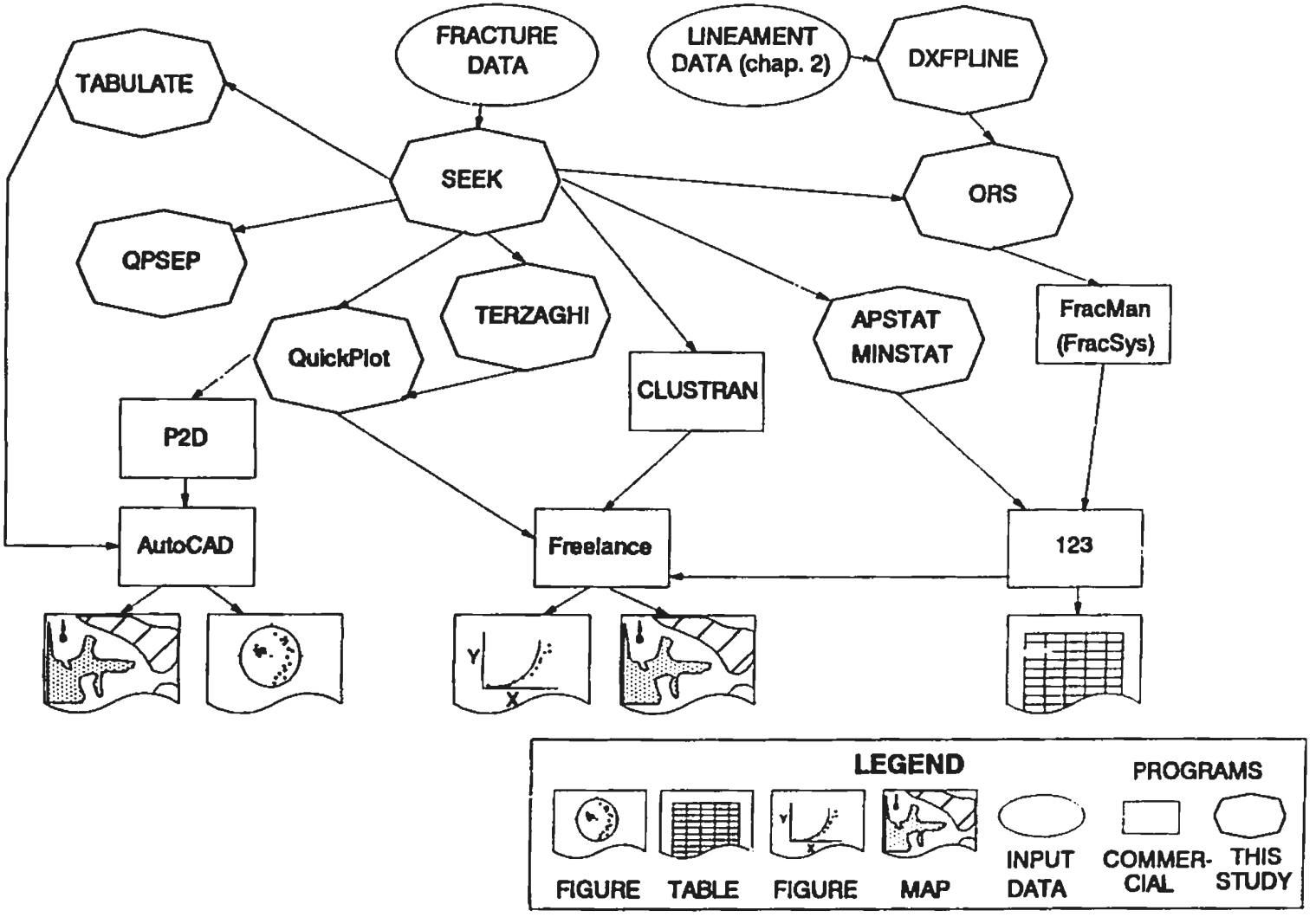

FIGURE 3.1 FLOWCHART OF DATA AND PROGRAMS USED IN CHAPTER 3. COMMERCIAL PROGRAMS AS FIGURE 2.2. FracMan - FRACTURE ANALYSIS; CLUSTRAN - CLUSTER ANALYSIS; SAS - STATISTICAL (* INCLUDES PROGRAMS BY ROULEAU, 1984 - SEE TEXT FOR DETAILS).

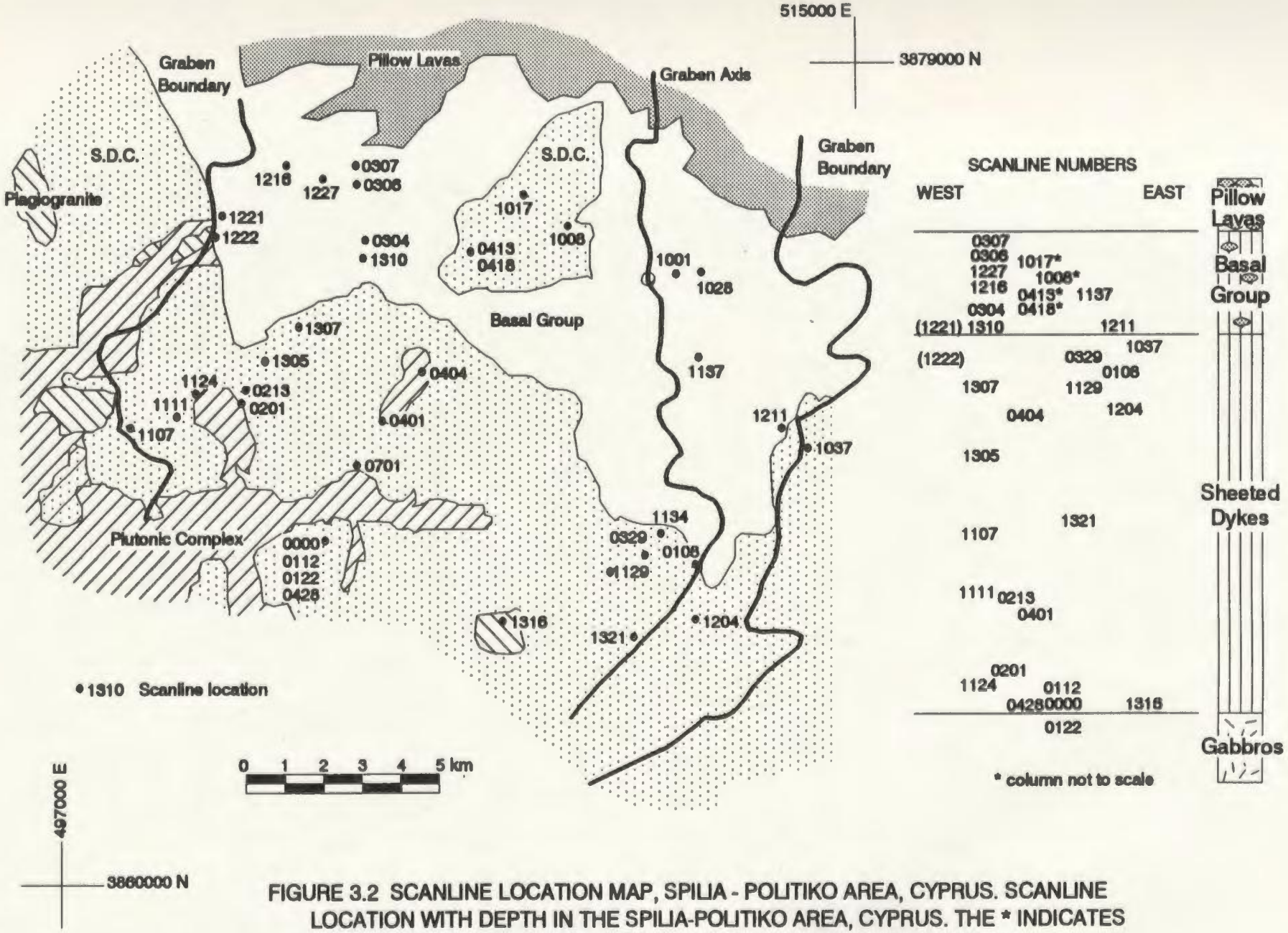

FIGURE 3.2 SCANLINE LOCATION MAP, SPILIA - POLITIKO AREA, CYPRUS. SCANLINE LOCATION WITH DEPTH IN THE SPILIA-POLITIKO AREA, CYPRUS. THE * INDICATES SCANLINES WITHIN THE SHEETED DYKE INLIER IN THE BASAL GROUP.

recorded; the listing of the fracture data is presented in Appendix A.1. Fractures were mapped in all dyke domains as defined in Section 2.3.2, with the exception of domain 1. No scanline fracture data were collected in domain 1 because, during field work, this area lay outside the study area and was not mapped.

The scanline locations were chosen in a variety of geological settings including: minimally altered dykes; dykes altered entirely to epidosites; dykes proximal to gabbros and plagiogranites; and areas proximal to faults (Table 3.1). Most of the scanline fracture measurements (76%) were taken from sheeted dykes. The remaining fracture measurements came from gabbro (13%), plagiogranite (6%), and pillow lavas (5%). The data from the different lithologies were kept separate for the analyses. The analyses concentrated on the fracture data collected from the sheeted dykes.

The outcrop traces of fractures recorded during the scanline mapping were drawn on overlays of photographs taken of the outcrops prior to the scanline survey. The following characteristics were measured from each fracture: distance to fracture from start of scanline; fracture type; orientation; trace length; censoring (fracture interaction with the outcrop edge) and termination mode (fracture interaction with other fractures); mineral filling; roughness (large scale fracture curvature and small scale fracture aperture variations); rock type; and width or aperture of the fracture (Appendix A.1 includes pictoral descriptions of some of the terminology of fracture characteristics). Various schemes have been formulated to classify rock discontinuity characteristics (Hodgson, 1961; International Society for Rock Mechanics (ISRM), 1978; Nelson, 1979; Hancock, 1985). This study used the terminology outlined by ISRM (1978).

TABLE 3.1 Scanline Field Relations

Scanline #	Scanline Length (m)	# of Fractures	Rock Type	Related Features	Location (graben)	Location (strat.)
0000	18	76	diabase	fault	west	base SDC
0108	30	88	epidosite	near fault	west	top SDC
0112	26	90	diabase	near gabbro/fault	west	base SDC
0122	110	291	gab/plag	gabbro	west	base SDC
0201	10	31	diabase		west	base SDC
0213	30	117	epidosite		west	base SDC
0301	7	14	diabase		west	BG
0302	13	47	diabase		west	BG
0303	7	13	diabase		west	BG
0304	6	14	diabase		west	BG
0306	10	11	diabase		west	BG
0307	10	21	diabase		west	BG
0328	10	20	diabase	shear zone	west	top SDC
0401	20	68	epidosite		west	SDC
0404	20	18	epidosite		west	SDC
0413	30	59	diabase		west	SDC inlier
0418	20	33	diabase		west	SDC inlier
0428	60	195	diabase	near fault	west	base SDC
0701	30	69	epid/gab	gabbro	west	base SDC
1001	30	93	diabase		east	top BG
1008	18	73	diabase		west	SDC inlier
1017	22	67	diabase		west	SDC inlier
1028	30	114	diabase		east	top BG
1037	30	96	epidosite		Makheeras	top SDC
1107	25	79	epidosite		west	base SDC
1111	30	121	epidosite	near gabbro	west	base SDC
1124	24	96	epidosite		west	base SDC
1128	30	105	diabase		west	top SDC
1134	30	68	epidosite		west	top SDC
1137	30	75	diabase		east	BG
1204	25	94	diabase		east	SDC
1211	28	139	diabase	near fault	east	base BG
1216	30	104	dia/pill		west	BG
1221	30	106	dia/gab	plagiogr.	west	base BG
1222	30	94	dia/plag	plagiogr.	west	plagiogr.
1227	20	61	diabase		west	BG
1305	15	39	epidosite		west	SDC
1307	20	51	diabase		west	SDC
1310	12	54	diabase		west	SDC
1316	30	108	diabase	near plagiogr.	west	gab/SDC
1321	30	109	epidosite		west	SDC
Total (41)	1036	3221				

Notes
SDC = Sheeted Dyke Complex
BG = Basal Group
plag = plagiogranite
gab = gabbro
dia = diabase
pill = pillow lava
SDC inlier = is within the BG
west = western half of the Mitsero Graben
east = eastern half of the Mitsero Graben
Makheeras = domain to the east of the Mitsero Graben

The following fracture types were noted in the study area: joints (regular planar discrete features); fractures (irregularly shaped discrete features); and faults (larger scale discrete features showing evidence for movement). Dyke margin contacts are a special case of joints with the attached genetic significance of being cooling joints. Veins are fractures containing a mineral infilling.

3.3 EVALUATION OF FRACTURE DATA

The fracture characteristic data are evaluated in the remainder of this chapter by comparing the various fracture characteristics on a per-scanline and per-domain basis. The evaluation of fracture data includes a discussion of sources of bias, fracture apertures, the grouping of fracture data based on orientation, fracture mineral filling, fracture termination mode, fracture trace lengths and fracture frequency in the study area. The trace length analysis results are important in determining fracture radius distributions which are used in the determination of fractured rock permeability (Section 4.3).

3.3.1 Sources of Bias

Fracture data collected during the course of this study are biased as a result of 1) the method employed to collect fracture measurements; 2) the orientation of the measurement surface (outcrop) and the orientation of the scanline with respect to the fractures and the outcrop surface; 3) interaction of the edge of the outcrop with fractures and artificially imposed trace length truncation. These are dealt with in the following three sub-sections.

3.3.1.1 *Scanline Versus Area Mapping*

Fractures can be mapped through one of two methods, 1) the scanline or 2) the area mapping method. The scanline method was defined earlier. The area mapping method involves mapping all fractures within an area on an outcrop by noting the fracture endpoint locations, rather than the fracture-scanline intersection point (done in the scanline method).

Fracture mapping over an area of outcrop, as well as along a scanline, was done in two areas to compare the two mapping methods (Appendix A.6). The area mapping technique is superior to the scanline mapping method, but it is more time consuming. The fracture orientations and trace lengths mapped by the scanline and area-mapped method give similar distributions of data points, as long as two or more non-parallel scanlines were used along each outcrop. In the present study, fractures were measured at each outcrop along at least two scanlines of different orientations. The scanline method of mapping fractures is scale-independent as long as the length of the scanline is much longer than the mean trace length of the fractures (Dershowitz and Hurda, 1992); this is the case with the scanline mapping performed for this study, since mean trace lengths were of the order of 2.5 metres whereas scanline lengths were in general 30 metres (See Section 3.3.6 for trace length discussion and Appendix A.1 for scanline lengths).

3.3.1.2 *Orientation Bias*

Orientation bias is the result of the preferential measurement of those fractures whose orientations lie at a high angle to the scanline (Terzaghi, 1965). This results in a blind

zone of orientations within 25° of the scanline orientation in which the fracture population is undersampled. The blind zones for each scanline area are plotted in Appendix A.4. From these plots it is evident that the region of overlapping blind zones for the individual outcrops is small. Terzaghi (1965) proposed a method to overcome the orientation bias. The method implies that, 1) the fractures are regularly spaced; 2) they are parallel; and 3) they are persistent beyond the limit of the sampling area. These assumptions are not valid for this fracture data set. The Terzaghi approach was applied to the fracture data of one scanline mapped outcrop to test its usefulness (Appendix A.6). The results were compared with the set of fracture data collected by area mapping the same outcrop. This comparison showed that the Terzaghi correction to these data resulted in an emphasis of certain of the fracture orientations which were not present in the area mapped fracture data. Hence, the Terzaghi correction was not considered useful for the interpretation of these data. Thus, the bias correction as proposed by Terzaghi (1965) was not performed on the data set from the field area.

As an alternative to the Terzaghi approach, to reduce orientation bias, fractures were measured along at least two, roughly orthogonal, scanlines on the same outcrop. Most scanline measurements were taken from vertical road-side outcrops, since these provided the freshest rock surfaces. However, in many cases the outcrop orientation varied on the scale of the scanline survey and, in several cases, adjacent outcrops were used at a particular location.

3.3.1.3 *Trace Length Bias*

Trace length biases include size bias, censoring bias and trace length truncation bias (Baecher and Lanney, 1978; Rouleau, 1984; and Rouleau and Gale, 1981). Size bias results from the greater probability that fractures with long trace lengths will intersect a scanline, causing preferential sampling of those fractures. However, since shorter fractures are less likely to intersect other fractures, their contribution to the overall permeability of the rock is probably not as significant as that of the longer fractures. This is supported by the permeability calculations done in Section 4.3, which show an insignificant difference in the calculated permeability between networks of fractures, all with sizes greater than 1 metre, and those with fractures greater than 0.01 metres.

A fracture is said to be censored when one or both ends of its fracture trace is(are) obscured by the edge(s) of an outcrop. Censoring bias is preferentially present in fracture data sets with longer fractures since they are more likely to extend beyond the boundaries of the sampling area obscuring one or both ends of the fracture (Baecher, 1980).

Trace length truncation bias is introduced by intentionally setting a cutoff value for the minimum length of fracture to be measured. In other studies, trace length cutoffs of 0.5 metres (Rouleau, 1984) and 0.01 metres (Priest and Hudson, 1981) metres were used. The cutoff length is imposed since time limitations generally preclude the mapping of every fracture if adequate coverage of the field area is to be obtained. In this study, a cutoff value of 0.25 metres was used. The trace length truncation and censoring are accounted for in the trace length analysis (Section 3.3.6).

In summary. the fracture data collected in the Spilia-Politiko area are biased by the data collection method. However, as shown above, the scanline method of mapping fractures appears to sample adequately all orientations of fractures since the fractures were measured using more than one non-parallel scanline along outcrops of varying orientations. Whereas the area mapping method of fracture measurement would provide a larger sample of fractures at a particular location, it is more time consuming and it, like the scanline mapping fracture method, requires the sampling of multiple outcrop orientations in order to reduce orientation bias. The trace length size bias was not corrected but its effects, with regard to the permeability determinations, are minimal (Section 4.3). Thus the fracture data set, while biased, is deemed to be adequate for a reasonable estimation of permeability.

A conventional method of fracture analysis is to divide fractures into sets on the basis of their orientations. This is done in the case of conjugate joint sets or fracture patterns related to geological structures (e.g. Spencer, 1977). Recall that this method was used to determine the boundaries of the dyke domains in the study area (Section 2.3.2). The fracture data, in this study, are divided into subsets on the basis of three parameters: fracture aperture, fracture orientation, and fracture type.

3.3.2 Fracture Aperture

Fracture aperture was one of the characteristics measured in the field. The measured apertures will be used in the permeability calculations (Section 4.3). The field-measured fracture aperture was the average width of the fracture mineral filling perpendicular to the long dimension of the fracture exposed at the outcrop surface, measured at several locations along the accessible length of the fracture. The

measurements, done using a millimetre scale, have an uncertainty of 0.2 millimetres. Fracture apertures are quite variable along the length of individual fractures, therefore it is difficult to obtain a representative value of fracture aperture in the field.

Several studies (e.g. Snow, 1965, 1969) suggest that the distribution of fracture apertures is best represented by log-normal distribution. A histogram of fracture apertures for fractures containing mineral fillings (Figure 3.3), indicates that they may be approximated by a log-normal distribution. However, the standard deviation of fracture apertures for all fractures and filled fractures is too large to ascertain whether this is indeed the case. That for unfilled fractures is smaller and a log-normal distribution appears to reasonably fit the data. The mean fracture apertures range from 1.1 to 11.0 millimetres (Table 3.2). These values are used later in the stochastic generation of fracture networks for the purpose of determining permeability (Section 4.3).

Thin sections of fracture filling material in the sheeted dykes show that mineral filling phases commonly consist of euhedral crystals (e.g. epidote rosettes such as seen in Plate 3.1). These crystals show no effects of impediment to growth due to contact with the opposite fracture wall. This indicates that the fractures were open to at least the width of the filling mineral crystals perpendicular to the long axis of the fracture. Therefore, apertures of fractures containing euhedral mineral fillings may represent a minimum estimate of the aperture when the fracture was utilized by circulating hydrothermal fluids. If fractures were open repeatedly with mineral filling occurring each time, then the width of the aperture during any opening event may be less than the total eventual width of the fracture.

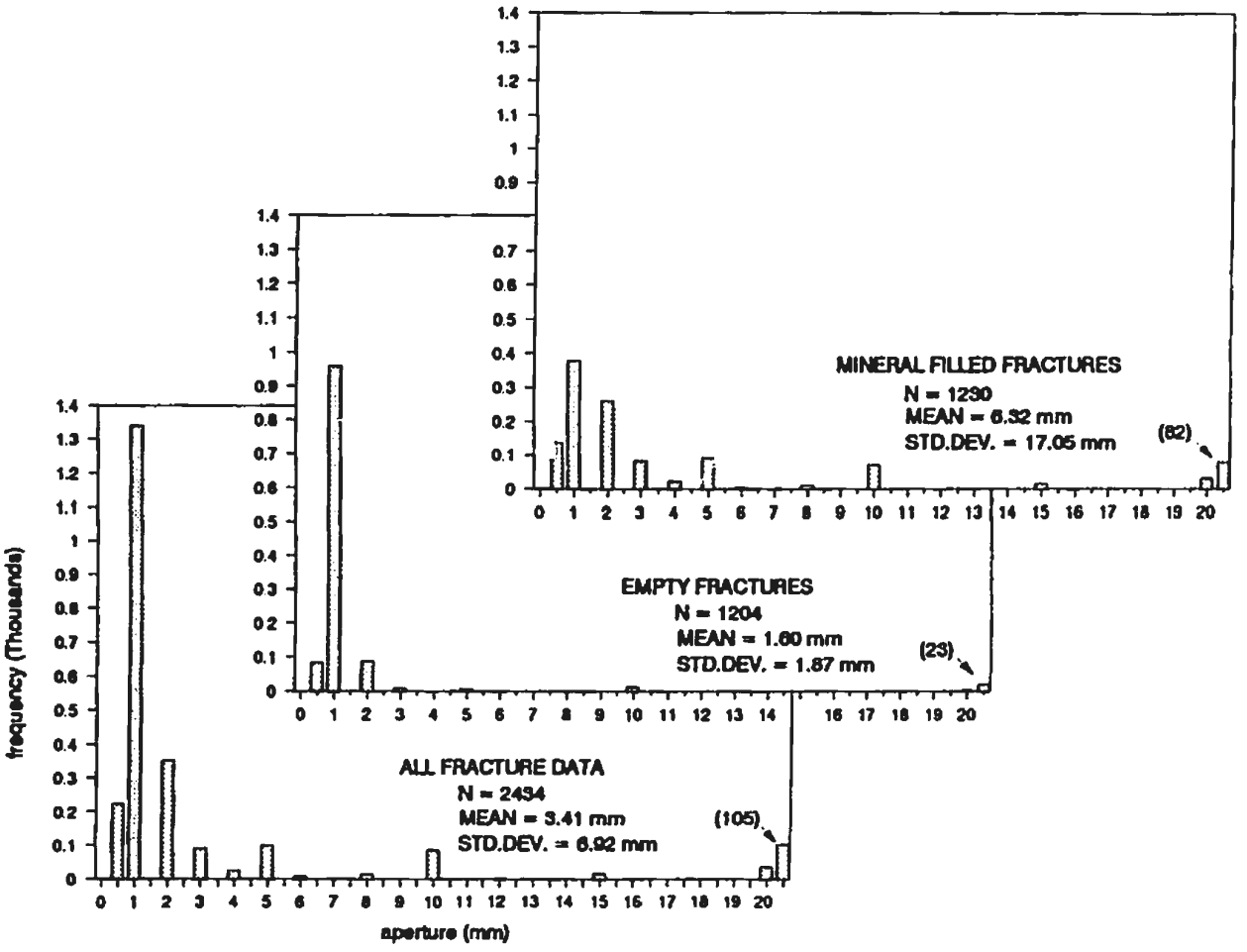

FIGURE 3.3 FRACTURE APERTURE HISTOGRAMS, SPILIA - POLITIKO AREA, CYPRUS. NUMBER IN BRACKETS IS NUMBER OF FRACTURES WITH APERTURES GREATER THAN 20mm. MEAN AND STANDARD DEVIATIONS BASED ON LOG BASE 10 TRANSFORMED DATA (SEE TABLE 3.11 FOR EXPLANATION).

TABLE 3.2 FRACTURE APERTURE VERSUS DYKE ORIENTATION AND MINERAL FILLING

Scanline	Data Type	Mean Dyke Orientation Az.	Dip	Average Aperture (mm) All Fractures	Filled Fractures #	Filled Fractures Mean	Filled Fractures Std.Dev.	Unfilled Fractures	VALUES	Average Aperture (mm) Fracture Mineral Filling Epidote	Zeolite	Calcite	Total Unfilled
0000	Dyke //	95	62	2.1	8	2.1	5.9	2.1		2.4	1.8		
	Rest			1.9	59	1.8	2.5	1.9					
0108	Dyke //	118	61	3.8	52	3.7	2.7	2.8		3.2	1.6		0.5
	Rest			2.6	8	1.2	4.0	1.4					
0112	Dyke //	102	40	1.1	12	1.0	7.3	0.0		2.0	0.9		0.4
	Rest			1.3	50	1.4	7.0	1.1					
0122	Dyke //	95	62	3.9	91	4.0	7.0	3.1		6.0	2.7		0.3
	Rest			3.8	79	3.6	5.0	2.4					
0401	Dyke //	85	75	1.7	45	2.0	6.1	0.8		2.1	0.7		0.2
	Rest			2.4	2	0.3	5.1	2.4					
0413	Dyke //	96	45	1.4	41	1.4	4.4	0.7		1.4			0.2
	Rest			1.2	3	0.5	3.8	1.1					
0418	Dyke //	n/a							=	2.6	12.2		0.1
	Rest			2.9	31	2.9	4.6	2.6					
0428	Dyke //	102	40	0.8	37	0.7	4.0	0.5		1.0	0.9		0.3
	Rest			0.9	81	1.0	3.7	0.8					
1037	Dyke //	125	85	2.4	25	2.2	2.2	1.8		2.0		1.0	1.5
	Rest			2.0	0	3.0	1.0	1.7					
1124	Dyke //	75	32	3.0	25	2.0	2.2	2.3		8.9	1.7	1.0	1.6
	Rest			1.6	2	1.0	1.0	1.5					
1134	Dyke //	125	43	5.1	27	5.7	2.3	4.2		6.7		2.5	1.6
	Rest			5.9	9	11.0	3.5	4.6					
1137	Dyke //	247	62	1.9	9	2.0	1.9	1.6		2.7			1.1
	Rest			3.9	6	1.6	2.9	1.5					
1222	Dyke //	258	80	1.6	16	1.4	2.1	1.7		1.4		1.0	1.2
	Rest			1.3	2	2.0	1.0	1.2					
1321	Dyke //	153	60	2.9	54	2.9	2.7	1.8		2.9			1.0
	Rest			2.9	0	2.0	1.0	1.9					
Area 1*	Dyke //	248	61	1.7	34	1.7	1.8	1.5		1.8		1.0	1.1
	Rest			1.6	38	1.6	2.3	1.2					

NOTE: all apertures were calculated as log-transformed values, and then presented in arithmetic form

* Area 1 = Area mapped fractures at scanline 1137 location.

n/a Scanlines 0112 and 0418 contained no mappable dyke margins.

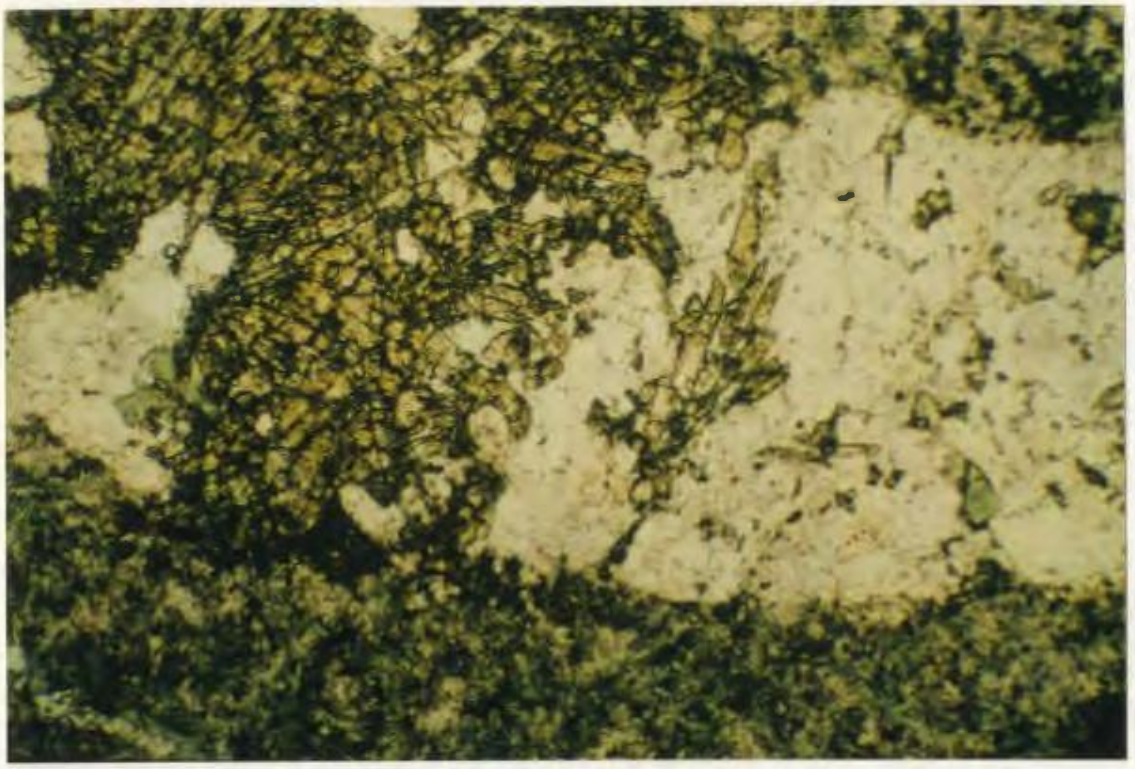

PLATE 3.1A Thin section in plane polarized light showing fracture filling minerals including quartz and epidote. Note euhedral crystal shapes of epidote. Field of view 2.2 x 3.3 mm^2.

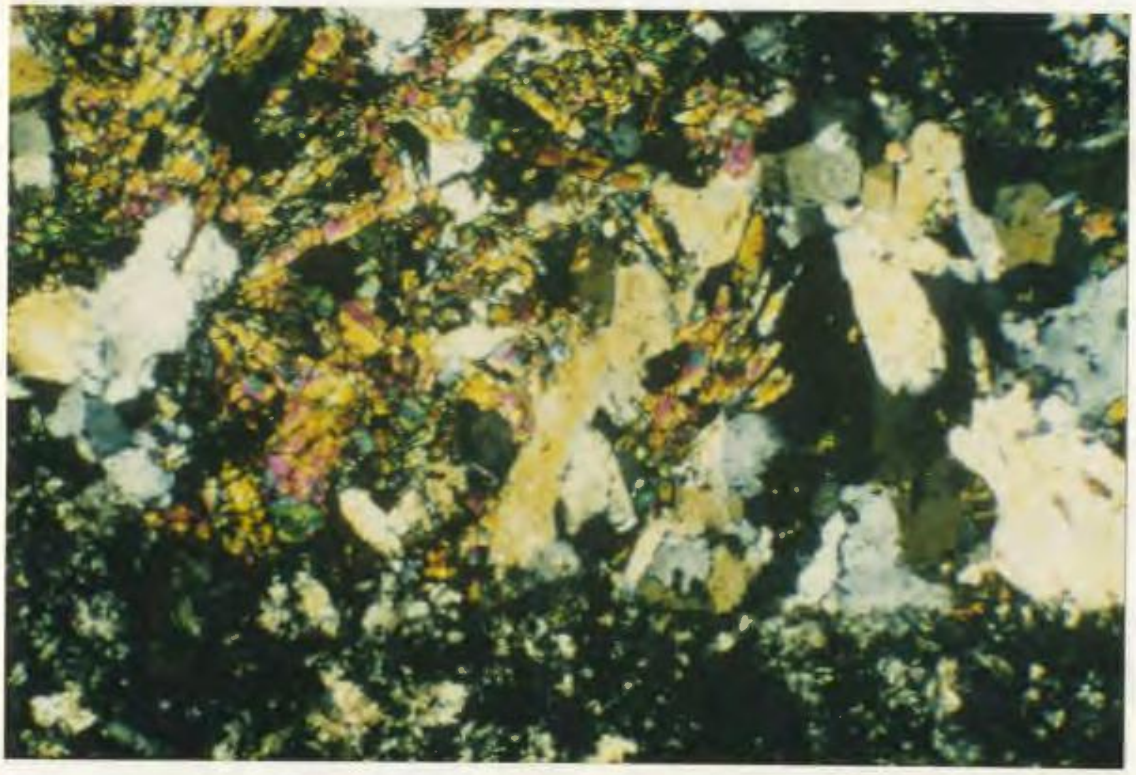

PLATE 3.1B Same section as Plate 3.3A but under cross polarized light. Field of view 2.2 x 3.3 mm^2.

Comparison of filled-fracture apertures between dyke-parallel (±30°) and non-dyke-parallel fractures (Table 3.2) demonstrates that dyke-parallel fractures generally have a greater average aperture. Assuming that dykes are injected vertically, this means that vertical fractures were open to a greater extent during hydrothermal fluid circulation than were other, non-vertical fractures. This is to be expected in an extensional regime where the maximum compressive stress is vertically oriented. The implication is that fluids would be more likely to circulate in the vertical plane. This implication is further discussed in Sections 4.3.2 and 6.3.5.

3.3.3 Fracture Orientation

An analysis of the orientations of fractures was undertaken to subdivide fractures by orientation at each of the scanline locations, to assess differences in the orientations of fractures within and between dyke domains, and to determine the origin of the fractures. Fractures owe their existence to stresses applied to a rock body. Their orientations are the result of the orientation of the applied stresses and the type of stress (i.e. tensional or compressional). Fracture orientations are expected to show axial symmetry about the mean stress direction in a pure tension stress field (Dershowitz and Einstein, 1988). The orientation of shear related tension gashes would be symmetric about a plane (Wilson, 1982). The orientation of fractures formed as a result of contraction, stress relief, and thermal effects are related to the anisotropy of these processes. Multiple processes will result in complex orientation patterns (Dershowitz and Einstein, 1988).

The initial step in the analysis of fracture orientations was to determine whether the data fell into clusters, were uniformly distributed or whether they followed some other

distribution such as a girdle distribution (Woodcock and Naylor, 1983). Stereographic projections of fracture orientation data by dyke domain (Appendix A.3.1) reveal that, although a lot of scatter is present, there is one dominant cluster of fractures per domain. The mean orientations of the dominant fracture cluster in each of the domains are similar to the mean dyke orientations for those domains. This implies that fracture formation in the sheeted dykes is, to a large extent, controlled by cooling on contraction along the dyke margins after dyke injection.

The fracture orientations were analysed on the basis of the dyke domains established in Section 2.3.2. The orientations of dykes for each scanline area, are shown in Figure 3.4. The fractures within each domain are treated together except for the fractures in domain 4. To facilitate interpretation, domain 4 was divided into a southern area containing the scanlines along a road section west of Alona in a gabbro body in the sheeted dykes (refer to Figure 2.1 for locations), and a northern area containing the remainder of the data. The dykes and gabbros in the Alona section are separated, by a steeply dipping, normal, northwest-southeast trending fault.

Contoured stereographic projections of the fracture orientation data were used to divide the fracture data into sets. Orientations of set boundaries were determined by including all fractures within the contour level representing twice the concentration of a uniform distribution, into one set (Robin and Jowett, 1986; van Everdingen et al., 1992). This method enabled the division of fractures into sets represented by clusters or girdles.

The fracture orientation data in domain 6 contain two subsets, one represented by a cluster distribution, the other by a girdle distribution (Figure 3.5). The mean orientation of the cluster (marked by a filled star on Figure 3.5) lies within 10° of the

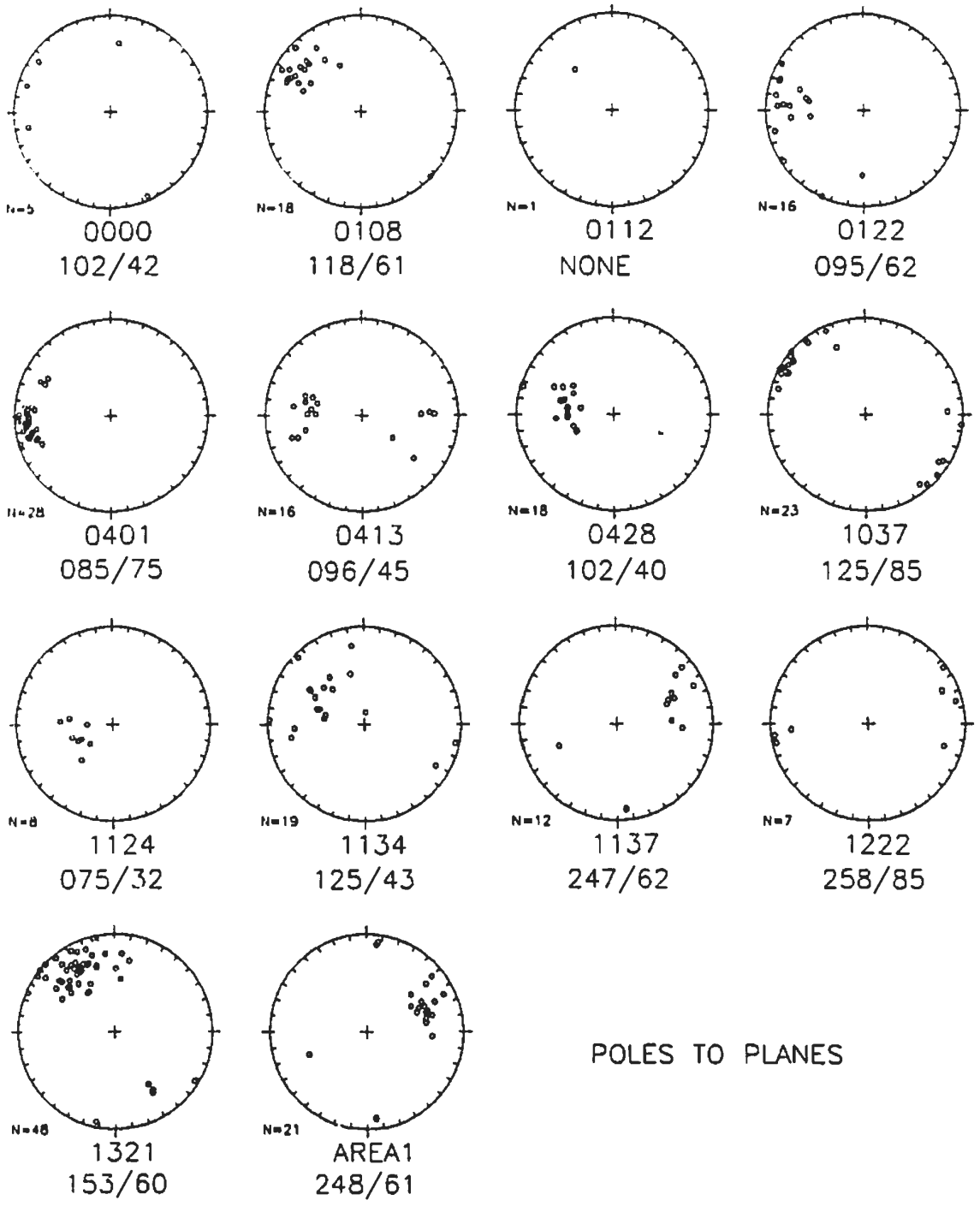

FIGURE 3.4 DYKE ORIENTATIONS BY SCANLINE. MEAN DYKE ORIENTATION BELOW EACH STEREONET. AREA1 IS AT LOCATION 1137. SEE TEXT FOR FURTHER EXPLANATION.

axis drawn through the girdle data subset. This implies that the cluster-related fractures are approximately orthogonal to the girdle-related fractures. In an effort to explain this distribution of girdle and cluster data, the spatial relationships of the domain 6 data were plotted on the stereographic projection in Figure 3.5. This figure shows that both the girdle and the cluster distributions are present in all three scanlines of domain 6 indicating a domainal rather than local relationship. This same cluster/girdle relationship is seen in eight areas (Figure 3.6 and Table 3.3): 1) scanline 1204; 2) scanline 1211; 3) central domain 4 (comprising scanlines 0304, 0401 and 0404); 4) Alona dyke section scanlines; 5) scanline 0213; 6) scanline 1124; 7) scanline 1305; and 8) domain 6 (scanlines 1001, 1028 and 1037). The fractures within the cluster distribution encompass the majority of dyke contacts (compare Figures 3.4 and 3.5), tend to end in intact rock or extend beyond the outcrop edge, and tend to contain epidote mineral filling. Those fracture data associated with the girdle distribution generally terminate against other fractures, have shorter trace lengths, smaller apertures, and preferentially contain calcite as a mineral filling (Table 3.4). Fracture trace lengths are further discussed in Section 3.3.6.

In domain 6, which lies east of the Mitsero graben axis, the girdle axis and cluster mean pole are east dipping (Figures 3.5 and 3.6). At sites in the western half of the Mitsero graben (dyke domains 4 and 5), the girdle axis and the cluster mean pole are west dipping (Figure 3.6). The poles of the cluster distributions lie close ($\pm 10°$) to the axes of the girdle distributions in all cases. The fact that the cluster/girdle relationship occurs throughout the study area indicates that this effect is not due to, for example, the local emplacement of a gabbro body, such as in the vicinity of domain 6 near Ayios Epiphanios. The other scanlines, sharing this relationship, lie at distances of up to 12 kilometres from this gabbro body, far beyond its range of influence. The most probable explanation is that the cluster of data points represents

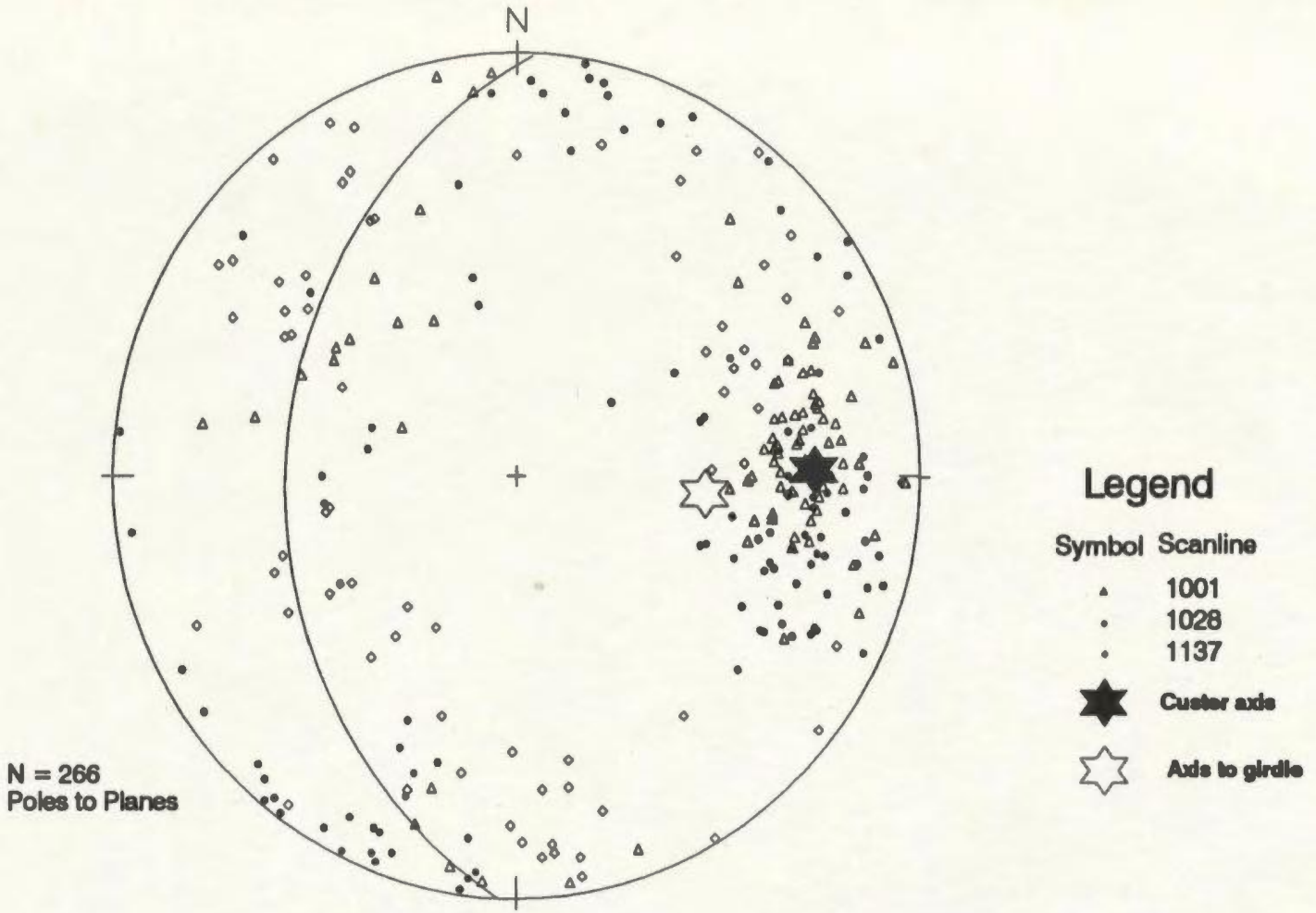

FIGURE 3.5 SPATIAL DISTRIBUTION OF ORIENTATION DATA IN DOMAIN 6 BY SCANLINE.

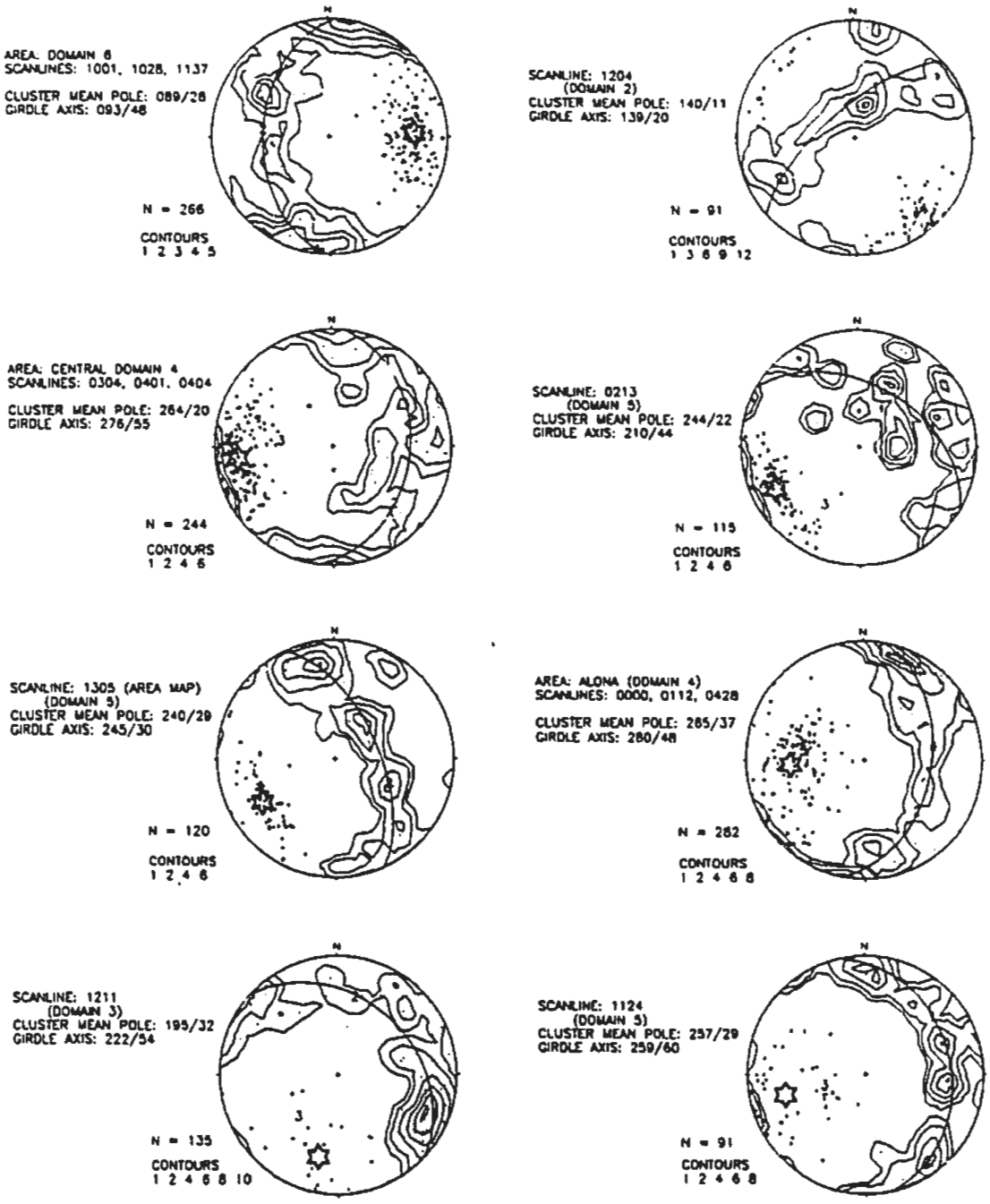

FIGURE 3.6 CLUSTER/GIRDLE RELATIONSHIPS FOR DOMAIN 6, CENTRAL DOMAIN 4, ALONA, AND SCANLINES 1204, 0213, 1305, 1211 AND 1124. STAR IS CLUSTER MEAN POLE; 1, 2, 3 ARE THE EIGEN VECTORS FOR THE GIRDLE DISTRIBUTION; N IS THE TOTAL NUMBER OF DATA POINTS ON THE STEREOGRAPHIC PROJECTION. CONTOUR INTERVALS ARE MULTIPLES OF A UNIFORM DISTRIBUTION.

Domain	Area	Orientation Distribution			
		Cluster	Girdle	None	Too Few
2	0108	Y			
	1316,1321 1037	Y			
	1204	Y	Y		
	0329				Y
3	1129	Y			
	1134		Y		
	1211	Y	?		
4	West			Y	
	1227	Y			
	Central	Y	Y		
	1310	Y			
	East			Y	
	Alona D.	Y	Y		
	Alona G.	Y			
5	0201				Y
	0213	Y	?		
	1107,1111	Y			
	1124	Y	Y		
	1221,1222	Y			
	1305	Y	Y		
	1307		Y		
6	1001,1028 1137	Y	Y		

Table 3.3. Orientation distributions for scanlines and dyke domains - West comprises scanlines 1216, 1221 and 1222; Central comprises scanlines 0304, 0401, 0404; East comprises 0306, 0307, 0413, 0418, 0701, 1008, 1017 scanlines. Alona D. represents the dyke section, and Alona G. the adjacent gabbro section. 'Y' means the column property is present and '?' indicates a weak presence. The shaded cells show scanlines or areas containing both a cluster and a girdle distribution of fracture orientations.

TABLE 3.4 Cluster / Girdle Distributions of Scanline Fracture Data

Scanline:	1204		1211		0304, 0401, 0404		0000, 0112, 0122, 0428		0213		1124		1305		1001, 1028, 1137	
Domain:	2		3		4		4		5		5		5		6	
Total N:	91		135		155		282		115		91		120		266	
Distribution:	Cluster	Girdle	Cluster	Girdle	Cluster	Girdle	Cluster	Girdle	Cluster	Girdle	Cluster	Girdle	Cluster	Girdle	Cluster	Girdle
Cluster Az.	120°–160°		330°–360°		040°–135°		025°–150°		020°–120°		020°–145°		015°–120°		212°–326°	
N:	60	31	22	113	155	89	128	154	93	22	46	45	66	54	147	119
Fracture Type																
contact	33%	3%	0%	10%	26%	10%	14%	1%	34%	0%	17%	0%	32%	0%	44%	5%
fracture	5%	0%	5%	3%	12%	4%	9%	7%	10%	9%	17%	4%	18%	24%	10%	11%
joint	62%	94%	95%	88%	58%	82%	75%	84%	53%	91%	63%	96%	50%	76%	46%	83%
Termination Mode:																
Both ends free	13%	3%	0%	3%	5%	2%	8%	4%	10%	9%	4%	2%	20%	2%	10%	2%
'T' junction	35%	16%	36%	48%	36%	38%	44%	49%	38%	18%	30%	20%	42%	17%	30%	42%
'H' junction	17%	71%	55%	24%	2%	19%	15%	30%	9%	73%	39%	78%	14%	80%	8%	41%
Splay	3%	0%	0%	1%	3%	1%	2%	1%	2%	0%	4%	0%	0%	0%	7%	1%
Mineral Filling																
none	65%	39%	95%	94%	25%	33%	23%	22%	57%	64%	43%	76%	68%	59%	86%	82%
calcite	28%	23%	5%	2%	0%	4%	0%	0%	26%	27%	4%	7%	15%	20%	3%	3%
epidote	7%	0%	0%	0%	64%	43%	36%	29%	19%	14%	4%	2%	18%	20%	8%	16%
zeolite	0%	0%	0%	4%	15%	17%	55%	61%	4%	0%	43%	13%	0%	0%	5%	0%
chlorite	0%	0%	0%	0%	1%	2%	3%	1%	0%	0%	0%	0%	0%	0%	1%	3%
pyrite	0%	0%	0%	0%	17%	18%	0%	1%	0%	0%	0%	0%	0%	0%	1%	4%
celadonite	0%	0%	0%	0%	0%	0%	0%	0%	0%	0%	0%	0%	0%	0%	0%	0%
hematite	0%	0%	0%	0%	3%	1%	7%	5%	0%	0%	2%	7%	0%	0%	0%	0%
magnetite	0%	0%	0%	0%	0%	0%	0%	0%	0%	0%	0%	0%	0%	0%	0%	0%
quartz	0%	0%	0%	0%	0%	0%	0%	0%	0%	0%	7%	0%	2%	0%	0%	0%
Large Scale Roughness:																
planar	93%	84%	91%	90%	90%	85%	87%	78%	80%	91%	89%	96%	86%	94%	71%	87%
undulating	7%	3%	0%	1%	1%	0%	2%	1%	6%	5%	7%	0%	0%	0%	21%	6%
curved	0%	10%	9%	9%	5%	13%	7%	18%	5%	0%	0%	2%	8%	0%	7%	7%
stepped	0%	0%	0%	0%	0%	0%	0%	0%	0%	0%	0%	0%	2%	0%	0%	0%
irregular	0%	0%	0%	0%	4%	1%	1%	2%	8%	5%	4%	0%	2%	6%	0%	0%

Note: percentages are based on the total number of fractures (N) within a particular cluster or girdle

fractures that formed either as dyke cooling margins or following the fabric of the rock parallel to the margins. The girdle distribution of points, which lie roughly perpendicular to the cluster fractures, are then most likely the poles to the columnar jointing cooling fractures in the interior of the dykes (Figure 3.7). The columnar joints perpendicular to dyke margins are commonly seen in the field area.

The division of fracture data into subsets was performed only on those fractures containing a mineral filling and also excluded those containing only calcite. This was done because unfilled fractures were unlikely to have been interconnected with the fracture network at the time of on-axis hydrothermal circulation. Calcite-filled fractures were also not included in the fracture sets because it is a late mineral phase formed during late, probably off-axis, hydrothermal circulation (see discussion in Section 5.3); the paleo-permeability analysis (Section 4.3) is only concerned with fluid flow during hydrothermal circulation at the spreading axis.

Two sets of fractures were extracted from the fracture data per scanline area: 1) fractures which have similar orientations to the dykes within the individual areas; and 2) the remaining fractures. The second set includes cooling fractures formed within the dyke perpendicular to the dyke margins as well as some non-systematic fractures. These non-systematic fractures were included in the fracture analysis because they contributed to the fracture network as fluid conduits since they were filled with minerals derived from hydrothermal alteration. Only those scanline areas with fracture data subsets containing more than 30 fractures were used to give statistically meaningful results. The fracture subsets, from the fourteen scanline areas with greater than 30 fractures, are plotted on stereographic projections in Figure 3.8.

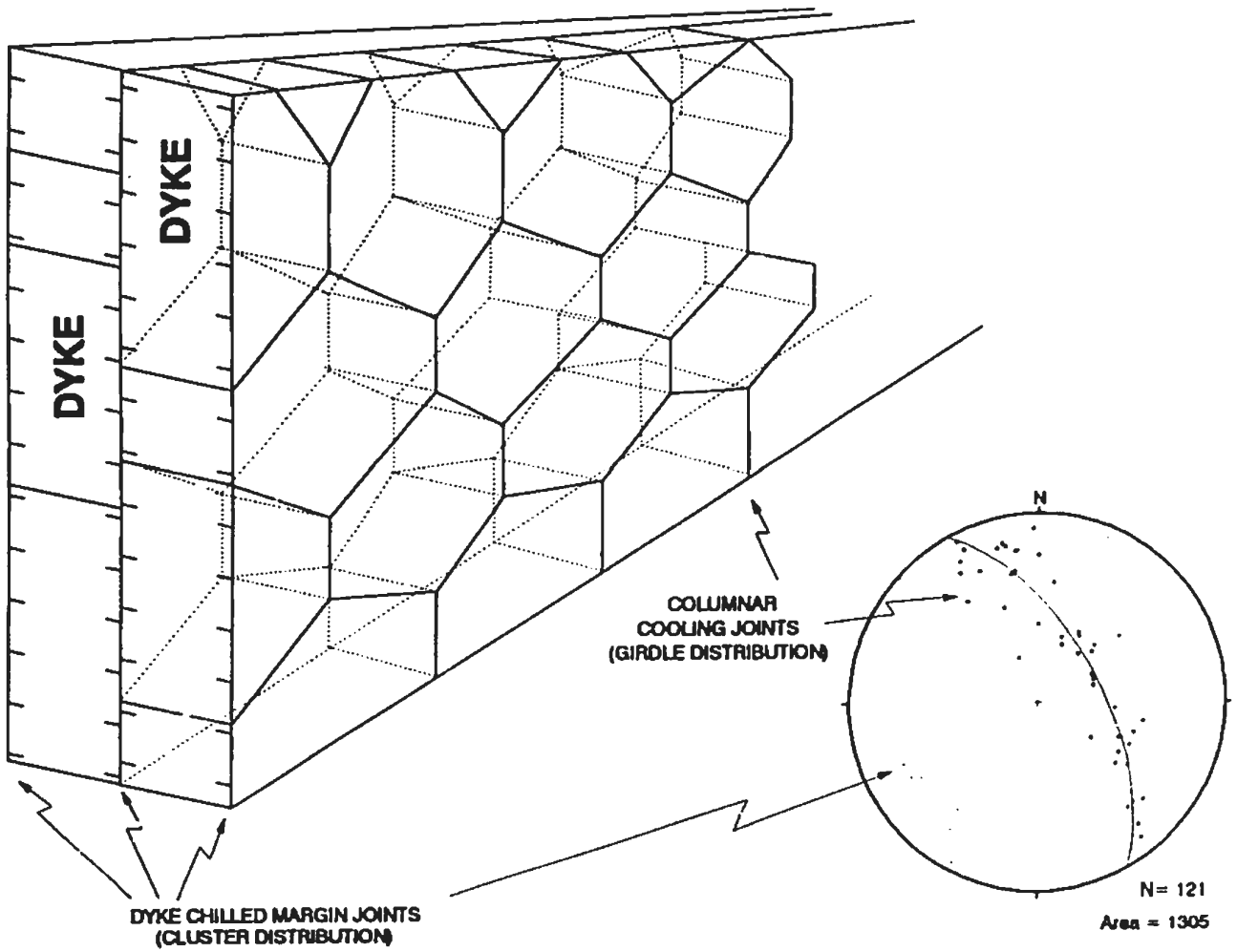

FIGURE 3.7 SCHEMATIC DIAGRAM TO ILLUSTRATE INTERNAL COLUMNAR JOINTING IN DYKES

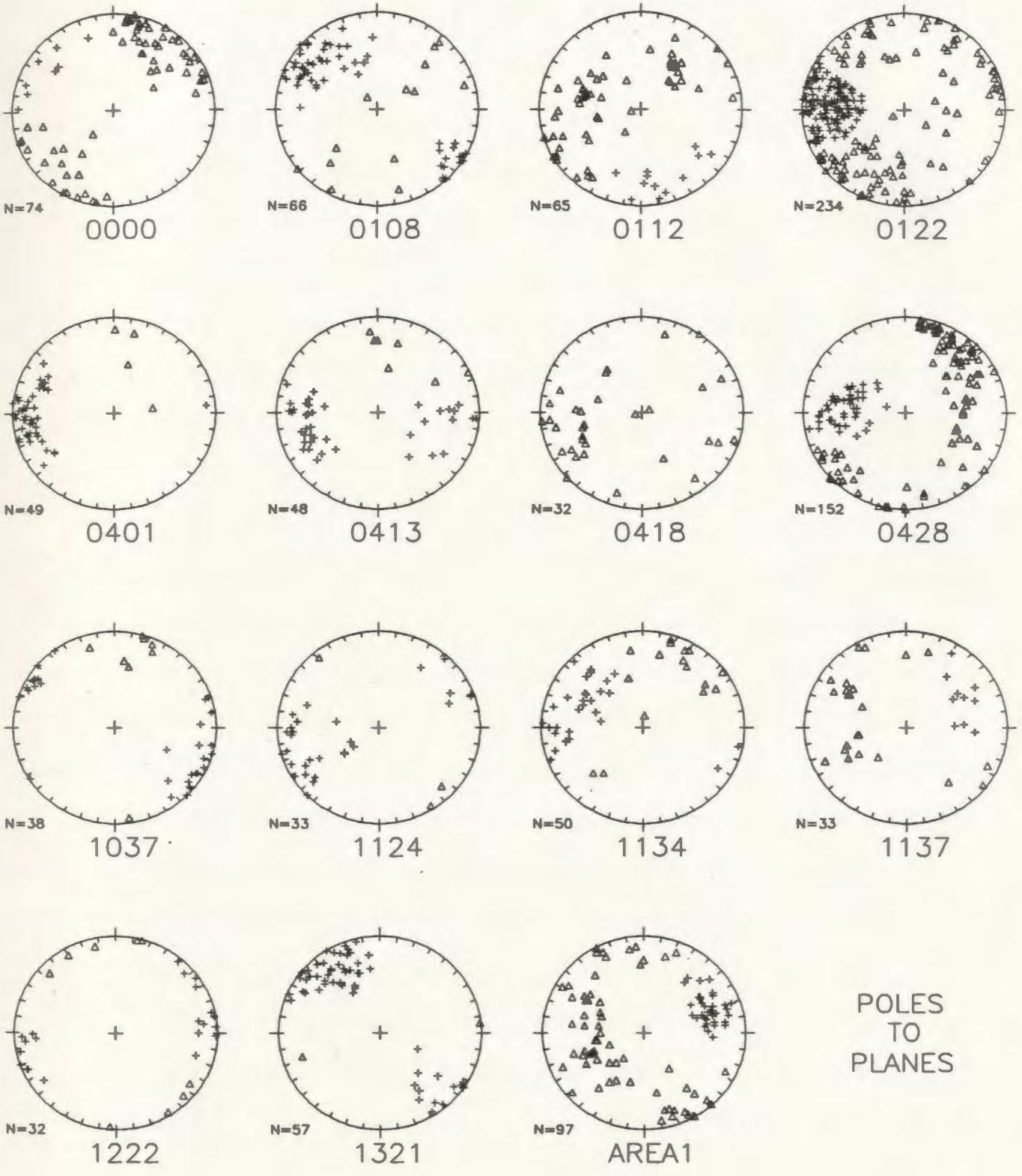

FIGURE 3.8 FRACTURE SETS BY SCANLINE. CROSSES ARE FRACTURES SUB-PARALLEL TO DYKES, TRIANGLES ARE OTHER FRACTURES. SEE TEXT FOR FURTHER EXPLANATION.

The present orientation of the fracture subsets is different from their orientation when they were still part of the sub-seafloor oceanic crust. Since that time, the fractures have undergone rotation due to graben formation and uplift of the ophiolite (Section 2.3.3). On the basis of field evidence such as columnar jointing in the interior of dykes and chilled margins along the edges of dykes, most fractures, appear to be related to the initial cooling and contraction of the dykes after their emplacement. Therefore the resultant fracture subsets were rotated to remove the effects of ophiolite uplift and graben formation (Figure 3.9). The 90° counter-clockwise rotation of the ophiolite (Section 2.2.2) affects the entire ophiolite in the same manner, therefore this rotation is not done.

The rotations performed on the fracture data were done in the two steps outlined in Section 2.3.3: 1) rotation of the fractures 3° in a clockwise fashion about a 090° (with respect to north) trending horizontal axis to remove the effects of the ophiolite uplift; and 2) rotation of the fractures about a horizontal north-south trending axis (parallel to the Mitsero graben axis) by either 19° or -16° for those scanlines situated on the west and east sides of the graben axis, respectively, to remove the effects of the graben formation. Scanline 1037 resides in the Makhaeras domain, outside the Mitsero graben, and does not appear to have been rotated during the graben formation, therefore it did not have the second correction applied. Scanline 0108, 1134 and 1321 lie in the vicinity of the portion of the graben axis which trends at an angle of 045° with respect to north, therefore they were rotated along an axis trending 045° rather than 0°.

Fracture orientation data plotted by sub-domain (Appendix A.3.1) as defined in Section 2.3.2, reveals that the relationship between fracture orientations and dyke orientations is similar from area to area. For example, scanline 1129, on the west side

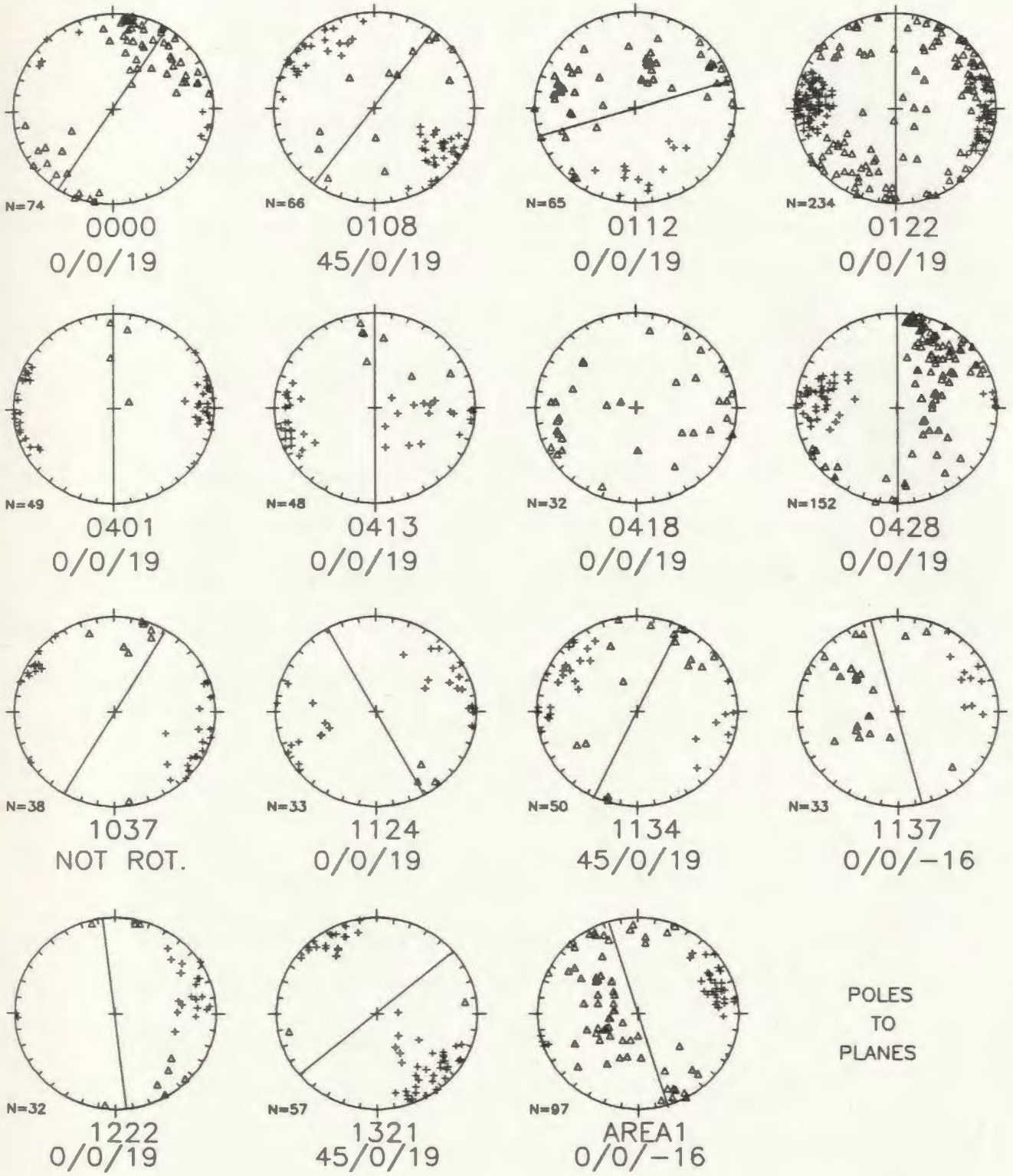

FIGURE 3.9 ROTATED FRACTURES BY SCANLINE. USING SAME SYMBOLS AS IN FIGURE 3.8. AMOUNT OF SECOND ROTATION GIVEN UNDER EACH PLOT (E.G. 0/0/19 = AXIS TREND/AXIS DIP/AMOUNT OF RIGHT-HANDED ROTATION). LINES ARE MEAN STRIKE OF CLUSTER (+).

of the graben axis in domain 2B, has dyke-parallel fractures presently dipping steeply to the southeast, whereas scanline 1204, on the east side of the graben axis in domain 2A, has the dyke parallel fractures presently dipping steeply to the northwest (Figure 3.10). From Figure 3.10, it can be seen that a 35° rotation about a horizontal axis oriented 045° will bring the fractures in scanline 1129 to a very similar orientation as those in scanline 1204. This 35° rotation is equal to the sum of the rotation of the western graben half (19°) and the eastern graben half (16°), needed to bring the dykes in each graben half back to the vertical (the rotations that the various portions of the Mitsero graben have undergone are dicussed in Section 2.3.3). This tends to corroborate the method (Section 2.3.3) of determining the amount of dyke rotation. The rotation axis used here is not north-south (i.e. 000°) because the graben axis trends north-east (045°) possibly as a result of the South Troodos Transform Fault, south of Apliki. A significant result of the fracture study is that prior to the graben formation and ophiolite uplift, the study area appears to have had similar fracture orientations, with respect to dyke orientations, in all scanline areas, implying a similar stress field during fracture formation for the whole of the study area.

The previous fracture orientation analysis dealt exclusively with fractures in the sheeted dykes and gabbros. Field work in pillowed and extrusive volcanic rocks of the Basal Group and of the Upper and Lower Pillow Lavas showed that systematic scanline fracture mapping was not feasible in these areas. This was because the highly curved nature of the fractures made the orientation measurements at the scanline-fracture intersections meaningless. The pillow units tend to have curved cooling fractures along their margins. The interiors of pillows tend to be highly fractured (probably cooling related) - these fractures may be curved or planar and are oriented radially about the centre of the pillow. In certain areas, the pillows are highly brecciated ('auto-brecciated'; Robinson, pers. comm., 1985), probably during

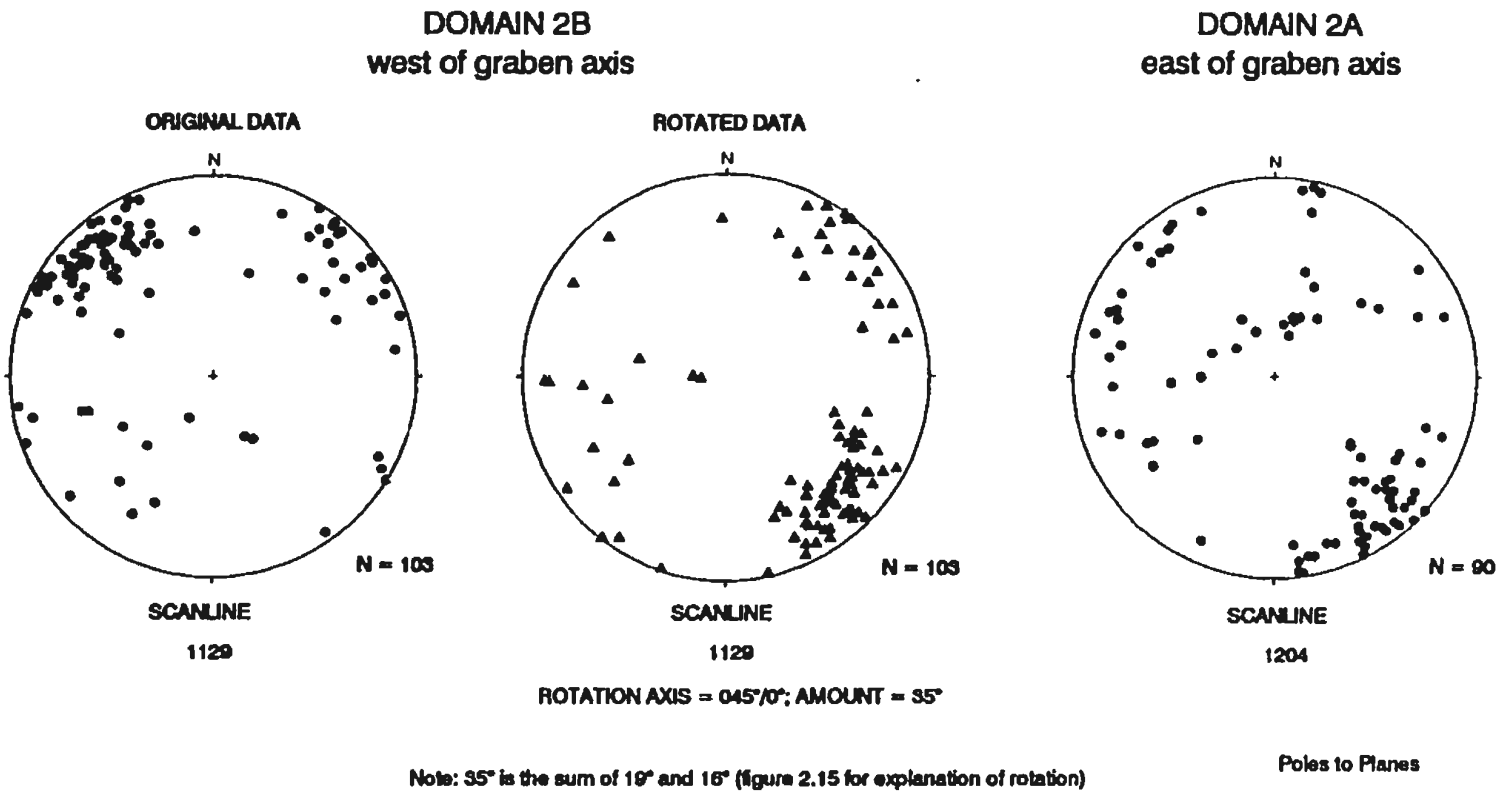

FIGURE 3.10 COMPARISON OF FRACTURE ORIENTATIONS WITHIN SUBDOMAINS 2A AND 2B.

the cooling process. Flow units exhibit fracturing perpendicular to the upper and lower margins of the unit. Since this study is concerned primarily with the sheeted dykes, fracturing in the pillowed and flow units is not treated further.

3.3.4 Fracture Filling Minerals: Type and Distribution

The precipitation of minerals in fractures is indicative of the passage of fluids. Many of the mineral fillings in fractures in the study area, especially epidote and quartz, were precipitated by hydrothermal fluids (Section 5.4). In order, to determine the extent of hydrothermal fluid circulation throughout the study area, it is necessary first to determine the spatial and temporal inter-relations of fracture filling minerals.

The oblique exposure of the ophiolite in the study area means a depth section through the ophiolite can be studied (up-section is to the north). Information on fracture characteristics throughout the section can be used, by analogy, to provide information on fracture characteristics and conditions that may have existed in a vertical section of oceanic lithosphere. For example, variations in fracture mineral filling are dependent on the temperature and fluid compositions, as well as which fractures are open at the time of fluid circulation.

The fracture-filling minerals include epidote, zeolites, quartz, calcite, chlorite, pyrite, and minor occurrences of hematite, magnetite, jasper, celadonite and clay minerals. Their modal abundances vary with proximity to hydrothermally altered zones and with rock type. For example, the concentration of epidote vein-filling increases in the immediate vicinity (within 20 metres) of epidosite zones and zeolites are more common in gabbros than in diabases. Celadonite-filling is restricted to the Pillow

Lava units, with rare occurrences in the upper part of the Basal Group in the study area. Rare occurrences of 5 centimetre wide hematite and magnetite veins were noted in areas of extensive epidote mineralization. Clay minerals were seen mainly in areas of faulting, as part of the gouge, and in the Pillow Lava units as alteration products of the extrusive rock. Plate 3.1 shows a typical relationship of vein filling material to the diabase. The vein is filled with euhedral epidote and anhedral to subhedral quartz. In many fractures the epidote forms rosettes which nucleate from the walls of the fracture (Plate 3.1).

Fracture frequency does not change with depth or laterally throughout the study area (Figure 3.11; and discussed later in section 3.3.7). There is an increase in the occurrence of fracture-filling minerals from the top to the bottom of the Sheeted Dyke Complex (from the volcanic rocks in the north to the gabbroic rocks in the south) (see Appendix A.3.2.2 and A.3.2.3) which is, therefore, correlated with a reduction in the number of fractures devoid of mineral filling with increased depth in the section (e.g. compare the northern (higher) and southern (lower) portions of domain 4) (Table 3.5).

The variations with depth in fracture mineral filling abundances are indicated in Figure 3.12 and Table 3.5 and then discussed in the following paragraphs.

The orientations of fractures filled with epidote tend to form clusters in all domains and have orientations similar to dyke margins for all dyke domains. Twice as many fractures in domains 2 and 4 (30%) contain epidote as do those in domains 3, 5 and 6 (15%). This may be because fractures in domains 2 and 4 lie deeper in the section. No consistent variation in frequency of epidote veining is observed in an east-west direction, however, the abundance of epidote is lowest higher in the section,

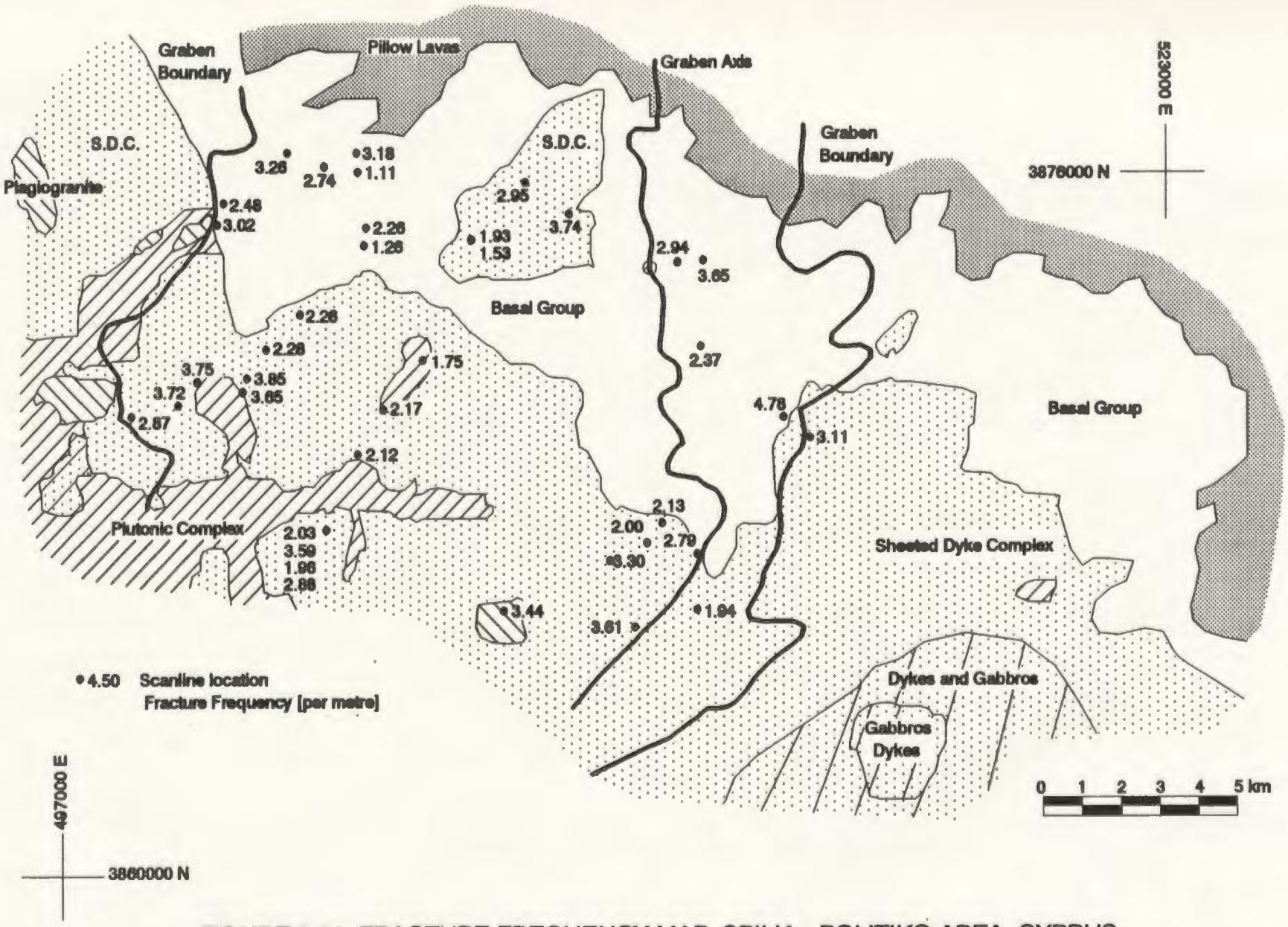

FIGURE 3.11 FRACTURE FREQUENCY MAP, SPILIA - POLITIKO AREA, CYPRUS.

TABLE 3.5 FRACTURE FILLING BY DYKE DOMAIN. EACH CELL CONTAINS THE FOLLOWING INFORMATION: LINE 1 – NUMBER OF MINERAL FILLED FRACTURES; LINE 2 – % OF DOMAIN'S FRACTURES WITH THAT MINERAL FILLING; LINE 3 – WHERE POSSIBLE, THE MEAN ORIENTATION OF THE FRACTURES FOR THAT MINERAL. 'w' INDICATES WEAK CLUSTERING ABOUT THE MEAN. DOMAIN 4 WAS SUBDIVIDED INTO NORTH (4N) AND SOUTH (4S) SUBSETS. N IS NUMBER OF FRACTURES IN EACH DOMAIN.

MINERAL	DYKE DOMAINS					
	2 N=508	3 N=302	4N N=715	4S N=646	5 N=719	6 N=266
NONE	235 43% 320°/79°	169 55% 292°/69°	406 52% 213°/79°	119 14% 000°/59°w	483 65% 234°/90°	223 79% 274°/59°
EPIDOTE	179 33%	62 18%	199 25% 087°/79°	235 27% 100°/50°	112 15% 060°/69°	33 12% 120°/59°
ZEOLITE	25 5% 120°/70°	6 2% 120°/69°	42 5% 082°/69°	404 47% 090°/69°	51 7% 327°/79°	7 2%
CALCITE	87 16%	77 22%	51 7% 087°/79°	0 0% 100°/50°	69 9% 060°/69°	9 3% 120°/59°
CHLORITE	4 1%	0 0%	5 1%	52 6% 090°/50°	2 <1%	4 1%
PYRITE	8 1%	7 2% 140°/79°	53 7% 069°/59°	2 <1%	0 0%	7 2%
CELADONITE	2 <1%	0 0%	0 0%	0 0%	0 0%	0 0%
HEMATITE	7 1%	0 0%	24 3% 087°/79°w	52 6% 100°/50°	20 3% 222°/89°	0 0%
MAGNETITE	0 0%	5 1%	0 0%	0 0%	0 0%	0 0%
QUARTZ	1 <1%	0 0%	4 1%	0 0%	11 1% 234°/89°	0 0%

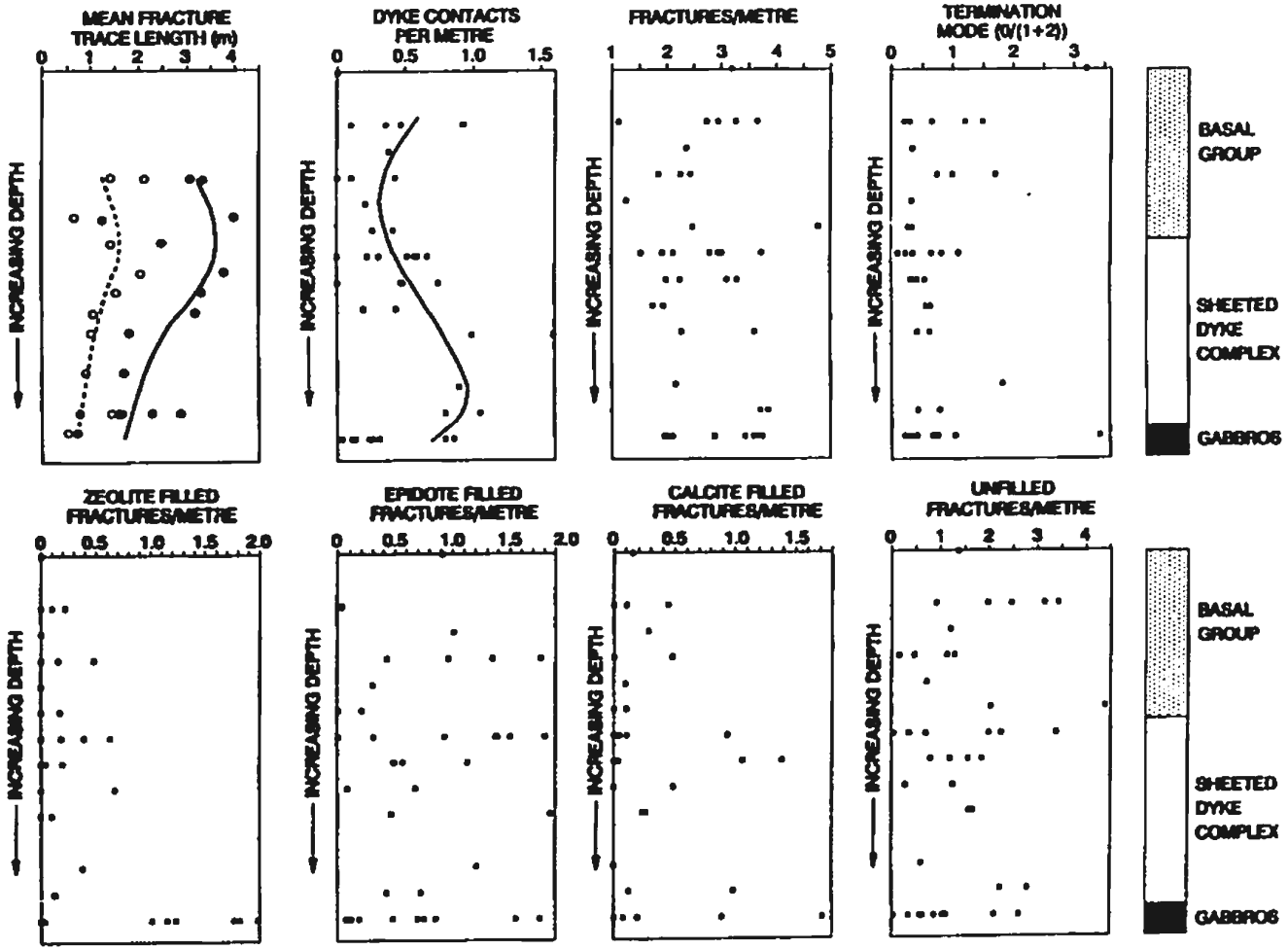

FIGURE 3.12 VARIATION WITH DEPTH OF VARIOUS FRACTURE PROPERTIES INCLUDING TRACE LENGTH, DYKE AND FRACTURE FREQUENCY, TERMINATION MODE, AND ZEOLITE, EPIDOTE, CALCITE AND UNFILLED FRACTURES IN THE SPILIA-POLITIKO AREA. TRACE LENGTHS ARE SUBDIVIDED INTO DYKE PARALLEL (FILLED CIRCLES; SOLID LINE) AND OTHER (OPEN CIRCLES; DOTTED LINE) FRACTURES. DEPTHS ARE RELATIVE DEPTHS BASED ON SCANLINE LOCATION IN THE FIELD AREA (REFER TO SCHEMATIC STRATIGRAPHIC COLUMNS TO RIGHT). SMOOTHED LINES ON GRAPHS CONNECT MEANS OF THE DATA POINTS AT EACH DEPTH.

especially in the Basal Group. Epidote is more common in the area of epidosites (Figure 3.13). In some epidosites, even though the rock is largely composed of epidote, epidote veining is not as common (i.e. scanline area 1107 - see Figure 3.2 for scanline number locations). Epidote is also common in the gabbros.

Zeolites are quite rare within the Sheeted Dyke Complex, away from the lower boundary to the Plutonic Complex, and in the Basal Group. Fractures containing zeolites have similar orientations as those containing epidote, especially in domain 4. Zeolite abundance increases sharply in the gabbros and dykes of the southern portion of domain 4 (Figure 3.14 and 3.12).

The frequency of calcite vein filling is greatest in the vicinity of shear zones and plagiogranites (Figure 3.15). No calcite was noted in the gabbros. Its distribution shows no consistent east-west variation. In general, calcite-filled fractures tend to be oriented 30° to 90° away from dyke orientations in domains 3 and 4, and have similar orientations to those of the dykes in domains 2 and 5. Many of the calcite vein orientations do not cluster with the mean dyke orientations (Figure 3.16). The orientation of fractures containing calcite coincides with those containing epidote and zeolites in domain 3, and with those containing epidote in domain 5. In places where cross-cutting relations can be discerned, calcite always post-dates epidote mineral filling. In fractures containing both epidote and calcite, the calcite always post-dates the epidote.

Mineral filled fractures in the dyke section, excluding those containing only calcite, (Alona area, domain 4) fall into two groups, a cluster with mean pole at 284°/45° (dyke-parallel) and a girdle with axis trending 278°/51°, whereas those in the gabbro section (Alona area, domain 4) lie in one cluster, whose mean pole trends 277°/45°,

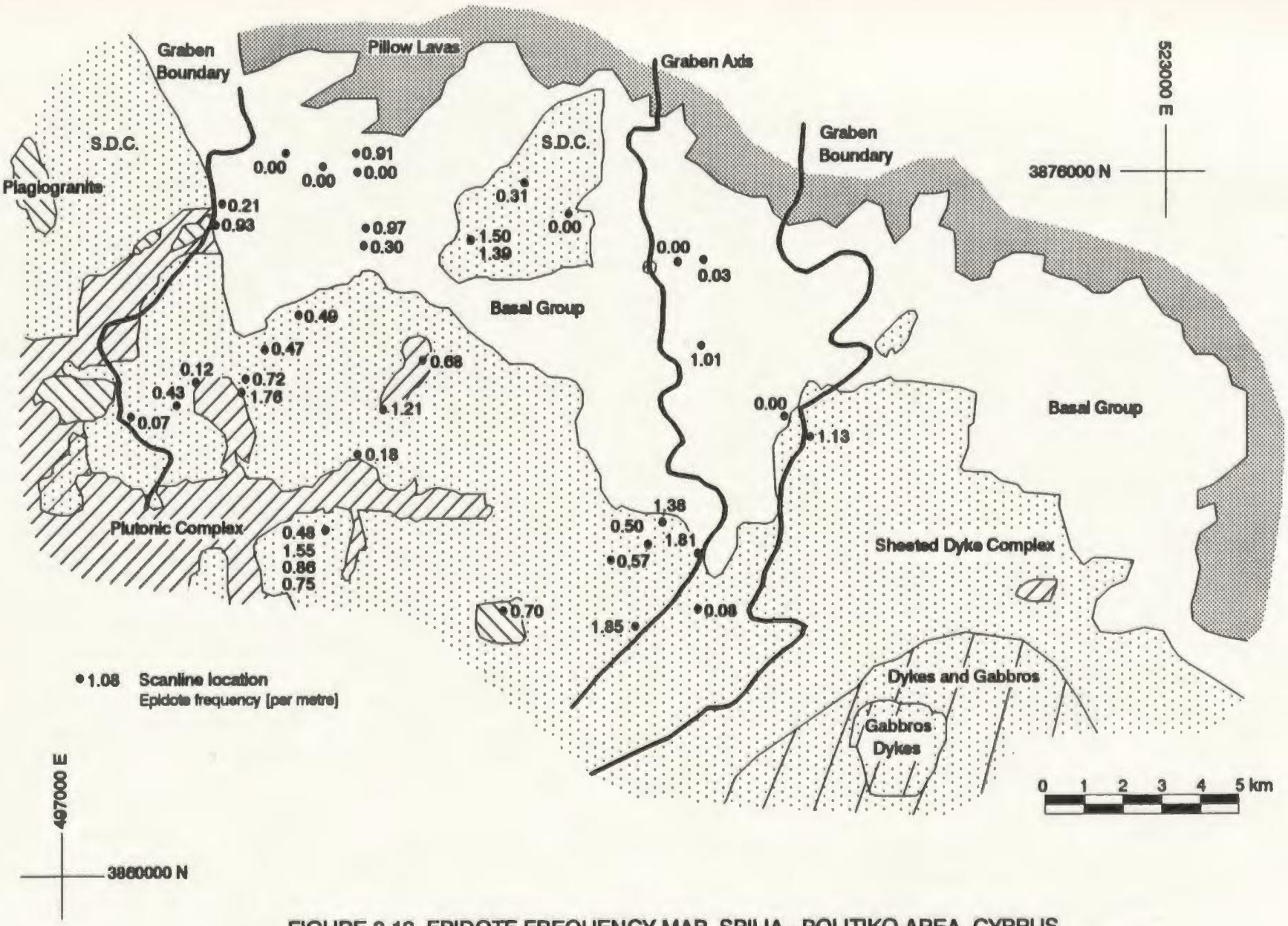

FIGURE 3.13 EPIDOTE FREQUENCY MAP, SPILIA - POLITIKO AREA, CYPRUS.

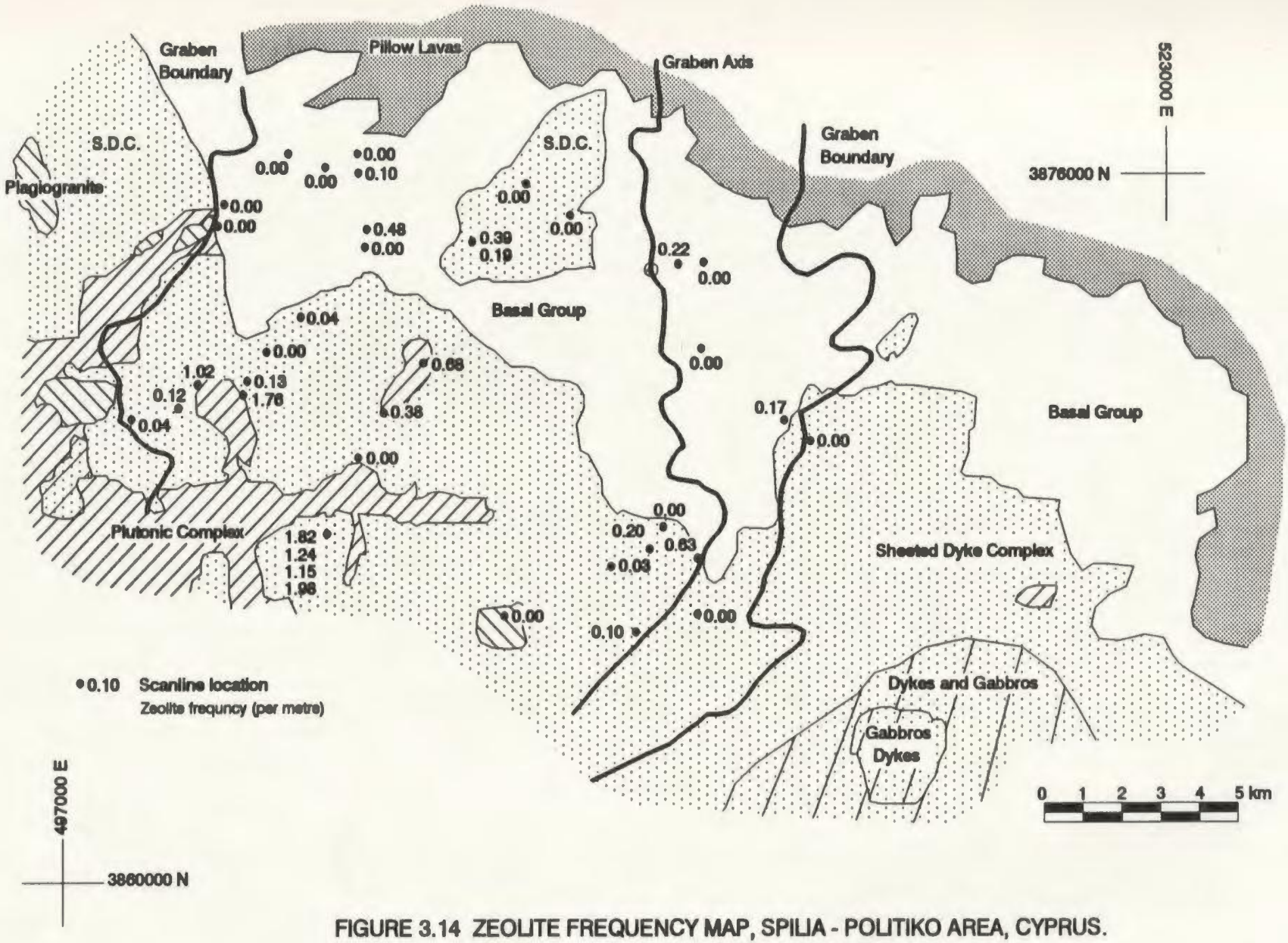

FIGURE 3.14 ZEOLITE FREQUENCY MAP, SPILIA - POLITIKO AREA, CYPRUS.

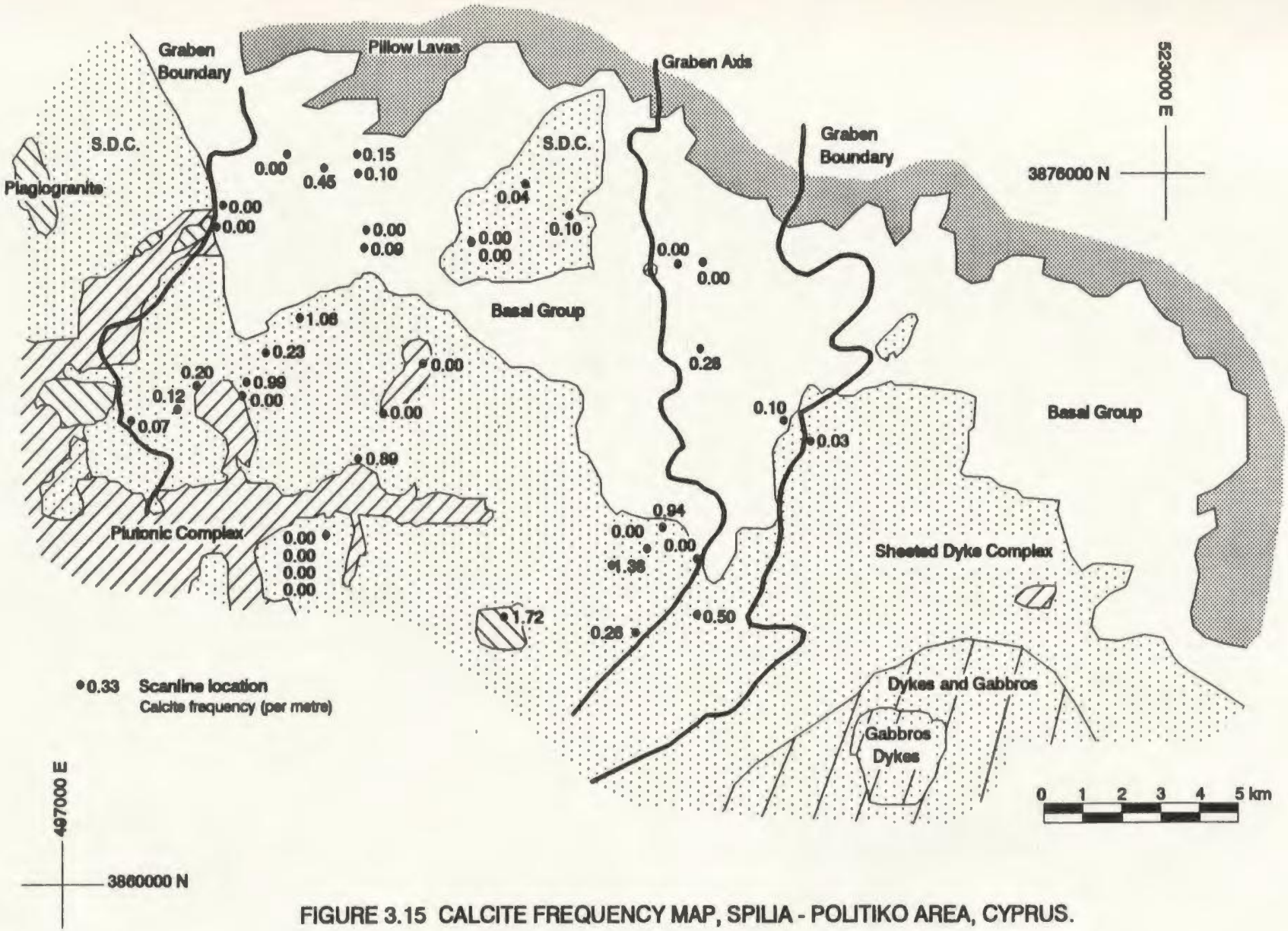

FIGURE 3.15 CALCITE FREQUENCY MAP, SPILIA - POLITIKO AREA, CYPRUS.

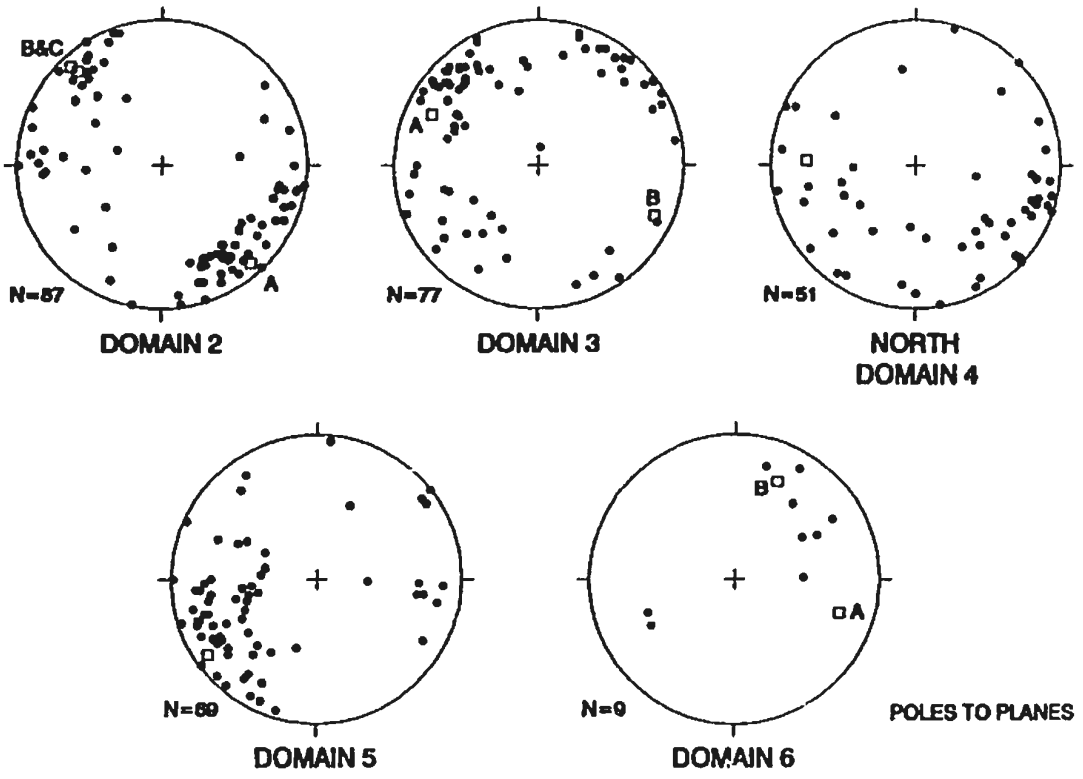

FIGURE 3.16 CALCITE VEIN ORIENTATIONS BY DOMAIN

similar to that of the dyke-parallel fractures (Figure 3.17). The field relations indicate that the gabbro was emplaced into the dykes; the gabbro may have intruded along the normal fault which lies at the eastern edge of the gabbro body. The existing sheeted fabric in the dykes (284°/45°) may have dictated the fracturing in the isotropic gabbros. The girdle set of fractures within the dykes (axis trend: 278°/51°) was not dominant in controlling fracturing within the gabbro, and were probably cooling fractures internal to the dykes.

Unfilled fractures have similar orientations to filled fractures (Figure 3.18 and Appendix A.3.1 (plots of complete orientation data set by domain)). In domain 6, fractures with no mineral filling comprise 83% of all fractures in the domain, for the other domains this varies from 18% to 76% (Table 3.6). Fractures containing no mineral infilling constitute 51% of the complete data set. The majority of fractures in the eastern portion of domain 4 (scanlines: 0306, 1216, and 1227) and the northern portion of domain 3 (1001, 1008, and 1028) contain no mineral filling. The frequency of fractures containing no mineral filling is also higher and more variable near the top of the section in the Basal Group, especially in the area east of the sheeted dyke inlier; it is lowest near the base of the Sheeted Dyke Complex. The southern portion of domain 4 (Alona section) contains a much greater proportion of fractures that contain mineral filling, than the northern portion of domain 4.

Fractures devoid of mineral filling imply they were either not present, closed, or not interconnected to the fracture network at the time of hydrothermal circulation, or the fluid chemistry may have been such that nothing was precipitated in the fracture. The similarity of orientations of filled and unfilled fractures may indicate a similar origin for both. Unfilled fractures in the northern (upper) part of the study area indicate an absence of hydrothermal fluid circulation in large parts of the upper sheeted dykes (in

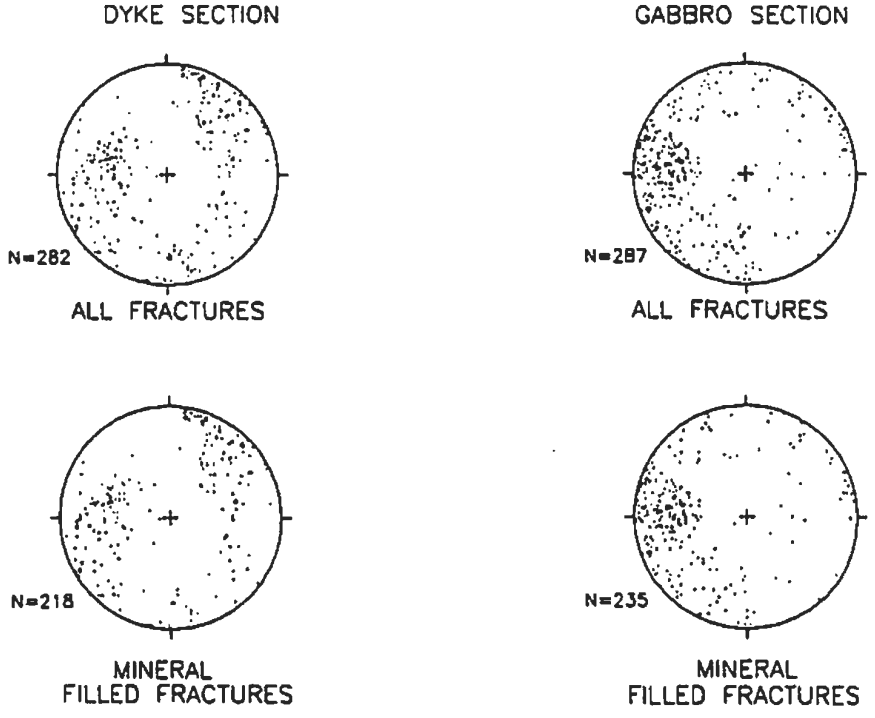

FIGURE 3.17 ALONA SECTION DYKES AND GABBROS. TOP PLOTS = ALL FRACTURES LOWER PLOTS = MINERAL FILLED FRACTURES (EXCLUDING FRACTURES CONTAINING ONLY CALCITE).

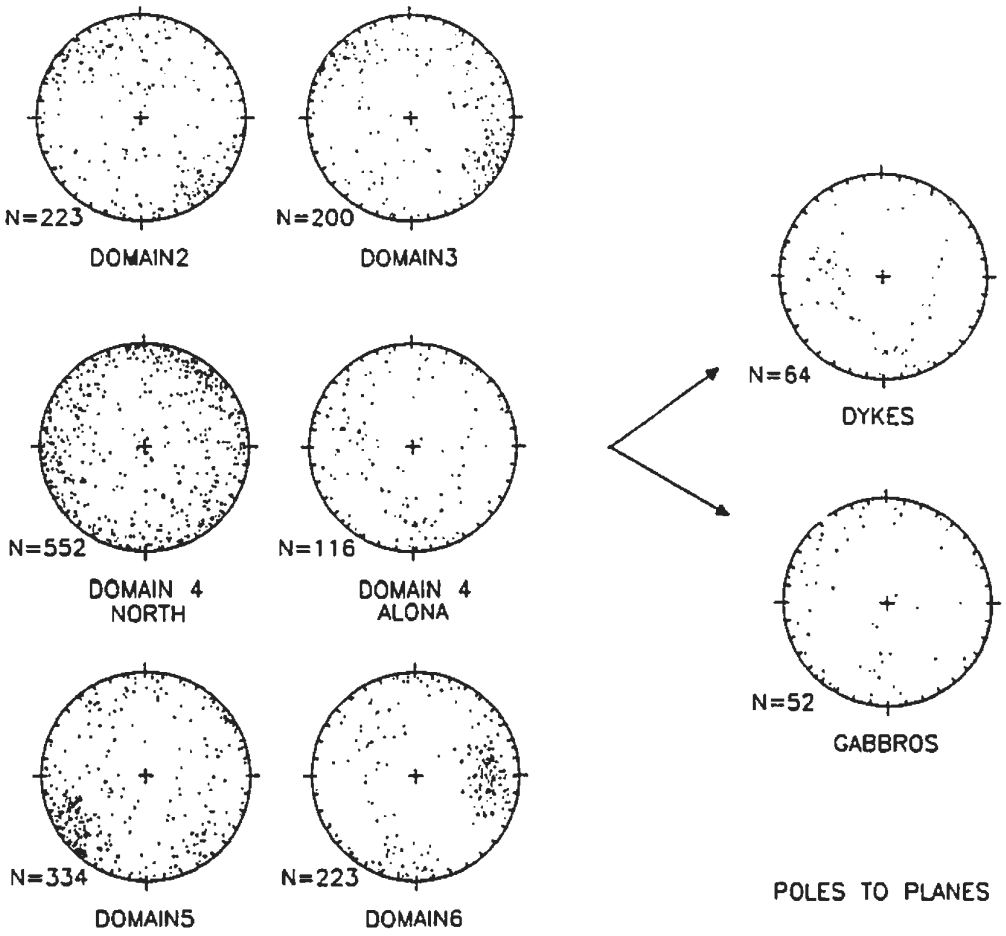

FIGURE 3.18 ORIENTATIONS OF UNFILLED FRACTURES BY DOMAIN. SOUTHERN PART OF DOMAIN 4 (ALONA) IS SUBDIVIDED INTO DYKES AND GABBROS.

	Dyke Domains					
	2 N=515	3 N=312	4N N=726	4S N=652	5 N=734	6 N=282
None	223 46%	200 62%	552 60%	119 18%	334 64%	223 83%
None + calcite	296 61%	245 76%	594 65%	117 18%	384 74%	222 83%

Table 3.6. Number of fractures containing no minerals as a percentage of all fractures (numbers taken from Figures A.1.2 and A.3.2.2.

the Basal Group) (implications of this are further discussed in Section 6.3.6). The frequency of unfilled fractures is the greatest in the eastern half of the Mitsero Graben (Figure 3.19). When this is compared to the contour map of the concentration of mines, gossans and mineral occurrences (Figure 4.3), it is seen that this area coincides with a low in the concentration of mineralization. Possible explanations for this include: the fractures may have been closed in this area at the time of hydrothermal fluid circulation or not interconnected to the fracture network; or the heat supply in this area was not great enough to sustain fluid circulation for the time needed to form mineral deposits, as well as, precipitates in the fractures. Because unfilled fractures are assumed not to have been utilized by fluids and therefore did not contribute to the hydrothermal circulation system, these fractures were identified and factored out of the data set during the later trace length (Section 3.3.6), intensity (Section 4.3.3.1), and permeability calculations (Section 4.3).

3.3.5 Fracture Termination Mode

Fracture termination mode refers to how the fracture ends. Possible termination modes include: 1) both ends free (mode 0); 2) forming a T-junction with another fracture (mode 1); 3) forming an H-junction with other fractures (mode 2); 4) one (mode 3); and the rare cases of both ends (mode 4) splayed and 5) fracture termination against a fracture at one end and splayed at the other (mode 5). Of these, the most common was the T-junction; except in domain 5 where it was the H-junction (Table 3.7). Fracture termination modes are mainly of use in inferring relative age of fracture formation.

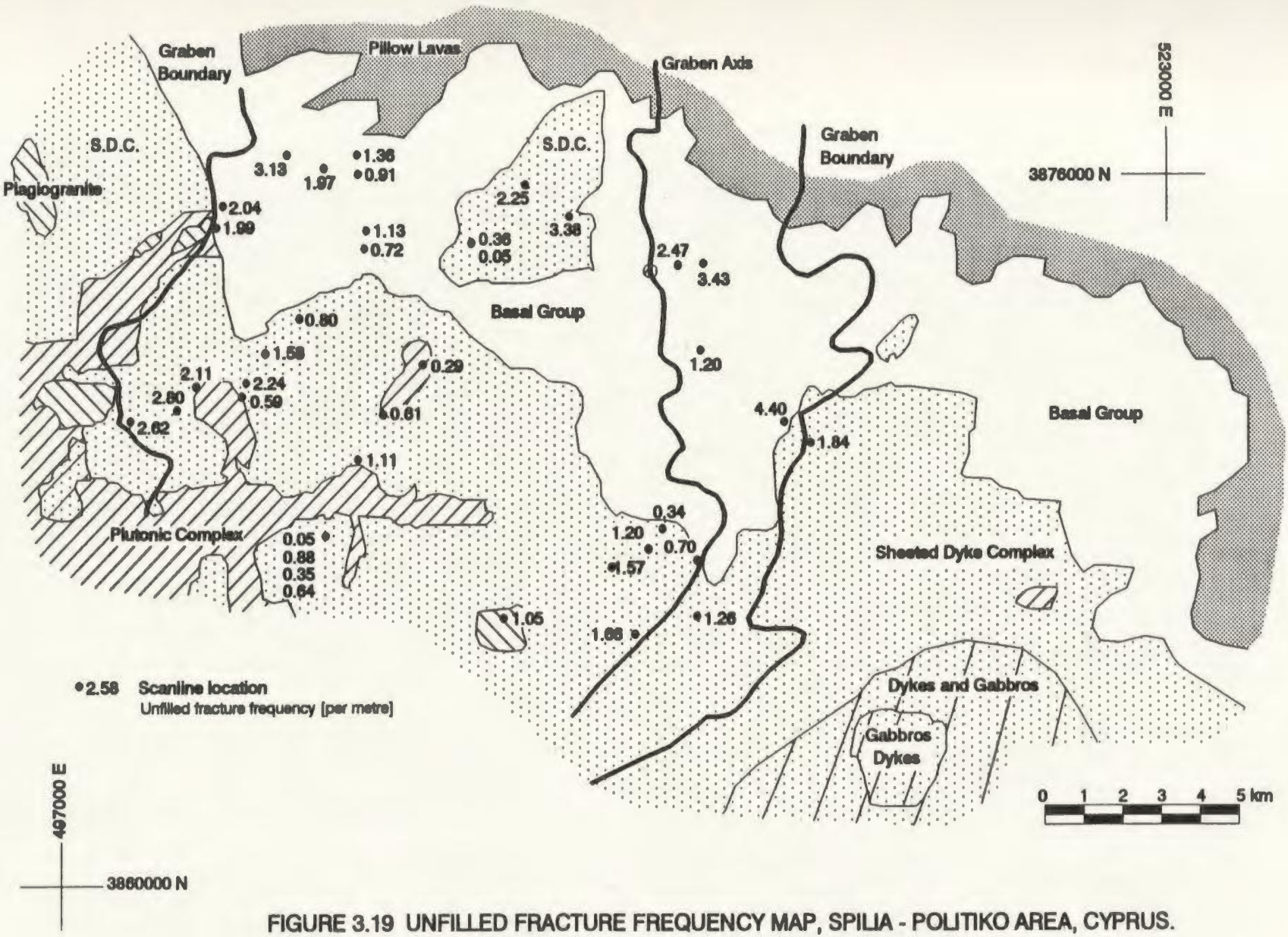

FIGURE 3.19 UNFILLED FRACTURE FREQUENCY MAP, SPILIA - POLITIKO AREA, CYPRUS.

Term. Mode	Dyke Domain 2 N=522	3 N=374	4N N=976	4S N=768	5 N=549	6 N=283
0	43 135/80	10	38	36 105/65	34 060/75	17 270/75
1	174 135/75	160 135/70 225/85	351 045/85	269 050/85	159 060/75	95 270/70
2	136	86	263	126 225/75	176	61 010/75
3	3	1	7	9	4	11
4	1	0	0	3	0	0
5	0	1	0	0	0	0

Table 3.7 Fracture termination mode by dyke domain. Termination mode: 0 = both ends free; 1 = 'T' junction; 2 = 'H' junction; 3 = one end splayed; 4 = both ends splayed; 5 = 'T' and splay. Each cell contains the number of fractures within a particular termination mode, followed by the orientation of the mean plane if the data are clustered about a means. Note that fractures with a censoring of '2' (both ends obscured) have no termination mode assigned to them.

Fractures that have both ends free can form anywhere in the rock. It is likely these fractures are the oldest, since subsequently forming fractures would be more likely to terminate against a pre-existing fracture. These fractures are less abundant than T- or H-junction fractures. Fractures that terminate against another fracture (T- or H-junctions) are assumed to have formed later than the fracture they terminate against. Thus, fracture termination mode can be used as a crude indicator of the relative age of fracture formation. A plot of the ratio of the number of fractures with both ends free to the sum of the number of fractures with T- and H-junctions, can thus indicate the presence of areas of relatively younger (low ratio value) or older fractures (high ratio value). No consistent variation was noted across the study area in an east-west direction (Figure 3.20). There is no overall variation in termination mode with depth in the Sheeted Dyke Complex (Figure 3.12). There is also no significant variation in termination mode by rock type. All termination mode types have the same distribution by trace length (Table 3.8). Table 3.9 indicates that mode 1 (T-junction), mineral-filled fractures are the most common in the study area.

From the stereographic plots of the termination modes of fractures by scanline and dyke domain (Appendix A.3.6), it is apparent that fractures with both ends free tend to follow cluster distributions, whereas the orientation of H- and T-junction termination mode fractures are more uniformly distributed, yet their mean orientations are very similar. The more uniform distribution of T- and H- mode fractures may be the result of fracture formation over a longer period of time, such that fractures that formed later have a greater variation in their orientation.

On average 92% of all fractures (by scanline) terminated against another fracture (Table 3.10). Since fracture frequency appears to be fairly uniform along measured outcrops, the fracture data set is highly connected, that is, most fractures are

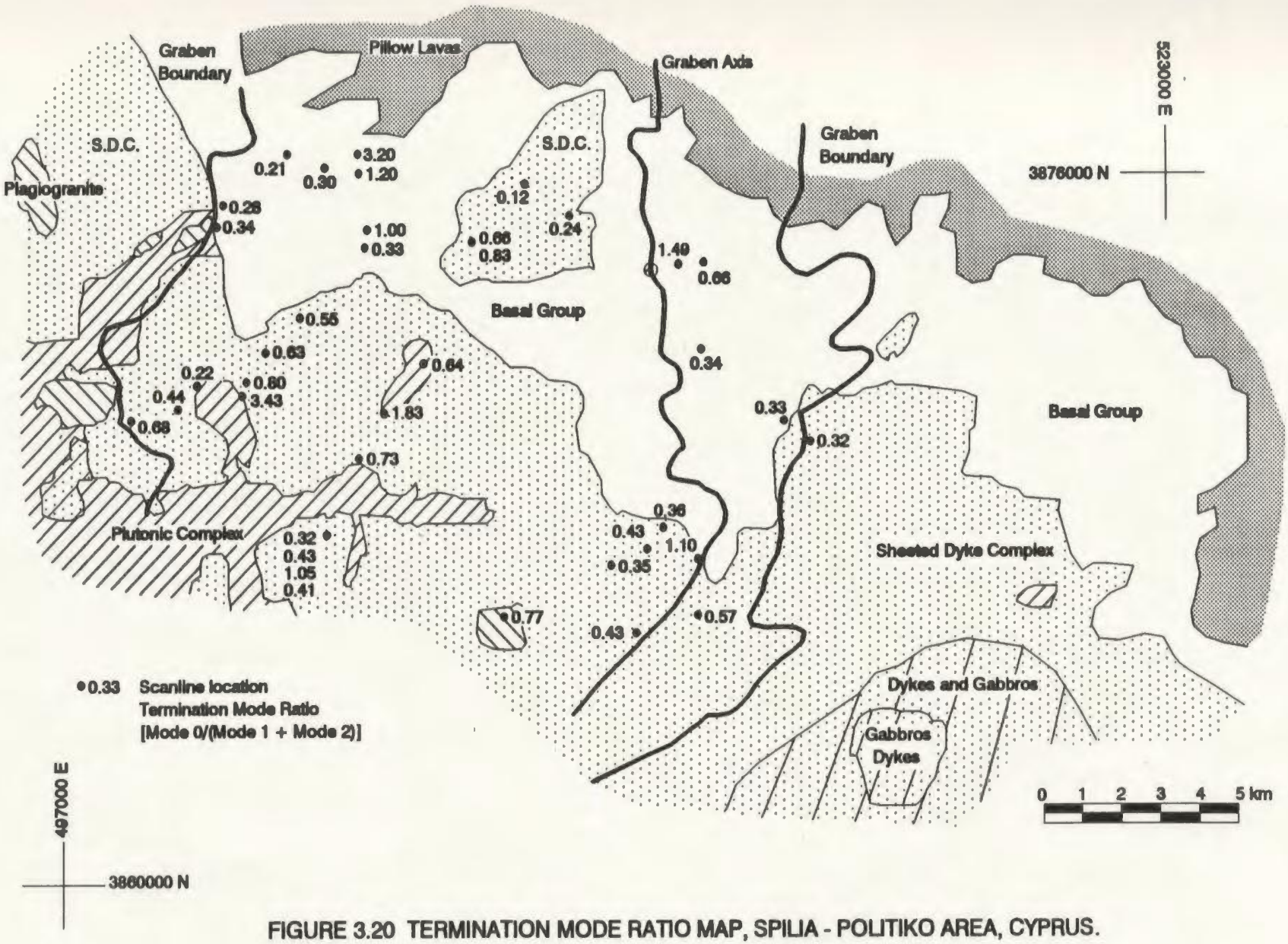

FIGURE 3.20 TERMINATION MODE RATIO MAP, SPILIA - POLITIKO AREA, CYPRUS.

TABLE 3.8 Trace Length versus Termination Mode For Complete Data Set

Number of fractures per cell

Trace Length	Termination Mode 0	1	2	3	4	5	–	Total
<0.5	4	23	63	1		1	16	108
0.5–1.0	11	176	364	6	1	2	64	624
1.0–2.0	54	456	273	11		2	100	896
2.0–3.0	35	219	75	8			112	449
3.0–4.0	23	140	22	8			133	326
4.0–5.0	10	43	5		1		127	186
5.0–6.0	4	29	4				116	153
6.0–7.0	2	12					74	88
7.0–8.0		3					39	42
8.0–9.0	1	3					14	18
9.0–10.0		2					12	14
>10.0	6	3	2		2		27	40
Total	150	1109	808	34	4	5	834	2944

Percentage of fractures normalized to column totals

Trace Length	Termination Mode 0	1	2	3	4	5	–
<0.5	2.67	2.07	7.80	2.94		20.00	1.92
0.5–1.0	7.33	15.87	45.05	17.65	25.00	40.00	7.67
1.0–2.0	36.00	41.12	33.79	32.35		40.00	11.99
2.0–3.0	23.33	19.75	9.28	23.53			13.43
3.0–4.0	15.33	12.62	2.72	23.53			15.95
4.0–5.0	6.67	3.88	0.62		25.00		15.23
5.0–6.0	2.67	2.61	0.50				13.91
6.0–7.0	1.33	1.08					8.87
7.0–8.0		0.27					4.68
8.0–9.0	0.67	0.27					1.68
9.0–10.0		0.18					1.44
>10.0	4.00	0.27	0.25		50.00		3.24
Total	100	100	100	100	100	100	100

Percentage of fractures normalized to row totals

Trace Length	Termination Mode 0	1	2	3	4	5	–	Total
<0.5	3.70	21.30	58.33	0.93		0.93	14.81	100
0.5–1.0	1.76	28.21	58.33	0.96	0.16	0.32	10.26	100
1.0–2.0	6.03	50.89	30.47	1.23		0.22	11.16	100
2.0–3.0	7.80	48.78	16.70	1.78			24.94	100
3.0–4.0	7.06	42.94	6.75	2.45			40.80	100
4.0–5.0	5.38	23.12	2.69		0.54		68.28	100
5.0–6.0	2.61	18.95	2.61				75.82	100
6.0–7.0	2.27	13.64					84.09	100
7.0–8.0		7.14					92.86	100
8.0–9.0	5.56	16.67					77.78	100
9.0–10.0		14.29					85.71	100
>10.0	15.00	7.50	5.00		5.00		67.50	100

Termination mode:

0	ends free	2	H'	4	splay + 'T'
1	T'	3	splay	5	double splay

Trace Length: is in metres

– censored

TABLE 3.9 Mineral Filling versus Termination Mode For Complete Scanline Data Set

Number of fractures per cell

Term mode	Mineral Filling										Total
	Zeolite	Epidote	Calcite	Chlorite	Pyrite	Hematite	Magnetite	Clay	Celadonite	None	
0	15	37	27	3	2	3	0	1	0	90	178
1	150	229	130	13	40	34	4	6	0	595	1201
2	79	118	57	7	8	13	0	2	2	565	851
3	5	6	1	2	0	2	0	0	0	19	35
4	1	1	0	0	0	0	0	0	0	2	4
5	2	2	0	0	0	0	0	0	0	3	7
–	87	219	62	26	23	53	1	9	0	401	881
Total	339	612	277	51	73	105	5	18	2	1675	3157

Percentage of fractures normalized to column totals

Term. Mode	Mineral Filling									
	Zeolite	Epidote	Calcite	Chlorite	Pyrite	Hematite	Magnetite	Clay	Celadonite	None
0	4.42	6.05	9.75	5.88	2.74	2.86		5.56		5.37
1	44.25	37.42	46.93	25.49	54.79	32.38	80.00	33.33		35.52
2	23.30	19.28	20.58	13.73	10.96	12.38		11.11	100.00	33.73
3	1.47	0.98	0.36	3.92		1.90				1.13
4	0.29	0.16								0.12
5	0.59	0.33								0.18
–	25.66	35.78	22.38	50.98	31.51	50.48	20.00	50.00		23.94
Total %	100	100	100	100	100	100	100	100	100	100

Percentage of fractures normalized to row totals

Term mode	Mineral Filling										Total
	Zeolite	Epidote	Calcite	Chlorite	Pyrite	Hematite	Magnetite	Clay	Celadonite	None	
0	8.43	20.79	15.17	1.69	1.12	1.69		0.56		50.56	100
1	12.49	19.07	10.82	1.08	3.33	2.83	0.33	0.50		49.54	100
2	9.28	13.87	6.70	0.82	0.94	1.53		0.24	0.24	66.39	100
3	14.29	17.14	2.86	5.71		5.71				54.29	100
4	25.00	25.00								50.00	100
5	28.57	28.57								42.86	100
–	9.88	24.86	7.04	2.95	2.61	6.02	0.11	1.02		45.52	100

TABLE 3.10 TERMINATION MODE STATISTICS BY SCANLINE USING MINERAL FILLED FRACTURES.

Scanline Mapping	Total** #	Termination Mode 0	1,2	%***
0000	74	2	58	96.7
0108	66	5	27	84.4
0112	68	1	44	97.8
0122	238	15	110	88.0
0401	49	3	18	85.7
0413	48	3	32	91.4
0418	32	4	18	81.8
0428	152	11	114	91.2
1037	38	0	26	100.0
1124	37	0	30	100.0
1134	44	0	35	100.0
1137	36	2	24	92.3
1222	32	0	21	100.0
1321	56	4	45	91.8
Total	970	50	602	92.3
Area Mapping				
Area1*	98	5	85	94.4

* Area1 = AREA MAPPED FRACTURES AT SCANLINE 1137
**Total = TOTAL MINERAL FILLED FRACTURES
*** % TERMINATION = TM1,2 / (TM1,2 + TM0)*100
NOTE: SOME FRACTURES WERE CENSORED AT BOTH ENDS, THUS A TERMINATION MODE WAS NOT MEASURED.

connected to other fractures. Permeability of fractured rock is enhanced by high connectivity of fractures (discussed further in Section 4.3).

3.3.6 Fracture Trace Length

In this section fracture trace lengths measured in the study area are analyzed to arrive at the distribution type and parameters (mean and standard deviation) describing the fracture trace lengths. Fracture size distributions will be derived in Section 4.3.3.2, using the fracture trace length distributions determined here. The relationship of fracture type and fracture mineral filling to fracture trace length is also examined with respect to the division of fractures into the dyke-parallel and dyke-normal sets (done in Section 3.3.3).

Fracture trace length distributions are dependent on the processes forming the fractures. A spatially uniform process would result in exponential trace length distributions, whereas multiple processes (such as breakage) may result in log-normal distributions of fracture trace lengths (Dershowitz and Einstein, 1988).

The mean orientations of the fracture data subsets (Section 3.3.3) are very similar for all the scanlines. To provide a summary of the trace length data, they were combined by set. The shape of the histograms in Figure 3.21 suggests both the log-normal and the exponential distribution may be fit to the fracture trace length data. This is also suggested in a literature review by Baecher and Lanney (1978) and a study by Rouleau (1984).

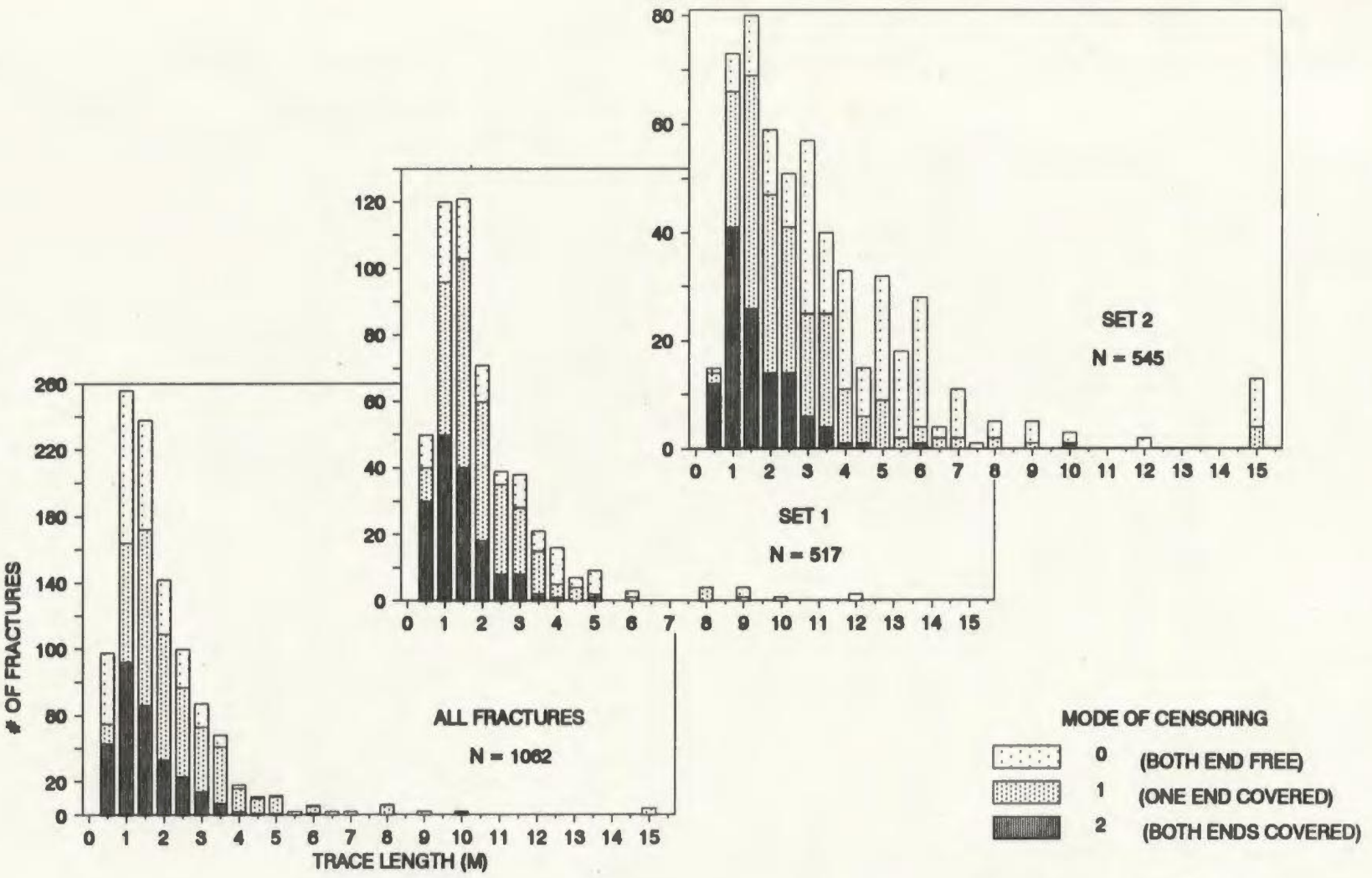

FIGURE 3.21 TRACE LENGTH HISTOGRAMS BY SET AND LEVEL OF CENSORING. SET 1 FRACTURES HAVE NON-DYKE PARALLEL ORIENATIONS; SET 2 FRACTURES ARE SUBPARALLEL TO DYKES. STATISTICS ARE SUMMARIZED IN TABLE 3.11.

Methods proposed by various authors to overcome trace length biases were summarized by Rouleau (1984). This study follows the data collection approach of Rouleau (1984) and also, in common with that author, uses Baecher's (1980) method of maximum likelihood to correct for trace length bias. This method uses a closed form expression to estimate the mean of a progressively censored sample assuming an exponential distribution of fracture trace lengths. Since there is no closed form expression available for the log-normal distribution (Baecher and Lanney, 1978), the mean and standard deviation of the $\log_e$ transformed trace length were estimated using a commercially available program which provides a fracture size analysis routine (FracMan produced by Golders Associates, Inc. (Dershowitz et al., 1991)). The mean and standard deviation of the original trace length distribution were then estimated following the method presented in Bury (1975, p.279).

The mean of an exponential distribution and the mean and standard deviation of a log-normal distribution, based on the trace length data, were computed (Table 3.11). The estimate for the mean of the exponential model, included correction for trace length truncation and censoring. Size bias was not corrected for because no simple method has been derived to estimate the parameters of the exponential and the log-normal models that also accounts for the censoring and truncation bias (Rouleau, 1984). This error may be important for the case of line-sampled data (Priest and Hudson, 1981; and Pahl, 1981) but its effects are reduced by the observation that in general the outcrops which were used in the scanline surveys had widths that were at least 2 times greater than the mean trace length.

On the basis of Chi-square and Kolmogorov-Smirnov goodness-of-fit tests, the FracMan program (Dershowitz et al., 1991) indicated that a log-normal distribution provides a better fit of the trace length data than does an exponential distribution. The

TABLE 3.11 FRACTURE TRACE LENGTH STATISTICS

	ALL DATA (N = 1062)			SET 1 (N = 517)			SET 2 (N = 545)		
CENSORING = =	0	1	2	0	1	2	0	1	2
N	284	448	330	163	238	116	121	210	214
NORMAL									
SUM (M)	376.71	1014.39	1300.2	196.6	446.64	294.02	180.11	567.75	1006.18
MAX (M)	10	15	15	4.8	9	12	10	15	15
MEAN (M)	1.326	2.264	3.940	1.206	1.877	2.535	1.489	2.704	4.702
STD.DEV. (M)	1.004	1.901	2.947	0.793	1.329	2.335	1.213	2.312	2.964
LOG-NORMAL*									
LN(μ)		0.261			0.139			0.375	
LN(STD.DEV.)		0.351			0.316			0.345	
μ (M)		1.381			1.208			1.544	
STD.DEV. (M)		0.500			0.391			0.549	
	BIAS CORRECTED PARAMETERS								
EXPONENTIAL**									
μ (M)		9.226			5.500			14.246	

* PARAMETERS FOR THE LOG-NORMAL DISTRIBUTION WERE COMPUTED USING FRACMAN (DERSHOWITZ ET AL, 1991)
THE ESTIMATED MEAN AND STANDARD DEVIATION WERE COMPUTED FROM THE FOLLOWING FORMULAE:

$$\mu = \text{EXP}(\text{LN}(\mu) + \text{LN}(\text{STD.DEV.})^2/2)$$

$$\text{STD.DEV} = \text{SQUARE ROOT } \{\text{EXP}(2\text{LN}(\mu) + \text{LN}(\text{STD.DEV.})^2)\{\text{EXP}(\text{LN}(\text{STD.DEV.}^2)-1]\}$$

** EXPONENTIAL MODEL MEANS WERE CALCULATED FROM: μ = SUM (CENS0 +CENS1 + CENS2)/NUMBER OF CENS0) - 0.25
(WHERE SUM IS THE TOTAL LENGTH OF FRACTURES FOR EACH LEVEL OF CENSORING, AND
0.25 IS THE TRACE LENGTH TRUNCATION).

results (Table 3.11) show that the mean trace lengths of Set 2 (dyke-parallel cluster) are longer (mean trace lengths (1.5 metres (log-normal model); 14.2 metres (exponential model)) than those of Set 1 (girdle distribution of orientations) (1.2 metres (log-normal model); 5.5 metres (exponential model)). Censoring of 75% to 95% of all fractures results in the estimation of a long mean trace length in the exponential model.

Fracture trace lengths are related to fracture plane size (see discussion in Section 4.3.3.2). Longer fracture trace lengths are indicative of greater fracture radii and thus possibly greater interconnectivity of fractures. The association of longer fracture trace lengths and greater fracture apertures (Section 3.3.2) with dyke parallel fractures also indicates an anisotropy in the permeability parallel to the dyke margins (Section 4.3). The result that the log-normal distribution provides a better fit to the trace length data is used in the determination of the fracture radii distributions in Section 4.3.3.1.

Trace lengths were measured at three different scales in the study area using the area mapping method. These included the 1137 scanline area (data presented in Appendix A.6), remotely sensed lineament and fault maps from the literature for the study area (Figure 2.11 and 2.12), and remotely sensed lineaments of the whole ophiolite (Figure 2.3A and B). The trace length distributions for the three different sampling scales have similar forms (Figure 3.22). This suggests that the trace length population may be self-similar as a result of the different scales of mapping. By extension, this similarity may continue down to the microscopic scale as well (Jaeger and Cook, 1969). The ophiolite, and therefore the study area, is fractured at all scales of measurement.

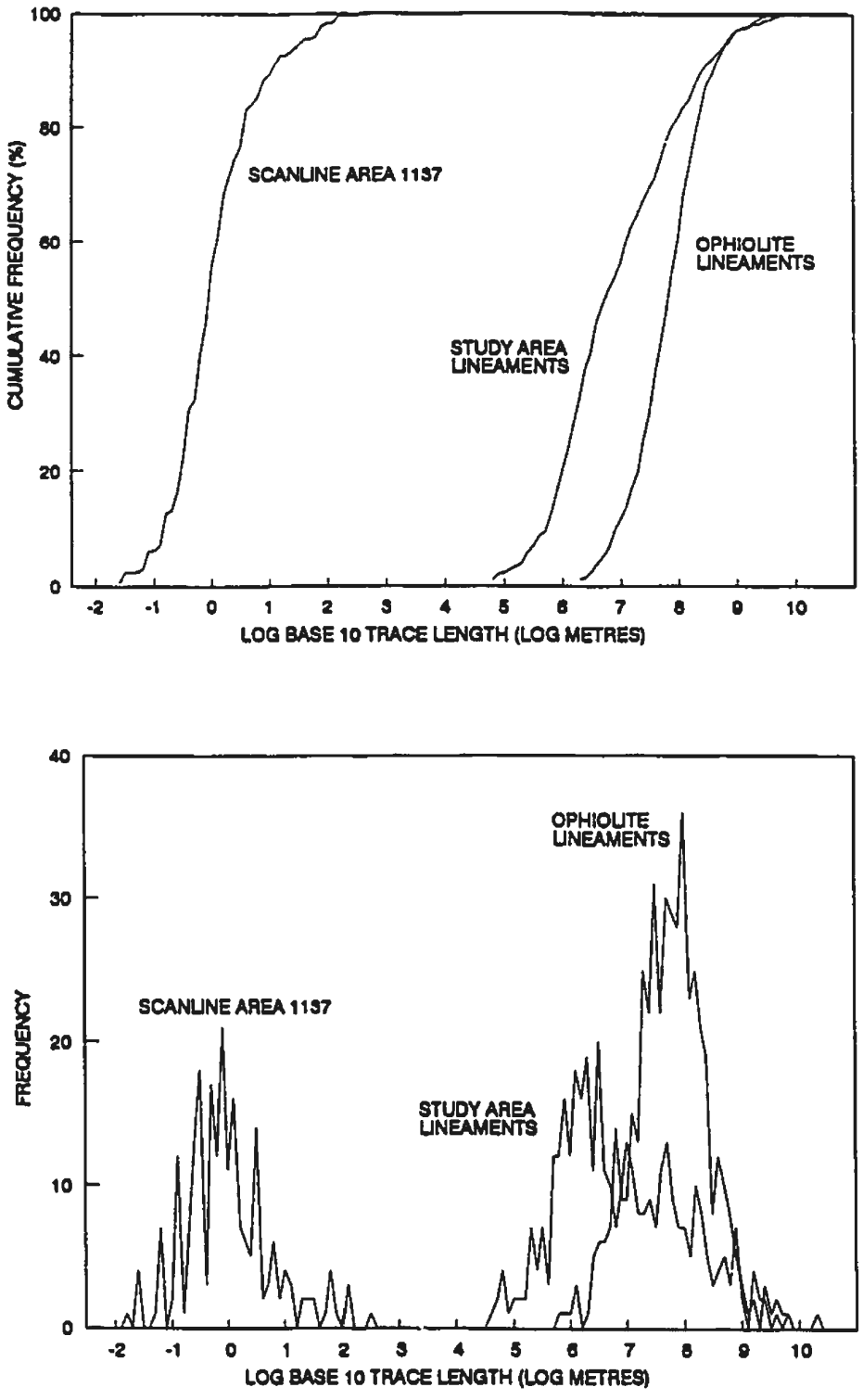

FIGURE 3.22 LINEAMENT AND FRACTURE TRACE LENGTH DISTRIBUTIONS.

The 20 to 50 metre scale of sub-seafloor packer-test permeability studies (i.e. Deep Sea Drilling Project Hole 504B; Becker, 1991) is on a similar scale to that of the outcrop fracture mapping done during the course of this study. The permeabilities to be determined in the study area will be compared with those from beneath the present-day seafloor (Section 4.3).

3.3.6.1 *Mineral Filling By Trace Length*

Since longer fractures are more likely to intersect other fractures, they are more likely to be conduits for hydrothermal circulation. Thus there may be a correlation between hydrothermal mineral filling and fracture trace length. For that reason, a comparison was made of fracture trace length and fracture mineral filling.

Plots of mineral filling versus fracture trace length by dyke domain are presented in Appendix A.3.3 for domains 2 through 6. The statistics are presented in Table 3.12. They demonstrate that, whereas there are differences between type of mineral filling and associated fracture trace length within individual domains, the differences are not consistent from domain to domain. The mean trace lengths of fractures filled with epidote and zeolite are longer than those filled with calcite (exception: domain 6). It should be noted that there is considerable overlap in the standard deviations of the trace lengths (Appendix A.3.3). In all of the domains, fractures without mineral filling have an average trace length of 1.61 metres. The mean trace lengths for unfilled fractures within each domain is less than the mean trace length for filled fractures. The longest fracture trace lengths are generally associated with the dyke margins (compare Appendix A.3.4 and A.3.5). Assuming that the dykes were originally vertical (Section 2.3.2), these fractures were likely open to hydrothermal

TABLE 3.12 AVERAGE MINERAL FILLING VERSUS TRACE LENGTH STATISTICS

FILLING MINERAL	DOMAIN 2		3		4		5		6	
	# OF FRACS.	MEAN LENGTH (metres)	# OF FRACS.	MEAN LENGTH (metres)	# OF FRACS.	MEAN LENGTH (metres)	# OF FRACS.	MEAN LENGTH (metres)	# OF FRACS.	MEAN LENGTH (metres)
EPIDOTE	179	2.15	62	2.75	434	2.31	113	1.94	33	1.63
ZEOLITE	25	2.98	6	2.94	446	1.86	51	1.04	7	2.09
CHLORITE	4	3.1	0		57	2.03	2	1.24	4	1.01
CALCITE	87	1.88	77	2.26	51	1.76	69	1.75	9	3.98
HEMATITE	7	1.99	0	-	76	2.65	20	1.59	0	-
MAGNETITE	0	-	5	2.38	0	-	0	-	0	-
PYRITE	8	3.38	7	2.29	55	2.5	0	-	7	1.52
CLAY	6	2.76	0	-	9	2.22	2	4.14	2	2.18
NONE	235	1.62	189	1.44	522	1.58	484	1.66	223	1.72

TRACE LENGTH VALUES CALCULATED IN LOG TRANSFORMED FORM AND PRESENTED IN ARITHMETIC VALUES IN METRES.

circulation at the time of active spreading or extension perpendicular to the ridge axis. Thus mineral fillings deposited by hydrothermal fluids are more likely to be associated with sub-vertical fractures which have the longest trace lengths in the study area.

3.3.7 Fracture Frequency

Fracture frequency, regardless of fracture orientation, along all scanlines, varies from 1.11 to 4.78 fractures per metre (Figure 3.11). In all but two of the fourteen scanlines with more than 30 mineral filled fractures, the filled-fracture frequency is much greater than the unfilled-fracture frequency (Table 3.13). There is no strong consistent variation in an east-west direction (Figure 3.11), although there is a slight increase in fracture frequency in a north-south direction (Figures 3.11 and 3.12). The fracture frequency appears to be somewhat higher in the southwest. The frequency of dyke contacts (the number of dyke margins per metre of scanline survey) increases further to the south in the field area. In the eastern half of the graben structure, the dyke margin frequency is higher then in the western half. However, in the south-west the dyke margin frequency is higher deeper in the section (Figure 3.23), this is not the case in the eastern portion of the field area. Fracture frequency is further discussed in Section 4.3.3.1 with regard to the determination of fracture intensity in order to calculate permeability. Fracture frequency along the measured length of scanline, presented in Appendix A.3.8, indicates fairly consistent frequencies. These plots were produced using a moving average 5 metre wide window in 1 metre increments along the length of the scanline. Some of the areas show cyclical frequencies (e.g. scanline 0000, 0112, 0428, and 1316); the lows coincide with the dyke margins whereas higher frequencies coincide with the interiors of dykes.

TABLE 3.13 FRACTURE FREQUENCY BY SCANLINE

Scanline	Length (m)	Total #	Total Frequency	Unfilled #	Unfilled Frequency	Filled* #	Filled* Frequency
0000	37.4	76	2	2	0.1	74	2
0108	31.5	88	2.8	22	0.7	66	2.1
0112	25.1	90	3.6	22	0.9	68	2.7
0122	148.2	290	2	52	0.4	238	1.6
0401	31.3	68	2.2	19	0.6	49	1.6
0413	30.6	59	1.9	11	0.4	48	1.6
0418	21.6	33	1.5	1	0	32	1.5
0428	67.6	195	2.9	43	0.6	152	2.2
1037	30.9	96	3.1	57	1.8	38	1.2
1124	25.6	96	3.7	54	2.1	37	1.4
1134	32	68	2.1	11	0.3	44	1.4
1137	31.7	75	2.4	38	1.2	36	1.1
1222	31.1	94	3	62	2	32	1
1321	30.2	109	3.6	50	1.7	57	1.9

*NOTE: THE FILLED COLUMNS INCLUDE FILLED FRACTURES BUT EXCLUDE THOSE ONLY FILLED WITH CALCITE. FREQUENCY = # / LENGTH

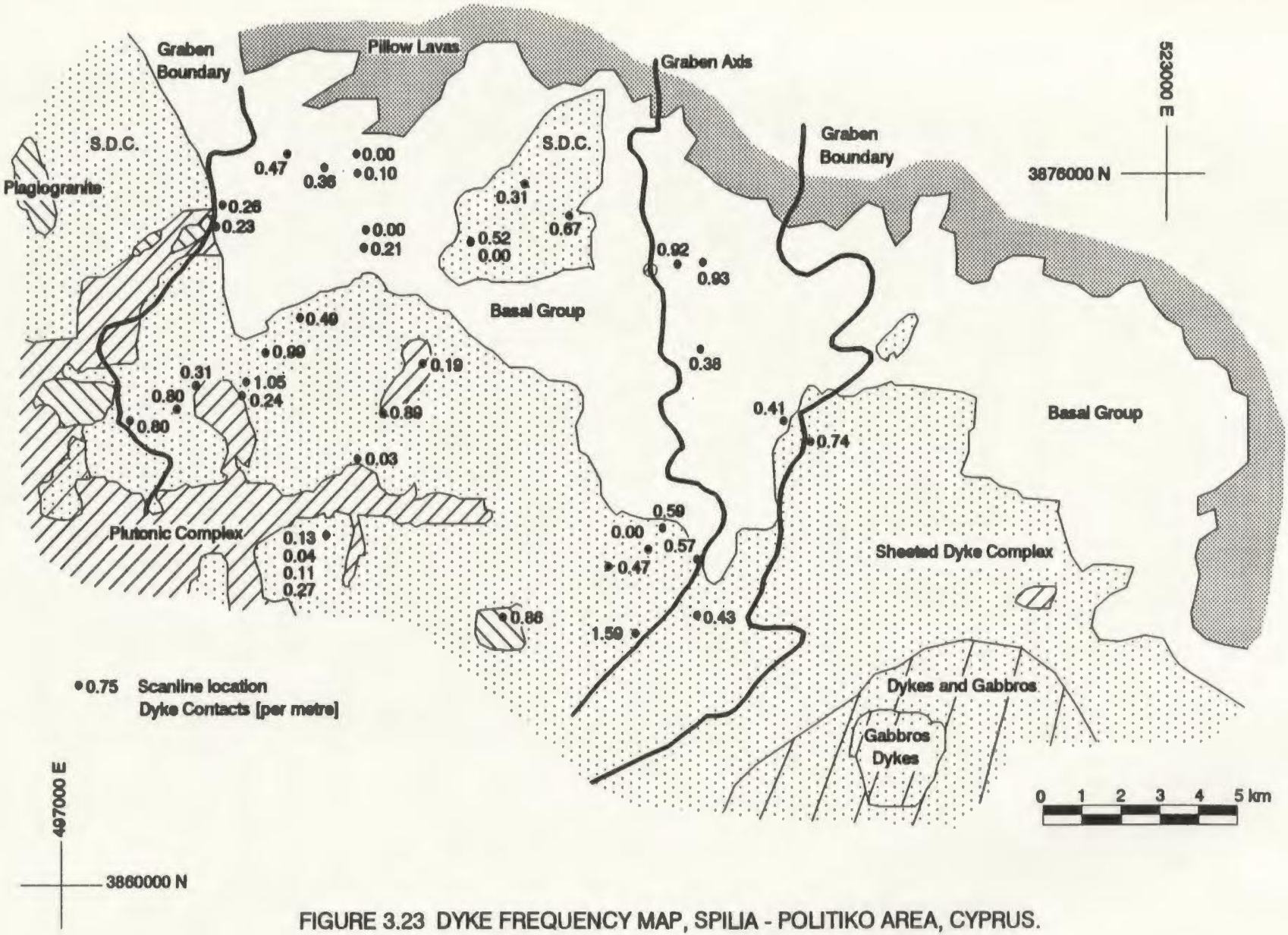

FIGURE 3.23 DYKE FREQUENCY MAP, SPILIA - POLITIKO AREA, CYPRUS.

3.4 SUMMARY

Many characteristics of the fractures in the study area have been discussed in this chapter. The fracture characteristics measured in the field area are summarized as follows:

(1) Aperture: fracture apertures appear to follow a log-normal distribution. Euhedral minerals in fractures indicate fractures were open beneath the seafloor, during hydrothermal fluid circulation. Vertical and sub-vertical fractures tend to have opened to a greater extent than non-vertical fractures, in agreement with stress conditions in an extensional spreading-ridge environment.

(2) Fracture orientation: in the sheeted dykes, fracture orientations tend to fall in cluster/girdle relations interpreted to reflect their formation as cooling fractures along dyke margins (cluster) and in the interior of dykes (girdle). Rotation of fracture orientations are consistent with those of the dyke orientations (Section 2.3.2) from domain to domain suggesting the majority of fractures in the area predate graben formation. There is a tendency for fractures in a cluster distribution to be longer, dyke-parallel, and to be filled with epidote, whereas fractures in girdle distributions tend to have shorter trace lengths, have H-junction termination modes, and be filled with calcite.

(3) Mineral filling:49% of measured fractures contained a mineral filling. The frequency of mineral filling increases with depth in the ophiolite. Domain 6 fractures are 83% unfilled, unfilled fractures in the other domains account for 18 to 76% of the total. Epidote occurs throughout the field area at all levels but is more concentrated in domains 2 and 4 (30% of filled fractures) than in domains 3, 5 and 6 (15% of filled fractures). Calcite is more concentrated in areas of shear zones and plagiogranites. Calcite deposition always post-dated

epidote and zeolite deposition. Epidote and zeolites in fractures show no consistent cross-cutting relations, indicating either variable hydrothermal conditions or contemporaneous deposition over wide areas. Hydrothermal epidote in dyke-parallel fractures implies that these fractures were open during hydrothermal circulation and crustal accretion whereas calcite in fractures perpendicular to the dyke margins implies these fractures were open during uplift of the ophiolite.

(4) Termination mode: Fractures with mineral filling tend to coincide with fractures of termination mode 0 (both ends free), whereas unfilled fractures tend to have T- and H-junction termination modes. Fractures with H-junction termination modes were more randomly oriented than those with both ends free or one end abutting against another fracture (T).

(5) Trace length: The calculated mean trace lengths by orientation set is 1.2 metres (log-normal distribution) or 5.5 metres (exponential distribution) (set #1) and 1.5 metres (log-normal distribution) or 14.2 metres (set #2); with a mean of 1.4 metres (log-normal distribution) or 9.2 metres (exponential distribution) for the entire data set. The trace length distributions at different scales of measurement (scanline, study area, ophiolite) show similarities in their distribution and all appear to be best modelled by a log-normal type of distribution.

(6) Fracture type versus trace length: dyke margin fractures tend to have longer trace lengths. Fractures with trace lengths less than 2 metres tend to be more randomly oriented.

(7) Mineral filling versus trace length (by domain): the mean fracture trace lengths of the various mineral fillings are different, yet there is significant overlap in the standard deviations of each population within, as well as between, domains. Unfilled fractures in all domains have a mean trace length of 1.6 metres.

4. APPLICATION OF FRACTURE CHARACTERISTICS TO ROCK PROPERTIES

4.1 INTRODUCTION

Fluids circulating in a rock mass may utilize different fractures or sets of fractures at different times. This implies that the permeability of the rock changes through time. Permeability is an intrinsic property of fractured rock, dependent on the amount of interconnected space in a rock, be it primary porosity or secondary fracture porosity. The permeability, in part, controls the direction and magnitude of fluid flow through a rock mass. Fracture properties, as described and characterized in the previous chapter, are applied here to estimate the relative age of fracturing and stress conditions, and to determine bulk rock permeability.

The bulk permeability of fractured rock is a measure of the ability of fluids to circulate through the rock. Bulk rock permeability has been determined in past studies of the oceanic crust in several Deep Sea Drilling Project boreholes (e.g. 504B, Anderson and Zoback, 1982). Only Nehlig and Juteau (1988) have previously attempted to determine the permeability of ancient oceanic lithosphere. They calculated permeability for the Semail ophiolite, Oman, and the values they determined were much greater than those determined from DSDP boreholes. In the present study, three methods of determining permeability are applied to the data from the Spilia-Politiko field area.

The permeability calculations required a number of computer programs to be written, including PARAPLAT and SNOWPERM (Section 4.3). Additional programs were written to simulate fracture trace lengths from a given distribution of fracture radii

(ELLIPSE) (Section 4.3.3.2). The flow chart in Figure 4.1 shows the relative use of each of the programs. The program codes are listed in Appendix D, and are accompanied by a short description of the programs, their input requirements and their output results.

4.2 RELATIVE AGES OF FRACTURES

The age of fractures is important to calculating the permeability, because the fracture data collected in the field reflect an integrated history of hydrothermal fluid circulation. It was not possible, from the field data, to establish clear cross-cutting relations for the age of formation in more than 2% of the fracture intersections. This precluded the possibility of establishing the fracture age relationships in a quantitative manner. Since most fractures are thought to have formed by contraction as a result of cooling, they most likely formed at roughly the same time. This study is more concerned with the utilization history of the fractures.

Observation of relative ages based on mineral filling and sequences of mineral filling within fractures resulted in determination of a simple fracture utilization history. Fractures containing epidote were likely infilled at an earlier time than those containing calcite (refer to Section 3.4.4). Multiple utilization of individual fractures also bore out the same relationship, with epidote pre-dating calcite. The relationship between epidote and zeolite filled fractures is ambiguous; they may be contemporaneous. In many cases it was not possible to determine the age relations (of either formation or utilization) between neighbouring fractures.

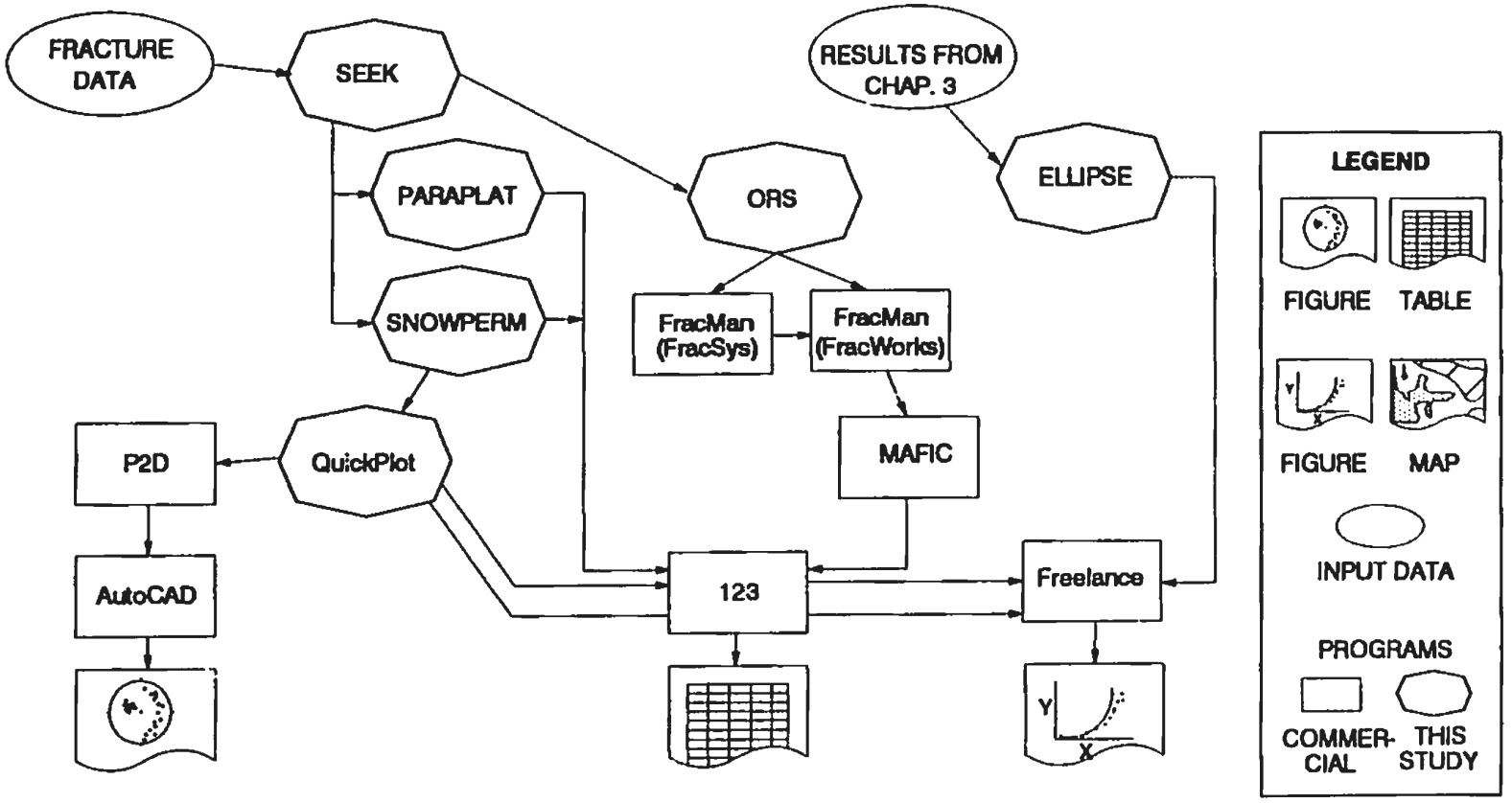

FIGURE 4.1 FLOWCHART OF DATA AND PROGRAMS USED IN CHAPTER 5. COMMERCIAL PROGRAMS AS IN FIGURE 2.2 AND 3.1. MAFIC = FRACTURE FLOW MODELLING PROGRAM.

In conclusion, it was, in general, not possible to determine the relative ages of formation of fractures. Since a majority of the fractures appear to be related to the cooling of the dykes, it is assumed these fractures formed quite early, soon after the dyke cooled enough to allow brittle deformation to take place. The relative ages of fracture filling by circulating fluids indicates that both epidote and zeolites precede calcite deposition in fractures.

4.3 PALEO-PERMEABILITY

In this section, permeability is calculated from the measured fracture properties of the rock in the Spilia-Politiko area. The permeability that is determined in the following sections is a paleo-permeability because only fractures containing a mineral filling, evidence of past fluid circulation, are used in the calculations. The purpose of this section is to determine whether the sheeted dykes of Layer 2B oceanic crust and those of the Troodos ophiolite have similar hydrogeological properties. The hydrogeological properties from the Spilia-Politko area are then used to extrapolate to sub-seafloor hydrogeological conditions discussed in Section 6.3.

Intrinsic permeability, k, is based solely on the rock properties. Hydraulic conductivity, K, however, incorporates properties of both the rock and the fluid,

$$K = \frac{k\rho g}{\mu} \quad \ldots\ldots\ldots\ldots\ldots\ldots \quad (4.1)$$

where ρ is the fluid density, g is the acceleration due to gravity, and μ is the dynamic viscosity of the fluid (Freeze and Cherry, 1979). Permeability may be determined from field measurements during well tests (e.g. pumping tests or slug tests; Kruseman and de Ridder, 1983), or from calculations based on orientations and apertures of

actual fractures (e.g. Snow, 1965) or on simulated fracture networks (e.g. Dershowitz et al., 1991). In the Spilia-Politiko field area, hydrothermal sub-seafloor circulation is thought to have occurred in the late Cretaceous (Staudigel et al., 1986). Present fluid circulation conditions may not bear any relation to the circulation of the past, nor to the conditions of interest for this study. Field measurements during well tests are therefore not a suitable means of determining paleo-permeability, instead, calculations based on fracture characteristics, will be used to estimate paleo-permeability.

Bulk rock permeability includes two components; the fracture permeability and the matrix permeability. The permeability of unfractured igneous rock is of the order of 10^{-21} to $10^{-24}m^2$, whereas the permeability of fractured igneous rock can be up to 10 or 12 orders of magnitude greater (Section 1.1; Freeze and Cherry, 1979). Permeabilities measured as part of the Deep Sea Drilling Project at various boreholes range from 10^{-12} to $10^{-17}m^2$ for Layer 2B (e.g. Anderson and Zoback, 1982). The difference between fracture and matrix permeability is great enough that the matrix permeability can be considered negligible, and the bulk of the fluid flow will thus be through the fractures. The fractured nature of the rocks of the Sheeted Dyke Complex (and of the extrusive and plutonic rocks) in the study area dictates that their permeability is controlled by the fractures.

It was assumed for this and subsequent permeability calculations of the study area, that the fracture apertures are uniform across the fracture plane. This assumption is, strictly speaking, not valid, since fracture apertures vary across the fracture plane (Gale, 1987). It was not possible to collect field data on apertures that would reflect these variations.

It is simpler to treat a fractured rock mass as an equivalent porous medium if the size of the area of interest is much larger than the dimensions of the largest fractures. This is the assumption used in previous numerical studies (e.g. Fehn et al., 1983). These earlier studies did not have access to a fracture database, such as presented in Chapter 3, for the oceanic crust. The determination of the size of such a representative elemental volume also depends on the fracture interconnectivity. The finite size of fractures strongly affects fracture network interconnectivity and, as a result, the permeability. Permeabilities are calculated for rocks, beneath the seafloor in present day systems (e.g. Anderson and Zoback, 1982), on the basis of packer tests, which measure flow rates through sealed-off intervals, whose borehole lengths are of the order of 30 metres. At this scale the permeability is fracture controlled and cannot be accurately approximated by a porous medium equivalent. Fractures were measured at a similar scale in the field area. Therefore permeabilities calculated for the individual fractured rock blocks, in this study, will be based on a fractured medium permeability.

The permeability of hand samples of diabase, while not tested, appears low on the basis of the few micro-fractures seen in thin sections in areas away from macro-scale fractures. A difficulty here is that testing of hand samples results in the determination of a present-permeability not a paleo-permeability.

Various methods have been presented in the literature describing the calculation of fractured rock permeability (e.g. Snow, 1965, 1969). This study applies three different methods to the Spilia-Politiko area. (1) The simplest method is a parallel-plate model (Norton and Knapp, 1977) in which the permeability is based on a single set of parallel fractures. (2) Snow (1965, 1969) presented a model in which permeability could be calculated from the apertures and orientation of various sets of

parallel fractures. A model by Bianchi and Snow (1969) is an extension of Snow's (1965, 1969) model, that accounts for all fractures regardless of set affinity. Both methods 1 and 2, are deterministic in that they use the properties (aperture and orientation) of the measured fractures in the calculations. (3) Dershowitz et al. (1991) developed a model in which the calculation of permeability is based on the stochastic generation of fracture sets using fracture distribution parameters such as fracture size, shape, and orientation. In such a model the location, orientation, and apertures of fractures are statistically equivalent to the observed fractures.

Each of these three methods will be used to calculate the permeability of the fractured rock mass within the Sheeted Dyke Complex. The resultant paleo-permeabilities from these methods are compared with each other and, in Chapter 6, with permeability determinations from Deep Sea Drilling Project and Ocean Drilling Program bore hole tests and from the Semail ophiolite.

4.3.1 Parallel-Plate Method

The longest fracture traces and those with the largest apertures are oriented sub-parallel to the dyke margins (Chapter 3). The dykes in the study area are now tilted to varying degrees as a result of rotation during the formation of the Mitsero graben (Chapter 2). Hydrothermal fluid circulation is thought to pre-date the formation of this graben structure (Chapter 2 and 5). If the dykes were originally vertical then the dyke margin fractures were originally vertical, and there will be a tendency toward vertical fluid migration. A parallel-plate model for fluid flow, can therefore be used to calculate permeability in the dykes. This method, however, assumes that cross-flow

(flow in directions other than dyke-parallel), is negligible, and that fractures are continuous within the region of interest.

From the discussion in Chapter 3 it is apparent that not all fractures are parallel to the dykes; that is, there is more than one set of fractures. Fractures are not continuous throughout the measurement region, as evidenced by the trace length distributions determined in Chapter 3. The assumption of continuous fractures results in an overestimation of the permeability magnitude, while ignoring the effects of other fractures may underestimate the permeability. This method is not appropriate for the Spilia-Politko area, especially where there is more systematic fracture data available to do a more detailed permeability calculation. Nevertheless, since this method was used by Nehlig and Juteau (1988) to calculate paleo-permeability for the Semail ophiolite, Oman, it will also be applied to the Spilia-Politiko area data. This enables direct comparison of results from the two ophiolites.

The parallel plate model of Norton and Knapp (1977) uses D'Arcy's law (D'Arcy, 1856) for flow through porous media (Figure 4.4A). Appendix A.7 gives a detailed description of this method of permeability calculation. A listing of the program PARAPLAT, used to apply the parallel plate model is given in Appendix D.

The results of applying this method to the data of the Spilia-Politiko study area, using those mineral filled fractures whose orientation falls within 20° of the mean dyke orientations for each domain, is summarized by domain in Table 4.1 (full results are in Appendix A.7.1). The set of dyke-parallel fractures was too small to use. Therefore, a somewhat greater dispersion (20°) about the mean dyke orientation was used to form the set of 'dyke-parallel' fractures. For fractures containing a mineral filling (excluding those containing only calcite) an overall parallel-plate mean

TABLE 4.1 AVERAGE PERMEABILITY MAGNITUDES BY DOMAIN AN FRACTURE MINERAL FILLING - PARALLEL PLATE METHOD

Domain	All Minerals Permeability (m^2)	No Minerals Permeability (m^2)	Epidote Permeability (m^2)	Zeolite Permeability (m^2)	Calcite Permeability (m^2)
2	1.917E-09	2.399E-10	6.124E-10	1.520E-09	1.746E-09
3	4.720E-10	8.524E-11	3.310E-09	3.874E-12	2.378E-10
4	1.214E-08	4.394E-12	1.491E-08	7.064E-10	7.924E-12
5	9.352E-09	3.264E-09	4.105E-08	8.353E-09	9.277E-09
6	3.865E-09	9.362E-10	2.963E-08	2.294E-08	7.010E-09

Permeability in units of m^2.
Values are the mean of the log-transformed permeability from permeability calculations presented in Appendix A.7.1.
All values are in exponential notation, for example 8.8E-07 is 0.00000088.

PAGINATION ERROR.

TEXT COMPLETE.

ERREUR DE PAGINATION.

LE TEXTE EST COMPLET.

NATIONAL LIBRARY OF CANADA.

CANADIAN THESES SERVICE.

BIBLIOTHEQUE NATIONALE DU CANADA.

SERVICE DES THESES CANADIENNES.

permeability of $3.3x10^{-9}m^2$ was calculated. On a per-mineral basis the mean calculated permeability varies from $8.2x10^{-9}m^2$ to $9.5x10^{-10}m^2$ for epidote and zeolite filled fractures respectively. The calculated permeability was consistently lower in domains 3 and 4 than in the other domains. The calculated permeability values for the different mineral-filled fractures can be equated to a time integrated permeability covering different stages during the hydrothermal process.

The permeability calculated for epidote-filled fractures is of roughly the same order of magnitude as that for all fractures from throughout the study area. The permeability calculated for the zeolite- filled fractures was slightly higher in the south west of the study area (Alona road section), than elsewhere. This area is characterized by gabbros containing more zeolite-filled fractures.

A small decrease in the parallel-plate (vertical) permeability is noted with increased depth in the sheeted dyke section (10^{-9} to 10^{-10}). This decrease is closely tied to the decrease in the fracture apertures with depth (Section 3.3.2).

4.3.2 Bianchi and Snow Method

Most rock contains fractures of varying orientations. These may be subdivided into multiple sets of sub-parallel fractures. A model presented by Snow (1965, 1969) allows the incorporation of multiple sets of parallel fractures, by calculating the permeability from the sum of the permeabilities of separate sets. Bianchi and Snow (1969) extended this approach to include all fractures regardless of their orientation. This latter approach is followed here.

The Bianchi and Snow (1969) method was applied to the Spilia-Politiko area fracture data for the following six sub-sets: (1) all fractures; (2) unfilled fractures; (3) filled fractures; (4) epidote-filled fractures; (5) zeolite-filled fractures; and (6) calcite-filled fractures. In addition, the method was also applied to these six sub-sets for all fractures within 20° of the mean dyke orientation of the station, for a total of twelve subsets. This latter subdivision was done for comparison with the results from the parallel-plate method (in the previous section 4.3.1). The fracture orientation data used in these calculations, were rotated, as outlined in Section 2.3.3, to remove the effects of graben formation and ophiolite tilt. A listing of the program, SNOWPERM, used to apply the Bianchi and Snow (1969) model, is given in Appendix D.

Permeability is represented mathematically as a tensor, of nine terms. The tensor can be diagonalized to its three principal components which coincide with the magnitudes of the maximum, intermediate and minimum flow. These are the eigen values of the tensor and are, by convention, referred to as the maximum permeability (k_1); intermediate permeability (k_2); and minimum permeability (k_3). The eigen vectors associated with the eigen values give the orientations of the principal permeabilities.

Average permeability magnitudes, calculated by this method range from 3.1×10^{-12} to $1.2 \times 10^{-6} m^2$ for the Spilia-Politiko area (Table 4.2A). The orientations of the principal permeability directions for the six sets of fractures (using all fractures, as noted above) show a very consistent k_3 orientation of roughly 256°/13°. The maximum and intermediate principal permeabilities, k_1 and k_2, on the other hand, show considerable variation for the various subsets (Table 4.2B). The six sets of fractures within 20° of the mean dyke orientations have a consistent k_3, oriented parallel to the poles of the mean dyke orientation for each of the areas, constrained by the choice of fracture set (i.e. dyke-parallel fractures). The calculated permeability

TABLE 4.2A AVERAGE PERMEABILITY MAGNITUDES – BIANCHI AND SNOW (1969) METHOD

Complete Data Set	Mean	Maximum	Minimum	Fractures Within 20° of Mean Dyke Orientations	Mean	Maximum	Minimum
All fractures	1.2E−06	1.7E−02	1.6E−09	All fractures	1.0E−09	1.3E−04	2.2E−18
Unfilled fractures	2.9E−09	1.3E−04	4.2E−18	Unfilled fractures	3.1E−12	1.3E−04	5.7E−18
Filled fractures	1.6E−07	1.7E−02	1.6E−12	Filled fractures	1.2E−09	1.5E−05	2.2E−18
Epidote filled fractures	1.6E−07	1.7E−02	1.0E−12	Epidote filled fractures	9.2E−10	1.5E−05	2.2E−18
Zeolite filled fractures	4.9E−09	1.7E−02	2.2E−18	Zeolite filled fractures	1.1E−09	1.7E−06	1.1E−11
Calcite filled fractures	5.2E−10	7.0E−05	6.1E−18	Calcite filled fractures	3.7E−11	1.8E−07	9.6E−13

Average permeability = (k1 + k2 + k3)/3

Values are average in each case of all scanline loactions.
Permeability values in m^2

TABLE 4.2B AVERAGE PERMEABILITY ORIENTATIONS – BIANCHI AND SNOW (1969) METHOD

Complete Data Set	k1	k2	k3	Fractures Within 20° of Mean Dyke Orientations	k1	k2	k3
All fractures	121/79	347/06	260/14	All fractures	120/74	021/46	277/15
Unfilled fractures	106/80	340/08	247/07	Unfilled fractures	049/71	152/69	278/14
Filled fractures	091/79	185/00	267/13	Filled fractures	111/71	041/66	277/19
Epidote filled fractures	129/71	355/04	267/19	Epidote filled fractures	099/73	088/70	278/20
Zeolite filled fractures	053/72	150/43	241/14	Zeolite filled fractures	104/64	106/68	277/25
Calcite filled fractures	353/67	116/51	251/11	Calcite filled fractures	122/75	007/54	268/16

k1, k2 are in girdle distributions

Average k1, k2, k3 were computed from the k1, k2, and k3 values for each scanline.
All values are in exponential notation, for example 8.8E−07 is 0.00000088

magnitudes and directions for all twelve subsets of the data for each scanline are summarized in Table 4.2 and are given in full in Appendix A.7.

Permeability anisotropy (defined in Figure 4.2), which is the ratio of k_1 to k_2 to k_3, indicates that in 82% of cases $k_1 \approx k_2 > k_3$ and in 18% of the cases $k_1 > k_2 > k_3$. These results are tabulated in Appendix A.7 and are only summarized here. The values were transformed to $\log_{10}$, since the results spanned 16 orders of magnitude. The lowest value of the ratios of $\log_{10}(k_1)$ to $\log_{10}(k_3)$ was 0.27 whereas that for $\log_{10}(k_2)$ to $\log_{10}(k_3)$ was 0.10; the highest values of the ratios of $\log_{10}(k_1)$ to $\log_{10}(k_3)$ and of $\log_{10}(k_2)$ to $\log_{10}(k_3)$ were both 7.68. These data indicate that the permeability tensor is anisotropic with $k_1 \approx k_2 > k_3$. This is caused by the existing anisotropy of dyke-parallel fractures in the dyke fabric.

The main conclusion to be drawn from these observations and calculations is that fluid circulation was most likely mediated by dyke-parallel fractures, and thus occurred largely in the vertical plane. This is demonstrated by the fact that the minimum principal permeability k_3 tends to be parallel to the pole to dyke planes, and thus, the maximum and intermediate principal permeability directions lie in the plane of the mean dyke orientations. The maximum and intermediate permeability magnitudes tend to be very similar and significantly larger than the minimum principal permeability magnitude.

The permeability orientation results by domain in the Spilia-Politiko area, plotted on stereographic projections, reveal that the maximum and intermediate principal orientation directions closely follow the mean dyke orientations for each domain (compare Figure 2.9 and principal permeability orientations by domain figures in Appendix A.7.2). This consistency holds for all six sets (all, filled, unfilled,

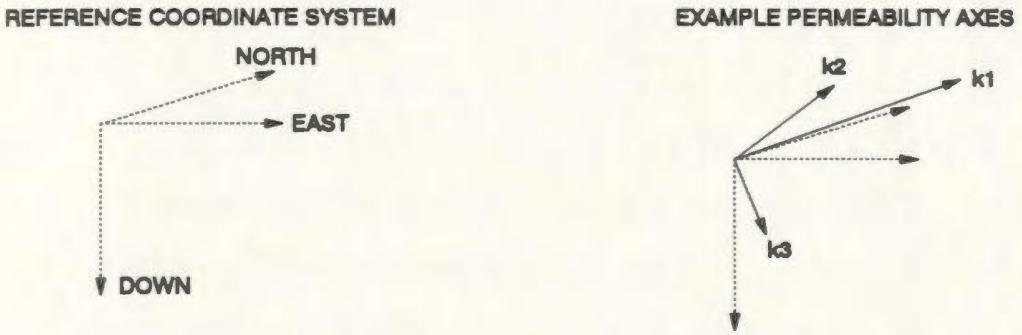

PERMEABILITY ELLIPSOID

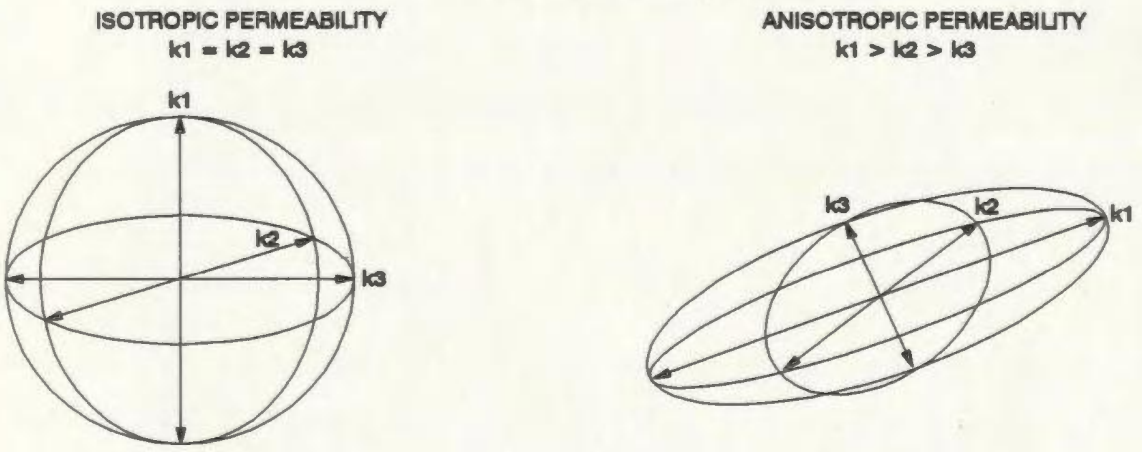

ANISOTROPY NOTATION

k1 / k3 : k2 / k3 : 1 (k3 / k3)

IF PERMEABILITY RANGE IS LARGE USE THE FOLLOWING FOR ANISOTROPY:

log(k1) / log(k3) : log(k2) / log(k3) : 1 (log(k3) / log(k3))

FIGURE 4.2 PERMEABILITY ANISOTROPY DEFINITION. k1, k2, AND k3 ARE THE PRINCIPAL PERMEABILITY AXES. BY CONVENTION k1 = MAXIMUM, k2 = INTERMEDIATE, k3 = MINIMUM.

epidote-filled, zeolite-filled, and calcite-filled fractures (Note: filled fractures are a subset of the 'all' fracture set)), although the principal permeability directions for the calcite are somewhat more variable from domain to domain.

The averaged principal permeability magnitudes by area throughout the study area are listed, by domain, in Table 4.3. The permeabilities are the arithmetic means of log transformed permeabilities for each scanline; the raw data can be found in Appendix A.7. The permeability magnitudes of the all- and filled-fracture sets for each domain are very consistent. The calculated permeabilities for epidote-filled fractures are higher in domains 3 and 4 and lowest in domains 2 and 5. The permeability for calcite-filled fractures is lowest in domains 4 and 5 and higher in domains 2, 3, and 6. It should be stressed at this point that intrinsic permeability tends to vary by the decade (Bear, 1979; Clauser, 1992), and thus the powers of ten are important rather than the units.

To determine the possible effects of faults on the magnitude and direction of permeability and direction for a particular location, the fracture data for scanline location 1129 (a typical example) were modified to include a hypothetical fault with a progressively larger aperture (Table 4.4). The initial data set of 53 fractures gave permeability magnitudes of 2.9×10^{-8}, 2.2×10^{-8} and $8.0 \times 10^{-9} m^2$ for k_1, k_2, and k_3, respectively. The associated permeability directions were 154°/67°, 047°/07°, and 314°/22°. The apertures ranged in size from 0.01 to 20 mm (mean = 2.5 mm). As Table 4.4 demonstrates, replacing the 20 mm aperture with first a 100 mm aperture and then incrementing this stepwise by 100 mm, results in the fault permeability becoming larger than that of the original fractures when the aperture of the fault increases to 400 mm, a difference of 2.2 orders of magnitude with the original mean aperture size. It should be noted that the apertures used in the calculations are

TABLE 4.3 AVERAGE PERMEABILITY MAGNITUDES BY DOMAIN AND FRACTURE MINERAL FILLING - BIANCHI AND SNOW (1969) METHOD)

COMPLETE FRACTURE DATA SET

ALL FRACTURES

Domain	kave	k1	k2	k3
2	1.9E-07	4.1E-07	3.7E-07	4.1E-08
3	7.8E-07	5.7E-06	5.6E-06	1.5E-08
4	1.0E-06	3.6E-06	3.3E-06	8.6E-08
5	2.9E-07	1.5E-06	1.4E-06	1.2E-08
6	2.5E-08	9.6E-08	9.4E-08	1.7E-09

UNFILLED FRACTURES

Domain	kave	k1	k2	k3
2	5.0E-09	1.3E-08	1.1E-08	8.9E-10
3	3.5E-08	3.1E-07	3.1E-07	4.3E-10
4	2.6E-10	1.2E-09	1.1E-09	1.5E-11
5	2.2E-08	1.5E-07	1.4E-07	5.6E-10
6	7.8E-10	1.4E-09	1.1E-09	3.2E-10

FILLED FRACTURES

Domain	kave	k1	k2	k3
2	8.5E-08	3.6E-07	3.3E-07	5.3E-09
3	2.3E-08	6.0E-08	4.6E-08	4.3E-09
4	3.5E-07	1.6E-06	1.5E-06	1.7E-08
5	1.3E-08	4.6E-08	4.2E-08	1.1E-09
6	1.2E-09	9.1E-09	9.0E-09	2.4E-11

EPIDOTE-FILLED FRACTURES

Domain	kave	k1	k2	k3
2	8.6E-09	1.5E-08	1.4E-08	1.3E-09
3	2.4E-07	1.4E-06	1.4E-06	6.6E-09
4	9.8E-07	3.7E-06	3.5E-06	7.3E-08
5	6.5E-09	2.9E-08	2.7E-08	3.4E-10
6	9.7E-08	4.3E-07	4.3E-07	4.9E-09

ZEOLITE-FILLED FRACTURES

Domain	kave	k1	k2	k3
2	4.3E-09	1.4E-08	1.3E-08	4.5E-10
3	1.7E-11	3.7E-11	3.3E-11	4.3E-12
4	2.0E-07	6.9E-07	6.6E-07	1.8E-08
5	5.3E-10	6.6E-09	6.1E-09	3.7E-12
6	1.8E-09	4.1E-08	4.1E-08	3.7E-12

CALCITE-FILLED FRACTURES

Domain	kave	k1	k2	k3
2	1.7E-08	9.9E-08	9.5E-08	5.3E-10
3	9.0E-09	3.6E-08	3.1E-08	6.6E-10
4	1.4E-11	5.1E-11	5.0E-11	1.1E-12
5	6.0E-10	3.2E-09	3.2E-09	2.1E-11
6	9.3E-08	4.3E-07	4.3E-07	4.4E-09

FRACTURES WITHIN 20° OF MEAN ORIENTATION

ALL FRACTURES

Domain	kave	k1	k2	k3
2	3.0E-09	3.4E-08	3.3E-08	2.3E-11
3	4.8E-11	1.6E-10	1.5E-10	4.7E-12
4	3.5E-09	3.4E-08	3.4E-08	3.7E-11
5	3.0E-10	8.7E-09	8.6E-09	3.8E-13
6	8.2E-13	3.3E-12	3.2E-12	5.1E-14

UNFILLED FRACTURES

Domain	kave	k1	k2	k3
2	5.9E-14	3.1E-13	3.1E-13	2.1E-15
3	4.1E-12	1.4E-11	1.4E-11	3.5E-13
4	3.0E-13	2.9E-12	2.8E-12	3.3E-15
5	1.9E-10	1.3E-08	1.3E-08	3.9E-14
6	8.2E-13	3.3E-12	3.2E-12	5.1E-14

FILLED FRACTURES

Domain	kave	k1	k2	k3
2	2.6E-09	3.4E-08	3.3E-08	1.5E-11
3	4.3E-09	1.3E-08	1.2E-08	5.3E-10
4	1.8E-08	1.3E-07	1.3E-07	3.9E-10
5	4.8E-11	2.4E-10	2.4E-10	1.7E-12
6	n/d	n/d	n/d	n/d

EPIDOTE-FILLED FRACTURES

Domain	kave	k1	k2	k3
2	1.0E-10	4.9E-10	4.9E-10	4.7E-12
3	4.3E-09	1.3E-08	1.2E-08	5.3E-10
4	2.4E-08	1.6E-07	1.6E-07	5.5E-10
5	3.5E-11	1.9E-10	1.9E-10	1.2E-12
6	n/d	n/d	n/d	n/d

ZEOLITE-FILLED FRACTURES

Domain	kave	k1	k2	k3
2	2.8E-07	9.3E-07	9.0E-07	2.6E-08
3	n/d	n/d	n/d	n/d
4	6.5E-10	2.5E-09	2.5E-09	4.3E-11
5	1.2E-11	4.4E-11	4.3E-11	9.0E-13
6	n/d	n/d	n/d	n/d

CALCITE-FILLED FRACTURES

Domain	kave	k1	k2	k3
2	1.7E-10	2.2E-09	2.2E-09	1.1E-12
3	2.9E-10	5.0E-09	5.0E-09	8.9E-13
4	5.0E-12	5.6E-11	5.6E-11	4.0E-14
5	4.4E-13	3.3E-11	3.3E-11	4.0E-15
6	n/d	n/d	n/d	n/d

All permeability values are in units of m^2
Values are the mean of the log transformed permeabilities from permeability calculations listed in Appendix A.7.2
All values are in exponential notation, for example 8.8E-07 is 0.00000088
kave = average of the three principal permeabilities, k1, k2, and k3.

TABLE 4.4 EFFECT OF FAULT SIZE ON PERMEABILITY

EXAMPLE AREA: SCANLINE 1129
53 FILLED FRACTURES
APERTURE RANGE: MIN = 0.01 mm; MAX = 20 mm
SCANLINE LENGTH = 30.5 m (1.74 FRACTURES/METRE)

Fault Aperture (mm)	k1 (m^2) az/dip	k2(m^2) az/dip	k3(m^2) az/dip
20	2.9E−08 154°/67°	2.2E−08 047°/07°	1.6E−08 317°/24°
100	4.2E−06 153°/65°	4.18E−08 050°/07°	1.6E−08 317°/24°
200	3.3E−05 153°/65°	3.3E−5 054°/16°	1.6E−08 317°/24°
300	1.12E−4 145°/66°	1.12E−4 123°/65°	1.6E−08 317°/24°
400	2.67E−4 141°/66°	2.67E−4 133°/65°	1.6E−08 317°/24°
500	5.22E−4 140°/66°	5.22E−4 134°/66°	1.6E−08 317°/24°
600	9.02E−4 139°/66°	9.02E−4 134°/66°	1.59E−08 317°/24°
700	1.4E−3 138°/66°	1.4E−3 136°/66°	1.57E−08 317°/24°
800	2.13E−3 138°/66°	2.13E−3 136°/66°	1.56E−08 317°/24°

IF AREA CONTAINS ONLY ONE FRACTURE ORIENTED 137°/66° WITH AN APERTURE OF 100 mm THEN THE RESULTANT PERMEABILITY IS:

	k1	k2	k3
MAGNITUDE:	2.01E−3	2.01E−3	2.78E−6
ORIENTATION:	138°/66°	137°/66°	317°/24°

NOTE: IT IS NOT POSSIBLE TO RESOLVE 1ST AND 2ND EIGEN VECTORS (PERMEABILITY DIRECTIONS) FOR A POLE TO ONE PLANE.

ALL VALUES USE EXPONENTIAL NOTATION
E.G. 8.8E−07 IS 0.00000088

hydraulic apertures, whereas the field measured apertures are in fact fracture widths. Hydraulic aperture is the effective width of the aperture available to fluid flow. This aperture is generally less than the fracture width due to fracture surface roughness and variation in the height of fracture asperities (Tsang, 1992).

The method of Snow and Bianchi (1969) does not take into account the problem of finite, non-continuous fractures, so that the calculated permeability magnitudes over-estimate the actual permeability. The assumption of continuous fractures throughout the region of interest implies that the fractures intersect and are thus all interconnected, which is not the case. The incorporation of fracture size would affect fracture interconnectivity and as a result the permeability, since the larger interconnected fractures would contribute more to the overall permeability. This can only be addressed by a method which takes into account both the size of fractures and fracture interconnection (as done in the following section).

4.3.3 Discrete-Fracture Geometric Modelling

Discrete fracture geometric modelling involves the stochastic generation of sets of fractures based on input values, or distributions of values, for various fracture properties (such as fracture orientation, aperture, and size). The location in space of these fractures is decided by choosing a particular model of fracture generation. This section describes the stochastic generation of fracture networks, in the Spilia-Politiko study area, and the permeabilities calculated based on those networks.

There are two approaches to describing fracture characteristics: (1) disaggregate; and (2) aggregate characterization (Dershowitz and Einstein, 1988). In the former,

TABLE 4.5 JOINT SYSTEM MODELS (AFTER DERSHOWITZ AND EINSTEIN, 1988)

MODEL	AUTHOR	FRACTURE CHARACTERISTICS IN MODEL				
		SHAPE	SIZE	TERMINATION AT INTERSECTIONS	COPLANAR FRACTURES	SET ORIENTATION
ORTHOGONAL	SNOW, 1965	RECTANGLE	UNBOUNDED	NO	YES	PARALLEL
BAECHER	BAECHER ET AL., 197	CIRCLE OR ELLIPSE	BOUNDED	YES	NO	STOCHASTIC
VENEZIANO	VENEZIANO, 1978	POLYGON	BOUNDED	YES	YES	STOCHASTIC
DERSHOWITZ	DERSHOWITZ, 1984	POLYGON	BOUNDED	YES	YES	STOCHASTIC

fracture characteristics are treated and described separately, whereas in the latter, joint-system models are used to describe the interdependence of fracture characteristics. The disaggregate characterization, followed in Chapter 3, describes joint properties such as persistence (outcrop trace length), planarity (refer to Appendix A.1 for definition), location, intensity and orientation. This characterization is a necessary step to choosing the appropriate joint-system model in the aggregate characterization approach.

Various joint-system models exist in the literature (Table 4.5). The orthogonal joint model is exemplified by that of Snow (1965, 1969), described in Section 4.3.1. The fracture characterization performed in Chapter 3, shows that fractures tend to be non-coplanar and thus non-parallel (i.e. internal dyke cooling fractures). The fractures are of finite length and are thus bounded (Table 3.11). Fractures also tend to terminate at fracture intersections with other fractures (Table 3.10). The joint-system model which includes most of these characteristics, is the Baecher model (Table 4.5). It, however, does not allow for fracture termination at fracture intersections. A modification by Dershowitz et al. (1991) removes this shortcoming. In general, the selection of a particular joint system model is subjective and not necessarily directly based on the results of field sampling procedures (Dershowitz and Einstein, 1988).

The Baecher joint-system model with revised terminations of fractures at intersections, is incorporated into the FracMan program (Dershowitz et al., 1991). This program stochastically generates fracture networks based on values of, or statistical distributions of, fracture parameters input by the user. These parameters include choice of joint model, fracture size distribution, fracture orientation distribution, fracture transmissivity, and fracture intensity. Of these parameters, the

orientation distribution and the fracture intensity were discussed in Chapter 3. Fracture size is discussed in the following section (4.3.3.1).

Fracture transmissivity is normally determined through measurements during packer tests in wells (e.g. Kruseman and de Ridder, 1983). This is not feasible in the present study. Fracture transmissivities are in part dependent on the fracture aperture, which was measured in the field (Chapter 3.4.3). The transmissivity, T, of a fracture is the hydraulic conductivity, K_f, of the fracture times its width (aperture), 2b (Freeze and Cherry, 1979),

$$T = 2bK_f \quad \ldots\ldots\ldots\ldots\ldots\ldots \quad (4.2)$$

where the hydraulic conductivity, K_f is (Rißler, 1978),

$$K_f = \frac{\rho g(2b)^2}{12\mu} \quad \ldots\ldots\ldots\ldots\ldots\ldots \quad (4.3)$$

where ρ is the fluid density, g is the acceleration due to gravity and μ is the dynamic viscosity of the fluid. Therefore the transmissivity of a fracture becomes (Rißler, 1978),

$$T = \frac{\rho g(2b)^3}{12\mu} \quad \ldots\ldots\ldots\ldots\ldots\ldots \quad (4.4)$$

For example, for a 1mm wide fracture ($2b = 10^{-3}$m) and water at 20°C, $\rho = 998.23$ kg/m^3, $\mu = 1.002 \times 10^{-3}$kg/ms and g=9.81 m/s, the transmissivity of that fracture is 8.144×10^{-4}m^2/s.

The rock mass permeability depends on the degree to which pathways are interconnected in a fracture network. If the fractures do not intersect then there are no interconnected pathways and the permeability will be controlled by that of the rock

matrix. There is a critical minimum level of interconnectivity needed before fluid circulation can occur in a fracture network (de Marsily, 1984). The information needed to generate the fracture networks and the results of the permeability calculations are presented in Section 4.3.3.3.

The following two sections describe the preprocessing needed to perform the paleo-permeability calculations. The fracture intensity must be determined for each area. The trace length of a fracture is dependent on the size of the fracture plane. To model the fractures in three dimensions it is necessary to convert the fracture trace length distributions (Chapter 3) to fracture radius distributions.

4.3.3.1 *Fracture Intensity*

To determine the paleo-permeability of a fractured rock mass it is necessary to determine the fracture intensity of the rock mass. In three dimensions, fracture intensity can be defined as one of, 1) the number of fractures per unit volume, 2) the area of fractures per unit volume, or 3) the volume of fractures per unit volume of rock (Dershowitz and Herda, 1992). There are several approaches to determining fracture intensity in a rock volume, these include the distance approach and the density approach as described below.

The distance approach computes distances between fracture intersections along a scanline (Rouleau, 1984). This approach has come to mean the calculation of fracture spacings (Kiraly, 1970; ISRM, 1978). Fracture spacing is defined as the perpendicular distance between adjacent sub-parallel fractures (ISRM, 1978). Since the data subsets in this study are only partially defined on the basis of orientation, fractures subdivided

into sets, earlier in this chapter, are not necessarily sub-parallel. Thus this method of determining the amount of fractures in a rock mass cannot be applied to these data. Fracture spacing, determined for the fractures in the dyke-parallel set of fractures, is presented in Appendix A.3.8.2.

The density approach requires the computation of fracture frequency (fracture intersections per unit length of scanline) (Rouleau, 1984). This value is a one-dimensional measure which needs to be related to one of the three volume measures of fracture intensity listed above. The number of fractures per unit volume is scale dependent. This measure changes with the size of the region of interest for regions smaller than the maximum fracture size. The size of fractures is taken to be the radius of a circular fracture of equivalent area (Dershowitz and Herda, 1992). The second and third measures of fracture intensity are not scale-dependent since they are based on fracture size. The third measure requires knowledge of the fracture aperture. Dershowitz and Herda (1992) suggest the use of the total fracture area per unit volume of rock, which they refer to as P_{32} (Persistence of fractures in a three dimensional measurement region using two dimensional fractures, that is excluding thickness), for modelling of three dimensional fracture networks. In this study the density approach was adopted using the area of fractures per unit volume measure. The computation of the parameters in this approach is further outlined below.

The fracture data collected in this study were collected along scanlines (one dimension). Fracture frequency along a scanline, although dependent on fracture orientation, is independent of fracture size and as a result also scale independent (Dershowitz and Herda, 1992). To be able to estimate a measure of fracture area per unit volume for the data in this study, use must be made of the relation between the scanline fracture frequency and the area of fractures per unit volume (Dershowitz and

Herda, 1992). P_{32} is related to the fracture spacing S_f by a constant C_p (Dershowitz and Herda, 1992),

$$P_{32} = C_p S_f \quad \ldots\ldots\ldots\ldots\ldots\ldots \quad (4.5)$$

C_p is dependent on the distribution of fracture orientation relative to the sampling line along which S_f is measured.

Estimation of the P_{32} measure from the scanline fracture data from the Spilia-Politiko area followed the approach set out by Dershowitz et al. (1991) in their program, FracMan (Figure 4.3). In this approach, an intial P_{32} is chosen, arbitrarily, to be 1, the fractures are generated by sampling the fracture data set with replacement using a bootstrap method (Efron, 1982). In the bootstrap method, simulated fracture orientations are obtained directly from the fracture data set. For each fracture simulated in the model an orientation is selected at random, with replacement, from the data set. A dispersion based on a Fisher distribution (Fisher, 1956) with a dispersion parameter, κ=20 is added to that orientation. The simulated fracture orientation is then chosen from that distribution.

To locate fracture centres in the generation region, the revised Baecher model (Baecher et al., 1977) which allows for fracture termination at fracture intersections was used. The probability that fractures terminate when intersecting another fracture was based on the fracture termination percentages taken from the field data (Table 3.10).

The frequency of filled fractures (Table 3.14) along a scanline will be used in the estimation of the fracture intensity. In present fracture modelling studies, it is the fractures which conduct fluids that are of interest. In this study, which is interested in

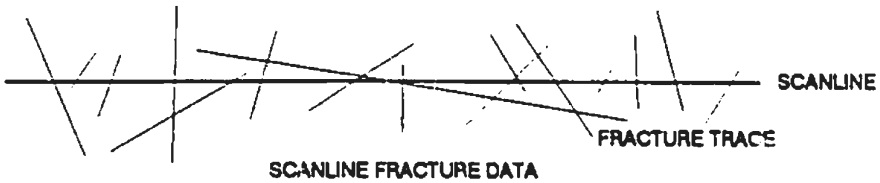

SCANLINE FRACTURE DATA

CALCULATE POPULATION FRACTURE INTENSITY = $\frac{\text{\# OF FRACTURES}}{\text{SCANLINE LENGTH}}$

ARBITRARILY ASSUME A VALUE FOR P32 = 1

$$P32 = \frac{\text{TOTAL AREA OF FRACTURES}}{\text{TOTAL VOLUME}}$$

GENERATE FRACTURES IN A GENERATION VOLUME BY SAMPLING RAW DATA SET UNTIL FRACTURE INTENSITY IN GENERATION VOLUME = P32

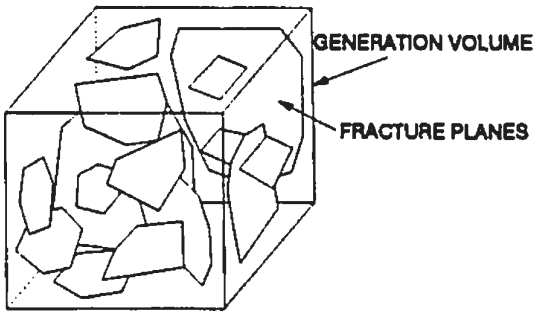

SIMULATE A BOREHOLE IN GENERATION REGION
MEASURE NUMBER OF FRACTURE INTERSECTIONS IN BOREHOLE

COMPUTE FRACTURE INTENSITY = $\frac{\text{\# OF INTERSECTIONS}}{\text{PER UNIT LENGTH OF BOREHOLE}}$

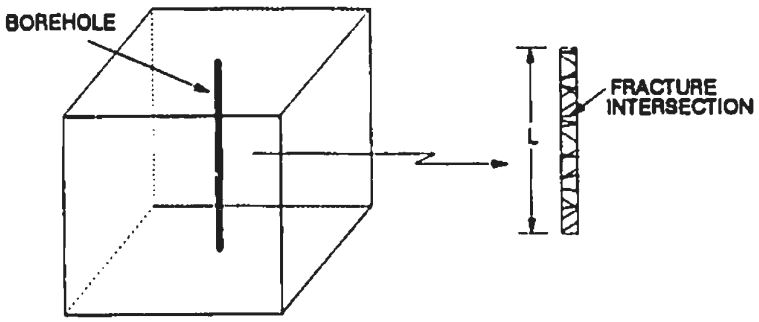

CALCULATE RATIO, Cp = $\frac{\text{FRACTURE INTENSITY}}{\text{ASSUMED P32}}$

P32 FOR ACTUAL FRACTURE POPULATION THEN IS:

$$P32 = \frac{\text{POPULATION FRACTURE INTENSITY}}{Cp}$$

FIGURE 4.3 SCHEMATIC SHOWING THE PROCESS FOR DETERMINATION OF THE FRACTURE AREA PER UNIT VOLUME MEASURE FROM THE SCANLINE FRACTURE DATA.

paleo-permeabilities, the filled fracture intensity is analogous to the intensity of conductive fractures, since fractures with a mineral filling are assumed to have conducted fluids in the past. The fractures used in the simulations for the fracture intensity determination were the mineral-filled fractures from the study area (excluding those fractures containing only calcite). These fractures are assumed to have conducted fluids at some time in their history. Thus, the calculated value for P_{32}, is actually a value for the conductive P_{32}. Boreholes cutting the fracture generation region were simulated with the program. The conductive fracture intensity was calculated from the number of fractures intersecting these simulated boreholes. The values of the ratio, C_p, in this study, of the assumed P_{32} and the simulated fracture intensity, fall in the range of 1.3 to 1.8 (Table 4.6). Dershowitz and Herda (1992) found that C_p for most fracture geometric patterns varies between 1 and 3. The estimated P_{32} for the actual fracture data set is,

$$P_{32} = f_{c(m)} C_p = f_{c(m)} \frac{P_{32(s)}}{f_{c(s)}} \quad \ldots\ldots\ldots\ldots \quad (4.6)$$

where $P_{32(s)}$ is the initially chosen P_{32}, $f_{c(m)}$ is the measured conductive fracture intensity, while $f_{c(s)}$ is the simulated conductive fracture intensity. The simulation indicates the average value for P_{32} is about 1.08 (with a standard deviation of ± 0.4) (Table 4.6).

4.3.3.2 *Fracture Shape and Size*

Knowledge of the shape and size distribution of fracture planes is of importance in determining the rock permeability. Fracture trace lengths, measured at an outcrop, depend on the shape and size of the fracture plane, and the distance between the

TABLE 4.6 FRACTURE INTENSITY BY ROCK VOLUME

SCAN-LINE	MEASUREMENT LINE LENGTH (m)	DATA TYPE	# OF FILLED FRAC.	FILLED* FREQ. (1/m)	SIMULATION #-	INITIAL P32 (1/m)	Cp (m)	MODEL P32**** (1/m)
0000	37.4	DYKE //	8	0.214	412	1.0	1.456	0.147
		REST	63	1.684	386	1.0	1.554	1.084
0108	31.5	DYKE //	52	1.651	398	1.0	1.508	1.095
		REST	13	0.413	411	1.0	1.460	0.283
0112	25.1	DYKE //	12	0.478	415	1.0	1.446	0.331
		REST	54	2.151	371	1.0	1.617	1.330
0122	148.2	DYKE //	133	0.897	389	1.0	1.542	0.582
		REST	102	0.688	393	1.0	1.527	0.451
0401	31.3	DYKE //	45	1.438	389	1.0	1.542	0.932
		REST	4	0.128	375	1.0	1.600	0.080
0413	30.6	DYKE //	41	1.340	390	1.0	1.538	0.871
		REST	7	0.229	384	1.0	1.563	0.146
0418	21.6	DYKE //						
		REST	32	1.481	397	1.0	1.511	0.980
0428	67.6	DYKE //	44	0.651	403	1.0	1.489	0.437
		REST	105	1.553	396	1.0	1.515	1.025
1037	30.9	DYKE //	30	0.971	428	1.0	1.402	0.693
		REST	8	0.259	382	1.0	1.571	0.165
1124	25.6	DYKE //	30	1.172	424	1.0	1.415	0.828
		REST	3	0.117	399	1.0	1.504	0.078
1134	32.0	DYKE //	32	1.000	434	1.0	1.382	0.723
		REST	18	0.563	394	1.0	1.523	0.369
1137	31.7	DYKE //	10	0.315	447	1.0	1.342	0.235
		REST	23	0.726	455	1.0	1.319	0.550
1222	31.1	DYKE //	21	0.675	418	1.0	1.435	0.470
		REST	10	0.322	427	1.0	1.405	0.229
1321	30.2	DYKE //	55	1.821	419	1.0	1.432	1.272
		REST	2	0.066	423	1.0	1.418	0.047
	AREA (m^2)		FILLED* LENGTH	INTENSITY (m/m^2)				
AREA 1 ***	59.4	DYKE //	64.88	1.092	412	1.0	1.456	0.750
		REST	67.05	1.129	446	1.0	1.345	0.839

* FRACTURES USED ARE MINERAL FILLED BUT EXCLUDE THOSE ONLY FILLED WITH CALCITE. FREQUENCY = #/LENGTH
FILLED LENGTH = SUM OF FILLED FRACTURE TRACE LENGTHS

** SIMULATIONS DONE USING FracMan (DERSHOWITZ ET AL., 1991) WITH FOLLOWING CONDITIONS:
1) ENHANCED BAECHER MODEL WITH REVISED TERMINATION HANDLING
2) TERMINATION PROBABILITY SET USING TABLE 3.12 VALUES
3) BOOTSTRAP SAMPLING OF MEASURED FIELD DATA
4) INTERSECTIONS SIMULATED USING 3 SIMULATED ORTHOGONAL BOREHOLES FOR TOTAL 600 M LENGTH GENERATION VOLUME = 100MX100MX100M
5) Cp = Assumed P32*Borehole length/(# of intersections)
6) P32 = TOTAL FRACTURE AREA PER UNIT VOLUME OF ROCK IN UNITS OF 1/m

*** AREA 1 = AREA MAP OF SCANLINE LOCATION 1137

**** MODEL P23 = FILLED FREQUENCY/Cp

\- # OF FRACTURE INTERSECTIONS IN SIMULATED BOREHOLES

centre of the fracture and the intersection with the outcrop surface (the further the intersection is from the fracture centre, the shorter the resultant trace length).

It is not possible to directly observe the shape of the fracture plane or the distribution of the fracture sizes from (isolated) outcrops. The simplest fracture shape is the circle. Anisotropy in the stress field may result in the formation of an elliptical fracture with its long axis oriented perpendicular to the least compressive stress.

To simulate the process of fracture trace length determination as a result of the intersection of fracture planes with an outcrop surface, the program ELLIPSE (listing in Appendix D) samples a distribution of lengths representing the length of the long axis of an elliptical fracture to produce a sample population of ellipses whose long axis half-lengths vary according to the input distribution. To determine what type of distribution of fracture radii could have produced the measured fracture trace length distribution, a variety of distribution types were sampled. The various input fracture radii distributions included log-normal, exponential, Weibull, bi-modal, and square. A consistent aspect ratio (the ratio of the long axis half-length, a, to the short axis half-length, b) is used in each simulation. Four different aspect ratios of fractures were tested: 1 (circle); 0.7; 0.4; and 0.1 (extreme ellipse). The results were binned by trace length to produce trace length histograms (see figures and tables presented in Appendix A.8).

The histograms indicate that the output trace length distribution tends to follow the input fracture radius distribution. Exceptions to this are the exponential distribution which appears somewhat truncated at shorter trace lengths, and the square distribution in which the trace length distribution is truncated at both the lower and the upper end

of the distribution. The means of the resultant trace length distributions are similar to the means of the input fracture radii distributions.

The results for the various trials (using the aspect ratios and size distributions given above), demonstrate that the simulations best matching the field trace length data (Figure 3.21) are the log-normal distribution (aspect ratio between 0.4 and 0.7 (approximately 0.6)), and the Weibull distribution (aspect ratio = 0.4). The other distributions do not match the data. Because it is not clear, on the basis of this data set, what the controls are on the orientations of the long axes of the fracture ellipses, the fracture network modelling using FracMan is done using circular fractures of equivalent areas.

The parameters of a log-normal fracture radius distribution of circular fractures are the mean and standard deviation. These parameters can be estimated through the program FracMan (Dershowitz et al., 1991). To determine these parameters, an assumed distribution of fracture radii with associated parameters of the mean and standard deviation is chosen. A random sampling of this distribution produces fracture trace lengths which are then tested for goodness of fit with the actual field-measured trace length data using either the Kolmogorov-Smirnov or Chi-squared goodness-of-fit-tests. In comparing simulated and measured trace lengths, the program uses simulated traces which are censored by the edge of the mapped area, and are not recorded if they are less than the specified minimum cutoff size. This method thus accounts for fracture trace length censoring and truncation.

The results of using this program (FracMan) on the data set, from the Spilia-Politiko area are presented in Table 4.7. The best fits to the field data were obtained using a log-normal distribution of fracture radii. The mean fracture radius for the complete

TABLE 4.7 FRACTURE RADIUS DETERMINATION BY TRACE LENGTH SAMPLING

SCANLINE LOCATION	DYKE DOMAIN	DYKE PARALLEL FRACTURES				OTHER FRACTURES			
		RADIUS		STATISTICS		RADIUS		STATISTICS	
		MEAN	STD.DEV.	K-S*	CHI-SQUARE	MEAN	STD.DEV.	K-S*	CHI-SQUARE
0000	4	2	2	90.8	99.9	2	2	90.6	99.9
0108	2	3.1	0.1	18.6	99.4	3.5	0.6	17.6	70.4
0112	4	no dykes				1.7	1.4		58.9
0122	4	2.2	1.7	11	35.2	2.1	1.5	16.9	33.6
0401	4	3.1	0.5	29.6	91	1.9	1.2	29.3	99.2
0413	4	3.5	0.1	46	100	2.1	2	12.3	79.6
0418	4	no dykes				2.6	2.5	24.5	96.8
0428	4	3.5	3	11	82.9	1.5	1.3	34.8	83.1
1037	2	2	2	37.1	99.3	1	1.3	64.1	97.7
1124	5	1	2	98.1	99.3	0.45	0.2	58.3	77.6
1134	3	5.3	3	44.3	99.2	3	4.8	43.2	79.8
1137	6	3.5	0.1	75.4	91.2	0.8	0.3	80.5	88
1222	5	2	1.5	7.9	95.7	3	2	49.1	99.6
1321	2	2	1.5	57.2	94.3	1	1.5	16.8	96.2

NOTE: *K-S = KOLMOGOROV-SMIRNOV GOODNESS-OF-FIT TEST
SIMULATION OF FRACTURE RADII IS BASED ON ASSUMING A MEAN AND STANDARD DEVIATION OF A LOG-NORMAL DISTRIBUTION OF FRACTURE RADII AND THEN SAMPLING THE FRACTURE TRACE LENGTH DATA. THE SIMULATION CALCULATES A SIMULATED DISTRIBUTION OF FRACTURE TRACE LENGTHS WHICH IS THEN COMPARED TO THE ORIGINA DATA USING THE KOLMOGOROV-SMIRNOV AND CHI-SQUARE GOODNESS-OF-FIT TESTS.

data set was 2.1 metres. The means varied from 1.4 to 5.3 metres, with those for the dyke-parallel fractures greater than for the other fractures (Table 4.7). The difference in mean fracture radius between dyke-parallel and other fractures was smallest for domain 4 locations and largest in domain 6. From north to south in the field area there was not much variation in the estimated mean fracture radius. In general there did not seem to be significant variation in the mean fracture radius from area to area, indicating that similar processes were operating in all areas. This also indicates that the stress conditions for fracture formation did not vary significantly with depth in the section or laterally across the area (see Section 4.4).

4.3.3.3 *Method of Permeability Determination*

The calculation of bulk fractured rock permeabilities was performed using the FracMan (Dershowitz et al., 1991) and MAFIC (Miller, 1990) programs. This pair of programs was developed by Golder Associates Incorporated, to generate fracture networks and simulate fluid flow and particle transport in nuclear waste repositories in fractured rock. Since the purpose here is to compute fractured rock permeabilities, these programs are well suited to this purpose.

The following paragraphs outline the method used to generate the fracture networks and to subsequently model fluid flow through these networks. A more complete description of the use of these programs is given in Dershowitz et al. (1991) and Miller (1990). Both these programs are still under development by Golder Associates Incorporated.

Fracture properties (determined in Chapter 3 and in the previous section), used in the generation of fracture networks, are tabulated in Table 4.8. The fracture data for each area were subdivided into two sets, as outlined in Chapter 3, dyke parallel and other fractures. The input data files to FracMan contain the raw orientation and trace length data for each fracture in a particular set. Since these networks are stochastically generated, it is necessary to generate multiple networks for each data set and then to average the results. Therefore twenty fracture networks were generated from each fracture data set using FracMan macro files. A macro file contains values of the various fracture parameters to be used in the fracture network generation, and the necessary commands to run the simulation. These commands are the same as those that would have to be typed in from the computer keyboard. An example macro file is listed in Appendix D. To simplify the generation of fracture orientations, especially those fractures which plot in a girdle distribution (Chapter 3) in the program, the data sets were each sampled using the bootstrap method (Efron, 1982), by the FracMan program, until the desired intensity of fractures was present in the generation region. Fracture transmissivities were calculated, as described above, from the fracture apertures (Table 4.8).

Once a fracture network has been generated, it is necessary to apply boundary conditions to the generation region. The generation region is a cube (in this study the cube dimensions used were 25 m x 25 m x 25 m). The easiest method to determine permeability of the rock block is based on d'Arcy's law. This involves knowing the heads at either end of the region of interest and the total flux, driven by the head gradient, through the region (Figure 4.4B). Using this method, two (opposing) boundaries of the cube have fixed heads. One head is set greater than the other to establish a flow gradient (in the direction of the lower head). The remaining four boundaries of the cube are set to no-flow boundaries; this means there is no flow

TABLE 4.8 FRACTURE MODEL DATASET**

Parameter	Common values		Individual Scanline Conditions							
			0000		0108		0112		0122	
Subdivision of Data Sets	1) Dyke parallel fractures 2) Remaining fractures in data set		Subdivide into	%	Subdivide into	%	Subdivide into	%	Subdivide into	%
		Dyke //		11		80		18		57
		Rest		89		20		82		43
Fracture Intensity Measure	P32	Total	1.231		1.378		1.661		1.033	
value (1/m)	varies (refer to	Dyke //	0.147		1.095		0.331		0.582	
	Table 3.15)	Rest	1.084		0.283		1.330		0.451	
Fracture Size Distribution	Truncated Log-normal									
Fracture Size Measure	Radius									
Mean (m)	(Data from Table 4.6)	Dyke //	2.00	2.00	3.10	0.10	2.00	2.00	2.20	1.70
Standard Deviation (m)		Rest	2.00	2.00	3.50	0.60	1.45	2.00	2.10	1.50
Minimum (m)	1 m									
Maximum (m)	20 m									
Aspect ratio	1 (circular)									
Termination (%)	(Data from Table 3.10)		97		84		98		88	
Fracture Aperture	Log-Normal Distribution	Dyke //	2.10	5.90	3.70	2.70	1.00	7.30	4.00	7.00
(mm)	(Data from Table 3.2)	Rest	1.80	2.50	1.20	4.00	1.40	7.30	3.60	5.00
	given as mean and standard deviation									
Fracture Transmissivity *	Log-Normal Distribution	Dyke //	0.00754	0.16727	0.04125	0.01603	0.00081	0.31682	0.05212	0.27935
(m^2/s)	(calculated from fracture aperture)	Rest	0.00475	0.01273	0.00141	0.05212	0.00223	0.31682	0.03800	0.10180
	given as mean and standard deviation									

NOTES: (On additional information required for the fracture network modelling)
Conceptual Fracture Model: BART (Enhanced Baecher Model with revised termination process)
Generation Volume: Box (Size: 25m x 25m x 25m)
Orientation Distribution: Bootstrap sampling (Fisher Dispersion Parameter for bootstrap method = 20)
The total P32 values for each scanline area is the sum of the P32 values of each of the subsets for the scanline.

* Fracture transmissivity is calculated using the following formula
$Tf = Kf \times 2b$ where $Kf = d\ g\ (2b)^3 / 12\ u$
Kf = fracture conductivity; 2b = fracture aperture; Tf = fracture transmissivity
at 20 degrees C, water density, d = 998.23 kg/m^3; absolute viscosity, u = 1.002 x 10^-3 Pa s (or kg/m s)
acceleration due to gravity, g = 9.81 m/s^2

** The first three pages of this table deal with the fracture data set excluding calcite only fractures.

TABLE 4.8 FRACTURE MODEL DATASET (continued)

Parameter	Individual Scanline Conditions											
	0401		0413		0418		0428		1037		1124	
Subdivision of Data Sets	Subdivide into	%	Subdivide into	%	One Set		Subdivide into	%	Subdivide into	%	Subdivide into	%
		92		85				30		79		91
		8		15				70		21		9
Fracture Intensity Measure	1.012		1.017		0.98		1.462		0.858		0.906	
value (1/m)	0.932		0.871				0.437		0.693		0.828	
	0.080		0.146		0.98		1.025		0.165		0.078	
Fracture Size Distribution:												
Fracture Size Measure:												
Mean (m)	3.10	0.50	3.50	0.10	2.60		3.50	3.00	2.00	2.00	1.00	2.00
Standard Deviation (m)	1.90	1.20	2.10	2.00	2.50		1.50	1.30	1.50	1.30	0.45	0.20
Minimum (m)												
Maximum (m)												
Aspect ratio												
Termination (%)	86		91		82		91		100		100	
Fracture Aperture	2.00	6.10	1.40	4.40			0.70	4.00	2.20	2.20	2.00	2.20
(mm)	0.30	5.10	0.50	3.80	2.90	4.60	1.00	3.70	3.00	1.00	1.00	1.00
Fracture Transmissivity *	0.00652	0.18486	0.00223	0.06938			0.00028	0.05212	0.00867	0.00867	0.00652	0.00867
(m^2/s)	0.00002	0.10803	0.00010	0.04469	0.01986	0.07927	0.00081	0.04125	0.02199	0.00081	0.00081	0.00081

TABLE 4.8 FRACTURE MODEL DATASET (continued)

Parameter	1134		1137		1222		1321	
Subdivision of Data Sets	Subdivide into	%	Subdivide into	%	Subdivide into	%	Subdivide into	%
		64		30		68		96
		36		70		32		4
Fracture Intensity Measure	1.092		0.785		0.699		1.319	
value (1/m)	0.723		0.235		0.470		1.272	
	0.369		0.550		0.229		0.047	
Fracture Size Distribution								
Fracture Size Measure								
Mean (m)	5.30	3.00	3.50	0.10	2.00	1.50	2.00	1.50
Standard Deviation (m)	3.00	4.80	0.80	0.30	3.00	2.00	1.50	1.50
Minimum (m)								
Maximum (m)								
Aspect ratio								
Termination (%)	100		92		100		92	
Fracture Aperture	5.70	2.30	2.00	1.90	1.40	2.10	2.90	2.70
(mm)	11.00	3.50	1.60	2.90	2.00	1.00	2.00	1.00
Fracture Transmissivity *	0.15083	0.00991	0.00652	0.00559	0.00223	0.00754	0.01986	0.01603
(m^2/s)	1.08400	0.03492	0.00334	0.01986	0.00652	0.00081	0.00652	0.00081

TABLE 4.8 FRACTURE MODEL DATASET (continued)***

Parameter	0213		0701		1129		1134		1316	
Subdivision of Data Sets	Subdivide into	%	Subdivide into	%	Subdivide into	%	Subdivide into	%	Subdivide into	%
		73		24		16		20		7
		27		76		84		80		91
Fracture Intensity Measure	0.56		0.58		0.91		0.71		1.08	
value (1/m)	0.4088		0.1392		0.1456		0.142		0.0756	
	0.1512		0.4408		0.7644		0.568		0.9828	
Fracture Size Distribution										
Fracture Size Measure										
Mean (m)	2.00	2.00	1.80	0.30	2.00	1.40	4.50	2.70	1.50	2.30
Standard Deviation (m)	0.50	0.50	2.00	1.70	2.40	2.70	2.C0	2.30	1.80	2.00
Minimum (m)										
Maximum (m)										
Aspect ratio										
Termination (%)	91		88		97		100		82	
Fracture Aperture	2.80	3.44	1.74	1.50	1.49	1.45	5.98	3.45	3.64	3.82
(mm)	2.49	2.15	2.35	2.64	1.61	2.32	6.31	3.31	2.04	2.10
Fracture Transmissivity *	0.01788	0.03315	0.00429	0.00275	0.00269	0.00248	0.17242	0.03344	0.03928	0.04540
(m^2/s)	0.01257	0.00809	0.01057	0.01499	0.00340	0.01017	0.20462	0.02953	0.00691	0.00754

*** Note: this portion of the table contains the data for the calcite filled fractures.

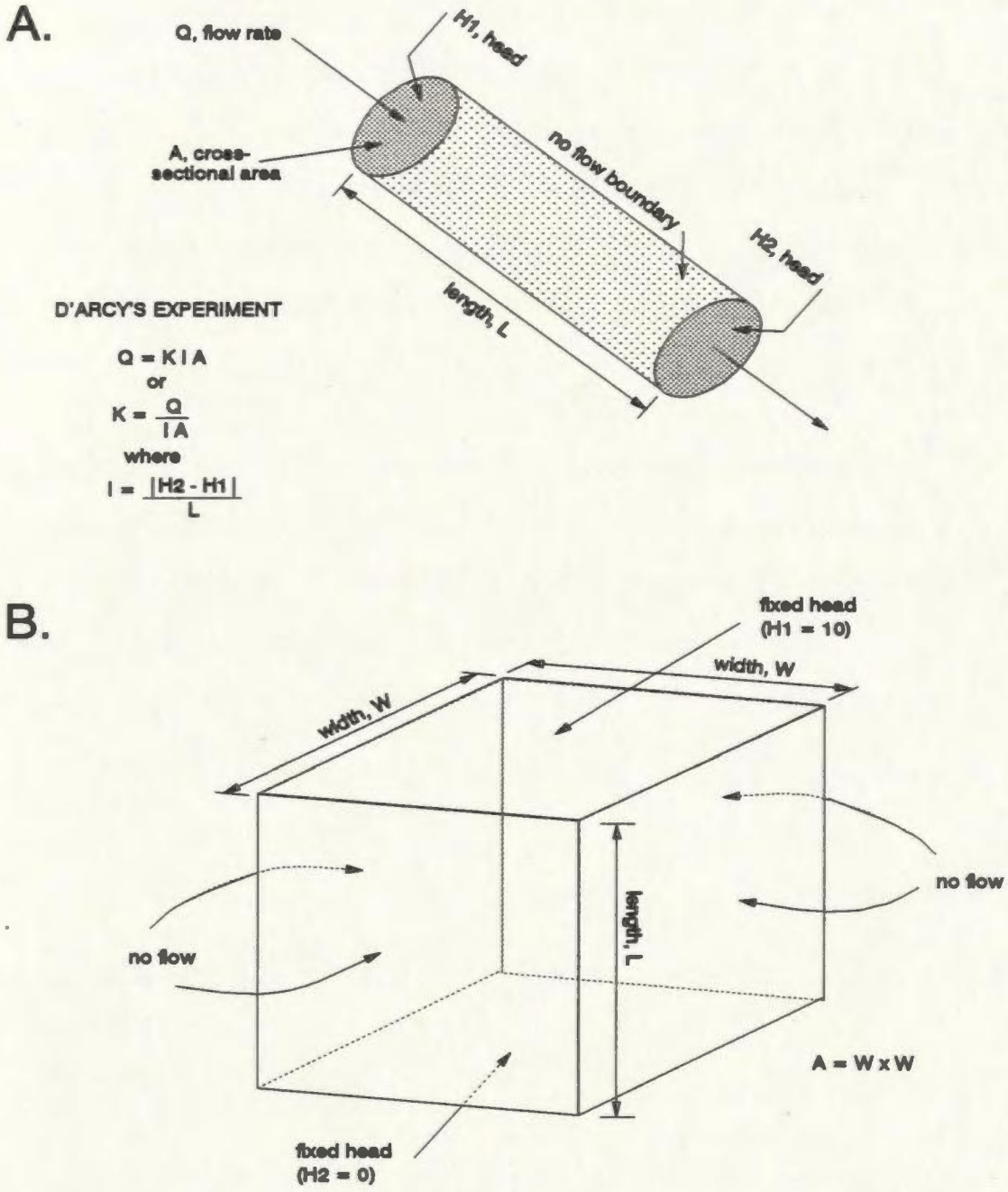

FIGURE 4.4 BOUNDARY CONDITIONS APPLIED TO THE FRACTURE NETWORKS.
A. D'ARCY'S LAW AND EXPERIMENT WITH A SAND FILLED CYLINDER
B. FRACTURE NETWORK GENERATION REGION AND BOUNDARY CONDITIONS.

across those boundaries. The program FracMan or an auxiliary program, MeshMonster (Dershowitz et al., 1991), is used to generate the finite element network from the fracture locations in the fracture network and the boundary conditions. The program MAFIC (Miller, 1990) is then used to calculate the total flow through the region. MAFIC (Miller, 1990) uses a finite element approach to solve for nodal heads and fluxes in the three dimensional fracture networks. The bulk permeability of the cube is calculated as follows. From D'Arcy's law we know that,

$$Q = K\,I\,A \quad \ldots\ldots\ldots\ldots\ldots\ldots \quad (4.7)$$

where Q is the discharge rate (in this case the units used are: cubic metres per second), K is the hydraulic conductivity (in metres/second), A is the area of the cube face through which the discharge is taking place, and I is the hydraulic gradient, $I = [h_1 - h_2]/L$, where h_1 and h_2 are the heads at opposite ends of the cube and L is the distance between the ends of the cube. Solving for the hydraulic conductivity, K, results in,

$$K = \frac{Q}{I\,A} \quad \ldots\ldots\ldots\ldots\ldots\ldots \quad (4.8)$$

By rearranging equation (4.1) we know that the intrinsic permeability, k, is related to the hydraulic conductivity as follows,

$$k = \frac{K\,\mu}{\rho\,g} \quad \ldots\ldots\ldots\ldots\ldots\ldots \quad (4.9)$$

where $\mu = 1.002 \times 10^{-3}$ kg/ms, $\rho = 1000$kg/m^3, and g = 9.81 m/s^2. Thus $k = K \times 1.02 \times 10^{-7}$ (for water at 20°C) (Freeze and Cherry, 1979). For a cube 25 metres on a side and with an hydraulic gradient of (10 - 0)/25 = 0.25, the conversion from discharge, Q, to intrinsic permeability, k, is,

$$k = Q \times 4.08 \times 10^{-10} \quad \ldots\ldots\ldots\ldots \quad (4.10)$$

Fracture sizes in the FracMan simulations were truncated so that all fractures with radii smaller than 1 metre were left out of the flow modelling. This was done to reduce the computer memory and time requirements. Several simulations were run using a non-truncated set of fractures, that is, all fractures regardless of size were included. The resultant flow through the network was within the same order of magnitude as that for the truncated data set (i.e. $7.6 \times 10^{-1} m^3/s$ for the truncated network versus $7.4 \times 10^{-1} m^3/s$ for the non-truncated network). This shows that the smaller fractures (i.e. those with less than 1 metre radius) do not contribute significantly to the fracture network interconnectivity.

4.3.3.4 *Paleo-Permeability*

The calculation of paleo-permeability in the fractured rock of the Spilia-Politiko area, using the method outlined above, was done for two groups of fractures. The first group included all fractures that contained a mineral filling but excluded those fractures containing only calcite. This first set of permeability calculations was done using 14 of the scanline mapped areas which contained more than 30 fractures with mineral infillings. The permeabilities calculated for this group are based on mineral-filled fractures which are shown to have been utilized by high temperature, probably on-axis hydrothermal fluids (Section 5.3.4). The second group encompassed those fractures containing calcite. This group contains 9 scanline areas, five of which were also used in the first set of calculations. Calcite, always the latest phase to form, probably resulted from low-temperture, off-axis circulation of fluids (Appendix C.1). Thus, this latter set of permeabilities are thought to be representative of off-axis permeabilities.

The permeabilities calculated in the following sections assume that all fractures were open at the same time. However, these fractures may have opened episodically during the life of the hydrothermal system, in which case the calculated permeabilities are a maximum which may not be achieved. Further calculations presented in Section 4.3.3.4.3 address this issue.

4.3.3.4.1 On-Axis Permeability

The results of the permeability study for the first group of calculations are shown in Figure 4.5 and Table 4.9. They show a variation of the vertical permeability, at each location, from 10^{-8} to $10^{-12}m^2$. It can be seen that there is a small decrease in the calculated permeability with increased depth in the sheeted dyke section (increasing depth is to the south) on the map displaying permeability by location (Figure 4.5). The mean calculated permeability at sites containing epidosites is almost two orders of magnitude (2.7×10^{-8} versus 7.0×10^{-10}), higher than that in unaltered diabase dykes. This is because the amount of fractures containing hydrothermal minerals, as well as their apertures, in epidosite outcrops is higher, than that in the diabase outcrops (Section 5.2.1).

The calculated permeability of both the epidosite and diabase sections decreases with depth. The highest permeability was calculated for scanline area 1134 in the vicinity of the Apliki shear zone, whereas the lowest permeabilities were calculated near Alona near the gabbro section.

Flow laterally through the fracture networks (north-south and east-west) was in all cases less than that for the vertical flow. In most cases this difference was one or two

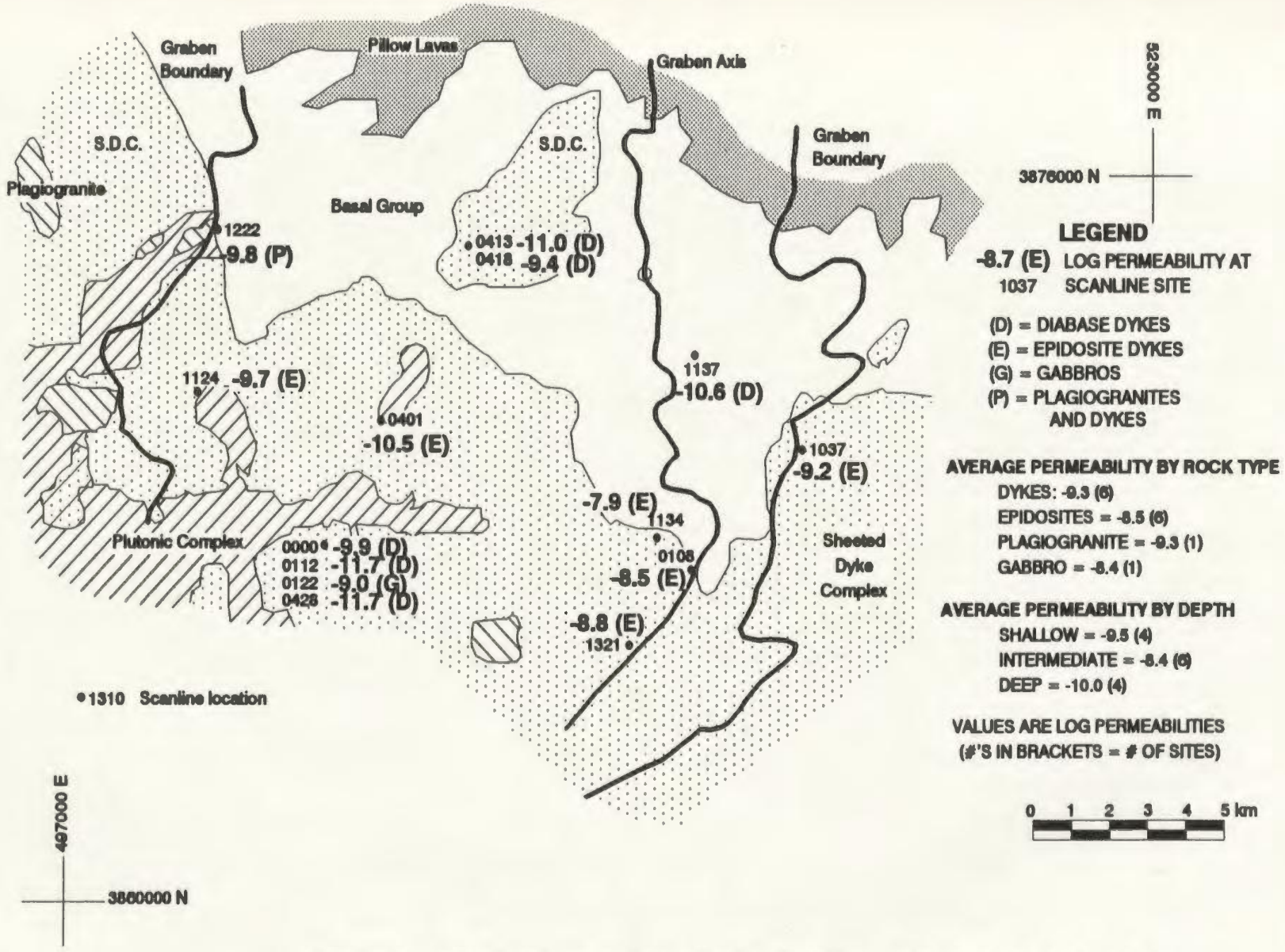

FIGURE 4.5 PERMEABILITY VARIATION IN THE SPILIA - POLITIKO AREA, CYPRUS.

TABLE 4.9 PERMEABILITY MODELLING RESULTS

Scanline	Permeability (m^2) Vertical Mean	Vertical Std.dev.	East–West Mean	East–West Std.dev.	North–South Mean	North–South Std.dev.
0000	5.55E–10	3.42E–10	7.72E–11	8.12E–11	6.19E–11	5.28E–11
0108	2.09E–08	1.27E–08	9.95E–10	9.86E–10	1.60E–09	1.16E–09
0112	9.69E–12	5.89E–12	8.67E–13	8.20E–13	9.45E–13	6.40E–13
0122	3.80E–09	2.36E–09	5.48E–10	4.95E–10	6.10E–10	8.28E–10
0401	2.07E–10	1.31E–10	1.79E–11	1.54E–11	1.16E–11	1.22E–11
0413	5.14E–11	3.26E–11	2.05E–12	1.33E–12	1.09E–11	1.97E–11
0418	1.99E–09	1.38E–09	1.83E–10	1.51E–10	1.50E–10	1.12E–10
0428	5.93E–12	4.02E–12	1.05E–12	2.75E–12	1.08E–12	8.91E–13
1037	2.39E–09	1.49E–09	2.64E–10	2.73E–10	3.01E–10	2.60E–10
1124	4.80E–10	3.12E–10	8.36E–11	9.90E–11	1.23E–10	9.38E–11
1134	7.73E–08	4.80E–08	3.99E–09	1.87E–08	8.69E–09	6.96E–09
1137	1.11E–10	6.91E–11	8.34E–12	5.89E–12	1.55E–11	1.27E–11
1222	4.95E–10	3.09E–10	1.45E–10	5.19E–10	4.21E–11	5.84E–11
1321	7.09E–09	4.34E–09	7.21E–10	9.32E–10	8.32E–10	5.75E–10

MEAN AND STANDARD DEVIATION BASED ON 20 SIMULATIONS FOR EACH AREA

orders of magnitude. This, again, is the result of the anisotropy caused by the dyke-parallel fractures.

4.3.3.4.2 Off-Axis Permeability

Calcite fillings commonly occur in fractures in the pillows and less commonly in the sheeted dykes of DSDP drill hole 504B (Alt et al., 1989) and in the Spilia-Politiko area. In the study area, calcite fillings represent a late phase of low temperature, possibly off-axis fluid circulation (Appendix C.1). Calcite fillings in some areas were precipitated on pre-existing epidote, while calcite-filled fractures in other areas contain only calcite. The re-use of fractures indicates that either 1) these fractures were still open after the first phase of hydrothermal circulation depositing epidote, had ceased, or 2) they were reopened during off-axis circulation possibly during formation of the Mitsero graben. Precipitation of calcite into empty fractures implies the creation of new fractures or connection of pre-existing fractures to the overall fracture network. The occurrence of calcite fracture-fillings, in the study area, is most common in the area of the Apliki shear zone and near plagiogranite bodies. It is likely that the emplacement of the plagiogranite bodies and the formation of shear zones resulted in the formation of new fractures.

The permeability of the calcite-filled fractures in the study area was determined, using the FracMan/MAFIC programs as outlined previously, for the purposes of comparison with off-axis oceanic crust permeabilities. Of the data sets used in the previous permeability calculations (this section) only five contain calcite-filled fractures (1037, 1124, 1134, 1137, and 1321). The proportion of calcite-filled fractures to the total number of mineral-filled fractures in these data sets varies from 3% (scanline 1037) to

53% (scanline 1134) (Table 4.10). The permeabilities for four of the areas (1037 [3%], 1124 [12%], 1137 [24%], and 1321 [14%]; numbers in brackets are the percentage of calcite bearing fractures as a proportion of total number of mineral filled fractures) ranged from 6.9×10^{-18} to $4.0 \times 10^{-20} m^2$ (Table 4.10), which are 8 to 10 orders of magnitude less than in the previous calculations. This indicates a large decrease in the permeability of the Sheeted Dyke Complex, possibly a result of hydrothermal mineral precipitation.

Four other data sets, which did not contain significant amounts of hydrothermal minerals such as epidote, contain 30 or more calcite filled fractures (0213, 0701, 1129, 1316). The calculated permeabilities of these areas, and that of 1134, containing larger proportions of calcite-filled fractures (0213 [60%], 0701 [88%], 1129 [80%], 1134 [53%], and 1316 [72%]; Table 4.10), ranged from 8.0×10^{-10} to $1.6 \times 10^{-8} m^2$. These were comparable to the permeabilities calculated for the hydrothermal mineral filled fractures (excluding those fractures that contained only calcite). These five areas are associated either with plagiogranite bodies (0213, 0701, 1129, and 1316) or shear zones (1134, near Apliki).

For all these areas, there is no correlation between the occurrence of calcite-filled fractures and whether the host rock is epidosite or diabase. Calcite, a late phase, over-prints earlier hydrothermal fracture fillings, implying, by association, that the plagiogranite occurrences and shear zones may be late as well. In the remaining areas measured in the field area, calcite-filled fractures represent less than 2% of the mineral-filled fractures.

TABLE 4.10 PERMEABILITY CALCULATIONS USING CALCITE–FILLED FRACTURES

SCANLINE	AFFINITY	Fractures					Permeability, k (m ^ 2)	
		Total Number	# filled (Exclude calcite only)	Total # Calcite	# Calcite Only	Calcite and Other	Filled (Exclude calcite only)	Calcite Filled
0213	epidosite	117	49	30	22	8	n.d.	7.95E–10
0701	epidosite	69	31	29	24	5	n.d.	5.23E–10
1037	epidosite	96	39	1	1	0	2.39E–09	4.01E–20
1124	epidosite	96	37	5	5	0	4.8E–10	5.30E–19
1129	diabase/shear zone	105	53	44	35	9	n.d.	3.06E–10
1134	epidosite	68	53	30	7	23	7.73E–08	1.59E–08
1137	diabase/A.Koroni	75	33	9	0	9	1.11E–10	6.90E–18
1316	diabase/plagiogranite	108	72	54	49	5	n.d.	1.19E–09
1321	epidosite	109	58	8	1	7	7.09E–09	4.80E–19

n.d. calculations not done

4.3.3.4.3 Effects of Variation in Fracture Density and Fracture Aperture

Several fracture and permeability simulations were run on the fracture data from areas 0108 and 0413 in order to determine the sensitivity of the calculated permeability to changes in the fracture density and fracture aperture distribution. The input values and permeability results are shown in Table 4.11.

The permeability calculations done in this section with reduced fracture density show what the permabilities may have been during a single phase of hydrothermal circulation at an instant in time, rather than an integrated permeability. It should be noted that the reduction levels in fracture density of 25% and 75% were arbitrarily chosen since there is no data available that allows the assignment of fractures to a particular hydrothermal event. The results indicate that permeability decreases with decreased fracture density. Factors, other than fracture size and transmissivity, such as the fracture interconnectivity, will also affect the permeability.

Reducing the fracture density, through a reduction in the P_{32} value, to 75% and 25% of the original value, resulted in a reduction of the permeability by one to two orders of magnitude.

Further reduction in the fracture density below 25% of the original value resulted in a drop of the fracture interconnectivity below a critical threshold. Below this threshold the number of available interconnected pathways becomes insufficient to support fluid circulation through the rock mass (de Marsily, 1984). At this point it is likely that flow through the fractures is similar to that of flow through the rock matrix.

TABLE 4.11 SENSITIVITY ANALYSIS RESULTS

Scanline	Fracture Density (P32) (% of originial)					
	100%		75%		25%	
	Permeability (m^2)					
	Mean	Std.dev.	Mean	Std.dev.	Mean	Std.dev.
0108	2.09E−08	1.27E−08	1.33E−08	9.14E−10	3.32E−10	5.91E−11
0413	5.14E−11	3.26E−11	2.40E−11	1.31E−11	4.69E−13	4.26E−13

Scanline	Transmissivity (m^2/s) (% of original)*					
	100%		75%		25%	
	Permeability (m^2)					
	Mean	Std.dev.	Mean	Std.dev.	Mean	Std.dev.
0108	2.09E−08	1.27E−08	1.50E−08	7.44E−10	3.50E−09	3.69E−10
0413	5.14E−11	3.26E−11	2.74E−11	6.74E−12	3.97E−12	1.24E−12

*for aperture to transmissivity conversion see Table 4.8

Permeability varies as the square of the fracture aperture. This means fracture aperture variations will have a large affect on the calculated permeability. Reducing the fracture aperture through a reduction in transmissivity was done to, firstly, determine the effects of aperture variation on the resultant permeability; and secondly, to simulate the effects of fluid circulation through fractures which had been used and partially infilled by a previous phase of fluid circulation (and mineral growth). Fracture apertures measured in the field (Section 3.3.2) are based on the complete fracture width. Thus multiple hydrothermal events utilizing a particular fracture may each be able to access a fracture aperture which is only a fraction of the total fracture width.

Some fractures contain multiple mineral fillings. The total fracture aperture at the end of the initial hydrothermal circultory phase is then equivalent to the width of the first mineral to be precipitated in the fracture. This total aperture was not necessarily the fracture aperture at any one time period in time. However, because of a lack of evidence to the contrary, these apertures can be used to calculate permeabilities that may have been present during the time period of an initial phase of hydrothermal circulation. Observation of fractures in thin section indicated, that in a fracture filled with two minerals (containing epidote and later quartz), the epidote filling occupied between one quarter and three-quarters of the fracture apertures. Reducing the mean of the fracture aperture distribution, to 75% and 25% of the original value, resulted in a reduction of the permeability by two to three orders of magnitude.The previous calculations of permeability (Section 4.3.3.4.1) assumed that all fractures filled with high temperature hydrothermal minerals were formed during the same phase of hydrothermal fluid circulation. Since hydrothermal fluid circulation was thought to take place at the same time as the formation of the sheeted dykes (e.g. field relationships shown in Plate 2.2), some fractures may not have existed at the time of

a particular phase of hydrothermal fluid circulation. This implies firstly, that if multiple phases of hydrothermal fluid circulation occurred in a particular area, not all fractures were present or available as fluid conduits; and secondly, that the calculated permeability in Section 4.3.3.4.1 is an integrated permeability which may not have been realized during any one specific hydrothermal event.

4.3.3.5 *Comparison of the Methods of Permeability Determination*

The results of the three methods of determining permeability in the fractured rocks in the Spilia-Politiko area are presented in Table 4.12. These results indicate that the FracMan/MAFIC method generally gives the lowest permeabilities. The FracMan/MAFIC permeabilities are considered to be more reasonable results because they take into account discontinuous fractures, and fracture interconnectivity, which the other two methods do not address. However, the FracMan/MAFIC results are critically dependent, as are the other two methods, on the fracture apertures. The field-measured fracture apertures are not good estimates of the true apertures for the following reasons: 1) fracture apertures are not constant over the fracture plane; 2) apertures measured in the field are not hydraulic apertures, which are invariably less; 3) asperities on the fracture plane result in channelization of flow (Tsang and Tsang, 1989) which will reduce the effective hydraulic aperture. For this reason, and because the permeability is dependent on the cube of the fracture aperture, it is necessary, in present studies to validate the modelling results through actual flow tests conducted in the field. In this study, it is not possible to do this, for reasons previously outlined (Section 4.3).

TABLE 4.12 COMPARISON OF CALCULATED PERMEABILITIES BETWEEN
1) PARALLEL PLATE METHOD
2) BIANCHI AND SNOW (1969) METHOD
3) FRACMAN/MAFIC METHOD

SCANLINE	LOG-PERMEABILITY (m^2) PARALLEL PLATE	BIANCHI AND SNOW	FRACMAN MAFIC
0000	-8.91	-9.53	-9.86
0108	-7.54	-6.54	-8.49
0112	-8.89	-7.79	-11.70
0122	-7.00	-6.24	-8.97
0401	-7.77	-6.68	-10.46
0413	-8.70	-8.23	-10.98
0418	-6.73	-5.91	-9.42
0428	-10.22	-8.35	-11.72
1037	-10.40	-8.51	-9.24
1124	-7.57	-10.07	-9.77
1134	-8.15	-8.36	-7.86
1137	-9.89	-7.01	-10.61
1222	-10.55	-8.30	-9.84
1321	-7.96	-7.04	-8.79

NOTE: LOG-PERMEABILITIES ARE LOG BASE 10
E.G. -8.91 = 1.26 X 10E-09

Comparison of the stochastic method of determining fractured rock permeabilities to the previous two deterministic methods, reveals the following:

1) The magnitudes of the permeabilities are lower than those calculated with the two deterministic methods; they are closer to the permeabilities determined beneath the seafloor (e.g. Anderson and Zoback, 1982);
2) The use of finite fracture radii means that fracture interconnectivity becomes an important parameter in determining the flow through a simulated block. This more closely approaches reality than do the assumptions of continuous fractures in the region of interest as assumed by the other methods;
3) The MAFIC flow modelling method of permeability determination precludes being able to calculate the principal permeability directions. This can only be calculated directly from the fracture properties, a capability that has not been included in the program FracMan. The principal permeability directions were determined through the Bianchi and Snow (1969) method. Those results, though, are biased as a result of the initial assumption of fracture continuity in the region of interest;
4) The stochastic method is more computation intensive than the deterministic methods. A minimum of a SUN workstation with 32 megabytes of random access memory, using the UNIX operating system was needed to run the simulations;
5) The stochastic method has the capability to model three dimensional systems of fractures without deterministic knowledge of every fracture within the rock block. This is a great advantage, in that it is not possible to measure every fracture in a block of rock. This method does mean that several simulations must be made of every dataset in order to obtain statistically representative results.

While all three methods result in permeabilities that are several orders of magnitude greater than those measured at the present-day seafloor, the stochastic fracture network generation method gives results closest to those at the seafloor and makes the least assumptions. The method of determining permeability at the seafloor, through down-hole packer tests, gives a bulk permeability magnitude; principal permeability directions can not be determined from this. It should be remembered that the bore-hole tests were done at off-axis locations. The Bianchi and Snow method does result in the calculations of principal permeability directions, but it makes the assumption of continuous fractures. Better field data, especially with respect to fracture apertures are needed to be able to compute permeabilities that approach the magnitude of those at the seafloor. To be able to compare these results with permeabilities in presently active hydrothermal areas, bore-hole tests should be done in the vicinity of, or on, ridge axes.

4.4 STRESS CONSIDERATIONS

When a rock mass, not bounded by a free surface (i.e. wholly contained within a larger rock mass), is subjected to a stress field that causes it to exceed its tensile strength, a minimum of five sets of fractures form (some more important than others) to overcome space problems (Paterson, 1978). Thus, it is quite complicated to unravel the paleo-stress conditions. A problem encountered with the data from the study area is that there do not appear to be multiple sets of fractures within the various domains.

To establish the stress field orientation at some point in the history of the rock mass, it is necessary to identify at least two contemporaneous conjugate fracture sets, assuming that there was a free surface nearby (Scheidegger, 1982). As can be seen

from the stereographic projections of the various scanlines and domains (Appendix A.3.1), it is not possible, in general, to identify more than one clustered set of fractures.

As discussed in Chapter 3, fractures noted in the study area consist of roughly three types: 1) dyke margin cooling fractures; 2) columnar jointed cooling fractures; and 3) remaining fractures which do not fit into either type 1 or type 2. Type 1 fractures are formed when hot magma is juxtaposed against older relatively cold rocks (in this case other dykes). Their orientations reflect formation in a rock with a well-developed sheeted fabric, and so do not necessarily indicate the stress field orientation. Type 2 fractures form later than type 1 fractures as a result of contraction-on-cooling of the dyke, and so reflect local thermal stresses and room considerations but not a regional stress field. The remaining fractures show no well-developed pattern (i.e. conjugate sets), and their formation times likely spanned several stress field orientations.

The study area is composed almost entirely of sheeted dykes indicative of formation in an extensional environment. In such an environment the least compressive stress is oriented parallel to the direction of spreading and, it is believed, parallel to the normal to the dykes.

Thus, on the basis of the analogy to the present day oceanic lithosphere, the stress field was probably oriented such that S_1 (maximum compressive stress) was vertical and parallel to the sheeted dyke margins; S_2 (intermediate compressive stress) was horizontal and parallel to the dyke margins; whereas S_3 (minimum compressive stress) was perpendicular to the dyke margins and the spreading ridge axis. The fracture data do not allow further refinement of this interpretation.

4.5 SUMMARY

In summary, the following points can be stated concerning the foregoing sections of this chapter:

(1) Relative fracture ages (cross-cutting and filling) based on the timing of fluid utilization of the fracture, for the study area, demonstrate that epidote fillings were the first to form, while calcite fillings were the last to form.

(2) From the viewpoint of modelling fracture networks in three dimensions, a better measure of fracture intensity is that of total fracture area per unit rock volume. Estimates of this measure indicate a fracture intensity of 1.08 m^2/m^3.

(3) Fractured rock permeabilities were calculated via three methods: parallel-plate; Bianchi and Snow (1969); and discrete-fracture modelling. The first method gave permeabilities of the same order as those calculated by the same method for the Semail ophiolite, but they underestimated permeabilities measured from borehole testing in the oceanic crust by seven orders of magnitude. The Bianchi and Snow method gave results, for dyke-parallel fractures, similar to those of the parallel-plate method. When all fractures were taken into account the resulting permeabilities were higher by one or two orders of magnitude. The permeability calculated using the discrete-fracture method were lower than those for the parallel-plate method but only slightly lower than those calculated for the Bianchi and Snow (1969) method.

(4) Permeabilities decrease deeper in the section, as expected, based on calculations done via all three methods. The permeabilties based on hydrothermally filled fractures are several orders of magnitude higher than those based on calcite filled fractures. An exception is for sections near shear zones and

plagiogranites, where permeabilities based on calcite-filled fractures are of similar magnitude to the hydrothermal mineral-filled fractures.

(5) Reduction in both fracture density and fracture aperture to 25% of their original value, results in the reduction of the calculated permeability of between one and three orders of magnitude.

(6) Permeability anisotropy resulting from the calculations indicates that, in the absence of faults, the major fluid pathways are along dyke-parallel fractures.

(7) Principal permeability directions tend to rotate in a clockwise direction from north to south in the study area. This is thought to be due to lateral movement along the South Troodos Transform Fault.

(8) Fracture shape: the fracture trace length distribution is better estimated by elliptical log-normally distributed fractures of aspect ratio 0.6, than by circular fractures or other distributions.

(9) Fracture radius: the measured distribution of fracture trace lengths was found to be estimated well by log-normally distributed fracture radii with a mean of 1.6 to 2.6 metres. There was no significant variation from area to area.

(10) Stress: in an extensional environment where dykes are thought to form in vertical sheets, the least compressive stress is in the horizontal plane parallel to the direction of spreading, whereas the intermediate and maximum compressive stresses lie in a vertical plane parallel to the spreading axis.

5. NATURE AND DEVELOPMENT OF THE SHEETED DYKE COMPLEX

5.1 INTRODUCTION

In this chapter, a model is presented for the nature and development of the sheeted dyke complex of the Troodos ophiolite based on the structural framework, the fracture characteristics and the perceived hydrothermal history of the Spilia-Politiko area discussed in Chapters 2 through 4.

The Sheeted Dyke Complex in the Troodos Ophiolite is analogous to Layer 2B sheeted dykes of the oceanic crust (Cann, 1974, Kennett, 1982). Layer 2B crust (Figure 1.1) forms the interface or distribution system for the transport of magma from the magma chamber at depth (Layer 3) to the extrusive volcanic rocks on the seafloor (Layer 2A). In the following sections, the development of the sheeted dyke complex is presented using a series of idealized schematic drawings that illustrate a model for the development of the magma chamber, formation and deformation of the sheeted dykes, and the development of fracture and permeability characteristics that affect hydrothermal circulation in the ocean crust, based on the data presented in the previous chapters. The properties of the sheeted dyke complex, including tectonic features, fracture and permeability characteristics, and hydrothermal alteration as inferred from the Spilia-Politiko area, are summarized in Table 5.1.

TABLE 5.1 SHEETED DYKE COMPLEX PROPERTIES

TECTONIC FEATURES

dyke formation

- multiple (different) contemporaneous magma sources
- orientation controlled by ridge orientation and presence of transform fault

graben structure formation

- dependent on magma budget and rate-of-extension relationships
- on-axis - preservation if ridge jump occurs
- off-axis - preserved in record; may cross-cut dyke strike
- generally asymmetric - may be related to presence of subduction zone

faulting

- extensional
  - spreading ridge related - normal (dip in part related to spreading rate)
  - graben related - normal
- strike-slip
  - related to shear along transform fault

FRACTURE CHARACTERISTICS

apertures

- log-normally distributed
- decrease with depth
- remain open at depth - as a result of fluid pressure
- dyke parallel fractures open further - dependent on stress field orientation

utilization

- 50% of fractures not used by fluids - probably not interconnected

size

- log-normal distribution of outcrop-scale fracture radii (mean = 2 metres)
- ranges from microscopic to mega-scale (30 kilometres)
- distribution is log-normal at all scales of measurement

termination

- younger fractures abut against older fractures
- most fractures terminate against another - large degree of interconnectivity
- most fractures related to contraction cooling of the dyke after injection
- late stage fracturing more common at shallow crustal levels
- shallow crustal levels likely have more than one generation of fracturing

intensity

- greater than 1 metre^2 of fracture surface area per 1 metre^3 of rock volume
- no change with depth in the sheeted dykes

orientation

- follows cluster (dyke-parallel) or girdle (columnar joint) distribution
- dependent on amount of rotation during graben formation

TABLE 5.1 SHEETED DYKE COMPLEX PROPERTIES (CONTINUED)

HYDROTHERMAL ALTERATION FEATURES

fluid circulation
- 300° to 360°C average fluid temperatures
- seawater salinities
- phase separation at depth beneath layer 2B in plagiogranites
- possible phase separation above layer 2B in stockwork
- 50% of fractures not affected by fluid circulation

fracture opening
- vertical fractures open during extension - high temperature fluid circulation
- horizontal fractures open during uplift - waning hydrothermal circulation

hydrothermal cell dimensions
- upflow: 150 metres (dyke parallel) by 50-100 metres (perpendicular)
- overall: assumed ~4 kilometre diameter elongate parallel to dyke strike

hydrothermal cell location
- fault controlled
- dependent on heat source location and shape (point or line source)

material source for ore deposits
- diabase dykes - leached of metals and altered to become epidosites

distribution of circulation
- related to ridge axis, heat source shape and size - uniformly distributed

PERMEABILITY CHARACTERISTICS

dyke parallel
- $6.9 - 4.5 \times 10^{-10}$ metres^2
- little spatial variation

permeability tensor
- anisotropic ($K_1 \approx K_2 > K_3$) - dyke parallel

permeability timing
- reduces with time

faults
- control permeability if 2 orders of magnitude > fracture permeability

5.2 THE TROODOS OPHIOLITE AS AN OCEANIC ANALOGUE

The Troodos ophiolite is thought to represent oceanic crust (Anonymous, 1972; Church, 1972), although, historically there has been much controversy over whether it represents a mid-ocean ridge (MOR) or a supra-subduction zone (SSZ) environment (Gass, 1990) (Section 2.2.1). It is now accepted that the Troodos ophiolite formed in a supra-subduction zone setting (e.g. Malpas et al., 1990). In general, extensional environments in SSZ settings are on a smaller scale than the mid-ocean ridge systems. However, like MOR settings, they show both fast (e.g. Lau Basin, Nautilau Group, 1990) and slow (e.g. Tyrrhenian Sea, Kastens et al., 1988) spreading characteristics. Consistent sub-parallel dyke strikes show that regional, rather than local, stress fields were dominant, and that dykes were passively injected from magma chambers along tension planes (e.g. Gass, 1990). Well-defined linear magmatic anomalies have been found both in SSZ environments (Scotia Sea; Barker and Hill, 1981) and in MOR environments (e.g. Atwater and Molnar, 1973). The geochemical signature of the rocks in a SSZ setting differs from that of MOR rocks by enrichment in components derived from the downgoing slab of lithosphere. The physics of heat flow and crustal formation, however, are not likely to be different from those at mid-ocean ridges.

Oudin and Constantinou (1984) and Oudin et al. (1981) found that common textural and paragenetic evidence from the sulfide deposits of the East Pacific Rise and the Troodos ophiolite, Cyprus, suggests that the genetic processes forming the deposits were the same. The physical processes of crustal accretion which occurred in the Troodos ophiolite are likely to have been similar to those occurring at accretionary boundaries, be they in MOR or SSZ settings (Section 2.2.1).

TABLE 5.2 Comparison of slow versus fast spreading rates at spreading centres (after Macdonald, 1983; and other sources referred to in text). Abbreviations: LVZ = Low Velocity Zone, OSC = Over Lapping Spreading Centre, MC = Magma Chamber.

Spreading Rate ==>	Fast	Slow	Troodos Ophiolite
Spreading rate (% of all ridges)	9–18cm/yr (56%)	1–5cm/yr (44%)	?
Axial seismic LVZ	Yes	No	?
Seismic reflection off magma chamber	Yes (inferred depth = 1–3 km; width = 1–3km; length to 10km)	Yes (inferred depth = 5–10 km; width = 5–10km)	Multiple, small (0.5–3km) MC
Axial gravity anomaly	Interpretation = MC	Interpretation no MC; mechanically strong	?
Inferred eruption rates	50–500 yrs	1000–10000yrs	?
Hydrothermal activity	Common 300–350 deg.C	Yes >300deg.C	Yes (>300 deg.C)
Thermal models	Most models support steady state MC	Most models suggest transient MC	Probably transient MC
Depth of axial zone	Smoothly varying	Highly variable, rough	?
Temperature gradient	High (oscillatory pattern on flanks)	Low	?
Axial valley	No (axial high)	Yes (axial graben)	Graben structures present (infer axial valley)
Axial neovolcanic zone	High degree on continuity along strike (shield volcano)	Highly discontinuous (string of volcanoes)	?
Axial relief	Small 50–100m	Large 100–2000m	Sediment/extrusive boundary has low relief
Transform spacing (ridge offsets > 30km)	90km (OSC's) 500km	50km 170km	?
Fault facing direction	Inward=outward dipping	Inward dipping dominant	?
Maintenance of transform fault pattern	Unstable for small offset; OCS's common	Stable	?
Propagating rifts	Common	Rare	?
Extension	Magmatically controlled	Magmatic and tectonic	Magmatic and tectonic
Petrologic data	Infer steady state MC	Infer steady state MC	Infer transient multiple MC
Seismic data	Infer steady state MC with thin melt layer	Infer transient MC	?

Much confusion exists in the literature regarding the relative spreading rate of the Troodos oceanic crust during its formation. Table 5.2 compares the Troodos ophiolite with fast and slow spreading oceanic crust. Fast spreading for the Troodos paleo-spreading environment has been proposed on the basis of the low sediment/extrusive interface relief (Cleintaur et al., 1977; Allerton and Vine, 1991); large areas of undeformed dykes, probably formed during long periods of uninterrupted magma injection (Allerton and Vine, 1991); and small rotations of dykes, such as seen in the Makhaeras (Figure 1.2) dyke domain and other areas of the Troodos ophiolite, indicative of long periods of magmatism keeping pace with spreading rates (MacDonald, 1982). Intermediate spreading rates have been proposed on the basis of comparison of fault throws between the Mathiati area and mid-ocean spreading centres (Boyle and Robertson, 1984). Slow spreading rates have been proposed on the basis of similarities between the dimensions of the Solea graben with throws of 300-800 metres along normal faults, and those of mid-Atlantic ridge valleys (Varga and Moores, 1985). Chapter 2 showed that the Troodos ophiolite probably formed in an intermediate to fast spreading environment punctuated by periods of tectonic thinning and low to no magma budget.

5.3 NATURE AND DEVELOPMENT OF THE SHEETED DYKE COMPLEX

The formation of the Sheeted Dyke Complex in the Troodos ophiolite depended on the rate of supply of magma, and stress conditions. An increased magma budget may have resulted in magmatic spreading, possibly at a fast rate. Periods of a decreased magma budget may have been concomitant with tectonic (amagmatic) spreading. Both magmatic and tectonic spreading appear to have contributed to formation of the

Troodos ophiolite: large areas of steep, undeformed dykes in the Makhaeras domain imply a continuous magma supply, whereas the formation of grabens and rotations of dykes about strike-parallel axes implies lack of a magma supply accompanied by tectonic stretching (Chapter 2).

5.3.1 Magma Chamber Model

Field work in the Plutonic Complex, of the Troodos ophiolite, showed that magma chamber sizes are 0.5 to 3 kilometres in their long (paleo-horizontal) dimensions, (Dunsworth, 1989; Dunsworth and Calon, 1984). Studies of cryptic layering in the plutonic rocks in the CY-4 drill hole (Browning et al., 1989; Sinton and Detrick, 1992) show that the melt portion of the magma chambers may have only been a few tens to a few hundreds of metres thick. Evidence from hydrothermal alteration (Sections 5.3.5) also suggests discrete small magma chambers existed in the Troodos crust.

Magma chambers beneath the seafloor were historically considered to be large bodies with sizes of the order of major transform fault spacings (e.g. Gass, 1979). Recent work in ophiolites, such as in the plutonic section of the Troodos ophiolite (Dunsworth, 1989; Malpas et al., 1989a), and seismic reflection surveys of oceanic crust (Detrick et al., 1987; Kent et al.,1990; Morton and Sleep, 1985) which indicate the magma chambers are multiple, smaller, transient bodies with melt layer widths and thicknesses of 800-1200 metres and 10-50 metres, respectively.

The geochemistry of the sheeted dykes is highly variable, but, this variance is not correlated with either temporal or spatial relationships (Section 2.3.2.2 and Appendix B.2). The observed variation in the geochemistry of the dykes implies that multiple injections from at least two chemically different sources of magma operated contemporaneously.

The field evidence, in the form of extensive syn-kinematic, large-scale, high-angle faulting, extending as far down as the residual mantle section (Calon, pers. comm., 1989) in the Troodos ophiolite, suggests a deep-seated brittle-ductile transition and a low thermal gradient. This, for the nature of the intrusions and the faults in the Troodos ophiolite suggests that small, transient magma chambers utilized fault systems in the crust (Figure 5.1)(Sinton and Detrick, 1992). The implications of small transient bodies for the formation of the crust and the development of fracture and hydrothermal systems are: increased chemical variability in the sheeted dyke population over small areas; the formation of interfingering dykes from different sources; and the formation of localized hydrothermal circulation cells. These implications result partly because these magma bodies are point sources of heat both in space and time.

5.3.2 Formation of the Sheeted Dyke Complex

Dyke orientations in the Spilia-Politiko area can be used to define dyke domains (Section 2.3.2.1). Abrupt changes in dyke trend define the domain boundaries; abrupt changes in dyke dip define the boundaries of sub-domains. The formation of discrete dyke domains in the Sheeted Dyke Complex of the Spilia-Politiko area, typically 3 to

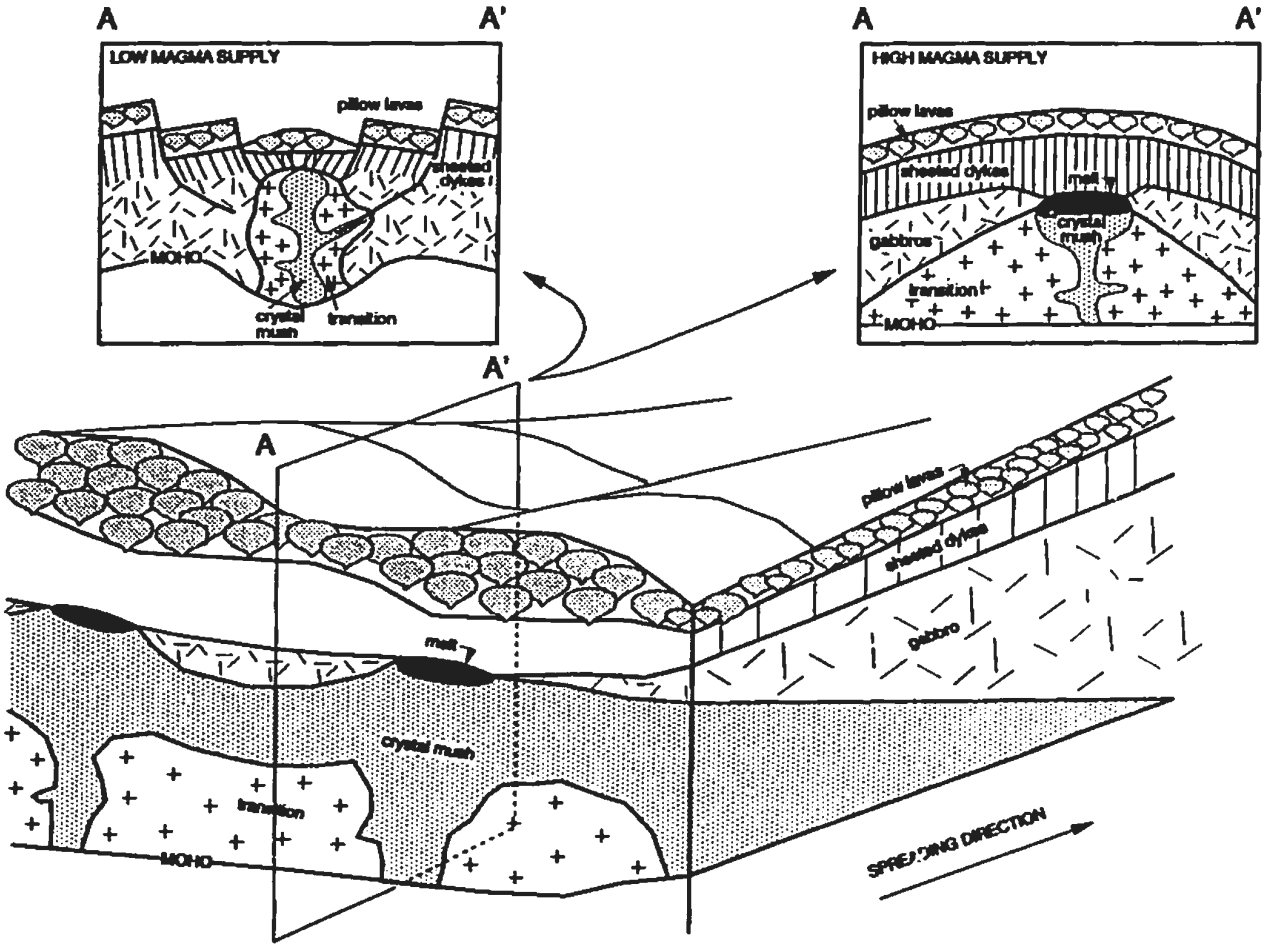

FIGURE 5.1 MAGMA CHAMBER MODEL (AFTER SINTON AND DETRICK, 1992). SECTIONS SHOW TWO END-MEMBER CASES: A) LOW MAGMA BUDGET - AMAGMATIC EXTENSION AND B) HIGH MAGMA BUDGET - MAGMATIC EXTENSION.

5 kilometres across, most likely reflects periods of continued spreading when there was no change in the orientation of the local stress field at the spreading centre. Abrupt changes in dyke orientation at the domain boundaries, typically over 500 metres, imply rapid changes in the stress field orientation or long periods of low to no magma budget accompanied by gradual change in the stress field orientation with respect to dyke formation. The former is favoured since long periods with no magma budget would be accompanied by amagmatic extension and rotation of dykes. This implies that the amount of dip-rotation of the dykes should change abruptly at the domain boundaries which is not the case. Local variations of dyke orientations are greatest near the boundaries of rock units such as at the transitions between the extrusive/sheeted dyke and the gabbro/sheeted dyke (Section 2.3.2.1). This likely reflects anisotropy in the stress field due to contrasting lithology.

The number of dyke margins measured along a scanline increases toward the south of the Spilia-Politiko area (Figure 3.12). Whereas this may indicate a decrease in dyke width with depth, it may also reflect increased splitting of the dykes with depth through intrusion by other dykes. Pulses of magma injected into the crust from a magma chamber are more likely to split pre-existing partially molten cores of dykes nearer the magma source resulting in a greater number of dyke margins. Dyke width may be controlled by the regional principal stress field at the time of dyke emplacement and the pressure of the intruding magma (Helgason and Zentilli, 1985).

At the seafloor, pillow and flow sequences generally lie horizontally or dip a few degrees (Rona, 1984). Near right-angle contacts between pillow and flow sequences and the sheeted dykes (e.g. near Ayia Marina and near Ayios Epiphanios), indicate that the dykes were injected vertically into the crust (Section 2.3.3), assuming the

extrusive volcanic rocks were originally horizontal. Dykes, in the field area, commonly have only one chilled margin. Opposite sides of the same dyke are often separated by a few metres to tens of metres by intervening dykes. This indicates that injection occurred either along the centres of split dykes or along existing dyke margins. Dykes often show striae, related to the injection of the magma, trending at low angles, and elongated vesicles whose elongation directions vary from vertical to sub-horizontal (e.g. near scanline 1111 - Spilia-Lagoudhera road and at scanline 1137 - Ayia Koroni section). The mode of migration is dependent on the magma pressure and the conduits available for magma transport. This phenomenon in the Troodos ophiolite was alluded to by Baragar et al. (1987) and Nash (1979), and has recently been shown on the basis of anisotropy of magnetic susceptibility data (Staudigel et al., 1992). Lateral injection of magma which subsequently rises to form vertical sheets should not significantly affect the final dyke orientation. Late dykes cutting the volcanics are rare in the study area, implying that late dykes did not penetrate the full thickness of the crust or, more likely, that off-axis volcanism was uncommon.

Dykes form when magma from a magma chamber is injected into the overlying crust along planes of tension (e.g. fractures and faults), in a narrow zone of intrusion (Kidd and Cann, 1974; Rosencrantz, 1982) at the spreading ridge axis. The ridge axis and transform fault orientations control the orientation of dykes. Dyke planes lie parallel to the spreading ridge axis and form planes of pre-existing weakness in the crust for subsequently injected dykes (Figure 5.2A).

Near a ridge-transform intersection (RTI), the principal stress orientations rotate and are different from those at the ridge axis far from the RTI. This results in the

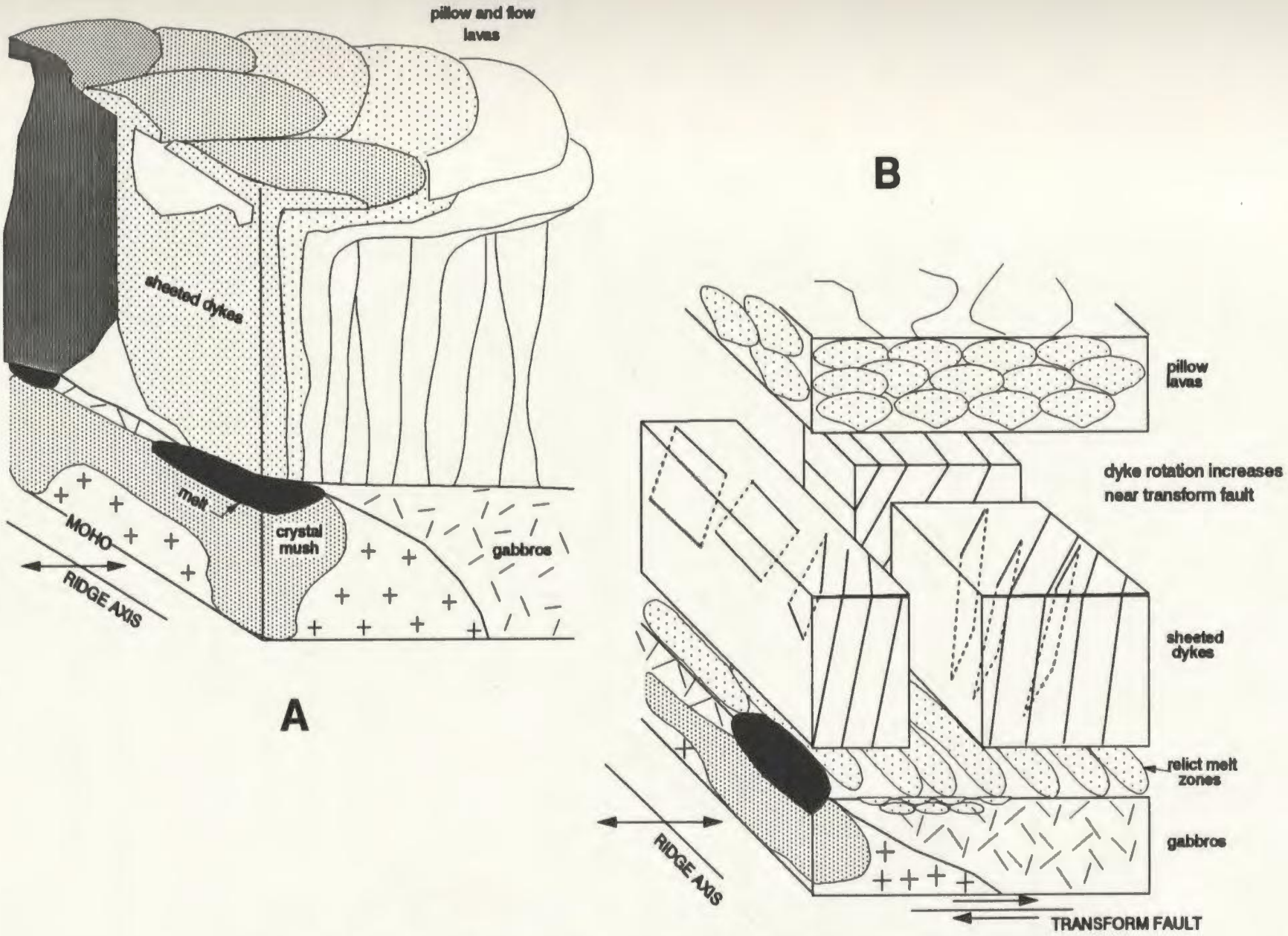

FIGURE 5.2 DYKE EMPLACEMENT (A) AWAY FROM AND (B) NEAR A TRANSFORM FAULT.

injection of dykes at increasing angles to the ridge axis, nearer the RTI (Figure 5.2B; Section 2.3.2). Oceanic transform faults can affect newly forming dykes at distances up to 10 kilometres from the transform zone (Karson, 1987). Dyke orientations in the Spilia-Politiko area are not always parallel to the assumed north-south trending ridge axis but show consistent change in orientation to the south toward the South Troodos Transform Fault (STTF). Dyke orientations in the Spilia-Politiko field area suggest that the effects of the STTF on dyke emplacement extend 12 kilometres to the north of the fault zone (Section 2.3.2). More than two thirds of strike-slip faults trend north-south perpendicular to the trend of the STTF (Table 2.2).

An upward bulge in the crust at the ridge axis, due to either asthensopheric upwelling or magma buoyancy, may cause the development of an axial caldera (Haymon et al., 1991). In either case, the brittle dyke sequence is cut by ridge-parallel normal faults during upwelling. Movement of dyke blocks along these faults results in the formation of an axial caldera. Continued magmatic spreading causes these faulted blocks to move up and over the caldera walls and then eventually down towards the abyssal plain. This involves reverse fault motion through reactivation of the previously formed normal faults (inversion tectonics) (Figure 5.3).

Karson (1987), on the basis of field work in the Bay of Islands ophiolite, Newfoundland, suggested that dyke orientations are controlled by shear along transform faults and by the depth to the brittle/ductile transition. These conditions result in the dyke orientations shown in Figure 5.4A, where, dykes at shallow depths form in tension gashes trending away from the RTI, and dykes below the brittle/ductile transition trend progressively more toward the RTI. MacLeod et al. (1990), on the basis of observations in the Troodos ophiolite, suggest that dyke

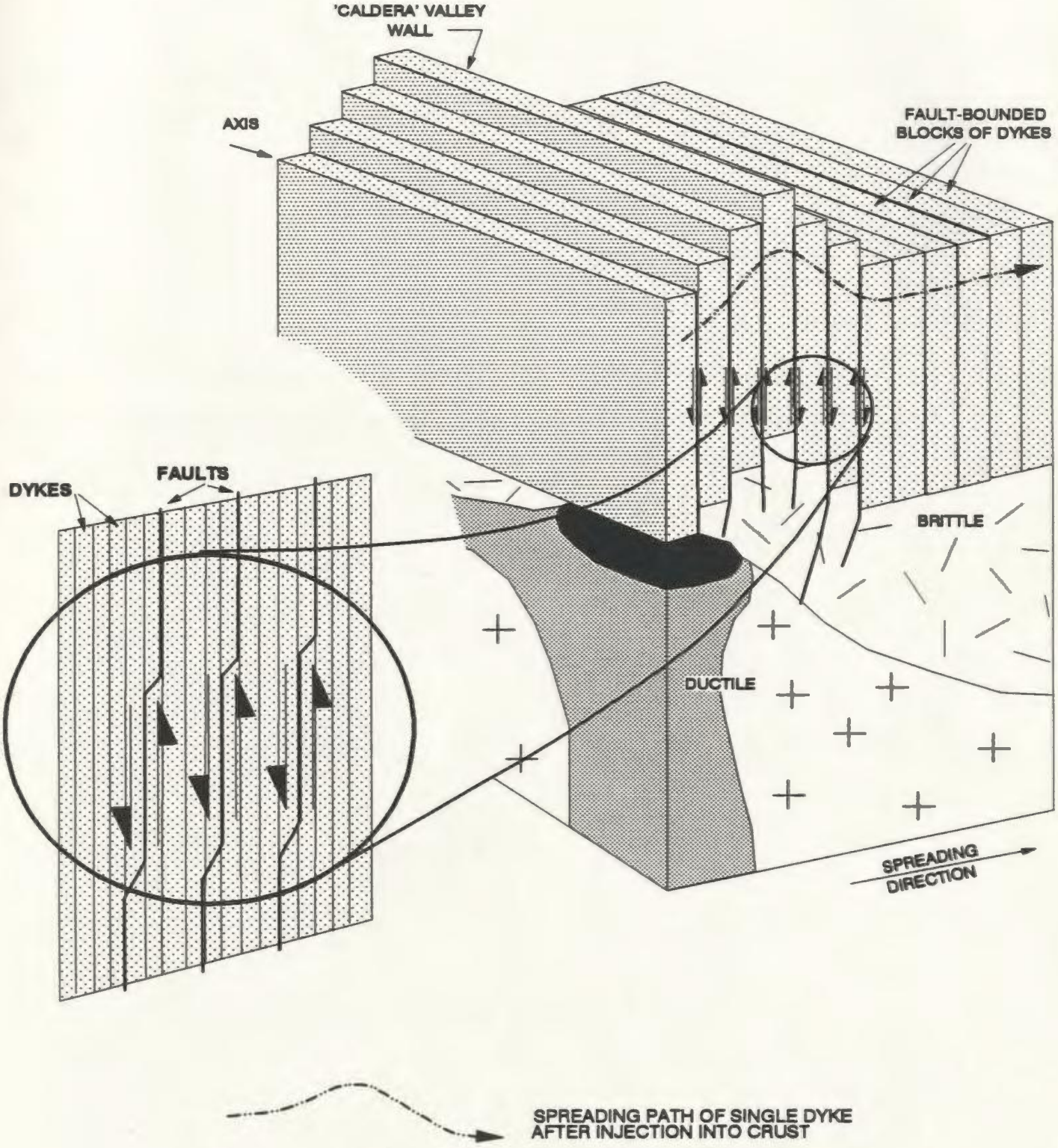

FIGURE 5.3 DYKE EMPLACEMENT AT A RIDGE AXIS FAR FROM A TRANSFORM FAULT. SCENARIO OF PERFECT ISOSTATIC READJUSTMENT. FILL PATTERNS FOR LOWER CRUST AS IN FIGURE 6.1.

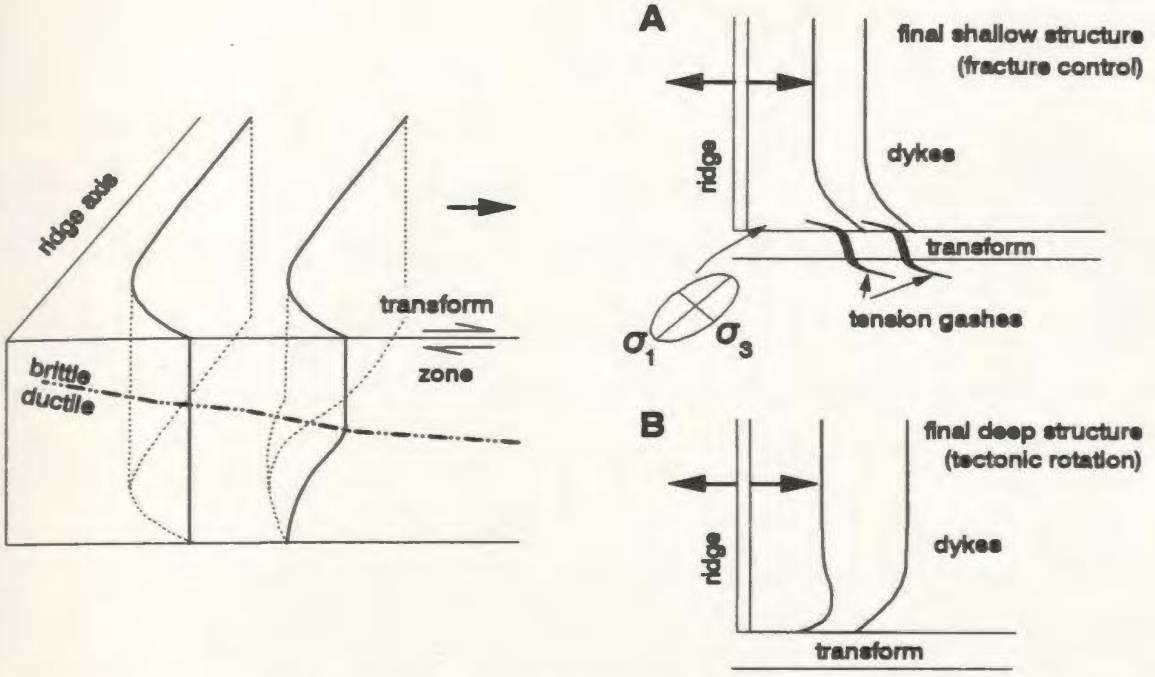

FIGURE 5.4A DYKE CHARACTERISTICS NEAR A RIDGE-TRANSFORM INTERSECTION, USING A SINISTRALLY OFFSET TRANSFORM WITH DEXTRAL SHEAR (AFTER KARSON, 1987; ALLERTON AND VINE, 1991). A) SHOWS SHALLOW DYKE ORIENTATION CONTROLLED BY TENSION GASHES; B) SHOWS DEEPER DYKE ORIENTATION CONTROLLED BY TECTONIC ROTATIONS. BOTH A AND B SHOW LATE STAGES AFTER SOME SPREADING.

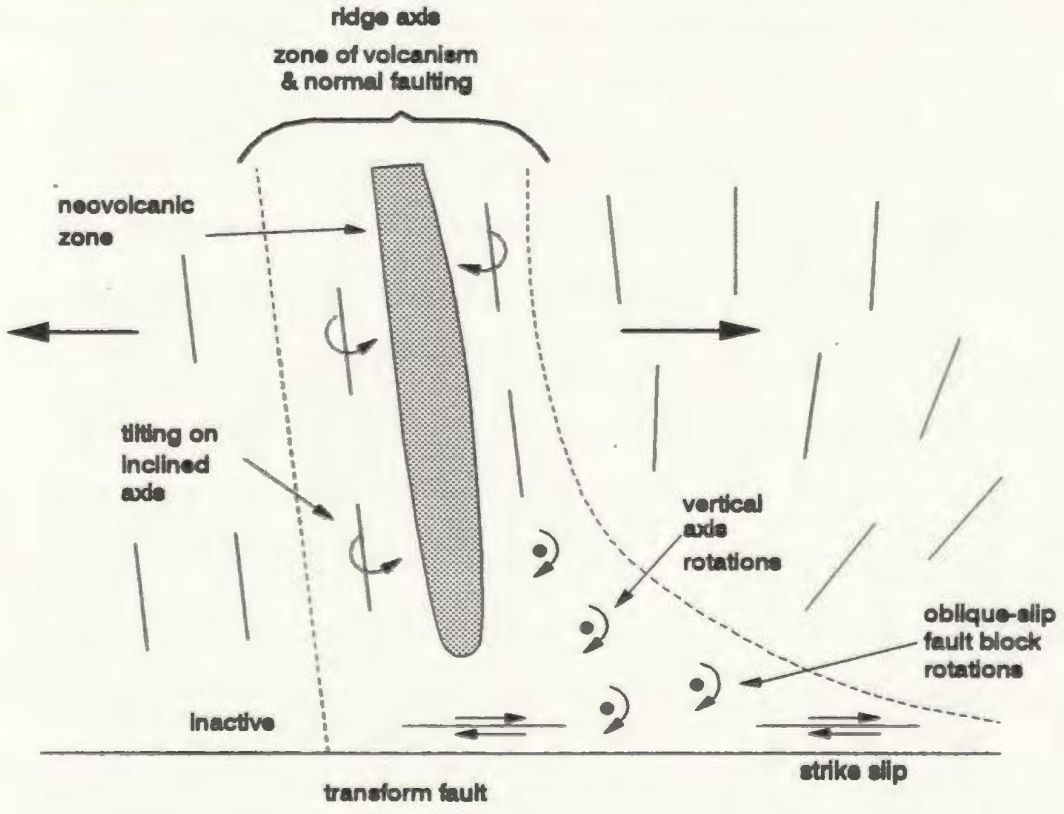

FIGURE 5.4B DYKE ORIENTATION AFTER INJECTION AT A RIDGE-TRANSFORM INTERSECTION (AFTER MACLEOD ET AL., 1990).

orientations are controlled entirely by tectonic rotations in the vicinity of the RTI (Figure 5.4B). They state that virtually all the of rotation of the dykes is accommodated in the vicinity of the RTI, whereas, Karson's (1987) model implies that continued rotation, in the active transform zone, will take place at depth, but not in the brittle zone. The continued clockwise swing of dyke orientations in the Spilia-Politiko area toward the south (e.g. Figure 2.6), tends to support the MacLeod et al. (1990) deduction.

Dykes thought to be injected vertically into the crust may later tilt. The tilting of dykes occurs either through block faulting (Verosub and Moores, 1981) or through subsidence (Cann, 1974; Rosencrantz, 1982). Dewey and Kidd (1977), using a similar model, noted that the dykes could also remain vertical due to the perfect isostatic adjustment to loading.

The style of tilting may depend on the balance between tectonic stretching and magmatic outflow (Karson, 1987; Karson et al., 1992). If there is episodic magmatic activity, this may lead to block faulting during the tectonic stretching phase, and subsidence during the magmatic outflow stage, causing dykes to dip toward the axis. The weight of the overlying lava pile causes subsidence, in turn causing dykes to rotate away from the axis. This style of deformation is noted in Iceland where dykes rotated away from the spreading axis (Bodvarsson and Walker, 1964).

Dykes at and beyond the edges of the Mitsero graben in the Spilia-Politiko field area, are near vertical (Figure 2.14). Since these areas were the least affected by the graben formation, which is thought to be a late event in the history of the Spilia-Politiko area (Sections 2.3.4 and 5.3.3), they may represent original dyke dips. This implies the

dykes formed and remained in a vertical position throughout the magmatic spreading process (Figure 5.3), and were isostatically adjusted without changes in their dip. This also implies that during spreading away from the axis and the axial caldera, dykes moved along steeply dipping faults. The steeply dipping Gourri fault zone on the eastern margin of the Mitsero graben, may be an example of the steeply dipping faults in this figure. Hydrothermal mineralization is seen along this fault zone indicating its presence early in the history of the area. Later tectonic stretching events will change the dyke dips away from the vertical. The model of Dewey and Kidd (1977) applies only to dykes near a high magma budget ridge axis, and so is not valid for spreading ridges with intermittant or low magma budgets, since it does not predict further tectonic rotations of dykes.

Rosencrantz (1982) stated the sheeted dyke complex is the lid or brittle roof zone of the magma chamber. He ascribed all dyke rotations to subsidence of the overlying lava pile. The findings of this study, however, show that most of the rotation can be ascribed to amagmatic stretching (Section 2.3.3). This is the direct consequence of axial fault formation and off-axis graben formation caused by tectonic stretching.

5.3.3 Graben Formation

The grabens in the Troodos ophiolite were defined, in this and other studies (e.g. Varga and Moores, 1985), on the basis of the dyke facing directions. Dykes dipping toward each other, over large areas, define a graben axis, whereas dykes dipping away from each other define the graben boundaries.

Graben structures may form in both on- and off-axis positions as a result of crustal tectonic extension during periods of low magma budget. However, the formation of on-axis grabens is contemporaneous with the formation of the sheeted dykes at the ridge axis. Thus, the trend of the graben axis is likely similar to that of the sheeted dykes, since both formed under the same regional stress conditions. Graben structures are of finite extent perpendicular to the axis. This means that material forming at the ridge axis, within the graben structure, will eventually spread beyond the edge of the graben. Material passing the edge of the graben, on its way toward the abyssal plain, is likely re-rotated along pre-existing faults.

The Solea graben, to the west of the Spilia-Politiko area, is thought to have formed on-axis at a spreading ridge (Figure 5.5) (e.g. Varga and Moores, 1985). Hydrothermal alteration in the graben is thought to post-date the graben formation and perhaps to be associated with an off-axis position because of its asymmetric shape with respect to the graben axis (Schiffman et al., 1987). The shape of the hydrothermal alteration pattern, however, could have formed on-axis, if crustal accretion in the area occurred in a direction oblique, rather than perpendicular, to the graben axis at slow spreading rates (Atwater and Macdonald, 1977).

Off-axis grabens post-date hydrothermal circulation and are superimposed on the pre-existing fabric of the crust. The trend of the axis of these late structures is not necessarily the same as that of the dykes. The off-axis graben axis was likely oriented perpendicular to the direction of extension at the time of its formation; this orientation may be different from that of the dykes.

A. ON-AXIS GRABEN FORMATION
LOW MAGMA BUDGET
e.g. Solea graben

STEP 1. ON-AXIS FORMATION OF DYKES AND GRABEN

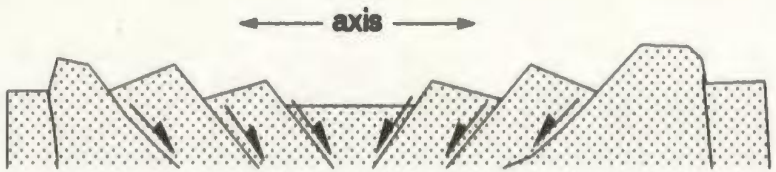

Implications:

- low magma budget leads to amagmatic extension and tilting
- crosscutting dykes in axis area in Solea graben, since area is still volcanically active.
- high magma budget leads to the formation of continuous dyke sequences

B. OFF-AXIS GRABEN FORMATION
HIGH MAGMA BUDGET
e.g. Spilia-Politiko area

STEP 1. ON-AXIS FORMATION OF DYKES AND AXIAL CALDERA

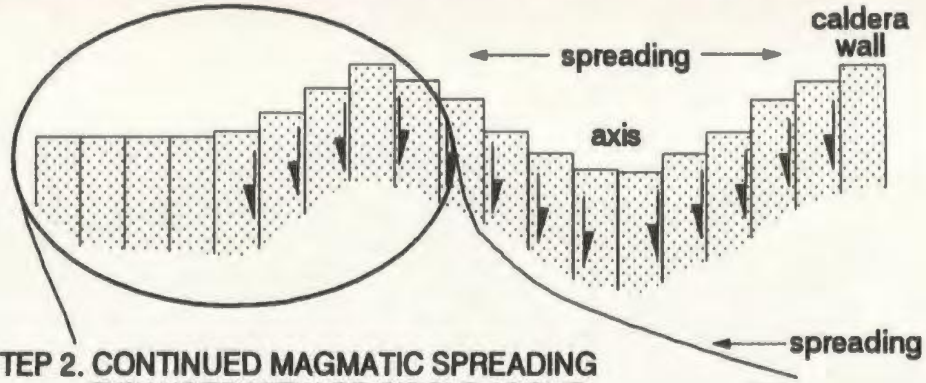

STEP 2. CONTINUED MAGMATIC SPREADING
EXPANDED VIEW OF CIRCLE ABOVE

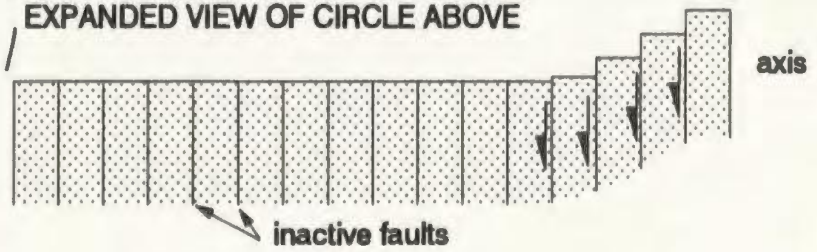



STEP 3. DECREASE IN MAGMA SUPPLY LEADING TO AMAGMATIC SPREADING.

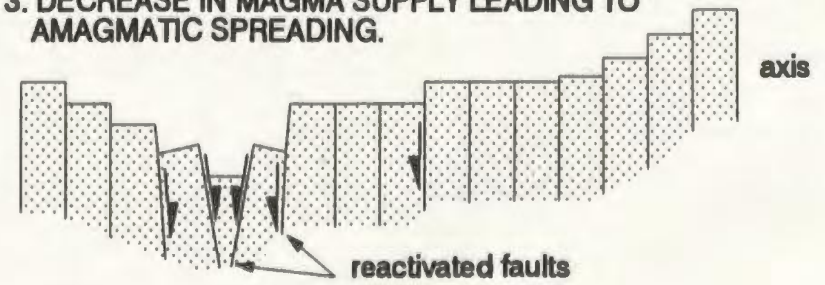

FIGURE 5.5 ON- AND OFF-AXIS GRABEN FORMATION. SPILIA-POLITIKO AREA HAS A COMPOSITE HISTORY OF MAGMATIC SPREADING FOLLOWED BY AMAGMATIC STRETCHING TO FORM THE MITSERO GRABEN. THE SOLEA GRABEN FORMED ON-AXIS DURING AMAGMATIC STRETCHING RESULTING FROM A LOW MAGMA BUDGET.

The present dip of the dykes implies that tectonic extension in the Spilia-Politiko study area caused the formation of the Mitsero graben. More than half the dip-slip faults in the field area trend east-west perpendicular to the graben axis (Table 2.2). Dyke dips are near vertical at the eastern and western boundaries of the graben. In the east-central portion of the field area dykes dip toward each other on opposite sides of a roughly north-south trending line (Figure 2.7). This line is defined as the Mitsero graben axis. The graben axis cuts across the dyke domains and therefore the graben is likely an off-axis late phenomenon (Figure 2.6). Although it is not possible to date the faulting in the field area, non-mineralized faults following the graben axis trend also indicate that graben formation may post-date hydrothermal circulation. If the graben had formed on-axis, the pattern of hydrothermal alteration (Section 5.3.5) would be expected to be symmetrical about the graben axis; it is not.

The Mitsero graben formed through rotation of dykes about an axis, largely parallel to the dyke strike. In the southern portion of the field area, the dyke strike swings from north-south to notheast-southwest, probably as a result of shear along the South Troodos Transform Fault (Section 2.3.2.1). The graben axis also swings to the west but to a lesser extent, again implying formation of the graben under different (later) stress conditions than the dykes. The later super-position of the graben axis on dykes, that had been rotated to some extent already, means that the total rotation of the graben axis will be less than that of the dykes.

Rotation, causing dip changes in the orientations of the dykes, appears to have occurred along faults which are planar at the outcrop scale. The map pattern of the faults suggests the fault traces converge to an area south-east of Palekhori (Figure 2.20). This implies the planar faults may have rotated, forming overall listric

trajectories. The depth of such a listric detachment zone seems to lie within the gabbros, rather than within the sheeted dykes implying cold crust, again, and off-axis graben formation. This is corroborated by the highly altered zone in the drill core of hole CY-4 south of Palekhori (Section 2.3.4), which is possibly a zone of detachment. To the west in the Solea graben, which formed on-axis, the detachment zone lies at the base of the sheeted dykes (Moores et al., 1990). That the Mitsero graben formed off-axis, and not on-axis, suggests that spreading rates in the Spilia-Politiko area were higher than those in the Solea graben area at the time of formation of the dykes, probably a result of more or longer lived (possible replenished) magmatic heat sources.

The Mitsero graben dykes experienced less rotation than did their Solea graben counterparts (Table 2.1); this may be explained in the following manner. An axial graben formed along the ridge axis, resulting in the rotations of dykes along horizontal axes toward the ridge axis, in both the Spilia-Politiko area and the Solea graben. In the Solea graben case, the amagmatic extension added to the net rotations that the dykes had experienced during the formation of the axial caldera. In the case of the Mitsero graben, the material constituting the axial caldera moved off-axis as a result of magmatic extension, back-rotating as the material passed the axial caldera boundary toward the abyssal plain. With the onset of amagmatic extension, the faults were reactivated and a graben structure formed in an off-axis position. However, the later rotations of the dykes, during the formation of the graben, were added to back-rotated dykes.

It appears possible that amagmatic or tectonic extension occurred in three major graben areas: the Solea graben; the Mitsero graben; and the Larnaca graben. The

east-west extension calculated for the Solea graben, whose present width is 15 kilometres, is 45% (Varga, 1991). In the Mitsero graben the average east-west extension is calculated as 12% over a present width of 16 kilometres (Section 2.3.3). The Larnaca graben, which is the least studied graben to date, has an estimated present width of 10 kilometres and an estimated 100% extension (Allerton and Vine, 1991). On the basis of these figures, almost 14 kilometres of the present-day exposure was produced through amagmatic stretching including faulting and block rotation. Some of this tectonic spreading occurred on-axis (Solea graben) and some off-axis (Mitsero graben).

Injection of dykes with different orientations into an area of pre-existing dykes as a result of a ridge jump, can produce areas with complicated and difficult to interpret magnetic lineation patterns. If such a multiply injected dyke package were further affected by superposition of a graben structure, a result of tectonic extension of the crust in an off-axis position, the resulting dyke pattern is further complicated. This may in part explain the somewhat chaotic orientations derived from paleo-magnetic studies of Deep Sea Drilling Project boreholes (e.g. DSDP hole 504B, Kinoshita et al., 1989) and the dyke orientations in the Spilia-Politiko area in domain 6 (Section 2.3.2.1). Domain 6 is defined by two sets of dykes oriented at roughly 90° to each other, one set of which shows affinity to domains 4 and 3B.

5.3.4 Significance of the Spilia-Politiko Area Dyke Domains

A tectonic model for the Spilia-Politiko area must explain the following points: 1) the swing in domain dyke orientations from NE-SW in the east to NW-SE in the west of the field area, 2) the graben axis features including its swing to the west in the south

and the observation that it cross-cuts dyke domain boundaries, 3) the formation of the Solea, Mitsero and Larnaca grabens in the Troodos ophiolite, and 4) the distribution of hydrothermal cells in the Spilia-Politiko field area. The tectonic framework developed in Chapter 2 for the Spilia-Politiko area suggests that the sheeted dykes formed on-axis, rather than off-axis as suggested by Gass and Smewing (1973), at an intermediate to fast spreading axis near a transform fault. The Mitsero graben structure formed off-axis, possibly through reactivation of earlier faults which formed on-axis. This area, thus, reflects an interplay of strike-slip faulting (along the South Troodos Transform Fault) and magmatic and amagmatic extension.

The dyke domains, delineated (Section 2.3.2) in the Sheeted Dyke Complex of the Spilia-Politiko area, have abrupt boundaries implying that they formed in distinct stages. The following model for the formation of the dyke domains (Section 2.3.2) utilizes the dyke rotation model of MacLeod et al. (1990) (Section 5.3.2). Dykes were injected, parallel to the ridge axis, at a dextrally offset spreading ridge north of the, sinistrally slipping, South Troodos Transform Fault (STTF) (Time 1 in Figure 5.6). These were dykes presently belonging to domains 2 and 5. East of the of the ridge axis (inactive corner of the ridge-transform intersection (RTI)), dykes were not rotated about a vertical axis; there may be rotation of dykes, about a horizontal axis, toward the ridge axis (domain 2). In the active corner of the RTI, west of the ridge, continued slip along the STTF resulted in the counter-clockwise, tectonic rotation of dykes forming domain 5 (cf. Figure 2.6).

The dykes of domain 4, at present, trend north-south, parallel to the paleo-ridge axis. This implies they have undergone no rotations about a vertical axis (Figure 2.6). An explanation for this is that a ridge jump occurred, after the formation of domains 2

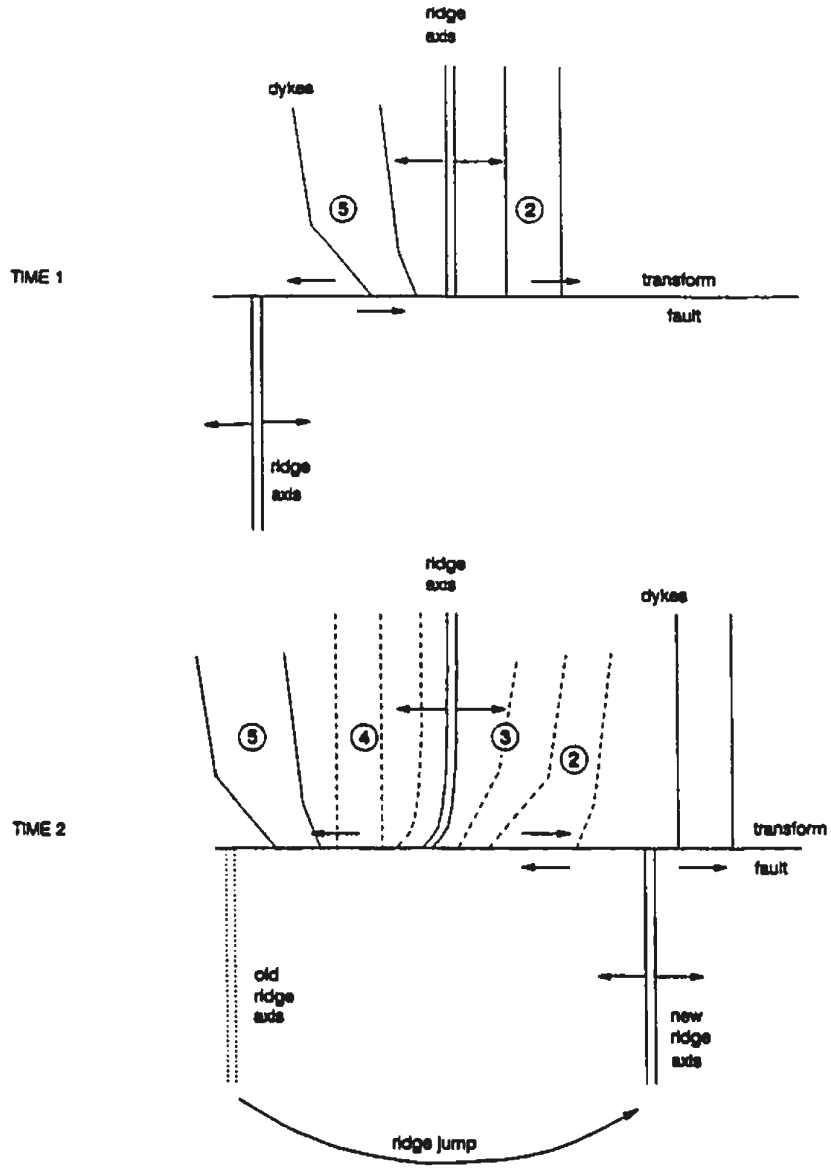

Time 3 may have involved a jump of the northern ridge axis segment to the east.



FIGURE 5.6 SCHEMATIC OF DYKE ORIENTATION RESULTING FROM A RIDGE JUMP ALONG A TRANSFORM FAULT.

and 5, of the ridge axis south of the STTF (Time 2 - Figure 5.6). The relative sense of motion of the ridge-transform system would now be reversed, from that of Time 1, to a sinistrally offset, dextrally slipping ridge. Following this ridge jump, the dykes of domains 3 and 4 were injected. The dykes of domain 4, located on the inactive side of the RTI, were not rotated, whereas, those of domain 3, on the active side of the RTI, were rotated about a vertical axis in a clockwise manner (viewed from above). The dykes rotated as blocks along roughly north-south trending strike slip faults (cf. Figure 2.18). These faults make up, in part, the boundaries for the dyke domains.

During the injection of dykes at the ridge axis, an axial caldera structure may have formed in conjunction with the formation of normal faults along the margin of the caldera structure.

With waning injection into the crust, as the magma chamber cooled, the rate of magma injection no longer provided the quantities of material needed to match the spreading rate; the spreading became amagmatic. As a result, the crust extended tectonically through rotations of the sheeted dyke section about a roughly horizontal axis, oriented sub-parallel to the ridge axis. This period of tectonic rotation may have succeeded a ridge jump to the east to form the Larnaca graben. Thus, the extension event forming the Mitsero graben, took place on the western flank of another (Larnaca) spreading ridge. It is possible the dykes of domain 6B formed during this period of amagmatic extension, possibly coincident with the emplacement of the small gabbro body which is located on the Mitsero graben axis in the vicinity of Ayios Epiphanios (Figure 2.1).

This curvature of the Mitsero graben axis indicates that, whereas the graben faults may have formed at the ridge axis, the graben axis was formed as a result of dextral slippage along the transform fault. The axis of the Mitsero graben cross-cuts the dyke domain boundaries; that is, the dykes were rotate to a greater degree than the axis. This implies that the dykes preceded the graben axis by a sufficient amount of time, allowing them to rotate to a greater amount before the super-position of the graben structure.

The main points of this model include: 1) formation of dykes in domains 2 and 5 at a dextrally offset, sinistrally slipping ridge; 2) a ridge jump to the east of the ridge axis to the south of the STTF, causing a shift to a sinistrally offset, dextrally slipping ridge; 3) this resulted in the formation of domains 3 and 4 and the pattern of dyke strikes presently seen in the field area; 4) formation of the Mitsero graben post-dates dyke formation at the ridge axis, as indicated by the cross-cutting relations of the graben axis and the dyke domains; 5) a detachment zone may be present in the Plutonic Complex (south of Palekhori - Section 2.3.4), its location in the gabbros indicates sufficient cooling of the crust to allow brittle deformation of the Plutonic Complex. Such conditions may have existed off-axis, away from crustal heat sources.

At the greater scale of the Troodos ophiolite, a sinistrally offset ridge near a dextrally slipping transform fault resulted in the on-axis formation of the Solea graben (Time 1, Figure 5.7). This is indicated by large dyke rotations and, possibly contemporaneous, hydrothermal alteration. Although Schiffman et al. (1987) stated that the alteration occurred off-axis, it is possible to envisage axis heat-source migration consistent with the pattern of hydrothermal alteration seen in the Solea graben (Section 5.3.3). A shallow detachment (at the base of the sheeted dykes - Moores et al., 1990; Varga,

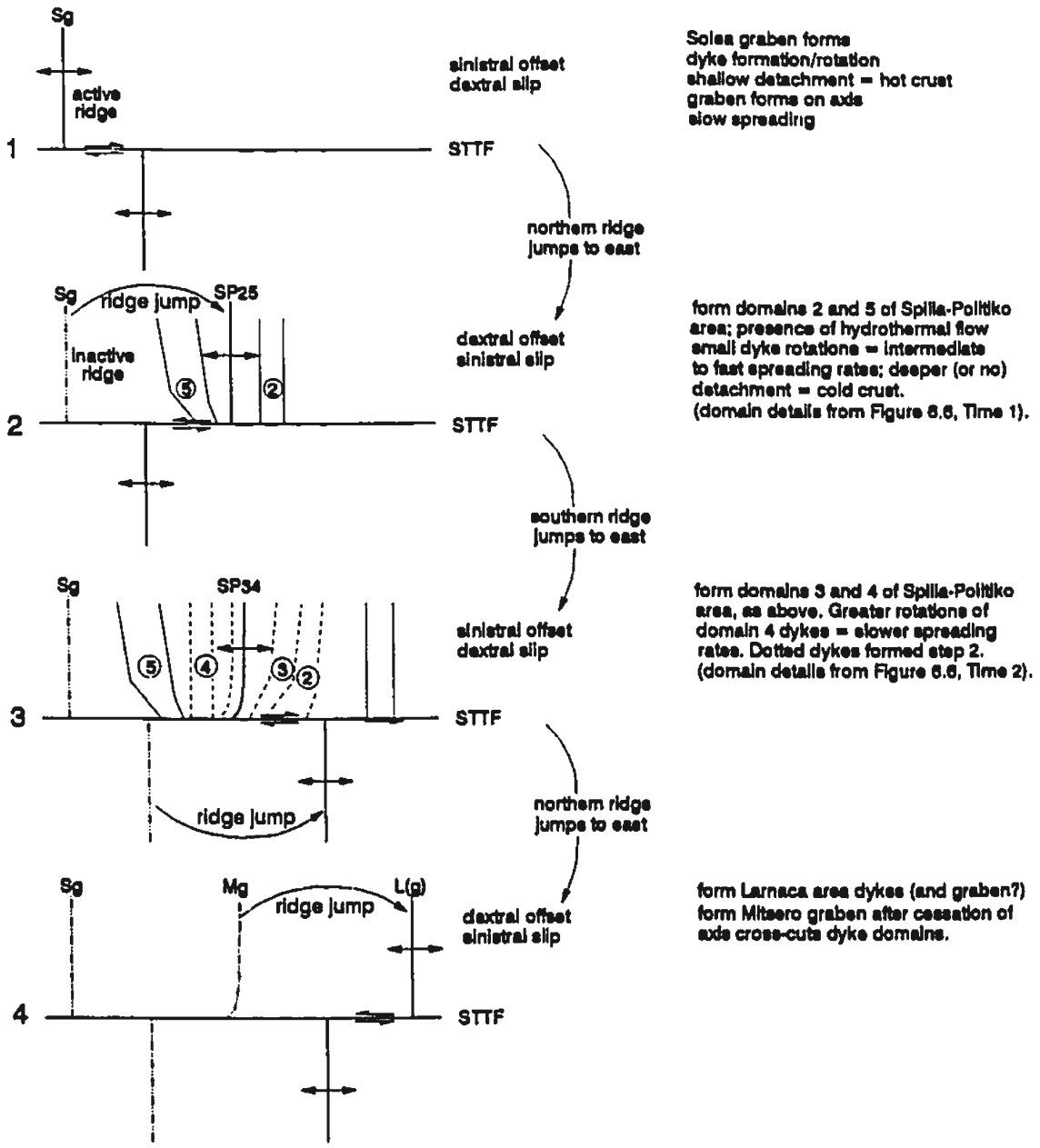

FIGURE 5.7 TROODOS DYKE DOMAIN FORMATION HISTORY. Sg = SOLEA GRABEN; SP25 = SPILIA-POLITIKO AREA DOMAINS 2 AND 5; SP34 = SPILIA-POLITIKO AREA DOMAINS 3 AND 4; Mg = MITSERO GRABEN; L(g) = LARNACA DYKES AND POSSIBLY GRABEN; STTF = SOUTH TROODOS TRANSFORM FAULT.

1991) indicates the presence of a shallow brittle/ductile transition zone which implies formation of the transition zone in a hot crust (i.e. on-axis) shortly after its formation.

A jump to the east of the ridge north of the transform fault initiated spreading in the Spilia-Politiko area forming the dykes of domains 2 and 5 (Time 2, Figure 5.7). Dyke rotations of smaller magnitudes than in the Solea graben (average present dips of 80° in the Mitsero graben) may indicate higher magmatic spreading rates. Following a ridge jump to the east of the ridge axis south of the transform fault, domains 3 and 4 formed (Time 3, Figure 5.7). Greater rotations of the domain 3 and 4 dykes (average dips of 70°) may show slower spreading rates. Lastly a ridge jump to the east of the ridge axis north of the transform fault initiated spreading in the Larnaca graben area (Time 4, Figure 5.7).

Cessation of magmatic spreading and continued extension resulted in the formation of the Mitsero graben. The lack of surface exposure of a detachment feature in the Mitsero graben (such as seen in the Solea graben), and its possible existence at deeper structural levels (Section 2.3.4) suggests a deeper brittle/ductile transition, implying the crust was cold, and thus off-axis, during graben formation. The axis of the graben cross-cuts dyke domain boundaries (Section 2.3.2.1), which also implies off-axis formation of the graben structure. The pattern of epidosites noted in the field is different in each domain. On-axis formation of a graben would control the location of hydrothermal cells. There is, however, no symmetrical relationship between the Mitsero graben and the epidosite pattern, implying the two are not related.

5.3.5 Hydrothermal Circulation

Many hydrothermal features seen at modern spreading centres, such as metal-sulfides and hydrothermal fluids discharging from vents, are preserved in the Troodos ophiolite in the form of metal sulfide ore deposits and chimney structures (Lydon, 1984; Oudin and Constantinou, 1984; Vibetti, 1985, pers. comm.). Fluid passage in fractures is recorded by the precipitation of secondary minerals. Fluid circulation, upon initiation of convection, will initially be up toward the discharge zone and then recharge down to the heat source. In a homogeneous, isotropic, porous medium a radial pattern of flow, in the hydrothermal circulation cell, is implied. The fracture/fault system biases the permeability into directions parallel to the ridge axis along dyke margins and perpendicular to the ridge axis along shallowly dipping portions of listric normal faults (Section 4.3).

Hydrothermal convective systems have been described as consisting of five parts (Figure 5.8): 1) recharge area; 2) downflow zone; 3) feeder zone; 4) upflow zone; 5) stockwork and discharge zone (Lydon, 1988). Recharge zones will preferentially occur in sediment-free areas, because the sediments form a low permeability cover on the extrusive volcanic rocks of the oceanic crust. The downflow zone is thought to occur along faults and fractures where permeability is highest. Areas in the Troodos ophiolite characterized by the complete alteration of dykes to epidosite (assemblage of epidote and quartz) are considered to be areas of intense water-rock interaction (Richardson et al., 1987; Schiffman et al., 1990). These assemblages indicate high water-rock ratios at relatively high temperatures (Bowers and Taylor, 1985; Mottl, 1983). These areas are considered to be the feeder and upflow zones to the hydrothermal ore deposits (Varga and Moores, 1985) and may be the source of the

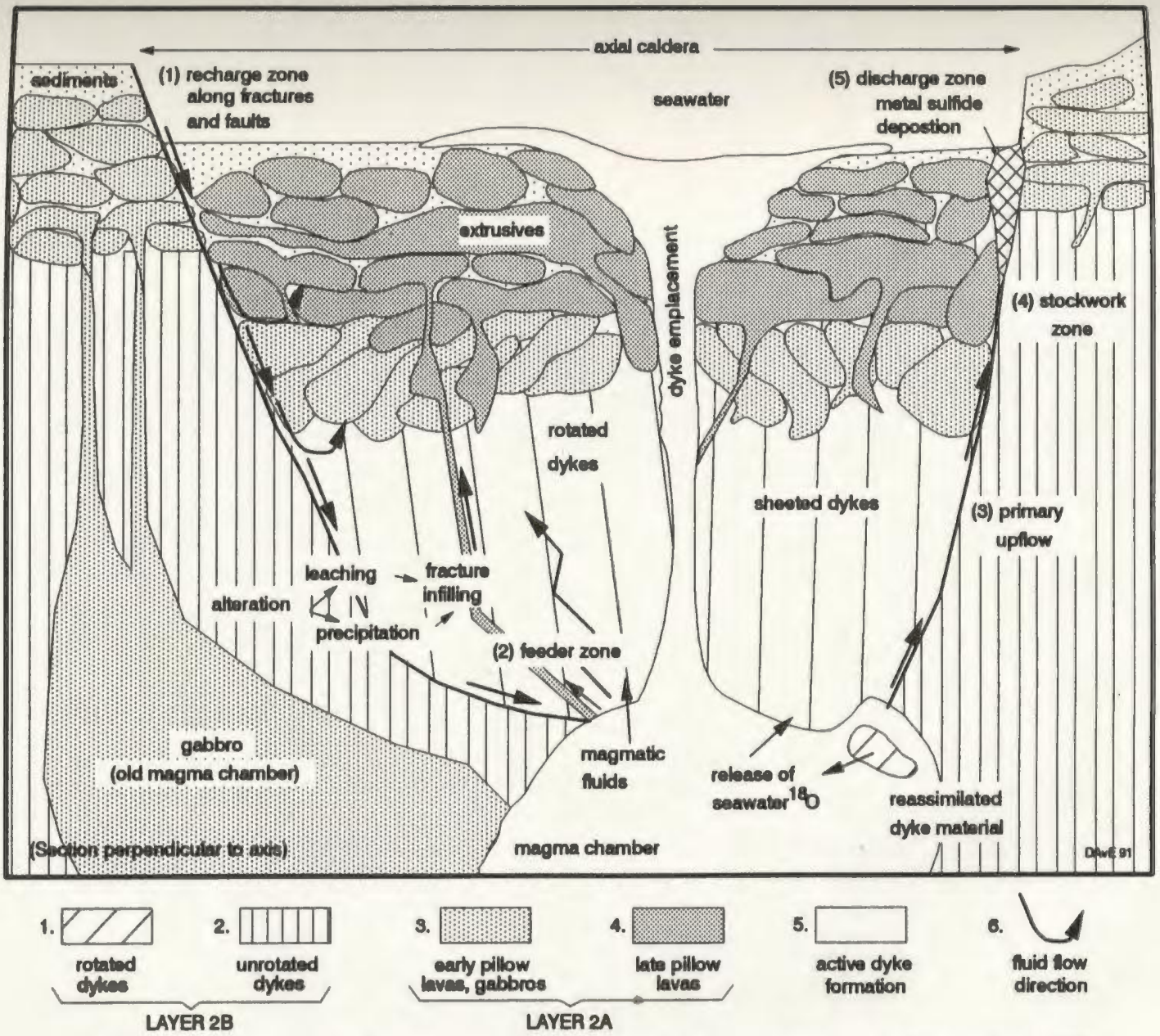

FIGURE 5.8 SCHEMATIC DIAGRAM OF A SPREADING CENTRE, SHOWING THE MAIN PARTS OF A GENERALIZED HYDROTHERMAL SYSTEM. SEE TEXT FOR DISCUSSION.

metals found in the metal-sulfide deposits in the Pillow Lavas (Richardson et al, 1987; Schiffman et al., 1990). Narrow pipe-like, fault controlled, epidosite bodies seen throughout the field area, indicate upflow zones may be narrow features, probably related to the adiabatic rise of fluids.

In the Spilia-Politiko area, epidosites were noted at all levels of the Sheeted Dyke Complex and the Basal Group (Figure 5.9). An occurrence of epidosite was also noted in the Lower Pillow Lavas east of Ayia Marina. Richardson et al. (1987) reported that epidosites occur only at the base of the sheeted dyke complex. This implies they are unlikely to be root zones for the hydrothermal circulation cells as he suggested. Rather, they constitute remnants of fluid pathways in the dyke section and to a limited extent, in the pillow lavas (such as in the area to the east of Ayia Marina where an area of pillow lavas has been completely epidotized). From the distribution of epidosites shown in Figure 5.9, one is lead to believe, instead, that they were conduits that were preferentially used by the circulating hydrothermal fluids (also Harper et al., 1988).

The highly brecciated, high permeability stockwork and discharge zones lie at the upper end of the upflow zone. They tend to channel flow causing fluids to largely by-pass areas outside the newly created higher permeability zone which would not undergo as much alteration as the higher permeability zone. The shear zone situated near Apliki village, in the vicinity of the Mitsero graben axis, is such a case. There, within 100 metres of the shear zone, there is no appreciable alteration. The discharge zone is an area where precipitation of metal sulfides occurred when hot saturated hydrothermal fluids came into contact with the downflowing cold, and as yet unmodified seawater, altering the mineral solubility. The extrusives in some mines

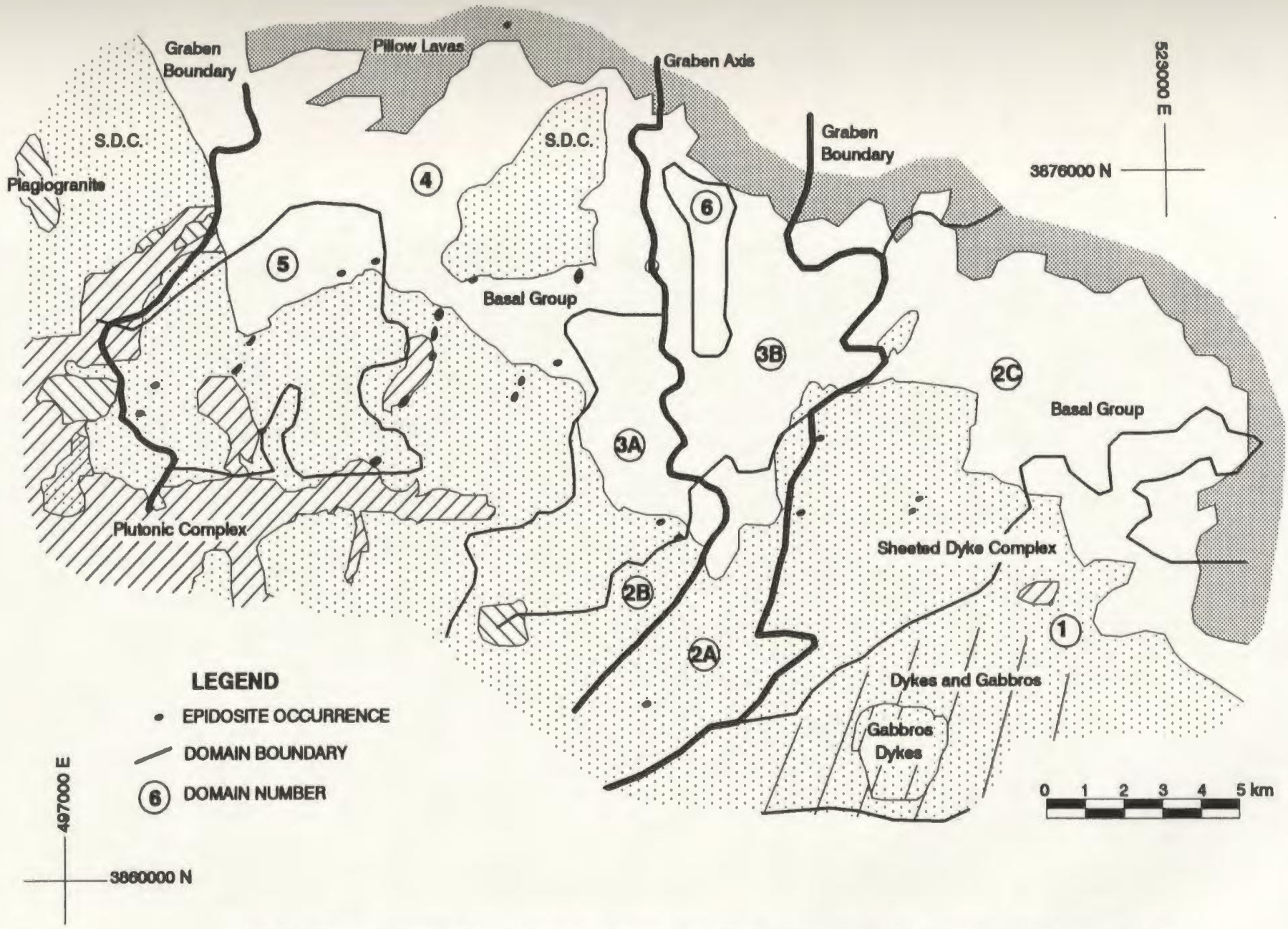

FIGURE 5.9 EPIDOSITE OCCURRENCE MAP, SPILIA - POLITIKO AREA, CYPRUS.

(e.g. Agrokipia and Mathiati mines), locally have fresh glass on pillow margins, demonstrating the degree to which hydrothermal alteration can vary in intensity (Gillis, 1986).

In the field area, epidote mineralization is associated with dyke margins (Section 3.3.4). Since it is assumed that the dykes were formed in a vertical orientation (Section 2.3.3 and Varga, 1991), this implies that vertical (dyke-parallel) fractures were open and more available to fluid passage than fractures normal to the plane of the dykes. This type of environment is present at the ridge axis during extension.

Calcite, a late precipitation product, related to the waning stages of hydrothermal circulation, tends to be found in fractures perpendicular to dyke planes which implies that unloading of the crust was taking place at the time of calcite precipitation. Permeability calculations show that fracture permeabilities for those fractures containing calcite, are less than for those containing epidote, suggesting a decrease in the rock permeability over time (Sections 4.3.3.4.1 and 5.3.5).

Fractures without mineral fillings represent 51% of all fractures (Table 3.5A). They are most commonly found at the top of the sheeted dyke section in the Basal Group. These fractures were not utilized by hydrothermal fluids because they: 1) were not interconnected to the general fracture network, or 2) formed after the cessation of hydrothermal fluid circulation. The first option appears the most reasonable because open, empty fractures cross-cutting hydrothermal mineral filled fractures, as would be expected if a later generation of fractures developed, are not seen in the field area. This implies that approximately half of the fractures do not contribute greatly to fluid circulation and, therefore, to crustal cooling.

High temperature, high water-rock ratio conditions result in the conversion of diabase dykes to epidosite (epidote-quartz-chlorite assemblages), a widespread phenomenon in the Sheeted Dyke Complex of the Troodos ophiolite. The distribution of epidosite is a direct indication of the distribution of hydrothermal circulation cells (Richardson et al., 1987).

Epidosites generally are fine to medium grained rocks consisting of epidote + quartz +/- chlorite; accessory minerals include sphene, magnetite, and locally, actinolite or pyrite. Epidosites are entirely lacking in relict igneous textures, consisting of a mosaic of anhedral to prismatic epidote and lobate quartz +/- skeletal magnetite (which may be replaced by sphene). Near the edges of epidosites, rare occurrences of relict pyroxene demonstrate that the epidosites formed through the alteration of the diabase dykes. In the Spilia-Politiko area, epidosites comprise roughly 30-50% of an outcrop area whereas the remainder of the outcrop consists of less altered diabase dykes. The epidosites form primarily in areas of light to dark grey competent dykes, with rare occurrences in dark brown weathered, friable dykes. The epidosite outcrops are roughly 6% more fractured than non-epidosite, diabase outcrops (based on the scanline fracture surveys; Chapter 3). Epidosite has a striped alteration pattern paralleling the dyke orientation which, in general, do not crosscut dyke margins. The most intense alteration seems to be concentrated in the coarsest portions of the dyke. The distribution of epidote in some cases suggests that the matrix permeability is locally significant to allow alteration of the rock on a large scale. This implies either long fluid residence times, which does not seem likely in view of fluid flow rates seen at analogous seafloor hydrothermal areas (e.g. MacDonald et al., 1980 or Von Damm, 1990), or, more likely, greater intergranular permeability in the coarser grained cores of some dykes, possibly along grain boundary cracks. Epidote veins

have an up to 3 centimetres wide alteration halo (generally less than 1 centimetre). The average size of an epidosite occurrence, in the study area, ranges from 50 to 100 metres perpendicular to the strike of the dykes, and, where it was possible to map, roughly 150 metres parallel to the dyke strike. Most epidosites occur in the vicinity of faults, although associated fault surfaces do not always contain evidence, such as hydrothermal minerals, for the passage of fluids.

Epidosites are strongly depleted in Cu and Zn (Richardson et al., 1987). Richardson et al. (1987) conclude that circulating water stripped 90% of the Cu, 50% of the Zn and 40% of the Mn from the rock. During the formation of a large sulfide deposit the water/rock ratio in the epidosite is as high as 20 (Richardson et al., 1987). On the basis of Cu concentrations in average diabase dykes (averaging 56 ppm - using analyses from Baragar et al. (1989)), mean ore body spacings of 4.4 kilometres implying a reservoir diameter of 4.4 kilometres - measured from published maps also Spooner and Bray, 1977), approximate crustal sheeted dyke thickness of 2 kilometres (Moores and Jackson, 1974), and average fracture densities of 3 fractures per metre (see fracture frequency plots in Appendix A.3.8), each with a 2 centimetre reaction halo, only 6% of the total Cu (43% of the Cu in the reaction halos) would be required to produce a 5.5 million tonne ore deposit at 2.25% Cu. This rough calculation was done to show that, although not every fracture has a large reaction halo, on a volumetric basis, there is no necessity to invoke a mantle or magmatic source to account for the metals found in the Cyprus ore deposits.

Occurrences of epidosites in the Mitsero graben (Figure 5.9) are aligned parallel to river valleys, along a northeast-southwest trend. Lineaments from the remotely sensed images coincide with these valleys (Section 2.3.1), suggesting that the occurrence of

the epidosites is controlled by the location of major lineaments or faults. Epidosites were not seen outside of the valley roadcut outcrops. Whereas this implies that they are restricted to the vicinity of major faults, it does not totally preclude the possibility, that because of poor outcrop availability, they may also exist elsewhere.

An example of massive epidotization associated with faulting occurs in the Lower Pillow Lavas east of Ayia Marina, with an area of 50 metres by 60 metres, about 250 metres from a large scale lineament (Peristerona River valley). Samples similar to those observed east of Ayia Marina have been collected from the mid-Atlantic ridge. These were originally glassy basalts, that were altered at high (200° to 350°C) temperatures, to chlorite-quartz-epidote-rich assemblages which may have come from a narrow zone of discharge of hydrothermal fluids (Stakes and O'Neil, 1982).

Mines, gossans, mineral occurrences and epidosites occur in greater concentrations west of the Mitsero graben axis (Figure 5.10). This asymmetric pattern, with respect to the graben axis, does not agree with a graben model in which the graben formed on the ridge axis, supporting earlier statements that it formed off-axis by amagmatic extension (Section 2.3.5).

Epidosites in the field area are spaced, in a north-south direction, 2.3 kilometres apart, and, in an east-west direction, 4.1 kilometres apart in the western portion of the Mitsero graben (Figure 5.9). In the eastern portion of the Mitsero graben the spacings are 5.3 kilometres (N-S) and 5.2 kilometres (E-W), respectively. These are average distances using all the epidosite data; it should be noted that the epidosites likely did not form at the same time, thus these spacings are to be taken only as possible indicators of hydrothermal cell spacing.

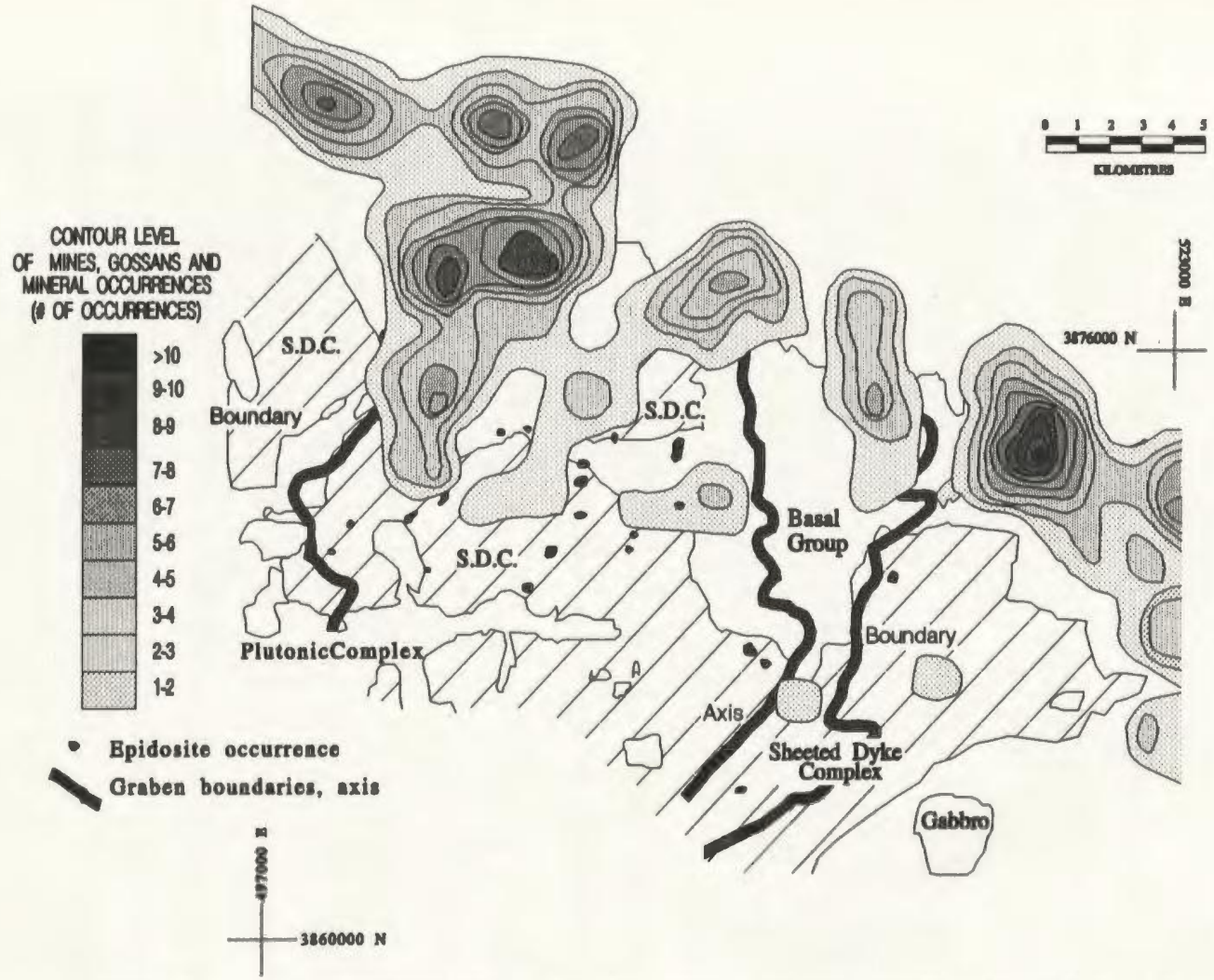

FIGURE 5.10 CONTOUR MAP OF THE MINES, GOSSANS AND MINERAL OCCURRENCES IN THE SPILIA - POLITIKO AREA, CYPRUS.

The extent of hydrothermal cells is based on the spacing of the epidosites (at depth) and the ore deposits (at shallower crustal levels in the extrusive volcanic rocks). Their locations were thus controlled, first, by the heat source location, and second, by the fracture characteristics of the crust overlying the heat source.

The size of hydrothermal cells was likely controlled by the size of the underlying heat source. The average size of each hydrothermal cell is estimated by the spacing between the epidosites (up-flow zones), in a north-south direction (parallel to the spreading-ridge axis) since ridge-parallel cells may have been contemporaneous. The present-day lateral spacing (ridge-normal) of the epidosites is probably dependent on the paleo-spreading rate and the spacing of major faults. Using the distances between mines, gossans, and mineral showings in the Spilia-Politiko area, the average spacing of hydrothermal upflow zones appears to have been 2.3 kilometres west of the graben axis and 5.3 kilometres east of the axis. The difference between spacings on either side of the graben axis implies fewer and possibly larger hydrothermal cells on the eastern side of the graben. Two possible causes could be, (1) that the Mitsero graben, east of the graben axis, is narrower and therefore fewer alteration zones are seen, and (2) that the dyke section is thicker in the eastern half of the graben, which may have lead to lower thermal gradients. The pattern of epidosite occurrences in the field area is not symmetric about the graben axis, which would be expected if the graben formed on axis. This indicates that the graben is a post-hydrothermal-circulation feature, so that the hydrothermal cell distribution and the graben axis are unrelated. However, faults that controlled the flow of hydrothermal fluids may have been re-activated during the formation of the graben structure. Many of the mineralized faults seen in the field area contained striae on the secondary mineral surfaces implying motion along the fault after mineral precipitation took place.

The spacing of hydrothermal upflow zones differs from domain to domain in the Spilia-Politiko area (Figures 5.10 and 5.11), suggesting that the heat sources in each domain may be different. The epidosites of domain 5 formed along a line parallel to the spreading direction (Figure 5.9), implying the influence of a single, probably intermittent, heat source (Figure 5.11A). At a later time, the epidosites in domain 4, situated along lines perpendicular to the spreading direction, may have formed under the influence of multiple, along-axis, heat sources (Figure 5.11B). This suggests that over time more heat sources developed along the spreading axis, or that a single heat source spread out along the ridge axis perhaps as a result of increased magma input to the system. The low number of simultaneous heat sources in domain 5 suggests generation of domain 5 during a period of low magma budget immediately following a ridge jump. Later, during the generation of domain 4, the number of active magma chambers increased as the new spreading ridge became established. The ridge jump may have been followed by an influx of magma, causing an increase both in the amount of spreading and in the hydrothermal activity. Domains 2 and 5 formed contemporaneously, as did domains 3 and 4 (Section 5.3.4), however, the number of occurrences of epidosites noted in the field in domains 2 and 3 are too low to discern a pattern similar to those seen in domains 4 and 5. Field mapping of epidosites during this study did not extend into the Makhaeras domain (the far eastern portions of domains 2 and 3).

There does not appear to be any systematic shifting of the heat source along the ridge axis, as would be indicated by a shift in the epidosite alteration pattern to the north or south parallel to the spreading axis. The pattern of epidosites in domain 4 is more indicative of simultaneous heat sources along the axis rather than a shifting of a heat source through time.

Figure 5.11 Hydrothermal fluid circulation. Patterns in the section below the sheeted dykes are the same as in Figure 5.1. Positioning of the hydrothermal vent fields are based on the patterns of epidosites noted in the field area. Fluid down flow occurs along stepped faults with an overall dip that is less steep than the dykes (Section 2.3.4) A. Early stage fluid circulation (domain 5) with a single heat source which is periodically replenished. B. Later stage fluid circulation (domain 4) with multiple heat sources which are periodically replenished. Between replenishment hydrothermal activity is much reduced as indicated by the vent spacing perpendicular to the spreading direction. Refer to text for further explanation.

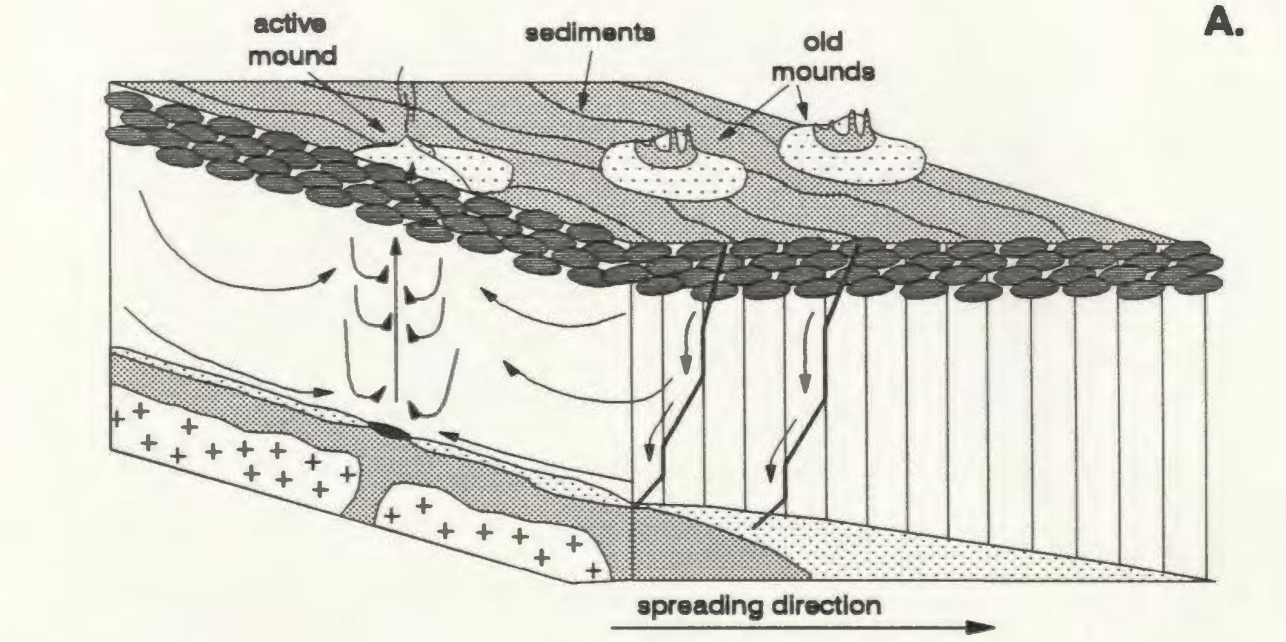
A.
active mound
sediments
old mounds
spreading direction

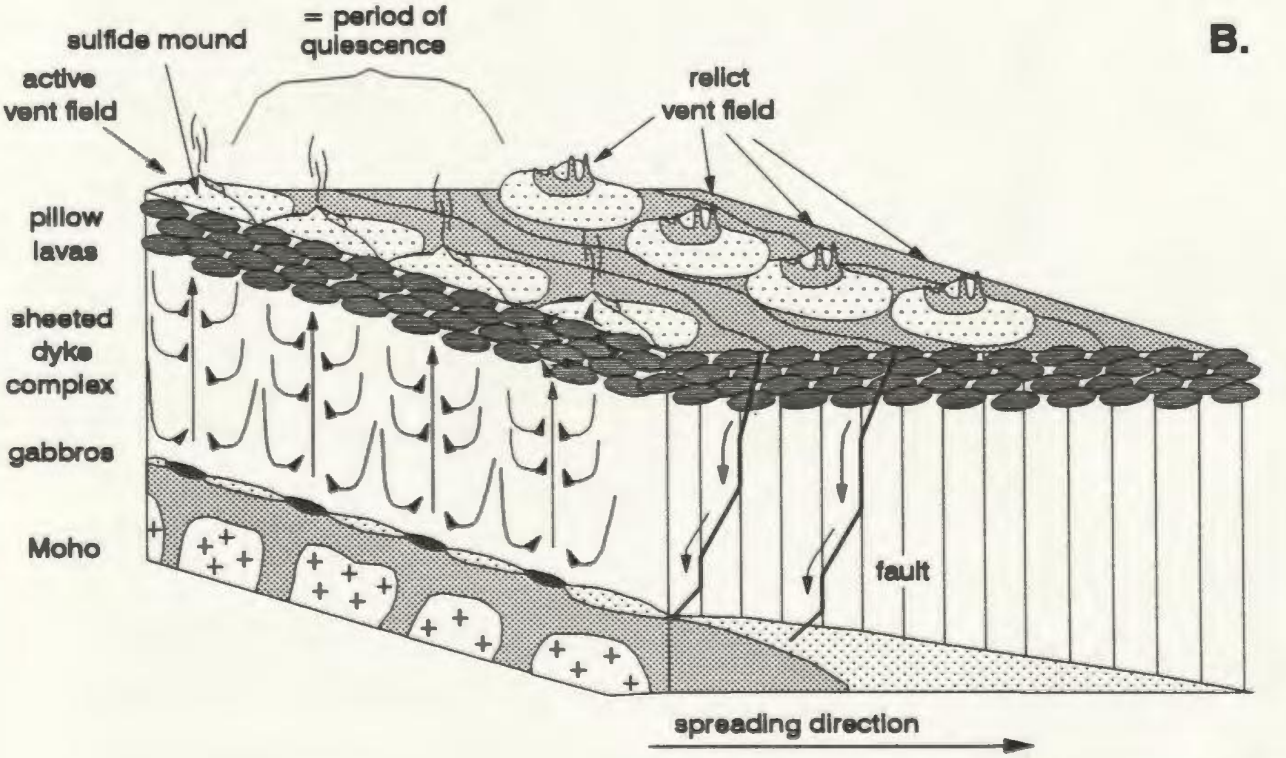
B.
sulfide mound
= period of quiescence
active vent field
relict vent field
pillow lavas
sheeted dyke complex
gabbros
Moho
fault
spreading direction

NOT TO SCALE

5.3.5.1 *Hydrothermal Fluid Properties*

Previous fluid inclusion thermometric studies in the Troodos ophiolite have demonstrated that hydrothermal fluids had near-seawater salinities and temperatures of 350°C (Spooner and Bray, 1977; Richardson et al., 1987; Cowan and Cann, 1988; Schiffman and Smith, 1988; Vibetti et al., 1989; Kelley et al., 1992) (Appendix C.2). These match outflow temperatures measured at hydrothermal vents on the present-day seafloor (MacDonald et al., 1980; MacDonald, 1986). Strontium isotope studies indicate a major component of seawater was present in the system (Staudigel et al., 1986). Analyses of fluid inclusions in plutonic rocks of the Troodos ophiolite indicate possible boiling or phase separation of fluids (Kelley et al., 1992). In the Sheeted Dyke Complex, uncorrected homogenization temperatures of 350°C were documented in fluid inclusions in hydrothermal quartz (Richardson et al., 1987). These conditions are similar to those inferred from present-day spreading axes (Haymon and Koski, 1987; Jehl, 1974; Kelley and Delaney, 1987).

Temperature and salinity of the hydrothermal fluids that cirulated in the sheeted dykes, in the study area, were estimated from fluid inclusions in secondary minerals, such as quartz and epidote in 27 samples from the Sheeted Dyke Complex (Appendix C.2). Fluid inclusion homogenization temperatures ranged from 160° to 400°C. Temperature ranges, as large as 100°C, within various cross-cutting planes of fluid inclusions at individual locations show that fluids passed through the rocks at different times and temperatures, during the life-cycle of the hydrothermal system. The consistency of fluid inclusion homogenization temperature maxima indicates little variation in the hydrothermal conditions throughout the sheeted dyke section. Inclusion homogenization temperatures measured from fractures, with different

orientations, in the same vicinity (i.e. within 10 metres of each other) are very similar, demonstrating that these fractures sampled similar fluids during their history.

Temperature/salinity relationships from the study area (Figure 5.12), indicate that salinity is independent of temperature. Since all fluid inclusions homogenized to the liquid phase, it is assumed that no phase separation occurred in the Sheeted Dyke Complex. The samples from the deepest part of the section at a particular temperature have the lowest salinities and those samples from the shallower parts of the section have higher salinities. However, the expected large variation in salinities in individual samples is not seen. Salinity of the fluids trapped in the rock may have been increased through a variety of processes including brine separation at depth, filtering of the fluids, or during the formation of hydrous phases such as epidote, chlorite and hornblende in the dykes as the fluid moved upward in the section. Increasing salinity of fluid inclusions higher in the section may be due to continued loss of water from the fluid in hydration reactions taking place in the wall rock of the dykes or from mixing and/or filtering of the fluid by the rock.

Salinities in a plagiogranite sample (CA86-9) just west of Spilia near the base of the Sheeted Dyke Complex, contained diverse salinities ranging from 1.6 to 20 wt.% NaCl equivalent. Salinities, if sufficiently diverse within a particular sample, can indicate that phase separation took place concentrating the salts in the liquid phase (= brine separation) which corresponds to boiling. The very high measured salinities suggest that the trapped fluids may have been derived through mixing of unmodified seawater and a phase-separated fluid (modified seawater) originating deeper in the section in the Plutonic Complex (Kelley et al., 1992). It was not possible to obtain enough data points to establish a trend. Cowan and Cann (1988) reported a similar

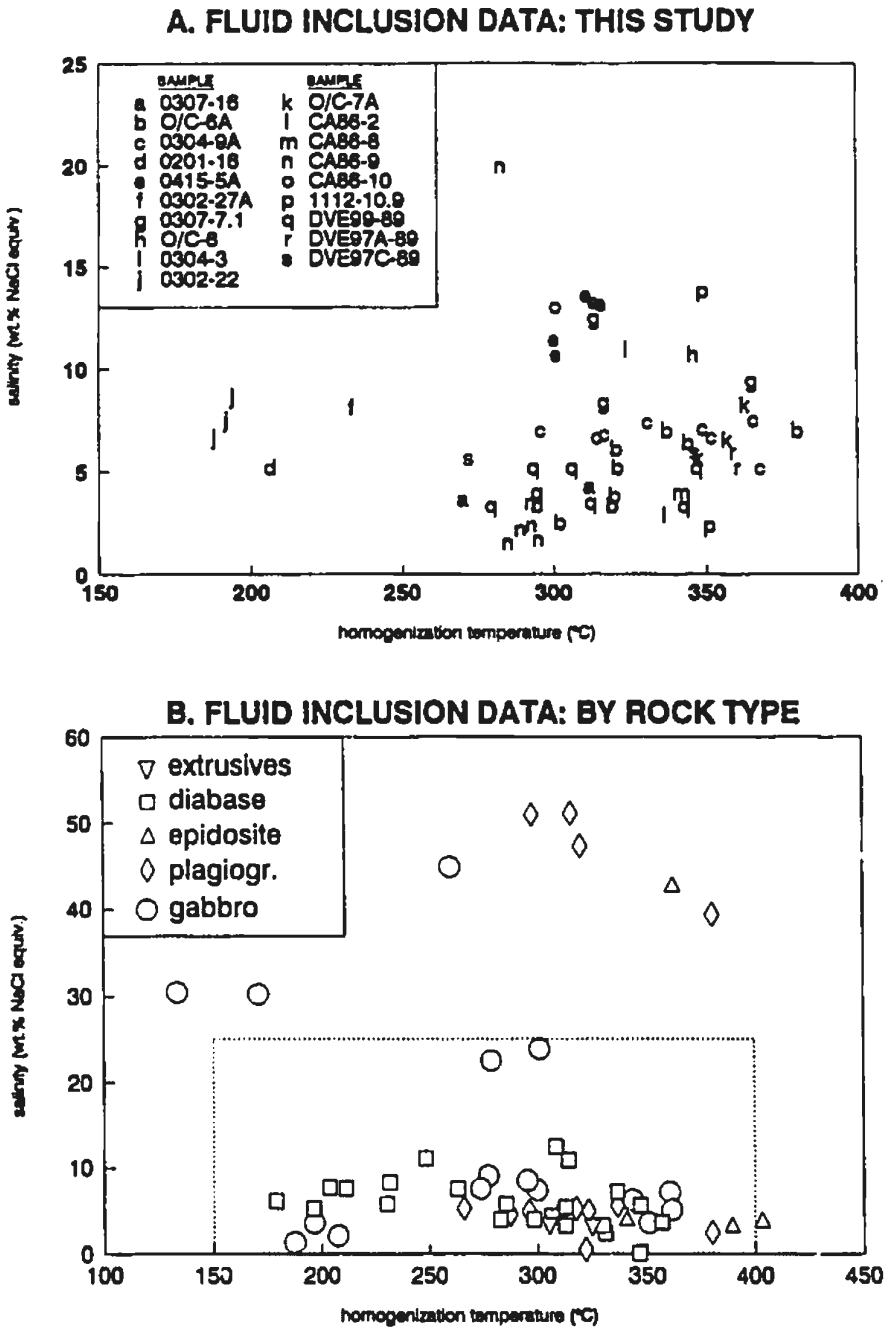

FIGURE 5.12 FLUID INCLUSION HOMOGENIZATION TEMPERATURE VERSUS SALINITY DATA FROM THE SPILIA-POLITIKO AREA, TROODOS OPHIOLITE, CYPRUS. A. DATA FROM THIS STUDY (SEE FIGURE 5.5 FOR LOCATIONS). B. DATA COMPILED FROM THIS STUDY, COWAN AND CANN (1987), KELLEY ET AL. (1991), RICHARDSON ET AL. (1987), SCHIFFMAN AND SMITH, 1988, SPOONER AND BRAY, 1977 AND VIBETTI ET AL. (1989). DOTTED LINE ENCLOSES AREA OF A ABOVE.

occurrence in plagiogranites near Platanistasa which they describe as representing a phase separated fluid (temperature = 500-525°C, salinity = 0.05 and 54-57wt% NaCl) which mixed with seawater. Phase separation is a necessary step in the generation of variable salinity black-smoker fluids and has been used to explain the development of fluids in the Southern Juan de Fuca Ridge (Von Damm, 1988).

5.3.5.2 *Interpretation of Fluid Inclusion Data*

The development of stacked convection cells, one overlying the other, separated by an impermeable horizon of silicified material was suggested by Sleep (1983). Sealing of fractures by quartz would be caused by decreasing quartz solubility with increasing temperature. Two locations near Gourri (Figure 2.1), along the Gourri fault zone (eastern margin of the Mitsero graben), were the only occurrences noted, of silicified dyke material, not nearly enough to consider dividing the entire hydrothermal system into separate cells. Fluid inclusion temperatures do not support separate cells, as there is no systematic temperature variation with depth in fluid inclusions in the sheeted dykes. There may, however, be separate hydrothermal circulation cells between the sheeted dykes and the underlying gabbros and plagiogranites (Kelley et al., 1992).

Bischoff and Rosenbauer (1989) presented a two tiered model of hydrothermal convection: the lower level is a high temperature (400-500°C), brine-rich ($NaCl$-KCl-$CaCl_2$) cell in the plutonic rocks; the upper level is at a lower temperature (300-400°C), with fluids of seawater salinities (NaCl) in the dykes. The two cells are separated by a density contrast at a double diffusive interface. The base of the lower cell is an ephemeral cracking front. The thermal barrier imposed by the brine layer prevents shallower fluids from attaining temperatures greater than 360°C. In the

lower cell the fluids boil; the vapour phase migrates upward and mixes with the upper fluids. In the lower cell recycling of brines results in progressive alteration, although rapid microcrack healing at high temperatures may prevent prolonged circulation of the brines (Brantley et al., 1990). The upper cell is a one-pass system. Circulation of acidic fluids leaches metals and albitizes the plagiogranites. The fluids are enriched in Ca and depleted in Na. Low temperature and salinity fluid inclusions cross-cut brine bearing microfractures implying downward migration of the cracking front during waning of the heat source. Kelley et al. (1992) showed that fluid inclusion data from the top of the Plutonic Complex supports the model of Bischoff and Rosenbauer (1989).

The consistent temperatures and salinities of the samples in the sheeted dykes would fall in the upper circulation cell of Bischoff and Rosenbauer (1989). Variation in salinities in the plagiogranite sample supports the existence of the brines in the lower part of the hydrothermal system.

The abundance of fractures does not vary with stratigraphic level in the sheeted dyke complex. Outcrops without any fracture infillings exist only in the Basal Group, whereas fracture infilling minerals are most common in epidosite areasa. Towards the base of the Sheeted Dyke Complex, fracture mineral fillings nearly ubiquitous. It is therefore likely that hydrothermal fluids passed from diffuse conduits deeper in ther section, into more concentrated zones up towards the seafloor. This also implies discrete zones of hydrothermal flow existed in the upper part of the Troodos crust. Goldfarb and Delany (1988) described an anastomosing array of fractures, with large open fractures (stockworks) near the seafloor extending down to the gabbros, fed by

smaller and smaller conduits which become more numerous with depth to preserve the flow.

A possible history of fracture utilization for the the Sheeted Dyke Complex would include: 1) downflow into the crust through a system of faults which extended at least as far down as the magma chambers (Dunsworth, 1989); 2) diffuse flow of hydrothermal fluids upward through the interconnected fracture network; 3) precipitation of hydrothermal minerals, such as epidote, quartz, and chlorite, in the fractures eventually causing them to be blocked to further flow; 4) the formation of new fractures, or enhancement of pre-existing, favourably situated (sub-vertically oriented) fractures, to form concentrated upflow zones; and 5) decreased efficiency of heat transfer, due to an increasingly thick insulating sediment cover, forcing fluids to migrate laterally in the highly permeable extrusive sequence. In such a scenario, vertical fluid migration in concentrated upflow zones in the dykes and lateral migration in the extrusive volcanic rocks (point 4 and 5), may have resulted in the formation of the mines, gossans, and mineral showings seen in the Spilia-Politiko area. It is expected that the late stage, post-hydrothermal (off-axis), interconnected fracture network would be of a very low permeability (cf. Rosenberg and Spera, 1992). At this stage, the permeability may have been below the critical level needed to support fluid circulation (de Marsily, 1984). The pattern of epidosites reflects the distribution of hydrothermal circulation cells which are a function of ridge processes such as the number of magma chambers operating at any one time and their relative sizes. Epidote is ubiquitously connected with hydrothermal fluid circulation and thus occurs early in the life of hydrothermal systems. Calcite forms late, possible during the waning stages of hydrothermal circulation. The spatial variation of fracture

mineral filling implies that hydrothermal circulation is diffuse at depth, becoming more focussed along discrete zones further up section.

5.4 REGIONAL TECTONIC SETTING FOR THE TROODOS OPHIOLITE

Interpretation of the regional tectonic setting of the Troodos ophiolite is complicated by the many tectonic belts in the Mediterranean (Dilek and Moores, 1990). Various authors (e.g. Clube et al., 1985; Moores et al., 1984; Robertson and Woodcock, 1986) presented models, often conflicting, to explain the observations in the eastern Mediterranean area. Many of the conflicts arise out of problems with determining the timing of initiation of the subduction zone south of Cyprus, whether the Eratosthenes seamount could have stopped subduction, and the timing of the accretion of the Mammonia and Kyrenia terranes. The unravelling of these problems is largely beyond the scope of this project. Figure 5.13 chronicles one possible scenario within which the Troodos ophiolite and the constituent dyke domains of the Spilia-Politiko area may have formed.

The Troodos ophiolite, like most other ophiolites of the eastern Mediterranean Sea and elsewhere, formed in a supra-subduction zone environment (Moores et al., 1984; Dilek and Eddy, 1992). In the early Cretaceous (less than 119 Ma), a north dipping subduction zone south of present-day Turkey aided in the closing of the Tethys Ocean (Robertson and Woodcock, 1986). Subduction of younger Cretaceous crust was followed by that of older thicker Tertiary crust. This may have caused roll-back of the subduction zone to the south causing stretching of the asthenospheric wedge. Extension in the supra-subduction zone initiated the formation of the Troodos Crust

Figure 5.13 Tectonic setting of the Troodos ophiolite. Modified from Clube et al. (1985), Moores et al. (1984) and Robertson and Woodcock (1986). Panel 1 (Santonian (<92 Ma)) shows a subduction zone in the Tethys sea, along the south coast of what is now Turkey. Panel 2 (Santonian (92 Ma)) shows the formation of a suture along the former subduction zone in the north, and the formation of a new subduction zone to the south in the Tethys sea. Panel 3 (Campanian (92-90 Ma)) describes the initiation of crustal accretion. The area of the circle is the area of formation of the Troodos crust. Below the panel the circles show the development of the Troodos crust with the associated ridge jumps (further detailed in Figure 5.7). Panel 4 (Maastrichtian (73-65 Ma)) indicates the impingement of the subduction zone with the African plate to the east and the counter-clockwise rotation of the African plate. In Panel 5 (late Maastrichtian to Paleocene (to 55 Ma)) the Mammonia complex is accreted to the Troodos crust. The Troodos crust rotates in a counterclockwise direction. Panel 6 (late Eocene) indicates the cessation of subduction and initiation of thrust faulting to the east. Strike slip faulting occurs along the suture zone causing the accretion of the Kyrenia terrane to the Troodos crust. The Eratosthenes seamount causes subduction to stop and may have initiated the uplift of the Troodos ophiolite.

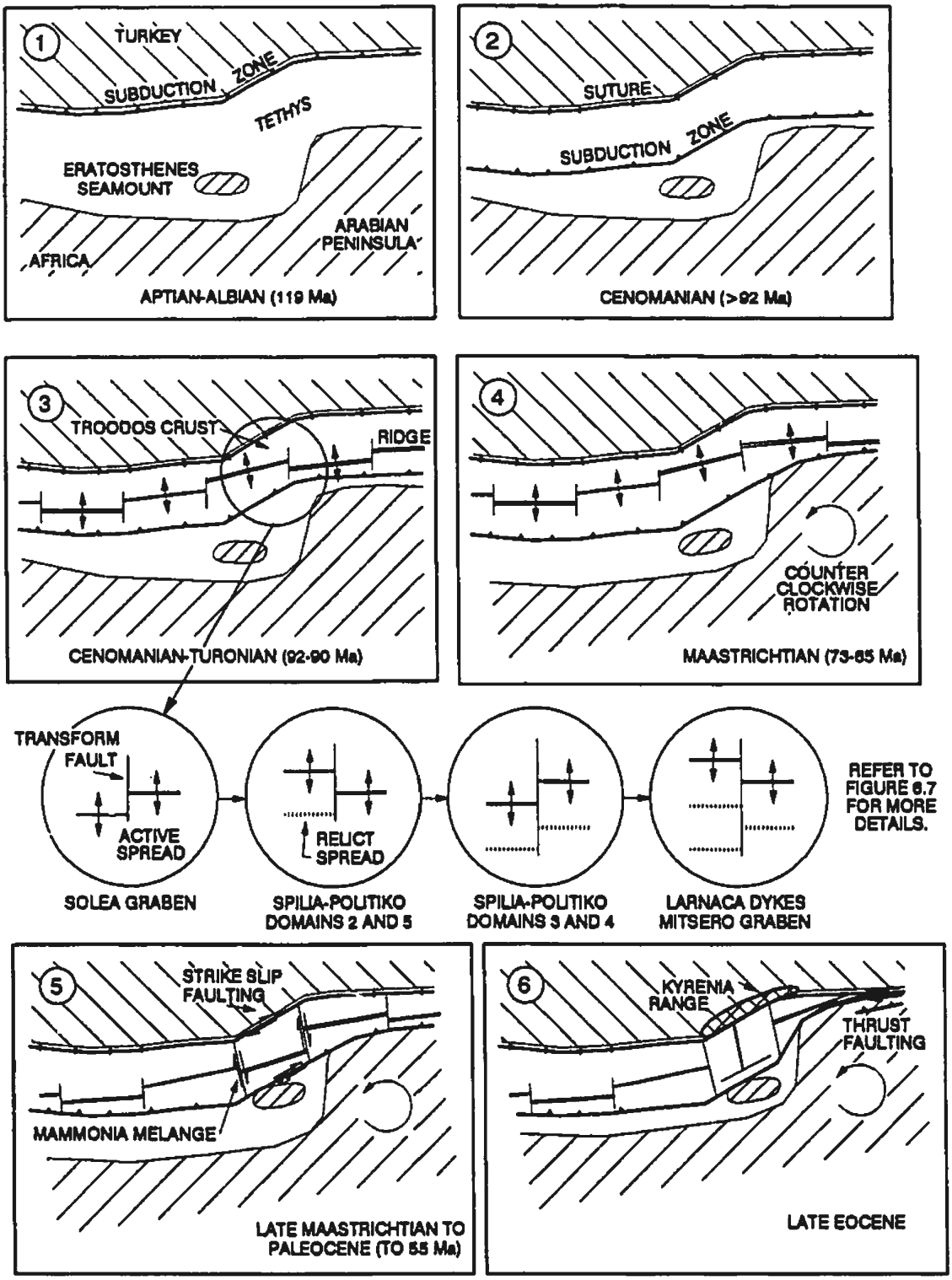
1
TURKEY
SUBDUCTION ZONE
TETHYS
ERATOSTHENES SEAMOUNT
ARABIAN PENINSULA
AFRICA
APTIAN-ALBIAN (119 Ma)
2
SUTURE
SUBDUCTION ZONE
CENOMANIAN (>92 Ma)
3
TROODOS CRUST
RIDGE
CENOMANIAN-TURONIAN (92-90 Ma)
4
COUNTER CLOCKWISE ROTATION
MAASTRICHTIAN (73-65 Ma)
TRANSFORM FAULT
ACTIVE SPREAD
RELICT SPREAD
SOLEA GRABEN
SPILIA-POLITIKO DOMAINS 2 AND 5
SPILIA-POLITIKO DOMAINS 3 AND 4
LARNACA DYKES MITSERO GRABEN
REFER TO FIGURE 6.7 FOR MORE DETAILS.
5
STRIKE SLIP FAULTING
MAMMONIA MELANGE
LATE MAASTRICHTIAN TO PALEOCENE (TO 55 Ma)
6
KYRENIA RANGE
THRUST FAULTING
LATE EOCENE

(Robertson and Woodcock, 1986). The subduction zone, situated beneath the Troodos Crust dips to the north (Ben Avraham and Nur, 1986). The 92-90 Ma period saw the formation of a minimum 120 kilometres wide zone of Troodos crust (present-day width of the ophiolite) (Blome and Irwin, 1985; Robertson, 1990; Staudigel et al., 1986). The dyke domains and grabens, described in Chapter 2 and Section 5.3.4, formed during this period.

Initially the Troodos spreading-ridge axis was oriented in a east-west direction (Moores and Vine, 1971; Allerton and Vine, 1991; Gass, 1990). The cessation of spreading and the subsequent 90° counter-clockwise rotation of the Troodos microplate (Allerton and Vine, 1989; Clube et al., 1985), over a period of 25 Ma from the latest Cretaceous (Maastrichtian) to the Paleocene, may have been caused by: 1) possible roll-back and subsequent impingement of the subduction zone with the African continental crust (Moores et al., 1984); 2) collision with a micro-continent, preserved in part as the Eratosthenes Seamount (Gass, 1979); and 3) the continued northward movement and counter-clockwise rotation of the African continent (Sclater et al., 1977).

The Tethys Sea appeared to have closed from the south-east to the north-west (e.g. Robertson and Woodcock, 1986). Closure in the south-east resulted in the obduction through thrust faulting of the Semail ophiolite in Oman. In the north-west the closure of the ocean basin may have halted in the late Eocene due to the attempted subduction of a micro-continent (possibly the Eratosthenes Seamount; e.g. Ben-Avraham and Nur, 1986; Robertson and Woodcock, 1986). The Troodos ophiolite was uplifted but was not split into fault-bounded thrust slices as was the Semail ophiolite, Oman; the

subduction process ceased before collision with the African continent in the Troodos region.

The Troodos ophiolite has undergone detachment and roughly 90° of counter-clockwise rotation (Clube et al., 1985; Robertson and Woodcock, 1986). Uplift and emplacement of the oceanic lithosphere formed new fractures and fracture zones (Section 2.3.1 and Figure 5.14). Two sets of large-scale lineaments cross-cut the igneous-sediment boundary, implying late formation, that may be related to the uplift of the ophiolite to its present position. The two remaining sets of large-scale fractures (interpreted from lineaments) are of pre-uplift origin, before the accumulation of significant sedimentary deposits (Section 2.3.1). These large-scale fractures may have formed during extension and ridge jump episodes since they are associated with hydrothermal alteration; other lineaments of these sets may be related to later graben formation.

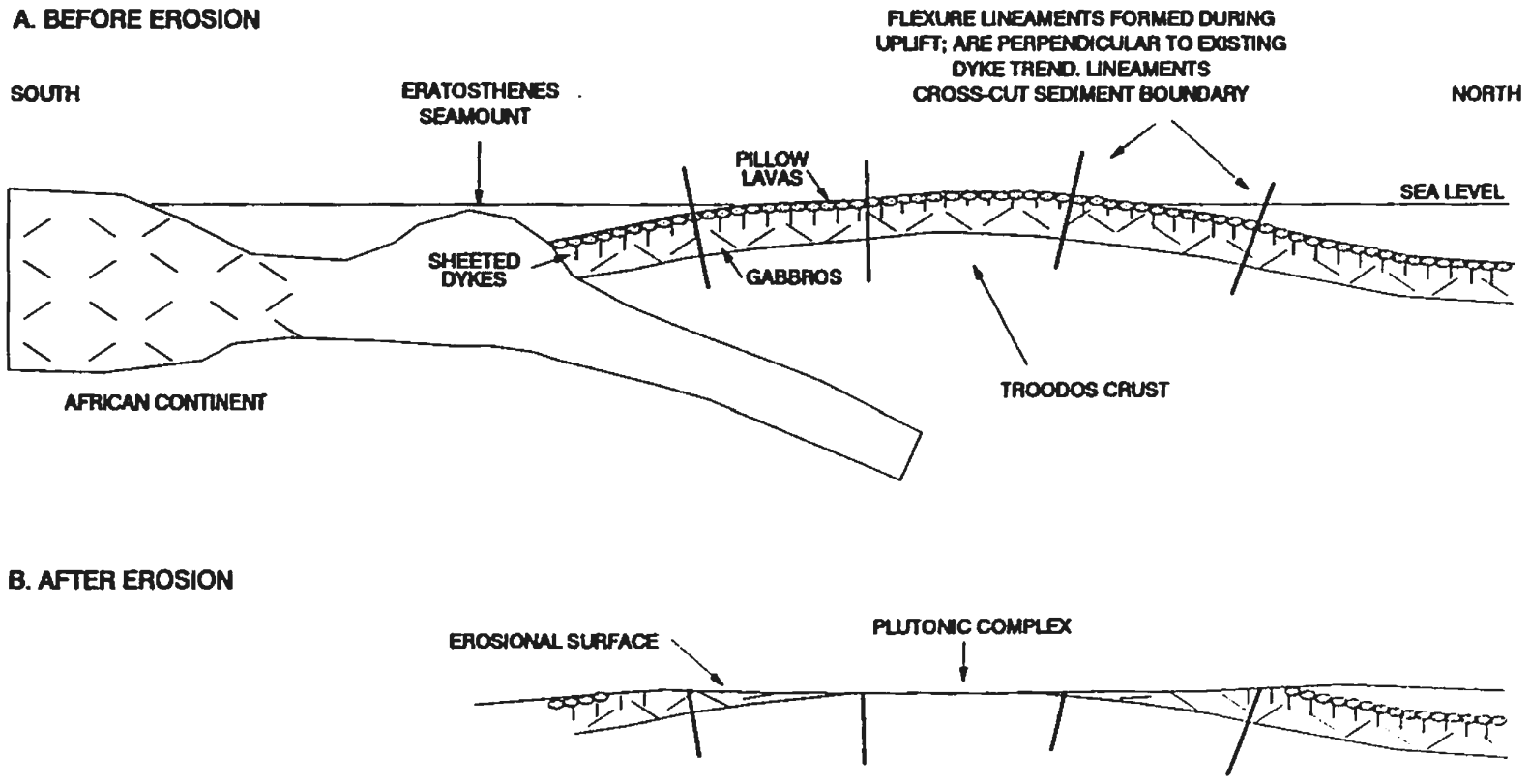

FIGURE 5.14 OPHIOLITE UPLIFT SHOWN IN A NORTH-SOUTH SECTION. FLEXURE IN AN EAST-WEST DIRECTION WAS VERY SIMILAR. LINEAMENTS ARE SETS 1 AND 3 AS DESCRIBED IN CHAPTER 2.2.1. THEY ARE UPLIFT RELATED AND CROSS-CUT THE IGNEOUS-SEDIMENTARY BOUNDARY.

6. FRACTURE AND PERMEABILITY CHARACTERISTICS OF THE SHEETED DYKE COMPLEX: IMPLICATIONS

6.1 INTRODCUTION

Fracture characteristics are important in controlling the directions and volumes of hydrothermal fluid flow through the sheeted dyke complex. These characteristics were used in Chapter 4 to determine the fractured rock permeability of the sheeted dyke complex. In this chapter the fracture characteristics of the sheeted dyke complex will be discussed in the context of their formation in oceanic crust and a model will be presented for the permeability structure of the sheeted dyke complex. Comparisons of the permeability results from Chapter 4 will be made with those from drilling efforts in the oceanic crust; the implications of these comparisons for permeability of the oceanic crust will be discussed.

6.2 FRACTURE CHARACTERISTICS

Fractures form as a result of applied stresses, be they thermal, fluid or mechanical. Fractures that were paragenetically early in the Spilia-Politko field area were divided into two groups based on orientation, origin, aperture and trace length. The two groups are 1) dyke-parallel cooling fractures, and 2) dyke-interior columnar cooling fractures (Figures 3.7 and 6.1). As the magma is injected into the crust it comes into contact with colder wall rock (previously formed dykes), and rapidly cools. During this process, contraction of the rock causes the formation of the dyke margin and internal columnar jointing fractures. Fractures sub-parallel to the dyke margins are in general longer, have greater apertures and have a tendency to be filled by paragenetically early epidote;

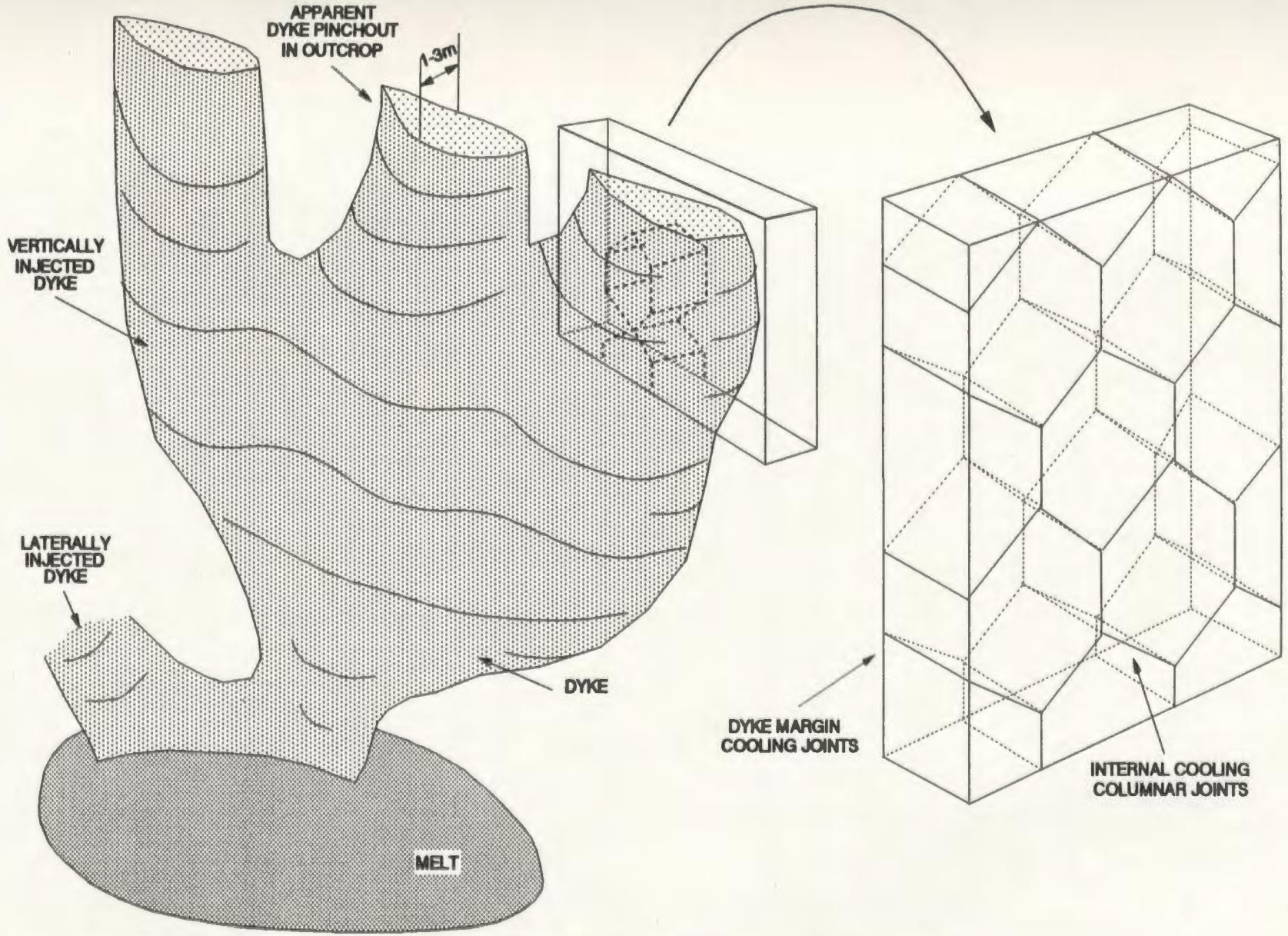

FIGURE 6.1 EARLY FRACTURE FORMATION IN SHEETED DYKES. SEE FIGURE 3.6 FOR FRACTURE ORIENTATION IN RELATION TO ORIGIN.

fractures in the interiors of dykes are shorter, have smaller apertures and are likely to be filled by paragenetically late calcite (Sections 3.3.4 and Appendix C.1).

The majority of fractures appear to have formed as a result of the contraction with cooling of the sheeted dykes. It was not always possible to determine the origin of fractures. This, however, does not affect the determination of the fracture permeability, since only those fractures that contained hydrothermal mineral fillings were used in the permeability calculations. These filled fractures existed at the time of hydrothermal fluid circulation independent of the mode of their formation. Fractures which formed late in the history of the area may have orientations similar to earlier fractures because anisotropies, such as existing fractures in the rock, influence the position and orientation of late fractures. Randomly oriented late fractures may have formed due to re-adjustment, during rotation, of fault-bounded dyke blocks.

Fracture frequency does not strongly change either with depth or laterally (Section 3.3.7). Fracture termination mode indicates that later fractures may have formed higher in the section (Section 3.3.5). This implies that there was minimal additional fracturing at depth.

In the sheeted dykes, fracture apertures decrease with depth, from 3 down to 2 millimetres, and fractures parallel to dyke margins have larger apertures than other fractures, by about 0.5 millimetres on average. This implies that fluid circulation will concentrate along dyke-parallel margins. Decrease in fracture aperture with depth is directly related to the increase in confining pressure with depth. Fracture mineral fillings do, however, indicate that fractures were open at depth (Section 3.3.2). Mean fracture trace lengths decrease with depth, from about 3 down to 1.5 metres (Figure 3.12). Fracture frequencies (and fracture intensities) are higher, deeper in the sheeted dykes.

This means that fluid circulation may be more diffuse in the deeper sections of Layer 2B (refer to Section 5.3.5) due to more numerous, yet smaller, fractures at depth.

The majority of fractures mapped in the northern portion of the Basal Group contain no mineral filling (Section 3.3.4). This may be the result of concentration of hydrothermal upflow into narrow, well defined zones. Fractures outside these zones would remain unaffected by hydrothermal upflow. They may act as conduits for recharging seawater. Roughly 50% of all fractures measured do not contain evidence for fluid passage (Table 3.6). The fractures containing no mineral fillings are concentrated in areas with the steepest dykes, lowest concentration of mines, gossans, and mineral showings, and the thickest dyke section. In these areas, only a few instances of leaching of material from fractured wall rock were noted in the sheeted dykes. A thick dyke section would result in shallower thermal gradients. Fluids would not traverse the section as quickly, meaning there is less chance of forming significant amounts of mineral deposits.

The extent of similarities in fracture characteristics in the field area (Chapter 3), implies that processes operating beneath the seafloor are similar over large areas. This also implies that, although the thermal state of the crust is variable, such as near a ridge-transform intersection (RTI), fracture chracteristics near a RTI are similar to those far from the RTI because dyke cooling stresses appear to operate on the scale of individual dykes. Dyke margin orientations are affected by the regional stress field and thus by proximity to a RTI but the internal fracturing of dykes depends on the thermal characteristics of dykes and not the external stress field.

Fracture characteristics such as fracture aperture, orientation, trace length, and mineral filling are discussed further in the following section in the context of the permeability of the sheeted dyke complex

6.3 PERMEABILITY

The primary permeability in hand specimens from the Spilia-Politiko area is too small for the rock matrix to act as fluid conduits (Section 4.3). Fractures provide most of the fluid conduits through the rock. The permeability of these conduits varies with time and depth. The decrease in the calculated vertical permeabilities with depth (parallel-plate method - Section 4.3.1) shows that the extent of interconnected fractures, with significant effective apertures available for fluid circulation, decreases with depth in the sheeted dykes. The relatively few fractures filled with late calcite indicate that late-stage permeabilities were lower in the sheeted dykes.

The permeability structure of sheeted dykes is quite variable. Figure 6.2 shows the relative permeabilities for the various rock types in the upper oceanic crust. Within the dykes, the permeability anisotropy remains at a relatively constant orientation, whereas their magnitudes get smaller with increasing depth. The permeability directions within the sheeted dykes are highly dependent on the orientations of the dykes. The directions of maximum and intermediate principal permeability are invariably oriented parallel to the dyke margins (Appendix A.7.2). This is suppported by the observation that dyke parallel fractures have the largest apertures (Section 3.3.2) and that these fractures also have the longest trace lengths implying the largest fracture radii (Section 4.3.3.2). The permeability directions are consistent within domains and differ from domain to domain, as expected (Section 4.3).

The vertical permeability in the gabbros (scanline 0122) is several orders of magnitude higher than in the sheeted dykes. In this area, a network of fine fractures filled with hydrothermal minerals and epidotization of parts of the gabbros, may be the result of the

Figure 6.2 Principal Permeability Directions in Layer 2B oceanic crust. k1, k2, k3 are the maximum, intermediate, and minimum principal permeabilities. Line lengths (labelled k1, k2, k3 at right of diagram) of permeability ellipsoids (represented by three orthogonal lines) are indicative of relative permeability magnitudes and directions. Longer lines indicate greater permeability. Along dyke planes permeability is greatest in two directions within the plane (longest lines). and smallest perpendicular to the plane (shortest line). Heavy arrows in the block diagram show hydrothermal fluid circulation. Note rotation of permeability ellipsoid near the ridge-transform intersection (RTI) with respect to those further away from the RTI. Permeability in the dykes decreases with depth (decreasing ellipsoid size with depth) Permeability in the epidosites is greater (larger ellipsoid) than that in the dykes (smaller ellipsoid), whereas in the sediments the permeability is very low (small ellipsoid). Patterns in the pillow lavas serve to differentiate different pillows and flows. Patterns in the crustal section below the sheeted dykes are the same as in Figure 5.1.

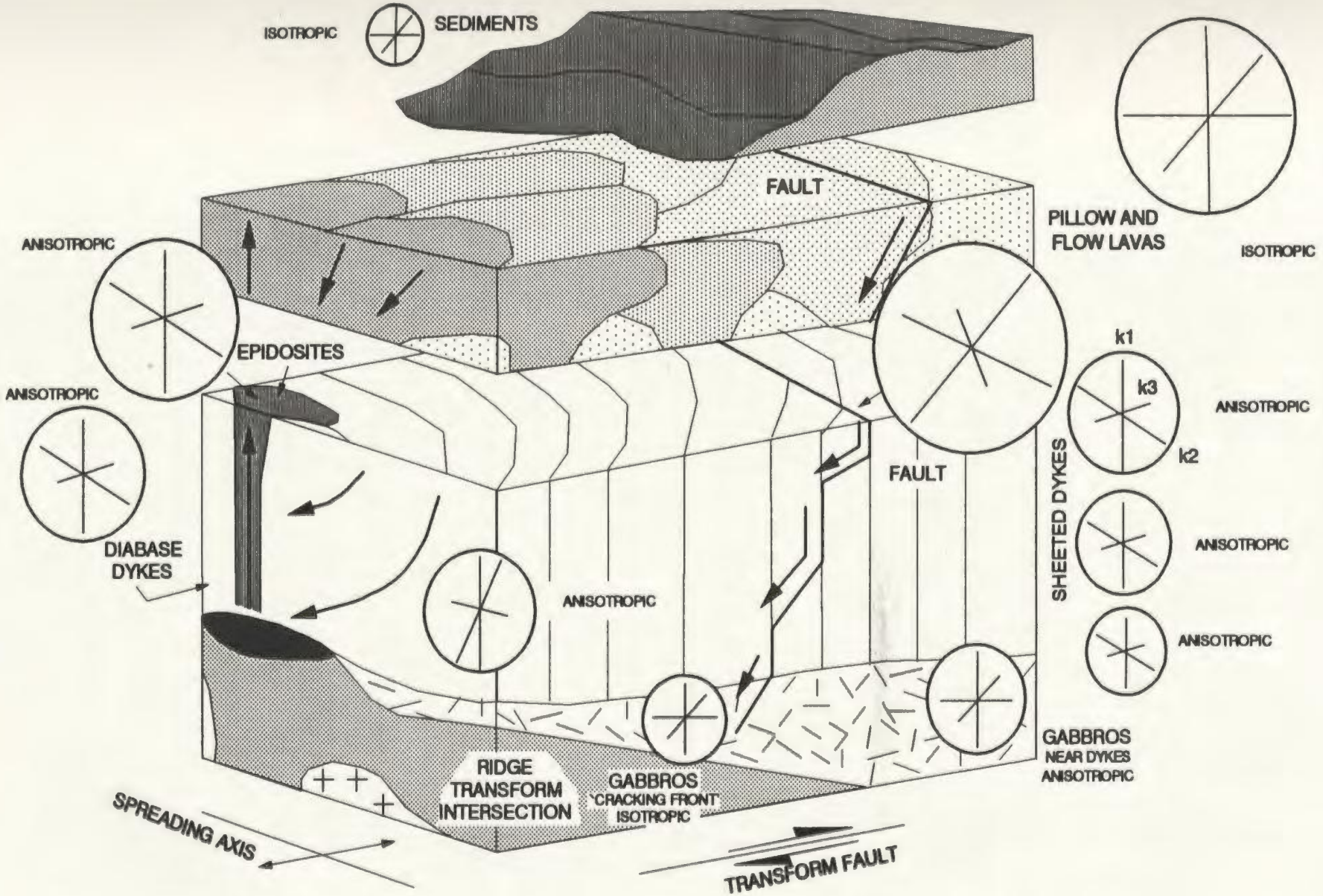
ISOTROPIC
SEDIMENTS
FAULT
PILLOW AND
FLOW LAVAS
ISOTROPIC
ANISOTROPIC
EPIDOSITES
ANISOTROPIC
k1
k3
k2
ANISOTROPIC
FAULT
SHEETED DYKES
DIABASE
DYKES
ANISOTROPIC
ANISOTROPIC
ANISOTROPIC
GABBROS
NEAR DYKES
ANISOTROPIC
RIDGE
TRANSFORM
INTERSECTION
GABBROS
'CRACKING FRONT'
ISOTROPIC
SPREADING AXIS
TRANSFORM FAULT

formation of a progressively advancing cracking front as postulated by Lister (1983). Areas where a 'cracking-front' has formed, have isotropic permeabilities, that is, the permability is the same in all directions at any point. In other gabbros (scanline 0112), where fracturing is also influenced by the injection of dykes from a new magma chamber, the fracture pattern and the permeability direction, reflect that of the dykes.

Mapping of fractures in extrusive volcanic rocks demonstrates there is an absence of a directional fabric (Section 3.3.3). As a result, the permeability in the pillow lavas is isotropic. This is due to their random, highly fractured nature. The permeability of the overlying sedimentary cover is very low and may be isotropic if there are no sedimentary structures, such as layering, present. Areas of little or no sediment cover become areas of vertical hydrothermal flow (discharge or recharge) whereas beneath sedimented areas hydrothermal circulation is laterally oriented assuming layering of contrasting lithologies.

Faults, which are open to the circulation of fluids and connected to the overall fracture network, tend to control permeability (Section 4.3.2). The presence of a high-permeability zone such as a fault, with an effective aperture at least two orders of magnitude greater than the average effective aperture in the area containing the fault, would result in the fluids primarily utilizing the fault (Section 4.3.2). That faults or permeable shear zones can be the major conduits for fluids in the sheeted dykes, is supported by the association of epidosites with major faults and lineaments (Section 5.2). However, the common occurrence of secondary mineralization in fractures, and the apparent lack of significant numbers of outcrop-scale mineralized faults, implies that much of the flow did pass through the outcrop-scale fracture systems. The unmineralized outcrop scale faults may not have been connected to the fracture network or they may have been the site of hydrothermal recharge (down-flow).

Whereas outcrop-scale faults do not seem as important in relation to the discharge portion of hydrothermal circulation cells, large-scale (100's of metres to kilometres in trace length) faults interpreted from lineaments from satellite imagery (Section 2.3.1), do appear to control the location of the epidosites. This implies that large-scale faults play a major role in the siting of hydrothermal circulation cells.

Fractures filled with minerals imply that some of the fractures were blocked to fluid circulation at some point in time. This in turn would have caused a decrease in the bulk permeability of the rock as the number of open interconnected fractures decreased. If, at this stage, sufficient heat was still present to drive fluid circulation, the fluid circulation would either 1) concentrate in the remaining open fractures in the network; or 2) create new fractures as a result of anomalously high fluid pressures; or 3) be relegated to the upper reaches of the oceanic crust, in the highly fractured extrusive rocks.

It is not possible, on the basis of field work in the Spilia-Politiko area to unequivocally decide whether fluids were largely confined to existing or newly-formed fractures, because new fractures would likely have similar orientations to pre-existing fractures and be filled with similar mineral assemblages. New fractures may have formed in areas such as the breccia zone, near Apliki village, which suggests the presence of anomalous fluid pressures caused fracturing of the rock. Anomalous fluid pressures imply that more permeable flow conduits were blocked allowing the pressure to build up.

The permeability of the rocks of the sheeted dyke complex decreased through time (Section 4.3) as fractures became filled with minerals deposited by circulating hydrothermal fluids. The permeability decreased in areas utilized by on-axis hydrothermal fluids (Section 4.3.3.4.1). Later circulation of cooler, calcite-precipitating

fluids, off-axis, occurred under very low permeability conditions (Section 4.3.3.4.2). These later conditions may be similar to those encountered in oceanic crust in off-axis Deep Sea Drilling Project boreholes (e.g. DSDP hole 504B).

The permeability calculations done on the basis of calcite-filled fractures (Section 4.3.3.4.2), indicated that formation of shear zones and formation of plagiogranite bodies lead to the formation of additional fractures. These are implied to have formed late because of their association with calcite. Their formation may be linked with the formation of the Mitsero graben structure.

Contemporaneity of hydrothermal circulation and sheeted dyke formation implies that some fractures may not have existed during early pulses or phases of hydrothermal circulation. Thus, the actual permeability of the system may have been lower than that calculated, in this study, based on modelling using all of the mineral-filled fractures. In order to model the effect of having fewer fractures on the permeability the fracture density (P_{32}) was reduced to 75% and 25% of its original field-mapped value (Section 4.3.3.4.3 and Table 4.11). These results demonstrated that the permeability is reduced by only one to two orders of magnitude even when the fracture density is dropped to 25% of its original value. Below this 25% level, there was a sharp drop in the modelled permeability to $10^{-23}m^2$ indicating a critical threshold below which the fracture interconnectivity is too low to support continuous pathways through the rock mass. A second important parameter that affects the calculated permeability is the fracture aperture. If multiple fluids had utilized the same fractures, the actual fracture apertures would be less at the time of fluid circulation than are presently preserved fracture widths used in the permeability calculations. In order to model the effect on permeability of having smaller apertures, the fracture transmissivity was reduced to 75% and 25% of the original value. The resultant permeability fell by only two to three orders of magnitude

(Section 4.3.3.4.3 and Table 4.11). Though abitrarily selecting reductions in size of the fractureset and aperture width have no physical basis in reality, the resultant change in the calculated permeability of only 1 to 3 orders of magnitude indicate that the permeability modelling for the Troodos sheeted dyke complex yields values that are relatively insensitive to the modelling parameters, therefore lending greater credibility to the results.

Lateral variations in permeability throughout the sheeted dyke complex appear to be mediated by the formation of faults. Characteristics of fracturing appear to have been very similar from area to area in the crust (Chapter 3), resulting in similar permeabilities in different areas at the same level in the crust.

6.4 PERMEABILITY COMPARISON AND IMPLICATIONS FOR OCEANIC CRUST

Comparisons of the results from the three methods of permeability calculations (Chapter 4) were made to assess their validity and the implications of these results with respect to the permeability structure of the oceanic crust. These three methods were, to reiterate, the parallel plate method (Norton and Knapp, 1977), a matrix addition method (Bianchi and Snow, 1969), and the stochastic fracture simulation method (Dershowitz et al., 1991).

Of the many holes drilled into the oceanic crust as part of the The Deep Sea Drilling Project (DSDP) and Ocean Drilling Program (ODP) only DSDP hole 504B penetrates well into the sheeted dykes of Layer 2B of the oceanic crust. DSDP drill hole 504B was drilled approximately 200 kilometres off the Costa Rica ridge axis in 6 Ma old crust (Anderson and Zoback, 1982). The permeability determined from *in situ* packer tests in

the sheeted dykes is approximately $10^{-17}m^2$ (Becker, 1991; Figure 6.3). Open fractures are those that contribute to the present permeability in hole 504B ocean crust, whereas other fractures may be sealed by the precipitation of minerals from hydrothermal fluids. The presence of both open and closed fractures means that permeabilities determined from *in situ* bore hole packer tests, in off-axis boreholes, are not likely to be representative of the permeability of the rock during the on-axis hydrothermal circulation. Comparison of the permeability calculations from ophiolites with permeability determinations from the sheeted dykes in the present day oceanic crust are hampered by the fact that there is only a single borehole in all the world's oceans that extends well into the sheeted dykes, that being DSDP hole 504B. Until more holes are drilled to these depths in the oceanic crust, it will not be possible to verify whether the permeabilities estimated from hole 504B are representative of oceanic crust as a whole, however it is the only *in situ* data available for comparison with this study of the Troodos ophiolite.

6.4.1 Parallel Plate Method Results

Comparison of the parallel plate method results with permeability data from borehole packer tests in the Deep Sea Drilling Project boreholes, shows that these results are larger by roughly seven orders of magnitude (Figure 6.3) then the *in situ* tests on the modern seafloor. However, the parallel-plate method of calculating permeability has yielded similar results for the sheeted dykes of the Semail ophiolite, Oman (Nehlig and Juteau, 1988). They estimated flow porosity using Norton and Knapp's (1977) parallel-plate fracture model, to be of the same order of magnitude as those estimated by this study, that is, of the order of $10^{-10}m^2$ ($3x10^{-10}$ to $7x10^{-9}m^2$). Norton and Knight (1977) showed that permeabilities greater than $10^{-19}m^2$ are conducive to fluid circulation in

Figure 6.3 Bulk Permeabilities of oceanic crust. Data from various studies: (1) Anderson and Zoback (1982); (2) Becker (1989, 1991); (3) Chapman (pers. comm., 1982); (4) Davis et al. (1991); (5) Freeze and Cherry (1979); (6) Johnson, (1980); (7) Nehlig and Juteau (1988); (8) Williams et al. (1986); The following results are from this study: (9) Parallel plate model and Bianchi and Snow (1969) methods (Sections 4.3.1 and 4.3.2); (10) Dyke permeability from FracMan/MAFIC results (Section 4.3.3); (12) Calcite filled fracture permeability from FracMan/MAFIC results (Section 4.3.3). Star is the lower permeability limit calculated through the reduction of fracture densities and apertures. Schematic stratigraphic column of Layer 1 (sedimentary rocks) and 2 (pillow and flow units and sheeted dykes) of the Troodos ophiolite is included for reference.

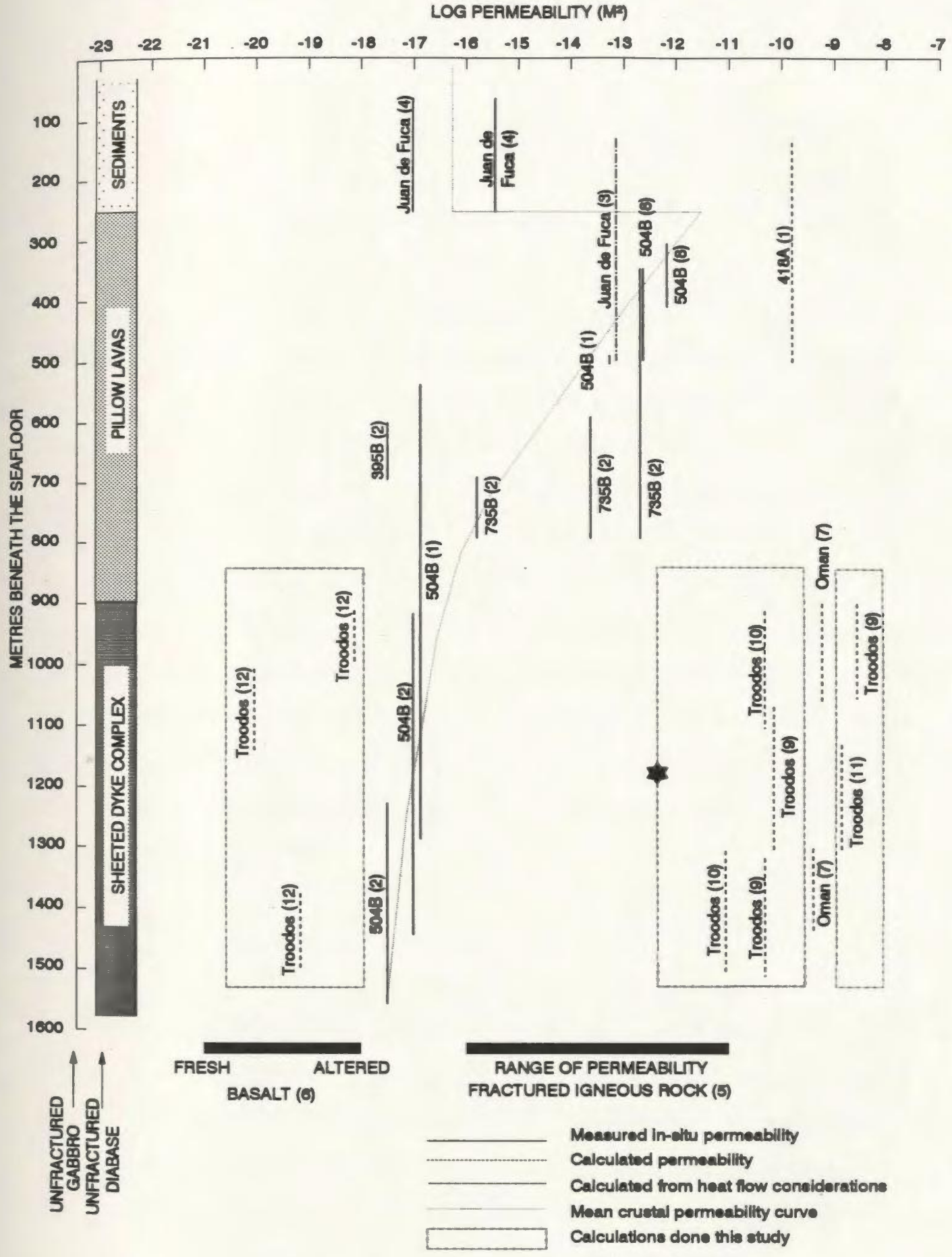
LOG PERMEABILITY (M²)
-23
-22
-21
-20
-19
-18
-17
-16
-15
-14
-13
-12
-11
-10
-9
-8
-7
METRES BENEATH THE SEAFLOOR
100
200
300
400
500
600
700
800
900
1000
1100
1200
1300
1400
1500
1600
SEDIMENTS
PILLOW LAVAS
SHEETED DYKE COMPLEX
UNFRACTURED GABBRO
UNFRACTURED DIABASE
Juan de Fuca (4)
Juan de Fuca (4)
Juan de Fuca (3)
504B (6)
504B (6)
418A (1)
504B (1)
735B (2)
735B (2)
735B (2)
395B (2)
504B (1)
504B (2)
504B (2)
Troodos (12)
Troodos (12)
Troodos (12)
Troodos (10)
Troodos (9)
Troodos (10)
Troodos (9)
Troodos (9)
Oman (7)
Oman (7)
Troodos (11)
Troodos (9)
FRESH
ALTERED
BASALT (6)
RANGE OF PERMEABILITY
FRACTURED IGNEOUS ROCK (5)
Measured in-situ permeability
Calculated permeability
Calculated from heat flow considerations
Mean crustal permeability curve
Calculations done this study

plutonic environments, which is the case for the Spilia-Politiko area of the Troodos ophiolite and the Semail ophiolite.

6.4.2 Matrix Addition Method Results

Comparison of the averaged permeability values calculated by the Bianchi and Snow (1969) method for the dyke-parallel fractures with the results from the parallel-plate model, also dyke-parallel (compare Table 4.1 and 4.3), indicates that the parallel-plate method results in slightly higher calculated permeabilities. When all fractures filled with hydrothermal minerals, and not only the dyke-parallel fractures, are taken into account, the permeability values calculated by the Bianchi and Snow (1969) method are higher than those calculated by the parallel-plate method, as expected. Calculated permeabilities do not show any significant variation from area to area. The Bianchi and Snow (1969) method does not give a better estimate of the permeability magnitude of Deep Sea Drilling Project borehole test results, than the parallel-plate method. It does give an estimate of the principal permeability directions. This estimate is biased by the assumption that all fractures are continuous throughout the area.

6.4.3 Stochastic Method Results

The permeabilties calculated on the basis of those fractures filled with high temperature hydrothermal minerals such as epidote and quartz are roughly seven orders of magnitude greater than those calculated from DSDP hole 504B (Figure 6.3). Even when reducing the number of fractures and aperture widths to 25% of the measured values in the field, the calculated permeability in this study is approximately 5 orders of magnitude greater

than those in hole 504B. This difference may be because 1) all filled fractures are taken into account in the calculations for this study whereas not all fractures may be open at any one specific time, or 2) the open, interconnected fractures in DSDP 504B are a subset of those that were open during ridge crest hydrothermal circulation, some of which have now been sealed. The permeability calculations done in this study using a reduced fracture set (Section 4.3.3.4.3) indicate that the permeabilities may be realistic, which implies the DSDP hole 504B permeabilities were higher at the ridge crest during hydrothermal circulation than they are now.

Permeabilities determined on the basis of calcite filled fractures, demonstrated that they were smaller than those computed from the borehole packer tests in DSDP drill hole 504B (Figure 6.3) but by no more than two orders of magnitude. This also infers that the 504B permeabilities are probably not representative of the original on-axis fracture permeability of the sheeted dykes, at the time of hydrothermal circulation.

Permeabilities determined on the basis of reduced apertures (Section 4.3.3.4.3) were still several orders of magnitude greater than the permeability calculated from the DSDP hole 504B packer tests. The simulated variations in aperture do not bring the calculated permeabilities into the range of those from hole 504B. This implies the permeabilities calculated here may be realistic and, as well, that the permeability in active hydrothermal areas at spreading ridges are probably significantly higher than those in off-axis positions. This again assumes that the Troodos ophiolite is a useful analogue for present oceanic crust. Since DSDP hole 504B is off-axis, permeabilities determined in this hole more likely reflect off-axis rather than on-axis conditions.

6.5 CONCLUSIONS

The present state of knowledge concerning sheeted dyke complexes lies in three areas: 1) theory of dyke formation (based on fracture mechanics and magmatic processes) (e.g. Karson, 1987; Pollard, 1987); 2) geochemistry of dykes in relation to oceanic crust formation (e.g. Baragar et al., 1989); and 3) large-scale tectonic processes in the deformation of dyke complexes (e.g. Allerton and Vine, 1991; Varga and Moores, 1985). The fracture mechanics approach (in point 1), is concerned with the fracture processes of the crust into which the magma is injected during the formation of dykes. This study is more concerned with the effects of processes acting after the formation of dykes in a sheeted dyke complex. These effects include the faulting and rotation of dykes within a sheeted dyke complex, the circulation of hydrothermal fluids and its scale, and the permeability structure of the sheeted dyke complex.

The principal contributions of this study, concerning the sheeted dykes of the Troodos ophiolite, can be presented in four groups as follows:

I. Formation and deformation of dyke domains:

1) ridge jumps, possibly during periods of amagmatic stretching, are used to account for the differing orientations of dyke domains near ridge-transform intersections;
2) continued vertical dyke orientations away from the ridge axis imply translation-without-rotation of dykes and/or re-rotation of the dykes as they spread beyond the axial caldera boundary;
3) permeability directions are greatly affected by dyke orientation. An on-axis graben which formed through listric faulting or rotation of planar normal

faults will have more shallow dipping conduits available for the lateral circulation of fluids than will an area where the graben formed off-axis.

II. Fracture characteristics of the sheeted dykes:

1) fracturing of the dykes in the sheeted dyke complex occurs very early in its history. Most fractures are cooling-related, either parallel to the chilled dyke margins or internal columnar cooling joints;
2) dyke parallel fractures are longer, have greater apertures, and contain a greater proportion of high temperature hydrothermal minerals, such as epidote, than do the internal columnar jointing fractures;
3) unfilled fractures in the upper portions of the sheeted dyke complex imply concentration of hydrothermal upflow in narrow zones. These zones are preserved as epidosites in ophiolite complexes;
4) filled fractures lower in the sheeted dyke complex imply hydrothermal fluids were more diffuse in their distribution at depth;
5) fracture apertures and trace lengths decrease with depth in the sheeted dyke complex.

III. Hydrothermal circulation in the sheeted dyke complex:

1) points II.3 and II.4 imply that hydrothermal fluid circulation starts in a more diffuse network at depth and then becomes concentrated in narrow zones as they rise through the sheeted dyke complex;
2) hydrothermal fluid temperatures throughout the sheeted dyke complex are consistent, about 360°C. The fluids did not undergo phase separation

within the sheeted dyke complex, although they may have done so in the plagiogranites below the dykes;

IV. Permeability variations within the sheeted dyke complex:

1) although fracture frequency and intensity (Sections 3.3.7 and 4.3.3.1) increase with depth, the effect of the decrease in fracture aperture with depth on permeability is much greater, resulting in permeability decrease with depth in the sheeted dyke complex;
2) areas altered to epidosites have higher permeabilities than do unaltered diabase dykes. Permeability anisotropy is strongly directed with the maximum and intermediate permeability directed parallel to the dyke margins.
3) permeability of hydrothermal mineral-filled fractures (on-axis) was of the order of $10^{-10}m^2$; later (off-axis) permeabilities, based on calcite-filled fractures dropped to $10^{-19}m^2$. Later formation of shear zones and intrusion of plagiogranites resulted in locally higher permeabilities.
4) Not all fractures may have been present during particular phases of hydrothermal activity, and not all fractures may have been open to the extent measured in the study area, however, calculated permeabilities nevertheless are substantially more than those seen in DSDP hole 504B. This implies permeability decreases as the crust moves off-axis.

In summary then, the magma supply and the prevailing stress field strongly influence the development of a sheeted dyke complex in the ocean crust. The complex develops in three stages: (1) **on-axis** injection of dykes is limited by the magma budget; the stress field orientation controls their orientation, this includes proximity to structures such as transform fault zones; (2) **intermediate stage of spreading** where the dykes move off-

axis and experience deformation due to possible subsidence, normal faulting related to axial caldera formation, and later reactivation of the faults as the dykes pass over the ridge valley walls; and (3) off-axis tectonic stretching related to periods of low or no magma budget, resulting in the formation of graben structures.

The permeability-porosity structure of the dykes changes within this period from low porosity-low permeability just after magma injection, to high permeabilities related to the formation of dyke cooling fractures. As the dykes move away from the injection point, faults form and hydrothermal fluid circulation will begin leaching elements from the rock and precipitating minerals in the fractures, in addition to internal rock iso-chemical mineralogy changes. The formation of hydrothermal upflow zones is restricted to narrow zones of increased permeability above a heat source. The hydrothermal upflow zones may narrow higher in the sheeted dyke section.

The direction of greatest permeability is directed parallel to the dyke margins. During hydrothermal fluid circulation it is these fractures that are more likely to be open. Porosity and permeability eventually decrease as the fractures are filled. Late, off-axis circulation probably occurs only in the upper reaches of the crust in the highly permeable volcanic section beneath a low permeability sedimentary cover. Low temperature (late) circulation may result in the precipitation of calcite. Additional fracturing, following the orientation of pre-existing fractures, may occur during the formation of the graben structure. Circulating cooler fluids, utilizing these later conduits, fill the fractures with calcite or possibly zeolite minerals.

6.6 RECOMMENDATIONS

The following list contains both suggestions to fine tune the work presented in this thesis and recommendations to extend this work in further studies.

(1) The domain boundaries established in Chapter 2 need to be 'ground-truthed'. That is, determine the cross-cutting relationships of dykes at the domain boundaries. Determine the role of faults with respect to domain boundaries. Dyke cross-cutting relations at the domain boundaries may also establish whether the relative domain ages (Section 5.3.4) are correct.

(2) More detailed mapping of faults may allow the identification of faults related to the formation of an axial caldera and those related to the formation of the Mitsero graben. Evidence for this may be found through a systematic study of slickensides on fault mineral-coated and uncoated surfaces.

(3) Further structural mapping in the study area is needed to collect strong evidence for the presence and location of a detachment zone. Fracture characteristics (such as fracture orientation and mineral filling) in the area of a detachment zone may indicate the timing of hydrothermal circulation with respect to the detachment.

(4) Further fracture measurements should be done on the basis of the area-mapping method (Section 3.3.1.1) in order to develop a less biased data set. Determine, through further field work, the shapes of fracture planes and their relation to different lithologies. Fracture mineral filling relationships to the wall rock need to be examined in greater detail to determine the extent of the interaction between fluid flow in the fractures and alteration in the rock matrix.

(5) Fracture mapping should be undertaken in domain 1 to determine the effects of the South Troodos Transform Fault (STTF) on the fracture pattern and on the spatial variability of hydrothermal circulation with respect STTF.

(6) A better method of determining the fracture apertures in the field needs to be developed. Such a method would require the measurement of aperture variations along fractures in order to incorporate the fluid channeling into an aperture model. Perhaps this would be a combination of existing laboratory fracture aperture variation data with a field model of apertures. This is very important in the determination of accurate and precise paleo-permeabilities.

(7) Determine the relations between the plutonic suite, the epidosites and the ore deposits. This may provide a method of determining the longevity of the hydrothermal systems, through knowledge of the cooling rates of the plutons and the rates of formation of the ore deposits.

(8) A transect across a hydrothermally altered epidosite zone, to measure fluid inclusion temperatures and oxygen isotope variations, to establish the lateral extent of an up-flow zone. This would help to determine the effects of the fracture system on the radii of hydrothermal systems.

(9) In order to develop a coherent numerical model for hydrothermal circulation in the area, information is required on the permeability at a greater number of locations. This information could be integrated into a dual-porosity model. Such a dual-porosity model would be one where the outcrop-scale, calculated permeabilities would provide a porous medium equivalent permeability, whereas large faults, fault zones, and other 'ground-truthed' lineaments would provide the large-scale fracture permeability to model the field area.

(10) Permeability information is needed from active hydrothermal areas at spreading ridge axes. This information has proven highly elusive, since the act of drilling into an active system changes its permeability characteristics.

(11) Further work may involve cross-hole packer tests in multiple boreholes in present-day oceanic crust in order to determine the control fractures have on the flow of fluids. Permeability data are also needed from active hydrothermal areas.

This may also establish the suitability of studying ophiolites as anlogues of oceanic crust in terms of their physical properties. There is a need for greater links between work done on ophiolites and that done on oceanic crust.

REFERENCES

Adamson, A.; 1985; Basement Lithostratigraphy, Deep Sea Drilling Project Hole 504B; in Anderson, R. N., Honnorez, J., Becker, K. et al. (eds.) Initial Reports of the Deep Sea Drilling Project; U.S. Government Printing Office, Washington, v83 p121-128.

Agar, S.M.; 1990; Fracture Evolution in the Upper Ocean Crust: Evidence From DSDP Hole 504B; in Knipe, R. J., Rutter, E. H. (eds.) Deformation Mechanisms, Rheology and Tectonics; Geological Society Special Publication n54 p41-50.

Allen, C. R.; 1975; The Petrology of a Portion of the Troodos Plutonic Complex, Cyprus; Unpublished Ph.D. thesis, Cambridge University 243p.

Allerton, S.; 1989; Distortions, Rotations and Crustal Thinning at Ridge-Transform Intersections; Nature; v340 p626-628.

Allerton, S., and Vine, F.J.; 1987; Spreading Structure of the Troodos Ophiolite, Cyprus: Some Paleomagnetic Constraints; Geology v15 p593-597.

Allerton, S., and Vine, F.J.; 1991; Spreading Evolution of the Troodos Ophiolite, Cyprus; Geology v19 p637-640.

Alt, J.C., Anderson, T.F., Bonnell, L., and Muehlenbachs, K.; 1989; Mineralogy, Chemistry and Isotope Compositions of Hydrothermally Altered Sheeted Dikes: ODP Hole 504B, Leg 111; in Becker, K., Sakai, H. et al. (eds.) Proceedings of the Ocean Drilling Program v111 p27-40.

Alt, J.C., Honnorez, J., Laverne, C., and Emmermann, R.; 1986; Hydrothermal Alteration of a 1Km Section Through the Upper Oceanic Crust, D.S.D.P. Hole 504B: Mineralogy, Chemistry and Evolution of Seawater Basalt Interactions; Journal of Geophysical Research v91 nB10 p10309-10335.

Anderson, R.N., and Zoback, M.D.; 1982; Permeability, Underpressures and Convection in the Oceanic Crust Near the Costa Rica Rift, Eastern Equatorial Pacific; Journal of Geophysical Research v87 nB4 p2860-2868.

Anonymous; 1972; Ophiolites (Penrose Conference Participants); Geotimes v17 p24-25.

Atwater, T., and Macdonald, K.C.; 1977; Are Spreading Centres Perpendicular to Their Faults?; Nature v270 p715-719.

Atwater, T., and Molnar, P.; 1973; Relative Motion of the Pacific and North American Plates Dedduced From Sea Floor Spreading in the Atlantic, Indian and South Pacific Oceans; in Proceedings of the Conference on Tectonic Problems of the San Andreas Fault System, Stanford University Publs., Geol. Seis. vol 13 p136-148.

Axen, G.J.; 1988; The Geometry of Planar Domino-Style Normal Faults Above a Dipping Basal Detachment; Journal of Structural Geology v10 n4 p405-411.

Baecher, G.B.; 1980; Progressively Censored Sampling of Rock Joint Traces; Mathematical Geology v12 n1 p33-40.

Baecher, G.B., and Lanney, N.A.; 1978; Trace Length Biases in Joint Surveys; 19th U.S. Rock Mechanics Symposium p56-65.

Baecher, G.B., Lanney, N.A., and Einstein, H.H.; 1977; Statistical Description of Rock Properties and Sampling; Proceedings of the 18th U.S. Symposium on Rock Mechanics, American Institute of Mining Sciences, 5C1-8.

Baragar, W.R. A., Lambert, M.B., Baglow, N., and Gibson, I.L.; 1989; Sheeted Dykes From CY-4 and Surface Sections: Troodos Ophiolite; in Gibson, I. L., Malpas, J., Robinson, P. T., Xenophontos, C. (eds.) Cyprus Crustal Study Project: Initial Report, Hole CY-4; Geological Survey of Canada, Ottawa, G.S.C. Paper 88-9 p69-106.

Barker, P.F., and Hill, I.A.; 1981; Back-Arc Extension in the Scotia Sea; Philosophical Transactions of the Royal Society of London vA300 p249-262.

Bear, J.; 1979; Hydraulics of Groundwater; McGraw Hill International Book Co., 567p.

Bear, L.M.; 1960; The Geology and Mineral Resources of the Akaki-Lythrodondha Area; Cyprus Geological Survey Memoir 3, Nicosia, Cyprus, 122p.

Becker, K.; 1989; Measurements of the Permeability of the Sheeted Dykes in Hole 504B ODP Leg 111; in Becker, K., Sakai, H., et al. (eds.) Proceedings of the Ocean Drilling Program Scientific Results; Texas A&M University, v111 p317-355.

Becker, K.; 1991; In-Situ Bulk Permeability of Oceanic Gabbros in Hole 735B, ODP Leg 118; in Von Herzen, R. P., Robinson, P. T., et al. (eds.) Proceedings of the Ocean Drilling Program, Scientific Results; Ocean Drilling Program, Texas A&M University, v118 p333-347.

Ben-Avraham, Z., and Nur, A.; 1986; Collisional Processes in the Eastern Mediterranean; Geologische Rundschau v75 n1 p209-217.

Berman, R.G., Brown, T.H., and Greenwood, H.J.; 1985; An Internally Consistent Thermodynamic Data Base For Minerals in The System Na2O - K2O - CaO - MgO - FeO - Fe2O3 - Al2O3 - SiO2 - TiO2 - H2O - CO2; Atomic Energy of Canada Limited Technical Report, Ottawa, v377 62p.

Bianchi, L., and Snow, D.T.; 1969; Permeability of Crystalline Rock Interpreted From Measured Orientations and Apertures of Fractures; Annals of Arid Zone v8 n2 p231-245.

Biju-Duval, B., Lapierre, H., and Letrouzey, J.; 1976; Is the Troodos Massif (Cyprus) Allochthonous?; Bulletin Societé Géologique de France v18 p1347-1356.

Bischoff, J.L., and Rosenbauer, R.J.; 1984; The Critical Point and Two Phase Boundary of Seawater 200-500°C; Earth and Planetary Science Letters v68 p172-180.

Bischoff, J.L., and Rosenbauer, R.J.; 1989; Salinity Variations in Submarine Hydrothermal Systems by Layered Double Diffusive Convection; Journal of Geology v97 p613-623.

Bishopp, D.W.; 1952; Some New Features of the Geology of Cyprus; 19th International Geological Congress n17 p13-18.

Blome, C.D., and Irwin, W.P.; 1985; Equivalent Radiolarian Ages From Ophiolitic Terranes of Cyprus and Oman; Geology v13 p401-404.

Bodvarsson, G., and Walker, G.P.L.; 1964; Crustal Drift in Iceland; Geophysical Journal of the Royal Astronomical Society v8 n3 p285-300.

Bonhommet, N., Roperch, P., and Calza, F.; 1988; Paleomagnetic Arguments For Block Rotations Along the Arakapas Fault (Cyprus); Geology v16 p422-425.

Bowers, T.S., and Taylor, H.P.; 1985; An Integrated Chemical and Stable Isotope Model of the Origin of Mid-Ocean Ridge Hot Spring Systems; Journal of Geophysical Research v90 nB14 p12583-12606.

Boyle, J.F., and Robertson, A.H. F.; 1984; Evolving Metallogenesis at the Troodos Spreading Axis; in Gass, I. G., Lippard, S. J., Shelton, A. W. (eds.) Ophiolites and Oceanic Lithosphere; Geological Society of London Special Publication, v13 p169-181.

Brantley, S.H., Evans, B., Hickman, S.H., and Crerar, D.A.; 1990; Healing of Microcracks in Quartz: Implications For Fluid Flow; Geology v18 p136-139.

Browning, P., Roberts, S., and Alabaster, T.; 1989; Fine Scale Modal Layering and Cyclic Units in Ultramafic Cummulates From the CY-4 Borehole, Troodos Ophiolite: Evidence For an Open System Magma Chamber; in Gibson, I.L., Malpas, J., Robinson, P.T., Xenophontos, C. (eds.) Cyprus Crustal Study Project: Initial Report, Hole CY-4, Geological Survey of Canada Paper 88-9, p193-220.

Bury, K.V.; 1975; Statistical Models in Applied Science; John Wiley and Sons, New York, 625p.

Cann, J.R.; 1974; A Model For Oceanic Crustal Structure Developed; Geophysical Journal of the Royal Astronomical Society v39 p169-187.

Carr, J.M., and Bear, L.M.; 1960; The Geology and Mineral Resources of the Peristerona-Lagoudhera Area; Cyprus Geological Survey Memoir 2, Nicosia, Cyprus, 79p.

Charlaix, E., Guyon, E., and Rivier, N.; 1984; A Criterion For Percolation Threshold in Random Array of Plates; Solid State Communications v50 n11 p999-1002.

Church, W.R.; 1972; Ophiolite: Its Definition, Origin as Oceanic Crust and Mode of Emplacement in Orogenic Belts With Special Reference to the Appalachians; in The Ancient Oceanic Lithosphere; Department of Energy Mines and Resources, Ottawa; Earth Physics Branch, n3 v 42 p71-86.

Church, W.R., and Stevens, R.K.; 1971; Early Paleozoic Ophiolite Complexes of the Newfoundland Appalachians as Mantle Oceanic Sequences; Journal of Geophysical Research v76 n5 p1460-1466.

Clauser, C.; 1992; Permeability of Crystalline Rocks; EOS Transactions v73 n21 p233, 237-238.

Cleintaur, M.R., Knox, G.J., and Ealey, P.J.; 1977; The Geology of Cyprus and its Place in the East Mediterranean Framework; Geologie en Mijnbouw v56 n1 p66-82.

Clube, T.M. M., Creer, K.M., and Robertson, A.H. F.; 1985; Paleorotation of the Troodos Microplate, Cyprus; Nature v317 p522-525.

Cowan, J.C., and Cann, J.R.; 1988; Supercritical Two Phase Separation of Hydrothermal Fluids in the Troodos Ophiolite; Nature v333 n6170 p259-261.

Craig, H.; 1957; Isotopic Standards For Carbon and Oxygen and the Correction Factors For Mass Spectrometric Analysis of Carbon Dioxide; Geochimica et Cosmochimica Acta; v12 p133-149

Crawford, M.L.; 1981; Phase Equilibria in Aqueous Fluid Inclusions; in Hollister, L. S., Crawford, M. L. (eds.) Short Course in Fluid Inclusions: Applications to Petrology; Mineralogical Association of Canada, Calgary, p75-99.

D'Arcy, H.; 1856; Les Fontaines Publiques de Ville de Dijon; Victor Dalmont, Paris.

Davis, E.E., Goodfellow, W.D., Bornhold, B.D., Adshead, J., Blaise, B., Villinger, H., and LeCheminant, G.M.; 1987; Massive Sulfides in a Sedimented Rift Valley Northern Juan de Fuca Ridge; Earth and Planetary Science Letters v82 p49-61.

Davis, E.E., Horel, G.C., MacDonald, R.D., Villinger, H., Bennett, R.H., and Li, H.; 1991; Pore Pressures and Permeabilities Measured in Marine Sediments With a Tethered Probe; Journal of Geophysical Research v98 nB4 p5975-5984.

de Marsily, G.; 1984; Flow and Transport in Fractured Rocks: Connectivity and Scale Effect; International Association of Hydrology Memoirs: Proceedings of the International Congress on Hydrogeology of Rocks of Low Permeability, Tucson v17 p267-277.

Delaney, J.R., Mogk, D.W., and Mottl, M.J.; 1987; Quartz-Cemented Breccias From the Mid-Atlantic Ridge: Samples of a High Salinity Hydrothermal Upflow Zone; Journal of Geophysical Research v92 nB9 p9175-9192.

Dershowitz, W.S. and Einstein, H.H.; 1988; Characterizing Joint Geometry With Joint System Models; Rock Mechanics and Rock Engineering v21 p21-51.

Dershowitz, W.S., and Herda, H.H.; 1992; Interpretation of Fracture Spacing and Intensity; Proceedings 33rd U.S. Rock Mechanics Symposium 10p.

Dershowitz, W., Lee, G., and Geier, J.; 1991; User Documentation FracMan Interactive Discrete Feature Data Analysis, Geometric Modelling, and Exploration Simulation; Golder Associates, Inc., Redmond, Washington, 139p.

Detrick, R.S., Buhl, P., Vera, E., Mutter, J., Orcutt, J., Madsen, J., and Brocher, T.; 1987; Multi-Channel Seismic Imaging of a Crustal Magma Chamber Along the East Pacific Rise; Nature v326 p35-41.

Dewey, J.F., and Kidd, W.S.F.; 1977; Geometry of Plate Accretion; Geological Society of America Bulletin v88 n7 p960-968.

De Wiest, R.; 1966; Geohydrology; Wiley New York 336p.

Dilek, Y., and Eddy, C.A.; 1992; The Troodos (Cyprus) and Kizildag (S.Turkey) Ophiolites as Structural Models For Slow-Spreading Ridge Segments; Journal of Geology v100 p305-322.

Dilek, Y., and Moores, E.M.; 1990; Regional Tectonics of the Eastern Mediterranean Ophiolites; in Malpas, J., Moores, E. M., Panayiotou, A., Xenophontos, C. (eds.) Ophiolites: Oceanic Crustal Analogues Proceedings of the Symposium 'Troodos 1987'; Geological Survey Department, Ministry of Agriculture and Natural Resources, Nicosia, Cyprus, p295-309.

Dilek, Y., Thy, P., Moores, E.M., and Ramsden, T.W.; 1990; Tectonic Evolution of the Troodos Ophiolite Within the Tethyan Framework; Tectonics; v9 n4 p811-823.

Dunsworth, S.M.; 1989; Multiple Intrusion and Deformation Within the North-Western Quandrant of the Plutonic Complex, Troodos Ophiolite, Cyprus; Unpublished M.Sc. Thesis, Memorial University of Newfoundland, 274p.

Dunsworth, S.M., and Calon, T.J.; 1984; Relationships Between Deformation and Magmatism in the Plutonic Complex, Troodos Ophiolite, Cyprus; Geological Association of Canada - Mineralogical Association of Canada Joint Annual Meeting Program With Abstracts v9 p59.

Efron, B.; 1982; The Jacknife, the Bootstrap, and Other Resampling Plans; S.I.A.M. Monograph n38 Society of Industrial and Applied Mathematics, 92p.

Faure, G.; 1977; Principles of Isotope Geology; John Wiley and Sons; New York 467p.

Fehn, U., Green, K.E., Von Herzen, R.P., and Cathles, L.M.; 1983; Numerical Models for the Hydrothermal Field at the Galapagos Spreading Center; Journal of Geophysical Research v88 nB2 p1033-1048.

Fisher, R.; 1956; Dispersion on a Sphere; Royal Society of London Proceedings v217 p295-305.

Francheteau, J., Armijo, R., Cheminee, J.L., Hekinian, R., Lonsdale, P., and Blum, N.; 1992; Dyke Complex of the East Pacific Rise Exposed in the Walls of Hess Deep and the Structure of the Upper Oceanic Crust; Earth and Planetary Science Letters v111 p109-121.

Freeze, R.A., and Cherry, J.A.; 1979; Groundwater; Prentice Hall, Inc, Englewood Cliffs, N.J., 604p.

Fritz, P.; 1976; Oxygen and Carbon Isotopes in Ore Deposits in Sedimentary Rocks; in Wolf, K. H. (ed.) Handbook of Strata-bound and Stratiform Ore Deposits; v2 Chapter 7 p191-217.

Gale, J.E.; 1987; Comparison of Coupled Fracture Deformation and Fluid Flow Models With Direct Measurements of Fracture Pore Structure and Stress-Flow Properties; in Farmer, I.W., Daemen, J.S.K., Desai, C.S., Glass, C.E., and Neuman, S.P.; 28th U.S. Symposium on Rock Mechanics, Tucson, Arizona, p1213-1222.

Gass, I.G.; 1979; The Troodos Massif: Its Role in the Unravelling of the Ophiolite Problem and Its Significance in the Understanding of Constraints on Plate Margin Processes; in Panayiotou, A. (ed.) Ophiolites: International Symposium 1979; Geological Survey Department, Nicosia, Cyprus, p23-35.

Gass, I.G.; 1990; Ophiolites and Oceanic Lithosphere; in Malpas, J., Moores, E. M., Panayiotou, A., Xenophontos, C. (eds.) Ophiolites: Oceanic Crustal Analogues Proceedings of the Symposium 'Troodos 1987'; Geological Survey Department, Ministry of Agriculture and Natural Resources, Nicosia, Cyprus, p1-12.

Gass, I.G., and Smewing, J.D.; 1973; Intrusion, Extrusion and Metamorphism at Constructive Margins: Evidence From the Troodos Massif, Cyprus; Nature v242 p26-29.

George, R. P. J.; 1975; The Internal Structure of the Troodos Ultramafic Complex, Cyprus; Unpublished Ph.D. thesis, University of New York (Stony Brook) 196p.

Gillett, S.; 1986; CLUSTRAN: Extract Clusters From Axial Data Sets Using the Algorithm of Shanley and Mahtab; Instruction Manual For the Commercial CLUSTRAN Software Package; 2214 Road 34, Pasco, Washington, 99301 U.S.A. 20p.

Gillis, K.M.; 1983; Low Temperature Alteration of the Extrusive Sequence, Troodos Ophiolite, Cyprus; Geological Association of Canada Program With Abstracts pA27.

Gillis, K. M.; 1986; Multistage Alteration of the Extrusive Sequence, Troodos Ophiolite, Cyprus; Unpublished Ph.D. thesis, Dalhousie University, Halifax, Nova Scotia 387p.

Goldfarb, M.S., and Delaney, J.R.; 1988; Response of Two Phase Fluids to Fracture Configurations Within Submarine Hydrothermal Systems; Journal of Geophysical Research v93 nB5 p4585-4594.

Greenbaum, D.; 1972; Magmatic Processes at Ocean Ridges: Evidence From the Troodos Massif, Cyprus; Nature, Physical Science v238 p18-21.

Gregory, R.T., and Taylor, H.P. Jr.; 1981; An Oxygen Isotope Profile in a Section of Cretaceous Oceanic Crust, Samail Ophiolite, Oman: Evidence for $\delta^{18}O$ Buffering of the Oceans by Deep (>5 km) Seawater-Hydrothermal Circulation at Mid-Ocean Ridges; Journal of Geophysical Research v86 nB4 p2737-2755.

Hancock, P.L.; 1985; Brittle Microtectonics: Principles and Practice; Journal Structural Geology v7 p437-457.

Harper, G.D.; 1982; Evidence For Large Scale Rotations at Spreading Centers From the Josephine Ophiolite; Tectonophysics v82 p25-44.

Harper, G.D.; 1985; Tectonics of Slow Spreading Mid-Ocean Ridges and Consequences of a Variable Depth to the Brittle/Ductile Transition; Tectonics v4 n4 p395-409.

Harper, G.D., Bowman, J.R., and Kuhns, R.; 1988; A Field, Chemical and Stable Isotope Study of Subseafloor Metamorphism of the Josephine Ophiolite California-Oregon; Journal of Geophysical Research v93 nB5 p4625-4656.

Haymon, R.M., Fornari, D.J., Edwards, M.H., Carbotte, S., Wright, D., and Macdonald, K.C.; 1991; Hydrothermal Vent Distribution Along the East Pacific Rise Crest (9°09'-54'N) and Its Relationship to Magmatic and Tectonic Processes on Fast-Spreading Mid-Ocean Ridges; Earth and Planetary Science Lettres v104 p513-534.

Haymon, R.M., and Koski, R.A.; 1987; Comparison of the Bayda Massive Sulfide Deposit, Oman Ophiolite With Eastern Pacific Ridge Axis Sulfide Deposits; Unpublished Manuscript.

Heaton, T.H. E., and Sheppard, S.H. F.; 1977; Hydrogen and Oxygen Isotope Evidence for Sea-Water-Hydrothermal Alteration and Ore Deposition, Troodos Complex, Cyprus; in Volcanic Processes in Ore Genesis; Special Publication N.7 Geological Society of London p42-57.

Helgason, J. and Zentilli, M.; 1985; Field Characteristics of Laterally Emplaced Dikes: Anatomy of an Exhumed Miocene Dike Swarm in Reydarfjördur, Eastern Iceland; Tectonophysics v115 p247-274.

Herzig, P.M., Hannington, M.D., Scott, S.D., Mallotis, G., Rona, and P., Thompson, G.; 1990; Gold-Rich Sea-Floor Gossans in the Troodos Ophiolite and on the Mid-Atlantic Ridge; Economic Geology and Bulletin of the Society of Economic Geologists V86 n8 p1747-1755.

Hodgson, R.A.; 1961; Classification of Structures on Joint Surfaces; American Journal of Science v259 p493-502.

Holser, W.T.; 1984; Gradual and Abrupt Shifts in Ocean Chemistry During Phanerozoic Time; in Holland, H.D., Trendall, A.F. (eds.) Patterns of Change in Earth Evolution, Dahlem Konferenzen Springer Verlag, Berlin; p123-145.

Hudson, J.A., and Priest, S.D.; 1979; Discontinuity Rock Mass Geometry; International Journal of Rock Mechanics, Mining Sciences and Geomechanics Abstracts v16 p339-362.

Hurst, S.D., Moores, E.M., and Karson, J.A.; 1988; Solea Graben Troodos Plutonic Complex: A Fossil Nodal Basin at a Ridge Transform Intersection?; Geological Society of America Abstracts With Programs pA166.

Hyndman, R.R., Von Herzen, R.P., Erickson, A.J., and Jolivet, J.; 1976; Heat Flow Measurements in Deep Crustal Holes on the Mid Atlantic Ridge; Journal of Geological Research v81 p4053-4060.

International Society for Rock Mechanics (ISRM); 1978; Suggested Methods For the Quantitative Description of Discontinuities in Rock Masses; Commission on Standardization of Field Tests; International Journal of Rock Mechanics, Mining Science and Geomechanics Abstracts v15 p319-368.

Jackson, J.A., and White, N.J.; 1989; Normal Faulting in the Upper Continental Crust: Observations From Regions of Active Extension; Journal of Structural Geology v11 n1/2 p15-36.

Jacobson, R.S.; 1992; Impact of Crustal Evolution on Changes of the Seismic Properties of the Uppermost Ocean Crust; Reviews of Geophysics; v30 n1 p23-42.

Jaeger, J.C., and Cook, N.C.; 1969; Fundamentals of Rock Mechanics; Methuan and Company, New York, New York, 513p.

Jehl, V.; 1974; Fluid Inclusions in Some Metamorphosed Oceanic Rocks From the North Atlantic; Commission of Ore Forming Fluids in Inclusions; Fluid Inclusion Research Abstract p88.

Johnson, D.H.; 1980; Crack Distribution in the Upper Oceanic Crust and Its Effects Upon Seismic Velocity, Seismic Structure, Formation Permeability and Fluid Circulation; Geophysical Program AK-50 University of Washington, Seattle, Washington; Initial Reports of the Deep Sea Drilling Project v51-53 Part 2 p1479-1490.

Karson, J.A.; 1987; Factors Controlling the Orientation of Dykes in Ophiolites and Oceanic Crust; in Halls, H. C., Fahrig, W. F. (eds.) Mafic Dyke Swarms; Geological Association of Canada, Ottawa, Special Paper 34 p229-241.

Karson, J.A., Hurst, S.D., and Lonsdale, P.; 1992; Tectonic Rotations of Dikes in Fast-Spread Oceanic Crust Exposed Near Hess Deep; Geology v20 p685-688.

Kastens, K., Mascle, J., Auroux, C., Bonatti, E., Broglia, C., Channell, J., Curzi, P., Emeis, K.-C., Glaçon, G., Hasegawa, S., Hieke, W., Mascle, G., McCoy, F., McKenzie, J., Mendelson, J., Müller, C., Réhault, J.-P., Robertson, A., Sartori, R., Sprovieri, R., and Torii, M.; 1988; O.D.P.Leg 107 in the Tyrrhenian Sea: Insights into Passive Margin and Back Arc Basin Evolution; Geological Society of America Bulletin v100 p1140-1156.

Kelley, D.S., and Delaney, J.R.; 1987; Two Phase Separation and Fracturing in Mid-Ocean Ridge Gabbros at Temperatures Greater Than 700°C; Earth and Planetary Science Letters v83 p53-66.

Kelley, D.S., Robinson, P.T., and Malpas, J.G.; 1992; Processes of Brine Generation and Circulation in the Oceanic Crust: Fluid Incusion Evidence From the Troodos Ophiolite, Cyprus; Journal of Geophysical Research v97 nB6 p9307-9322.

Kennett, J.P.; 1982; Marine Geology; Prentice-Hall, Inc., Englewood Cliffs, N.J., 813p.

Kent, G.M., Harding, A.J., and Orcutt, J.A.; 1990; Evidence for a Smaller Magma Chamber Beneath the East Pacific Rise at 9° 30' North; Nature v304 p650-653.

Kidd, R.G. W., and Cann, J.R.; 1974; Chilling Statistics Indicate an Ocean Floor Spreading Origin For the Troodos Complex, Cyprus; Earth and Planetary Science Letters v24 p151-155.

Kinoshita, H, Furuta, T., and Pariso, J.; 1989; Downhole Magnetic Field Measurements and Paleomagnatism, Hole 504B, Costa Rica Rift; in Becker, K., Sakai, H. et al. (eds) Proceedings of the Ocean Drilling Program Scientific Results v111 p147-156.

Kiraly, L.; 1970; Statistical Analysis of Fractures (Orientation and Density); Geologische Rundschau v59 p125-151.

Kruseman, G.P., and de Ridder, N.A.; 1983; Analysis and Evaluation of Pumping Test Data; International Institute for Land Reclamation and Improvement, Wageningen, The Netherlands, Bulletin 11, 2nd edition, 200p.

Kyser, T.K.; 1987; Equilibrium Fractionation Factors For Stable Isotopes; in Kyser, T. K. (ed.) Short Course in Stable Isotope Geochemistry of Low Temperature Fluids; Mineralogical Association of Canada, Saskatoon, v13 p1-84.

LaPointe, P.R., and Hudson, J.A.; 1985; Characterization and Interpretation of Rock Mass Joint Patterns; Geological Society of America Special Paper 199 37p.

Lewis, B.T. R.; 1983; The Process of Formation of Ocean Crust; Science v220 p151-157.

Lister, C.R. B.; 1972; On the Thermal Balance of a Mid-Ocean Ridge; Geophysical Journal of the Royal Astronomical Society v26 p515-535.

Lister, C.R. B.; 1983; The Basic Physics of Water Penetration into Hot Rock; in Rona, P., Bostrom, K., Laubier, L., Smith, K. (eds.) Hydrothermal Processes at Seafloor Spreading Centers; Plenum Publishing Corp., p141-168.

Long, J.C. S., and Billaux, D.M.; 1987; From Field Data to fracture Network Modelling - An Example Incorporating Spatial Structure; Water Resources Research v23 n7 p1201-1216.

Lonsdale, P.; 1977; Structural Geomorphology of a Fast Spreading Rise Crest: The East Pacific Rise Near 3°25' South; Marine Geophysical Researches v3 p251-293.

Lydon, J.W.; 1984; Some Observations on the Morphology and Ore Textures of Volcanogenic Sulphide of Cyprus; Current Research Part A Geological Survey of Canada 84-1A p601-610.

Lydon, J.W.; 1988; Ore Deposit Models - 14 Volcanogenic Massive Sulphide Deposits Part 2: Genetic Models; Geoscience Canada v15 n1 p43-65.

MacDonald, K.C.; 1982; Mid Ocean Ridges: Fine Scale Tectonic, Volcanic and Hydrothermal Processes Within the Plate Boundary Zone; Annual Review of Earth and Planetary Sciences v10 p155-190.

MacDonald, K.C.; 1983; A Geophysical Comparison Between Fast and Slow Spreading Centers: Constraints on Magma Chamber Formation and Hydrothermal Activity; in Rona, P., Bostrom, K., Laubier, L., Smith, K. (eds.) Hydrothermal Processes at Seafloor Spreading Centers; Plenum Press, New York, p27-51.

Macdonald, K.C.; 1986; The Crest of the Mid Atlantic Ridge: Models For Crustal Generation Processes and Tectonics; in Vogt, P. C., Tucholke, B. E. (eds.) Geology of North America: The Western North Atlantic Region (Decade of North American Geology); Geological Society of America, vM p51-68.

MacDonald, K.C., Beckerk, K., Speiss, F.N., and Ballard, R.D.; 1980; Hydrothermal Heat Flux of the "Black Smoker" Vents on the East Pacific Rise; Earth and Planetary Science Letters v48 p1-7.

MacLeod C.J.; 1990; Role of the South Troodos Transform Fault in the Rotation of the Cyprus Microplate: Evidence From the Eastern Limassol Forest Complex; in Malpas, J., Moores, E. M., Panayiotou, A., Xenophontos, C. (eds.) Ophiolites: Oceanic Crustal Analogues Proceedings of the Symposium 'Troodos 1987'; Geological Survey Department/Ministry of Agriculture and Natural Resources, Nicosia, Cyprus, p75-86.

MacLeod, C.J., Allerton, S., Gass, I.G., and Xenophontos, C.; 1990; Structure of a Fossil Ridge-Transform Intersection in the Troodos Ophiolite; Nature v348 p717-719.

MacLeod, C.J., Robertson, A.H. F., Allerton, S., Browning, S., Gass, I.G., Taylor, R.N., Vine, F.J., and Xenophontos, C.; 1992; Comment on "Tectonic Evolution of the Troodos Ophiolite Within the Tethyan Framework" by Y.Dilek, P.Thy, E.M. Moores, and T.W. Ramsden and reply; Tectonics v11 n4 p910-923.

Mahtab, M.A., and Yegulalp, T.M.; 1982; A Rejection Criterion For Definition of Clusters in Orientation Data; in Goodman, R. E., Heuze, F. E. (eds.) Issues in Rock Mechanics; 23rd United States Symposium on Rock Mechanics, Berkeley, California p116-123.

Makris, J.; 1983; Deep Structure of the Eastern Mediterranean Deduced From Refraction Seismic Data (Abstract); EOS American Geophysical Union Transactions v62 p6247.

Malpas, J.M., and Brace, T.; 1987; Geological Map of the Amiandos-Palekhori Area, 1:10,000 Scale; Geological Survey Department, Cyprus and Centre For Earth Resources Research, Memorial University of Newfoundland, Canada, 2 Sheets.

Malpas, J., Brace, T., and Dunsworth, S.M.; 1989a; Structural and Petrologic Relationships of the CY-4 Drill Hole of the Cyprus Crustal Study Project; in Gibson, I.L., Malpas, J., Robinson, P.T., Xenophontos, C. (eds.) Cyprus Crustal Study Project: Initial Report, Hole CY-4; Geological Survey of Canada Paper 88-9 p39-68.

Malpas, J.G., Calon, T., and Xenophontos, C.; 1987; Plutonic Rocks of The Troodos Ophiolite; in Xenophontos, C., Malpas, J. G. (eds.) Field Excursion Guidebook, Symposium 'Troodos 1987' Ophiolites and Oceanic Lithosphere; Geological Survey Department, Nicosia, Cyprus, p158-181.

Malpas, J., Case, G., and Moore, P.; 1989b; The Geology of the Area Immediately Surrounding the CY-4 Borehole of the Cyprus Crustal Study Project; Cyprus Crustal Study Project: Initial Report, Hole CY-4 p31-38.

Malpas, J.M., Moores, E.M., Panayioutou, A., and Xenophontos, C.; 1990; Ophiolites: Oceanic Crustal Analogues Proceedings of the Symposium 'Troodos 1987'; Cyprus Geological Survey Department/Ministry of Agriculture, Nicosia, 733p.

McCallum, J.E., and Robertson, A.H. F.; 1990; Pulsed Uplift of the Troodos Massif - Evidence From the Plio-Pleistocene Mesaoria Basin; in Malpas, J., Moores, E. M., Panayiotou, A., Xenophontos, C. (eds.) Ophiolites: Oceanic Crustal Analogues Proceedings of the Symposium 'Troodos 1987'; Geological Survey Department/Ministry of Agriculture and Natural Resources, Nicosia, Cyprus, p217-230.

McClain, J.S., Chin, C., and Moores, E.M.; 1990; Seismic Velocities in Young Oceanic Crust: Constraints on Models For the Development of Permeability and Water Penetration; in Malpas, J., Moores, E. M., Panayiotou, A., Xenophontos, C. (eds.) Ophiolites: Oceanic Crustal Analogues Proceedings of the Symposium 'Troodos 1987'; Geological Survey Department/Ministry of Agriculture and Natural Resources, Nicosia, Cyprus, p577-584.

McCrea, J.M.; 1950; On the Isotope Chemistry of Carbonates and a Paleotemperature Scale; Journal of Chemical Physics v18 p849-857.

McKenzie, D.P., and Sclater, J.G.; 1969; Heat Flow in the Eastern Pacific and Seafloor Spreading; Bulletin Volcanologique v33-1 p101-118.

Miller, I.; 1990; User Documentation MAFIC Matrix/Fracture Hydraulic Interaction Code With Solute Transport; Golder Associates, Inc., Redmond, Washington, 49p.

Miyashiro, A.; 1973; The Troodos Ophiolite Complex Was Probably Formed in an Island Arc Complex; Earth and Planetary Science Letters v19 p218-224.

Moores, E.M., and Jackson, E.D.; 1974; Ophiolites and Oceanic Crust; Nature v250 p136-139.

Moores, E.M., Robinson, P.T., Malpas, J.M., and Xenophonotos, C.; 1984; Model for the Origin of the Troodos Massif, Cyprus and Other Mid East Ophiolites; Geology v12 p500-503.

Moores, E.M., Varga, R.J., Verosub, K.L., and Ramsden, T.; 1990; Regional Structure of the Troodos Ophiolite Dike Complex; in Malpas, J. M., Moores, E. M., Panayioutou, A., Xenophontos, C. (eds.) Ophiolites - Oceanic Crustal Analogues Proceedings of the Symposium 'Troodos 1987'; Geological Survey Department/Ministry of Agriculture and Natural Resources, Nicosia, Cyprus, p639-653.

Moores, E.M., and Vine, F.J.; 1971; The Troodos Massif, Cyprus and Other Ophiolites as Oceanic Crust: Evaluation and Implications; Royal Society of London, Philosophical Transactions vA268 p443-466.

Morton, J.L., and Sleep, N.H.; 1985; Seismic Reflections From a Lau Basin Magma Chamber; in Scholl, D. W., Vallier, J. L. (eds.) Geology and Offshore Resources of Pacific Island Arcs - Tonga Region, Circum Pacific Council For Energy and Mineral Resources; Circum Pacific Council for Energy and Mineral Resources, Houston, Texas, v2 Earth Sciences Series p441-453.

Mottl, M.J.; 1983; Metabasalts, Axial Hot Springs, and the Structure of Hydrothermal Systems at Mid-Ocean Ridges; Geological Society of America Bulletin, v94 p161-180.

Muehlenbachs, K., and Clayton, R.N.; 1976; Oxygen Isotope Composition of the Oceanic Crust and its Bearing on Seawater; Journal of Geophysical Research v81 n23 p4365-4369.

Murton, B.J.; 1986; Anomalous Oceanic Lithosphere Formed in a Leaky Transform Fault: Evidence From the Western Limassol Forest Complex, Cyprus; Journal of the Geological Society of London v143 p845-854.

Nash, D.; 1979; An Interpretation of Irregular Dyke Forms in the Itvidleq Shear Zone West Greenland; in Korstgård, J.A. (ed.) Nagssugtoquidian Geology; Rapport Grønlands Geologiske Undersøgelse n89 p77-83.

Nautilau Group; 1990; Hydrothermal Activity in the Lau Basin; EOS Abstracts Transactions of the American Geophysical Union; v71 n18 p678-679.

Nehlig, P., and Juteau, T.; 1988; Flow Porosities, Permeabilities and Preliminary Data on Fluid Inclusions and Fossil Geothermal Gradients in the Crustal Sequence of the Sumail Ophiolite (Oman); Tectonophysics v151 p199-221.

Nelson, R.A.; 1979; Natural Fracture Systems: Description and Classification; American Association of Petroleum Geologists Bulletin v63 n12.

Nicolas, A., and Violette, J.F.; 1982; Mantle Flow Structures at Oceanic Spreading Centres: Models Derived From Ophiolites; Tectonophysics v81 p319-339.

Norrell, G.T., and Harper, G.D.; 1988; Detachment Faulting and Amagmatic Extension at Mid-Ocean Ridges: The Josephine Ophiolite as an Example; Geology v16 p827-830.

Norton, D., and Knapp, R.; 1977; Transport Phenomena in Hydrothermal Systems: the Nature of Porosity; American Journal of Science v277 p913-936.

Norton, D., and Knight, J.; 1977; Transport Phenomena in Hydrothermal Systems: Cooling Plutons; American Journal of Science v277 p937-981.

Ohle, P.; 1951; The Influence of Permeability on Ore Distribution in Limestone and Dolostone; Economic Geology v46 p667-706.

Ohmoto, H., and Rye, R.O.; 1974; Hydrogen and Oxygen Isotope Compositions of Fluid Inclusions in the Kuroko Deposits, Japan; Economic Geology v69 p947-953.

Oudin, E., and Constantinou, G.; 1984; Black Smoker Chimney Fragments in Cyprus Sulfide Deposits; Nature v308 p349-353.

Oudin, E., Picot, P., and Pouit, G.; 1981; Comparison of Sulfide Deposits From the East Pacific Rise and Cyprus; Nature v291 p404-407.

Pahl, P.J.; 1981; Estimating the Mean Length of Discontinuity Traces; International Journal of Rock Mechanics Mining Sciences and Geomechanics Abstracts v18 p221-228.

Panayioutou, A.; 1979; Ophiolites: International Symposium; Cyprus Geological Survey Department, Nicosia, 781p.

Parker, R.L., and Oldenburg, D.W.; 1973; Thermal Model of Ocean Ridges; Nature Physical Science v242 p137-139.

Paterson, M.S.; 1978; Experimental Rock Deformation - The Brittle Field; Springer Verlag, New York, p254.

Pearce, J.A.; 1975; Basalt Geochemistry Used to Investigate Post Tectonic Environments on Cyprus; Tectonophysics v25 p41-67.

Pearce, J.A.; 1983; Role of the Sub-Continental Lithosphere in Magma Genesis at Active Continental Margins; in Hawkesworth, C. J., Norry, M. J. (eds.) Continental Basalts and Mantle Xenoliths; Shiva Publishing Limited, London, p230-249.

Pearce, J.A., and Cann, J.R.; 1973; Tectonic Setting of Basic Volcanic Rocks Determined Using Trace Element Analyses; Earth and Planetary Science Letters v19 p290-300.

Pearce, J.A., and Norry, M.J.; 1979; Petrogenetic Implications of Ti, Zr, Y, and Nb Variations in Volcanic Rocks; Contributions to Mineralogy and Petrology; v69 p33-47.

Perkins, E.H., Brown, T.H., and Berman, R.G.; 1986; PTX-System: Three Programs For Calculation of Pressure-Temperature-Composition Phase Diagrams; Computers and Geosciences v12 p749-755.

Piteau, D.R.; 1970; Geological Factors Significant to the Stability of Slopes Cut in Rock; South African Institute of Mining and Metallurgy Symposium on Planning Open Pit Mines, Johannesburg p33-53.

Pollard, D.D.; 1987; Elementary Fracture Mechanics Applied to the Structural Interpretation of Dykes; in Halls, H. G., Fahrig, W. F. (eds.) Mafic Dyke Swarms; Geological Association of Canada, Ottawa, Canada, v34 Special Paper p5-24.

Poole, A.J., Shimmield, G.B., and Robertson, A.H. F.; 1990; Late Quaternary Uplift of the Troodos Ophiolite, Cyprus: Uranium Series Dating of Pleistocene Coral; Geology v18 p894-897.

Potter, R.W.; 1977; Pressure Corrections For Fluid Inclusion Homogenization Temperatures Based on the Volumetric Properties of the System NaCl - H_2O; Journal of Research of the United States Geological Survey v5 n5 p603-607.

Priest, S.D., and Hudson, J.A.; 1976; Discontinuity Spacings in Rock; International Journal of Rock Mechanics, Mining Sciences and Geomechanics Abstracts v13 p135-148.

Priest, S.D., and Hudson, J.A.; 1981; Estimation of Discontinuity Spacing and Trace Length Using Scanline Surveys; International Journal of Rock Mechanics Mining Sciences and Geomechanics Abstracts v18 p183-197.

Ramsden, T.; 1987; The Structural Geology and Paleomagnetism of the Sheeted Dyke Complex in the Mitsero-Arakapas Area, Troodos Ophiolite, Cyprus; Unpublished M.Sc. thesis, University of California (Davis), California 114p.

Rautenschlein, M., Jenner, G., Hertozen, J., Hofmann, A.W., Kerrich, R., Schmincke, H.-U., and White, W.M.; 1985; Isotopic and Trace Element Composition of Volcanic Glass From the Akaki Canyon, Cyprus: Implications For the Origin of the Troodos Ophiolite; Earth and Planetary Science Letters v75 p693-383.

Richardson, C.J., Cann, J.R., Richards, H.G., and Cowan, J.G.; 1987; Metal Depleted Root Zones of the Troodos Ore Forming Hydrothermal Systems, Cyprus; Earth and Planetary Science Letters v84 p243-253.

RISE Project Group (Spiess, F.N., MacDonald, K.C., Atwater, T., Ballard, R., Carranza, A., Cordoba, D., Cox, C., Diaz Garcia, V.M., Francheteau, J., Guerrero, J., Hawkins, J., Haymon, R., Hessler, R., Juteau, T., Kastner, M., Larson, R., Luyendyk, B., MacDougall, J.D., Miller, S., Normark, W., Orcutt, J., Rangin, C.); 1980; East Pacific Rise: Hot Springs and Geophysical Experiments; Science v207 n4438 p1421-1432.

Rißler, P.; 1978; Determination of the Water Permeability of Jointed Rock; Wittke, W. (ed.) Publication of the Institute for Foundation Engineering, Soil Mechanics and Water Ways Construction RWTH (University) Aachen, Germany, v5 151p.

Robertson, A.H. F.; 1977; Tertiary Uplift History of the Troodos Massif, Cyprus; Geological Society of America Bulletin v88 p1763-1772.

Robertson, A.H. F.; 1990; Tectonic Evolution of Cyprus; in Malpas, J., Moores, E. M., Panayiotou, A., Xenophontos, C. (eds.) Ophiolites: Oceanic Crustal Analogues Proceedings of the Symposium 'Troodos 1987'; Geological Survey Department/Ministry of Agriculture and Natural Resources, Nicosia, Cyprus, p235-251.

Robertson, A.H. F., and Hudson, J.D.; 1974; Pelagic Sediments in the Cretaceous and Tertiary History of the Troodos Massif, Cyprus; Special Publications Institute of the Association of Sedimentologists v1 p403-436.

Robertson, A.H. F., and Woodcock, N.H.; 1979; Tectonic Setting of the Troodos Massif in the Eastern Mediterranean; in Panayiotou, A. (ed.) Ophiolites Proceedings of an International Ophiolite Symposium; Geological Survey Department, Nicosia, Cyprus, p36-49.

Robertson, A.H.F., and Woodcock, N.H.; 1986; The Role of the Kyrenia Range Lineament, Cyprus, in the Geological Evolution of the Eastern Mediterranean Area; in Reading H.G., Watterson, J., White, S.H. (eds.) Major Crustal Lineaments and Their Influence on the Geological History of the Continental Lithosphere; Philosophical Transactions of the Royal Society of London vA317 p141-177.

Robin, P.-Y., and Jowett, E.C.; 1986; Computerized Density Contouring and Statistical Evaluation of Orientation Data Using Counting Circles and Continuous Weighting Functions; Tectonophysics v121 n2-4 p204-233.

Robinson, P.T., and Malpas, J.; 1990; The Troodos Ophiolite of Cyprus: New Perspectives on its Origin and Emplacement; in Malpas, J., Moores, E. M., Panayiotou, A., Xenophontos, C. (eds.) Ophiolites: Oceanic Crustal Analogues Proceedings of the Symposium 'Troodos 1987'; Geological Survey Department/Ministry of Agriculture and Natural Resources, Nicosia, Cyprus, p13-26.

Robinson, P.T., Melson, W., and Schmincke, H.-U.; 1983; Volcanic Glass Compositions of the Troodos Ophiolite, Cyprus; Geology v11 p400-404.

Roedder, E.; 1979; Fluid Inclusions as Samples of Ore Fluids; in Barnes, H. L. (ed.) Geochemistry of Hydrothermal Ore Deposits; Wiley Interscience, New York, N.Y., 2nd edition p684-737.

Roedder, E.; 1984; Fluid Inclusions; in Ribbe P.H. (ed.) Reviews in Mineralogy; Mineralogical Society of America, v12 644p.

Romm, E.S.; 1966; Fluid Flow in Fractured Rocks; Moscow, Nedra (in Russian).

Rona, P.A.; 1984; Hydrothermal Mineralization at Seafloor Spreading Centers; Earth Sceince Reviews v20 p1-104.

Rona, P.A., Thompson, G. Mottl, M.J., Karson, J.A., Jenkins, W.J., Graham, D., Mallette, M., Von Damm, K.L., and Edmond, J.M.; 1984; Hydrothermal Activity at the Trans-Atlantic Geotranverse Hydrothermal Field, Mid-Atlantic Ridge Crest at 26°N; Journal of Geophysical Research v89 nB13 p11365-11377.

Rona, R.A. Denlinger, R.P., Fisk, M.R., Howard, K.J., Taghin, G.L., Klitgord, K.D., McClain, J.S., McMurray, G.R., and Wiltshire, J.C.; 1990; Major Off-Axis Hydrothermal Activity on the Northern Gorda Ridge; Geology v18 p493-406.

Rosenberg, N.D., and Spera, F.J.; 1992; Hydrothermal Convection at Mid-Ocean Ridges: The Role of Permeability Distribution and Chemical Buoyancy; in Delaney, J., Dick, H., Norton, D. (conveners) RIDGE Theoretical Short Course Tucson, Arizona, January 1992, Abstracts p6-7.

Rosencrantz, E.J.; 1980; The Geology of the Northern Part of North Arm Massif, Bay of Islands Ophiolite Complex, Newfoundland: With Application to Upper Oceanic Crust Lithology Structure and Genesis; Unpublished Ph.D. thesis, State University of New York (Albany) 318p.

Rosencrantz, E.J.; 1982; Formation of Uppermost Oceanic Crust; Tectonics v1 n6 p471-494.

Rouleau, A.; 1984; Statistical Characterization and Numerical Simulation of a Fracture System - Application to Groundwater Flow in the Stripa Granite; Unpublished Ph.D. thesis, University of Waterloo, Ontario 216p.

Rouleau, A., and Gale, J.E.; 1981; Characterizing Orientation, Spacing and Length of Fractures For Hydrogeological Purposes - Application to the Gneissic Bedrock at Chalk River; Atomic Energy of Canada Limited Report, Pinewa, Manitoba.

Scheidegger, A.E.; 1982; Principles of Geodynamics; Springer Verlag, New York, p395.

Schiffman, P., Bettison, L.A., and Smith, B.M.; 1990; Mineralogy and Geochemistry of Epidosites From the Solea Graben, Troodos Ophiolite, Cyprus; in Malpas, J. M., Moores, E. M., Panayioutou, A., Xenophontos, A. (eds.) Proceedings of the Symposium 'Troodos 1987'; Geological Survey Department/Ministry of Agriculture and Natural Resources, Nicosia, Cyprus, p673-684.

Schiffman, P., and Smith, B.M.; 1988; Petrology and Oxygen Isotope Geochemistry of a Fossil Seawater Hydrothermal System Within the Solea Graben, Northern Troodos Ophiolite, Cyprus; Journal of Geophysical Research v93 nB5 p4612-4624.

Schiffman, P., Smith, B.M., Varga, R.J., and Moores, E.M.; 1987; Geometry, Conditions and Timing of Off-Axis Hydrothermal Metamorphism and Ore Deposition in the Solea Graben; Nature v325 p423-425.

Sclater, J.G., and Francheteau, J.; 1970; The Implications of Terrestrial heat Flow Observations on Current Tectonic and Geochemical Model of the Crust and Upper Mantle of the Earth; Geophysical Journal of the Royal Astronomical Society v20 p509-542.

Sclater, J.G., Hellinger, S., and Tapscott, C.; 1977; The Paleo-bathymetry of the Atlantic Ocean From the Jurassic to the Present; Journal of Geology v85 p509-522.

Shanley, R.J., and Mahtab, M.A.; 1976; Delineation and Analysis of Clusters in Orientation Data; Mathematical Geology v8 n1 p9-23.

Simmons, G., and Richter, D.; 1976; Microcracks in Rocks; in Strens, R. G. J. (ed.) The Physics and Chemistry of Minerals and Rocks; John Wiley and Sons, NATO Advanced Study Institute, New Castle-Upon Tyne, p105-137.

Simonian, K.D. and Gass, I.G.; 1978; Arakapas Fault Belt, Cyprus; a Fossil Transform Fault; Geological Society of America Bulletin v89 p1220-1230.

Sinton, J.M., and Detrick, R.S.; 1992; Mid-Ocean Ridge Magma Chambers; Journal of Geophysical Research v97 nB1 p197-216.

Sleep, N.H.; 1983; Hydrothermal Convection at Ridge Axes; in Rona, P. Bostrom, K., Laubier, L., Smith, K.L. (eds.) Hydrothermal Processes at Seafloor Spreading Centers; Plenum Press, New York and London, p71-82.

Smewing, J.D., Simonian, K.O., and Gass, I.G.; 1975; Metabasalts From the Troodos Massif, Cyprus: Genetic Implication Deduced From Petrography and Trace Element Geochemistry; Contributions to Mineralogy v51 p49-54.

Snow, D. T.; 1965; A Parallel Plate Model of Permeable Fractured Media; Unpublished Ph.D. thesis, University of California (Berkeley) 331p.

Snow, D.T.; 1969; Anisotropic Permeability of Fractured Media; Water Resources Research v5 n6 p1273-1288.

Spencer, E.W.; 1977; Introduction to the Structure of the Earth; McGraw Hill Book Company, New York, 640p.

Spooner, E.T. C.; 1977; Hydrodynamic Model For the Origin of the Ophiolitic Cupriferous Pyrite Ore Deposits of Cyprus; in Gass, I. G. (ed.) Volcanic Processes in Ore Genesis; Geological Society of London Special Publication 7, p58-72.

Spooner, E.T. C., and Bray, C.J.; 1977; Hydrothermal Fluids of Seawater Salinity in Ophiolitic Sulfide Ore Deposits in Cyprus; Nature v266 p808-812.

Stakes, D.S., and O'Neil, J.R.; 1982; Mineralogy and Stable Isotope Geochemistry of Hydrothermally Altered Oceanic Rocks; Earth and Planetary Sceience Letters v57 p285-304.

Staudigel, H., Gee, J., Tauxe, L., and Varga, R.J.; 1992; Shallow Intrusive Directions of Sheeted Dykes in the Troodos Ophiolite: Anisotropy of Magnetic Susceptibilty and Structural Data; Geology v20 p841-844.

Staudigel, H., Gillis, K.M., and Duncan, R.; 1986; K/Ar and Rb/Sr Ages of Celadonites From the Troodos Ophiolite, Cyprus; Geology v14 p72-75.

Strens, M.R., and Cann, J.R.; 1986; A Fracture-Loop Thermal Balance Model of Black Smoker Circulation; Tectonophysics v122 p307-324.

Terzaghi, R.D.; 1965; Sources of Error in Joint Surveys; Geotechnique v15 p287-303.

Thy, P., Brooks, C.K., and Walsh, J.N.; 1985; Tectonic and Petrogenetic Implications of Major and Rare Earth Element Chemistry of Troodos Glasses, Cyprus; Lithos v18 p165-178.

Trimmer, D., Bonner, B., Heard, H.C., and Duba, A.; 1980; Effect of Pressure and Stress on Water Transport in Intact and Fractured Gabbro and Granite; Journal of Geophysical Research v85 nB12 p7059-7071.

Tsang, Y.W.; 1992; Usage of "Equivalent Apertures" For Rock Fractures as Derived From Hydraulic and Trace Tests; Water Resources Research v28 n5 p1451-1455.

Tsang, Y.W., and Tsang, C.F.; 1989; Flow Channelization in a Single Fracture as a 2D Strongly Heterogeneous Permeabile Medium; Water Resources Research v25 n9 p2076-2080.

van Everdingen, D.A., van Gool, J.A. M., and Vissers, R.; 1992; QuickPlot: A Microcomputer Based Program For Processing of Orientation Data; Computers and Geosciences v18 n2/3 p183-287.

Varga, R.J.; 1991; Modes of Extension at Oceanic Spreading Centers: Evidence From the Solea Graben, Troodos Ophiolite, Cyprus; Journal of Structural Geology v13 n5 p517-537.

Varga, R.J., and Moores, E.M.; 1985; Spreading Structure of the Troodos Ophiolite, Cyprus; Geology v13 p846-850.

Varga, R.J., and Moores, E.M.; 1990; Intermittent Magmatic Spreading and Tectonic Extension in the Troodos Ophiolite; in Malpas, J., Moores, E. M., Panayiotou, A., Xenophontos, C. (eds.) Ophiolites: Oceanic Crustal Analogues Proceedings of the Symposium 'Troodos 1987'; Geological Survey Department/Ministry of Agriculture and Natural Resources, Nicosia, Cyprus, p37-52.

Veizer, J.; 1988; Continental Growth: Comment on "The Archean-Proterozoic Transition: Evidence From Guyana and Montana" by Gibbs, A.K., Montgomery, C.W., O'Day, P.A., Ersher, E.A.; Geochimica Cosmochimica A p789-792.

Verosub, K.L., and Moores, E.M.; 1981; Tectonic Rotations in Extensional Regimes and Their Paleomagnetic Consequences For Oceanic Basalts; Journal of Geophysical Research v86 nB7 p6335-6349.

Vibetti, N.J., Kerrich, R., and Fyfe, W.S.; 1989; Hypersaline Fluids Discovered in the Troodos Ophiolite; in Gibson, I. L., Malpas, J., Robinson, P. T., Xenophontos, C. (eds.) Cyprus Crustal Drilling Project: Initial Report, Hole CY-4; Geological Survey of Canada, Ottawa, Paper 88-9 p229-234.

Von Damm, K.L.; 1988; Systematics of and Postulated Controls on Submarine Hydrothermal Solution Geochemistry; Journal of Geophysical Research v93 nB5 p4551-4561.

Von Damm, K.L.; 1990; Seafloor Hydrothermal Activity: Black Smoker Chemistry and Chimneys; Annual Reviews of Earth and Planetary Science v18 p173-204.

Weiss, R.F., Lonsdale, P., Lupton, J.E., Bainbridge, A.E., and Craig, H.; 1977; Hydrothermal Plumes on the Galapagos Rift; Nature v267 p600-603.

Welhan, J.A., and Craig, H.; 1983; Methane, Hydrogen and Helium in Hydrothermal Fluids at 21° North on the East Pacific Rise; in Rona, P., Bostrom, K., Laubier, L., Smith, K. (eds.) Hydrothermal Processes at Seafloor Spreading Centers; Plenum Press, New York, p391-409.

Wilkens, R.H., Fryer, G.J., and Karsten, J.; 1991; Evolution of Porosity and Seismic Structure of Upper Oceanic Crust: Importance of Aspect Ratios; Journal of Geophysical Research v96 nB11 p17981-17995.

Williams, C.F., Narasimhan, T.N., Anderson, R.N., Zoback, M.D., and Becker, K.; 1986; Convection in the Oceanic Crust: Simulation of Observations From Deep Sea Drilling Project Hole 504B, Costa Rica Rift; Journal of Geophysical Research v91 nB5 p4877-4889.

Williams, D.L., Von Herzen, R.P., Sclater, J.P., and Anderson, R.N.; 1974; The Galapagos Spreading Centre: Lithospheric Cooling and Hydrothermal Circulation; Geophysical Journal of the Royal Astronomical Society v38 p587-608.

Wilson, G.; 1982; Introduction to Small Scale Geological Structures; George Allen and Unwin, Boston 128p.

Wilson, R.A. M., and Ingham, F.T.; 1959; The Geology of the Xeros-Troodos Area With an Account of the Mineral Resources; Cyprus Geological Survey Department Memoir 1, Nicosia, Cyprus, 135p.

Withjack, M.O., and Scheiner, C.; 1982; Fault Patterns Associated With Domes - An Experimental and Analytical Study; American Association of Petroleum Geologists Bulletin v66 n3 p302-216.

Woodcock, N.H., and Naylor, M.A.; 1983; Randomness Testing in Three Dimensional Orientation Data; Journal of Structural Geology v5 n5 p539-548.

APPENDICES

A. METHODOLOGY AND DATA PRESENTATION

A.1 FRACTURE MEASUREMENTS AND SCANLINE PHOTOGRAPHS

A.1.1 *Methodology*

Suitable areas for scanline mapping were chosen based on the availabiity of relatively unweathered outcrops. As a result most scanlines were located along recent roadcuts.

The scanline mapping procedure started with the laying of a measuring tape along the outcrop surface. To minimize data bias, two scanlines were used, one approximately vertical, the other sub-horizontal. Where possible, a 30 m distance was mapped. The orientation of each scanline was noted.

The characteristics of all fractures with lengths greater than 0.25 m and cutting the scanline, were measured. Measured characteristics include the following: distance along scanline, fracture type, orientation, trace length, censoring, termination, mineral filling and, where possible, the relative ages of minerals and consistency of mineral filling along the fracture, large and small scale surface roughnesses, rock type hosting the fracture, grain size of the rock, and the fracture width. Other observations, for example slickenside measurements, were also noted where possible.

Area mapping proceeded much the same way, except that all fractures within a 2 m high by roughly 30 m long area were mapped. In this case, the start and end coordinates of the fractures were noted in addition to the above-mentioned characteristics.

The Universal Transverse Mercator grid zone for the field area is 36S with the origin at Longitude 33°East and Latitude 0° (equator), using false coordinates of origin 500,000 metres East and 0 metres North. The 100,000 metre square identifications are VD and WD. In this study all UTM coordinates will be given as in the following example: 506000 E, 3870000 N (Easting and Northing). This was done to facilitate the plotting data of points on computer drawn maps. The topographic maps used in this study were Series 717, Sheets 10,11,12,18,19,20, Edition I-GSGS published by the Department of Survey, Ministry of Defence, United Kingdom in 1973; available through the Department of Lands and Surveys, Cyprus.

A.1.2. *Scanline Locations (U.T.M. coordinates)*

Scanline Identifier	Dyke Domain	Easting (m)	Northing (m)
0000	4	503190	3866060
0108 - 0111	2	511550	3865500
0112	4	503364	3866050
0122	4	503130	3866137
0124	4	503122	3866139
0201	5	500820	3869330
0213 - 0215	5	501175	3869950
0301 - 0304	4	503670	3873300
0306	4	503500	3874580
0307	4	503510	3875040
0329	2	510700	3865750
0401 - 0403	4	504200	3868890
0404	4	504800	3869660
0418 - 0419	4	506568	3873050
0413 - 0415	4	506517	3873037
0428	4	503300	3866075
0701 - 0704	4	503780	3867830
0801	4	503600	3873190
1001 - 1006	6	511575	3872900
1008 - 1011	4	508800	3874150
1017 - 1021	4	507750	3874675
1028 - 1031	6	512400	3872900
1037 - 1038- 1208-1210	2	514800	3868100
1107 - 1110	5	498150	3868850
1111 - 1116	5	498700	3869100
1124 - 1127	5	499025	3869750
1129 - 1132	3	509200	3864950
1134 - 1136	3	511000	3866250
1137 - 1203	6	511850	3870850
1204 - 1207	2	512150	3863900
1211 - 1215	3	514050	3868550
1216 - 1220	4	500750	3875150
1221A - F	5	500125	3873800
1222A - E	5	499650	3873300
1227 - 1231	4	502600	3874750
1305 - 1306	5	501400	3870700
1307 - 1309	5	502300	3871550
1310 - 1315	4	503400	3873050
1316 - 1320	2	507500	3863650
1321 - 1327	2	510275	3863450

For location see Figure A.1

A.1.3. *Format Used For Scanline Data*

The following section outlines the use of symbols in the SCANLINE data set: (the formats are in the Description column in brackets and are as follows: I = integer, F = real, A = character)

Col #	Possible Symbols	Description
1	1	Data line to follow (I1)
	2	Photo location data line to follow (I1)
	3	Comment line to follow(I1)
2-5	integer	Photo number (I4) the first two numbers refer to the film number and the last to the frame number
6	character	Scanline identifier (1A)
7-9	integer	Scanline trend in the plunge direction (I3)
10-11	integer	Scanline plunge down from the horizontal = +ve (I2)
12-14	integer	Fracture number found on corresponding photo (I3)
15-19	real	Distance from start of scanline in metres (F5.2)
20-21	JT	Joint - regular (2A)
	CN	Contact - between rock types (2A)
	VN	Vein - filled fracture (2A)
	FR	Fracture - irregular (2A)
22-24	integer	Fracture trend in plunge direction (I3)
25-26	integer	Fracture plunge (down from the horizontal = +ve) (I2)
27-30	real	Fracture trace length in metres (F4.2)
31	0	Both ends free
	1	One end covered = Censoring (I1)
	2	Both ends covered
32	0	Both ends free
	1	'T' junction
	2	'H' junction = Termination (I1)
	3	splayed at one end
	4	splayed both ends
33-42	character	Mineral filling of fracture (3A) accommodate up to three minerals per fracture. Place in order of decreasing abundance. Presently used symbols:

(Format for scanline data continued)

Col #	Symbols	Description	
		Z=zeolite, E=epidote, K=chlorite, H=hematite, P=pyrite, J=jasper, C=calcite, X=clay, R=rubble, U=unknown, '-'=none Format is 1%A2%A3%AC (col 33-42) where: 1,2,3 are the three most important minerals % is the relative abundance A is the relative age with respect to the other minerals (1,2,3) C is the consistency of composition along the fracture (1 to 0: 1=poor; 5=reasonable; 0=very good).	
43	S	Smooth	
	U	Undulating	Large scale fracture
	C	Curved	roughness (1A)
	P	Planar	
44	S	Smooth	Small scale roughness (1A)
	R	Rough	
45	G	Gabbro	
	T	Trondjhemite	Host rock type (1A)
	D	Dyke rock	
	P	Extrusives (pillows)	
46	F	Fine	
	M	Medium	Grain size of host rock
	C	Coarse	of fracture (1A)
47-49	real	Fracture aperture in millimetres (F3.1)	
50-80	character	Additional comments	

Note: In the raw field data the first 11 columns are for simplicity put on a separate line prefixed by a '2' in column 1 (one for each scanline)followed on the next lines by the data for each fracture (column 11 onwards). Lines starting with a '3' in column 1 are considered comment statements.

The data format for the area mapped data sets is slightly different from the above layout: col 15-19 contains the X coordinate of the start of the fracture; columns 50-80 contain the Y start, X end and Y end coordinates of the fracture (Format F5.3 e.g. 21.03).Fracture numbering in these files is in ascending order except where fractures measured by the scanline method are encountered: their numbers are those used in the scanline data set (for purposes of cross-referencing).

On the following pages the scanline data are presented using the above format.

Flag (1): 1=fracture data; 2=scanline data; 3=comments

Scanline data: (Numbers in brackets refer to column numbers in coding form)

Locator (2-5): Photo label

Scan line (6): Labels A, B, C, etc. for scanlines used (label on overlay)

Scan trend (7-9): 0-360 azimuthal scanline trens (0=north)

Scan plunge (10-11): 0-90 inclination (0=horizontal)

Fracture data:

Fracture number (12-14): Sequential labels; marked on overlay

Scan dx (15-19): Distance (+/-0.01m) where fracture crosses scanline

Fracture type (20-21): Rock contact=cn; joint=jt; vein=vn; fracture zone=fz

Orientation (22-24,25-26): Dip direction: 0-360 azimuthal bearing (0=north)
Dip 0-90 inclination (0 = horizontal)

Trace length (27-30): To nearest 0.2m - may continue off photo, minimum length measured 0.2m

Censoring type (31):

0: both ends free

1: one end covered

2: both ends covered

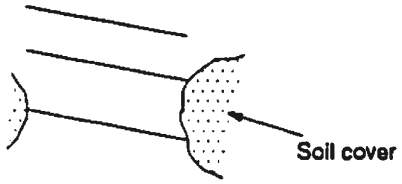

Termination type: (32):

0: both ends free

1: end against another joint

2: both ends against joints

3: one end splays

4: both ends splay

5: one end splays the other ends against a joint

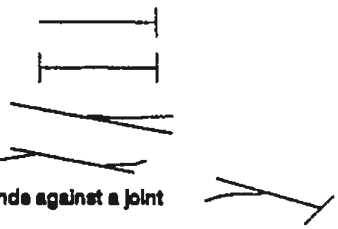

blank if censoring is 2

Infilling (33-42): e=epidote; z=zeolite; c=calcite; k=chlorite; p=pyrite; r=rubble; n=none
q=quartz; h=hematite; x=clay; m=magnetite; l=celadonite; j=jasper
followed by %/10 of total minerals in fracture; relative age

Roughness (43): Large scale (L):

s=stepped u=undulating

c=curved p=flat plane

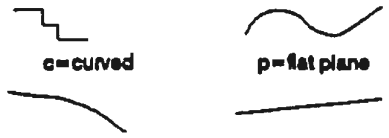

Small scale (S):

r=rough k=slickensided s=smooth



Rock type (45): g=gabbro; t=trondjhemite; d=dyke; p=pillows and lava flows

Rock grain size (46): f=fine; m=medium; c=coarse

Fracture width (47-49): Present width of fracture/vein (mm)

Comment (50-80): Relation details, slickenside orientations, etc.

Coding convention for scanline mapping

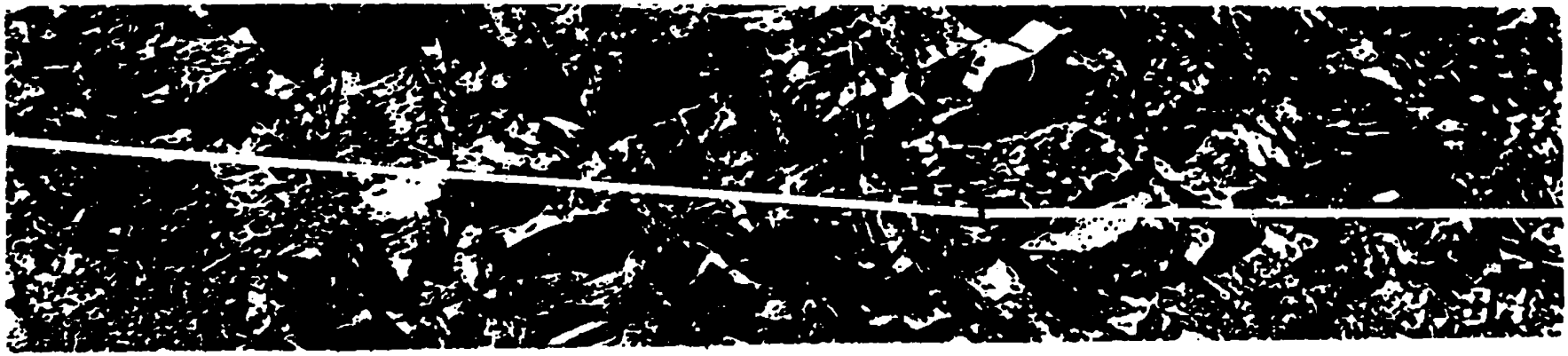

A. PHOTOGRAPH

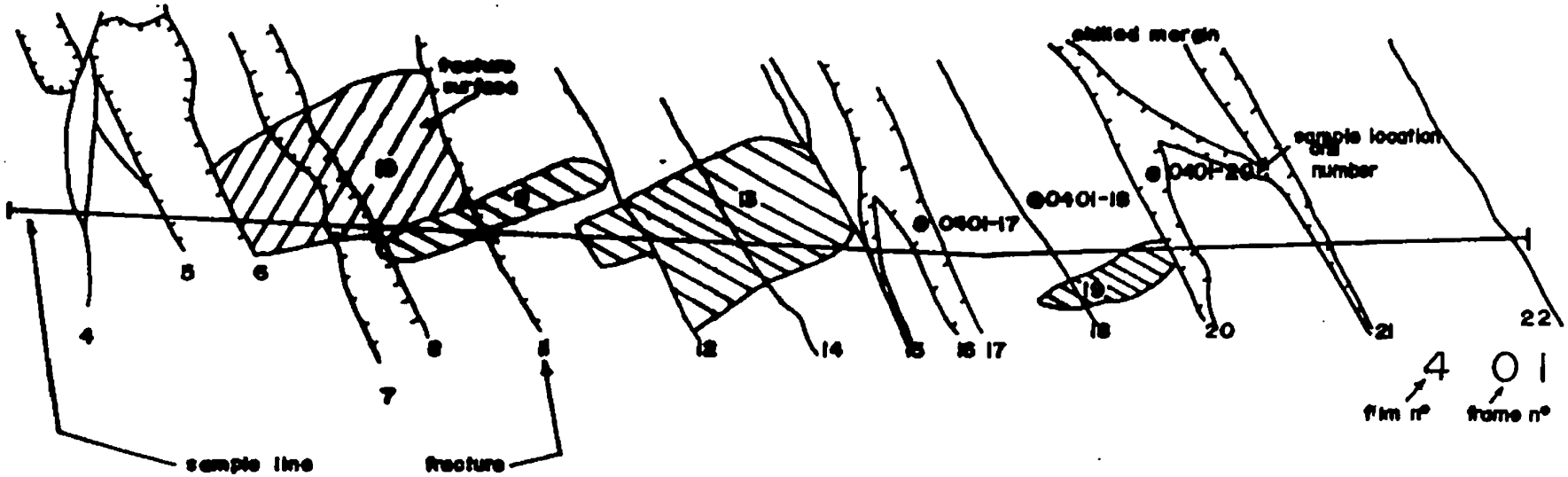

EXAMPLE OF FRACTURE SAMPLING B. OVERLAY

FIGURE 4

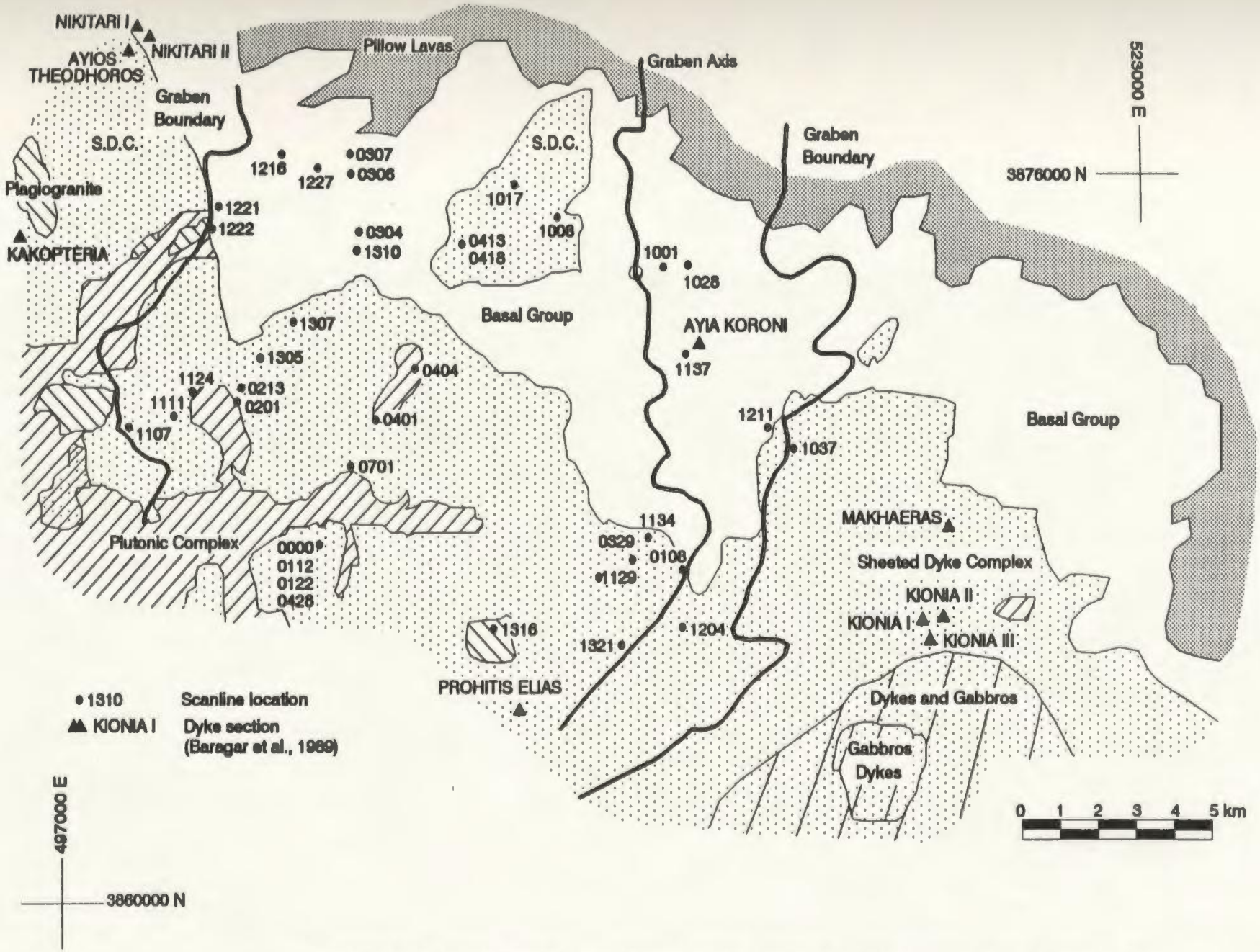

SCANLINE AND DYKE LOCATION MAP, SPILIA - POLITIKO AREA, CYPRUS.

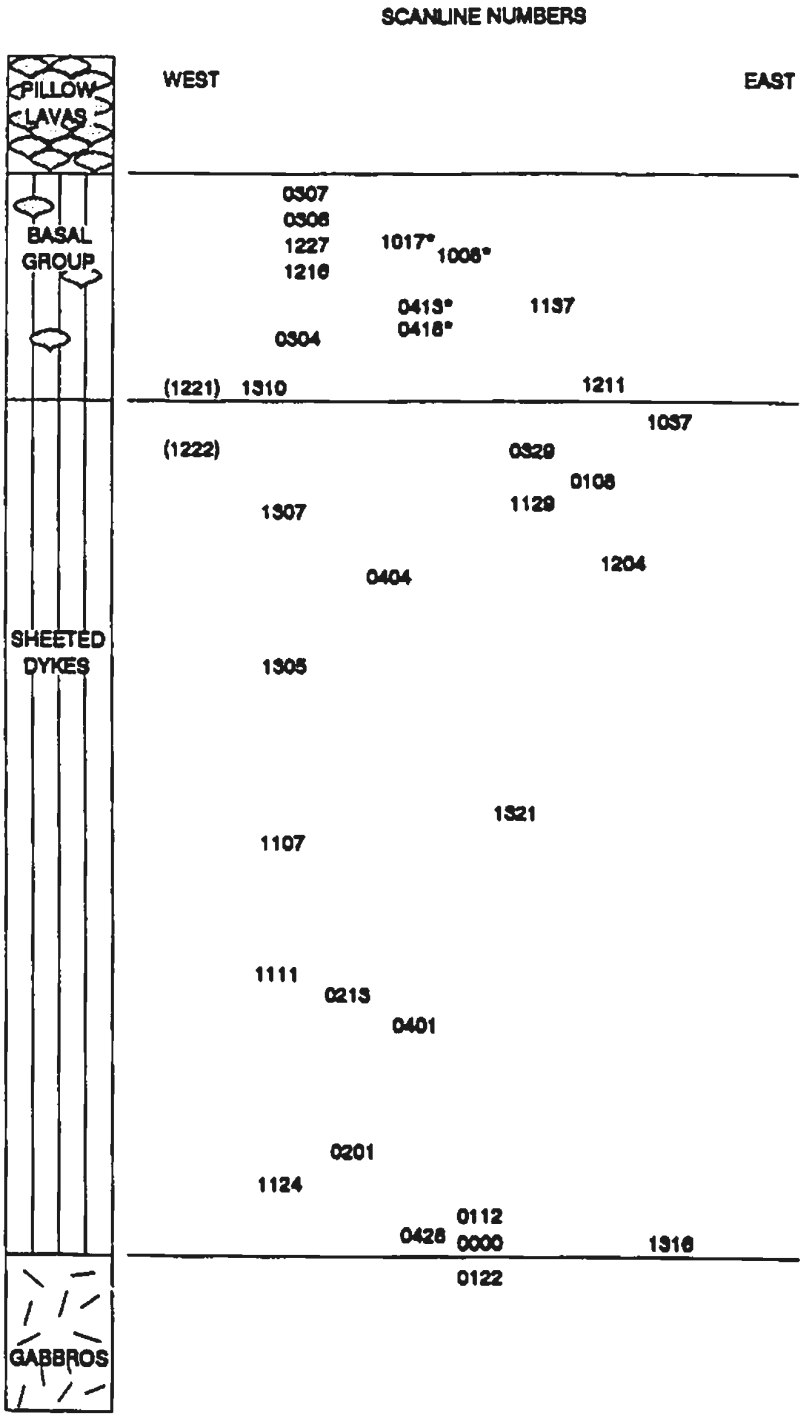

SCANLINE LOCATION WITH DEPTH IN THE SPILIA-POLITIKO AREA, CYPRUS
* INDICATES SCANLINES WITHIN THE SHEETED DYKE INLIER IN THE BASAL GROUP.

Scanline Fracture Measurements

(using the format outlined on the previous pages)
Note: the data are presented in a two column format

```
0000000001111111111222222222233333333344444444445555555556
12345678901234567890123456789012345678901234567890123456789
3in ravine between outcrops of 0124 0130 and 0119 0121 no photo
20000c02324
3begins at stone wall near road
1    00100.19j001771.202-e      pedm
1    00204.50j334400.682-z      pedm  patchy z (1mm)
1    00304.45j251800.752-z      pedm001
1    00404.58j206550.532-z      pedm001
1    00505.30j281750.852-z  r   pedm010
1    00605.90j205541.4002z      pedm006
1    00706.30m1087910.02-e      pedm005gabbro/dyke contact
1    00806.90j027630.6011z      pedm002alichnosites 014/62
1    00907.20j299380.382-z  e   pedm  patchy z and e (e on z)
1    01007.30j258731.052-z      pedm  patchy z
1    01107.90j180701.312-z      pedm001patchy z
1    01207.83j236860.752-z      pedm0.5patchy z
1    01308.06j237781.1011z      pedm0.5
1    01408.80j196671.8302z      pedm001
1    01508.90j318410.5511e      pedm  patchy e
1    01608.60j251842.0011z      pedm001
1    01709.30j205661.7011z      pedm002
1    01809.30j052531.1602z  e   pedm002minor e
1    01909.45j055601.7002e  z   pedm001
1    02010.00j222450.6002z      pedm002
3end of line a at 10.00m
20000c04036
1    02111.20j072871.5511z      pedm0.1minor patchy z
1    02211.45j035450.8411e      pegm0.5
1    02312.00j213792.4002z      pedm001
1    02413.20j004781.3511z      pegm002
1    02513.40j196830.7210z      pegm002
1    02614.35j232801.8011z      urgm002cuts dyke also
1    02714.90j039261.5011z      pegm005cuts dyke also
1    02815.10j0a5822.0011z  e   pegm001
1    02915.65j035693.2011z      pegm002
1    03016.30j039852.7011z  e   pegm001minor e
1    03118.70j130602.1002z      pegm001
1    03219.30j203811.4002z      pegm001
1    03319.40j211691.0502z      pegm003
1    03419.80j029860.9502z      pegm008
1    03519.90j052741.0011z      pegm003
3end of line b at 20.00m line c starts at 00.00m same place
20000c01224
1    03600.30j092830.6302z      pegm0.1u=grey mineral
1    03700.35j246850.4902z      pegm003
1    03800.86j188800.5711z      pegm003
1    03900.95j218530.532-z      pegm005
1    04001.15j010870.762-e      pegm006
1    04101.39j214680.3801z      pegm003
1    04201.77j196820.6802z      urgm002
1    04304.56j190831.7811z      pegm003
1    04404.79m188600.3401u      pegm025dyklet 1cm wide with
3chalk like material in it (SAMPLE R-54)
1    04505.20j200630.7302z      pegm003
1    04605.50j192901.3811z      pegm002
1    04705.98j022830.7702z      pegm001patchy z
1    04804.68m125802.3511z  e   pegm012joint with dyklet in it e on r
1    04904.87j140751.1022z      pegm001patchy open
1    05006.67j018801.2610z      pegm004crosses into dyke
1    05106.80m336853.602-e      crgm000light
1    05204.95j030881.3411z      pedm000patchy z
1    05307.50j192871.302-e      pedm002patchy z
1    05407.85j044630.6102z      pegm005
310.20 to 10.80 network of 1cm wide z veins crosscutting at 80deg
3two sets of 7 separated by 5cm
3rest covered by rubble/debris
1    05510.78j012850.5411z      pedm  patchy z
1    05610.99j188870.2511z      pedm002
1    05711.26j018800.4511z      pedm004
1    05811.55j212890.6011z      pedm001
1    05911.78j190850.762-e      pedm0.5
1    06011.72j126801.202-e  z   pedm0080.5mm thick z
1    06111.90j232600.9502z  e   pedm001
1    06212.13j162680.6702z  e   pedm0.5dyke getting coarser
1    06312.37j188830.8302z      pedc001
1    06412.47j230800.5202z  e   pedc003minor e
1    06513.28j196780.5502z      pedc001
1    06613.33j226500.4805z      undc001patchy open epieye cut or
3terminated by fracture
1    06713.47m222850.4601z      undc002
1    06813.50j196730.4302z  e   pedc001minor e
1    06913.50j072850.3001z      pedc002
1    07013.64j188850.6102z  e   pedc001minor e
1    07113.71j078602.6202z  z   pedc012e on z on rock e in middle
3epidote dominant
1    07214.04j242700.4002z      pedm001
1    07314.22m080752.2211e  z   pedm010e gabbro/dyke z on rock wall
3e on contact
1    07415.03j300851.3501z      undm002crosscuts dyke/gabbro contact
1    07515.38j219830.9011z      pegm001
1    07617.46j102753.4011e  z   pegm015z on e on rock
30302 line 40m 175 deg and 29m 206 deg from end of line c (photo 0301)
203026219200
1    00100.00j078691.3802z      pedm
1    00200.20j325450.8511e  k   pedm  minor k wavy surface
3wave trend 253/20
1    00300.36j072690.8011e  u   pedm  u=red coating minor & patchy e
1    00400.50j174901.652-e      pedm001open
1    00501.10j350821.753-u      pedm  u=red coating
1    00600.70j060811.3010u      pedm0.5u=red coating
1    00700.90j150020.302-e      pedm0.5light 0.1mm e coating
1    00801.35j358890.6311u      pedm0.5u=red coating
1    00901.00j062812.202-u      pedm0.5u=red coating
1    01001.76j350881.0501u      pedm0.5very light red coating
1    01102.00j358880.852-u      pedm0.1u=red coating; covered
1    01201.96j289990.9011e      pedm0.1covered light coloured sandy e
1    01301.90j052752.6013u  h   pedm0.1patchy red & oxides
1    01402.65j001870.302-u      pedm001open red=u
1    01502.10j074652.302-e  u r  pedm005mainly e u=red
3which spills over from fracture 016
1    01603.10j339881.702-u      pedm  u=red coating
1    01703.10j239560.6012u      pedm  v.light coating red
1    01803.37j013842.002-u      pedm  light to v. light red coat
1    01902.45j100451.2511e      pedm001rock in area more fractured
3then elsewhere as with fracture 015
1    02003.35e100722.202-e      pedm020zone of 001mm
3wide epidote veins in places to 10mm wide
1    02103.35e052781.8011e      pedm020e 020
1    02204.10e075722.702-e  u   pedm020e 020 u=sulfate or zeolite?
1    02304.30e045892.802-e  r   pedm030zone contains dyke rubble
3broken off walls (angular) rock between 020 and 023 contains
3irregular 0.1mm epidote veins
3end of page #23 start of page #24
1    02404.80e077712.6011e      pedm0.5
1    02504.90e069862.202-e      pedm0.1
1    02605.16e071782.102-e      pedm0.1epidote pod 2cm diam
3rock between 023 and 026 contains 1% pyrite
1    02704.60j106643.0012e      pedm002open
1    02806.10j301422.602-e  z   pedm  patchy zeolite
1    02906.05j093702.3010e      pedm001
1    03007.30j064731.552-e      pedm0012veins each 0.2 mm wide
1    03108.00j060901.802-e      cnd001dyke contact
1    03208.10j060801.802-e      cnd001dyke contact
3    03308.10zone stretches to 11.40m (off the photo which
3stops at 9.00m) contains abundant pyrite (1mm diam.) epidote
```

```
In highly weathered andesite cutting thoroughly silicified
20801419200
|       05411.44m042651.552-e          pxfm005
|       05511.70j042701.332-e          pxfm001
|       05612.18j052691.952-e  p  z    pxfm030some of e and z veins
Small scale pyrite veins
|       05712.74j025790.752-e          pxfm   patchy e
|       05812.49j046751.902-e          pxfm001patchy  e in pxfm 1cm diam
End of line d at 13.30m
20801e04650
|       00100.00j311391.8002s          cxfm   patchy z
|       00200.43j027770.4802s          pxfm0.5minor epidote
|       00300.86j023850.6002s          pxfm001cpxm
|       00401.80j080801.5811s          pxfm001
|       00502.45m251871.902-e          pxf0.1tight  small dyke
35cm wide crossed with sulfides
Mrom 2.45m to 5.70m is an intrusive flow(ecomm?) vesicular pyrite
Vesicles infilled with some epidote no chilled margins seen
|       00605.70j067861.872-e          pxf002cpxm
|       00706.00j066871.602-e          pxfm001cpxm
|       00806.10j045791.2011e          pxfm002
|       00906.53j063801.702-e          pxfm030down to 10mm
|       01006.80j039751.2711e          pxfm0.1patchy  e cpxm
20112n17304
|       00100.00j223861.7511s          pxfm0.1tight silicksnides 209/86
|       00200.24j186541.2511s          pxfm0.1tight
|       00301.25j122822.8002s          pxfm0.1patchy  e
|       00401.30j058873.2011s  e  u    pxfm0.1e cm z cm rock u=red
|       00501.70j154280.6002s          pxfm0.1v. patchy e
|       00602.00j060853.6011s  e       pxfm005mostly z patchy e (1%) rock in
Xphases healed e in adjacent veins truncated by zeolite veins i.e. 007
Xis cut by 006
|       00702.10j188521.2611e          pxfm010e tight hairline
|       00802.30j063782.7511s  u       pxfm005u=rare  red
|       00902.65j050903.0011s          pxfm005
|       01003.30j102491.7511e          pxfm005e patchy in places
|       01102.85j034741.2011s          pxfm003
|       01203.90j094501.1911e          pxfm   patchy e
|       01303.40j262801.8511s          pxfm003
|       01404.30j133422.1511e          pxfm0.1v.patchy  e
|       01504.50j272992.7502s          cxfm002cpxm
|       01605.40j110512.702-e  z  k    pxfm008patchy  coverage some u=red
|       01705.25j230891.3511s          pxfm005
|       01805.45j078712.452-e  u       pxfm010u=red
|       01905.60j125443.402-e  e  k    pxfm015minor k
|       02006.00j127510.7302e  k       pxfm0.1patchy  e v minor k
|       02106.30j073892.7010s  u       pxfm0.1patchy  z minor u=red
|       02206.60j110501.102-e          pxfm   v patchy z
|       02307.10j072790.6011s  e  u    pxfm001patchy  zeo(red)
|       02407.40j104480.9002s  e  u    pxfm0.5as above
|       02507.40j349840.7502s          pxf008
|       02608.25j105732.0002s  u  e    pxfm003v minor e (u=red)
|       02707.85m138472.1011s          pxfm001dyke  contact
|       02808.25j148591.7011e          pxfm003
End of line e at 9.00m this line line 65m bearing 158 deg from photo 0113
20115n15600
|       00100.00j130892.4011s          pxfm0.1cpxm
|       00200.00j205702.4001s          pxfm0.5patchy  z
|       00300.30j310431.6001s          pxfm001
|       00400.70j344781.1511s          pxfm0.1patchy  z
|       00500.90j077353.083-e  h       pxf010dyke  contact hematite=h
|       00601.30j306563.2011s          pxfm0.5
|       00701.10j042842.2002s          pxfm0.1patchy  z
|       00801.40j104721.5002s          pxfm001
|       00902.70j098500.8003s          pxfm002
|       01001.40j208542.9002s          pxfm0.5
|       01101.90j037760.8003-e         pxfm0.2
|       01202.60j009712.3011s          pxfm0.1patchy
|       01303.00j108472.2011h          pxfm0.1Fe oxides=h
|       01403.60j064503.602-e  u  e    pxfm001central portion of zeolite
Vein network in angular dyke fragments over 10cm u=red mineral
|       01505.30j000840.6002s          pxfm010reached  zone with e
|       01605.65j108430.802-e          pxfm003
|       01705.65j021600.852-e          pxfm0.1patchy  zeolites
|       01805.90j353593.003-e  u       pxfm015u=red=v.  minor
End of line e at 05.90m k connects on to 0116
20116n13102
|       00100.00j100524.352-e  z  h    pxgm010fracture  completely
Xfilled with epidote on rock minor hematite (rust) = edge of 24cm
Xthick dyke gabbroic center other side also epidote
|       00200.00j355553.002-e          pxgm0.1patchy  zeolite
|       00300.40j110571.9010m          prg m001tight to cpxm
|       00400.45j010471.5511s          pxgm
|       00500.65j350704.502-h          pxgm002mostly  nothing. very minor
Xzeolite stains
|       00601.00j329714.502-e  h       pxgm008minor h
|       00701.20j333833.5011s          pxgm0.1
|       00801.30j352629.5011s          pxgm0.1
|       00901.45j358862.1002s          pxgm005cpxm
|       01001.80j055451.2011s          pxgm
|       01101.94j227334.8002s          urgm010varies  hairline to 1cm
Xthick epidote vein is truncated against other epidote veins
Xremaining hematite in places (v. small patches)
|       01201.95j346660.8602s          pxgm
|       01302.10j000643.5011s          pxgm001
|       01403.01j341890.602-e          pxgm   patchy e
|       01503.10j358630.8502s          pxgm
|       01603.50j115572.5011e  h       pxgm040patches  of hematite
|       01704.30j086602.002-e          pxf200small  diabase dykelet dk=dyke
|       01804.90j104572.5011s          pxgm0.1tight
|       01905.15j089712.0011s          urgm0.1patchy  zeolite
|       02005.15j084080.3002h          pxgm0.1patchy  hematite
|       02104.10j080361.3511e          pxf0.1cover  by white cement
Xcoming of dyke (6cm thick dyke)
Mracture 022 doesn't connect the sample line but has hematite coating
Xis curved gabbro surface 076/77 1.5m long trace it terminates against
Mracture 021
|       02306.10j359611.1011s          pxgm
|       02406.60j093450.752-e          urgm
|       02506.75j358661.1511e          pxgm0.1thin  coating epidote
|       02607.60j108331.0011e          pxgm0.1patchy  epidote
End of line a at 07.40m
20116n05500
|       02800.50j083741.152-h          pxgm   patchy Fe oxidation
Y***check out numbering on photo here as there are two 026 fractures***
|       02700.70j034220.702-e          pxgm001
|       01301.10
|       02701.30j233411.3502e  h       pxgm005
|       02801.50m216463.1502s          pxgm004
|       01101.70
|       02901.80m224331.1002s          pxgm005up  to 20mm
|       03002.05m236331.9002s          pxgm015down  to 001mm
|       03102.15h224449.002-e  h       pxgm100h  on rock e on h=hematite
|       03202.40j248880.7002s          pxgm
|       03302.50m220521.2002s          pxgm002mafic  against e veins l=lreeg
|       03402.65j241900.4002s          pxgm0.1tight
|       03503.17h211820.6002s          cxgm0.1tight
|       03603.35j250511.252-e  h       cxgm025h=hematite  in e on rock
|       03703.50j036021.0511s          pxgm
|       03803.57h210480.602-e          pxgm002
|       03903.66h216470.352-e          pxgm001
|       04003.41h215490.7002s          pxgm0.5
|       04103.39h212480.5502s          pxgm001
End of line b at 03.40m
Xthe start of line c line 52m bearing 130 deg from end of photo 0118
Xthe epidote veins seem to be related to the intrusion of the dykes as they
Xphoto 01-22 line 60m at 326 deg and then 60m at 310 deg from ravine rock
Xbetween alcan and polystipes
Xtype is med cse gr gabbro  sample line starts at 0.00m
20122n31400
|       00100.00j148002.400s          cxgm   med to cre gabbro
|       00200.36j1040800.802s          cxgm   hairline cpxm
|       00300.75j0886402.113s  e  k    cxgm   z=.9 e=.05 k=.05
Xtail end of fracture terminated by blasting
|       00401.04j0936306.02-e  r  e    xrgm   z=.6 e=.1 rust=.3
|       99901.04j0936304.011s  r  e    xrgm   subparallel to 004
|       00501.40j0846600.802s          cxgm
|       00601.70j1363802.401s          pxgm   similar to 001
|       00702.60m0904306.02-e  e       cxgm020z=.4 e=.4 loose
|       00802.50m2548001.611s          cxgm050six  veins z well bonded
|       00902.62j001450.4501s          pxgm   epidoty zeolite
|       01002.80j003480.6001s          pxgm001z=small  vein
|       01102.90j136780.6002s          cxgm   tight
|       01203.03j004480.8002s          cxgm
End of line a at 3.03m start of b at 3.03m goes to 6.50m
20122n30607
|       01303.13j240482.6101s          cxgm001patchy  z
|       01403.42j1636302.011s          pxgm
|       01504.10j0843301.002s          pxgm   silicksnides 132/26
|       01604.25j2802401.802s          pxgm
|       01704.57h0786405.02-e          pxgm   z covers .6 of surface
Mracture zone covers 04.50m to 4.65m
|       99804.95j0737304.011s  e       pxgm   silicksnides 088/74 curves to
Xbottom. vein fill zeolite in middle epidote on rock wall surfaces
|       01805.00j150703.6002s          pxgm
|       01906.00 s093761.5011s        cxgm002tight
|       02006.30j068525.402-e  z       cxgm   e on rock z b/t silicksnides 1
|       02106.50 s0967802.72-e  e      cxgm   e on rock z on e
End of line b at 6.50m start of c at 6.50m goes to 10.10m
20123e28710
```

1 02207.00m0905305.511s r crgm040up to 0.1m wide
1 02307.25 s0708001.411s crgm
1 02407.40 s2368201.511s r crgm030joins 023 to match dip
3in places filled with s and rubble from gabbro split off host no epidote
1 02508.00 s0588401.911s e crgm slickensides 132/61 s on e on
1 02608.24 s2488201.601s prgm040sharp well defined surface
1 02708.35js0688205.52-s e urgm patchy e more common s on rock
1 02808.40js2008801.52-s prgm surf subparallel to sampleline
1 02909.05js0708802.201s crgm
1 03009.92js083701.4510s prgm001epidote fills joint
3end of line e 10.1m start line d at 10.1m goes to 12.14m edge of photo
3matches photo 0533
20124428100
1 03110.40js1006704.52-s crgm050east edge of alteration zone
1 03210.70m0926804.52-s e r prgm300 varies to 0.3m wide
3in highly altered and crushed zone spotty epidote along rock surfaces filled
3with s
1 03311.45 s2588801.411e s crgm e on rock minor s
3rock mass from 10.4m to 14.2m is highly fragmented with zeolite veining
3dominant (multiple layering of zeolite?)
1 03412.00js0788001.211s prgm
1 03512.75s0698201.903s urgm s fills vein fracture
3ends as e series of splays
1 03613.15m2578202.811s crgm020distinct upper part s filled
1 03713.45m2588804.020r s e crgm050zone of strong alteration
3varies 7 to 3 cm in width e on rock s on e mixed with rubble
1 03813.90js0878201.911s crgm subparallel veins
1 03914.02js0688600.811s s crgm
1 04014.07js2538604.02-e s crgm s on e (dominant) on rock
1 04114.16js0968803.011s e prgm s in center and around e
1 04214.20js1587500.702s prgm s as scale on surface
1 04314.60js1448401.101s crgm
1 04414.90m2628801.400s prgm fine fracture/vein
1 04515.20js2458401.411s prgm010beyond s
1 04615.40js2508403.011s crgm 6 fractures between 046 and 04
1 04715.95m0748003.021e s crgm040minor e and s from 2 to 4 cm
1 04816.35m0908006.02-s crgm edge of fracture zone extends
1 04918.20m1008003.02-s e crgm connect to 0.1m wide dyke
318.8m to 19.8m covered in gravel
1 05019.80js2428502.42-s prgm
1 05119.10js1587201.510s crgm series of subparallel s veins
3sample line d ends at 20.0m line e starts at 0.0m goes to 5.30m connects to d
20124s13306
1 05200.35js1118401.82-s prgm003s crystallized in from edges
3leaving a line down the center of the fracture
1 05300.55js0888301.211s prgm003
1 05401.00js0847303.02-s e prgm0401 to 4cm wide minor e
1 05501.10js0988801.82-s e crgm minor s and e on surface
1 05601.20js1867801.02-s prgm
1 05701.60m0428001.22-s crgm subparallel to sample line
1 05801.87js1608801.22-s prgm
1 05902.10js0928502.22-s crgm100highly altered
1 06002.30 s0988501.111s crgm002joins 059
1 to 0.2cm thick
1 06102.90js2468801.702s e crgm100to 4cm wide very altered
1 06203.33js0978001.211s e crgm altered clay gouge
3061 062 063 have split a small 10cm wide dyke
1 06303.45s2718400.411s crgm s in dyke center
1 06403.70js0888802.72-s crgm100highly altered zone
1 06503.70js0708201.42-s e u crgm020dark green= amphibole?
1 06604.00js1088401.811s s crgm045s some pyx and amph
1 06704.30js0878802.52-s crgm highly altered
1 06804.80js1158701.511s s crgm005s=.9 s.1
1 06905.17js0958202.72-s crgm
3end of line e at 5.3m start of line f at 5.3m goes to 14.0m
20125f13200
1 07005.40js0065201.12-s prgm
1 07105.60s1108502.510s prgm minor e
1 07205.75s1057502.810s prgm patchy crs
1 07306.40m1038202.02-e s crgm Fe oxide staining
1 07406.45m1307201.711s e crgm filled with s on surface of
3rock some epidote pods throughout
1 07507.40s1088402.211s e crgm tight
1 07607.35m0958000.811s e crgm minor e veins
1 07707.75js1148302.32-s e prgm005s cm e on rock
3to 10cm long epidote veins (scale on surface)
1 07809.10m1188202.12-s e prgm vertical e crosscuts e series
3horizontal epidote veins (3) s is mixed with e
1 07909.60m1724502.511s e prgm upper portion mostly s
1 08010.95js1907501.602s prgm
1 08111.10js1048601.611s e prgm s on rock e in center
1 08211.30js1048601.001s prgm
1 08311.55m0927604.02-s e pstf altered zone on contact with d
3wedge of gabbro cuts dyke (not completely through) dyke=v.fine diabase
1 08412.00m0947003.02-s pstf
1 08512.60m1208303.52-s e crgm cm dyke e near top
1 08613.25m1108003.52-e s prgm ss=top e and s vein=bottom
3contact to gabbro/dyke=sharp epidote interzone
1 08713.45js3527701.311s prgm
1 08813.60js0588201.402s prgm
3top line f at 14.00m start line g at 0m goes to 10.2m and connects to f
20126g14200
1 08900.25js0018703.02-s crgm005patchy s
1 09000.40js1068701.72-e s prgm s on e on rock
1 09101.40s157800.952-s prgm
1 09202.60m0015703.52-e crt contact g to t
1 09302.90js098580.852-e prt
1 09402.95js186651.252-s prt
1 09503.30js1055301.02-e prt
1 09603.65s1135201.810s crt 002light
1 09703.40s193751.0511s e crt minor epidote
1 09803.90js194850.602-e e prt 001
1 09903.90js144603.002-e h prt 020s=sandy
1 10005.12m 2.002-h s prt? highly oxidized e in pods
3epidote and hematite zone extends from 4.50m to 5.75m
1 10106.00js1186401.52-s prt 0.1
1 10206.74js0915301.22-s prt 0.1
1 10307.05js3564101.02-s prt
1 10408.00ss 02.01 e h prt of sandy epidote
3weathered at top by rust colored Fe oxides up to 5cm thick
1 10508.40m102301.252-s prt 001even coverage of e
1 10609.25s111551.302-s e crt alchemsides 116/55
1 10709.70js096561.852-s s prt s on e on rock
1 10810.20js1096503.22-s s h prt 010
3 109 no contact (prt) zeolite rich zone with serpentinite
3epidote and Fe oxides
1 11004.36js005851.602-s h crt 003forget this one earlier
20127h14001 start at 0.00m end 7.50m
1 11100.97js1005303.92-s e k prtm100mostly 1mm upto 10cm wide
1 11201.07js08710.852-s prtm002
1 11301.24 s1154001.513s k u prtm005s=red carbonate?
1 11401.10s3345102.511s crtm0.1light
1 11501.48s306810.7502s crtm0.1light crosscuts 116
1 11601.57js0994804.02-s e prtm120mcrrows down to 5cm
1 11701.70js2254002.42-s prtm0.1light
1 11801.44s132811.2502k crtm001minor chlorite
1 11902.30js0956003.02-s e h crtm050minor epidote and Fe oxides
1 12002.50js0975804.02-s s h prtm020massive e minor s and h
3 this is a zone of mainly epidote forming an irregular surface in the
3tremdjhomite. It is mixed with some zeolites and iron oxides so out-
3pidates. Rock is coated with Fe oxides overlain by epidote (light green
3to dark green) zeolites are rare. Zone goes from 2.50m to 4.10m and
3extends vertically over the whole outcrop (>4.0m)
1 12104.60js0885304.02-e k prtm010start e pod lower down pod of
3epidote crosses sample line 4.50m to 5.30m contains chlorite (?)- dark
3green and epidote at the top of the pod
1 12206.40js1166204.02-e h k prtm005minor h & k
3west edge of epidote pod zone. Bordered by zeolites spilling over to
3east joint surfaces on outcrop
1 12308.84js0785801.511e s prtm0.1minor e & s tight
1 12407.10js0898504.02-e h e prtm030alichemsides 002/26 minor e
1 12507.30js0925703.21le s prtm002s cm patchy e(s also on rock)
3end of line at 7.50m
20128i11209 start 0.0m end 3.0m
1 12600.00js0906403.010s s prtm0.1light
1 12700.00js3567502.511e prtm very minor patchy e
1 12800.40s1177302.901e crtm0.1e staining on rock about
30.5cm beyond fracture
1 12900.55js0805602.011e prtm002mmepidote on rock
1 13001.20m0578704.02-e s prtm0.1minor & s tight
3dyke is faulted off just above sample line cut by plane of tremdjhomite
3infilling of fracture near top of fracture near top contains more e
3between the joint is bordered by tremdjhomite on both sides
1 13101.24m077830.5011e e h crtm050minor e major k minor h
1 13201.75m094643.5020h e prt0.1light
3end of page #8 start of page #9
1 13302.60s0655403.02-e h crt1010
1 13402.70s0944603.02-e k h crtm010k=dark green
1 13500.00s0893301.602s k crtm003minor s & k
3end of sample line i at 3.0m
20128j33206 start 3.0m end 6.80m
1 13600.00js2341001.902s prtm0.1light
1 13700.50js1033503.811h s crtm002minor zeolite
1 13800.40js000800.872-s h prtm001s on rock h on s
1 13900.80js1415302.32-h k crtc005many ho chlorite
1 14004.35js1357001.710s s prtc001minor s to tight
1 14104.20js2522601.011e h crtc020h cm rock cm e (open along h)
1 14204.67js1157600.411s prtc002open
1 14305.30js0924602.52-e h k prtc005 143s doesn't match sample lin
1 14405.10js1678300.411s prtc

```
1        14926.50j0903701.52-h  e     prdm001
1        14887.30m1004704.02-h  k e  prm  minor k & e
3contact track to trondjhemite zone contact in places trondjhemite is
3highly weathered and crumbly elsewhere it is competent
1        14707.30h1014702.011e  h     prtz020zone continues to 7.70m contai
3rubble epidote and iron oxides
1        14808.40j1084503.02-e  h k  arm005irregular surface minor k
1        14908.70j3052201.702a        prtz030zone of e and trondjhemite
1        15009.00j1135402.411e        prtz020fairly tight higher up k is
3(thicker as it passes through a highly altered trondjhemite patch (approx.
30.5m in diameter)
1        15108.20j2713401.62-e  p     prtz030p=pyrite substantial in t and e
3end of sample line j at 9.0m start line k at 0.0m end at 9.0m
20129z13300
1        15200.70j0986002.610a  k     prtz001widens where k contacts 150
1        15300.80j0434701.32-e  k     prtz  faint/rare e and k
1        15401.70h0834501.310a        crtz030zone of highly altered trondjh
1        15502.00j1002500.753-e  k e  prtz  minor zin
3from 2.10m to   m there is a highly altered rust colored epidote containg
3trondjhemite
1        15602.830l1107503.52-e       prtz0.1tight
1        15704.35m3198701.510k  e     prtz001
1        15805.00j0845003.52-e  k     crtz001
3end of page #9 start page #10
1        15905.30j0864502.02-k  e     prtz001mainly k
1        16005.85j0903701.12-e  k h   prtz001mainly e but patchy
1        16106.10j087500.502-k  e     prtz001mainly k
1        16205.00h1248803.52-e  e     crtz010widens at bottom to a 10cm wid
3of networked zeolite veins cutting trondjhemite and epidote
1        16306.50j0733801.011k        prtz0.1tight
1        16406.60j1014802.82-e        prtz010
3end of line k at 9.0m
3photo 0130 is missing here but will be added later
3line A line between line K (0129) and (0131)
20130z13900
1        00101.70j082573.003-e  e h  prgz  alichannidze 165/10
3patchy e and h (hematite)
1        00202.00j087542.003-k        prgz0.2sample
1        00302.20j113472.002-e        prgz0.2patchy zeolites
1        00403.10j160842.003-e        prgz001
1        00504.80j071560.752-k        prgz001
1        00605.60j112763.002-h  k     prgz001possible k sample
1        00706.00m299392.1011e        lrgz004
1        00806.40m192533.9003e        lrgz005zeolite vein sample
1        00906.75j094663.002-e  k     prgz001zone 20 cm wide
3with chlorite on rock to 0.5mm thick and zeolite veins
3to 004 zone wide *sample
1        01007.30j094603.003-e        prgz0.1patchy zeolites
3at 8.30m a 30 cm diam. remote of pyroxene crystals in a
3more leucocratic (trondjhemitic?) finer rock
1        01109.00j073653.002-h        prgz001008 crosscuts this one
3h+Fe oxides
1        01209.10j070741.2002e        prgz002
1        01309.90j077703.002-e        prgz001
1        01410.42j128722.5010e        prgz001open
3end of line e at 10.80 m commente to line 1 (0130)
3end of page #41 start of page #42
20131z12901  start at 0.0m end at 4.7m
1        16500.20j0447404.02-e  e     prgz010
1        16600.70m300850.7002e  e     prgz015e on z on rock
1        16700.50m2254601.302e        prgz005
1        16801.25j0557304.02-e  e k   prgz010
1        16901.80j0127502.02-h        prgz  very minor patchy h
1        17001.70j0408401.211e        prgz002
1        17102.10j3598602.711e  h     prgz001gabbro leucocrac patchy zones
3almost pegmatitic with very fine patches in k
1        17202.75m1118402.511e        crgz010irregular vein
1        17303.80j1065304.02-e        prgz020network z veins in gabbro
3from 3.0m to 3.8m is a network of zeolite veins randomly pseudo vertically
3oriented in gabbro with minor h
1        17404.80j1136603.011k  e     prgz010contains 7 cm diameter e pod
1        17504.70j2607301.811e        prgz010contains 2 cm diam. e pod
3end of sample line l at 4.7m
20131z01400 start 4.7m end 9 0m
1        17605.10h0517903.511h  z     crgz005
1        17705.95h0876302.011e  e     crgz030alichannidze 345/15
1        17806.55j0246201.02-k        prgz001
1        17906.90j0404001.02-k        prgz001
1        18007.30m    04.511k         crgz100
3curved zone containing h and rusty chlorite
1        18107.30j0564801.011k  e     prgz001
1        18207.82j0483504.02-e  k z   crgz020
1        18308.00j0468003.02-k  e h   crgz005minor z & h
1        18408.75j0284500.42-e  k     prgz0.1tight
3end of page #10 start page #11
1        18509.00j0454501.611k  e h   crgz003
1        18608.80j0527501.452-k  e     prgz001very minor e
1        18708.80m0787503.011z        crgz010
3end of sample line m at 9.0m
20131z09400  start 9.0m end 12.0m
1        18809.50j0487003.02-e  k e   crgz080
1        18909.80h1664506.02-e  e h   crgz015
1        19010.30h1624801.711z        crgz005zone between 189 and 190
3contains network of zeolite veins approx. 2mm thick
1        19110.25j2147701.511e  z     prgf001contains purple mineral
3the purple mineral is found in similar trending fractures below the sample
3line between 9.7m and 10.6m the coating is very thin and in places looks
3piece orientation  :21470 alichannidze 279/51
3end                :21470 alichannidze 269/58
1        19212.00m0269001.911k  z     prtf250encountered slice of trond-
3jhemite out of by fault
3end of sample line m at 12.0m
20132z07000
1        00100.00j0433390.0011k  e h   prtm010k bands in rock e in cracks(?)
1        00200.50j1026703.011e        prtm005open
1        00301.80m108579.002-k  k e   crtm010minor k rare e
1        00401.65j0924001.202e  k     crtm020
1        00503.30h077399.0011e  e     prgz010
1        00603.55j1044503.010e        prgz0.1tight
1        00704.30h1096101.511e  k     prgz0.1 - sample
1        00804.35j0232004.502e        prgz0.1tight
1        00905.10j1296302.911e        prgz0.2specks of epidote
1        01005.55j021841.7513e  e     crgz004e on sides e in center
1        01105.85j231831.8013e        crgz002
1        01206.50j326591.1016e        prgz
1        01306.00j1125805.011e        prgz0.5minor zeolites
1        01406.70h215641.8002e        crgz002
1        01507.22j111451.8011e        prgz020varies in width
1        01607.52j106449.002-e        prgz0.1tight e at lower end small pod
1        01707.95h0506405.012e  e k   crgz020e in pods (width 0.1 to 2cm)
1        01809.25j057109.002-e        prgz060massive epidote - sample
1        01902.95j0042003.22-e        prgz0.1tight end of altered zone
1        02010.00j1004107.02-e  h     prgz020mainly epidote
1        02100.00j0704507.02-e  z     prtm020
3 contains unknown purple mineral on alichannidzd surface
3zone 003 and 019 contain epidote rock - is transitional between gabbro
3and trondjhemite
3end of line a at 10.00m
20133z05300
1        00100.60j023571.1011e        prgz  amphibole crystals 2cm long
1        00201.05j106595.0011e        prgz0.1
1        00301.10j044870.9002e        prgz0.1
1        00401.70j133702.2011e        prgz0.1
1        00501.70j034483.2511e        crgz005
1        00602.10j069791.3011e        prgz001
1        00702.60j320601.1001e        prgz0.1
1        00803.20h025871.6001e        crgz008
1        00903.40h035703.3511e        crgz003
1        01003.80j270802.7011e        prgz  gabbro more leucocratic
1        01103.80j010790.802-e        prgz
1        01204.10j190733.5011e        prgz0.1
1        01304.40j238781.3511e        prgz0.1
1        01405.10h216720.4001e        prgz002
1        01505.15j212650.6502e        prgz002
1        01605.20j049474.002-e  e     prgz0030.1 to 010mm
3epidote is in pods within the zeolite vein occurring mainly on rock (z on e)
1        01705.60j010571.4011e        prgz0.1
1        01805.90j220800.7302e        prgz0.1
1        01906.10j014581.2002e        prgz0.1
1        02006.20j005384.502-e        prgz002
1        02106.90j356701.4011e        prgz
1        02207.50j215800.9011e        prgz004
1        02308.00j051890.9511e        prgz003open in center
3showing crystal growths inward - SAMPLE
1        02407.45j008414.002-e        prgz  largely covered
1        02508.40j105564.002-e  e     prgz002up to 010mm v.minor e
1        02609.55h211895.002-e        lrgz004gabbro is more leucocratic in
3within 5cm of fracture on either side
1        02710.20h022762.0002e        crgz002
3end of line e at 10.80m
20134z24002
1        02810.80j103563.302-e        prgz001
1        02911.40j000741.3511e        prgz001zone 5cm wide of zeolite veins
3each 001mm wide
1        03012.40j040811.4011e        prgz005varies 0.1 to 10mm
1        03112.10j273440.7002e        prgz002below031 is a narrow
3trondjhemitic dyke ? SAMPLE
1        03312.55j019701.9011e  h     prgz007minor Fe oxides
1        03412.55h108363.402-e        prgz003
1        03513.10j138543.002-e        prgz003
```

1 00614.35j043790.8002n pegz
1 03714.45j213830.8002n pegz001
1 00815.10m084452.902-e pod005dyke 10cm wide gabbro inclusi
3dyke - or is it transjhumite SAMPLE
1 09e5.70j078552.203-e pegz002series of z veins to 5cm wide
3some one vein to 020mm wide
1 04015.45j031871.7502n pegz001
1 04116.00j087713.002-e orgz001edge of zone 009
1 04215.80j019630.9502n pegz001
1 04316.30j083611.5010n pegz008formed due to partial
3injection of transjhumite dyke
1 04416.50m084632.6611n orgz0.1light small 5cm dyke
1 04516.20j196891.1511n pegz001open
1 04617.20j082492.252-e e pegz001z minor hairline epidote veins
3leaching of host gabbro around joint associated with epidote formation? SAMPLE
1 04718.10j105662.002-e pegz0.5
1 04817.80j096802.202-e pegz002e 010 mm wide vein
1 04919.00j012531.702-e pegz001
1 05019.30j103502.802-e z pegz030minor z e pods to 20cm long
1 05118.84j035861.1011n pegz001
1 05219.80j016571.3511n pegz002
3end of line b at 20.00m
20124s02822
1 00103.50m1117901.111e ued0.1light cm-dyke/gabbro
3covered intervalfrom 4.0m to 5.30m
1 00205.80j1637401.52-n pegn
1 00306.15j1407803.211n pegn003
1 00406.70j1728003.111n pegn003series of three veins
1 00508.71j1547805.02-e e k pegn015minor k and e
3altered e and k extends 2cm either side of fracture into rock. veins in
3zeolite filled. some epidote pods to west and cross cuts small 10cm
3wide dyke
1 00610.10j0607901.211n pegn003g almost transjhumitic
1 00708.80j0727804.004n pegn016massive epidote locally
1 00812.40j097748.0020n z urg002veins to 1cm e cm rock
3e cm e runs subparallelto zone line from 12.5m to 14.2m
1 00914.90j009590.7011n pegn001
1 01015.12j031640.6011n pegn001
1 01117.20j0917606.02-e e orgn020minor e at 17.5m a series of
3splays come off the fracture filled with z and e each to 2mm wide
20201s09201
1 00100.00j244861.4011n pedm002open
1 00200.40j042773.502-n pedm
1 00300.42j339712.8011n pedm
1 00401.00m070733.402-e pedm010series 4to5 fractures cm
3filled with epidote w/ alteration zone ~2cm into rock either side of fracture
1 00501.30j087852.5002n pedm002in places e elsewhere nothing
1 00601.40j143791.7502n undm001
1 00702.35j333621.102-k z pedm0.1chlorite?
1 00802.70j032551.402-k pedm0.1patchy minor chlorite
1 00903.11j054702.102-e e pedm002e=z in amount
1 01003.30j054701.202-e pedm001
1 01103.53j063703.502-e z pedm020
1 01203.70j079803.502-e z pedm003v minor z
1 01303.87j074763.502-e pedm006
1 01404.00j330820.802-e pedm0.5
1 01504.10m009643.502-e pedf patchy v. minor e chilled margin
1 01604.60j039730.482-e pedf off white zeolite
1 01704.60b112890.902-e cedf003
1 01804.64b116840.2510n cedf001
1 01904.96j301691.8811z e pedm0.1patches of e
1 02005.14j327850.632-e pedm1.5
1 02105.60j319720.482-e cedm0.5
1 02206.02m070601.902-e pedf005
1 02306.07j320863.202-e e pedm001patchy e
1 02406.13j002700.302-e pedm0.5
1 02506.30j307900.3011n pedm0.1light
1 02606.75j114790.952-e pedm010
1 02707.05b334091.402-e bedm002
1 02807.60j020700.952-e pedf
1 02907.80j136890.922-e pedf006z is lower?
3end of page 051 start of page 052
3zone is a breccia filled with angular dyke fragments (1cm diam) extending
3over 3cm
20201s09201
1 03008.13b327810.7011z cedm002
1 03108.46b143870.902-e pedm010
3zone from 7.85 m to 9.50m is highly fractured dyke angular fragments
3with numerous zeolite veins but in a largely covered interval so
3can't see vein continuity spacing = 10cm vertical to subvertical
3section 02-13 to 02-15 8.5km south of Xylotox
20213s08102
1 00100.35m049664.502-e pedf001open
1 00200.36j055662.6010n pedm001open
1 00300.16j046691.1010n pedm001open
1 00400.45m055734.502-e pedf001
1 00500.90j073651.4010n pedm001open zone of 4 joints
3over 50cm all open zone filled highly fractured
1 00601.30m061644.502-e2 e2 2pedf001
1 00701.75m07664
32.4 to 2.9m is a dyke rubble brecciated w/ epidote=2%
1 00802.40j077704.502-e bedm500rubble zone
1 00902.90m072594.502-e pedf001
1 01002.95j064583.2010e6 e4 8pedm005SAMPLE
3epidosite band starts at 3.2 to 4.65m
1 01103.10j233800.7002e6 e4 7pedm001
1 01203.15j273640.8001n pedm001
1 01303.37j243871.0002n undm001discoloration either side of
3of fracture SAMPLE
1 01403.50j072562.0511n undm001discolor sides of fracture
1 01503.95j078891.3511n undm001discolor sides of fracture
1 01603.90j075841.0001e0 9undm002SAMPLE
1 01704.30j249612.0511e0 9pedm002
1 01804.60j066691.7510n pedm001
1 01904.95m087664.502-e pedf001
1 02005.30m079664.502-e pedf001
1 02104.75j146770.4002e0 7pedm j.u.
1 02205.25j205480.5502e0 7pedm j.u.
1 02305.50b009842.1013e6 e4 5pedf050fractures some rubble
1 02405.67m081784.502-e1 1pedf002
1 02505.90j074670.7011n pedm001
1 02605.95j042641.3011e0 2pedm001
1 02706.50j030602.8011n pedm001
1 02807.30j034723.1011n pedm001
1 02907.35m056723.002-e0 2pedf001
1 03007.40j243861.1502n pedf002open
1 03107.50j046660.7002n undm001
1 03207.95m092704.502-e pedf001
1 03308.25m073702.002-e0 2pedm001
1 03408.50j073803.0002n pedm001
1 03508.65j068633.1011n pedm001
1 03609.10j064703.5011e0 3pedm001
1 03709.45j067652.5011n pedm001
1 03809.85j039764.502-e0 3pedm001
1 03910.00m070644.502-e pedf001
1 04009.40j257291.6002n pedm001
1 04110.40m071654.502-e pedf001
1 04210.70m081594.502-e pedf001
1 04311.10m066704.502-e pedm001
3end of line a photo 02-13 start of line b photo 02-14
20214s07204
1 04411.70j031641.3001n pedm001faulty to epidosite
1 04511.90j160561.7002n pedm001
1 04611.29j046700.8001n pedm001
1 04711.20j292871.0802n pedm001
1 04812.00m082334.502-e8 e2 5pedf002
1 04912.22j042630.8002n cedm001
1 05011.20j232331.4502n pedm j.u.
1 05112.45j065641.1000n pedm001'start' of epidosite
1 05212.65j067024.502-e pedm001
1 05312.85j252851.2510n pedm001
1 05413.05j059711.5010n undc001
1 05513.45m035704.502-e0 7undf001
3epidosite dyke very fractured zone content
1 05613.65j076434.502-e0 1pedm001
1 05713.80j022351.4502n cedm j.u.
1 05813.60j123330.4502n pedm j.u.
1 05914.10j077682.1001n pedm001
1 06014.25m070734.502-e pedf001
1 06114.50j078654.502-e0 1pedm001
1 06214.60j054664.0011e0 1pedf001
1 06314.65m054644.502-e pedf001
3from 14.65 to 30.00m dykes are highly fractured friendly wasthered the major
3fractures will be measured
1 06415.45m069804.502-e pedf001
1 06515.60j059671.2011e0 7pedm002
1 06616.00b114870.4001e0 0bedc010
1 06716.35j045711.3000e0 4pedm003087 older than 066
1 06816.75m084804.502-e pedm001hard to get orientation
1 06917.10b273291.1510e0 0bedm002
1 07017.50b070741.2010e0 0bedm002
1 07117.90j300741.7011e0 7pedm002
1 07218.40b114881.0511e0 0bedf003
1 07318.50b053894.502-r7 e3 0bedf200
1 07418.70m108854.502-e pedf001
1 07518.90j027641.4002n pedm001
1 07619.10j204800.8501e0 1pedm001
1 07719.40j024821.4502r7 e3 2pedm001
1 07819.90m088794.502-e undm001
1 07920.00j072701.3511e0 5pedm002

```
1       08020.60m064792.5011e       pedm060small dykiet
1       08121.50m067752.8011e       pedm030small dykiet
3end of line b photo 02-14 start of line c photo 02-15
202154c24702
1       08221.45j029821.8511c0      1cedc002
1       08221.95j042641.8011e       pedc001
3epidosite band starts 22.05 to 22.5m
1       08422.50m070754.502-c0      1pedc002
1       08522.80k066430.5502c0      0ledc002
1       08623.056068770.7001c0      0ledc002
1       08723.156063770.6003c0      0ledc002
1       08823.278068661.6011c0      0pedc002
1       08923.406081620.7501c0      0pedc002
1       09023.706085730.8001c0      0pedc002
1       09123.80m072674.502-c6  c4  3pedc002
3start of epidosite band
1       09224.006273770.4502c0      0pedc002
1       09324.80j051654.502-e       pedm030small dykelet not epidotized
1       09423.30m051703.502-e       pedf040small dykelet not epidotized
1       09525.45j031723.0001e       pedm001
1       09625.85j098701.1011c0      1pedm001
1       09726.00j035744.502-c0      0pedm002
1       09826.30m039714.502-c7  a3  8pedm003e cm rck c cm e
1       09926.75j096734.502-e       pedm001bdy to epidosite
1       10026.95j070862.8011e0      1pedm002cpm e conc. to side SAMPLE
1       10127.00j181262.5002e       pedm003cpm
1       10227.80j069494.502-e       pedm001end of epidosite band
1       10327.70j027705.002-e0  c2  7pedm004103 younger than 104
1       10428.00m066714.502-e       pedm001
1       10528.20j063423.5021e       pedm001start of epidosite band
1       10627.80j064651.4511e       pedm040sp.band in gr mod.dyke
1       10728.60j054732.4011e0      5pedm003
1       10829.10j057462.1011e0  c1  7pedm045
1       10929.55m049753.8011e       pedf001dyke
1       11028.85m050753.8011e       pedf001some dyke as 109
3end of section star of vertical section crosses coastline at 13.80m (it crossed
3 at 1.50m
202149v13200
1       11100.05j319641.1002e       pedm001
1       11200.40j277340.3502e       pedm001
1       05700.80j022351.4502e       cedm  j.s.
1       11300.85j095860.4002e       pedm  j.s.
1       11401.30j206520.6002e       pedm  j.s.
1       11501.35j320870.6502e       pedm002cpm
1       056[..30j076434.502-e0      1pedm001
3end of section. 30-10-89 D.A.v.E.
20301c18700
3         1 irregular contact dyke to pillow aperture <0.1mm
1       00200.07j031891.002-e       pedm0.1sulfate infill
1       00301.60j287731.802-p   e   pedm  patchy pyrite and calcite
1       00400.80j073631.6511e   p   pedm003
1       00501.40j239851.701|e   p   pedm001trace e and p
1       00601.30j050822.2011e   p k pedm003possible k
1       00701.90j274691.802-e   e   pedm  calcite crystals
1       00802.20j198876.002-e   r   pedm0.1to 030
3calcite around angular pieces of dyke
1       00902.50j058862.7511e   p   pedm015e and p fund smaller
3veins cut at right angles (0.1mm width)
1       01003.40j247873.0011e       pedm002patchy e
1       01103.90j250853.1011e       pedc003sandy e silicasnides 340/05
1       01204.10j244903.4011e       pedc001sandy e
3end of page 021 start of page 022
3between 011 and 012 rubble zone of dyke (angular) fragments
3 in fracture 011  SAMPLE
1       01303.60j204831.002-e       pedm003
1       01404.90j254781.702-e   k p pedm  patchy e and p k covers k?
3part of pillow even though it has a joint surface SAMPLE
1       01506.20m1345210.002e   r p pedm030
3throughout the "pillow zone" (014) the rock is highly veined (0.1mm wide)
3filled with pyrite and sometimes epidote. these are planar veins 3 to
34 cm apart in all directions (photo) close up slide (CY#3 film)
20304a16104
1       00100.00r171980.9502e       pedm002cpm dyke=vesicular
1       00200.50j082867.402-e   a r pedf030some of brecciated
3rubble dyke with laterahial e and a between fracture 002 and 003
3surface shows sulfate weathering, mineral veins run parallel to
3subparallel to the dyke contact. a few crossout the dyke contact
3locally (i.e. fracture #   )some seems to be alteration of dyke
3material
1       00300.00j090857.002-e   s r pedf030as above
1       00400.50j094677.002-e       pedf001patchy e
1       00502.50j345380.902-e       pedm  patchy e light coating
1       00602.70j152842.6011e       pedm0.5cpm
1       00703.70j203677.002-e   p   pedm0021 epidote pod also some
1       00804.20j339417.002-e       pedm002
1       00902.806126651.5001e   p s pedm002minor s and p
1       01004.20j238630.462-e       pedm
1       01104.60j050843.5011e       pedm001pillow margin partly?
1       01204.60j353152.0002e       cedm004cpm pillow margin
1       01306.20j345351.5011e       cedm002
1       015   j098802.2511p   u     pedm250silicasnides 008/12 some of py
3dark green mineral(off the sample line compare to fault to north
3of sample line (left of photo i.e. 30cm from 00.00m)
3end of line a at 6.20m line b starts at 00.00m 73m bearing 161 from
20306a33601
1       00100.80m315698.002-e       pedf  silicasnides 032/30
3contact pillows/dyke
1       00201.17j313898.002-e       pedf  v patchy calcite dyke contact
1       00302.10j028778.002-e       pedm001cpm
1       00402.40j028843.0011e       pedm001
1       00502.60j032813.0011e       pedm001
1       00604.75j007711.3002e       pcpd001joint within pillow
3minor zeolite very patchy
1       00709.30j274852.0011e       cpm010mainly rubble filled
1       00808.70j198887.002-e       pcpm010mainly rubble filled
1       00909.30j195858.002-e       pcpm010mainly rubble filled
1       01009.60j017817.002-e       pcpm010mainly rubble filled
1       01109.90j001752.6011e       cpm010
3fractures 008 to 011 veen in an angular brecciated zone cemented
3together (by what?) SAMPLE 0306-10 pillows were about 1m diam vesicular

3fine to medium grained
3end of line a photo 0306 at 10.00m
20307a13602
1       00100.250176764.002-h       cpm  silicasnides 086/03
1       00200.25j351705.002-e       pcpm  rock is enclosed dyke rock
3but has a rounded brecciated appearance contains vesicles and pyrite
3definite pillow rubble with pillows and pillow fragments (to 25cm diam)
1       00301.25j170735.002-e       pcpm002cpm
1       00401.80j122643.2010e       vcpm  pillow rock contains pyrite
3and epidote in vesicles
1       00502.65j330406.502-e       pcpm
1       00602.10j184401.102-h       cpm  silicasnides 095/00
1       00702.60j134605.002-e       pcpm
1       00803.20j266803.702-e       pcpm
1       00903.30j172741.802-e       pcpm
1       01003.70j334871.9011k       pcpm  k=dark green mineral
1       01104.10m169866.002-e       pcpm
1       01204.60m334776.002-e   p z pcpm  silicasnides 316/77
3the zone from 011 to 012 (50cm) is one joint zone containing cobble
3island rubble with abundant pyrite epidote; rounded fragments and silicasnides
3at the edges of the joint, much rust alteration as coating and some chlorite
3surface of 012 because of silicasnide is relatively smooth
1       01304.556094814.0001e   h   pcpm015planar zone free of larger
3rubble running through shear zone (m)
1       01405.45j148356.002-e       pcpm0.1
1       01505.70j318831.6010e       pcpm0.1
1       01606.60j119803.7011r       pcpm010rubble fill zon 012
3pillowy vesicles are infilled with epidote (lining) then calcite
3then pyrite zones are infilled with zeolites
1       01706.40j353706.502-e   h z pcpm005z=calcdonite v.patchy
1       01807.50j330712.4011e   p h pcpm002p and h on rock (e on p & h)
1       01908.30j158364.1011h       pcpm001h=iron oxides
1       02009.55j079864.5010e       pcpm002v. minor calcite
1       02106.60j172842.3010e   p   pcpm002
20329a07704
1       00100.15j136841.7511h   p   pedm  silicasnides 046/05
1       00200.75j220700.5002h   z e pedm005cpm minerals more in rock
3than in fracture
1       00300.50j315504.5010e   h   pedm002
1       00401.05j298342.3011e       pedm001cpm
1       00501.80j069712.3510e       uedm001
1       00602.60j058521.1002e       pedm001cpm
1       00702.10j300465.1011k   e   pedm001patchy infill
1       00803.20j010881.2511e       pedm001cpm
1       00903.30j114606.002-e   k r pedm008sulfate weathering also some p
1       01003.30j329811.010e        pedm002
1       01104.40j160851.9011e       uedm001
1       01205.70j255655.5011e       uedm0.1
1       01306.20j195861.5011e       pedm0.5
1       01406.95j179542.9011e       pedm0.5
1       01507.45j247882.1111e   p r pedm001
1       01607.80j037676.0011e   p r pedc001some from 015 to 016 of
3rubble and rounded pebbl - also fragments with small epidote veins in between
1       01708.50j313584.5011e       cedm001cpm
1       01809.00j105861.7010e       pedm001
1       01909.60j319840.7011e       pedm  silicasnides 048/06
1       02010.00j23389
3problem - the measurements are of fractures not representative to the flow
3regime since most contain no mineralization whereas the rock is chock full of
```

3epidote (i.e. not a coating) as vesicle fill also there is abundant pyrite
3and mobile mineralization again not on or on fracture surfaces at least not
20401a10110
1 00100.00j076772.7011s pedm001patchy s
1 00200.57j109876.002-e pedm002r=rubble
1 00300.41h084701.7001e z pedm002patchy z
1 00401.10j096906.002-e pedm005
1 00501.55m076781.8011e ped1002
1 00602.10m086742.9011e ped0.1tight
1 00702.80m092776.002-e ped0.1tight
1 00803.00m080676.002-e ped0.1patchy e
1 00903.10j201361.0511s pedm
1 01002.00j194741.3011e pedm patchy e
1 01103.57m096716.002-e ped0.1tight
1 01204.55j071774.0011e u pedm0.1u=red e=patch
1 01304.70j192711.452-e pedm
1 01405.05h111646.002-e p pedm0.5patchy z and p
1 01505.75m086774.002-h ped0.1small dyklet Fe oxides
1 01606.05m095676.002-e ped0.1
1 01706.20m096786.002-e pedm001epm next dyke is green
3with epidote alteration - SAMPLE
1 01806.87j094783.1510s pedm010closed e filled dyke
1 01907.45j196440.902-e p pedm patchy pyrite
1 02007.67m086816.002-e ved00112 cm dyke
1 02108.60m091756.002-e vedm0.110 cm dyke
1 02209.75j092786.002-e pedm0.1epm
3within dyke very epidote rich with some pyrite sulfate weathering & plenty
3of Fe oxide alteration on surface
1 02310.10m091856.0021s ped0.1
1 02410.80m089746.0021s ped0.1
1 02511.10j111592.9011e cedm020
1 02611.24m116696.002-e ped030pods of epidote
3end of line a at 11.30m
3end of page #24 start of page #25
3this line (b) starts 1.30m beyond line a of photo 0401
20402a12103
1 00100.35j095476.002-e pedm001some of 3 or 4 z veins
1 00200.64m078726.002-e pedm0.1tight
1 00301.20j075482.5011e pedm010down to 0.1m
1 00400.50j181771.0011s pedm001
1 00502.00m088456.002-e z p pedm040some of e some z & p
1 00602.75m073685.0011e ped005
1 00703.30m075763.2011e pedm020epidote rich diabase
1 00804.10j076746.002-e pedm001
1 00904.60m073886.002-e pedm001dyke rich in e
1 01004.80j074876.002-e pedm0.2
1 01105.60m121645.002-e p pedm030sulfate staining
1 01206.15m116645.002-e p pedm015e with disemm. pyrite
1 01306.70m076735.002-e pedm0.1tight
1 01407.70m077735.002-e pedm0.110cm wide dyke
1 01508.20j087875.002-e pedm002
1 01609.15j092835.002-e pedm001
1 01709.60j092805.002-e pedm010
3end of line b at 9.70m
20403a11200
1 00100.12j114665.002-e k pedm002sulfate coating
3narrow 1cm wide shear zone
1 00200.70j086642.0011p e pedm003
1 00300.60j264321.6002s pedm0.1epm minor e coating
1 00401.70j086701.4011s pedm0.1patchy z
1 00502.20m084764.0011s ped0.1tight
1 00601.73j183730.752-e pedm
3rock "impregnated" with epidote but not the later 10cm wide dyke (005)
1 00702.30m083774.0011s pedm0.1
1 00802.70m087864.002-e pedm002patchy z
1 00903.40j265804.002-e pedm001rubble zone 10cm wide
3rounded fragments patchy z (0.1 to 1.0mm)
1 01003.70j100874.002-e pedm0.5
1 01103.95j086781.3010s pedm001rock to east contains
3pyrite patches 5cm diam. with 1.0mm crystals (subhedral)
1 01204.10h127751.0511e ledm005down to 001mm
1 01304.65m080661.4010s p pedm002
1 01405.40m072705.002-e pedm001epm
1 01505.05j054611.3011e pedm0.5
1 01605.15j056601.2011e pedm0.5vscj impregnated with e
1 01706.70j052774.002-e z u pedm0.5chlorite/epidote 142/02 u=red
1 01806.80j098751.202-e u z pedm0.1epm u=red
1 01907.40h098850.902-e pedm001
1 02007.63h089890.4001p pedm002
1 02108.30j083735.002-e z pedm001chlorite/epidote 165/24
1 02208.85j088773.1001e pedm0.5
1 02309.25m080825.002-e pedm040down to 001
1 02409.80m094764.902-e ped030
3pyrite in fine grained chilled dyke east to epidote zone in contact area
1 02510.50j103715.002-e ped001

20404a07000
1 00100.25m076882.2010s irgm002
1 00200.60m351341.0011s crgm002
1 00301.60m003451.4011s crgm002
3whole gabbro shot through by narrow (0.5mm) zeolite veins with
3average 2cm spacing random orientation most trending approximately
3030/56 some minor patches of epidote on joint surfaces (137/80)
1 00402.90m061744.002-e prgm001between rubble and
3competent gabbro SAMPLE
1 00502.25m003871.8511s prgm
1 00602.75j259454.3011e crgm010epm
1 00703.40j112571.002-e prgm u=blue gray mineral SAMPLE
1 00804.50j302325.0011h prgm003epm h=Fe oxides
1 00906.30m106795.002-z u e prgm100chlorite/oxides 007/08
3to dyke from gabbro z=clay u=leached rock
1 01006.65m113743.0011s e u crgm050zone of leaching SAMPLE
1 01107.60j081735.002-e pedm0.1epm
1 01208.00j112752.3011e pedm patchy e chlorite/oxides 024/06
1 01308.30j118812.202-e cedm001
1 01408.50j130780.7011e pedm
1 01509.70j186781.2511s pedm001
1 01608.80j271332.7011s z pedm010some of e over 5cm zones
3sides of fracture SAMPLE
1 01709.80j077603.002-e z pedm010minor z
1 01810.30m088821.8001e ledm010epidote in rock in vein area
3SAMPLE
20413a09503
1 00100.20j258331.5002s pedc001dyke light gray SAMPLE
3late dyke crosscuts joint v. fine grained gray with disseminated pyrite
1 00200.30m075903.0011s ped0.1chilled margin
1 00300.80j077583.1011e z p pedm002minor z and p
1 00401.10j096753.2011e z p cedm002
1 00502.40m098605.002-e p ped015z and p beside small dyke
3or chilled margin 2.5cm wide SAMPLE
1 00602.55j240552.3011e p cedm001minor p
1 00702.90j077822.1001e p ledm001
1 00803.70j075674.0011e p pedm005minor p
1 00904.10j067674.2011e p pedm001
1 01004.50j088402.0011e p pedm001
1 01104.90j245893.0010s pedm001
1 01205.75j274863.0002s e pedm001u=red minor e and u SAMPLE

1 01305.50j175749.9011p pedm0.1
1 01406.15j274831.3010e cedm0.5
1 01506.856090741.9011e z ledm002
1 01606.40m269510.8002s z pedm001chilled margin
1 01706.60m267600.9002s z pedm001chilled margin
1 01806.80m269451.0002s z pedm001chilled margin
1 01907.170276641.2501e z pedm0.12 hairline veins
1 02007.40h265691.8011e z pedm0.1
1 02107.765108832.0010s z pedm010
1 02207.875091761.1011e pedm015
1 02307.90j304671.7002s pedm001v. minor e
1 02410.20j087676.0011s pedm006epm
1 02510.45j105547.002-e pedl001tight chilled margin
3end of line c at 11.0m (0413)
20414a09100
1 00111.05m092403.8011s ped0.1tight
1 00211.80j196642.3011p e cedm minor e disseminated p
1 00313.40m104507.602-e ped0.1tight
1 00413.60m105407.002-e pedm0.1tight
1 00513.80m110457.002-e pedm0.1tight
1 00614.00m109527.002-e pedm0.1tight
1 00715.00m096446.802-e pedm001p in rock
1 00816.00j108567.102-e pedm0.1veins epidote
3joint is cut by dyke
1 00915.70m306335.0011e p pedm0.1
1 01016.40m310595.0011e p pedm0.1
3dyke between 9 and 10 epidote throughout rock as with minor pyrite
1 01116.70j094577.002-e pedm003
1 01217.40j082991.4002s pedm004
1 01317.70j326461.1001e pedm001minor e
1 01418.50j101597.002-e pedm0.1minor e
1 01519.30j180640.9002p e ledm patchy e and p
1 01620.25j051667.0011e p pedm003
1 01720.50j063727.002-e pedm002minor e
3end of line b (0414) at 23.50m start of line c (0415) at 00.00m is
30.25m from the end of line b (0414)
20415c10000
1 00100.30j178451.002-p e pedm minor e disseminated p
1 00200.80m072656.002-e ped0012 e veins
1 00301.40h052603.3011e s pedm001
1 00401.95j064643.3010s pedm0.1tight
1 00502.60j061496.002-e p s pedm030minor p patchy s
1 00602.90j194091.3011p pedm p throughout rock

```
1       00703.20j065425.002-e  p     pnkm004
1       00803.40j068585.002-e  p     pnkm004
1       00904.00j089593.2011e        cnkm002
1       01004.70j186571.7002n        cnkm   cooling joint
1       01105.60j051677.0011e        pnkm001
1       01206.60j060676.0011e  p     pnkm007p ln e
1       01307.656092723.0011s        pnkm002
1       01408.80m071607.002-e  s     pnk003chilled margin silicinoxides 02
1       01509.10m092477.003-e        pnkm0.1tight
1       01609.90j047476.902-e        pnkm030down to 002mm
1       01710.15j090553.5013e        pnkm001
3end of line e (0415) at 10.80m 0418 stays 20m bearing 098deg from
20418e08400
1       00100.00j092505.002-e        pnkm0.1minor patchy e
1       00200.45j079053.0011e        cnkm001
1       00301.40j064544.3010r  e     pnkm001v minor e
1       00402.20j067543.0010e  r     pnkm030mainly rubble
1       00503.10j083881.102-e  s     pnkm010
1       00603.80j063776.002-e        cnkm001zone 20cm wide contains
3epidote veins 001mm wide
1       00704.60j047902.5011e        cnkm001
1       00805.44j085815.003-r  h e   pnkm001h+Fe oxides
1       00905.95j322751.6502e  r     pnkm001
1       01006.00j017751.2011e        pnkm0.2
1       01106.20j054681.3511e        pnkm010
1       01207.02j106722.5011e  h     pnkm001
1       01307.35j075513.3011e        pnkm008
1       01408.40h078492.102-e        cnkm010
1       01509.60j053611.0010e        pnkm005
3zone between 013 and 015 network of veins subvertical braided
3in angular highly fractured dykes
1       01609.70j336440.9002e        pnkm002
1       01710.25j140453.502-e        pnkm0022 e veins
1       01810.74j046552.3511e        pnkm002
1       01911.40j143461.5011e  p     pnkm001
1       02012.50m109375.002-e  s p   pnkm   zone continues to 14.10m
3containing angular to subrounded pebble size fragments around which is
3epidote and zeolites
3end of line e at 12.50m start of line b (0419)
3either side of the shear zone the dykes are weathering a darker rust
3purple colour
20419e08400
1       02101.50j059545.002-e        pnkm015thick z vein
1       02201.75j287851.1001e        pnkm010
1       02302.05j292711.0002e        pnkm008
1       02402.20j294021.0502e        pnkm025
1       02502.30j250071.3002e        pnkm008
1       02602.92j213091.3011e        pnkm002
1       02703.25j061681.3011e        pnkm005
1       02803.58j080754.2011e        pnkm040
3the zone between 021 and 028 contains many random fractures these included
3are only the ones to intersect the line
1       02904.40j093552.3001e        pnkm001
1       03005.30j196731.902-e        pnkm001
1       03106.50j016902.002-e        pnkm0.1tight
1       03207.00j096804.502-r  e     pnkm010
1       03309.10j246742.0010e        pnkm0.4
3there are fractures between 032 and 033 but they are open and contain
3no mineralisation and are only short and all interconnected
3beyond the dykes are more competent as in 0414 and 0415 though they
3weather a more reddish rust brown there is still common epidote veining
3(along joints) though not as pervasive as in 0418 and 0419. 89 paces (162m)
3further up the road is a small shear zone (50cm wide) otherwise fairly
3competent dykes
3line a line 33.6m at 131 degrees from 0116 (towards Alcan)
20428a10110
1       00100.10j181402.8511s        prgm001open
1       00200.20j098821.752-e        prgm001open
1       00301.50j103382.802-e        prgm
1       00402.30j338631.3011e        prgm
1       00502.70j079750.752-e  s     prgm0.5patchy e and minor s
1       00603.80j063472.102-e        prgm
1       00704.70j052501.202-e        prgm004silicinoxides 142/00
1       00807.65m107872.002-e        pnk030dyke
1       00908.35j100631.3511s        prgm002
1       01008.80j078562.102-e  e     prgm002v.minor patchy e
1       01109.20j102371.302-e        prgm001patchy e
1       01210.45j084420.4011e        prgm0.1possible e sample
1       01311.80j110376.002-e        prgm001minor e blebs
3zone is about 20 cm wide
3end of line e at 13m line b cuts e at 11.80m lying along
3fracture 013
20428b05000
1       01401.50j261401.0511e  h     prgm010h+rust oxides
1       01502.00j226461.3511e  h     prgm010related to 014 ?
1       01602.40j100801.0511h        prgm0.1h+rust oxides
1       01703.40m341721.4001s        orgm010varying width to 0.5
3line b crosses line e at 04.30m on b
1       01804.00m228770.452-e        prgm002
3end of line b at 05.0m
20429c09706
1       01900.00m100400.002-e        pnkf
1       02000.00m240700.502-e        pnkm001
1       02100.15j307390.602-e        pnkm
1       02200.50j207801.302-e        cnkm001
1       02301.27j225800.902-e        pnkm001
1       02401.50j117433.802-e        pnkm0.1
1       02501.50j084742.002-e        pnkm0.1
1       02602.70j036421.5011s        pnkm0.1
1       02703.90j066351.7011s        pnk0.1
20429c09706
1       02804.10m067343.002-e        pnk0.1dyke contact
3dyke between 024 and 028 is highly fractured
1       02905.10j211641.7011s        pnkm010
1       03004.95j080830.5511s        pnkm002
1       03105.15j080830.4002s        pnkm0.5
1       03205.51j244881.0002s        pnkm001
3end of line e at 5.70m start of line d (0430)
20430d07100
1       03305.70j312511.1502s        pnkm
1       03406.40j343651.6002s        pnkm
1       03506.556080992.3502s        pnkm004
1       03607.25j043864.002-e        pnkm003
1       03707.40j199803.0011s        pnkm001
1       03807.40m104482.5011s        pnkm0.1chilled margin patchy z
1       03907.40j329441.6011s        pnkm
1       04008.50j220652.5010s        pnkm0.1patchy z
1       04108.43j287441.7511s  e     pnkm   v minor z and e
1       04209.25j080682.202-e        pnkm001
1       04309.806066843.502-e        pnkm001zone 10cm wide
1       04410.356/232803.502-e  e     pnkm001minor e
1       04509.30j250431.8011e        pnkm0.1v.minor e
1       04610.95j234540.502-e  z     pnkm0.1minor e rare z
1       04711.20j300770.702-e        pnkm001
1       04812.00j223602.3011s        pnkm0.1patchy e
1       04911.50m107448.002-e        pnk0.1tight
1       05012.05m074363.0011s        pnk0.1tight
3049 and 050 are the same as 001 and 002 on 0118
20118A06601
1       00100.20j2118001.802s        cnkm001
1       00200.27j2008001.102s        cnkm001
1       00300.30j2066603.111s        pnkm001
1       00400.40j133301.6511s        pnkm   very rare z
1       00500.65j2018402.102s  e     pnkm   patchy z rare e
1       00601.13m145715.010s         pnk0.1tight chilled margin
1       00701.15j3065201.111s        pnkm   v rare z
1       00801.70m2274704.011s  e     cnkm005network of veins
3zone is about 15cm wide at the bottom to 1cm wide upwards
3where it contains epidote similar to 009
1       00901.40m0566504.02-s  e     pnkm005silicinoxides 058/65
3epidote is on the rock but zeolites are throughout the epidote
1       01001.50m0874015.03-s        pnk0.1chilled margin
1       01102.00m228700.9702s        pnkm005dogleg of 008
1       01202.10m1002815.011s        pnk0.1
1       01302.80j0367300.011s        cnkm002
1       01403.00m118015.020s  h e   pnkm002rusty appearance
1       01503.40m0853015.020s  e     pnkm0.1h\ 014 & 015 z
3zone dyke v altered/weathered - rusty appearance
1       01604.10j240081.5011e  p     pnkm   small dyke fed from
3dyke b\ 014 & 015 (?) filled with e veins and some pyrite
3crystals. dyke width 1 to 15cm
1       01704.40j244600.4002s  e     pnkm0.1
1       01804.30m1264215.011e        pnk0.5patchy e
1       01904.40j047900.8002s        pnkm0.1
1       02005.00j302440.6011s        pnkm
1       02105.15j028400.9002s        pnkm0.1
1       02205.50j350800.4011s        pnkm
1       02305.806089303.2013s        pnkm0.1
1       02405.806056731.8002s        pnkm0.1open in places epidote
1       02506.60h115422.1502s        cnkm0.1tight faint rust
1       02606.20j260450.6002s        pnkm
1       02706.60j253500.5302s        pnkm
1       02806.60j006610.6002s        pnkm
1       02906.406051490.7502s        cnkp0.1
3end of line e at 6.60m
3end of f line d (0429) at 12.05m start of line a (0431)
20431a06002
1       00100.25j220781.2011s        pnkm0.1
1       00200.50j091271.5010s        pnkm0.1open
1       00301.00j210851.2011s        pnkm001open
```

1 00401.30m118398.002-e z j pxfm010j=jasper
1 00501.45j047792.6011z pxfm0.5
20431e06002
1 00602.35j083791.2011z pxfm0.1
3end of line a (0431) at 2.35m start line a (0432) at 2.35m
20432e06000
1 00702.50j045701.4511z pxfm001
1 00703.00j249661.3002z pxfm0.5check duplicate 007
1 00803.20j211741.6011z pxfm0.5patchy z
1 00903.10j087730.6002z pxfm0.5patchy z
1 01003.566070721.4002z pxfm001open
1 01103.85j334570.902-e pxfm
1 01203.908j259573.3013z u e pxfm0.5v. minor e several
3parallel fractures u=red
1 01303.93j256521.5011z pxfm patchy 50% of surface
1 01404.156085411.8002z pxfm001
1 01504.806063442.3011e z pxfm0.5e cm rock
1 01605.50j359461.502-e pxfm001
1 01704.90j092652.9001z e pxfm001e cm rock z cm e
1 01805.05j073572.1001e z pxfm001open e cm rock
1 01905.21j084632.5011z pxfm0.5open
1 02005.50j089731.3011z pxfm0.5open
1 02105.26j242731.7511z pxfm0.5
1 02206.00j036641.7511z pxfm001
1 02306.45j219751.4011z pxfm001
1 02407.00j188843.502-e pxfm005some about 5 cm wide
3example
1 02507.20j029841.552-e u pxfm0.5silicimarbles 10R/6D
3u=grey
1 02606.50j104625.0010e pxfm002
1 02706.85j096504.0011z pxfm0.1chilled margin 5cm wide
1 02807.65j211781.5011z pxfm patchy z
1 02907.85j200794.0011z pxfm001
1 03008.20j226673.0011z pxfm1.5
1 03107.75j102522.7011e u z pxfm0.1u=red (Fe oxides)
1 03207.95j139341.7011e z ixfm001
1 03308.94j263502.9002z pxfm0.1patchy z
1 03408.15j072203.0011z pxfm0.1
1 03508.97j099384.5011z e u pxfm001patchy e and u (=red)
3dyke rubble zone 35cm wide rounded pebble size dyke fragments
3veins of z with epoxy e and red mineral
20432e06002
1 03609.90j077305.0021z pxfm0.5
1 03710.40j096426.0011e z u pxfm001u=red
1 03811.70m096405.4011z u pxfm0.1chilled margin
3end of line a (0432) at 11.70m start of line b (0433)
20433e06000
1 03911.75j198851.3011z e pxfm0.5patchy e
1 04012.46j288441.3011z e pxfm0.1
1 04112.48j1054510.02-e pxfm0.1tight chilled margin
1 04212.906091701.1011z pxfm001
1 04313.70j011892.5011z u pxfm0.1u=grey mineral
1 04413.75j041824.002-e r pxfm010z mixed with dyke rubble
1 04514.00j346801.1011z pxfm
1 04614.30j304471.1011z pxfm0.1patchy z
1 04714.70j005901.8011z pxfm002open
1 04815.01j068581.9011z cxfm001
1 04914.70j192791.8011z ixfm002
1 05016.01j226810.9002z pxfm001
1 05116.50j046904.2010z pxfm001
1 05216.85j226891.8511z pxfm001
1 05317.55j200802.4002z pxfm001
1 05417.70m290439.002-e pxfm0.1chilled margin
3end of line b at 17.70m commons to 0121
20121e05502
1 05108.00j198832.3711z pxf 0.5off photo edge patchy z
1 05200.00j296302.1511z cxf
1 05300.00j1084015.02-e cxf 005
1 05409.50j240801.4511z pxf
1 05500.90j307881.1010z pxf minor z film
1 05600.95j348770.9402z pxf
1 05708.90j257521.7511z cxf cooling fracture
1 05801.35j190800.7502z pxf 005
1 05901.20j214741.7511z e pxf 0.5minor e tight
1 06001.75j116781.7711z cxf 001small fracture zone
1 06101.92j210831.3502z cxf 004
1 06202.05j200801.9011z e cxf 0.5e=.5
1 06302.09j210801.9511z e cxf 0.5patchy z minor e tight
1 06402.20j322850.7811z cxf surface cxnt of z
1 06502.80j240432.1011z pxf 0302 to 30mm crushed rock
1 06603.30j293572.5511z e cxf minor z cxf e
1 06703.40j200822.2002z e cxf 005 minor e cm rock z cm e
1 06803.80j192851.8510z e pxf 002
1 06904.10j194822.1502z pxf 002
1 07004.00m0904015.02-e pxf dyke chilled margin minor z
1 07104.20j221452.8002z cxf 005zeolite filled
1 07204.55j201853.3011z e cxf 1.5minor e
1 07304.80j347740.9502z cxf 002
1 07404.75j189882.6802z e cxf 001e cm rock
1 07505.15j096642.9510z cxf 005e vein to joint
1 07605.230059852.8502z cxf 001
1 07705.50j342830.8502z pxf
1 07805.40j211721.3500z cxf minor zeolites
1 07905.55j010901.7500z cxf minor zeolites
1 08005.80j296671.052-e e pxf patchy e
1 08105.90j002855.0011z cxf fracture zone
1 08206.15j257506.0011z
1 08306.15j000901.1001z
1 08406.40j1046015.014z
1 08507.20j1145315.014z
1 08607.80j314682.002-e
1 08707.91j229833.2001z
1 08808.50j147712.502-e
1 08908.70j226641.4502z
1 09008.95j1145003.011z
3end of line a at 9.0m start of line b at 9.0m goes to 12.2m
20120e21006
1 04109.25 z225821.1002z cxf 002
1 04209.356/220852.5011z cxf 002
1 04309.85j207822.3011z pxf fractures zone over middle 0.5
1 04410.10j208501.2702z pxf 0.5minor z
1 04510.20j201741.9010z pxf 001
1 04610.35m085351.0003z e cxf z cm e cm rock
1 04711.30m1054515.011z e pxf z cm e cm rock
1 04810.35 z100454.5002z e cxf fracture spray between 046 & 0
1 04911.00j272481.7011z e pxf minor z cxf e
1 05012.260/1094715.010z z z pxf 005z lines rock e & z mixed local
1 05111.206012891.9511z pxf 00220cm wide zone of 2mm fracture
1 05211.89j189802.1011z pxf
312.3m on photo is 27m bearing 244 deg from review cxf 0.00m on photo 0121

3to 18m bearing 58 deg from photo 0118
20435e02711
1 00100.00j190821.1311e pxfm001
1 00200.256015903.0011z e pxfm001
1 00301.10j189861.1311z pxfm001
1 00402.00j268481.302-e z pxfm
1 00502.30j001871.5911z pxfm002
1 00603.20j192784.0011z pxfm0023 veins of zeolite
1 00703.45j206721.0011z pxfm001
1 00804.10j197592.2011z pxfm001open
1 00903.80j107160.7011e pxfm005
3end of line a (0435) at 4.20m
20435e20004
3minor zone between 6.90m and 8.10m weathers rust brown
3remains dyke rubble zeolites minor epidote tennis 080/45 deg
3dyke material chloritized highly sheared angular fragments
3zeolite veining network around fragments cxns=2 term=- roughly
3section north of Pinnacleton near intersection Alithinos-Kato Meni
20701a34402
1 00100.60m198840.802-e pxe bit mafic & less mafic por-
3rions Gabbro? SAMPLE
1 00200.82j198892.202-e pxe j.s.
3pingiogranite very rare common epidote in rock varies mafic to less mafic
1 00301.30j145892.002-e pxe j.s.
1 00401.60j317832.102-e pxe j.s.
1 00501.606513060.9010e pxe001
1 00601.606192850.8010e pxe001
1 00702.20j185822.002-e pxe001
1 00802.40j116810.8010e0 4pxe001
1 00902.906/112861.3011e0 5pxe002
1 01002.906/009760.7511e pxe001
1 01102.958/351431.1011e0 5pxe002
1 01203.60j179862.202-e pxe001
1 01303.70j181822.202-e pxe j.s.
1 01404.30j352872.002-e pxe001
1 01504.50j188902.002-e pxe001
1 01604.4 j138670.9002e pxe001
1 01704.90j005892.802-e pxe001
1 01804.80j334642.902-e0 5pxe002
1 01905.10j000792.1011e0 5pxe002
1 02005.30j330892.802-e7 e3 5pxe001con rock e cm e
1 02105.558/048705.002-e5 r5 5pxe050134/10 fault?
3see back of original sheet for fault orientation
3increase in epidote near fault blackened zone of clayey material network of
3calcite veins comes off fault lower side
1 02206.00j122891.0002e pxe j.s.
1 02306.50j301662.3011e0 4pxe002
1 02407.10j112861.5511e pxe001
1 02509.40j339611.1002e pxe001

3end of line a photo 07-01 start of line b photo 07-02
207022833505
1 02610.20|c088361.8002e0 8pvn002
1 02710.30|c032442.8011e0 8pvn003
1 02810.70|c324861.202-e pvn001
1 02913.00|c284771.3011e0 5pvn001
1 03013.80|c098010.02-e pbx 017/08 j.s.
1 03114.10|c218542.3011e pvn j.s.
1 03214.30|c139121.7002e pvn002open
1 03315.60|c270821.4511e pvn
1 03416.60|c197740.9011e pvn j.s.
3no fracture 035 forgot it!
1 03617.05|c114873.3010e0 6pvn003
3end of line b photo 07-02 start of line c photo 07-03
207030c32502
1 03718.90|c312835.002-e0 7pbx 227/36 downstep
1 03818.90|c330792.8011e0 5pvn005moved slick.
1 03920.60|c263791.1011e0 1pvn j.s.
1 04019.90|c339851.3002e pvn002open
1 04121.70|c283867.002-e0 el 3pbx 196/24 j.s.
1 04221.70|c178530.8011e pvn001
1 04322.35|c261895.0910e pvn001
1 04422.80|c186436.002-e pvn j.s.
1 04523.50|c036721.2511e0 8pvn002
1 04623.60|c222905.0002e0 5pbx 315/32 j.s.
1 04723.90|c216511.3511e pvn j.s.
3end of line c photo 07-03 start of line d photo 07-04
207040d31402
1 04824.60|c176402.5302e pvn j.s.
1 04925.10|c330820.8502e0 6pvn001open
1 05025.60|c262892.7002e pvn002open
1 05125.70|c213900.8011e pvn j.s.
1 05226.60|c285702.8011e0 el 8pbx030203/28 possible pyr
1 05327.00|c287841.2611e0 7pvn001
1 05428.05|c172561.8010e0 pvn002
1 05527.60|c289892.3010e0 el pvn007
1 05629.10|c276710.02-e6 e4 4pbx 309/09 j.s.
1 05728.80|c250791.1011e0 7pvn001
1 05828.20|c182440.8011e pvn j.s.
1 05929.50|c356940.7002e pvn j.s.
1 06029.80|c019780.9402e pvn j.s.
3end of line d photo 07-04 start of line e photo 07-01 vertical section at
30m (crossed at 1.77m)
207014c07033
1 02100.00
1 06100.61|c030641.6001e0 5pvn002
1 06201.00|c061533.0001e pvn001
1 06301.25|c066452.1002e0 2pvn002
1 06401.34|c079270.5003e pvn001
1 06501.65|c055393.1002e0 1pvn001
1 06601.90|c077431.3002e0 3pvn002
1 06702.15|c051830.9001e0 3pvn001
1 06802.65|c277821.3003e0 4vn003
1 02502.70
3end of section 28-10-89. D.A.v.E.
3section 0.7km up A.Epiphanius road from Palekhori-Nicosia highway turnoff
3start measuring at 1.5m on tape
21001e08003
1 00101.50m251581.703-e vn0001
1 00201.90m251641.703-e vn0001
1 00302.00m257462.202-e vnp001vugs filled w calcite
1 00402.20|c257650.8003e pvpx001pillow screen difficult to
3id. but has rind to right margin
1 00502.50m246702.103-e vn0001
1 00602.85m246782.503-e vn0001
1 00703.20|c246702.403-e pvn0002open
1 00803.40|c180940.4402e pvdm002open
1 00903.65|c254878.7511e vn0001
1 01004.20|c260643.203-e pvdm001
1 01104.55|c243480.9010e pvdm001
1 01204.65|c251461.6911e pvdm001
1 01304.75|c258421.1011e pvdm001
1 01404.85m230613.102-e pvpx001
1 01504.97m258371.7011e vn0001
1 01605.20|c258601.7011e pvdm001
1 01705.50|c282432.402-e pvdm001
1 01805.90|c272551.2003e pvdm001
1 01906.25|c275611.2002e pvdm j.s.
1 02006.34|c268742.102-e pvdm002open
1 02106.40|c141360.603-e vndm j.s.
3end of line a photo 1001 start line b photo 1002-continuation of line a
21002e08003
1 02206.60|c151350.3511e vndm j.s.
1 02307.13|c274644.003-e pvdm005open
1 02407.20|c278632.1002e pvdm001subsidiary of #025
1 02507.45m261615.002-e pvdm001contact zone very fine grained
1 02607.60|c005860.5002e pvdm
1 02707.78m270675.002-e pvdm002very fine grained contact
1 02807.95|c279541.1202e vndm002open
1 02908.27|c099681.0511e pvdm001
1 03008.80|c278632.1011e pvdm001
1 03108.35|c221701.3011e vndm001
1 03209.00m247695.002-e pvdm001
1 03309.10|c179811.7511e vndm j.s.
1 03410.90m272655.002-e pvdm
1 03511.30m300664.502-e vnpx001margin to pillow rubble
3end of line b photo 1002 start of line c photo 1003 note 0.5m gap b/t photos
21003c08003
1 03611.85m264674.502-e vndm001
1 0371i.85|c143490.802-e pvdm j.s.
1 03813.20m271485.502-e vnpx001pillow rubble
1 03913.50m269555.502-e vndm001
1 04013.80m284605.402-e vnpx001mass of pillows and rinds
1 04114.80m255655.402-e vndm001
1 04215.10|c257742.0501e pvdm001
1 04315.70|c284750.402-e0 1pvdm005c 1cm thick; over 5cm random
3orientation of crystals 1mm long
1 04416.00|c280503.202-e0 1pvdm001SAMPLE of vein
1 04516.45m267615.002-e vnpx001pillow vesicles filled with
3zeolites; vesicles more common near rim/process filled with calcimicte
3end of line c photo 1003 start of line d photo 1004 continuation of line c
21004d08003
1 04616.80|c282691.0003e pvpx
1 04716.85|c259650.7001e pvpx
1 04816.90|c291800.8001e pvpx
1 04917.40m263402.502-e0 1vndm020dyktet centre part filled in
3places with zeolites;rusty pillows
1 05019.90|c102561.803-e cvpx
1 05120.25|c250811.7011e0 5pvpx002
3end of line d photo 1004 start of line f photo 1005 note 0.2m gap b/t photos
21005e08003
1 05220.40m270492.802-e vndm001
1 05320.75|c276642.402-e0 0vndm002
1 05420.55|c114490.602-e pvdm j.s.
1 05521.20|c017750.8502e pvdm
1 05621.40m271802.302-e vndm002
1 05721.80m279792.202-e vndm001
1 05822.40|c264555.002-e0 5pvdm001spotty zeolites throughout
1 05923.10m249625.002-e vndm001
1 06023.00|c251373.1010e pvdm001
1 06123.90m258553.502-e0 2pvdm002
1 06224.20|c283504.202-e pvdm001
1 06324.65|c273583.1011e pvdm0012 fractures parallel 1cm apart
1 06424.85|c273441.0502e pvdm001
1 06524.95|c278543.002-e pvdm001
1 06625.20m264521.5011e pvdm001small dyktet
1 06725.30m265551.5011e pvdm001
1 06825.70|c267543.002-e pvdm001
3end of line e photo 1005 start line f photo 1006 note gap of 1.2m b/t photos
3next 2 fractures in gap b/t photos
1 06925.95|c264542.1013e pvdm001
1 07026.80|c261692.2011e pvdm001
21006f08003
1 07127.15|c264701.3002e0 1pvdm001
1 07227.60|c112250.6002e pvdm j.s.
1 07328.20m264594.002-e vndm001small dyktet margin
1 07428.25m266634.002-e vndm001small dyktet margin
1 07528.55|c262544.002-e pvdm001zeolites near lower part of
3fracture in neighboring fractures
1 07629.30m270629.502-e pvdm001
1 07729.60|c272701.9011e pvdm001
3vertical section photo 10-05 0.7km from turnoff to A.Epiphanius
21005v35170
1 06100.00
1 10800.15|c139570.5302e pvdm j.s.
1 10900.15|c014660.5302e pvdm j.s.
1 11000.45|c010831.3502e pvdm j.s.
1 11100.45|c121441.3002e pvdm j.s.
1 11200.90|c124450.8002e pvdm j.s.
1 06200.60
1 06300.92
1 06401.10
1 11300.90|c152870.8502e pvdm j.s.
1 06501.30
1 11401.30|c178850.4002e pvdm j.s.
1 11501.60|c128441.0502e pvdm j.s.
1 06601.70
1 06701.90
1 11602.00|c341830.6002e pvdm j.s.
3end of line v end of section 17-10-89

3section 10-08 to 10-12 4.6km west of A.Epiphanios - sheeted dyke inlier
21008s29000
1 00100.00m125480.7502n pedm j.s.
1 00200.20m142600.9502n pedm j.s.
1 00300.60j142650.5511n pedm j.s.
1 00400.80m063562.502-n pedm001
1 00501.70m084392.502-n pedm001
3note: dykes here are v.fractured & very friable
1 00602.10j115760.5511n pedm001
1 00702.25j125800.5511n pedm001
1 00802.30j142890.6011n cedm001
1 00902.45j320860.8011n pedm001
1 01002.60m150782.502-n pedm001
1 01102.80m141510.7511n pedm001
1 01203.00m174642.502-h0 8pcym001h=rust <1mm
3pillow screen not v. vesicular plenty of chilled margins but hard to i.d.
3individual pillows due to friability
1 01305.10j101841.8011n cepm001
1 01405.35j098542.502-n pcym001
1 01503.95j116810.6002n cepm001
1 01604.65j116870.5002n cepm001
1 01705.40j341860.8002n pcym001
1 01805.50j307800.7702n pcym001
3end of line a photo 10-08 start of line b photo 10-09
21109b28900
1 01906.00j299342.7011n cepm001
1 02006.40j066710.7002n pcym001
1 02106.80j313660.6002n cepm001
1 02207.30m073442.502-n pedm010rubble zone
3entering zone of dyke rubble = sheer
1 02307.72j308640.8002n pedm002rubble
1 02408.05m131652.502-n cedm001
1 02507.60m145432.502-n cedm001
1 02608.40j098821.1011n pedm001
1 02708.60j113882.0002n cedm001
1 02808.40j088160.8002n pedm001
1 02909.10j121550.5502n 6pedm001
1 03007.15j333480.9002n pcym001
1 03106.70j296660.7502n cedm001
3end of line b photo 10-09 start of line c photo 10-10
21010c27800
1 03209.80j091600.8002n cepm001
1 03309.75m097830.6002-0 8pcym001
1 03410.05m102752.7011n cepm010
1 03510.20j229230.5002n pedm j.s.
1 03610.52m119722.502-r0 0pedm700shear zone w/ dyke rubble
3zone back of sheet for fault relations
1 03711.30j097831.1013n pedm001
1 03811.35j224830.8511n pedm001
1 03911.70j133702.542-n cedm001
1 04011.95j196430.5002n pedm j.s.
1 04112.25j103981.8002n pedm001
1 04212.10j300640.6502n cedm001
1 04312.30j094861.6002n pedm001
1 04412.50m112582.502-n pedm001
1 04513.40j210730.4002n pedm j.s.
1 04613.10j340421.5002n pedm001
1 04713.80j120610.6002n pedm j.s.
3end of line c photo 10-10 start of line d photo 10-12
21012d28000
1 04814.20j212080.6002n cedm j.s.
1 04914.20j116661.2011n pedm001
1 05014.35j115600.5002n pedm001vesicular dyke no filling
1 05114.55j304650.9002n cedm001
1 05214.90j120640.4002n pedm001
1 05315.85j118701.1011n pedm001
1 05415.20j020781.1502n pedm j.s.
1 05515.50m128572.502-n pedm001
1 05616.00j223630.4002n pedm001
1 05716.15j274800.5002n pedm001
1 05816.20j208760.5502n pedm j.s.
1 05916.25j124530.7011p0 6pedm j.s.
1 06016.85j082701.1011n pedm001
1 06117.00j226460.6011p0 8pedm j.s. p=rusty pyrite=1mm
1 06217.00j132680.6011n pedm j.s.
1 06317.20j223800.5002n pedm j.s.
1 06417.20j123720.6011n pedm j.s.
1 06517.30j114591.8011n pedm001
1 06617.95j134610.6002n pedm001
1 06718.10m122602.502-n pedm001
3end of line d photo 10-11
3vertical section crosses sunshine at 15.8m (it's crossed at 1.1m)
21011v25240
1 06800.00j309150.5002n pedm001
1 06900.00j210890.5002n pedm j.s.
1 07000.30j010590.5502n pedm001
1 07100.35j207640.5002n pedm j.s.
1 07200.74j181500.6002n pedm001
1 05501.45
3end of section 11-08 to 11-11. 7-11-89 D.A.v.H.
3section west of A.Epiphanios 10-17 to 10-21 near Kato Moni/Plasmiotes Rd.
3note: photos 10-18 to 10-21 were printed in reverse by accident
21017s02000
1 00100.70m0361114.02-n ued002
3dykes are rust colored fresh=light grey med. gr. aphyric
1 00200.25j092880.4002n pedm j.s.
1 00302.45j300830.9002n pedm j.s.
1 00402.45j280520.7502n pedm j.s.
1 00502.60j193880.6002n pedm001
1 00603.00j010870.6502n pedm001
1 00702.40j227540.5502n pedm001
1 00803.20j007740.5002n pedm001
1 00903.50j349700.3002n pedm j.s.
1 01003.50j242080.2502n pedm j.s.
1 01104.10j315730.9002n pedm j.s.
1 01204.05m207341.3002n pedm001
1 01304.40j045690.6002n pedm001
1 01404.40j271830.4002n pedm001
1 01504.20m226221.3002n pedm j.s.
1 01604.85j346790.5502n pedm j.s.
3end of line a photo 10-17 start of line b photo 10-18
21018b19200
1 01704.95j066960.6002n pedm j.s.
1 01805.30m253983.402-r0 e4 9pedm200163402 rubble zone patchy ep
3zone back of sheet above 50cm left lateral offset
1 01905.80j275740.5002n0 8pedm001
1 02005.80m000720.902-n pedm j.s. east follow contact
1 02106.20m250780.902-n pedm001
1 02206.50j172870.5502n pedm j.s.
1 02306.50j107820.4502n cedm j.s.
1 02407.15j340851.7002n cedm j.s.
1 02508.10j338832.0011n pedm001
3end 0of page 92 start of page 93
1 02608.25j214770.8002n pedm001
1 02708.50j197850.8002n pedm001
3end of line b photo 10-18 start of line c photo 10-19
21019c00100
1 02809.40m262196.002-n pedm001
1 02909.45j281770.8002n pedm j.s.
1 03009.90j346830.8002n pedm j.s.
1 03110.46j196781.0002n pedm001
1 03210.70j269851.0502n pedm j.s.
1 03311.75m014881.3511n pedm001
1 03411.80j283430.6502n0 1pedm j.s.
1 03512.20j264801.2002n0 2pedm j.s.
1 03612.57m014991.0011n pedm001
1 03713.20j194800.6011n pedm001
1 03813.20j270820.4802n pedm j.s.
1 03913.50j134851.3011n pedm001
1 04013.72j330811.2011n pedm001
1 04113.95j155861.2002n pedm001
1 04214.05j250750.5511n pedm j.s.
1 04314.30j164891.7011n pedm001
1 04414.80j160301.8011n pedm001
1 04514.90j254640.8002n5 p4 u1 6pedm j.s. u=br.green=unleachies?
3end of line c photo 10-19 start of line d photo 10-20
21020d18004
1 04615.25j192782.6011n pedm j.s.
1 04716.10j314750.8011n pedm j.s.
1 04816.30j215811.2511n0 2pedm j.s.
1 04917.30j353781.4011n pedm001
1 05018.20j239750.8511n pedm j.s.
3end of line d photo 10-20 start of line e photo 10-21
21021e17400
1 05118.95j133892.502-r0 0pedm030rubbly zone
1 05219.80m042055.2011n ped001
1 05319.50j301720.8002n0 0pedm002
1 05420.00j140840.8002n0 0pedm002
1 05520.50j261851.8002n pedm j.s.
1 05620.32j172870.7002n pedm001
1 05720.50j028890.5002n pedm001
1 05820.70j132880.5002n pedm001
1 05922.10j202890.7002n0 0pedm010
3end of line e photo 10-21 start of line v photo 10-17 vertical section
3crosses zone line at 1.0m (it is crossed at 1.2m)
21017v12082
1 06000.50j302282.8002n pedm001
1 06100.20j107831.7502n cedm j.s.
1 00100.85
1 06201.00j005490.8001n0 0pedm001z=clay

1 08301.35j317030.5002s0 0andm001
1 08401.70j078751.7001e8 r2 0pedm022r may be clay as well SAMPLE
1 08501.20h055330.5002s0 0pedm002
1 08600.60h085048.5511e0 0pedm002SAMPLE
3end of section. 8-11-99. D.A.v.E.
3start of sandline swapping 7-10-1999 turnoff to A.Epiphaneia-Paleldori road
21028e06104
1 00100.00m253400.0000m pedf002adjacent dykes filled w pyrite
1 00200.42j090401.3011n pedf001
1 00300.85m281422.1001n pedf001crosses pillow/dyke bdy
1 00400.87j301600.4011n sedm001
1 00501.00h282540.8011n pedm001healed fracture
1 00601.05h130700.252-e pedm f.o.
1 00701.20h284600.4000m pedm002open
1 00801.05j082400.4511n pedm f.o.
1 00901.30h022002.5511n pedm003
1 01001.85m254391.1011n sedf001margin to pillow on right
1 01102.20m287806.002-e pedf002
1 01202.50j270702.6013n pedf001
1 01302.55j272751.5011n pedf001
1 01402.47h038871.4010n sedf001
1 01502.30h198750.7011n sedf001
1 01603.10m280776.002-e sedf001
1 01703.10j167400.352-e pedf f.o.
1 01803.40h096891.0502n sepm001to pillow screen
1 01903.40m082861.2011n sedm001
1 02004.05h284681.2502n pedm001
1 02104.40m286844.5010n pedf002dyke margin epidote altered
1 02204.65m271644.5010n pedf001
1 02304.70h054831.5001n pedf002open
1 02404.95j008761.0503n pedf001older than small dyke
1 02505.10j220871.8003n pedf001
1 02605.20j100310.7011n pedf001
1 02705.30j261631.4010n pedf001
1 02805.75j021881.1511n pedf001
1 02906.00m298854.5011n pedc001volcanic coarse dyke
1 03006.30h261585.502-e sedc010R-fault;contact to dyke
1 03107.00h234891.5511n pedm002
1 03206.95h207831.4711n pedm001
1 03307.70m289412.5011n pedf001small dyke
1 03407.75m290402.5011n pedm001
1 03507.30j190891.8011n pedm001
1 03608.30j182831.4011n pedm001
1 03708.70m026893.3011n pepf002
1 03809.10h2333410.02-e pedm002
3start line B photo 1029 continuation of line A photo 1028
21029e06104
1 03908.80h226803.4013e0 pedm003
1 04009.20j041830.6011n pedm most S (40 to 44)part of epicy
1 04109.45j022803.2011n pedm
1 04209.44j023802.1011n pedm001
1 04309.80j043831.4011n pedm001
1 04409.90j034893.502-e pedm001
1 04510.00j027802.802-e pedm001
1 04610.20j030861.4011n pedm
1 04710.25j299872.2000m pedm001
1 04810.45j274032.1002m pedm001
1 04910.85j297710.9511n pedm
1 05011.00j284761.1002m pedm001
1 05111.35j203800.8002m pedm001
1 05210.80j286710.9511n pedm001
1 05311.45m284606.502-e pedm001
1 05410.70j290404.502-e pedm001
1 05511.80j008891.3011n pedm001
1 05612.60j194823.9002m pedm001
1 05712.80m290712.3010m sedf001
1 05813.00m287802.3010m sedm001
1 05913.00h024000.6002m pedm001
1 06013.30h191853.5911n pedm001
1 06113.30h130870.7511n pedm001
1 06213.80m289577.002-e pedf001
1 06313.90j290353.2013n pedf001
1 06414.50j190871.0502n pedm001
1 06514.65h290646.802-e pedm001
1 06615.00j007660.9402n pedm
3start line e photo 1030 continued from line e photo 1029
21030e06104
1 06715.50m284605.202-e pedm001
1 06815.50j028700.6502n pedm001
1 06915.55j108310.4011n pedm001
1 07015.90j273661.4011n sedm001
1 07116.10j004840.7302n pedm001
1 07216.40m279035.002-e pedm001
1 07316.60j080421.3011n pedm001
1 07417.30j016000.9902n pedm001
1 07517.50j020641.2002n pedm001
1 07618.20j193851.2002n pedm001
1 07718.50m281666.002-e pedf001light green alteration halo
3in rock - SAMPLE #077
1 07818.90m301616.002-e pedm001
1 07919.10j019840.7011n pedm001
1 08019.40j025540.5802n pedm001
1 08119.90m290485.002-e pedm001
1 08220.00j184800.702-e pedm
1 08320.40j310611.6300n pedm001
1 08420.75j280452.1013n pedm001
3end line e photo 1030 start line d photo 1031
21031d06104
1 08521.40j295611.2011n pedm001
1 08622.20j188702.0011n pedm001
1 08722.85m288565.802-e pedm001
1 08823.00j176801.7511n pedm001
1 08923.40h235801.3502n sedm001may be blasting fracture
1 09023.80h299541.4005n pedm001
1 09124.35m270575.002-e pedm001greenish halo - clay
1 09224.60h284602.3013n sedm001
1 09325.05m286655.002-e pedm001contact zone contains frags of
3dyke or pillow
1 09425.20h290850.6003n pedm001
1 09525.50j240840.7511n pedm001
1 09625.70j252883.5011n pedm001
1 09726.10m287754.202-e pedm001
1 09826.30h039891.2511e0 1pedm001epidote blob in fracture
3lower part of fracture becomes contact to dyke
1 09926.30j238383.0003n pepm010
1 10026.70j242504.302-e cepf005
1 10126.75m298721.3502n pedm001
1 10227.50j284664.0011n sedm001
1 10327.90j167340.4511n pedm001
1 10428.50m061840.8011n sedm001SAMPLE highly altered pillow
1 10528.20j276714.002-e pedm001
1 10628.80m271854.002-e rubble zone pillow and dyke
3fragments to 29.20m
1 10729.20m282814.002-e pedm
3A.Epiphaneia vertical section (10-30) near the turnoff on Nicosia-Paleldori
21030a33070
1 10600.20j168601.1002n pedm f.o.
1 07700.40
1 07800.80
1 10701.20j284520.8001n pedm001
1 08001.65
1 08101.75
1 07902.00
3end of section 18-10-99 D.A.v.E.
3section east of Gourri on road to Makhaeras 1037-1038; 1208 to 1210
21037e31302
1 00100.10j137771.8011n pedm002Open
1 00200.10j030122.1002n pedm002open
1 00300.20j172760.5702n pedm f.o.
1 00400.45j278881.4002n pedm f.o.
1 00500.70j111091.8502n pedm003open
1 00600.70j019750.3002n pedm f.o.
1 00701.30j131811.9302n pedc002open
1 00801.53j319772.0011n pedc001open
1 00901.90j057890.4002e0 8pedc f.o.
1 01002.05j236741.0711n pedm f.o.
1 01102.25j123761.6511n pedm002open
1 01202.35j159890.4002n pedm002open
1 01302.55j129790.7002n pedm001open
1 01402.75j164760.9511e0 7pedm f.o.
1 01503.20m322803.502-e0 2pedm001
3this is an epidosite dyke: basal is from 0.9 to 2.0m.end of line e photo 1037
3note gap bet 4.0 and 5.4m following fractures not on photo
1 01604.15m319852.4010n pedm030small dykelet dk.br.zond.
1 01704.45m159853.502-e sedf001small dykelet as above
1 01804.70m276883.502-e sedf001
1 01904.90j315893.502-e0 9pedf009
1 02005.15j092880.5402n pedm f.o.
1 02105.45j114801.0202n pedm f.o.
1 02205.40j294480.900200 8pedm001l-leached SAMPLE
1 02305.50j004890.5202n pedm f.o.
21038b13102
1 02406.05j124801.0502e0 8pedm002leach halo
1 02506.40j281862.1011e0 8pedm009
1 02606.90j011780.9002n pedm f.o.
1 02707.20m157453.502-e pedf001f.o.
1 02806.65j317630.700200 0pedm002
1 02907.80j254610.4002n pedm001
1 03007.80j223610.9002n pedm f.o.
1 03108.30m120863.002-e pedm001like grey green sand dyke

1 09208.96jt114822.0011e0 0pedm002
1 09309.35m118991.6511n pedf001
1 09409.60m127821.6011n pedf001some dyke as 003
1 09509.70m126802.0811n pedf004small dyklet
1 09609.95m118943.0321-b0 1pedf050
1 09710.65tr122831.6911e0 8pedm003large sp. xnals
1 09810.80m128875.502-n pedf001v.fine gr dyke epidosite
1 09911.65jt122753.2011e0 1pedm002leached zone epidositeSAMPLE
1 10011.75m118793.502-n pedf001dk.br.f.dyke
1 10112.10jt132891.8011n pedf001
1 10212.40jt188391.0302n0 6pedf j.s.
1 10312.70jt295871.102-e0 1pedm001
1 10412.25jt031491.2502n pedm002open 044 younger than 043
1 10513.30jt287831.702-n pedm002open
3end of line b photo 12-08 start of line c photo 12-08
21208c13102
1 04613.90m268743.102-e0 3pedm j.s.
1 04714.70m131893.202-e0 7pedm002SAMPLE
1 04815.10jt286891.2002e0 7pedm002
1 04915.20m119893.302-n pedf001
1 05015.85m142873.302-n pedf001
1 05115.90jt300842.2002e0 8pedm002
3end of line c photo 12-08 start of line d photo 12-09
3note gap bet photo from 15.9 to 17.4m
1 05216.20jt290831.3502e0 8pedm002epidosite dyke
1 05316.50jt283741.9502e0 5pedm003open as well
1 05416.80m142943.502-n pedf001chill toward dyke to right
1 05517.10jt296782.5011n pedf001mod.dk.br.dyke
1 05617.20jt000750.6002n pedm001
21209d13102
1 05717.65jt322883.0011n pedm001
1 05818.45m310873.502-e0 3pedm001epidosite
1 05918.50jt308811.5002e0 1pedm001open
1 06018.95jt000640.9002n pedm001open
1 06119.40jt352852.3011e0 5pedm003
1 06219.90m119783.2011e0 5pedm002
1 06320.00jt252852.5011e0 8pedm j.s.
1 06420.40jt173890.9002n pedm j.s.
1 06521.00jt109892.902-e0 8pedm001
1 06621.00jt176851.6011n pedm002open
1 06722.40m108829.2002e0 3pedm001
3end of line d photo 12-09
3note gap bet 22.4 and 24.50 in photo
1 06822.60m303793.802-e0 8pedm003
1 06922.80jt205762.0002e0 3pedm j.s.
1 07022.95jt322872.0002n pedm002open
1 07123.90jt340862.0011n pedm002open
3start of line e photo 12-10
21210e13102
1 07224.65jt093820.7011n pedm j.s.
1 07324.75jt206521.1502n pedm j.s.
1 07425.00jt144891.1511e0 8pedm003
1 07525.30jt142851.2511n pedm001
1 07626.00jt116871.6002n pedm j.s.
1 07726.50jt312891.2002n pedm002open
1 07826.60jt130851.1002n pedm003open
1 07926.65jt194891.0502e0 7pedm j.s.
1 08026.70jt288821.0502n pedm003open
1 08127.05m301825.502-e0 2pedm004blob of epidote
1 08227.40jt261870.4502e0 5pedm j.s.
1 08327.50jt198700.8502n pedm j.s.
1 08427.70jt252871.3011e0 1pedm j.s.
1 08528.15jt310883.502-e0 9pedm003
1 08628.55jt140811.2511n pedm001
1 08728.70jt093892.0011n pedm001
1 08828.40jt196770.9502n pedm j.s.
1 08929.20m123833.002-e0 2pedf001
1 09029.50jt016771.8002n pedf001
3end of section.
3start of vertical section f photo 1208 3crosses line at 13.10m (it's crossed at 1.3m
21208f02454
1 09100.00jt024291.5002n pedm001open
1 09200.00jt192541.2002e0 3pedm j.s.
1 09300.26jt022351.1002n pedm001open
1 09400.55jt198840.5002e0 4pedm j.s.
1 09501.00jt204090.8002n pedm001
1 09601.35jt203830.8002e0 3pedm j.s.
3end of section 31-10-89. D.A.v.E.
3section 11-07 to 11-10 3km east of turnoff from Sylia/Kannavis
21107n28602
1 00100.00m032837.002-n pedm j.s.
1 00200.40m042837.002-n pedm j.s.
1 00300.75m052857.002-n pedf j.s.
1 00401.20jt060882.6010n pedf001
1 00501.40jt059843.0011n pedf001
1 00601.95jt047781.7010n pedf001
1 00702.20m042857.002-n pedm001
1 00803.00jt056882.6011n pedm002open
1 00903.40jt058844.002-n pedm002open
1 01003.70jt061893.1011n pedm001open
1 01104.40jt032703.7011n pedm001
1 01205.90m059777.002-n pedm j.s.
3end of line e photo 11-07 start of line b photo 11-08
21108b10608
1 01306.20m058827.002-n pedm002open
1 01406.30jt059791.2011n pedm j.s.
1 01507.05m054797.002-n pedm001massive epidosite dyke
1 01607.30m054897.002-n pedm002open
1 01707.95jt066774.0010n pedm j.s.
1 01808.20jt064893.0010n pedm001
1 01908.45jt335721.3011n pedm j.s.
1 02008.50jt343400.8502n pedm002
1 02108.75t094833.0011n pedm002
1 02209.35t288855.3011n pedm001
1 02309.70jt322800.7002n pedm j.s.
1 02410.40m059857.002-n pedm j.s.
1 02510.50jt328761.1002n pedm j.s.
1 02611.90m070787.002-n pedm002small breccia zone
1 02712.30jt000763.1011n pedm j.s.
1 02812.60jt142872.2002n pedm j.s.
1 02913.10m058897.002-n pedf into monpidolaned dyke j.s.
3this dyke is dk.gr.f.aplyrie
3end of line b photo 11-08 start of line c photo 11-09
21109c10006
1 03013.30jt061740.6502n pedf001
1 03113.40jt044801.0502n pedf001
1 03213.74jt042722.2011n pedf j.s.
1 03313.95jt305701.0002n pedf j.s.
1 03414.10jt281742.2011e0 8pedm002
1 03514.80jt048831.1011n pedm j.s.
1 03615.30m045866.002-e0 ei 2pedf040
1 03715.30jt346852.2011n pedf j.s.
1 03815.606025891.9511b0 5shelf 115/00 h=sed<1mm j.s.
1 03916.50m048867.002-n pedf001
1 04016.60jt024820.9511b0 2pedf 113/05 h=sed<1mm j.s.
1 04117.35jt144770.7002n pedf j.s.
1 04217.75jt049860.9002n pedf j.s.
1 04316.80jt148731.5011n pedf001
1 04416.70jt331710.6002n pedf j.s.
3end of line e photo 11-09 start of line d photo 11-10
21110d09804
1 04517.75jt149800.7002n pedf j.s.
1 04617.85jt070681.6011n pedm002open
1 04718.15jt145720.8002n pedm j.s.
1 04818.30m040831.0010n pedm010small breccia zone
1 04918.60mh227841.4010n pedm010rock is epidosized
3see back of sheet for fault orientation 227/84 and 234/87 (subsidiary)
1 05019.00m050866.002-n pedf001
1 05119.30jt316870.8002n pedf j.s.
1 05219.30jt225870.6011b0 3pedf j.s.
1 05319.65jt046862.8011e0 2pedf j.s.
1 05420.05m065815.002-n pedf j.s.
1 05520.50jt046815.002-n pedm j.s.
1 05620.80jt072811.3002n pedm j.s.
1 05721.20jt072701.5011n pedm j.s.
1 05820.95jt049894.002-n pedf j.s.
1 05921.60m067663.002-n pedf001
1 06022.00jt054781.0000e0 6pedm020
1 06122.30m255823.502-n pedf001
1 06222.75m040840.6011n pedf001zones w/ minor epidosite in
3mod. dyke
1 06323.30jt046860.7011n pedm j.s.
1 06423.50m236853.002-n pedm001partly epidosite
1 06523.80m054873.002-n pedf001partly epidosite
1 06624.30jt020763.002-n pedf f.dk.gr.dyke j.s.
1 06724.40m064893.002-n pedf001
1 06824.70m066833.002-n pedm j.s.
1 06925.00jt038881.8011n pedm j.s.
1 07025.40jt295742.5011n pedm j.s.
3epidosite basal starts at 25.7m at end of o/c=1m from last contact(SAMPLE)
3end of section start of vertical section 11-07 crosses near 5.0m
21107v25645
1 07100.00jt315401.3002n pedm j.s.
1 07200.10jt130420.8502n pedm j.s.
1 07300.80jt292281.8002n pedm j.s.
1 07401.00jt330602.3002n pedm j.s.
1 07501.15jt140701.7002n pedm j.s.
1 07601.70jt316440.8002n pedm j.s.
1 07701.70jt147710.8002n pedm j.s.

```
1       07802.15j300302.3002n       pxdm  j.s.
1       07902.15j161890.9302n       pxdm  j.s.
3end of vertical section.
3end of section 11-07 to 11-10. 1-11-89 D.A.v.E.
3east of section 11-11 to 11-16 40m east of Split6/Kennevin turnoff
21111c22808
1       00100.05m234897.002-e       pxdm001f.-sand.lim  gr.aphyricdyke
1       00200.20j328840.9002n       pxdm  j.s.
1       00301.90m052747.002-e       pxd1001
1       00401.75j043861.1002n       pxd1002
1       00502.15j039891.9011n       pxd1001
1       00602.40m060895.002-e       pxdm001epidosite zone starts 2cm in
1       00702.10j342791.0002n       pxdf  j.s.
1       00802.55j310800.7002n       pxdf  j.s.
1       00903.00j222811.4011e0      3pxdf  j.s.
1       01003.50m235815.002-e0      1pxd1001
1       01103.90j055891.2000n       pxdm001
1       01204.30j042772.801-e       pxdm001
1       01304.50j144651.8002n       pxdm  j.s.
1       01405.00m233843.002-e       pxdm001
1       01505.10j235842.0511n       pxdm001
1       01605.35m250742.2011n       pxdm001
1       01705.55m077824.0011n       pxdm001
3end of line a photo 11-11 start of line b photo 11-12 gap to 6.15m
1       01805.90j066792.0002n       pxdm001start of epidosite ends 6.3m
21112c20405
1       01906.15j042893.002-e       pxdm001
1       02006.40m046853.002-e       pxd1001
1       02106.50j064900.4002n       cxd1001
1       02206.90j143761.3002n       pxdm  j.s.
1       02306.70j239892.5010n       pxdm001start epidosite
1       02407.80j254892.8010n       pxdm001end epidosite
1       02507.50j322701.5002n       pxdm  j.s.
1       02608.10j039850.8001n       pxdm001
1       02708.40m222893.002-e       pxdm001
1       02808.30j026701.8011h0      2pxd1001116/43  h=rod
1       02908.50j254850.4000n       pxdm001
1       03008.75m046743.002-e       pxd1001
1       03108.95h223980.5302n       pxd1001
1       03209.20j298420.8302n       pxd1001
1       03309.40h017851.1011e0      3pxdm001
1       03410.20j237813.302-e       pxdc001
1       03508.10j148729.0011n       pxdm001
1       03610.70j299591.1002n       pxdc  j.s.
1       03710.40h300821.7002n       pxdc  j.s.
1       03811.25h052892.8011e0      1pxdc020
1       03911.50j043651.1011n       pxdc001
3end of line b photo 11-12 start of line c photo 11-13
21113c21710
1       04011.80j009820.5502n       pxdm001
1       04112.20j331670.9502n       pxdm  j.s.
1       04212.80m039893.002-e0      1pxd1002
1       04313.10j328411.2002n       pxdm  j.s.
1       04413.20h040862.0511e0      8pxdm002
1       04513.42j043892.0002n       pxd1001
1       04613.55m042843.502-e       pxd1001dyke is very fractured
1       04713.75m023893.502-e       pxd1001
1       04814.00j308822.1002n       pxdm  j.s.
1       04914.30j040732.2002e0      1pxdm002
1       05014.40j045891.4502n       pxdm002cpxm
3section will be continued in a later file. 1-11-89. D.A.v.E.
3continuation of 11-11 to 11-16 section east of Split6
21113c21708
1       05114.80h237871.9511n       lxdm002cpxm
1       05215.05h234852.502-e       pxdm001start of epidosite band
1       05315.10j183852.502-e       pxdm001end of epidosite band
1       05415.45m038853.0011n       pxd1001lite grey dyke
1       05516.40j046841.0010n       pxd1001
3end of line c photo 11-13 start of line d photo 11-14
21114c21708
1       05615.80m046843.0011n       pxd1001
1       05716.05h037880.7002e6  q4  4lxdm001SAMPLE
1       05816.10m224803.002-e       pxd1001
1       05917.05j070723.0011n       pxdm001
1       06017.30j326801.4002n       pxdm  j.s.
1       06117.35j054801.5011n       pxdm001
1       06217.55m054783.002-e       pxdm001
1       06317.70m210893.002-e       pxdm001
1       06417.80m230853.002-e       pxdm001margin partly epidotized
1       06517.90j278830.7002n       pxdm  j.s.
1       06618.65j000860.5002e0      1pxdm  j.s.
1       06719.75h041870.3000n       pxdm001
1       06818.85h237850.6510n       pxdm001
1       06918.90m217832.502-e       pxd1001
1       07018.90h146471.1002n       pxd1001
1       07119.60j168880.5502n       pxdm  j.s.
1       07219.40j029811.4011e0      9pxdm  j.s.
1       07319.95m344852.502-e       pxdf140small dykes
1       07419.90j022851.1002e0      3pxd1001
1       07519.75j199871.8002e0      5pxd1001
1       07621.00j07?.?40.7002n      pxdf  j.s.
1       07721.30h05387.9.9001e0     4pxdm001
1       07820.10j060201.1001n       pxd1001
21115d21708
1       07921.40j030833.002-e0      0pxdm010
1       08021.75m037833.002-e       pxd1001
1       08122.10m028803.002-e       pxd1001
1       08222.30j201770.8002e0      1pxdm  j.s.
1       08322.60j201881.8011n       pxdm001
1       08422.80j200851.2011n       pxdm001
1       08522.90j019712.2011n       pxdm002cpxm
1       08623.00j191730.3002n       pxdm001
1       08723.25j067881.3011n       pxdm  j.s.
1       08823.70j204721.1002e0      pxdm001226/71  h=rod Fe
1       08923.80m233802.2011n       pxd1001
1       09024.00m004812.2011n       pxd1001
1       09124.05j019811.0011e0      1pxd1001
1       09224.30j018821.8011n       pxdm002cpxm
1       09324.40h230890.4502n       pxdm001
1       09424.570222830.9002n       pxdm001
1       09524.70h238880.8002n       pxd1001
1       09624.65m234883.002-e       pxd1001
1       09724.80j039832.0511n       cxd1001cpxm
1       09825.10j050880.4011q0      9pxdm002
1       09925.20j232892.502-e0      8pxdm005
1       10025.70j318710.8002n       pxgf  j.s.gabbro screen
1       10126.50j039832.002-e       pxg1001
1       10226.80j029851.4001q0      8pxgm  j.s.
1       10327.60j310750.8502n       pxgm  j.s.
3acro surf. under sl 32715 (sl=scanline)   with clinozoisite 326/15 (1115d)
1       10427.60j050842.202-e       pxgm  j.s.
1       10527.95j053861.4011q0      8pxgm  j.s.
1       10627.40h031870.5402e0      0pxgm002sm  calcium fracture sm sheet
1       10728.40j243802.0002e0      2pxgm  j.s.:zeolite?
1       10828.40j166671.3002n       pxgm  j.s.
3end of line d photo 11-15 start of line e photo 11-16
21116c18905
1       10928.50j356602.202-e0      8pxgm002SAMPLE
1       11029.10j325700.5002n       pxgm  j.s.
1       11129.50j264871.0002e0      6pxgm  j.s.
1       11229.70j059862.1002e0      7pxgm  j.s.
1       11330.50j047860.4502q0      6pxgm  j.s. q=qz? SAMPLE
3end of section start of vertical section v photo 11-11 crosses scanline
3at 4.2m (it is crossed at 1.2m)
21111v31702
1       11400.00j130090.9002q0      7pxdm002
1       11500.00j138541.4802n       pxdm  j.s.
1       11600.55j330361.8002n       pxdm  j.s.
1       01300.55
1       11701.25j317281.9002n       pxdm  j.s.
1       11801.25j134890.4502n       pxdm  j.s.
1       11901.55j159680.8001n       pxdm  j.s.
1       12002.00j320590.7002n       pxdm  j.s.
3end of vertical section
3section 11-24 to 11-27 0.7km from Split6/Sarandi turnoff
21124s11403
1       00100.10h125532.002-e       pxdm035small fault zone no offset
1       00201.10j174791.0002n       pxdm002cpxm
1       00301.30j181731.0002n       pxdm002cpxm
1       00401.30m090212.002-e       pxdm001dyke pebble size rubble
1       00501.50j004891.0002n       pxdm002cpxm
1       00601.80j219570.4002n       pxdm  j.s.
1       00702.00j184830.5502n       pxdm  j.s.
1       00802.30j341831.3002n       pxdm002cpxm
1       00902.30j089891.6011n       pxdm002cpxm
1       01002.10j069861.4011n       pxdm002cpxm
1       01102.75j253610.5011n       pxdm  j.s.
1       01202.75j168750.5511n       pxdm  j.s.
1       01303.00j252520.6002n       pxdm  j.s.
1       01403.00j324830.5502n       pxdm  j.s.
1       01503.30m064304.802-e       pxd1001epidote
1       01603.35j250610.6002n       pxdm  j.s.d
1       01703.35j188811.3002n       pxdm  j.s.
1       01804.00m065304.802-e       pxdm001end of sp.band
3fracture later than band
1       01900.40j072870.7511e0      7pxdm001cpxm
1       02003.50j082750.8511n       pxdm001cpxm
1       02103.85j273401.1011e0      5pxdm001
1       02204.15j279800.4502e0      8pxdm  j.s.
1       02304.50j090810.4502n       pxdm0?i
```

```
1       02404.55j278631.0611e0      7pedm001
1       02504.80j090890.7002e0      5pedm  j.s.
1       02604.90j186700.8002m       pedm  j.s.
1       02705.25j082860.7802m       pedm001
1       02805.50j082530.7002m       pedm001
1       02905.75j272550.6402m       pedm001
1       03006.00j060338.002-e       vein001not continuous fracture
1       03106.00j016210.4402m       pedm001zoned as conduit rock halo
3SAMPLE
1       03206.10j085760.5511e0      0pedm002
1       03306.20j087730.7511e0      0pedm002harder than calcite
3#033 and #032 lower than #033 & #030
1       03406.90j052353.002-e0      6pedm002end of sp. band (top of it)
1       03506.95j280893.0003m       pedm001
3end of line a photo 11-24 start of line b photo 11-25
21125b11403
1       03607.35j323802.2802m       pedm001
1       03707.40j066841.3002e0      5pedm001
1       03807.65j094600.7502e0  e1  5pedm002
1       03907.70j243550.8502m       pedm  j.s.
1       04008.10j349560.5002m       pedm002open
1       04108.40j320640.7011m       pedm002
1       04208.50j277300.7511m       pedm001
1       04308.70j328830.3011e0      9pedm001
1       04408.80j189430.7002m       pedm  j.s.
1       04509.30j062261.103-b6  e4  3pedm  j.s. <1mm
3end of work day. 3-11-89. D.A.v.E.
3continuation of 11-24 to 11-27 near Sarandi
1       04609.90j063450.9803e0      8pedm002a-mo? or calcite? SAMPLE
1       04710.20m072361.0400m       pedf001small dyklet
1       04810.18j230860.5502e0      6pedm001
1       04910.50j027690.7002m       pedm001
1       05010.50j341700.5702m       pedm001
1       05111.10m097374.502-e       pedf001
1       05211.20j174840.8502m       pedm  j.s.
1       05311.60j320702.1011m       pedm  j.s.
1       05411.30b059871.1002q0      4pedm002
1       05511.95j050710.7013q0      6pedm001SAMPLE
1       05611.90j307640.8802m       pedm002open
1       05712.20j189680.8502m       pedm  j.s.
1       05812.25j238540.5002m       pedm002
1       05913.10j056772.3011e0      6pedm002
1       06012.95j074890.7511e0      5pedm002
1       06113.10j073830.8011e0      6pedm002
1       06213.35j108430.4002e0      6pedm002
1       06313.50j061710.7011e0      1pedm001
1       06413.50j048730.7001e0      1pedm001
1       06513.60j061560.6502e0      2pedm001
3end of line b photo 11-25 start of line c photo 11-26
21126c09402
1       06614.50j099340.5002e0      5pedm001
1       06714.70j220740.4502m       cedm  j.s.
1       06815.30b070302.0002m       ledm001boundary b/t epdyke & normal
1       06915.50b139371.3002m       pedm  fracture surface
1       07016.15b120620.8302m       ledm001
1       07116.65b249860.6702e0      7pedm002
1       07216.95b045890.4402e0      8pedm010SAMPLE
1       07317.05j330851.7511m       pedm  j.s.
1       07417.30j251630.4502e7  e3  5pedm  <1mm j.s.
1       07517.60j324840.5002m       pedm  j.s.
1       07617.90j214630.6002e6  b4  7pedm  <1mm j.s.
1       07718.00j315750.5002e0      1pedm  <1mm j.s.
1       07819.40m049259.502-e       pedf001
3end of line c photo 11-26 start of line d photo 11-27
21127d09602
1       07920.30j051361.1005e0      8pedm002network of veins parallel to
3contact.
1       08018.40b052262.2001e0      8pedm040epidote concentrated in vein
3part of rubble zone b/t dyke contacts
1       08121.10j222850.5002e0      9pedm  <mm j.s.
1       08221.30j343680.5502e0      9pedm  <1mm h-rust j.s.
1       08321.95j207630.6002m       pedm  j.s.
1       08422.10j141830.8502e0      1pedm001
1       08522.40m094452.1000m       pedm050
1       08622.85j090750.7002e0      2pedm002
1       08723.20j099750.8502e0      2pedm001
1       08823.30j087800.6011e0      2pedm002
3zeo veins z-cut epidosite zone-later. epidosite confined to convact part
3of dyke material
1       08923.75m041401.1001m       vedm001contact to rubble zone
3end of line d photo 11-27 start of vertical line v photo 11-24 at 5.4m
3it is crossed at 1.55m)
21124v02000
1       05100.23
1       09000.50j250890.9002m       pedm001
1       09100.75j107691.0502m       pedm001
1       03401.00
1       03001.30
1       02701.55
1       02801.90
3end of session.4-11-89. D.A.v.E.
3start to line a photo1129 1.45km south of Aplikl towards Palakhori (on the
3Palakhori-Nizzala highway)
21129a09301
1       00100.00m116615.002-m       pedm001
1       00200.00j214725.001-m       pedm  j.s.
1       00300.35m116745.002-m       pedf001
1       00400.65j125661.3002e0      1pedf001
1       00500.90j114321.4001m       pedm001
1       00601.00j128801.3011e0      5pedm005
1       00701.30j142755.003-e01s12  9pedm001silicimesidae 053/04
1       00802.00j199452.302-m       pedm  j.s.
1       00901.65j122841.1511e3  c5  1pedm001open
1       01002.10j119823.3011e0  c1  2pedm001silicimesidae 032/20
1       01102.30j135571.3011e0      7pedm001
1       01202.60m141763.102-e7  p2 c1 4pedm001silicimesidae 053/09
1       01303.15m139816.002-e0  c2  8pedm010silicimesidae 047/12
1       01403.50m139711.3011m       pedm  j.s.
3also contains 1cm wide very fine grained dyklet at margin
1       01504.50m140434.8011e0      1pedf001
1       01604.75m140454.8011m       pedf001
1       01705.00j133602.402-e0      3pedm001
1       01805.25j222551.1011m       pedm  j.s.
1       01905.25m137667.002-e0      9pedm020silicimesidae 059/27
3network veins in dyke margin SAMPLE of
v.f. gr. dyke margin & epidote veining
1       02006.30j128837.002-e0      2pedm005dyke weathers spheroidally
3locale like microgabbro SAMPLE contains many horizontal fractures filled with
3calcite only 1mm wide
1       02106.55j140791.1002e0      1pedm001
1       02206.60j148700.4002e81e22  3pedm001
1       02306.75j143745.0011e7  e3  2pedm005
3end of line a photo 1129 start of line b photo 1130
21130b09301
1       02407.00j142741.0002m       pedm001
1       02507.50j252862.3011m       pedm001open
1       02607.60j325852.1002e0      1pedm001
1       02707.85j132711.3011e0      7pedm002
1       02808.10j074542.3011e0      3pedm002
1       02908.20j075542.3011e0      3pedm002
1       03008.40j1407510.02-e0      6pedm002
1       03108.60j202755.0011e0      8pedm002
1       03208.95j132731.4511e0      1pedm001
1       03309.20j148620.6002m       pedm  j.s.
1       03409.50j144851.8011m       pedm  j.s.
1       03510.20j212880.6002m       pedm  j.s.
1       03610.10j060421.9011e8  e2  3pedm002
1       03710.35m1476610.02-e8  c2  7pedm001
1       03810.85j116850.3011m       pedm001
1       03910.90j117870.7011m       pedm001
1       04011.10j109870.5502m       pedm001
1       04111.30j131753.8011e0      4pedm001
1       04211.70j043540.6002m       pedm  j.s.
1       04311.80j150710.5002m       pedm  j.s.
1       04412.05j120850.5002m       pedm001
1       04512.60j077802.1011e0      7pedm001
1       04612.65j262800.6002m       pedm001
3micro gabbro? in places has epidote crystals & calcite as replacement (or
3vugs)?
1       04713.30j070880.6511e0      6pedm001
1       04813.70j042393.0011e0      8pedm002
1       04914.20j138803.1011e0      1pedm001
1       05014.70j218861.3011m       pedm001
1       05115.20j157850.6002m       pedm001
3this part (1m) has boundary fractured but has no fractures >0.5m in length
1       05215.50m1257710.02-m       pedf001
3end of line b photo 1130 start line c photo 1131
21131c09301
1       05315.80j330301.9011m       pedm001
1       05416.10j221760.6002e0      3pedm001
1       05516.40j121875.0011m       pedm001
1       05616.50m1386110.020m       pedf001
1       05716.70j156661.0011m       pedf  j.s.
1       05817.35j050812.1011e0      2pedm001
1       05917.60j172824.002-e6  c4  5pedm  j.s.
1       06018.40j157710.702-m       pedm  j.s.
1       06118.45j244830.3011e0      8pedm001
1       06218.70j233803.3011e0      9pedm010
1       06318.95j233877.0011e0      9pedm015
1       06418.90m136458.002-e0      5pedf010
```

```
1       06519.10j130611.3011a       pod001
1       06619.40j124721.3011a       pedm001
1       06719.80j153433.1011e0      5pedm001
1       06819.80j148795.1011e0      3pedm001
1       06920.40j120661.0011e0      8pedm002
1       07020.40j125741.3011e0      9pedm005
1       07121.10j234842.5011e0      5pedm002cuts 6070; 6071 = younger
1       07221.70j132740.5011a       pedm  j.s.
1       07322.10j221831.102-a       pedm  j.s.
1       07422.10j128778.002-e0      3pedm001
1       07522.25j151748.002-a       undm001
1       07622.40j142770.6511a       pedm001
1       07722.40j233580.6002a       pedm  j.s.
1       07822.50j142680.7011e0      3pedm  j.s.
1       07922.70j233690.6511a       pedm  j.s.
3end of line a photo 1131 start line d photo 1132
21132d09301
1       08023.00j133740.7002a       pedm  j.s.
1       08123.40j133753.0010a       pedm001
1       08223.70j136792.1011e0      1pedm001v.light surface dusting
1       08325.90j130660.702-a       pedm  j.s.
3overburden (telephone pole) to 25.3m
1       08425.30j299841.1011a       pedm001
1       08525.35j119088.002-a       pedm050cms of fractures 1cm apart
1       08625.70j154870.5011e8      1pedm001v.light surface dusting
1       08726.80j081842.0011a       pedm001
1       08827.00j226703.0002e0      1pedm001v.light surface dusting
1       08927.45j215791.2011e0      1pedm001
1       09027.80j218840.9010e0      6pedm001
1       09127.90j221853.0011e0      5pedm001
1       09228.00m133819.002-a       pod001
3interval to 29.5m too much rubble to get a measurement = gabbro screen
1       09329.50m301996.0011a       undf001
1       09429.90m128792.9021a       pod001small dyke1et
1       09530.05j294801.5011e0      5pedf001
1       09630.20j244763.0011e0      2pedm001
1       09730.30j153840.5002e0      5pedm001
1       09830.70j240872.0011e0      1pedm001
3end of section. D.A.v.E. 11-10-89
3vertical section 1.9km toward Palaikhori from Aplidi 11-29
21129v15030
1       09400.45j029200.5002a       pedm002open
1       09700.00
1       09900.40j041590.5002a       pedm002open
1       09600.85j333280.5502a       pedm001
1       09700.85j030880.4002a       pedm001
1       09801.30j024590.4002a       pedm001
1       09901.10
3end of section 19-10-89
3section 1.45km north of Aplidi on Palaikhori-Nicosia highway 1134-1136
21134s27202
1       00100.00j070875.4011e0  e1  8pedf010black dyke
1       00200.20j210811.3011e6  e4  9undf  j.s.
1       00301.30m109403.8011e0      8undf  j.s. grey green dyke
1       00401.40j174381.7002e0      7undf  j.s.
1       00501.50j140682.6002e6  e3|p1  4undm  olichnosites 058/25
3note this may be just preferential orientation of crystals since the
3plane is not too extensive
1       00602.30j193472.0011e6  p4  5pedm  j.s.
1       00701.40j343763.8002e0      4pedm002
1       00803.70j052711.1011e0      3pedm002
1       00903.50j197851.4011e7  e3  4pedm  j.s.
1       01005.30j099741.8011e7  e2 p1 8pedm015network of veins SAMPLE
3some extends to 7.7m increasing in concentration of epidote veining until
3it starts the epidotized dyke
1       01106.20j039522.2011e7  e2 m1  3pedm022m=magnetite
1       01206.30j112691.4011e6  e4  7pedm015SAMPLE
3d011 older than d012 (re-cutting relation. In general calcite filled
3fractures cut epidote fractures
1       01306.808046388.0011e81e22  5pedm008fault fracture existed befor
3 fracture 010 filled but moved after it was filled.
1       01407.10m143509.002-e0      1pedf005
1       01507.70m1383912.02-e0      4pedm005transition to epidosite 8.3m
3SAMPLE
1       01608.10j093841.2011a       pedm001
1       01709.10j234651.1011e0      8pedm  j.s.
1       01809.15j295439.0011a       pedm002open - late
1       01909.90j336111.0002a       pedm  j.s.
1       02009.75j241721.2002e0      8pedm001
1       02110.05j090810.6002e0      8pedm010cms of 1mm wide fractures
1       02210.40j104802.0002e0      9pedm002
3end of line a photo 11-34 start of line b photo 11-35
21135b27202
1       02311.30j134651.8011e8  e2 m  6pedm  j.s.
1       02412.20j138631.2011e9  e1 m  6pedm005j.s.
1       02511.50j030424.0002e0      1pedm001open
1       02612.80m099351.502-e0      1pedm002
1       02713.20m1033-3.0002a       pedf020small dyke1et
1       02813.74j257771.3002a       pedf001
1       02914.70j208791.1011e7  p2 e1  2pedm  j.s.
1       03015.10j112539.002-e8  e2  1pedm001open
1       03116.40j214653.4011e5  e3 p2  2pedm  j.s.
1       03216.40m1074315.02-a       pedm001
1       03316.50j333751.1501e0      0pedm010trails perpendicular to frac
3fracture also contains wall rock dyke fragments
1       03416.90m300751.5002e0      5pedm050parts of dyke1et shared to e
1       03517.40j116541.402-e71c32  5pedm  j.s.
1       03617.90m118483.2011e71c32  3pedf020a on contact c x-cuts e
1       03718.35m1215515.02-e91e12  9pedf010
1       03819.05m1314605.011e0      2pedf002
1       03919.40j211671.3011a       pedf  j.s.
1       04019.40j153521.1011e8  e2  4pedm  j.s.
1       04119.85m0806615.02-e0      5pedf005
1       04219.90j081633.3011e0      4pedm004
3end of line b photo 1135 start of line c photo 1136
21136c27202
1       04320.40m086624.002-e0      1pedf005
1       04420.60j060651.0011e6      1pedm002
1       04520.90m122565.5011e71c32  4pedf005
1       04621.65j043761.2002a       pedm001
1       04721.70j029820.9502a       pedm001
1       04821.70j074793.1002e0      5pedm002
1       04921.70m282856.002-e0      6pedf005small dyke near contact of
1       05021.80m093893.2002e0      9pedf008larger dyke
1       05122.55m171700.002-e0      9pedf0156
3covered under overburden to 26.20m
1       05226.20m189103.002-e6  e3 p1  6undf100cms of dyke margin
1       05327.30j030722.3002e0      3pedm003
1       05427.40m165430.02-e9  e1   7pedf010
1       05524.80m1358610.02-e7  m3   7pedf010
1       05628.30j106551.2002e6  e3 e2  6pedf005mixed minerals: u=red
SAMPLE
1       05728.50j086702.2001e6  e4   1pedm005
1       05829.70j070661.0002-e0      1pedm003
1       05929.60j238601.5011e0      1pedm  j.s.
1       06030.00j198810.6011e9  e1  2pedm  j.s.
3end of line c photo 1136. end of section 1134 to 1136. D.A.v.E.10-10-89
3start of vertical section 11-34 to 11-36 near Aplidi in sharp corner
21135v00861
1       06100.00j210691.5502e0      1pedm  e<1mm j.s.
1       06200.70j100421.6502a       pedm002open
1       06300.90j126471.7502a       pedm001
1       01501.20
1       01401.90
1       01302.30
1       01102.80
1       06402.00j234930.4511e0      0pedm005
3end of section 19-10-89section 5.6km north of Aplidi on the Palaikhori-Nicosia
highway: 100m north
3of the Ayia Kereni church. Section is covered page 83 of the Treadon '87
3fieldguide book
21137s00101
1       00100.00m354770.9011a       pedf001small dark late dyke margin
1       00200.05m354780.9011a       pedf001small dark late dyke margin
1       00300.50j132601.202-a       pedm  j.s.
1       00400.55j195700.7002a51e33k224pedm005pyrite  diseam w/in dyke
1       00500.45m245300.0011a       pedm001
1       00601.50j268402.5011e4  e4 k 20pedm005small  e blob 5cm long
1       00701.80j066700.552-e0      4pedm  j.s.
1       00802.25j180651.0002e0      1pedm002
1       00902.85j235923.5002e0      4pedm001epidote alteration halo to
3either side of fracture
1       01003.32j345710.9002a       pedm002open
1       01100.20j116400.452-e0      4pedm  j.s.
1       01204.00j126760.6011a       pedm  j.s.
1       01305.95j217552.1010e61e42  5pedm003c cm e cm rock
1       01404.00j059450.5011e6  k4  3pedm  j.s.
1       01504.40j072510.8511e0      1pedm  j.s.
1       01604.55j154811.1010e0      1pedm  j.s.
1       01705.50m244785.2011a       undm  j.s.
1       01806.25j127350.502-e0      1pedm  j.s.
1       01906.25j018500.402-a       pedm  j.s.
1       02006.80j020081.2502a       pedm001
1       02107.70j253526.0011a       pedm002open
1       02207.90j219870.9011a       undm  j.s.
1       02308.90j120562.6011e6  p4  1undm  j.s.
1       02408.90j324601.1002e62p41  5pedm002
1       02509.35j248834.4011e0      1undm001
1       02610.40m242548.0011e71c2  p1  3undm005
3end of line a photo 1137 start of line b photo 1138.
```

21138h00108
1 02710.50N060538.0011e0 c1 1cmbm0305cm wide fault zone curved
3to vertical near the top of outcrop - at bottom in light grey dyke & horiz
1 02811.00N238465.302-e0 c2 1pmbm002
1 02911.05m230781.5011n cmbm001margin=epidote halo
1 03011.60N124591.0011p0 e1 1pmbm j.o. SAMPLE
1 03111.80N330891.1002n pmbm001
1 03212.10m274572.802-n0 e1 7mpf002clay=altered volc. glass
1 03313.05N210782.5002e0 e4 4cmbm SAMPLE
1 03415.00N238686.5011e0 e4 1pmbm001
1 03514.40N120560.952-e pmbm j.o.
1 03614.60N001590.9011n pmbm j.o.
1 03715.30N121551.1002p0 1pmbm j.o.
1 03815.90N008400.6011n pmbm j.o.
1 03916.35N034861.5011n pmbm j.o.
1 04016.90N141861.602-e pmbm001
1 04117.30N148712.0011n pmbm001
3end of line b photo 1138 start of line c photo 1202
21202c00108
1 04218.10N080401.4002e0 1cmbm j.o.
1 04317.95N359762.2002n pmbm001
1 04418.30N356802.1002n pmbm001
1 04518.65N355642.5002n pmbm001
1 04618.80m0695412.02-e0 c1 1prpm005epidote not common
1 04720.05N350860.9002n prpm001
1 04820.20N001720.8002n prpm001
1 04921.20N309863.4011e0 1pmbm001rare epidote
1 05021.20N029341.1011n pmbm j.o.
1 05122.25N118690.9311e0 1pmbm j.o.
1 05222.70m231688.002-n pmf001
1 05323.80N151851.2011e5 k5 1pmf j.o.
1 05424.40N150800.5011n pmf j.o.
1 05524.45N349581.3002n pmf001
1 05625.50N350642.8002n umf001
1 05725.80m346555.602-n pmbm
3end of line c photo 1202 start of line d photo 1203
21203d00108
1 05825.90m249465.5011n pmf001
1 05927.80m267478.002-e0 1pmbm002epidote rare
1 06027.70N128641.0511e5 p5 1pmbm j.o.
1 06127.80N011611.0511n pmbm j.o.
1 06228.50N149800.9502n pmbm j.o.
1 06328.50N040471.3002n pmbm j.o.
1 06429.00N150720.8002n pmbm001j.o.
1 06529.30N350802.002n pmbm001
1 06629.70N267003.502n pmbm001
3end of line d photo 1203. end of section. D.A.v.E. 9-10-89
3vertical section near Ayin Koreni
21137v27868
1 06700.00N058400.5502n umbm j.o.
1 02800.30
1 01200.50
1 06801.00N041340.5302e0 4pmbm j.o. c=1mm
1 01301.05
1 06901.50N081390.7002e0 p1 3pmbm j.o. calp<1mm
1 07001.10N297780.4502e0 1pmbm j.o.
1 01701.65
1 07102.00N124780.6011e0 4pmbm<1mm
3end of section 19-10-89
3section 12-04 to 12-06 by the kmobi runoff near Pharmakia
21204s16802
1 00100.23N312410.5304n pmbm001light grey dyke
1 00200.30N312420.6003n pmbm001
1 00300.50N312801.5020n pmbm001epidote nodule at one end
1 00400.80N330800.4013n pmbm001
1 00501.25m328693.203-n pmf001
1 00601.10N203270.4002n pmbm001
1 00701.70N.034802.8011n pmbm001
1 00802.15N354733.1011n pmbm001
1 00902.50N250781.0502n pmbm j.o.
1 01003.10m320821.1010n pmf020small dykelet
1 01102.89N315801.3012n pmbm001
1 01203.80m112773.502-e0 1umf001v.minor epidote
1 01304.35N311891.9001e0 1pmbm001
1 01404.00N087430.7302e0 3cmbm j.o. mineral=1mm thick
1 01504.40N331753.502-e0 9pmbm003
1 01604.30N195252.2502n pmbm001
1 01705.20N215305.2002n pmbm001
1 01804.90N042601.2502n pmbm j.o.
1 01905.90N352874.302-e0 2pmbm002
1 02006.20m332844.002-n umf001basalt
1 02106.50N141721.0811e0 1pmbm j.o.
1 02206.75m318761.0011n pmf010small dykelet
1 02306.90N110720.4502n pmbm j.o.
3end of line a photo 1204 start of line b photo 1205

21205a16004
1 02407.15N104810.5002e0 1pmbm001
1 02507.45N119761.1011e0 1pmbm001
1 02607.45m136721.2511n pmf020small dykelet
1 02708.10N113751.0002n pmbm j.o.
1 02808.30m333875.002-e pmf
1 02908.35N333875.0003-e pmbm001
1 03008.50m347805.002-e pmf001v.patchy epidote on j.o.
3in this older dyke
1 03108.65N133743.5011e0 1pmbm002
1 03208.80N331731.1001e pmbm001
1 03309.00N314702.1011e pmbm001
1 03409.50N349801.1002n pmbm001
1 03509.80m329675.502-e pmbm001
1 03610.30N191871.0001e pmbm001
1 03710.50N194850.6010e pmbm001
1 03810.70N188840.7511e pmbm001
1 03? .0.30N082591.3002n pmbm001
1 04010.75N087690.8502e0 1pmbm001
1 04111.30m097713.2011e0 1pmbm001
1 04212.04m304615.002-e pmf001
3new outer a dyke which is highly fractured (fragments no larger than
35cm) the interstices are filled with calcite
no visible epidote zone seen
3to 13.50m. Dyke is fine to med. aphyric greenish colour weathers dark rust
3calcite veins up to .5cm wide thrown in all orientations
3end of line b photo 1205 start of line c photo 1206
21206c16804
1 04313.50m134836.002-e pmbm001
1 04413.65N342753.202-e0 6pmbm002
1 04514.00N203410.6502n pmbm001
1 04614.00N333800.4301e0 3pmbm002
1 04714.50N146803.0011e0 5pmbm001
1 04814.65N144791.5010e0 0pmbm002SAMPLE
1 04914.90N324823.2010e0 6pmbm001
1 05013.05N326772.8001e0 5pmbm001
1 05115.75N136812.7010e0 2pmbm001
1 05216.70m328425.502-e0 7pmf100zone of calcite veins
3trending parallel to dyke trend contaminating to 3mm thick
1 05317.00N339760.9502n pmbm001
1 05417.50m314491.702-e pmpm001v.small pillow screen which
3contains no large fractures but common epidote and some calcite as vug fill
1 05518.20m319571.602-e pmbm001
1 05618.350N316891.7000e0 5pmbm002
1 05718.80N301611.0001e0 1umbm001
1 05819.05m193740.7511n umf040small dykelet
1 05919.60N318641.5011e0 5pmbm002
1 06019.80m326775.2020n pmbm001
1 06120.75m317706.0020n pmbm001
3end of line c photo 1206 start of line d photo 1207
1 06221.00N301731.8311n pmbm001
1 06321.60N288681.5011n pmbm001
1 06421.65N312652.0511n pmbm001
1 06522.05N352821.1511n pmbm001
1 06622.10N232781.4002e0 2pmbm002
1 06722.40N196461.30 pmbm001
1 06822.10N102671.0502n pmbm j.o.
1 06923.40m323556.502-n pmbm001
1 07024.00m320844.502-e pmbm001
1 07124.20N290771.7011n pmbm001
1 07223.20N246674.502-e0 4pmbm j.o.
1 07324.30N072791.2001n pmbm j.o.
1 07424.70N315660.7002n pmbm002open
1 07524.75N314650.6802n pmbm002open
1 07625.20m309784.002-n pmbm001can't spot upper end
1 07725.40N053401.2002e0 2pmbm j.o.
1 07821.60N024773.2011e0 2pmbm001
3end of line d photo 1207 start of line e photo 1207.line e crosses d at 22.2m
1 07900.00N189222.5002n pmbm002open
1 08000.45N128201.5502n pmbm002open
1 08100.80N229480.8502n pmbm001
1 08201.05N236920.7002n pmbm001
1 08301.25N156202.3002n pmbm001
1 08401.55N198241.9002n pmbm001
1 06402.00
3end of line e. end of section. 16-10-89. D.A.v.E.
3vertical section near Pharmakia 12-04
21204v25959
1 07800.00N092301.5502n pmbm001
1 07900.10N078711.8002n pmbm j.o.
1 01600.30
1 01700.65
1 01800.70
1 08000.95N198181.0502n pmbm001
1 08101.00N053640.7002e0 1cmbm j.o.

1 08201.20|s151281.8502n pedm001
1 08301.40|s110270.8002s0 3sedm j.s.
3end of section 19-10-89 D.A.v.E.
3section W. of Gouri off main road (Kalokhorio-Pharmakies) photos 1211-1215
21211s14900
1 00100.30|s138804.202-n pedm001
1 00200.35|s335892.7011n pedm001cpm
1 00301.05|s304875.002-n pedm001
1 00400.60|s129831.2011n pedm001
1 00500.85|s294880.3811n pedm001
1 00600.75|s234840.4502n pedm001
1 00701.05|s227650.4502n pedm j.s.
1 00801.30|s302810.5611n cedm j.s.
1 00901.35|s232890.7511n pedm001
1 01001.50|s068270.7502n pedm001
1 01101.70|s172560.9001n pedm001
1 01201.60|s314610.6711n pedm001
1 01301.85|s282700.4502n pedm001
1 01401.91|s308800.4003n pedm001
1 01502.10|s303652.4511n pedm001
1 01602.15|s289451.8511n pedm001
1 01702.30|s303681.1601n pedm001
1 01802.40|s299591.9001n pedm001
1 01901.45|s227671.3011n pedm j.s.
1 02002.10|s225760.4802n pedm j.s.
1 02102.70|s296891.3011n pedm001
1 02202.72|s228980.7302n pedm j.s.
1 02305.05|s306631.152-n pedm001
1 02405.40|s149516.002-n pedm001j.s. is fine & black
1 02503.40|s132541.1011n pedm001
1 02603.80|s294761.9041n pedm001
1 02704.10|s287773.0511n pedm001
1 02804.20|s294853.1511n pedm001
1 02904.40|s316830.8301n pedm001
1 03004.50|s137881.6002n pedm001
1 03104.70m304785.002-s0 1pedm001dyke becomes v rubbly zone
3of fracturing 0.2m wide
3note that numbers 002 thru 007 are missing - due to mismumbering
3end of line a photo 1211 start of line b photo 121-
21212b13908
1 03805.00|s258455.002-n sedm j.s.
1 03905.70|s180861.2511n pedm j.s.
1 04005.90|s339671.2011n pedm002cpm
1 04106.35|s304772.2511n pedm001zone of many fractures close
3ly spaced over 0.1m @1 per cm
1 04206.95m294805.002-n pedm001contact zone to left very
3fractured east dyke zone competent light grey
1 04306.70|s356360.3002n pedm002cpm
1 04406.60|s246860.9511n pedm001
1 04507.00|s012871.1511n pedm001
1 04607.25|s209801.102-n pedm j.s.
1 04707.30|s295680.902-n pedm j.s.
1 04807.40|s304755.802-n pedm001
1 04907.55m306685.802-s0 1pedf001
1 05008.10|s296885.402-n pedm001
1 05108.40|s124892.5002n pedm j.s.
1 05208.30|s011832.002-n pedm001
1 05307.60|s198590.5002n pedm j.s.
1 05408.70|s307700.702-n pedm002cpm
1 05509.05|s306780.922-n pedm j.s.
1 05609.20m315842.8011n pedm001
1 05709.30|s291482.7011n pedm j.s.
1 05809.20|s059751.1811n pedm001
1 05909.30|s254581.2502n pedm j.s.
1 06009.70|s068340.8502n pedm j.s.
3end of line b photo 1212 start of line c photo 1213 note gap between 9.7 and
311.4m in photo coverage = not measureable rubble
1 06110.70m 5.0002n sedm v.irregular contact zone is
3drawn on 1212 photo overlay - material is highly fractured no mineralisation
3(v.minor zeolites) chill to right
21213c14802
1 06212.50m253615.302-n pedf001
1 06312.75|s170760.5511n pedf001
1 06413.20|s262530.952-n pedm001
1 06513.50|s285675.302-n pedm001
1 06613.62|s321662.0011s0 3sedm001
1 06713.35|s260850.452-s0 1pedm alkkmonzdiss 349/14 j.s.
1 06814.20|s259461.7011n pedm j.s.
1 06914.45|s134705.502-n pedm001
1 07014.20|s215771.1011n sedm001
1 07114.80|s129861.5002n pedm001
1 07215.00m306881.4010n pedm005small dykelet
1 07315.20|s030421.7002n pedm001
1 07415.35|s140823.0011n sedm001
1 07515.00|s280644.502-n sedm001continues from small dykelet
3cpm
1 07615.60|s283861.3011n pedm001
1 07715.80|s272651.1001n pedm001
1 07816.00|s110761.3002n pedm001
1 07916.22|s302771.7511n pedm001
1 08016.20|s187301.2002n pedm j.s.
1 08116.55|s345490.8011n pedm j.s.
3end of line c photo 1213 start of line d photo 1214 note gap between 16.55
3to 17.50m
1 08216.90|s046760.4511n pedm j.s.
1 08317.40|s232621.7011n pedm j.s.
21214d12902
1 08417.40|s272603.402-n pedm001
1 08517.50|s290671.9011n pedm001
1 08617.70|s312862.1011n pedm001
1 08717.80|s303582.5011n pedm001
1 08817.85|s332503.0011n sedm001
1 08918.20|s276800.8515n pedm001
1 09018.35|s280690.7515n pedm001
1 09118.45|s314591.7011n sedm001
1 09218.70|s287711.3011n sedm001
1 09318.80|s141862.4011n pedm001
1 09419.00|s081891.8502n pedm001
1 09519.10|s288702.7001n pedm001
1 09619.20|s314680.9302n pedm001
1 09719.12|s135551.2002n pedm001
1 09819.50
1 09819.35|s108850.7011n sedm001
1 09919.50|s192331.4011n pedm j.s.
1 10019.70|s290700.3502n pedm j.s.
1 10120.10|s238370.4502n pedm j.s.
1 10220.10m141598.002-n pedf002cpm
1 10320.55|s281631.8002n pedm001
1 10420.80|s179691.5011n sedm j.s.
1 10520.70|s299521.0002n pedm001
1 10620.90m301664.802-n pedm001
1 10720.95|s017980.5402n pedm001
1 10820.70|s100751.5302n pedm003cpm
1 10921.50|s248761.4011n pedm002cpm
1 11021.90|s142800.5302n pedm001
1 11122.30|s288670.9511n pedm001
1 11222.85m315756.002-n pedm001
1 11323.60m285456.002-n pedf001
3end of line d photo 1214 start line e photo 1215
21215e12902
1 11424.85|s286753.0010s0 2pedm002
1 11524.20|s257481.3502n pedm j.s.
1 11624.30|s176700.7302n sedm j.s.
1 11724.80|s292730.8011n pedm001
1 11825.20|s122880.7011s0 7pedm002
1 11925.20m286844.802-n pedm001
1 12025.35|s295890.7002n pedm001
1 12125.45|s272730.6002n pedm001
1 12225.75|s301542.3011n pedm001
1 12326.20|s290672.2011n pedm001
1 12425.90|s213830.3502n pedm j.s.
1 12526.25|s299773.0501n pedm001
1 12626.40|s278771.4211n pedm001
1 12726.75|s280851.1011n pedm001
1 12826.75|s094151.7502n pedm001
1 12927.00|s125682.2011s0 5pedm001
1 13026.90|s355840.8002n pedm001
1 13127.20|s297711.8011n pedm001
1 13227.50|s262691.8511n pedm002cpm
1 13327.50|s138303.6011n pedm001
3end of section and photo 1215 at 26.70m D.A.v.E. 14-10-89 (locked keys in car)
3start of vertical section at turnoff to Gouri
21214v21274
1 13400.00|s254361.2002n pedm001cpm
1 13500.00|s186560.6002n pedm j.s.
1 13600.00|s036550.5502n pedm j.s.
1 13700.40|s333480.5001n pedm001
1 13800.50|s009150.4502n pedm001
1 13900.80|s026541.4502n pedm001
1 14001.00|s012501.2002n pedm001
1 10201.30
1 09901.45
1 14101.45|s016702.402-n pedm001
1 14201.65|s018570.4502s0 4sedm001
3end of vertical section. 17-10-89 D.A.v.E.
3section 1.9km south of A.Yeoryios photos 12-16 to 12-20
21216s01009
1 00100.10m216765.0010n sedf100small dykelet
1 00200.80m159866.002-n pedf001
1 00301.10|s299843.5001n pedf001

1 00401.65j016821.0502s0 3pnt001rust stains orange red
1 00501.40j179890.8701s pnt001
1 00601.75m348662.6011s cryp001entering pillow screen
1 00702.05j227800.5002s prpm j.s.
1 00802.05j359460.4502s prpm j.s.
1 00902.20j074900.4502s prpm001
1 01002.35m208804.0011s pnbm001
3this dyke is very fractured - fractures are less than 25cm long
1 01102.70j200783.5011s pnbc001
1 01202.80j208800.9011s pnbc001
1 01303.00j209711.0511s pnbc001
1 01403.20j206711.5011s pnbc001
1 01503.30j207810.5011s pnbm001
1 01603.35m209866.0020s prpm001contact to pillow/flow screen
1 01703.45j325810.4011s prp001
1 01803.90j272812.8011s prpm j.s.
1 01904.25j322860.6502s prpm j.s.
1 02004.25j256791.2602s prpm j.s.
1 02104.55j170810.3502s prpm001
1 02204.80j338740.7511s prpm001
1 02304.90j188741.3011s prpm001
1 02405.00j306840.8502s rvpm001
1 02505.00j061901.3502s prpm001
1 02605.80j327853.1011s prpm001
3end of line a photo 12-16 start of line b photo 12-17
21217b00407
1 02706.18m221596.002-s pnbc001
1 02806.80j212842.7511s pnbc001
1 02906.90j224751.0011s pnbc001
1 03007.00j190713.2011s pnbc001
1 03107.45m215776.002-s prpm001pillow/flow screen
1 03208.00r310842.3011s prpm002-rpm
1 03308.45r144871.9011s prpm001
1 03408.80r344811.8511s prpm001
1 03509.30r172893.1011s prpm001
1 03608.50j251756.002-s prpm j.s.
1 03709.70m049886.002-s pnbc001dyke
1 03809.90j209842.0511s pnbc001
1 03910.15j249791.0511s pnbc001
1 04010.40m221716.002-s prpm001pillow/flow screen
1 04110.70r330851.5011s prpm001
1 04210.90r178871.1501s prpm001
1 04311.30r339891.4002s prpm001
1 04411.60r316831.1502s prpm001
1 04511.30j271692.0011s prpm j.s.
1 04611.90j267682.2011s prpm j.s.
1 04712.60r008874.0011s prpm001rpm
3end of line b photo 12-17. Note gap between 12-17 and 12-18 (12.6m to 14m)
3following fractures are from gap area and therefore not on photos
1 04813.00r204803.0510s prpm001
1 04913.50r329661.1002s urpm001
1 05013.75r334590.5502s urpm001
1 05114.00r356650.7001s crpm001
3start of line a photo 12-18
21218c01002
1 05214.40j330605.502-s prpm001
1 05313.70j259801.3511s prpm j.s.
1 05414.50m223786.002-s pnbc001dyke looks same as before
1 05514.80j227701.1011s pnbc001
1 05615.20j227752.2011s prpc001
1 05715.35m028806.002-s prpm001
1 05815.60r188701.0011s crpm001
1 05915.72r008640.8511s urpm001
1 06016.12r012771.0511s prpm001
1 06116.50j270721.8011s prpm j.s.
1 06216.50j309652.2011s prpm001
1 06316.95j240660.7511s prpm j.s.
1 06417.50j230731.2611s prpm001
1 06517.50m231612.1011s pnbc001 j.s.
1 06617.40j349433.1002s pnbm001possible fault no slic.
3more highly fractured and scanline too low to get crossing fractures
1 06719.40m222809.5011s pnbm001
1 06820.20j237770.6011s pnbm001
1 06920.50j165880.4511s pnbm001
1 07020.70j238750.4011s pnbm001
3end of line a photo 12-18 start of line d photo 12-19
21219d01400
1 07120.90j152831.0511s pnbm001
1 07222.00j331701.4011s cnbm j.s.
1 07321.60j142650.7002s pnbm001
1 07422.75j210811.3011s pnbm001
1 07522.95m233866.002-s pnbc001
1 07623.45j052891.8511s pnbm001
1 07723.60j234752.1011s pnbm001
1 07824.15j206771.1511s pnbm001
1 07924.50j277771.2511s pnbm j.s.
1 08024.65j322813.5011s pnbm001
1 08124.40j034384.5002s pnbm001
1 08224.90j026671.7011s pnbm001
1 08325.00j228661.2011s pnbm j.s.
1 08425.45j216751.7011s pnbm j.s.
1 08525.50j028372.4002s pnbm001
1 08626.10j357354.0011s cnbm001
1 08726.80j021750.5502s pnbm j.s.
1 08827.80j297481.1002s pnbm j.s.
1 08927.80j021662.5002s pnbm001
3end of line d photo 12-19 start of line e photo 12-20
21220e00802
1 09028.30j080891.2502s pnbm001
1 09128.60j274500.5511s pnbm001
1 09228.60j068632.0510s pnbm001
1 09329.20j314521.2311s pnbm j.s.
1 09429.10j268850.652-s pnbm j.s.
1 09529.85m191645.5011s prpm001
3screen fractures continue into the pillow screen not many see photo
3end of line e photo 12-20 start of line f photo 12-19 (vertical section)
3screens main scanline at 26.50m
21219v10167
1 09600.20j293550.4002s pnbm j.s.
1 09700.20j230530.4502s pnbm j.s.
1 09800.20j100850.8002s pnbm j.s.
1 09900.65
1 09900.65j10085 02s pnbm j.s.
1 10001.10j29653 02s pnbm j.s.
1 10101.35j09289 02s pnbm j.s.
1 08601.80
1 08702.00
3end of section.21-10-89. D.A.v.E.
3section 3.9km south of A.Yeoryios 12-21a to 12-21e
21221a19408
1 00100.10j061880.3002s prpm j.s.
1 00200.30j212852.0502s prpm002rpm
1 00000.55j342890.7002s prpm001
1 00401.50j251672.5002s prpm001
1 00500.90j222820.8002s prpm001
1 00601.55j174120.6002s prpm001
1 00702.95j182830.7502s prpm j.s.
1 00803.05j153840.9002s prpm j.s.
1 00903.30j233811.302-s prpm001rpm and covered by rubble
3scanline blinked due to o/c exposure
21221e20000
1 01002.25j307750.7002s prpm001rpm
1 01103.55j232891.5511s prpm001rubble covered
1 01204.00j057720.4002s prpm j.s.
1 01304.40m129216.5011s urpm001white dyke SAMPLE
3contains some epidote; there is another similar dyke below containing more ep
1 01405.50j068890.8502s prpm j.s. cuts wh. dyke
1 01505.60j294751.0502s prpm001
1 01606.20j233892.2011s prpm001
1 01706.70m057836.002-s pnbc001blue-grey fresh dyke
1 01806.90j180710.7511s pnbm j.s.
1 01906.95j176741.0011s pnbm j.s.
1 02007.20j068700.4011s pnbm j.s.
1 02107.25j211661.0011s pnbm001
1 02207.90j183782.102-s0 1pnbm j.s.
1 02308.20j074892.202-s pnbm j.s.
1 02409.00j146735.302-s0 9pnbm alkhornblde 058/12;s=1mm
3j.s.
1 02508.80j156741.0001s0 9pnbm j.s.;s=1mm
1 02609.10j100755.502-s cnbm j.s.
1 02709.50j147763.0011s tnbm j.s.
1 02810.20j150831.2002s pnbm j.s.;alkhornblde 180/15
1 02910.40m074855.502-s pnbc001to more competent dykes
3had to relay scanline due to o/c accessibility line lower along contact
3end of line a photo 12-21a start of line b photo 12-21b
21221b18402
1 03011.00j230830.4011s prpc j.s.
3gabbro with plagioclase xenocrysts
1 03102.00j022891.2011s prpc001
1 03212.20j202804.5011s prpc001
3epidote is fairly common in the gabbro but most is not fracture fill also is
3more restricted to plagioclase portions
1 03312.70j213781.2011s0 2prpc003rpm
1 03412.80j148991.7002s prpc001
1 03513.05j197822.5011s prpc001
1 03613.70j055742.8011s prpc001fine+cm gabbro + plagioc.
1 03714.10j014591.9002s0 1prpc001mostly rpm
3end of line b photo 12-21b start of line c photo 12-21c this area is a fine
3minkmesh of fine and coa gabbro with 'sweats' of leucocratic material (plag
3biogranite containing abundant epidote

21221c18400
1 03815.10j344751.2011n prgm001
1 03914.40j318991.6011n prgm001
1 04015.80j340841.4002n prgm001
1 04115.35j322780.5011n prgm001
1 04215.35j234890.8002n prgm001
1 04316.20j329820.8302n prgm001
1 04416.50j281801.1002n prgm001
1 04517.00j210820.5302n prgm001
1 04617.35j130771.4002n prgm001
3end of line c photo 12-21e start of line d photo 12-21d
21221d00306
1 04718.00j311891.7302n prgm001
1 04818.35j220792.0002n prgm001
1 04918.50j219741.1002n prgm001
1 05018.70j204782.2002n prgm001
1 05118.85j201881.5302n prgm001
1 05218.95j173842.5002n prgm001
1 05320.00j267713.002-n pmf001v.fine dyke rust brown
1 05419.20j110860.4002n prgm001
1 05519.30j295641.6002n prgm001
1 05620.00j188871.1002n prgm001cpen
1 05720.40j174891.3002n prgm001cpen
3new line orientation due to o/c coverage
21221d14115
1 05820.65j173863.8011n prgm001
1 05921.05j172891.6002n prgm001
1 06021.30j172841.5302n prgm001
1 06121.10j174781.3802n prgm001
1 06221.15j220700.9301n prgm001
1 06321.60j149801.1702n prgm001
1 06421.70j095821.1011n prgm j.s.
1 06521.90j008534.8011n prgm001
1 06622.00m168835.002-e0 2pmf002
1 06722.45m176865.002-n prgc001
1 06822.40j212800.7002n prgc001
1 06923.00j216791.3502n prgc001
1 07023.10j201771.3511n prgc001
1 07123.50j226731.1011n prgc001
1 07223.75j212721.4511n prgc001
1 07324.00m194844.202-b0 9pmf001alicinnsides 283/12
3breccia pebble size clasts/b-ax alteration either side of contact
3leached angular rubble interior
3end of line d photo 12-21d
3start of line e photo 12-21e
21221e03902
1 07424.50m175794.202-b0 9pcbm002minor calcite
1 07524.52j082822.0011b0 9pcbm001alicinnsides 355/20
1 07624.80j044823.6011n pmf001
1 07724.85j138500.3502n0 8pmf001
1 07825.30j164834.102-b0 8pmf001
1 07925.50j200784.102-b0 7pmf001alicinnsides 111/02
1 08025.70j210844.102-b0 5pmf001alicinnsides 121/12
1 08126.40j176794.002-e0 6pmf001
1 08226.50j072711.8311b0 3pmf001
1 08326.80m180852.2011e0 4pmf001dyke darker grey
1 08427.27m209874.002-b0 4pmf001
1 08527.35m212774.002-n pmf001
1 08627.60j230854.002-b0 2pmf001j.s.
1 08727.70j150804.002-n pmf alicinnsides 062/12 j.s.
3silicic unmeasd in downstep direction
1 08827.80j161713.002-n pmf j.s.
1 08928.10j161702.1011n pmf j.s.
1 09028.30m089854.202-n prgf001into gabbros
1 09128.50j192841.3011n prgc001alicinnsides 280/12
1 09228.50j234851.0011n prgf j.s.
1 09328.80j156751.4002n prgf j.s.
1 09428.90m230801.3011n prgm060fracture zone
1 09529.30j158771.4311n prgm j.s.
1 09629.70j164830.4502n prgc j.s.
1 09729.50j264800.9002n prgc001
1 09830.00j174801.4011n prgc j.s.
3end of line e 12-21e start of vertical section photo 12-21e
21221v33377
1 09900.35j206971.5311n prgc001
1 09900.45
1 10000.55j261410.7002n orgc001
1 10100.80j333100.6002n orgc001
1 10200.95j138050.5002n orgc001
1 10301.05j333060.5302n orgc001
1 10401.35j329130.4302n orgc001
1 10501.65j329130.8302n orgc001
3note that any increase in the number of fractures in the later part of the
3section may be due to the outcrop being more covered by overburden in the
3begining of the section

3end of section. 21-10-89. D.A.v.E.
3section 4.02km S of A.Yeoryios 12-22e to 12-22f
21222e07208
1 00100.30j136810.6002n prgm fracture surface
1 00200.60j035842.3011n prgm001
1 00300.80j235811.0602n prgm001
1 00401.10j077844.002-n prgm001alicinnsides 165/18
1 00501.65j195892.0511q0 1prgm alicinnsides 349/14 j.surf.
3end of line b photo 12-22b start of line c photo 12-22c
21222c24400
1 00601.65j134781.3002n0 1prgm j.s.
1 00701.90j212851.8002n prgm j.s.
1 00801.91j066852.1002n0 2prgm alicinnsides 337/08 j.surf.
1 00902.15m256824.502-n cnkm001
1 01002.30j260891.0502n0 3prkm001
1 01102.55j220813.2011n pmf j.s.
1 01202.70j272881.0002n0 4pmf j.s.
1 01302.90j266890.8002n0 1pmf j.s.
1 01403.04j084830.8702n pmf j.s.
3highly fractured zone to 3.70m pieces too small to measure - fractures < 25cm
1 01503.80j022850.9002n pmf j.s.
1 01604.00j017841.5002n pmf j.s.
1 01704.10j045862.9011n cnf002open
1 01804.30j084764.002-n1 1pmf001entering fine rubble zone
3pebble size rounded dyke material
1 01904.47m078854.002-n0 1prgm001
3no epidote in rubble zone just along edge. Gabbro boundary to plagiogranite
3obscure in places see transitional gradation to leached looking gabbro
1 02004.70j328854.4011n0 4pmc remember t=trondjhemite
1 02104.60j108130.3502n0 3pmc specular hematite j.surf.
1 02205.20j040854.0010n prm001
1 02305.40j227844.0011n prm001
1 02405.60j098841.3002n prm001
1 02506.40j222872.4002n vrm001
3highly fractured zone of pglgogr. to 0.60m parallel to #025 & #026
1 02606.90j223854.0011n prm001
1 02707.10j130811.8002n0 1prm j.s.
1 02807.40j253841.0702n prm001
1 02907.75j049723.1011n prc001
1 03008.20m246735.002-n pmf090small dyke
1 03108.80m083863.5011n pmf060small dyke
1 03208.65j015960.6002n crm j.s.
1 03309.05h070893.4011n0 9prm005
3end of line e photo 12-22e start of line d photo 12-22d
21222d24206
1 03410.15m286713.002-n0 6pmf010small dyke
1 03510.50j257853.002-n0 6prm001
3At #034 &#035 highly fractured brecciated plagiogr. zone narrows to
310cm upwards
1 03610.60j261723.002-n0 1prm001
1 03711.10j062831.1002n prm001
1 03811.40j230790.6002n prm001
1 03911.65j054852.8011n prm001
1 04011.80j087813.0011n0 1prm001
1 04112.40j190772.6011n prm j.s.
1 04212.42j314821.0711n0 1prm002
3zone up to #040 highly fractured mostly parallel to #040 #036
1 04312.60j194861.4011n prc001
1 04412.80j218793.002-n prm001
1 04512.90j306781.0602n0 8prm j.s.
1 04613.30j004870.4002n0 8prm j.s.
1 04713.40j219773.002-n prm001
1 04813.65j228751.1010n prm001
1 04914.10j083891.8511n prm002open
1 05014.30j160861.7002n prm001
1 05115.05h066862.1511n prm001
1 05215.65j066844.302-n0 5prm j.s.
1 05315.80j093814.502-n prm j.s.
1 05416.90j193872.902-n0 6prm002j.s.
1 05516.30j223860.6512n prm j.s.
3end of line d photo 12-22d start of line e photo 12-22e
21222e24700
1 05617.00j220852.2511n0 1prm001
1 05717.20j265883.0011n prm001
1 05817.60j084875.002-n prm001
1 05917.80j087871.7011n prm001
1 06018.10j126861.7011n prm001
1 06118.50j128790.8411n prm j.s.
1 06218.50j228810.5511n0 4prm j.s.
1 06318.70j229811.4011q8 n2 1prgm001j.s.
1 06419.05j103891.1511n prgm001
1 06519.10j167801.0011n0 1prgm j.s. ; a<1mm
1 06619.40h049891.1011n prgm002
1 06719.80h046813.1511n prgm j.s.
1 06820.20h212831.4711n prgm001

1 06920.40jc250362.1002a prm001
1 07020.70jc140791.2202a prm j.s.
1 07121.70fc080872.0011a prm001
3fractured zone from 21.55m to 21.70m
1 07221.00jc238361.4002a prm001
1 07322.10fc266460.7001a prm001
1 07422.75jc076790.8011a prm001
1 07522.40jc255301.3011a prm001
1 07623.30jc089706.502-c0 1prm001
1 07724.10jc055765.202-c0 1prm001
1 07823.40jc270701.1002c0 1prm001
3end of line e photo 12-22e start of line f photo 12-22f
21222f24800
1 07924.30jc068904.202-c prm001
1 08025.10jc083784.0011a prm001
1 08125.20jc177851.4011a prm001
1 08225.60jc054894.502-c crm j.s.
1 08325.20jc082601.3511a prm001
1 08426.20jc232833.002-c prm001
1 08526.60jc086651.7502a prm001
1 08627.70jc086650.3002a prm001
1 08728.40cm0866815.02-c0 1prd001
3looks like epidosite dyke with very leached (plagiogr.) to south side of
3dyke rubble shear (?) zone is epidote rich
3rubble zone contacts on about 20cm into gabbro
1 08829.00cm2348615.02-c0 3prgn001
1 08929.10jc264760.9002c0 9prgn004
3for last 90cm of section very rubbly no coherent samples; overburden cover
3end of line f photo 12-22f start of vert section on photo 12-22c at 7.45m
3crosses line at 1.25m (vert. line)
21222v33047
1 09000.40fr331100.4001a prdm001
1 09100.556r332120.5002a prdm001
1 09200.55fr264361.4001a prdm001
1 02701.20
1 09302.056r042280.4002a prdm001
3end of section. 23-10-89. D.A.v.E.
3section 12-27 to 12-31 on forest road between Xylistos/Lagoudhera road and
3Vyzakia/Kannavia road
21227a35400
3start of coastline is in brecciated dyke (frags in place) cm = pillow frag
1 00100.60cm335551.2511a cst001
1 00201.10jc040841.4011a pstf j.s.
1 00301.40cm334503.002-c pst001
1 00401.30jc164890.8811a pst001
1 00502.00jc321611.9511c0 1pst001
1 00602.20jc330151.4002c0 1pst001
1 00702.30cm332463.002-b0 1pst001rust stain
1 00803.00jc125440.5802a pstf j.s.
1 00903.10jc312701.2802a pst001
1 01003.30jc318404.502-c pst001
1 01103.30jc029664.002-c pst001
1 01203.10jc226510.8002a pstf j.s.
1 01303.50jc242711.5510a pstf j.s.
1 01403.90cm315405.002-c prgn001
3entering shear breccia zone of dyke rubble and pillows=highly frag screen
1 01504.40fc047891.8511a crgn008cpen
3pillow margins visible;minor calcite and weathered pyrite
3end of line a photo 12-27 start of line b photo 12-28
21228b35400
1 01606.30jc134732.7011a prgn001
1 01705.75jc001760.5002a prgn003pillow margin filled with
3pillow rubble sand to pebble sized
1 01806.20jc055701.7511a crgn001
1 01907.60jc032781.1511a crgn001
1 02008.50jc349481.0002c0 2prp001h=rust
3end of line b photo 12-28 start of line c photo 12-29
21228c35400
1 02108.90jc309534.002-c prp001
1 02209.30jc245710.6802a prpf j.s.
1 02309.50jc145540.6501a prp001
1 02409.55jc309680.8202c0 1prpf j.s.
1 02509.60jc229661.8002c0 1prpf j.s.
1 02609.60jc308551.902-c0 1prp001
1 02709.80jc308501.002-c0 1prpf j.s.
1 02809.85jc066820.7511a crpf j.s.
1 02910.70fc212890.8511a pst001
1 03011.10jc280352.2002c0 1cstf j.s.
1 03111.25fc197801.3002a cst002cpen
1 03211.50jc264510.5502a pstf silicmarbles 348/07 j.s.
1 03311.75jc318520.5002c0 4pstf j.s.
3end of line c photo 12-28 start of line d photo 12-29
21230d35900
1 03411.80jc322592.8010a prp001
1 03511.90jc309513.0011a crp001
1 03612.40jc310600.7011a pstf j.s.
1 03712.60jc186890.7502a pst002cpen
1 03812.90jc306801.1011a pst001
1 03911.90cm034393.0011a cst001
1 04013.40jc309690.5511a pst001
1 04113.75jc289780.4511c6 p4 3pstf j.s.
1 04214.80fc288730.6002a pstf j.s.
1 04314.60cm035420.8511a cstf j.s.
1 04415.10cm314664.0011p6 d4 2prp001silicmarbles 237/24 j.s.
3this may be a faulted contact hard to tell no offset indicators d=calcdranite
3end of line d photo 13-29 start of line e photo 13-31
21230e35900
1 04516.60jc281691.6011p0 1prpf j.s.
1 04616.65jc292700.5502c0 8pstf j.s.
1 04716.75jc292640.7202a pstf j.s.
1 04816.80jc199690.8802a pstf j.s.
1 04916.30cm300672.8002a pst001silicmarbles 211/02
3fracture #49 is not on the photo
1 05017.90jc280503.1011a prpf silicmarbles 007/04 j.s.
1 05118.90jc314840.7010a prp001
3entering zone of pillow rubble leached grey on the surface up to 19.30m
1 05219.70jc336830.7002a prp001
1 05319.80jc338850.6002a prp001
1 05419.85jc324781.2011a prp001
1 05520.30jc331752.1011a prp001
1 05620.60jc150672.7511a prp001
3end of line e photo 12-30 start of vertical section 12-27 crosses zone
3line at 3.85 (fault is crossed at 1.60m)
21227v25270
1 05700.27jc213080.6002a pst002cpen
1 01100.50
1 01000.72
1 05801.20jc149390.6002a pst001
1 01401.65
3end of section 12-27 to 12-30. D.A.v.E.24-10-89
3start of page 40 photos 1305 to 1307 section 7.4km south of Xylistos
21305a25204
1 00100.00jc072594.0010a prdc001
1 00200.80cm069616.002-c prdc001
1 00304.90jc001760.9511c0 5prdc j.s.
1 00402.00fc160443.502-c0 0prdc002
1 00503.80cm065676.002-c62c41 8prdc002
1 00604.30cm070576.002-c prd001
1 00705.10jc070551.0002a prd001
1 00805.50cm040576.002-c6 c4 1prd001
1 00905.85cm056705.0011c0 1prd001
1 01006.10fc052503.1011a prd001
1 01107.10fc073561.1011c0 8prd001
3end of line a photo 13-06 start of line b photo 1306
21306b25204
1 01207.20cm051563.0811a prd001
1 01308.20cm032576.002-c prd001
1 01408.00jc039592.7011a cst001
1 01508.70jc052594.5011a prd001
1 01609.10jc057572.002-c prd050small dyke
1 01709.45jc048883.8011a prd001
1 01809.55jc045693.8011a prd001
1 01909.90jc044703.7002a prd001
1 02010.15cm082923.0011a prd001
1 02111.00jc055572.1010c0 8prd001
1 02211.45jc043554.5011a prd001
1 02311.80cm062623.8010a prd003small dyke
1 02412.05jc036800.6511c0 1prdm001
1 02512.70cm043475.002-c prd001small dyke
1 02613.25cm055563.8011c0 1prd001
1 02713.50cm057623.8011a prd001
1 02813.65cm059682.5011a cst001
1 02913.85cm051494.0011c0 1cst001
1 03014.00cm053925.1011a prd001
1 03114.85cm057579.502-c cst001s=stopped
1 03215.25cm069585.502-c prd001
3end of line b photo 13-06 start of line c photo 13-06 vertical section
21306v15556
1 03000.00
1 03300.30jc312660.8502a prdm j.s.
1 03400.50jc172700.8002a prdm j.s.
1 03500.90jc341630.8002a prdm j.s.
1 03601.20jc168730.8002a prdm j.s.
1 03701.50jc288450.7502a prdm j.s.
1 03101.80
3end of section. 25-10-89. D.A.v.E.
3start of page 38. Section 1307-1309 5.3km south of Xylistos
21307a24000
1 00100.00jc076701.111c0 0cist002348/12
1 00200.00fc076390.7511c0 0prd001

1 00300.25j306830.4002e0 0pxd001
3d003 is older than d002 (c cuts e)
1 00400.50j112621.0011e0 e2 7pkd100107.405
1 00500.656049695.002-e6 e4 6pxd002
1 00600.90j041523.202-e0 7pxd002
1 00701.60mJ15909.002-e2 e2 8pxd010
1 00801.90j116343.002-e pxd002open
1 00902.50j297541.1511e pxd001
1 01002.90j315670.3502e pxd001
1 01102.90j000990.3502e pxd001
1 01203.65j023821.5011e0 5pxd001zone of epidotization in
3rock parallel to joint about 20cm thick
1 01304.70j186852.1511e0 2pxdf j.s.
1 01404.75mJ03303.002-e6 e3 z1 8pxd010
1 01505.906119451.3011e0 7chlf 025/06 j.s.
3slick. measurement taken in direction of downstep
1 01606.05j087530.9502e pxdf j.s.
1 01706.65j083424.002-e0 6phlf 022/24 j.s.
1 01807.00j076471.4002e0 6phlf 003/16 j.s.
1 01907.70m070473.5010e0 e2 6pxd100
3zone of intense brecciation and epidotization which passes out into
3competent dyke;there is a small dyke intruding about .3m wide very epidot-
3ized and broken up.
1 02008.65m094312.9010e0 7phlf 032/16 j.s.
1 02109.15j052661.1511e0 6pxd001
1 02209.55j058461.1011h0 9phlf 342/29 j.s. h=
3rust
1 02309.65j070590.9002e0 9pxd030
3end of line a photo 13-07 start of line b photo 13-08
21308d03002
1 02410.80m083372.2011e7 e3 7pxd001
1 02511.60m016415.0010e6 e5 5pxd002
1 02610.65j194691.3411e pxdf j.s.
1 02711.75m048500.4002e pxd001
3series of small dykes. epidotized in .25m wide zone
1 02812.30j051493.0002e0 1pxd001
1 02912.55j061491.2202e61e32 4pkd002346/16
1 03012.95j353851.0002e pxdf j.s.
1 03113.25m024405.002-e pxd001
3locally there are blobs of epidote in rock sometimes mixed w/ qtz SAMPLE
1 03213.70j072410.8502e9 z1 7pxd002
1 03314.20j140701.0002e0 7pxdf c<1mm j.s.
3end of line b photo 13-08 start of line c photo 13-09
21308e04504
1 03414.60m016474.2011e pxd001
1 03515.15m080683.502-e0 7pxd005
1 03615.60j084691.7511e0 8pxd004
3calcite stain grew out into fracture - fracture was open at time of pptn
1 03716.10j090822.3011e0 6phlf 004/06 j.s.
3slick measurements taken in downstep direction
1 03817.25j100470.6011e pxdf j.s.
1 03915.60j145410.7002e pxdf j.s.
1 04018.50j077342.1011e0 2pxdf j.s.
1 04119.90m018273.502-e pxdf j.s.
1 04220.40j150571.602-e pxdf j.s.
1 04320.80j155581.602-e pxdf j.s.
1 04420.60j064801.602-e pxdf j.s.
3beyond this the dykes are too fractured to get measurements
3end of line c photo 13-09 start of line d photo 13-09. vertical section
21309e34060
1 03100.00
1 04300.45j031501.0002e0 5pxd001
1 02800.80
1 04401.25j117331.1002e0 3pxdf j.s.
1 04700.85j345800.8002e pxd001
1 02301.45
1 04802.85j166701.3011e pxdf j.s.
3end of section. 25-10-89. D.A.v.E.
3section 13-10 to 13-15 along Xylotex- Lagoudhera highway
21310e03900
1 00100.606051633.8010e0 9pxp005
1 00201.20j144784.002-e pxpf j.s.
1 00301.90j028563.0011e9 h1 6pxp002
1 00403.40j032713.1010e pxp001
1 00503.60j037713.0011e9 h1 3pxp001
1 00605.35j213092.6011e urp001
1 00706.00j121552.2011e pxpf j.s.
1 00807.10j045482.8013e9 e1 3pxp003
1 00908.50j030591.0511e0 8pxp002
1 01008.70j088880.8202e urpx j.s.
3end of line a photo 13-10 start of line b photo 13-11
21311b03900
1 01113.10j048805.0011e0 2pxp002
1 01213.30j041754.0011e0 2pxp002
3in intensely rubbled zone of pillow frags sp. only along margins of zone
1 01314.15j031851.0302e pxp001
1 01414.80j030672.2011h0 1pxp001
1 01515.20j278880.8301e pxp001
1 01615.40j268820.6801e pxp001
1 01715.90j082521O.02-e6 e1 h1 7pxp050
3rubble (fault?) zone
1 01817.206094510.02-e7 e2 h1 7pxp400
3epidotized fragments; anstomosing veins of rubble (clay) most epidote is in
3fragments not in interstices
1 01918.20j066303.011e0 9pxp005
3end of line b photo 13-11 start of line c photo 13-12 #18 &#19 on this ?
21312e03900
1 02018.30m081609.02-e0 3pxd001
1 02119.10m079810O.02-e0 3pxp001
3zone of highly fractured epidotic dyke banded over 5cm intervals
1 02220.50j080150.7002e pxp001pillowed
3end of line c photo 13-12 start of line d photo 13-13
21313d03900
1 02321.60j260892.0511e pxp001
1 02422.10m066754.0011e0 7pxd005silicksmicides 342/19
3into another epidotic dyke
1 02522.45j079712.202-e pxdm001
3margin to epidotic to south is not margin to north is epidotic6
1 02623.37j032792.3010e0 0pxdm010
1 02723.70j079701.5511e pxdm001
1 02824.15j073743.0011e pxdm001
1 02924.90m078651.352-e0 7pxp005
1 03025.50j073714.5011e pxp001
3zone pillow grain size is fine but the frags are pebble to cobble sized
3#030 is part of large shear or fault
1 03126.75j060565.0011e pxdm001
1 03227.60j050510.02-e pxp001
3bA 031 and 032 epidotized dyke block is caught between shears. hanging wall
3is not epidotized but footwall is heavily epidotized to fracture #017
1 03329.20j081804.0011e pxpm001
1 03429.55j080853.5011e pxpm001
3pillow/dyke contacts are chilled to dyke (normal)
3most fractures in gap bA 13-13 and 13-14 gap=1.20m
1 03500.00j278830.6002e0 8pxpf slickensides 008/00 j.s.
21314e04600
1 03604.50j199892.2011e pxp005open
1 03706.90m055402.0011q5 e5 2pxp003
1 03807.806044661.1002e pxd001SAMPLE
3zone of 6 parallel fractures about 1cm apart
1 03908.50j035822.1001e0 0pxd001
1 04008.90j071711.1002e0 1pxd001
3dyke highly fractured there are two prominent fractures (039 & 040)
3calcite crosses epidote fractures therefore calcite is late
1 04109.05j008873.2011e pxd001
1 04209.15j034820.8002e pxd001
1 04309.60j272750.3002e pxd001
1 04410.10j184891.7211e0 2pxdf j.s. e<1mm
1 04510.55m065673.202-e undf001
1 04610.70m042361.0002e0 3undf001
1 04710.85m061582.1002e undf001
3the last three contacts are all chilled one very fine slivers of dykes faulted
1 04811.50m071342.5002e undf j.s.
3end of line e photo 13-14 start of line f photo 13-15 at 16.40m of scanline
21315f03060
1 04900.45j266650.5002e pxdm001
1 05000.65j287580.3001e pxdm001
1 05101.00j298591.0902e pxdm001
1 05201.10j015810.02-e0 8pxdm005
1 05301.50j260300.5502e pxdm001
1 05401.70j255530.5602e pxdm001
3end of section 13-10 to 13-15 at 2.0m
324-10-89. D.A.v.E.
3section up road 300m from CY-4 toward Agros (13-16 to 13-20 start at 0.5m
21316a30408
1 00102.80j028813.0002e0 2pxdm j.s.
1 00200.50j040461.3000e undf003small dark grey dyke1et
1 00301.50j340761.3001e0 5pxdm001
1 00401.45j264500.4501e0 7pxdm001
1 00502.00j323671.1001e0 8pxdm002
1 00602.25j135670.9300e0 7pxdm001
1 00702.60j118640.9802e0 4pxdm001
1 00802.10j268461.0010e0 6pxdm002
1 00902.40j159861.5502e0 8pxdm001
1 01002.85m329702.2011e pxd001small branch dyke1et
1 01102.95m330675.002-e pxd001
1 01200.50j153710.8502e pxd001
1 01300.35j300640.8002e pxd001
1 01403.85j297580.4003e0 9pxd003
1 01504.25j136554.002-e0 8pxd004SAMPLE
3from 3.95m to 5.95m dyke highly fractured veining (calcite) parallel

3no margins. sheeted look. 1 or 2 patches v rare epidote.
1 01404.656/086700.7002e0 8pedi002
1 01704.806/310992.2000e0 0pedi002
1 01805.00m331680.9010n pedi001
1 01904.956/352800.8500e0 0pedi001
1 02005.40m317702.5002e0 1ped1001
1 02105.80m330738.002-e0 2pedm001
1 02206.10m340848.003-e pedm001
3end of line a photo 13-16 start of line b photo 13-17
21317b29507
3new gap in photos between 6.40m and 8.40m following 4 fractures in gap no
3not on photos
1 02306.40m322772.6010n pedi030small dyklet
1 02407.256/322800.6000n pedm001
1 02507.30j326675.0000e0 6pedm002
1 02607.90m330676.5000n pedi020small dyklet
3the rest of the fractures are on the photo
1 02708.50j200714.7011n pedm j.s.
1 02809.006/308801.1310e0 5pedm002
1 02909.10j317781.5710e0 2pedm002very patchy
1 03009.27m327661.360-e0 1pedi005leached dyke like area of
3same material as host dyke
1 03110.30j020522.0002n pedm001
1 03211.106/301850.5511n pedm001
1 03311.506/102870.6611n pedm001
1 03411.506/168890.6011n pedm001
1 03511.706/341760.9810e0 8pedm002
1 03611.80m311724.0011e0 4pedc004sp.vein along contact
1 03712.00j328663.502-e0 6pedi010
1 03812.30j340733.002-e0 5pedi020quite variable width 0-60mm
1 03912.40m324663.002-e0 2pedm002
1 04012.60j123433.9010e0 7pedm002
1 04111.40j210395.0002n pedm j.s.
1 04212.60j228360.5002n pedm j.s.
1 04312.70j325641.4010e0 2pedm001
1 04413.00j342813.1010e0 5pedm001leached zone around fracture
1 04513.20m336644.002-e6 e4 5pedm010calc mined (.1 to 3 cm wide)
1 04613.40m319761.3011e0 4pedm001
3white dyke in this area highly fractured - probably due to intrusion
3of dyke. sp. vein freq. increases near dykes. calcite veins cross cut - later
313.40m is anastamozing calcite veins
1 04713.80m325693.002-e0 3pedm002
1 04814.10m332603.002-e0 5pedm002
1 04914.30m336710.7011n pedm001
3end of line b photo 13-17 start of line c photo 13-18
21318c29504
1 05014.406/339653.0011e0 0pedm001
1 05114.456/343603.0011e0 0pedm001
1 05214.506/335602.2011e0 0pedm001
1 05314.90m322995.202-e6 e4 1pedm001
1 05415.20j021871.7002n pedm001
1 05516.256/324691.4011e0 2pedm001
1 05616.55j142852.0010e0 7pedm001
1 05716.60j342891.0010e0 7pedm001
1 05816.50j354251.9002n pedm001
1 05916.80j323191.7511e0 7pedm0031-2mm sp. halo
1 06017.20j179851.2011n pedm001
1 06117.85m144783.502-e0 8pedm003
3to 18.65m zone of very fractured dyke - many 1/5cm anastamozing calcite veins
3to 1cm wide most 1-3mm. dyke fine to med gr. dark grey green weather light
3 some rare epidote mixed in with calcite
1 06218.65m326775.502-e9 e1 7pedm003
1 06319.106/281751.8811e0 0pedm004
1 06419.60j045710.7502n
1 06519.70j144702.9002e0 6pedm001
1 06620.05m314603.002-e pedm001small dyklet 5cm long
3end of line c photo 13-18 start of line d photo 13.19
21319d29201
1 06720.20j307719.502-e0 8pedm003
1 06820.406/326630.6002e0 8pedm002
1 06920.90m320601.3011e0 5pedm001
1 07021.156/323590.5501e0 5pedm002
1 07121.256/281830.7002e0 6pedm002
1 07221.406/327652.5011e0 6pedm002
1 07321.506/263450.6011e0 8pedm003
1 07421.85m282811.0511n pedi010small dyklet
1 07522.006/095801.0001e0 6pedm002
1 07622.20j216830.6502n pedm j.s.
1 07722.60m310603.002-e0 pedm002
1 07823.25m289783.002-e0 6pedi002
1 07923.30j042700.8002n pedm j.s.
1 08022.90j306581.9011e0 7pedm002
1 08123.556/293821.6011e0 8pedm001
1 08223.956/254813.002-e6 e2 8pedm060 rubble zone
1 08324.306/287701.4011e0 0pedm002
1 08434.406/280711.3511e0 0pedm002
1 08534.506/270891.4511e0 0pedm002
1 08634.656/296771.3511e0 0pedm002
1 08734.706/282702.3011e0 8pedm002
1 08834.856/280851.2011e0 7pedm002
1 08925.006/287825.0011e0 8pedm002
1 09025.10j030542.0002e0 7pedm002
1 09125.156/270803.502-e0 8pedm002
1 09225.306/091743.502-e0 6pedm002
1 09325.80m301703.502-e0 8pedm003
1 09426.206/090892.902-e6 e4 8pedm040offset along contact (d093)
3by 5cm. hanging wall is downthrown
1 09526.60m315704.502-e pedi003open
3ends of line d photo 13-19 start of line e photo 13-20
21320e29201
1 09626.80m316754.202-e0 3pedm008
1 09727.506/289791.1011e0 5pedm003
1 09827.70j334621.9011n pedm001
1 09928.10j317754.302-e0 0pedi030rubble dyke zone
1 10029.10j320712.0011n pedm001
1 10129.406/330641.9511e0 8pedm006
1 10229.906/095580.7511e0 8pedm002
3end of line e photo 13-20 start of vertical line f photo 13-17
21317e04649
1 10300.00j222812.6511n pedm001
1 03400.85
1 10400.80j219882.8002n pedm001
1 10500.556/049551.0502n mdm001
1 04001.20
1 10601.45j053350.3502n pedm001
3end of section. 18-10-89. D.A.v.E.
3section south of the mine of old Apilil village photos 13-21 to 13-27
21321a35101
1 00100.00j058791.3011n pedm j.s. e stain on rx
1 00200.60j119741.1502e0 9pedm002
1 00300.00j162540.9511e0 7pedm004
1 00400.70j120760.9011e0 4pedm001
1 00501.30m128784.002-e pedi001dyke=clay v.f. lite blue gr
1 00601.40m153664.002-e pedi001
1 00701.30j171712.3010n pedm001
1 00801.90j134743.802-e0 4pedm030patchy e to 4cm thick
1 00901.95m141864.002-e pedi001
1 01001.95j144511.2202n pedm j.s.
1 01102.30j104871.1011e0 6pedc005
1 01202.60j120860.8002e0 1pedi001
1 01302.90j153441.9011e0 e1 7pedi003
1 01402.92m153464.502-e0 1pedi001
1 01503.10j028290.5502n pedm001
1 01603.60j172560.4002e0 9pedm001
1 01703.90e164700.3502n vedm001
1 01803.80j072700.5002e0 3pedm e<1mmj.s.
1 01904.05j155602.2002e9 p1 8pedm003silicimmiden 107/49 hanging
3wall moved down.epidosite band to 4.45m
1 02004.20j151630.4002n pedm j.s.
1 02104.45m328546.002-e0 5pedm003
1 02204.456/328830.6011e0 0medi002with 1 cm halo
3new epidosite dyke. end of line 1 photo 13-21 start of line b photo 13-22
21322b35104
1 02304.75j160800.7011e0 0pedm002
1 02405.20j144711.2511e0 0pedm004
1 02505.40j295341.1502e0 0pedm001
1 02605.75j161554.0011e0 0pedm004silicimmiden 103/38
1 02705.60j308821.5002e0 6pedm002
1 02805.90j264881.9511e0 1medm002j.s.
1 02906.45m148406.002-e9 p1 9pedc020
1 03006.70e158310.3501n pedi001
1 03106.96e168870.5510e0 8pedc001epidosite band to 8.00
1 03207.10e333341.1002n pedi001
1 03307.80m134562.1011n pedi001
1 03408.10m135546.002-e pedi001
1 03508.40m132506.002-e pedi001
1 03608.70m122546.002-e pedi001
1 03708.40e163651.7511e9 q1 8pedm001v.minor qtz
1 03808.75e139841.0010e0 7pedm003 w/ 50mm halo
1 03909.55m186455.002-e pedm001
1 04009.40j260760.5502n pedm j.s.
3end of line b photo 13-22 start of line c photo 13-23
21323c33908
1 04110.15m130708.0002e9 e1 7pedm002
1 04209.75m146992.2011n pedm001
1 04309.90m150602.2011n pedm001
1 04410.30j146990.2011e9 e1 8pedm003
1 04510.95m132666.002-e pedi001
1 04611.30m134656.002-e pedi001
1 04711.40m138643.3011n pedi001

```
1       04811.50m196699.2010a       unit001dyke/sist 6cm wide
1       04911.90m012841.1011a       unit001dyke v.dark black w/ minor
3 epidote veins no fracture fill minerals
1       05012.55m142761.1011a       unit001 as 0049
3end of line c photo 13-25 start of line d photo 13-24
21324/32906
1       05112.95m135793.2011e0      3pmt020possibly calcite as well
3v.minor calcite. SAMPLE
1       05212.55m152843.2011e0      3pmt020epidosite band
1       05313.15ft172701.2011e0     3pmt005
1       05413.30m146406.002-a       pmt001
1       05513.85m140644.2011a       pmt001late unmineralized dyke
1       05613.95m146704.2011a       pmt001
1       05714.05m148661.2011a       pmt001small short late dyke
1       05814.75m152616.002-e0      3pmt002mnr.vein=5mm
1       05914.90N331683.1011e91e1   3pmt0036mlt offset=normal 2cm
3along 252/21
1       06015.00j280370.6002a       pmtn001
1       06115.30j012891.1511e0      3pmtn  j.s.;e=1mm
1       06215.45m152646.0021e0      3pmtn0036dyke contains pyr phases
3SAMPLE
1       06316.00m13830
3epidote veins have 2mm halos
3end of line c photo 13-24 start of line d photo 13-25
21325s33706
1       06416.40j030840.5002a       pmtn  j.s.
1       06516.50m192831.9011a       pmtn001
1       06617.40m129891.7011e0      4pmtn001
1       06717.50ft132852.4010e9  e1 3pmtn0023SAMPLE
1       06817.80j135631.0011e0      3pmtn001
1       06917.95m133436.002-e0      1pmtn001small dyklet 2cm wide
1       07018.00j202830.6302a       pmtn001main dyke weathers spheroidally
1       07118.50m126872.5011e91e1   4pmtn004small dyklet 2cm wide
1       07219.10m126641.7511e9  e1  4pmtn002
1       07318.90ft130791.1011e0     3pmtn001
1       07419.50m167877.002-a       unit001
1       07520.20m328637.002-a       unit001
1       07620.20m327807.002-e8  z2  3pmt030clay=dyke gouge
3end of line e photo 13-25 start of line f photo 13-26
21326/33209
1       07720.40j144553.5011e0      2pmtn002
1       07820.55j305890.9511e0      3pmtn020
1       07920.80j174650.9311a       pmtn001
1       08021.00j308801.8011e0      5pmtn015
1       08121.05m143521.9011e0      5pmt006
1       08221.75j323790.7511e0      1pmt001
1       08322.10j140692.0511e0      2pmtn001
1       08422.25ft318461.0505e0     3pmtn002
1       08522.70ft143531.8505e0     3pmtn001
1       08623.05m142681.3011a       unit001
1       08723.21ft139832.5011e0     9pmtn002
1       08823.50ft140673.0011e8  e2 3pmtn002complicated dyke relations
3very white dyke intrudes epidote cross cuts them =pisgiogranite? SAMPLE
1       08923.70m134891.5010a       unit001white dyke
1       09024.20m164791.0010a
1       09124.30j158751.4010e0      3pmt005
1       09224.60j111831.9011e0      4pmtn005
1       09324.85j142803.1011e81e22  7pmtn010
1       09424.80j161772.6013e0      7pmtn005
1       09525.00m164714.2011a       pmtn001
3end of line e photo 13-26 start of line g photo 13-27
21327g32402
1       09625.70m174708.003-a       pmtn001
1       09726.80j022311.8002a       pmtn  j.s.
1       09826.95ft281821.7010a      unkn001
1       09927.90m164903.402-a       cmtn001open
1       10028.40j180571.5011a       pmtn001
1       10129.10j286800.6911a       pmtn004
1       10229.30m302861.3511e0      3pmtn005
1       10329.50m114871.2011e8  e2  7pmtn001
1       10428.45m165382.0002a       pmtn001
1       10529.30m182551.0011a       pmtn001
3end of line g photo 13-27 start of line h photo 13-25
3vertical section cuts horizontal section at 16.55m
21325v06082
1       10530.40ft128800.5001e0     0pmtn002
1       10700.70j354310.4302a       pmtn001
1       10800.80j271820.7302a       pmtn  j.s.
1       06500.90
3end of section. 17-10-89 D.A.v.H.20303b15004


1       00100.80j105821.7011a       pmt0.1phaneso structure - photo
1       00200.00j182892.5011a       pmt0.1cms 1 pillow steps
3at margin of pillow
1       00300.00pl    1.002-a  p    cry0005cms in fracture but
3plenty of pyrite on surface and vesicle filling epidote
3average size of pillows 1m long diameter smooth rounded ellipsoidal
3vesicles filled with pyrite and epidote SAMPLE
1       00401.20ft133612.0011a      pmt0.1crosses dyke and pillow
1       00500.21j003873.002-a       pmt0.1crosses dyke and pillow
1       00604.40m267430.02-c  e p  pmt006chilled margin
3dykes show chilled margins against the pillows seem highly pyritic
3intrusive material is included in the dykes therefore dykes intrude
3the pillow
1       00703.406/263803.0013a      pmt0.1
1       00804.20j120661.1013a       pmt001
1       00904.25j101691.3513a       pmt001
1       01004.80m260855.002-a       pmt001borders pillow rubble
3seems filled with pyrite SAMPLE
1       01104.00j092742.002-h       pmt002hematite
3may join onto 000 cannot tell for sure it does cross 010 and cuts
3both pillow and dyke
1       01206.00m083846.002-e  h    pmt020contact to pillow
3pillows are an included block in the dyke
1       01307.00ft096767.002-e  p r  pmt100widens to 50cm
3is a shear zone examining platy particles~0.5mm thick and rounded
3pebbles(diam=1cm) contains pyrite and epidote
3end of line b at 07.50m line c photo 0301 starts 40m 163 deg and  20108s14100

1       00100.106/313754.102-e      unkn010
1       00200.556r177634.002-e      unkn010
1       00301.50ft135585.002-e  e   cmtn050to 001mm highly fractured
1       00401.78ft001731.2002a      pmtn001open
1       00502.106/298753.0011e      pmtn010
1       00602.206r165412.4002a      pmtn001v. minor z
1       00702.57ft156602.8002a  z   pmtn003
1       00803.056r170463.0002a      pmtn002open on places
1       00901.90j226561.3511a       pmtn  dyke joint surface
1       01002.845r341441.4502a  e   pmtn001minor e and z
1       01105.50j230850.303-a       pmtn
1       01205.70j323500.6001a       pmtn
1       01309.37m112722.5010a       pmt005small dyke (margin)
1       01403.35m126672.5010a       pmt002no 013
1       01503.945r345751.0002a  h   pmtn010minor h and h
1       01604.506/305645.503-e      pmtn002minor e in rubble
1       01704.36m119505.003-e       pmt005patchy e
1       01804.50m110545.003-e       pmt003patchy e
1       01905.32m133664.002-e  z    pmt002widens at bottom to 10cm
3wide rubble zone infilled with epidote and sulfate (weathering) coming
1       02005.336/006352.6511a      unkn0.516cm wide zone
1       02106.066/298895.503-e  e   pmtn005open fracture zone
3rubble infill zones? and questionable epidote
1       02207.42ft131905.502-e      pmtn006
1       02307.906r300401.7011a  e   cmtn004e cm r z cm and in e
1       02408.51m127823.5002a       pmt001truncated by fracture
1       02508.62m114603.5002a       pmt002
1       02609.40ft087845.502-a      pmtn0.1light
1       02709.506/045472.5010a      cmtn003minor z at west end
3end of sample line a at 9.50m
3end of the second file cyprus2.dat connects to cyprus3.dat
3start of file cyprus3.dat connects from file cyprus2.dat
3line b line 1.45m bearing 141 deg from line a photo 0108 (9.5m)
20109s14100
1       00100.30ft178271.6511a      pmtn001open
1       00200.50ft328815.503-a      pmtn001
1       00300.10j222752.802-e       cmtn  ribbed surface (dis???)
1       00401.54ft126474.302-a      unkn005open rubble
1       00502.106r317885.502-a  p e pmtn005
1       00602.346r318854.001-e  e   pmtn003
1       00702.806r117761.4011a      cmtn003open
1       00802.856r140700.8011a      cmtn002open
1       00902.976r110872.5011a      cmtn001open
1       01003.056r115681.1011a      cmtn0.1tight
1       01103.30j018640.8002a       pmtn0.1cooling joint
1       01203.40j280403.7502a       pmtn0.1cooling joint
3where is fracture 013 ??
1       01403.92m118815.502-e       pmtn010
1       01504.06m120755.502-e  z    pmtn005
1       01604.25ft109841.1511e      unkn002
1       01704.50ft120731.7011e      unkn002
1       01804.40m119665.0011e       unt001
1       01904.91m132625.0011e       unt006contact to rubble
3zone goes until 020 filled with rounded dyke rubble e p hematite sulfate
3cm surface
1       02005.70m116705.502-e       unt002
1       02106.10m114712.4511e  z    pmtn005minor z
1       02206.206/307735.002-e  z   cmtn005
1       02306.70ft125715.002-e  z   pmtn002
1       02406.80j295745.002-e       cmtn004
1       02507.036r113842.1011a      cmtn0.1
```

```
1       02608.00fr299875.002-e  x     urdm004
1       02708.50fr299301.3011n        crdm0.1
1       02809.40fr144122.0011e        crdm002
3end of line b at 10.00m on photo 0109 start line c at 10.00m
20110c14100
1       00110.55jt142444.5011e  u     prdm005u=clay?
1       00210.78fr312780.9502e        crdm002
1       00311.12fr121821.6002e  z     crdm005series of 3 fracture veins
1       00411.31jt183460.8511n        prdm
1       00512.20fr254785.002-z        prdm002open slickensides 344/02
1       00611.75fr150635.002-e        urdm0.5network veins
1       00712.51fr091655.502-e        prdm003
1       00812.27fr135851.7002e        crdm012
1       00912.75fr114895.502-z        urdm001patchy z at lower end
3in veins about 001mm wide
1       01013.06cm134845.502-e  r     prdm001zone r 20mm wide
1       01113.45jt237290.8011e        prdm0.5patchy surface cont of e
1       01214.35jt127900.5010n        prdf001open
1       01314.50cm313894.502-n        prdm0.1tight
1       01414.70fr184675.502-n        urdm0.5open
1       01514.35jt040621.552-e        prdm0.5
1       01614.90jt244341.652-r        prdm  v.patchy oxides
1       01714.80fr028842.002-e        urdm0.1numerous (9)
3hairline cracks continuous over width of (14.65 to 15.0) epidote
3filled parallel to dyke contact
3end of line c at 16.00m start line d at 0.00m (end of line c)
20111d14100
1       00100.21jt119701.4011e  x     prdm010x=clay
1       00200.70cm156445.0011e  p h   prdm007possible clays
1       00301.08fr152390.9002n        crdm001
1       00401.38fr152333.5011x        urdm010
1       00501.75fr143742.40  e x     urdm006
1       00602.55cm145704.502-e        urdm005start of series (9) SAMPLE
3epidote vein 1 to 5 mm wide between 006 and 007 (contact rubble to
3dyke which cross cuts shear zone)
1       00702.70cm145555.002-e  h     urdm001dyke to rubble
1       00802.83fr222821.252-e  h     crdm
1       00903.20fr229860.7011n        urdm001
1       01003.35fr158795.502-e        urdm001minor e
1       01104.10jt112542.1511e  x z   prdm045minor x and z
1       01204.85jt301851.5511e        prdm001
1       01305.47jt304892.5010e  x     prdm030001 to 030mm
1       01406.40jt052900.852-e        prdm
1       01506.30jt303906.402-e        urdm001to005
3some joint surfaces show plumose structures, joint surfaces show epidote
3veins throughout to 0.1m thick
1       01606.84jt127846.002-e  r     prdm005minor e (to 010)
1       01707.25jt107712.1011e  p     crdm002minor e and p
```

---- End of Scanline Fracture Measurements ----

The following pages present a tabulation of the number of occurrences of each of the values that each measured fracture characteristic can assume. The last page of the table presents the frequencies of occurrenceof various (including dyke contact frequency, fracture frequency, terminatioan mode ratio, and zeolite, epidote, chlorite, hematite calcite and unfilled (none) fracture frequecnies) fracture properties normalized to scanline length. These results are used in the construction of Figures 3.11, and 3.21 to 3.26.

Fracture Characteristics : Spilia - Politiko Area, Troodos Ophiolite, Cyprus

Scanline #	Scanline Length (m)	#	Fracture Type: joint	fracture	alteration zone	contact	vein	splay	fault zone	fault	#
0000	37.4	76	70	0	0	5	1	0	0	0	76
0102	31.5	88	21	48	0	18	0	0	1	0	88
0112	25.1	90	77	5	0	1	4	0	0	0	87
0122	148.2	291	196	34	11	16	14	9	9	1	290
0201	8.5	31	22	6	0	2	0	0	0	0	30
0213	30.4	117	71	11	0	32	0	0	2	0	116
0301	6.2	14	13	0	0	0	0	0	0	0	13
0302	19.3	47	38	7	0	2	0	0	0	0	47
0303	7	13	6	2	0	3	0	0	1	0	12
0304	6.2	14	12	2	0	0	0	0	0	0	14
0306	9.9	11	10	0	0	1	0	0	0	0	11
0307	6.6	21	17	1	0	0	0	0	0	1	19
0329	10	20	19	1	0	0	0	0	0	0	20
0401	31.3	68	34	5	0	28	1	0	0	0	68
0404	10.3	18	10	0	0	2	6	0	0	0	18
0413	30.6	59	36	7	0	16	0	0	0	0	59
0418	21.6	33	31	1	0	0	0	0	0	0	32
0428	67.6	195	149	18	0	18	6	2	2	0	195
0701	32.5	69	60	5	0	1	0	0	0	0	66
1001	31.6	93	54	3	0	29	0	0	0	0	86
1008	19.5	73	56	1	0	13	0	0	0	0	70
1017	22.7	67	53	5	0	7	0	0	0	0	65
1028	31.2	114	57	22	0	29	0	0	0	0	108
1037	30.9	96	72	1	0	23	0	0	0	0	96
1107	27.5	79	52	3	0	22	0	0	0	0	77
1111	32.5	121	78	16	0	26	0	0	0	0	120
1124	25.6	96	72	10	0	8	0	0	0	0	90
1129	31.8	105	88	0	0	15	0	0	0	0	103
1134	32	68	44	0	0	19	0	0	0	0	63
1137	31.7	75	55	3	0	12	0	0	0	0	70
1204	48.4	94	66	3	0	21	0	0	0	0	90
1211	29.1	139	120	4	0	12	0	0	0	0	136
1218	31.9	104	70	16	0	15	0	0	0	0	101
1221	42.7	106	93	0	0	11	0	0	1	0	105
1222	31.1	94	71	15	0	7	0	0	0	0	93
1227	22.3	61	47	3	0	8	0	0	0	0	58
1305	17.1	39	17	3	0	17	0	0	0	0	37
1307	22.6	51	34	3	0	11	0	0	0	0	48
1310	42.8	54	39	1	0	9	0	0	2	0	51
1316	31.4	108	42	36	0	27	0	0	1	0	106
1321	30.2	109	43	16	0	48	0	0	0	0	107
Total (41)	1206.8	3221	2215	317	11	534	32	11	19	2	3141

Fracture Characteristics : Spilia - Politiko Area, Troodos Ophiolite, Cyprus

Scanline #	Fracture Length (m) 0-1	1-2	2-3	3-4	4-5	5-6	6-7	7-8	8-9	9-10	>10	#
0000	40	24	8	3	0	0	0	0	0	0	1	76
0108	11	18	16	6	8	27	2	0	0	0	0	88
0112	25	27	20	13	4	0	0	0	0	1	0	90
0122	39	102	54	50	25	8	5	2	1	5	0	291
0201	13	8	3	7	0	0	0	0	0	0	0	31
0213	22	33	14	11	36	1	0	0	0	0	0	117
0301	0	7	2	3	0	0	1	0	0	0	1	14
0302	11	23	12	1	0	0	0	0	0	0	0	47
0303	0	4	3	2	0	1	1	1	0	0	1	13
0304	3	2	3	1	0	0	0	5	0	0	0	14
0306	0	1	2	2	0	0	0	2	4	0	0	11
0307	0	4	2	3	4	3	5	0	0	0	0	21
0329	3	6	4	0	2	2	2	0	0	0	1	20
0401	4	14	5	3	9	13	20	0	0	0	0	68
0404	1	6	4	2	2	3	0	0	0	0	0	18
0413	4	13	5	11	2	5	6	13	0	0	0	59
0418	1	13	7	4	3	4	1	0	0	0	0	33
0428	29	77	38	19	10	3	3	0	2	1	13	195
0701	17	20	21	4	0	3	1	1	0	0	2	69
1001	27	23	16	9	7	11	0	0	0	0	0	93
1008	46	11	16	0	0	0	0	0	0	0	0	73
1017	41	18	4	1	0	1	1	0	0	0	1	67
1028	32	33	14	10	9	7	7	1	0	0	1	114
1037	23	35	15	23	0	0	0	0	0	0	0	96
1107	17	19	10	11	2	5	3	12	0	0	0	79
1111	33	37	25	21	1	2	0	2	0	0	0	121
1124	63	18	8	2	3	0	0	0	1	1	0	96
1129	32	24	13	12	3	7	2	3	4	1	4	105
1134	8	26	6	10	2	3	1	0	1	3	8	68
1137	30	18	11	4	1	4	2	0	4	0	1	75
1204	24	36	8	10	5	8	3	0	0	0	0	94
1211	49	47	16	8	4	11	3	0	1	0	0	139
1216	31	33	14	9	3	3	11	0	0	0	0	104
1221	29	39	13	5	13	5	2	0	0	0	0	106
1222	19	31	12	13	13	3	1	0	0	0	2	94
1227	23	17	6	5	4	1	0	0	0	0	0	61
1305	9	2	4	10	4	5	5	0	0	0	0	39
1307	14	19	5	9	2	2	0	0	0	0	0	51
1310	11	9	12	9	5	2	0	0	0	2	4	54
1316	26	31	14	23	7	2	1	0	2	0	0	106
1321	26	37	11	10	8	1	12	3	1	0	0	109
Total (41)	843	965	476	359	201	156	101	45	21	14	40	3221

Fracture Characteristics : Spilia - Politiko Area, Troodos Ophiolite, Cyprus

Scanline #	Censoring: 0	1	2	#	Termination: 0	1	2	3	4	5	#
0000	32	28	16	76	18	31	26	0	0	1	76
0108	16	33	39	88	46	28	14	0	0	0	88
0112	31	36	23	90	27	36	27	0	0	0	90
0122	50	111	130	291	146	105	34	5	1	0	291
0201	2	6	23	31	24	5	2	0	0	0	31
0213	40	37	40	117	51	39	25	2	0	0	117
0301	1	7	6	14	6	7	1	0	0	0	14
0302	5	15	27	47	29	11	6	1	0	0	47
0303	0	6	7	13	7	3	0	3	0	0	13
0304	3	4	7	14	7	5	2	0	0	0	14
0306	1	4	6	11	6	4	1	0	0	0	11
0307	1	8	12	21	16	5	0	0	0	0	21
0329	3	16	1	20	6	12	2	0	0	0	20
0401	4	21	43	68	44	23	1	0	0	0	68
0404	1	11	6	18	7	11	0	0	0	0	18
0413	12	28	19	59	23	28	9	1	0	0	59
0418	7	15	11	33	15	13	5	0	0	0	33
0428	47	104	44	195	55	96	38	4	2	0	195
0701	22	28	19	69	29	24	16	0	0	0	69
1001	31	19	43	93	55	19	18	1	0	0	93
1008	40	20	13	73	14	19	39	1	0	0	73
1017	45	16	6	67	7	18	42	0	0	0	67
1028	35	53	26	114	41	45	17	10	0	1	114
1037	47	27	22	96	23	26	47	0	0	0	96
1107	24	30	25	79	32	24	23	0	0	0	79
1111	59	33	29	121	37	33	51	0	0	0	121
1124	66	21	9	96	17	23	53	2	0	1	96
1129	26	56	23	105	27	55	23	0	0	0	105
1134	27	27	14	68	18	29	21	0	0	0	68
1137	30	32	13	75	19	30	26	0	0	0	75
1204	46	26	22	94	33	26	32	2	1	0	94
1211	53	58	28	139	34	62	40	1	0	2	139
1216	34	58	12	104	18	59	27	0	0	0	104
1221	50	34	22	106	23	36	47	0	0	0	106
1222	35	38	21	94	24	38	32	0	0	0	94
1227	27	26	8	61	14	24	23	0	0	0	61
1305	9	20	10	39	15	17	7	0	0	0	39
1307	19	20	12	51	18	17	16	0	0	0	51
1310	19	25	10	54	13	25	15	1	0	0	54
1316	37	45	26	108	47	39	22	0	0	0	108
1321	27	60	22	109	32	53	21	1	0	2	109
Total (41)	1064	1262	895	3221	1123	1201	851	35	4	7	3221

Fracture Characteristics : Spilia - Politiko Area, Troodos Ophiolite, Cyprus

Scanline #	Primary Mineral filling								#
	zeolite	epidote	chlorite	hematite	pyrite	clay	calcite	none	
0000	63	8	1	2	0	0	0	2	76
0108	11	51	1	0	0	1	0	22	88
0112	29	32	0	5	0	0	0	22	88
0122	145	62	18	12	0	0	0	52	290
0201	12	12	2	0	0	0	0	5	31
0213	3	18	0	0	0	1	24	68	116
0301	0	11	0	0	1	0	1	1	14
0302	1	26	0	11	0	0	0	9	47
0303	0	2	0	1	0	0	0	9	13
0304	0	6	0	0	1	0	0	7	14
0306	1	0	0	0	0	0	1	9	11
0307	0	6	1	3	0	0	1	9	21
0329	1	3	1	2	0	0	0	12	19
0401	7	37	0	2	2	0	0	19	68
0404	6	5	0	2	0	2	0	3	18
0413	0	42	0	1	5	0	0	11	59
0418	2	27	0	0	0	0	0	1	33
0428	125	23	1	2	0	0	0	43	195
0701	0	5	0	0	0	1	25	36	67
1001	7	0	0	0	0	1	0	78	86
1008	0	0	0	1	2	0	2	66	72
1017	0	6	0	0	0	3	1	51	66
1028	0	1	0	0	0	0	0	107	109
1037	0	35	1	0	0	0	1	57	94
1107	1	1	0	3	0	0	2	72	79
1111	4	14	0	2	0	0	4	91	115
1124	25	1	0	3	0	0	5	54	88
1129	0	16	0	0	0	0	37	50	103
1134	0	38	0	0	0	0	13	11	62
1137	0	29	0	0	2	1	1	38	71
1204	0	4	0	0	0	0	24	61	89
1211	5	0	0	0	0	0	3	128	136
1216	0	0	0	1	0	0	0	100	101
1221	0	9	0	9	0	0	0	87	105
1222	0	28	0	1	0	0	0	62	91
1227	0	0	0	2	2	0	10	44	58
1305	0	7	0	0	0	0	3	27	37
1307	0	7	0	1	0	0	20	18	48
1310	0	9	0	3	0	0	4	31	50
1316	0	21	0	0	0	0	50	33	106
1321	0	55	0	0	0	0	2	50	107
Total (41)	448	657	26	69	15	10	234	1656	3141

Fracture Characteristics : Spilia - Politiko Area, Troodos Ophiolite, Cyprus

Scanline #	Secondary Mineral filling								#
	zeolite	epidote	chlorite	hematite	pyrite	clay	calcite	none	
0000	5	10	0	0	0	0	0	0	16
0108	8	5	0	4	3	4	0	0	26
0112	2	5	1	12	0	0	0	0	20
0122	25	57	19	15	1	0	0	0	121
0201	3	3	0	0	0	0	0	0	6
0213	1	4	0	0	0	0	6	0	11
0301	0	0	1	0	4	0	2	0	9
0302	1	0	1	4	1	0	0	0	8
0303	0	1	0	1	2	0	0	0	4
0304	2	0	0	1	2	0	0	0	5
0306	0	0	0	0	0	0	0	0	0
0307	0	0	0	2	3	0	0	0	5
0329	1	1	1	1	3	0	0	0	7
0401	4	1	1	2	5	0	0	0	13
0404	1	1	0	1	0	1	0	0	4
0413	11	4	0	0	13	0	0	0	28
0418	2	2	0	2	1	0	0	0	9
0428	8	26	1	8	1	0	0	0	45
0701	0	1	0	0	0	0	4	0	6
1001	0	0	0	0	0	0	0	0	0
1008	0	0	0	0	0	0	0	0	0
1017	0	1	0	0	1	0	0	0	3
1028	0	0	0	0	0	0	0	0	0
1037	0	0	0	0	0	0	0	0	0
1107	0	1	0	0	0	0	0	0	1
1111	0	0	0	0	0	0	0	0	0
1124	1	2	0	1	0	0	0	0	4
1129	1	2	0	0	1	0	6	0	10
1134	0	5	0	1	2	0	16	0	24
1137	0	3	2	0	4	0	8	0	17
1204	0	0	0	0	0	0	0	0	0
1211	0	0	0	0	0	0	0	0	0
1216	0	0	0	0	0	0	0	0	0
1221	0	0	0	0	0	0	0	0	0
1222	0	1	0	0	0	0	0	0	1
1227	0	0	0	0	1	0	0	0	1
1305	0	1	0	0	0	0	1	0	2
1307	1	4	0	0	0	0	4	0	9
1310	0	4	0	2	0	0	0	0	6
1316	0	1	0	0	0	0	4	0	5
1321	3	1	0	0	2	1	6	0	13
Total (41)	80	147	27	57	50	6	57	0	439

Fracture Characteristics : Spilia - Politiko Area, Troodos Ophiolite, Cyprus

Scanline #	Tertiary Mineral filling								#
	zeolite	epidote	chlorite	hematite	pyrite	clay	calcite	none	
0000	0	0	0	0	0	0	0	0	0
0108	1	1	0	1	0	0	0	0	3
0112	0	2	2	4	0	0	0	0	8
0122	1	8	8	13	0	0	0	0	31
0201	0	0	0	0	0	0	0	0	0
0213	0	0	0	0	0	0	0	0	0
0301	0	0	1	0	2	0	0	0	3
0302	1	0	0	0	0	0	0	0	2
0303	0	0	0	0	1	0	0	0	2
0304	1	0	0	0	0	0	0	0	3
0306	0	0	0	0	0	0	0	0	0
0307	0	0	0	1	0	2	0	0	3
0329	0	1	0	0	0	0	0	0	4
0401	1	0	0	1	1	0	0	0	3
0404	0	1	0	1	0	0	0	0	2
0413	1	0	0	0	2	0	0	0	3
0418	0	1	0	0	1	0	0	0	2
0428	1	2	1	2	0	0	0	0	7
0701	0	0	0	0	0	0	0	0	0
1001	0	0	0	0	0	0	0	0	0
1008	0	0	0	0	0	0	0	0	0
1017	0	0	0	1	0	0	0	0	1
1028	0	0	0	0	0	0	0	0	0
1037	0	0	0	0	0	0	0	0	0
1107	0	0	0	0	0	0	0	0	0
1111	0	0	0	0	0	0	0	0	0
1124	0	0	0	0	0	0	0	0	0
1129	0	0	0	0	0	0	1	0	1
1134	0	1	0	0	4	0	1	0	6
1137	0	0	2	0	1	0	0	0	3
1204	0	0	0	0	0	0	0	0	0
1211	0	0	0	0	0	0	0	0	0
1216	0	0	0	0	0	0	0	0	0
1221	0	0	0	0	0	0	0	0	0
1222	0	0	0	0	0	0	0	0	0
1227	0	0	0	0	0	0	0	0	0
1305	0	0	0	0	0	0	0	0	0
1307	0	0	0	0	0	1	0	0	1
1310	0	0	0	2	0	0	0	0	2
1316	0	0	0	0	0	0	0	0	0
1321	0	0	0	0	0	0	0	0	0
Total (41)	7	17	14	26	12	3	2	0	90

Fracture Characteristics : Spilia - Politiko Area, Troodos Ophiolite, Cyprus

Scanline #	Small Scale Roughness			#	Large Scale Roughness				#
	rough	slickenside	smooth		stepped	curved	undulating	planer	
0000	76	0	0	76	0	2	4	69	75
0108	88	0	0	88	0	19	21	48	88
0112	87	0	1	88	0	3	3	80	86
0122	288	0	0	288	13	81	6	185	285
0201	31	0	0	31	0	4	1	25	30
0213	116	0	0	116	0	6	7	95	108
0301	14	0	0	14	0	0	0	14	14
0302	47	0	0	47	0	3	0	44	47
0303	13	0	0	13	0	1	0	12	13
0304	14	0	0	14	0	2	0	12	14
0306	11	0	0	11	0	2	0	9	11
0307	21	0	0	21	0	2	1	18	21
0329	19	0	0	19	0	1	3	15	19
0401	68	0	0	68	0	1	2	63	66
0404	18	0	0	18	0	5	0	11	16
0413	56	0	3	59	0	6	0	50	56
0418	33	0	0	33	0	4	0	29	33
0428	186	0	0	186	0	30	2	152	184
0701	60	7	0	67	0	1	0	66	67
1001	66	0	20	86	0	5	23	58	86
1008	72	0	0	72	0	15	2	55	72
1017	65	1	0	66	0	5	1	59	65
1028	51	0	57	108	0	5	11	92	108
1037	96	0	0	96	0	2	2	92	96
1107	73	2	3	78	1	6	2	69	78
1111	115	2	3	120	0	2	0	116	118
1124	90	0	1	91	0	1	3	85	89
1129	96	0	7	103	0	4	2	97	103
1134	34	0	30	64	0	4	1	59	64
1137	54	0	17	71	0	8	4	59	71
1204	89	0	1	90	0	3	5	82	90
1211	135	0	1	136	0	12	2	122	136
1216	101	0	0	101	0	5	4	92	101
1221	105	0	0	105	0	7	2	96	105
1222	93	0	0	93	0	4	1	88	93
1227	58	0	0	58	0	9	1	48	58
1305	36	0	1	37	1	3	0	33	37
1307	38	9	1	48	0	2	0	46	48
1310	50	0	4	54	0	1	5	48	54
1316	103	0	2	105	0	5	1	99	105
1321	105	0	1	106	0	10	6	90	106
Total (41)	2971	21	153	3145	15	291	128	2682	3116

Fracture Characteristics : Spilia - Politiko Area, Troodos Ophiolite, Cyprus

Scanline #	Rock Type					Grain Size			
	gabbro	plagiogr.	dyke	pillow lavas	#	fine	medium	coarse	#
0000	32	0	44	0	76	0	67	9	76
0108	0	0	88	0	88	11	77	0	88
0112	40	0	48	0	88	4	82	1	87
0122	208	61	19	0	288	9	140	123	272
0201	0	0	31	0	31	7	24	0	31
0213	0	0	116	0	116	25	73	18	116
0301	0	0	14	0	14	0	12	2	14
0302	0	0	47	0	47	4	43	0	47
0303	0	0	11	2	13	13	0	0	13
0304	0	0	14	0	14	3	11	0	14
0306	0	0	5	6	11	3	8	0	11
0307	0	0	0	21	21	0	21	0	21
0329	0	0	19	0	19	0	19	0	19
0401	0	0	68	0	68	14	54	0	68
0404	10	0	8	0	18	0	18	0	18
0413	0	0	59	0	59	7	51	1	59
0418	0	0	33	0	33	0	33	0	33
0428	17	0	169	0	186	10	133	0	143
0701	0	67	0	0	67	1	12	54	67
1001	0	0	74	12	86	7	78	1	86
1008	0	0	58	14	72	0	72	0	72
1017	0	0	66	0	66	2	64	0	66
1028	0	0	104	4	108	26	80	2	108
1037	0	0	96	0	96	17	75	4	96
1107	0	0	78	0	78	31	47	0	78
1111	14	0	106	0	120	38	77	5	120
1124	0	0	91	0	91	4	87	0	91
1129	0	0	103	0	103	13	90	0	103
1134	0	0	64	0	64	21	43	0	64
1137	0	0	67	4	71	9	62	0	71
1204	0	0	89	1	90	11	79	0	90
1211	0	0	136	0	136	5	131	0	136
1216	0	0	56	45	101	8	79	14	101
1221	73	0	32	0	105	23	48	34	105
1222	19	56	18	0	93	12	77	4	93
1227	0	0	32	26	58	52	6	0	58
1305	0	0	37	0	37	26	6	5	37
1307	0	0	48	0	48	48	0	0	48
1310	0	0	24	30	54	40	14	0	54
1316	0	0	105	0	105	21	83	1	105
1321	0	0	106	0	106	30	68	8	106
Total (41)	413	184	2383	165	3145	555	2244	286	3085

Fracture Characteristics : Spilia - Politiko Area, Troodos Ophiolite, Cyprus

Scanline #	Aperture (mm) 0	0-5	5-10	10-100	>100	#
	0	5	10	100		
0000	8	8	10	6	0	32
0108	8	8	23	11	0	50
0112	15	15	17	12	2	61
0122	92	92	36	60	8	288
0201	5	5	7	4	0	21
0213	9	9	2	8	2	30
0301	3	3	0	2	0	8
0302	10	10	2	6	0	28
0303	0	0	1	3	1	5
0304	2	2	0	0	3	7
0306	2	2	5	5	0	14
0307	11	11	2	2	0	26
0329	3	3	2	0	0	8
0401	5	[illegible]	6	12	0	28
0404	4	4	4	6	1	19
0413	5	5	4	5	0	19
0418	1	1	10	9	0	21
0428	51	51	16	8	0	126
0701	24	24	2	2	0	52
1001	30	30	2	1	0	63
1008	18	18	2	2	1	41
1017	28	28	1	3	1	61
1028	17	17	3	2	0	39
1037	27	27	0	3	0	57
1107	46	46	2	5	0	99
1111	38	38	2	2	1	81
1124	32	32	2	4	0	70
1129	21	21	7	6	0	55
1134	21	21	18	14	1	75
1137	38	38	4	1	0	81
1204	18	18	1	5	1	43
1211	34	34	1	0	0	69
1216	28	28	0	1	1	58
1221	26	26	0	1	0	53
1222	28	28	2	3	0	61
1227	24	24	1	0	0	49
1305	8	8	0	2	0	18
1307	23	23	3	4	1	54
1310	6	6	6	2	1	21
1316	9	9	6	9	0	33
1321	12	12	8	8	0	40
Total (41)	790	790	220	239	25	2064

Fracture Characteristics : Spilia - Politiko Area, Troodos Ophiolite, Cyprus

Scanline #	Combinations of Characteristics								
	contacts /metre	fracture frequency	term. mod 0/(1+2)	zeolite /metre	epidote /metre	chlorite /metre	hematite /metre	calcite /metre	none /metre
0000	0.13	2.03	0.32	1.82	0.48	0.03	0.05	0.00	0.05
0108	0.57	2.79	1.10	0.63	1.81	0.03	0.16	0.00	0.70
0112	0.04	3.59	0.43	1.24	1.55	0.12	0.84	0.00	0.68
0122	0.11	1.96	1.05	1.15	0.86	0.30	0.27	0.00	0.35
0201	0.24	3.65	3.43	1.76	1.76	0.24	0.00	0.00	0.59
0213	1.05	3.85	0.80	0.13	0.72	0.00	0.00	0.99	2.24
0301	0.00	2.26	0.75	0.00	1.77	0.32	0.00	0.48	0.16
0302	0.10	2.44	1.71	0.16	1.35	0.05	0.78	0.00	0.47
0303	0.43	1.86	2.33	0.00	0.43	0.00	0.29	0.00	1.29
0304	0.00	2.26	1.00	0.48	0.97	0.00	0.16	0.00	1.13
0306	0.10	1.11	1.20	0.10	0.00	0.00	0.00	0.10	0.91
0307	0.00	3.18	3.20	0.00	0.91	0.15	0.91	0.15	1.36
0329	0.00	2.00	0.43	0.20	0.50	0.20	0.30	0.00	1.20
0401	0.89	2.17	1.83	0.38	1.21	0.03	0.16	0.00	0.61
0404	0.19	1.75	0.64	0.68	0.68	0.00	0.39	0.00	0.29
0413	0.52	1.93	0.66	0.39	1.50	0.00	0.03	0.00	0.36
0418	0.00	1.53	0.83	0.19	1.39	0.00	0.09	0.00	0.05
0428	0.27	2.88	0.41	1.98	0.75	0.04	0.18	0.00	0.64
0701	0.03	2.12	0.73	0.00	0.18	0.00	0.00	0.89	1.11
1001	0.92	2.94	1.49	0.22	0.00	0.00	0.00	0.00	2.47
1008	0.67	3.74	0.24	0.00	0.00	0.00	0.05	0.10	3.38
1017	0.31	2.95	0.12	0.00	0.31	0.00	0.04	0.04	2.25
1028	0.93	3.65	0.66	0.00	0.03	0.00	0.00	0.00	3.43
1037	0.74	3.11	0.32	0.00	1.13	0.03	0.00	0.03	1.84
1107	0.80	2.87	0.68	0.04	0.07	0.00	0.11	0.07	2.62
1111	0.80	3.72	0.44	0.12	0.43	0.00	0.08	0.12	2.80
1124	0.31	3.75	0.22	1.02	0.12	0.00	0.16	0.20	2.11
1129	0.47	3.30	0.35	0.03	0.57	0.00	0.00	1.38	1.57
1134	0.59	2.13	0.36	0.00	1.38	0.00	0.03	0.94	0.34
1137	0.38	2.37	0.34	0.00	1.01	0.13	0.00	0.28	1.20
1204	0.43	1.94	0.57	0.00	0.08	0.00	0.00	0.50	1.26
1211	0.41	4.78	0.33	0.17	0.00	0.00	0.00	0.10	4.40
1216	0.47	3.26	0.21	0.00	0.00	0.00	0.03	0.00	3.13
1221	0.26	2.48	0.28	0.00	0.21	0.00	0.21	0.00	2.04
1222	0.23	3.02	0.34	0.00	0.93	0.00	0.03	0.00	1.99
1227	0.36	2.74	0.30	0.00	0.00	0.00	0.09	0.45	1.97
1305	0.99	2.28	0.63	0.00	0.47	0.00	0.00	0.23	1.58
1307	0.49	2.26	0.55	0.04	0.49	0.00	0.04	1.06	0.80
1310	0.21	1.26	0.33	0.00	0.30	0.00	0.16	0.09	0.72
1316	0.86	3.44	0.77	0.00	0.70	0.00	0.00	1.72	1.05
1321	1.59	3.61	0.43	0.10	1.85	0.00	0.00	0.26	1.66
Total (41)	0.44	2.67	0.80	0.44	0.68	0.06	0.13	0.24	1.37

Note: the last row contains the mean value for each column.

A.2 SAMPLES COLLECTED

A.2.1. *Sampling Methodology*

Sampling was conducted throughout the study area, but was concentrated in the areas of the scanlines. Sampling included host rocks and vein fillings. Where possible, oriented samples were collected. The following pages list the collected samples along with a short field description, possible use for the sample and a location in UTM coordinates (see Appendix A.1 for a description of the UTM coordinates used).

A.2 SAMPLES COLLECTED

Sampling was conducted throughout the study area, but concentrated in the areas of the scanline surveys. Sampling included host rocks and mineral fillings. The locations of the samples are given in accompanying map. The location of each sample is given in U.T.M. coordinates in the listing below. A short field description of the sample and what the sample was used for is given as well.

DVE289
Location: 3.7km S of Lagoudhera turnoff at Sarandi turn (500071.3E,3869749N)
Description: oriented, f.gr.dyke adjoining calcite vein
+ unoriented epidote altered rock
Use: geochemistry

DVE4889
Location: 13-27-096 (scanline photo 13-27, fracture 096) area (510330.4E,3863344N)
Description: dyke sample with epidote veins
Use: thin section, geochem

DVE6689
Location: 1227-1231 (502597E,3874746N)
Description: calcite vein 11m S of section toward ravine
Purpose: stable isotope analysis

DVE7089
Location: 0.68mi N of Platanistasa/Alithinou turnoff (504236.5E,3868934N)
Description: calcite veins cross-cut epidote sample near gabbro screen
Use: thin section

DVE7689
Location: 0.5mi S of Xyliatos (excavation) (503662.3E,3876194N)
Description: calcite in pillow
Purpose: stable isotope analysis

DVE9789
Location: 400m from Sarandi/Spilia turnoff A: (498398.8E,3868915N) B: (498398.8E,3868916N) C: (498312.6E,3868965N)
Description: A - epidosite margin quartz? vein; B - diabase epidote quartz vein and zeolite; C - diabase and epidote vein
Use: fluid inclusion, thin section

DVE9889
Location: 450m from Sarandi/Spilia turnoff (498184.8E,3869043N)
Description: red stain on 'poured' epidosite dyke
Use: thin section

DVE9989
Location: 470m from Sarandi/Spilia turnoff (498184.8E,3869043N)
Description: A - non-epidosite oriented 330/44; B - epidosite oriented 280/25; C - margin of dyke with zeolite vein
Use: thin section; fluid inclusion, geochemistry

DVE10189
Location: 550m from Sarandi/Spilia turnoff (498106.2E,3868943N)
Description: oriented 007/88 epidote/zeolite vein in diabase
Use: fluid inclusions, thin section

DVE12689
Location: Akaki Canyon (p23.5 #2 notebook) (516256.9E,3877356N)
Description: calcite veins
Purpose: stable isotope analysis

DVE131A89

Location: 1990paces N of Pharmakas (513223.7E,3866690N)
Description: orienteed 165/63 chloritized dyke
Use: thin section, geochemisrty

DVE141A89

Location: 4.5miles S of Atamas restaurant near E1134 (511150E,3866302N)
Description: epidotized dyke
Use: thin section

DVE15689

Location: 3.7 miles S of Kato Moni (A.Ep. bridge) (505092.3E,3869992N)
Description: lightly epidotized grey dyke near fault oriented 102/84
Use: thin section, geochemistry

— end of DVE series of samples —

The next series of samples are keyed to the photo numbers of the scanlines. Their location is thus presented in the first four digits of the sample number; the remaining digits refer to the particular fracture number or, if followed by a 'm', to the distance in metres along the scanline.

0109-19/20

Description: Fe oxidized dyke with pyrite
Use: thin section

0111-8

Description: altered dyke with dissem. pyrite; zeolite in cavity
Use: thin section

0113-4

Description: medium leached dyke
Use: thin section

0113-6

Description: chlorite vein, zeolite + Fe oxide in dyke
Use: thin section

0113-8

Description: zeolite + epidote + Fe oxide coating dyke
Use: thin section, X.R.D.

0113-19

Description: fine dyke; zeolite + epidote mixed vein
Use: thin section

0115-14

Description: Fe oxide + zeolite vein in greenish dyke
Use: X.R.D.

0116-3

Description: epidote vein on surface on crs/med dyke
Use: thin section

0116-11

Description: 3mm epidote vein in gabbro
Use: thin section

0116-14

Description: epidote veins in medium gabbro (or coarse dyke(?))
Use: thin section

0116-21

Description: fine dyke with chilled margin
Use: thin section, X.R.D.

0116-31(2)
Description: plagiogranite; leached around epidote veins
Use: thin section

0126-110
Description: fine plagiogranite epidote coating and chlorite
Use: thin section

0127-112
Description: fine plagiogranite with epidote, amphibole(?), pyx(?)
Use: X.R.D.

0130-2
Description: chlorite, rust weathering in slickensided coarse gabbro
Use: thin section

0131-191
Description: Fe oxide (purple) in slickensided gabbro
Use: X.R.D.

0132-6
Description: coarse gabbro
Use: thin section

0132-18
Description: coarse gabbro epidote veins and Fe oxides, chlorite
Use: thin section

0132-21
Description: fine quartz and plagiclase bands in plagiogranite
Use: thin section, X.R.D.

0134-29
Description: (leucocratic) gabbro
Use: thin section

0134-48
Description: 1cm zeolite vein in coarse gabbro
Use: thin section

0201-4
Description: coarse dyke contact to epidote vein
Use: thin section

0201-7
Description: leucocratic coarse dyke chlorite vein surface and calcite surface
Use: thin section

0201-16
Description: med dyke 5mm epidote vein, calcite vein surface
Use: thin section, fluid inclusion

0301-14(2)
Description: epidote fracture fill (sandy); pyrite and epidote veining on fine dyke, parallel pyrite veins
Use: thin section

0302-11/12
Description: two joint surfaces: 1 epidote, 1 hematite
Use: thin section, X.R.D.

0302-14
Description: leuco dyke hemaite joint surface coating
Use: X.R.D.

0302-20
Description: epidote veins, minor pyrite, altered dyke
Use: thin section

0302-22
Description: epidote, chlorite veins altered dyke
Use: thin section, fluid inclusion

0302-27
Description: calcite, epidote in fine dyke
Use: thin section, fluid inclusion

0302-28
Description: fine greenish dyke calcite surface coat
Use: X.R.D.

0302-33.2
Description: epidote, pyrite vessicle fill: pillow carapace
Use: thin section

0303-12
Description: epidote alteration in pillow; relict vessicles, epidote, clay alteration of pillow
Use: thin section

0304-3
Description: parallel epidote veins, filled vessicles in dyke; pervasive alteration = dark green
Use: thin section, fluid inclusion

0304-7
Description: vertically stretched vessicles in dyke with epidote fracture fill
Use: thin section

0304-9
Description: sandy epidote dyke from breccia zone
Use: thin section, fluid inclusion

0304-14
Description: epidote, clay vein fill
Use: X.R.D.

0306-A
Description: calcite in vessicles of medium brown grey pillow
Use: thin section

0306-4
Description:
Use: thin section

0306-6
Description: rust coating on dark grey fine dyke
Use: geochem

0306-10
Description: brecciated pillow rubble
Use: thin section

0307-2
Description: angular dyke breccia: calcite, epidote, chlorite, pyrite
Use: thin section, fluid inclusion

0307-7.1
Description: chlorite, epidote, calcite, fill of joint (rubble)
Use: thin section, fluid inclusion

0307-11A
Description: epidote + rubble middle of breccia zone in joint
Use: thin section

0307-16
Description: chlorite, calcite, epidote in pillow rubble
Use: fluid inclusion

0307-18A
Description: epidote nodule, with calcite and pyrite
Use: thin section

0308-1
Description: chlorite, epidote from zone between two pillows
Use: thin section

0401-17
Description: disseminated pyrite in fine dyke
Use: thin section

0401-18
Description: epidote in coarse dyke
Use: thin section

0401-20
Description: chlorite blebs + epidote in medium dyke
Use: thin section

0401-23
Description: dyke with chilled margin
Use: thin section

0401-26
Description: epidote vein blob from vein with zeolites
Use: thin section

0403-6
Description: epidote throughout medium dyke
Use: thin section

0403-17
Description: epidote in slickensieded fine dyke
Use: thin section, fluid inclusions

0403-23
Description: sandy epidote in fine dyke
Use: thin section

0404-4
Description: zeolite vein in Fe oxidized dyke
Use: thin section

0404-7
Description: grey clay in coarse dyke
Use: X.R.D.

0404-16
Description: epidote vein and 2 pieces outside fracture 16
Use: thin section

0413-1
Description: pyrite, chlorite in medium gabbro
Use: thin section

0413-2
Description: epidote in fine clayey dyke
Use: thin section

0413-5
Description: dyke with epidote vein
Use: thin section

0413-15
Description:epidote + Fe oxide in fine dyke
Use: thin section, X.R.D.

0414-18
Description
Use: thin section

0415-5
Description: epidote (vein and throughout) with pyrite in dyke
Use: thin section, fluid inclusions

0419-21
Description: white mineral: quartz + calcite
Use: X.R.D.

0432-18
Description: zeolite vein in dyke rubble of medium dyke
Use: thin section

0432-25
Description: zeolite coating and grey clay on dyke surface
Use: thin section, X.R.D.

0432-35
Description: zeolite vein and gabbro pod in dyke
Use: X.R.D

0801-36
Description: epidote in leached host dyke
Use: thin section

1037A-1.14m
Description: same as GC23 early epidosite dyke (coarse)
Use: thin section

1110-22.75m
Description: relation b/t epidosite and chilled dyke margin
Use: thin section

1112-032
Description: dyke - epidotized in coarse areas oriented 313/64
Use: thin section

1112-10.9m
Description: epidosite sample 2 pieces
Use: fluid inclusions, thin section

1126-16.3A&B
Description: contact b/t epidosite and normal dyke gradation b/t 2 pieces (same dyke)
Use: thin section

1134-012
Description: fracture fill epidote, magnetite and calcite (fragile)
Use: thin section

1134-010
Description: fracture fill epidote zeolite calcite and magnetite - oriented 075/84
Use: fluid inclusions, thin section

1134-015
Description: complete fracture: quartz,epidote,magnetite,calcite
Use: thin section

1136-055
Description: Fe-oxide with calcite ± quartz and fracture fill and dyke fragments
Use: thin section

1138-030
Description: dyke fragment with pyrite vein surface
Purpose: stable isotope analysis

1222C-012

Description: fine grained aphyric dyke not oriented
Use: thin section, geochemistry

1305A-004

Description: 2 pieces coarse epidote and transition b/t epidotized and non-epidotized dyke oriented 340/60
Use: thin section, geochemistry

— end of scanline series of samples —

The following samples were taken from the road outcrops near the village of Apliki by a large shear zone.

O/C-2

Location: (510950E,3865850N)
Description: fracture coating: epidote + hematite; fine dyke
Use: thin section

O/C-5

Location: (510750E,3865750N)
Description: calcite, epidote, hematite in dyke
Use: thin section

O/C-6

Location: (510700E,3865750N)
Description: fine dyke with epidote pods, zeolite, jasper in vugs dyke altered to clay; 3 dyke generations
Use: thin section, fluid inclusions

O/C-7A

Location: (510550E,3865650N)
Description: fine dyke with 2cm wide eidote vein
Use: thin section, fluid inclusions

— End of the Apliki Shear zone samples —

Start of the GC series of samples. These were primarily collected for the purposes of dyke geochemistry.

GC9

Location: 4.25km on forest road (Spilia to Sarandi) from '4-way' intersection going east) (498700E,3869100N)
Description:
Use: geochemistry

GC11

Location: photo 10-28 (512376.2E,3872817N)
Description: 'fresh' dyke
Use: geochemistry

GC14A

Location: 11-34 to 11-36 (511043.7E,3866116N)
Description: less epidotized dyke
Use: thin section, geochemistry

GC17

Location: diorite cupola top of mountain (506745.7E,3867057N)
Description: 2 pieces dyke (1 for me) of dyke above cupola
Use: thin section, geochemistry

GC24

Location: near 10-38 (515064.4E,3868139N)
Description: late dyke dark grey aphyric fine grained
Use: thin section, geochemistry

GC27

Location: 11-24 - 7.4m (499139.2E,3869788N)
Description: fine gr. aphyric dyke
Use: thin section, geochemistry

GC33

Location: 100m SE of 10-21 (504998.3E,3866532N)
Description: competent dyke sample
Use: geochemistry

GC36

Location: 1304 paces N of Pharmakas (512906.7E,3865437N)
Description: dyke
Use: thin section, geochemistry

GC41

Location: 0.3miles N of Atamas restaurant (511880.8E,3869821N)
Description: very weathered dyke rust brown
Use: thin section, geochemistry

GC42

Location: 2.6miles S of Atamas restaurant (As DVE13989) (511525.7E,3867866N)
Description: dyke
Use: thin section, geochemistry

GC43

Location: 6.6miles S of Atamas("6.6" on Palekhori map) (509438.7E,3865076N)
Description: dyke (same area as DVE14689)
Use: thin section, gechemistry

GC44

Location: 6.0 miles S of Kato Moni (A.Ep. bridge turnoff) (501738.7E,3870466N)
Description: microgabbro epidote veins parallel dyke trend
Use: geochemistry

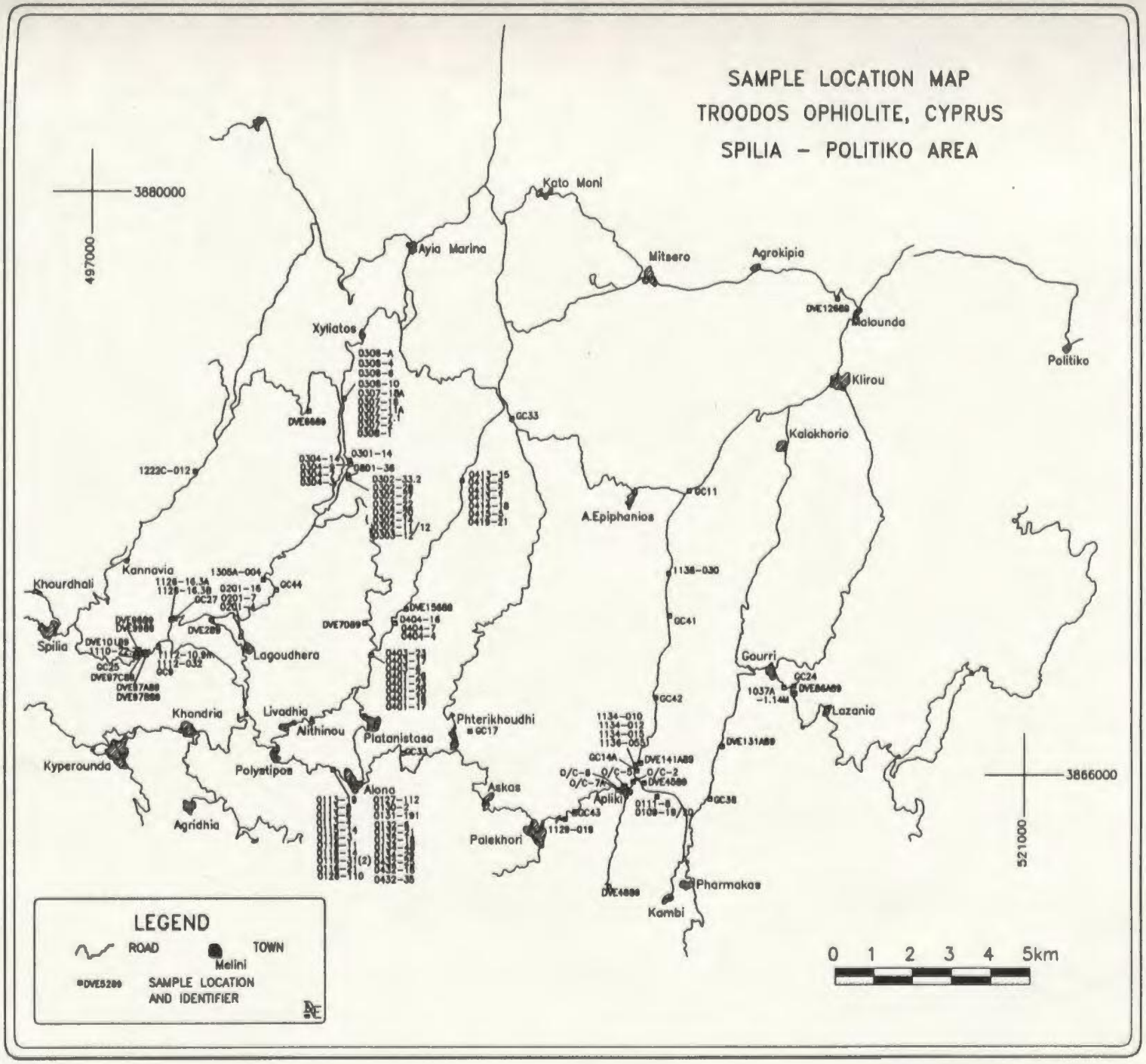
SAMPLE LOCATION MAP
TROODOS OPHIOLITE, CYPRUS
SPILIA – POLITIKO AREA
3880000
497000
3866000
521000
Kato Moni
Ayia Marina
Mitsero
Agrokipia
Malounda
Politiko
Klirou
Kalokhorio
Xyliatos
A.Epiphanios
Kannavia
Khourdhali
Spilia
Lagoudhera
Gourri
Lazania
Khandria
Livadhia
Aithinou
Platanistasa
Phterikhoudhi
Kyperounda
Polystipos
Alona
Askas
Apliki
Agridhia
Palekhori
Pharmakas
Kambi
0 1 2 3 4 5km
LEGEND
ROAD
TOWN
Melini
SAMPLE LOCATION AND IDENTIFIER

A.3 FRACTURE CHARACTERISTICS

A.3 FRACTURE CHARACTERISTICS

A.3.1 *Plots of All Scanline Data*

All stereographic projection in the appendices are equal area, lower hemisphere plots of poles to fracture planes.

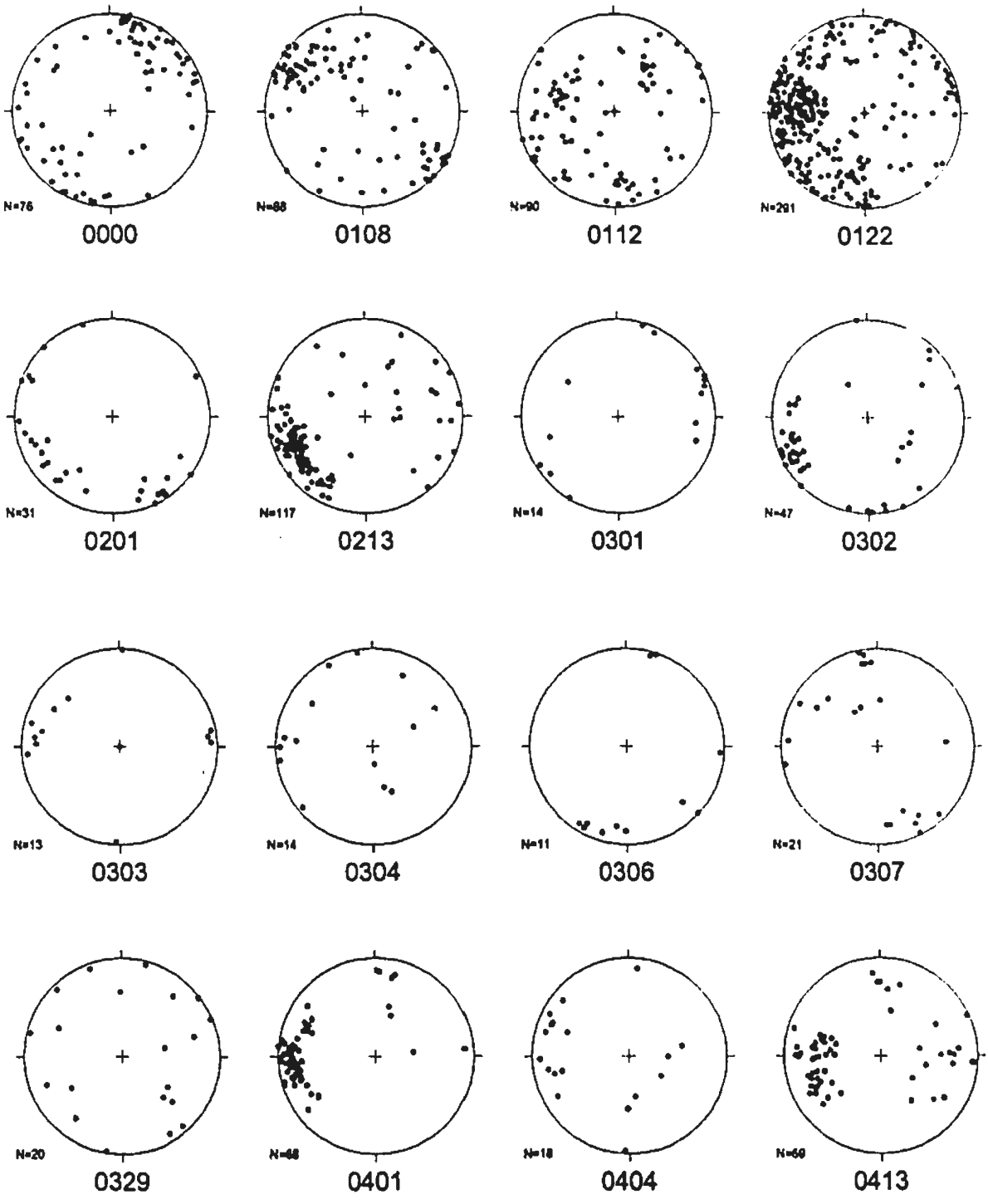

ALL SCANLINE FRACTURE DATA

Poles to Planes

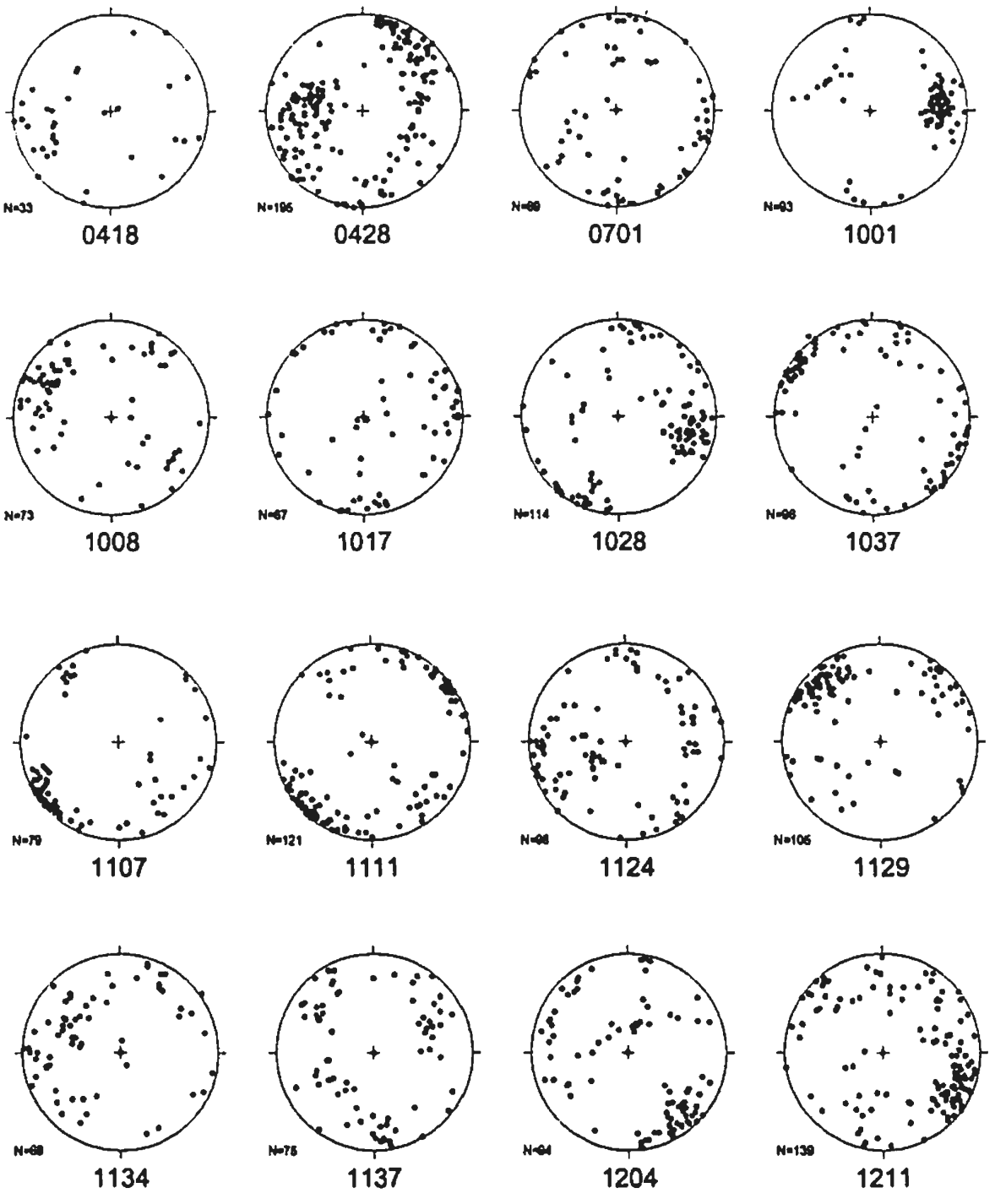

ALL SCANLINE FRACTURE DATA

Poles to Planes

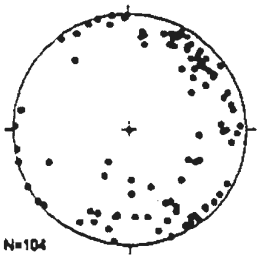

1216

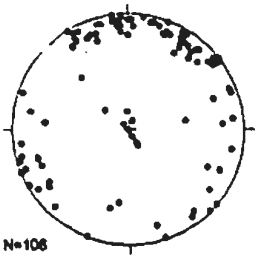

1221

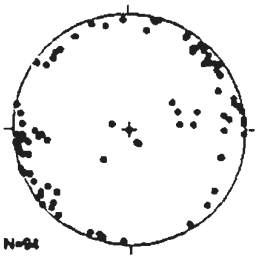

1222

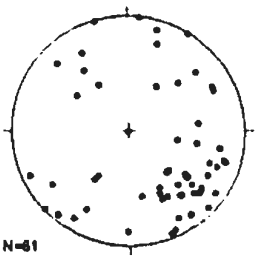

1227

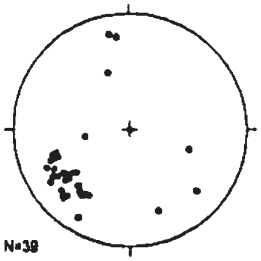

1305

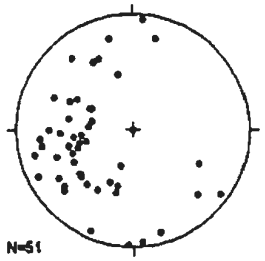

1307

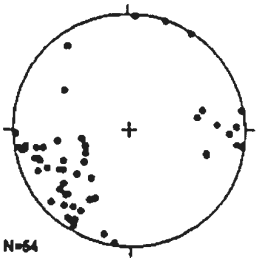

1310

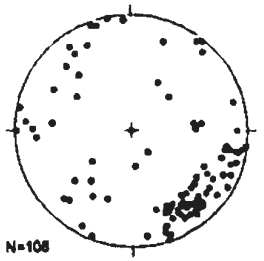

1316

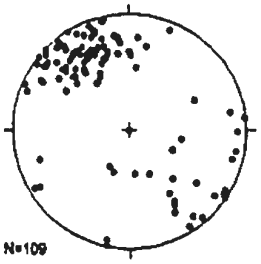

1321

ALL SCANLINE FRACTURE DATA

Poles to Planes

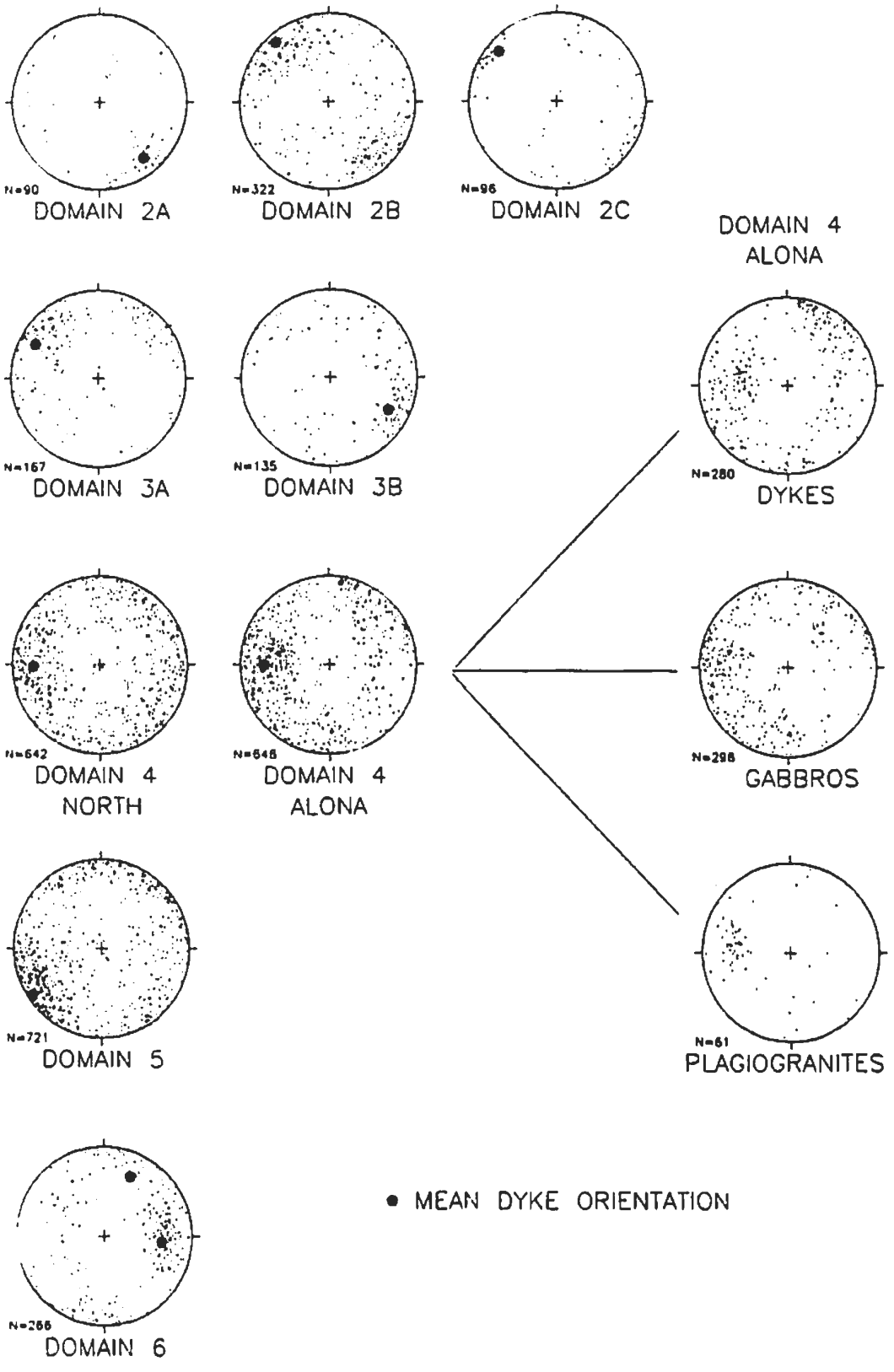

ALL FRACTURE DATA BY DOMAIN

A.3 Fracture Characteristics

A.3.2 *Fracture Filling Minerals vs. Orientation*

STEREO PLOT SYMBOL USAGE

FOR STEREOGRAPHIC PROJECTIONS IN APPENDICES:
A.3.2; A.3.4; A 3.5; AND A.3.6 SCANLINE DATA

TRACE LENGTH

SYMBOL	TRACE LENGTH
○	less than or equal to 2M
●	greater than 2M

FRACTURE TYPE

SYMBOL	TYPE
·	contact
△	vein
+	fracture
○	joint
□	fault

FRACTURE FILLING MATERIALS

SYMBOL	MATERIAL
•	none
△	calcite
+	epidote
○	zeolite
●	chlorite
▽	hematite/goethite
▼	pyrite
□	magnetite
■	quartz/jasper
◇	celadonite
◆	clay

TERMINATION MODE

SYMBOL	MODE (See text for description)
•	0
△	1
+	2
○	3
□	4

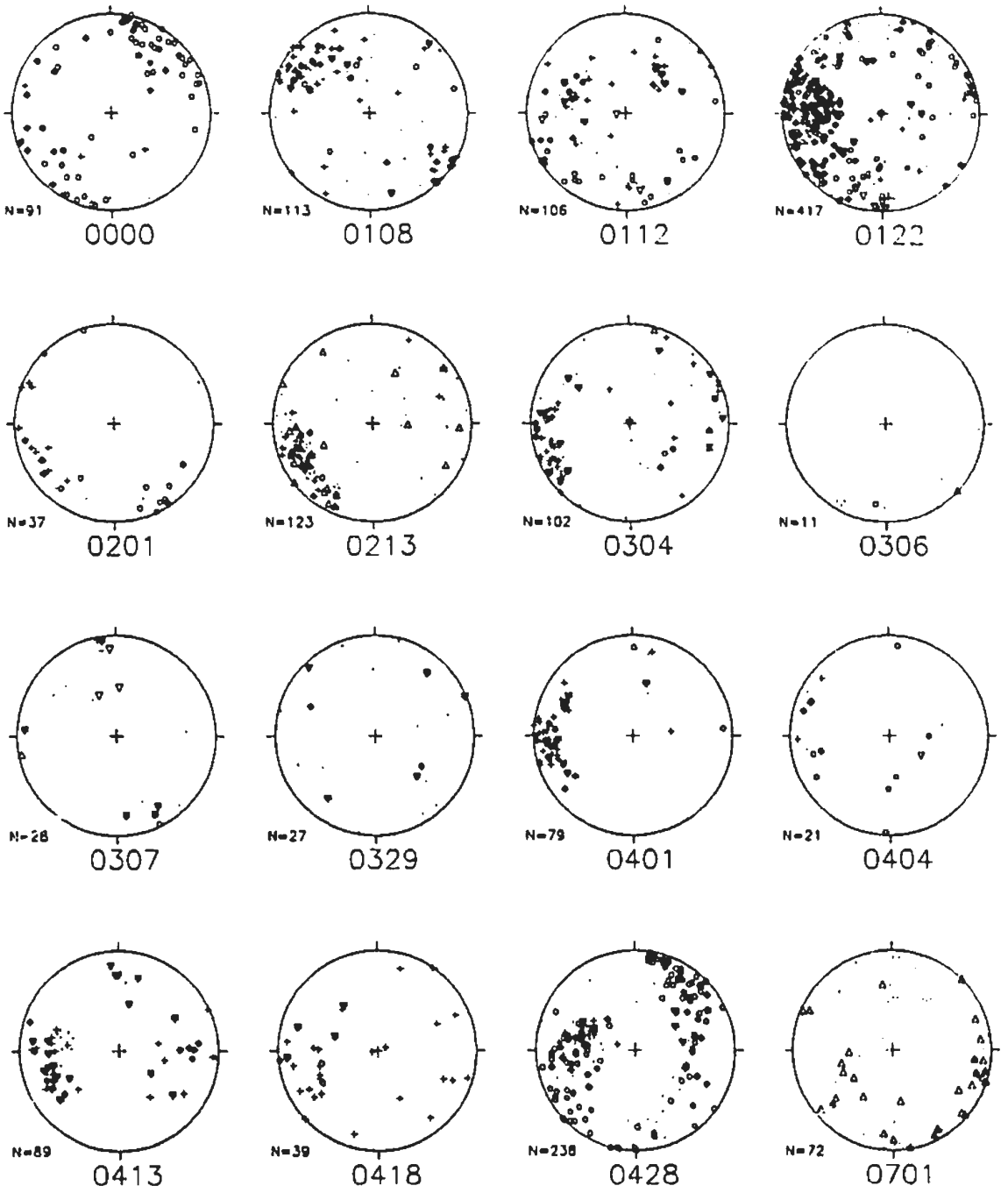

MINERAL FILLING BY SCANLINE

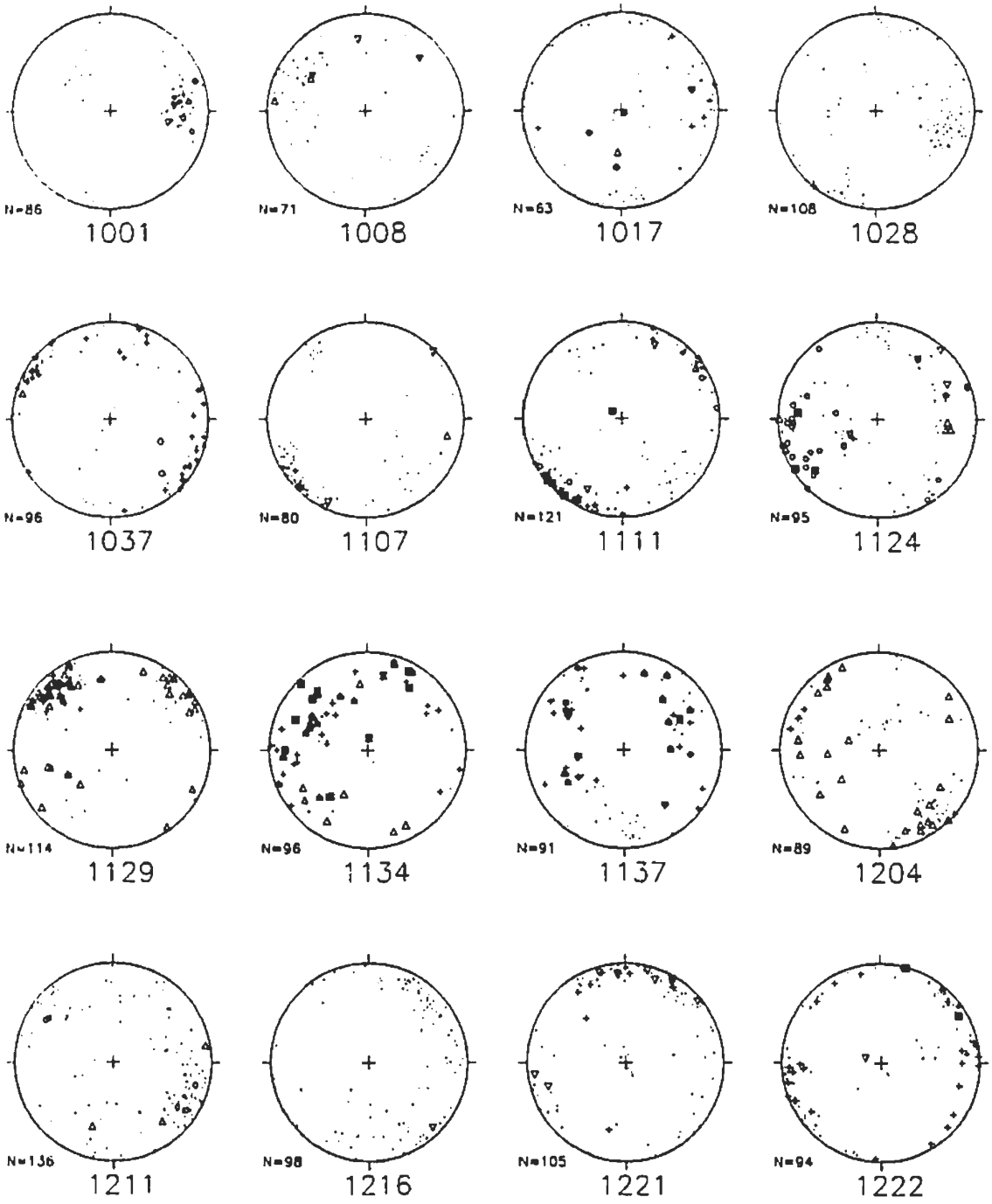

MINERAL FILLING BY SCANLINE

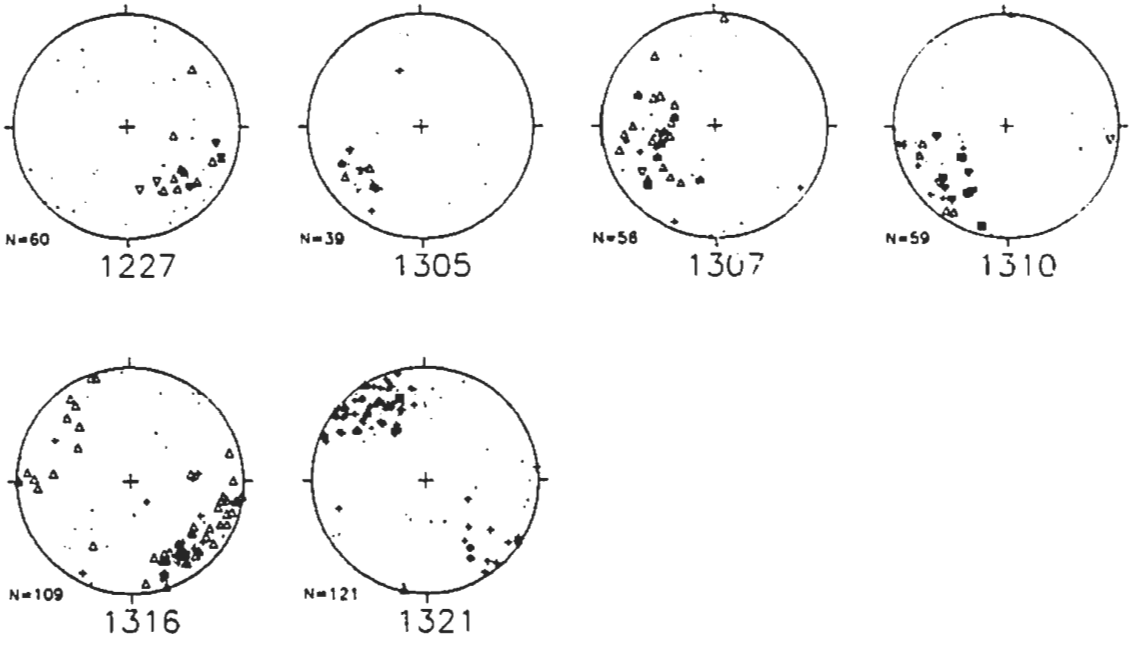

MINERAL FILLING BY SCANLINE

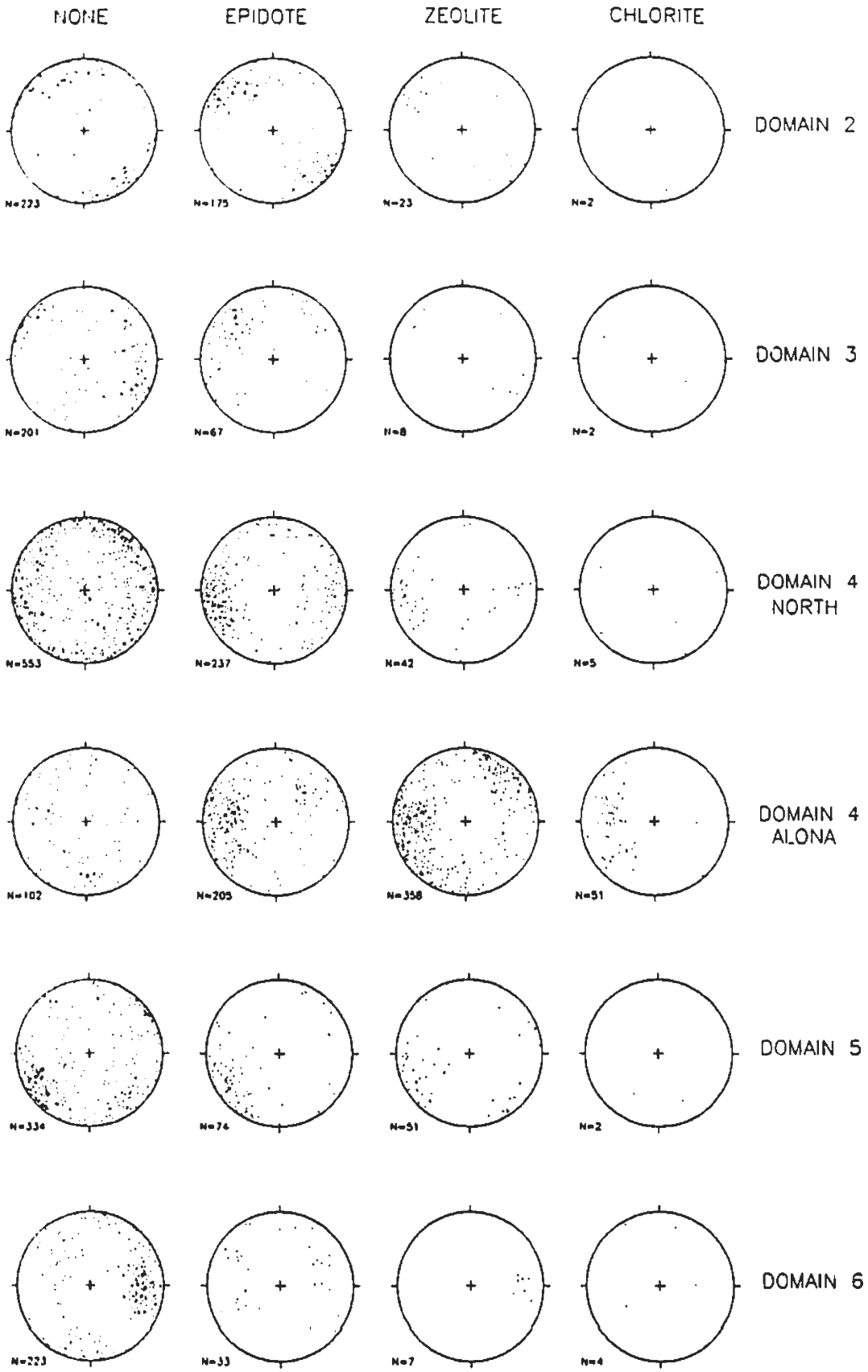
NONE
EPIDOTE
ZEOLITE
CHLORITE
DOMAIN 2
N=273
N=175
N=23
N=2
DOMAIN 3
N=201
N=67
N=8
N=2
DOMAIN 4 NORTH
N=553
N=237
N=42
N=5
DOMAIN 4 ALONA
N=102
N=205
N=358
N=51
DOMAIN 5
N=334
N=74
N=51
N=2
DOMAIN 6
N=223
N=33
N=7
N=4

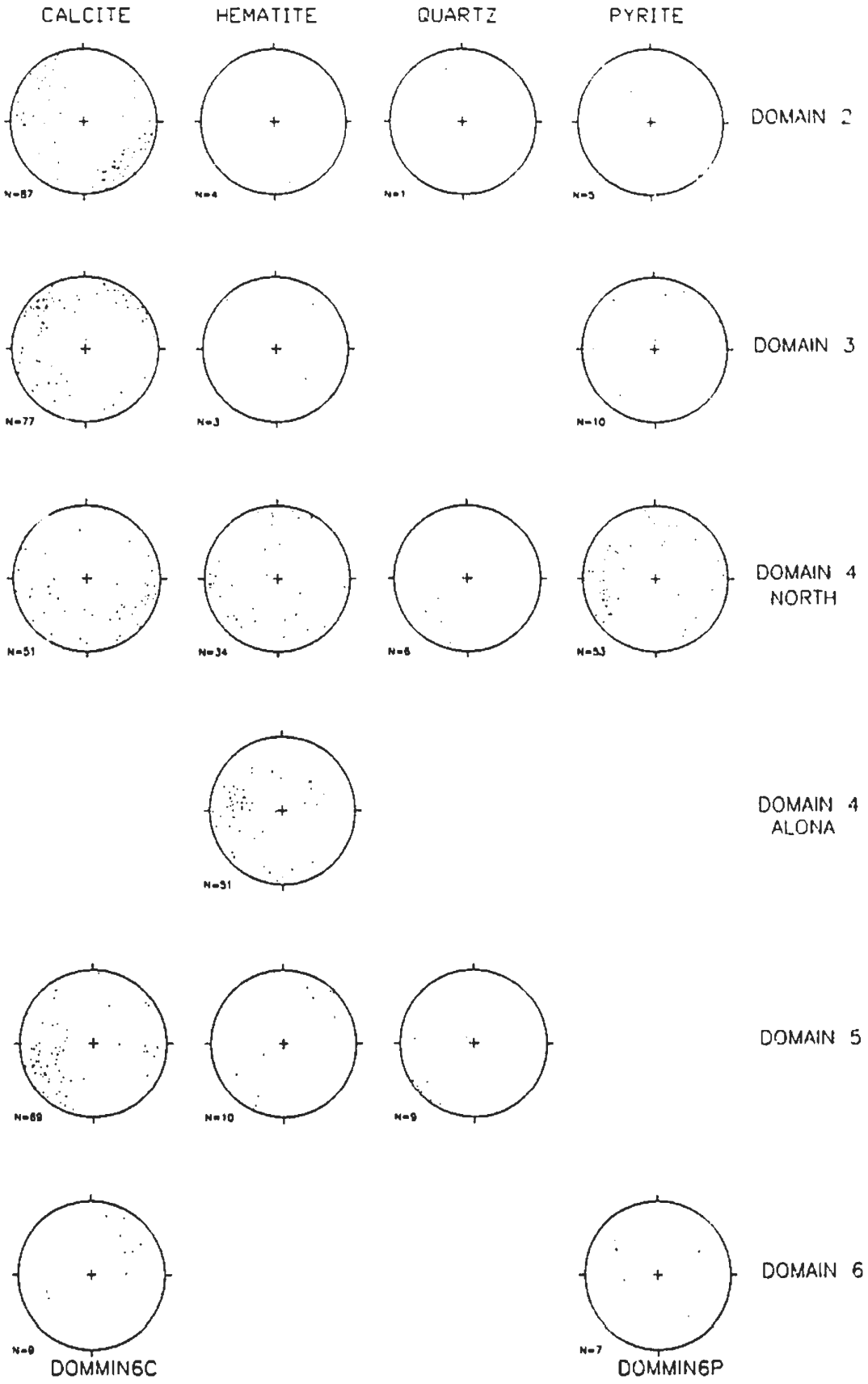
CALCITE
HEMATITE
QUARTZ
PYRITE
N=87
N=4
N=1
N=5
DOMAIN 2
N=77
N=3
N=10
DOMAIN 3
N=51
N=34
N=6
N=53
DOMAIN 4 NORTH
N=31
DOMAIN 4 ALONA
N=69
N=10
N=9
DOMAIN 5
N=9
DOMMIN6C
N=7
DOMMIN6P
DOMAIN 6

MAGNETITE CELADONITE CLAY

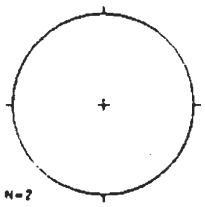

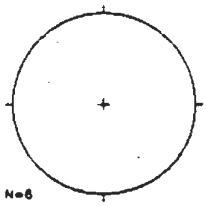

DOMAIN 2

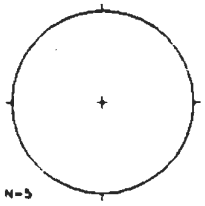

DOMAIN 3

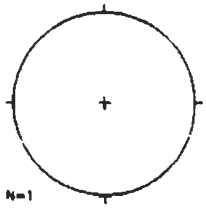

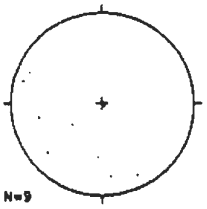

DOMAIN 4
NORTH

DOMAIN 4
ALONA

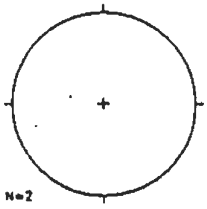

DOMAIN 5

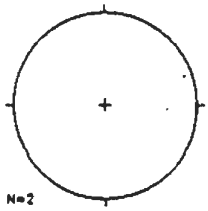

DOMAIN 6

A.3 Fracture Characteristics

A.3.3 *Fracture Filling Minerals vs. Trace Length*

Mineral Filling Versus Trace Length Statistics

Trace length values were used in their log transformed form for calculations. They are presented as arithmetic values in metres

Domain 2

Mineral	#	Mean	Average Deviation	Standard Deviation	Skewness	Kurtosis	Max. Length	Min. Length
epidote	179	2.15	2.44	2.09	0.73	0.44	8	0.4
zeolite	25	2.98	3.14	1.79	0.33	3.08	5.5	0.5
chlorite	4	3.1	3.1	2.25	0.62	0.15	6	1
calcite	87	1.88	2.1	1.86	0.75	0.39	8	0.43
hematite	7	1.99	2.42	2.49	0.84	0.17	5	0.5
magnetite	0							
pyrite	8	3.38	3.38	1.73	0.99	0.12	6	1.75
clay	6	2.76	2.76	1.72	1.66	0.32	7	1.4
none	235	1.62	2.06	2.17	1.18	0.43	10	0.3

Domain 3

Mineral	#	Mean	Average Deviation	Standard Deviation	Skewness	Kurtosis	Max. Length	Min. Length
epidote	62	2.75	2.99	2.47	1.14	0.39	15	0.45
zeolite	6	2.84	3.31	2.2	0.44	0.35	5.6	0.7
chlorite	0							
calcite	77	2.26	2.6	2.27	1.07	0.58	15	0.45
hematite	0							
magnetite	5	2.38	2.38	2.3	2.43	0.33	10	1.2
pyrite	7	2.28	2.28	1.49	0.51	0.32	3.4	1.1
clay	0							
none	189	1.44	2	2.27	1.66	0.63	15	0.35

Domain 4

Mineral	#	Mean	Average Deviation	Standard Deviation	Skewness	Kurtosis	Max. Length	Min. Length
epidote	434	2.31	2.57	2.15	1.02	0.83	30	0.3
zeolite	446	1.86	2.17	2.04	1.05	1.13	15	0.25
chlorite	57	2.03	2.32	2.12	1.11	0.81	15	0.4
calcite	51	1.76	2.08	2.07	1.29	0.73	10	0.45
hematite	76	2.65	2.83	2.04	0.75	1.62	15	0.3
magnetite	0							
pyrite	55	2.5	2.8	2.33	1.12	0.99	30	0.4
clay	9	2.22	3.39	3.02	0.64	0.16	9.5	0.5
none	522	1.58	2.11	2.27	1.41	0.58	16	0.25

Domain 5

Mineral	#	Mean	Average Deviation	Standard Deviation	Skewness	Kurtosis	Max. Length	Min. Length
epidote	113	1.94	2.35	2.24	0.82	0.72	15	0.25
zeolite	51	1.04	1.71	1.31	1.71	0.41	4.5	0.4
chlorite	2	1.24	1.24	1.19	1	0.06	1.4	1.1
calcite	69	1.75	2.16	2.16	0.95	0.3	8	0.4
hematite	20	1.59	2.24	2.34	0.82	0.23	4.2	0.35
magnetite	0							
pyrite	0							
clay	2	4.14	4.14	1.13	1	0.06	4.5	3.8
none	484	1.66	2.12	2.16	1.01	0.4	9.5	0.3

Domain 6

Mineral	#	Mean	Average Deviation	Standard Deviation	Skewness	Kurtosis	Max. Length	Min. Length
epidote	33	1.63	2.3	2.67	1.53	0.32	12	0.45
zeolite	7	2.09	2.72	2.31	0.4	0.53	5	0.4
chlorite	4	1.01	1.71	2.02	1.28	0.13	2.5	0.5
calcite	9	3.98	4.31	2.45	0.58	0.36	12	0.7
hematite	0							
magnetite	0							
pyrite	7	1.52	1.68	2.3	2.75	0.56	8	0.7
clay	2	2.18	2.18	1.42	1	0.06	2.8	1.7
none	223	1.72	2.13	2.17	1.07	0.4	10	0.25

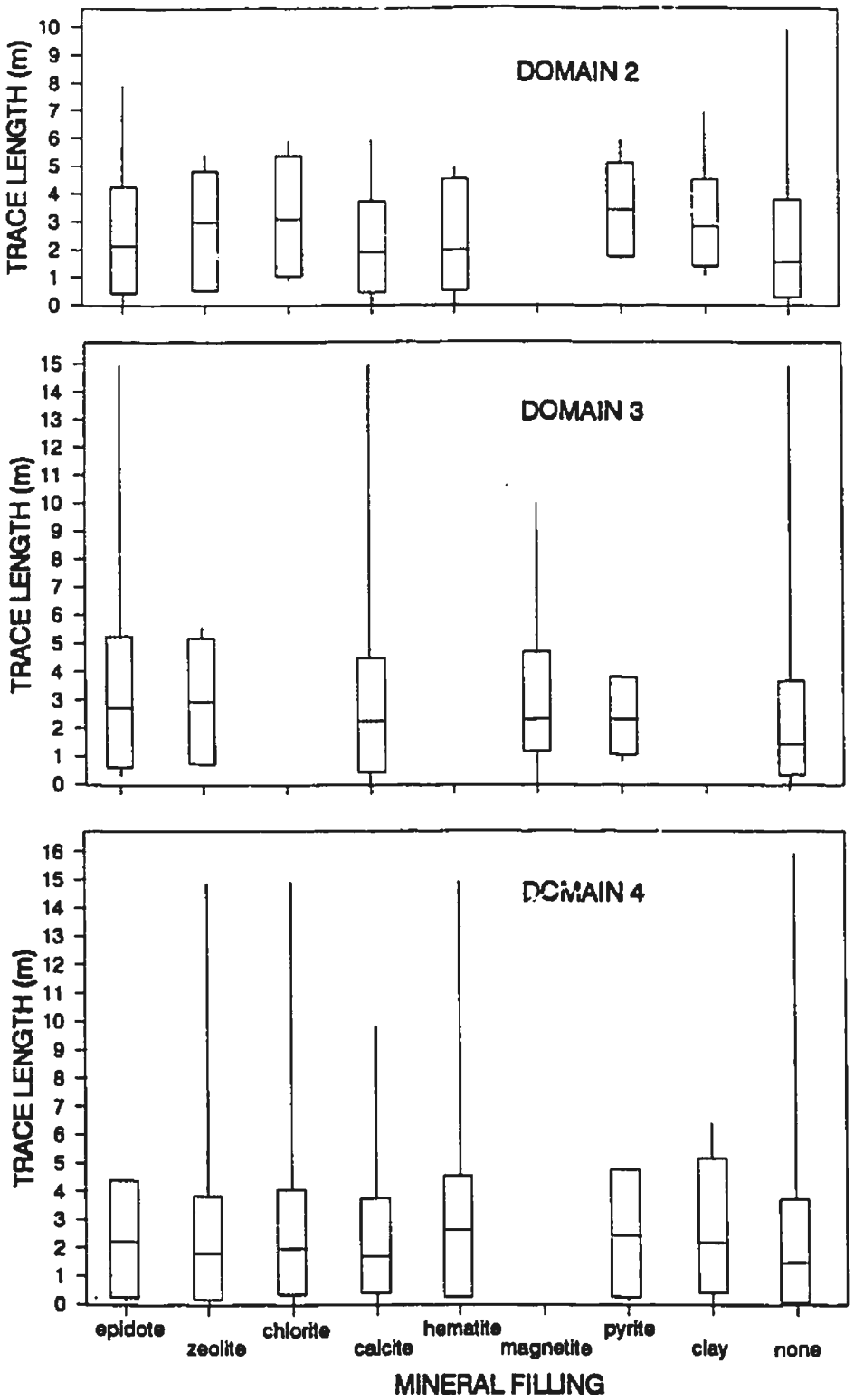
DOMAIN 2
TRACE LENGTH (m)
0 1 2 3 4 5 6 7 8 9 10
DOMAIN 3
TRACE LENGTH (m)
0 1 2 3 4 5 6 7 8 9 10 11 12 13 14 15
DOMAIN 4
TRACE LENGTH (m)
0 1 2 3 4 5 6 7 8 9 10 11 12 13 14 15 16
epidote
zeolite
chlorite
calcite
hematite
magnetite
pyrite
clay
none
MINERAL FILLING

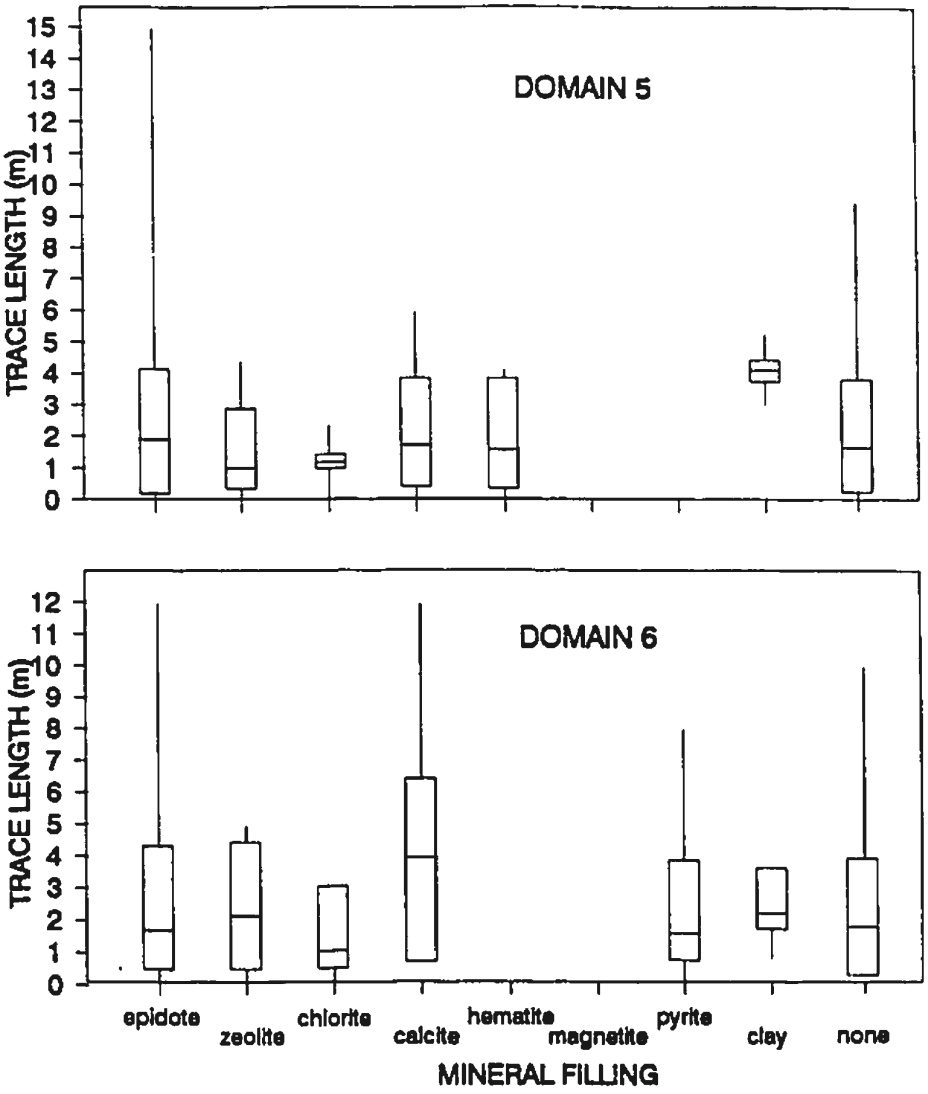

Note: the boxes on the graphs represent the standard deviation about the mean (the line in the centre region of the box). The lines outside the box represent the maximum and minimum values encountered if they fell outside the range of the standard deviation.

The trace length values were used in their log transformed form for the calculations. The values are presented as arithmetic values.

Mineral Filling versus Trace Length For Complete Scanline Data Set

Number of fractures per cell

Trace Length	Mineral Filling										Total
	Zeolite	Epidote	Calcite	Chlorite	Pyrite	Hematite	Magnetite	Clay	Celadonite	None	
<0.5	20	25	8	1	2	2				118	176
0.5-1.0	74	87	41	8	7	10		3	2	434	666
1.0-2.0	118	189	90	19	20	26	3	2		498	965
2.0-3.0	62	93	44	6	15	18	1	4		233	476
3.0-4.0	35	86	44	7	5	18		4		160	359
4.0-5.0	11	49	17	4	3	19		1		97	201
5.0-10.0	17	79	29	5	19	10		5		173	337
>10.0	2	10	7	1	2	3	1			14	40
Total	339	618	280	51	73	106	5	19	2	1727	3220

Percentage of fractures normalized to column totals

Trace Length	Mineral Filling									
	Zeolite	Epidote	Calcite	Chlorite	Pyrite	Hematite	Magnetite	Clay	Celadonite	None
<0.5	5.90	4.05	2.86	1.96	2.74	1.89				6.83
0.5-1.0	21.83	14.08	14.64	15.69	9.59	9.43		15.79	100.00	25.13
1.0-2.0	34.81	30.58	32.14	37.25	27.40	24.53	60.00	10.53		28.84
2.0-3.0	18.29	15.05	15.71	11.76	20.55	16.98	20.00	21.05		13.49
3.0-4.0	10.32	13.92	15.71	13.73	6.85	16.98		21.05		9.26
4.0-5.0	3.24	7.93	6.07	7.84	4.11	17.92		5.26		5.62
5.0-10.0	5.01	12.78	10.36	9.80	26.03	9.43		26.32		10.02
>10.0	0.59	1.62	2.50	1.96	2.74	2.83	20.00			0.81
Total	100	100	100	100	100	100	100	100	100	100

Percentage of fractures normalized to row totals

Trace Length	Mineral Filling										Total
	Zeolite	Epidote	Calcite	Chlorite	Pyrite	Hematite	Magnetite	Clay	Celadonite	None	
<0.5	11.36	14.20	4.55	0.57	1.14	1.14	0.00	0.00	0.00	67.05	100
0.5-1.0	11.11	13.06	6.16	1.20	1.05	1.50	0.00	0.45	0.30	65.17	100
1.0-2.0	12.23	19.59	9.33	1.97	2.07	2.69	0.31	0.21	0.00	51.61	100
2.0-3.0	13.03	19.54	9.24	1.26	3.15	3.78	0.21	0.84	0.00	48.95	100
3.0-4.0	9.75	23.96	12.26	1.95	1.39	5.01	0.00	1.11	0.00	44.57	100
4.0-5.0	5.47	24.38	8.46	1.99	1.49	9.45	0.00	0.50	0.00	48.26	100
5.0-10.0	5.04	23.44	8.61	1.48	5.64	2.97	0.00	1.48	0.00	51.34	100
>10.0	5.00	25.00	17.50	2.50	5.00	7.50	2.50	0.00	0.00	35.00	100

A.3 Fracture Characteristics

A.3.4 *Trace Length vs. Orientation*

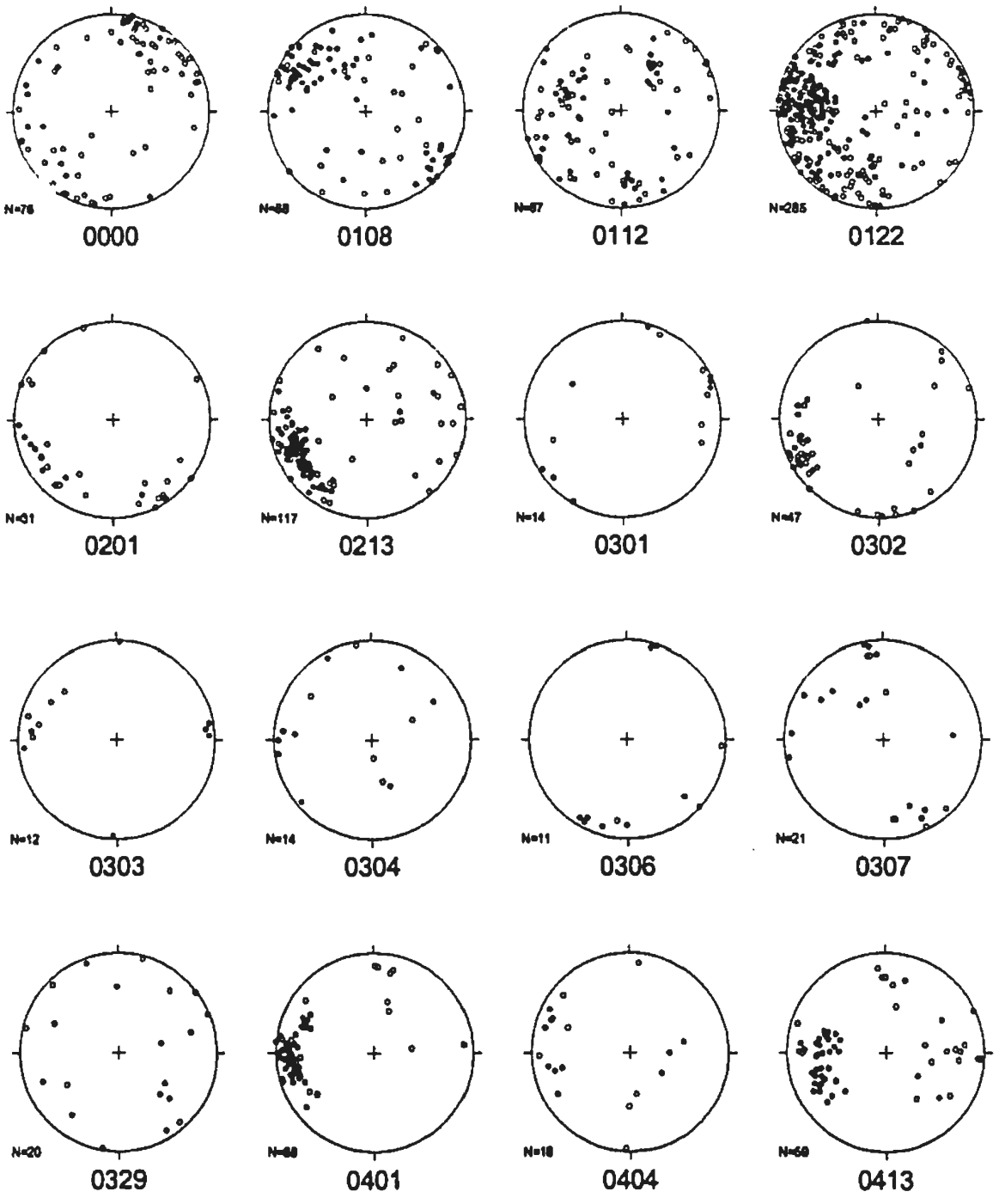

TRACE LENGTH (OPEN CIRCLE <= 2M; CLOSED CIRCLE > 2M)

ALL SCANLINE FRACTURE DATA

Poles to Planes

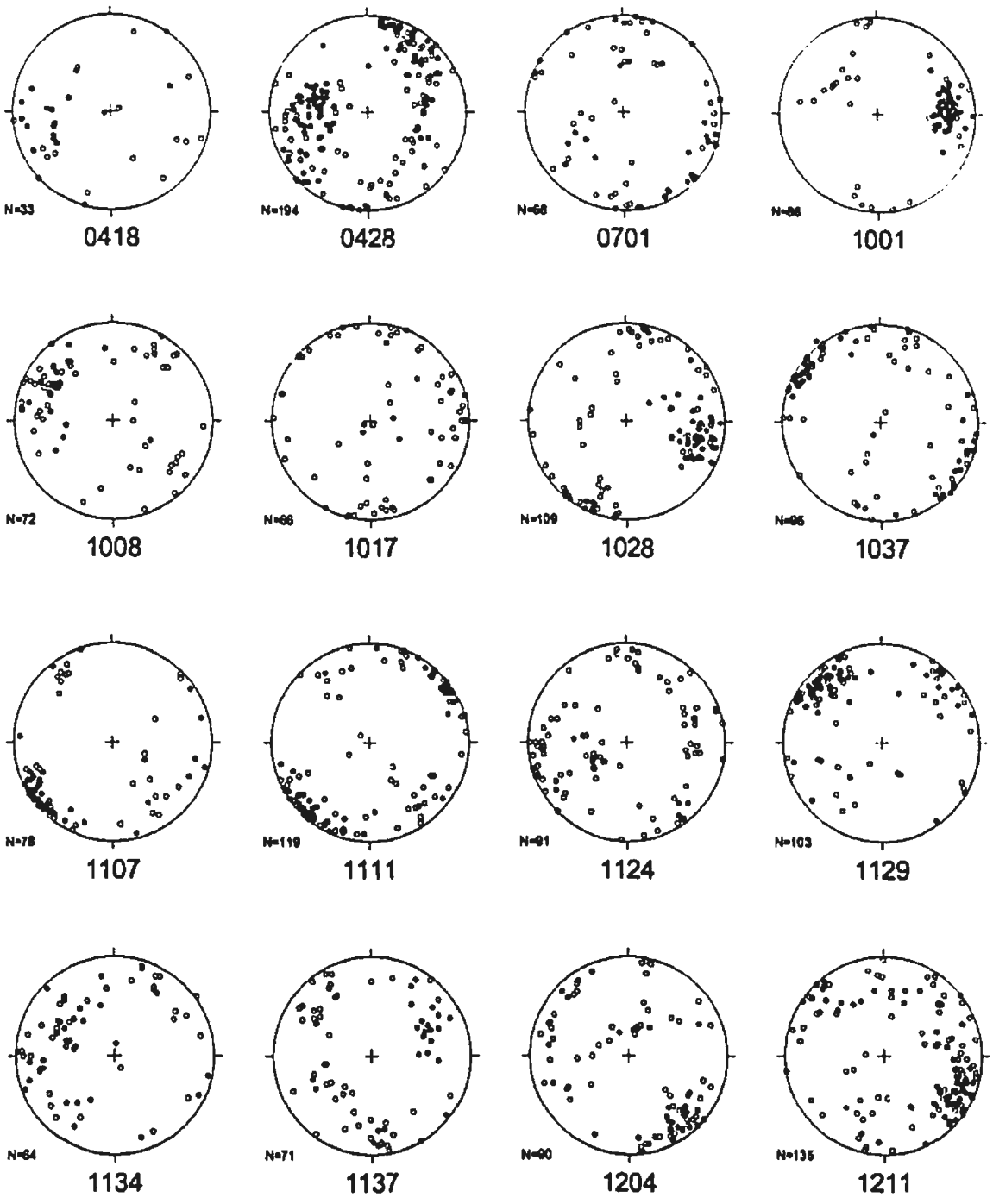

TRACE LENGTH (OPEN CIRCLE <= 2M; CLOSED CIRCLE > 2M)

ALL SCANLINE FRACTURE DATA

Poles to Planes

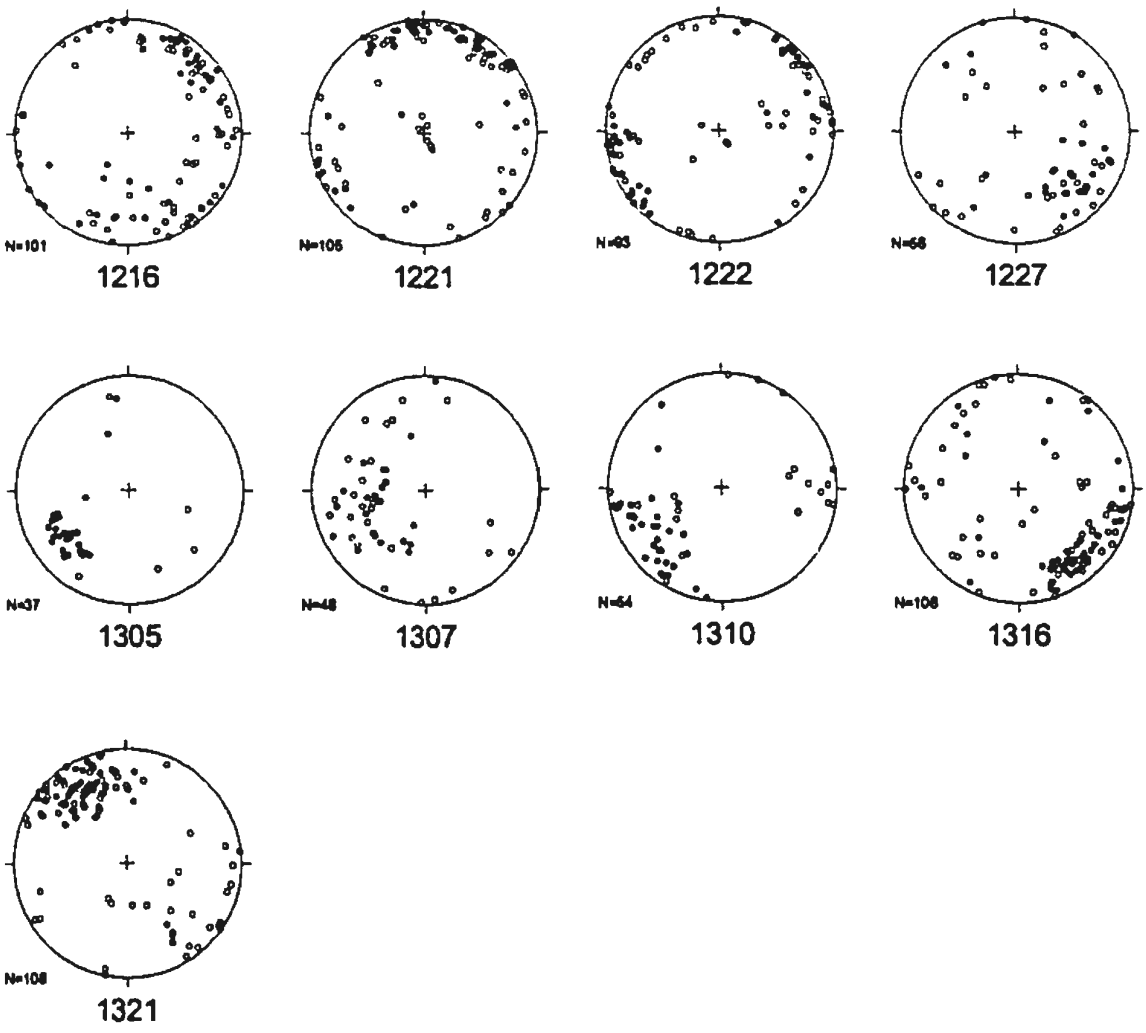

TRACE LENGTH (OPEN CIRCLE <= 2M; CLOSED CIRCLE > 2M)

ALL SCANLINE FRACTURE DATA

Poles to Planes

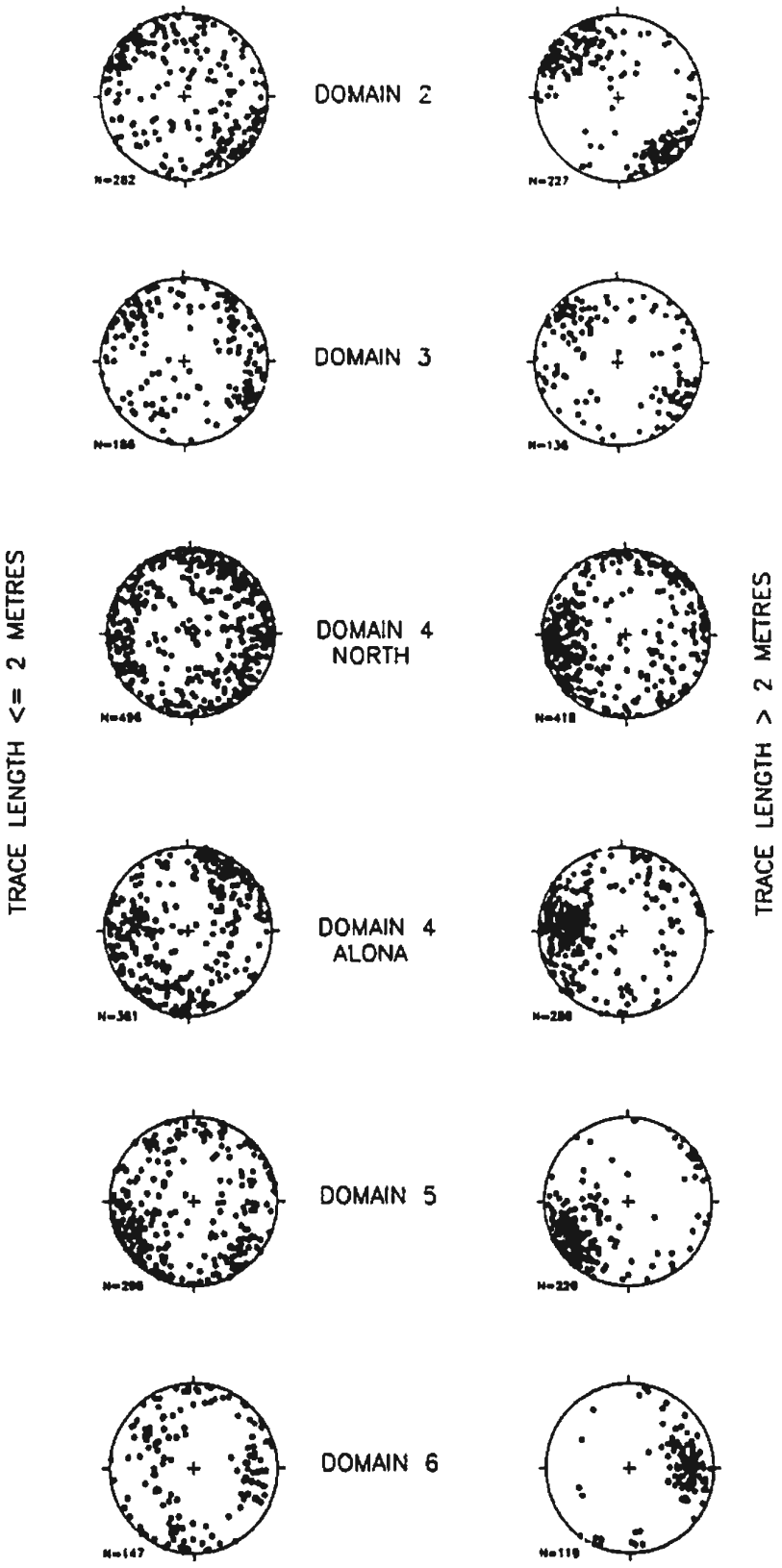

TRACE LENGTH BY DYKE DOMAIN

A.3 Fracture Characteristics

A.3.5 *Fracture Type vs. Orientation*

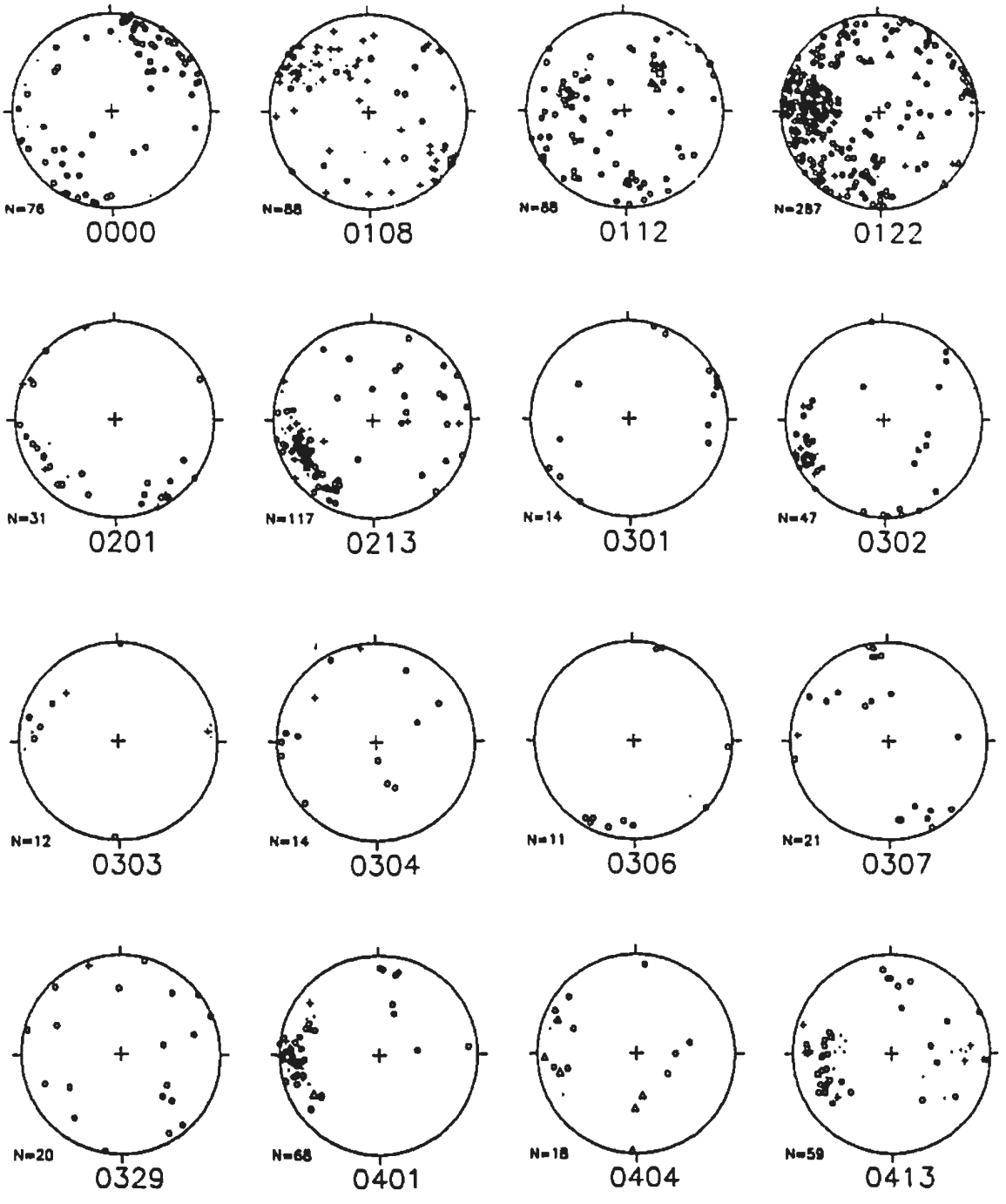

FRACTURE TYPE BY SCANLINE

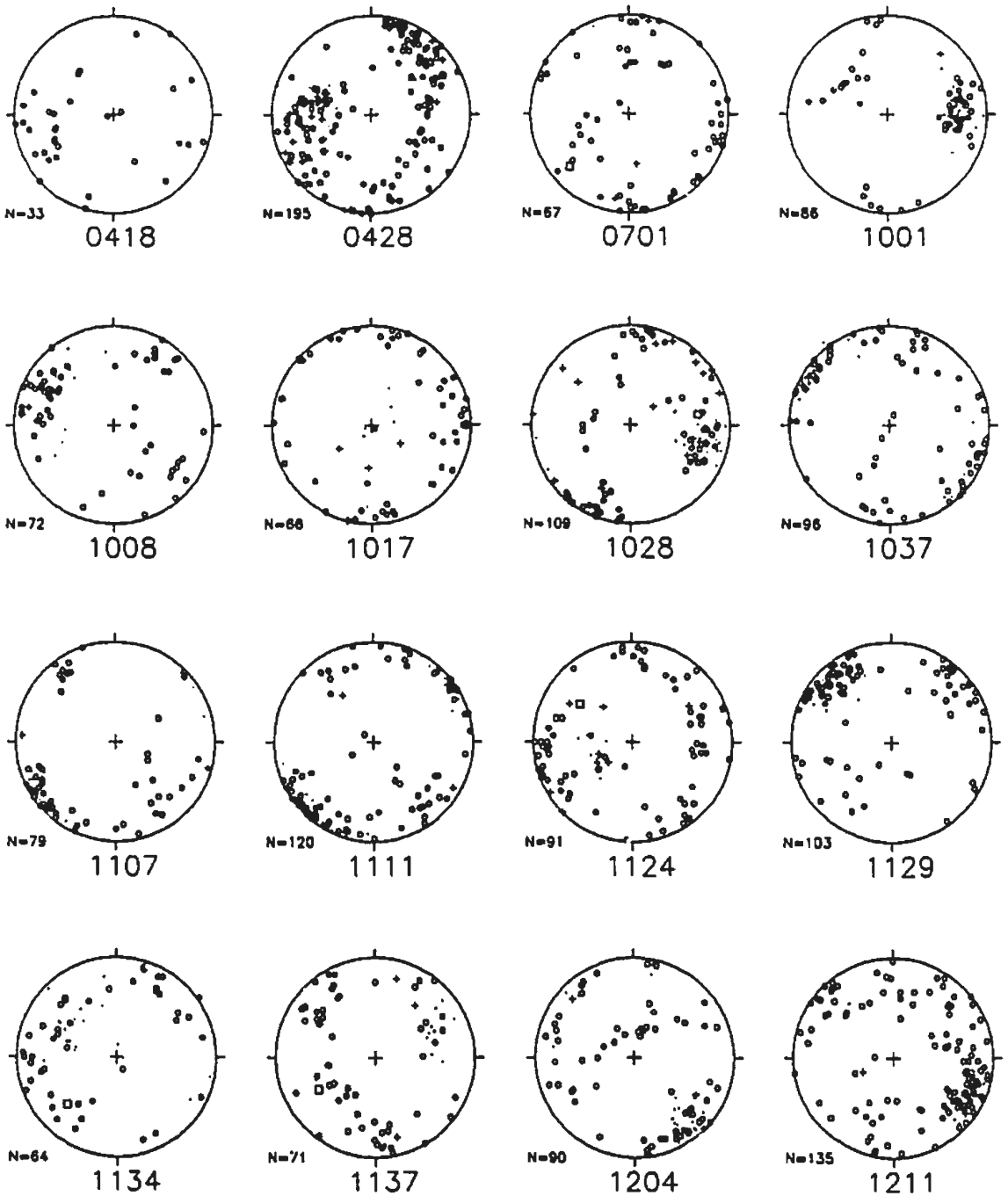

FRACTURE TYPE BY SCANLINE

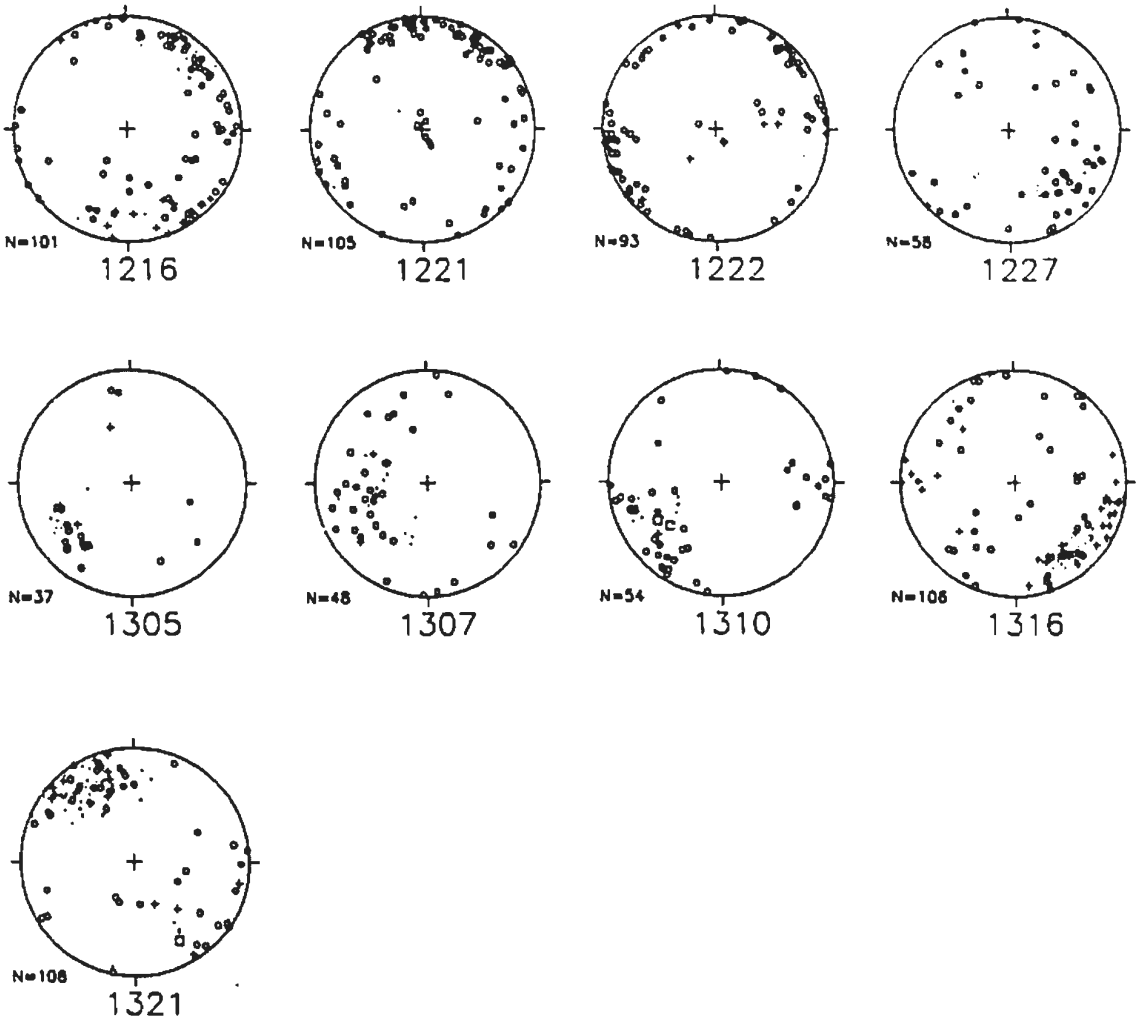

FRACTURE TYPE BY SCANLINE

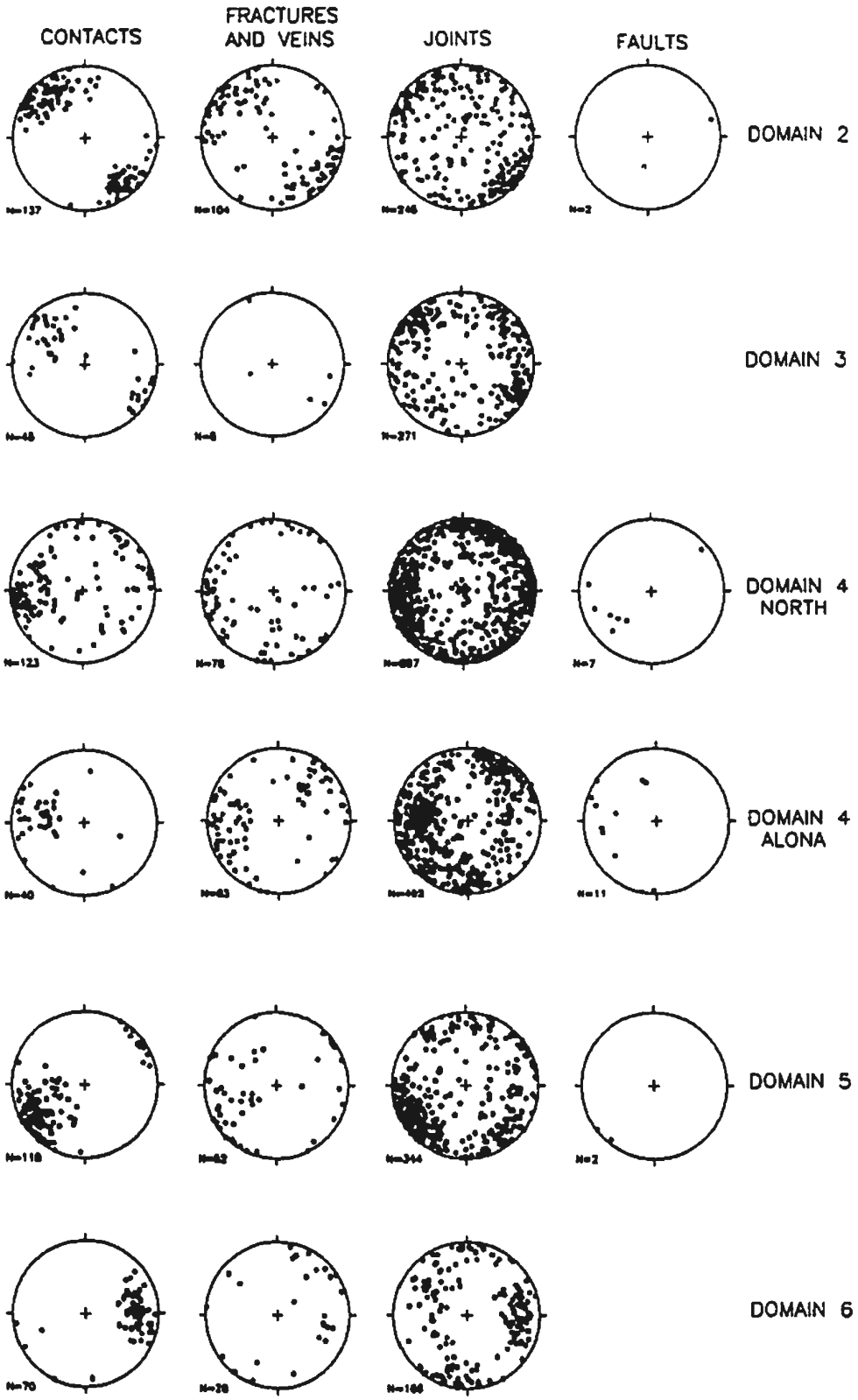

FRACTURE TYPE BY DYKE DOMAIN

A.3 Fracture Characteristics
A.3.6 *Termination Style vs. Orientation*

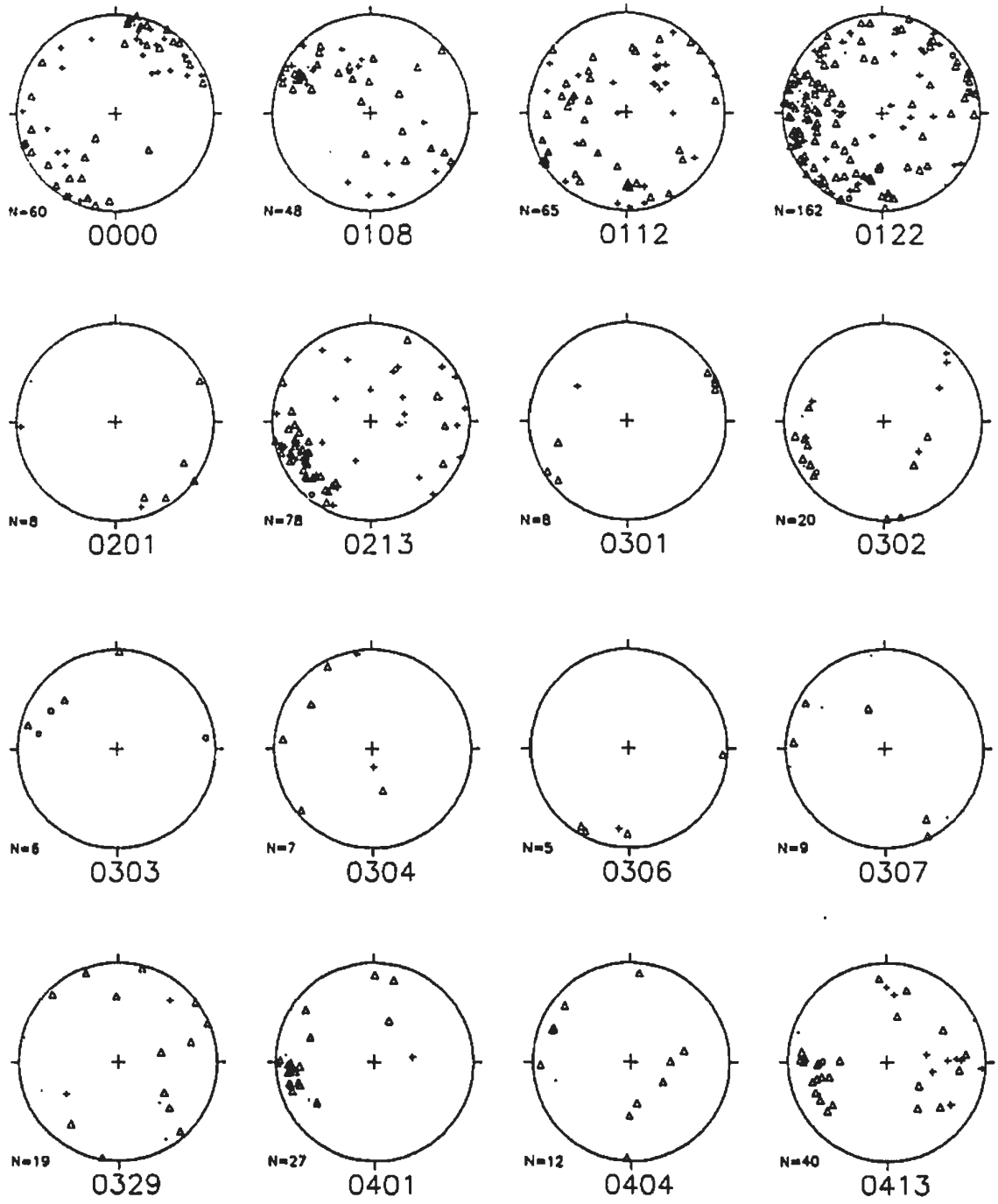

TERMINATION MODE BY SCANLINE

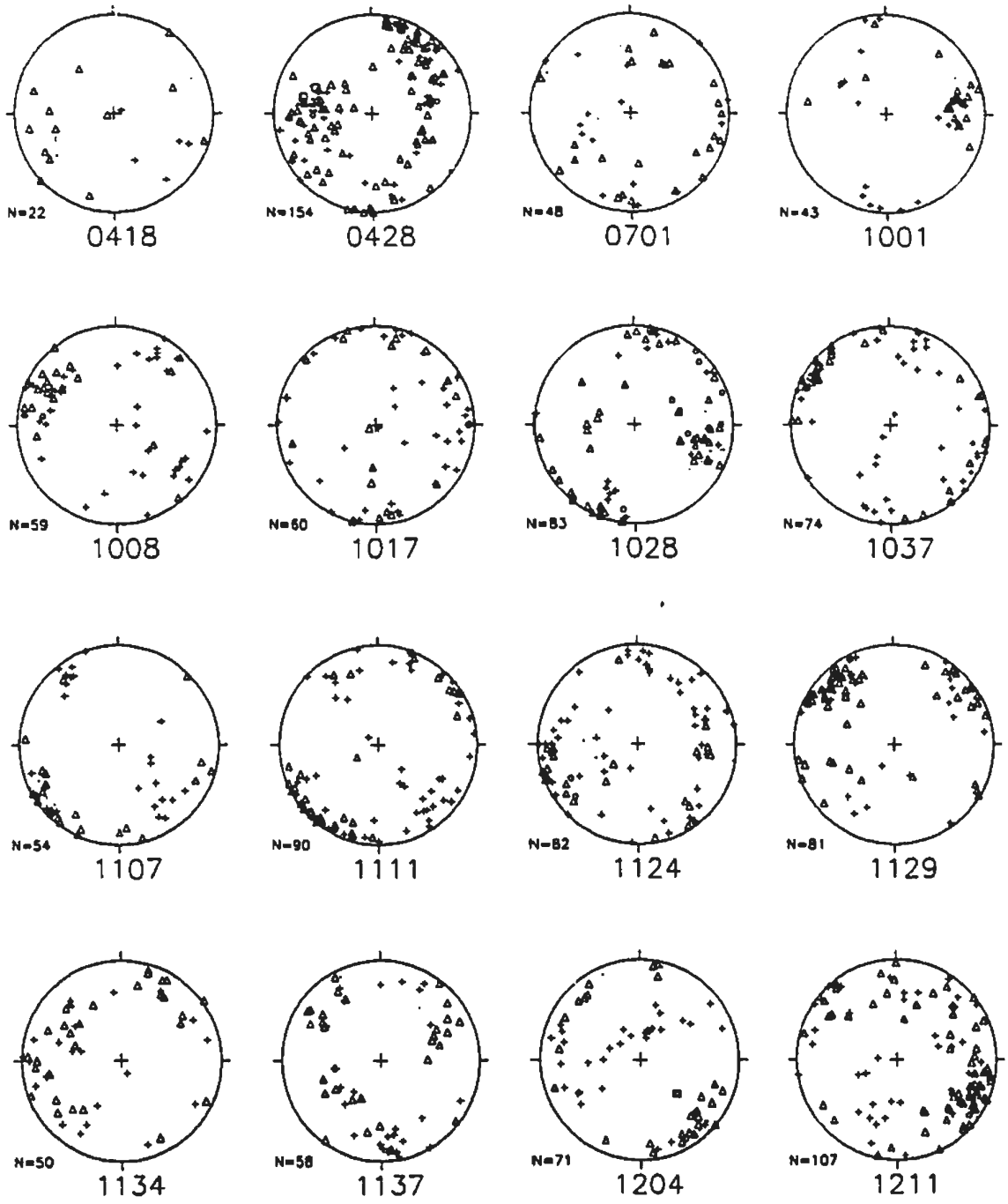

TERMINATION MODE BY SCANLINE

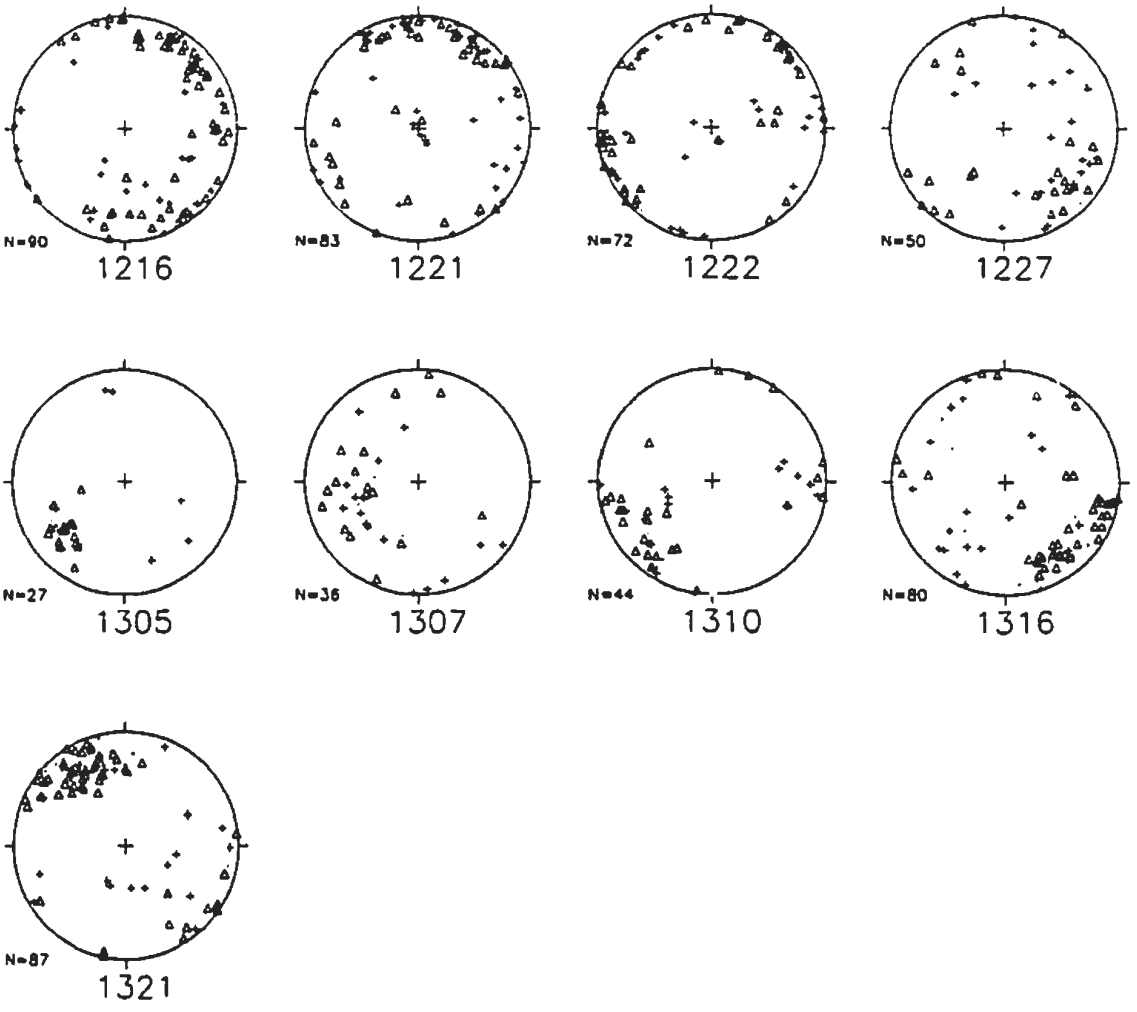

TERMINATION MODE BY SCANLINE

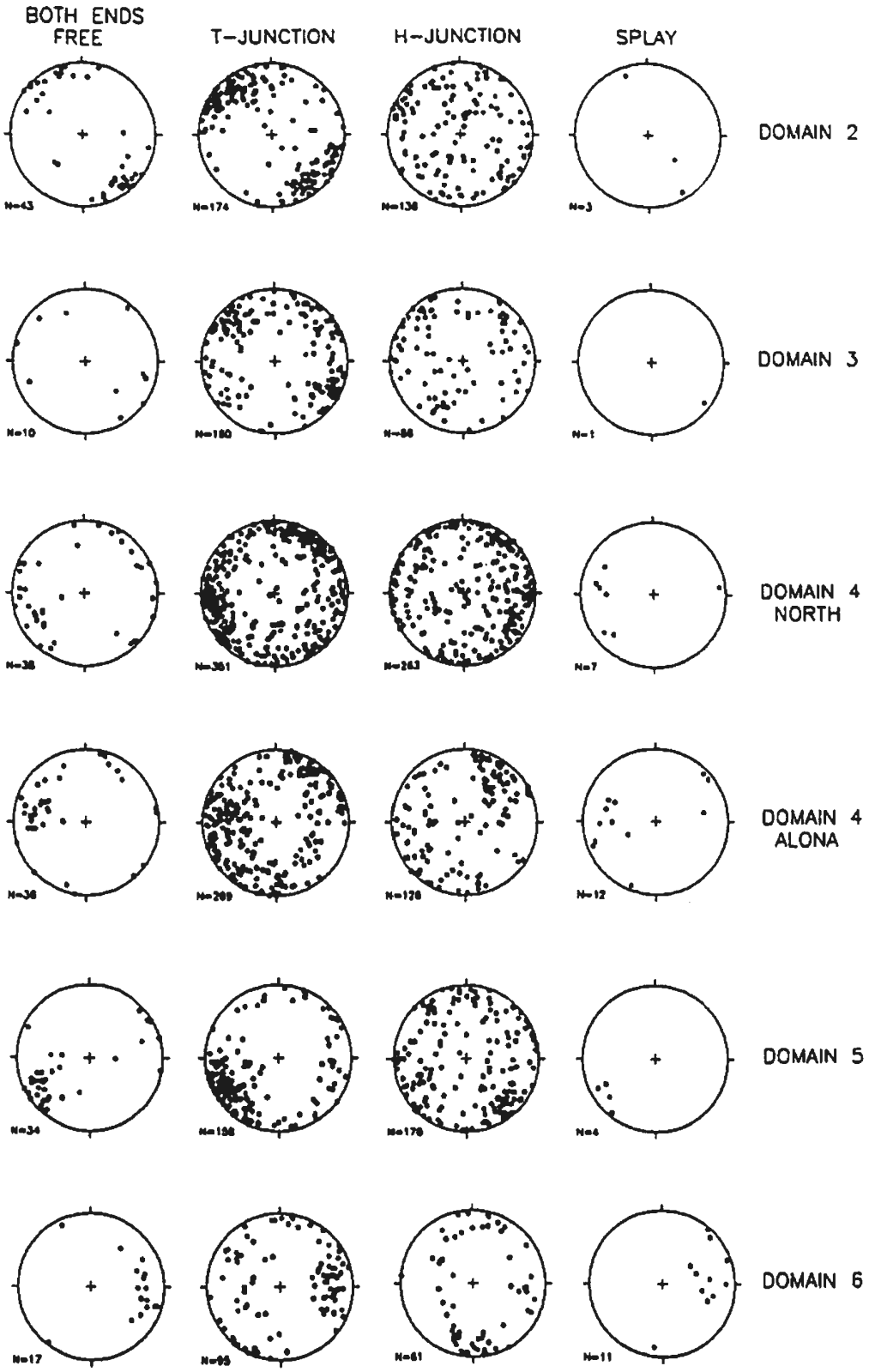

TERMINATION MODE BY DYKE DOMAIN

A.3 Fracture Characteristics

A.3.7 *Trace Length vs Censoring and Termination*

A.3.7.1 *Trace Length Histograms For Each Scanline By Set*

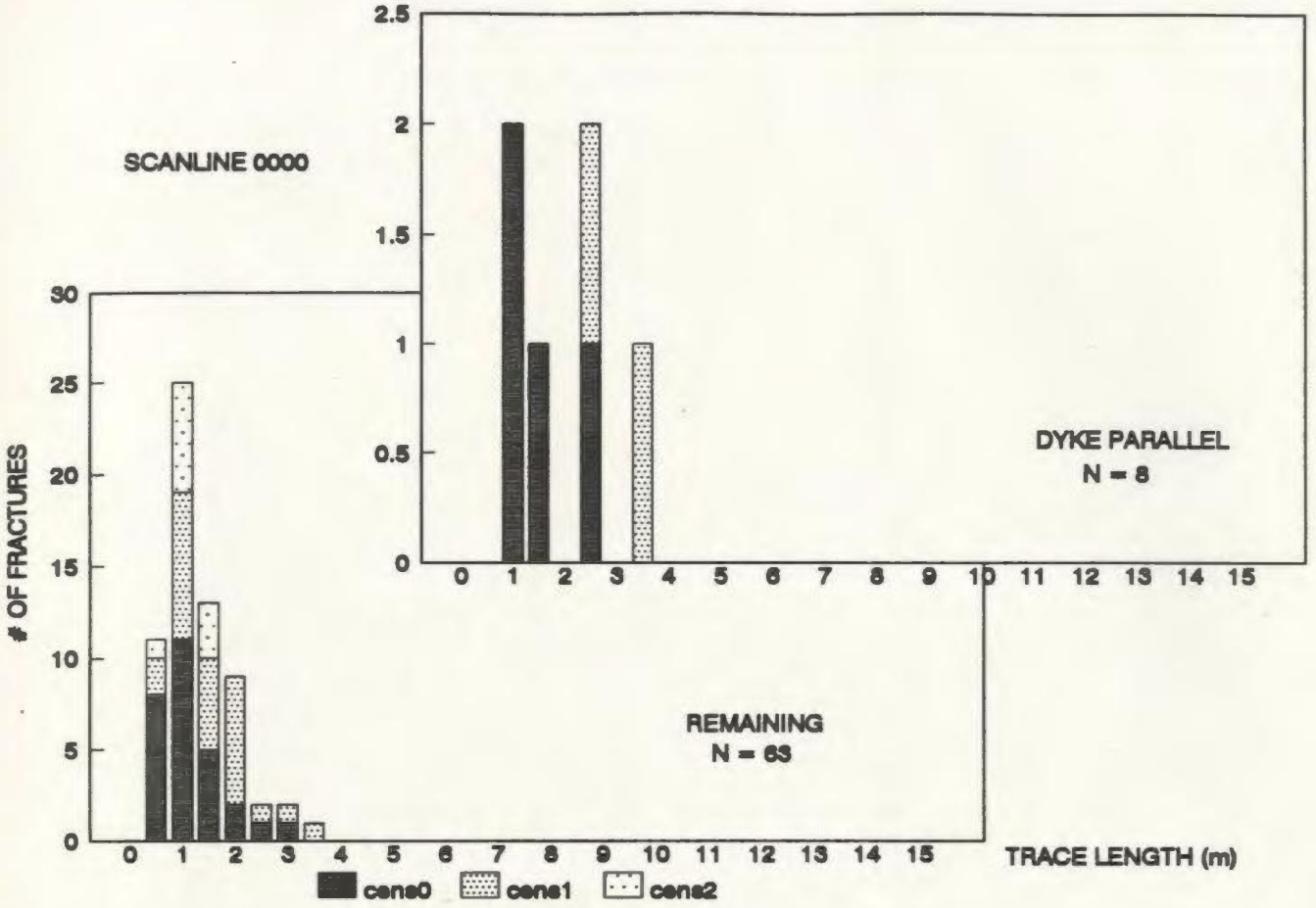
SCANLINE 0000
OF FRACTURES
TRACE LENGTH (m)
DYKE PARALLEL
N = 8
REMAINING
N = 63
cens0
cens1
cens2

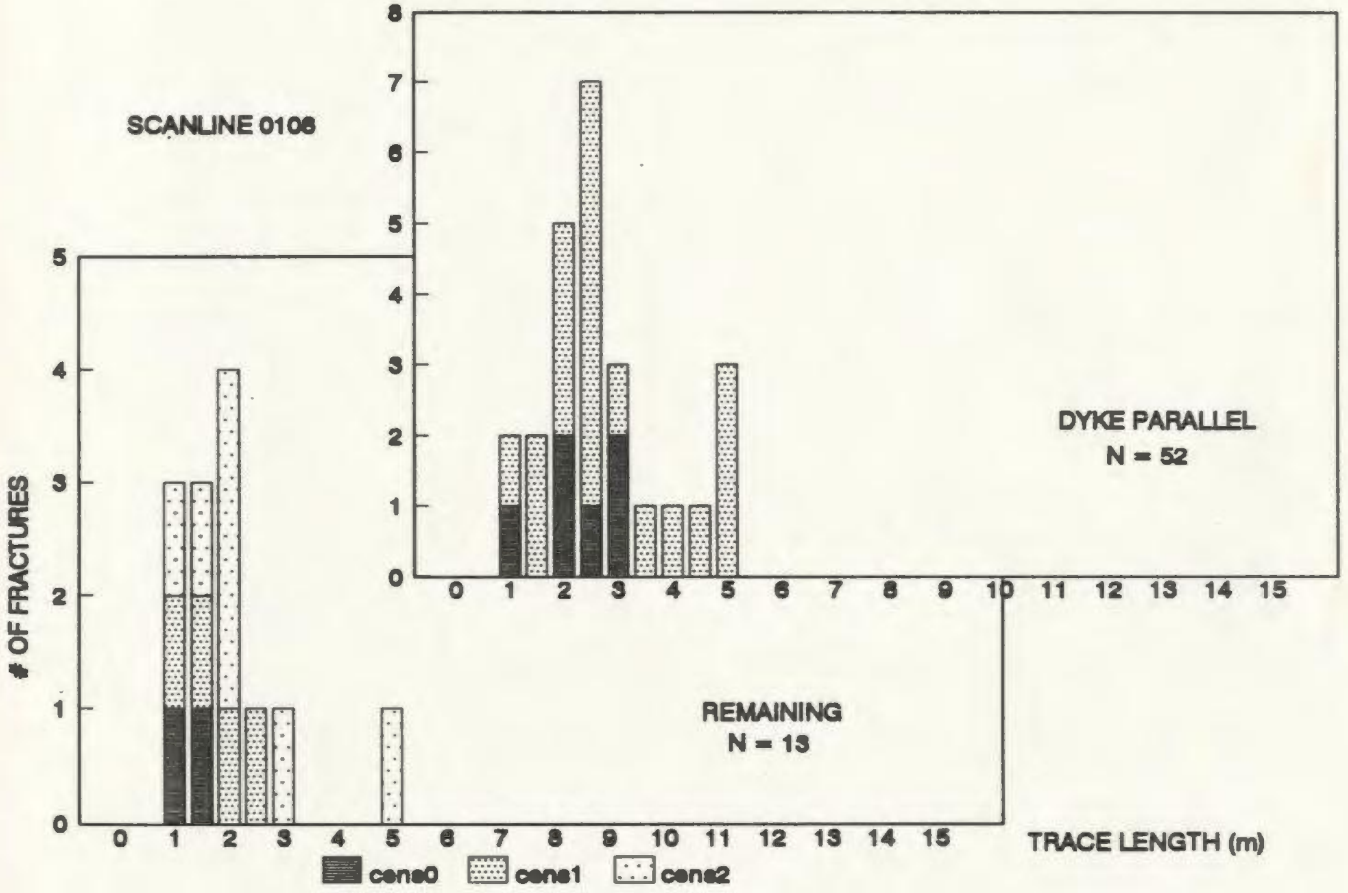
SCANLINE 0106
OF FRACTURES
TRACE LENGTH (m)
DYKE PARALLEL
N = 52
REMAINING
N = 13
cens0
cens1
cens2

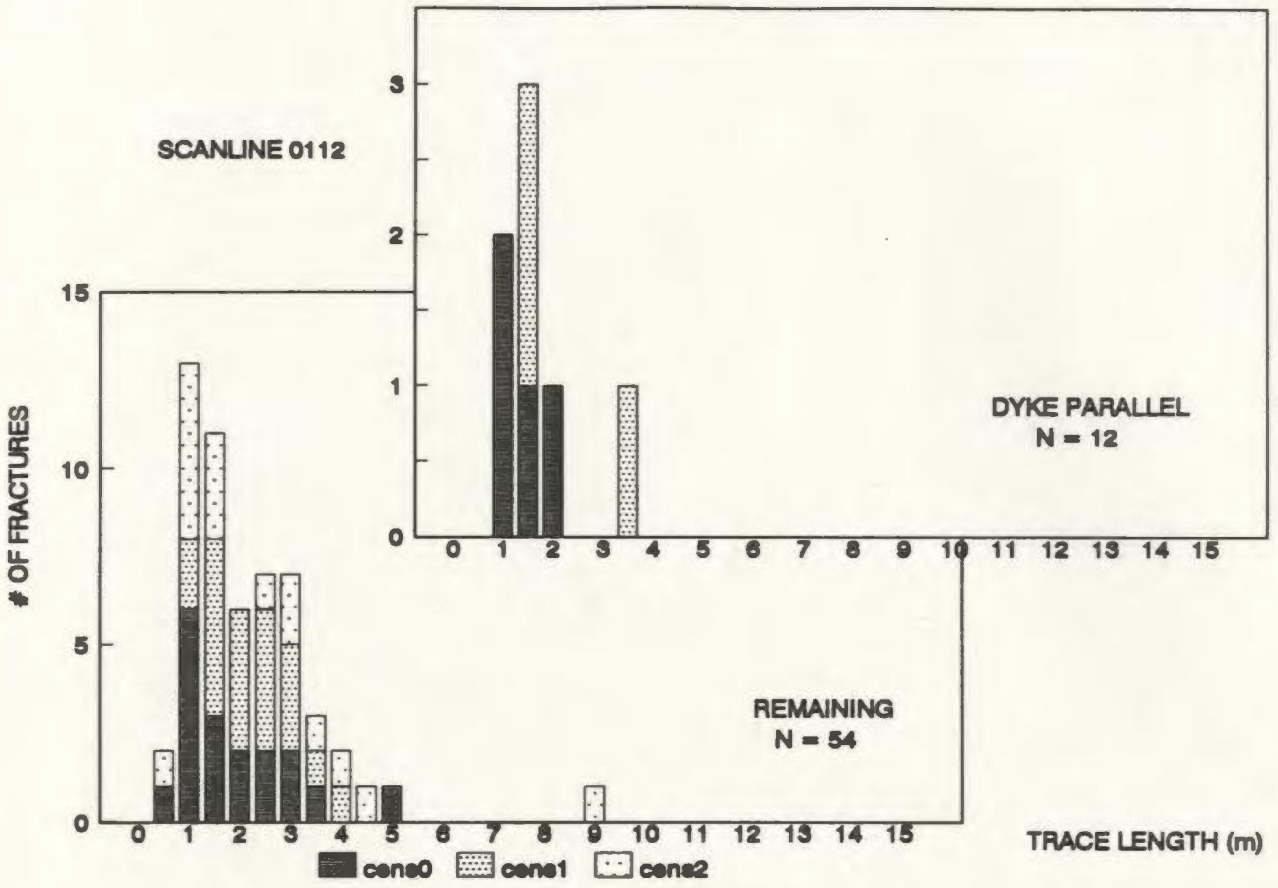
SCANLINE 0112
OF FRACTURES
DYKE PARALLEL
N = 12
REMAINING
N = 54
TRACE LENGTH (m)
cens0
cens1
cens2

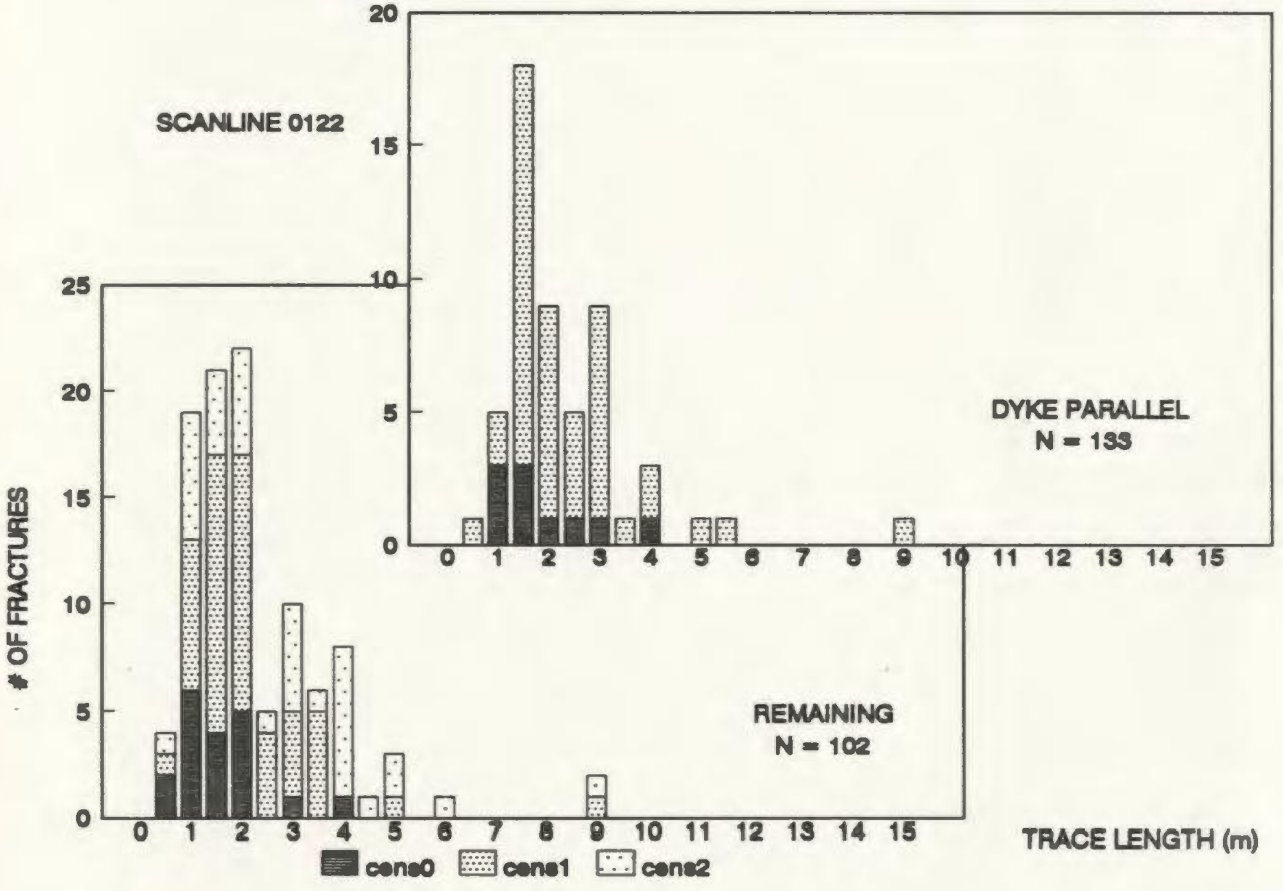
SCANLINE 0122
OF FRACTURES
DYKE PARALLEL
N = 133
REMAINING
N = 102
TRACE LENGTH (m)
cens0
cens1
cens2

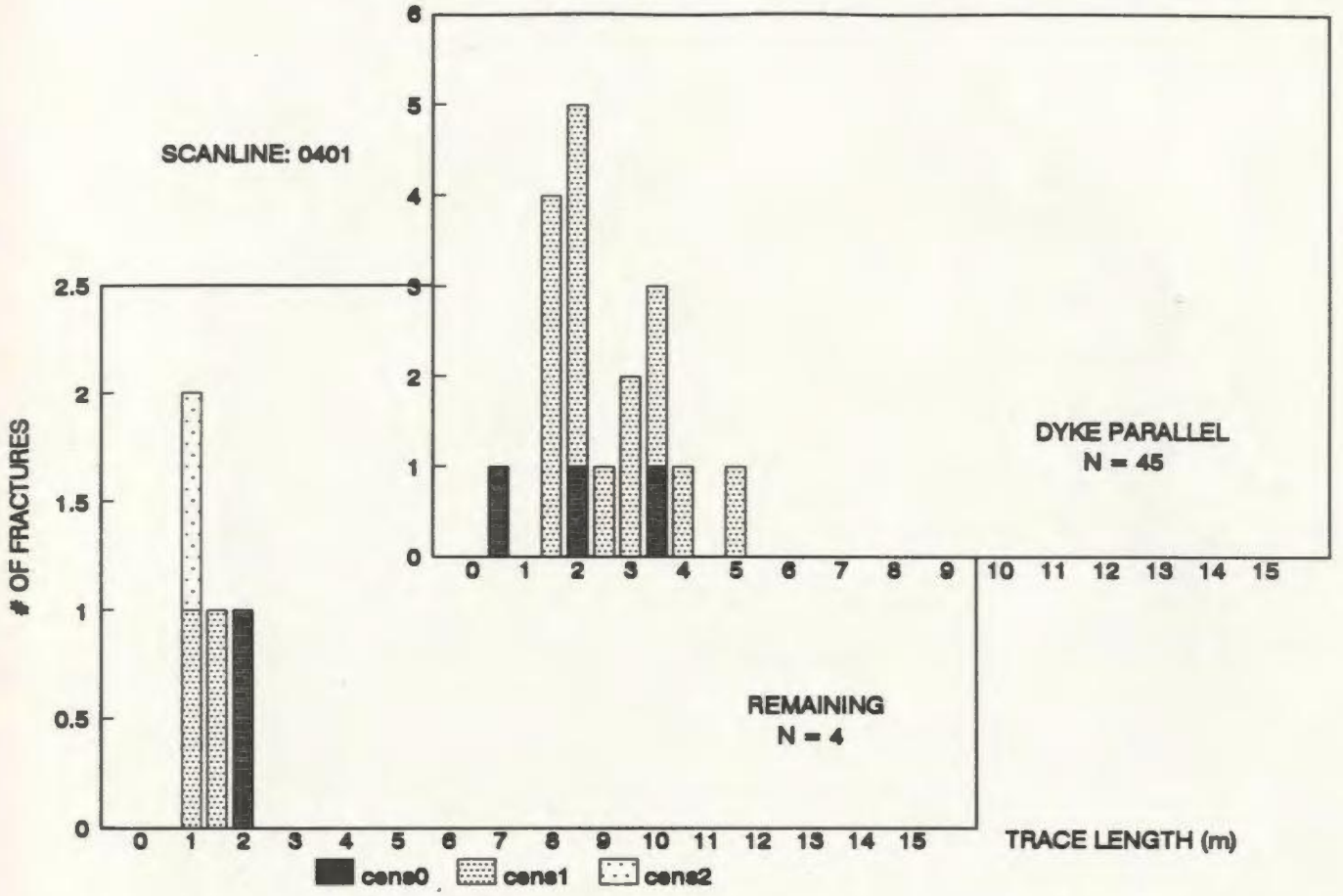
SCANLINE: 0401
OF FRACTURES
DYKE PARALLEL
N = 45
REMAINING
N = 4
TRACE LENGTH (m)
cens0
cens1
cens2

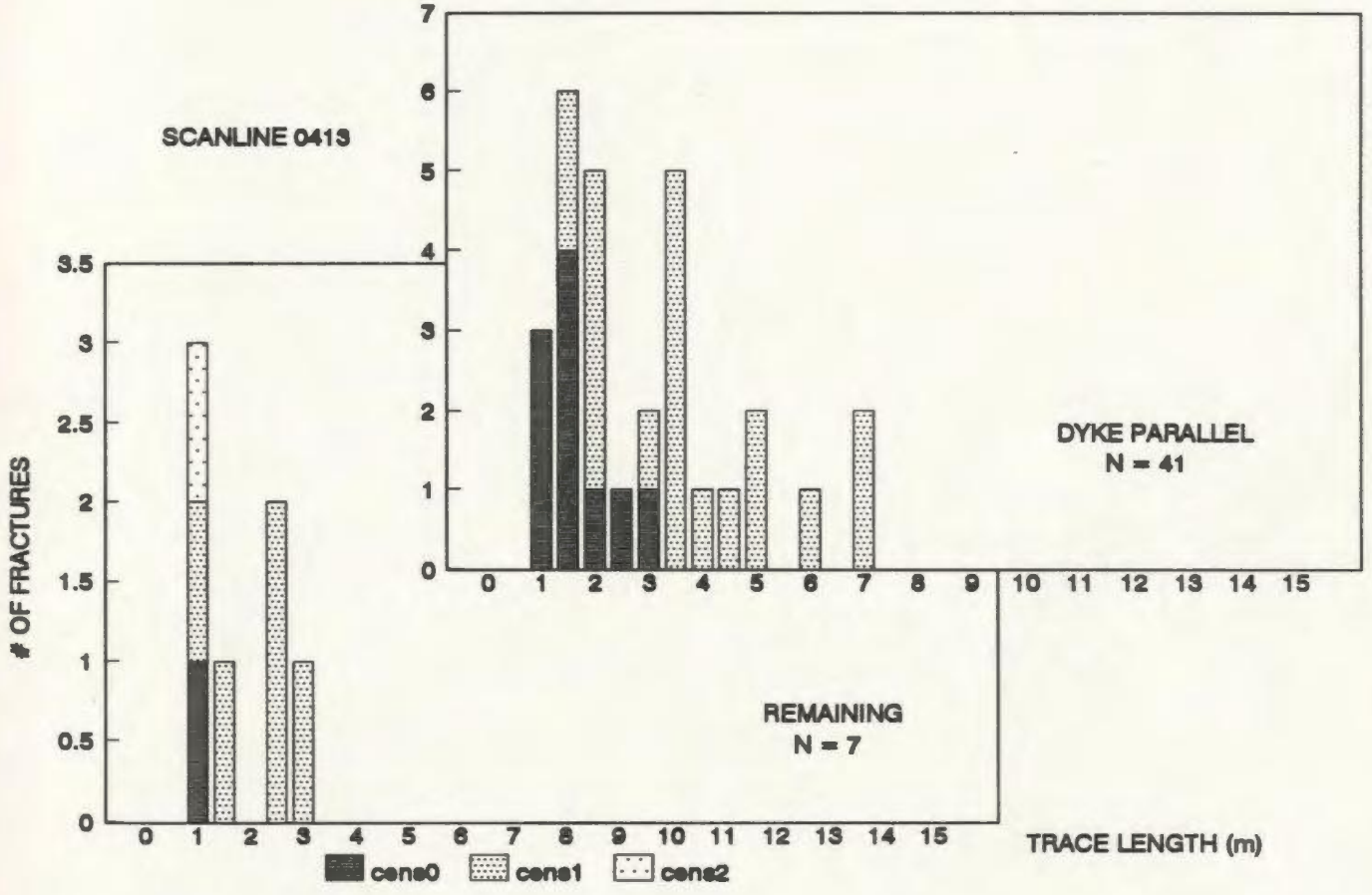
SCANLINE 0413
OF FRACTURES
DYKE PARALLEL
N = 41
REMAINING
N = 7
TRACE LENGTH (m)
cens0
cens1
cens2

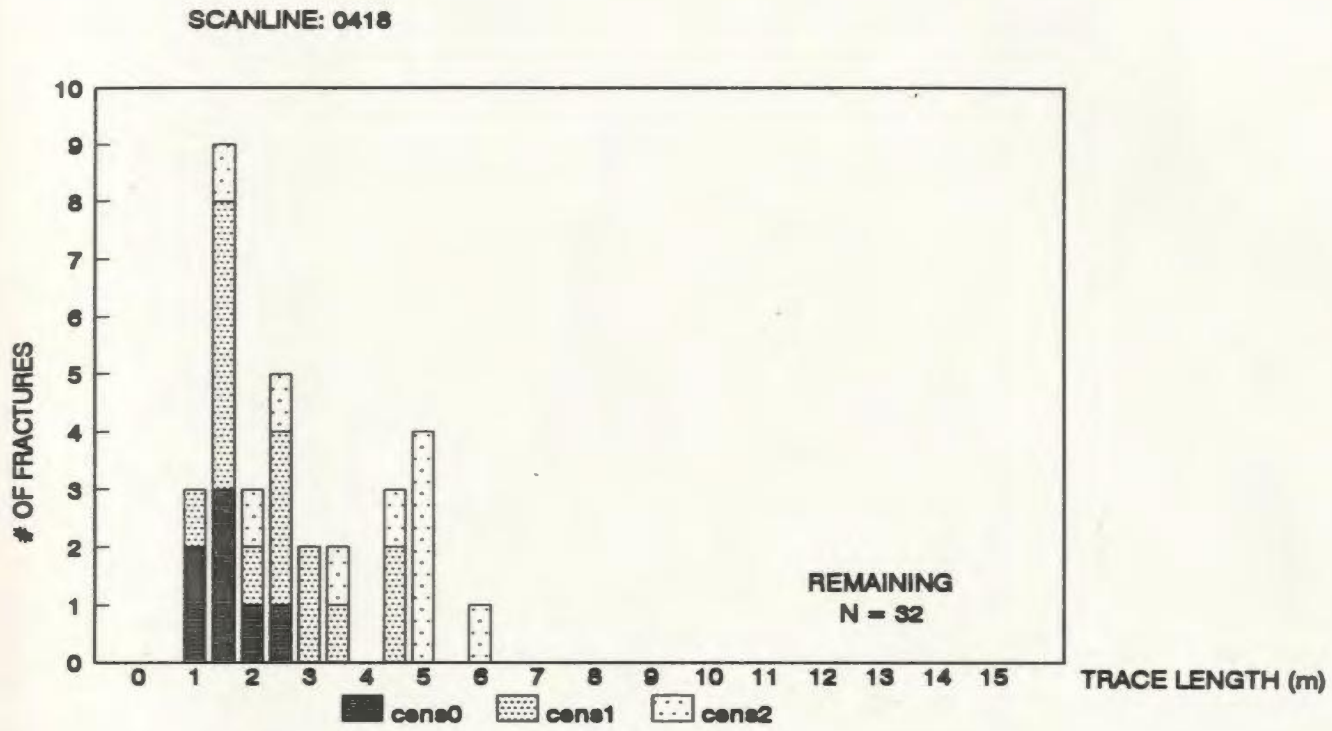
SCANLINE: 0418
OF FRACTURES
REMAINING
N = 32
TRACE LENGTH (m)
cens0
cens1
cens2

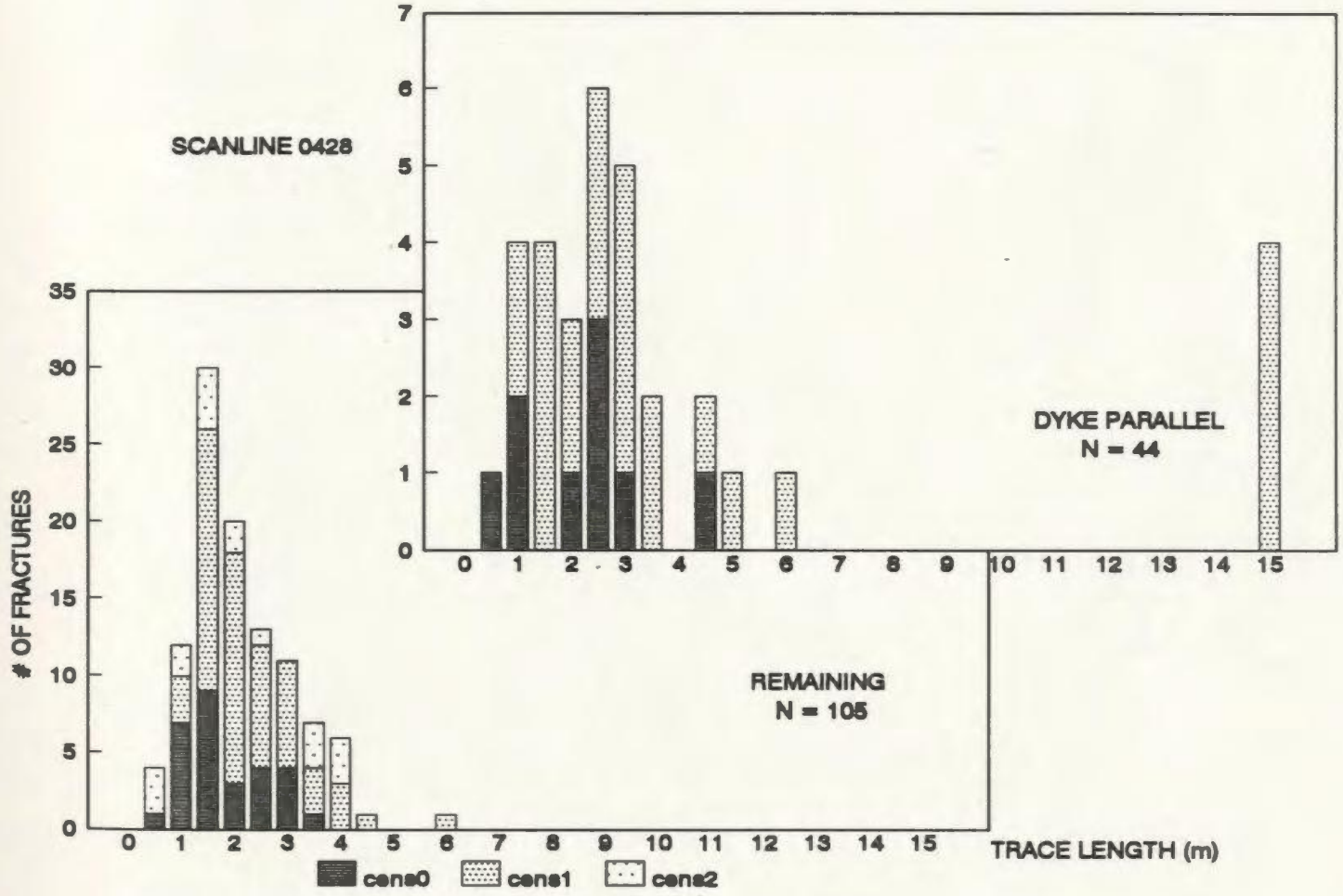
SCANLINE 0428
OF FRACTURES
DYKE PARALLEL
N = 44
REMAINING
N = 105
TRACE LENGTH (m)
cens0
cens1
cens2

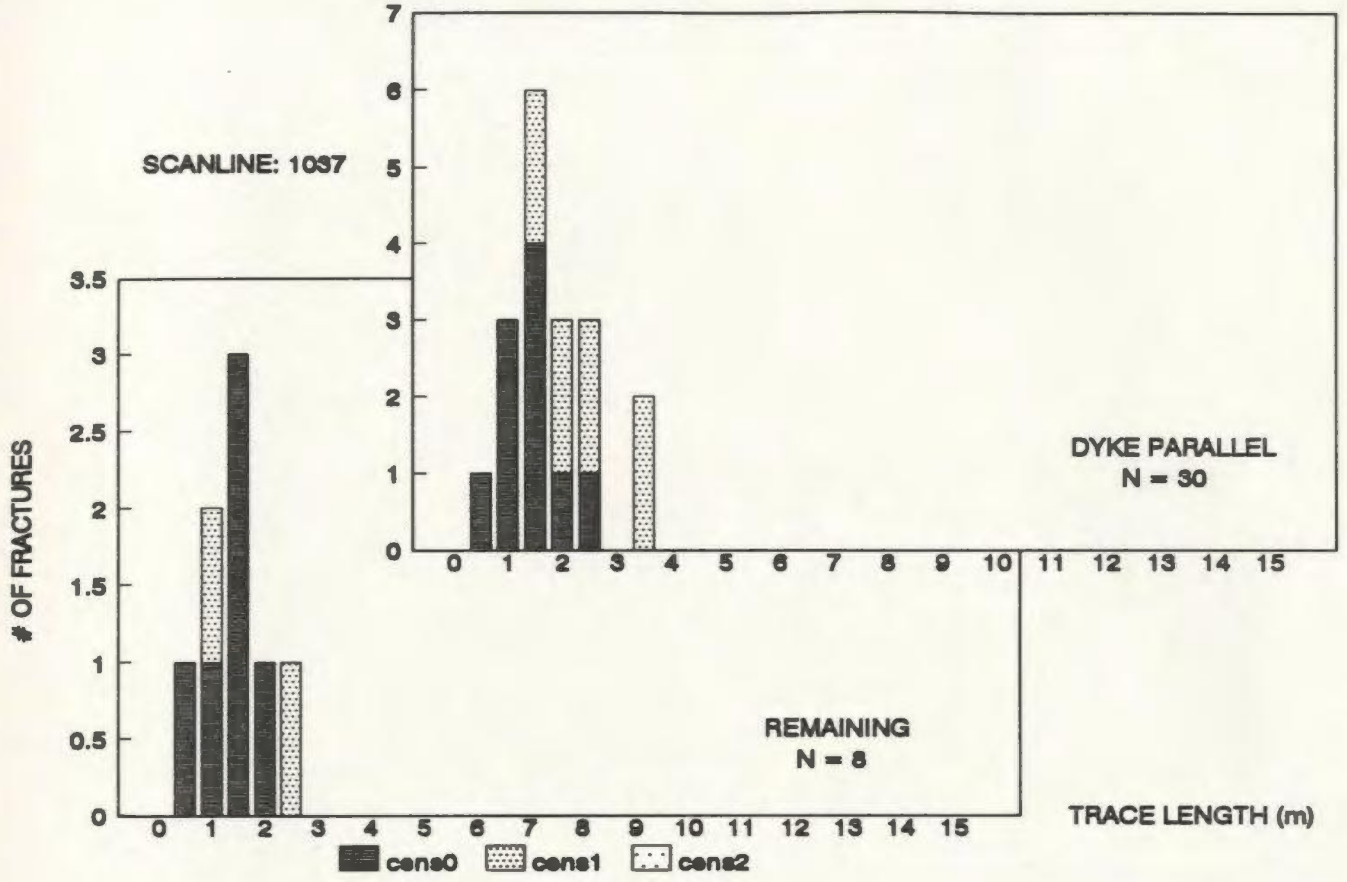
SCANLINE: 1037
OF FRACTURES
TRACE LENGTH (m)
DYKE PARALLEL
N = 30
REMAINING
N = 8
cens0
cens1
cens2

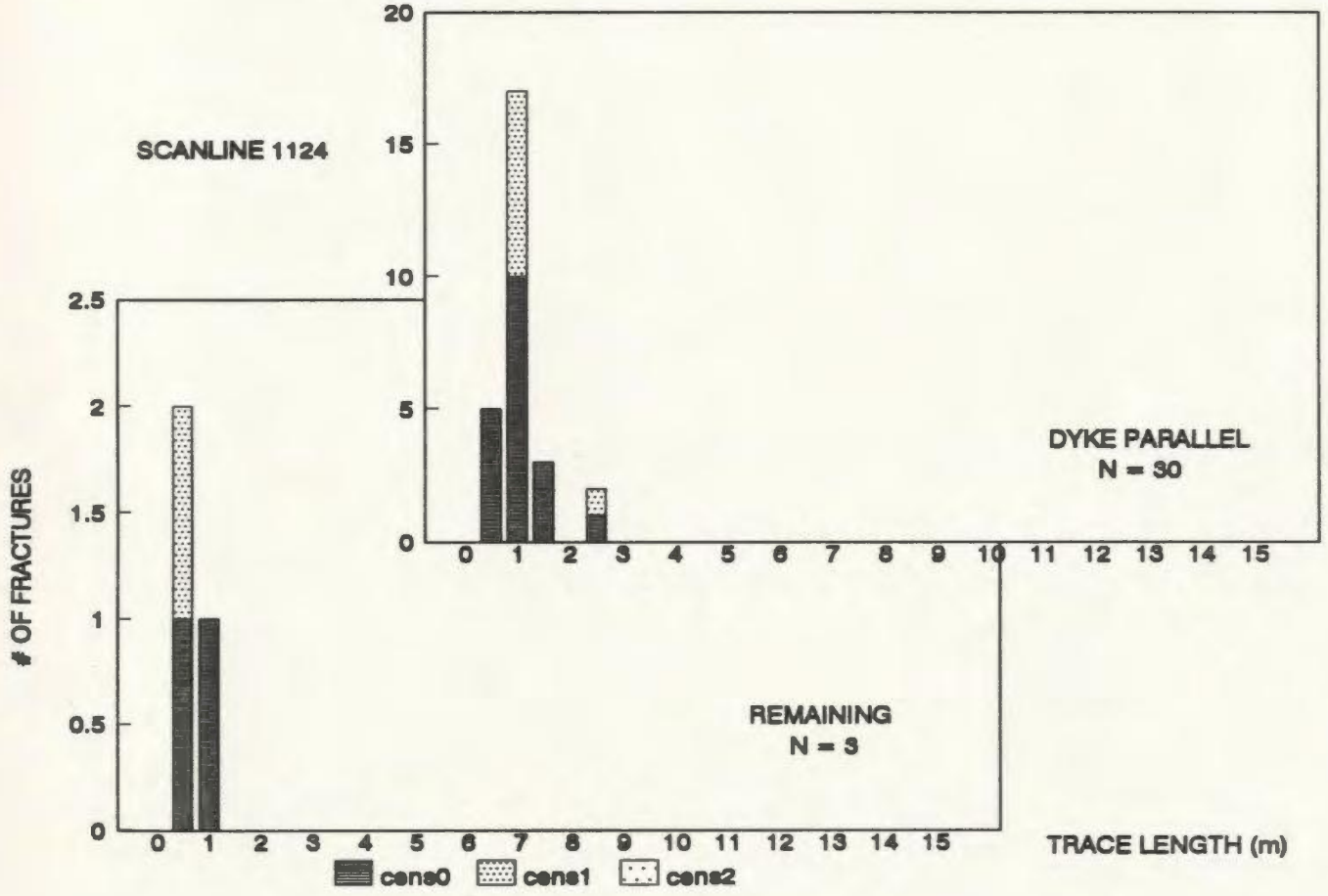
SCANLINE 1124
OF FRACTURES
TRACE LENGTH (m)
DYKE PARALLEL
N = 30
REMAINING
N = 3
cens0
cens1
cens2

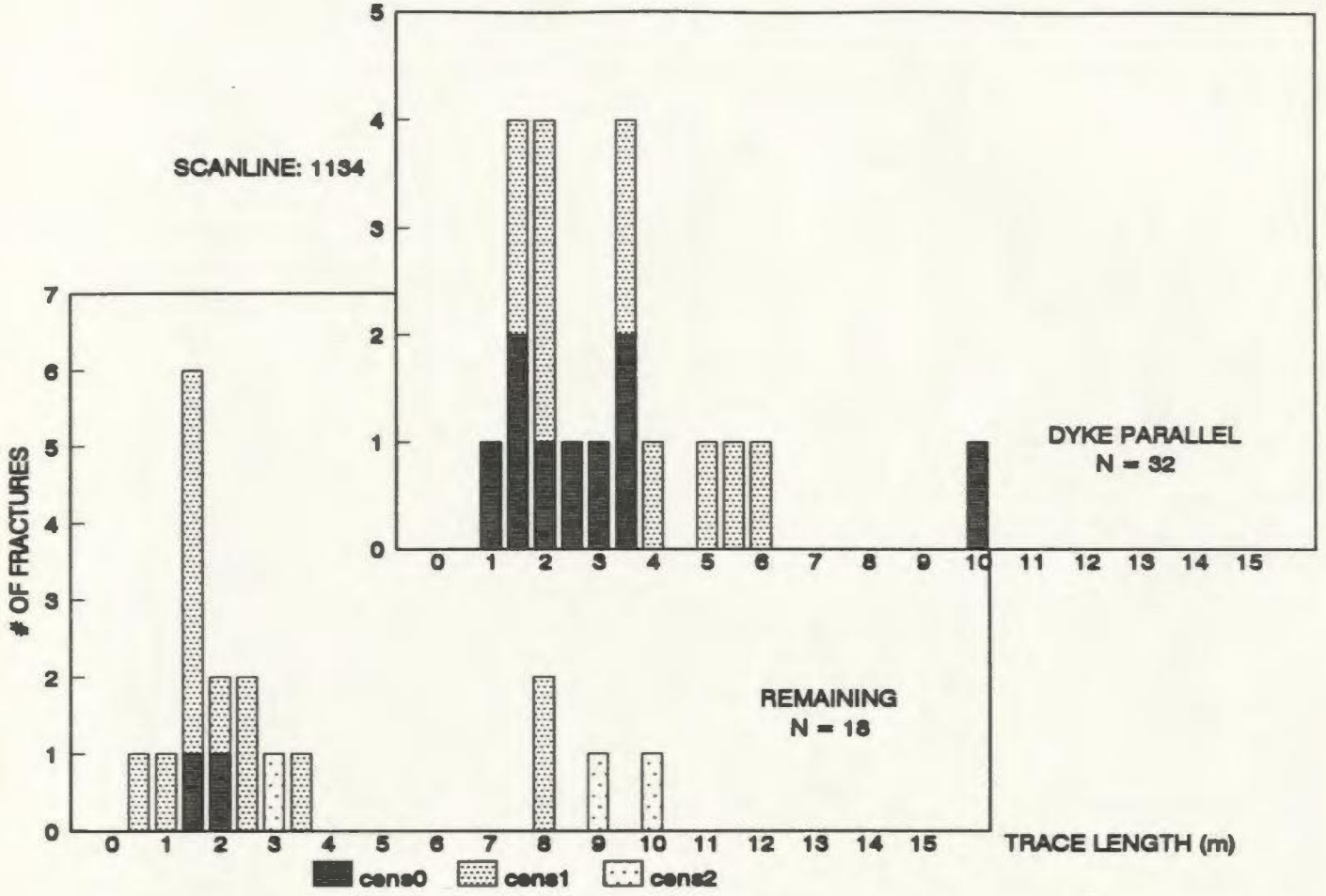
SCANLINE: 1134
DYKE PARALLEL
N = 32
REMAINING
N = 18
# OF FRACTURES
TRACE LENGTH (m)
cens0
cens1
cens2

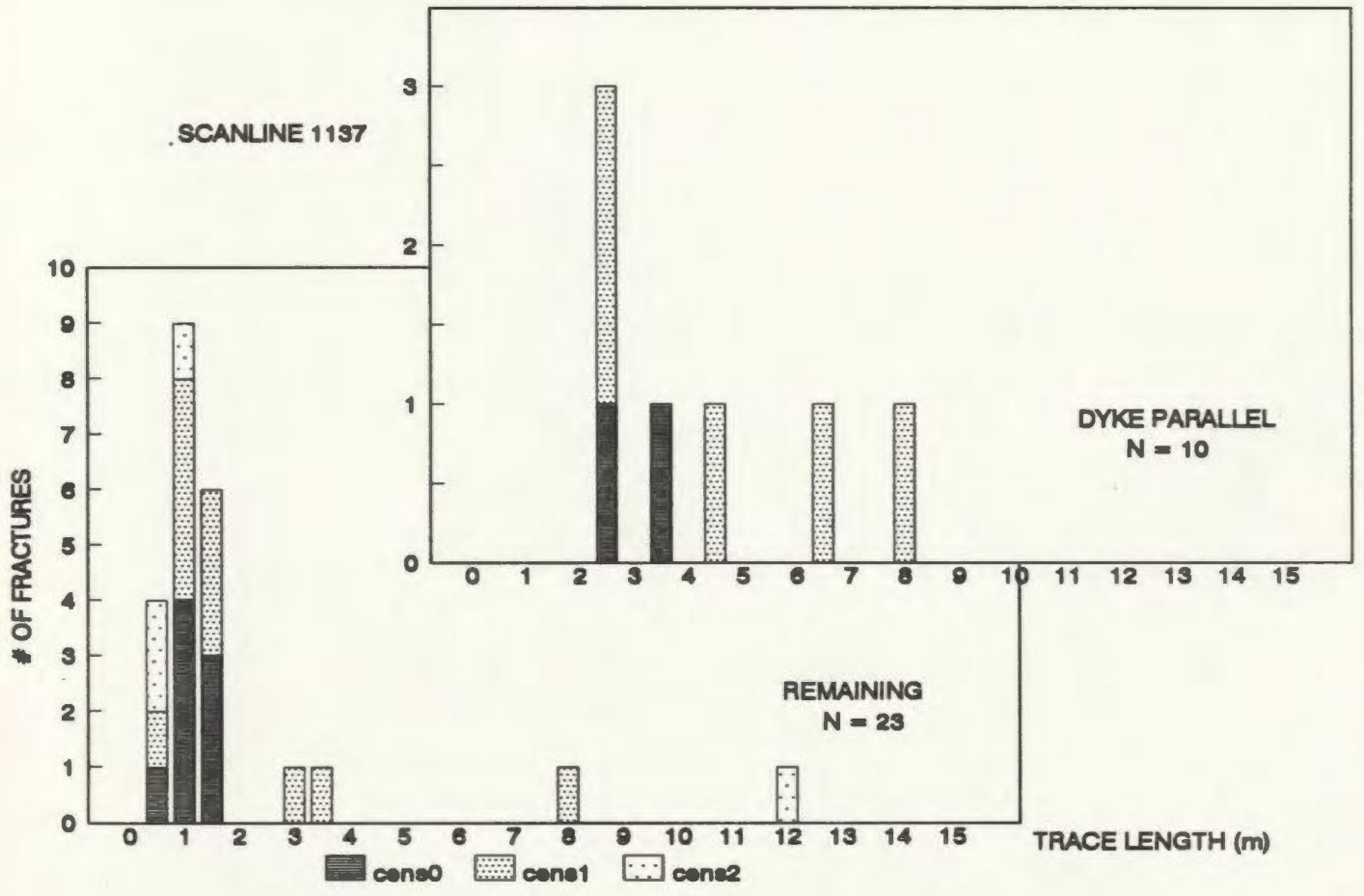
SCANLINE 1137
DYKE PARALLEL
N = 10
REMAINING
N = 23
# OF FRACTURES
TRACE LENGTH (m)
cens0
cens1
cens2

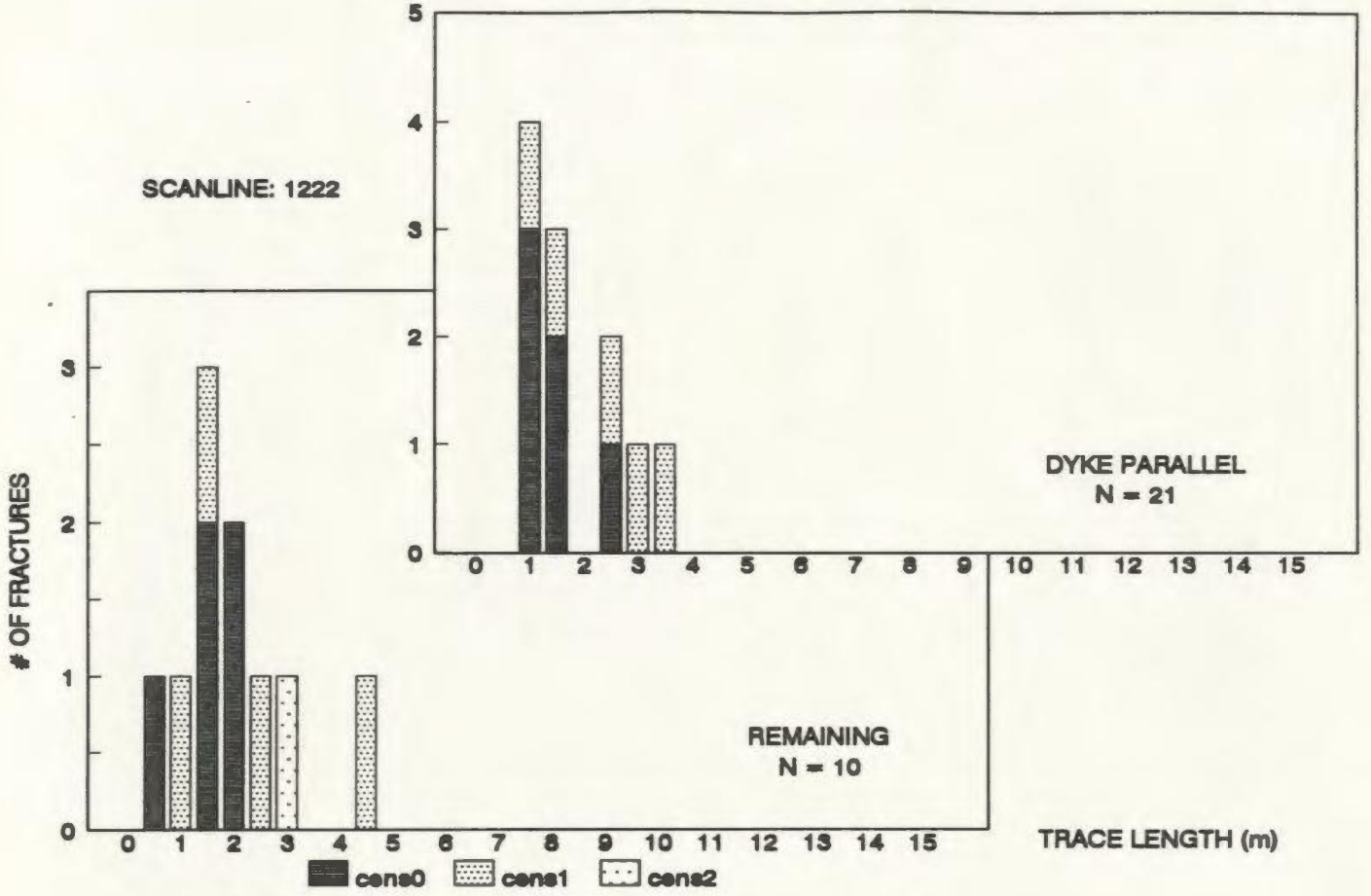
SCANLINE: 1222
DYKE PARALLEL
N = 21
REMAINING
N = 10
# OF FRACTURES
TRACE LENGTH (m)
cens0
cens1
cens2

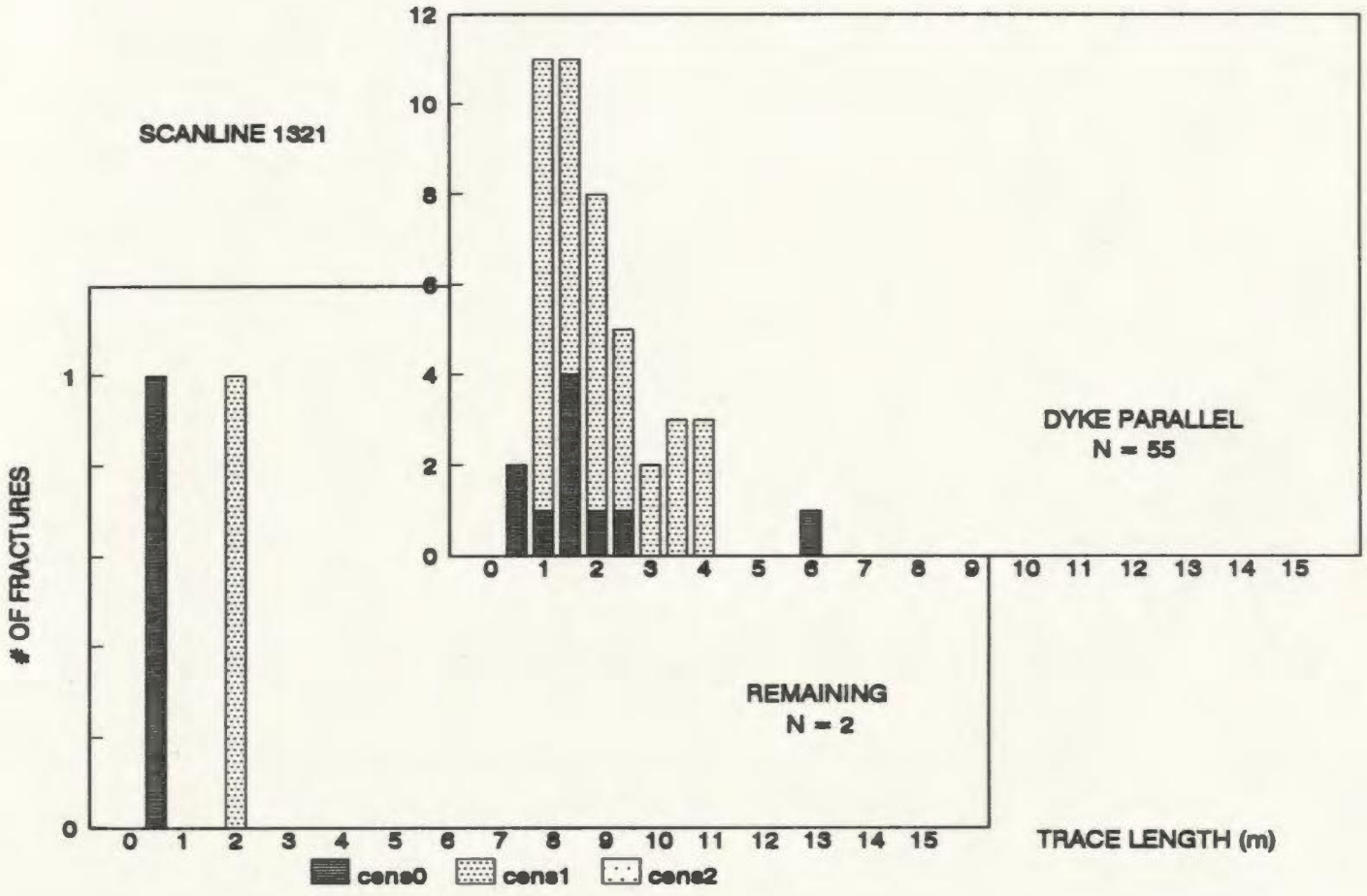
SCANLINE 1321
DYKE PARALLEL
N = 55
REMAINING
N = 2
# OF FRACTURES
TRACE LENGTH (m)
cens0
cens1
cens2

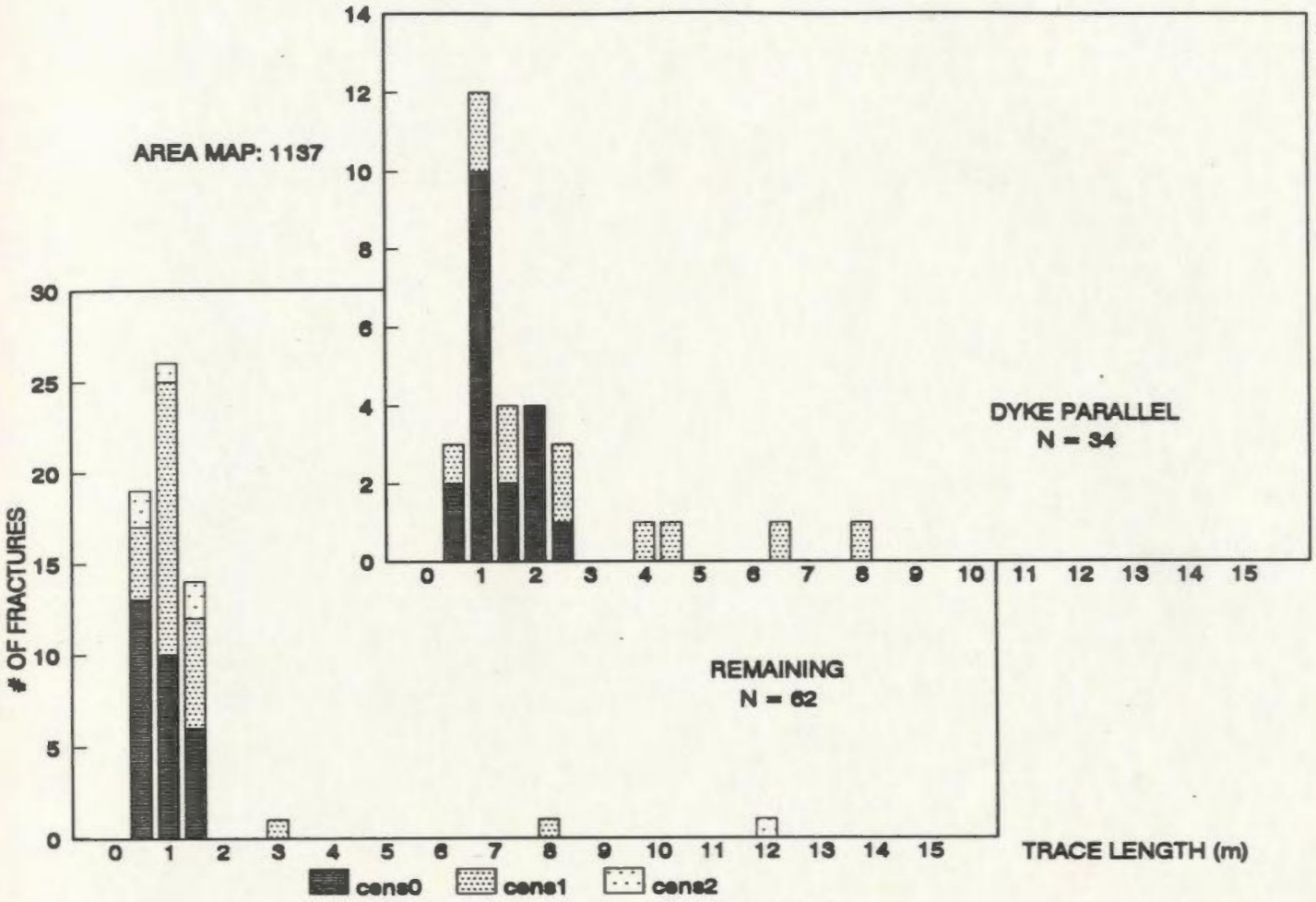
AREA MAP: 1137
DYKE PARALLEL
N = 34
REMAINING
N = 62
# OF FRACTURES
TRACE LENGTH (m)
cens0
cens1
cens2

A.3 Fracture Characteristics

A.3.7 *Trace Length vs Censoring and Termination*

A.3.7.2 *Trace Length Histograms BY Domain By Set*

The trace length histograms by domain are stckaed bar graphs broken down by censoring and termination. Each domain is also identified with a nearby town name (these are seen in Figure 3.1).

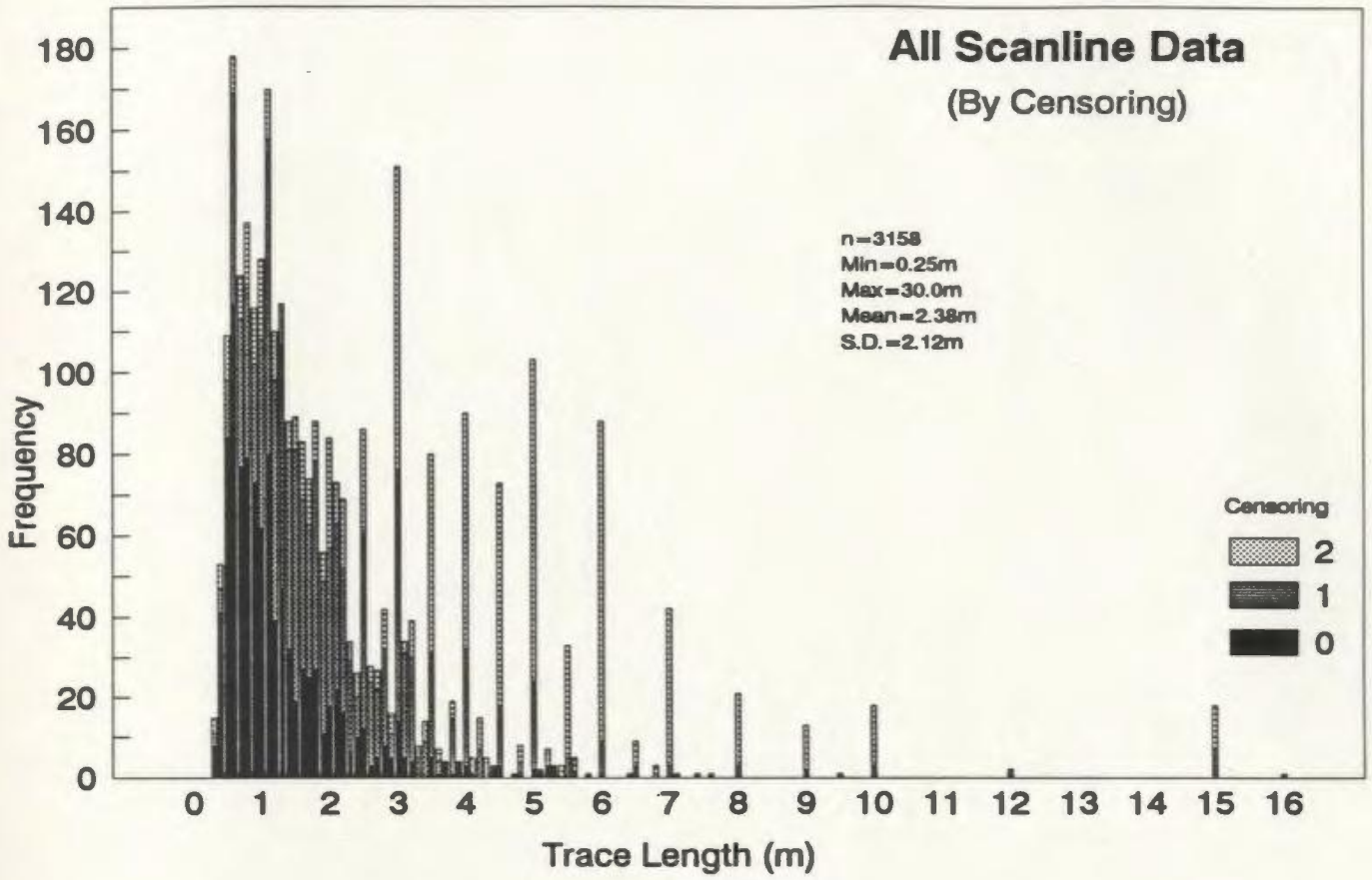
All Scanline Data
(By Censoring)
n=3158
Min=0.25m
Max=30.0m
Mean=2.38m
S.D.=2.12m
Censoring
2
1
0
Frequency
Trace Length (m)

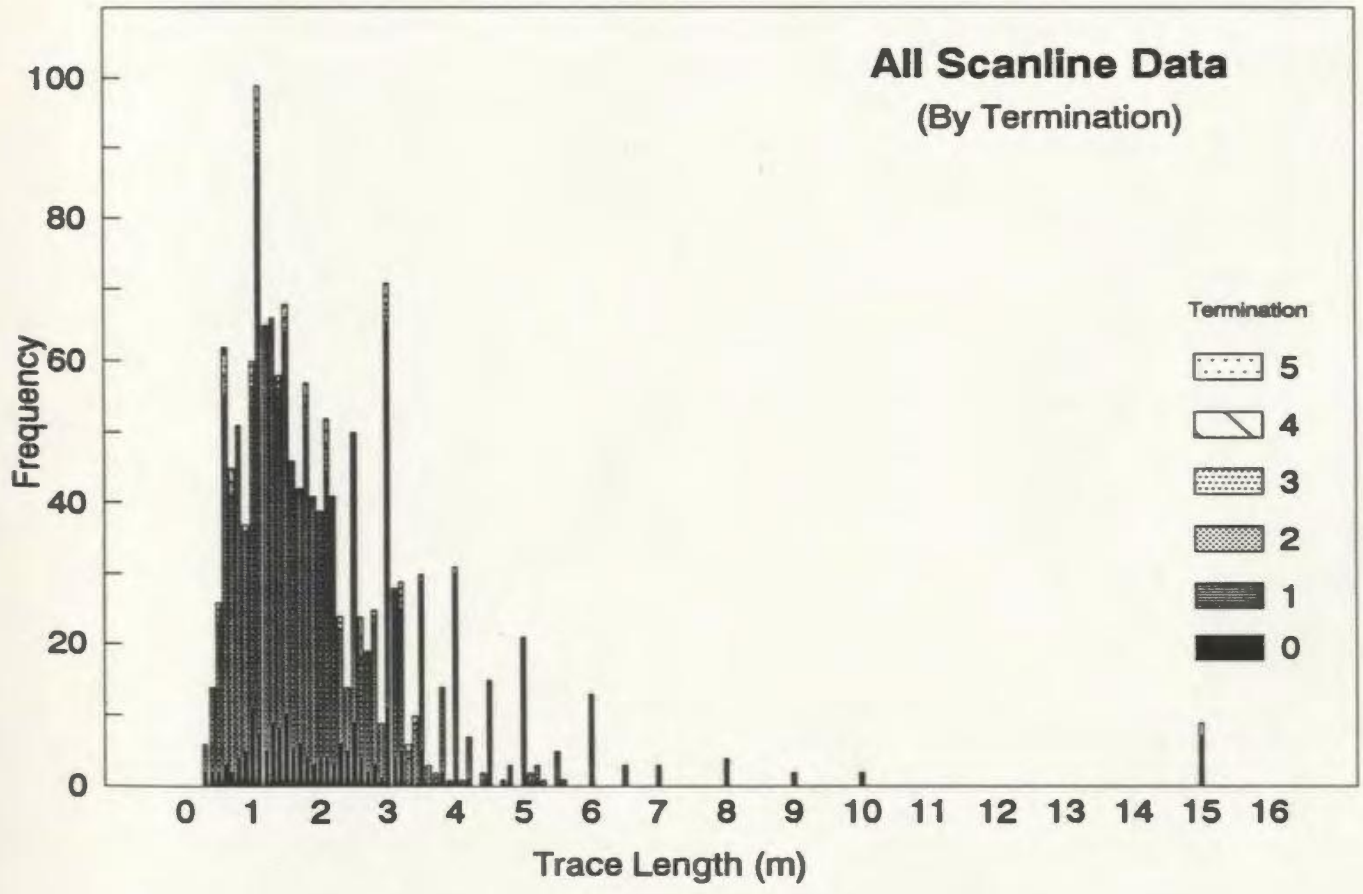
All Scanline Data
(By Termination)
Termination
5
4
3
2
1
0
Frequency
Trace Length (m)

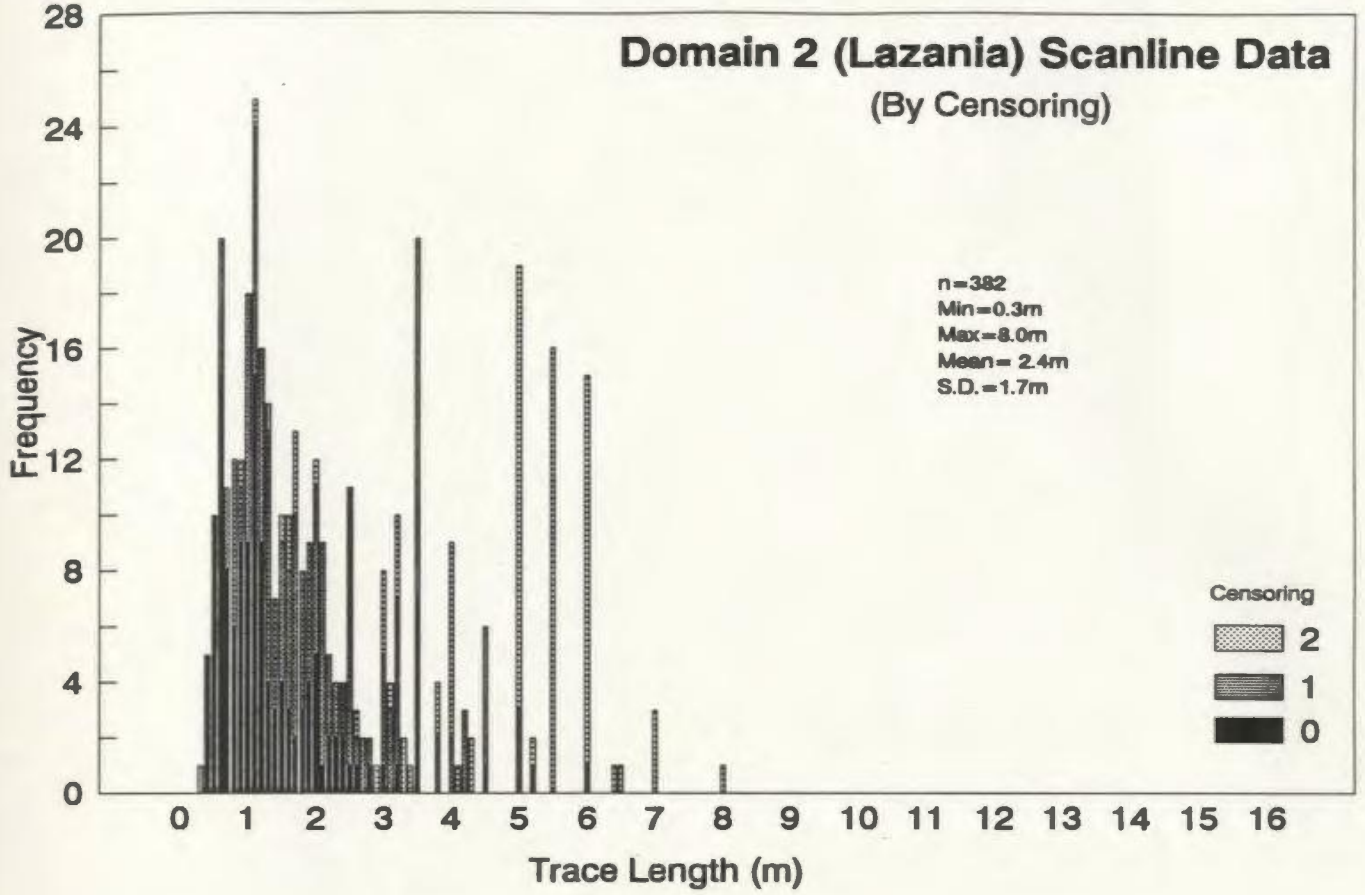
Domain 2 (Lazania) Scanline Data
(By Censoring)
n=382
Min=0.3m
Max=8.0m
Mean= 2.4m
S.D.=1.7m
Censoring
2
1
0
Frequency
Trace Length (m)
0 1 2 3 4 5 6 7 8 9 10 11 12 13 14 15 16
0 4 8 12 16 20 24 28

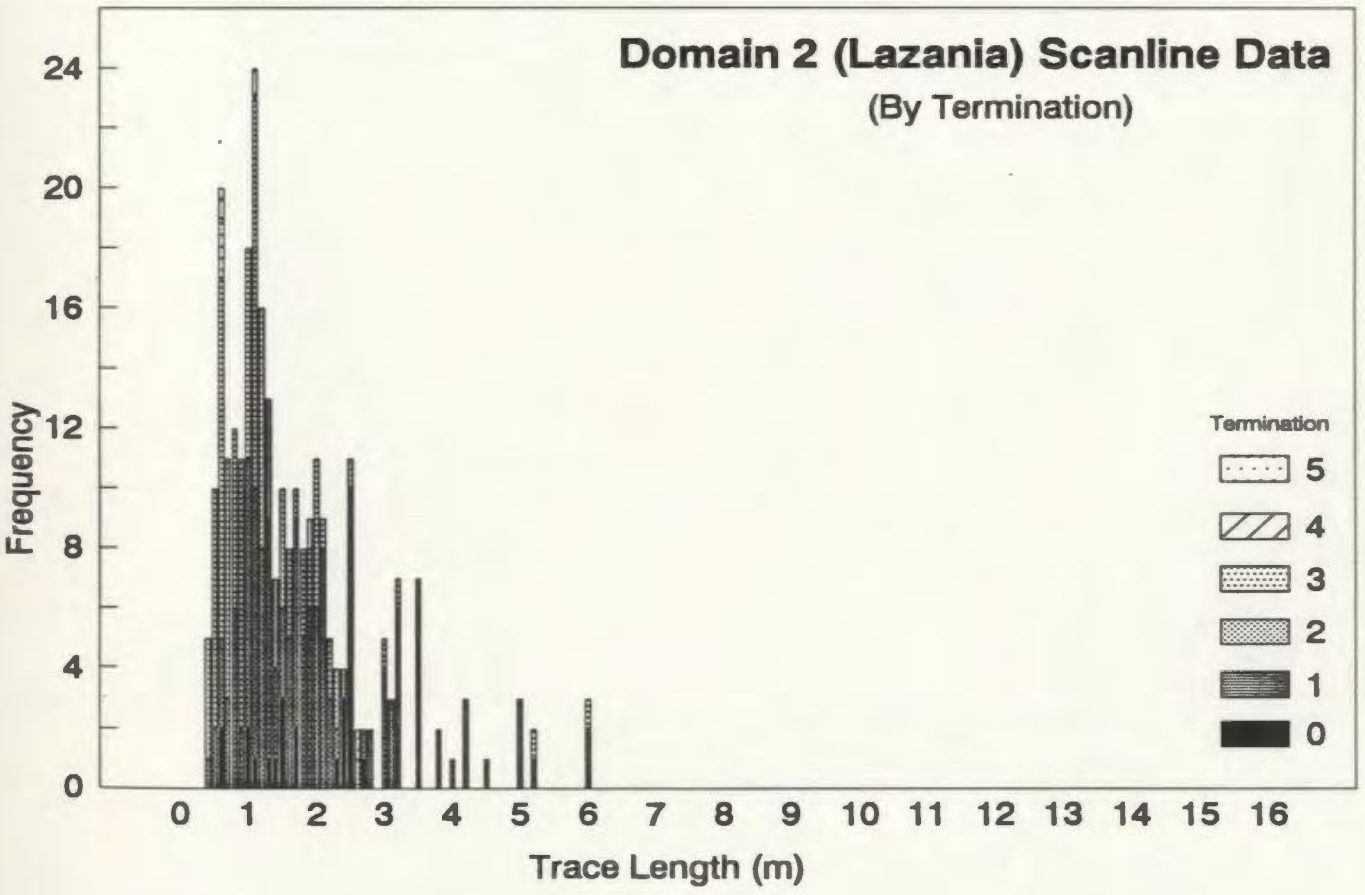
Domain 2 (Lazania) Scanline Data
(By Termination)
Termination
5
4
3
2
1
0
Frequency
Trace Length (m)
0 1 2 3 4 5 6 7 8 9 10 11 12 13 14 15 16
0 4 8 12 16 20 24

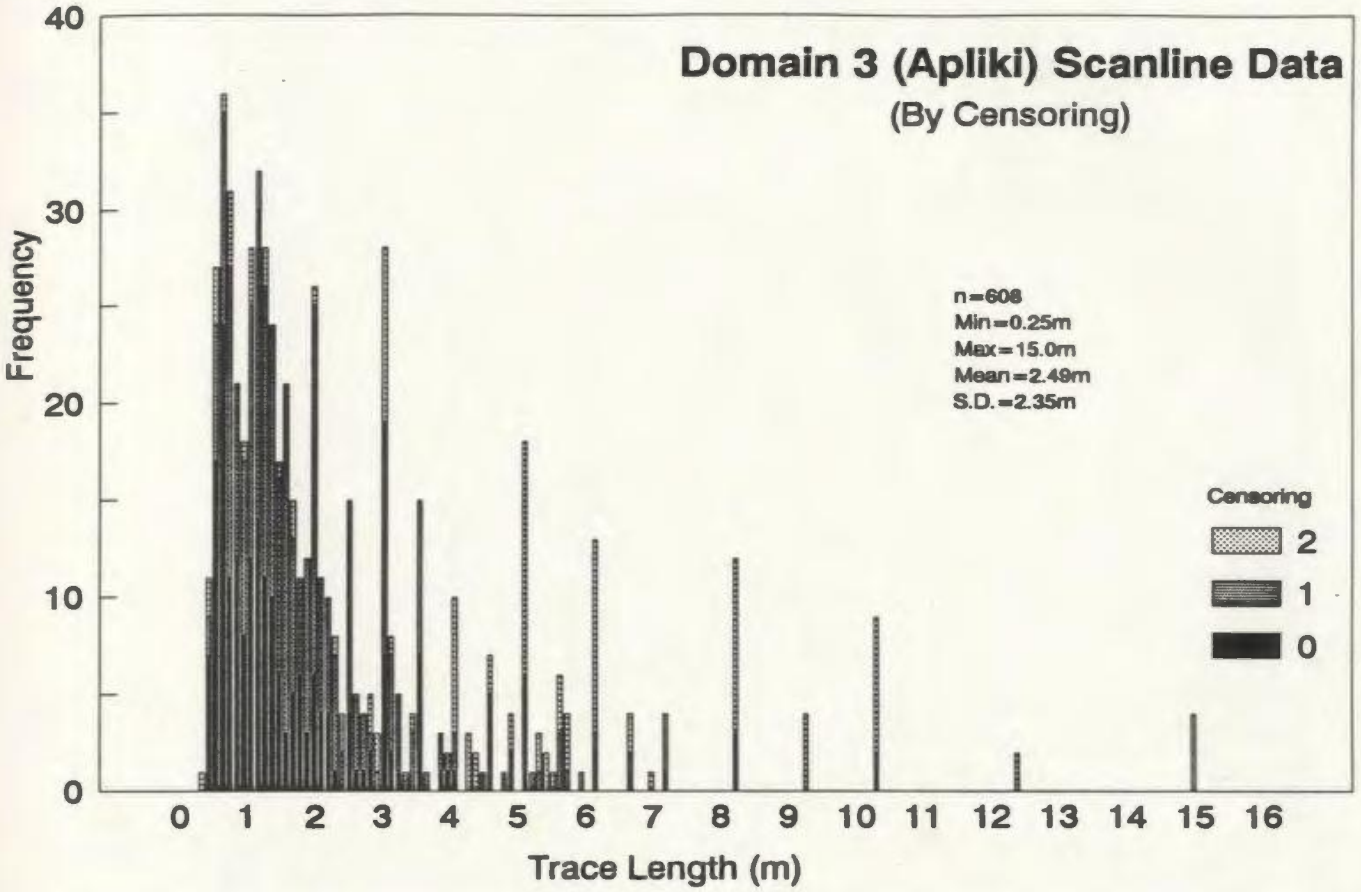
Domain 3 (Apliki) Scanline Data
(By Censoring)
n=608
Min=0.25m
Max=15.0m
Mean=2.49m
S.D.=2.35m
Censoring
2
1
0
Frequency
Trace Length (m)

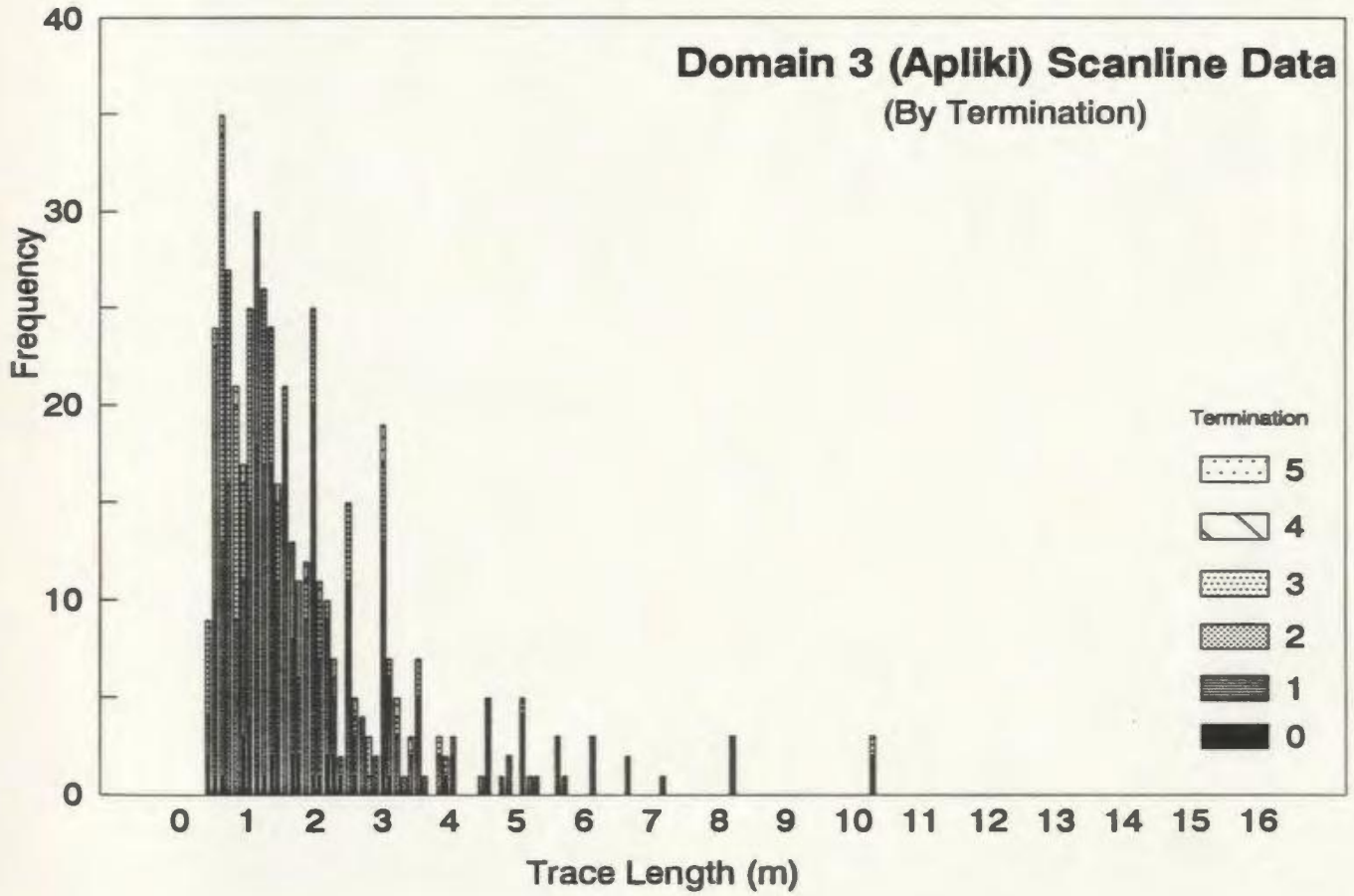
Domain 3 (Apliki) Scanline Data
(By Termination)
Termination
5
4
3
2
1
0
Frequency
Trace Length (m)

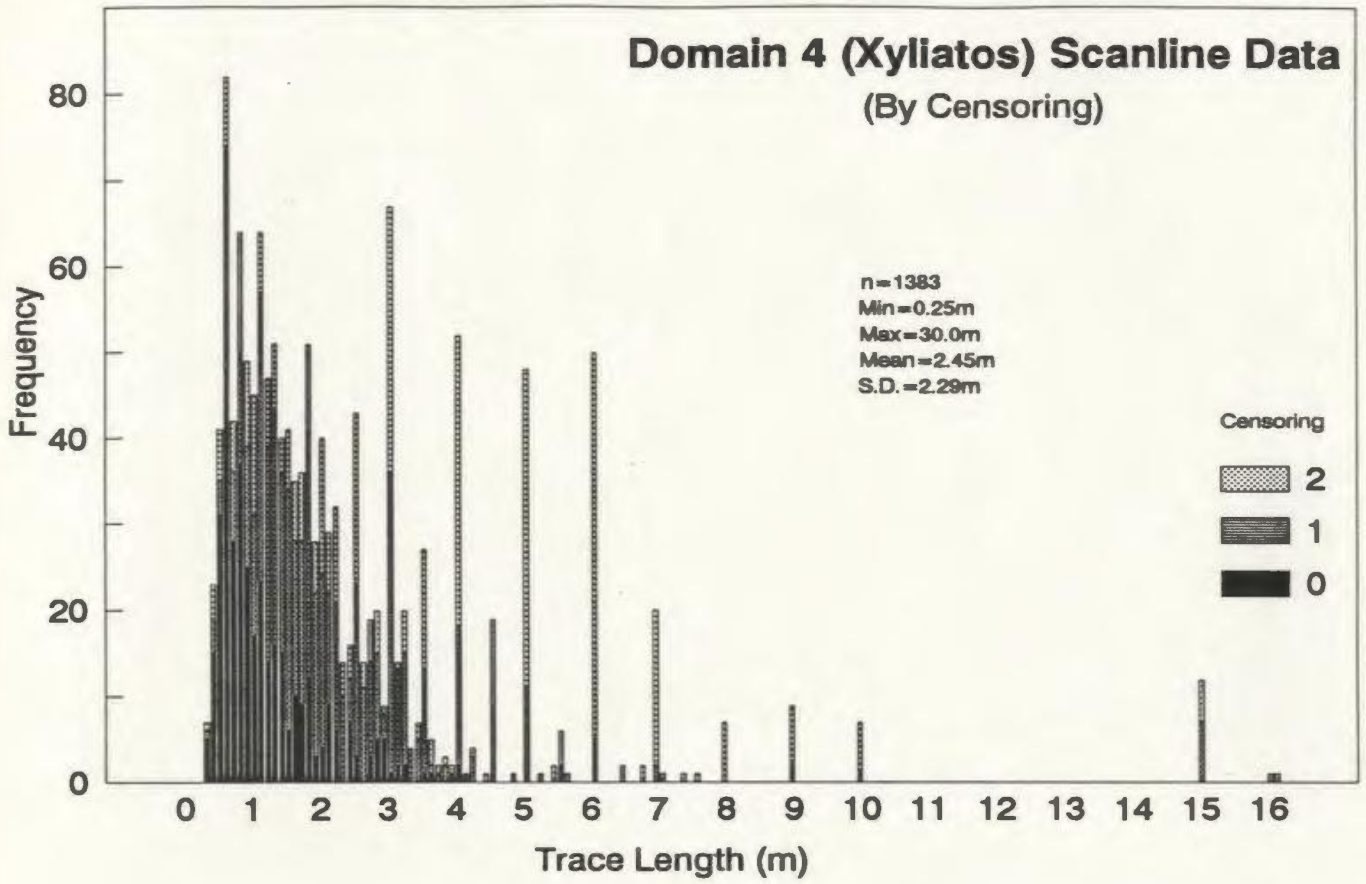
Domain 4 (Xyliatos) Scanline Data
(By Censoring)
n=1383
Min=0.25m
Max=30.0m
Mean=2.45m
S.D.=2.29m
Censoring
2
1
0
Frequency
0
20
40
60
80
0 1 2 3 4 5 6 7 8 9 10 11 12 13 14 15 16
Trace Length (m)

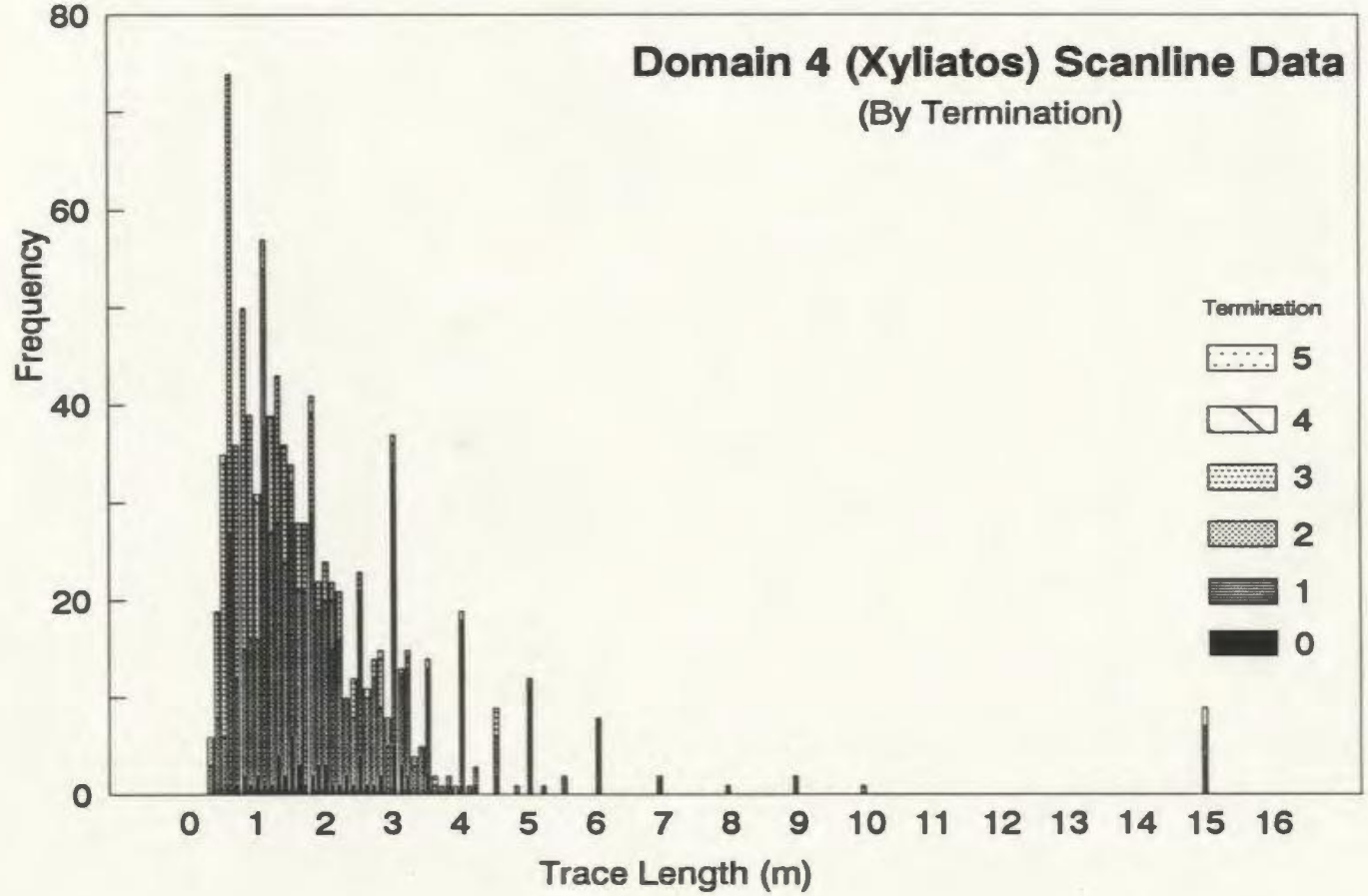
Domain 4 (Xyliatos) Scanline Data
(By Termination)
Termination
5
4
3
2
1
0
Frequency
0
20
40
60
80
0 1 2 3 4 5 6 7 8 9 10 11 12 13 14 15 16
Trace Length (m)

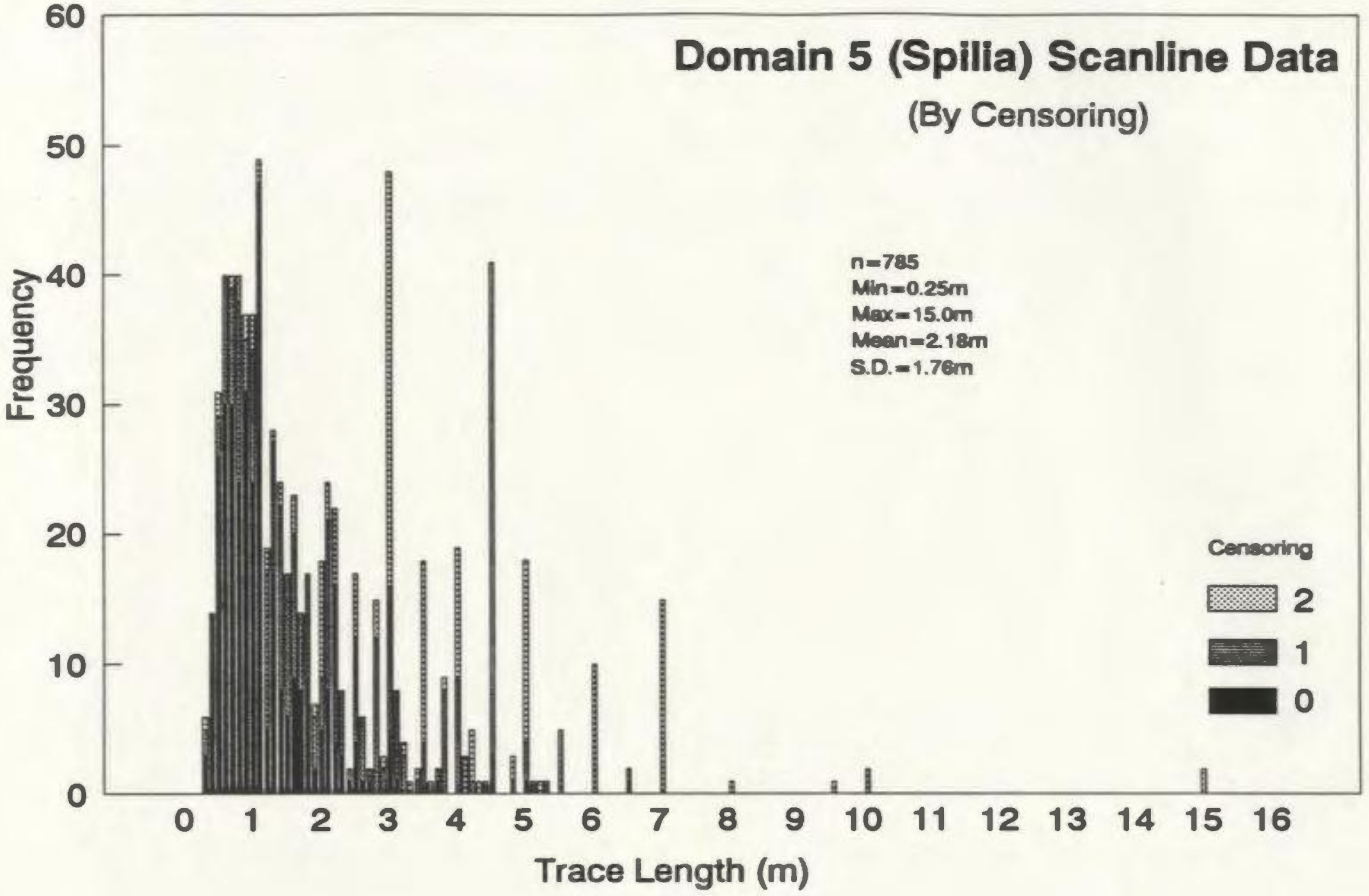
Domain 5 (Spilia) Scanline Data
(By Censoring)
n=785
Min=0.25m
Max=15.0m
Mean=2.18m
S.D.=1.76m
Censoring
2
1
0
Frequency
Trace Length (m)
0 10 20 30 40 50 60
0 1 2 3 4 5 6 7 8 9 10 11 12 13 14 15 16

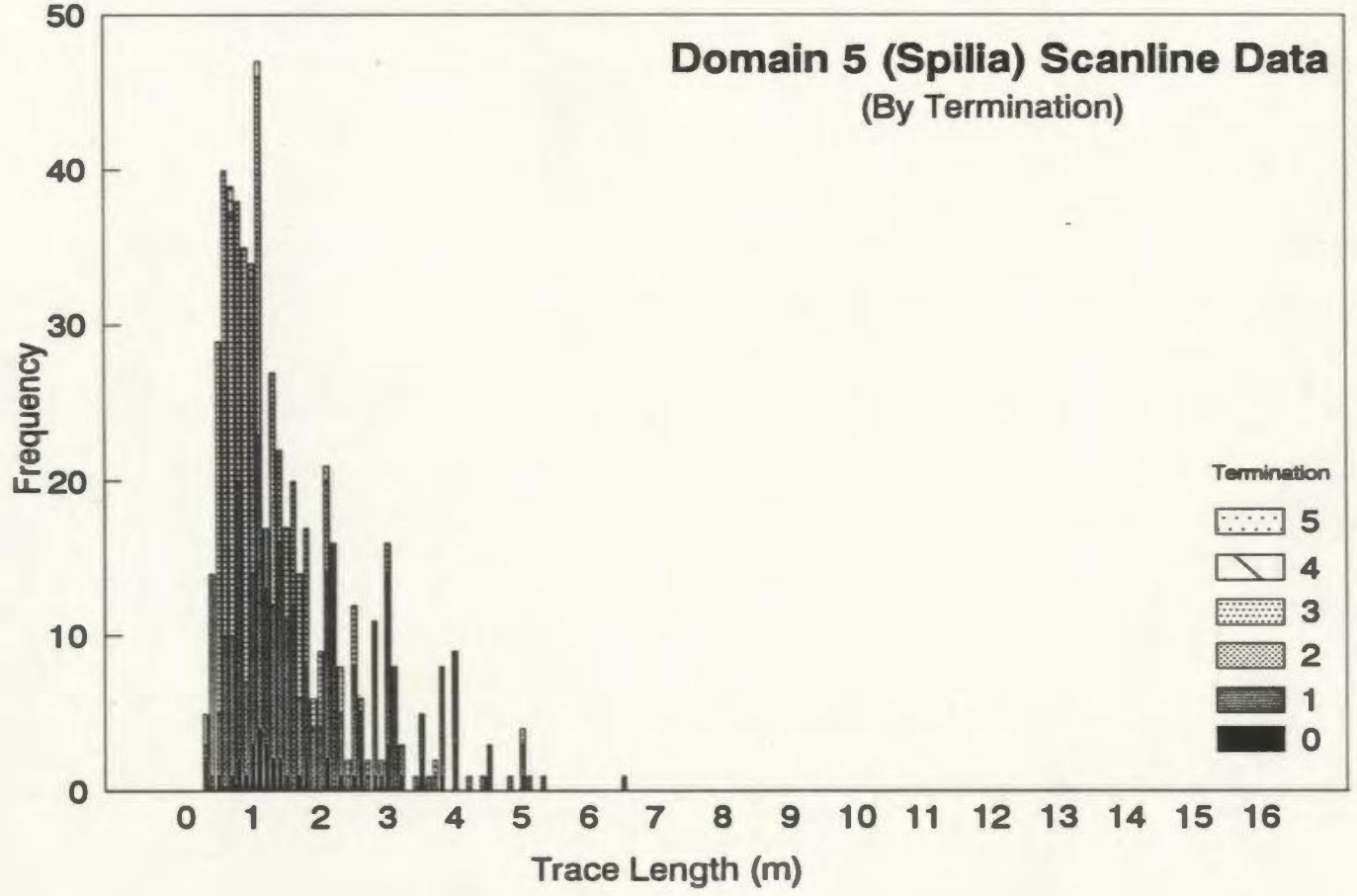
Domain 5 (Spilia) Scanline Data
(By Termination)
Termination
5
4
3
2
1
0
Frequency
Trace Length (m)
0 10 20 30 40 50
0 1 2 3 4 5 6 7 8 9 10 11 12 13 14 15 16

A.3 Fracture Characteristics
A.3.8 *Fracture Frequency and Spacing*
A.3.8.1 *Fracture Frequency*

Joint/fracture frequency is presented as a moving average along each scanline. This moving average uses a 5 metre window which is moved along the scanline in 1 metre increments.

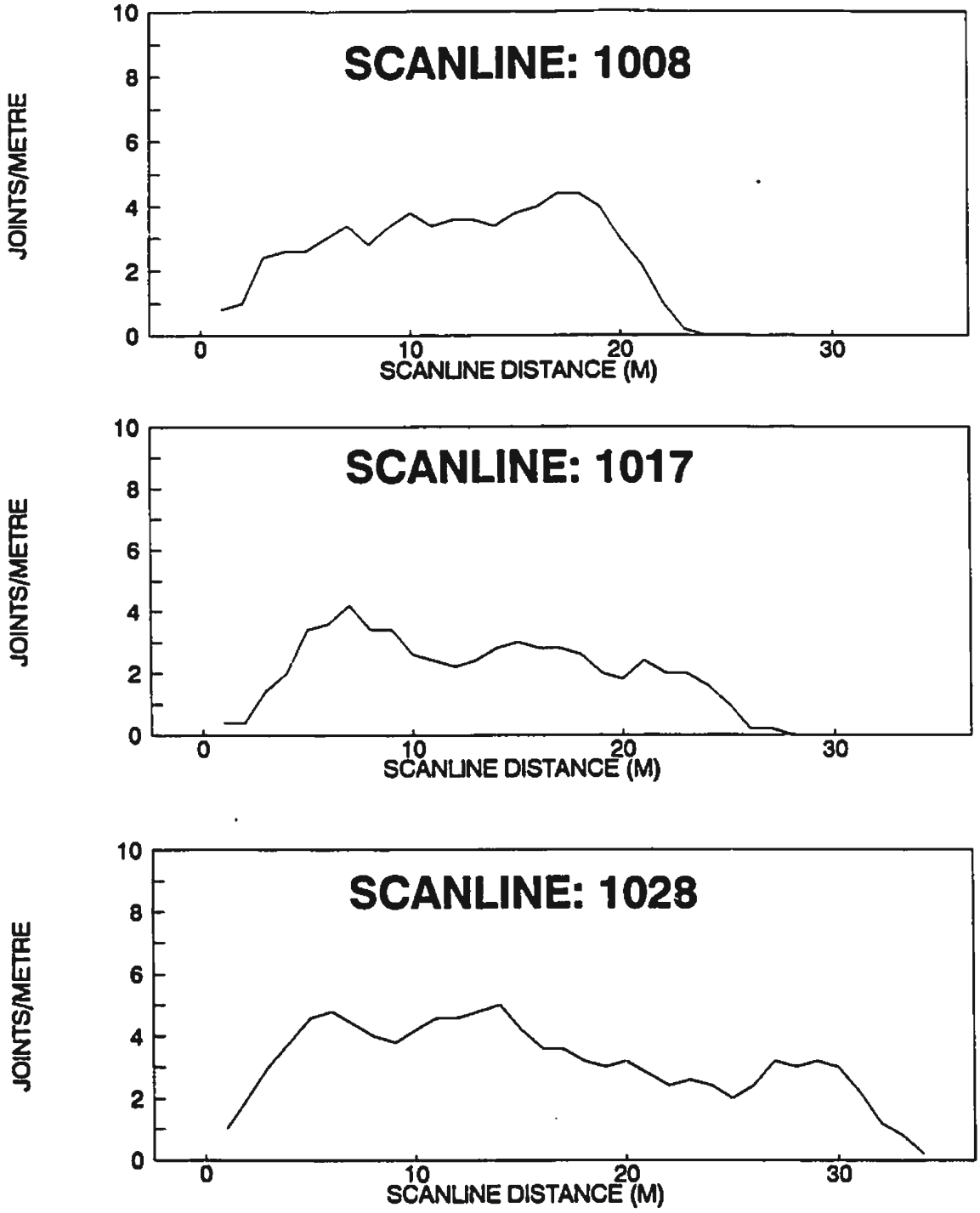

Fracture frequency expressed as moving averages using 5M window in 1M increments

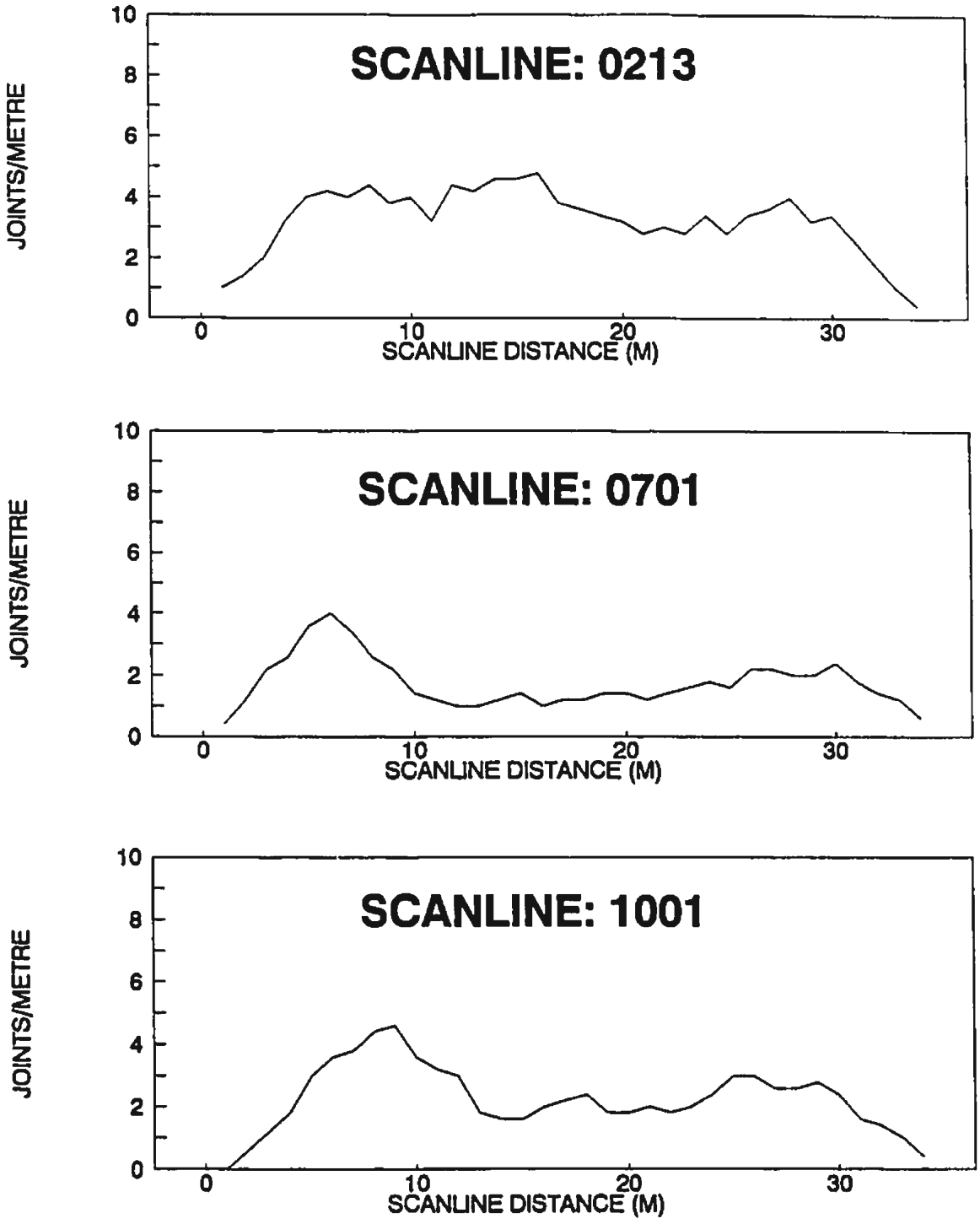

Fracture frequency expressed as moving averages using 5M window in 1M increments

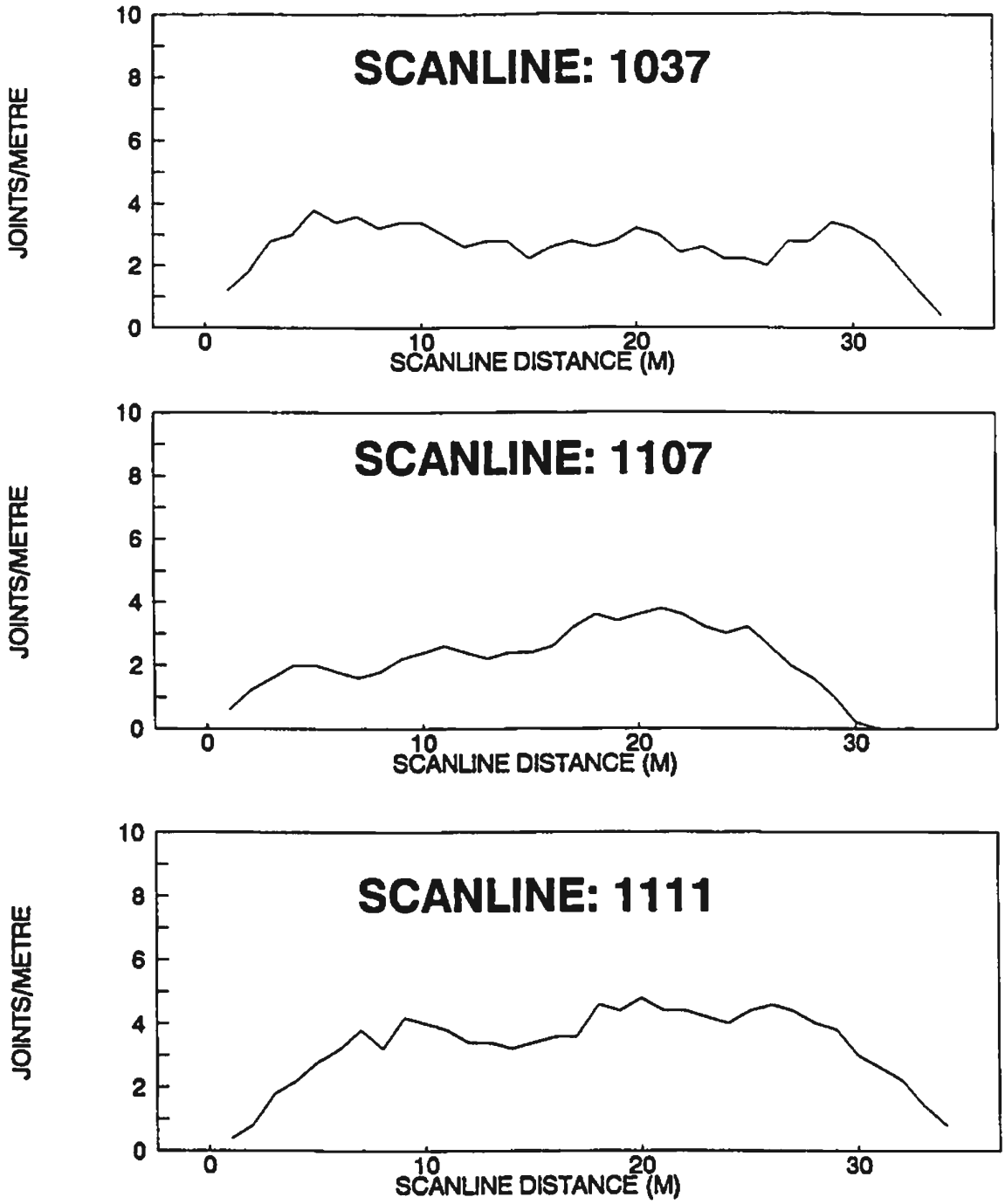

Fracture frequency expressed as moving averages using 5M window in 1M increments

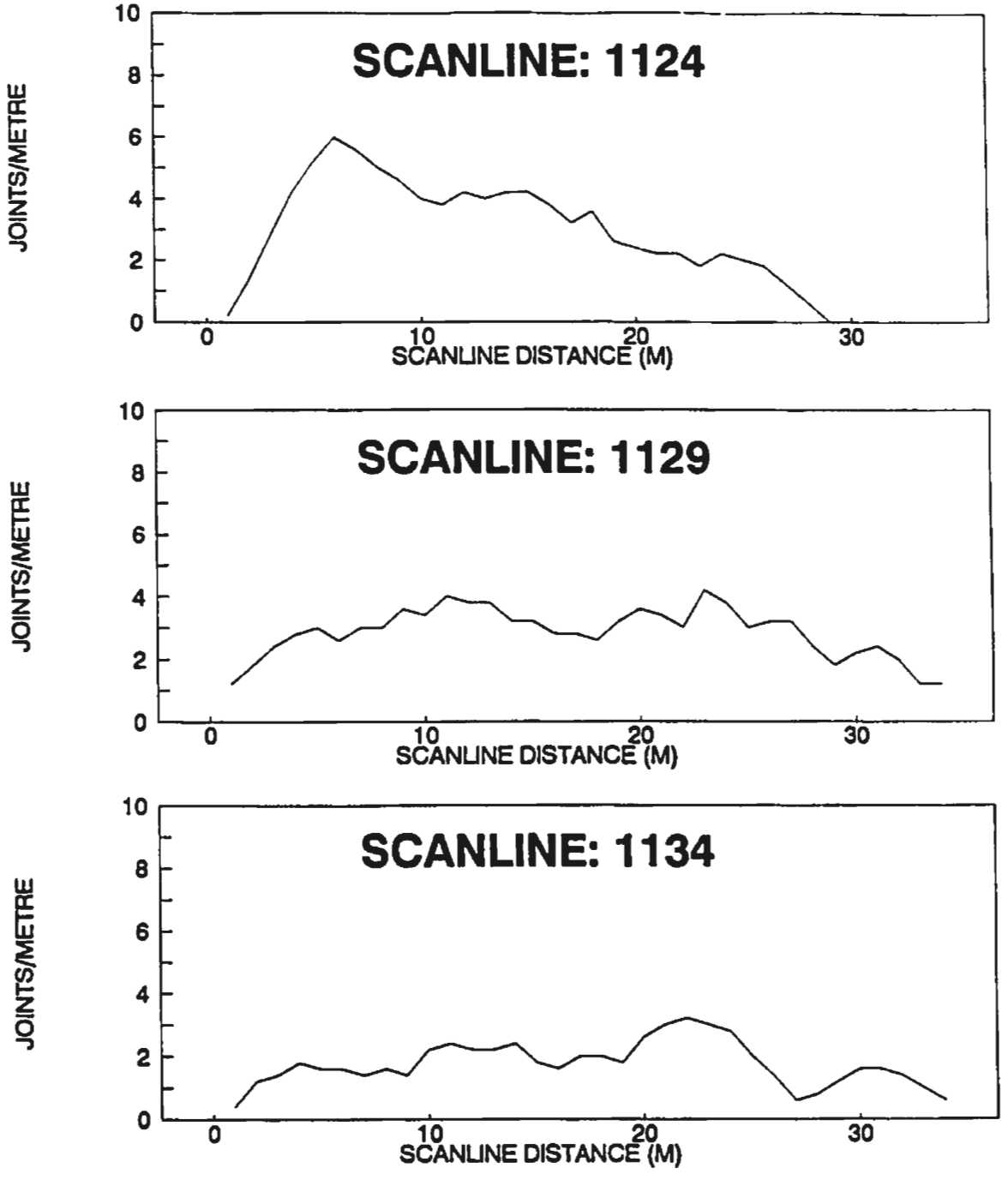

Fracture frequency expressed as moving averages using 5M window in 1M increments

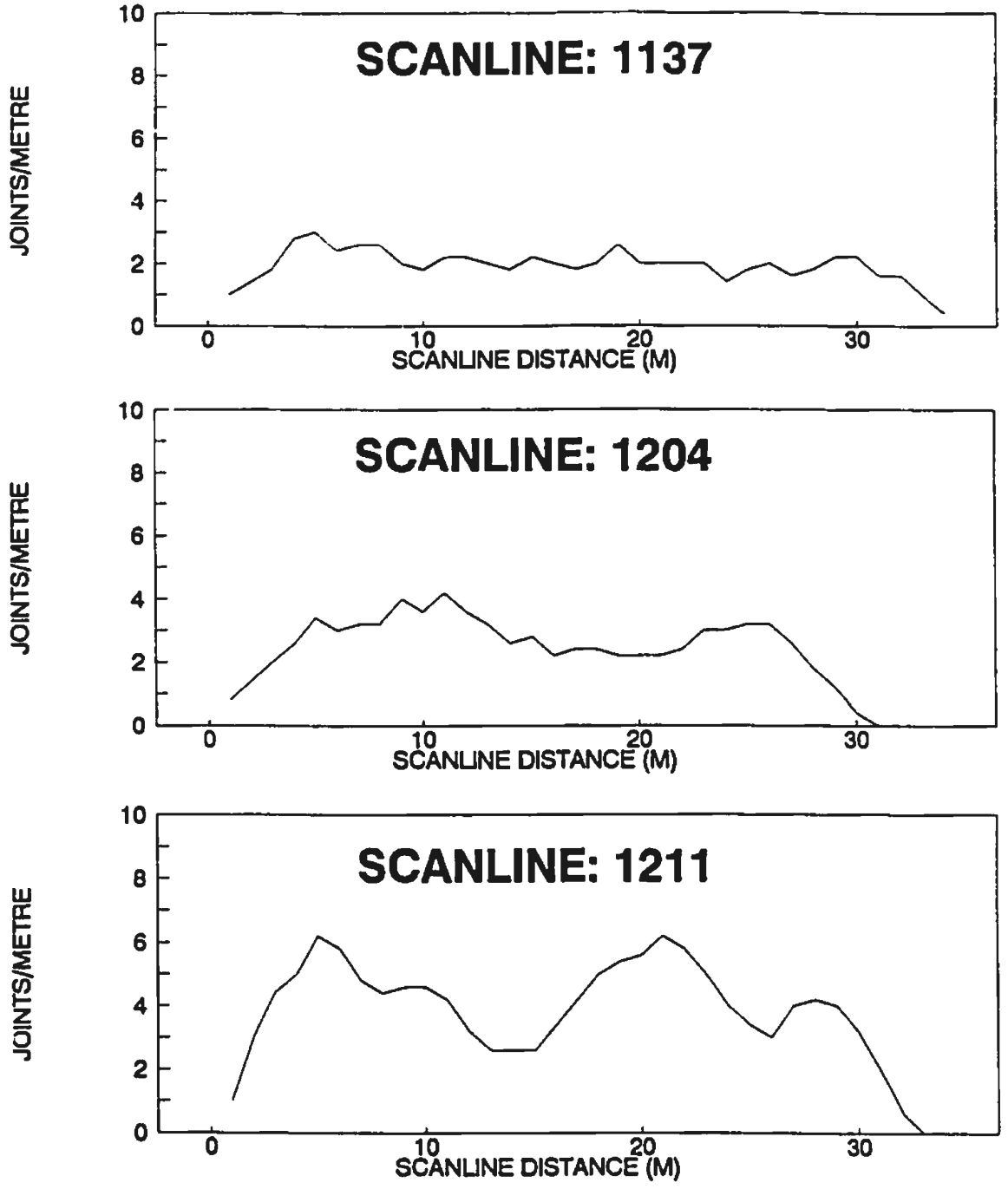

Fracture frequency expressed as moving averages using 5M window in 1M increments

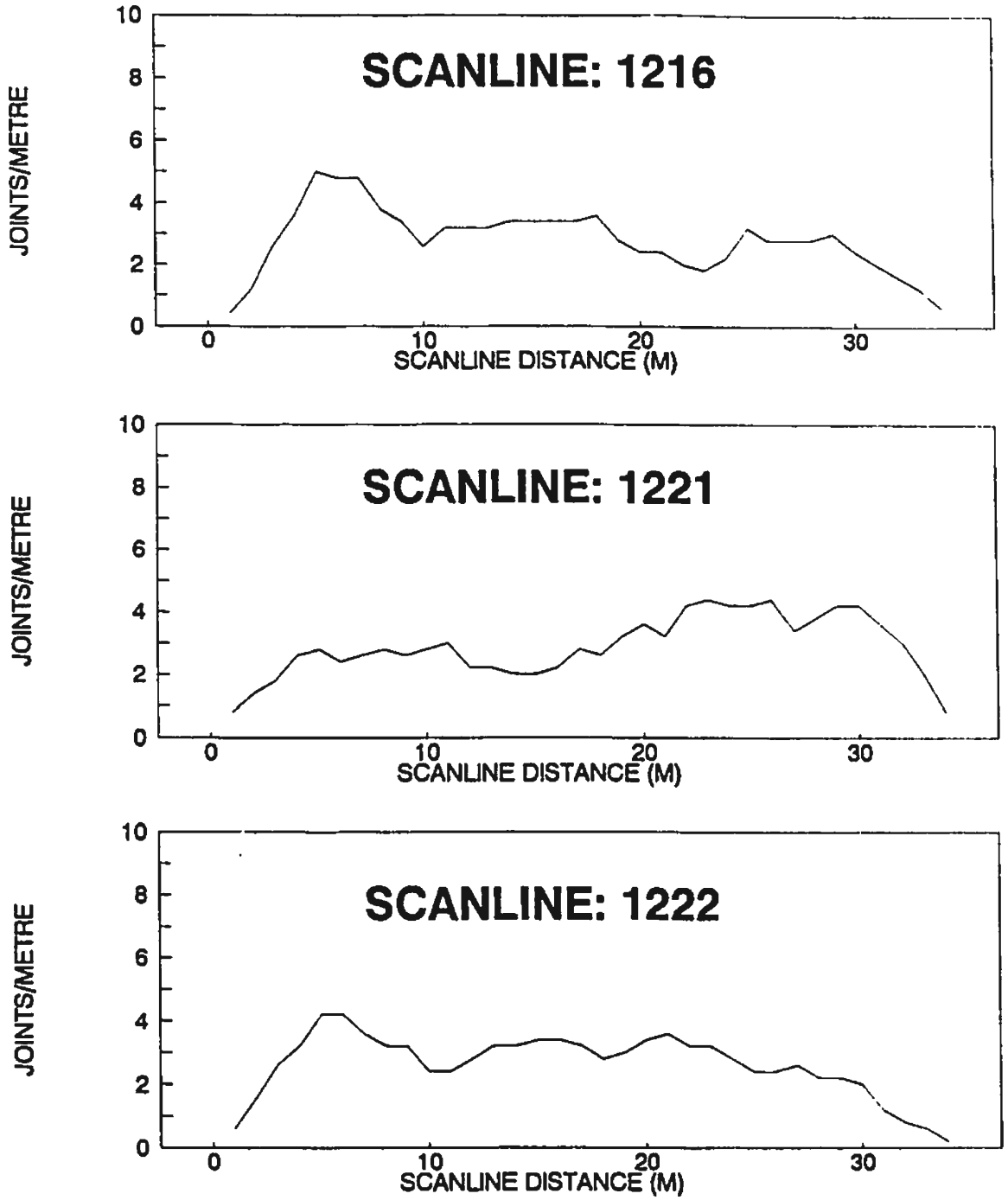

Fracture frequency expressed as moving averages using 5M window in 1M increments

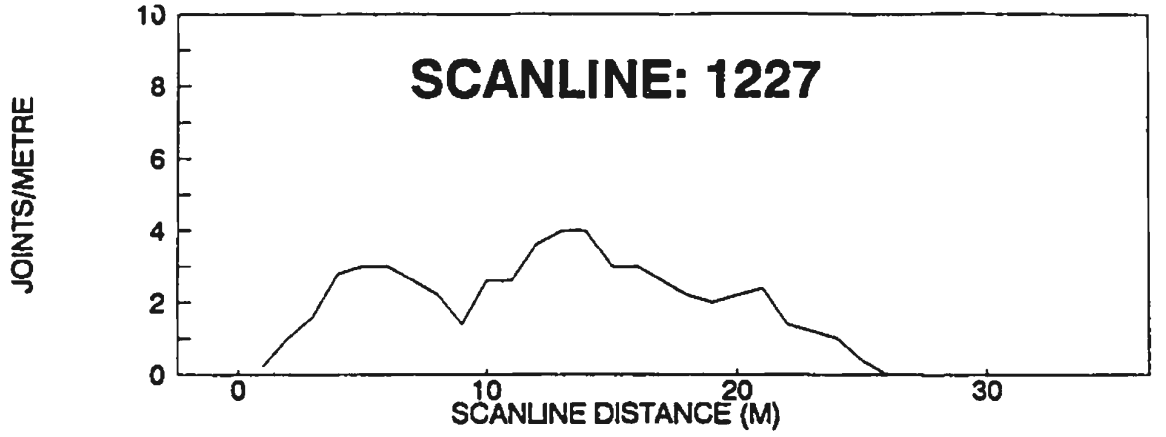

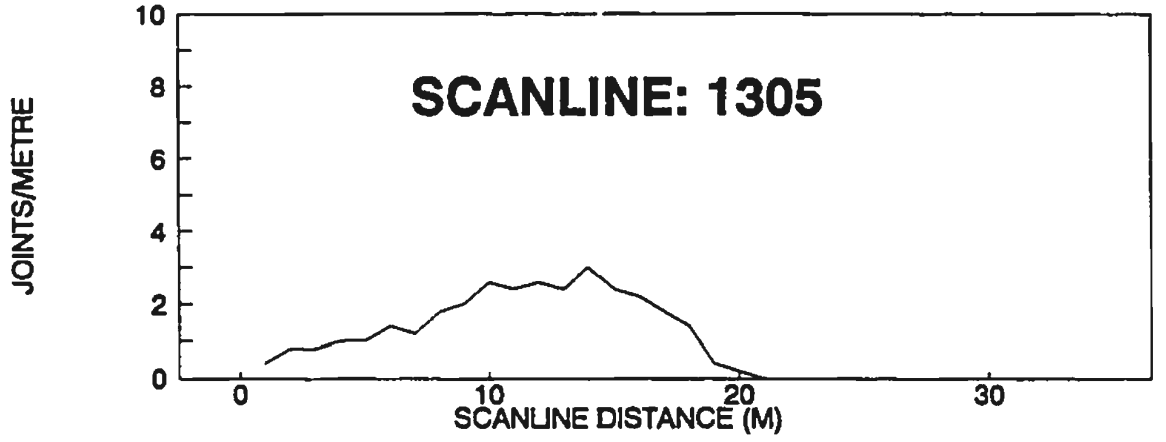

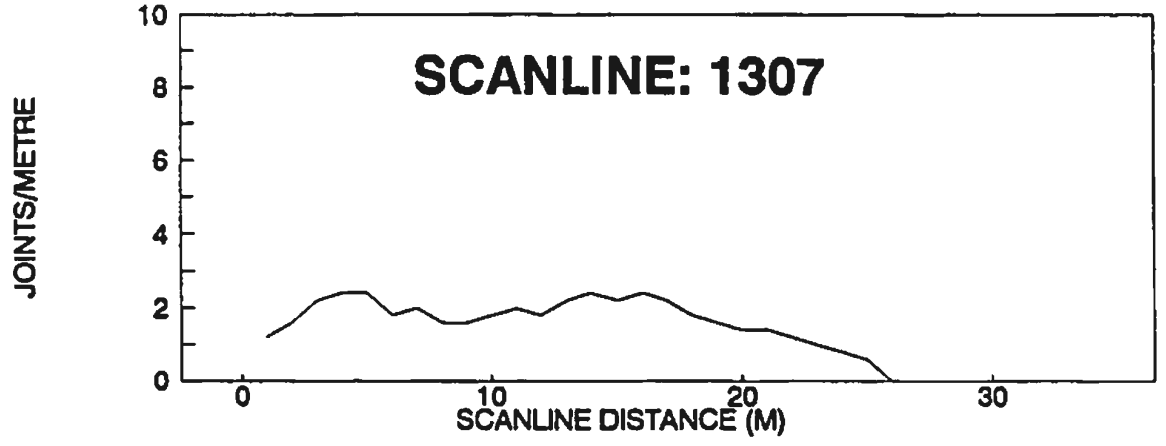

Fracture frequency expressed as moving averages using 5M window in 1M increments

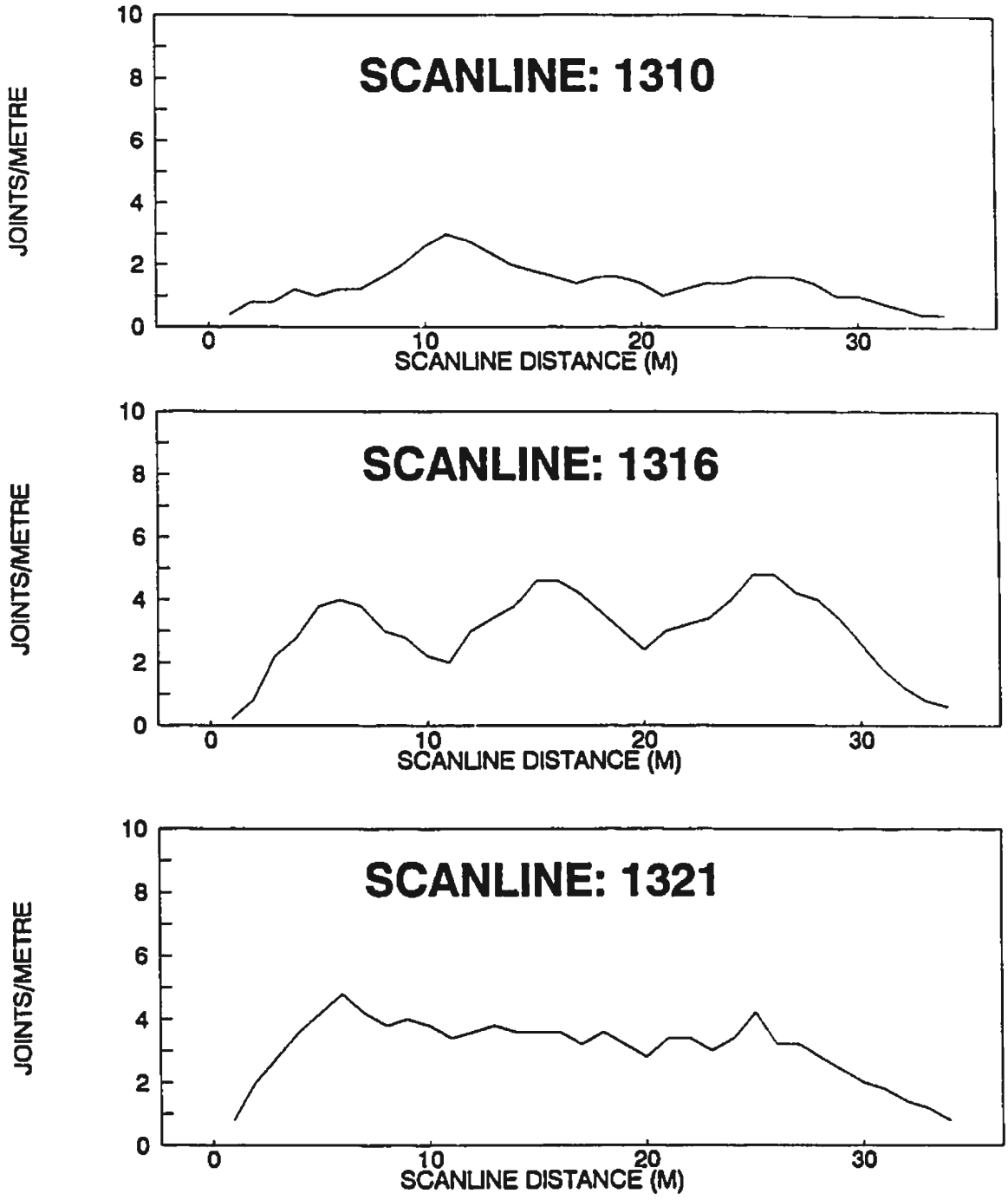

Fracture frequency expressed as moving averages using 5M window in 1M increments

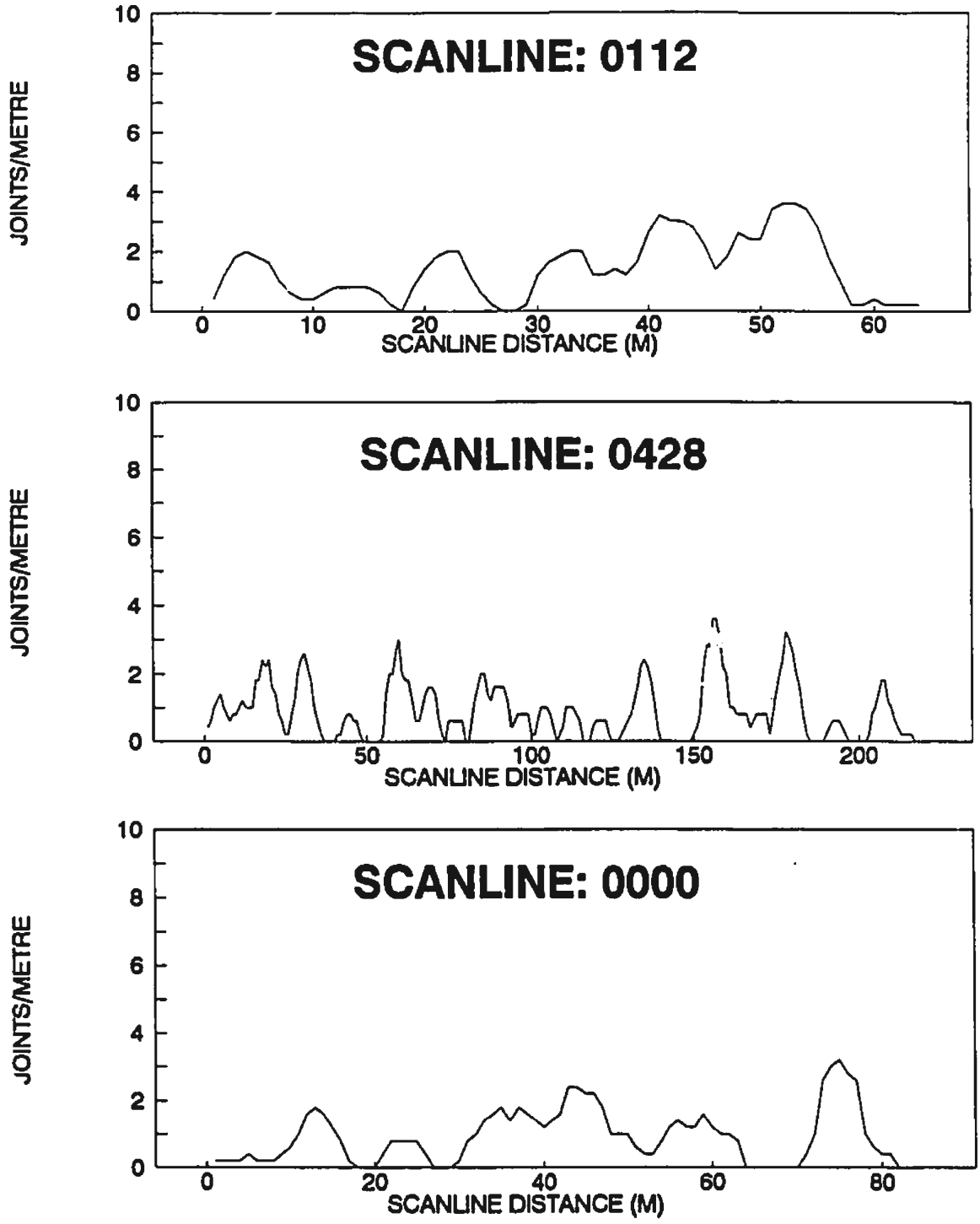

Fracture frequency expressed as moving averages using 5M window in 1M increments

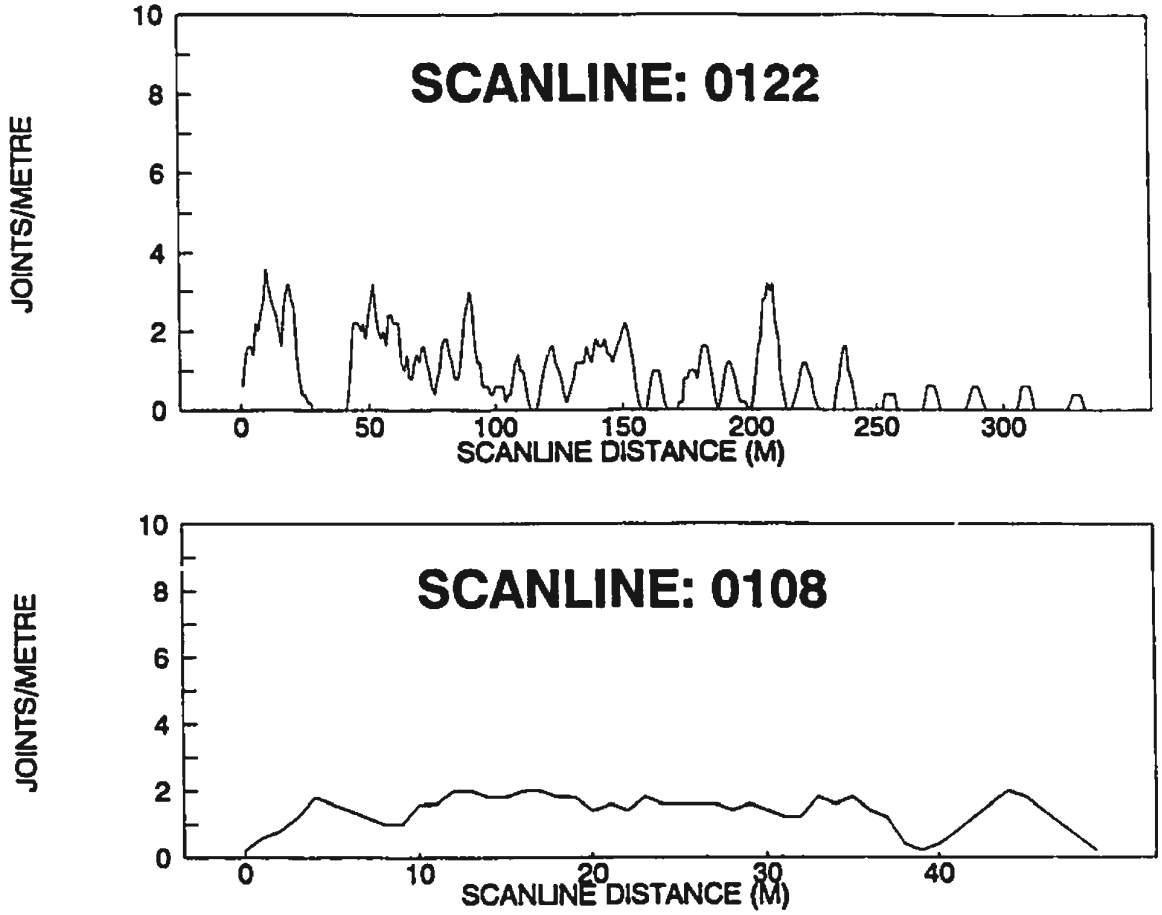

Fracture frequency expressed as moving averages using a 5M window in 1M increments

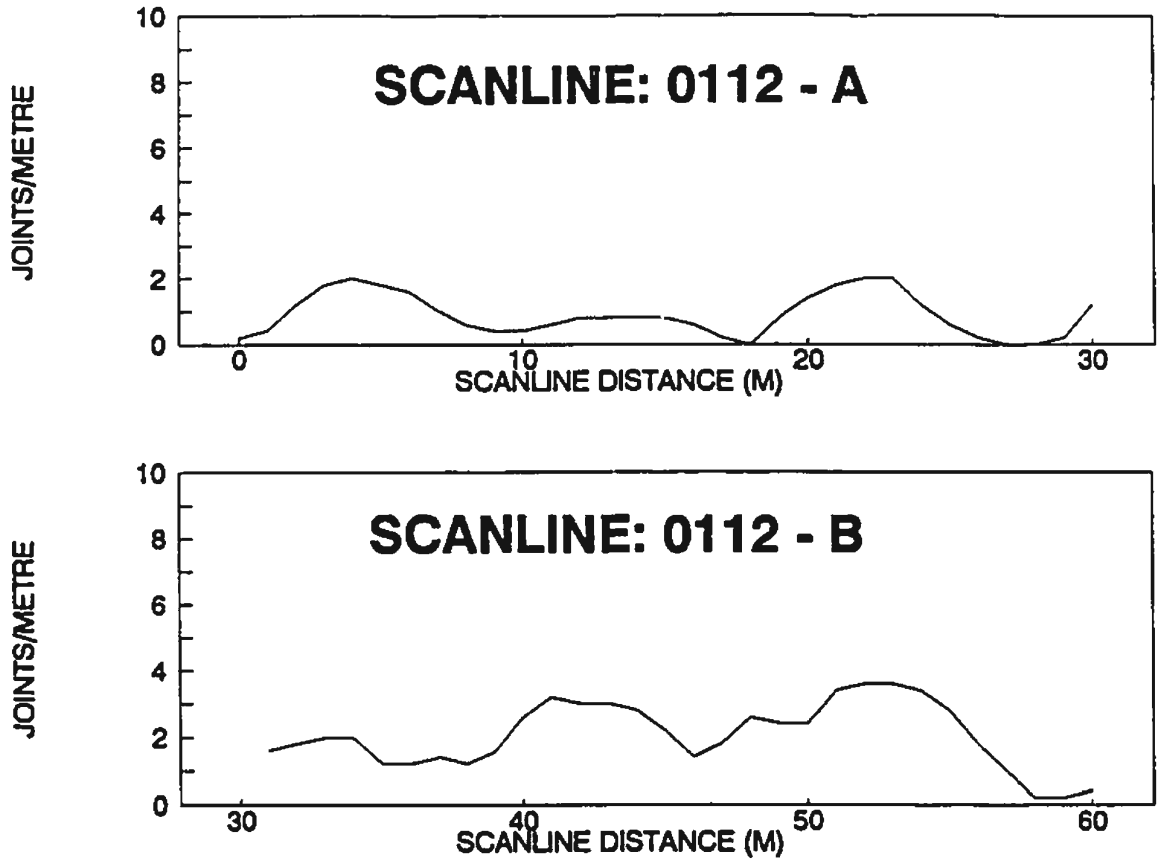

(Note: 0112 - B is a continuation of 0112 - A)

Fracture frequency expressed as moving averages using a 5M window in 1M increments

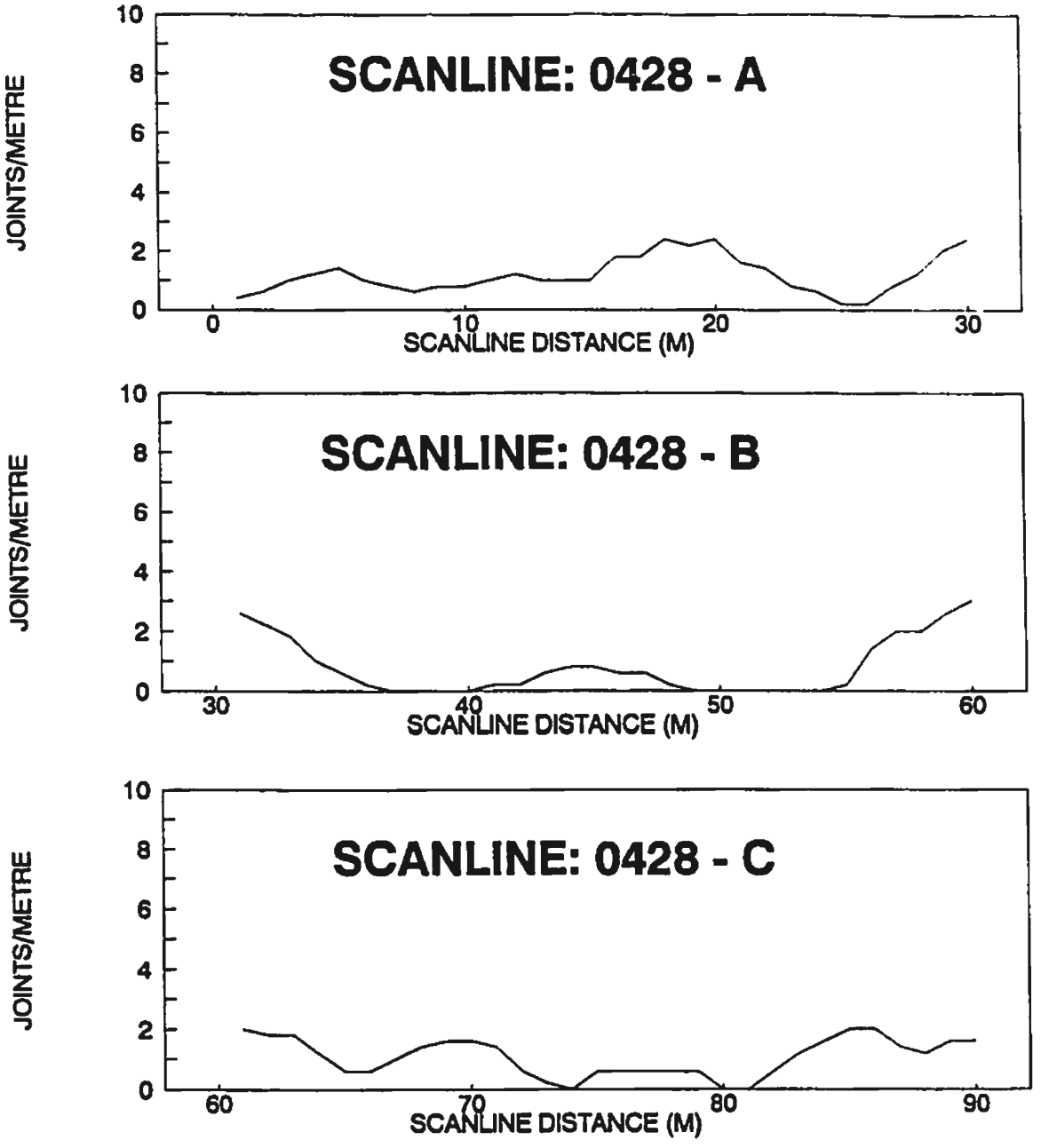

(Note: 0428 connects from 0112 and to 0122)

Fracture frequency expressed as moving averages using a 5M window in 1M increments

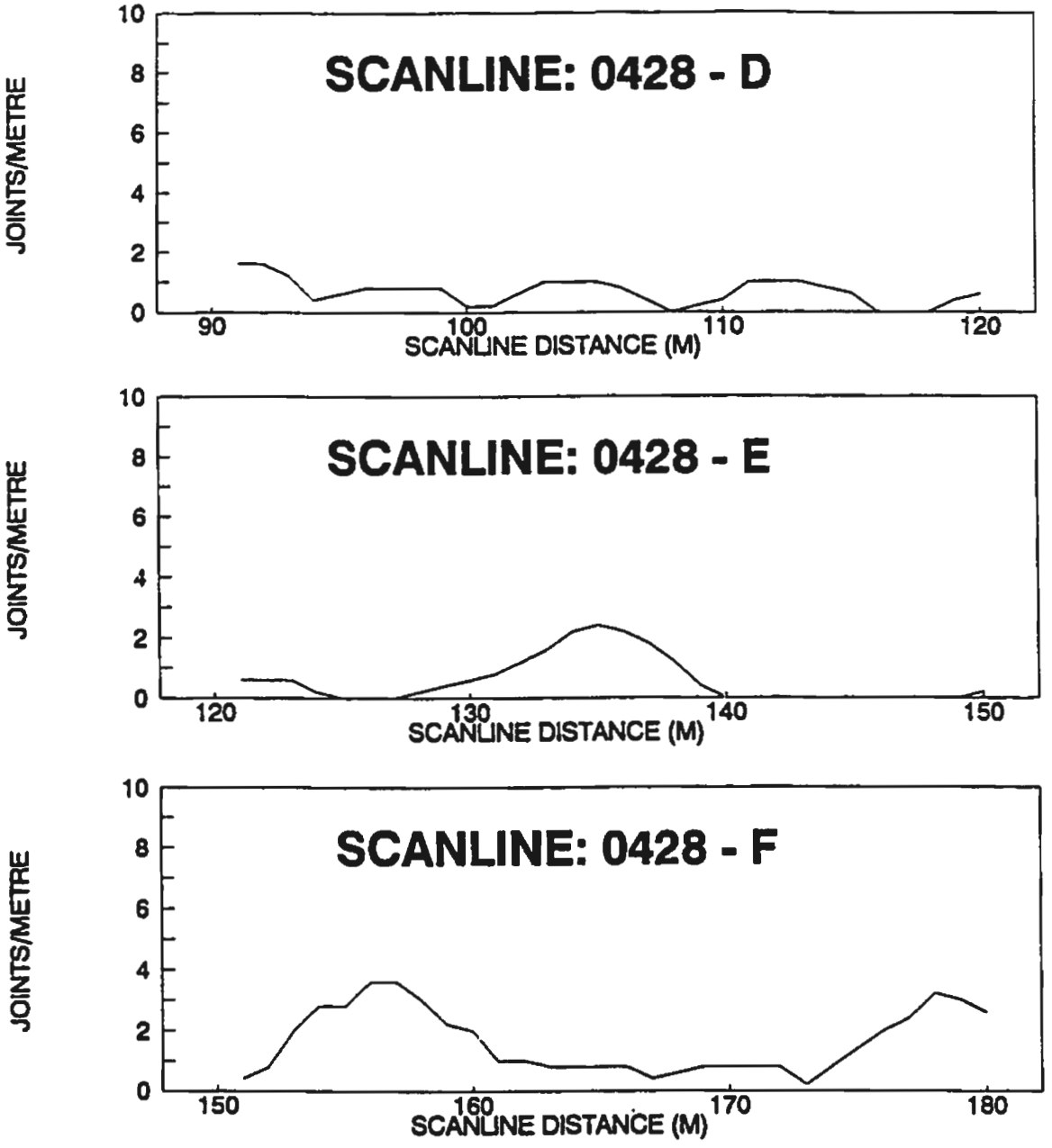

(Note: 0428 connects from 0112 and to 0122)

Fracture frequency expressed as moving averages using a 5M window in 1M increments

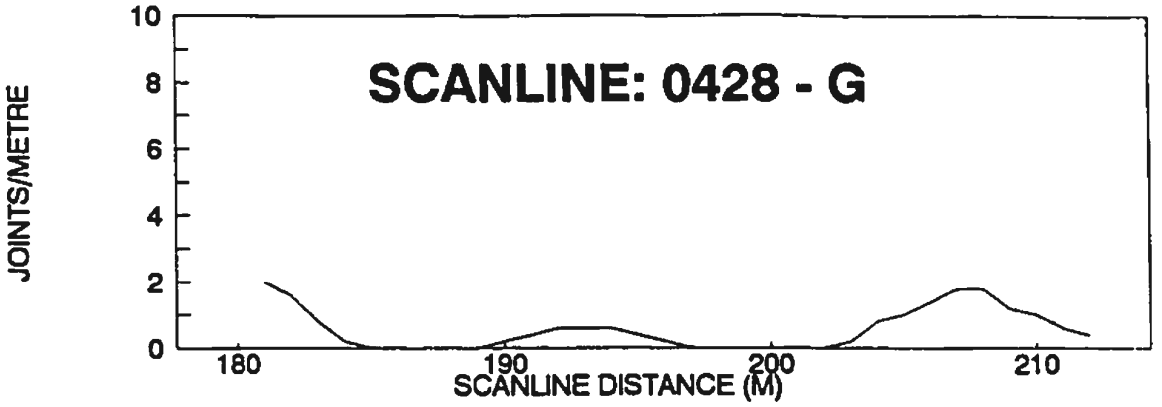

(Note 0428 connects from 0112 and to 0122)

Fracture frequency expressed as moving averages using a 5M window in 1M increments

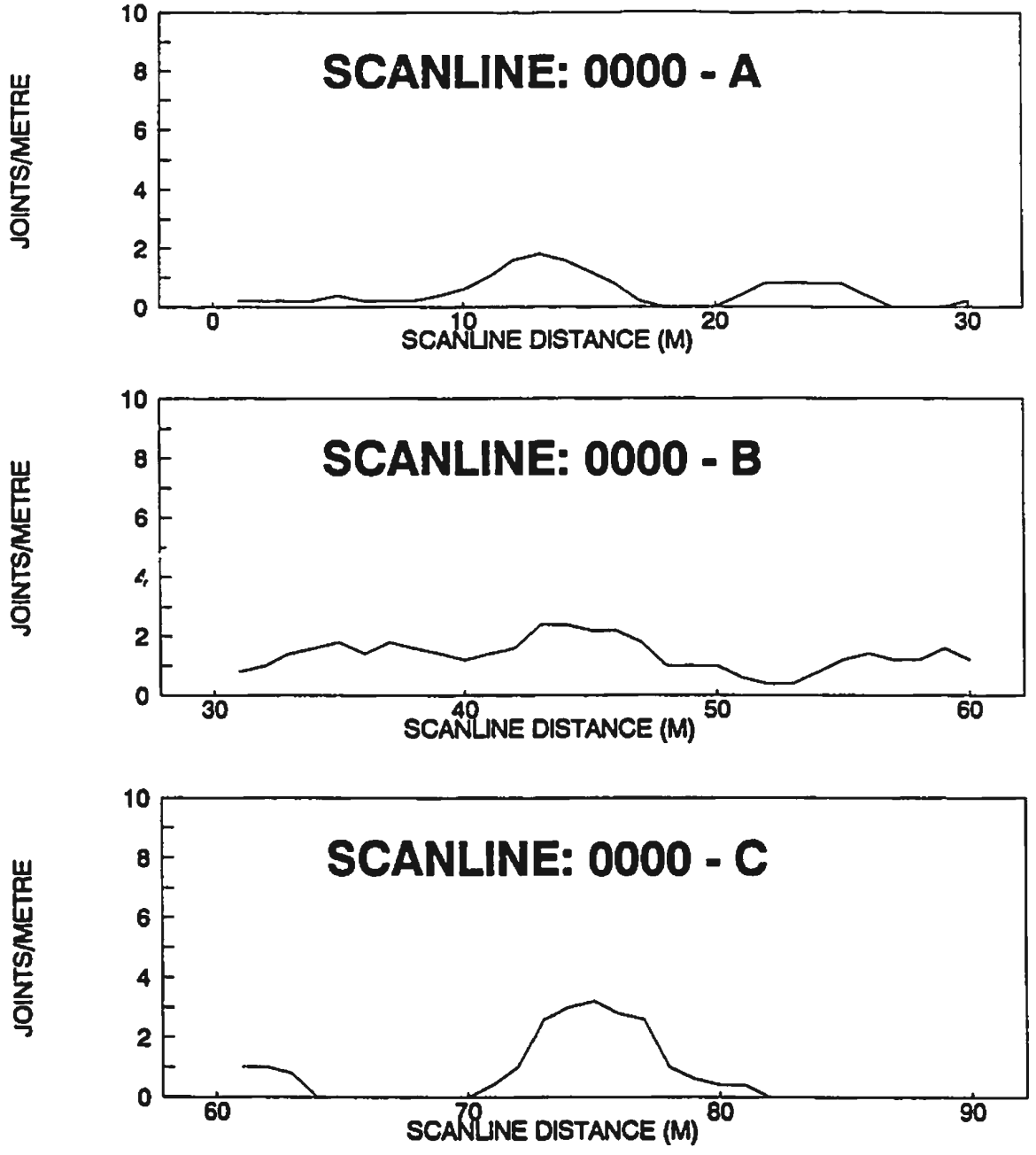

(Note: 0000 is between 0428 and 0122 at right angles)

Fracture frequency expressed as moving averages using a 5M window in 1M increments

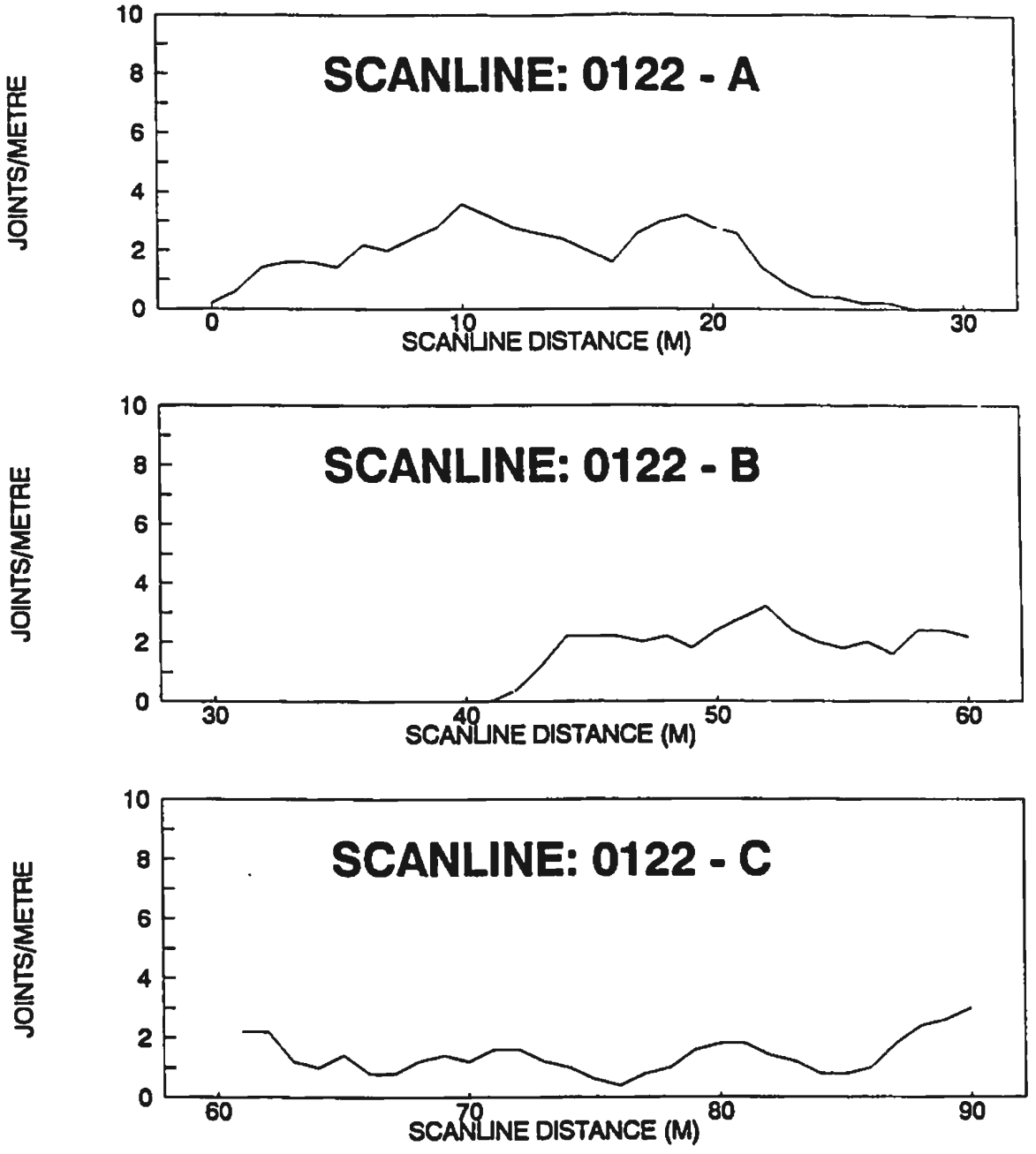

(Note: 0122 connects from 0112 and 0000)

Fracture frequency expressed as moving averages using a 5M window in 1M increments

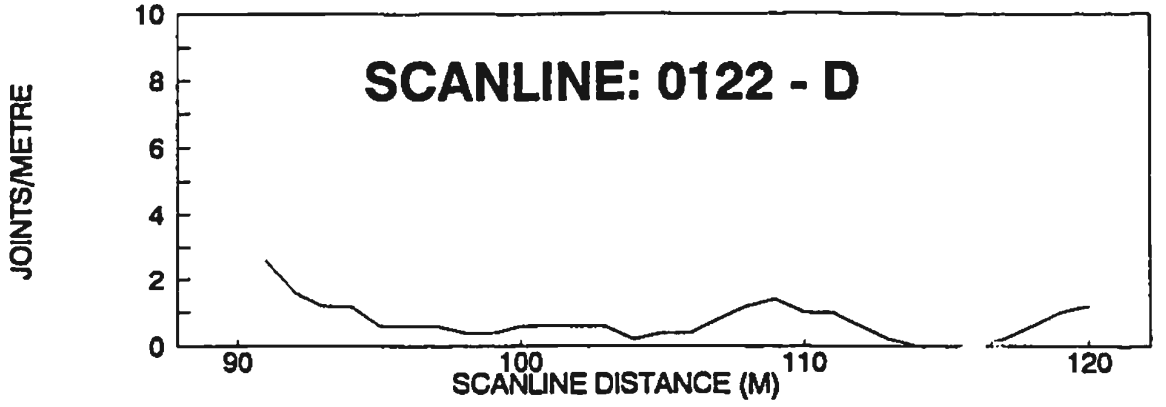

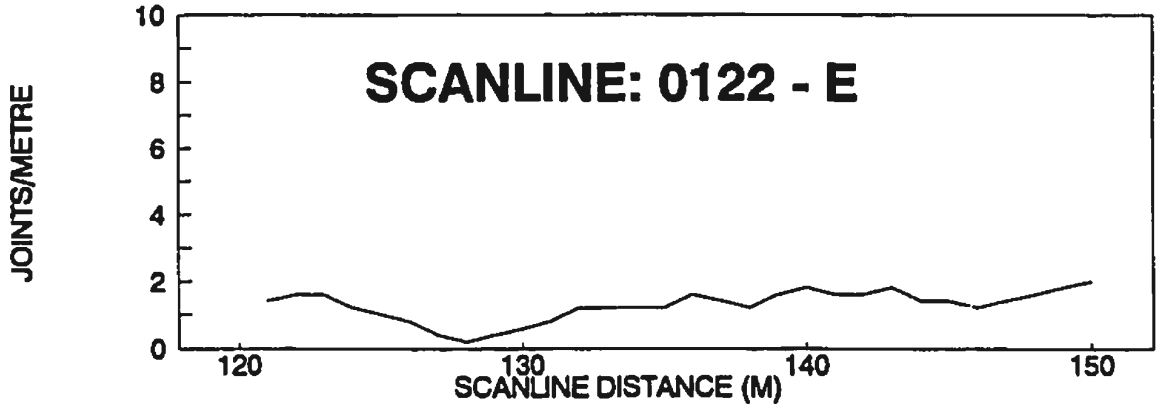

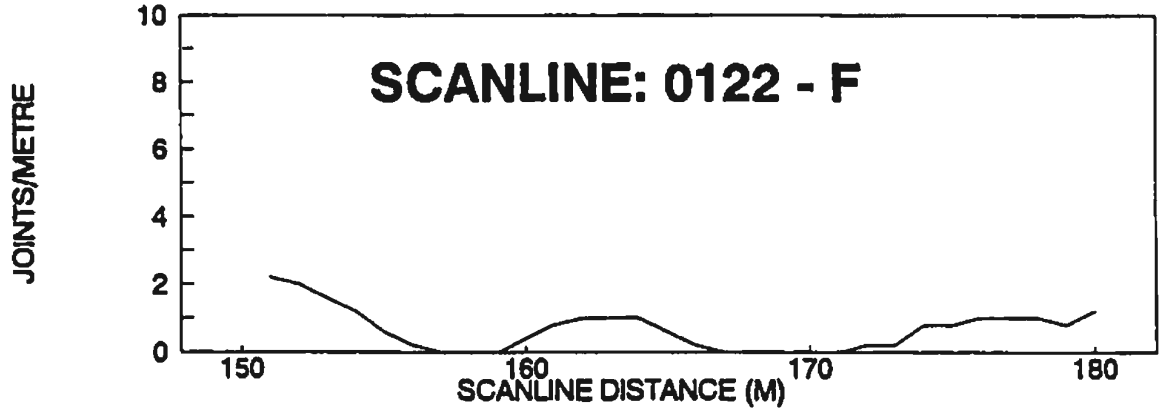

(Note: 0122 connects from 0429 and 0000)

Fracture frequency expressed as moving averages using a 5M window in 1M increments

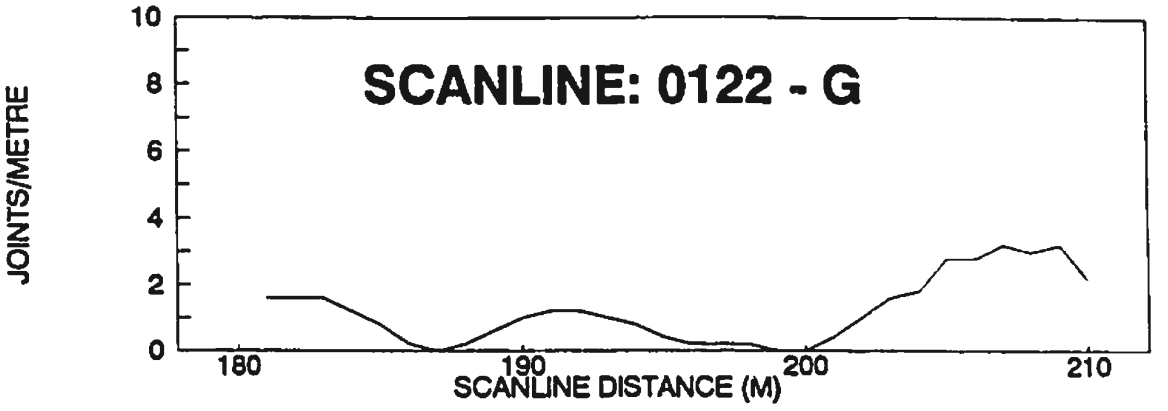

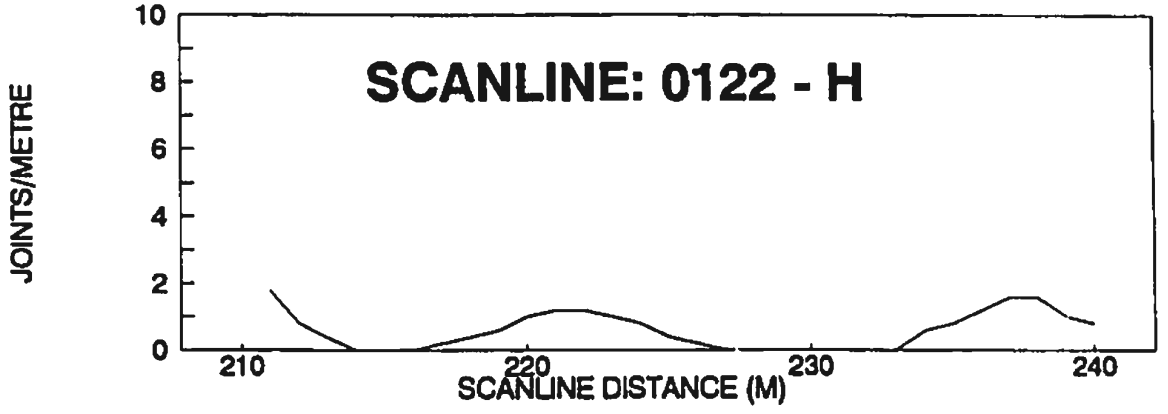

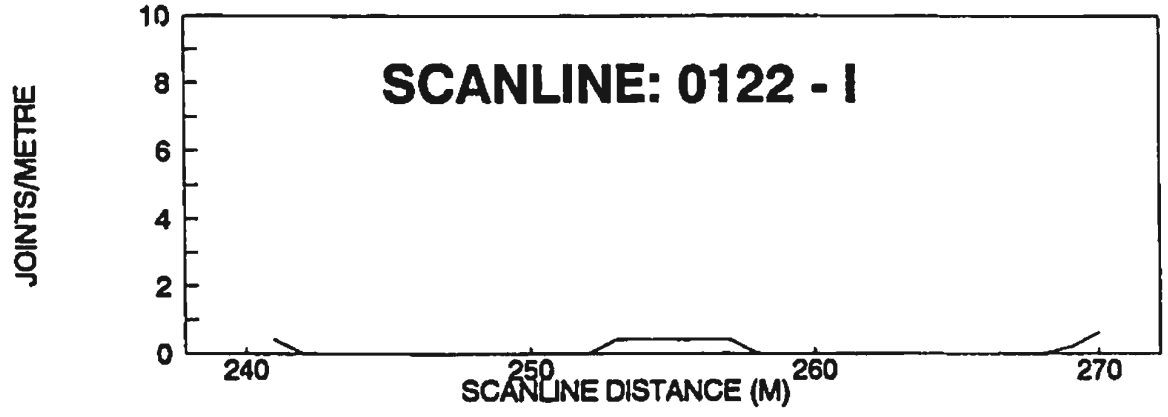

(Note: 0122 connects from 0428 and 0000)

Fracture frequency expressed as moving averages using a 5M window in 1M increments

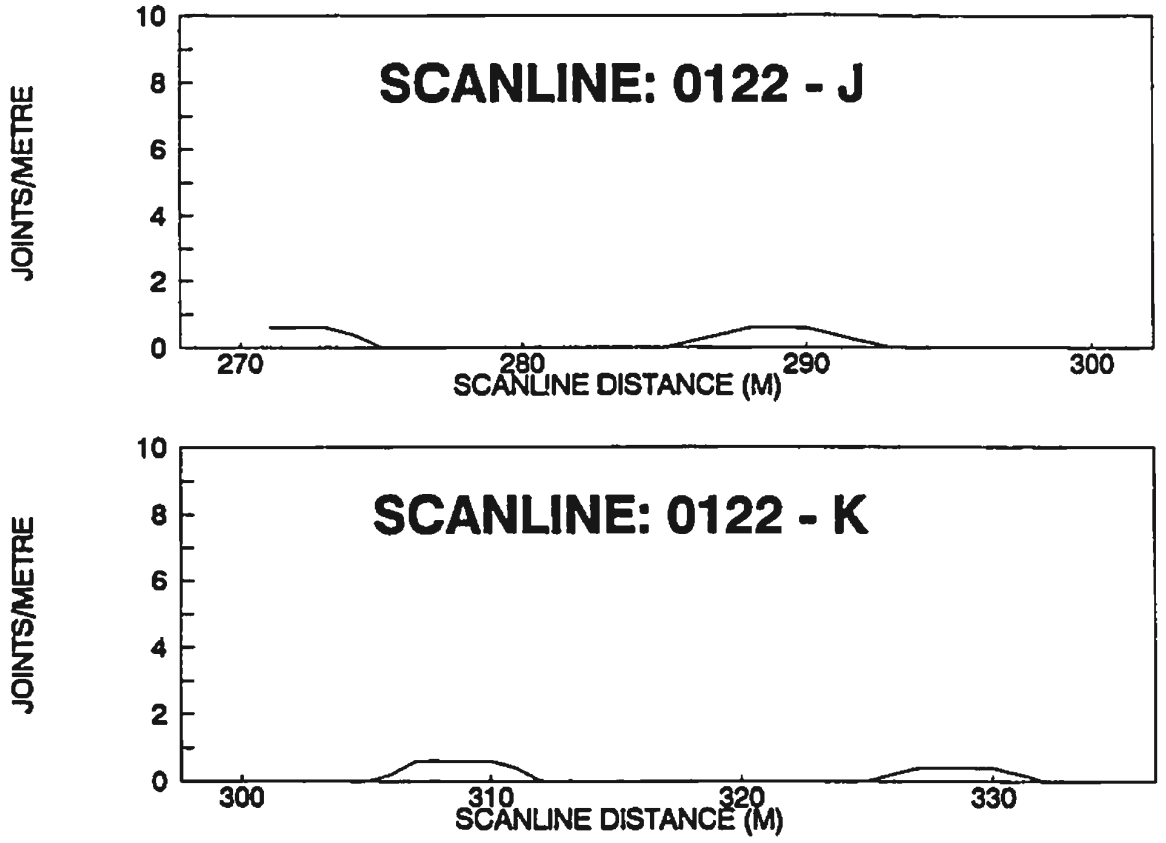

(Note: 0122 connects from 0428 and 0000)

Fracture frequency expressed as moving averages using a 5M window in 1M increments

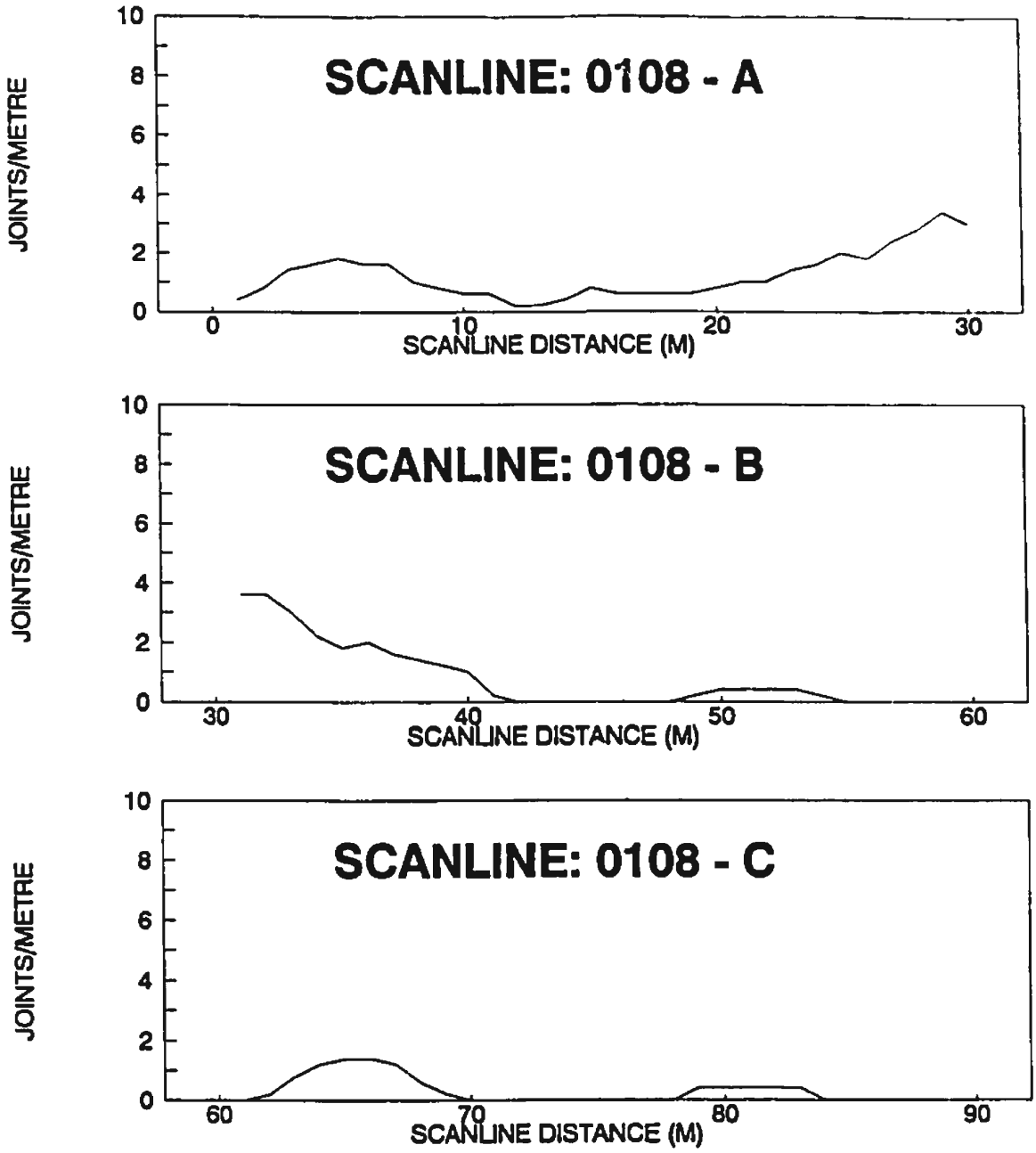

(note: 0108 - A to 0108 - D are continuous)

Fracture frequency expressed as moving averages using a 5M window in 1M increments

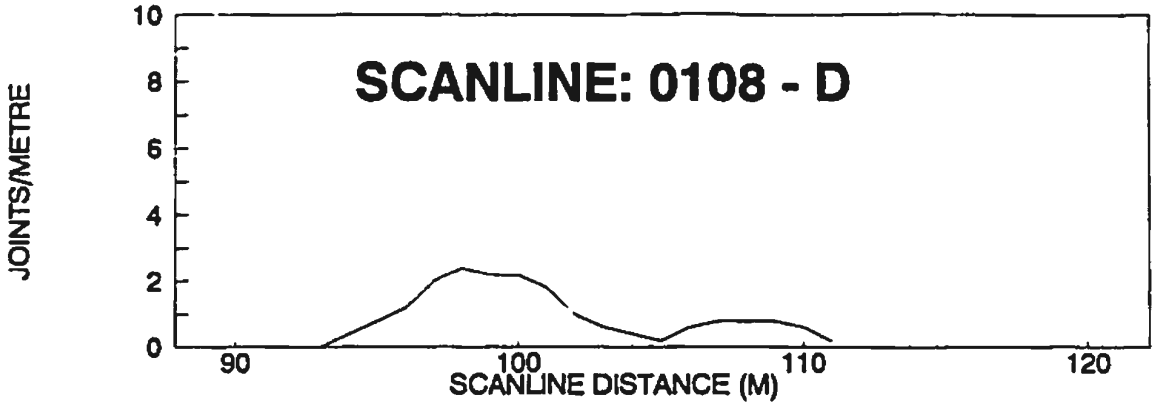

(Note: 0108 - A to 0108 - D are continuous)

Fracture frequency expressed as moving averages using a 5M window in 1M increments

A.3 Fracture Characteristics
A.3.8 *Fracture Frequency and Spacing*
A.3.8.2 *Fracture Spacing*

Fracture spacing was calculated for the fracture sets delineated in Chapter 3.4.3. Spacing calculated for the girdle (other fractures) distributions is not meaningful because the fractures are not sub-parallel.

Spacing analysis determines the mean distance between consecutive fractures of a set of sub-parallel fractures along a scanline. The International Society of Rock Mechanics (ISRM) (1978) defines spacing to be the perpendicular distance between adjacent rock discontinuities. Since fractures within a set are roughly parallel, the spacing can be calculated as the perpendicular distance between fractures within that set.

The fracture data set was truncated at the lower end (at 0.25 metres); this means that any calculated spacing will overestimate the actual spacing. A simple count of the number of fractures with trace lengths less than 0.25 metres does not suffice to correct the calculated spacings. This is because the scanline distances and the orientations of these counted fractures are not known. However fractures shorter than 0.25 metres may not be important to the fluid circulation, therefore the fracture spacing will be calculated on the available fracture data set.

The fracture spacings were computed as follows: extract scanline orientations, scanline distance for each scanline and the mean orientation of the fracture set to which the chosen fracture belongs (for further details see Rouleau, 1984). These results were than used in a series of SAS (SAS Institute, 1985) programs (adapted from SPACE.SAS, LNORM.SAS, and EXPON.SAS by Rouleau, 1984).

The perpendicular spacing is the product of the distance between pairs of fractures (length) and the cosine of the angle, ϕ. between the scanline (subscript, s) and the pole to the fracture plane (subscript, f) which is the vector dot product of the direction cosines (k, l, and m) of the two vectors (the scanline and the fracture plane),

$$spacing = length \times \cos(\phi) \quad \ldots\ldots\ldots \text{(A.3.8.1.1)}$$

where

$$\cos(\phi) = k_s \cdot k_f + l_s \cdot l_f + m_s \cdot m_s \quad \ldots\ldots\ldots \text{(A.3.8.1.2)}$$

The main statistics of the distribution of fracture spacing are plotted by scanline and for the complete data set in Table A.3.8.1. The mean spacing for the complete data set is 0.82 metres.

The exponential and log-normal distributions were fit to the data set. The estimate of the parameter of the exponential distribution is the inverse of the value for the mean spacing, while the parameters for the log-normal distribution are the mean and standard deviation of the log of the spacing (Rouleau, 1984). The Kolmogorov-Smirnov goodness-of-fit test was applied to these models in the plots shown in Figure A.3.8.1. The straight line on the plot is a reference line with a slope of one. The closer the data lie to this line, the better the fit of the chosen theoretical distribution. The results of this analysis shows that the data are better represented by a log-

normal distribution. The log-normal distribution of the data set indicates that they are not randomly distributed (Priest and Hudson, 1976). That the data are best represented by a log-normal distribution indicates that a multiplicatory process, such as breakage, may have produced the fractures (Dershowitz and Einstein, 1988). An better fit to the exponential distribution would have indicated the fractures were produced through a uniform process.

Truncation of trace lengths biases the data sets toward longer trace lengths. In order to establish the effect of the trace length truncation on the spacing, the following analysis was carried out. The trace length data for each scanline were progressively truncated toward higher trace lengths. The original truncation during field measurement was 0.25 metres, subsequent truncations were set at 0.4, 0.6, 0.8, 1.0, 1.2, and 1.4 metres. The results are tabulated by scanline and for the combined data set in Table A.3.8.2. A plot of the mean spacing against trace length truncation shows that the mean spacing is not significantly altered with increase in the size of the trace length truncation (Figure A.3.8.2). Exceptions to this are: 0000, 0418, 1124 and 1222. The mean spacing for a trace length truncation of 0 metres was estimated from Figure A.3.8.2 as 0.82 metres.

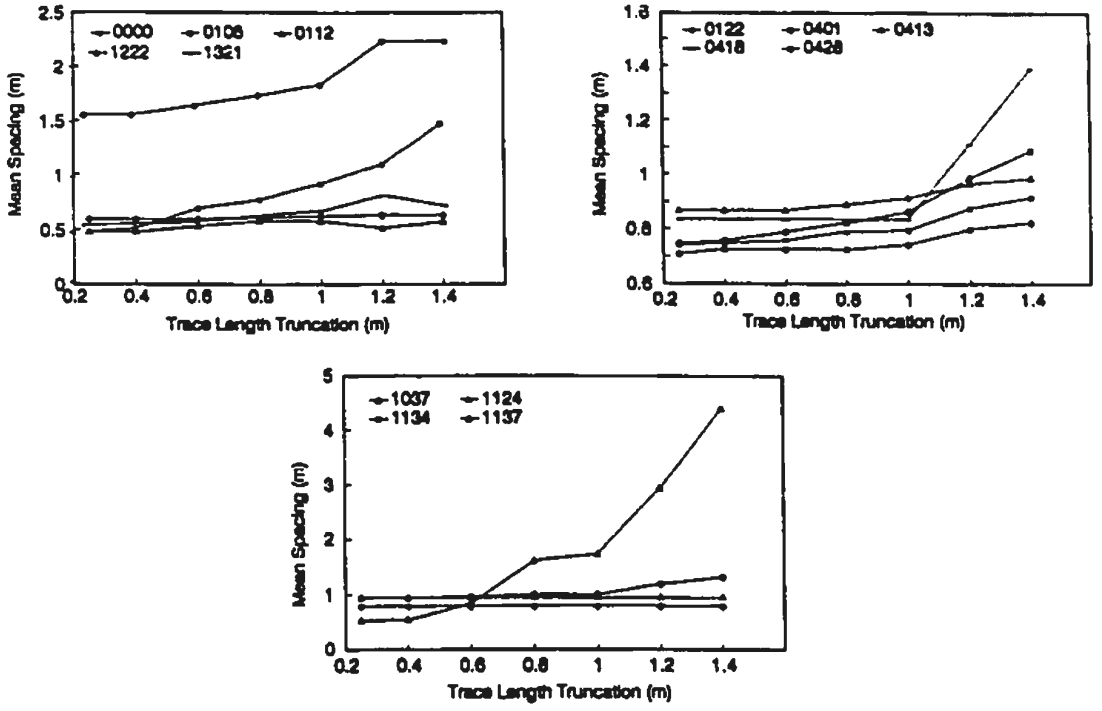

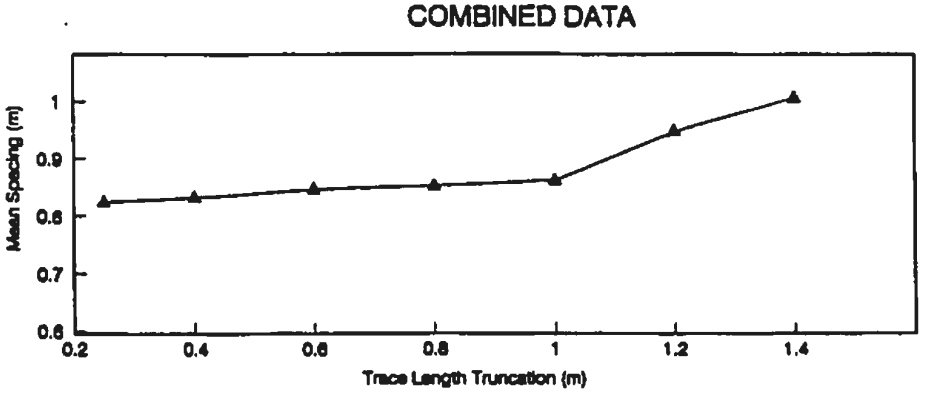

FIGURE A.3.8.2.1 DYKE PARALLEL FRACTURE SPACING AS A FUNCTION OF TRACE LENGTH TRUNCATION.

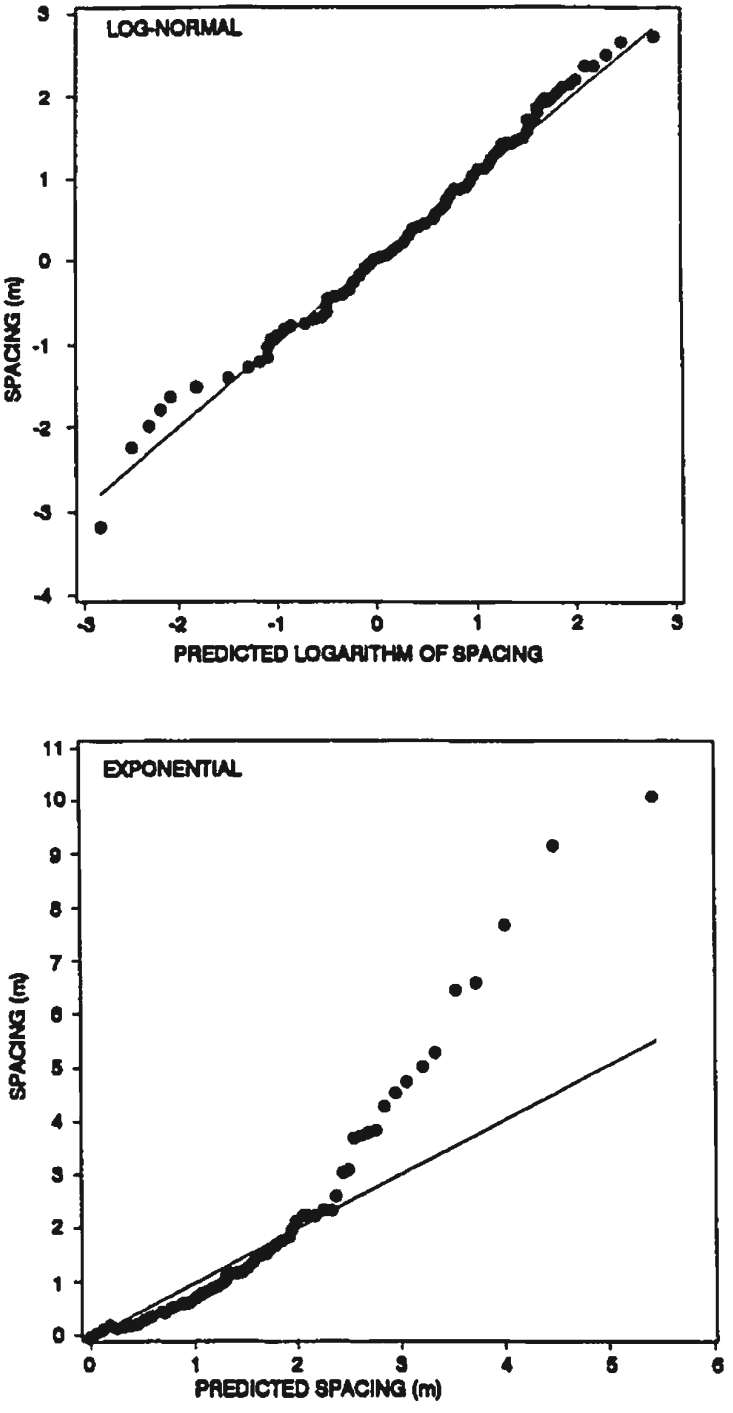

FIGURE A.3.8.2.2 QUANTILE PLOTS FOR EXPONENTIAL AND LOG-NORMAL MODELS FITTED TO THE SPACING DISTRIBUTIONS OF DYKE PARALLEL FRACTURES.

TABLE A.3.8.1 DYKE PARALLEL FRACTURE SPACING STATISTICS

Scanline	Spacing					Log Spacing			Lognorm Di	Expon. Di	Critital Di at 0.01*
	Max	Min	Mean	Std.Dev.	Skewness	Mean	Std.Dev.	Skewness			
0000	3.760	0.070	0.479	0.661	3.231	−1.270	0.974	0.565	0.049	0.109	0.212
0108	2.830	0.090	0.593	0.548	2.419	−0.856	0.844	−0.156	0.005	0.069	0.231
0112	2.150	0.060	0.474	0.645	2.024	−1.432	1.166	0.635	0.024	0.198	0.404
0122	4.270	0.070	0.742	0.788	2.032	−0.782	1.004	0.071	0.040	0.074	0.137
0401	4.360	0.090	0.708	0.873	3.364	−0.771	0.906	0.138	0.069	0.143	0.249
0413	6.690	0.090	0.867	1.336	3.704	−0.668	0.933	0.686	0.026	0.130	0.261
0418	2.670	0.180	0.836	0.666	1.768	−0.448	0.764	−0.037	0.016	0.090	0.352
0428	6.580	0.080	0.747	1.097	4.253	−0.797	0.945	0.443	0.028	0.095	0.191
1037	2.310	0.100	0.936	0.639	0.589	−0.367	0.881	−0.711	0.002	0.039	0.303
1124	1.800	0.070	0.518	0.484	1.411	−1.075	0.958	0.039	0.035	0.046	0.313
1134	2.320	0.120	0.782	0.879	1.995	−0.696	1.063	0.253	0.290	0.158	0.669
1137	3.790	0.180	0.940	1.201	2.127	−0.572	0.975	1.185	0.093	0.256	0.514
1222	9.120	0.100	1.568	2.253	2.364	−0.420	1.401	0.177	0.624	0.169	0.352
1321	4.330	0.080	0.570	0.719	3.620	−1.008	0.907	0.411	0.123	0.105	0.240

TABLE A.3.8.2 SPACING AS A FUNCTION OF TRACE LENGTH TRUNCATION BY SCANLINE

Scanline	Truncation Length (m)						
	0.25	0.40	0.60	0.80	1.0	1.2	1.4
0000	0.479	0.454	0.611	0.772	0.917	1.093	1.487
0108	0.593	0.479	0.479	0.489	0.500	0.511	0.511
0112	0.474	0.367	0.339	0.373	0.373	0.243	0.277
0122	0.742	0.686	0.697	0.717	0.723	0.777	0.770
0401	0.708	0.753	0.753	0.753	0.772	0.836	0.860
0413	0.867	0.713	0.713	0.733	0.754	0.800	0.825
0418	0.836	0.807	0.807	0.807	0.807	1.094	1.391
0428	0.747	0.652	0.685	0.720	0.759	0.837	0.891
1037	0.936	0.828	0.847	0.887	0.887	0.898	1.019
1124	0.518	0.541	0.678	1.335	1.380	3.900	–
1134	0.782	0.782	0.782	0.782	0.782	0.782	0.782
1137	0.940	0.641	0.641	0.641	0.641	0.641	0.641
1222	1.568	1.568	1.650	1.742	1.838	2.232	2.232
1321	0.570	0.423	0.434	0.468	0.498	0.600	0.611

NOTE: SPACING VALUES ARE IN METRES
CELLS CONTAINING '–' INDICATE NO DATA VALUES.

A.3 Fracture Characteristics
A.3.9 *Orientation Cluster Analysis*

A cluster analysis was performed on the individual scanline data using the IBM-PC based program CLUSTRAN (Gillett, 1986). The following pages of this section give stereographic projection plots for each of the scanlines. Different symbols were used to differentiate between the sets chosen by CLUSTRAN. This was done because the choices made by CLUSTRAN were not always obvious. The cluster analysis algorithm of CLUSTRAN is based on the work of Shanley and Mahtab (1976) and Mahtab and Yegulalp (1982).

The method used in this study to subdivide the orientation data into sets was based on the use of contoured stereographic projections. The contour levels on the contoured stereographic projections are in multiples of a uniform distribution.

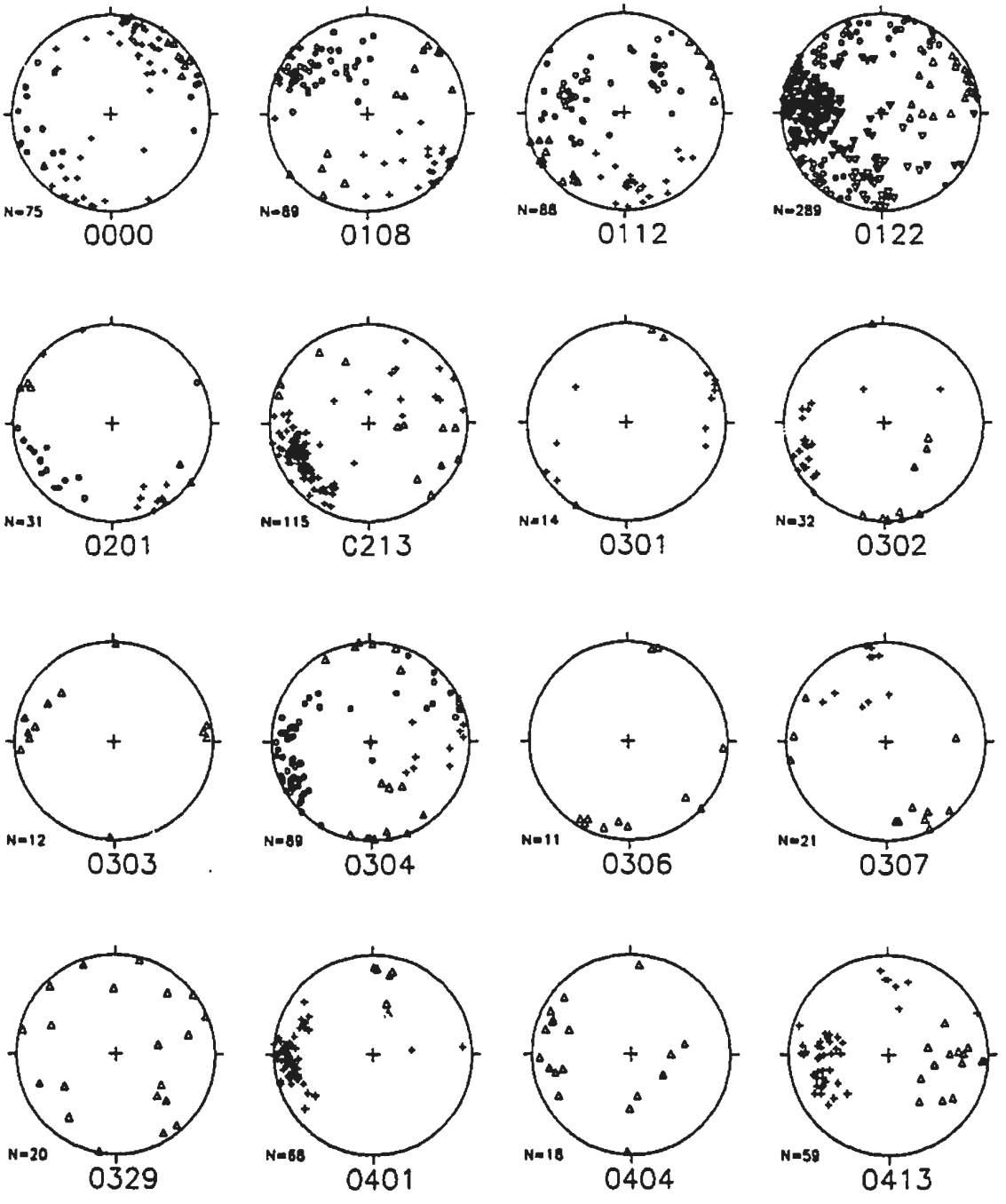

CLUSTRAN BASED SCANLINE CLUSTER ANALYSIS

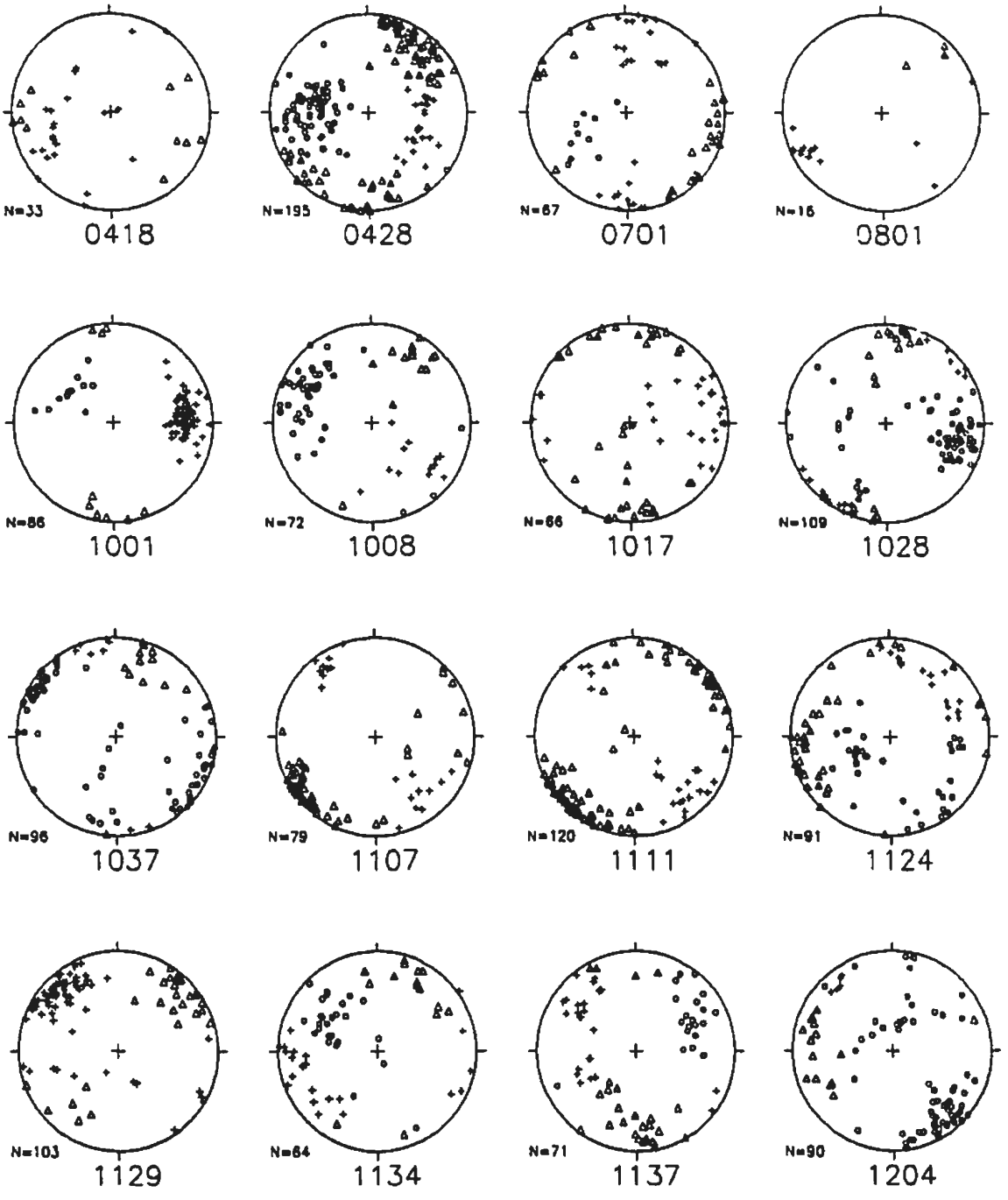

CLUSTRAN BASED SCANLINE CLUSTER ANALYSIS

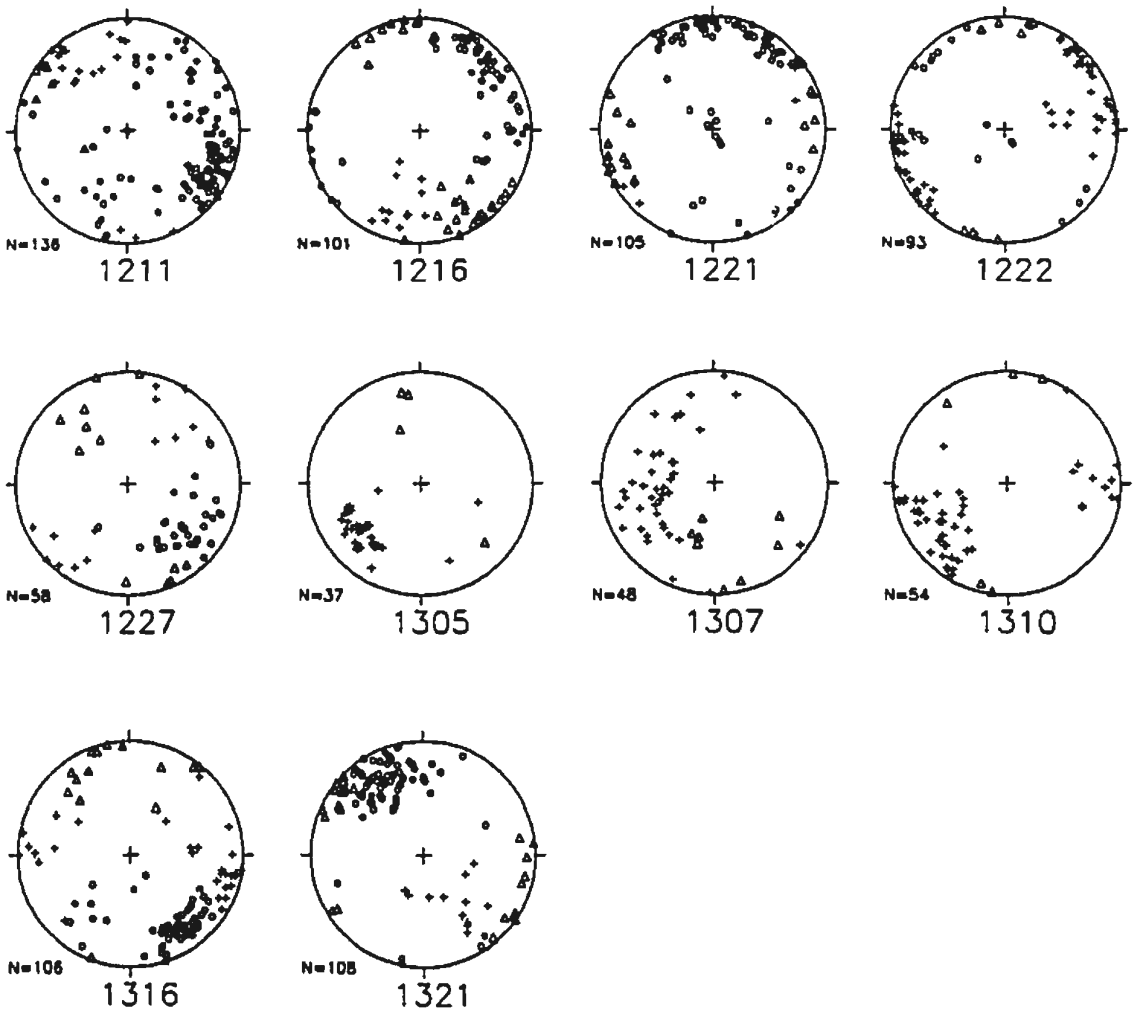

CLUSTRAN BASED SCANLINE CLUSTER ANALYSIS

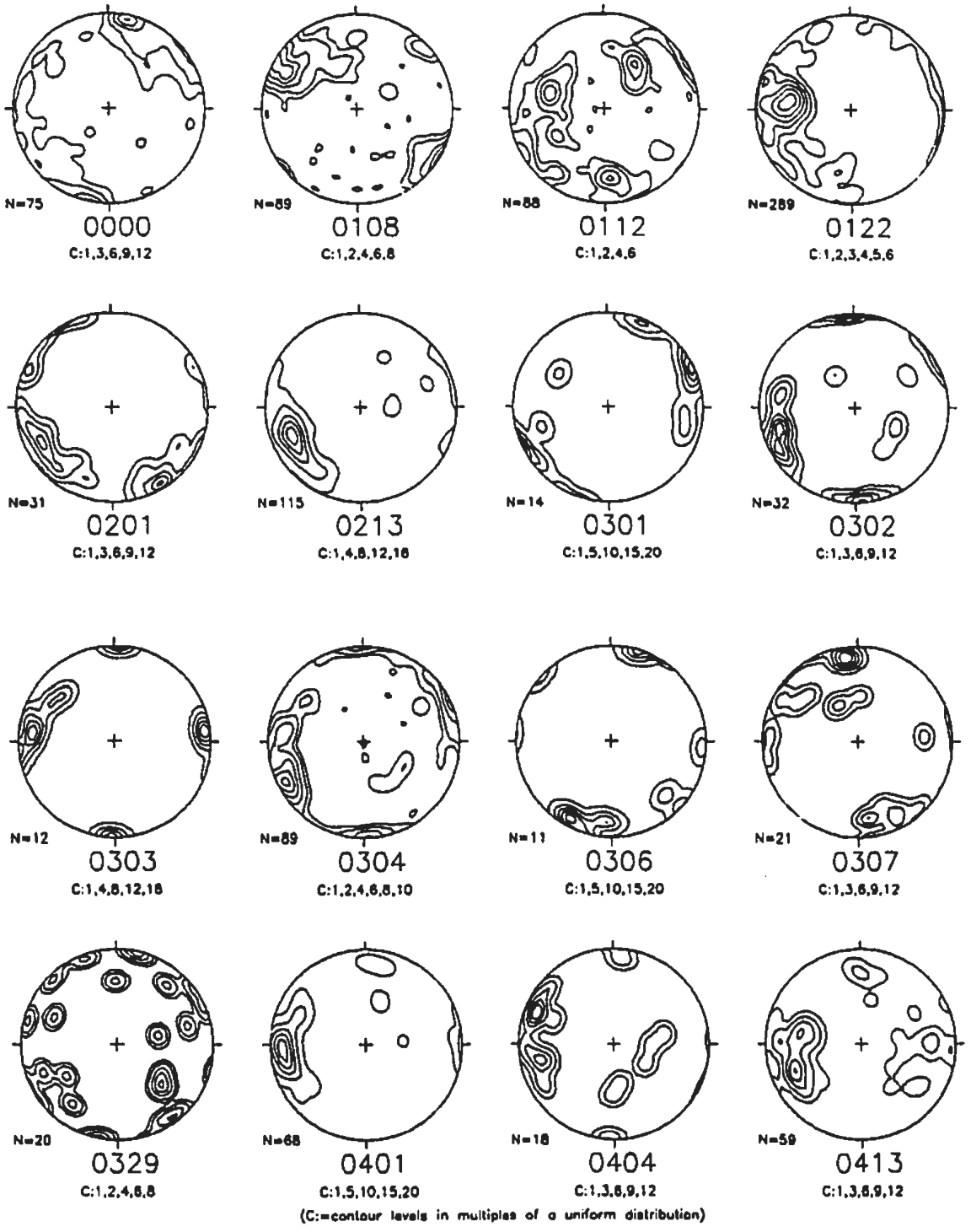

(C:=contour levels in multiples of a uniform distribution)

CONTOUR BASED SCANLINE CLUSTER ANALYSIS

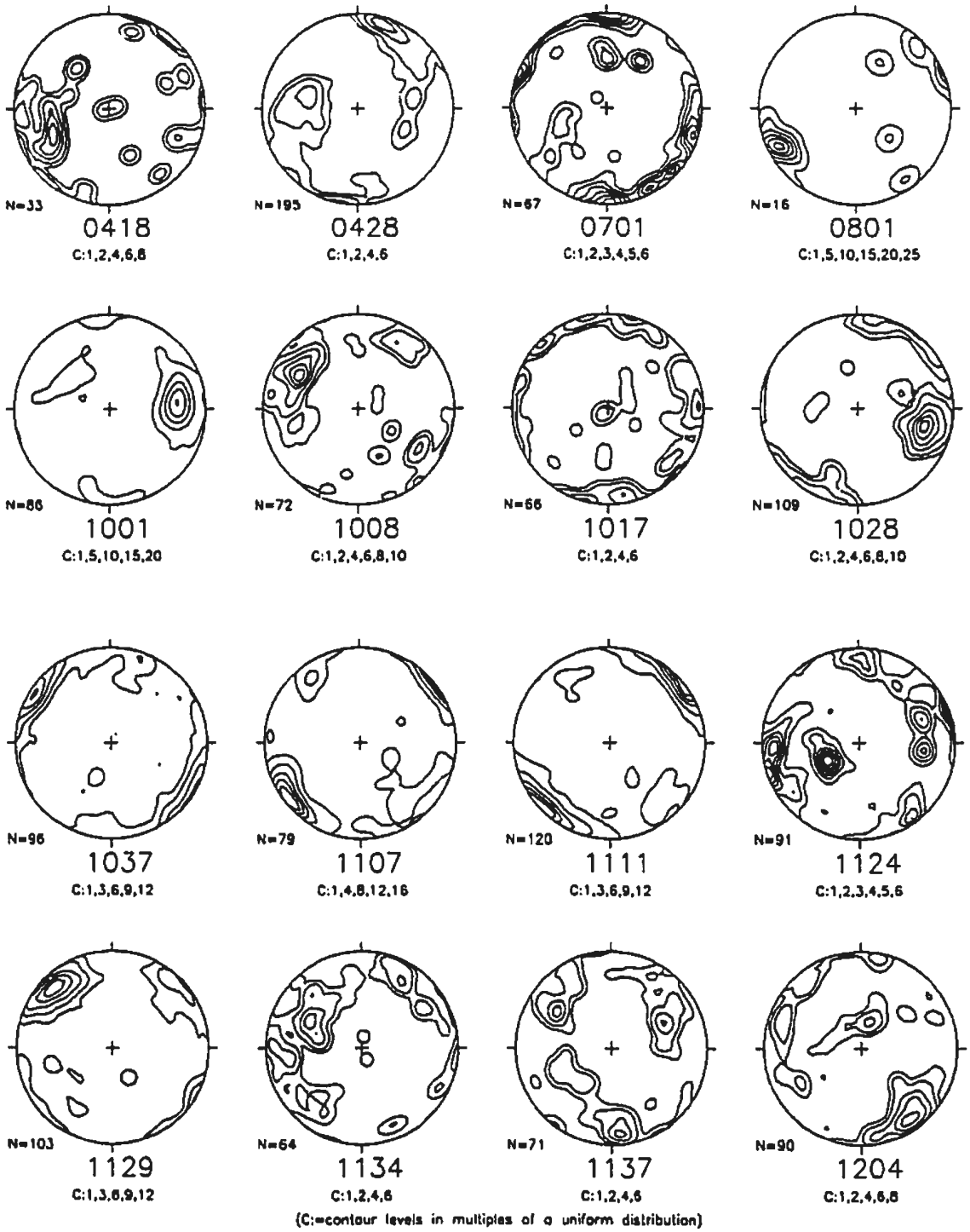

(C:=contour levels in multiples of a uniform distribution)

CONTOUR BASED SCANLINE CLUSTER ANALYSIS

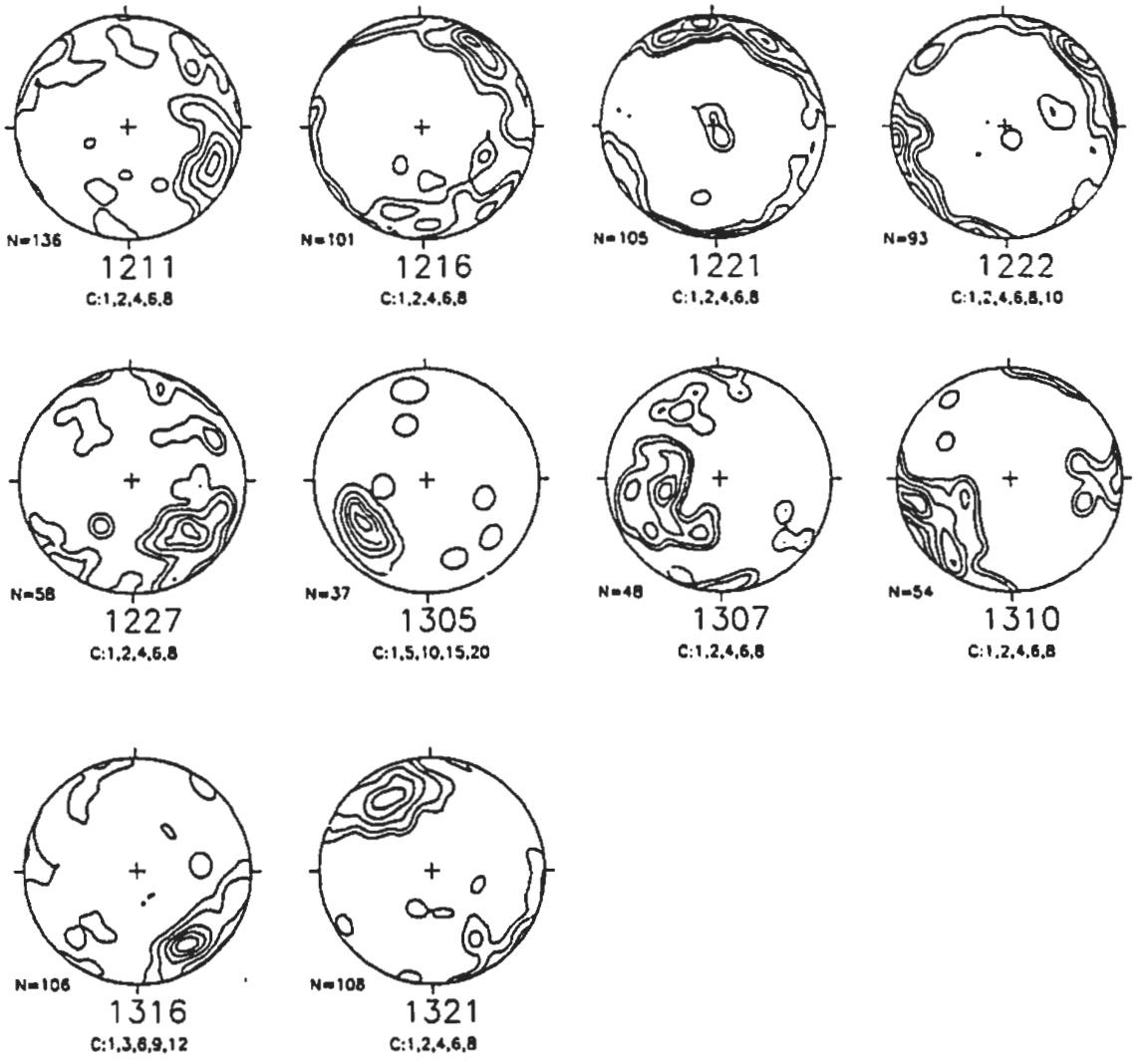

(C:=contour levels in multiples of a uniform distribution)

CONTOUR BASED SCANLINE CLUSTER ANALYSIS

A.3 Fracture Characteristics

A.3.10 *Termination Mode Ratios vs. Mineral Filling Presence*

Termination Mode versus Presence of Mineral Filling

		Termination Mode						Termination Mode Ratios					
		0		1		2		0/1		0/2		2/1	
Scanline	n	Min.	None	Min	None	Min.	None	Min.	None	Min.	None	Min.	None
0108	89	4	1	45	25	9	5	0.09	0.04	0.44	0.20	0.20	0.20
0329	32	1	3	8	17	1	1	0.11	0.18	1.00	3.00	0.11	0.06
1037	147	0	1	37	62	17	30	0.00	0.02	0.00	0.03	0.46	0.48
1204	128	4	5	29	58	7	25	0.14	0.09	0.57	0.20	0.24	0.43
1316	142	15	5	65	35	9	13	0.23	0.14	1.67	0.38	0.14	0.37
1321	160	4	5	81	49	8	13	0.05	0.10	0.50	0.38	0.10	0.27
1129	159	1	2	75	58	7	16	0.01	0.03	0.14	0.13	0.09	0.28
1134	101	0	0	67	13	14	7	0.00	0.00	0.00	0.00	0.21	0.54
1211	210	1	2	7	160	1	39	0.14	0.01	1.00	0.05	0.14	0.24
0112	128	1	1	68	31	20	7	0.01	0.03	0.05	0.14	0.29	0.23
0428	292	11	3	196	43	31	8	0.06	0.07	0.35	0.38	0.16	0.19
0000	118	3	0	89	0	26	0	0.03		0.12		0.29	
0122	305	15	3	199	53	20	15	0.08	0.06	0.75	0.20	0.10	0.28
0201	15	1	0	6	6	2	0	0.17	0.00	0.50		0.33	
0301	17	1	0	15	0	1	0	0.07		1.00		0.07	
0302	39	2	0	28	2	5	2	0.07	0.00	0.40	0.00	0.18	1.00
0303	9	0	0	0	9	0	0		0.00				
0304	14	0	0	4	8	0	2	0.00	0.00		0.00		0.25
0306	10	0	0	1	8	1	0	0.00	0.00	0.00		1.00	
0307	14	2	2	10	0	0	0	0.20					
0401	55	3	0	39	12	1	0	0.08	0.00	3.00		0.03	
0404	23	1	0	20	2	0	0	0.05	0.00				
0413	76	4	1	55	7	8	1	0.07	0.14	0.50	1.00	0.15	0.14
0418	42	4	0	32	0	6	0	0.13		0.67		0.19	
0701	88	4	4	35	29	7	9	0.11	0.14	0.57	0.44	0.20	0.31
1008	117	0	0	6	72	2	37	0.00	0.00	0.00	0.00	0.33	0.51
1017	121	1	0	17	61	9	33	0.06	0.00	0.11	0.00	0.53	0.54
1028	145	0	10	3	115	0	17	0.00	0.09		0.59		0.15
1227	97	0	3	15	56	7	16	0.00	0.05	0.00	0.19	0.47	0.29
1310	85	2	1	27	40	3	12	0.07	0.03	0.67	0.08	0.11	0.30
0213	141	4	7	48	57	6	19	0.08	0.12	0.67	0.37	0.13	0.33
1107	101	1	6	10	61	0	23	0.10	0.10		0.26		0.38
1111	174	0	6	35	82	13	38	0.00	0.07	0.00	0.16	0.37	0.46
1124	158	0	3	48	54	19	34	0.00	0.06	0.00	0.09	0.40	0.63
1216	176	0	4	1	144	1	28	0.00	0.03	0.00	0.15	1.00	0.19
1221	166	0	0	12	107	2	45	0.00	0.00	0.00	0.00	0.17	0.42
1222	145	1	2	30	79	12	21	0.03	0.03	0.08	0.10	0.40	0.27
1307	70	4	0	33	17	9	7	0.12	0.00	0.44	0.00	0.27	0.41
1305	51	1	2	12	29	0	7	0.08	0.07		0.29		0.24
1001	80	0	5	3	54	1	17	0.00	0.09	0.00	0.29	0.33	0.31
1137	114	2	0	38	48	10	16	0.05	0.00	0.20	0.00	0.26	0.33
ALL	4354	98	87	1550	1783	295	561	0.06	0.05	0.33	0.16	0.19	0.32

Note: Min. = Presence of mineral filling; None = Absence of mineral filling Note: Blanks signify denominator values of zero.

A.4 BLIND ZONE STEREOGRAPHICS PROJECTIONS

Blind zones are defined as the angular band that lies 20° to either side of the scanline orientation (Terzaghi, 1965). The following stereographic projections show the orientation of the blind zone for each scanline or scanline area. The hatched area is the area of the blind zone. This zone is undersampled because fractures whose orientations lie parallel or subparallel to that of the scanline, will be less likely to be intersected by the scanline than those fractures that lie perpendiclular to the scanline.

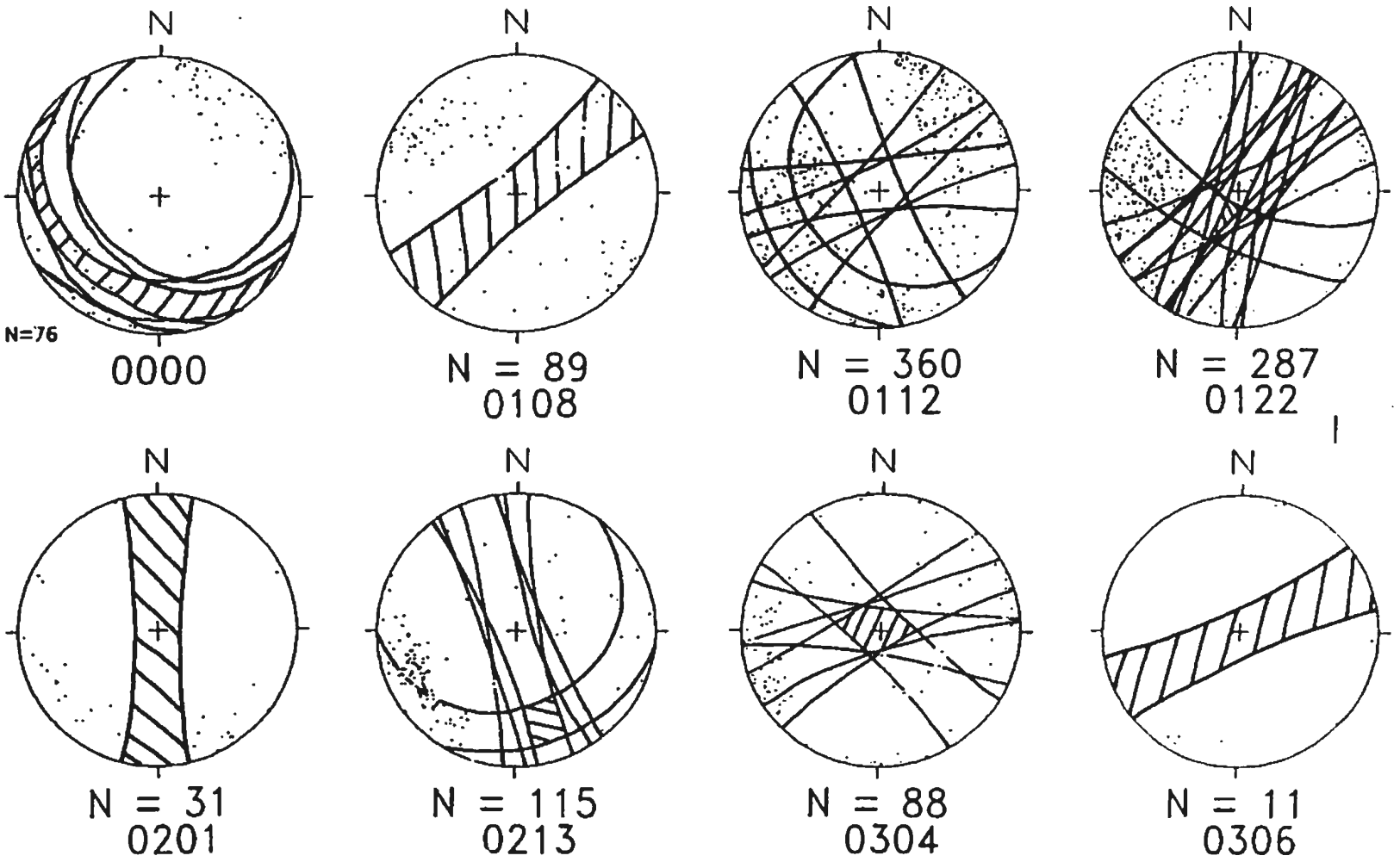

BLIND ZONE DELINEATION

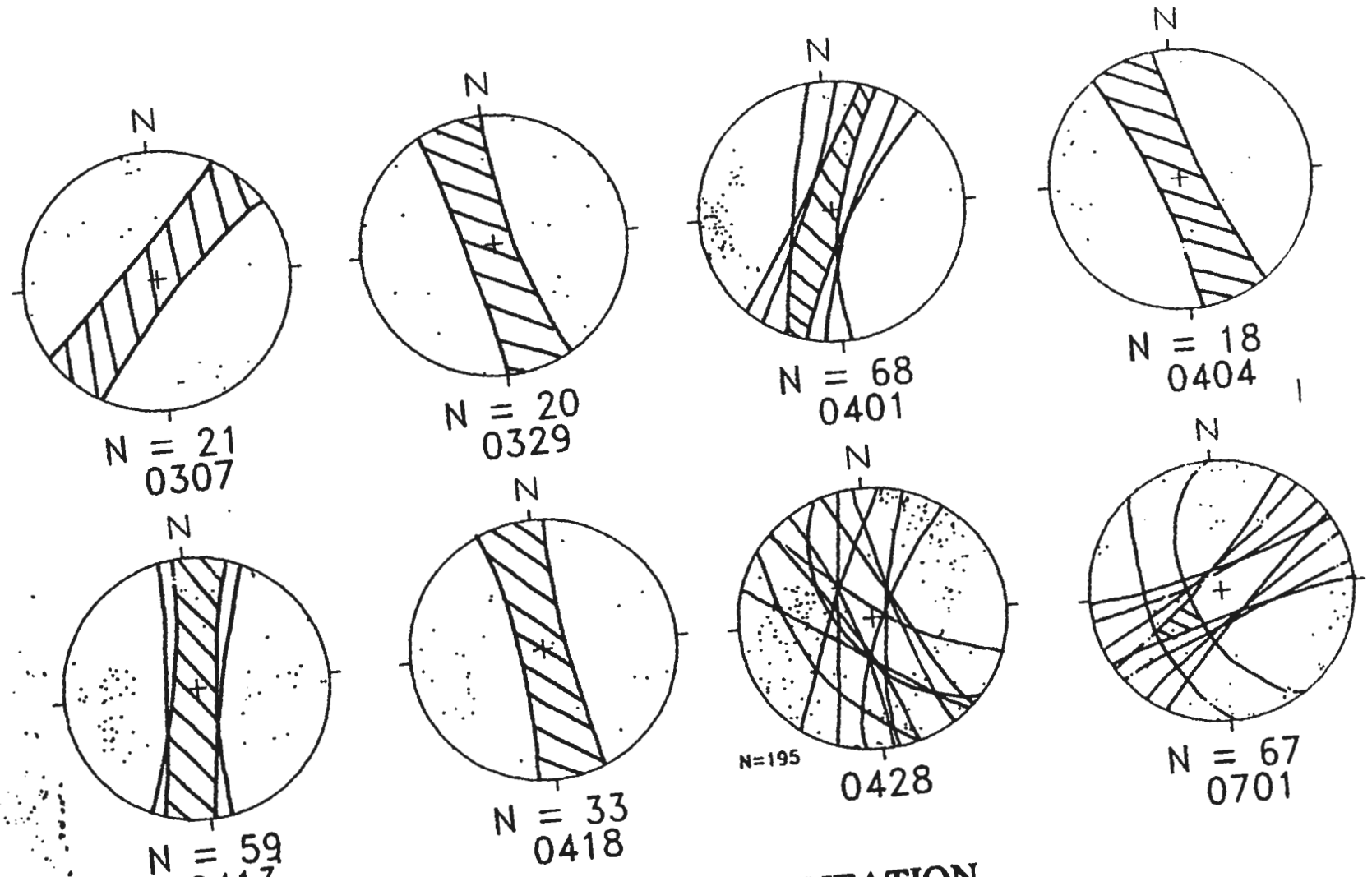

BLIND ZONE DELINEATION

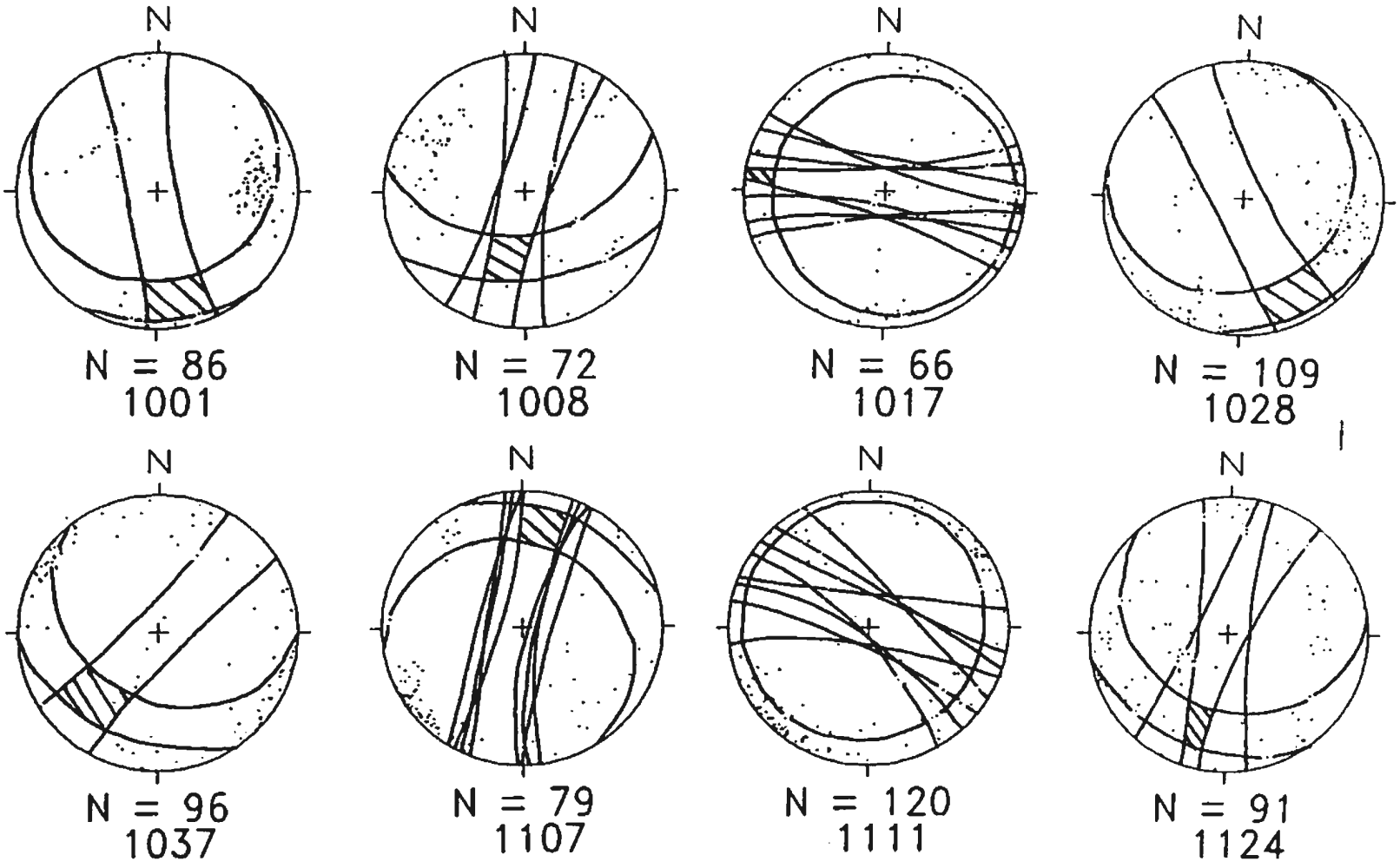

BLIND ZONE DELINEATION

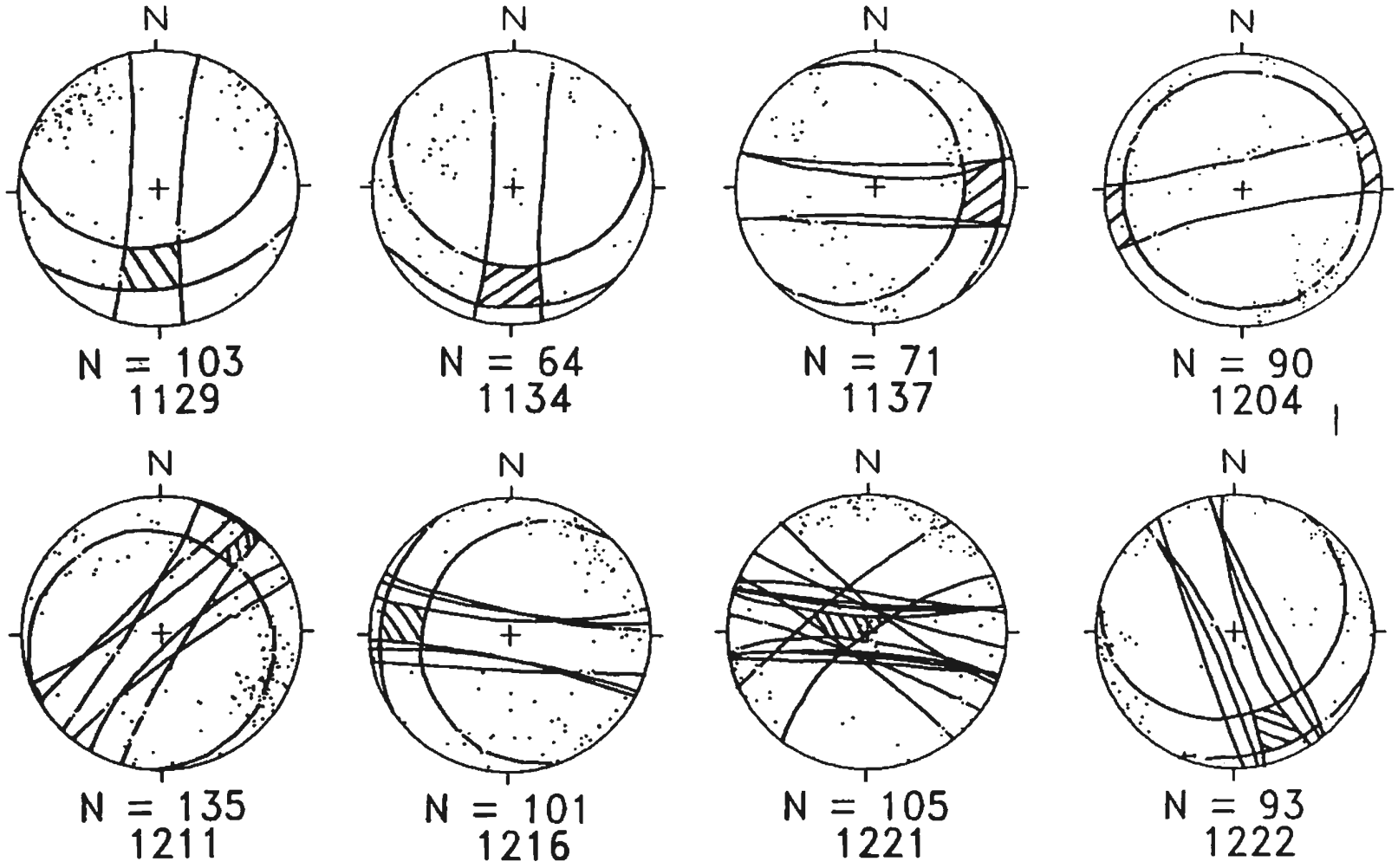

BLIND ZONE DELINEATION

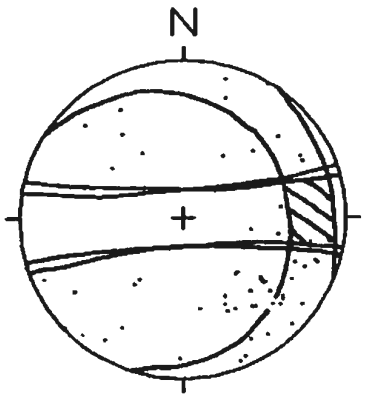

N = 58
1227

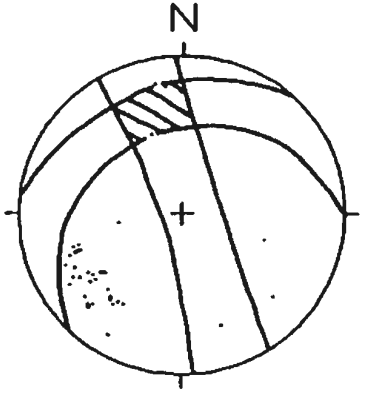

N = 37
1305

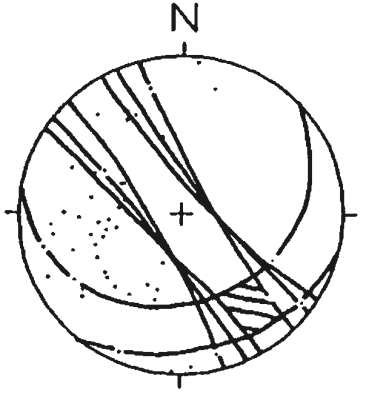

N = 48
1307

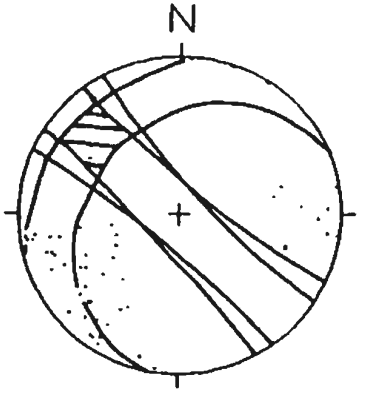

N = 54
1310

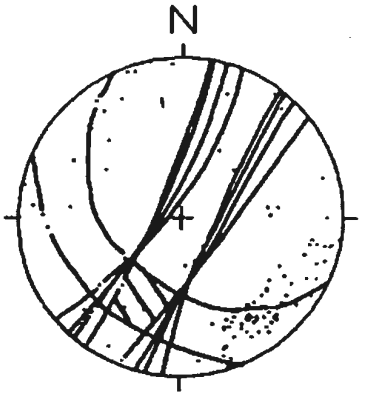

N = 106
1316

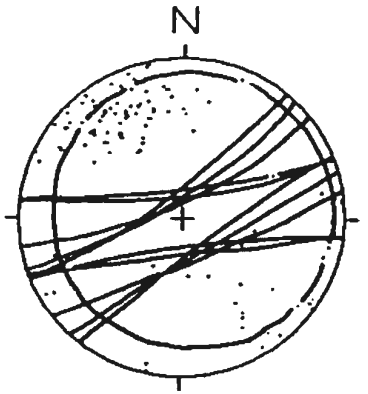

N = 108
1321

BLIND ZONE DELINEATION

A.5 SLICKENSIDE LINEATIONS

The scanline locations can be found on the scanline location map. The other locations are descriptions and can be found in relation to village names (such as listed on Figure 3.1). The data listing gives first the fault plane orientation (labelled: Plane) followed by the slickenside lineation (labelled: Slick).

Plane Slick Plane Slick Plane Slick Plane Slick

Scanline: 0108
254 78 344 02

Scanline: 0112
223 86 209 86 049 69 047 68

Scanline: 0118
056 65 058 65 052 50 142 00 029 84 108 60 027 63 014 62

Scanline: 0123
086 35 132 26 075 75 088 74 068 52 140 22 058 84 132 61
111 55 116 55 089 85 002 26 067 63 345 15 214 70 279 51
214 70 269 58 082 57 165 10

Scanline: 0213
093 75 176 25

Scanline: 0301
250 85 340 05

Scanline: 0304
096 80 008 12

Scanline: 0306
315 69 032 30 176 76 086 03 184 40 095 00 334 77 316 77

Scanline: 0329
136 84 046 05 319 84 048 06

Scanline: 0403
052 77 142 02

Scanline: 0404
083 73 165 24 106 79 007 08 112 75 024 06

Scanline: 0415
071 60 049 58

Scanline: 0701
048 70 134 10 289 80 017 08 312 83 227 36 283 86 196 24
225 89 315 32 285 76 203 28 276 73 309 69

Scanline: 1011
127 53 153 55

Scanline: 1018
255 88 165 02

Scanline: 1021
346 75 075 03 131 68 045 09 260 80 170 02

Plane	Slick	Plane	Slick	Plane	Slick	Plane	Slick

Scanline: 1107
025 89 115 00 024 82 113 05

Scanline: 1108
241 81 331 02 009 81 279 01 253 76 336 25 083 89 354 07

Scanline: 1111
026 70 116 43 204 72 226 71 327 15 326 15 075 87 164 3
234 79 169 65

Scanline: 1125
212 76 283 55

Scanline: 1129
142 75 053 04 119 82 032 20 141 76 053 09 135 81 047 12
137 66 059 27

Scanline: 1134
140 68 058 23 030 55 306 05

Scanline: 1205
135 80 057 52 296 79 212 27 130 56 081 44

Scanline: 1211
260 85 349 14 336 58 337 57

Scanline: 1216
251 59 168 12

Scanline: 1221
146 75 058 12 150 85 180 85 194 84 283 12 082 82 355 20
200 78 111 02 210 84 121 12 150 80 062 12 192 84 280 12

Scanline: 1222
077 84 165 18 195 89 349 14 066 85 337 08

Scanline: 1227
264 51 348 07 314 66 237 24 300 67 211 02 280 50 007 04
277 71 004 09 298 80 024 9

Scanline: 1307
076 76 348 12 112 62 025 05 119 45 025 06 083 42 022 24
076 47 003 16 094 31 032 16 058 66 342 29 061 49 346 16
090 62 004 06

Scanline: 1310
066 75 342 19 278 83 008 00

Scanline: 1321
155 60 107 49 161 55 103 38

Area: Diorite Cupola N.E. of Phterikhoudi
071 48 069 46 056 34 342 09

Area: 2 km west of 1107
238 89 162 27

Plane Slick Plane Slick Plane Slick Plane Slick

Area: 6.4 km S of 1011
114 56 175 34

Area: Shear zone at Apliki Village
279 87 009 00 044 75 320 20 083 85 354 05 038 77 337 64 116 84 027 07 075 78 349 16 093 54 102 54

Scanline: Askas
026 66 324 45

Area: 2 km north of Pharmakas
316 70 316 70 322 80 232 02 315 87 212 4

Area: 4 km north of Pharmakas
286 61 219 35 060 89 060 89 062 80 151 06 274 88 185 28
318 85 280 84 277 84 188 07

Area: Cemetary at Ayios Epiphanios
281 65 280 62

Area: Ayia Koroni
358 83 086 12

Area: 1.1 km north of Apliki
084 64 002 15

Area: 0.5 km north-east of Palekhori
109 46 183 16

Area: 2.9km south of Ayios Epiphanios/Kato Moni turnoff
175 65 092 16 024 86 298 25 110 55 197 05

Area: 4.42 km south of Xyliatos
323 85 050 28 110 31 156 19

Area: 5 km south of Xyliatos
129 74 046 26 044 55 132 04 126 74 041 20 141 44 052 01
340 79 060 39 341 84 065 41 321 81 046 26 038 52 060 50

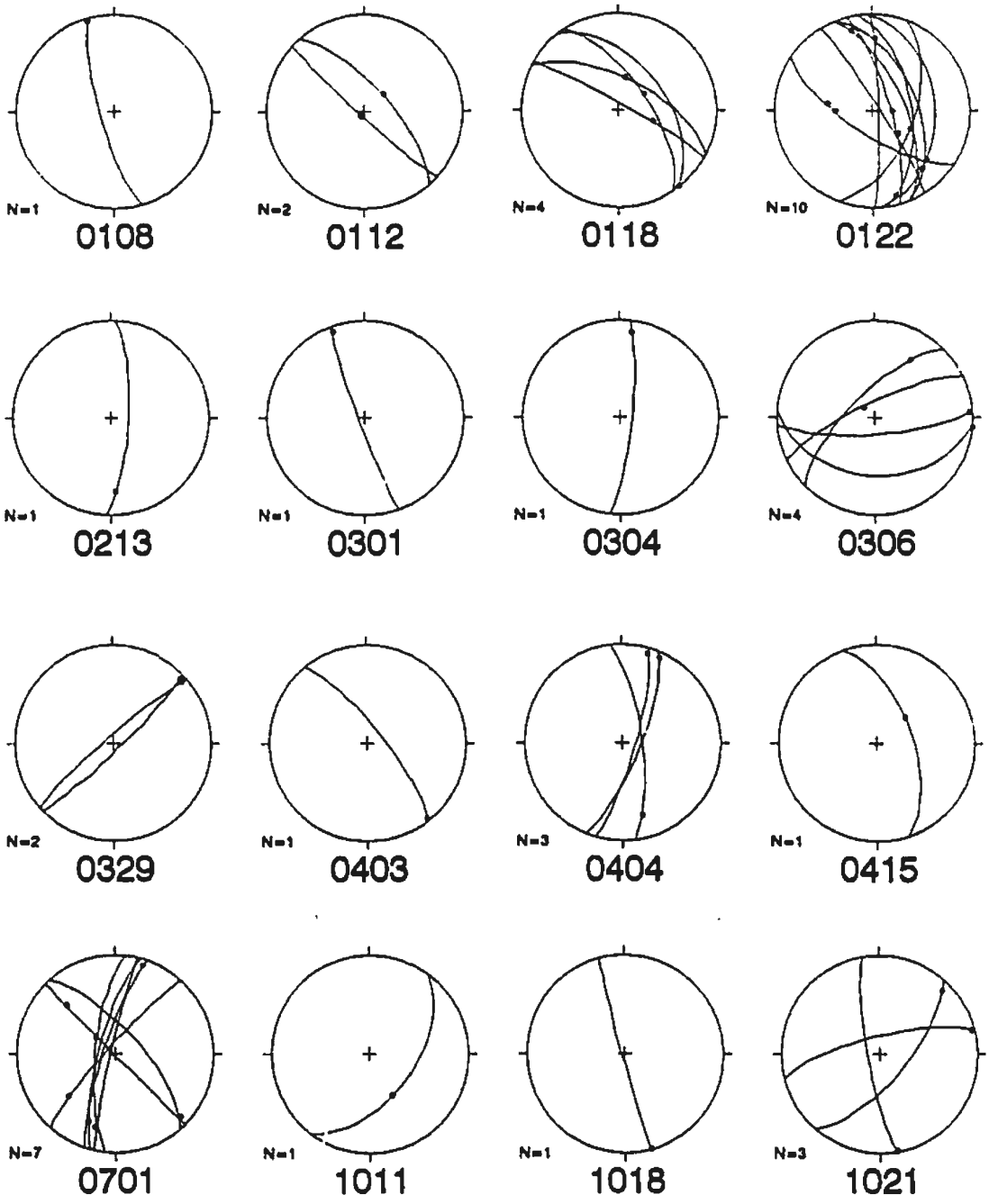

SLICKENSIDE LINEATIONS

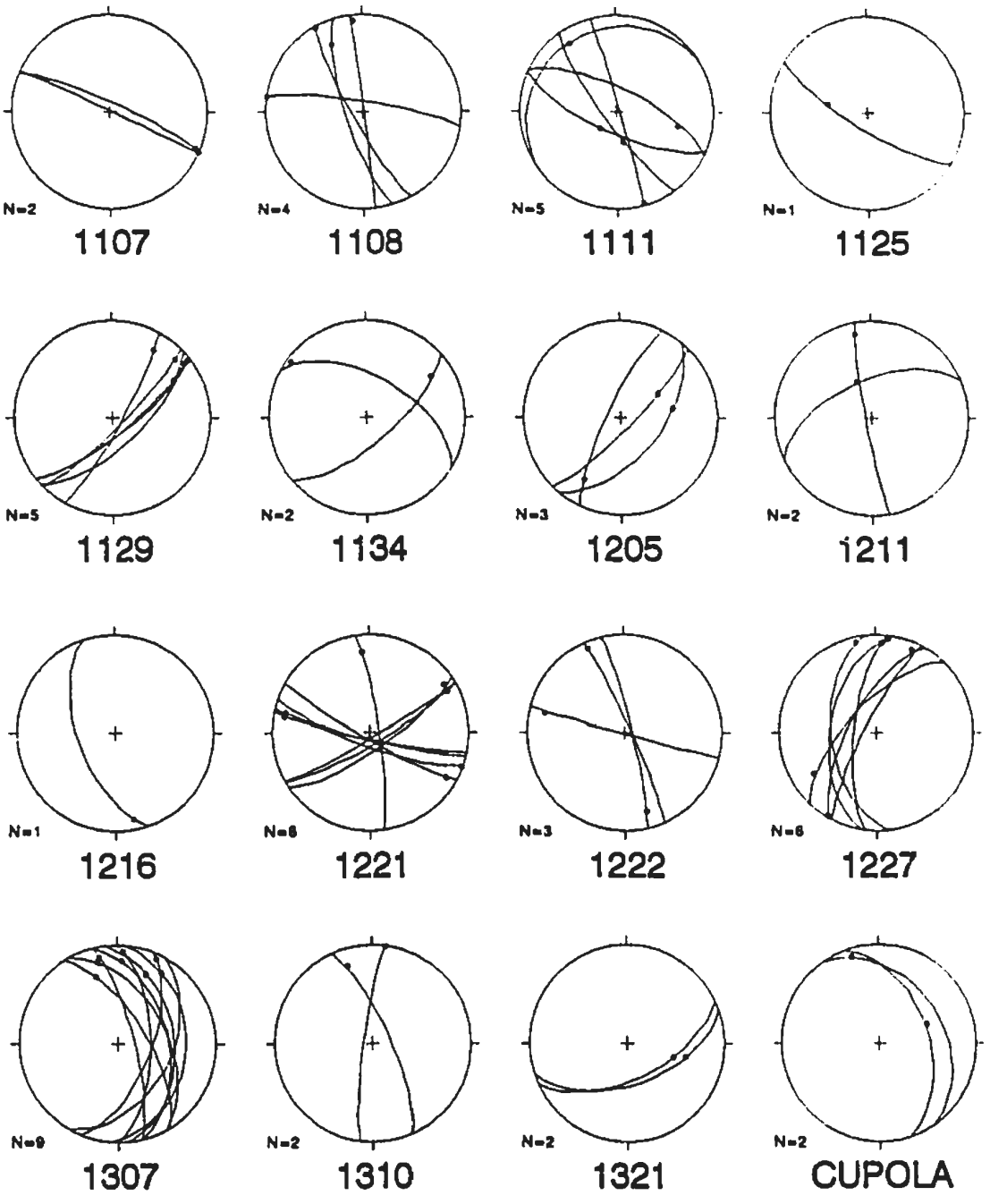

SLICKENSIDE LINEATIONS

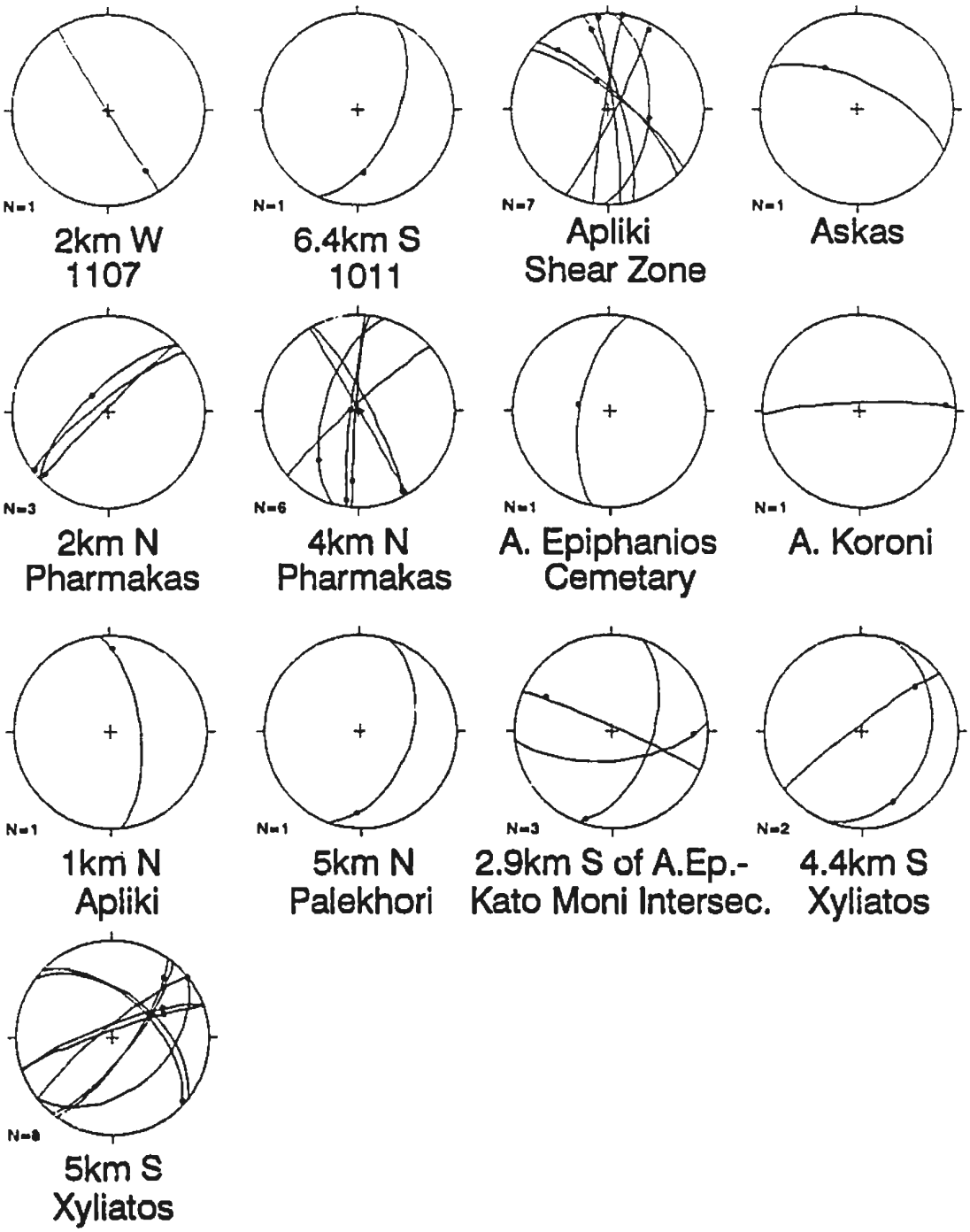

SLICKENSIDE LINEATIONS

A.6 FRACTURE AREA MAPPING

The area mapping method of measuring fracture characteristics was done at two sites, 1137 and 1305. The following four pages show the fracture area and scanline maps for these two areas. The distance along the outcrop is shown at the base of the map. There is no vertical exaggeration in the maps. The distribution of fracture orientations are shown on the following page to compare the area and scanline mapping methods. The comparison of fracture trace length distributions and the tabulated fracture properties between the two methods is shown on the following pages. The last page in this section shows the effect of applying the Terzaghi (1965) correction to the scanline 1137 fracture orientation data and is compared to the area mapped fracture data of site 1137.

AREA 1 (SCANLINE 1137)

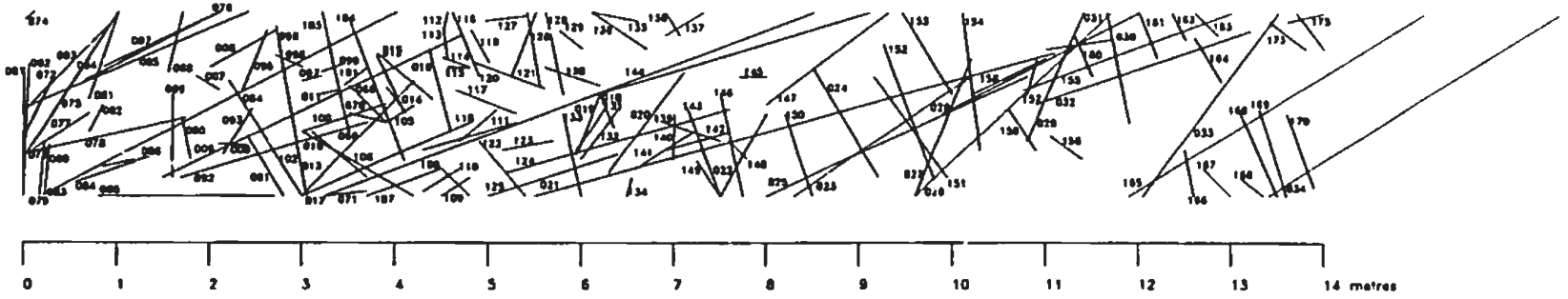

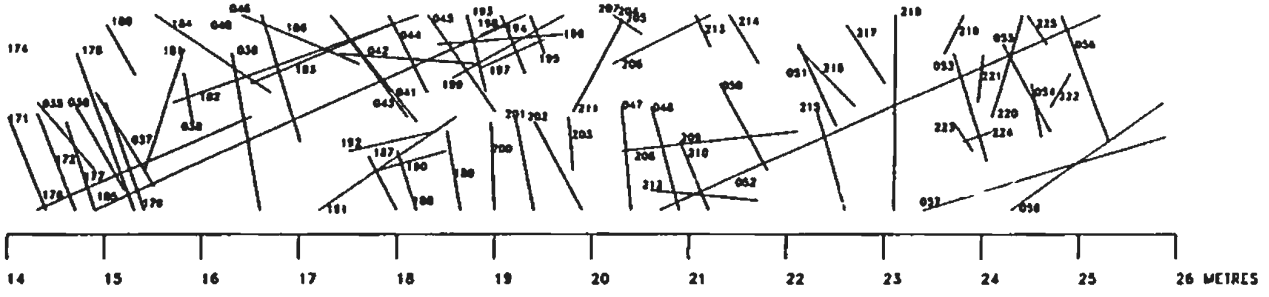

SCANLINE 1137

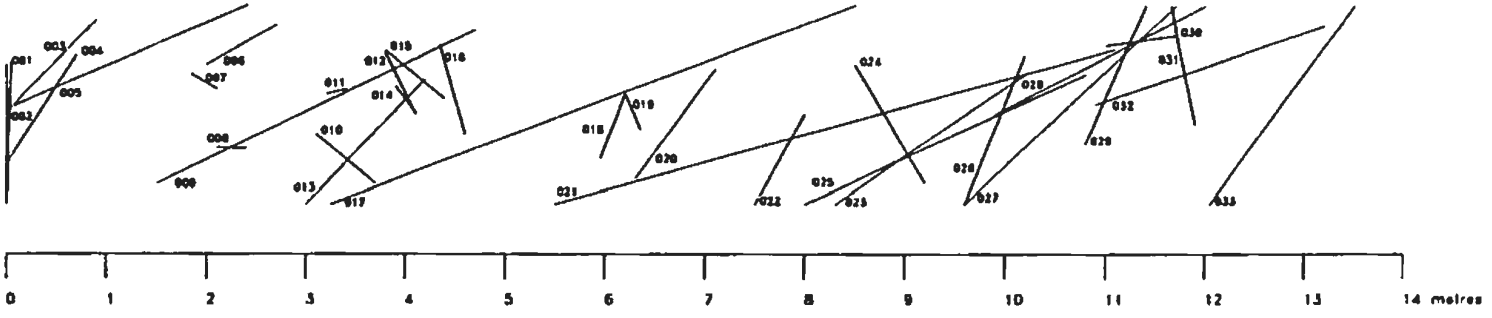

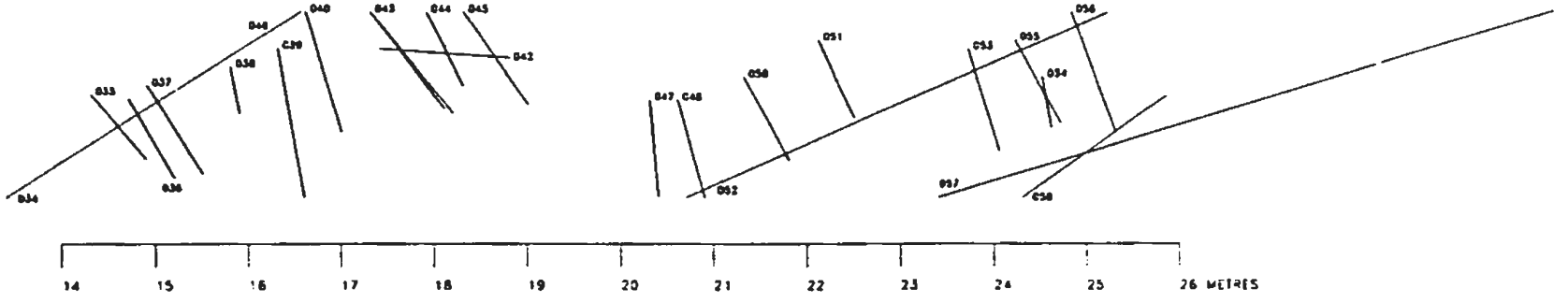

AREA 2 (SCANLINE 1305)

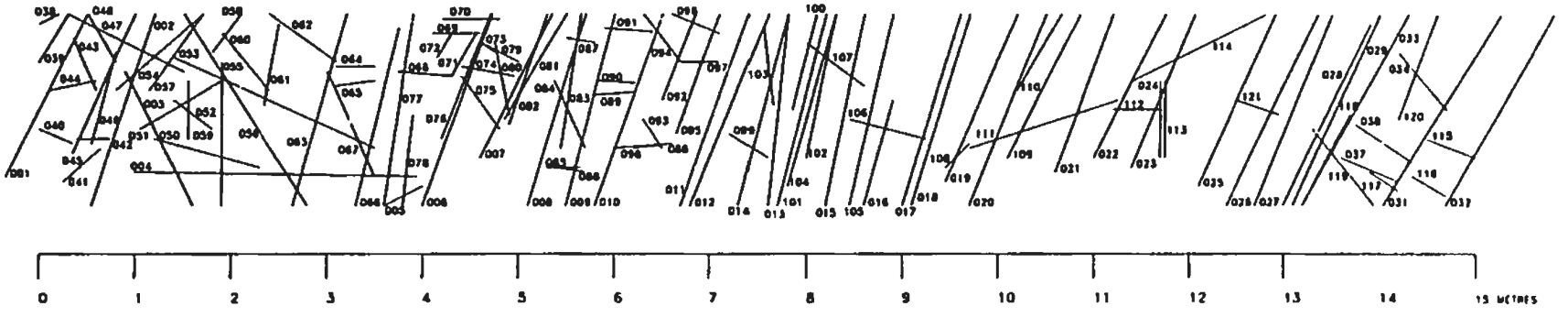

SCANLINE 1305

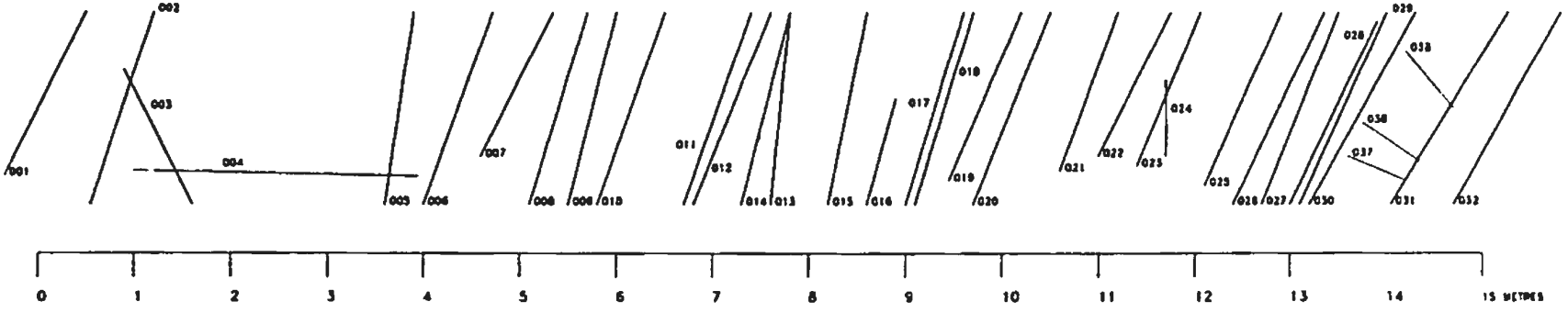

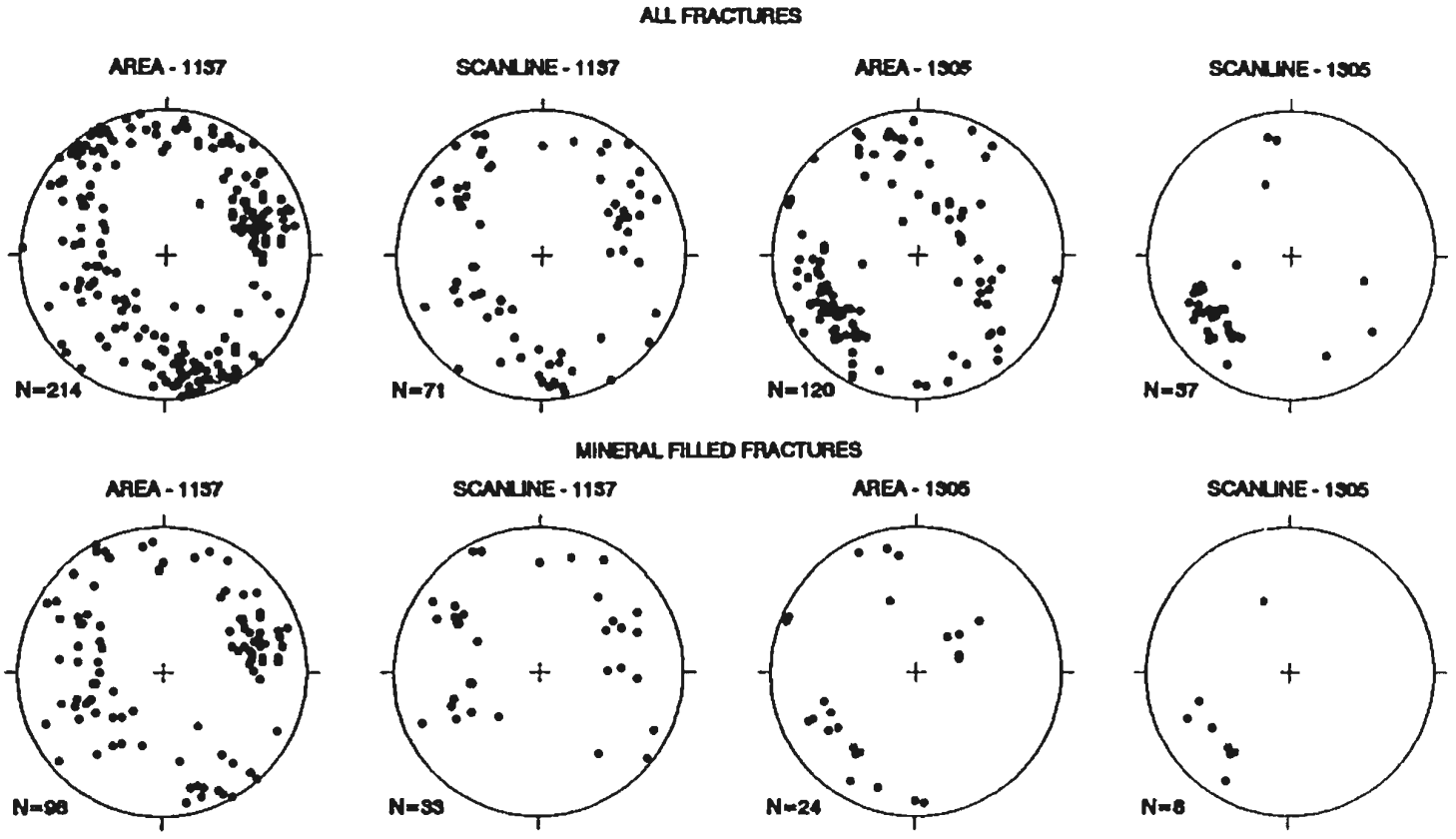

Poles to Planes

AREA VERSUS SCANLINE FRACTURE MAPPING

TRACE LENGTH HISTOGRAMS

Area versus Scanline Mapping

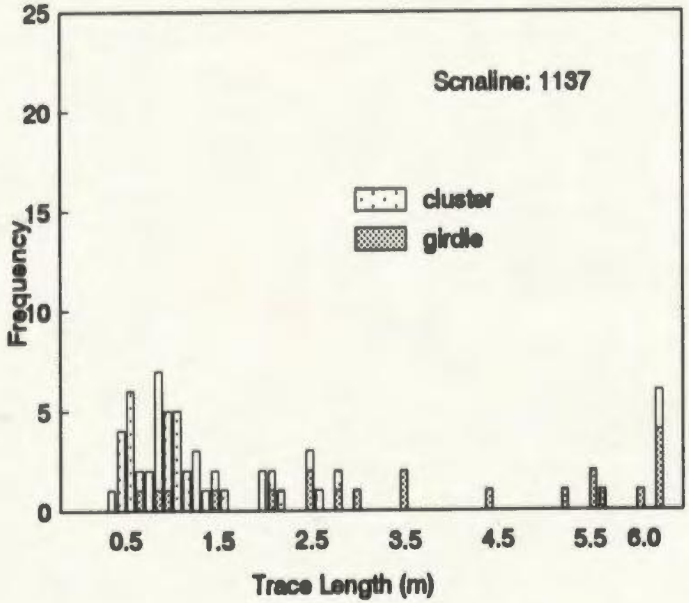

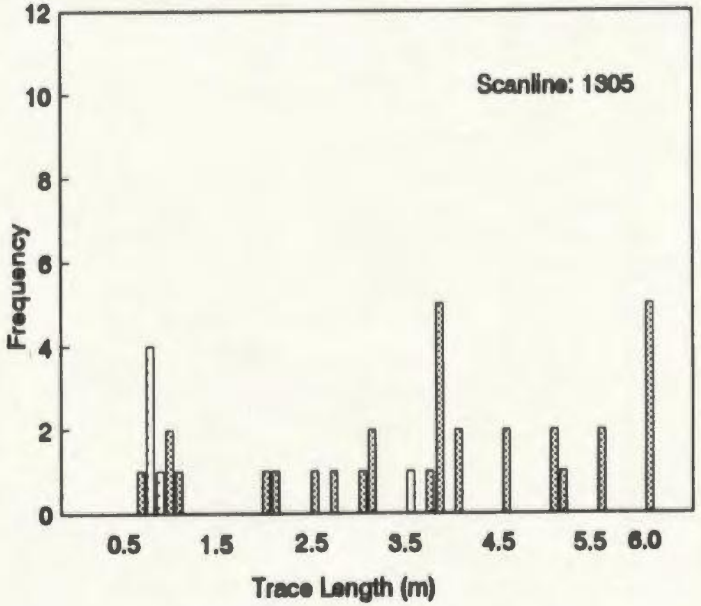

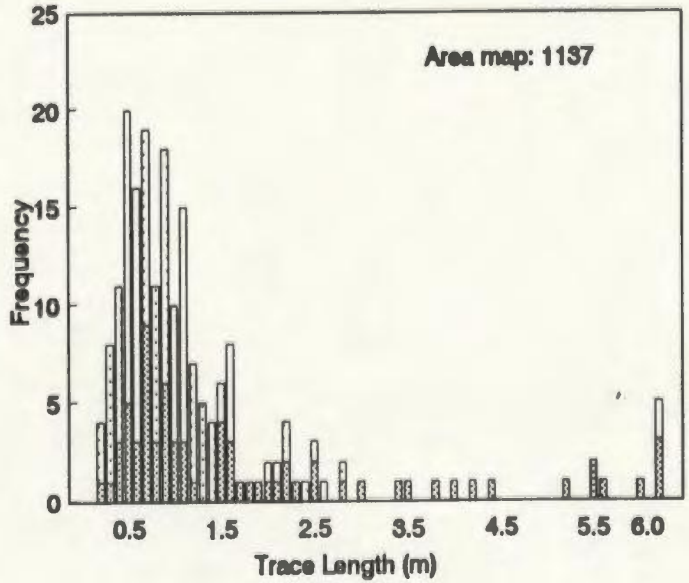

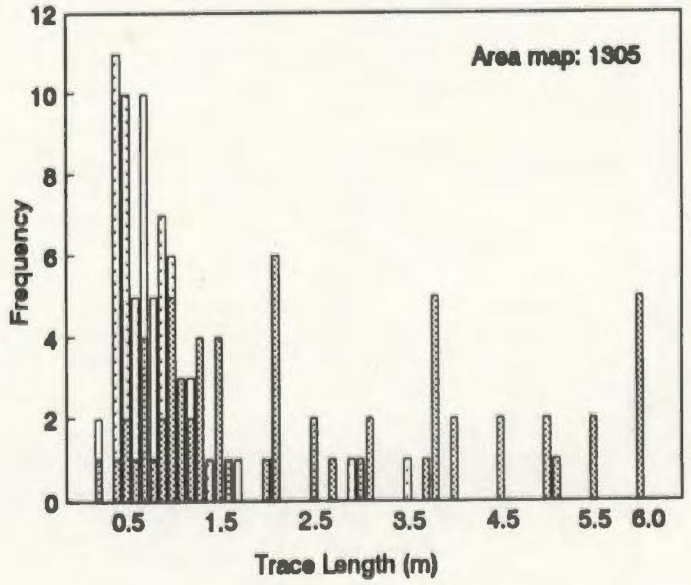

Scanline versus Area Mapping: Tabulated Properties

Location Set	1137-S Cluster	1137-S Girdle	1137-A Cluster	1137-A Girdle	1305-S Cluster	1305-S Girdle	1305-A Cluster	1305-A Girdle
#	21	45	70	126	30	6	64	44
Type								
contact	9	3	16	3	16	0	21	0
fracture	2	1	19	16	2	1	12	9
joint	10	41	35	107	12	5	31	35
Trace Length								
< =2m	4	39	49	118	6	6	32	42
> 2m	17	7	22	9	25	1	32	2
Term. Mode								
0	1	1	5	2	3	0	12	1
1	10	19	22	62	16	0	28	7
2	5	18	35	54	2	5	8	35
3	0	0	1	0	0	0	0	0
Mineral Filling								
none	9	28	33	73	21	5	45	27
epidote	12	17	35	38	7	1	10	9
calcite	7	2	7	3	4	0	10	8
zeolite	0	0	0	0	0	0	0	0
pyrite	1	5	6	25	0	0	0	0
chlorite	2	2	1	2	0	0	0	0
celadonite	0	0	0	0	0	0	0	0
hematite	0	0	0	0	0	0	0	0
magnetite	0	0	0	0	0	0	0	0
quartz	0	0	1	0	0	0	1	0
clay	1	0	2	4	0	0	0	0
Large scale Roughness								
planar	14	41	62	117	26	6	57	42
undulating	2	2	2	1	0	0	0	0
curved	5	3	7	8	3	0	5	0
stepped	0	0	0	0	1	0	1	0
irregular	0	0	0	1	0	0	1	2
Mean Length	4.13	1.51	1.95	1.05	3.71	1.07	2.47	0.75
Std. Dev.	2.32	1.95	1.86	1.27	1.73	1.03	1.76	0.61

Note: S = scanline mapped data
A = area mapped data
Cluster = cluster distribution of data
Girdle = girdle distribution of data

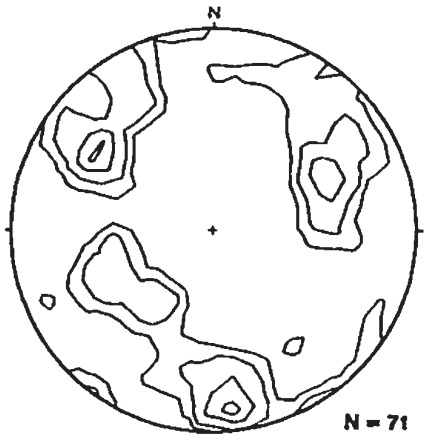

Contours:
1 2 4 6

ORIGINAL
SCANLINE
DATA

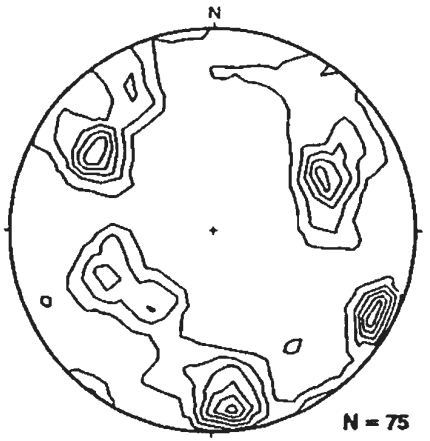

Contours:
1 2 3 4 5 6

TERZAGHI
CORRECTED
SCANLINE DATA

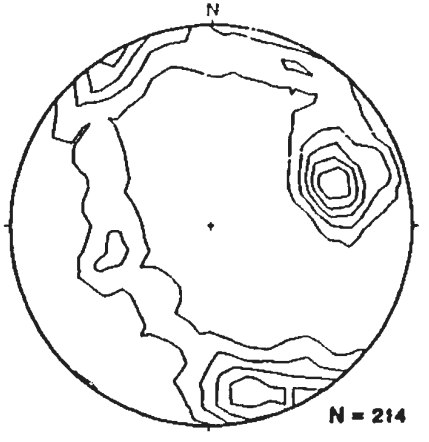

Contours:
1 2 3 4 5

Poles to Planes

AREA MAPPED
DATA

EFFECT OF TERZAGHI CORRECTION AT SCANLINE LOCATION 1137

A.7 PERMEABILITY CALCULATION RESULTS

Formulation of Parallel-Plate Flow

(after Norton and Knapp, 1977; Snow, 1965, 1969).

The parallel plate model of Norton and Knapp (1977) uses the analogy of d'Arcy's Law for flow through porous media (Figure 4.10A),

$$Q = \frac{-k\nabla\Omega}{\eta} \quad \ldots\ldots\ldots\ldots\ldots\ldots (A.7.1)$$

and a formulation for the volume flow rate from n parallel fractures,

$$Q = \frac{-nd^3\nabla\Omega}{12\eta} \quad \ldots\ldots\ldots\ldots\ldots\ldots (A.7.2)$$

to derive intrinsic permeability for fracture controlled flow,

$$k = \frac{nd^3}{12} \quad \ldots\ldots\ldots\ldots\ldots\ldots (A.7.3)$$

where Q is the flow rate, d is the fracture aperture, η is the fluid viscosity, Ω is the fluid potential, ∇ is the gradient operator, and k is the intrinsic permeability of the fractured rock.

Similarly, Snow (1969), derived a formulation for discharge, Q,

$$Q = -\frac{b^2}{3}\frac{g}{\nu}L(2b)I \quad \ldots\ldots\ldots\ldots\ldots\ldots (A.7.4)$$

where, L is the length of the sides of a cube, with parallel plate conduits of aperture 2b, separated by non-conductive solid material. L(2b) is the area and I is the hydraulic gradient, parallel to the conduits. From this, the hydraulic conductivity, K is,

$$K = \frac{b^2}{3}\frac{g}{\nu} \quad \ldots\ldots\ldots\ldots\ldots\ldots (A.7.5)$$

The total discharge, Q, of N such conduits is,

$$Q = -\frac{2}{3}b^3\frac{g}{\nu}NLI \quad \ldots\ldots\ldots\ldots\ldots\ldots (A.7.6)$$

If apertures in each of the conduits remain constant in all directions then

$$Q = -\frac{2}{3}\frac{g}{\nu}LI\sum_{i=1}^{N} b_i^3 \quad \ldots\ldots\ldots\ldots\ldots\ldots (A.7.7)$$

The equivalent porous medium flow is given by D'Arcy's law,

$$Q = KAI = -k\frac{g}{\nu}L^2I \quad \ldots\ldots\ldots\ldots\ldots\ldots (A.7.8)$$

where A is the area (WxW) of a side of the cube. If equations (A.7.7) and (A.7.8) are equated and solved for the permeability, k, then following is obtained,

$$k = \frac{2}{3}\frac{1}{L}\sum_{i=1}^{N} b_i^3 \quad \ldots\ldots\ldots\ldots\ldots\ldots (A.7.9)$$

and if the average fracture spacing, S, is known, the fracture intrinsic permeability becomes,

$$k = \frac{2}{3}\frac{1}{S}\frac{1}{N}\sum_{i=1}^{N} b^3 \quad \ldots\ldots\ldots\ldots\ldots\ldots \text{(A.7.10)}$$

since $\mathbf{L} = \mathbf{S} \bullet \mathbf{N}$.

Comparison between the two formulations (Snow, 1969 and Norton and Knapp, 1977) shows that the two methods give identical results, since Norton and Knapp's (1977) **d** is equal to the **2b** of Snow (1969). Nehlig and Juteau (1988) used the Norton and Knapp (1977) equation with a 'porosity', $\mathbf{P} = \mathbf{nd}$, equal to the number of fractures times the average aperture such that,

$$k = \frac{Pd^2}{12} = \frac{nd^3}{12} \quad \ldots\ldots\ldots\ldots\ldots\ldots \text{(A.7.11)}$$

It should be noted that these permeabilities are not strictly fracture permeabilities but are bulk fractured rock permeabilities which take into account the fracture 'porosity', that is the amount of fracturing per unit length of rock face. The bulk rock permeability is dependent on the length of occupied rock space between fractures assuming a negligible matrix permeability.

Formulation of Bianchi and Snow (1969) Method

Permeability in the Bianchi and Snow (1969) model, is calculated on the basis of the direction cosines of fracture orientations, the fracture aperture, and a weight based on the angle of the fracture to the sampling line (to account for the bias toward measuring fractures whose normals are parallel to the sampling line, and to take account of the relative density of fractures over the length of the sampling line). The weighting scheme assumes that each fracture is repeated at a distance **l** along the scanline, where **l** is the scanline length such that,

$$W = l|n_i D_i| \quad \ldots\ldots\ldots\ldots\ldots\ldots \text{(A.7.12)}$$

The permeability of a particular sampling line area is the sum of the individual fracture contributions, N (Snow, 1969),

$$k_{ij} = \frac{2}{3l}\sum_{i=1}^{N} \frac{b^3}{|n_i D_i|}(\delta_{ij} - m_{ij}) \quad \ldots\ldots\ldots\ldots\ldots\ldots \text{(A.7.13)}$$

where $\mathbf{k_{ij}}$ is the permeability tensor, **b** is the half-aperture, $\mathbf{n_i}$ and $\mathbf{D_i}$ are the direction cosines, respectively, of the normal to the fracture and of the scanline, δ_{ij} is the Kronecker delta (which is 1 for i=j and 0 for $i \neq j$), and $\mathbf{m_{ij}}$ is the matrix containing terms summing the direction cosines of each fracture. The equivalent permeability is then calculated as the sum of the values obtained from all the scanline surveys for a particular station, divided by the number of scanlines, M, at that station (Bianchi and Snow, 1969),

$$k_{ij} = \frac{1}{M}\sum_{l=1}^{M}\frac{2}{3l}\sum_{i=1}^{N}\frac{b^3}{|n_i D_l|}(\delta_{ij}-m_{ij}) \quad \ldots\ldots\ldots\ldots \text{(A.7.14)}$$

Diagonalization of the k_{ij} permeability tensor results in the three principal (orthogonal) permeability directions and magnitudes, k_1, k_2, and k_3 (the eigen vectors and eigen values of the k_{ij} matrix).

A.7 PERMEABILITY CALCULATION RESULTS
A.7.1 PARALLEL PLATE METHOD

FRACTURE PERMEABILITY MAGNITUDES - PARALLEL PLATE METHOD*

Scanline	Scanline Length (m)	Mean Dyke Azimuth (°)	Mean Dyke Dip (°)	# of fractures	Epidote #	Epidote Trace Length (m) Mean	Epidote Trace Length (m) Max.	Epidote Trace Length (m) Min.	Epidote Aperture (mm)	Epidote Spacing (m)	Epidote Permeability (m^2)	Zeolite #	Zeolite Trace Length (m) Mean	Zeolite Trace Length (m) Max.	Zeolite Trace Length (m) Min.	Zeolite Aperture (mm)	Zeolite Spacing (m)	Zeolite Permeability (m^2)
0000	37.4	138	82	76	1	2.3	2.3	2.3	12	0.03	3.650E-09	1	2.3	2.3	2.3	12	0.03	3.650E-09
0108	31.5	127	67	88	25	3.7	6	0.8	7.8	0.79	3.139E-08	7	3.9	5.5	1.6	10.1	0.22	1.908E-08
0112	25.1	138	47	90	4	2	3.4	0.8	4.6	0.16	1.293E-09	1	3.4	3.4	3.4	15	0.04	1.121E-08
0122	148.2	90	72	291	43	2.7	8	0.5	17.7	0.29	1.341E-07	63	2.8	8	0.8	13.1	0.43	7.964E-08
0201	8.5	56	63	31	8	2.4	3.5	0.3	5.6	0.94	1.377E-08	3	2	3.5	0.5	7.3	0.35	1.144E-08
0213	30.4	68	70	117	13	3.5	4.5	1	5.3	0.43	5.305E-09	2	3.3	4.5	2	1.5	0.07	1.850E-11
0301	6.2	68	70	141	3	2.2	2.8	1.6	7	0.46	1.383E-08							
0302	19.3	81	79	47	16	1.9	2.8	0.8	10.1	0.83	7.118E-08							
0303	7	262	88	13	1	30	30	30	60	0.14	2.571E-06							
0304	6.2	262	88	14														
0306	8.9	316	69	11														
0307	6.6	315	69	21	2	4.2	6	2.4	1	0.30	2.525E-11							
0329	10	315	69	20								1	4.5	4.5	4.5	2	0.10	6.667E-11
0401	31.3	88	75	88	24	4	6	0.9	7	0.77	2.192E-08	6	3.5	6	1.6	1.2	0.19	2.760E-11
0404	10.3	79	77	18	2	2.4	3	1.8	10	0.19	1.618E-08	2	3.1	4	2.2	1.5	0.19	5.461E-11
0413	30.6	87	71	59	17	4	7	1.1	3.5	0.56	1.985E-09	4	3.8	7	1.9	2.3	0.13	1.325E-10
0418	21.6	87	71	33	6	3	4.5	1.1	22	0.28	2.465E-07	1	1.1	1.1	1.1	10	0.05	3.858E-09
0428	67.6	96	49	195	15	6.6	15	0.6	1.6	0.22	7.574E-11	19	6.3	15	1.4	1	0.28	2.342E-11
0701	32.5	168	84	69														
1001	31.6	263	63	93								6	3	5	1.3	4.5	0.19	1.442E-03
1008	19.5	117	62	73														
1017	22.7	269	79	67	5	1.4	3.6	0.5	40.2	0.22	1.192E-06							
1028	31.2	281	68	114														
1037	30.9	146	68	96	3	1.8	3.2	0.9	1.7	0.10	3.975E-11							
1107	27.5	55	84	79	2	3.5	6	1	30	0.07	1.636E-07							
1111	32.5	17	89	121	8	1.3	3	0.5	2.3	0.18	1.872E-10							
1124	25.6	71	35	96	1	2.2	2.2	2.2	40	0.04	2.083E-07	2	2	3	1.1	1	0.08	6.510E-12
1129	31.8	138	71	105	15	3.3	10	0.6	3.4	0.47	1.545E-09	1	5	5	5	1	0.03	2.621E-12
1134	32	127	60	68	12	4.9	15	1.2	6.1	0.38	7.093E-09							
1137	31.7	257	70	76	4	5.4	8	2.8	2.3	0.13	1.279E-10							
1204	48.4	323	79	94	1	1.9	1.9	1.9	1	0.02	1.722E-12							
1211	29.1	308	77	139								2	5.3	5.6	5	1	0.07	5.727E-12
1216	31.9	223	80	104														
1221	42.7	145	81	106														
1222	31.1	258	88	94	8	1.5	3	0.8	1.1	0.26	2.853E-11							
1227	22.3	344	56	61														
1305	17.1	58	59	39	4	4.2	8	1.1	1.3	0.23	4.283E-11							
1307	22.6	60	49	51	4	2.3	3.5	0.9	34.3	0.18	5.952E-07	1	0.9	0.9	0.9	2	0.04	2.950E-11
1310	42.8	65	60	54	3	6.3	10	4	19	0.07	4.006E-08							
1316	31.4	321	71	108	14	3	8	0.6	4.6	0.45	3.617E-09							
1321	30.2	151	71	109	27	2.7	6	0.6	5.3	0.89	1.109E-08	1	3.1	3.1	3.1	10	0.03	2.759E-09
										Mean	5.027E-09						Mean	2.685E-10
										Max.	2.571E-06						Max.	7.964E-08
										Min.	1.722E-12						Min.	2.621E-12

* This method assumes parallel, continuous fractures (one orientation set)
All fractures within 20° of the mean dyke orientation were taken as subparallel to the dykes.
The permeability was calculated using: $k = n * d^3 / 12$
where n = # of fractures per metre
d = the fracture aperture in metres
permeability calculations for fractures of zero aperture were not performed.

FRACTURE PERMEABILITY MAGNITUDES - PARALLEL PLATE METHOD (CONTINUED)*

Baseline	Calcite							All Minerals							No Minerals						
	#	Trace Length (m)			Aperture (mm)	Spacing (m)	Permeability (m^2)	#	Trace Length (m)			Aperture (mm)	Spacing (m)	Permeability (m^2)	#	Trace Length (m)			Aperture (mm)	Spacing (m)	Permeability (m^2)
		Mean	Max.	Min.					Mean	Max.	Min.					Mean	Max.	Min.			
0000								2	1.7	2.3	1.1	6.5	0.05	1.224E-09							
0108								26	3.7	6	0.8	7.5	0.83	2.902E-08	5	2.2	3.6	1.1	1	0.15873	1.323E-11
0112								4	2	3.4	0.8	4.6	0.16	1.293E-09	1	2.1	2.1	2.1	1	0.039841	3.320E-12
0122								81	2.7	9	0.5	13	0.55	1.001E-07	5	2.5	3	1	1.2	0.033738	4.869E-12
0201								9	2.2	3.5	0.3	4.9	1.06	1.038E-08		3.5	3.5	3.5			
0213	16	2.5	4.5	0.8	17.3	0.63	2.271E-07	28	2.8	4.5	0	10.5	0.82	8.885E-08	40	3.3	4.5	0.7	19.9	1.315789	8.641E-07
0301								3	2.2	2.8	1.6	7	0.48	1.383E-08							
0302								19	1.9	2.8	0.8	8.6	0.58	5.218E-08	6	1.7	1.8	1.4	1.7	0.310881	1.273E-10
0303								1	30	30	30	60	0.14	2.571E-08	2	4	5	3	0.6	0.285714	5.143E-12
0304																					
0306								1	8	8	8	0	0.10			8	8	8			
0307								3	3.4	6	1.8	0.7	0.45	1.289E-11	1	1.6	1.6	1.6	0.1	0.151515	1.263E-14
0329								1	4.5	4.5	4.5	2	0.10	6.667E-11	3	5.1	10	0.7	1	0.3	2.500E-11
0401								31	3.8	6	0.4	5.8	0.99	1.695E-08	16	5.3	6	2.5	0.3	0.511182	1.150E-12
0404								4	2.8	4	1.8	5.8	0.38	6.314E-09	1	5	5	5	0.1	0.097087	8.091E-15
0413								17	4	7	1.1	3.5	0.56	1.885E-08	2	6.5	7	6	3.5	0.065359	2.335E-10
0418								7	3.3	5	1.1	19	0.32	1.852E-07							
0428								28	5.6	15	0.6	1.2	0.41	5.864E-11	9	8.3	15	1.8	0.2	0.133136	8.876E-14
0701															4	1.5	2.2	0.8	0.5	0.123077	1.282E-12
1001								7	2.8	5	1.3	4.1	0.22	1.272E-09	48	2.8	5.5	0.7	1.1	1.550633	1.720E-10
1006	1	0.6	0.6	0.6	1	0.05	4.274E-12	3	1.3	2.5	0.8	233.7	0.15	0.00016364	22	1.4	2.7	0.5	1.2	1.128205	1.625E-10
1017								5	1.4	3.8	0.5	40.2	0.22	1.192E-08	7	0.9	1.8	0.4	0.3	0.30837	6.938E-13
1028															43	3.4	7	0.4	1	1.378205	1.149E-10
1037								3	1.8	3.2	0.9	1.7	0.10	3.975E-11	14	2	3.5	0.6	4.1	0.453074	2.602E-09
1107	1	6	6	6	45	0.04	1.939E-07	3	3.3	6	1	20	0.11	7.273E-08	40	3.8	7	0.6	1.4	1.454645	3.328E-10
1111	1	1.1	1.1	1.1	1	0.03	2.664E-12	8	1.3	3	0.5	1.8	0.28	1.346E-10	7	2.3	3.5	0.6	1.3	0.215385	3.943E-11
1124								3	2.1	3	1.1	14	0.12	2.680E-08	8	3.8	8	1	2.2	0.234375	2.080E-10
1129	21	3.8	10	0.5	2.5	0.66	8.599E-10	30	3.5	10	0.5	2.8	0.84	1.726E-09	23	2.8	10	0.5	2.7	0.723327	1.186E-09
1134	8	5	15	1.2	6.4	0.25	5.461E-09	12	4.8	15	1.2	6.1	0.38	7.093E-09	2	8.4	15	1.5	1	0.0625	5.208E-12
1137	2	7.3	8	6.5	3	0.08	1.420E-10	4	5.4	8	2.8	2.3	0.13	1.279E-10	3	5.5	6	5.2	0.7	0.084637	2.705E-12
1204	8	2.7	5.5	0.4	14.1	0.17	3.861E-08	9	2.6	5.5	0.4	12.7	0.19	3.174E-08	21	2.8	6	0.6	2.4	0.433884	4.888E-10
1211	1	2	2	2	1	0.03	2.664E-12	3	4.2	5.6	2	1	0.10	8.691E-12	36	2.1	6	0.3	1	1.202749	1.002E-10
1216															29	2.5	5	0.5	4.3	0.809091	6.023E-09
1221								3	3.5	5.5	1	0.3	0.07	1.691E-13	11	1.8	4	0.8	0.3	0.257611	5.796E-13
1222								8	1.5	3	0.8	1.1	0.26	2.853E-11	4	3.4	5	1.1	23.3	0.128617	1.368E-07
1227	1	1.4	1.4	1.4	1	0.04	3.737E-12	3	1.8	2	1	1	0.13	1.121E-11	3	2.1	3	1.3	1	0.134529	1.121E-11
1306	4	5.3	6	4	1.3	0.23	4.283E-11	6	4.3	6	1.1	1.2	0.35	5.053E-11	20	4	6	1	4.9	1.188591	1.147E-08
1307	8	1.7	3.2	0.8	1.1	0.35	3.926E-11	12	1.9	3.5	0.8	12	0.53	7.648E-08	1	0.6	0.6	0.6	1	0.044248	3.687E-12
1310	2	1.2	1.4	1.1	2	0.05	3.115E-11	8	3.8	10	1.1	8	0.19	1.136E-08	8	3.8	10	1.5	1	0.21028	1.752E-11
1318	22	2.5	5.2	0.6	2.8	0.70	1.026E-08	34	2.6	8	0.6	4.8	1.08	1.062E-08	12	3.2	8	0.6	6.8	0.382166	1.001E-08
1321	4	3.1	6	0.8	2.3	0.13	1.343E-10		2.6	6	0				22	3.1	7	0.3	0.8	0.728477	4.425E-11
						Mean	2.606E-10						Mean	3.187E-08						Mean	4.070E-11
						Max.	2.271E-07						Max.	0.00016364						Max.	8.641E-07
						Min.	2.564E-12						Min.	1.691E-13						Min.	8.091E-15

* This method assumes parallel, continuous fractures (one orientation set)
All fractures within 20° of the mean dyke orientation were taken as subparallel to the dykes.
The permeability was calculated using: $k = n * d^3 / 12$
where n = # of fractures per metre
d = the fracture aperture in metres
permeability calculations for fractures of zero aperture were not performed.

A.7 PERMEABILITY CALCULATION RESULTS
A.7.2 BIANCHI AND SNOW (1969) METHOD

The following table presents the permeability calculation results from the SNOWPERM program (Appendix D). The column headings are as follows: area refers to the scanline mapping location number; kave is the permeability average determined from the three principal permeabilities, k1, k2, k3; Az1, Dip1, Az2, Dip2, Az3, Dip3 are the principal permeability directions associated with k1, k2, k3, respectively; '#Ap.=0.01' is the number of apertures whose field aperture was measured as 0, these apertures were set to 0.01 for the permeability calculations since the log of 0 is undefined; MinAp and MaxAp are the minimum and maximum apertures measured at that scanline location. Each page of the table is based on a grouping of fractures: All, Unfilled, All Filled, Epidote-filled, Zeolite-filled, Calcite-filled; and on all orientations or dyke parallel orientations ($\pm 20°$ of the mean dyke orientation for that scanline location). Following the table are the principal permeability orientation stereographic projections for the previously mentioned groups for each scanline location. The next set of tables lists the permeability magnitudes and anisotropy for each of the groupings. The last set of stereographic projections show the principal permeability orientations plotted for each of the groupings by dyke domain.

Fracture Permeability Magnitude and Orientation Using the Method of Bianchi and Snow (1969)

* Indicates non-unique permeability directions due to large range in aperture.

All Fractures Area	#	kave	k1	Az1	Dip1	k2	Az2	Dip2	k3	Az3	Dip3	#Ap. =0.01	MinAp	MaxAp
0000	76	3.02E-07	6.51E-07	155	71	6.29E-07	20	14	6.72E-08	286	13	8	0.01	25
0108	88	4.32E-07	1.05E-06	46	19	1.03E-06	162	62	7.46E-08	304	31	8	0.01	50
0112	88	2.14E-06	4.32E-06	161	24	3.73E-06	39	51	6.08E-08	266	29	13	0.01	200
0122	287	4.08E-06	7.26E-06	117	59	6.19E-06	305	31	1.51E-06	213	4	89	0.01	250
0201	31	9.06E-08	1.58E-07	74	71	1.19E-07	337	3	3.97E-08	246	19	5	0.01	20
0213	117	5.14E-06	2.06E-04	141	50	2.02E-04	359	33	3.29E-08	255	19	9	0.01	500
0301	14	4.16E-07	1.09E-06	143	50	1.03E-06	40	10	6.43E-08	302	38	3	0.01	30
0302	47	9.05E-07	1.92E-06	116	71	1.71E-06	349	11	2.25E-07	256	15	10	0.01	50
0303	12	7.78E-06	2.74E-05	180	24	2.68E-05	25	64	6.42E-07	274	10	0	0.1	100
0304	14	4.44E-03	2.54E-02	152	79	2.52E-02	356	11	1.37E-04	265	4	2	0.01	600
0306	11	3.66E-08	6.06E-08	312	62	4.33E-08	109	8	1.67E-08	200	3	2	0.01	10
0307	21	1.95E-08	5.14E-08	55	77	4.88E-08	187	9	2.98E-09	279	9	11	0.01	15
0329	20	4.92E-09	8.11E-09	155	54	6.98E-09	36	20	1.74E-09	294	28	3	0.01	8
0401	68	7.14E-07	1.55E-06	105	70	1.43E-06	4	4	1.65E-07	272	19	5	0.01	50
0404	18	1.96E-06	1.17E-05	189	35	1.16E-05	33	53	5.55E-08	287	12	4	0.01	100
0413	59	1.36E-07	4.62E-07	29	45	4.51E-07	133	13	1.21E-08	235	42	5	0.01	30
0418	33	1.23E-06	2.81E-06	359	28	2.57E-06	132	53	2.58E-07	256	23	1	0.01	60
0428	195	5.06E-06	8.09E-06	186	45	6.32E-06	336	41	2.52E-08	80	15	51	0.01	30
0701	67	4.70E-07	7.97E-07	352	57	5.68E-07	157	32	2.30E-07	252	7	22	0.01	50
1001	86	8.05E-08	4.60E-07	248	59	4.58E-07	349	7	2.47E-09	83	30	23	0.01	20
1008	72	1.31E-05	8.41E-04	48	44	8.41E-04	193	40	3.19E-09	299	18	17	0.01	700
1017	66	7.48E-06	2.81E-05	178	84	2.77E-05	346	6	5.38E-07	76	1	27	0.01	200
1028	109	1.89E-09	4.39E-09	198	34	4.26E-09	309	29	4.21E-10	70	43	12	0.01	10
1037	96	9.54E-08	3.15E-07	44	69	3.11E-07	210	21	8.86E-09	302	5	27	0.01	50
1107	79	6.39E-08	2.61E-07	126	66	2.58E-07	319	24	3.86E-09	227	5	46	0.01	40
1111	120	2.63E-07	4.02E-06	321	69	4.02E-06	156	20	1.13E-09	64	5	37	0.01	140
1124	91	5.11E-07	1.16E-06	43	27	1.07E-06	140	14	1.08E-07	255	58	27	0.01	50
1128	103	9.26E-08	2.21E-07	111	64	2.13E-07	209	1	1.68E-08	299	6	19	0.01	50
1134	64	1.50E-05	1.05E-04	211	9	1.05E-04	120	4	3.03E-07	9	80	17	0.01	100
1137	71	9.73E-08	4.31E-07	339	13	4.27E-07	87	52	5.01E-09	240	35	33	0.01	50
1204	90	7.58E-07	2.09E-06	285	41	2.00E-06	37	37	1.04E-07	149	27	14	0.01	100
1211	135	3.37E-07	7.83E-06	358	61	7.83E-06	142	24	6.26E-10	239	15	30	0.01	5
1216	101	6.35E-06	1.60E-05	268	68	1.60E-05	130	17	1.00E-10	36	14	25	0.01	100
1221	105	3.95E-08	4.43E-07	319	6	4.43E-07	196	78	3.13E-10	50	10	25	0.01	60
1222	93	4.62E-07	1.39E-06	170	38	1.33E-06	325	49	5.34E-08	70	12	27	0.01	90
1227	58	1.23E-09	2.22E-09	136	1	2.07E-09	239	85	4.00E-10	45	5	21	0.01	8
1305	37	6.53E-08	4.86E-07	352	33	4.85E-07	115	40	1.18E-09	238	32	6	0.01	50
1307	48	3.53E-07	2.85E-06	146	15	2.85E-06	40	43	5.39E-09	250	43	20	0.01	100
1310	54	1.15E-05	1.26E-04	45	45	1.26E-04	312	3	9.33E-08	219	45	5	0.01	400
1316	105	3.06E-06	5.38E-06	338	76	4.16E-06	203	10	1.28E-06	111	10	3	0.01	60
1321	108	8.20E-08	1.67E-07	50	4	1.43E-07	197	86	3.25E-08	320	2	11	0.01	30

Fracture Permeability Magnitude and Orientation Using the Method of Bianchi and Snow (1969)

* Indicates non-unique permeability directions due to large range in aperture.

Unfilled Fractures Area	#	kave	k1	Az1	Dip1	k2	Az2	Dip2	k3	Az3	Dip3	#Ap. = 0.01	MinAp	MaxAp
0000	2	2.27E-18	6.3E-18	52	70	5.9E-18	260	18	3.1E-19	167	9	2	0.01	0.01
0108	22	3.00E-10	5.1E-10	148	48	4.1E-10	42	13	1.3E-10	301	38	3	0.01	5
0112	22	9.54E-07	0.000037	77	60	0.000037	173	5	6.4E-10	266	30	9	0.01	200
0122	52	7.92E-08	7.4E-08	166	45	7.4E-08	330	44	9.0E-11	68	8	24	0.01	40
0201	5	4.26E-12	8.9E-11	218	86	8.9E-11	334	2	9.6E-15	64	4	3	0.01	2
0213	68	1.62E-05	0.000192	46	68	0.000192	183	10	1.2E-07	267	20	6	0.01	500
0301														
0302	9	2.01E-10	7.8E-10	333	2	7.7E-10	67	67	1.3E-11	242	23	1	0.01	5
0303	8	3.37E-11	7.0E-11	174	47	6.2E-11	12	42	8.8E-12	274	9	0	0.1	1
0304	7	1.21E-09	3.1E-09	262	0	3.0E-09	352	18	1.9E-10	171	72	1	0.01	4
0306	9	3.66E-08	6.1E-08	312	82	4.3E-08	109	6	1.9E-08	200	3	1	0.01	10
0307	9	4.44E-12	8.8E-11	82	8	8.8E-11	201	73	1.1E-14	350	15	6	0.01	2
0329	12	1.91E-10	3.5E-10	276	78	3.3E-10	61	10	6.0E-11	152	7	1	0.01	2
0401	19	2.95E-12	9.1E-12	23	63	8.8E-12	167	23	3.2E-13	263	15	3	0.01	1
0404	3	1.10E-09	1.2E-08	203	29	1.2E-08	312	31	1.0E-11	79	45	0	0.1	10
0413	11	6.51E-11	5.6E-10	123	52	5.6E-10	350	28	8.9E-13	247	23	1	0.01	6
0418														
0428	43	4.15E-09	3.3E-08	194	48	3.3E-08	20	42	6.6E-11	287	3	20	0.01	30
0701	36	2.18E-10	3.3E-10	164	3	2.8E-10	72	40	1.1E-10	258	49	17	0.01	2
1001	77	3.84E-09	6.3E-09	251	61	4.2E-09	8	13	2.1E-09	102	25	23	0.01	5
1006	68	3.91E-09	7.2E-09	29	39	6.3E-09	147	30	1.3E-09	263	37	15	0.01	10
1017	51	1.28E-10	1.9E-10	267	1	1.7E-10	357	9	6.5E-11	169	81	23	0.01	2
1028	107	1.95E-09	4.4E-09	198	33	4.2E-09	309	29	4.0E-10	70	43	12	0.01	10
1037	57	4.21E-08	1.3E-07	44	35	1.3E-07	212	55	4.4E-09	310	6	15	0.01	40
1107	72	9.03E-09	2.4E-08	130	67	2.3E-08	336	21	1.4E-09	242	9	42	0.01	20
1111	91	1.66E-07	4.0E-06	160	50	4.0E-06	330	40	2.8E-10	64	5	27	0.01	140
1124	54	1.42E-07	4.5E-07	82	44	4.4E-07	182	10	1.5E-08	281	44	19	0.01	50
1129	50	6.19E-08	2.0E-07	35	57	1.9E-07	206	33	6.4E-09	299	4	17	0.01	50
1134	11	2.03E-09	1.9E-08	20	5	1.9E-08	113	34	2.2E-11	283	56	2	0.01	20
1137	38	6.22E-11	9.8E-11	275	50	6.6E-11	174	9	3.7E-11	76	38	16	0.01	2
1204	61	7.57E-08	1.5E-07	217	72	1.4E-07	98	9	2.1E-08	5	15	8	0.01	40
1211	127	3.29E-07	7.8E-06	358	61	7.8E-06	142	24	5.8E-10	239	15	29	0.01	5
1216	100	6.30E-06	1.6E-05	268	68	1.6E-05	130	17	9.8E-11	36	14	25	0.01	100
1221	87	3.80E-06	4.4E-07	319	7	4.4E-07	194	78	2.8E-10	50	10	22	0.01	60
1222	62	4.60E-07	1.4E-06	170	38	1.3E-06	325	49	5.3E-08	70	12	14	0.01	90
1227	44	1.20E-09	2.2E-09	135	4	2.1E-09	263	83	3.8E-10	45	5	13	0.01	8
1306	27	5.97E-08	4.9E-07	353	34	4.8E-07	117	39	9.1E-10	238	32	5	0.01	50
1307	18	9.52E-11	1.5E-10	68	24	9.5E-11	221	64	6.2E-11	333	10	10	0.01	2
1310	31	2.39E-10	3.7E-10	292	59	2.6E-10	140	28	1.4E-10	43	12	4	0.01	5
1316	32	8.95E-07	8.4E-06	41	40	8.4E-06	247	47	1.0E-08	142	13	6	0.01	50
1321	60	9.15E-11	1.3E-10	64	7	8.7E-11	328	39	6.9E-11	182	50	8	0.01	1

Fracture Permeability Magnitude and Orientation Using the Method of Bianchi and Snow (1969)

* Indicates non-unique permeability directions due to large range in aperture.

Filled Fractures Area	#		kave	k1	Az1	Dip1	k2	Az2	Dip2	k3	Az3	Dip3	#Ap. =0.01	MinAp	MaxAp
0000		74	3.02E-07	6.5E-07	155	71	6.3E-07	20	14	6.7E-08	286	13	6	0.01	25
0108		66	4.31E-07	1.0E-06	46	19	1.0E-06	162	52	7.4E-08	304	31	5	0.01	50
0112		66	2.33E-06	6.4E-06	176	32	6.1E-06	283	26	3.3E-07	44	46	4	0.01	100
0122		236	4.07E-05	0.000073	117	59	0.000042	306	31	0.000015	213	4	65	0.01	250
0201		26	9.06E-06	1.6E-07	74	71	1.2E-07	337	3	4.0E-08	246	19	2	0.01	20
0213		49	1.93E-06	0.000013	323	5	0.000013	127	85	4.1E-06	233	1	3	0.01	200
0301		13	4.16E-07	1.1E-06	143	60	1.0E-06	40	10	6.4E-08	302	38	3	0.01	30
0302		38	9.04E-07	1.9E-06	116	71	1.7E-06	349	11	2.3E-07	256	15	9	0.01	50
0303		4	7.78E-06	0.000027	180	24	0.000027	25	64	6.4E-07	274	10	0	2	100
0304		7	4.44E-03	0.025366	152	79	0.025224	356	11	0.000137	265	4	1	0.01	600
0306		2	8.55E-14	1.0E-11	40	68	1.0E-11	281	10	6.7E-16	187	19	1	0.01	1
0307		12	1.94E-06	5.1E-06	53	77	4.9E-06	187	9	2.9E-09	279	9	5	0.01	15
0329		8	4.30E-09	7.9E-09	159	51	6.7E-09	37	23	1.5E-09	293	29	2	0.01	8
0401		49	7.14E-07	1.5E-06	105	70	1.4E-06	4	4	1.7E-07	272	19	2	0.01	50
0404		15	1.85E-06	0.000012	187	39	0.000012	30	49	4.6E-06	287	12	4	0.01	100
0413		48	1.36E-07	4.6E-07	30	45	4.5E-07	133	13	1.2E-06	235	42	4	0.01	30
0418		32	1.23E-06	2.8E-06	359	28	2.6E-06	132	53	2.6E-07	256	23	1	0.01	60
0428		152	2.69E-06	5.0E-06	158	19	4.5E-06	277	64	8.7E-09	67	29	31	0.01	30
0701		31	4.70E-07	8.9E-07	352	57	5.7E-07	157	32	2.3E-07	252	7	5	0.01	50
1001		7	3.91E-09	4.1E-06	336	29	4.1E-06	210	46	3.5E-11	83	30	0	1	20
1008	*		2.36E-06	0.000841	193	41	0.000841	92	70	1.9E-11	299	18	2	0.01	700
1017		15	7.48E-06	0.000028	179	84	0.000028	346	6	5.4E-07	76	1	4	0.01	200
1028		2	5.06E-12	4.2E-11	310	32	4.2E-11	150	56	7.6E-14	46	10	0	1	3
1037		39	1.40E-06	1.9E-07	46	79	1.9E-07	206	11	8.0E-11	296	4	12	0.01	50
1107		7	3.64E-06	2.4E-07	131	48	2.4E-07	320	42	8.6E-10	226	5	4	0.01	40
1111		29	4.57E-09	1.3E-06	336	76	1.3E-06	148	14	5.7E-10	239	2	10	0.01	20
1124		37	1.28E-07	7.1E-07	136	3	7.1E-07	44	26	4.1E-09	232	64	8	0.01	40
1129		53	1.72E-06	2.9E-06	154	67	2.2E-06	47	7	8.0E-09	314	22	2	0.01	20
1134		53	1.49E-05	0.000105	212	9	0.000105	121	4	3.0E-07	9	80	15	0.01	100
1137		33	9.68E-06	4.3E-07	339	13	4.3E-07	87	62	4.9E-09	240	35	17	0.01	50
1204		29	6.94E-06	1.9E-06	354	59	1.9E-06	244	12	8.9E-11	148	28	6	0.01	100
1211		8	4.62E-11	6.9E-11	25	65	4.2E-11	257	24	3.4E-11	155	24	1	0.01	2
1216															
1221		18	5.22E-11	9.3E-11	152	75	7.8E-11	289	11	2.0E-11	21	10	3	0.01	3
1222		31	7.86E-10	2.1E-09	330	65	2.0E-09	198	17	1.2E-10	102	17	13	0.01	10
1227		14	6.33E-12	1.8E-11	9	45	1.7E-11	253	24	8.5E-13	144	36	6	0.01	1
1306		10	1.66E-10	3.4E-10	123	38	3.0E-10	227	18	4.5E-11	337	47	1	0.01	2
1307		30	3.51E-07	2.9E-06	146	15	2.9E-06	41	43	5.3E-09	250	43	10	0.01	100
1310		23	1.16E-05	0.000128	46	45	0.000128	312	3	9.3E-08	219	45	2	0.01	400
1316		72	2.35E-06	4.2E-06	338	76	3.4E-06	192	12	8.9E-07	100	8	0	1	60
1321		58	9.19E-08	1.7E-07	50	4	1.4E-07	197	86	3.2E-08	320	2	3	0.01	30

Fracture Permeability Magnitude and Orientation Using the Method of Bianchi and Snow (1969)

* indicates non-unique permeability directions due to large range in aperture.

Epidote filled Fractures

Area	#	kave	k1	Az1	Dip1	k2	Az2	Dip2	k3	Az3	Dip3	#Ap.=0.01	MinAp	MaxAp
0000	18	1.73E-07	6.1E-07	35	56	6.0E-07	186	31	1.4E-08	286	13	2	0.01	15
0108	57	4.18E-07	1.0E-06	45	18	1.0E-06	161	53	6.9E-08	303	31	3	0.01	50
0112	39	2.23E-06	6.3E-06	176	33	6.1E-06	284	26	2.9E-07	44	46	2	0.01	100
0122	126	1.06E-06	0.000016	162	22	0.000017	39	53	3.6E-06	264	28	39	0.01	200
0201	15	4.56E-08	1.2E-07	53	70	1.2E-07	156	5	6.5E-09	247	18	1	0.01	20
0213	22	1.39E-07	4.0E-07	124	42	3.8E-07	329	45	1.8E-08	226	13	0	1	50
0301	11	4.16E-07	1.1E-06	143	50	1.0E-06	40	10	6.4E-08	302	38	2	0.01	30
0302	26	9.04E-07	1.9E-06	116	71	1.7E-06	348	11	2.3E-07	256	15	4	0.01	50
0303	3	7.78E-06	0.000027	180	24	0.000027	25	64	6.4E-07	274	10	0	20	100
0304	6	4.12E-03	0.024837	144	82	0.024724	355	7	0.000113	265	4	1	0.01	600
0306														
0307	6	1.38E-08	4.2E-08	27	68	4.1E-08	181	20	1.5E-09	274	9	2	0.01	15
0328	5	4.14E-09	7.9E-09	157	52	6.5E-09	36	22	1.4E-09	293	30	0	1	8
0401	38	7.03E-07	1.5E-06	105	70	1.4E-06	3	4	1.6E-07	272	19	2	0.01	50
0404	7	1.83E-06	0.000012	187	40	0.000012	30	48	4.5E-08	287	12	2	0.01	100
0413	46	1.36E-07	4.6E-07	30	45	4.5E-07	133	13	1.2E-08	235	42	3	0.01	30
0418	30	1.21E-06	2.8E-06	359	28	2.5E-06	133	53	2.5E-07	256	23	1	0.01	60
0428	51	5.51E-09	8.6E-09	159	12	6.5E-09	252	13	3.0E-09	28	72	9	0.01	10
0701	6	1.83E-08	3.6E-07	200	18	3.6E-07	339	67	4.6E-11	106	14	2	0.01	50
1001														
1008														
1017	7	4.31E-06	0.000028	165	10	0.000027	338	80	1.1E-07	75	1	4	0.01	200
1028														
1037	35	2.46E-10	5.2E-10	257	85	4.8E-10	34	4	5.8E-11	124	4	12	0.01	4
1107	2	3.62E-08	2.4E-07	131	47	2.4E-07	320	42	6.5E-10	226	5	0	20	40
1111	14	3.99E-09	1.3E-08	336	78	1.2E-08	149	12	4.0E-10	239	2	4	0.01	20
1124	3	1.71E-08	7.1E-07	12	21	7.1E-07	108	15	9.9E-12	232	64	1	0.01	40
1129	16	3.79E-09	1.9E-08	225	4	1.9E-08	126	67	1.5E-10	317	22	2	0.01	20
1134	44	1.48E-06	0.000105	211	9	0.000105	121	4	2.9E-07	9	80	13	0.01	100
1137	32	9.68E-08	4.3E-07	339	13	4.3E-07	87	52	4.9E-09	240	35	16	0.01	50
1204	4	3.73E-12	1.2E-11	48	68	1.1E-11	201	19	4.0E-13	294	10	0	1	1
1211														
1218														
1221	9	3.26E-11	6.3E-11	172	77	5.7E-11	291	7	9.6E-12	22	12	3	0.01	3
1222	29	7.86E-10	2.1E-09	330	65	2.0E-09	198	17	1.2E-10	102	17	11	0.01	10
1227														
1305	8	1.57E-10	3.3E-10	123	38	3.0E-10	228	18	3.9E-11	338	47	1	0.01	2
1307	11	3.15E-07	2.9E-06	154	7	2.8E-06	56	46	3.9E-09	250	43	0	1	100
1310	13	1.13E-05	0.000128	43	45	0.000128	311	2	8.9E-08	219	45	1	0.01	400
1318	21	5.78E-07	1.7E-06	3	72	1.6E-06	181	17	7.2E-08	271	1	0	1	40
1321	58	9.19E-08	1.7E-07	50	4	1.4E-07	197	86	3.2E-08	320	2	1	0.01	30

Fracture Permeability Magnitude and Orientation Using the Method of Bianchi and Snow (1969)

* indicates non-unique permeability directions due to large range in aperture.

Zeolite filled Fractures

Area	#	kave	k1	Az1	Dip1	k2	Az2	Dip2	k3	Az3	Dip3	#Ap.=0.01	MinAp	MaxAp
0000	68	8.11E-08	1.5E-07	23	40	1.4E-07	165	43	2.5E-08	275	20	5	0.01	15
0108	20	2.86E-07	9.3E-07	102	53	9.0E-07	206	10	2.8E-08	303	35	1	0.01	50
0112	31	4.76E-08	6.2E-08	64	58	5.5E-08	175	13	3.2E-08	272	29	1	0.01	15
0122	171	3.79E-06	0.000071	117	60	0.00006	304	30	0.000013	212	3	56	0.01	250
0201	15	7.54E-08	1.3E-07	78	70	9.9E-08	332	6	3.3E-08	240	19	1	0.01	20
0213	4	8.11E-08	2.4E-07	123	45	2.4E-07	315	44	9.3E-12	219	6	0	1	50
0301														
0302														
0303														
0304	3	4.12E-03	0.024837	144	82	0.024724	355	7	0.000113	265	4	0	2	600
0306														
0307														
0329	2	6.63E-10	1.5E-09	287	47	1.4E-09	147	36	1.4E-10	41	21	0	2	5
0401	12	1.24E-08	3.5E-07	36	61	3.5E-07	152	14	1.5E-11	248	25	0	0.1	40
0404	7	5.20E-09	1.7E-08	312	26	1.6E-08	213	17	5.1E-10	93	58	1	0.01	10
0413	12	3.71E-08	1.9E-07	24	43	1.9E-07	133	20	1.4E-09	241	41	0	0.1	30
0418	4	1.83E-08	4.6E-08	358	30	4.4E-08	119	42	3.1E-09	246	33	1	0.01	15
0428	134	1.99E-08	4.3E-08	164	31	4.1E-08	295	47	4.5E-09	57	26	29	0.01	30
0701														
1001	6	1.86E-09	4.1E-08	225	54	4.1E-08	342	18	3.7E-12	83	30	0	1	20
1008														
1017														
1028														
1037														
1107														
1111	4	6.70E-14	1.1E-11	337	56	1.1E-11	121	27	2.4E-18	220	17	3	0.01	2
1124	26	1.90E-09	5.4E-09	135	14	5.2E-09	327	76	2.5E-10	226	3	4	0.01	10
1128														
1134														
1137														
1204														
1211	5	1.74E-11	3.7E-11	205	20	3.3E-11	26	70	4.3E-12	295	1	0	1	2
1216														
1221														
1222														
1227														
1305														
1307														
1310														
1318														
1321	3	4.23E-10	1.8E-09	231	2	1.8E-09	126	81	2.4E-11	321	9	0	3	10

Fracture Permeability Magnitude and Orientation Using the Method of Bianchi and Snow (1969)

* Indicates non-unique permeability directions due to large range in aperture.

Calcite filled Fractures

Area	#		K1	Az1	Dip1	K2	Az2	Dip2	K3	Az3	Dip3	#Ap. = 0.01	MinAp	MaxAp
0000														
0108														
0112														
0122														
0201														
0213	30	1.63E-06	0.000013	143	10	0.000013	330	80	2.6E-06	233	1	2	0.01	200
0301	3	4.03E-15	1.4E-14	278	70	1.4E-14	107	20	3.4E-16	16	3	2	0.01	0.1
0302														
0303														
0304														
0306														
0307														
0329														
0401														
0404														
0413														
0418														
0428														
0701	29	6.25E-08	3.6E-07	7	30	3.6E-07	217	57	1.9E-09	106	14	5	0.01	50
1001														
1008	2	2.30E-12	5.2E-12	182	35	4.8E-12	46	47	4.9E-13	289	23	0	1	1
1017														
1028														
1037														
1107	2	7.80E-09	2.2E-07	325	68	2.2E-07	133	21	1.0E-11	225	4	0	2	40
1111	4	3.36E-11	1.9E-10	319	73	1.9E-10	141	17	1.1E-12	51	1	0	1	5
1124	5	2.93E-12	6.5E-12	344	34	5.8E-12	200	50	6.7E-13	87	16	2	0.01	1
1129	44	7.77E-09	1.2E-08	157	72	6.1E-09	330	18	4.6E-09	61	2	1	0.01	15
1134	30	6.92E-06	0.000106	176	10	0.000106	266	2	6.4E-06	9	80	11	0.01	100
1137	8	9.30E-08	4.3E-07	339	12	4.3E-07	86	52	4.4E-09	240	36	1	0.01	50
1204	24	6.68E-08	1.9E-06	341	61	1.9E-06	241	6	7.9E-11	148	28	6	0.01	100
1211	3	1.06E-11	3.5E-11	6	57	3.4E-11	104	4	9.7E-13	196	33	1	0.01	1
1216														
1221														
1222														
1227	10	2.43E-12	9.0E-12	310	56	8.9E-12	46	4	1.8E-13	139	33	7	0.01	1
1305	4	1.01E-11	3.3E-11	357	42	3.3E-11	130	36	9.3E-13	241	26	0	1	2
1307	24	3.73E-09	1.0E-08	39	16	1.0E-08	140	36	5.0E-10	288	51	9	0.01	10
1310	4	3.95E-10	1.5E-09	99	64	1.5E-09	308	23	2.8E-11	213	11	0	1	10
1316	53	9.71E-07	3.1E-06	186	68	3.1E-06	346	21	9.4E-08	79	6	0	1	60
1321	8	7.64E-11	1.6E-10	230	8	1.4E-10	123	66	2.0E-11	324	24	1	0.01	3

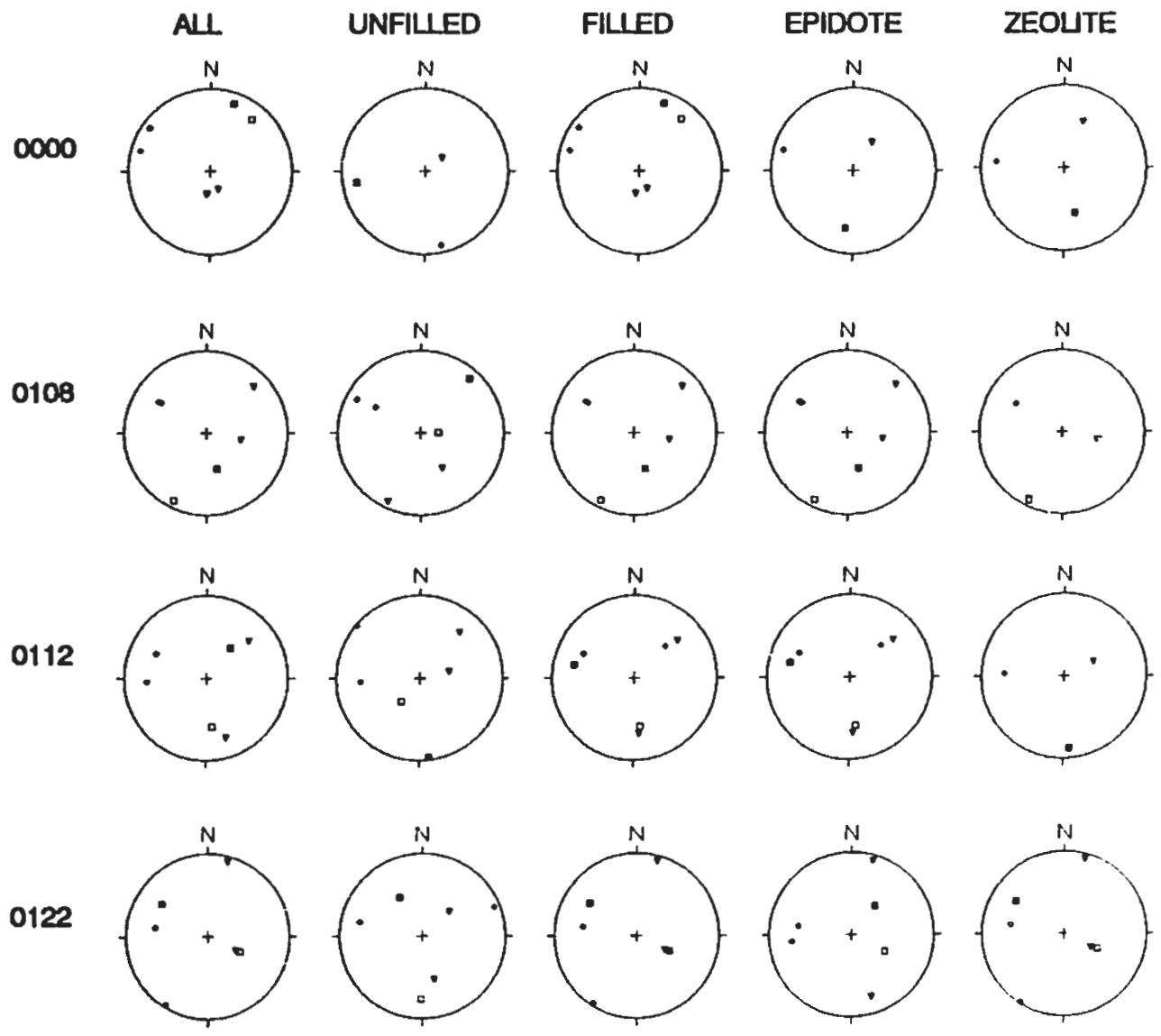

PRINCIPAL PERMEABILITY ORIENTATIONS

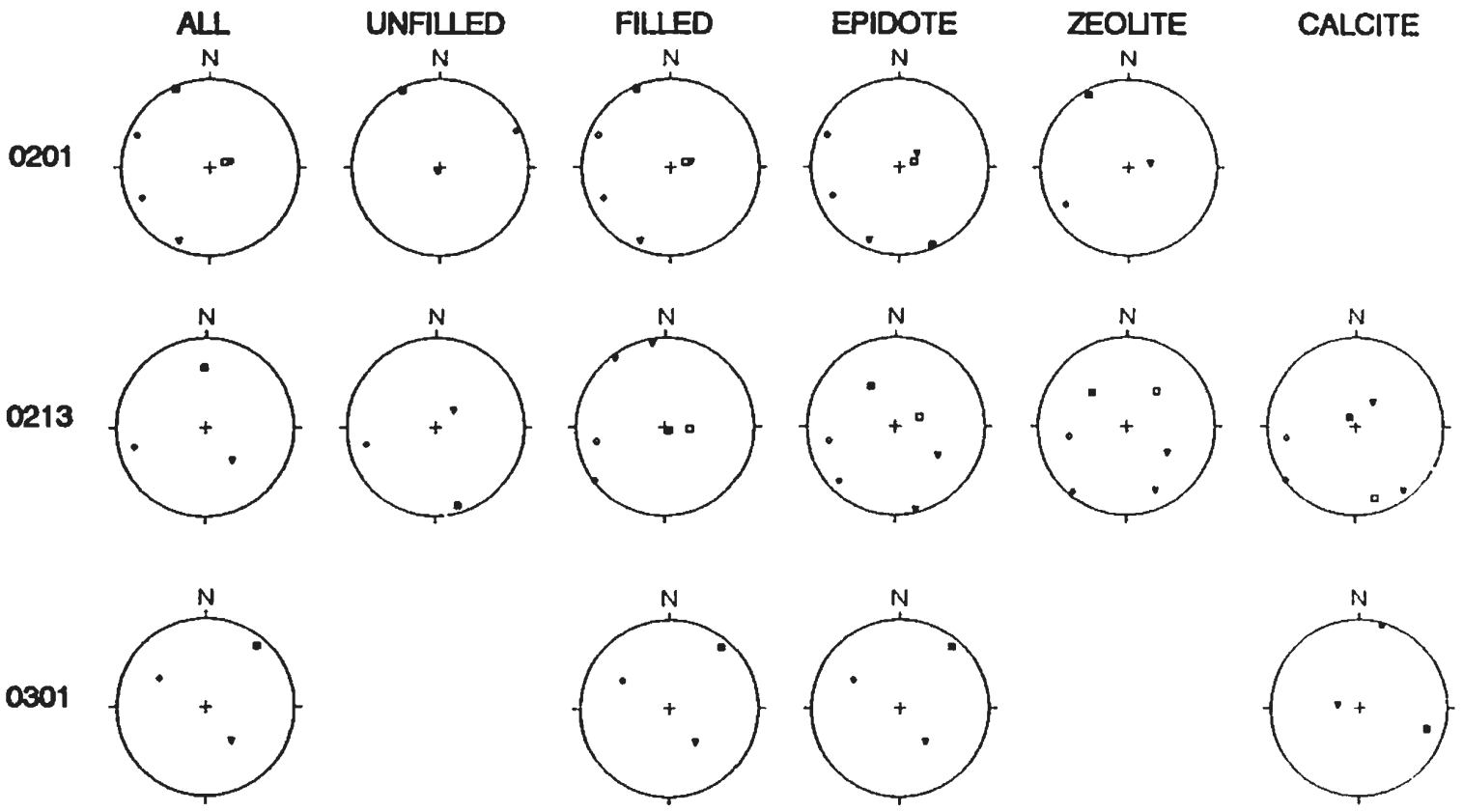

PRINCIPAL PERMEABILITY ORIENTATIONS

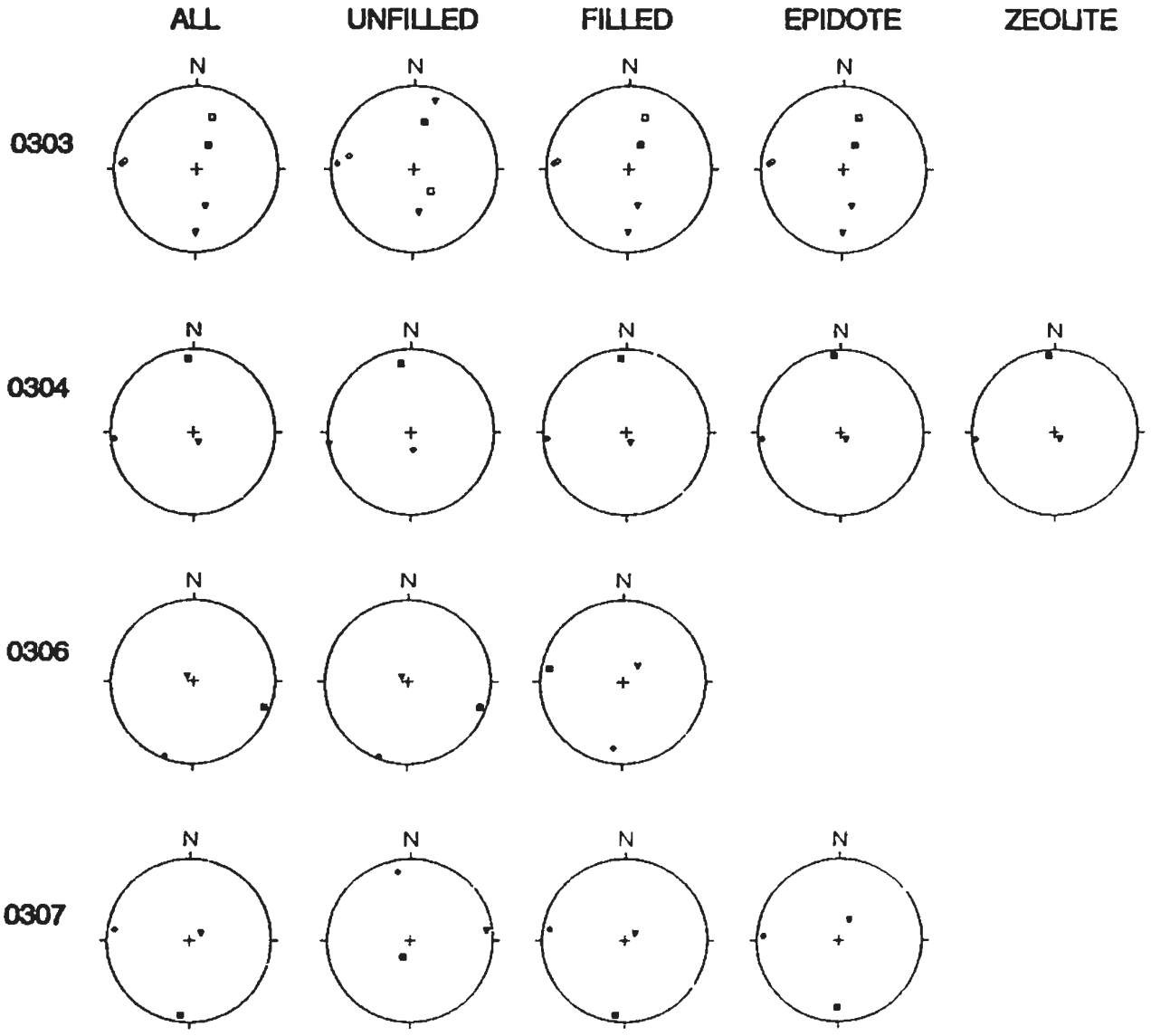

PRINCIPAL PERMEABILITY ORIENTATIONS

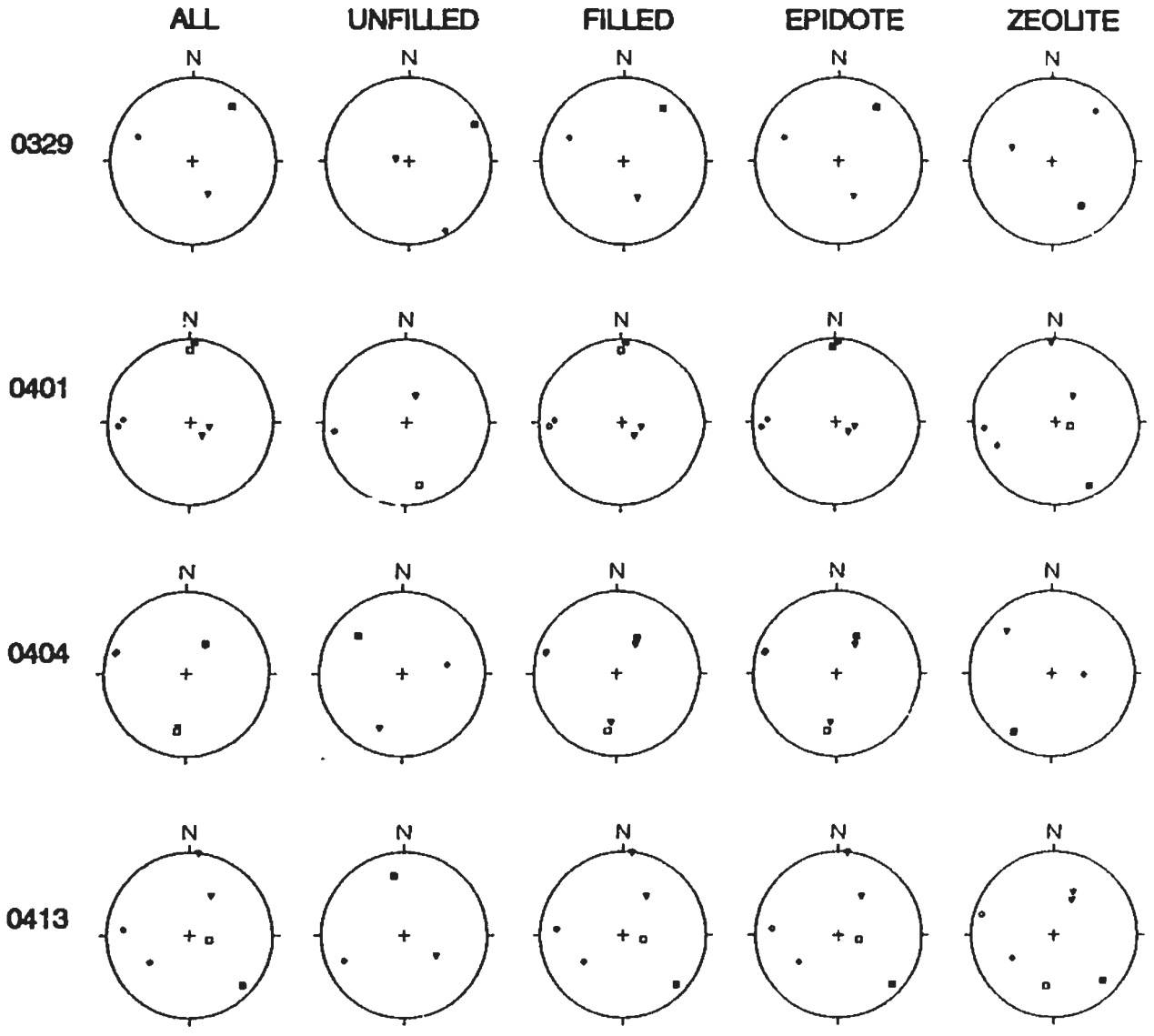

PRINCIPAL PERMEABILITY ORIENTATIONS

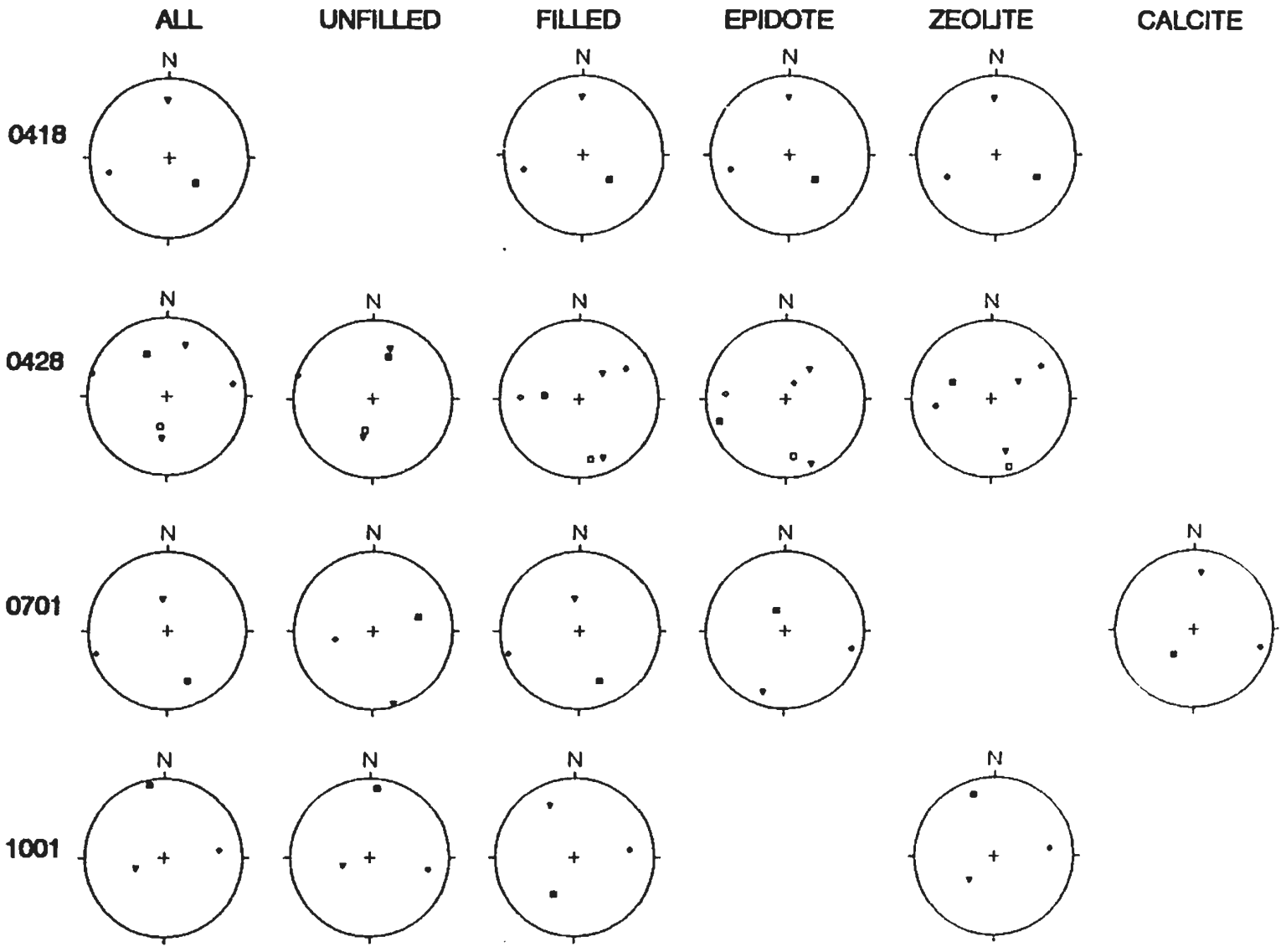

PRINCIPAL PERMEABILITY ORIENTATIONS

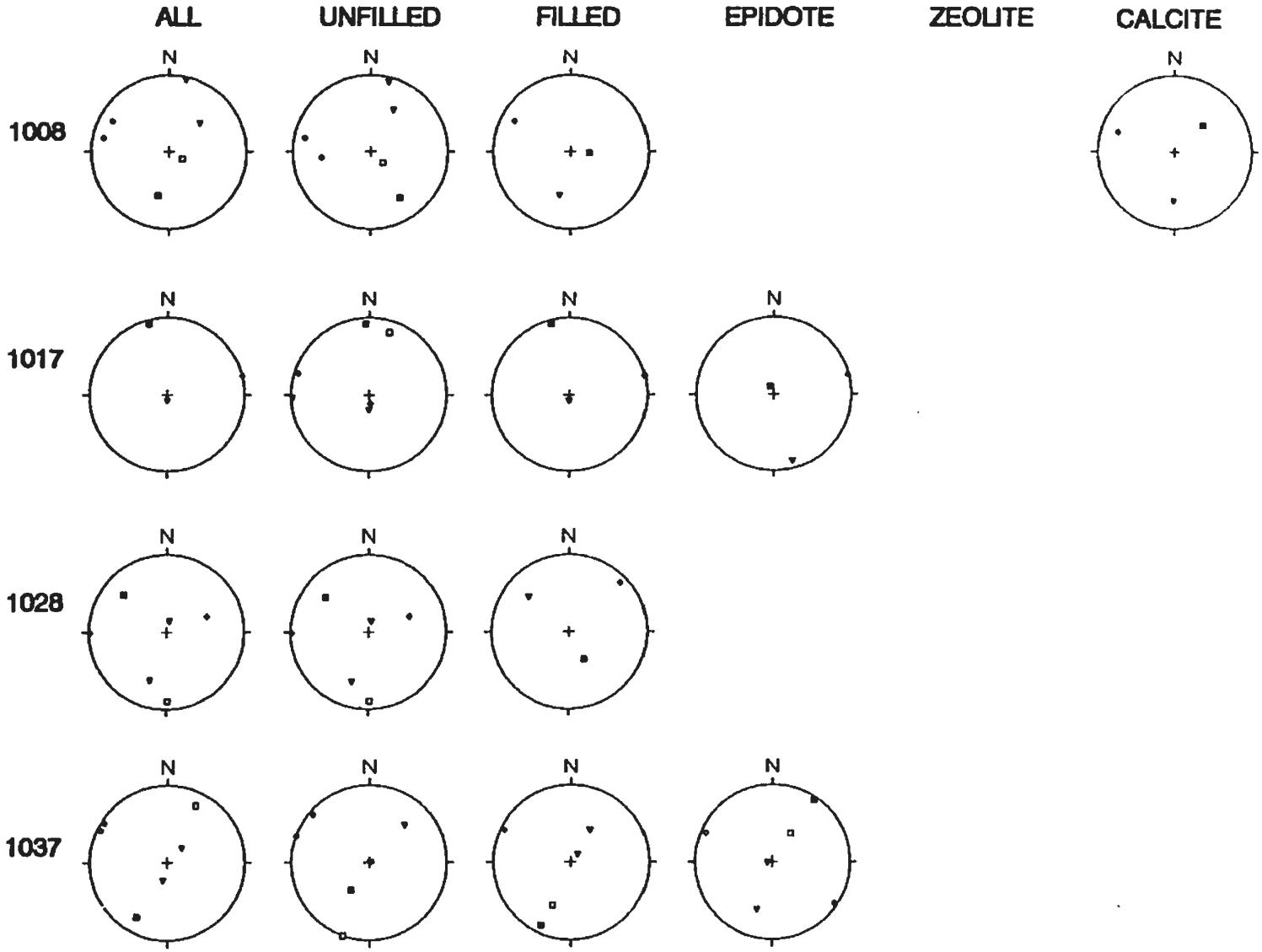

PRINCIPAL PERMEABILITY ORIENTATIONS

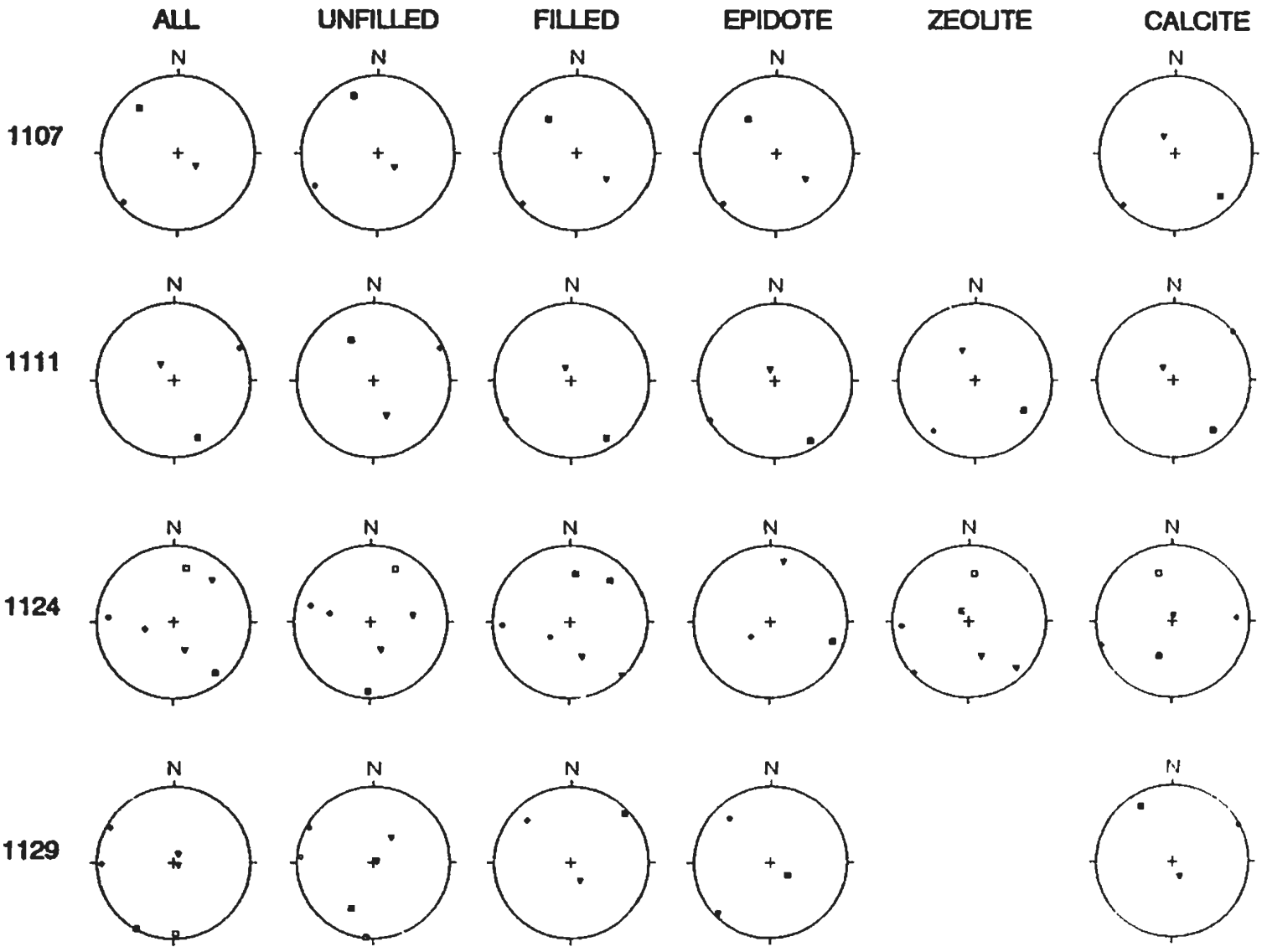

PRINCIPAL PERMEABILITY ORIENTATIONS

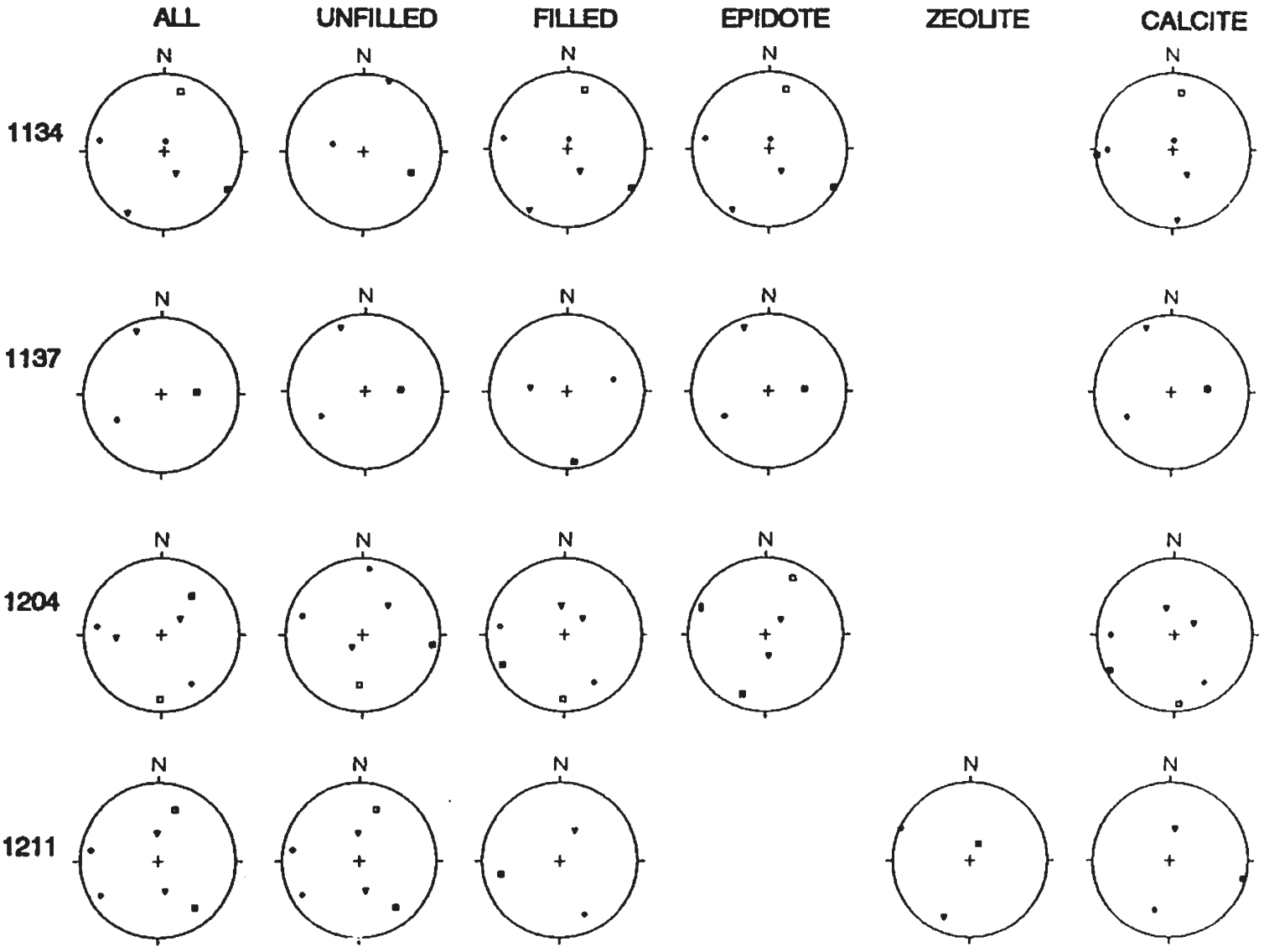

PRINCIPAL PERMEABILITY ORIENTATIONS

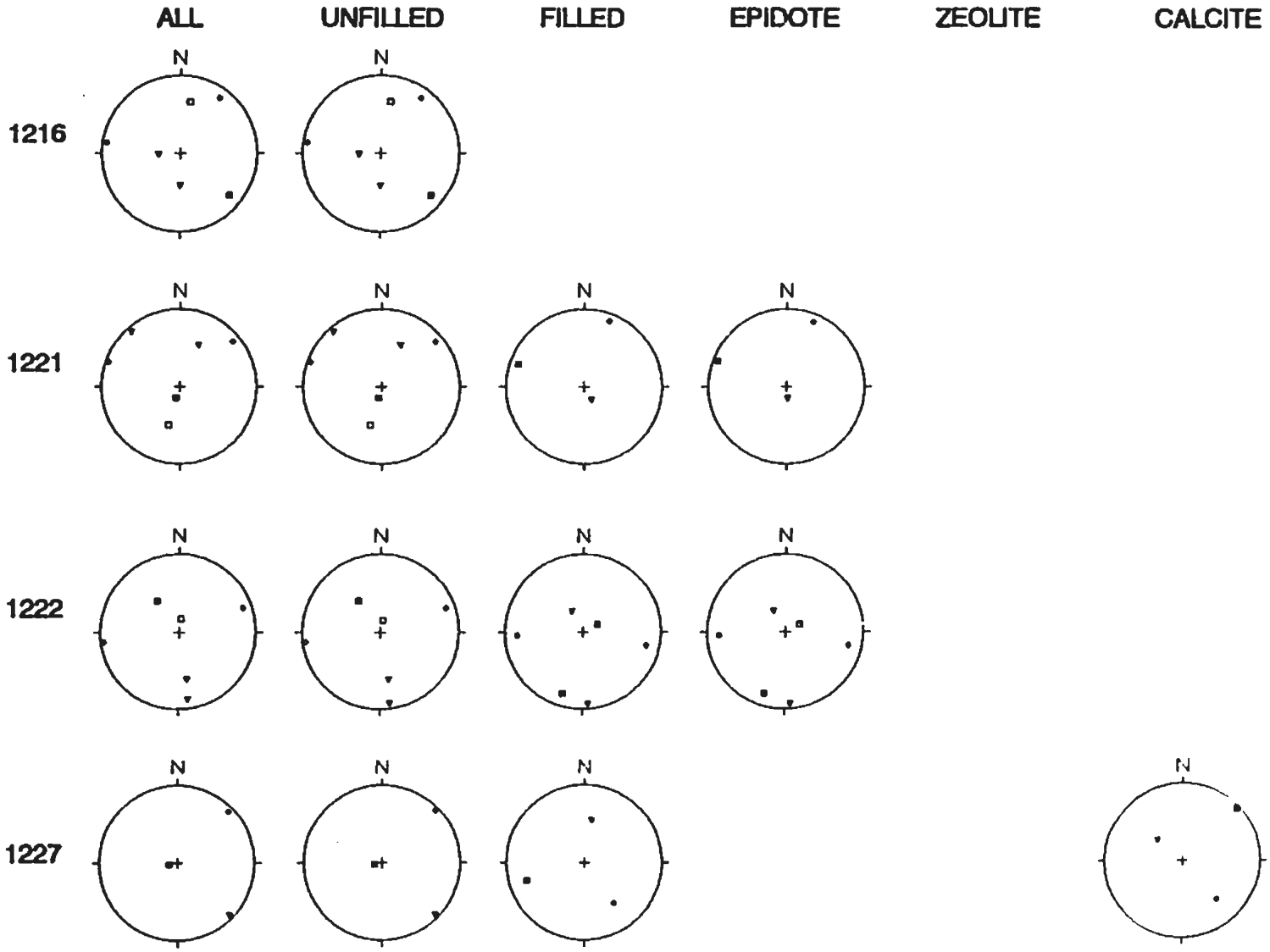

PRINCIPAL PERMEABILITY ORIENTATIONS

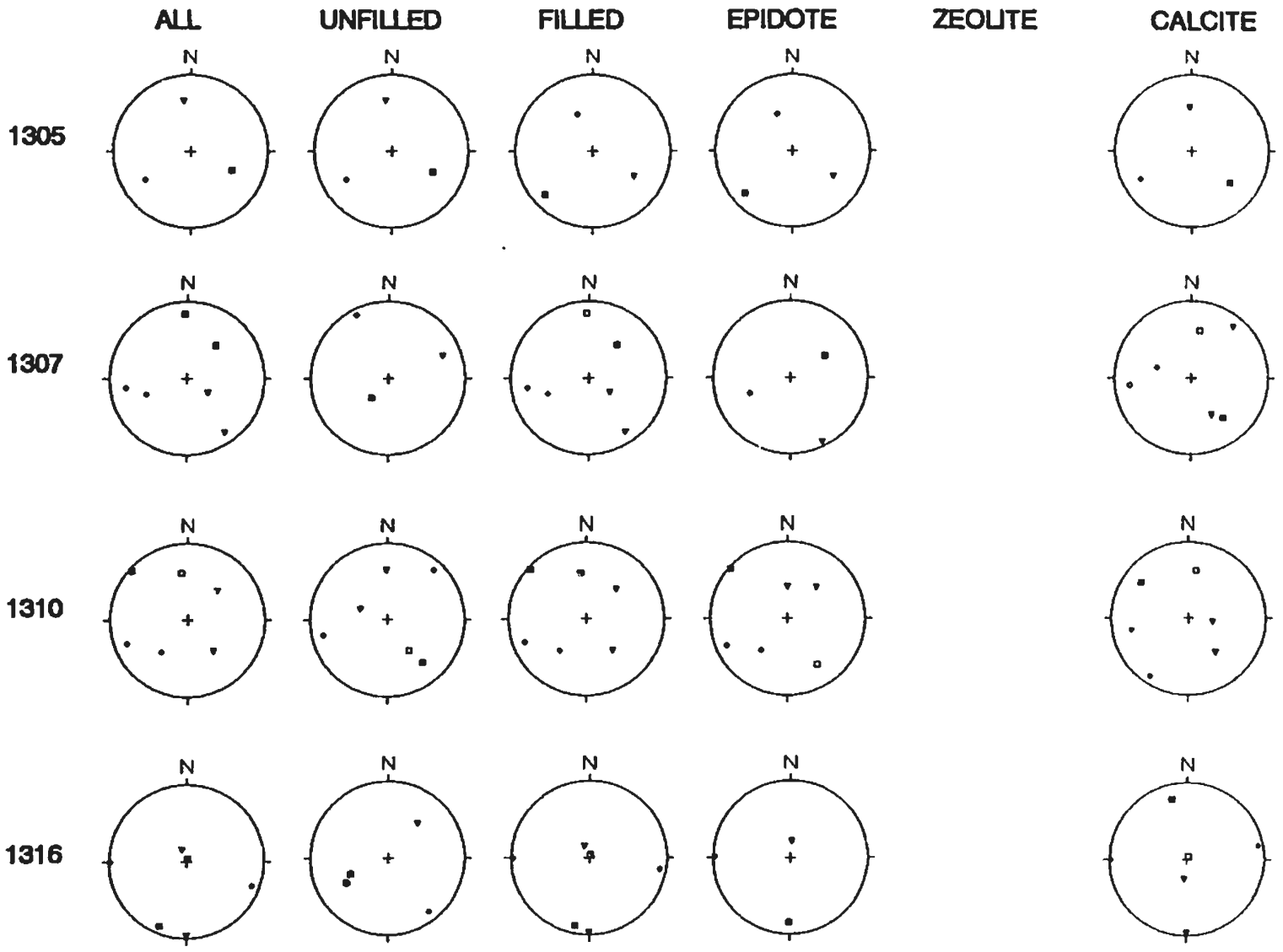

PRINCIPAL PERMEABILITY ORIENTATIONS

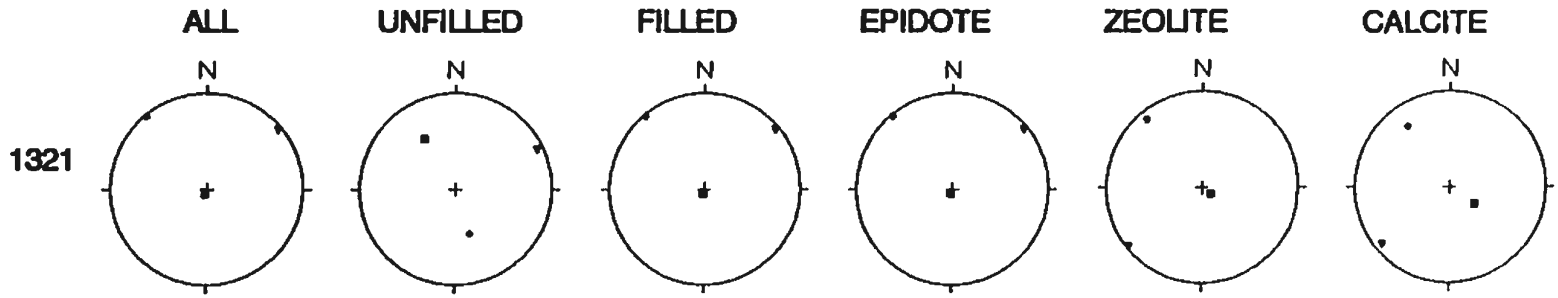

PRINCIPAL PERMEABILITY ORIENTATIONS

Fracture Permeability Magnitude and Anisotropy Using the Method of Bianchi and Snow (1969)

All Fractures

Area	K1	K2	K3	log K1/K3:	K2/K3:	K3/K3
0000	6.51E-07	6.29E-07	6.72E-08	0.99	0.97	0.00
0108	1.05E-06	1.03E-06	7.46E-08	1.15	1.14	0.00
0112	4.32E-05	3.73E-05	6.08E-06	0.85	0.79	0.00
0122	7.28E-05	6.19E-05	1.51E-05	0.68	0.61	0.00
0201	1.58E-07	1.19E-07	3.97E-08	0.60	0.48	0.00
0213	2.05E-04	2.02E-04	3.29E-06	1.79	1.79	0.00
0301	1.09E-06	1.03E-06	6.43E-08	1.23	1.20	0.00
0302	1.92E-06	1.71E-06	2.25E-07	0.93	0.88	0.00
0303	2.74E-05	2.68E-05	6.42E-07	1.63	1.62	0.00
0304	2.54E-02	2.52E-02	1.37E-04	2.27	2.27	0.00
0306	6.06E-08	4.33E-08	1.87E-08	0.51	0.37	0.00
0307	5.14E-08	4.88E-08	2.98E-09	1.24	1.21	0.00
0328	8.11E-09	6.98E-09	1.74E-09	0.67	0.60	0.00
0401	1.55E-06	1.43E-06	1.65E-07	0.97	0.94	0.00
0404	1.17E-05	1.16E-05	5.55E-08	2.32	2.32	0.00
0413	4.62E-07	4.51E-07	1.21E-08	1.58	1.57	0.00
0418	2.81E-06	2.57E-06	2.58E-07	1.04	1.00	0.00
0428	8.09E-08	6.32E-08	2.52E-08	0.51	0.40	0.00
0701	7.97E-07	5.68E-07	2.30E-07	0.54	0.39	0.00
1001	4.60E-07	4.58E-07	2.47E-09	2.27	2.27	0.00
1008	8.41E-04	8.41E-04	3.19E-09	5.42	5.42	0.00
1017	2.81E-05	2.77E-05	5.38E-07	1.72	1.71	0.00
1028	4.39E-09	4.26E-09	4.21E-10	1.02	1.01	0.00
1037	3.15E-07	3.11E-07	8.86E-09	1.55	1.55	0.00
1107	2.61E-07	2.58E-07	3.86E-09	1.83	1.82	0.00
1111	4.02E-06	4.02E-06	1.13E-09	3.55	3.55	0.00
1124	1.16E-06	1.07E-06	1.08E-07	1.03	1.00	0.00
1129	2.21E-07	2.13E-07	1.88E-08	1.12	1.10	0.00
1134	1.05E-04	1.05E-04	3.03E-07	2.54	2.54	0.00
1137	4.31E-07	4.27E-07	5.01E-09	1.93	1.93	0.00
1204	2.09E-06	2.00E-06	1.04E-07	1.30	1.28	0.00
1211	7.83E-06	7.83E-06	6.26E-10	4.10	4.10	0.00
1216	1.60E-06	1.60E-06	1.00E-10	4.20	4.20	0.00
1221	4.43E-07	4.43E-07	3.13E-10	3.15	3.15	0.00
1222	1.39E-06	1.33E-06	5.34E-08	1.41	1.40	0.00
1227	2.22E-09	2.07E-09	4.00E-10	0.75	0.71	0.00
1305	4.86E-07	4.86E-07	1.18E-09	2.61	2.61	0.00
1307	2.85E-06	2.85E-06	5.39E-09	2.72	2.72	0.00
1310	1.28E-04	1.28E-04	9.33E-08	3.14	3.14	0.00
1316	5.38E-06	4.16E-06	1.28E-06	0.62	0.51	0.00
1321	1.67E-07	1.43E-07	3.25E-08	0.71	0.64	0.00

All Fractures - Within 20° of Mean Dyke Orientations

Area	K1	K2	K3	log K1/K3:	K2/K3:	K3/K3
0000	9.8E-09	9.8E-09	2.6E-13	4.57	4.57	0.00
0108	9.4E-07	9.1E-07	2.9E-08	1.52	1.50	0.00
0112	2.3E-07	2.3E-07	8.6E-11	3.42	3.42	0.00
0122	2.5E-06	2.5E-06	3.0E-08	1.92	1.91	0.00
0201	1.1E-08	1.1E-08	8.7E-12	3.11	3.11	0.00
0213	0.000191	0.000191	9.0E-12	7.32	7.32	0.00
0301						
0302	8.5E-07	8.4E-07	9.4E-09	1.96	1.95	0.00
0303	0.000022	0.000022	1.2E-08	3.25	3.24	0.00
0304						
0306						
0307						
0328						
0401	7.1E-07	7.0E-07	1.9E-08	1.58	1.58	0.00
0404	0.00001	0.00001	3.6E-09	3.45	3.45	0.00
0413	1.8E-08	1.8E-08	6.4E-10	1.45	1.44	0.00
0418						
0428	3.3E-08	3.3E-08	8.2E-11	2.61	2.61	0.00
0701						
1001						
1008	2.4E-09	2.4E-09	3.0E-12	2.91	2.91	0.00
1017	1.3E-06	1.3E-06	7.1E-14	7.25	7.25	0.00
1028	3.3E-12	3.2E-12	5.1E-14	1.81	1.80	0.00
1037	1.8E-07	1.8E-07	8.7E-13	5.33	5.33	0.00
1107						
1111						
1124	2.2E-10	2.1E-10	1.3E-11	1.23	1.21	0.00
1129	4.2E-12	4.0E-12	2.6E-13	1.21	1.18	0.00
1134	1.3E-08	1.2E-08	5.3E-10	1.38	1.36	0.00
1137						
1204	2.7E-11	2.6E-11	1.1E-12	1.41	1.39	0.00
1211	7.3E-11	7.2E-11	7.5E-13	1.98	1.98	0.00
1216	2.0E-16	2.0E-16	1.1E-18	2.24	2.24	0.00
1221	6.1E-12	6.1E-12	2.6E-18	6.36	6.36	0.00
1222	3.2E-07	3.2E-07	1.2E-12	5.43	5.43	0.00
1227						
1305						
1307	4.5E-10	4.5E-10	8.7E-13	2.72	2.72	0.00
1310	2.6E-10	2.7E-10	3.6E-12	1.88	1.88	0.00
1316	2.7E-07	2.7E-07	1.1E-11	4.40	4.40	0.00
1321						

Fracture Permeability Magnitude and Anisotropy Using the Method of Bianchi and Snow (1969)

Unfilled Fractures

Area	K1	K2	K3	log K1/K3:	K2/K3:	K3/K3
0000	6.3E-10	5.9E-10	3.1E-10	1.30	1.28	0.00
0108	5.1E-10	4.1E-10	1.3E-10	0.59	0.50	0.00
0112	0.000037	0.000037	6.4E-10	4.76	4.76	0.00
0122	7.4E-08	7.4E-08	9.0E-11	2.92	2.92	0.00
0201	8.9E-11	8.9E-11	9.6E-15	3.97	3.97	0.00
0213	0.000192	0.000192	1.2E-07	3.22	3.22	0.00
0301						
0302	7.8E-10	7.7E-10	1.3E-11	1.76	1.76	0.00
0303	7.0E-11	6.2E-11	8.8E-12	0.90	0.85	0.00
0304	3.1E-09	3.0E-09	1.9E-10	1.22	1.21	0.00
0306	6.1E-08	4.3E-09	1.9E-08	0.51	0.37	0.00
0307	8.8E-11	8.8E-11	1.1E-14	3.90	3.90	0.00
0329	3.5E-10	3.3E-10	6.0E-11	0.77	0.75	0.00
0401	9.1E-12	6.8E-12	3.2E-13	1.45	1.44	0.00
0404	1.2E-08	1.2E-08	1.0E-11	3.07	3.07	0.00
0413	5.6E-10	5.6E-10	8.9E-13	2.80	2.80	0.00
0418						
0428	3.3E-08	3.3E-08	6.6E-11	2.70	2.69	0.00
0701	3.3E-10	2.8E-10	1.1E-10	0.46	0.38	0.00
1001	6.3E-09	4.2E-09	2.1E-09	0.47	0.30	0.00
1008	7.2E-09	6.3E-09	1.3E-09	0.74	0.68	0.00
1017	1.9E-10	1.7E-10	6.5E-11	0.46	0.42	0.00
1028	4.4E-09	4.2E-09	4.0E-10	1.03	1.02	0.00
1037	1.3E-07	1.3E-07	4.4E-09	1.47	1.46	0.00
1107	2.4E-08	2.3E-08	1.4E-09	1.24	1.22	0.00
1111	4.0E-06	4.0E-06	2.8E-10	4.15	4.15	0.00
1124	4.5E-07	4.4E-07	1.5E-08	1.49	1.48	0.00
1128	2.0E-07	1.9E-07	6.4E-09	1.49	1.47	0.00
1134	1.9E-08	1.9E-08	2.2E-11	2.95	2.95	0.00
1137	9.8E-11	6.6E-11	3.7E-11	0.42	0.25	0.00
1204	1.5E-07	1.4E-07	2.1E-08	0.87	0.82	0.00
1211	7.8E-06	7.8E-06	5.8E-10	4.13	4.13	0.00
1216	1.6E-06	1.6E-06	9.8E-11	4.21	4.21	0.00
1221	4.4E-07	4.4E-07	2.8E-10	3.20	3.20	0.00
1222	1.4E-06	1.3E-06	5.3E-08	1.42	1.40	0.00
1227	2.2E-09	2.1E-09	3.8E-10	0.76	0.73	0.00
1305	4.9E-07	4.8E-07	9.1E-10	2.73	2.73	0.00
1307	1.5E-10	9.5E-11	6.2E-11	0.37	0.19	0.00
1310	3.7E-10	2.6E-10	1.4E-10	0.41	0.26	0.00
1316	8.4E-06	8.4E-06	1.0E-08	2.92	2.92	0.00
1321	1.3E-10	8.7E-11	6.9E-11	0.27	0.10	0.00

Unfilled Fractures - Within 20° of Mean Dyke Orientation

Area	K1	K2	K3	log K1/K3:	K2/K3:	K3/K3
0000						
0108	6.4E-11	6.4E-11	5.2E-13	2.09	2.09	0.00
0112	3.9E-15	3.9E-15	1.3E-18	3.48	3.48	0.00
0122	1.6E-10	1.6E-10	7.4E-13	2.33	2.33	0.00
0201						
0213	0.000191	0.000191	1.0E-12	8.28	8.28	0.00
0301						
0302	8.6E-18	8.6E-18	1.6E-26	7.72	7.72	0.00
0303	2.0E-11	2.0E-11	9.5E-16	4.33	4.33	0.00
0304						
0306						
0307						
0329						
0401	9.1E-12	6.8E-12	3.2E-13	1.45	1.44	0.00
0404						
0413						
0418						
0428	3.3E-08	3.3E-08	4.1E-13	4.91	4.91	0.00
0701						
1001						
1008	2.4E-09	2.4E-09	2.9E-12	2.92	2.92	0.00
1017	5.4E-16	5.4E-16	5.1E-19	3.03	3.03	0.00
1028	3.3E-12	3.2E-12	5.1E-14	1.81	1.80	0.00
1037	4.3E-11	4.3E-11	1.7E-13	2.41	2.40	0.00
1107						
1111						
1124	8.3E-11	8.2E-11	1.1E-12	1.90	1.89	0.00
1128	2.8E-12	2.6E-12	1.6E-13	1.23	1.21	0.00
1134						
1137						
1204	1.1E-17	1.1E-17	1.0E-19	2.02	2.01	0.00
1211	7.3E-11	7.2E-11	7.5E-13	1.98	1.98	0.00
1216	2.0E-16	2.0E-16	1.1E-18	2.24	2.24	0.00
1221	6.1E-12	6.1E-12	2.6E-18	6.36	6.36	0.00
1222	3.2E-07	3.2E-07	8.4E-13	5.58	5.58	0.00
1227						
1305						
1307						
1310	1.3E-11	1.3E-11	2.3E-13	1.75	1.75	0.00
1316						
1321						

Fracture Permeability Magnitude and Anisotropy Using the Method of Bianchi and Snow (1969)

Filled Fractures

Area	K1	K2	K3	log K1/K3:	K2/K3:	K3/K3
0000	6.5E-07	6.3E-07	6.7E-08	0.99	0.97	0.00
0108	1.0E-06	1.0E-06	7.4E-08	1.15	1.14	0.00
0112	6.4E-06	6.1E-06	3.3E-07	1.29	1.27	0.00
0122	0.000073	0.000062	0.000015	0.68	0.61	0.00
0201	1.6E-07	1.2E-07	4.0E-08	0.60	0.48	0.00
0213	0.000013	0.000013	4.1E-09	2.50	2.50	0.00
0301	1.1E-06	1.0E-06	6.4E-08	1.23	1.20	0.00
0302	1.9E-06	1.7E-06	2.3E-07	0.93	0.88	0.00
0303	0.000027	0.000027	6.4E-07	1.63	1.62	0.00
0304	0.025356	0.025224	0.000137	2.27	2.27	0.00
0306	1.0E-11	1.0E-11	5.7E-18	6.26	6.26	0.00
0307	5.1E-08	4.9E-08	2.9E-09	1.25	1.23	0.00
0329	7.9E-09	6.7E-09	1.5E-09	0.72	0.65	0.00
0401	1.5E-06	1.4E-06	1.7E-07	0.97	0.94	0.00
0404	0.000012	0.000012	4.6E-08	2.40	2.40	0.00
0413	4.6E-07	4.5E-07	1.2E-08	1.59	1.57	0.00
0418	2.8E-06	2.6E-06	2.6E-07	1.04	1.00	0.00
0428	5.0E-08	4.5E-08	8.7E-09	0.76	0.71	0.00
0701	8.0E-07	5.7E-07	2.3E-07	0.54	0.39	0.00
1001	4.1E-08	4.1E-08	3.5E-11	3.07	3.07	0.00
1008	0.000841	0.000841	1.9E-11	7.65	7.65	0.00
1017	0.000028	0.000028	5.4E-07	1.72	1.71	0.00
1028	4.2E-11	4.2E-11	7.6E-14	2.74	2.74	0.00
1037	1.9E-07	1.9E-07	8.0E-11	3.38	3.38	0.00
1107	2.4E-07	2.4E-07	8.6E-10	2.44	2.44	0.00
1111	1.3E-08	1.3E-08	5.7E-10	1.38	1.35	0.00
1124	7.1E-07	7.1E-07	4.1E-09	2.24	2.24	0.00
1129	2.9E-08	2.2E-08	8.0E-09	0.56	0.43	0.00
1134	0.000105	0.000105	3.0E-07	2.55	2.55	0.00
1137	4.3E-07	4.3E-07	4.9E-09	1.94	1.94	0.00
1204	1.9E-06	1.9E-06	8.9E-11	4.34	4.34	0.00
1211	6.9E-11	4.2E-11	3.4E-11	0.30	0.09	0.00
1216						
1221	9.3E-11	7.8E-11	2.0E-11	0.67	0.60	0.00
1222	2.1E-09	2.0E-09	1.2E-10	1.24	1.22	0.00
1227	1.8E-11	1.7E-11	8.5E-13	1.31	1.30	0.00
1306	3.4E-10	3.0E-10	4.5E-11	0.88	0.82	0.00
1307	2.8E-06	2.8E-06	5.3E-09	2.73	2.73	0.00
1310	0.000128	0.000128	9.3E-08	3.14	3.14	0.00
1316	4.2E-06	3.4E-06	8.9E-07	0.68	0.59	0.00
1321	1.7E-07	1.4E-07	3.2E-08	0.71	0.64	0.00

Filled Fractures - Within 20° of Mean Dyke Orientation

Area	K1	K2	K3	log K1/K3:	K2/K3:	K3/K3
0000	9.8E-09	9.8E-09	2.6E-13	4.57	4.57	0.00
0108	9.4E-07	9.1E-07	2.9E-08	1.52	1.50	0.00
0112	2.3E-07	2.3E-07	8.6E-11	3.42	3.42	0.00
0122	2.5E-06	2.5E-06	3.0E-08	1.92	1.91	0.00
0201	1.1E-08	1.1E-08	8.7E-12	3.11	3.11	0.00
0213	1.9E-10	1.9E-10	4.5E-12	1.63	1.62	0.00
0301						
0302	8.5E-07	8.4E-07	9.4E-09	1.96	1.95	0.00
0303	0.000022	0.000022	1.2E-08	3.25	3.24	0.00
0304						
0306						
0307						
0329						
0401	7.1E-07	7.0E-07	1.9E-08	1.58	1.58	0.00
0404	0.00001	0.00001	3.6E-09	3.45	3.45	0.00
0413	1.8E-08	1.8E-08	6.4E-10	1.45	1.44	0.00
0418						
0428	3.5E-10	3.4E-10	6.6E-12	1.72	1.71	0.00
0701						
1001						
1008						
1017						
1028						
1037	1.8E-07	1.8E-07	1.5E-13	6.08	6.08	0.00
1107						
1111						
1124	1.4E-10	1.3E-10	6.4E-12	1.34	1.32	0.00
1129						
1134	1.3E-08	1.2E-08	5.3E-10	1.38	1.38	0.00
1137						
1204	2.7E-11	2.6E-11	1.1E-12	1.41	1.39	0.00
1211						
1216						
1221						
1222	6.5E-12	6.5E-12	6.3E-14	2.01	2.01	0.00
1227						
1306						
1307	4.5E-10	4.5E-10	8.7E-13	2.72	2.72	0.00
1310	2.6E-10	2.6E-10	3.2E-12	1.92	1.91	0.00
1316	2.7E-07	2.7E-07	1.1E-11	4.40	4.40	0.00
1321						

Fracture Permeability Magnitude and Anisotropy Using the Method of Bianchi and Snow (1969)

Epidote filled Fractures

Area	K1	K2	K3	log K1/K3:	K2/K3:	K3/K3
0000	6.1E-07	6.0E-07	1.4E-08	1.63	1.62	0.00
0108	1.0E-06	1.0E-06	6.9E-08	1.18	1.17	0.00
0112	6.3E-06	6.1E-06	2.9E-07	1.34	1.32	0.00
0122	0.000018	0.000017	3.6E-06	0.71	0.68	0.00
0201	1.2E-07	1.2E-07	6.5E-09	1.28	1.26	0.00
0213	4.0E-07	3.9E-07	1.8E-08	1.35	1.33	0.00
0301	1.1E-06	1.0E-06	6.4E-08	1.23	1.20	0.00
0302	1.9E-06	1.7E-06	2.3E-07	0.93	0.88	0.00
0303	0.000027	0.000027	6.4E-07	1.63	1.62	0.00
0304	0.024837	0.024724	0.000113	2.34	2.34	0.00
0306						
0307	4.2E-08	4.1E-08	1.5E-09	1.43	1.42	0.00
0329	7.9E-09	6.5E-09	1.4E-09	0.76	0.68	0.00
0401	1.5E-06	1.4E-06	1.6E-07	0.97	0.93	0.00
0404	0.000012	0.000012	4.5E-08	2.41	2.41	0.00
0413	4.6E-07	4.5E-07	1.2E-08	1.59	1.57	0.00
0418	2.8E-06	2.5E-06	2.5E-07	1.04	1.00	0.00
0428	6.6E-09	6.5E-09	3.0E-09	0.46	0.34	0.00
0701	3.6E-07	3.6E-07	4.8E-11	3.87	3.87	0.00
1001						
1008						
1017	0.000028	0.000027	1.1E-07	2.42	2.41	0.00
1028						
1037	5.2E-10	4.8E-10	5.8E-11	0.96	0.92	0.00
1107	2.4E-07	2.4E-07	8.5E-10	2.45	2.45	0.00
1111	1.3E-08	1.2E-08	4.0E-10	1.51	1.49	0.00
1124	7.1E-07	7.1E-07	9.9E-12	4.85	4.85	0.00
1129	1.9E-08	1.9E-08	1.5E-10	2.11	2.10	0.00
1134	0.000105	0.000105	2.9E-07	2.56	2.55	0.00
1137	4.3E-07	4.3E-07	4.9E-09	1.94	1.94	0.00
1204	1.2E-11	1.1E-11	4.0E-13	1.46	1.45	0.00
1211						
1216						
1221	6.3E-11	5.7E-11	9.6E-12	0.82	0.77	0.00
1222	2.1E-09	2.0E-09	1.2E-10	1.24	1.22	0.00
1227						
1305	3.3E-10	3.0E-10	3.9E-11	0.94	0.89	0.00
1307	2.9E-06	2.8E-06	3.9E-09	2.87	2.87	0.00
1310	0.000128	0.000128	6.9E-08	3.16	3.16	0.00
1316	1.7E-06	1.6E-06	7.2E-08	1.37	1.35	0.00
1321	1.7E-07	1.4E-07	3.2E-08	0.71	0.64	0.00

Epidote filled Fractures - Within 20° of Mean Dyke Orientation

Area	K1	K2	K3	log K1/K3:	K2/K3:	K3/K3
0000						
0108	9.4E-07	9.1E-07	2.9E-08	1.52	1.50	0.00
0112	2.3E-07	2.3E-07	8.6E-11	3.42	3.42	0.00
0122	2.4E-06	2.4E-06	2.6E-08	1.96	1.96	0.00
0201	1.1E-08	1.1E-08	8.7E-12	3.11	3.11	0.00
0213	9.6E-11	9.4E-11	2.8E-12	1.53	1.52	0.00
0301						
0302	8.5E-07	8.4E-07	9.4E-09	1.96	1.95	0.00
0303	0.000022	0.000022	1.2E-08	3.26	3.24	0.00
0304						
0306						
0307						
0329						
0401	6.9E-07	6.7E-07	1.5E-08	1.67	1.66	0.00
0404	0.00001	0.00001	3.6E-09	3.45	3.45	0.00
0413	1.8E-08	1.8E-08	6.4E-10	1.45	1.44	0.00
0418						
0428	2.4E-10	2.4E-10	1.8E-12	2.12	2.12	0.00
0701						
1001						
1008						
1017						
1028						
1037	1.4E-11	1.4E-11	3.1E-14	2.65	2.64	0.00
1107						
1111						
1124						
1129						
1134	1.3E-08	1.2E-08	5.3E-10	1.38	1.36	0.00
1137						
1204	9.5E-12	9.4E-12	1.2E-13	1.91	1.90	0.00
1211						
1216						
1221						
1222	6.5E-12	6.5E-12	6.3E-14	2.01	2.01	0.00
1227						
1305						
1307						
1310	2.1E-10	2.1E-10	2.9E-13	2.85	2.85	0.00
1316						
1321						

Fracture Permeability Magnitude and Anisotropy Using the Method of Bianchi and Snow (1969)

Zeolite filled Fractures

Area	K1	K2	K3	log K1/K3:	K2/K3:	K3/K3
0000	1.5E-07	1.4E-07	2.5E-08	0.79	0.76	0.00
0108	9.3E-07	9.0E-07	2.8E-08	1.53	1.51	0.00
0112	6.2E-08	5.5E-08	3.2E-08	0.29	0.24	0.00
0122	0.000071	0.00006	0.000013	0.75	0.67	0.00
0201	1.3E-07	9.9E-08	3.3E-08	0.60	0.48	0.00
0213	2.4E-07	2.4E-07	9.3E-12	4.41	4.41	0.00
0301						
0302						
0303						
0304	0.024837	0.024724	0.000113	2.34	2.34	0.00
0306						
0307						
0329	1.5E-09	1.4E-09	1.4E-10	1.02	0.97	0.00
0401	3.5E-07	3.5E-07	1.5E-11	4.37	4.37	0.00
0404	1.7E-08	1.6E-08	5.1E-10	1.52	1.51	0.00
0413	1.9E-07	1.9E-07	1.4E-09	2.13	2.13	0.00
0418	4.6E-08	4.4E-08	3.1E-09	1.17	1.15	0.00
0428	4.3E-08	4.1E-08	4.5E-09	0.98	0.95	0.00
0701						
1001	4.1E-08	4.1E-08	3.7E-12	4.04	4.04	0.00
1008						
1017						
1028						
1037						
1107						
1111	1.1E-11	1.1E-11	2.4E-18	6.67	6.67	0.00
1124	5.4E-09	5.2E-09	2.5E-10	1.34	1.32	0.00
1129						
1134						
1137						
1204						
1211	3.7E-11	3.3E-11	4.3E-12	0.93	0.88	0.00
1216						
1221						
1222						
1227						
1305						
1307						
1310						
1316						
1321	1.8E-09	1.6E-09	2.4E-11	1.88	1.88	0.00

Zeolite filled Fractures - Within 20° of Mean Dyke Orientation

Area	K1	K2	K3	log K1/K3:	K2/K3:	K3/K3
0000						
0108	9.3E-07	9.0E-07	2.8E-08	1.55	1.53	0.00
0112						
0122	2.5E-06	2.5E-06	3.0E-08	1.92	1.92	0.00
0201						
0213	1.6E-11	1.6E-11	1.4E-13	2.05	2.04	0.00
0301						
0302						
0303						
0304						
0306						
0307						
0329						
0401	5.7E-11	5.6E-11	1.3E-12	1.66	1.65	0.00
0404						
0413	2.3E-09	2.2E-09	7.2E-11	1.51	1.50	0.00
0418						
0428	1.3E-10	1.3E-10	1.3E-12	1.98	1.98	0.00
0701						
1001						
1008						
1017						
1028						
1037						
1107						
1111						
1124	1.2E-10	1.2E-10	5.6E-12	1.33	1.31	0.00
1129						
1134						
1137						
1204						
1211						
1216						
1221						
1222						
1227						
1305						
1307						
1310						
1316						
1321						

Fracture Permeability Magnitude and Anisotropy Using the Method of Bianchi and Snow (1969)

Calcite filled Fractures							Calcite filled Fractures - Within 20° of Mean Dyke Orientation						
Area	K1	K2	K3	log K1/K3:	K2/K3:	K3/K3	Area	K1	K2	K3	log K1/K3:	K2/K3:	K3/K3
0000							0000						
0108							0108						
0112							0112						
0122							0122						
0201							0201						
0213	0.000013	0.000013	2.6E-08	2.70	2.70	0.00	0213	9.2E-11	9.2E-11	1.3E-12	1.84	1.84	0.00
0301	1.4E-14	1.4E-14	3.4E-16	1.61	1.60	0.00	0301						
0302							0302						
0303							0303						
0304							0304						
0306	9.2E-18	9.2E-18	7.3E-26	7.10	7.10	0.00	0306						
0307	1.3E-10	1.3E-10	7.5E-19	8.23	8.23	0.00	0307						
0329							0329						
0401							0401						
0404							0404						
0413							0413						
0418							0418						
0428							0428						
0701	3.6E-07	3.6E-07	1.9E-09	2.28	2.28	0.00	0701						
1001							1001						
1008	5.2E-12	4.8E-12	4.9E-13	1.03	0.99	0.00	1008	2.4E-12	2.4E-12	8.3E-20	7.46	7.46	0.00
1017							1017						
1028							1028						
1037	1.6E-12	1.6E-12	4.1E-20	7.59	7.59	0.00	1037	1.6E-12	1.6E-12	4.1E-20	7.59	7.59	0.00
1107	2.2E-07	2.2E-07	1.0E-11	4.33	4.33	0.00	1107						
1111	1.9E-10	1.9E-10	1.1E-12	2.24	2.24	0.00	1111						
1124	6.5E-12	5.8E-12	6.7E-13	0.99	0.94	0.00	1124	2.4E-12	2.4E-12	9.4E-20	7.40	7.40	0.00
1129	1.2E-08	8.1E-09	4.6E-09	0.43	0.24	0.00	1129						
1134	0.000105	0.000105	6.4E-08	3.21	3.21	0.00	1134	5.0E-09	5.0E-09	9.9E-13	3.70	3.70	0.00
1137	4.3E-07	4.3E-07	4.4E-09	1.99	1.99	0.00	1137						
1204	1.9E-06	1.9E-06	7.9E-11	4.39	4.39	0.00	1204	1.8E-11	1.8E-11	1.1E-13	2.22	2.22	0.00
1211	3.5E-11	3.4E-11	9.7E-13	1.56	1.55	0.00	1211						
1216							1216						
1221							1221						
1222							1222						
1227	9.0E-12	8.9E-12	1.8E-13	1.70	1.69	0.00	1227						
1305	3.3E-11	3.3E-11	9.3E-13	1.55	1.55	0.00	1305						
1307	1.0E-08	1.0E-08	5.0E-10	1.31	1.30	0.00	1307	1.7E-10	1.7E-10	5.0E-13	2.53	2.52	0.00
1310	1.5E-09	1.5E-09	2.8E-11	1.73	1.72	0.00	1310	5.6E-11	5.6E-11	4.0E-14	3.14	3.14	0.00
1316	3.1E-06	3.1E-06	9.4E-08	1.52	1.51	0.00	1316	2.7E-07	2.7E-07	1.1E-11	4.40	4.40	0.00
1321	1.6E-10	1.4E-10	2.0E-11	0.90	0.86	0.00	1321						

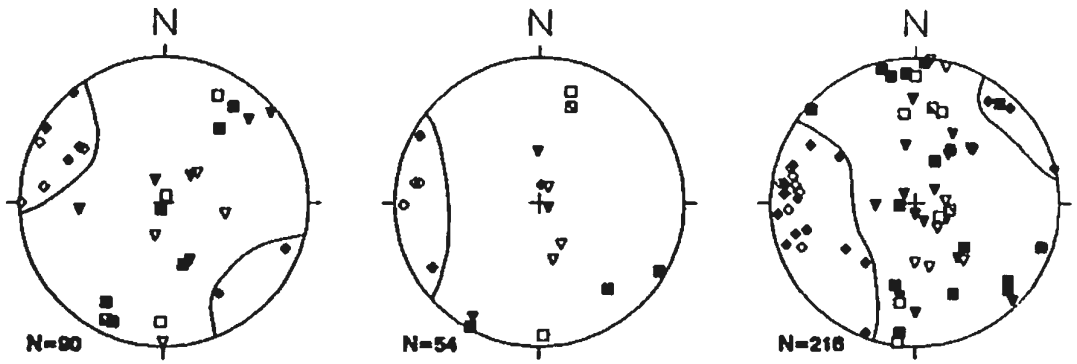

PRINCIPAL PERMEABILITY ORIENTATIONS (BY DOMAIN) FOR ALL FRACTURES. CLOSED SYMBOLS ARE PRINCIPAL PERMEABILITY DIRECTIONS FOR ALL FRACTURES. OPEN SYMBOLS FOR DYKE PARALLEL FRACTURES. TRIANGLES = k1; SQUARES = k2; DIAMONDS = k3. LINES ON PLOT OUTLINE k3 ORIENTATIONS. DATA USED ARE THE MEANS FROM EACH OF THE SCANLINES.

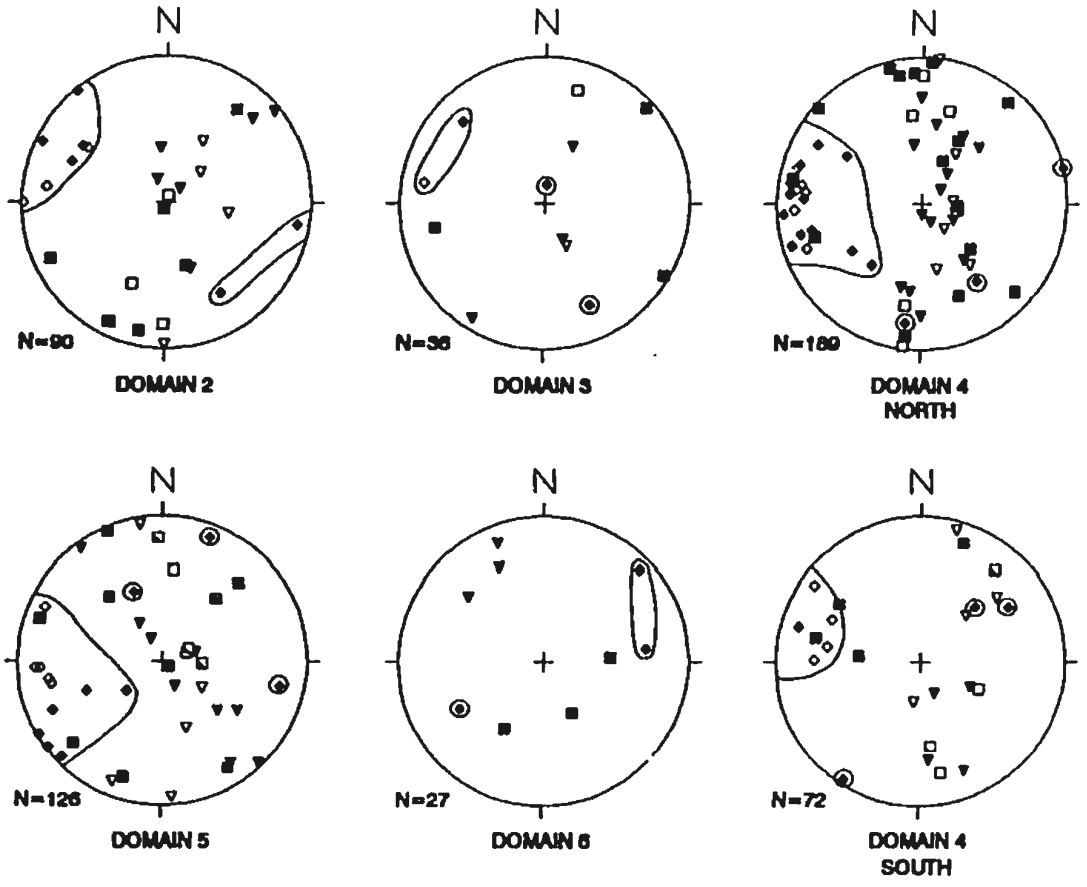

PRINCIPAL PERMEABILITY ORIENTATIONS (BY DOMAIN) FOR FILLED FRACTURES. CLOSED SYMBOLS ARE PRINCIPAL PERMEABILITY DIRECTIONS FOR ALL FRACTURES. OPEN SYMBOLS FOR DYKE PARALLEL FRACTURES. TRIANGLES = k1; SQUARES = k2; DIAMONDS = k3. LINES ON PLOT OUTLINE k3 ORIENTATIONS. DATA USED ARE THE MEANS FROM EACH OF THE SCANLINES.

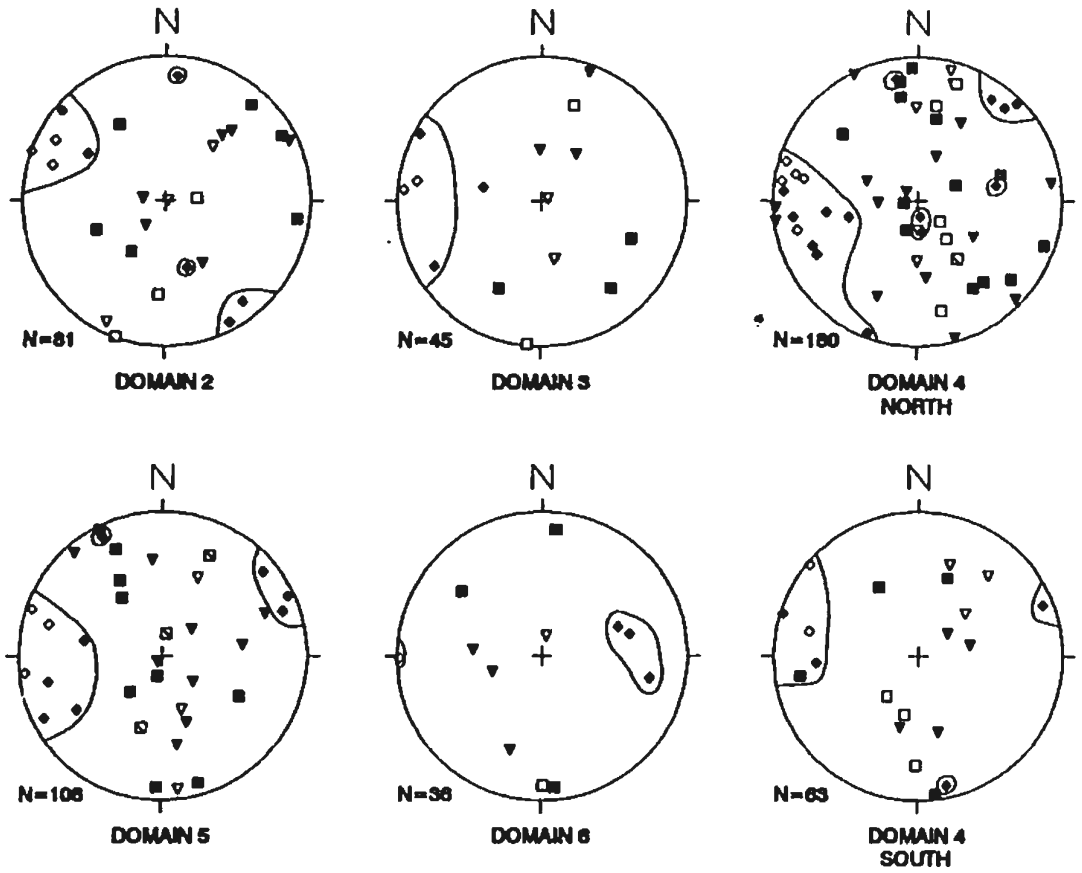

PRINCIPAL PERMEABILITY ORIENTATIONS (BY DOMAIN) FOR UNFILLED FRACTURES. CLOSED SYMBOLS ARE PRINCIPAL PERMEABILITY DIRECTIONS FOR ALL FRACTURES. OPEN SYMBOLS FOR DYKE PARALLEL FRACTURES. TRIANGLES = k1; SQUARES = k2; DIAMONDS = k3. LINES ON PLOT OUTLINE k3 ORIENTATIONS. DATA USED ARE THE MEANS FROM EACH OF THE SCANLINES.

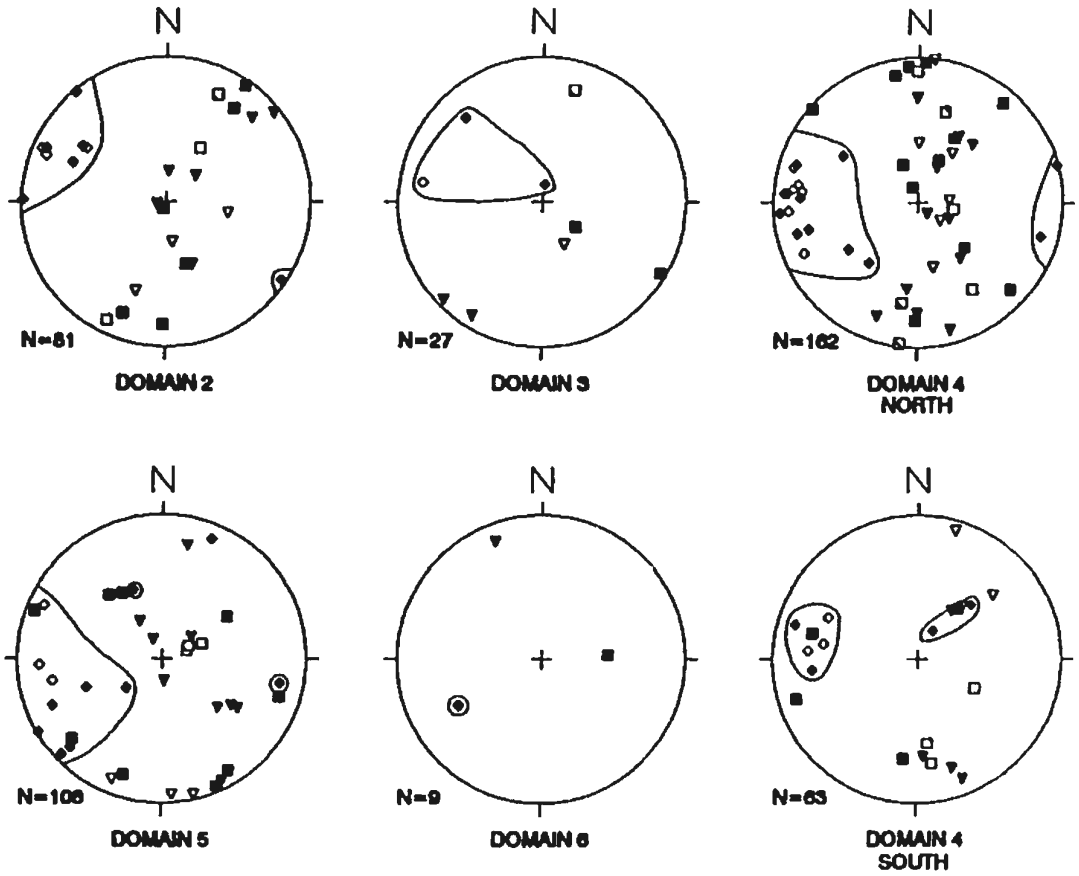

PRINCIPAL PERMEABILITY ORIENTATIONS (BY DOMAIN) FOR EPIDOTE-FILLED FRACTURES. CLOSED SYMBOLS ARE PRINCIPAL PERMEABILITY DIRECTIONS FOR ALL FRACTURES. OPEN SYMBOLS FOR DYKE PARALLEL FRACTURES. TRIANGLES = k1; SQUARES = k2; DIAMONDS = k3. LINES ON PLOT OUTLINE k3 ORIENTATIONS. DATA USED ARE THE MEANS FROM EACH OF THE SCANLINES.

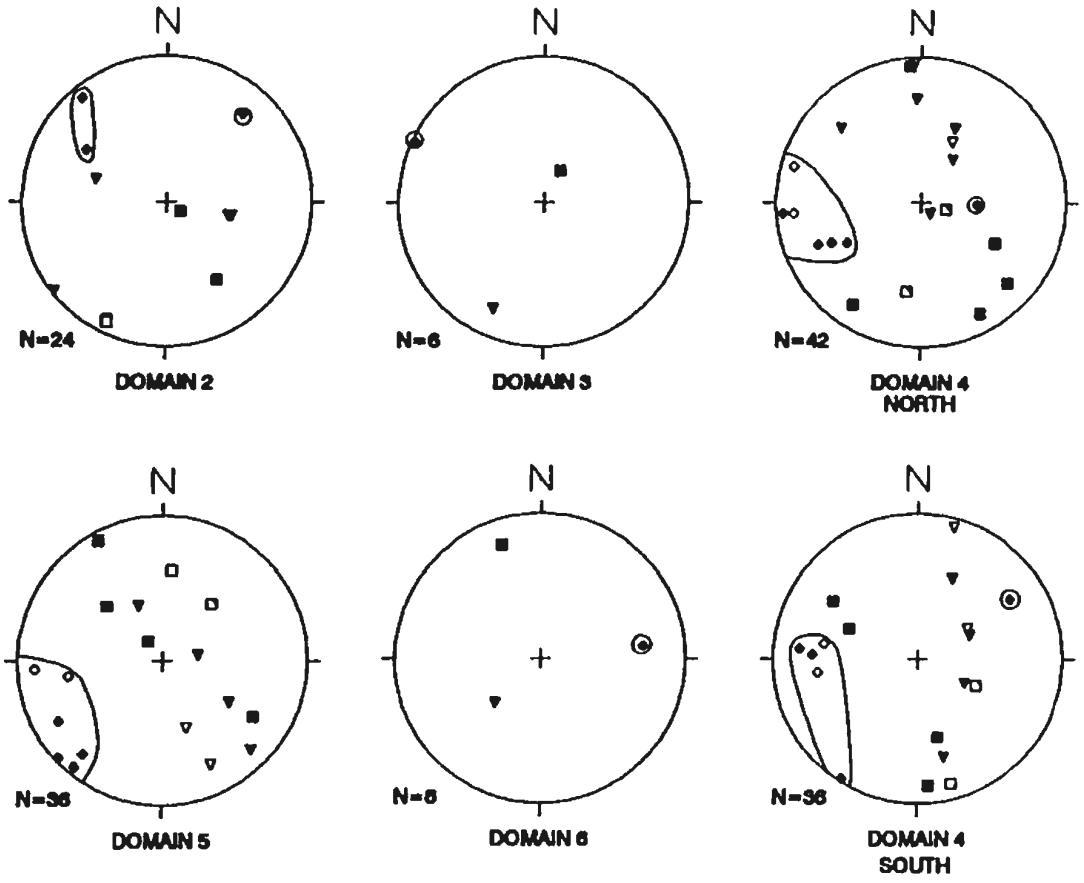

PRINCIPAL PERMEABILITY ORIENTATIONS (BY DOMAIN) FOR ZEOLITE-FILLED FRACTURES. CLOSED SYMBOLS ARE PRINCIPAL PERMEABILITY DIRECTIONS FOR ALL FRACTURES. OPEN SYMBOLS FOR DYKE PARALLEL FRACTURES. TRIANGLES = k1; SQUARES = k2; DIAMONDS = k3. LINES ON PLOT OUTLINE k3 ORIENTATIONS. DATA USED ARE THE MEANS FROM EACH OF THE SCANLINES.

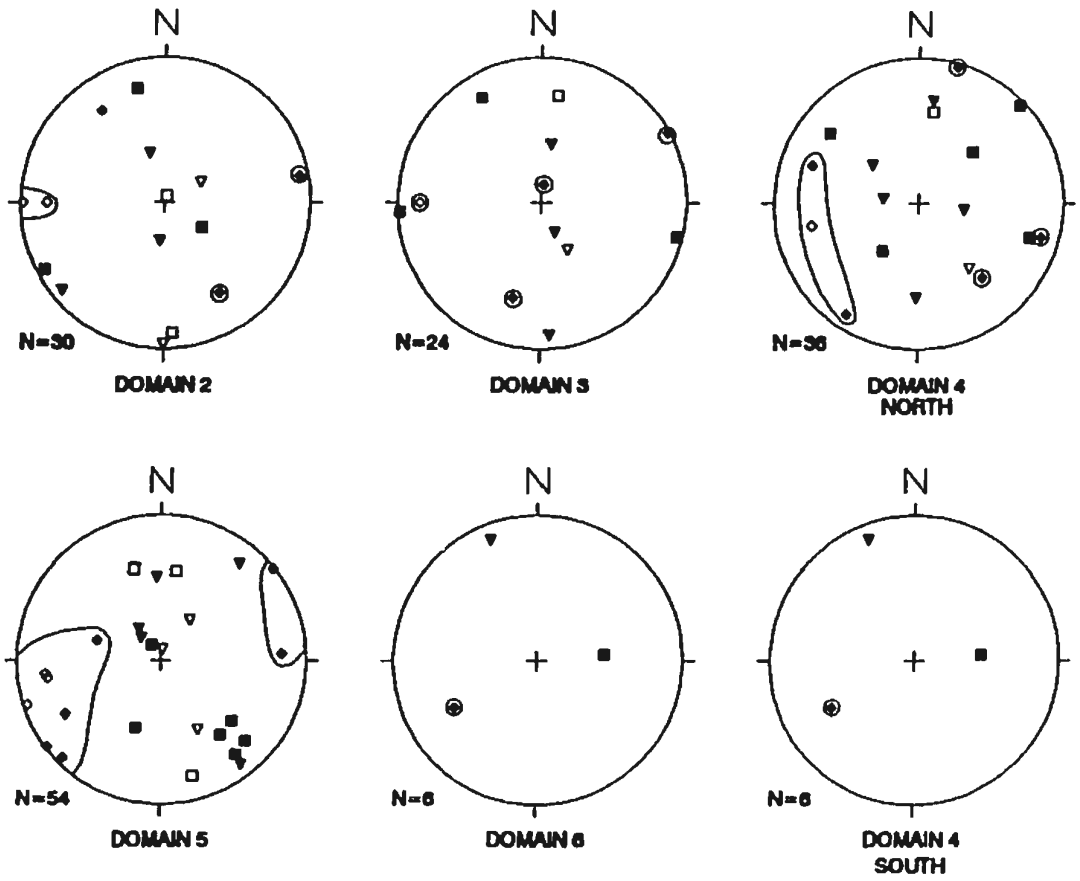

PRINCIPAL PERMEABILITY ORIENTATIONS (BY DOMAIN) FOR CALCITE-FILLED FRACTURES. CLOSED SYMBOLS ARE PRINCIPAL PERMEABILITY DIRECTIONS FOR ALL FRACTURES. OPEN SYMBOLS FOR DYKE PARALLEL FRACTURES. TRIANGLES = k1; SQUARES = k2; DIAMONDS = k3. LINES ON PLOT OUTLINE k3 ORIENTATIONS. DATA USED ARE THE MEANS FROM EACH OF THE SCANLINES.

A.8 TRACE LENGTH SIMULATION

Fracture Size and Shape

The relationship between the radius of a circular fracture and the fracture trace length produced by intersection of a fracture with an outcrop surface is given by Charlaix et al. (1984),

$$l^2 = r^2 - \frac{z^2}{\sin^2\beta} \quad \ldots\ldots\ldots\ldots\ldots\ldots \text{(A.7.15)}$$

where l is the half fracture trace length, r is the fracture radius, z is the vertical distance from the centre of the circular fracture to the outcrop plane and ß is the angle between the fracture plane and the outcrop surface (Figure A.7.1A). The angle of intersection has no effect on the resulting fracture trace length. It was assumed, for simplicity, that all fractures intersect the outcrop surface at right angles so that $\sin(ß)=1$.

The formulation for calculating trace length from elliptical fractures is given in the following paragraphs. This is a more general formulation than that of equation (A.7.16).

The equation of a line representing the outcrop-fracture intersection is (refer to Figure A.7.1B),

$$y = mx + B \quad \ldots\ldots\ldots\ldots\ldots\ldots \text{(A.7.17)}$$

where m is the slope and B is the y-intercept. The equation of an elliptical fracture is,

$$\frac{x^2}{a^2} + \frac{y^2}{b^2} = 1 \quad \ldots\ldots\ldots\ldots\ldots\ldots \text{(A.7.18)}$$

where a is the half length of the long axis and b is the half length of the short axis. Solving for y equation (A.7.18) becomes,

$$y = \sqrt{(1-\frac{x^2}{a^2})b^2} \quad \ldots\ldots\ldots\ldots\ldots\ldots \text{(A.7.19)}$$

To find the points P(x,y) and Q(x,y) (Figure A.7.1B), take the square of equation (A.7.19) and equate with the square of the equation (A.7.17) and then solve the quadratic equation for x,

$$x = \frac{-2mB \pm \sqrt{(2mB)^2 - 4(m^2 + \frac{b^2}{a^2})(B^2 - b^2)}}{2(m^2 + \frac{b^2}{a^2})} \quad \ldots\ldots\ldots\ldots \text{(A.7.20)}$$

The trace length of the fracture plane-outcrop surface intersection is determined from the following equation,

$$\overline{PQ} = \sqrt{(Px - Qx)^2 + (Py - Qy)^2} \quad \ldots\ldots\ldots\ldots \text{(A.7.21)}$$

Both circular and elliptical fractures were used to generate various distributions of fracture trace lengths in order to determine from what type of distribution of fracture

radii the measured fracture trace length distribution in the field area could have originated. Input distributions of fracture radii included normal, exponential Weibull, bimodal and square. For each distribution of ellipses a series of randomly oriented lines, representing outcrop surfaces, is generated at random distances from the origin (see Figure A.7.1B). The program determines whether the lines cut the ellipses. A simulated line which lies entirely outside the ellipse boundaries will result in an imaginary solution; such a line is ignored in the further calculations. This method biases the result toward sampling the larger fracture radii, very much as that of sampling fractures on an outcrop in the field.

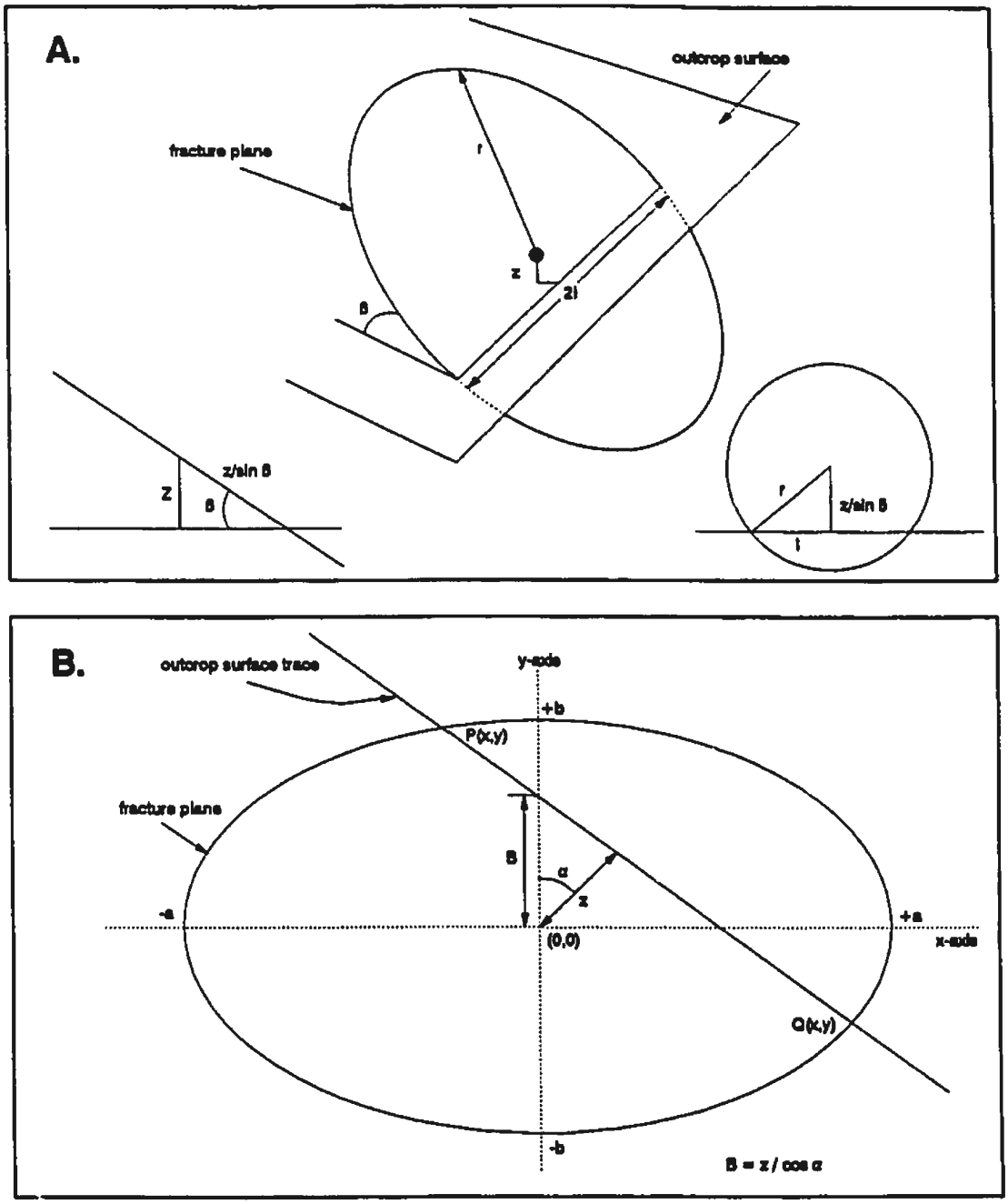

FIGURE A.7.1 TRACE LENGTH SIMUATION USING CIRCULAR AND ELLIPTICAL FRACTURE SHAPE
A. CIRCULAR FRACTURE. r IS FRACTURE RADIUS, β IS ANGLE OF INTERSECTION BETWEEN FRACTURE PLANE AND OUTCROP, z IS THE HEIGHT OF THE CIRCLE CENTRE ABOVE THE OUTCROP PLANE, AND 2l IS THE LENGTH OF THE FRACTURE PLANE-OUTCROP SURFACE INTERSECTION (AFTER CHARLAIX ET AL., 1984).
B. ELLIPTICAL FRACTURE PLANE. LINE PQ IS THE FRACTURE PLANE-OUTCROP INTERSECTION.

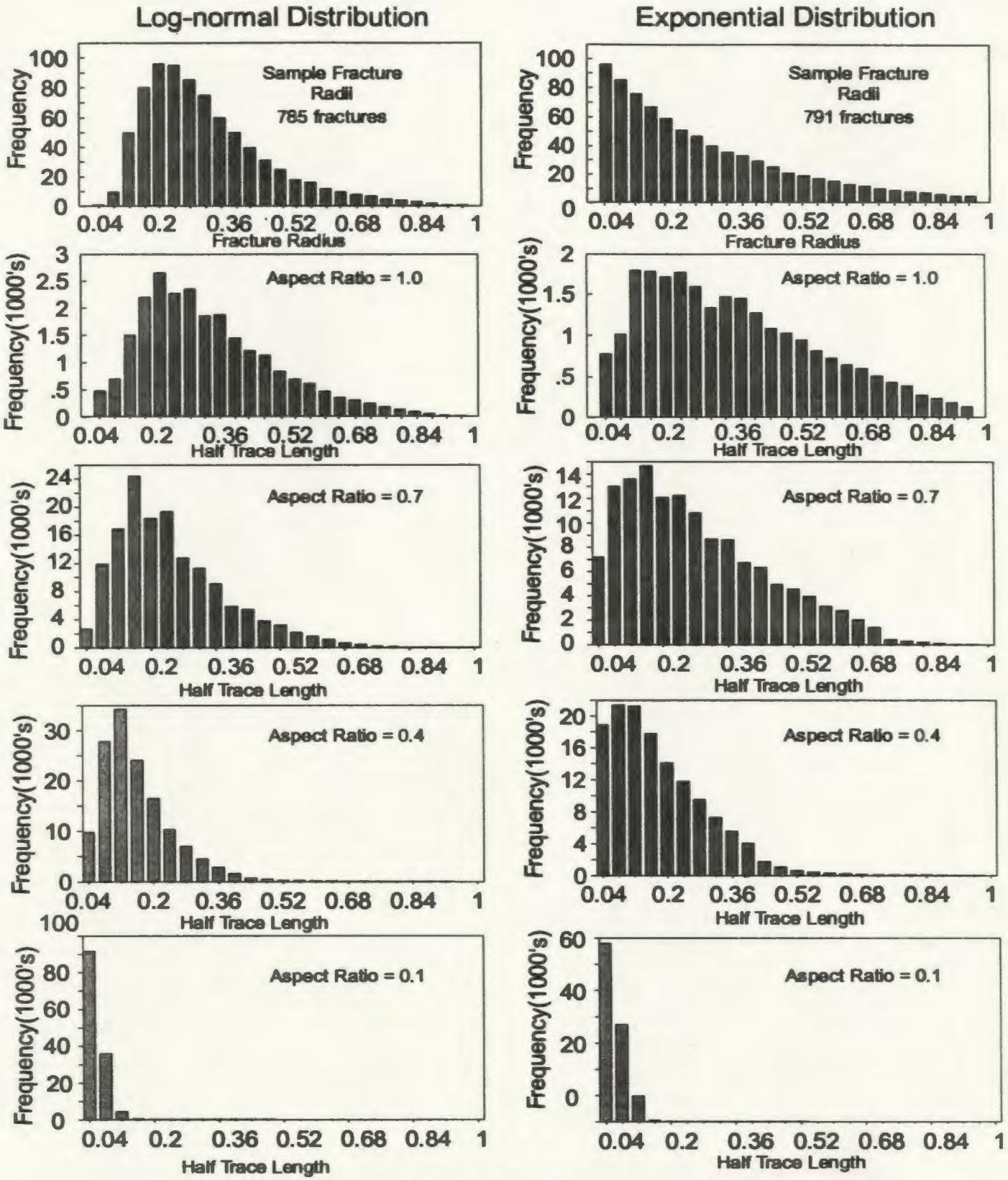

FRACTURE TRACE LENGTH SIMULATION. TOP HISTOGRAM IN EACH COLUMN ARE THE INPUT FRACTURE RADIUS DISTRIBUTION. THE REMAINING HISTOGRAMS ARE RESULTANT TRACE LENGTH DISTRIBUTION FOR ELLIPSE ASPECT RATIOS 1.0, 0.7, 0.4, AND 0.1.

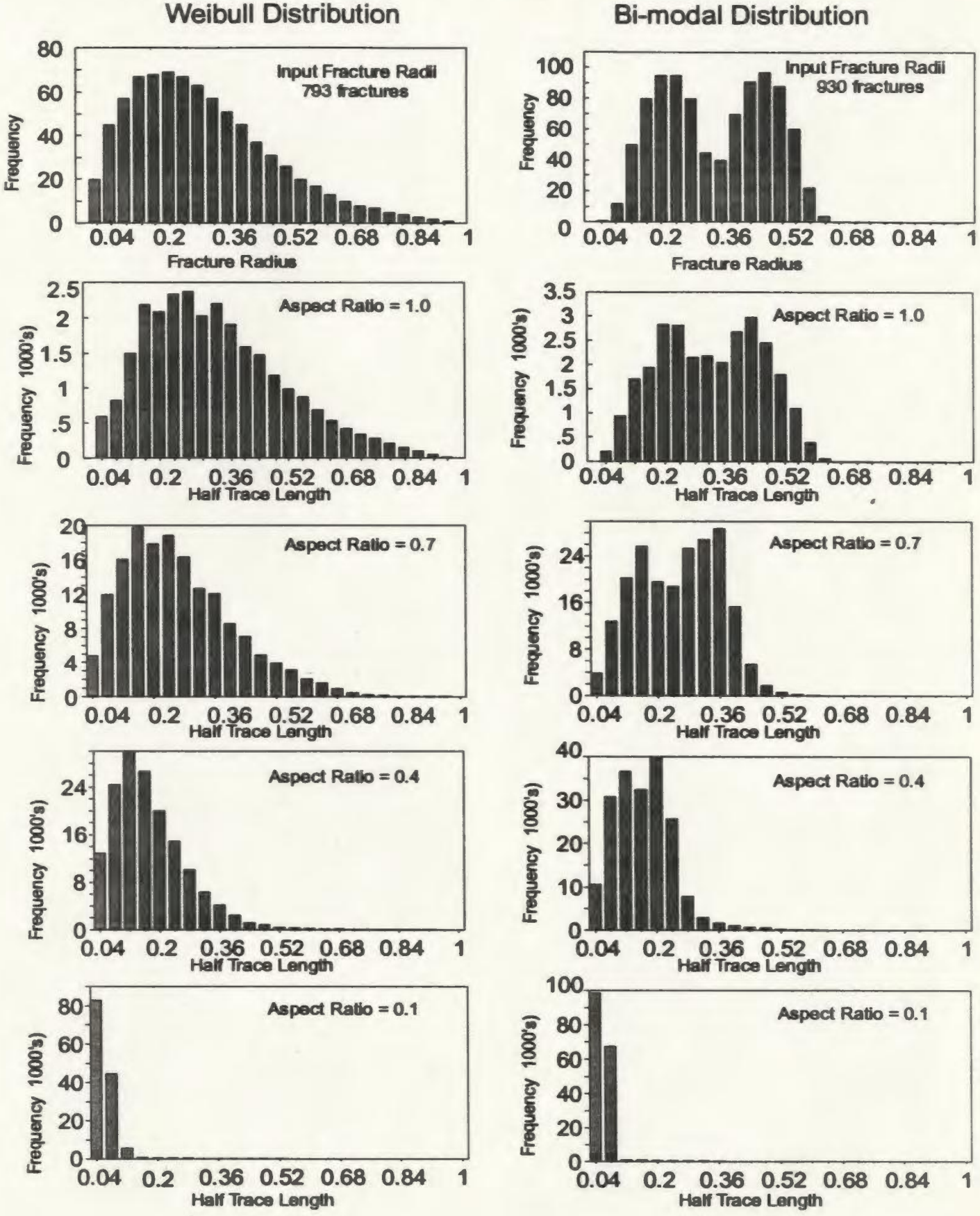
Weibull Distribution
Bi-modal Distribution
Input Fracture Radii
793 fractures
Input Fracture Radii
930 fractures
Frequency
Fracture Radius
Aspect Ratio = 1.0
Aspect Ratio = 0.7
Aspect Ratio = 0.4
Aspect Ratio = 0.1
Frequency 1000's
Half Trace Length

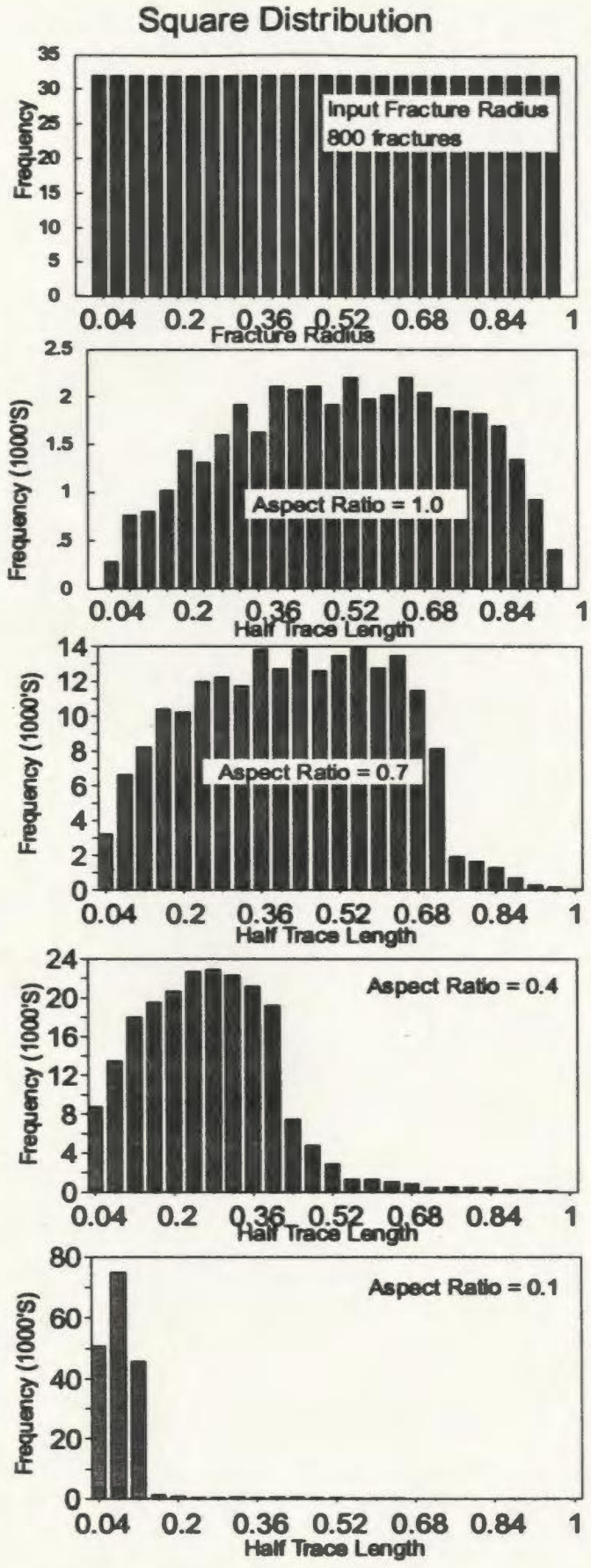
Square Distribution
Input Fracture Radius
800 fractures
Frequency
Fracture Radius
Aspect Ratio = 1.0
Frequency (1000'S)
Half Trace Length
Aspect Ratio = 0.7
Aspect Ratio = 0.4
Aspect Ratio = 0.1

B. DYKE DATA

B.1 DYKE ORIENTATION DATA

The standard approach of plotting orientations on a stereographic projection is difficult to apply meaningfully to an area whose domains are to be delineated on the basis of those orientations. A more useful approach is to treat each orientation separately by plotting them on a map and then interpreting the trends. Various methods of plotting dyke orientations (three-dimensional vectors) on a map (two dimensional surface) were implemented to extract information concerning domains.

Dyke orientation data (listed on the following pages) were obtained from various sources:

(1) Field data: 848 measurements

(2) Geological Map of the Amiandos-Palekhori Area compiled by Malpas, J. and Brace, T.; 1987; Geological Survey Department, Cyprus (Scale 1:10,000): 638 measurements (Sheeted Dyke Complex) and 313 measurements (Gabbro and Plagiogranite areas)

(3) Geological map of the Peristerona-Lagoudhera area in Carr, J.M. and Bear, L.M.; 1960; The Geology and Mineral Resources of the Peristerona-Lagoudhera Area; Geological Survey Department, Cyprus, Memoir #2 (Scale 1:31,680): 1068 measurements - dip azimuth only, dip was not available

(4) Geological map of the Akaki-Lythrodondha area in Bear, L.M.; 1960; The Geology and Mineral Resources of the Akaki-Lythrodondha Area; Geological Survey Department, Cyprus, Memoir #3 (Scale 1:31,680): 355 measurements

(5) Ramsden, T.W.; 1987; The Structural Geology and Paleomagnetism of the Sheeted Dyke Complex in the Mitsero-Arakapas Area, Troodos Ophiolite, Cyprus; Unpublished M.Sc. thesis, University of California, Davis (Scale 1:25,000): 409 measurements.

Total number of dyke orientation data points collected:

2250 orientations (Dip-Azimuth, Dip)
313 orientations (Dip-Azimuth, Dip) Dykes in gabbros
1068 orientations (Strike only) (from the Memoir #2 map)
3631 Total number of data points

Of these, 2250 measurements were within the Sheeted Dyke Complex and the Basal Group in the Spilia-Lythrodondha field area and consisted of both dip-azimuth and dip values. These dyke data were digitized from the maps to obtain their locations (in Universal Transverse Mercator grid eastings and northings).

Basic statistics of the dyke domains as delineated in Chapter 3 are presented below. This is followed by the listing of the dyke orientation data and a map of the dyke orientation data showing the relationship of the individual dykes to the dyke domains.

DYKE DOMAIN ORIENTATION DATA: SPILIA - POLITIKO AREA, TROODOS OPHIOLITE, CYPRUS

EIGEN ANALYSIS

DOMAIN	# Pts.	Eigen-values	Eigenvectors as Cosines:			Coordinates of Endpoints:		
1	194	0.7138	L: 0.9332	0.1210	-0.3382	Az.: 340.93	80.14	242.18
		0.1081	M: -0.3226	0.6965	-0.6409	Dip: 9.09	45.01	43.56
		0.1061	N: 0.1580	0.7073	0.6891			
2	513	0.7995	L: 0.7122	0.0155	-0.7018	Az.: 315.89	85.50	224.77
		0.1086	M: -0.6904	0.1965	-0.6963	Dip: 7.30	78.63	8.66
		0.0919	N: 0.1271	0.9804	0.1506			
3	411	0.7359	L: 0.4393	-0.0801	0.8947	Az.: 296.50	117.31	26.52
		0.1450	M: -0.8812	0.1551	0.4466	Dip: 10.05	79.95	0.16
		0.1191	N: 0.1745	0.9846	0.0028			
4	537	0.7338	L: 0.0075	0.2742	-0.9616	Az.: 270.47	56.12	173.51
		0.1533	M: -0.9062	0.4084	0.1094	Dip: 25.01	60.53	14.57
		0.1129	N: 0.4227	0.8707	0.2515			
5	419	0.7955	L: -0.5789	0.5198	-0.6283	Az.: 234.11	337.68	138.26
		0.1281	M: -0.8001	-0.2134	0.5606	Dip: 9.05	55.82	32.64
		0.0764	N: 0.1573	0.8272	0.5394			
6	129	0.5703	L: 0.2808	0.9145	-0.2912	Az.: 70.78	336.93	236.91
		0.3572	M: 0.8053	-0.3896	-0.4469	Dip: 31.47	6.26	57.77
		0.0725	N: 0.5221	0.1091	0.8459			
6A	66	0.8637	L: -0.2756	-0.9488	0.1547	Az.: 107.67	198.35	291.61
		0.0769	M: 0.8650	-0.3148	-0.3906	Dip: 24.79	1.48	65.16
		0.0594	N: 0.4193	0.0258	0.9075			
6B	63	0.8397	L: 0.8157	0.1487	-0.5590	Az.: 23.27	279.43	153.90
		0.1212	M: 0.3509	-0.8955	0.2738	Dip: 27.38	24.80	51.50
		0.0391	N: 0.4599	0.4195	0.7826			

FISHER ANALYSIS

DOMAIN	# Pts.	Total*			Res. Dir. Cos.			95% Level (degrees)	K**
1	194	60.66	36.05	0.52	0.8597	0.5108	0.0074	13.40	1.56
2	513	142.34	73.63	-78.70	0.7973	0.4124	-0.4408	8.50	1.53
3	411	139.69	49.30	-99.39	0.7831	0.2764	-0.5572	7.93	1.76
4	537	233.04	9.58	-284.10	0.6340	0.0260	-0.7729	4.12	3.16
5	419	116.04	-48.99	-117.02	0.6749	-0.2850	-0.6806	8.25	1.69
6	129	52.72	26.89	61.96	0.6153	0.3138	0.7231	8.87	2.96
6A	66	25.97	-15.16	45.63	0.4752	-0.2775	0.8350	8.03	5.73
6B	63	26.75	42.05	16.33	0.5100	0.8018	0.3114	8.09	5.88

* Total resultant vector ; ** K = (N - 1) / (N - R)

Easting	Northing	Az.	Dip	Easting	Northing	Az.	Dip	Easting	Northing	Az.	Dip	Easting	Northing	Az.	Dip	Easting	Northing	Az.	Dip
509993.2	3872962	111	60	516004.5	3866360	142	60	508480	3867480	66	60	498423	3867560	245	75	502300	3871550	70	47
510048.7	3872964	111	75	516101.2	3866112	143	60	508536.4	3867364	72	60	498659.3	3867374	218	60	502300	3871550	94	31
510134	3873063	66	65	515750.9	3865257	141	70	508608	3867273	61	70	498530.8	3867332	218	65	502300	3871550	85	37
510206.1	3873166	48	45	515412.9	3865756	139	60	508633.8	3867161	66	60	498387.8	3867364	241	65	502300	3871550	18	41
510357.2	3873267	66	65	515466	3865964	142	70	508498.4	3867151	64	65	498368.1	3867267	238	55	502300	3871550	48	50
510388	3873219	116	70	514918.4	3865367	144	60	508286.2	3866960	64	70	498620.1	3867203	240	60	502300	3871550	24	40
510048.7	3872808	96	64	514586.4	3865533	329	90	508254.9	3866910	76	70	498466.3	3867138	240	70	502300	3871550	16	47
510237.7	3872789	100	58	515473	3866867	152	90	508182.3	3866869	67	65	498684.5	3867096	226	60	502300	3871550	80	66
510410.3	3872781	106	66	515984.3	3867126	153	60	508166.8	3866763	72	60	498655	3866859	255	60	502300	3871550	18	27
510466.8	3872882	111	74	515178	3867225	136	70	508131.7	3866716	66	60	498684.3	3866731	270	70	501400	3870700	69	61
510588.3	3872852	96	66	515296.9	3867428	134	70	508196.7	3866562	114	60	498804.6	3866763	65	70	501400	3870700	65	67
510680	3873022	95	90	513272.3	3867538	130	60	508241.8	3866465	123	50	498656.7	3866543	71	40	501400	3870700	70	57
510736.4	3873026	287	60	514540.1	3866590	134	70	508258.8	3866368	102	50	499122.7	3867536	234	65	501400	3870700	40	57
510815.5	3873336	300	50	515020.4	3867740	133	70	508285.3	3866301	106	65	499240.7	3867389	251	60	501400	3870700	96	70
510783.3	3873901	116	71	515192.7	3867905	136	90	508311.4	3866182	136	60	499235.3	3867140	217	75	501400	3870700	51	58
510840.2	3873049	87	36	515091	3868103	131	90	507988.8	3867490	66	60	499321.5	3867482	241	60	501400	3870700	32	57
511080.4	3873148	203	45	514752.2	3868131	271	75	507951.4	3867422	58	65	499366.7	3867719	229	75	501400	3870700	62	32
511296.8	3873208	187	40	513985.9	3868814	324	60	507897	3867343	75	70	499143.3	3867847	57	65	501400	3870700	62	62
511310.5	3872899	203	45	514757.1	3868836	290	60	507883.5	3867148	82	70	499074.4	3868023	51	65	501400	3870700	43	67
511469.4	3873208	274	35	514639.1	3868783	315	70	507859.8	3867028	66	70	499020.7	3868019	225	65	501400	3870700	55	56
511468.8	3872828	183	55	515166.7	3869183	328	70	507819.5	3866962	67	65	498997.8	3868143	65	60	501400	3870700	57	62
511182.6	3872874	279	35	515382.8	3868830	323	70	507758.4	3866873	56	75	499036	3868182	62	65	501400	3870700	59	66
510978.6	3872783	330	52	515360.1	3869375	319	70	507687	3866847	77	65	499081.8	3868256	36	60	501400	3870700	51	49
510834.5	3872705	90	25	516013.4	3868948	318	90	507754.5	3866805	53	65	498167.5	3868220	219	90	501400	3870700	53	52
511730.3	3872801	186	81	515864.1	3869184	325	90	507674	3866778	53	70	498148.7	3868295	53	85	501400	3870700	57	57
511865.8	3872868	283	80	516071.1	3869489	328	90	507681.8	3866820	74	55	499206.5	3868311	62	90	501400	3870700	69	58
512106.5	3872769	205	45	516350.7	3868290	144	65	507609.8	3866556	71	60	499404.8	3868297	51	75	503780	3867830	158	84
512272.7	3872899	186	70	516328.3	3868960	317	60	507633.1	3866406	74	45	499499.5	3868263	55	60	501175	3869950	49	66
512356.8	3872533	189	64	516533.5	3869196	310	90	507622.1	3866183	281	55	499628.5	3868177	63	70	501175	3869950	55	72
512431.4	3872788	281	65	516541.8	3868974	318	75	507648.3	3866136	44	35	499702.7	3868155	66	75	501175	3869950	61	64
512511.7	3872824	292	60	516323.8	3868327	328	90	507792.4	3865937	294	77	499773.1	3868064	53	85	501175	3869950	76	64
512664.7	3872915	297	70	515998	3868132	151	80	507842.8	3865898	290	77	499532.4	3868025	54	90	501175	3869950	72	59
511875.1	3871988	192	65	515584.3	3868029	331	90	507842	3865748	271	71	499586.4	3867925	43	80	501175	3869950	87	66
511666.5	3871765	204	48	515468.5	3868251	318	90	507796.2	3865704	296	75	499679	3867908	55	80	501175	3869950	79	66
511673.2	3871535	280	55	516710.8	3868367	311	90	507460.7	3865383	294	67	499757	3867770	241	80	501175	3869950	81	76
511978.1	3871389	195	48	517028.4	3868565	128	80	507603.2	3865952	294	85	499478.3	3867576	55	90	501175	3869950	56	72
511659.2	3871148	273	50	517447.7	3868850	145	80	507506.8	3865900	291	75	499647.5	3867725	49	80	501175	3869950	92	70
511983.2	3871077	215	60	517852.5	3868261	129	85	507423.9	3865829	293	81	499823.3	3867574	38	90	501175	3869950	73	70
511919.3	3870924	187	70	513056.9	3868236	328	90	507368.8	3865863	69	85	499785.3	3867481	51	90	501175	3869950	70	64
511891.5	3870716	196	60	513106.3	3868996	328	80	507286.1	3865819	95	90	499611	3867416	58	80	501175	3869950	71	65
511842.6	3870376	196	72	513474.7	3865306	328	80	507331.4	3865754	294	77	499663.3	3867666	50	80	501175	3869950	81	59
511637.2	3870005	194	75	513184	3864966	305	80	507310.2	3865672	288	70	499663.5	3867388	59	85	501175	3869950	88	70
514088.9	3874467	270	65	512882.3	3864818	328	80	507241.8	3865567	285	77	497429.4	3870088	49	90	501175	3869950	82	53
514086.3	3874671	66	69	512487.7	3865518	327	90	507174.1	3865562	282	70	497321.5	3870062	54	90	501175	3869950	35	70
514321	3874818	192	75	512205.3	3865148	328	70	507145.8	3865563	296	66	497182.8	3870143	46	75	501175	3869950	70	73
514206.6	3874152	274	74	511856.3	3865139	120	80	507201.5	3865706	296	69	497081.4	3869981	41	90	501175	3869950	54	64
514694	3874496	119	65	511913.2	3865116	304	80	507076.2	3865474	287	65	497239.7	3869947	50	70	501175	3869950	69	60
517121.6	3872735	96	75	511892.9	3865512	319	90	506998.7	3865753	120	65	496521.7	3869990	31	60	501175	3869950	84	80
517226.6	3872841	114	90	511115.6	3864963	143	60	507380.2	3867420	87	60	496445.2	3870111	68	85	501175	3869950	108	85
517331.5	3872279	109	80	511131.3	3865220	16	80	507375.9	3867279	64	75	496367.3	3870174	64	75	501175	3869950	65	79
516846	3870946	116	78	511284.3	3865625	323	40	507443.8	3867183	78	65	496412.5	3870234	61	50	501175	3869950	84	79
516517.3	3870465	113	90	511629.4	3866173	128	60	507446.5	3867137	66	60	496493.1	3870214	78	65	501175	3869950	87	75
516323.6	3870121	118	80	511595.9	3866279	99	90	507466.9	3867077	55	80	503122	3866139	100	80	501175	3869950	70	75
513856.4	3869918	185	75	510617.8	3865258	145	50	507526.5	3866963	70	70	503108	3866148	93	76	501175	3869950	72	67
511859.3	3869434	191	65	510423.4	3865790	93	60	507490.2	3866936	93	75	503108	3866148	94	70	501175	3869950	51	70
511519.8	3868819	299	90	510327.3	3865949	133	40	507471.3	3866880	64	65	503108	3866148	120	65	501175	3869950	59	71
511488.9	3868047	267	60	510391.6	3866204	128	60	507402.5	3866902	60	60	503108	3866148	110	60	501175	3869950	68	71
511560.9	3868024	95	75	510694.3	3866583	124	70	507344.9	3866833	110	66	503099	3866153	1	57	501175	3869950	49	75
511514.7	3867701	109	79	509679.8	3866062	92	60	507290.5	3866713	106	64	503099	3866153	102	50	501175	3869950	50	75
511493.3	3867682	67	78	510200.4	3866710	130	65	507217.1	3866499	107	60	503257	3866060	90	40	498150	3868850	32	63
511163.9	3867575	103	60	523564.3	3865009	92	90	507148	3866591	109	60	503255	3866056	65	35	498150	3868850	42	63
510980.3	3867507	101	63	523605.8	3865309	138	90	507013.6	3866564	102	74	503255	3866056	105	45	498150	3868850	52	65
510791.5	3867521	119	71	522694.7	3865406	148	60	507228.1	3866223	117	77	503099	3866169	97	87	498150	3868850	42	65
511053.9	3867346	110	59	522543.4	3865854	73	60	507147	3866133	122	40	503099	3866169	77	83	498150	3868850	59	77
510714.4	3867199	113	65	523412.2	3866076	153	65	507057	3866118	109	42	503099	3866169	94	64	498150	3868850	58	82
510467.2	3866976	149	70	523299.1	3866166	148	60	507073.1	3866068	126	53	503099	3866169	100	47	498150	3868850	54	79
510312.3	3866823	152	71	523661.4	3866151	140	60	506983.9	3866177	93	78	503070	3866190	28	90	498150	3868850	54	69
510415.3	3866837	115	65	523660.8	3866129	200	55	506878.3	3866316	109	80	503280	3866078	114	57	498150	3868850	59	65
511416.8	3867026	97	61	524356.3	3866382	144	30	506899.2	3866013	65	80	503280	3866075	87	40	498150	3868850	70	76
511285.9	3866957	64	68	524188.4	3866538	89	40	507083.7	3865963	138	70	503280	3866075	100	28	498150	3868850	58	69
511390.2	3866953	103	73	524828	3866818	130	70	506778.1	3866278	110	65	503280	3866075	118	50	498150	3868850	45	66
511143	3866739	80	65	523024.9	3866387	119	60	506948.3	3866351	93	71	503280	3866075	85	50	498150	3868850	48	66
511111.4	3866644	108	76	522329.9	3865857	181	60	506528.8	3866431	269	85	503280	3866075	126	42	498150	3868850	50	68
511076.6	3866576	107	50	522090.7	3865967	148	60	506553.1	3866221	293	90	503087	3866165	108	57	498150	3868850	65	61
511037.4	3866362	100	68	522456.9	3866361	178	60	506468.1	3866232	268	90	503122	3866139	111	79	498150	3868850	67	66
511042.5	3866296	115	55	522491.6	3866541	181	60	506389	3866363	87	75	511550	3865500	112	72	498150	3868850	165	82
513726	3866233	286	65	522920.7	3866804	141	60	506285.4	3866262	78	90	511550	3865500	126	67	498150	3868850	40	64
514114.3	3868196	310	70	522976	3867358	48	60	506200.2	3866156	77	75	511550	3865500	119	50	498150	3868850	214	65
513566.8	3868694	273	82	523663.3	3866948	142	30	506786.7	3867606	75	68	511550	3865500	110	54	498150	3868850	54	67
513613	3868674	94	90	524144.8	3866847	178	60	506729.2	3867515	79	76	511550	3865500	133	66	498150	3868850	64	69
513678.1	3868576	302	77	524437.4	3867676	174	60	506688.4	3867465	79	78	511550	3865500	127	62	498150	3868850	66	63
513994.7	3868518	302	70	524388	3867742	176	50	506638.8	3867429	70	73	511550	3865500	114	60	498700	3869100	216	69
513561.4	3868381	183	65	524084.8	3867878	182	60	506631.7	3867414	62	71	511554	3865498	116	61	498700	3869100	52	74
513735	3868398	315	78	523863.3	3868158	134	90	506469.8	3867444	90	63	511554	3865498	120	75	498700	3869100	60	69
513911.4	3868378	286	65	523834.6	3868512	135	60	506453.4	3867357	90	74	511554	3865498	119	66	498700	3869100	215	81
514311.3	3868753	286	82	525215.3	3868255	138	60	506526.7	3867319	99	70	511554	3865498	132	62	498700	3869100	217	84
514508.2	3868856	307	90	525539.9	3868452	134	60	506433.8	3867347	67	90	511554	3865498	119	70	498700	3869100	200	74
513494.9	3867963	276	64	525783.3	3868435	138	60	506771.3	3867206	93	79	511554	3865498	114	71	498700	3869100	77	82
513521.9	3867264	304	90	526050.1	3868468	144	50	506678.7	3867230	90	75	511558	3865498	134	84	498700	3869100	46	85
513604.1	3866957	301	90	525869	3869062	135	80	506349.1	3867313	269	88	511558	3865498	313	69	498700	3869100	228	69
513304.5	3867347	280	80	526003.8	3868240	129	60	506640.4	3867302	271	90	511563	3865494	156	44	498700	3869100	48	74
513267.2	3866951	312	77	525049.3	3868854	160	50	506085.9	3867495	83	80	511563	3865494	145	70	498700	3869100	39	69
513116.6	3866835	317	78	525016.8	3868921	150	70	506022.5	3867549	91	60	511563	3865494	145	55	498700	3869100	42	84
512866.6	3866587	304	60	525308.9	3868462	126	80	506083.4	3867549	86	86	503980	3873470	163	84	498700	3869100	25	89
512630.9	3866620	307	90	524583.1	3868363	132	80	506730.9	3867319	249	84	503980	3873470	190	85	498700	3869100	36	85

Easting	Northing	Az.	Dip	Easting	Northing	Az.	Dip	Easting	Northing	Az.	Dip	Easting	Northing	Az.	Dip	Easting	Northing	Az.	Dip
513001	3866382	333	90	524899.9	3868833	136	80	506529.8	3867532	84	76	503680	3873470	85	84	498700	3869100	48	84
508622.8	3864138	108	89	525382.7	3870007	130	70	505512.5	3867807	87	71	503600	3873190	82	65	498700	3869100	228	60
508848.7	3864307	124	65	520899.6	3868831	175	75	505434.8	3867566	74	75	503500	3874580	315	66	498700	3869100	54	78
508838.5	3864858	122	66	521233.1	3867065	157	70	505374.4	3867804	84	75	503364	3868050	138	47	498700	3869100	240	69
509175.8	3865235	124	84	521526.1	3867490	144	60	505337.3	3867575	92	70	503085	3868174	84	45	498700	3869100	212	65
509339.2	3865395	145	68	522011.8	3867637	178	60	505283.8	3867597	74	70	503085	3868174	84	63	498700	3869100	233	63
509401.2	3865456	120	77	522305.7	3868323	147	60	505210.5	3867600	82	68	504200	3868890	76	76	498700	3869100	206	65
509579.1	3865365	123	64	522996	3868901	142	50	505029.9	3867513	111	58	504200	3868890	66	74	498700	3869100	37	63
509843	3865480	149	71	522819.8	3869165	133	50	504168.8	3868123	84	75	504200	3868890	92	77	498700	3869100	26	60
509928.5	3865686	125	72	522984.8	3869449	134	80	504026.1	3868094	82	70	504200	3868890	80	67	498700	3869100	217	60
509917.1	3865960	134	60	523317.8	3869243	136	80	503884.4	3868107	66	70	504200	3868890	96	71	498700	3869100	4	61
510111.4	3865997	154	60	523478.7	3869394	131	55	503783.6	3868111	74	75	504200	3868890	66	77	498700	3869100	218	66
510269.7	3865725	130	48	523663.4	3869979	156	60	503717.7	3868078	70	60	504200	3868890	95	67	499025	3868750	60	21
510401.9	3865784	116	60	523990.7	3870224	122	70	504182.2	3868361	72	75	504200	3868890	96	76	499025	3868750	64	30
510488.7	3865814	122	71	522732.8	3870555	121	80	503831.2	3868023	78	80	504200	3868890	86	81	499025	3868750	65	32
510597.5	3865659	139	50	522684.8	3870856	130	75	503770.3	3868026	66	65	504200	3868890	91	75	499025	3868750	72	38
510534.9	3865564	135	68	522780.4	3870900	140	60	504125.8	3867675	81	80	504200	3868890	81	85	499025	3868750	97	37
510329.6	3865456	111	55	522885.7	3871110	137	60	504176.3	3867646	357	80	504200	3868890	88	74	499025	3868750	49	25
510102.5	3865371	114	63	523096.1	3871032	123	60	506359.8	3866360	66	75	504200	3868890	116	69	499025	3868750	64	45
510659.6	3865259	145	69	521998.8	3870869	86	70	506377	3866864	90	90	504187	3868890	76	72	499025	3868750	41	40
510540.6	3864946	112	64	521606	3869782	147	70	506551.2	3866826	94	85	504187	3868890	66	65	508800	3874150	125	58
510443.7	3864773	107	48	521165.8	3869736	146	70	506509.2	3866736	66	80	504187	3868890	73	66	508800	3874150	142	60
510492.5	3864596	148	50	520818.2	3869904	138	90	506351.4	3866576	77	82	504187	3868890	75	76	508800	3874150	63	58
510480.4	3864446	139	50	520932.9	3869788	132	90	506124.6	3865661	94	60	504187	3868890	73	66	508800	3874150	64	39
510531.1	3864259	151	60	520132.2	3869371	137	90	506496.2	3866415	66	72	504187	3868890	121	64	508800	3874150	150	78
510396.9	3864226	148	61	519447.9	3868712	131	90	506673.4	3866307	81	73	504187	3868890	116	64	508800	3874150	141	51
510369.7	3864143	140	74	519534.2	3868818	116	90	506057.5	3866232	85	63	504187	3868890	76	75	508800	3874150	174	64
510498.8	3863914	324	90	519312.6	3868506	136	90	506121.2	3866096	73	65	504187	3868890	77	73	498150	3868850	72	44
510501.3	3863803	145	50	520421.1	3867975	179	60	506236	3866348	66	65	503300	3868075	107	67	498150	3868850	131	65
510331.7	3863639	138	50	520443	3867950	135	60	506516.8	3866366	111	76	503290	3868078	100	40	498150	3868850	149	63
510296.3	3863457	343	55	520705.1	3867815	134	60	506561.3	3866425	90	78	503290	3868076	67	34	508800	3874150	112	58
511513.5	3864426	117	74	521053.3	3867904	137	60	506761.4	3866343	272	79	503285	3868078	104	48	508800	3874150	120	57
511002.7	3865969	116	60	521279.5	3868065	132	65	506280.3	3866139	66	79	503285	3868078	107	44	508800	3874150	122	30
511140.7	3865751	111	74	521496.8	3868581	129	60	506565.2	3866199	84	76	503285	3868076	74	38	507750	3874875	38	11
511235	3865607	115	73	522421.1	3869624	128	60	506269.8	3866001	101	47	503278	3868071	118	39	507750	3874875	243	34
511566.6	3865456	126	75	520897.1	3870106	140	70	505996.4	3864822	106	75	503270	3868068	96	40	507750	3874875	224	22
511579.3	3865533	96	90	521063.1	3870400	146	65	506125.8	3864617	61	53	503285	3868064	290	43	507750	3874875	3	72
511773	3865515	116	69	521465.3	3870712	137	90	506250.4	3864778	68	52	504177	3868895	84	78	507750	3874875	200	78
512192.1	3865437	133	66	521290.1	3871532	101	90	506439.7	3864718	90	54	504177	3868895	83	77	507750	3874875	166	19
512159.1	3865048	321	76	521111.1	3871706	110	70	506506.9	3864711	119	70	504177	3868895	67	68	507750	3874875	82	5
512240.8	3865083	118	70	521022.4	3871632	121	70	506581.9	3864760	103	64	504177	3868895	72	70	513759.3	3869876	294	66
512675.1	3865600	325	60	520259.2	3871913	93	90	506582.1	3864653	114	70	504177	3868895	80	82	513782.4	3869867	282	76
511474.3	3863320	326	60	520056.5	3871785	294	60	506665	3864927	60	58	504177	3868895	94	76	513781.9	3869050	311	39
511626.2	3863581	317	65	518168	3870276	114	60	506783.1	3864956	261	76	504600	3868960	61	74	513701.7	3869245	312	18
511691.3	3863932	306	61	518278.7	3870874	125	70	506788.8	3865019	261	60	504600	3868960	106	79	513701.7	3869245	125	61
511680	3864233	289	75	518386.9	3871411	138	90	506977.3	3865100	265	60	506517	3873037	75	50	513674.8	3869065	290	70
511665.4	3863096	314	76	517231.4	3870224	141	90	506947.1	3865019	273	76	506517	3873037	96	60	513635.1	3868952	168	64
511840.1	3863447	321	50	517080.8	3870033	116	90	506986.8	3864990	271	72	506517	3873037	181	51	513622.3	3868892	246	56
511964.6	3863572	298	90	517246.1	3870046	122	76	506855.3	3864656	269	70	506517	3873037	183	60	513619.7	3868730	307	67
512131.9	3863468	304	56	516904.3	3870011	132	90	506926.8	3864766	112	58	506517	3873037	181	65	513597.9	3868670	280	57
512063.6	3863670	305	79	516834.4	3870463	136	90	506994.8	3864909	66	61	506527	3873040	92	40	513623.5	3868604	279	70
512233.2	3863714	336	78	516463.3	3870086	136	90	507096.7	3864792	69	61	506527	3873040	104	50	513604.2	3868523	270	73
512490.2	3863636	304	90	516471.5	3870086	140	90	507147.8	3864679	69	76	506527	3873040	105	40	513604.2	3868523	16	48
512063.8	3863880	334	66	516425.9	3870356	139	90	506990.5	3864556	142	65	506527	3873040	110	45	513682.6	3868586	306	73
512437	3863944	306	70	517066.3	3870924	121	90	505797.2	3866061	61	60	506527	3873040	109	52	514193.7	3868406	286	72
512704.1	3864044	320	76	515609.2	3869643	320	70	505422.3	3866404	60	64	506527	3873040	96	44	514868.8	3867853	128	60
512982.7	3864203	324	90	515398.6	3869940	323	75	505400	3866247	34	78	506527	3873040	306	33	514863.5	3867852	310	65
513105.5	3864487	314	79	515054.8	3869807	328	60	505398.7	3866217	66	90	506527	3873040	310	59	514863.5	3867852	298	69
512992.2	3864646	310	90	515081.7	3870008	250	90	505304.8	3866162	93	88	506546	3873050	72	65	514072	3868377	285	67
513327.6	3864529	316	90	515180.6	3870428	270	90	505186.7	3866106	60	90	506546	3873050	71	60	513910.5	3868312	264	75
513493.5	3864301	312	84	515283.5	3870416	296	90	505056.1	3866152	67	90	506546	3873050	92	47	513645.3	3868163	331	73
512604.1	3864723	312	85	515747.3	3871618	310	75	505030.9	3866172	82	90	503190	3868060	106	79	513687.1	3867853	316	65
512323.7	3864446	307	90	515656.9	3871998	126	65	504984.2	3866114	216	55	503190	3868060	282	60	513617.1	3867921	319	60
512364.5	3864297	310	62	515789.6	3872642	55	65	505097.7	3866488	66	90	503190	3868060	125	60	513588.4	3867872	284	75
512230.7	3864562	126	60	515635	3872868	124	55	504821.2	3864636	66	40	503190	3868060	336	65	513403.2	3867277	266	61
512609.2	3865023	316	90	517752.2	3871772	123	90	504747.8	3864633	84	45	503190	3868060	80	75	513164.1	3866662	290	74
512607.3	3865017	315	90	518202.2	3872890	312	65	504686.7	3864763	96	65	500620	3869330	38	64	512827.9	3865261	315	67
513256.8	3865180	303	90	516623.6	3872914	317	70	504690	3864932	112	65	500620	3869330	70	60	512626	3865026	322	60
512476.8	3863016	317	90	516303.8	3873309	266	60	504784.4	3865037	104	58	503600	3873190	186	67	512540.9	3864906	306	66
512688.2	3863187	319	90	515671.9	3873495	82	70	504776.5	3865116	106	60	512400	3872900	187	40	512484.5	3864896	289	73
513340.9	3863203	310	85	515832	3873310	269	60	504756	3865238	78	66	512400	3872900	261	62	512428.2	3864634	132	74
513865.7	3863610	150	80	516075.2	3873122	266	90	504891.1	3865417	66	65	512400	3872900	196	39	512456.3	3864371	316	70
513860.9	3864216	142	86	516122.4	3873101	100	75	504658.6	3865651	96	66	512400	3872900	287	60	512467.9	3864216	316	69
513672.6	3864261	330	90	516077.6	3873324	141	75	504657.5	3865652	103	40	512400	3872900	280	77	512467.9	3864219	301	69
513823.3	3864366	142	85	514940.1	3872970	107	50	504625.3	3865710	79	30	512400	3872900	82	68	512394.6	3864159	175	84
514246.1	3863589	326	61	514797.7	3872263	92	70	504630.9	3865706	66	55	512400	3872900	288	84	512329.8	3863921	341	72
514891.7	3864367	324	90	514652.9	3871241	318	60	504676	3865785	112	45	512400	3872900	271	64	512238.7	3863764	335	63
514553.1	3864687	337	90	514751.3	3871204	323	90	504683.6	3865851	106	50	512400	3872900	296	65	512088.8	3863812	349	65
514765.2	3865426	150	76	514814	3871007	315	60	504616.4	3865666	60	45	512400	3872900	289	41	512243.9	3863974	138	67
515065.2	3865363	141	62	514858.8	3870736	293	70	504577.5	3865962	96	55	512400	3872900	290	40	512236.2	3864068	115	55
515403.2	3865209	129	76	513919.8	3872707	149	90	504469.1	3865943	106	65	512400	3872900	26	69	512234.9	3864188	228	55
515429.2	3865425	150	75	513643.1	3872751	322	65	504306.7	3866030	101	60	512400	3872900	284	60	512251.6	3864261	296	79
515784.3	3864531	142	74	513438.9	3873007	312	90	504287	3864679	90	60	512400	3872900	290	71	512277.2	3864361	310	70
515571.6	3863966	317	90	514176.1	3871100	252	60	504249.1	3864616	81	90	512400	3872900	267	60	512291.3	3864485	132	66
515621.6	3863726	160	82	514088.8	3871030	253	70	504126.1	3864666	66	60	512400	3872900	269	57	512206.3	3865263	60	65
515566.3	3863452	164	77	513657.2	3870871	304	60	504187.3	3864646	60	65	512400	3872900	284	60	512204.1	3865259	310	62
516003.3	3863460	156	82	513906.9	3869905	318	70	504006.9	3864532	96	70	512400	3872900	276	63	511974.7	3865494	135	76
515581.5	3862976	176	76	513691.1	3869880	321	60	503894.4	3864666	73	65	512400	3872900	261	66	511868.4	3865480	260	10
516116.5	3863126	139	82	513688.7	3869520	324	50	503825.3	3864633	96	50	512400	3872900	301	61	511837.8	3865602	128	89
510141.2	3863198	302	84	513749.7	3869373	275	50	503543.5	3864665	66	50	512400	3872900	290	48	511837.8	3865602	130	28
508404.2	3862975	354	83	513570.7	3869277	320	60	503690	3864619	66	60	512400	3872900	288	56	511836	3865630	129	84
517588.3	3862941	177	65	513604.1	3869066	297	60	503702.3	3864621	97	60	512400	3872900	270	57	511850.3	3865518	133	79
517449	3863232	157	60	514060.5	3869159	312	70	503722	3866612	66	50	512400	3872900	288	66	511841.4	3865511	120	66
517583.8	3863248	176	70	514076.4	3869026	276	60	503836	3865654	69	55	512400	3872900	183	76	511824.7	3865644	293	85
517730.7	3863302	181	80	513539.8	3868391	320	70	503891	3865756	74	50	512400	3872900	298	72	511824.7	3865644	149	76

Easting	Northing	Az.	Dip	Easting	Northing	Az.	Dip	Easting	Northing	Az.	Dip	Easting	Northing	Az.	Dip	Easting	Northing	Az.	Dip
518238.7	3862872	281	30	513517.8	3867765	321	90	503987.3	3868836	119	40	512400	3872900	61	84	511314.5	3865537	109	66
518056.7	3863004	142	55	513444.8	3867296	318	90	504084.1	3868575	109	50	512400	3872900	271	85	511187.8	3865730	107	53
518059.3	3863095	158	70	513627.7	3866978	325	90	504122.2	3868802	107	45	512400	3872900	282	81	511187.8	3865730	122	81
518100.4	3863526	139	65	512910	3866871	340	85	504072	3868795	107	45	511575	3872900	199	58	511082.5	3866180	84	90
518020.8	3863857	168	70	512746.4	3866993	337	70	504220.8	3868865	98	50	511575	3872900	199	64	511082.5	3866180	294	65
517909.8	3864234	173	71	512636.8	3865891	311	60	503987.4	3868185	108	35	511575	3872900	183	66	511112	3866349	113	64
517481.7	3864406	120	30	512348.5	3865966	131	60	504030.1	3868106	110	50	511575	3872900	204	70	511129.8	3866340	114	73
518001.7	3864417	182	55	512223.3	3866843	318	90	504126.2	3868084	110	45	511575	3872900	182	70	511215.8	3866577	104	53
517940.3	3864496	173	68	512396.8	3866745	317	65	504182.5	3868178	118	45	511575	3872900	220	61	511211.8	3866575	50	62
518036.5	3864518	139	45	512513.7	3866915	321	70	504151.1	3868258	107	45	511575	3872900	192	57	511444	3866842	109	63
518256.8	3864664	142	55	512397.4	3867230	322	60	504202.2	3868325	110	40	511575	3872900	189	61	511538.8	3867290	121	54
518410.6	3864446	170	75	512562	3867477	276	60	504275.6	3868367	123	50	511575	3872900	270	67	511532.4	3867268	346	22
518299.4	3864675	155	70	512798.5	3867837	252	90	504318.3	3868453	91	50	511575	3872900	203	69	511497.8	3867539	188	72
518171.3	3865039	150	70	512647.3	3868137	247	70	504277.7	3868486	104	35	511575	3872900	272	65	511604.2	3868202	273	59
518059.4	3865018	152	60	512765.2	3868831	274	60	504212.2	3868527	98	60	511575	3872900	300	66	511604.2	3868068	284	57
518171.3	3865200	111	69	513004.4	3868310	240	70	504185.8	3868580	98	60	511575	3872900	186	67	511865.7	3868877	284	49
518365.5	3865216	153	71	513116.3	3868610	234	60	504120.8	3868664	98	75	511575	3872900	271	48	511873.4	3868840	309	81
518175.7	3865374	122	75	512634.2	3870030	280	60	504102.5	3868742	82	60	511575	3872900	181	55	511873.4	3868840	347	62
517781.4	3865384	168	73	513006.2	3870345	296	70	504331.3	3868803	81	60	511575	3872900	284	60	511842.8	3870152	304	60
517902.8	3865943	157	78	512347.7	3870388	265	60	504418.3	3868851	98	75	511575	3872900	195	65	511538.8	3870239	280	70
517576.2	3866226	122	74	513161.6	3871000	302	60	504384.3	3868708	98	75	511575	3872900	183	61	511787.5	3870449	210	60
517636.4	3866367	185	65	512748.1	3871305	296	70	504647.7	3868728	85	60	511575	3872900	187	60	511787.5	3870449	208	60
517582	3866833	139	78	512557.7	3871383	294	65	504670.2	3868847	98	60	511575	3872900	270	49	514198.8	3874498	272	54
517942.8	3866813	127	73	512691.1	3872143	283	60	504590.8	3868966	95	50	511575	3872900	271	68	514198.8	3874489	282	84
518204.8	3866899	137	70	513136.2	3872810	282	60	504600.2	3868568	78	60	511575	3872900	279	78	511737.5	3872932	274	70
517845.9	3866780	142	72	512914.1	3873039	317	60	504668.7	3868648	95	60	511575	3872900	202	62	510786.3	3872443	166	85
517725.7	3866877	143	72	513106.9	3873244	284	70	504763.8	3868586	86	60	511575	3872900	192	55	510988.9	3872348	53	43
517774.4	3866864	130	69	513353.4	3873435	280	90	503781.8	3868731	94	90	511575	3872900	168	52	510899.2	3872236	292	62
517946.6	3867130	129	68	513437.3	3873595	297	80	503323.7	3864673	78	70	511575	3872900	185	55	510985.8	3872138	264	46
518505.5	3867200	143	80	512414.4	3873029	318	55	503225.8	3864811	107	45	511575	3872900	188	59	510906.8	3872082	29	12
518142.8	3867530	134	80	512131.3	3872800	301	70	503194.3	3864980	94	55	511575	3872900	184	63	510983.8	3871988	93	82
518339.1	3867571	120	85	511936	3872487	279	80	503168	3864984	88	50	511575	3872900	270	62	510983.3	3871951	276	84
518289.4	3867857	100	74	511857.2	3872133	255	80	503318.5	3864931	87	40	511650	3870850	354	77	511024.8	3871858	198	70
518578.8	3868611	137	66	511888	3871914	245	75	503234.7	3865060	78	45	511650	3870850	354	79	510915.8	3871755	270	81
518007.1	3868065	140	75	511636.2	3871661	318	70	503106.8	3865078	91	55	511650	3870850	205	50	510701.8	3865653	340	40
518235.8	3868291	143	70	511677.5	3871485	233	70	503023.5	3865175	77	50	511650	3870850	206	78	510624.8	3865520	286	78
518314.7	3868578	134	81	511686.4	3871365	135	60	503078.8	3865223	81	40	511650	3870850	208	54	510385.8	3865583	122	43
518326.1	3868448	136	65	511814.8	3871189	278	90	502997.2	3865250	90	45	511650	3870850	220	78	510276.2	3865619	135	75
518611	3868438	144	68	511800.1	3870539	245	80	502995.7	3865222	81	50	511650	3870850	274	57	509972.3	3865503	119	53
518448.4	3868255	132	70	511845.5	3870442	253	80	502872.3	3865282	73	40	511650	3870850	69	54	509972.3	3865503	122	43
518659.1	3868168	132	65	511750.5	3870227	238	60	502787.8	3865341	72	40	511650	3870850	218	68	509659.6	3865314	284	35
518880	3868378	115	71	511496.3	3870106	63	85	502907.9	3865539	67	35	511650	3870850	204	55	509660.9	3865314	110	58
517035.7	3868613	138	77	511683.9	3869755	232	90	502956.3	3865533	82	45	511650	3870850	201	48	509660.9	3865315	102	52
517239.5	3868795	130	63	511639.8	3869660	250	60	502970	3865902	66	40	511650	3870850	183	47	509492.9	3865081	10	87
515450.7	3865751	158	70	511820.5	3869224	287	80	502954.2	3865837	100	60	511000	3866250	109	40	509356.8	3865022	157	44
515350.7	3865996	149	71	511579.8	3869027	296	60	503174.1	3865953	78	30	511000	3866250	143	50	509060.9	3864930	109	46
515284.3	3865827	207	78	511975.9	3868506	303	60	503114	3866062	138	50	511000	3866250	138	39	509059.7	3864928	128	81
515081	3866142	279	79	511856.3	3868116	312	30	503324.3	3866065	138	60	511000	3866250	99	35	508880.2	3864902	120	60
515086.1	3866406	294	65	511720.4	3867973	306	90	503469	3866079	132	65	511000	3866250	103	34	508880.2	3864902	122	80
515272.8	3866870	355	80	511753.8	3867809	139	60	503302.3	3866453	100	35	511000	3866250	107	43	508804.8	3864873	287	70
515666.4	3866860	306	75	511606.5	3867827	132	90	503256.7	3866453	107	20	511000	3866250	300	75	508672.5	3864840	135	77
516121.7	3867107	218	84	511477.1	3867520	114	60	503138.1	3866454	102	40	511000	3866250	118	48	508532.8	3864281	325	44
515675.4	3867286	274	65	511336.3	3867128	136	60	503070.5	3866444	100	25	511000	3866250	121	55	507534.2	3863550	313	61
516078.7	3868487	116	81	511185.8	3866862	130	90	503042.4	3866374	110	45	511000	3866250	131	48	507706.8	3865142	278	85
515910.3	3868151	115	90	510847.1	3867526	137	60	503017.8	3866423	100	30	511000	3866250	80	66	507578.2	3865137	122	87
515724.2	3868602	10	90	509762.7	3867410	128	70	503145	3866878	84	40	511000	3866250	86	62	507432.9	3865115	324	74
516196.3	3868644	341	90	509957.1	3867819	119	70	503093.1	3866836	107	30	511000	3866250	122	56	507352.2	3865034	280	60
516514.8	3868692	78	90	509924.6	3868562	136	70	502970	3866566	87	15	511000	3866250	282	85	507281.2	3865107	25	89
516926.7	3868253	144	90	509774.9	3868433	143	90	502948	3866541	109	30	511000	3866250	93	69	510814.7	3873004	128	82
516419.8	3868114	136	67	509754.5	3868769	99	80	502918.8	3866511	109	50	511000	3866250	171	70	510564.5	3873077	103	74
516102.7	3867762	181	81	510001.1	3868790	107	30	502917.1	3866836	104	30	511000	3866250	281	10	510387.9	3873136	110	62
515777.9	3867587	159	74	510126.4	3868954	129	60	502877.5	3866868	121	25	511000	3866250	165	43	510223.9	3873160	104	77
515627.9	3867436	191	88	510621.9	3868917	117	60	502784.4	3866863	128	40	511000	3866250	135	88	510181.8	3873083	354	78
515404.5	3866787	235	80	510722	3868897	321	60	502738.8	3866375	134	50	509200	3864950	116	61	509877.9	3872940	87	91
515148.8	3866760	238	85	510656.4	3868990	146	60	502670.1	3866247	131	50	509200	3864950	116	74	509738.8	3873251	126	82
514948.1	3866810	248	78	511027.9	3869062	71	90	502687.5	3866156	128	60	509200	3864950	141	76	509701.1	3873475	110	87
514758.9	3866799	102	78	511254.2	3869499	71	90	502784.2	3866174	142	35	509200	3864950	135	81	509706.8	3873738	114	66
514624.6	3866287	6	80	511041.8	3869874	91	90	502814	3866166	143	45	509200	3864950	139	71	509707.5	3873738	128	78
514757.6	3866172	36	84	510866.8	3869899	59	90	502880.3	3866156	136	40	509200	3864950	142	43	509630.8	3873931	130	70
514606.2	3867978	335	85	511189.9	3869890	124	90	502927.1	3866172	137	50	509200	3864950	148	65	509534.5	3874184	113	52
514600.4	3867878	42	90	511356.8	3871248	322	90	502518.4	3866269	128	50	509200	3864950	137	66	509378.9	3874140	150	57
515010.6	3867778	32	83	511233.8	3871208	81	90	502485.7	3866258	87	55	511000	3866250	147	68	509274.4	3874167	331	70
515248.4	3867224	183	80	510931.1	3871529	90	70	502378.5	3866333	116	40	511000	3866250	125	77	509274.4	3874167	148	62
509124.5	3862208	181	70	511194	3870954	128	65	502288	3866348	87	63	511000	3866250	158	61	509215.5	3874119	116	66
509288.6	3862128	208	77	510919.8	3871545	95	90	502188.5	3866402	80	70	511000	3866250	136	65	509086.8	3874130	106	75
509398.2	3862202	144	76	511473.9	3871997	316	50	502130.9	3866344	93	55	511000	3866250	132	61	508897.7	3874236	116	57
509452.5	3861960	310	81	511578.1	3871899	280	60	502090.5	3866330	90	50	511000	3866250	301	69	508823.4	3874125	142	52
509548.3	3862257	300	84	510674.2	3872330	94	90	501897.7	3866290	106	75	511000	3866250	128	79	508823.4	3874125	131	70
509548.3	3862531	116	76	510846.3	3872854	87	70	501902.8	3866308	96	70	514050	3868550	304	78	508823.4	3874125	106	80
509700.4	3862281	302	82	510866.1	3872803	121	90	501354.5	3865868	109	90	514050	3868550	294	80	508838.8	3874135	141	52
509879	3862196	305	88	510932.8	3872887	47	90	501590.1	3865914	106	55	514050	3868550	306	68	508710.6	3874084	121	65
510148.2	3862332	308	83	510671	3872756	120	80	501658.1	3865898	99	60	514050	3868550	315	54	508509.4	3874162	124	55
509629.9	3861754	342	90	511094.7	3873048	276	65	501379.3	3865824	94	90	514050	3868550	196	61	508172.4	3874328	129	45
509604.8	3861556	336	90	511649.7	3873022	299	60	501699.3	3865276	94	90	514050	3868550	306	68	508007.1	3874151	104	68
509726.3	3861192	334	87	511736.4	3873456	291	40	501599	3864738	287	85	514050	3868550	141	59	508039.2	3874388	118	70
509838.9	3861177	332	90	511503.2	3873687	101	90	502259.8	3864486	273	80	514050	3868550	301	68	508035.3	3874388	116	56
509876.4	3861099	10	85	511422.7	3873430	237	90	502367.8	3864424	276	80	514050	3868550	315	75	507970	3874484	123	50
509774.8	3860931	340	78	511141.1	3873831	139	90	502320.2	3866561	90	45	514050	3868550	265	65	507964.8	3874479	95	36
509897.1	3860847	337	74	510923.8	3873135	323	65	502382.6	3866848	93	66	514050	3868550	286	84	507973.8	3874484	138	30
509814.8	3860733	348	90	511440.8	3873781	327	90	502384.6	3866590	99	60	512150	3863900	328	69	507918.7	3874534	128	79
509841.5	3860540	343	88	511652.1	3874060	62	50	501276.8	3867722	234	75	512150	3863900	320	82	507882.3	3874581	145	80
510209	3861179	311	80	511388.9	3873990	333	30	501483.2	3867717	70	75	512150	3863900	112	77	507822.8	3874631	85	36
510393.4	3861180	328	82	511257.5	3874060	131	90	501512.3	3867628	80	90	512150	3863900	332	64	507823.9	3874631	107	63
510650.3	3861261	348	82	511007.7	3873851	250	90	501656.8	3867611	77	90	512150	3863900	318	78	507840.5	3874722	160	20
510821.8	3861412	344	79	511010.1	3874656	307	70	501789	3867507	48	60	512150	3863900	138	72	507840.5	3874722	92	24

Easting	Northing	Az.	Dip	Easting	Northing	Az.	Dip	Easting	Northing	Az.	Dip	Easting	Northing	Az.	Dip	Easting	Northing	Az.	Dip
511241.8	3861561	314	75	510650.4	3875496	85	90	501679.5	3867325	87	80	512150	3863900	333	87	507778.5	3875012	77	35
511234	3861636	344	67	510465.7	3875488	100	70	502239.9	3867310	83	70	512150	3863900	347	80	508810	3877837	43	27
511573.7	3861533	330	75	510050.7	3875168	78	80	502419.4	3867318	333	75	512150	3863900	329	87	508843.8	3869487	82	36
511862.3	3861448	346	80	510057.2	3874825	135	80	507328.2	3866504	180	90	512150	3863900	87	71	508848.2	3868468	90	40
512286.8	3861784	310	90	509699.3	3874636	116	80	502347.3	3867116	87	72	512150	3863900	304	81	508606.1	3868652	88	64
512246.7	3861896	310	90	509614.8	3874449	127	80	501977.8	3866878	231	90	512150	3863900	134	83	508396.4	3868031	72	84
512180.7	3862060	332	55	510237	3875017	113	90	501180.7	3866709	240	80	512150	3863900	329	82	508769.3	3868858	58	39
512277.1	3862223	332	90	510158.1	3875899	103	80	501238	3866581	236	80	512150	3863900	314	49	508618.1	3868820	217	74
512660.2	3862312	318	90	509922.1	3875529	92	70	501240.3	3866478	236	85	512150	3863900	319	57	508628.3	3868819	158	65
512634.3	3862554	312	80	509650.5	3875700	83	90	501234.2	3866330	243	80	512150	3863900	297	74	508628.3	3868818	70	76
512622	3861477	309	85	510158.7	3875536	100	90	501235	3866104	230	90	512150	3863900	328	77	508668	3868818	318	82
512647.8	3861389	337	90	510024.6	3876869	118	90	501183.8	3866102	228	90	512150	3863900	317	70	508668.8	3868813	215	88
512864	3861487	338	90	509851.3	3874181	105	70	501228.3	3867849	227	75	512150	3863900	323	55	508891	3868868	71	61
512899.6	3861262	78	74	510178	3874178	109	70	501168.3	3867858	230	80	512150	3863900	320	84	506764.2	3867017	70	61
512720.3	3861149	303	90	509991.3	3873901	107	70	501125.7	3867709	230	90	512150	3863900	309	78	506757.5	3867032	48	80
512754.8	3861148	336	90	509805.8	3873061	101	50	500957.3	3867812	58	80	510275	3863450	126	78	506758.8	3867023	348	68
512460.3	3861027	328	80	509882.2	3873482	64	70	500891.8	3867863	236	90	510275	3863450	155	68	506758.8	3867026	48	78
513186.4	3861174	143	81	510087.8	3872163	253	75	500893.3	3867806	243	90	510275	3863450	141	88	506945.6	3867077	87	97
513252.9	3861034	142	80	510399.2	3873263	300	85	500851.1	3867868	243	80	510275	3863450	153	46	507091.8	3867105	355	10
513129.3	3860860	160	69	509699.4	3871300	61	80	500821.1	3868044	227	90	510275	3863450	328	54	507123.8	3867081	18	31
513586.1	3861207	161	78	509944.8	3871189	114	85	500777.6	3868047	242	90	510275	3863450	148	40	507121.2	3867073	54	38
513606.2	3861265	133	85	510005.9	3870921	92	40	500608.8	3868375	63	80	510275	3863450	134	58	507227.5	3865098	25	89
513567	3861589	181	71	510283.1	3870133	313	50	500472.1	3868143	248	90	510275	3863450	135	54	507340.2	3865087	280	80
513728.5	3861765	148	85	510286.3	3870059	244	50	500353.3	3867913	248	85	510275	3863450	132	50	507422.1	3865113	324	74
513867	3861899	156	79	509786.2	3869961	325	80	500252.8	3868041	248	80	510275	3863450	122	54	507579.7	3865126	122	67
514169.6	3862143	163	83	509710.5	3870054	58	40	500136.4	3867416	225	85	510275	3863450	264	45	507691.1	3865137	278	85
514374.9	3862303	154	78	509727.8	3869837	268	90	500271.3	3867458	224	90	510275	3863450	150	70	504958.3	3868829	72	85
514413.8	3862468	124	85	509927.8	3869804	228	90	500185.7	3867438	170	80	510275	3863450	148	59	504958.3	3868829	82	75
514805.9	3862148	155	70	510171.1	3869906	70	50	500189.8	3868587	278	75	510275	3863450	150	60	504982.2	3868881	284	68
515080.3	3862339	167	79	508902.8	3862870	329	80	500270	3868386	256	80	510275	3863450	132	68	504958.8	3868850	288	85
514949.5	3861756	256	76	508803.4	3862835	320	90	500182.5	3868354	283	80	510275	3863450	134	85	504950.7	3868860	282	85
515176.7	3861560	252	35	508842	3862867	307	90	500385.8	3865411	278	80	510275	3863450	158	64	504878.3	3868841	280	82
516028.2	3861864	169	79	509003.8	3862975	148	65	500571.7	3865555	283	90	510275	3863450	264	69	504986.5	3868850	256	94
517961.7	3862747	176	30	508726.7	3862970	337	85	500556.8	3865420	102	80	510275	3863450	12	84	504960.8	3868844	288	69
518318.9	3862800	268	45	508635.1	3862912	317	85	500500.9	3865300	282	70	510275	3863450	142	76	503341	3868129	100	34
518302.7	3862895	258	45	508618.3	3862836	317	75	500427.8	3865301	103	90	510275	3863450	156	79	503887.8	3867991	83	74
518850.8	3862827	269	35	508590.1	3862954	320	70	500405.4	3865218	82	85	510275	3863450	152	84	503912.1	3868117	74	85
517850.4	3862458	5	25	508532.1	3863021	308	80	501743.4	3868074	58	90	510275	3863450	148	40	504013.3	3868098	88	88
517856.2	3862268	250	35	508403	3863017	339	85	501936.1	3865547	90	90	510275	3863450	160	84	504207.9	3868036	88	78
518254.8	3861986	179	43	506387.4	3862943	358	65	502418.4	3866526	145	90	510275	3863450	148	70	503930	3868103	102	70
518195.3	3861821	250	20	506309.1	3862834	347	70	504041	3866929	272	85	510275	3863450	148	68	504169.5	3868883	189	80
518311.1	3861556	160	78	506703.4	3863305	189	80	503882.3	3867209	122	25	510275	3863450	152	61	504188.2	3868883	86	75
518338.9	3860896	338	81	506855.5	3863385	148	90	504881.8	3864713	89	90	510275	3863450	152	64	504795.7	3868814	78	73
518586.7	3860762	157	70	506895.4	3863305	132	90	504783.4	3866852	90	80	510275	3863450	138	59	504795.7	3868814	97	58
518893.5	3860587	156	71	506921.5	3863163	145	90	504916.8	3866556	229	38	510275	3863450	258	63	505049.3	3868970	70	75
518373.1	3861409	187	85	506754.8	3863456	117	85	504802	3866511	219	68	510275	3863450	129	89	505048.3	3868970	96	65
518543.9	3860761	171	78	506546.9	3863497	165	90	497005.8	3866854	223	75	510275	3863450	133	63	505483.3	3870827	74	55
518743.9	3860519	159	85	506473	3863578	306	80	496936.4	3866[illegible]99	256	65	510275	3863450	126	87	505483.3	3870825	74	52
517169	3860564	313	80	506401.9	3863591	296	90	496932.8	3866[illegible]29	332	70	510275	3863450	126	64	505525.8	3871027	80	55
517246	3860326	165	81	506383	3863966	98	85	497000.5	3866483	248	80	510275	3863450	167	67	505763.8	3871490	39	84
517355.4	3860240	161	80	506576.1	3863731	128	70	497020.8	3866518	244	85	510275	3863450	328	63	505762.5	3871480	84	40
517462.8	3860287	263	74	506620.6	3863897	141	80	497283.7	3866223	238	70	510275	3863450	327	60	506089.6	3871736	55	74
517800.6	3860500	172	80	506463.8	3863916	131	65	497360	3866427	226	85	510275	3863450	143	52	506088.6	3871734	83	40
517817.4	3860447	141	80	506476.6	3863943	316	80	497350.1	3866499	230	90	510275	3863450	142	68	506233.6	3871937	87	35
513439.3	3860854	344	85	506445.2	3864069	135	85	497340.4	3866820	225	90	510275	3863450	134	69	506222.3	3871926	87	35
513823.7	3860865	170	80	506296.8	3863951	307	80	497224.3	3866862	220	85	510275	3863450	181	79	506223.5	3871926	68	85
513577.7	3860786	133	90	506319.3	3864099	128	75	497244.8	3866894	244	80	510275	3863450	164	71	506222.3	3871929	76	81
513516.9	3860972	156	85	506249	3864283	124	90	497292.4	3866870	230	85	510275	3863450	174	70	506222.3	3871929	81	47
513652.8	3860738	157	69	506080	3864281	119	85	497436.8	3866850	223	85	510275	3863450	164	58	506222.3	3871929	90	60
513786.7	3860652	165	75	506023	3864374	116	75	497502.7	3866848	229	90	510275	3863450	302	68	506520.6	3872311	86	51
513897.4	3860342	156	60	506018.9	3864419	123	65	497572.1	3866732	239	75	510275	3863450	114	67	506520.6	3872311	60	60
514057.8	3860212	119	84	507901.3	3864367	123	70	497596.3	3866794	243	50	510275	3863450	165	58	506551.3	3872388	114	44
514201.5	3860131	269	66	507866.6	3864290	130	75	497648.1	3866857	230	85	510275	3863450	288	55	506575.7	3872540	115	69
514222.6	3860058	120	90	507783.9	3864301	116	80	497733.8	3866724	243	35	507500	3863850	329	78	506584.7	3872747	135	70
514571	3859947	159	85	507883.2	3864309	114	90	497618.7	3866706	234	90	507500	3863850	330	67	506584.7	3872747	130	76
513098.9	3859965	167	85	507535.9	3864272	111	70	497614.8	3866126	236	85	507500	3863850	331	69	506584.7	3873046	155	37
513268.4	3859929	170	70	507480.7	3864248	118	85	497708.8	3866150	224	85	507500	3863850	317	70	506983.2	3873870	109	30
513861.1	3859781	266	70	507812.8	3864040	117	75	497771.4	3866197	36	13	507500	3863850	330	73	506983.2	3873866	95	21
514673.2	3859568	306	85	507504.2	3863867	315	80	497819.2	3866070	45	80	507500	3863850	340	84	507053.3	3874107	108	78
514769.7	3859595	312	90	507350.8	3864196	117	85	497823	3866105	40	90	507500	3863850	322	77	507053.3	3874107	90	44
514536.9	3859476	339	78	507382.8	3864048	125	70	497849.7	3866202	48	90	507500	3863850	330	67	507053.3	3874107	95	36
514913.3	3859364	8	75	507383.5	3863998	129	90	497843	3866829	66	60	507500	3863850	327	66	502520.1	3867316	45	50
515208.4	3859982	338	55	507398.1	3863916	141	60	497884.8	3866885	53	85	507500	3863850	311	72	501043.8	3867506	52	67
515238.8	3859805	22	78	508449.5	3864152	314	75	497892.6	3866707	53	75	507500	3863850	324	66	500978.8	3867716	58	70
515281.4	3859854	22	61	508447.2	3864412	117	75	498086.4	3866720	47	85	507500	3863850	336	64	500922	3875241	243	65
515287.3	3859833	0	79	506085.2	3864566	132	80	496125.1	3866740	235	75	507500	3863850	318	78	500907.9	3875244	84	17
515360.8	3859825	186	35	508048.3	3864871	111	80	496054.7	3866863	48	75	507500	3863850	326	69	500316	3874076	58	60
515816.9	3859890	175	45	507848.6	3864734	95	84	496139.8	3866966	61	85	507500	3863850	332	60	503477.3	3876437	128	84
517370.9	3859766	5	50	507711.3	3864731	140	78	496160.7	3866950	235	35	507500	3863850	336	71	502646.8	3875321	272	66
515512.2	3859647	152	84	507841	3864668	118	78	496283.5	3866970	54	80	507500	3863850	322	59	502693.2	3874962	304	54
516667.8	3859560	157	90	507387.1	3864589	134	58	496360.8	3866970	45	75	507500	3863850	144	78	500921	3875225	243	85
516605.4	3859252	340	68	507230.4	3864735	93	75	496431	3866906	239	65	507500	3863850	328	77	500609.5	3875203	84	17
516629.3	3859186	344	75	507460	3864783	105	75	496549.5	3866966	236	90	507500	3863850	314	80	500331.2	3874087	156	74
516277.3	3859016	5	64	507501.2	3864735	121	61	496606.4	3866966	48	90	507500	3863850	320	60	500353	3874088	190	78
516533.6	3858991	1	63	507566.1	3864812	154	67	497413.2	3866150	233	75	507500	3863850	282	81	500332.5	3873854	75	80
516426.2	3856788	353	80	507736.4	3864871	104	83	497470.4	3866099	236	75	507500	3863850	310	60	499668.7	3873501	90	79
516566.9	3858621	235	66	507812.6	3864910	96	66	497523.8	3866056	237	75	507500	3863850	288	78	499806.5	3873347	184	71
516646.8	3858567	185	80	507571.5	3865004	82	75	497627.3	3866084	235	80	507500	3863850	301	70	497884.3	3871250	190	76
516226.2	3858530	265	77	507747.6	3865006	100	22	497739.9	3866119	232	75	507500	3863850	315	70	497449.8	3870463	58	80
516796.9	3858367	2	80	507833.3	3864985	90	11	497855.1	3866017	240	75	507500	3863850	318	75	497462.8	3868748	227	66
516920.5	3858277	351	25	507867.8	3865034	89	70	497732.5	3867908	244	80	514800	3868100	323	80	497804.2	3868711	56	80
517024.7	3858311	294	35	507896.7	3864995	92	73	497484.8	3867900	238	75	514800	3868100	319	65	498204.8	3868069	69	89
517172.3	3858158	296	50	506163.9	3865105	132	67	497170.1	3867778	268	70	514800	3868100	155	85	498314.8	3868063	209	81
517216.9	3858227	0	55	508212.5	3864898	98	42	497552.3	3867556	240	65	514800	3868100	276	88	498413.1	3868030	64	67
517332.1	3858185	340	70	508747.8	3864624	100	75	497676.6	3867720	248	85	514800	3868100	157	65	498621.8	3868060	197	78

Easting	Northing	Az.	Dip
517482.2	3857873	320	75
517882.1	3858281	343	70
518023.2	3858251	348	90
517802.2	3858008	334	75
517869.8	3858516	2	80
517940.3	3858486	158	75
517907.3	3858260	50	45
517258	3856587	31	80
517242.8	3856829	160	34
517154.8	3856804	168	65
514042.3	3857683	175	80
514251.3	3857804	107	60
514256.5	3857477	173	60
514485.8	3857272	188	45
510223.3	3856512	202	39
510434.8	3856437	313	60
510740.3	3856329	253	25
511085.8	3856244	245	35
511002.3	3856958	218	31
510672.9	3856927	3	85
510645.1	3856855	321	45
510611.4	3856426	220	67
510625.7	3856357	187	60
510654.2	3856223	329	90
510718.3	3857855	287	65
510740.9	3858004	0	90
510632.2	3857726	6	90
510693	3857426	205	65
510702.7	3857477	104	70
526203.8	3865639	283	60
524126.3	3864675	350	90
522723.3	3864761	187	60
521948.8	3865016	161	75
522097.5	3865272	180	45
521797.7	3865603	182	55
521383.3	3865636	187	60
520478.3	3865031	178	90
520444.7	3864932	175	90
520375.8	3864783	177	70
520189.2	3864701	181	80
519894.5	3865017	176	65
520105.8	3865481	328	60
520090.3	3865864	343	90
520812.8	3866057	181	65
520590.1	3866503	187	80
520742.1	3866584	172	80
519714.1	3866025	174	80
519801.9	3866483	170	80
519519.1	3866512	180	70
519935.2	3866906	124	70
520025.3	3866902	175	80
520083	3867003	178	65
520140.8	3867185	199	80
517830.4	3864788	154	80
518273.3	3865074	158	75
518299.3	3865282	150	60
517887.8	3865584	142	60
517507.6	3866120	148	60
517542.8	3866348	152	70
517547.7	3866573	158	80
518049	3866787	148	80
517842.8	3867024	147	80
518526.1	3867756	158	90
518438.1	3868019	127	90
518231.9	3867829	152	80
518411.5	3868287	148	70
518520.4	3868564	141	60
518502.5	3868415	122	80
518909.8	3868702	227	65
518438.4	3868501	140	70
509085.8	3867736	84	–
508639.4	3867886	86	–
508460.8	3868038	69	–
508289.4	3868548	66	–
508142	3868736	101	–
508709.1	3868287	87	–
508333.2	3867743	123	–
508016.4	3867722	58	–
507944.3	3868133	61	–
508148.4	3868175	109	–
508054.5	3868336	66	–
507869.2	3868428	120	–
507740.1	3868152	132	–
507578.1	3867990	93	–
507352.2	3867810	142	–
507382.6	3867762	66	–
507218.4	3868332	155	–
507466.3	3868757	104	–
507563.5	3869199	63	–
507696.4	3869081	80	–
507329.4	3868662	57	–
506803.6	3870332	118	–
506925.1	3870081	104	–
507450.1	3868827	127	–
507648.6	3868027	316	–

Easting	Northing	Az.	Dip
508842.5	3864511	125	75
508850.2	3864419	119	70
508777.6	3864368	103	90
508832.1	3864413	96	75
508768.8	3864258	130	65
508814.4	3864223	116	70
508748.8	3864150	104	75
508756.7	3864017	104	90
508586	3863848	248	75
509001.5	3864278	118	80
509072.8	3864287	109	80
508783.2	3864903	121	70
508820.8	3864845	90	85
508898.4	3864912	107	70
508888.5	3865035	111	85
509020.2	3865076	108	70
509237.8	3865265	113	80
509275.6	3865276	87	80
508462.1	3865503	128	80
508383.7	3865517	104	70
508490.4	3866189	112	60
508548.7	3866266	111	60
508645.3	3866364	133	70
508983.9	3866547	155	50
509710.8	3866906	125	70
509205.1	3867149	118	65
508145.2	3867101	100	60
508080.8	3866906	120	70
508665.2	3866819	108	70
508606.5	3866917	98	60
508825.4	3866826	108	70
508729	3866902	111	65
508708.3	3866489	128	65
508717.5	3866404	113	60
508734.1	3866303	124	80
508782.7	3866295	122	75
508850.2	3866241	117	70
508950.7	3866184	120	80
508938.3	3866107	127	55
508975.5	3865892	120	70
508901.9	3866211	108	65
508597.5	3866103	96	70
508665.3	3865966	119	75
508671.4	3865921	117	70
508611.1	3865780	122	60
508549.5	3865740	122	80
508713.9	3865535	106	75
508677.3	3865395	87	70
508537.4	3865261	114	80
508767.9	3865256	109	75
508573.5	3865166	109	60
508770.4	3865105	123	75
508542.1	3865111	127	55
508407.3	3865379	111	70
508316.5	3865623	109	60
508071.3	3865951	102	82
508002.8	3865578	105	55
508029.9	3865396	107	65
508054.7	3865352	99	43
508165.2	3865361	114	45
508023	3865266	111	65
507855.3	3865220	103	72
507737.7	3865331	111	68
507716.2	3865205	99	84
507885	3865144	150	78
508156.8	3867538	76	70
508206.7	3867353	75	55
508229.6	3867206	51	60
508258.2	3867087	58	80
508330.3	3867078	71	70
485468.8	3878817	33	–
485382	3878886	29	–
485388	3878886	21	–
485398.3	3878275	22	–
485409.8	3878434	24	–
485473.8	3878558	287	–
485621.1	3878513	273	–
485629.1	3878719	287	–
485452.4	3878898	40	–
485301.8	3878881	47	–
485299.4	3878337	16	–
485556	3877006	47	–
485696	3877045	203	–
485640.2	3877340	11	–
485742.2	3877543	353	–
485782.7	3877787	343	–
485982.1	3878975	78	–
485514.3	3878203	72	–
485747.5	3878394	87	–
485871.3	3878557	282	–
485109.8	3877151	42	–
486033.2	3877726	32	–

Easting	Northing	Az.	Dip
487725.4	3867706	239	80
487778.5	3867782	150	75
487821.9	3867880	84	75
487854.2	3867940	50	60
487858.8	3867873	218	60
487855.8	3867716	40	65
487856.3	3867863	207	63
488001.3	3867880	235	75
488043.5	3867706	231	65
488084.4	3867721	232	75
488152.3	3867868	234	65
488206.9	3867887	237	75
488274.8	3867728	180	70
488204.9	3867618	236	60
488182.2	3867388	236	60
488128.1	3867380	227	70
488132.5	3867315	231	65
488114.9	3867279	231	75
488023.9	3867273	247	70
487996.7	3867321	230	60
487929.3	3867310	236	60
487881.7	3867371	222	75
487877.6	3867429	231	50
487815.4	3867550	252	60
487875.8	3868369	49	75
488100.9	3868110	233	65
488131.2	3868169	58	60
488213.3	3868209	49	80
488289.9	3868200	48	85
488371.5	3868284	48	85
488432.3	3868325	38	80
488281.9	3868382	42	60
488358.8	3868472	45	90
488524.5	3868539	45	85
488582.4	3868589	53	85
488722.8	3868652	42	60
488805.9	3868968	48	90
488632.8	3869050	35	65
488748	3869022	57	65
488704.8	3869151	65	80
488783.5	3869189	48	85
488806.8	3869062	48	85
488896.8	3869109	47	85
489012.2	3869189	48	80
489086.2	3869108	47	85
489018.8	3868914	41	75
489290.1	3868056	43	75
488478.3	3868134	124	65
488609.2	3868154	48	75
488632.1	3868990	40	75
488712.2	3868917	38	70
488857.8	3868827	54	75
488895.4	3868832	43	65
488578.7	3868486	46	75
488614.3	3868483	40	85
488340.1	3867821	44	80
488398.8	3868008	56	75
488491.8	3867990	47	80
488578	3867972	43	75
488688.8	3867981	32	70
488784.8	3868053	53	80
488741.7	3868091	27	90
488806.1	3868156	58	75
488547.4	3868186	44	85
488691.9	3867838	48	85
488826.8	3867763	68	90
488636.8	3867557	214	85
488654	3867569	219	80
488498.7	3867494	238	80
503783.1	3878213	330	–
503678.9	3878030	357	–
503508.8	3878009	324	–
503548.9	3878360	133	–
502308.2	3878953	286	–
502852.3	3878975	310	–
502782.9	3878966	316	–
502796.7	3878918	304	–
502940.5	3878904	313	–
502896.9	3878063	307	–
503009.9	3878137	315	–
502832.3	3878188	316	–
502998.2	3878258	321	–
503126.9	3878268	319	–
503143.1	3878420	341	–
502087.8	3878907	65	–
502280.2	3878885	6	–
502117.9	3878885	350	–
502025.9	3878908	3	–
502535.3	3878472	4	–
502408.5	3878209	80	–
502883.6	3878341	98	–
502574	3878011	93	–
502612.7	3874929	322	–
502871.1	3874811	284	–

Easting	Northing	Az.	Dip
514800	3868100	120	66
514800	3868100	118	69
514800	3868100	127	62
514800	3868100	128	60
514800	3868100	118	66
514800	3868100	128	67
514800	3868100	118	79
514800	3868100	182	74
514800	3868100	131	69
514800	3868100	119	68
514800	3868100	142	67
514800	3868100	142	66
514800	3868100	310	67
514800	3868100	119	78
514800	3868100	106	62
514800	3868100	303	79
514050	3868550	301	62
514050	3868550	123	63
500750	3875150	234	76
500750	3875150	159	66
500750	3875150	348	66
500750	3875150	244	60
500750	3875150	241	66
500750	3875150	229	59
500750	3875150	235	77
500750	3875150	49	65
500750	3875150	229	71
500750	3875150	227	75
500750	3875150	28	60
500750	3875150	219	61
500750	3875150	228	60
500750	3875150	215	66
500750	3875150	259	64
500125	3873800	129	21
500125	3873800	57	63
500125	3873800	76	65
500125	3873800	166	63
500125	3873800	178	66
500125	3873800	256	64
500125	3873800	175	79
500125	3873800	180	65
500125	3873800	241	67
500125	3873800	238	77
500125	3873800	69	65
499650	3873300	194	62
499650	3873300	78	65
499650	3873300	204	73
499650	3873300	83	66
499650	3873300	266	71
499650	3873300	66	66
499650	3873300	216	66
502600	3874750	335	55
502600	3874750	334	50
502600	3874750	332	48
502600	3874750	315	40
502600	3874750	34	39
502600	3874750	35	42
502600	3874750	314	66
502600	3874750	300	67
503400	3873050	61	66
503400	3873050	79	61
503400	3873050	66	75
503400	3873050	78	65
503400	3873050	65	40
503400	3873050	65	67
503400	3873050	62	38
503400	3873050	61	58
503400	3873050	71	34
502300	3871650	115	50
502300	3871650	103	30
499467.7	3879709	47	–
499658.7	3879685	61	–
499717.8	3879683	66	–
499758	3879412	59	–
499620.3	3879182	42	–
499650.1	3878894	68	–
499750.1	3878376	61	–
499913.8	3878305	56	–
500158.7	3878459	62	–
500181.5	3877993	44	–
500258.8	3878018	48	–
500381.4	3878051	70	–
500449.5	3878054	91	–
500408.3	3878160	53	–
502434.1	3878843	82	–
502500.4	3878842	45	–
502590.1	3878731	84	–
502681.8	3878486	49	–
502685.5	3878564	60	–
502835.1	3878467	44	–
502824.8	3878596	40	–
502884.4	3878616	57	–
502981.4	3878627	50	–
503087.4	3878696	26	–
503214.3	3878562	79	–

Easting	Northing	Az.	Dip
498603.7	3868968	75	67
498630.8	3869036	230	87
498982.4	3868910	27	81
499073.2	3868936	18	70
499114.2	3869102	42	84
499080.8	3869296	28	89
499187.1	3868991	135	50
499187.1	3868991	52	86
499417.3	3869135	77	78
499600.3	3869192	74	68
499070.7	3869530	72	87
499092.4	3869783	80	25
499282.5	3869869	143	71
499398.2	3869902	81	25
499495.3	3869883	39	52
499407.1	3869800	21	28
500663.3	3869468	73	73
500640.9	3869266	80	60
500823.2	3869389	36	84
500784.8	3869844	50	80
500944.8	3869774	54	71
501186.5	3870015	67	71
501274.8	3869993	19	66
501410.4	3870035	62	60
501411.7	3870114	93	75
501572.8	3870152	52	71
501672.7	3870046	66	60
501672.7	3870046	66	50
501773.7	3870472	51	65
501698.2	3870852	230	88
501617.6	3871031	55	75
501617.6	3871031	26	67
501617.9	3871031	14	83
501816.9	3871280	58	82
502027	3871266	63	65
502012.9	3871410	61	57
502135.7	3871420	61	43
502168.2	3871424	51	27
502288	3871528	12	57
502348.8	3871523	54	47
502451.7	3871561	56	52
502483.9	3871657	46	72
502483.9	3871657	59	61
502657.2	3872182	51	64
502657.2	3872182	66	50
502946.8	3872305	49	57
503188	3872430	54	55
503233.3	3872504	64	44
503282.8	3872574	68	60
503377.9	3872664	53	45
503416.6	3872850	56	41
503430.3	3872944	91	35
503486.6	3873030	78	65
503623.5	3873276	225	16
503681.9	3873383	115	44
503750.2	3873440	71	60
503805.6	3873728	95	39
503844	3873985	74	71
503844	3873985	71	36
503812	3874096	115	47
503812	3874096	133	57
503815.6	3874231	79	67
503815.6	3874231	70	45
503563.4	3874386	241	44
504419.2	3871467	110	30
504435.9	3871456	140	28
504769.3	3870699	109	38
504218.4	3869758	74	50
507500	3863820	313	61
508021.3	3876499	87	–
507920.2	3876263	85	–
508180.3	3876407	24	–
508180.3	3876473	18	–
508373.3	3876566	3	–
508636.3	3876648	82	–
509177.3	3876853	102	–
509215.3	3876839	273	–
509275	3876796	276	–
509315.3	3876948	287	–
509544.8	3877036	284	–
509618.1	3877215	286	–
507925.3	3876243	89	–
508225	3875503	302	–
508343.6	3875550	310	–
508410	3875470	286	–
508395.5	3875687	293	–
508527.9	3875874	326	–
508417.3	3875936	295	–
508258.3	3876158	291	–
508375.3	3876272	293	–
508378.6	3876409	310	–
508668.5	3876232	293	–
508783.6	3876440	310	–
508776.5	3876504	316	–
508804.1	3876538	308	–

Easting	Northing	Az.	Dip	Easting	Northing	Az.	Dip	Easting	Northing	Az.	Dip	Easting	Northing	Az.	Dip	Easting	Northing	Az.	Dip
507748.8	3869510	324	-	496693.9	3877832	291	-	502881.9	3875180	144	-	503266.3	3878851	2	-	506373.7	3878811	92	-
506598.8	3870096	123	-	497533.8	3877878	4	-	502672.7	3875293	8	-	502780.8	3878866	57	-	506328.4	3878836	2	-
506402.3	3869852	133	-	497690.1	3878111	61	-	502787.1	3875370	14	-	503029.3	3878812	37	-	506427.8	3877148	90	-
506229.2	3869738	104	-	498017	3877806	44	-	502889.4	3875584	350	-	502898.8	3878222	39	-	506586	3877133	292	-
506956.7	3869147	135	-	498157.1	3877191	50	-	503131.8	3875552	325	-	503286.5	3878866	61	-	506678.7	3877313	89	-
506915.4	3868993	85	-	497987.7	3876899	259	-	503114	3875407	323	-	503476.3	3878927	59	-	506674	3877407	268	-
506754.9	3868722	104	-	498603.8	3876799	262	-	503334.4	3875356	313	-	503328.5	3879147	44	-	506819.3	3877723	73	-
506500.8	3868543	46	-	498408.7	3876566	233	-	503538.7	3875099	311	-	503139.8	3879372	40	-	506941.2	3877712	79	-
506506.2	3868436	117	-	498515.8	3876256	280	-	503399.8	3874918	324	-	503382.3	3879317	40	-	506859	3877539	87	-
506539.2	3868174	53	-	498505.8	3876133	90	-	503357	3874779	350	-	503505.4	3879157	5	-	507029.2	3877418	84	-
505937.5	3868784	59	-	498611.2	3875969	208	-	503956.4	3874859	328	-	503707.5	3879255	50	-	506906.1	3877328	95	-
505906.7	3868873	54	-	498429	3875564	253	-	503131	3874399	89	-	503987.1	3879292	203	-	507141.4	3877486	78	-
506289.9	3869050	85	-	498332.7	3875367	237	-	503286.2	3874163	88	-	503236.9	3879431	215	-	507180.8	3877562	310	-
506536.6	3869127	81	-	498207.3	3875261	236	-	503311.8	3874040	280	-	503048.8	3879497	216	-	507284.9	3877853	108	-
505901	3869215	88	-	499224.7	3875348	79	-	503899.5	3874451	77	-	503055.8	3879562	232	-	507420.7	3877408	85	-
505866.9	3869221	61	-	495381.5	3876803	35	-	504090.8	3874314	90	-	502911.8	3879749	208	-	507149.5	3876966	284	-
505842.7	3869397	68	-	495711.8	3876825	215	-	504032.7	3874386	310	-	502982.8	3879998	66	-	507273.8	3876813	269	-
505839.9	3869566	65	-	495885.8	3877010	236	-	504200.8	3873778	346	-	502981.2	3879825	49	-	507066.5	3876887	78	-
506045.3	3869903	64	-	495787	3877070	247	-	504289.2	3873389	286	-	503087.4	3879820	48	-	506477	3876851	76	-
506258.3	3869863	244	-	495848.9	3877732	33	-	504345.8	3873313	277	-	503239.4	3879776	50	-	506336.6	3877452	78	-
506496.5	3870073	260	-	496114	3877844	24	-	502945.3	3873947	347	-	503440.7	3879703	35	-	506225.2	3876885	282	-
506624.5	3870342	142	-	496355.3	3877753	49	-	502948.8	3873784	307	-	503492.4	3879748	228	-	505875.6	3876946	335	-
505983.4	3870073	145	-	496541.4	3877756	36	-	503829.3	3872994	93	-	503549	3879787	10	-	505891.8	3877019	239	-
505860	3870171	111	-	496527.7	3877818	36	-	504448.8	3873376	300	-	503820.7	3879810	49	-	505747.3	3877099	301	-
505803.8	3870256	38	-	496535.8	3878058	42	-	504375	3873814	334	-	503856.7	3879757	31	-	505790.9	3876818	116	-
505925.3	3870421	120	-	496671.7	3877900	18	-	504732.8	3873311	74	-	503982.4	3879799	42	-	505869.3	3876706	280	-
505406	3869916	87	-	496634.5	3878085	18	-	504773.8	3872927	248	-	504153	3879514	47	-	506047.6	3876893	309	-
505635.3	3869391	113	-	496736.8	3878007	46	-	504341.1	3873013	1	-	504229.9	3879730	69	-	506018.1	3876420	311	-
505249.7	3869935	95	-	496649.3	3877737	37	-	504406.4	3872861	83	-	504280.4	3879795	58	-	505801.4	3876508	117	-
505408.4	3870484	115	-	495799.2	3877975	44	-	504286.8	3872871	87	-	504338.2	3879811	54	-	505840.9	3876396	148	-
505392.3	3869029	103	-	495497.3	3878178	39	-	504387.8	3872474	6	-	504504.7	3880914	132	-	505681.7	3876269	140	-
505322.8	3868761	58	-	495509.4	3878336	27	-	504354.8	3872486	96	-	504484.2	3880840	3	-	505702.1	3876834	323	-
505673.5	3868875	71	-	495726.3	3878483	12	-	504339.4	3872182	47	-	506282	3872900	62	-	505866.9	3876960	316	-
505820	3868551	38	-	495659.1	3878591	57	-	504157.8	3872209	86	-	506449.2	3872886	66	-	506007.2	3876962	333	-
505827.3	3868457	65	-	495868.2	3878647	12	-	504737.4	3872084	73	-	506412.8	3872778	102	-	506053.3	3876915	69	-
505757.6	3868301	63	-	496095.4	3878659	73	-	504606.8	3872002	53	-	506315.9	3872876	93	-	506028.2	3876543	120	-
506087.1	3868152	72	-	496279.2	3878748	18	-	502733.2	3873296	132	-	506663.5	3872850	97	-	505539	3876140	262	-
506367.1	3868117	114	-	496485.6	3878619	29	-	502365.7	3873122	131	-	506597.3	3872829	82	-	505466.5	3876114	79	-
506324.6	3868005	59	-	496506.8	3878415	21	-	502535.9	3873085	87	-	506525.4	3872728	96	-	505403.4	3876469	52	-
506402.5	3867752	68	-	496569.2	3878756	69	-	502718.2	3872851	104	-	506284.5	3872920	88	-	505426	3876543	125	-
504979.9	3868148	46	-	496740.5	3878725	14	-	502660.3	3872330	148	-	506178.3	3872810	110	-	505312.2	3876298	101	-
504892.4	3868993	92	-	496894.3	3878304	356	-	502781.8	3872266	37	-	506024	3872812	138	-	504884.1	3876909	88	-
504748.2	3868918	88	-	497168.7	3878710	36	-	503090.8	3872419	45	-	507932.8	3872925	96	-	505158.5	3876890	283	-
505299.9	3868711	116	-	497303.1	3878733	48	-	502838.7	3873488	86	-	507784.7	3872894	90	-	505168.7	3873078	76	-
505207.5	3868346	95	-	497316.8	3878811	335	-	501676.5	3875287	284	-	507897.8	3872914	110	-	504957	3873430	330	-
506083.3	3867850	159	-	497277.2	3878167	39	-	502002.2	3874833	284	-	507545.2	3872962	77	-	504826.2	3873869	318	-
506137.6	3867706	66	-	495523.1	3878447	75	-	502181.1	3875003	101	-	507256.2	3872896	104	-	504786.6	3874122	273	-
505230.2	3868072	51	-	495643.8	3878159	78	-	502116.1	3874811	91	-	507484.7	3872871	103	-	504768.1	3874268	304	-
505461.1	3867861	41	-	496019.3	3878228	39	-	502289.7	3874862	90	-	507573.5	3872569	101	-	504356	3874400	47	-
504188.2	3869891	127	-	495424.4	3878700	43	-	502242.8	3874838	97	-	507697.8	3872887	111	-	504396.8	3874850	41	-
504200.5	3869432	126	-	495429.3	3878841	42	-	502351.5	3874795	64	-	507780	3872870	99	-	503942.3	3875464	327	-
504203.7	3869950	78	-	495511	3880077	37	-	502353.8	3874566	87	-	509177.1	3873383	93	-	504156.2	3875437	177	-
504255.6	3869734	90	-	495463.5	3880421	78	-	502418	3874271	284	-	509136.3	3873338	103	-	504096.5	3875386	3	-
504228	3871000	18	-	495409	3880814	64	-	501803.1	3875599	80	-	509034.1	3873368	96	-	504214.3	3875178	350	-
504482.4	3871132	49	-	495324.8	3881231	61	-	501466.8	3875720	314	-	508936.4	3873444	84	-	504203	3875119	345	-
504704.4	3870948	59	-	496301	3881078	42	-	501610.6	3875852	123	-	508905.8	3873311	110	-	504127.9	3874718	93	-
505013.9	3871220	49	-	496424	3880789	65	-	501488.5	3876024	72	-	508818.8	3873510	88	-	504297.5	3874625	21	-
505097.3	3871340	187	-	496348.3	3880577	49	-	501597.9	3876183	109	-	508782.2	3873498	102	-	504205.4	3874341	334	-
504949.9	3871544	88	-	496333.4	3880436	69	-	501673.3	3876215	284	-	508637.7	3873523	103	-	503898.5	3876289	338	-
505257.8	3871305	127	-	496525.2	3880931	51	-	501798	3876156	6	-	508313.3	3873491	104	-	503560.8	3876129	348	-
505394.7	3870930	111	-	496476.7	3881171	69	-	501848.7	3876111	71	-	508334.8	3873529	97	-	499218.3	3877984	228	-
505312.8	3870733	116	-	496648.3	3881118	58	-	501884.5	3876490	12	-	508211.8	3873545	137	-	499526.8	3877826	70	-
505224.5	3870337	103	-	496300.2	3880211	25	-	502133.5	3876379	45	-	508200.5	3873920	126	-	499574.2	3877643	87	-
503898.7	3872157	90	-	496513.1	3880194	34	-	502312.8	3876537	340	-	508215	3873752	111	-	498814	3876785	248	-
503863.5	3871638	58	-	496744.8	3880251	75	-	502306.3	3877558	52	-	508140.7	3873752	115	-	499113.8	3877067	236	-
503942	3871302	53	-	508806.1	3868366	92	-	501518.8	3876299	109	-	508161.2	3873915	100	-	499474.2	3877149	235	-
504096.8	3871122	48	-	509058.4	3868494	132	-	501344.3	3875978	67	-	508082.4	3873934	104	-	499745.1	3877429	83	-
503869.9	3870757	56	-	509078.8	3868782	84	-	501238.1	3876166	92	-	50..019.8	3874100	110	-	499788.8	3877226	271	-
503711.2	3870422	64	-	509227	3868366	86	-	501190.3	3876348	78	-	508035.8	3874304	105	-	499857.1	3877368	90	-
503406.5	3870342	51	-	509404.5	3868106	84	-	500858.8	3875723	83	-	508799.2	3874197	101	-	499803.9	3877071	65	-
504161.6	3870202	136	-	509590.1	3868118	83	-	500884.8	3875524	112	-	508682.8	3873915	114	-	499468.4	3881894	78	-
504001.2	3869910	41	-	509089	3868177	90	-	500934.2	3875269	22	-	508584.4	3873893	121	-	499420.8	3881739	59	-
503978.5	3869729	56	-	509363.4	3868041	95	-	501110.8	3875562	82	-	508615.1	3874117	111	-	499543.4	3881726	9	-
503781.4	3869693	45	-	509514.3	3868650	93	-	501199.2	3875572	73	-	508481	3874167	91	-	499469.4	3881399	69	-
503178.1	3871615	66	-	509642.8	3868524	131	-	501382.1	3875299	37	-	508411.8	3874230	100	-	499566.5	3881530	38	-
503482.4	3871653	73	-	509284.3	3868531	53	-	501657.8	3874648	3	-	508694.2	3874829	116	-	499687.5	3881649	95	-
503376.5	3869204	51	-	509414.2	3868381	90	-	501200.1	3874787	68	-	508603	3874854	111	-	499087.4	3882178	273	-
503567.8	3868911	287	-	509482.9	3868659	52	-	501375	3874753	64	-	508138.3	3874544	311	-	499185.8	3882304	89	-
503639.2	3868987	72	-	509678.3	3868942	91	-	501394.5	3874539	68	-	508317.5	3874867	131	-	499213.3	3881971	84	-
503847.3	3868093	82	-	509788.4	3868965	87	-	501463.4	3874809	89	-	508400.7	3874871	118	-	499038.3	3881770	77	-
503243.7	3868037	101	-	509970.4	3868843	139	-	501542.8	3874555	87	-	508518.8	3874875	134	-	499129.4	3881782	78	-
503012.8	3868215	100	-	509248	3870348	82	-	501673.3	3874396	82	-	508129.4	3875334	173	-	499208.4	3881720	83	-
503382.8	3868469	81	-	509286.8	3870135	145	-	501821.5	3874273	88	-	508383.8	3876287	121	-	499042.4	3881442	13	-
503887.4	3868497	142	-	509134.2	3870467	279	-	501887.3	3874248	96	-	508417.7	3876566	121	-	498851.3	3881325	7	-
503843.1	3868838	136	-	508896.8	3870977	82	-	501520.1	3874209	273	-	508436.7	3876522	88	-	498227.8	3881454	49	-
503820.5	3868447	138	-	508500	3870964	87	-	501455.3	3874309	96	-	508303	3876873	86	-	498417.3	3881485	44	-
503814.8	3868148	75	-	508403.2	3870831	148	-	501462	3874627	83	-	508676	3875701	318	-	498538.2	3881493	45	-
503140	3868194	83	-	508242.8	3871137	328	-	501754.3	3874471	291	-	509237.5	3876312	85	-	498653.1	3881851	60	-
503822.9	3868345	87	-	508748.3	3872009	130	-	500499.8	3876378	118	-	509402.3	3876365	103	-	498281	3882026	48	-
503756.5	3868168	71	-	508541.2	3871748	131	-	500394.7	3876322	133	-	509083.4	3876369	283	-	498478.1	3882007	51	-
504100	3868627	48	-	508640.4	3872291	99	-	500564.8	3876182	102	-	508300.2	3876219	347	-	498568.3	3882092	57	-
504055.5	3868200	58	-	509055.2	3872642	75	-	500735.7	3876357	126	-	508416.5	3876181	184	-	498302.8	3882166	84	-
501464.5	3870998	54	-	509156.6	3872431	300	-	500824.8	3876313	125	-	508518.2	3876336	92	-	498414.8	3882190	96	-
501483.2	3870842	40	-	509217.3	3872450	90	-	500766.7	3876061	118	-	508287.8	3875969	93	-	498758.1	3881479	101	-

Easting	Northing	Az.	Dip
501714.1	3870854	78	–
502033.3	3870400	80	–
502162.1	3870273	138	–
501818.1	3871380	58	–
501806.1	3871473	72	–
501731.1	3871706	61	–
502008.2	3871200	81	–
502106.4	3871841	31	–
502441.8	3871748	47	–
502829.8	3871768	89	–
502806.2	3871581	63	–
503221.8	3870238	61	–
503090.8	3869826	53	–
503549.9	3869878	108	–
501681.4	3870422	52	–
501710	3870084	61	–
502201	3869358	47	–
502254.5	3868844	55	–
502723.8	3868852	48	–
502825.3	3869321	38	–
502521	3869092	49	–
502708.2	3870399	47	–
502533.2	3868758	311	–
502533.2	3868873	58	–
502580.2	3868227	258	–
502702.5	3868268	49	–
502889.4	3868051	59	–
502509.7	3868847	91	–
502307.8	3868829	44	–
502508.8	3867848	58	–
502354.8	3867724	48	–
502122.4	3868747	67	–
502100.5	3868901	124	–
501850.2	3868989	45	–
501871.8	3868278	43	–
501359.2	3867831	48	–
501125.1	3868353	57	–
501394.1	3869686	77	–
500827.4	3869309	68	–
500837.3	3871144	58	–
500682.3	3870863	56	–
500495.7	3870764	47	–
500347.7	3870878	32	–
500106.8	3870588	54	–
501393.5	3870879	360	–
500828.8	3870847	32	–
501460.7	3870208	45	–
501247.1	3870084	48	–
501004.5	3869970	48	–
500718.5	3869874	58	–
499880.1	3870105	48	–
500111.4	3869969	50	–
499772.5	3869781	205	–
499336.5	3870958	40	–
499570.2	3871194	48	–
499874.4	3871407	39	–
499858.8	3871737	49	–
499830.8	3871823	218	–
499417.4	3872119	285	–
499738.1	3872483	83	–
499848.9	3872530	253	–
500083.9	3871847	81	–
499858.9	3871838	275	–
499791.3	3871493	50	–
499827.2	3871024	58	–
499150.5	3870828	48	–
498708	3870883	47	–
498347.3	3871022	100	–
498485.8	3870079	52	–
498130.5	3869851	47	–
497935.5	3868719	62	–
497806.1	3870218	32	–
499021.9	3869715	37	–
499177.2	3869503	23	–
498857.7	3869186	46	–
499254	3869179	47	–
499003.5	3869015	46	–
498500.9	3869078	66	–
498772.7	3868887	38	–
498544.8	3868801	44	–
498444.3	3868293	30	–
498702.3	3868182	71	–
498915.1	3868238	88	–
499183.7	3868279	65	–
498957.8	3868218	67	–
497307.8	3868827	212	–
497465.8	3868728	231	–
497468	3868530	224	–
497349.1	3868359	231	–
497332.9	3868059	240	–
497431.8	3867730	248	–
497632	3868053	238	–
498378.4	3868077	218	–
498136.9	3867885	227	–

Easting	Northing	Az.	Dip
508258.3	3872177	63	–
506485.8	3872258	82	–
508814.3	3872086	298	–
508553.8	3871827	84	–
508571.8	3871842	87	–
508834.5	3871312	150	–
509007.5	3871787	111	–
509086.8	3871489	113	–
509074.5	3871178	87	–
509208	3871008	128	–
509581.8	3874436	137	–
509588.7	3874358	124	–
509689.2	3874368	127	–
509557	3873853	88	–
509540.1	3873507	115	–
509468.3	3873313	328	–
509457	3873132	82	–
509482.8	3872858	80	–
509540.8	3872841	84	–
507836.8	3872200	58	–
508053	3872294	89	–
507848.8	3871873	80	–
507885.1	3871884	86	–
507887.5	3871300	38	–
508018.8	3871843	87	–
507524.5	3871189	106	–
507631.8	3871148	103	–
508224.1	3870763	88	–
508094.2	3870868	88	–
508280.4	3870338	117	–
508137.7	3869872	144	–
507348.2	3870483	54	–
507074.3	3870440	137	–
507188	3870890	109	–
508588.1	3870984	42	–
508849.9	3870982	270	–
507040.3	3871073	93	–
508934.7	3871544	47	–
508875	3871718	98	–
508959.5	3871748	248	–
508925.8	3871862	289	–
508843.5	3872083	127	–
508318.8	3871231	107	–
507681	3872183	132	–
508670.8	3872467	109	–
508770.8	3872271	131	–
508193.5	3871861	38	–
508219.8	3871599	73	–
508214.9	3871411	28	–
508410.2	3872430	75	–
508030.9	3872114	91	–
505947.8	3871929	63	–
505780.9	3871588	114	–
505854.2	3871395	109	–
505865.8	3872282	84	–
505683	3872487	85	–
505670.3	3871703	63	–
505087.7	3871744	87	–
505147.4	3872338	73	–
504874.7	3872711	72	–
504829.5	3872708	81	–
504723	3872858	79	–
504830.2	3872847	84	–
504822.1	3872877	6	–
504824.5	3873043	88	–
505370.8	3872317	159	–
504946.1	3872889	348	–
505050.8	3872814	299	–
505387	3873303	123	–
505572.8	3873874	109	–
505288.4	3873744	85	–
505409.8	3873702	94	–
505808.9	3873811	328	–
505828.1	3873781	323	–
505898.8	3873420	318	–
505428.3	3874383	288	–
505887.9	3874874	334	–
505809.7	3875309	323	–
506585	3876864	282	–
506830.1	3875848	109	–
506775.1	3875460	305	–
507034.7	3875431	108	–
507072.7	3875280	288	–
507215	3878301	287	–
507288.2	3875343	314	–
507484.3	3875891	113	–
507542.5	3875892	118	–
507583	3875858	281	–
507853	3875974	328	–
507140.8	3876272	117	–
507290.2	3876089	293	–
507821.5	3876824	127	–
507897	3876545	98	–
507880.8	3876587	98	–

Easting	Northing	Az.	Dip
501080.1	3876112	162	–
500874.7	3876036	80	–
499660.4	3877680	301	–
500130.3	3877782	108	–
500188.4	3877369	94	–
502309.4	3877402	82	–
500463.7	3877117	98	–
500803.8	3876881	82	–
500495.8	3876797	58	–
500870.3	3876804	148	–
500758.8	3876580	61	–
500332.7	3877780	110	–
500380.3	3877829	88	–
500480.2	3877898	113	–
500484.2	3877537	87	–
500602.2	3877154	94	–
500678.8	3877113	94	–
501204.1	3873902	87	–
501823.7	3873708	82	–
501137.2	3873877	84	–
501142.8	3873277	128	–
501254.2	3873021	63	–
501482.3	3873178	80	–
501503.5	3872817	78	–
501828.5	3873271	78	–
501898.2	3872843	278	–
501257.4	3873003	88	–
501234.8	3872879	64	–
501814	3872820	80	–
500948.8	3872481	82	–
500948.2	3872133	94	–
501056.5	3871887	82	–
500649.8	3872089	88	–
500587.5	3872283	124	–
501522	3872344	302	–
501860.5	3872229	277	–
502245	3872382	62	–
501834.4	3872944	331	–
502082.8	3872889	289	–
501234	3872053	61	–
501121	3871541	92	–
500082.8	3873473	61	–
500181.8	3872937	82	–
500338.3	3872138	68	–
500598.9	3872588	53	–
500584.3	3872882	82	–
500852.2	3872889	84	–
500400.5	3873448	30	–
500812.7	3873381	68	–
500881.9	3873486	87	–
500829.8	3873354	71	–
500758.5	3873288	45	–
500882.9	3873368	71	–
500875.8	3874848	348	–
501104.1	3874539	10	–
500749.1	3874732	38	–
500658.5	3874867	48	–
500477.1	3874469	28	–
500388.2	3874208	360	–
499854.3	3873989	84	–
500288.9	3874473	80	–
500178.6	3876084	298	–
500132.6	3876344	300	–
500378.3	3876333	273	–
500442.4	3876507	268	–
500283.3	3876073	323	–
500352.1	3876262	128	–
500253.6	3876884	93	–
500223	3876879	278	–
500483.6	3875817	274	–
500876.5	3876251	82	–
499885.6	3877045	80	–
499906.7	3875901	48	–
499786.5	3876096	61	–
499892.1	3877584	94	–
499689.4	3877269	98	–
497423.1	3880088	80	–
497479.5	3879929	58	–
499072.3	3876842	28	–
497981.2	3878774	42	–
497738.8	3878487	48	–
498115	3878409	22	–
498017.5	3878282	24	–
498130.3	3878045	238	–
498077.1	3878014	238	–
498055.4	3877970	88	–
498045.7	3877898	49	–
498830.2	3878034	51	–
498468.8	3877970	47	–
498488.1	3877882	73	–
498880.1	3878859	41	–
499040.5	3878481	38	–
499009.1	3877563	52	–
499117.8	3877577	4	–

Easting	Northing	Az.	Dip
508113.7	3875828	308	–
508408.9	3875883	103	–
507878.4	3875487	350	–
508231.5	3875832	109	–
508309.8	3875417	88	–
508401.1	3875325	102	–
508239.8	3875010	87	–
508399.8	3875004	109	–
508383.2	3874749	127	–
508484.3	3874523	189	–
508088.2	3874382	109	–
508012.7	3874283	171	–
507988.9	3875490	348	–
507599.3	3875284	107	–
507659.1	3875128	87	–
507721.3	3874978	88	–
5078[illegible].4	[illegible]874778	100	–
507742.3	3874568	104	–
507824.8	3874821	103	–
507789.9	3874434	98	–
507832	3874811	105	–
507856.1	3874285	98	–
507178	3872897	124	–
508086.8	3872838	88	–
508914.8	3872884	103	–
506782.7	3872817	97	–
506736.4	3872968	129	–
508631.2	3873018	128	–
508877.9	3872873	88	–
508488.1	3873134	282	–
508547.3	3873435	209	–
508835.3	3873823	283	–
506737.8	3873867	63	–
508345.4	3874383	330	–
508834.3	3874369	108	–
508880.3	3874232	318	–
508782.2	3874287	127	–
508843.8	3874157	89	–
508827.5	3874039	98	–
508818.3	3873744	262	–
508821.8	3873589	315	–
508812.9	3873868	305	–
508487.3	3874079	348	–
508370.4	3873998	287	–
508458.4	3873902	283	–
497858.7	3867781	51	–
498698.8	3867847	228	–
497125	3867894	243	–
498480.3	3867870	270	–
498401.1	3867918	243	–
498582	3867957	301	–
498785.1	3868068	220	–
498680.9	3868329	229	–
498386.3	3869978	40	–
498801.7	3869889	24	–
498898.5	3870102	59	–
498178.8	3870158	49	–
498338.3	3870411	34	–
498511.1	3870463	238	–
498872.3	3870983	47	–
498128.8	3871175	240	–
498210.2	3870952	63	–
498340.4	3871890	98	–
498847.3	3871295	244	–
498484.4	3871985	51	–
498881.4	3872338	58	–
498831.8	3872779	82	–
498029.8	3872478	92	–
495833.4	3873425	100	–
495853.7	3873247	288	–
495759.6	3873188	112	–
498217.4	3872480	137	–
498380.8	3872428	98	–
498462	3872931	69	–
498787.4	3873180	67	–
497011.8	3872905	68	–
498876.3	3873314	254	–
498928.8	3873488	78	–
497028.5	3873498	243	–
498888.1	3873782	61	–
497194.6	3873508	243	–
497178.4	3873488	78	–
497342.8	3873834	50	–
497532.7	3873807	224	–
497574.8	3873398	90	–
497683.8	3873389	83	–
497828.8	3873401	54	–
497813.7	3873438	49	–
497888.3	3873828	78	–
497888.4	3873888	281	–
498138.6	3873768	79	–
498090.8	3873448	68	–
498090.8	3873497	50	–
498172.5	3873505	60	–

Easting	Northing	Az.	Dip
498615.7	3881588	38	–
497018.8	3881701	91	–
497112.7	3881881	3	–
497154.8	3881548	330	–
497298.7	3881723	38	–
497483.1	3881844	217	–
498853.8	3881258	113	–
498853.7	3881284	118	–
497013.4	3881445	113	–
497088.8	3881297	120	–
497140.9	3881485	103	–
497320.1	3881517	135	–
497434.7	3881538	155	–
497582.4	3881581	183	–
497233.7	3881101	77	–
497293.9	3880817	80	–
497485.7	3880575	45	–
497470.2	3880489	42	–
497492.8	3880238	45	–
497987.5	3880423	47	–
498002.8	3881094	331	–
497988.3	3881058	350	–
497990.5	3880993	88	–
497940.7	3880848	48	–
498048.1	3880789	48	–
498184.9	3880781	270	–
498238.5	3881075	120	–
498428.2	3881039	183	–
498450	3880973	23	–
498423.3	3880922	45	–
498388.8	3880837	18	–
498289.4	3880509	38	–
498178.8	3880485	38	–
498348.1	3880372	59	–
498489.5	3880271	39	–
498884.7	3880854	50	–
498793	3880889	218	–
498821.3	3880820	128	–
498789.8	3880540	37	–
498780.7	3880504	54	–
498858.8	3880492	63	–
498838.2	3880232	26	–
498800.3	3880223	59	–
498881.4	3880222	14	–
499224.8	3880204	48	–
499395.8	3880098	48	–
498484.5	3879317	58	–
498488.5	3879448	35	–
498558.5	3879839	54	–
498933.4	3879279	62	–
499367.8	3878544	83	–
499823.5	3878448	89	–
499759.8	3878405	61	–
498359.4	3873463	84	–
498327	3873837	65	–
498412.8	3873735	47	–
498544.6	3873531	49	–
498412.8	3874078	59	–
498818.5	3874510	77	–
498892.4	3874019	72	–
499018.2	3874087	69	–
499160.2	3874023	59	–
499134.3	3874290	78	–
499203.1	3874393	81	–
498580.6	3874747	94	–
498842.9	3873867	42	–
497028.7	3873868	242	–
497008.8	3873502	244	–
496787.5	3874285	41	–
496540.8	3874339	51	–
496518.5	3874501	213	–
496284.8	3874547	74	–
496301.8	3874708	22	–
496277.5	3874899	37	–
496243.5	3875031	24	–
496844.2	3874575	45	–
496905.7	3874890	42	–
497087.5	3874901	47	–
496997.9	3875310	262	–
496845.8	3875405	55	–
496530.1	3875412	67	–
496353.6	3875445	27	–
496181.8	3875612	42	–
496133.5	3875417	51	–
496083.3	3875847	37	–
495733.6	3875824	24	–
495806.4	3875584	21	–
495897.2	3875897	19	–
495851	3875971	30	–
495823.8	3876019	30	–
496220.1	3875970	12	–

Note: a '–' in the Dip column indicates only azimuth data was available.

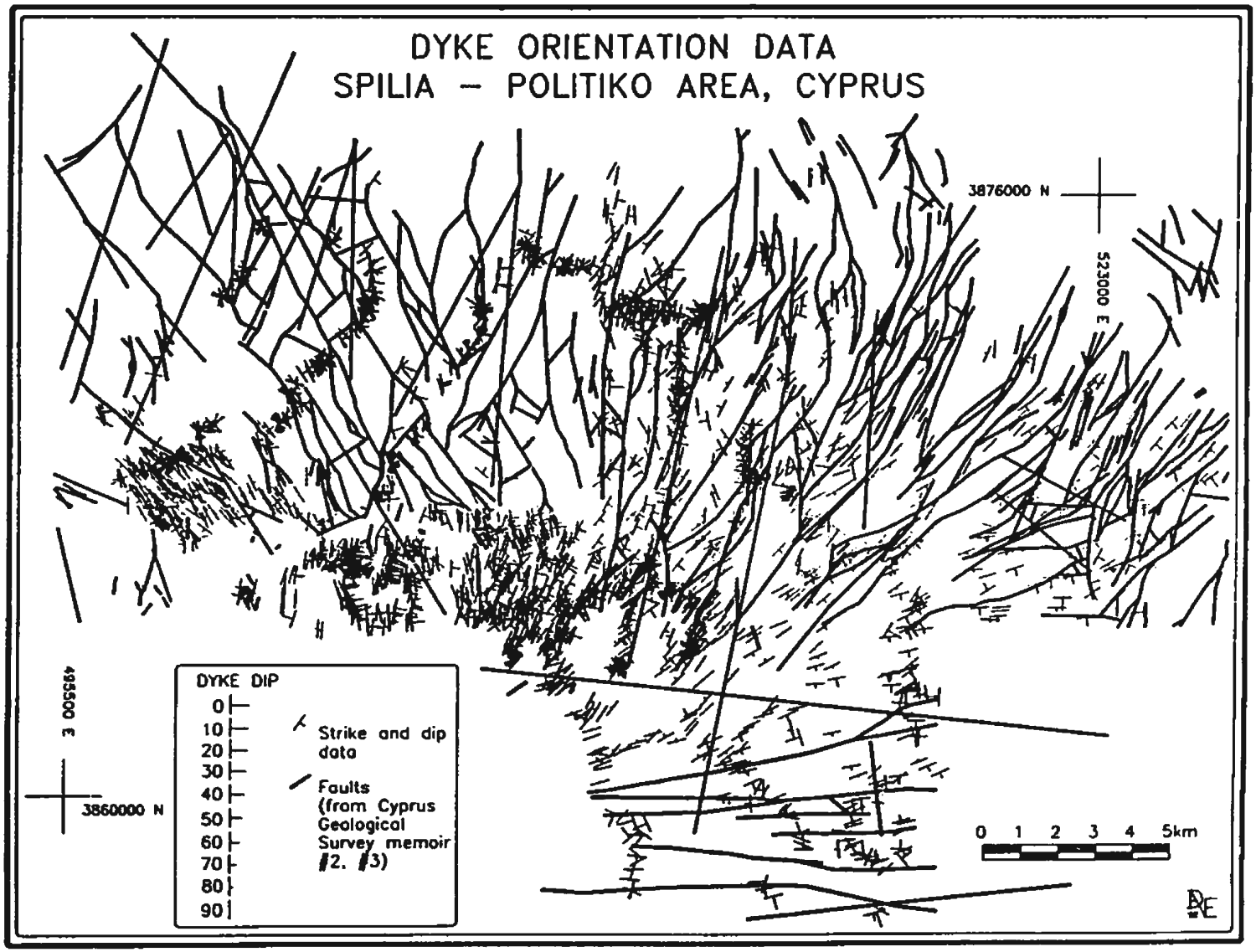
DYKE ORIENTATION DATA
SPILIA – POLITIKO AREA, CYPRUS
3876000 N
523000 E
493500 E
3860000 N
DYKE DIP
0
10
20
30
40
50
60
70
80
90
Strike and dip data
Faults (from Cyprus Geological Survey memoir #2, #3)
0 1 2 3 4 5km

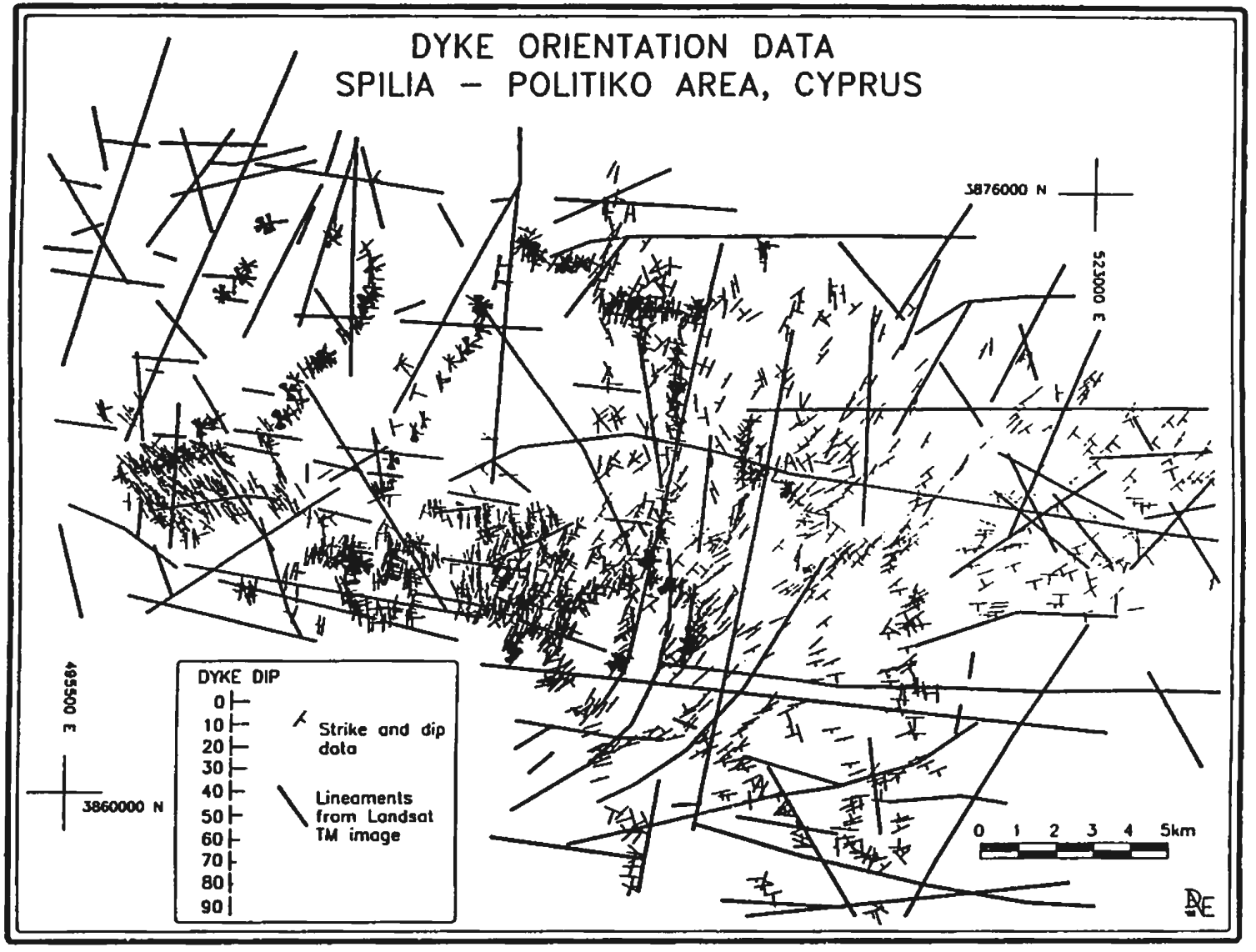
DYKE ORIENTATION DATA
SPILIA – POLITIKO AREA, CYPRUS
3876000 N
525000 E
495500 E
3860000 N
DYKE DIP
0
10
20
30
40
50
60
70
80
90
Strike and dip data
Lineaments from Landsat TM image
0 1 2 3 4 5km

B.2 DYKE GEOCHEMISTRY

Whole-rock major and trace element analyses from samples collected during the course of this study (Table B.3.1) as well as those published by Baragar et al. (1987) from ten road-cut sections (Figure B.1) were used. While variations are apparent in the data, these variations are not consistent with the dyke domains. Discrimination diagrams based on major elements show no consistent differences with respect to areal distribution of the dykes. For their data set an enrichment trend in FeO and TiO_2 is indicated. The dykes are mainly island arc tholeiites, with a minor number of mid-ocean ridge and calc-alkaline basalts. Dykes from the Kakopetria, Kionia and Prophitis Elias sections were more likely to fall into the calc-alkaline basalt field (on the basis of major elements, after Miyashiro, 1973).

The dyke analyses plot well within the island arc basalt field, with minor overlap into the mid-ocean ridge basalt field (Figure B.2, after Pearce and Norry, 1979). Mostly the dykes are are low potassium tholeiites (Figure B.3, after Pearce, 1975) with a very few falling within the ocean floor basalt field. With respect to trace elements, most dykes plot in the andesite-basalt field (Figure B.4). Of the dykes for which Zr analyses were available, those in the Kakopetria and Kionia-3 areas fall solidly within the low-K tholeiite field, while those in the Ayios Theodhoros, Prophitis Elias and Ayia Koroni sections are evenly distributed between the low-K tholeiite and ocean floor basalt fields of Pearce and Cann (1973) (Figure B.5). Plots of Mg# vs Sr/Y and Zr/Y vs Ti/Y (Figure B.6 and B.7, respectively) demonstrate that it is not possible to separate the dykes into domains on the basis of the geochemistry data.

The only differences from area to area appear on a TiO_2 vs CaO/Na_2O plot. These plots indicate that the sections at Nikitari, Ayios Theodhoros, Kakopetria and to a lesser extent Ayia Koroni have a low CaO/Na_2O ratio, while the Makheras, Kionia and Prophitis Elias sections have a higher mean CaO/Na_2O ratio. The overlap of the data, though, makes it difficult to make a clear distinction between the areas. It should be noted that both CaO and Na_2O are mobile components that are strongly affected by hydrothermal alteration processes. The differences in dyke compostion may simply be a reflection of the variation of alteration intensity in different locations.

In conclusion, the dyke chemistry neither supports nor refutes the dyke domain subdivisions. The geochemical data indicate that the dykes are low-K tholeiites within the island-arc basalt field. There may be depleted and/or undepleted suites represented by the dykes, but, the data distribution is continuous, obscuring possible domainal divisions on the basis of the dyke chemistry. Cross-cutting relationships of the dykes indicate depleted and undepleted dykes are not consistently age related (Baragar et al. 1987). The implication is that there were multiple magma sources operating contemporaneously within the dyke domains. These sources may have been replenished over time, from compositionally unchanged sources, to supply magma for all the domains within the field area.

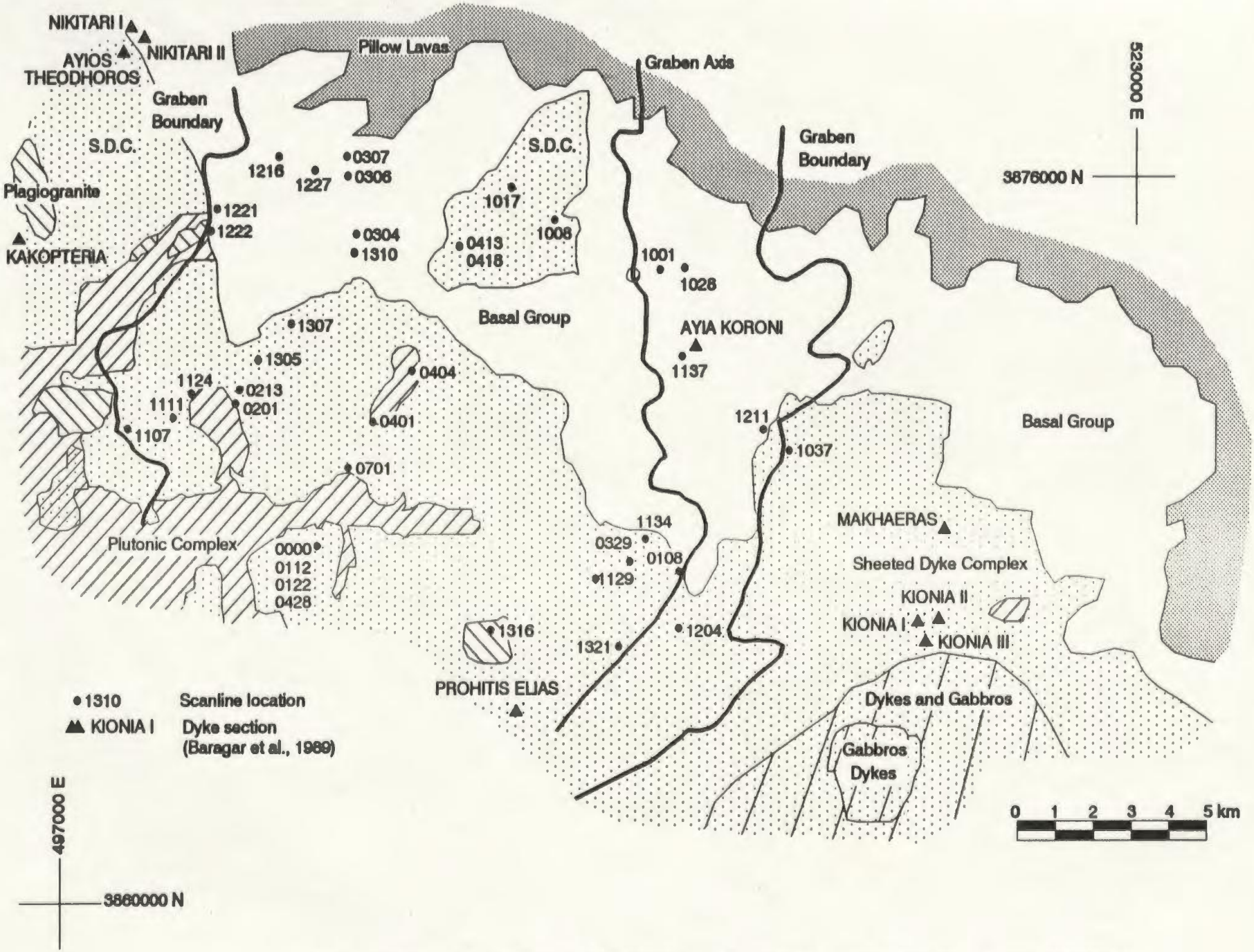

SCANLINE AND DYKE LOCATION MAP, SPILIA - POLITIKO AREA, CYPRUS.

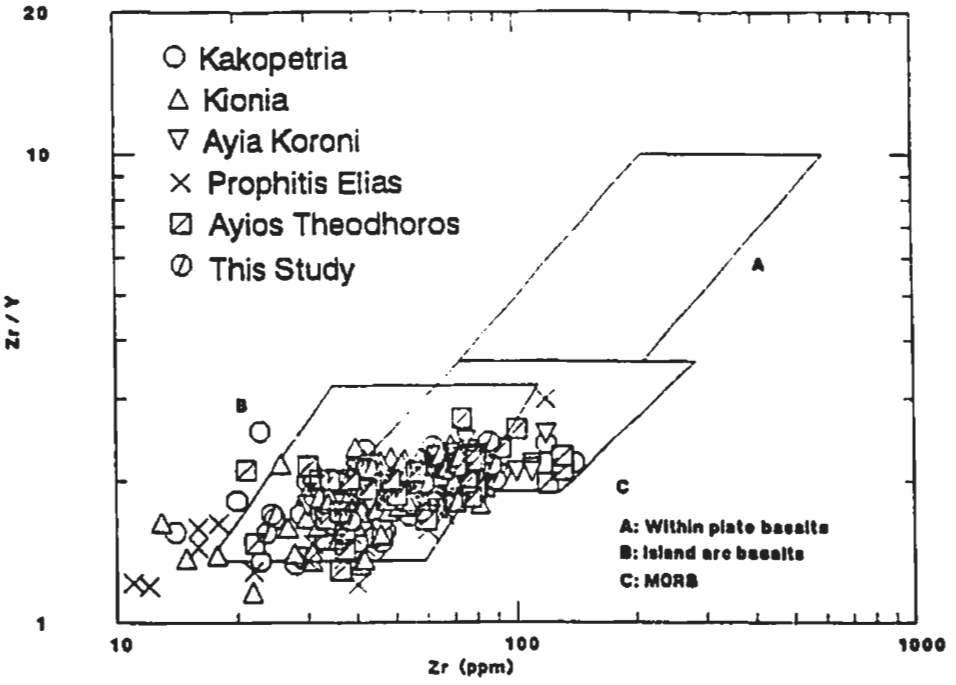

Zr/Y vs. Zr plot for the dyke sections of Baragar et al (1989) at Kakopetria, Kionia (1,2,3), Ayia Koroni, Makhaeras, Nikitari, Palekhori, Prophitis Elias, Ayios Theodhoros and this study.

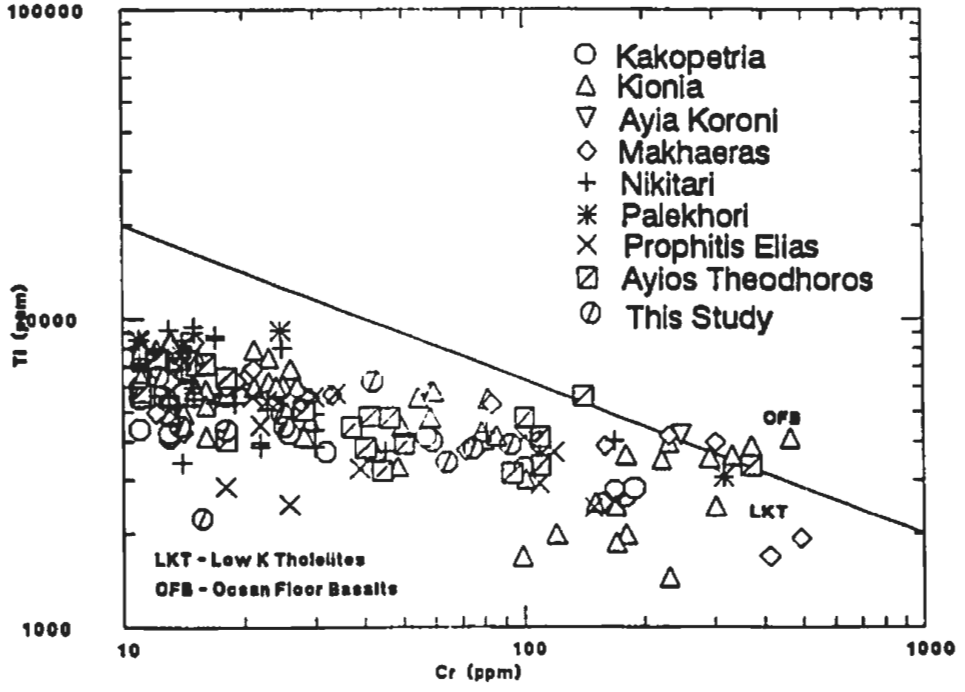

Ti vs Cr plot for the dyke sections of Baragar et al (1989) at Kakopetria, Kionia (1,2,3), Ayia Koroni, Makhaeras, Nikitari, Palekhori, Prophitis Elias, Ayios Theodhoros and this study.

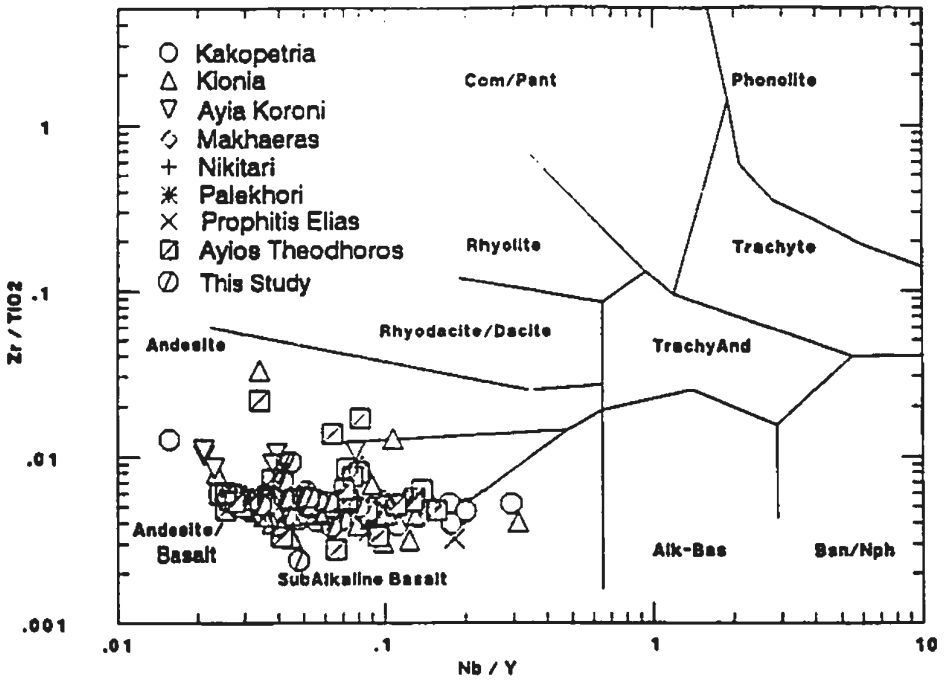

Zr/TiO2 vs. Nb/Y plot for the dyke sections of Baragar et al. (1989) at Kakopetria, Kionia (1,2,3), Ayia Koroni, Makhaeras, Nikitari, Palekhori, Prophitis Elias, Ayios Theodhoros and this study.

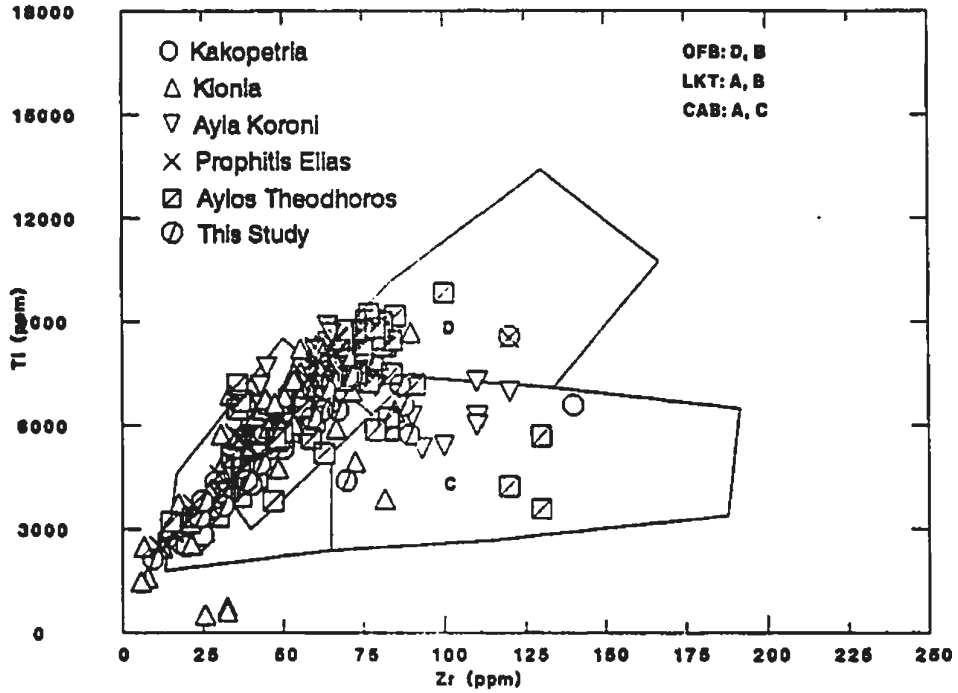

Ti vs. Zr plot for the dyke sections of Baragar et al. (1989) at Kakopetria, Kionia (1,2,3), Ayia Koroni, Makhaeras, Nikitari, Palekhori, Prophitis Elias, Ayios Theodhoros and this study.

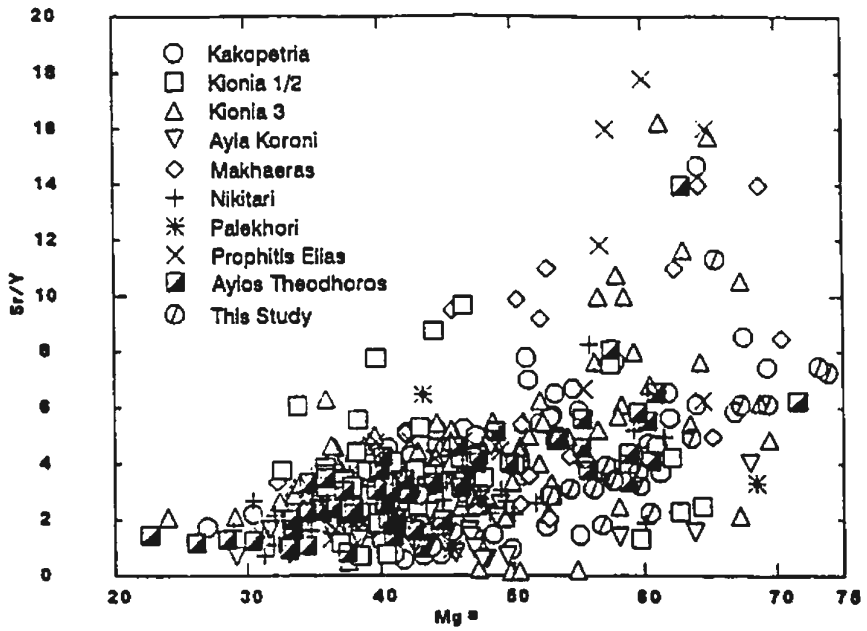

Mg# vs. Sr/Y plot for the dyke sections of Baragar et al. (1989) at Kakopetria, Kionia (1,2,3), Ayia Koroni, Makhaeras, Nikitari, Palekhori, Prophitis Elias, Ayios Theodhoros and this study.

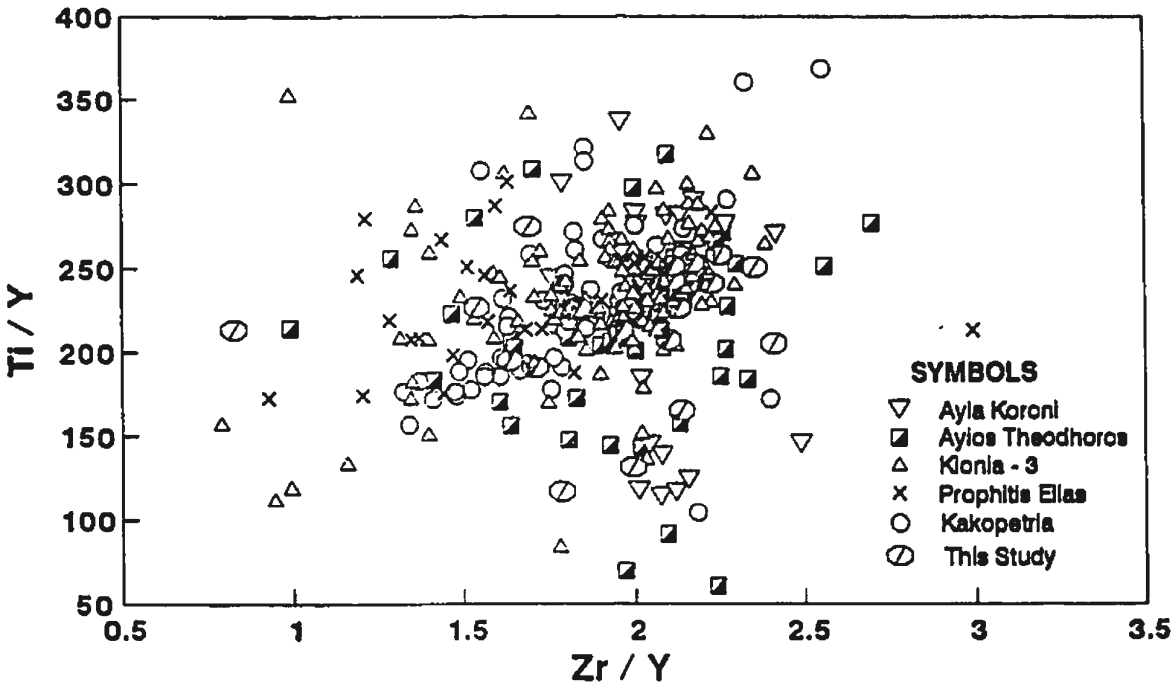

Plot of Zr/Y vs. Ti/Y for the dyke sections of Baragar et al. (1989) at Ayia Koronia, Ayios Theodhoros, Kionia-3, Prophitis Elias, Kakopetria and this study.

TABLE B.2.1 Whole rock geochemical analyses

Sample	GC9A	GC11	GC14A	GC17	GC24	GC27	GC33	GC36	GC41	GC42	GC43	GC44	DVE2A
SiO2	54.80	60.00	55.90	54.60	53.90	56.00	52.70	54.90	58.40	52.90	52.30	50.90	51.60
TiO2	0.74	0.98	1.24	1.10	0.58	1.20	0.38	1.10	1.12	1.34	0.64	0.66	0.84
Al2O3	14.90	13.80	13.50	14.50	16.00	14.30	14.40	14.10	14.00	13.90	15.50	16.00	14.80
Fe2O3	10.16	10.09	13.05	11.11	8.30	10.44	9.41	11.60	10.22	12.18	8.50	7.67	8.70
MnO	0.07	0.12	0.16	0.12	0.12	0.06	0.07	0.15	0.09	0.15	0.07	0.05	0.09
MgO	4.86	2.85	4.19	5.44	6.15	3.78	7.82	4.55	2.59	5.07	6.34	6.82	7.22
CaO	10.66	3.02	5.76	3.76	8.96	7.12	8.40	4.86	1.96	4.22	10.72	12.00	7.50
Na2O	2.34	4.90	3.32	4.48	3.64	3.58	1.29	4.68	5.28	4.34	1.48	1.15	0.42
K2O	0.24	0.46	0.48	0.21	0.32	0.23	0.56	0.87	0.02	0.13	0.21	0.20	0.72
P2O5	0.04	0.24	0.07	0.05	0.01	0.05	0.00	0.06	0.08	0.06	0.01	0.00	0.02
LOI	1.60	2.70	2.28	3.72	1.88	1.82	4.39	2.07	4.66	3.91	3.13	3.29	5.33
Total(%)	100.61	99.16	99.95	99.09	99.86	98.58	99.42	98.94	98.42	98.20	98.90	98.74	97.24
S	44	1429	68	490	60	49	36	43	92	181	43	31	26
Cl	42	42	42	78	258	54	77	199	56	36	64	70	83
Sc	40	26	29	39	42	35	52	32	30	38	51	36	43
V	369	228	443	480	311	342	303	457	189	506	320	282	326
Cr	18	b.d.	10	12	65	b.d.	16	5	b.d.	2	75	93	25
Ni	18.0	0.7	10.1	22.0	32.0	6.9	24.4	16.7	b.d.	10.9	34.1	43.4	32.5
Cu	b.d.	103.4	b.d.	101.4	2.3	0.7	b.d.	9.9	10.8	59.4	15.3	b.d.	b.d.
Zn	19.7	27.9	59.8	65.5	15.9	28.4	13.2	37.7	104.2	76.5	17.4	9.6	16.0
Ga	15.4	14.1	13.7	16.6	15.9	17.2	13.2	15.9	18.5	17.4	14.2	13.5	13.0
As	b.d.	b.d.	b.d.	b.d.	b.d.	b.d.	b.d.	b.d.	b.d.	b.d.	b.d.	1.6	5.0
Rb	1.1	1.6	2.1	1.2	1.6	1.0	2.6	4.3	b.d.	1.2	2.4	2.6	3.4
Sr	120.2	81.9	118.1	104.3	176.1	117.5	79.6	107.4	54.5	107.8	107.6	110.8	127.2
Y	23.2	44.5	30.7	26.4	15.4	28.0	10.7	31.8	40.6	31.8	17.0	14.5	20.1
Zr	39.9	89.1	65.1	62.2	23.8	63.1	8.9	67.0	87.2	69.3	31.3	24.6	42.6
Nb	1.3	1.9	1.6	1.0	1.0	1.7	0.5	1.6	1.7	1.2	1.4	0.9	0.7
Ba	b.d.	40	b.d.	b.d.	40	16	7	31	7	23	8	b.d.	8
Ce	20	36	40	32	19	23	26	26	34	14	7	32	27

Major element analyses (%) by A.A.; trace element analyses (ppm) by X.R.F.
b.d. = below detection limit

TABLE B.2.1 Whole rock geochemical analyses (continued)

Sample	DVE48	DVE99	DVE131A	DVE156	DVE0306.6	1222C–012	1305A–004
SiO2	59.30	55.80	54.10	56.10	53.40	63.30	52.30
TiO2	0.76	1.06	1.26	1.22	1.26	0.76	1.38
Al2O3	13.00	14.20	13.40	14.30	14.10	12.70	13.40
Fe2O3	10.56	10.78	12.58	11.37	12.18	9.23	14.54
MnO	0.15	0.07	0.14	0.14	0.12	0.02	0.07
MgO	4.55	4.95	5.34	4.13	6.52	1.81	4.73
CaO	8.52	8.00	2.96	5.80	1.98	3.74	4.48
Na2O	1.83	2.42	4.08	3.53	4.48	1.65	4.07
K2O	0.06	0.20	0.15	0.37	0.52	2.43	0.21
P2O5	0.01	0.10	0.06	0.07	0.08	0.14	0.07
LOI	1.15	1.79	4.43	1.96	4.69	3.03	2.76
Total(%)	99.89	99.37	98.50	98.99	99.31	98.81	98.01
S	20	18	9517	36	161	55	42
Cl	53	68	73	57	36	36	64
Sc	34	40	39	34	35	25	45
V	329	391	489	376	603	6	573
Cr	14	42	8	9	b.d.	26	11
Ni	8.2	16.4	6.4	16.1	11.3	b.d.	6.5
Cu	8.3	b.d.	597.0	b.d.	51.4	b.d.	b.d.
Zn	46.6	17.1	47.8	37.3	81.6	9.7	8.2
Ga	14.9	14.2	17.0	15.8	18.3	14.2	13.2
As	3.3	1.7	b.d.	b.d.	4.0	0.7	9.4
Rb	0.4	1.0	0.7	1.8	3.5	10.7	1.3
Sr	86.0	104.2	70.4	111.9	79.6	122.3	77.1
Y	23.4	29.9	33.4	35.7	31.4	38.7	29.6
Zr	38.5	58.8	71.4	86.2	70.2	69.5	71.9
Nb	1.2	1.2	1.6	1.5	1.6	1.7	1.2
Ba	8	5	14	29	9	23	2
Ce	17	15	19	31	40	26	34

Major element analyses (%) by A.A.; trace element analyses (ppm) by X.R.F.
b.d. = below detection limit

C. ISOTOPE AND FLUID INCLUSION DATA

C.1 STABLE ISOTOPE ANALYSES OF CALCITE

Calcite, on the basis of fracture filling and cross cutting relationships, was the latest mineral to be precipitated in the study area (refer to chapter 3). In an effort to determine whether the calcite is related to late hydrothermal fluid circulation (at or beneath the seafloor) or to later meteoric fluid circulation (post uplift), calcite samples were analyzed to determine their $^{13}C/^{12}C$ and $^{18}O/^{16}O$ isotopic composition.

The isotope data are reported as $\delta^{13}C$ and $\delta^{18}O$ values,

$$\delta = \left(\frac{R_{sample}}{R_{standard}} - 1\right) 1000 \quad \ldots\ldots\ldots\ldots \text{(C.1.1)}$$

where, R_{sample} is $^{13}C/^{12}C$ or $^{18}O/^{16}O$ in the sample and $R_{standard}$ is the corresponding ratio for the standard. The oxygen isotopic data in this study are reported using the standard δ notation, in units of parts per thousand, relative to the SMOW standard (Standard Mean Ocean Water) and the carbon relative to the PDB standard (Pee Dee Formation Belemnite) (Craig, 1957). The fractionation factor, α, is the isotopic partition coefficient for two phases such as a mineral and a coexisting fluid, and $\alpha_{A-B} = R_A / R_B$. From this and the above definition of δ it follows that,

$$\ln \alpha_{A-B} = \ln\left(1+\frac{\delta_A}{1000}\right) - \ln\left(1+\frac{\delta_B}{1000}\right) \quad \ldots\ldots \text{(C.1.2)}$$

which can be approximated by $1000 \ln \alpha_{A-B} \approx \delta_A - \delta_B$ since $\ln(1 + \epsilon) \approx \epsilon$ if $\epsilon \ll 1$. Fractionation factors are temperature dependent; thus, if one knows the isotopic composition of a sample and can make some assumptions about the isotopic composition of the coexisting fluid, the temperature of formation of the mineral can be determined. Fractionation factors as a function of temperature have been summarized by various workers (e.g. Kyser, 1987). The analyses were performed on a MAT 252 mass spectrometer in the Department of Earth Sciences, Memorial University of Newfoundland.

Four samples of calcite from fractures in the the dykes and pillow basalts yielded $\delta^{13}C$ values from +0.4 to +3.6 and $\delta^{18}O$ values from +13.2 to +27.9 (Figure 5.4). The four samples came from different depths through a stratigraphic section of the ophiolite. The data suggest that calcites in the Troodos ophiolite are similar to those that form in a marine environment, not a continental-meteoric environment (Fritz, 1976). Marine carbonates generally yield $\delta^{13}C$ values in the range of -3 to +4 and $\delta^{18}O$ values ranging from +22 to +35 whereas $\delta^{13}C$ and $\delta^{18}O$ in bulk average crustal carbon sources are -7 and +6 respectively (Faure, 1977; Fritz, 1976).

In order to calculate the isotopic composition of the fluid that formed the calcite, either temperature or the $\delta^{18}O$ value of the fluid needs to be estimated. If these carbonates formed in equilibrium with meteoric water with a $\delta^{18}O$ value between -5

and -10‰ at 1°C, then only the calcite with a $\delta^{18}O$ value of +27.9‰ could have formed from it. For the other three samples, regardless of temperature, the isotopic compositions of the water are not consistent with any possible near-coastal meteoric water.

If, on the other hand, the calcite formed in equilibrium with seawater, sample DVE-126-89 ($\delta^{18}O$ = +27.9) could have formed at temperatures of 17°C (Kyser, 1987) and the other calcite at temperatures between 75° and 135°C. Thus the simplest interpretation is that the $\delta^{18}O$ values of the calcite are indicative of seawater alteration at low temperatures between 17° and 135°C (Kyser, 1987), probably when the oceanic crust was in an off-axis position during the waning stages of hydrothermal circulation. These are the same conclusions reached by Alt et al. (1986) for calcite from DSDP Hole 504B that had isotopic compositions similar to those for calcite from the Troodos ophiolite. This suggests that fractures containing only calcite were unrelated to the high temperature or on-axis hydrothermal fluid circulation, or were they related to the uplift and emplacement of the ophiolite.

From the map (Figure C.1.1) it can be seen that sample 1138-030 and DVE-66-89 lie further to the south and consequently, because of the northerly dip of this part of the ophiolite, come from deeper in the section than the other two samples (DVE-76-89 and DVE-126-89). The deeper lying samples had lower $\delta^{18}O$ values ($\delta^{18}O$ = +13.2 and +17.3) than those shallower in the section ($\delta^{18}O$ = +18.9 and +27.9). This relationship of increasing $\delta^{18}O$ values higher in the section was also noted by Alt et al. (1986) in their analyses of calcite in DSDP hole 504B and by Gregory and Taylor (1981) for whole rock $\delta^{18}O$ analyses in the Semail ophiolite, Oman.

CARBON AND OXYGEN ISOTOPE
ANALYSES OF CALCITE

sample	$\delta^{13}C$ (PDB)	$\delta^{18}O$ (SMOW)
DVE-126-89	2.1	27.9
DVE-76-89	2.5	18.9
1138-030	0.4	17.3
DVE-66-89	3.6	13.2

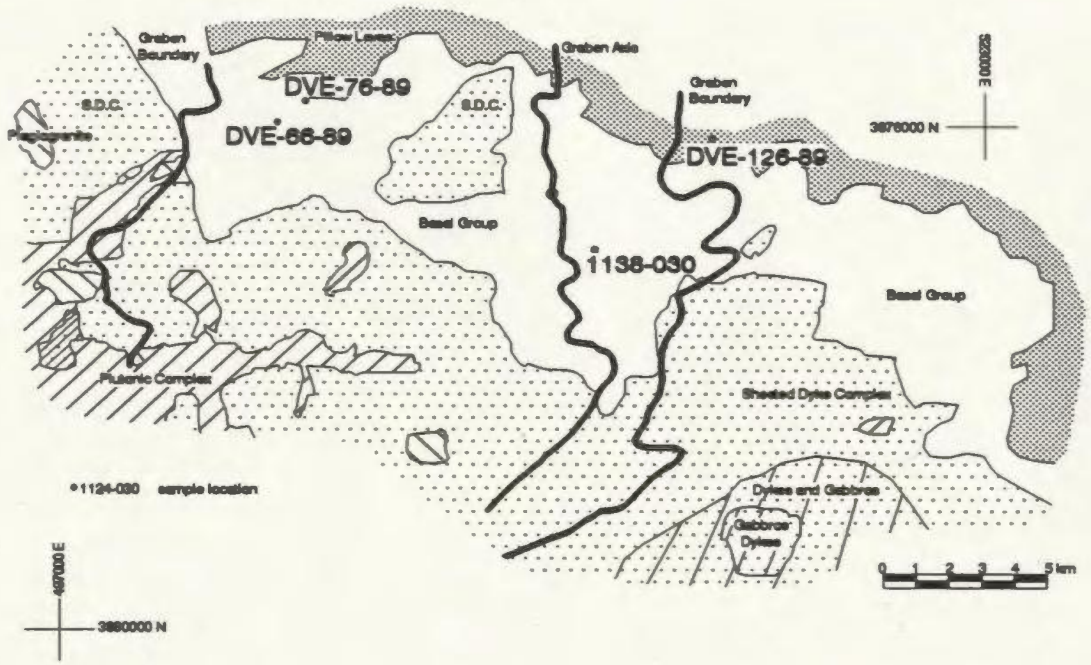

FIGURE C.1.1 CARBON AND OXYGEN ISOTOPA ANALYSIS RESULTS AND CALCITE SAMPLE LOCATION MAP, SPILIA - POLITIKO AREA, CYPRUS

C.2 FLUID INCLUSION ANALYSES

C.2.1 Methodology

The micro-thermometric analysis of fluid inclusions was done using a Fluid Inc. modified United States Geological Survey gas-flow heating-freezing stage operational within the temperature range -180°C to 500°C, using the procedures outlined in Roedder (1984). Homogenization temperature measurements were performed on individual fluid inclusions to obtain room-pressure trapping temperatures and salinities. During measurement of homogenization and freezing temperatures the samples were progressively heated in order to avoid inclusion decrepitation or phase changes caused by inclusion stretching. The temperatures reported have not been corrected for pressure unless specifically noted.

The accuracy of the combined thermocouple-heating/freezing stage was tested with synthetic fluid inclusions with known temperatures of phase transition (-56°C, O°C and 374.1°C), as well as, through the known melting temperatures of several compounds. The precision of the thermocouple and heating/freezing stage is 0.1°C. The homogenization and melting temperatures are reproducible to within 0.2°C.

The nomenclature used to describe inclusion behaviour during the heating and freezing procedures is that used by Roedder (1984). The last melting temperature (T_m) provides a measure of the solute salinity; and the homogenization temperature (T_h) is indicative of the minimum temperature at the time of fluid entrapment (Roedder, 1979; Crawford, 1981).

C.2.2 Fluid Inclusion Types and Results

The rock samples which were examined came from the western half of the Mitsero graben (Figure C.1). The vein samples studied contained quartz and epidote. Quartz veins are on the order of 1 millimetre wide; in some samples the mineral containing the fluid inclusions was within a vug in the host rock. Locally pyrite, hematite and jasper were seen.

The homogenization temperatures, and where possible, the last melting and eutectic temperatures were measured. These measurements, including fluid inclusion size, host minerals and salinities are presented in the following tables, as well as a compilation of the data from this study and that from the available literature and escriptions of the petrography of the fluid inclusion samples.

Of the 233 inclusions observed; 222 were within quartz and 11 were within epidote crystals. The sizes of the fluid inclusions varied from 3 to 40μm in their long dimension.

Two types of inclusions were seen: 1) two phase: liquid-vapour and 2) three phase: liquid-vapour-solid. All inclusions on which homogenization temperatures were measured, homogenized to the liquid phase.

Only two fluid inclusions were seen containing more than two phases. These (both in sample 0415-5A) were thought to be NaCl, based on the cubic form and the high relief of the solid phase. The included solid phase did not nucleate upon cooling, suggesting it was not a daughter mineral. The remainder of the fluid inclusions contained only two phases: fluid and vapour. There was no evidence for the presence of CO_2 in any of these inclusions, making a magmatic source for the fluids less likely.

In most cases the inclusions examined were secondary. Very few primary inclusions, identified by their isolated nature or by their occurrence in the growth zones of mineral phases, were identified. Secondary inclusions occurred in groups representing healed microfracture planes. Valid information can be obtained from secondary inclusions within a particular micro-fracture provided they have consistent liquid to vapour ratios (Roedder, 1984). This rule was observed in this study.

C.2.2.1 *Fluid Temperatures*

The homogenization temperatures for fluid inclusions varied from a minimum of 143°C to a maximum of 450°C. The mean temperatures for each sample range from 161° to 365°.

A histogram plot of all the fluid inclusion analyses (see histograms at the end of Appendix C.2) shows that there are three general populations of homogenization temperatures; 1) 190°-200°C, 2) 300°-320°C and 3) 350°-360°C. The largest population centres around 310°C. The highest homogenization temperatures for individual samples generally were similar at around 360°C; samples 0302-22 and 0302-27A are exceptions, their highest homogenization temperatures were 271°C and 259°C, respectivly.

C.2.2.2 *Fluid Composition*

Final melt temperatures were measured in 58 inclusions yielding weight-percent NaCl-equivalent salinities that varied from 1.6% to 20.0% (mean= 6.6%, standard deviation = 3.6%). This is based on the assumption that the melting solid is ice (H_2O) and not hydrohalite ($NaCl \cdot nH_2O$). In general, the salinities within a particular sample were fairly consistent, not varying by more than a few weight percent.

Salinities increase up-section: in the south (deeper in the sheeted dykes), salinities range from 2.4% (scanline area 1107) to 5.6% (shear zone near Apliki village);

whereas further to north, in the Basal Group mean salinities vary from 7.6% (scanline area 0307) to 12.5% (scanline area 0413).

C.2.2.3 *Estimated Pressures*

Temperature corrections for pressure can only be applied if the depth, and densities or compositions are known. No evidence for boiling was seen in the Sheeted Dyke Complex. This means that the homogenization temperatures did not lie on the boiling curve, which would have given a unique solution for the pressure. No estimates of pressure can be made from the inclusions themselves. Therefore, the pressure determination must be based on other sources of information.

Estimates of depth can be made from the thickness of the stratigraphic package and assuming that all hydrothermal activity had ceased by the time erosional processes started. The thickness of the overlying rock body is not well constrained, but it can be roughly estimated from map distances. It was assumed that fractures were interconnected to the seafloor so that the pressure was due wholly to hydrostatic, rather than lithostatic, effects. This was supported by the presence of 0.1 to 1.0 metre diameter angular dyke fragments floating in a vein network of epidote and quartz in a shear zone near the base of the Basal Group (at Apliki village) indicating fluid pressures in excess of lithostatic strength.

Calculations were done for various combinations of stratigraphic thickness, water depths, and lithostatic versus hydrostatic pressures. They were based on: 1) an average dip of the Upper and Lower Pillow Lava units of 8°; 2) four different water depths: 2000, 2200, 2400 and 2600 metres (from present day active hydrothermal areas including Valu Fa Ridge (Morton and Sleep, 1985), Juan de Fuca (Davis et al., 1987), Kane Fracture Zone (Delaney et al., 1987) and the East Pacific Rise (Welhan and Craig, 1983)); and 3) either a wholly hydrostatic case or a combination of hydrostatic and lithostatic pressure. In the latter case one must compute a combined water-rock pressure using,

$$P = [\rho_{water} \times d_{water} + \rho_{rock} \times d_{rock}]\, g \quad \ldots\ldots\ldots\ldots \quad (5.3)$$

where **P** = total pressure, ρ = density, and **d** = depth and **g** is the gravitational acceleration. This case provides a maximum pressure as it is believed that the fluid particle will not be subjected to as high a pressure as the adjacent rock particle. The hydrostatic case provides a minimum estimated pressure. The calculated pressures for the above combinations are presented in the last tables of this appendix. These pressures range from 340 bars (34.5 MPa) near the base of the Basal Group, in 2000 metres water depth in the hydrostatic case to 1095 bars (111 MPa) near the base of the sheeted dykes, in 2600 metres of water in the lithostatic case.

The final trapping temperatures were estimated using homogenization temperature corrections due to pressure conditions measured from published curves (Potter, 1977). The temperature corrections range from a minimum of 22° to a maximum of 119°C, which is a 6% to roughly 35% correction of the measured homogenization temperature. The pressure corrected temperatures are plotted in Figure C.3 and are discussed below.

To determine how reasonable the resulting temperatures at the various pressures were, a comparison was made with Bischoff and Rosenbauer's (1984) experimentally determined critical curve for seawater between 200° and 500°C and 0 to 500 bars (50.8 MPa) pressure. Since no evidence for boiling was seen in the fluid inclusion data set within the sheeted dyke complex, the curve provides a limit on the lowest possible pressures.

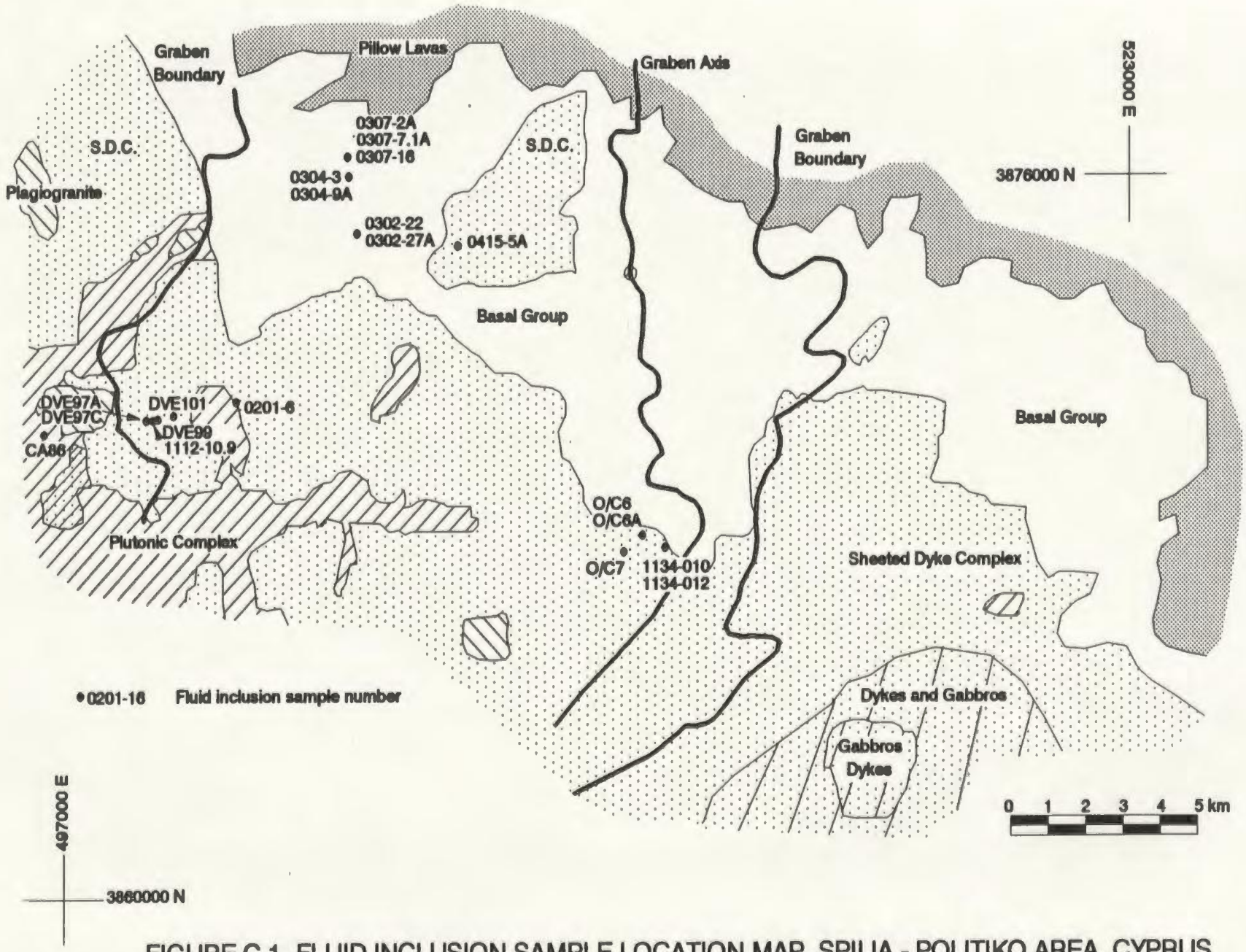

FIGURE C.1 FLUID INCLUSION SAMPLE LOCATION MAP, SPILIA - POLITIKO AREA, CYPRUS

Compiled Fluid Inclusion Results

Source of Data	Sample	Rock Type	Mineral	Th (°C)	N	Tm (°C)	Salinity Wt.% NaCl*
This study	O/C 6	diabase (vn**)	qtz	314.8	10	-7.2	10.7
	O/C 6A	diabase (vn)	qtz	312.2	32	-7.5 to -4.4	***2.6-7.0(9)
(Temperatures are mean for sample. For individual analyses see following table).	O/C 7	diabase (vn)	qtz	343.2	11	-3.5 to -5.3	5.7-8.3(3)
	0201-16	diabase (vn)	ep	196.8	2	-3.2	5.2
		diabase (vn)	qtz	380.4	1		
	0302-22	diabase (vn)	qtz	203.9	10	-4.2 to -5.6	6.7-8.7(3)
	0302-27A	diabase (vn)	qtz	318.2	2		
		diabase (vn)	qtz	184.8	2		
		diabase (vn)	qtz	232	3	-5.2	8.1
	0304-3	diabase (vn)	qtz	248.4	6	-7.4	11
	0304-9A	diabase (vn)	qtz	336.9	9	-3.2 to -4.8	5.2-7.8(7)
		diabase (vn)	qtz	190.6	1		
	0307-2A	diabase (vn)	qtz	298.2	8		
	0307-7.1A	diabase (vn)	qtz	301.1	10	-6.2	9.6(12)
		diabase (vn)	qtz	309.1	1	-6.4 to -8.7	8.4 - 12.9(2)
	0307-16	diabase (vn)	qtz	301.6	5	-2.2 to -2.6	3.7-4.3(2)
	0415-5A	epidosite (vn)	qtz	309.4	10	-7.2 to -8.7	10.7-13.7(5)
	1112-10.9	epidosite (gm,**)	qtz	331.6	8	-1.4	2.4
	1134-010	epidosite (vn)	qtz	352	3		
		epidosite (vn)	ep	212.5	4		
	1134-012	epidosite (vn)	ep	330.6	3		
		epidosite (vn)	qtz	161	1		
	DVE87A	epidosite (vn)	qtz	346.9	8	-3.2 to -3.7	5.2-6.0(2)
	DVE87C	diabase (vn)	qtz, ep	285.7	10	-3.2 to -3.6	5.4-5.6(2)
	DVE99	epidosite (vn)	qtz	307	14	-2.0 to -3.2	3.4-5.2(7)
	DVE101	diabase (vn)	qtz, ep	284.8	6		
	CAB6	plagiogr. (gm)	qtz	321.8	35	-1.0 to -18.5	1.7-20(9)
Cowan and Cann, 1988	Platanetasa	plagiogr. (gm)	qtz	380	20	-1	1.7
		plagiogr. (gm)	qtz	380	18	-42	39.7
Kelley et al., 1992	CY87-1	plagiogr. (gm)	qtz	317	46		50.2
		plagiogr. (gm)	qtz	317.3	17		6
	CY88-5	plagiogr. (gm)	qtz	320.9	21		46.8
		plagiogr. (gm)	qtz	336.3	28		5.2
	CY88-9	epidosite (gm)	qtz	382.2	55		42.5
		epidosite (gm)	qtz	386.1	68		3.2
		epidosite (gm)	ep	402.4	18		3.8
	CY88-17	u.gabbro (gm)	qtz	197	18		3.7
		u.gabbro (gm)	plag	207.1	7		2.1
	CY88-36	plagiogr. (vn)	qtz	322.8	123		4.2
		plagiogr. (vn)	qtz	296.7	37		4.2
	CY88-39	plagiogr. (vn)	qtz	282.9	42		3.8
	CY88-54	plagiogr. (gm)	qtz	297.8	18		50.4
		plagiogr. (gm)	qtz	266.6	22		4.5
	CY88-58	gabbro (gm)	amphi	343.7	6		6.2
	CY88-77	plagiogr. (gm)	qtz	287.5	25		3.9
	CY88-78	u.gabbro (vn)	qtz	330.1	20		3.2
	CY1017.62	gabbro (gm)	plag	187.7	40		1.2
	CY1181.75	gabbro (gm)	qtz	261.2	2		44.8
		gabbro (gm)	qtz	278.6	12		9
		gabbro (gm)	cpx	350.5	12		3.7
	CY10N.16	diabase (gm)	qtz	357.6	50		3.9
Richardson et al, 1987	Adelphi	epidosite (gm)	qtz	310	Total = 176		3.7-7.1%
		diabase (gm)	qtz	310			
Schiffman and Smith, 1988	Solea Graben	epidosite (gm)	qtz	340	Total = 74		4%
		epidosite (gm)	qtz?	300			
Spooner and Bray, 1977	Alestos Mine	Basal Group (vn)	qtz	325	61	-1.8	3.1
	Limni Mine	Pillow Lava (vn)	qtz	306	94	-1.9	3.2
		diabase (vn)	qtz	312.9	80	-2	3.4
Vibetti et al., 1989	CY-121	gabbro (vn), 970 m	qtz	230	8	-3.5	5.7
(Drillhole CY-4)			qtz	284	9	-4.8	7.8
	CY-120	gabbro (vn), 973 m	qtz	180	17	-3.8	6.1
			qtz	211	10	-4.7	7.4
	CY-118	gabbro (vn), 983.8 m	qtz	280	21	-19.6	22.4
			qtz	361	10	-4.5	7.2
	CY-004	diabase (vn), 1056 m	qtz	300	19	-4.7	7.4
			qtz	361	7	-3	4.9
			qtz	135	8	-31.6	30.4
	CY-006	Alt.diabase(gm) 1073	qtz	275	20	-4.7	7.4
	CY-024	gabbro (vn), 1186 m	qtz	295	15	-5.3	8.3
			qtz	172.1	8	-31.4	30.1
			qtz	301	3	-21.9	24.0

*weight% NaCl equivalent.

**vn = vein gm = groundmass

***number in brackets is number of analyses.

SAMPLE	ROCK TYPE	DESCRIPTION
O/C-6	DIABASE	shear zone, breccia. multiple dyke fragments from different dykes: some fine, some coarse grained. interstices filled with quartz and epidote. epidote has fine grained sandy texture to well developed euhedral crystals.
O/C-7A	DIABASE	altered diabase with zeolite and epidote vein and void filling quartz. late cross-cutting fine fractures some with calcite.
0201-16	DIABASE	altered diabase, matrix of chlorite and plagioclase. epidote, calcite vein. small fractures filled with inclusion rich quartz.
0302-22	DIABASE	altered dyke, epidote, quartz and chlorite. pale green epidote fracture fill, highly brecciated. both vein and groundmass fine grained. minor pyrite.
0302-27A	DIABASE	chlorite and epidote. dyke fragments. epidote fracture fill (similar to 302-22).
0304-3	DIABASE	altered dark green diabase. albite, chlorite and minor opagues with minor epidote.
0304-9A	DIABASE	breccia with fine grained glassy matrix containing plagioclase laths. quartz filling of vugs and veins. locally places quartz is highly fractured. some sausseritization of ground mass.
0307-2A	DIABASE	breccia; calcite, epidote, chlorite, pyrite and quartz. fragment interstices filled with epidote and quartz. vessicles increasing to outside of sample - may be pillow fragment.
0307-7.1	DIABASE	vessicles infilled with calcite. pillow fragment = rind. highly chloritized. epidote, pyrite in interior. diabase fragment = chloritized.
0307-16	DIABASE	pillow rubble. chlorite, calcite, epidote (forms euhedral rosettes), quartz.
0415-5A	EPIDOSITE	epidote (coarse grained in veins), pyrite (massive), quartz (vug infill).
1112-10.9	EPIDOSITE	coarse grained light green, no visible quartz or plagioclase.
1134-010	EPIDOSITE	epidote (vein), zeolite, calcite (in vein coarse grained, with possible malachite), magnetite (vein), quartz (minor in vein).
1134-012	EPIDOSITE	epidosite/diabase transition. fine grained calcite. magnetite in epidotized region.
DVE97A	EPIDOSITE	veins of quartz, magnetite, epidote. vein material intergrown. epidosite fine to medium grained. no visible sulfides.
DVE97C	DIABASE	chloritized diabase dyke, heavily veined with calcite, fine grained, no sulfides.
DVE99	EPIDOSITE	dyke margin; zeolite vein. host is fine grained, dark grey. no epidote, no sulfides.
DVE101	DIABASE	epidote veins; crystal perpendicular to vein walls; quartz vein with rare epidote crystals perpendicular to vein trend on wall rock. dyke is fine grained, and chloritized.
CA86	PLAGIOGRANITE	varies from fine grained dyke (CA86-1) with coarse epidote blebs to silicified bleached appearing (CA86-4) containing mafic fragments. may contain diabase xenoliths (with ill-defined boundaries).

Fluid Inclusion Sample Descriptions

The following table contains the results of the fluid inclusion analyses. The abbreviations used are as follows:

T.homo	Homogenization Temperature
T.melt	Last Melt Temperature
Host	the mineral hosting the fluid inclusion
Prim. Size	Size of primary inclusions
Sec. Size	Size of secondary inclusions
Vapour H_2O%	Vapour bubble size as a percentage of inclusion size
WT%NaCl equiv.	Weight percent based on an equivalent NaCl composition

The measurement of temperature, in the modified United States Geological Survey Heating/Freezing stage (by Fluid Inc.), was done through a thermocouple placed on the sample. It was found that the intensity of the light source did affect the measured temperature due to absorption of light energy by the thermocouple material. At low temperatures the difference in the measured temperature for no light source and a light source at +8V was 5°C. It was also noted that temperatures measured off a light mineral were different from temperatures measured off a dark mineral, again due to their different absorptive properties. Ideally the mineral crystal being investigated should have the same light absorptive properties as the thermocouple. These errors would be added to the measurement error. The light source temperature changes appear to be linear - a case could be made for subtracting this amount (5°C) from the temperature.

The effect of the microscope light voltage on the temperature recorded by the thermocouple is noted in Figure C.1.

Fluid Inclusion Data (Troodos Ophiolite, Cyprus)

Sample #	T.homo (C)	T.melt (C)	Host	Prim. Size	Sec. Size	Vapour H2O%	Daughter Mineral	WT%NaCl equiv.
O/C-6	338.1		qtz		12	30		
O/C-6	283.9		qtz		24	20		
O/C-6	323.2		qtz		8	20		
O/C-6	345.9	-7.2	qtz		24	10		10.7
O/C-6	352.9		qtz		15	15		
O/C-6	323.2		qtz		8	30		
O/C-6	258.1		qtz		8	20		
O/C-6	286.5		qtz		20	30		
O/C-6	291.2		qtz		20	20		
O/C-6	345.1		qtz		8	15		
O/C 6A	353.8		qtz		24	5		
O/C 6A	357.0		qtz		15	10		
O/C 6A	>403		qtz		15	15		
O/C 6A	359.4		qtz		24	30		
O/C 6A	351.0		qtz					
O/C 6A	350.0		qtz					
O/C 6A	351.0		qtz					
O/C 6A	225.3		qtz		30	5		
O/C 6A	225.4		qtz		30	2		
O/C 6A	380.0	-4.4	qtz		30	40		7.0
O/C 6A	344.1	-4.0	qtz		30	40		6.4
O/C 6A	223.1		qtz		40	3		
O/C 6A	310.5		qtz			20		
O/C 6A	321.0	-3.2	qtz		17	10		5.2
O/C 6A	320.6	-3.8	qtz		17	20		6.1
O/C 6A	337.2	-4.4	qtz		12	5		7.0
O/C 6A	333.9		qtz		17	10		
O/C 6A	334.7		qtz		17	2		
O/C 6A	277.8		qtz		12	5		
O/C 6A	298.4		qtz		15	7		
O/C 6A	306.2		qtz		12	5		
O/C 6A			qtz		12	15		
O/C 6A	298.9		qtz		12	20		
O/C 6A			qtz		12	15		
O/C 6A	292.3		qtz		3	12		
O/C 6A			qtz		12	5		
O/C 6A	294.6	-2.0	qtz		15	20		3.4
O/C 6A	302.2	-1.5	qtz		15	15		2.6
O/C 6A	320.0	-2.3	qtz		10	5		3.9
O/C 6A	296.1		qtz		15	5		
O/C 6A	310.1		qtz		10	15		
O/C 6A	319.1	-2.0	qtz		10	5		3.4
O/C 6A	293.0		qtz		10	5		
O/C 6A	299.1		qtz		12	5		
O/C 6A	290.2		qtz		15	30		
O/C 6A	313.0		qtz		12	10		
O/C-7A	362.8	-5.3	qtz		40	35		8.3
O/C-7A	356.8	-4.1	qtz		30	20		6.6
O/C-7A	371.0		qtz		24	10		

Fluid Inclusion Data (Troodos Ophiolite, Cyprus)

Sample #	T.homo (C)	T.melt (C)	Host	Prim. Size	Sec. Size	Vapour H2O%	Daughter Mineral	WT%NaCl equiv.
O/C-7A	339.4		qtz		24	10		
O/C-7A	290.6		qtz		24	10		
O/C-7A	347.3	-3.5	qtz		30	20		5.7
O/C-7A	343.1		qtz		20	10		
O/C-7A	352.1		qtz		12	15		
O/C-7A	357.0		qtz		12	10		
O/C-7A	342.0		qtz		6	10		
O/C-7A	346.6		qtz		6	15		
0201-16	187.1		ep	24		8		
0201-16	>450		ep	24		25		
0201-16	206.4	-3.2	qtz		17	20		5.2
0201-16	360.4		qtz		15	60		
0201-16			qtz		8	20		
0201-16			qtz		8	60		
0302-22	193.9	-5.6	qtz		30	2		8.7
0302-22	177.9		qtz		10	10		
0302-22	187.9	-4.2	qtz		30	5		6.7
0302-22	197.9		qtz		30	10		
0302-22	191.7	-4.8	qtz		30	10		7.6
0302-22	210.2		qtz		6	5		
0302-22	258.5		qtz		6	5		
0302-22	211.8		qtz		6	5		
0302-22	212.2		qtz		6	5		
0302-22	196.9		qtz		6	10		
0302-27A	271.4		qtz		20	10		
0302-27A	192.6		qtz		6	0		
0302-27A	233.2	-5.2	qtz		6	1		8.1
0302-27A	142.1		qtz		15	10		
0302-27A	188.8		qtz		15	10		
0304-3	140.0		qtz		20	15		
0304-3	171.2		qtz		12	10		
0304-3	183.2		qtz		8	10		
0304-3	323.9	-7.4	qtz		20	30		11.0
0304-3	337.5		qtz		12	20		
0304-3	334.5		qtz		12	20		
0304-9A	365.6	-4.8	qtz		17	15		7.6
0304-9A	330.8	-4.7	qtz		20	5		7.4
0304-9A	351.6	-4.2	qtz		15	20		6.7
0304-9A	316.7	-4.3	qtz		10	3		6.9
0304-9A	191.0		qtz		6	2		
0304-9A	314.2	-4.2	qtz		20	40		6.7
0304-9A	348.7	-4.5	qtz		17	15		7.2
0304-9A	367.9	-3.2	qtz		20	20		5.2
0304-9A	295.8	-4.4	qtz		15	10		7.0
0304-9A	340.8		qtz		20	15		
0307-2A	281.2		qtz		20	5		
0307-2A	305.4		qtz		20	10		
0307-2A	316.8		qtz		15	20		
0307-2A	284.5		qtz		30	15		

Fluid Inclusion Data (Troodos Ophiolite, Cyprus)

Sample #	T.homo (C)	T.melt (C)	Host	Prim. Size	Sec. Size	Vapour H2O%	Daughter Mineral	WT%NaCl equiv.
0307-2A	300.1		qtz		15	10		
0307-2A	280.1		qtz		10	10		
0307-2A	304.2		qtz		10	10		
0307-2A	291.6		qtz		15	15		
0307-2A	319.9		qtz		15	10		
0307-7.1A	365.1	-6.2	qtz		30	5		9.5
0307-7.1A	290.1		qtz			10		
0307-7.1A	291.4		qtz			10		
0307-7.1A	290.2		qtz			10		
0307-7.1A	313.4	-8.7	qtz		20	30		12.5
0307-7.1A	296.0		qtz		8	15		
0307-7.1A	305.1		qtz		12	10		
0307-7.1A	316.5	-5.4	qtz		30	15		8.4
0307-7.1A	294.1		qtz		6	30		
0307-7.1A	300.2		qtz		6	25		
0307-7.1A	314.0		qtz		6	10		
307-16	>410		qtz		24	20		
307-16	311.5	-2.6	qtz		24	10		4.3
307-16	269.8	-2.2	qtz		24	20		3.7
307-16	268.2		qtz		24	2		
307-16	>457		qtz		24	30		
0415-5A	311.1		qtz		24	5	NaCl	
0415-5A	310.9		qtz		20	10	NaCl	
0415-5A	316.0	-9.3	qtz		24	5		13.2
0415-5A	311.0	-9.7	qtz		17	5		13.7
0415-5A	310.7		qtz		17	7		
0415-5A	313.4	-9.4	qtz		24	10		13.3
0415-5A	314.5		qtz		30	15		
0415-5A	304.5		qtz		30	15		
0415-5A	301.1	-7.2	qtz		20	30		10.7
0415-5A	300.5	-7.8	qtz		20	30		11.5
1112-10.9	356.8		qtz		7	25		
1112-10.9	349.0		qtz		6	30		
1112-10.9	317.0		qtz		7	20		
1112-10.9	351.0	-1.4	qtz		8	25		2.4
1112-10.9	328.0		qtz		6	25		
1112-10.9	324.0		qtz		8	35		
1112-10.9	330.0		qtz		6	30		
1112-10.9	297.0		qtz		6	20		
1134-010	235.4		qtz		9	15		
1134-010	237.1		qtz		1	20		
1134-010	187.6		ep		4	20		
1134-010	190.0		ep		2	20		
1134-010	351.0		qtz		9	25		
1134-010	355.0		qtz		6	20		
1134-010	350.0		qtz		2	20		
1134-012	161.0		qtz		2	20		
1134-012	300.1		ep		3	20		
1134-012	305.3		ep		2	20		

Fluid Inclusion Data (Troodos Ophiolite, Cyprus)

Sample #	T.homo (C)	T.melt (C)	Host	Prim. Size	Sec. Size	Vapour H2O%	Daughter Mineral	WT%NaCl equiv.
1134-012	302.1		ep		1	20		
DVE97A-89	360.3	-3.2	qtz	10		30		5.2
DVE97A-89	359.0	-3.7	qtz		8	20		6.0
DVE97A-89	358.0		qtz		8	20		
DVE97A-89	358.9		qtz		10	25		
DVE97A-89	357.0		qtz		8	20		
DVE97A-89	359.0		qtz		8	20		
DVE97A-89	355.0		qtz		8	20		
DVE97A-89	354.0		qtz		10	20		
DVE97A-89	261.0		qtz		12	35		
DVE97C-89	219.0		ep	9		30		
DVE97C-89	298.0		ep		12	15		
DVE97C-89	270.1	-3.6	qtz		1	40		5.8
DVE97C-89	346.8	-3.3	qtz	2		45		5.4
DVE97C-89	269.8		qtz	1		35		
DVE97C-89	267.7		qtz	1		40		
DVE97C-89	299.9		ep	2		20		
DVE97C-89	355.6	(T.vap?)	qtz	2		45		
DVE97C-89	251.0		qtz		1	30		
DVE97C-89	279.5		qtz		1	30		
DVE99-89	306.0	-3.2	qtz		6	25		5.2
DVE99-89	308.8		qtz		3	25		
DVE99-89	279.5	-2.0	qtz		6	25		3.4
DVE99-89	312.2	-2.1	qtz		1	25		3.5
DVE99-89	303.0		qtz		6	30		
DVE99-89	305.0		qtz		2	25		
DVE99-89	301.0		qtz		2	20		
DVE99-89	308.0		qtz		12	20		
DVE99-89	306.0		qtz		9	25		
DVE99-89	294.5	-2.4	qtz		6	20		4.0
DVE99-89	293.3	-3.2	qtz		6	20		5.2
DVE99-89	290.8		qtz		6	20		
DVE99-89	342.6	-2.0	qtz		9	30		3.4
DVE99-89	346.9	-3.2	qtz		7	25		5.2
DVE101-89	236.8		qtz		3	25		
DVE101-89	237.9		qtz		6	25		
DVE101-89	279.8		qtz		3	20		
DVE101-89	278.1		qtz		3	20		
DVE101-89	290.0		ep		6	15		
DVE101-89	266.0		qtz		3	30		
CA86-2	336.2	-1.7	qtz		12	5		2.9
CA86-2	334.9		qtz		15	5		
CA86-2	197.5		qtz			5		
CA86-2	340.6		qtz			5		
CA86-2	313.3		qtz		15	12		
CA86-2	294.0		qtz			5		
CA86-2	296.2		qtz			5		
CA86-2	340.6		qtz		15	5		
CA86-2	337.0		qtz		10	5		

Fluid Inclusion Data (Troodos Ophiolite, Cyprus)

Sample #	T.homo (C)	T.melt (C)	Host	Prim. Size	Sec. Size	Vapour H2O%	Daughter Mineral	WT%NaCl equiv.
CA86-7	290.1		qtz		10	5		
CA86-7	308.9		qtz		10	5		
CA86-7	308.6		qtz		12	5		
CA86-7	305.1		qtz			5		
CA86-7	308.2		qtz		10	5		
CA86-7	318.2		qtz		12	5		
CA86-7	312.2		qtz		15	5		
CA86-7	312.8		qtz		10	5		
CA86-8	342.0	-2.4	qtz		15	20		4.0
CA86-9	283.1	-16.5	qtz		20	5		20.0
CA86-9	277.6		qtz		12	10		
CA86-9	285.0	-0.9	qtz		15	5		1.6
CA86-9	283.0		qtz		12	5		
CA86-9	292.7	-1.4	qtz		20	5		2.4
CA86-9	275.3		qtz		20	7		
CA86-9	292.0		qtz		20	7		
CA86-9	284.6		qtz		20	5		
CA86-9	280.0		qtz		15	5		
CA86-9	289.3	-1.3	qtz		15	5		2.2
CA86-9	292.5	-2.1	qtz		40	10		3.5
CA86-9	282.0		qtz		12	5		
CA86-9		-1.0	qtz		30	5		1.7
CA86-10	323.9		qtz		15	5		
CA86-10			qtz		8	5		
CA86-10	330.9		qtz		12	5		
CA86-10			qtz		12	5		
CA86-10	336.0		qtz		15	5		
CA86-10	328.9		qtz		15	5		
CA86-10	332.9		qtz		17	5		
CA86-10	322.0		qtz		15	5		
CA86-10	300.9	-9.2	qtz		15	5		13.1
CA86-10	329.8		qtz		15	5		

Fluid Inclusion Microscope Light Source Temperature Effects

Under Ambient Conditions (i.e. no heating)

Light Voltage	Thermocouple Temp.(°C)
0	23.1
1	23.1
2	23.1
3	23.2
4	23.9
5	24.9
6	25.9
7	27
8	28.3
9	29.3
10	30.8

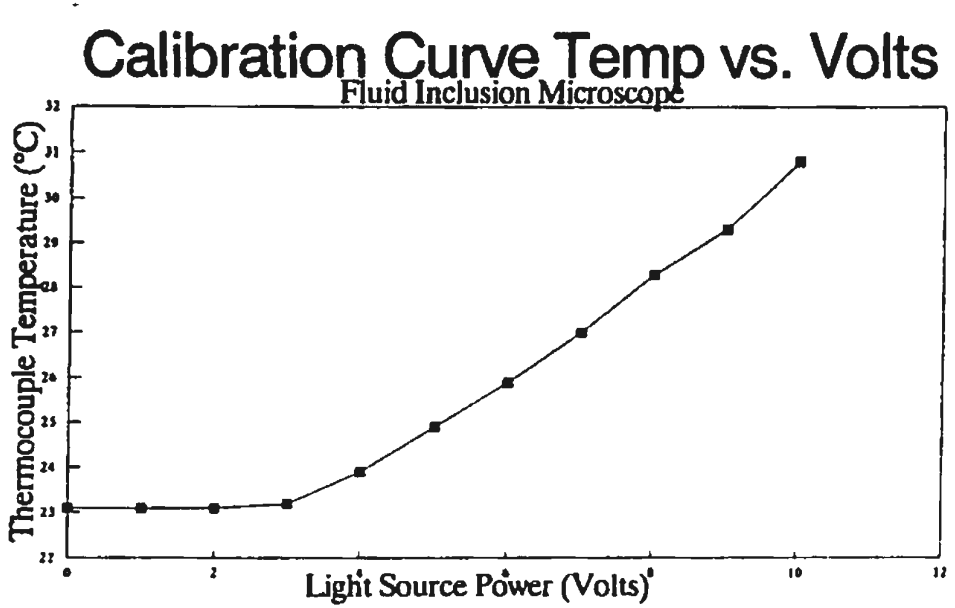

Figure C.1

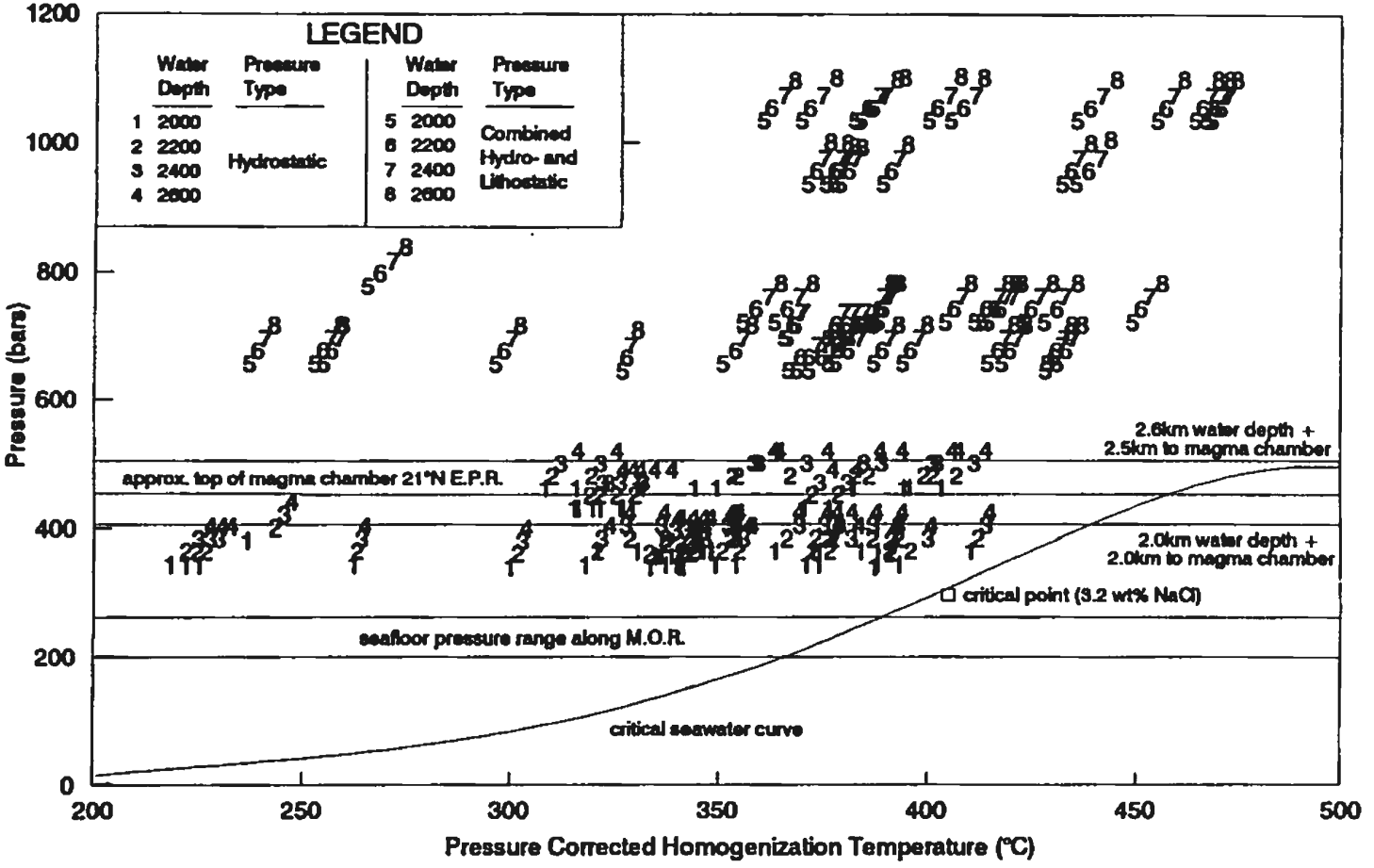

FIGURE C.3 HOMOGENIZATION TEMPERATURE VERSUS PRESSURE BASED ON FLUID INCLUSION DATA. CRITICAL SEAWATER CURVE AFTER BISCHOFF AND ROSENBAUER (1988) LOWER 2 HORIZONTAL LINES REPRESENT THE UPPER AND LOWER LIMITS OF SEAWATER DEPTHS ASSUMED IN THIS STUDY (2000 AND 2600 METRES RESPECTIVELY). MIDDLE UPPER LINE IS THE APPROXIMATE DEPTH OF AN EAST PACIFIC RISE MAGMA CHAMBER.

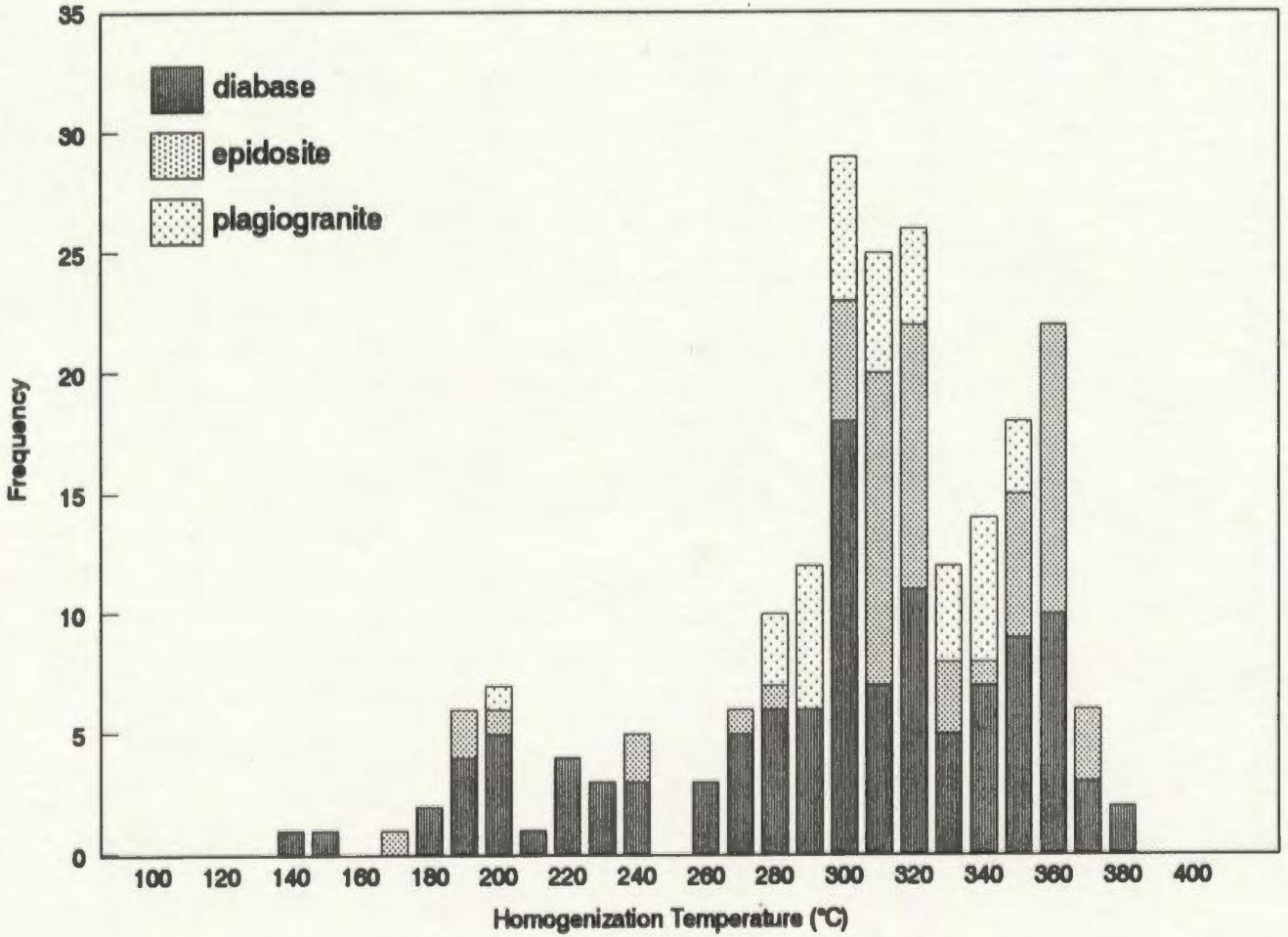

FIGURE C.2 HISTOGRAM OF FLUID INCLUSION HOMGENIZAION TEMPERATURES BY ROCK TYPE. TEMPERATURES ARE NOT CORRECTED FOR PRESSURE EFFECTS.

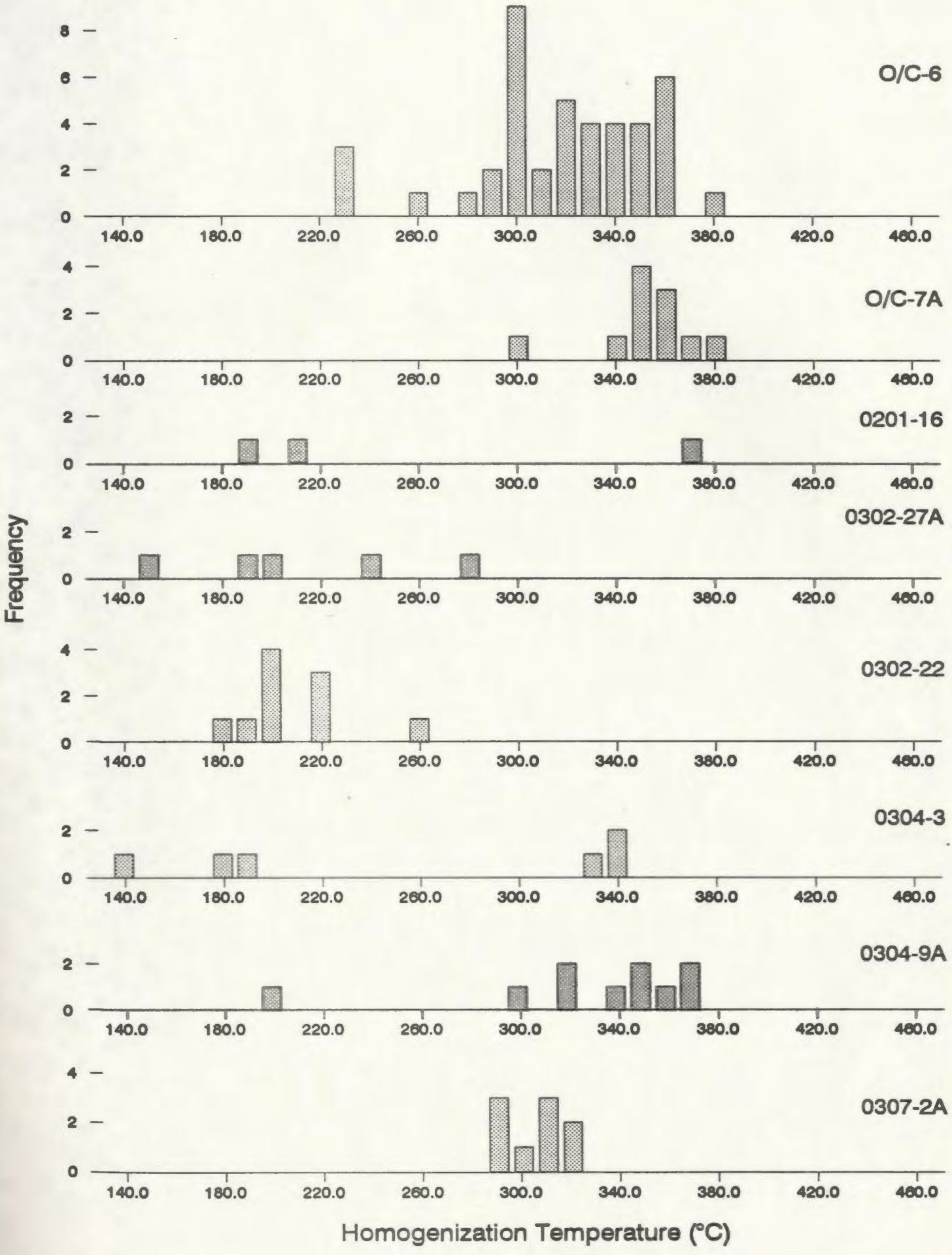
O/C-6
O/C-7A
0201-16
0302-27A
0302-22
0304-3
0304-9A
0307-2A
Frequency
Homogenization Temperature (°C)
140.0
180.0
220.0
260.0
300.0
340.0
380.0
420.0
460.0

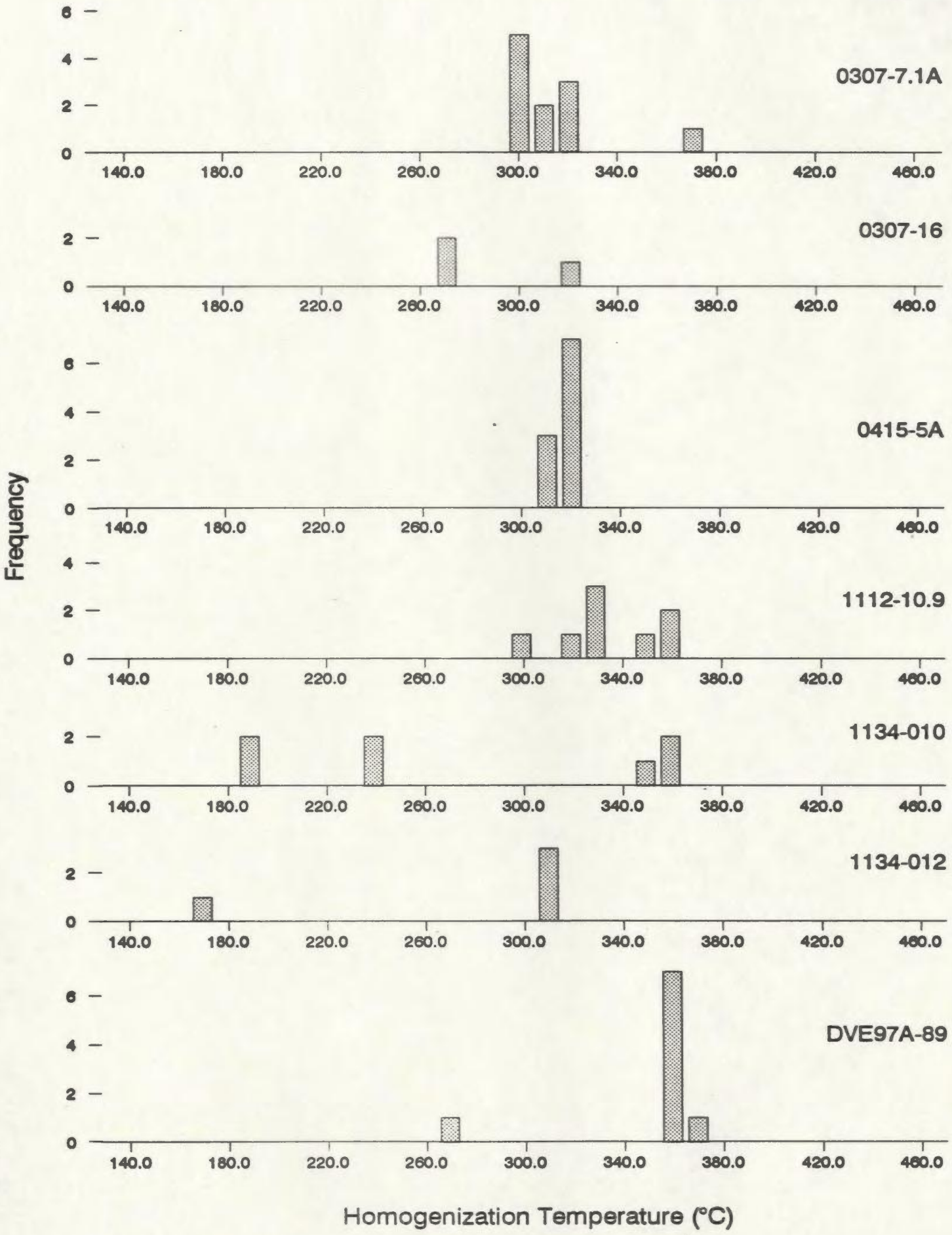
0307-7.1A
0307-16
0415-5A
1112-10.9
1134-010
1134-012
DVE97A-89
Frequency
Homogenization Temperature (°C)
140.0
180.0
220.0
260.0
300.0
340.0
380.0
420.0
460.0

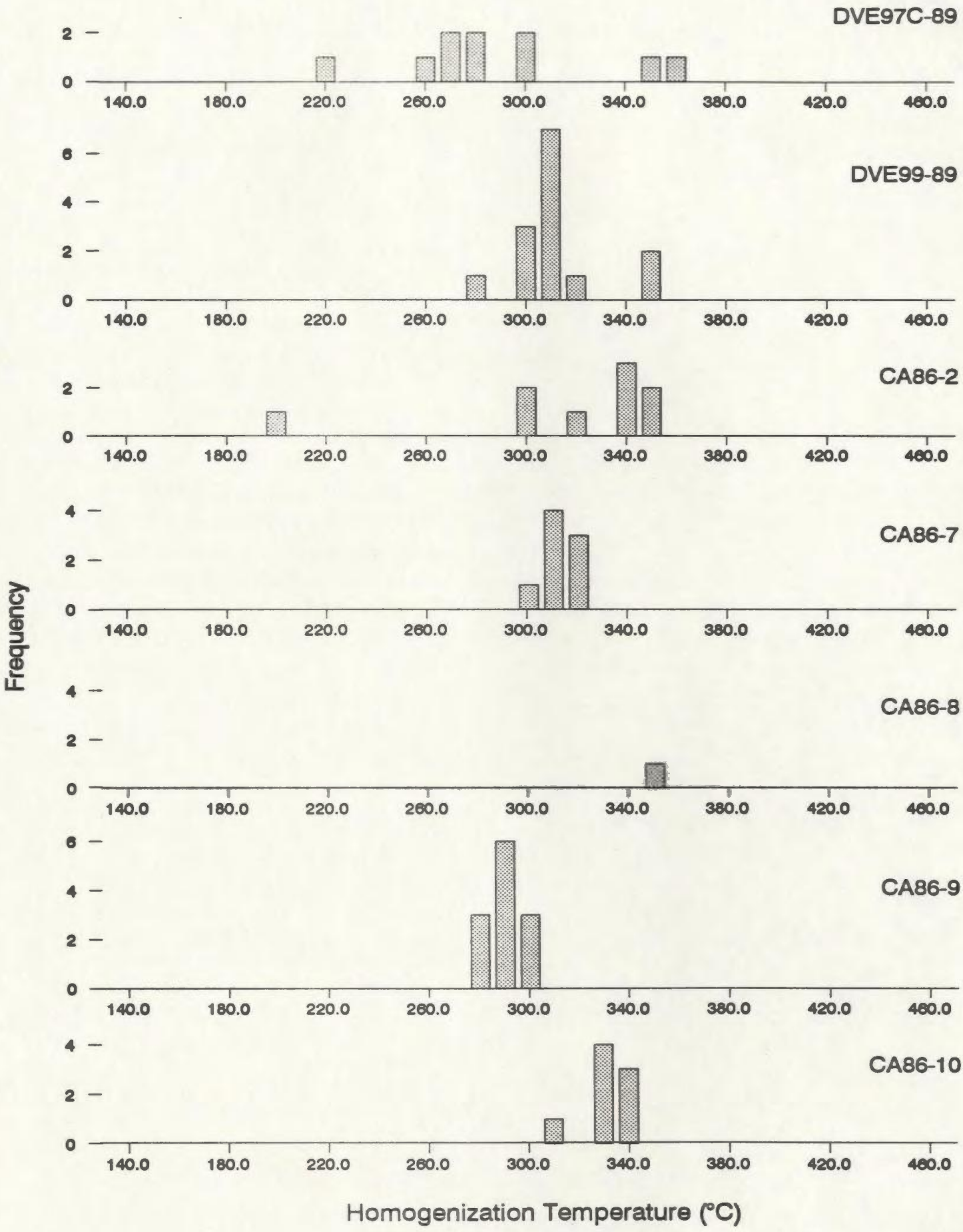
DVE97C-89
DVE99-89
CA86-2
CA86-7
CA86-8
CA86-9
CA86-10
Frequency
140.0
180.0
220.0
260.0
300.0
340.0
380.0
420.0
460.0
Homogenization Temperature (°C)

The following two pages show the calculation of the pressure corrected fluid inclusion temperatures. On the next page the first three columns give the sample name, inclusion homogenization temperature,, and the salinity (in weight % NaCl equivalent). The following four columns are the stratigraphic thicknesses for each sample, from the seafloor to the sample, estimated from geological maps of the area (e.g. Carr and Bear, 1960). The depth estimations are based on a sediment dip of 18°. The last four columns are the calculated pressures based on water depths of 2000, 2200, 2400, and 2600 metres and the assumption of either hydrostatic (columns 8 to 11) or lithostatic (columns 12 to 15) pressure conditions. For these determinations a seawater density of 1025 kg/m^3, and a rock density of 3300 kg/m^3, were assumed. The second page of the table gives the pressure corrected temperatures. These pressure corrections for temperature were measured from graphs by Potter (1977), for the cases as mentioned above. This includes all combinations of hydrostatic, lithostatic pressures and water depths of 2000, 2200, 2400, 2600 metres.

Fluid Inclusion Pressure Corrected Temperatures (cont'd)

Sample #	T.homo (°C)	Weight %NaCl equiv.	Pressure Corrected Temperatures: Hydrostatic Case Water Depth				Lithostatic Case Water Depth			
			2000m	2200m	2400m	2600m	2000m	2200m	2400m	2600m
O/C-6	345.9	10.7	373.9	375.9	378.9	381.9	412.9	415.9	418.9	420.9
O/C 6A	380.0	7.0	410.0	412.0	414.0	415.0	449.0	451.0	453.0	456.0
O/C 6A	344.1	6.4	372.1	373.1	375.1	376.1	411.1	414.1	417.1	419.1
O/C 6A	321.0	5.2	348.0	353.0	354.0	355.0	387.0	389.0	391.0	393.0
O/C 6A	320.6	6.1	347.6	352.6	353.6	354.6	386.6	388.6	390.6	392.6
O/C 6A	337.2	7.0	363.2	366.2	369.2	369.2	404.2	406.2	408.2	410.2
O/C 6A	294.6	3.4	320.6	328.6	327.6	328.6	355.6	358.6	361.6	364.6
O/C 6A	302.2	2.6	330.2	337.2	334.2	337.2	363.2	366.2	369.2	372.2
O/C 6A	320.0	3.9	346.0	354.0	353.0	354.0	388.0	389.0	390.0	392.0
O/C 6A	319.1	3.4	345.1	353.1	352.1	353.1	387.1	388.1	389.1	391.1
O/C-7A	362.8	8.3	387.8	392.8	392.8	393.8	427.8	430.8	432.8	435.8
O/C-7A	356.8	6.6	383.8	386.8	386.8	387.8	422.8	424.8	426.8	429.8
O/C-7A	347.3	5.7	372.3	377.3	377.3	378.3	414.3	417.3	420.3	422.3
0201-16	206.4	5.2	236.4	243.4	245.4	247.4	265.4	268.4	271.4	274.4
0302-22	193.9	8.7	224.9	228.9	229.9	232.9	254.9	256.9	258.9	259.1
0302-22	187.9	6.7	217.9	221.9	224.9	227.9	236.9	238.9	240.9	242.9
0302-22	191.7	7.6	221.7	224.7	227.7	230.7	252.7	254.7	256.7	259.7
0302-27A	233.2	8.1	262.2	263.2	264.2	265.2	296.2	298.2	300.2	302.2
0304-3	323.9	11.0	348.9	350.9	353.9	357.9	386.9	388.9	390.9	392.9
0304-9A	365.6	7.6	387.6	390.6	391.6	392.6	428.6	430.6	432.6	434.6
0304-9A	330.8	7.4	353.8	354.8	355.8	356.8	393.8	395.8	397.8	399.8
0304-9A	351.6	6.7	373.6	376.6	381.6	383.6	417.6	419.6	421.6	423.6
0304-9A	316.7	6.9	339.7	343.7	346.7	346.7	377.7	380.7	383.7	386.7
0304-9A	314.2	6.7	337.2	341.2	344.2	344.2	376.2	378.2	381.2	384.2
0304-9A	348.7	7.2	370.7	372.7	376.7	378.7	414.2	416.7	418.7	420.7
0304-9A	367.9	5.2	392.9	395.9	399.9	400.9	430.9	432.9	434.9	436.9
0304-9A	295.8	7.0	317.8	320.8	321.8	323.8	350.8	353.8	355.8	357.8
0307-7.1A	365.1	9.5	387.1	391.1	391.1	392.1	428.1	430.1	432.1	434.1
0307-7.1A	313.4	12.5	340.4	343.4	344.4	346.4	368.4	371.4	373.4	377.4
0307-7.1A	316.5	8.4	341.5	341.5	343.5	344.5	371.5	374.5	378.5	380.5
307-16	311.5	4.3	333.5	333.5	343.5	344.5	366.5	369.5	373.5	375.5
307-16	269.8	3.7	299.8	301.8	302.8	303.8	326.8	327.8	328.8	329.8
0415-5A	316.0	13.2	341.0	345.0	346.0	348.0	381.0	383.0	385.0	387.0
0415-5A	311.0	13.7	336.0	341.0	342.0	344.0	376.0	378.0	380.0	382.0
0415-5A	313.4	13.3	338.4	343.4	344.4	346.4	378.0	380.4	382.4	384.4
0415-5A	301.1	10.7	335.1	338.1	340.1	341.1	366.1	368.1	370.1	371.1
0415-5A	300.5	11.5	334.5	337.5	339.5	340.5	365.5	367.5	369.5	371.5
1112-10.9	351.0	2.4	403.0	407.0	411.0	414.0	464.0	466.0	468.0	470.0
DVE97A-89	360.3	5.2	395.3	401.3	402.3	407.3	468.3	470.3	472.3	473.3
DVE97A-89	359.0	6.0	394.0	399.0	401.0	406.0	467.0	469.0	471.0	472.0
DVE97C-89	270.1	5.8	308.1	310.1	312.1	316.1	360.1	362.1	365.1	369.1
DVE97C-89	346.8	5.4	381.8	385.8	388.8	393.8	454.8	456.8	458.8	459.8
DVE99-89	306.0	5.2	344.0	367.0	371.0	376.0	400.0	402.0	405.0	408.0
DVE99-89	279.5	3.4	315.5	319.5	321.5	325.5	369.5	371.5	374.5	377.5
DVE99-89	312.2	3.5	349.2	353.2	359.2	363.2	405.2	408.2	411.2	414.2
DVE99-89	294.5	4.0	331.5	334.5	359.5	364.5	383.5	386.5	389.5	392.5
DVE99-89	293.3	5.2	330.3	353.3	358.3	363.3	382.3	385.3	388.3	391.3
DVE99-89	342.6	3.4	381.6	382.6	384.6	388.6	435.6	438.6	441.6	444.6
DVE99-89	346.9	5.2	381.9	385.9	388.9	393.9	454.9	456.9	458.9	459.9
CA86-2	336.2	2.9	370.2	372.2	374.2	377.2	435.2	438.2	441.2	443.2
CA86-8	342.0	4.0	376.0	378.6	380.6	383.0	432.0	434.0	436.0	439.0
CA86-9	283.1	20.0	315.1	319.1	322.1	327.1	377.1	378.1	379.1	380.1
CA86-9	285.0	1.6	316.0	319.0	322.0	327.0	371.0	373.0	375.0	378.0
CA86-9	292.7	2.4	326.7	329.7	331.7	334.7	378.7	380.7	382.7	385.7
CA86-9	289.3	2.2	321.3	325.3	326.3	331.3	375.3	377.3	379.3	381.3
CA86-9	292.5	3.5	319.5	321.5	323.5	329.5	375.5	377.5	380.5	382.5
CA86-10	300.9	13.1	325.9	329.9	331.9	338.9	388.9	390.9	392.9	394.9

Pressure Correction of Fluid Inclusion Homogenization Temperatures

Sample #	T.homo (°C)	Weight %NaCl equiv.	Stratigraphic Thickness (m) * Pillows	Basal Gp.	Dykes	Total Thickness (m)	Hydrostatic Pressure (Bars) ** 2000.0 (m)	2200.0 (m)	2400.0 (m)	2600.0 (m)	Hydro- and Lithostatic Pressure (Bars) *** 2000.0 (m)	2200.0 (m)	2400.0 (m)	2600.0 (m)
O/C-6	345.9	10.7	1180.0	352.0	69.0	1601.0	362.8	383.0	403.1	423.3	720.8	741.0	761.1	781.3
O/C 6A	380.0	7.0	1180.0	352.0	69.0	1601.0	362.8	383.0	403.1	423.3	720.8	741.0	761.1	781.3
O/C 6A	344.1	6.4	1180.0	352.0	69.0	1601.0	362.8	383.0	403.1	423.3	720.8	741.0	761.1	781.3
O/C 6A	321.0	5.2	1180.0	352.0	69.0	1601.0	362.8	383.0	403.1	423.3	720.8	741.0	761.1	781.3
O/C 6A	320.6	6.1	1180.0	352.0	69.0	1601.0	362.8	383.0	403.1	423.3	720.8	741.0	761.1	781.3
O/C 6A	337.2	7.0	1180.0	352.0	69.0	1601.0	362.8	383.0	403.1	423.3	720.8	741.0	761.1	781.3
O/C 6A	294.6	3.4	1180.0	352.0	69.0	1601.0	362.8	383.0	403.1	423.3	720.8	741.0	761.1	781.3
O/C 6A	302.2	2.6	1180.0	352.0	69.0	1601.0	362.8	383.0	403.1	423.3	720.8	741.0	761.1	781.3
O/C 6A	320.0	3.9	1180.0	352.0	69.0	1601.0	362.8	383.0	403.1	423.3	720.8	741.0	761.1	781.3
O/C 6A	319.1	3.4	1180.0	352.0	69.0	1601.0	362.8	383.0	403.1	423.3	720.8	741.0	761.1	781.3
O/C-7A	362.8	8.3	1180.0	352.0	69.0	1601.0	362.8	383.0	403.1	423.3	720.8	741.0	761.1	781.3
O/C-7A	356.8	6.6	1180.0	352.0	69.0	1601.0	362.8	383.0	403.1	423.3	720.8	741.0	761.1	781.3
O/C-7A	347.3	5.7	1180.0	352.0	69.0	1601.0	362.8	383.0	403.1	423.3	720.8	741.0	761.1	781.3
0201-16	206.4	5.2	1180.0	352.0	241.0	1773.0	380.1	400.3	420.4	440.6	776.6	796.8	816.9	837.1
0302-2	193.9	8.7	1180.0	220.0	m	1400.0	342.6	362.7	382.9	403.0	655.6	675.8	695.9	716.1
0302-22	187.9	6.7	1180.0	220.0	m	1400.0	342.6	362.7	382.9	403.0	655.6	675.8	695.9	716.1
0302-22	191.7	7.6	1180.0	220.0	m	1400.0	342.6	362.7	382.9	403.0	655.6	675.8	695.9	716.1
0302-27A	233.2	8.1	1180.0	220.0	m	1400.0	342.6	362.7	382.9	403.0	655.6	675.8	695.9	716.1
0304-3	323.9	11.0	1180.0	220.0	m	1400.0	342.6	362.7	382.9	403.0	655.6	675.8	695.9	716.1
0304-9A	365.6	7.6	1180.0	220.0	m	1400.0	342.6	362.7	382.9	403.0	655.6	675.8	695.9	716.1
0304-9A	330.8	7.4	1180.0	220.0	m	1400.0	342.6	362.7	382.9	403.0	655.6	675.8	695.9	716.1
0304-9A	351.6	6.7	1180.0	220.0	m	1400.0	342.6	362.7	382.9	403.0	655.6	675.8	695.9	716.1
0304-9A	316.7	6.9	1180.0	220.0	m	1400.0	342.6	362.7	382.9	403.0	655.6	675.8	695.9	716.1
0304-9A	314.2	6.7	1180.0	220.0	m	1400.0	342.6	362.7	382.9	403.0	655.6	675.8	695.9	716.1
0304-9A	348.7	7.2	1180.0	220.0	m	1400.0	342.6	362.7	382.9	403.0	655.6	675.8	695.9	716.1
0304-9A	367.9	5.2	1180.0	220.0	m	1400.0	342.6	362.7	382.9	403.0	655.6	675.8	695.9	716.1
0304-9A	295.8	7.0	1180.0	220.0	m	1400.0	342.6	362.7	382.9	403.0	655.6	675.8	695.9	716.1
0307-7.1A	365.1	9.5	1180.0	186.0	m	1366.0	339.1	359.3	379.4	399.6	644.6	664.8	684.9	705.1
0307-7.1A	313.4	12.5	1180.0	186.0	m	1366.0	339.1	359.3	379.4	399.6	644.6	664.8	684.9	705.1
0307-7.1A	316.5	8.4	1180.0	186.0	m	1366.0	339.1	359.3	379.4	399.6	644.6	664.8	684.9	705.1
307-16	311.5	4.7	1180.0	186.0	m	1366.0	339.1	359.3	379.4	399.6	644.6	664.8	684.9	705.1
307-16	269.8	4.7	1180.0	186.0	m	1366.0	339.1	359.3	379.4	399.6	644.6	664.8	684.9	705.1
0415-5A	316.0	13.2	1180.0	344.0	m	1524.0	355.1	375.2	395.4	415.5	695.9	716.0	736.2	756.3
0415-5A	311.0	13.7	1180.0	344.0	m	1524.0	355.1	375.2	395.4	415.5	695.9	716.0	736.2	756.3
0415-5A	313.4	13.3	1180.0	344.0	m	1524.0	355.1	375.2	395.4	415.5	695.9	716.0	736.2	756.3
0415-5A	301.1	10.7	1180.0	344.0	m	1524.0	355.1	375.2	395.4	415.5	695.9	716.0	736.2	756.3
0415-5A	300.5	11.5	1180.0	344.0	m	1524.0	355.1	375.2	395.4	415.5	695.9	716.0	736.2	756.3
1112-10.9	351.0	2.4	700.0	1000.0	868.0	2568.0	460.2	480.4	500.5	520.7	1034.5	1054.7	1074.8	1095.0
DVE97A-89	360.3	5.2	700.0	1000.0	868.0	2568.0	460.2	480.4	500.5	520.7	1034.5	1054.7	1074.8	1095.0
DVE97A-89	359.0	6.0	700.0	1000.0	868.0	2568.0	460.2	480.4	500.5	520.7	1034.5	1054.7	1074.8	1095.0
DVE97C-89	270.1	5.8	700.0	1000.0	868.0	2568.0	460.2	480.4	500.5	520.7	1034.5	1054.7	1074.8	1095.0
DVE97C-89	346.8	5.4	700.0	1000.0	868.0	2568.0	460.2	480.4	500.5	520.7	1034.5	1054.7	1074.8	1095.0
DVE99-89	306.0	5.2	700.0	1000.0	868.0	2568.0	460.2	480.4	500.5	520.7	1034.5	1054.7	1074.8	1095.0
DVE99-89	279.5	3.4	700.0	1000.0	868.0	2568.0	460.2	480.4	500.5	520.7	1034.5	1054.7	1074.8	1095.0
DVE99-89	312.2	3.5	700.0	1000.0	868.0	2568.0	460.2	480.4	500.5	520.7	1034.5	1054.7	1074.8	1095.0
DVE99-89	294.5	4.0	700.0	1000.0	868.0	2568.0	460.2	480.4	500.5	520.7	1034.5	1054.7	1074.8	1095.0
DVE99-89	293.3	5.2	700.0	1000.0	868.0	2568.0	460.2	480.4	500.5	520.7	1034.5	1054.7	1074.8	1095.0
DVE99-89	342.6	3.4	700.0	1000.0	868.0	2568.0	460.2	480.4	500.5	520.7	1034.5	1054.7	1074.8	1095.0
DVE99-89	346.9	5.2	700.0	1000.0	868.0	2568.0	460.2	480.4	500.5	520.7	1034.5	1054.7	1074.8	1095.0
CA86-2	336.2	2.9	1130.0	434.0	700.0	2264.0	429.6	449.8	469.9	490.1	935.9	956.0	976.2	996.3
CA86-8	342.0	4.0	1130.0	434.0	700.0	2264.0	429.6	449.8	469.9	490.1	935.9	956.0	976.2	996.3
CA86-9	283.1	20.0	1130.0	434.0	700.0	2264.0	429.6	449.8	469.9	490.1	935.9	956.0	976.2	996.3
CA86-9	285.0	1.6	1130.0	434.0	700.0	2264.0	429.6	449.8	469.9	490.1	935.9	956.0	976.2	996.3
CA86-9	292.7	2.4	1130.0	434.0	700.0	2264.0	429.6	449.8	469.9	490.1	935.9	956.0	976.2	996.3
CA86-9	289.3	2.2	1130.0	434.0	700.0	2264.0	429.6	449.8	469.9	490.1	935.9	956.0	976.2	996.3
CA86-9	292.5	3.5	1130.0	434.0	700.0	2264.0	429.6	449.8	469.9	490.1	935.9	956.0	976.2	996.3
CA86-10	300.9	13.1	1130.0	434.0	700.0	2264.0	429.6	449.8	469.9	490.1	935.9	956.0	976.2	996.3

* Depth estimation used a dip of 10° to convert map distance to depth
P (bars) = P (Pascals) / 1.002*10^5 Pa
Pressure corrected temperatures measured tables by Potter (1977)

** To calculate hydrostatic pressure:
Assume seawater density of 1025 kg/m^3
P = density*(gravitational acc'n)*depth
= 1.025*(9.81)*depth (in Pascals)

*** To calculate lithostatic pressure:
1) seawater density is 1025kg/m^3)
2) rock density is 3300kg/m^3)
P = (water density*water depth + rock density *rock thickness)*gravitational acc'n
= (1.025*water depth + 3.300*rock thickness)*9.81

D. PROGRAMS

D.1 PROGRAM DESCRIPTION

The following is a listing of programs written in the course of this project. They are referenced in the flow charts of Figures 2.2, 3.1, and 5.1.1. A short description of each program is followed by the input requirements and the output file specifications. Unless otherwise noted, all input and output files are in ASCII (American Standards Association for Information Interchange) format. Graphics programs output files in the Lotus PIC format (e.g. QuickPlot, QPSEP, and ROSE). The following programs were all written and complied using the MicroSoft Corporation QuickBASIC editor and compiler for the IBM PC.

ANOVA

Purpose: Perform an analysis of variance test on a series of data sets to test whether the differences between and within sets are significant.
Input: 1 column of values separated by group labels.
Output: full table of test results.

APSTAT

Purpose: Calculate the mean apertures for various subsets of fracture data: all fractures, filled fracture, unfilled fractures, epidote, or zeolite or calcite filled fractures.
Input: 2 file types: 1 batch file containing the file names and the directory pathname, the raw data files containing the fracture data.
Output: table of mean apertures as outlined above for each scanline area.

CIRCLE

Purpose: Using the method outlined by Charlaix et al. (1984) compute fracture trace lengths based on sampling an input distribution of fracture radii.
Input: contains one column of fracture radii following a distributional form such as normal, log-normal, exponential, Weibull, square, and bimodal.
Output: binned numbers of fracture trace lengths.

DISTANCE

Purpose: to convert distances along scanlines in an area of multiple scanlines (each connected to the preceding line but with distance counting staring at zero) to consecutive distances.
Input: raw fracture characteristic data files

Output: fracture data files with modified distances.

DOMSEP

Purpose: Determines whether a point lies inside or outside of an irregularly shaped (closed) polygon.
Input: 2 files: one containing the raw dyke orientation and location data, the other containing the x, y coordinates of the domain boundaries.
Output: separated data file containing orientation and location values of all points falling within the domain boundary.

DXFPLINE

Purpose: Conversion of AutoCAD DXF files containing lineament information as polylines to give start and end coordinates of lines as well as their lengths and orientations.
Input: AutoCAD DXF format file
Output: #, X1, Y1, X2, Y2, Length, Orientation

GRID

Purpose: take raw dyke data (location and orientation) and calculate estimated dyke orientations at evenly spaced grid nodes. The program comprises several subprograms: GRIDDIG, GRIDEST, GRIDANGL.

GRIDDIG

Purpose: digitize orientation dip symbols from published maps.
Input: from a GTCO 24" x 36" digitizing table.
Output: azimuth, dip, easting, northing.

GRIDEST

Purpose: Estimate dyke orientations at evenly spaced grid points from the raw dyke orientation data. The resulting values were then plotted through either SURFACE II (contouring package for VAX systems), or through AutoCAD (AutoDesk). The orientation data were plotted using the QuickPlot stereographic projection program (van Everdingen et al., 1992).
Input: raw dyke orientation and location data
Output: estimated dyke orientations and nodal locations

Following is a more detailed description of the GRIDEST program:

The raw data proved difficult to interpret due to their nonuniform spatial distribution (see raw data plot, Figure B.1.2). Therefore, orientations were estimated for regularly spaced grid node points overlain on the data set, using the program GRIDEST. This was done by first picking a grid-node spacing such that the total number of grid points was roughly equal to the number of data points. Since the grid is rectangular and the data distribution is not, grid points on the periphery of the grid will have no corresponding data points and

thus, in the final analysis, will be dropped from the estimated data set. The final result is an estimated data set numbering roughly one third the number of data points, providing a minimal smoothing of the original data.

The estimation of orientation at a grid-node was done in four steps:

1) pick a search circle radius - to reduce the amount of smoothing this was generally picked as equal to the distance between grid nodes,

2) determine which points of the data set fall within the search circle periphery - different approaches for nearest neighbour searches are possible, but for simplicity, all neighbouring points found within the search circle were used. (this approach biases the resultant orientation if no neighbouring data points are found in some of the quadrants of the search circle),

3) assign a weight to each data point, dependent on its distance from the grid node whose orientation we are trying to estimate. Several different weighting techniques could be employed. A linear weighting was tried but it proved to smooth the data too much. An inverse exponential weighting was used. This weight was
then normalized to the total number of data points within the search circle radius, by

$$\vec{Z}_e=\sum_{i=1}^{n}\left[\frac{W_i Z_i}{W_T}\right], \qquad W_T=\sum_{i=1}^{n} W_i, \qquad \vec{Z}_i=\begin{bmatrix} Z_{i1} \\ Z_{i2} \\ Z_{i3} \end{bmatrix}$$

where vector Z_e is the estimated orientation at the grid node point, vector Z_i is the orientation at data point i within the search circle radius and is comprised of the three direction cosines, Z_j for $j=1,2,3$. n is the number of points falling within the search circle radius. The weight, W_i, applied to the data point using the weighting function in this case is,

$$W_i = \frac{1}{e^{10\frac{h_i}{r}}}$$

where h is the distance of the ith data point to the grid node point and r is the radius of the search circle, so that when $h/r=1$, $W\approx 0$ and when $h/r=0$, $W=1$. W_T is the sum of the weights of all data points that fall within the search circle perimeter. This is used to normalize the results to the number of data points.

4) convert the orientations to direction cosines and apply the appropriate

weights at each data point to its direction cosines. Then sum the direction cosines and convert back to an azimuth-dip orientation.

GRIDANGL

Purpose: To calculate the spherical angle between the orientations of dykes at adjacent node points.
Input: estimated dyke orientation data and nodal locations.
Output: angles and locations.

Following is a more detailed description of the GRIDANGL program:

The angle between two planes can be determined through the dot product of the normal vectors to each plane. This method allows angles between various planes in X-Y space to be monitored without referring to a reference point and thus it does not imply any mode of deformation.

Areal variations in orientation of dykes can be observed by several different methods. Determining the angle or dot product between the normals of two adjacent dykes (or adjacent data sampling points) is the simplest approach. Other methods include breaking the angular difference between the two points into two components (the simplest case - where no prior knowledge of the deformation history is known). One component represents rotation about a horizontal axis, the other about a vertical axis. This allows the determination of the difference in strike angle from point to point and then the difference in dip angle. Another method is to observe the angular difference (dot product) between points as above but to separate the results into two groups based on whether the total angular change is dominated by change in strike (implying rotation about a vertical axis) or whether it is dominated by change in dip angle (implying rotation about a horizontal axis.

MINSTAT

Purpose: Calculation of fracture mineral filling by trace length statistics. Statistics calculated include: mean, average and standard deviation, skewness and kurtosis, as well as, maximum and minimum trace lengths for each fracture filling mineral.
Input: 2 file types: batch files containing the file names (of the scanlines by domain) and the directory pathname; the raw data files containing the fracture data.
Output: mineral versus trace length statistics as outlined above for each domain.

ORS

Purpose: conversion of raw fracture data files to a format containing orientation and trace length for use by FracSys and FracWorks (FracMan).
Input: raw fracture characteristic data.
Output: orientation and scanline identifier and trace length (this is linked to a SVY survey file containing the particulars of the scanline such as length and orientation).

PARAPLAT

Purpose: Calculation of permeability using the parallel plate model presented by Norton and Knapp (1977).
Input: raw fracture characteristic data files and a batch file containing the names of the scanline data files.
Output: table of permeability data for each scanline including number of fractures, scanline length, mean dyke orientation, and permeability based on all, filled, unfilled, epidote, zeolite and calcite mineral fillings.

PREPROC

Purpose: Processes the raw fracture characteristic data files to separate the fractures based on different mineral fillings or whether the fractures are sub-parallel to dyke orientations, for use by ORS.
Input: raw fracture characteristic data and a batch file containing the names of the scanline data files to be used.
Output: chosen fracture characteristics.

QPSEP

Purpose: to graphically separate fracture data on the basis of orientation. The chosen results can be tabulated and output to either ASCII files or PIC files.
Input: raw fracture characteristic data.
Output: various possible formats: PIC, table output, fracture record output, or orientation data only output.

QuickPlot

Purpose: To plot, rotate, contour or statistically manipulate spherical orientation data. The program was produced by van Everdingen et al. (1992). Its listing is published in the same reference and thus will not be reproduced here (as it is rather lengthy).
Input: orientation data in an azimuth, dip or dip, azimuth or strike, dip formats.
Output: PIC format stereographic projection plots, statistical results tables, or rotated data orientations.

ROSE

Purpose: to plot rose orientation diagrams.
Input: azimuth orientation data in several file formats (e.g. from DXFPLINE, SEEK, QuickPlot). Can be run in batch mode to put multiple rose plots in one file.
Output: PIC graphics file.

SCRIPT

Purpose: to produce an AutoCAD compatible script file to plot symbols on a map (e.g. dip symbols with dip magnitude).
Input: 2 files: one containing location name and U.T.M. coordinates, the other containing azimuth and dip.
Output: SCR file to be read into AutoCAD using the SCRIPT command (needs the presence of a drawing file containing the symbol to be plotted).

SEEK

Purpose: to search the fracture characteristics data files based on various possible user selected parameters and extract matches to the search to an output file.
Input: raw fracture characteristic data files (see format in Appendix A).
Output: varies dependent on the choice of output parameters. Includes QuickPlot compatible files as well as files containing complete data records.

SNOWPERM

Purpose: to calculate rock intrinsic permeabilities based on fracture orientations and apertures using the Bianchi and Snow (1969) method.
Input: raw fracture characteristic data files. can also be run in batch mode with another file containing file location and names.
Output: permeability tensor (directions and magnitude).

SPACE

Purpose: to calculate the spacing between fractures of the same orientation set within one scanline area. Used in the SAS routines (SPACE.SAS, RKSPACE.SAS, and LNORM.SAS by Rouleau, 1984).
Input: batch file containing scanline areas to be treated, file containing the eigen values of the mean set orientations and of the scanline, fracture characteristic data file prepared by DISTANCE to have consecutive scanline distances.
Output: set number, spacing, angle between fracture and scanline.

TABULATE

Purpose: to compile for each scanline the totals of the number of fractures exhibiting each of the possible values for each parameter (e.g. length, mineral filling).
Input: raw fracture characteristics data files.
Output: table of frequency results for use in producing the frequency maps of chapter 3.

TERZAGHI

Purpose: to apply the Terzaghi correction factor (Terzaghi, 1965) to a set of orientation data.
Input: Azimuth dip data.
Output: Corrected azimuth dip data.

VAXCONV

Purpose: to convert GRID produced data files for use by the SURFACE II program on the VAX operating system (an example SURFACE II command file is given below).
Input: output files from the GRID programs containing location and orientation (azimuth and dip) of dykes.
Output: x,y coordinates of the dykes for plotting and angle values and locations for contouring.

Example SURFACE II command file:

```
TITL          DYKE ORIENTATIONS - TROODOS OPHIOLITE, CYPRUS
DEVICE        6,'DVAN'
IDXY          3104,11,4,1,2,3,-1,4,,,'(3F12.2,F2.0)'
POST          2,,0.05,,0
SIZCONTOUR    0,1270,1270
BOX           1000,5,1000,5,,495000,3856000,1
ROUTLINE      12,3104,'(2F12.2)'
POUTLINE
PERFORM
STOP
```

D.2 PROGRAM LISTINGS

The following are the BASIC code listings of the programs outlined in the previous section. Where code lines are too long to properly fit on the page, they have been truncated by an '@' symbol, the code for that line continues on the line following prefixed by the '@' symbol. To save space in printing these listings, spaces have been removed from many of the print statements. The codes are in the same order as that in the previous section.

```
'---ANOVA.BAS
'---Program to perform Analysis of Variance on multiple
'---groups with one dependent variable
'---By: D. van Everdingen  Date: 1 November 1988

DIM HIST(1000), POINTER(100), LABEL$(100),
GRPSUM(100), GRPSQR(100)
CLS
LOCATE 2, 5: PRINT "One-Way Analysis of Variance Program"
LOCATE 3, 2: PRINT "By D. van Everdingen  Date: November
1988"
LOCATE 1, 1: PRINT CHR$(218);
FOR II = 1 TO 47
PRINT CHR$(196);
NEXT II
PRINT CHR$(191)
LOCATE 4, 1: PRINT CHR$(192);
FOR II = 1 TO 47
PRINT CHR$(196);
NEXT II
PRINT CHR$(217)
FOR II = 1 TO 2: LOCATE 1 + II, 1: PRINT CHR$(179); :
NEXT II
FOR II = 1 TO 2: LOCATE 1 + II, 49: PRINT CHR$(179); :
NEXT II
LOCATE 5, 1
'---The data must be in one column separated by group labels
'---(Note: labels may not start with: a number, +, - or .,
'---all else are valid)
INPUT "Input name of file containing data: ", FILE1$
OPEN FILE1$ FOR INPUT AS #1
INPUT "How many groups are there in the data: ", GROUP
I = 1: K = 1: POINTER(1) = 1
WHILE NOT EOF(1)
INPUT #1, DATASTRING$
CHECK = ASC(MID$(DATASTRING$, 1, 1))
IF CHECK = 43 OR CHECK = 45 OR CHECK = 46 OR
(CHECK > 47 AND @
@ CHECK < 58) THEN
HIST(I) = VAL(DATASTRING$)
I = I + 1
ELSE
LABEL$(K) = MID$(DATASTRING$, 1, 10)
 IF K > 1 THEN
POINTER(K) = I
ELSE
POINTER(K) = I
END IF
K = K + 1
END IF
WEND
COUNTER = I - 1
'---fill the POINTER array with the size of each group
'---find the number of observations in the largest group
FOR I = 1 TO GROUP
POINTER(I) = POINTER(I + 1) - POINTER(I)
NEXT I
POINTER(GROUP) = COUNTER + POINTER(GROUP) + 1
FOR I = 1 TO GROUP
IF MAX < POINTER(I) THEN MAX = POINTER(I)
NEXT I
'---print out the input data
COLOR 1, 8: PRINT "Input Data": COLOR 7, 0
PRINT : PRINT "";
FOR I = 1 TO GROUP - 1
PRINT USING "\\"; LABEL$(I);
NEXT I
PRINT USING "\\"; LABEL$(GROUP)
START = 1: ENDING = 0
FOR J = 1 TO GROUP
START = START + POINTER(J - 1)
ENDING = ENDING + POINTER(J)
IF J = 1 THEN
XPOS = 1
ELSE
XPOS = J * 10 - 10
END IF
K = 1
FOR I = START TO ENDING
LOCATE 9 + K, XPOS
PRINT USING "#######.##"; HIST(I)
K = K + 1
NEXT I
NEXT J
LOCATE 12 + MAX, 1
'---Now we can start the data manipulation
'---POINTER contains the position of the
'---start of the new group of data
'---HIST contains the complete list of data
'---LABEL contains the labels for each group
K = 1: SUM = 0
DUMMY = POINTER(1)
FOR I = 1 TO COUNTER
SUMSQR = SUMSQR + (HIST(I) * HIST(I))
SUM = SUM + HIST(I)
IF I <= DUMMY THEN
GRPSUM(K) = GRPSUM(K) + HIST(I)
ELSE
K = K + 1
DUMMY = DUMMY + POINTER(K)
GRPSUM(K) = GRPSUM(K) + HIST(I)
END IF
NEXT I
SST = SUMSQR - (SUM * SUM) / COUNTER
SUMINT = 0
FOR I = 1 TO GROUP
SUMINT = SUMINT + (GRPSUM(I) * GRPSUM(I)) /
POINTER(I)
NEXT I
SSB = SUMINT - (SUM * SUM) / COUNTER
SSW = SUMSQR - SUMINT
```

```
'----calculate degrees of freedom
'----for Between
DFB = GROUP - 1
'-----for within
DFW = COUNTER - GROUP
'----for total
DFT = COUNTER - 1
'-----Means squared
SSBDF = SSB / DFB
SSWDF = SSW / DFW
'----F ratio
F = SSBDF / SSWDF
'----produce output table
COLOR 1, 8: PRINT "Source"; : COLOR 7, 0: PRINT " ";
COLOR 1, 8: PRINT "SumSquare"; : COLOR 7, 0: PRINT "";
COLOR 1, 8: PRINT "Degrees of"; : COLOR 7, 0
PRINT "";
COLOR 1, 8: PRINT "MeanaSquare"; : COLOR 7, 0: PRINT "";
COLOR 1, 8: PRINT "F": COLOR 7, 0
PRINT " ";
COLOR 1, 8: PRINT "Freedom": COLOR 7, 0
PRINT "Between ";
PRINT USING "##########.##"; SSB; DFB; SSBDF; F
PRINT "Within";
PRINT USING "##########.##"; SSW; DFW; SSWDF
PRINT
PRINT "Total";
PRINT USING "##########.##"; SST; DFT
PRINT ""
CLOSE #1
END
```

```
'----APSTAT.BAS
'----program to calculate aperture statistics
'----dimension arrays
DIM M$(10), T(10, 10), S(10, 4), LT(10, 10), LS(10, 2)
M$(1) = "0": M$(2) = "1": M$(3) = "2"
CLS
'----print title
PRINT "Aperture Statistics": PRINT
'----get input batch file name
INPUT "Enter batch file name: ", BF$
OF$ = "APSTAT.OUT"
CLOSE #1: CLOSE #3
OPEN BF$ FOR INPUT AS #1
OPEN OF$ FOR OUTPUT AS #3
PRINT "Output will be to: "; OF$
INPUT #1, Dir$
Dir$ = Dir$ + "\"
PRINT "Input directory: "; Dir$
WHILE NOT EOF(1)
  INPUT #1, F$
  CLOSE #2
  OPEN Dir$ + F$ FOR INPUT AS #2
  PRINT "Reading: "; F$
'----first pass to get the mean
  FOR I = 1 TO 10
    S(I, 1) = 0: S(I, 2) = 0
    S(I, 3) = 0: S(I, 4) = 1000
    LS(I, 1) = 0: LS(I, 2) = 0
  NEXT I
  WHILE NOT EOF(2)
    INPUT #2, D$
    IF MID$(D$, 1, 1) = "1" THEN
      FOR I = 1 TO 3
      IF MID$(D$, 80, 1) = M$(I) THEN
     IF VAL(MID$(D$,47,3))< >0 THEN
        V = VAL(MID$(D$, 47, 3))
        IF S(I, 3) < V THEN S(I, 3) = V
        IF S(I, 4) > V THEN S(I, 4) = V
             LV = LOG(V)
             S(I, 1) = S(I, 1) + V
             S(I, 2) = S(I, 2) + 1
             LS(I, 1) = LS(I, 1) + LV
          END IF
        END IF
      NEXT I
    END IF
  WEND
'----calc. mean aperture for each mineral
'----LS refers to the log transformed values
  FOR I = 1 TO 3
    IF S(I, 2) < > 0 THEN
      S(I, 1) = S(I, 1) / S(I, 2)
      LS(I, 1) = LS(I, 1) / S(I, 2)
    ELSE
      S(I, 1) = 0
      LS(I, 1) = 0
    END IF
  NEXT I
'----second pass to get other stats
'----to get first (absolute), 2ND, 3RD,4TH
'----moments of deviation form the mean
'----T(I,1)=average deviation
'----T(I,2)=variance
'----T(I,3)=skewness
'----T(I,4)=kurtosis
'----LT(I,7)=the log transformed T
  FOR I = 1 TO 10: FOR J = 1 TO 10
   T(I, J) = 0: LT(I, J) = 0
  NEXT J: NEXT I
  PRINT "Aperture Statistics": PRINT
  PRINT "Second pass to get four moments of deviation"
  PRINT "Re-reading file: "; F$
  CLOSE #2
  OPEN Dir$ + F$ FOR INPUT AS #2
  WHILE NOT EOF(2)
    INPUT #2, D$
    IF MID$(D$, 1, 1) = "1" THEN
    FOR I = 1 TO 10
    IF S(I, 1) < > 0 THEN
    IF MID$(D$, 80, 1) = M$(I) THEN
    IF VAL(MID$(D$,47,3)) < >0 THEN
          V = VAL(MID$(D$, 47, 3))
             LV = LOG(V)
             T(I, 5) = V - S(I, 1)
             T(I, 1) = T(I, 1) + ABS(V)
               T(I, 6) = T(I, 5) * T(I, 5)
               T(I, 2) = T(I, 2) + T(I, 6)
               T(I, 6) = T(I, 6) * T(I, 5)
               T(I, 3) = T(I, 3) + T(I, 6)
          T(I, 6) = T(I, 6) * T(I, 5)
          T(I, 4) = T(I, 4) + T(I, 6)
          T(I, 7) = T(I, 7) + 1
'----do the same for log transformed values
          LT(I, 5) = LV - LS(I, 1)
          LT(I, 1) = LT(I, 1) + ABS(LV)
          LT(I, 6) = LT(I, 5) * LT(I, 5)
          LT(I, 2) = LT(I, 2) + LT(I, 6)
          LT(I, 6) = LT(I, 6) * LT(I, 5)
          LT(I, 3) = LT(I, 3) + LT(I, 6)
          LT(I, 6) = LT(I, 6) * LT(I, 5)
          LT(I, 4) = LT(I, 4) + LT(I, 6)
          END IF
          END IF
        END IF
      NEXT I
    END IF
  WEND
  FOR I = 1 TO 3
    IF T(I, 7) > 1 THEN
'average deviation
      T(I, 1) = T(I, 1) / T(I, 7)
      T(I, 2) = T(I, 2) / (T(I, 7) - 1)
      var = T(I, 2)           'variation
'standard deviation
      T(I, 2) = SQR(var)
      IF var < > 0 THEN
        T(I, 3) = T(I, 3) / (T(I, 7) * T(I, 2) * T(I, 2) * T(I, 2))
'skewness
        T(I, 4) = T(I, 4) / (T(I, 7) * var * var) - 3  'kurtosis
      END IF
'----now do the same for the log transformed values
      LT(I, 1) = LT(I, 1) / T(I, 7)  'average deviation
      LT(I, 2) = LT(I, 2) / (T(I, 7) - 1)
      Lvar = LT(I, 2)           'variation
      LT(I, 2) = SQR(Lvar)      'standard deviation
      IF Lvar < > 0 THEN
        LT(I, 3) = LT(I, 3) / (T(I, 7) * LT(I, 2) * LT(I, 2) *
LT(I, 2))  'skewness
        LT(I, 4) = LT(I, 4) / (T(I, 7) * Lvar * Lvar) - 3
```

```
  'kurtosis
      END IF
    ELSE
      FOR J = 1 TO 10: T(I, J) = 0: LT(I, J) = 0: NEXT J
    END IF
  NEXT I
  CLS
  PRINT "Aperture Statistics (all values in mm) SCANLINE: ";
MID$(F$, 1, LEN(F$) - 4)
  PRINT
  PRINT "Set  #  Mean  Average  Standard  Skewness
Kurtosis  Max  Min"
  PRINT "            Deviation  Deviation"
  FOR I = 1 TO 3
    PRINT M$(I); "  ";
    PRINT USING "####"; T(I, 7);
    PRINT USING "######.##"; S(I, 1);
    FOR J = 1 TO 4
      PRINT USING "######.##"; T(I, J);
    NEXT J
    PRINT USING "######.##"; S(I, 3); S(I, 4)
    PRINT
  NEXT I
  PRINT "The following are the stats of the log transformed
apertures"
  PRINT "  The results are given as arithmetic values": PRINT
  PRINT "Set  #  Mean  Average  Standard  Skewness
Kurtosis"
  PRINT "            Deviation  Deviation"
  FOR I = 1 TO 3
    PRINT M$(I); "  ";
    PRINT USING "####"; T(I, 7);
    PRINT USING "######.##"; EXP(LS(I, 1));
    FOR J = 1 TO 4
      PRINT USING "######.##"; EXP(LT(I, J));
    NEXT J
    PRINT
  NEXT I
'-----Output to the file
  FOR I = 1 TO 3
    IF I = 1 THEN
      PRINT #3, MID$(F$, 1, 4); "  ";
    ELSE
      PRINT #3, "      ";
    END IF
    PRINT #3, M$(I); "  ";
    PRINT #3, USING "####"; T(I, 7);
    PRINT #3, USING "######.##"; S(I, 1);
    PRINT #3, USING "######.##"; T(I, 2);
    PRINT #3, USING "######.##"; EXP(LS(I, 1));
    PRINT #3, USING "######.##"; EXP(LT(I, 2))
  NEXT I
WEND
CLOSE

END
```

```
'----APERTURE.BAS
'----Program to produce results for TABLE 3.4 on
'----aperture filling output is in table form which
'----can be imported into Lotus (R) 123
'----By:D.A.v.E. 18.6.92
'----Subroutine declarations - not used in present
'----program. They are used in the commented out
'----section to calculate the mean dyke orientation.
DECLARE SUB DirCosToAzDip (Z1!, Z2!, z3!, Az!, Dip!)
DECLARE SUB AzDipToDirCos (A!, D!, X!, Y!, Z!)
'----Note: Input directory is set in the first DATA
'----statement at the end of the program
'----open output file
OF$ = "APERTURE.OUT"
OPEN OF$ FOR OUTPUT AS #3
'----print title
PRINT "Program to determine the mean aperture by orientation
PRINT "and fracture mineral filling. Results saved to "; OF$
'----read data directory name
READ Dir$
WHILE NOT EOF(1)
'----read file name and mean dyke orientation
READ F$, DykeAz, DykeDip
'----this section is only necessary if you still
'----want to calculate the mean dyke orientation
'----from the raw data then you must remember to
'----comment out the 2 READ statements
'CLOSE #2
'OPEN F$ FOR INPUT AS #2
'Ndyk = 0
'WHILE NOT EOF(2)
'INPUT #2, D$
'IF MID$(D$, 1, 1) = "1" THEN
'IF MID$(D$, 20, 2) = "cn" THEN
'Ndyk = Ndyk + 1
'Az = VAL(MID$(D$, 22, 3))
'Dip = VAL(MID$(D$, 25, 2))
'----convert Az and Dip to direction cosines sum
'----and convert back
'AzDipToDirCos Az, Dip, X, Y, Z
'XT = XT + X
'YT = YT + Y
'ZT = ZT + Z
'DirCosToAzDip XT, YT, ZT, DykeAz, DykeDip
'END IF
'END IF
'WEND
'----open file for orientation and aperture data
PRINT "Reading "; F$; "";
CLOSE #2
OPEN Dir$ + F$ FOR INPUT AS #2
'----initialize some variables
NoneNum1 = 0: NoneAp1 = 0: DykeNum1 = 0: DykeAp1 = 0
NoneNum2 = 0: NoneAp2 = 0: DykeNum2 = 0: DykeAp2 = 0
NoneNum3 = 0: NoneAp3 = 0: DykeNum3 = 0: DykeAp3 = 0
cnum = 0: cap = 0: znum = 0: zap = 0: cnum = 0: cap = 0
nnum = 0: nap = 0
WHILE NOT EOF(2)
NextOne:
INPUT #2, D$
IF MID$(D$, 1, 1) = "1" THEN
Az = VAL(MID$(D$, 22, 3))
Dip = VAL(MID$(D$, 25, 2))
Ap = VAL(MID$(D$, 47, 3))
'----because huge apertures are generally fracture
'----zones/faults and because they make too large
'----an influence on the mean, ignore fractures
'----with apertures > 99 mm
IF Ap > 99 THEN GOTO NextOne:
'----for aperture all fractures - dyke parallel
IF ABS(Az - DykeAz) < 30 AND ABS(Dip - DykeDip) < 30@
@ AND MID$(D$, 47, 3) <> "" THEN
DykeNum3 = DykeNum3 + 1
DykeAp3 = DykeAp3 + Ap
'----- remaining fractures
ELSE
NoneNum3 = NoneNum3 + 1
NoneAp3 = NoneAp3 + Ap
END IF
'----for filled fractures
IF MID$(D$, 33, 1) <> "n" THEN
IF ABS(Az - DykeAz) < 30 AND ABS(Dip - DykeDip) < 30
AND@
@MID$(D$, 47, 3) <> "" THEN
DykeNum1 = DykeNum1 + 1
DykeAp1 = DykeAp1 + Ap
ELSE
NoneNum1 = NoneNum1 + 1
NoneAp1 = NoneAp1 + Ap
END IF
END IF
'----for unfilled fracture
IF MID$(D$, 33, 1) = "n" THEN
IF ABS(Az - DykeAz) < 30 AND ABS(Dip - DykeDip) < 30
AND@
@MID$(D$, 47, 3) <> "" THEN
DykeNum2 = DykeNum2 + 1
DykeAp2 = DykeAp2 + Ap
ELSE
NoneNum2 = NoneNum2 + 1
NoneAp2 = NoneAp2 + Ap
END IF
END IF
'----calculate mean aperture by mineral filling
IF MID$(D$, 33, 1) = "e" OR MID$(D$, 36, 1) = "e" OR@
@MID$(D$, 39, 1) = "e" THEN
enum = enum + 1: eap = eap + Ap
ELSEIF MID$(D$, 33, 1) = "z" OR MID$(D$, 36, 1) = "z"@
@ OR MID$(D$, 39, 1) = "z" THEN
znum = znum + 1: zap = zap + Ap
ELSEIF MID$(D$, 33, 1) = "c" OR MID$(D$, 36, 1) = "c"@
@ OR MID$(D$, 39, 1) = "c" THEN
cnum = cnum + 1: cap = cap + Ap
ELSEIF MID$(D$, 33, 1) = "q" OR MID$(D$, 36, 1) = "q"@
@ OR MID$(D$, 39, 1) = "q" THEN
qnum = qnum + 1: qap = qap + Ap
ELSEIF MID$(D$, 33, 1) = "p" OR MID$(D$, 36, 1) = "p"@
@ OR MID$(D$, 39, 1) = "p" THEN
pnum = pnum + 1: pap = pap + Ap
ELSEIF MID$(D$, 33, 1) = "n" THEN
nnum = nnum + 1: nap = nap + Ap
END IF
END IF
WEND
'----print out mean aperture for dyke parallel
'----and other fractures
PRINT #3, MID$(F$, 1, 4);
PRINT #3, USING "####"; Ndyk; DykeAz; DykeDip;
```

```
PRINT USING "####"; Ndyk; DykeAz; DykeDip;
IF DykeNum1 < > 0 THEN
PRINT #3, DykeAp1 / DykeNum1;
PRINT DykeAp1 / DykeNum1;
ELSE
PRINT #3, 0!;
PRINT 0!;
END IF
IF NoneNum1 < > 0 THEN
PRINT #3, NoneAp1 / NoneNum1;
PRINT NoneAp1 / NoneNum1;
ELSE
PRINT #3, 0!;
PRINT 0!;
END IF
IF DykeNum2 < > 0 THEN
PRINT #3, DykeAp2 / DykeNum2;
PRINT DykeAp2 / DykeNum2;
ELSE
PRINT #3, 0!;
PRINT 0!;
END IF
IF NoneNum2 < > 0 THEN
PRINT #3, NoneAp2 / NoneNum2;
PRINT NoneAp2 / NoneNum2;
ELSE
PRINT #3, 0!;
PRINT 0!;
END IF
IF DykeNum3 < > 0 THEN
PRINT #3, DykeAp3 / DykeNum3;
PRINT DykeAp3 / DykeNum3;
ELSE
PRINT #3, 0!;
PRINT 0!;
END IF
IF NoneNum3 < > 0 THEN
PRINT #3, NoneAp3 / NoneNum3;
PRINT NoneAp3 / NoneNum3;
ELSE
PRINT #3, ;
PRINT ;
END IF
'----average aperture by mineral filling
IF enum < > 0 THEN
PRINT #3, eap / enum;
PRINT eap / enum;
ELSE
PRINT #3, 0;
PRINT 0;
END IF
IF znum < > 0 THEN
PRINT #3, zap / znum;
PRINT zap / znum;
ELSE
PRINT #3, 0;
PRINT 0;
END IF
IF cnum < > 0 THEN
PRINT #3, cap / cnum;
PRINT cap / cnum;
ELSE
PRINT #3, 0;
PRINT 0;
END IF
IF qnum < > 0 THEN
PRINT #3, qap / qnum;
PRINT qap / qnum;
ELSE
PRINT #3, 0;
PRINT 0;
END IF
IF pnum < > 0 THEN
PRINT #3, pap / pnum;
PRINT pap / pnum;
ELSE
PRINT #3, 0;
PRINT 0;
END IF
IF nnum < > 0 THEN
PRINT #3, nap / nnum
PRINT nap / nnum
ELSE
PRINT #3, 0
PRINT 0
END IF
WEND
CLOSE
END
'----Input file names, and mean dyke orientations
'----(-9 means no dykes) mean orientations from
'----visual inspection of plots to remove outliers
DATA "C:\DATA\FRACTURE\"
DATA "0000.DOC",095,62
DATA "0108.DOC",118,61
DATA "0112.DOC",-9,-9
DATA "0122.DOC",095,62
DATA "0401.DOC",085,75
DATA "0413.DOC",096,45
DATA "0418.DOC",-9,-9
DATA "0428.DOC",102,40
DATA "1037.DOC",125,85
DATA "1124.DOC",075,32
DATA "1134.DOC",125,43
DATA "1137.DOC",247,62
DATA "1222.DOC",258,80
DATA "1305.DOC",054,60
DATA "1321.DOC",153,60
DATA "AREA1.DOC",248,61
DATA "AREA2.DOC",055,59

'*****************************************
SUB AzDipToDirCos (A, D, X, Y, Z)
'
REM $DYNAMIC
Grad = 3.1415926544# / 180
'----If the dip is 90 then make it 89.9 to
'----preserve the azimuth
IF D = 90 THEN D = 89.9
'----Calculate direction cosines from
'----azimuth and dip
azimuth = A * Grad
Dip = D * Grad
Z = SIN(Dip)
Y = COS(Dip) * COS(azimuth)
X = COS(Dip) * SIN(azimuth)
'
END SUB

'*****************************************
```

```
SUB DirCosToAzDip (Z1, Z2, z3, Az, Dip)
'
Grad = 3.1415926534# / 180
'----convert direction cosines to azimuth dip
'-----to avoid division by 0 if z2=0, set az=90
IF Z2 = 0 THEN
Az = 90
ELSE
Az = ATN(ABS(Z1 / Z2)) / Grad
END IF
IF Z1 < 0 AND Z2 > 0 THEN
Az = 360 - Az
ELSEIF Z1 < 0 AND Z2 < 0 THEN
Az = Az + 180
ELSEIF Z1 > 0 AND Z2 < 0 THEN
Az = 180 - Az
END IF
hyp = SQR(Z1 * Z1 + Z2 * Z2)
'----if z1,z2=0 then the direction is
'-----vertical so to avoid division by
'----0 set dip=90
IF hyp = 0 THEN
Dip = 90
ELSE
Dip = ATN(z3 / hyp) / Grad
END IF
'----Just a safety precaution
IF z3 = 0 THEN Dip = 0
'
END SUB
```

```
'—CIRCLE.BAS
'----Program to compute fracture trace lengths
'----through random sampling of a fracture with
'----a unit radius. - The program produces a
'----histogram of binned frequencies of trace
'----lengths. These may be later fit to a
'----distribution. Associated file (e.g.) = LOGNORM.DAT
COMMON SHARED fracnum
COMMON SHARED frac(), lognorm()
COMMON SHARED bin(), binf(), bind()
RANDOMIZE (TIMER)
CLS
PRINT TAB(10); "Trace Length Simulation"
PRINT
PRINT "This program samples a population of fracture radii
randomly"
PRINT "to produce a population of fracture trace lengths."
PRINT "The fracture radii distribution is governed by a file"
PRINT "containing fracture radii in the range of 0 to 5 following
PRINT "some distribution. The first line contains the number of"
PRINT "values in each size bin separated by a space (25 total);"
PRINT "the second line contains the number of values to be read;"
PRINT "the Remaining lines contain the fracture radii values to"
PRINT "be sampled by the program. The output is a histogram of
PRINT "sampled radius distribution overlain on the total radius"
PRINT "distribution; a histogram showing the resulting fracture"
PRINT "trace length distribution; the binned results are put in an"
PRINT "output file for later plotting.": PRINT
Again:
INPUT "Enter name of file containing the distribution data: ", f$
OPEN f$ FOR INPUT AS #1
PRINT
INPUT "Use all fractures in distribution [Y/N]: ", fracuse$
IF UCASE$(fracuse$) = "N" THEN
PRINT
INPUT "Enter the number of fractures to sample: ", fracnum
END IF
'----dimension the arrays
DIM bin(50), binf(25), bind(25)
'----get first line of files containing the bins for the total set
FOR i = 1 TO 25
INPUT #1, bind(i)
NEXT i
INPUT #1, numpoints
IF UCASE$(fracuse$) = "Y" THEN fracnum = numpoints
'----dimension the arrays
DIM frac(fracnum), lognorm(numpoints)
SCREEN 3
CLS
'----Set the number of fractures to use
'----read in a lognormal distribution of values ranging from
'----0 to 5. Use this to generate the fracture radii between 0 and 1
'----plot the total fracture radius histogram
'----draw histogram axes
LINE (300, 100)-(300, 300): LINE (300, 300)-(700, 300)
LOCATE 1, 40: PRINT "Total Fracture Radius Histogram"
max = 0
FOR i = 2 TO 25
IF max < bind(i) THEN max = bind(i)
NEXT i
FOR i = 1 TO 25
y1 = 300 - 200 * bind(i) / max: y2 = 300
x1 = 300 + (i - 1) * 16
x2 = 300 + (i) * 16
LINE (x1, y1)-(x2, y2), , B
NEXT i
'----Read in the rest of the data
LOCATE 1, 1: PRINT "Reading "; f$; " (distrib. data)"
i = 0
CIRCLE (150, 100), 100, , , , .729
WHILE NOT EOF(1)
i = i + 1
INPUT #1, lognorm(i)
IF UCASE$(fracuse$) = "Y" THEN
frac(i) = lognorm(i) / 5
END IF
WEND
CLOSE #1
'----generate a distribution of fracture radii between 0 and 1
'----divide by 5 since the lognorm data range from 0 to 5
LOCATE 1, 1: PRINT "Generating fracture radii"
IF UCASE$(fracuse$) = "N" THEN
FOR i = 1 TO fracnum
Pointer = INT(RND(2) * numpoints)
frac(i) = lognorm(Pointer) / 5
'CIRCLE (150, 100), frac(i) * 100, , , , .729
NEXT i
END IF
'----draw circle center
'LINE (150, 95)-(150, 105): LINE (145, 100)-(155, 100)
'----now bin the radii
LOCATE !, 1: PRINT "Binning the fracture radii"
FOR j = 1 TO 25
FOR i = 1 TO fracnum
IF frac(i) >= ((j / 25!) - .04) AND frac(i) < ((j / 25!)) THEN
binf(j) = binf(j) + 1
END IF
NEXT i
NEXT j
'----plot the radius histogram
'----draw histogram axes
LINE (300, 100)-(300, 300): LINE (300, 300)-(700, 300)
LOCATE 2, 40: PRINT "Fracture Radius Histogram"
FOR i = 1 TO 25
y1 = 300 - 200 * binf(i) / max: y2 = 300
x1 = 300 + (i - 1) * 16
x2 = 300 + (i) * 16
LINE (x1, y1)-(x2, y2), , BF
NEXT i
'----generate random distances from the center of the circle for
'----population and calculate the associated trace lengths
FOR i = 1 TO 100
dum = INT(RND(1) * 10)
FOR zz = 1 TO dum: dum1 = RND(1): NEXT zz
z = (RND(1) - .5) * 2'----use range -1 to 1
x = 150 - z * 100
y1 = 30: y2 = 200
LINE (x, y1)-(x, y2)
'----calculate the intersecting line trace length, tr
FOR j = 1 TO fracnum
IF ABS(z) <= frac(j) THEN
tr = SQR(frac(j) * frac(j) - z * z)
'----now bin the trace lengths
FOR k = 1 TO 50
IF tr >= (k / 25 - .04) AND tr < (k / 25) THEN
bin(k) = bin(k) + 1
END IF
NEXT k
```

```
END IF
NEXT j
LINE (x, y1)-(x, y2), 0
NEXT i
'LOCATE 25, 1: PRINT "Press any key to continue";
'DO: LOOP UNTIL INKEY$ <> "": CLS
'----draw histogram axes
LINE (300, 100)-(300, 300): LINE (300, 300)-(700, 300)
'----find the max bin value and normalize to that
LOCATE 1, 1: PRINT "Fracture Trace Length Histogram"
max = 0
FOR i = 2 TO 50
IF max < bin(i) THEN max = bin(i)
NEXT i
FOR i = 1 TO 50
y1 = 300 - 200 * bin(i) / max: y2 = 300
x1 = 300 + (i - 1) * 16
x2 = 300 + (i) * 16
LINE (x1, y1)-(x2, y2), , B
NEXT i
LOCATE 1, 1: PRINT "Saving data to TRACEST.OUT"
OPEN "tracest.out" FOR OUTPUT AS #1
PRINT #1, "Fracture Radii Distribution"
PRINT #1, "Variation is from 0 to 1 in 25 intervals of 0.04"
PRINT #1, "Number of fractures: "; fracnum
FOR i = 1 TO 25: PRINT #1, binf(i): NEXT i
PRINT #1, "Fracture Trace Length Distribution"
PRINT #1, "Variation is from 0 to 1 in 25 intervals of 0.04"
PRINT #1, "The sample of fractures is sampled 100 times"
FOR i = 1 TO 50: PRINT #1, bin(i): NEXT i
LOCATE 25, 1: PRINT "Press any key to continue";
DO: LOOP UNTIL INKEY$ <> ""
SCREEN 0
CLOSE
END
```

```
'—DISTANCE.BAS
'—program to take the distances from the file minb.dat and
'——make them into a consequetive distance (i.e. 0.00 to x.xx m)
'—pick the distance columns 15 to 19
N = 300
DIM DISTANCE(N), FINALDIST(N)
DIM DATASTRING(N) AS STRING

OPEN "SCAN.AUT" FOR INPUT AS #3
WHILE NOT EOF(3)
INPUT #3, F$
FOR J = 1 TO N
DISTANCE(N) = 0
FINALDIST(N) = 0: DATASTRING$(N) = ""
NEXT J

OPEN F$ FOR INPUT AS #1
I = 1
WHILE NOT EOF(1)
INPUT #1, DATASTRING$(I)
DISTANCE(I) = VAL(MID$(DATASTRING$(I), 15, 5))
I = I + 1
WEND
I = I - 1
FINALDIST(1) = DISTANCE(1)
PRINT FINALDIST(1)
FOR J = 2 TO I
IF DISTANCE(J - 1) > DISTANCE(J) THEN
FINALDIST(J) = FINALDIST(J - 1) + DISTANCE(J)
A$ = "DIST(J-1) > DIST(J)"
ELSEIF DISTANCE(J - 1) < DISTANCE(J) THEN
FINALDIST(J) = FINALDIST(J - 1) + (DISTANCE(J) -@
@ DISTANCE(J - 1))
A$ = "DIST(J-1) < DIST(J)"
ELSEIF DISTANCE(J - 1) = DISTANCE(J) THEN
FINALDIST(J) = FINALDIST(J - 1)
A$ = "DIST(J-1) = DIST(J)"
END IF
PRINT USING "##.##"; DISTANCE(J);
PRINT " : ";
PRINT USING "###.##"; FINALDIST(J);
PRINT " : "; A$
NEXT J
OF$ = MID$(F$, 1, LEN(F$) - 3) + "OUT"
OPEN OF$ FOR OUTPUT AS #2
FOR J = 1 TO I
PRINT #2, MID$(DATASTRING$(J), 1, 14);
PRINT #2, USING "###.##"; FINALDIST(J);
PRINT #2, MID$(DATASTRING$(J), 20,
LEN(DATASTRING$(J)))
NEXT J
CLOSE #2
CLOSE #1

WEND
CLOSE #3

END
```

```
'—DOMSEP.BAS
'—Program to determine if a point lies within an enclosed
'—irregular polygonCreated 8-6-90D.A.v.E.

x = 500: y = 2300
DIM Bound#(x, 2), FileNm$(100)
DIM E#(y), N#(y), Az(y), Dip(y)
'—Clear screen
CLS
PRINT
PRINT "D O M A I N A L D A T A S E P A R A T I O N":
PRINT
PRINT "Uses two data files 1) containing the Easting and
Northing"
PRINT "coordinates of the boundary of the domain, 2) containing"
PRINT "the Easting, Northing, Azimuthal and Dip coordinated of"
PRINT "the data points (free format comma or space delimited)"
PRINT "to decide which data points fall within which domains"
BNum% = 0: DNum% = 0
'—Input data file name
PRINT
PRINT
PRINT "Enter name of data file (E,N,Az,Dip)(Q=Quit): "
INPUT ; ">> ", FD$
FD$ = UCASE$(FD$)
IF FD$ = "Q" THEN GOTO EndDomain:
OPEN FD$ FOR INPUT AS #3
I = 0
PRINT : PRINT "Use Batch mode [N]": Q$ =
UCASE$(INPUT$(1))
IF Q$ <> "Y" THEN
PRINT
PRINT "Enter name of file containing boundary points
(E,N)(Q=Quit): "
INPUT ">> ", FB$
FB$ = UCASE$(FB$)
IF FB$ = "Q" THEN GOTO EndDomain:
Flag% = 0
ELSE
PRINT
PRINT "Enter name of batch file of domain data names (Q=Quit)"
INPUT " >> ", BatchF$
BatchF$ = UCASE$(BatchF$)
IF BatchF$ = "Q" THEN GOTO EndDomain:
OPEN BatchF$ FOR INPUT AS #1
I = 0
WHILE NOT EOF(1)
I = I + 1
INPUT #1, FileNm$(I)
WEND
NumFiles% = I
CLOSE #1
Flag% = 1
END IF
I = 0
WHILE NOT EOF(3)
I = I + 1
INPUT #3, E#(I), N#(I), Az(I), Dip(I)
row% = CSRLIN
LOCATE row%, 1
IF I MOD 10 = 0 THEN PRINT "Reading data file "; FD$; "
record #"; I;
WEND
CLOSE #3
PRINT
DNum% = I
'—Check if the batch mode flag is set
IF Flag% <> 1 THEN NumFiles% = 1
FOR L = 1 TO NumFiles%
IF Flag% = 1 THEN FB$ = FileNm$(L)
PRINT FB$
OPEN FB$ FOR INPUT AS #1
FO$ = MID$(FB$, 1, LEN(FB$) - 3) + "DAT"
PRINT : PRINT "Output of chosen points will be to "; FO$:
PRINT
OPEN FO$ FOR OUTPUT AS #2
I = 0
WHILE NOT EOF(1)
I = I + 1
INPUT #1, Bound#(I, 1), Bound#(I, 2)
row% = CSRLIN
LOCATE row%, 1
IF I MOD 10 = 0 THEN
PRINT "Reading boundary file "; FB$; " record #"; I;
END IF
WEND
PRINT
CLOSE #1
'—Close the boundary and set the number of boundary points to
BNum%
Bound#(I + 1, 1) = Bound#(1, 1): Bound#(I + 1, 2) =@
@ Bound#(1, 2)
BNum% = I
'—Start looking for the nearest points to the boundary
FOR I = 1 TO DNum%
West = 0: East = 0
row% = CSRLIN
FOR J = 1 TO BNum%
IF J > 1 THEN
BMinus1# = Bound#(J - 1, 2)
BMinusE# = Bound#(J - 1, 1)
ELSE
BMinus1# = Bound#(BNum%, 2)
BMinusE# = Bound#(BNum%, 1)
END IF
'—Find pairs of boundary points that cross an east-west line
'—containing the data point. First case: boundary point lies on
line
IF Bound#(J, 2) = N#(I) THEN
'—Now check if the next two points on the boundary straddle it
'—or lie to one side
IF (BMinus1# > N#(I) AND Bound#(J + 1, 2) > N#(I)) OR@
@(BMinus1# < N#(I) AND Bound#(J + 1, 2) < N#(I)) THEN
IF Bound#(J, 1) < E#(I) THEN
West = West + 2
ELSE
East = East + 2
END IF
ELSE
IF Bound#(J, 1) < E#(I) THEN
West = West + 1
ELSE
East = East + 1
END IF
END IF
'Two boundary points straddle line
ELSEIF (Bound#(J, 2) > N#(I) AND BMinus1# < N#(I)) OR@
@(Bound#(J, 2) < N#(I) AND BMinus1# > N#(I)) THEN
```

```
IF BMinusE# < > Bound#(J, 1) THEN
slope# = (BMinus1# - Bound#(J, 2)) / (BMinusE# - Bound#(J, 1))
inter# = Bound#(J, 2) - (slope# * Bound#(J, 1))
pt# = (N#(I) - inter#) / slope#
ELSEIF BMinusE# = Bound#(J, 1) THEN
pt# = Bound#(J, 1): slope# = 0: inter# = 0
END IF
IF pt# < E#(I) THEN
West = West + 1
ELSE
East = East + 1
END IF
END IF
NEXT J
IF East MOD 2 = 0 AND West MOD 2 = 0 THEN
Choose$ = "no" ELSE Choose$ = "yes"
END IF
'——Write the values of points within the boundary to a file
IF Choose$ = "yes" THEN WRITE #2, E#(I), N#(I), Az(I),@
@ Dip(I)
NEXT I
CLOSE #2
NEXT L
PRINT : PRINT : PRINT "Finished."
EndDomain:
END
```

```
'---DXFPLINE.BAS
'---Program to take .DXF format files produced with AutoCAD
'---to produce a file containing the start and end points
'---of lineations. Note the original digitized file must be produced
'---using the PLINE function, so that the .DXF file contains the
'---sequence ENTITIES, 10, Xbegin, 20, Ybegin, 10, Xend, 20,
Yend.

DIM XB(1000), YB(1000), XE(1000), YE(1000), HIST(18)
CLS
RTD = 180 / 3.1415926544
LOCATE 2, 3: COLOR 8, 1
PRINT "AutoCAD .DXF Orientation Interpretation PLINE"
COLOR 7, 0
LOCATE 3, 7: PRINT "By: D. van EverdingenOct 1988"
LOCATE 1, 1: PRINT CHR$(218); : FOR II = 1 TO 47: PRINT
CHR$(196); : NEXT II
PRINT CHR$(191)
LOCATE 4, 1: PRINT CHR$(192); : FOR II = 1 TO 47: PRINT
CHR$(196); : NEXT II
PRINT CHR$(217)
FOR II = 1 TO 2: LOCATE 1 + II, 1: PRINT CHR$(179);
NEXT II
FOR II = 1 TO 2: LOCATE 1 + II, 49: PRINT CHR$(179);
NEXT II
LOCATE 6, 1
INPUT "Input the .DXF file name (no file extension): ", FILE1$
FILE$ = RTRIM$(FILE1$) + ".DXF"
OPEN FILE$ FOR INPUT AS #1
INPUT "Output file name: ", FILE2$
OPEN FILE2$ FOR OUTPUT AS #2
DO
INPUT #1, DUMMY$
LOOP UNTIL DUMMY$ = "POLYLINE"
FOR J = 1 TO 8: INPUT #1, DUMMY$: NEXT J
I = 1
WHILE NOT EOF(1)
INPUT #1, NUM$
IF NOT EOF(1) AND NUM$ = "10" THEN
INPUT #1, XB
INPUT #1, NUM$
IF NUM$ = "20" THEN INPUT #1, YB
FOR J = 1 TO 4: INPUT #1, DUMMY$: NEXT J
INPUT #1, NUM$
IF NUM$ = "10" THEN INPUT #1, XE
INPUT #1, NUM$
IF NUM$ = "20" THEN INPUT #1, YE
LOCATE 9, 1: PRINT "Lineation number "; I; " read."
LENGTH = SQR((XE - XB) ^ 2 + (YE - YB) ^ 2)
Y = ABS(YB - YE)
X = ABS(XB - XE)
'---If line is oriented NW-SE then add 90 degrees to the angle
IF XB > XE AND YB > YE THEN
ANGLE = ATN(X / Y) * RTD
ELSEIF XB < XE AND YB > YE THEN
ANGLE = ATN(Y / X) * RTD
ANGLE = ANGLE + 90
ELSEIF XB > XE AND YB < YE THEN
ANGLE = ATN(X / Y) * RTD
ANGLE = ANGLE + 90
ELSEIF XB < XE AND YB < YE THEN
ANGLE = ATN(Y / X) * RTD
END IF
'---Print results
PRINT #2, USING "####"; I;
PRINT #2, USING "#####.#####"; XB; YB; XE; YE; LENGTH;
PRINT #2, USING "###.#"; ANGLE
I = I + 1
END IF
FOR J = 1 TO 14: INPUT #1, DUMMY$: NEXT J
WEND
PRINT
PRINT "Output is in file: "; FILE2$
PRINT "It contains the following on each line of output:"
PRINT "1) Start X and Y coordinates of each line"
PRINT "2) End X and Y coordinates of each line"
PRINT "3) Length of each line"
PRINT "4) Angle of each line with respect to north (0-180)"
CLOSE #2
END
```

'—ELLIPSE.BAS

```
'Program to compute fracture trace lengths through random
'sampling of a fracture with a unit radius. - The program
'produces a histogram of binned frequencies of trace
'lengths. These may be later fit to a distribution.
' A s s o c i a t e d   f i l e s   =
LOGNORM.DAT,WEIBULL.DAT,EXPONEN.DAT
'SQUARE.DAT,BIMODAL.DAT
ON ERROR GOTO Generr:
'—dimension the arrays
DIM bin(50), binf(25), bind(25)
DIM BF$(5)
DIM xx(2), yy(2)
Pi = 3.141592654#: Flg = 0: Out$ = "N"
CLS
PRINT TAB(10); "Trace Length Simulation: ELLIPSES"
PRINT : PRINT "This program samples a population of"
PRINT "fracture radii randomly to produce a population"
PRINT "of fracture trace lengths. The fracture radii"
PRINT "distribution is governed by a file containing"
PRINT "fracture radii in the range of 0 to 5 following"
PRINT "some distribution. The first line contains the"
PRINT "number of values in each size bin separated by a"
PRINT "space (25 total); the second line contains the"
PRINT "number of values to be read; the remaining lines"
PRINT "contain the fracture radii values to be sampled"
PRINT "by the program. The output is a histogram showing"
PRINT "the sampled radius distribution overlain on the"
PRINT "total radius distribution; a histogram showing"
PRINT "the resulting fracture trace length distribution;"
PRINT "the binned results are put in an output file for"
PRINT "later plotting."
PRINT
l = 1: Batch = 0
INPUT "Enter filename for the distribution data: ", f$
f$ = UCASE$(f$)
IF f$ = "SCAN.AUT" THEN
  Batch = 1
  OPEN f$ FOR INPUT AS #1
  WHILE NOT EOF(1)
    BFNum = BFNum + 1: INPUT #1, BF$(BFNum)
  WEND
ELSE
  BFNum = 1: BF$(1) = f$
END IF
INPUT "Use all fractures in distribution [Y/N]: ", fracuse$
IF UCASE$(fracuse$) = "N" THEN
  INPUT "Enter the number of fractures to sample: ",
fracnum
END IF
Again:
INPUT "Enter aspect ratio (<=1, or 9 to cycle): ", Asp
IF Asp = 9 THEN
  cycle = 9
ELSE
  IF Asp <= 1 THEN
    Aspect = Asp
  ELSE
    GOTO Again:
  END IF
  cycle = 1
END IF
INPUT "Output to be used for Lotus 123 [Y/N]: ", Out$
Out$ = UCASE$(Out$)
'—loop for various distributions
FOR l = 1 TO BFNum
  CLOSE #1
  OPEN BF$(l) FOR INPUT AS #1
'—get first line of files containing bins for total set
FOR i = 1 TO 25
  INPUT #1, bind(i)
NEXT i
INPUT #1, numpoints
IF UCASE$(fracuse$) = "Y" THEN fracnum = numpoints
'—dimension the arrays
REDIM frac(fracnum), lognorm(numpoints)
'—set the screen mode 3=Herc 12=VGA
SCREEN 3
IF Nerr% = 5 THEN
  SCREEN 12: Nerr% = 0
END IF
IF Nerr% = 5 THEN
  SCREEN 0: Flg = 1
END IF
CLS
'—Get the number of fractures to use. Read in a
'—lognormal distribution of values ranging from 0 to 5.
'—Use this to generate the fracture radii between 0
'—between 0 and 1. plot the total fracture radius
'—histogram. Draw histogram axes
IF Flg = 0 THEN
  LINE (300, 50)-(300, 100)
  LINE (300, 100)-(700, 100)
END IF
LOCATE 1, 40
PRINT "Total Fracture Long Axis Histogram"
max = 0
FOR i = 2 TO 25
  IF max < bind(i) THEN max = bind(i)
NEXT i
FOR i = 1 TO 25
  y1 = 100 - 50 * bind(i) / max: y2 = 100
  x1 = 300 + (i - 1) * 16
  x2 = 300 + (i) * 16
  IF Flg = 0 THEN LINE (x1, y1)-(x2, y2), , B
NEXT i
'—Read in the rest of the data
LOCATE 1, 1: PRINT "Reading "; f$; " (distrib. data)"
i = 0
WHILE NOT EOF(1)
  i = i + 1
  INPUT #1, lognorm(i)
  IF UCASE$(fracuse$) = "Y" THEN
    frac(i) = lognorm(i) / 5
  END IF
WEND
i = 0
CLOSE #1
'—generate a distribution of fracture radii between
'—0 an 1. divide by 5 since the lognorm data range
'—from 0 to 5
LOCATE 1, 1: PRINT "Generating long axes"
IF UCASE$(fracuse$) = "N" THEN
  FOR i = 1 TO fracnum
    Pointer = 0
    WHILE Pointer = 0
      Pointer = INT(RND(2) * numpoints)
    WEND
    IF lognorm(Pointer) / 5 = 0 THEN STOP
```

```
    frac(i) = lognorm(Pointer) / 5
  NEXT i
END IF
'----now bin the radii
LOCATE 1, 1: PRINT "Binning the fracture long axes    "
FOR j = 1 TO 25
  FOR i = 1 TO fracnum
    IF frac(i) >= ((j / 25!) - .04) AND frac(i) < @
@((j / 25!)) THEN
      binf(j) = binf(j) + 1
    END IF
  NEXT i
NEXT j
'----plot the radius histogram
'----draw histogram axes
LOCATE 2, 40: PRINT "Fracture Long Axis Histogram"
FOR i = 1 TO 25
  y1 = 100 - 50 * binf(i) / max: y2 = 100
  x1 = 300 + (i - 1) * 16
  x2 = 300 + (i) * 16
  IF Flg = 0 THEN LINE (x1, y1)-(x2, y2), , BF
NEXT i
'----loop for several aspect ratios
FOR AspCyc = 1 TO cycle
  IF Asp = 9 THEN Aspect = AspCyc / 10
  LOCATE 3, 1: PRINT "Aspect ratio: "; Aspect
'----initialize some variables and arrays
  max1 = 0: min1 = 10: KK = 0
  FOR i = 1 TO 50: bin(i) = 0: NEXT i
  FOR ii = 1 TO 10
'-----run random number generator a number of times
    dum = INT(RND(1) * 10)
    FOR iii = 1 TO dum: dum2 = RND(1): NEXT iii
    ordeg = (RND(1) * 179)
'----convert degrees to radians
    Orient = ((90 - ordeg) / 180) * Pi
    IF Orient < 0 THEN Orient = Orient + 2 * Pi
    FOR i = 0 TO 50
      LOCATE 5, 1
      KK = KK + 1
      PRINT "Sampling (500) "; KK; "  "
'----generate distances from the origin for the
'----cross-cutting line run through the random number
'----generator a number of times
      dum = INT(RND(1) * 10)
      FOR iii = 1 TO dum: dum2 = RND(1): NEXT iii
      z = (RND(1) - .5) * 2   '----use range -1 to 1
'----the slope of the line, m is dY/dX
      m = SIN(Orient) / COS(Orient)
'----y-axis intercept of line is b=z/cos alpha where alpha is
'----line orientation - 90 degrees
      IF Orient < 90 THEN
        inter = Orient + 3.1415926549# / 4
      ELSE
        inter = Orient - 3.1415926549# / 4
      END IF
      B = z / COS(ABS(inter))
      IF (z < 0 AND m > 0) OR (z > 0 AND m > 0)
THEN
        B = B * -1
      END IF
'----for each ellipse the 2 intersection points of the
'----line and the ellipse must be found. Calculate where
'----the ellipse and the line coincide. equate the two
'----formulae and solve for the x values. this results
'----in a quadratic equation:
'----(ax^2+bx+c=0 solved by x=[-b+-root(b^2-4ac)]/2a)
'----from equating Y-line=mx+b and
'----Yellipse=sqr((1-x^2/a^2)b^2)
'----the short axis,b = aspect * a
      FOR j = 1 TO fracnum
        bax = Aspect * frac(j)
        part1 = -2 * m * B
        part2 = part1 * part1
        part2a = frac(j) * frac(j)
        part3 = (m * m + (bax * bax / part2a))
        part4 = 4 * part3 * (B * B - bax * bax)
'----if the line and the ellipse do not intersect then the
'----value of (part2-part4) will be negative (imaginary
'----root): ignore and continue
        IF (part2 - part4) >= 0 THEN
          part5 = SQR(part2 - part4)
          part6 = 2 * part3
          xx(1) = (part1 + part5) / part6
          xx(2) = (part1 - part5) / part6
          yy(1) = m * xx(1) + B
          yy(2) = m * xx(2) + B
'----calculate the distance between the two points
          dxx = xx(1) - xx(2): dyy = yy(1) - yy(2)
          tr = SQR((dxx * dxx) + (dyy * dyy))
          IF max1 < tr THEN max1 = tr
          IF min1 > tr THEN min1 = tr
'----now bin the trace lengths
          FOR k = 1 TO 50
            IF tr >= (k / 25 - .04) AND tr < (k / 25)
THEN
              bin(k) = bin(k) + 1
            END IF
          NEXT k
        END IF
      NEXT j
    NEXT i
  NEXT ii
'----start trace length output
'----draw histogram axes
  IF Flg = 0 THEN
    LINE (10, 100)-(10, 300)
    LINE (10, 300)-(710, 300)
  END IF
'----find the max bin value and normalize to that
  IF Asp = 9 THEN CLS
  LOCATE 1, 1: PRINT "Fracture Trace Length
Histogram"
  max = 0
  FOR i = 2 TO 50
    IF max < bin(i) THEN max = bin(i)
  NEXT i
  FOR i = 1 TO 50
    y1 = 300 - 200 * bin(i) / max: y2 = 300
    x1 = 10 + (i - 1) * 16
    x2 = 10 + (i) * 16
    IF Flg = 0 THEN LINE (x1, y1)-(x2, y2), , B
  NEXT i
  IF Asp <> 9 THEN
    of$ = MID$(BF$(i), 1, LEN(BF$(i)) - 3) + "OUT"
  ELSE
    of$ = MID$(BF$(i), 1, LEN(BF$(i)) - 5) + @
@LTRIM$(STR$(AspCyc)) + ".OUT"
  END IF
  LOCATE 23, 40: PRINT "Saving data to "; of$
```

```
  OPEN ofS FOR OUTPUT AS #1
  IF Out$ = "N" THEN
    PRINT #1, "Fracture Long Axis Distribution @
@(Ellipses) is "; MID$(fS, 1, LEN(fS) - 4)
    PRINT #1, "Variation is from 0 to 1 in 25 @
@intervals of 0.04"
    PRINT #1, "Ellipse aspect ratio (a/b) is "; Aspect
    PRINT #1, "Number of fractures: "; fracnum
    PRINT #1, "Len.  #."
    FOR i = 1 TO 25
      PRINT #1, USING "####.##"; i / 25; binf(i)
    NEXT i
    PRINT #1, "Fracture Trace Length Distribution"
    PRINT #1, "Variation is from 0 to 2 in 50 intervals of
0.04"
    PRINT #1, "The sample of fractures is sampled 100
times"
    PRINT #1, "Longest Fracture: "; max1; "  Shortest@
@ Fracture: "; min1
    PRINT #1, "Len.  #."
    FOR i = 1 TO 50
      PRINT #1, USING "####.##"; i / 25; bin(i)
    NEXT i
'----output for use in Lotus (R) 123
  ELSEIF Out$ = "Y" THEN
    FOR i = 1 TO 50: PRINT #1, bin(i): NEXT i
  END IF
  CLOSE #1
NEXT AspCyc
CLOSE
'----end batch loop
  KK = 0
NEXT l
'----display last plot and exit
FOR i = 1 TO 2000: NEXT i
SCREEN 0
END
'----error trapping routine
Generr:
Nerr% = ERR
RESUME NEXT
```

```
'----GRID.BAS
'----Rotation, Sorting, Gridding and Estimation of orientation
'----data positioned by x, y coordinates.
'----Creation date: 23-4-1990 D.A.v.E.
'----Header program for the sorting, rotation and estimation of
'----azimuth and dip values at grid node points.

COUNT% = 0
Startprgm:
c$ = "p"
WHILE INSTR("Q", c$) = 0
CLS
LOCATE 4, 25: PRINT "G R I DE S T I M A T I O N"
LOCATE 6, 20: PRINT "Created: 20-4-1990 D.A.v.E."

LOCATE 8, 26: PRINT "Choose one of the following:"
LOCATE 10, 17
PRINT "(1) Digitize data points (8) Nearest neighbors"
LOCATE 11, 17
PRINT "(2) Display locations (9) Angular change"
LOCATE 12, 17
PRINT "(3) Rotation (A) Convert for SURFII"
LOCATE 13, 17
PRINT "(4) Sorting(B) Convert for STEREO"
LOCATE 14, 17
PRINT "(5) Grid generation(C) Convert for GeoSoft"
LOCATE 15, 17
PRINT "(6) Estimation(D) History"
LOCATE 16, 17: PRINT "(7) Remove null points(E) Help"
LOCATE 18, 30: PRINT "(Q) Exit program"
LOCATE 19, 30: PRINT "(S) Shell to DOS"
LOCATE 21, 28: PRINT SPACE$(30)
IF type$ < > "" AND FO$ < > "" THEN
IF LEFT$(type$, 2) < > "Di" THEN
LOCATE 22, 10: PRINT "("; LTRIM$(type$); " in ";@
@ UCASE$(FO$); ")"
END IF
COUNT% = COUNT% + 1
IF COUNT% > 9 THEN
FOR I = 2 TO 9: text$(I - 1) = text$(I): NEXT I
COUNT% = 9
END IF
IF LEFT$(type$, 2) = "Di" THEN
text$(COUNT%) = " " + type$
ELSE
FOR I = LEN(F$) TO 1 STEP -1
IF MID$(F$, I, 1) = "\" THEN EXIT FOR
NEXT I
I = LEN(F$) - I
hf$ = MID$(F$, LEN(F$) - (I - 1), LEN(F$))
hfo$ = MID$(FO$, LEN(FO$) - (I - 1), LEN(FO$))
text$(COUNT%) = " Input data from " + UCASE$(hf$) + ". "@
@+ type$ + " in " + UCASE$(hfo$)
END IF
type$ = ""
END IF
LOCATE 21, 28
PRINT "Enter choice > > "; : c$ = UCASE$(INPUT$(1))
PRINT c$
'----Start timer
tSTART = TIMER

SELECT CASE c$
CASE "1"
type$ = "Digitize points"
tmp$ = "GRIDDIG"
CHAIN tmp$
CASE "2"
type$ = "Display point locations"
tmp$ = "GRIDPLOT"
CHAIN tmp$
CASE "3"
type$ = "Rotated result"
RotCoord
CASE "4"
type$ = "Sorted result"
InsertSort
CASE "5"
type$ = "Grid data"
Makegrid
CASE "6"
type$ = "Estimated results"
Estimate
CASE "7"
type$ = "Remove nulls"
Short
CASE "8"
type$ = "Nearest Neighbors"
Neighbor
CASE "9"
type$ = "Angular change"
GridAngle
CASE "A"
type$ = "VAX conversion"
VAXConvert
CASE "B"
type$ = "STEREO convert"
DigToSTEREO
CASE "C"
type$ = "GeoSoft convert"
GeoSoft
CASE "D"
type$ = "Display history"
CLS
LOCATE 5, 25: PRINT "D I S P L A Y H I S T O R Y"
LOCATE 8, 22: PRINT "(List of previous actions performed)"
FOR I = 1 TO COUNT%
LOCATE 9 + I, 1: PRINT "(";
PRINT USING "#"; I;
PRINT ") "; text$(I)
NEXT I
LOCATE 24, 28: PRINT "Press any key to continue"
DO: LOOP UNTIL INKEY$ < > ""
CASE "E"
OPEN "GRID.HLP" FOR INPUT AS #1
IF Nerr% = 53 THEN
Nerr% = 0
ELSE
CLS
WHILE NOT EOF(1)
INPUT #1, d$
PRINT d$;
WEND
LOCATE 25, 25: PRINT "Press any key to continue";
DO: LOOP UNTIL INKEY$ < > ""
END IF
CLOSE #1
CASE "Q"
```

```
CLS : GOTO EndPrgm:
CASE "S"
SHELL
CASE ELSE
END SELECT
'----Open timing file and dump timing data
OPEN "GRIDTIME.LOG" FOR APPEND AS #10
ISTOP = TIMER
PRINT #10, "Action: "; type$
PRINT #10, "Starting time: "; ISTART
PRINT #10, "Stopping time: "; ISTOP
PRINT #10, "Elapsed time:"; ISTOP - ISTART
PRINT #10, "End Date:"; DATE$
PRINT #10, "End Time:"; TIME$
PRINT #10, "----------"
CLOSE #10
'----Close timing file
WEND
GOTO EndPrgm:
'---- Error trapping
GenError:
Nerr% = ERR: pr% = CSRLIN: pc% = POS(0)
IF Nerr% <> 53 THEN
LOCATE 25, 1: PRINT "Error: "; Nerr%;
END IF
RESUME NEXT

EndPrgm:

END

'*****************************************
SUB AzDipToDirCos (A, d, X, Y, z)
'
REM $DYNAMIC
Grad = 3.1415926654# / 180
'----If the dip is 90 then make it 89.9 to preserve the azimuth
IF d = 90 THEN d = 89.9
'----Calculate direction cosines from azimuth and dip
azimuth = A * Grad
Dip = d * Grad
z = SIN(Dip)
Y = COS(Dip) * COS(azimuth)
X = COS(Dip) * SIN(azimuth)

END SUB

'*****************************************
SUB AzToDirCos (A, X, Y)

Grad = 3.1415926654# / 180
'----Calculate direction cosines from azimuth
azimuth = A * Grad
Y = COS(azimuth)
X = SIN(azimuth)
'
END SUB

'*****************************************
SUB CalcAngle (A1, A2, D1, D2, Theta)
Grad = 3.1415926654# / 180

IF D1 = 90 THEN D1 = 89.9
IF D2 = 90 THEN D2 = 89.9
AA1 = A1 * Grad
AA2 = A2 * Grad
DD1 = D1 * Grad
DD2 = D2 * Grad
x1 = COS(DD1) * SIN(AA1)
x2 = COS(DD2) * SIN(AA2)
y1 = COS(DD1) * COS(AA1)
y2 = COS(DD2) * COS(AA2)
Z1 = SIN(DD1)
Z2 = SIN(DD2)
T1 = x1 * x2
T2 = y1 * y2
T3 = Z1 * Z2
Theta = T1 + T2 + T3
IF (1 - Theta * Theta) < 0 THEN Theta = 1
Theta = ATN(SQR(1 - Theta * Theta) / Theta)
Theta = ABS(Theta / Grad)
END SUB

'*****************************************
SUB DigToSTEREO

DIM FileNm$(100)
ReEnter1:
CLS
PRINT "CONVERT ORIENTATIONS FOR STEREO"
PRINT
PRINT "Routine to separate dyke azimuth and dip values from the"
PRINT "location (E, N) for use in STEREO"
PRINT
PRINT "Batch mode [N]?": B$ = UCASE$(INPUT$(1))
IF B$ = "Y" THEN Batch% = 1
IF Batch% = 0 THEN
INPUT "Enter file name (Q=Quit to menu): ", F$
ELSE
PRINT "Enter batch file of files to be converted (Q=Quit)"
INPUT " >> ", F$
INPUT "Enter number of columns (4 or 5): ", Col%
END IF
IF UCASE$(F$) = "Q" THEN GOTO EndDig:
IF Batch% = 1 THEN
OPEN F$ FOR INPUT AS #1
I = 0
PRINT "Reading file names from "; F$
WHILE NOT EOF(1)
I = I + 1
INPUT #1, FileNm$(I)
WEND
NumFiles% = I
CLOSE #1
ELSE
 OPEN F$ FOR INPUT AS #1
 NumFiles% = 1
 END IF
 FOR I = 1 TO NumFiles%
 IF Batch% = 0 THEN
LINE INPUT #1, Data$
CLOSE #1: OPEN F$ FOR INPUT AS #1
PRINT "Example record from "; F$
PRINT ""; Data$
col2:
INPUT "Enter number of columns (4 or 5): ", Col%
IF Col% < 4 OR Col% > 5 THEN GOTO col2:
PRINT : INPUT "Enter output file name: ", FO$
ELSE
F$ = FileNm$(I)
```

```
OPEN F$ FOR INPUT AS #1
FO$ = MID$(F$, 1, LEN(F$) - 3) + "PLT"
END IF
OPEN FO$ FOR OUTPUT AS #2
PRINT "Reading data from "; F$
WHILE NOT EOF(1)
INPUT #1, A#, B#, c%, d%
PRINT #2, c%; d%
row% = CSRLIN
L = L + 1: LOCATE row%, 1: PRINT "Reading record "; L;
WEND
PRINT : L = 0
CLOSE #1: CLOSE #2
NEXT I
EndDig:
IF UCASE$(F$) = "Q" THEN FO$ = ""
END SUB

'*****************************************
SUB DirCosToAzDip (Z1, Z2, z3, Az, Dip)
'
Grad = 3.141592654# / 180
'----convert direction cosines to azimuth dip
'----to avoid division by 0 if z2=0, set az=90
IF Z2 = 0 THEN
Az = 90
ELSE
Az = ATN(ABS(Z1 / Z2)) / Grad
END IF
IF Z1 < 0 AND Z2 > 0 THEN
Az = 360 - Az
ELSEIF Z1 < 0 AND Z2 < 0 THEN
Az = Az + 180
ELSEIF Z1 > 0 AND Z2 < 0 THEN
Az = 180 - Az
END IF
hyp = SQR(Z1 * Z1 + Z2 * Z2)
'----if z1,z2=0 then the direction is vertical so to avoid division
'----by 0 set dip=90
IF hyp = 0 THEN
Dip = 90
ELSE
Dip = ATN(z3 / hyp) / Grad
END IF
'----Just a safety precaution
IF z3 = 0 THEN Dip = 0
'
END SUB

'*****************************************
SUB Estimate
'----Routine to estimate values of orientation at the nodes of
'----a grid whose endpts were computed using MakeGrid. Results
'----saved in file.GRD. Estimation based on a max. of 100
'----neighboring points
'----Arrays:
'----nb()= pointers to neighbor points in data location
'----arrays (east(),north())
'----dist() = distance from the local node to neighboring point
'----wt()= weight assigned to neighbor points on basis of
'----distance from node

DIM NBB(100), dist(100), wt(100)
CLS
LOCATE 2, 17: PRINT "NODAL VALUE ESTIMATION"
LOCATE 6, 1
sortflg% = 0
ON ERROR GOTO GenError:
PRINT "Directory Listing:": LOCATE 7, 1
FILES "*.SRT"
IF Nerr% = 53 THEN
Nerr% = 0
LOCATE pr% - 1, pc%
FILES
END IF
LOCATE 4, 10: INPUT ; "Enter data file name (Q=quit): ", F$
F$ = UCASE$(F$)
IF F$ = "Q" THEN GOTO EndEst2:
grid$ = MID$(F$, 1, LEN(F$) - 3) + "GRD"
ON ERROR GOTO GenError:
OPEN grid$ FOR INPUT AS #1
IF Nerr% <> 0 THEN
CLS : LOCATE 10, 1
PRINT "Can't find: "; grid$
PRINT "You must create a grid data file first (Option 4)."
PRINT "File must be in same directory as sorted data file"
CLOSE #1
GOTO EndEst:
ELSE
INPUT #1, ONumb%, xmin#, xmax#, ymin#, ymax#
INPUT #1, lftptx#, rhtptx#, lftpty#, rhtpty#
INPUT #1, da#, numx, numy
CLOSE #1
END IF
CLS
LOCATE 2, 17: PRINT "NODAL VALUE ESTIMATION"
LOCATE 4, 1: PRINT "Grid Parameters:"
LOCATE 5, 5
PRINT "XMIN= "; xmin#; TAB(30); "# nodes in X direction=@
@ "; numx
LOCATE 6, 5
PRINT "XMAX= "; xmax#; TAB(30); "# nodes in Y@
@direction= "; numy
LOCATE 7, 5
PRINT "YMIN= "; ymin#; TAB(30); "Total # of nodal points =
"; numx * numy
LOCATE 8, 5
PRINT "YMAX= "; ymax#; TAB(30); "# of data points= ";
ONumb%
LOCATE 9, 5: PRINT "Node spacing = "; da#
LOCATE 11, 1
INPUT "Enter search circle radius (multiples of node spacing): ",
r%
rad% = da# * r%
'----input data
wtfunc$ = "P"
WHILE INSTR("LE", wtfunc$) = 0
LOCATE 12, 1: PRINT SPACE$(79)
LOCATE 12, 1
INPUT "Use Linear or Exponential weighting [L/E]: ", wtfunc$
wtfunc$ = UCASE$(wtfunc$)
WEND
Col:
LOCATE 13, 1: PRINT SPACE$(79): LOCATE 13, 1
PRINT "Output # of neighbor points in estimate (col 5) [N]? "
Col5$ = UCASE$(INPUT$(1))
IF Col5$ = CHR$(13) THEN Col5$ = "N"
IF Col5$ <> "Y" AND Col5$ <> "N" THEN GOTO Col:

OPEN F$ FOR INPUT AS #1
```

```
n = 0
LOCATE 14, 15: PRINT "Inputting";
Numb% = 0
WHILE NOT EOF(1)
Numb% = Numb% + 1
INPUT #1, east#(Numb%), north#(Numb%), A(Numb%),@
@ Dip(Numb%)
IF Numb% MOD 10 = 0 THEN PRINT " .";
IF (Numb% - 10) MOD 100 = 0 THEN
LOCATE 14, 25: PRINT SPACE$(20): LOCATE 14, 25
END IF
WEND
LOCATE 14, 25: PRINT SPACE$(20)
CLOSE #1
IF ONumb% <> Numb% THEN
PRINT "Data set changed since grid was computed - continue [N]"
ans$ = UCASE$(INPUT$(1))
IF ans$ <> "Y" THEN GOTO EndEst:
END IF
FO$ = MID$(F$, 1, LEN(F$) - 3) + "ES"
IF wtfunc$ = "L" THEN
FO$ = FO$ + "L"
ELSEIF wtfunc$ = "E" THEN
FO$ = FO$ + "E"
END IF
OPEN FO$ FOR OUTPUT AS #1
'----start estimation loop
LOCATE 15, 15: PRINT "Estimating node: "
FOR xx# = lftptx# TO rhtptx# STEP da#
FOR yy# = lftpty# TO rhtpty# STEP da#
LOCATE 15, 32: PRINT SPACE$(37)
LOCATE 15, 32: PRINT "(X="; xx#; ", Y="; yy#; ")";
'----Set appropriate variables to zero
COUNT% = 0: wtflg% = 0: totalwt = 0
Z1 = 0: Z2 = 0: z3 = 0
FOR k = 1 TO 100: NBB(k) = 0: dist(k) = 0
wt(k) = 0: NEXT k
'----Search for all points in square of influence
FOR k = 1 TO Numb%
IF east#(k) >= (xx# - rad%) AND east#(k) <= (xx# + rad%)@
@ AND north#(k) >= (yy# - rad%) AND north#(k) <= (yy#@
@ + rad%) THEN
COUNT% = COUNT% + 1
'----(max count for array=100)
IF COUNT% < 100 THEN NBB(COUNT%) = k
END IF
NEXT k
'----Search for all neighbor (nb) points in square also within circle
'----of radius rad%
numpts = COUNT%
FOR k = 1 TO COUNT%
'----calculate distance from node to each point and check if point
'----within circle
dist(k) = SQR((east#(NBB(k)) - xx#) * (east#(NBB(k)) - xx#) +@
@(north#(NBB(k)) - yy#) * (north#(NBB(k)) - yy#))
IF dist(k) >= rad% THEN
NBB(k) = 0
numpts = numpts - 1
'----Write x,y,azimuth,dip,number of points in circle to disk
'----for points centered on node and don't estimate
ELSEIF dist(k) < .001 THEN
Az = A(NBB(k)): di = Dip(NBB(k)): numpts = 1
IF Col5$ = "Y" THEN
WRITE #1, CINT(xx#), CINT(yy#), CINT(Az), CINT(di), numpts
ELSE
WRITE #1, CINT(xx#), CINT(yy#), CINT(Az), CINT(di)
END IF
wtflg% = 1
END IF
NEXT k
IF wtflg% = 0 THEN
'----Check if there are dips = zero- truth table
'---- dipflg%nodipflg%
'----1) some dips = 011
'----2) all dips = 010
'----3) no dips = 0 00
'----
dipflg% = 0: nodipflg% = 0
FOR k = 1 TO COUNT%
IF NBB(k) <> 0 THEN
IF Dip(k) = 0 THEN
nodipflg% = 1
ELSE
dipflg% = 1
END IF
END IF
NEXT k
'----Based on the above loop eliminate dip=0 iff
'----there are dip<>0 present
IF dipflg% = 1 AND nodipflg% = 1 THEN
FOR k = 1 TO COUNT%
IF Dip(NBB(k)) = 0 AND NBB(k) <> 0 THEN
NBB(k) = 0
numpts = numpts - 1
END IF
NEXT k
END IF
'----From distance calculate weight (linear function if
distance=rad%
'----then wt=0, if distance=0 then wt=1)
FOR k = 1 TO COUNT%
IF NBB(k) <> 0 THEN '(legitimate point within circle)
IF wtfunc$ = "L" THEN '(linear weighting)
wt(k) = (rad% - dist(k)) / rad%
ELSEIF wtfunc$ = "E" THEN'(exponential weighting)
'----Exponential wieghting is *10 to scale it from 0-1 to 0-10: at
10 the
'----value of the function is 0.0000454 = sufficiently small (i.e. 0)
wt(k) = 1 / EXP(dist(k) * 10 / rad%)
END IF
totalwt = totalwt + wt(k)
END IF
NEXT k
'----Normalize weights to total weight
FOR k = 1 TO COUNT%
IF NBB(k) <> 0 THEN
wt(k) = wt(k) / totalwt
'----Convert azimuth,dip to direction cosines,apply
'----weights,and total
IF dipflg% = 1 THEN
AzDipToDirCos A(NBB(k)), Dip(NBB(k)), X, Y, z
Z1 = Z1 + X * wt(k)
Z2 = Z2 + Y * wt(k)
z3 = z3 + z * wt(k)
ELSEIF dipflg% = 0 AND nodipflg% = 1 THEN
AzToDirCos A(NBB(k)), X, Y
Z1 = Z1 + X * wt(k)
Z2 = Z2 + Y * wt(k)
z3 = 0
END IF
```

```
END IF
NEXT k
'----Convert estimated direction cosines back to azimuth, dip
DirCosToAzDip Z1, Z2, z3, Az, di
'----Write x,y,azimuth,dip,number of points in circle to disk
'----If there were no nearest neighbors to the node output -1,-1
IF numpts = 0 THEN
Az = -1: di = -1
END IF
IF Col5$ = "Y" THEN
WRITE #1, xx#, yy#, CINT(Az), CINT(di), numpts
ELSE
WRITE #1, xx#, yy#, CINT(Az), CINT(di)
END IF
END IF
NEXT yy#
NEXT xx#
CLOSE #1
LOCATE 16, 15: PRINT "Finished. Results in "; FO$
EndEst:
LOCATE 25, 25: PRINT "Press any key to continue";
DO: LOOP UNTIL INKEY$ <> ""
EndEst2:
IF F$ = "Q" THEN FO$ = ""
END SUB

'*****************************************
SUB GeoSoft

ReEnter2:
CLS : LOCATE 5, 1
PRINT "GRID - GEO:CONVERSION TO GEOSOFT"
PRINT
PRINT "Program to convert output files produced by GRID"
PRINT "for use by the GeoSoft mapping package."
PRINT "Created 27-5-90 D.A.v.E."
PRINT : INPUT "Enter data file name (Q=Quit): ", F$
IF UCASE$(F$) = "Q" THEN GOTO EndGeo:
'----If file not found
IF Nerr% = 53 THEN
Nerr% = 0
GOTO ReEnter2:
END IF
OPEN F$ FOR INPUT AS #1
LINE INPUT #1, Data$
LINE INPUT #1, Data$
PRINT "Example data record from "; F$
PRINT ""; Data$
PRINT "Note number of columns": PRINT
CLOSE #1
OPEN F$ FOR INPUT AS #1
PRINT "Choices:"
PRINT "1) Input E,N,Angle"
PRINT "2) Input E1,N1,E2,N2 (Strike)"
PRINT "3) Input E1,N1,E2,N2,0 (Az/Dip)"
INPUT ">> ", Choice%
FO$ = MID$(F$, 1, LEN(F$) - 3) + "GEO"
PRINT "Output will be to :"
IF Choice% = 1 OR Choice% = 3 THEN
PRINT ""; FO$;
PRINT " (Contains: LINE 1000; X1,Y1,Counter,Angle)"
OPEN FO$ FOR OUTPUT AS #2
END IF
IF Choice% > 1 THEN
FO1$ = MID$(F$, 1, LEN(F$) - 3) + "GE2"
PRINT ""; FO1$;
PRINT " (Contains: MDDF M; LINA X1,Y1 etc;@
@ X2,Y2;repeated)"
OPEN FO1$ FOR OUTPUT AS #3
END IF
J = 1
IF Choice% = 1 OR Choice% = 3 THEN
PRINT #2, "LINE "; J * 1000
END IF
IF Choice% > 1 THEN
PRINT #3, "MDFP .m."
END IF
WHILE NOT EOF(1)
I = I + 1
IF Choice% = 1 THEN
INPUT #1, e1#, n1#, Angle
ELSEIF Choice% = 2 THEN
INPUT #1, e1#, n1#, e2#, n2#
ELSEIF Choice% = 3 THEN
INPUT #1, e1#, n1#, e2#, n2#, d%
END IF
row% = CSRLIN
IF I MOD 10 = 0 THEN
LOCATE row%, 1: PRINT "Converting record #"; I;
END IF
IF Choice% = 1 OR Choice% = 3 THEN
IF I MOD 500 = 0 THEN
J = J + 1
PRINT #2, "LINE "; J * 1000
END IF
IF Choice% = 1 THEN
PRINT #2, USING "############"; e1#; n1#; I; Angle
ELSE
PRINT #2, USING "############"; e1#; n1#; I
END IF
END IF
IF Choice% > 1 THEN
PRINT #3, "LINA 0,";
PRINT #3, USING "######"; e1#;
PRINT #3, ",";
PRINT #3, USING "#######"; n1#;
PRINT #3, ",1,1,1.0,0,0.25,1"
PRINT #3, " ";
PRINT #3, USING "######"; e2#;
PRINT #3, ",";
PRINT #3, USING "#######"; n2#
END IF
WEND
PRINT : PRINT : PRINT "Finished."
PRINT "Press any key to continue"
DO: LOOP UNTIL INKEY$ <> ""
CLOSE #1: CLOSE #2: CLOSE #3
EndGeo:
END SUB

'*****************************************
SUB GridAngle
'----Program to find and compute the angular change in dyke
'-----orientation from one grid point to the next in the N-S
'-----and E-W directions from the estimated data set (Option
'----estimate) - the grid spacing is calculated from the data
'----input (can be changed; 0 input ends program)

'----Created 18-5-90 D.A.v.E. (further modified 6-6-90)
CLS
```

```
d = 2200
PI = 3.1415926554#
Grad = PI / 180
DIM NA(3, 3), NB(3, 3), NC(3, 3), LL(3), FO$(6)
'
CLS
PRINT "This program is designed for Troodos Ophiolite"
PRINT "Sheeted Dyke orientation data. Its use is to determine the"
PRINT "change in angular relations between neighboring data pts."
PRINT "The output files produced are:"
PRINT "(1) amount of angular change in the strike (horizontal @
@plane rotation"
PRINT "(2) amount of angular change in the dip (vertical plane@
@ rotation)"
PRINT "(3) amount of angular change (dot prod.) for strike@
@ dominated change"
PRINT "(4) amount of angular change (dot prod.) for dip@
@ dominated changes"
PRINT "(5) amount of angular change (dot prod.) for complete@
@ data set."
PRINT : PRINT "Created: 22-5-90 (D.A.v.E.)"
PRINT : PRINT
ReDoAngle:
INPUT "Do (R)otation only or rotation + (A)ngular change@
@ calculation: ", W$
W$ = UCASE$(W$)
IF W$ <> "R" AND W$ <> "A" AND W$ <> "Q"@
@ THEN GOTO ReDoAngle:
IF W$ = "Q" THEN GOTO EndAngle:
INPUT "Enter data file name (Q=Quit): ", F$
IF UCASE$(F$) = "Q" THEN GOTO EndAngle:
OPEN F$ FOR INPUT AS #1
LINE INPUT #1, Data$
PRINT "Example data record from "; F$
PRINT ""; Data$
AgainCol:
INPUT "Enter number of columns in data (4 or 5): ", Col%
IF Col% < 4 OR Col% > 5 THEN GOTO AgainCol:
'----Determine grid spacing
IF Col% = 4 THEN
INPUT #1, e1#, n1#, A, d
INPUT #1, e2#, n2#, A, d
ELSEIF Col% = 5 THEN
INPUT #1, e1#, n1#, A, d, c
INPUT #1, e2#, n2#, A, d, c
END IF
Gridsp = ABS(e1# - e2#)
IF Gridsp = 0 THEN Gridsp = ABS(n1# - n2#)
IF Gridsp <> 0 THEN
PRINT "Grid spacing to be used is "; Gridsp; "m Okay?[Y] "
END IF
GridQ$ = UCASE$(INPUT$(1))
IF GridQ$ = "N" THEN INPUT "Enter grid spacing: ", Gridsp
IF Gridsp = 0 THEN GOTO EndAngle:
'----Close and then reopen file
CLOSE #1
OPEN F$ FOR INPUT AS #1

IF W$ = "A" THEN
FO$(1) = MID$(F$, 1, LEN(F$) - 3) + "V"
FO$(2) = MID$(F$, 1, LEN(F$) - 3) + "H"
FO$(3) = MID$(F$, 1, LEN(F$) - 3) + "S"
FO$(4) = MID$(F$, 1, LEN(F$) - 3) + "D"
FO$(5) = MID$(F$, 1, LEN(F$) - 3) + "T"
FOR I = 1 TO 5
OPEN FO$(I) FOR OUTPUT AS #(I + 1)
NEXT I
ELSEIF W$ = "R" THEN
FO$(6) = MID$(F$, 1, LEN(F$) - 3) + "ROT"
OPEN FO$(6) FOR OUTPUT AS #2
END IF
'----Read in data file
CLS
PRINT "Reading data file: "; F$
I = 0
WHILE NOT EOF(1)
I = I + 1
IF Col% = 4 THEN
INPUT #1, east#(I), north#(I), A(I), Dip(I)
ELSEIF Col% = 5 THEN
INPUT #1, east#(I), north#(I), A(I), Dip(I), Dummy
END IF
WEND
Num% = I
'----Remove 5 degree uplift caused by up doming of TROODOS
PRINT "For Troodos the ophiolite trend is 110 deg,layers dip 5
PRINT " deg to N (Suggest right handed rotation:"
PRINT " Az=110,Dip=0,Angle of rotation=5)"
INPUT "Enter rotation axis azimuth: ", RAZI
INPUT "Plunge: ", RDIP
INPUT "Enter right-handed rotation angle: ", RAN
PRINT "Calculating rotation matrix"
'
IF RAZI = 0 AND RDIP = 0 AND RAN = 0 THEN GOTO
SkipRotate:
'
AA = RAZI * Grad: Dip = RDIP * Grad
D1 = PI / 2 - Dip: H = RAN * Grad
NA(1, 1) = COS(AA): NA(2, 1) = SIN(AA): NA(3, 1) = 0
NA(1, 2) = -SIN(AA): NA(2, 2) = CCS(AA): NA(3, 2) = 0
NA(1, 3) = 0: NA(2, 3) = 0: NA(3, 3) = 1
'
NB(1, 1) = COS(D1): NB(2, 1) = 0: NB(3, 1) = -SIN(D1)
NB(1, 2) = 0: NB(2, 2) = 1: NB(3, 2) = 0
NB(1, 3) = SIN(D1): NB(2, 3) = 0: NB(3, 3) = COS(D1):
GOSUB 4800
'
NB(1, 1) = COS(H): NB(2, 1) = -SIN(H): NB(3, 1) = 0
NB(1, 2) = SIN(H): NB(2, 2) = COS(H): NB(3, 2) = 0
NB(1, 3) = 0: NB(2, 3) = 0: NB(3, 3) = 1: GOSUB 4800
'
NB(1, 1) = COS(D1): NB(2, 1) = 0: NB(3, 1) = SIN(D1)
NB(1, 2) = 0: NB(2, 2) = 1: NB(3, 2) = 0
NB(1, 3) = -SIN(D1): NB(2, 3) = 0: NB(3, 3) = COS(D1):
GOSUB 4800
'
NB(1, 1) = COS(AA): NB(2, 1) = -SIN(AA): NB(3, 1) = 0
NB(1, 2) = SIN(AA): NB(2, 2) = COS(AA): NB(3, 2) = 0
NB(1, 3) = 0: NB(2, 3) = 0: NB(3, 3) = 1: GOSUB 4800
GOTO Rotatemathend:

4800 FOR J = 1 TO 3: FOR I = 1 TO 3
NC(I, J) = NB(1, J) * NA(I, 1) + NB(2, J) * NA(I, 2) + @
@NB(3, J) * NA(I, 3)
NEXT I: NEXT J
FOR J = 1 TO 3: FOR I = 1 TO 3: NA(I, J) = NC(I, J)
NEXT I: NEXT J
RETURN

Rotatemathend:
```

```
'----Now do the rotation
FOR I = 1 TO Num%
IF A(I) <> -1 THEN
AA = (A(I) + 180 MOD 360) * Grad: d = Dip(I) * Grad
L = SIN(d) * COS(AA)
m = SIN(d) * SIN(AA)
n = COS(d)
FOR J = 1 TO 3
LL(J) = NA(1, J) * L + NA(2, J) * m + NA(3, J) * n
NEXT J
AA = ATN(LL(2) / LL(1))
IF LL(1) < 0 THEN AA = AA + PI
d = ATN(((1 / LL(3)) ^ 2 - 1) ^ .5)
IF LL(3) < 0 THEN AA = AA + PI
A(I) = ((AA / Grad) + 180) MOD 360
Dip(I) = d / Grad
IF W$ = "R" THEN
PRINT #2, USING "##############"; east#(I); north#(I);@
@ A(I); Dip(I)
END IF
END IF
NEXT I
IF W$ = "R" THEN
CLOSE #1: CLOSE #2
GOTO EndAngle:
END IF
SkipRotate:
'----Find nearest neighbors to N,S,E,W,
PRINT "Determining change angle"
FOR I = 1 TO Num%
LOCATE 9, 1: IF I MOD 10 = 0 THEN PRINT " Using record
#"; I
'----Check if we are along the north or east map boundary
EFlg% = 0: NFlg% = 0
e = 525272.3 - east#(I): IF e < 10 THEN EFlg% = 1
n = 3876754 - north#(I): IF n < 10 THEN NFlg% = 1
'----No estimated data (Az=-1,Dip=-1)
IF A(I) = -1 AND Dip(I) = -1 THEN
EFlg% = 1: NFlg% = 1
END IF
FOR J = 1 TO Num%
Flag% = 0
'----east
IF EFlg% = 0 THEN
IF east#(J) = east#(I) + Gridsp AND north#(J) = north#(I)@
@ AND A(J) <> -1 THEN
'----Calculate midpoint
MidEE# = east#(I) + Gridsp / 2: MidEN# = north#(I)
'----Get azimuth b/t 0-180 and compare and print difference
A1 = A(I) MOD 180: A2 = A(J) MOD 180
VertRot = ABS(A1 - A2)
PRINT #2, USING "##############"; MidEE#; MidEN#; VertRot
'----Compare dips and print the difference - if dip azimuths are
'---->90 degrees apart then the dip differences must be added
'----together & then subtracted from 180:Az<90: |Az>90 |
'----(Dips opposite)                          |\   /|\
AbsVertRot = ABS(A(I) - A(J))
IF AbsVertRot <= 90 THEN
HorizRot = ABS(Dip(I) - Dip(J))
ELSE
HorizRot = 180 - (Dip(I) + Dip(J))
END IF
PRINT #3, USING "##############"; MidEE#; MidEN#;@
@ HorizRot
'----Calculate the difference angle by dot product
CalcAngle A(I), A(J), Dip(I), Dip(J), Theta
'----Separate the results based on dominant rotation mode and
'----print to file
'----VertRot dominant = strike direction rotation more important
'----HorizRot dominant = dip rotation - important to angular
'---- change
IF VertRot > HorizRot THEN
PRINT #4, USING "##############"; MidEE#; MidEN#; Theta
ELSEIF VertRot = HorizRot THEN
PRINT #4, USING "##############"; MidEE#; MidEN#; Theta
PRINT #5, USING "##############"; MidEE#; MidEN#; Theta
ELSE
PRINT #5, USING "##############"; MidEE#; MidEN#; Theta
END IF
'----Print all angular change results to another file
PRINT #6, USING "##############"; MidEE#; MidEN#; Theta
END IF
END IF
'----north (same method as above refer there for comments)
IF NFlg% = 0 THEN
IF east#(J) = east#(I) AND north#(J) = north#(I) +@
@Gridsp AND A(J) <> -1 THEN
MidNE# = east#(I): MidNN# = north#(I) + Gridsp / 2
A1 = A(I) MOD 180: A2 = A(J) MOD 180
VertRot = ABS(A1 - A2)
PRINT #2, USING "##############"; MidNE#; MidNN#;@
@ VertRot
AbsVertRot = ABS(A(I) - A(J))
IF AbsVertRot <= 90 THEN
HorizRot = ABS(Dip(I) - Dip(J))
ELSE
HorizRot = 180 - (Dip(I) + Dip(J))
END IF
PRINT #3, USING "##############"; MidNE#; MidNN#;@
@ HorizRot
CalcAngle A(I), A(J), Dip(I), Dip(J), Theta
IF VertRot > HorizRot THEN
PRINT #4, USING "##############"; MidNE#; MidNN#; Theta
ELSEIF VertRot = HorizRot THEN
PRINT #4, USING "##############"; MidNE#; MidNN#; Theta
PRINT #5, USING "##############"; MidNE#; MidNN#; Theta
ELSE
PRINT #5, USING "##############"; MidNE#; MidNN#; Theta
END IF
PRINT #6, USING "##############"; MidNE#; MidNN#; Theta
END IF
END IF
NEXT J
NEXT I
FOR I = 1 TO 6
CLOSE #(I)
NEXT I
PRINT : PRINT "Output is in:"
IF W$ = "A" THEN
PRINT ""; FO$(1); ": amount of rotation in vertical direction"
PRINT ""; FO$(2); ": amount of rotation in horizontal direction"
PRINT ""; FO$(3); ": change in orientation if strike dominated"
PRINT ""; FO$(4); ": change in orientation if dip dominated"
PRINT ""; FO$(5); ": change in orientation all data)"
ELSEIF W$ = "R" THEN
PRINT ""; FO$(6); ": data rotated by ("; RAN; "-"; RAZ; "/";
RDIP; ")"
FO$ = FO$(6)
END IF
PRINT : PRINT "Finished ": PRINT
```

```
PRINT : PRINT "Press any key to continue": DO: LOOP UNTIL
INKEY$ <> ""
EndAngle:
'
END SUB

'*****************************************
SUB InsertSort
'----Sorting routine - using the insertion sort method to sort
'----the first element in the data record - here east#().
'----Creation date: 18-4-1990 D.A.v.E.
'----Based on Stubbs & Webre;1985;Data Structures With Abstract
'----Data Types and Pascal;Brooks Cole Publ p274.

'----Enter data
ReEnter4:
CLS : LOCATE 2, 10
PRINT "S O R T I N G-I N S E R T I O N M E T H O D"
LOCATE 4, 10
PRINT "Enter file name containing numbers to be sorted
(Q=quit): "
LOCATE 5, 15: INPUT "> > ", F$
IF UCASE$(F$) = "Q" THEN GOTO EndSort:
'----If file not found
OPEN F$ FOR INPUT AS #1
IF Nerr% = 53 THEN
Nerr% = 0
GOTO ReEnter4:
END IF
FO$ = MID$(F$, 1, LEN(F$) - 3) + "SRT"
LOCATE 7, 10: PRINT "Output file name: "; FO$; " Okay? [Y]"
ans$ = UCASE$(INPUT$(1))
IF ans$ <> "Y" AND ans$ <> CHR$(13) THEN
LOCATE 7, 10: PRINT SPACE$(50)
LOCATE 7, 10: INPUT "Enter output file name >> ", FO$
END IF
OPEN FO$ FOR OUTPUT AS #2
n = 0
LOCATE 10, 25: PRINT "Inputting";
LOCATE 10, 35
WHILE NOT EOF(1)
n = n + 1
INPUT #1, east#(n), north#(n), A(n), Dip(n)
IF n MOD 10 = 0 THEN PRINT " .";
IF (n - 10) MOD 100 = 0 THEN
LOCATE 10, 35: PRINT SPACE$(20): LOCATE 10, 35
END IF
WEND
CLOSE #1
'----Sort data file using insertion method
LOCATE 11, 25: PRINT "Sorting";
LOCATE 11, 35
FOR k = n - 1 TO 1 STEP -1
L = n - k
J = k + 1
save = east#(k)
east#(n + 1) = save
'----remember elements in remmaining arrays
sy = north#(k): sa = A(k): sd = Dip(k)
north#(n + 1) = sy: A(n + 1) = sa: Dip(n + 1) = sd
IF L MOD 10 = 0 THEN PRINT " .";
IF (L - 10) MOD 100 = 0 THEN
LOCATE 11, 35: PRINT SPACE$(20): LOCATE 11, 35
END IF
WHILE save > east#(J)
east#(J - 1) = east#(J)
'----do the same to elements in the remaining arays
north#(J - 1) = north#(J): A(J - 1) = A(J): Dip(J - 1) = Dip(J)
J = J + 1
WEND
east#(J - 1) = save
'----do the same to elements in the remaining arays
north#(J - 1) = sy: A(J - 1) = sa: Dip(J - 1) = sd
NEXT k
'----Save sorted data to file
LOCATE 12, 25: PRINT "Saving"; : LOCATE 12, 35
FOR k = 1 TO n
WRITE #2, east#(k), north#(k), A(k), Dip(k)
IF k MOD 10 = 0 THEN PRINT " .";
IF (k - 10) MOD 100 = 0 THEN
LOCATE 12, 35: PRINT SPACE$(20): LOCATE 12, 35
END IF
NEXT k
CLOSE #2
'
EndSort:
IF UCASE$(F$) = "Q" THEN FO$ = ""
END SUB

'*****************************************
SUB Makegrid
'----Subroutine to determine grid boundaries and the necessary
'----number of nodes.
ReEnter5:
CLS
LOCATE 2, 28: PRINT "G R I DC R E A T I O N"
LOCATE 4, 1
PRINT "Reads data file, calc. the max. & min values in X, Y"
PRINT "directions, asks for grid spacing and calc number"
PRINT "of grid points needed in each direction"
ON ERROR GOTO GenError:
LOCATE 9, 1: PRINT "Directory Listing:": LOCATE 11, 1
FILES "*.SRT"
IF Nerr% = 53 THEN
Nerr% = 0
LOCATE pr% - 1, pc%
FILES
END IF
LOCATE 8, 15: INPUT ; "Enter data file name (Q=quit): ", F$
IF UCASE$(F$) = "Q" THEN GOTO EndGrid:
'----If file not found
IF Nerr% = 53 THEN
Nerr% = 0
GOTO ReEnter5:
END IF
OPEN F$ FOR INPUT AS #1
FO$ = MID$(F$, 1, LEN(F$) - 3) + "GRD"
'----Input data file; determine max and min easting and northing
xmax# = -10000000: ymax# = xmax#
xmin# = 10000000: ymin# = xmin#
CLS
LOCATE 10, 15: PRINT "Inputting";
k = 0
WHILE NOT EOF(1)
k = k + 1
INPUT #1, e#, n#, Az, Dip
IF xmin# > e# THEN xmin# = e#
IF ymin# > n# THEN ymin# = n#
IF xmax# < e# THEN xmax# = e#
IF ymax# < n# THEN ymax# = n#
```

```
IF k MOD 10 = 0 THEN PRINT " .";
IF (k - 10) MOD 100 = 0 THEN
LOCATE 10, 25: PRINT SPACE$(20): LOCATE 10, 25
END IF
WEND
Numb% = k
CLOSE #1
lenx# = xmax# - xmin#: leny# = ymax# - ymin#
'----Display data set limits
CLS
LOCATE 2, 28: PRINT "G R I DC R E A T I O N"
LOCATE 4, 1: PRINT "Data ranges in "; UCASE$(F$); ":"
LOCATE 5, 5: PRINT "XMIN= "; xmin#
LOCATE 6, 5: PRINT "XMAX= "; xmax#
LOCATE 7, 5: PRINT "YMIN= "; ymin#
LOCATE 8, 5: PRINT "YMAX= "; ymax#
LOCATE 9, 5: PRINT "# PTS.= "; Numb%
'----Input grid node point spacing (Guess if you have to)
Setspacing:
numx = 0: numy = 0
LOCATE 11, 1
INPUT "Enter grid spacing (Note:dX=dY): ", da#
'----Compute upper,lower,left,right grid limits (1*da# in from
'----data edges)
lftptx# = xmin# + da#: rhtptx# = xmax# - da#
lftpty# = ymin# + da#: rhtpty# = ymax# - da#
FOR k = lftptx# TO rhtptx# STEP da#: numx = numx + 1:
NEXT k
FOR k = lftpty# TO rhtpty# STEP da#: numy = numy + 1:
NEXT k
totalpts = numx * numy
PRINT
PRINT "Number of grid nodes in X direction: "; numx
PRINT "Number of grid nodes in Y direction: "; numy
PRINT "Total number of grid nodes: "; totalpts
PRINT
PRINT "Spacing okay? (# of nodes should be < # of@
@ data pts.) [N]";
ans$ = UCASE$(INPUT$(1))
IF ans$ < > "Y" THEN
LOCATE 11, 1
FOR I = 11 TO 17: PRINT SPACE$(79): NEXT I
GOTO Setspacing:
END IF
'----Output results to file.GRD
OPEN FO$ FOR OUTPUT AS #1
WRITE #1, Numb%, xmin#, xmax#, ymin#, ymax#
WRITE #1, lftptx#, rhtptx#, lftpty#, rhtpty#
WRITE #1, da#, numx, numy
CLOSE #1
EndGrid:
IF UCASE$(F$) = "Q" THEN FO$ = ""
END SUB

'*****************************************
SUB Neighbor

ReEnter6:
CLS
PRINT "Routine to compile number of nearest neihbors for grid"
PRINT "points and determine the average number and standard"
PRINT " deviation"
PRINT
PRINT "Enter file name to be checked (MUST be 5 col format): "
INPUT "(Q=Quit) > > ", F$
IF UCASE$(F$) = "Q" THEN GOTO EndNeighbor:
OPEN F$ FOR INPUT AS #1
'----If file not found
IF Nerr% = 53 THEN
Nerr% = 0
GOTO ReEnter6:
END IF
 WHILE NOT EOF(1)
 INPUT #1, A#, B#, c, d, e
 COUNT% = COUNT% + 1
 TOTAL = TOTAL + e
 SX2# = SX2# + e * e
 WEND
 AVERAGE = TOTAL / COUNT%
 SDEV = SQR((SX2# / COUNT%) - (AVERAGE * AVERAGE))
 PRINT "Total # pts="; COUNT%
 PRINT "Sum of Neighbors="; TOTAL
 PRINT "Average # of Neighbors="; AVERAGE
 PRINT "std.dev="; SDEV
 CLOSE #1
'
EndNeighbor:
END SUB
'
'*****************************************
SUB RotCoord
'----Program fragment to rotate from one orthogonal coordinate
'----system in x-y space to another by a straight linear
'----transformationwith a rotation axis centered on the
'---- origin (mutual origin)
'----Creation date: 20-4-1990 D.A.v.E.

Grad = 3.1415926534# / 180
'----Input data file name
ReEnter:
CLS
LOCATE 2, 5
PRINT "ROTATION OF COORDINATE SYSTEM"
LOCATE 4, 1
PRINT "Rotate coordinate system clockwise by an angle theta"
LOCATE 7, 1
PRINT "Enter file containing x,y coords to be rotated (Q=quit)"
LOCATE 8, 10: INPUT "> > ", F$
IF UCASE$(F$) = "Q" THEN GOTO EndRotCoord:
'----If file not found
IF Nerr% = 53 THEN
Nerr% = 0
GOTO ReEnter:
END IF
OPEN F$ FOR INPUT AS #1

FO$ = MID$(F$, 1, LEN(F$) - 3) + "ROT"
OPEN FO$ FOR OUTPUT AS #2
LOCATE 11, 1
PRINT "Enter clockwise (from north=0) rotation angle"
LOCATE 12, 10: INPUT "> > ", Theta
Theta = Theta * Grad
n = 0: LOCATE 14, 14: PRINT "Inputting,Computing and
Saving"; : LOCATE 14, 45
WHILE NOT EOF(1)
n = n + 1
INPUT #1, e#, n#, Az, Dip
no# = e# * COS(Theta) - n# * SIN(Theta)
nn# = e# * SIN(Theta) + n# * COS(Theta)
IF n MOD 10 = 0 THEN PRINT " .";
```

```
IF (n - 10) MOD 100 = 0 THEN LOCATE 14, 45: PRINT
SPACE$(20): LOCATE 14, 45
PRINT #2, USING "##########.##,"; nc#; nn#;
WRITE #2, Az, Dip
WEND
LOCATE 16, 14: PRINT "Finished. Results in "; FO$
LOCATE 25, 35: PRINT "Press any key to continue";
DO: LOOP UNTIL INKEY$ <> ""
CLOSE #1: CLOSE #2
EndRotCoord:
IF UCASE$(F$) = "Q" THEN FO$ = ""
END SUB

'*****************************************
SUB Short

ReEnter7:
CLS
PRINT
PRINT "Checks for null points on est. grid (dyke data), removes"
PRINT "them (all pts whose azimuth & dip were -1,-1) from file"
PRINT
INPUT "Enter file to remove null data points (Q=quit): ", F$
IF UCASE$(F$) = "Q" THEN GOTO EndShort:
OPEN F$ FOR INPUT AS #1
'----If file not found
IF Nerr% = 53 THEN
Nerr% = 0
GOTO ReEnter7:
END IF
FO$ = MID$(F$, 1, LEN(F$) - 3) + "SHT"
PRINT "Output will be in "; FO$
OPEN FO$ FOR OUTPUT AS #2
LINE INPUT #1, Data$
CLOSE #1: OPEN F$ FOR INPUT AS #1
PRINT "Example data record from "; F$
PRINT ""; Data$
col3:
INPUT "Enter number of columns in data record (4 or 5): ", Col%
IF Col% < 4 OR Col% > 5 THEN GOTO col3:
WHILE NOT EOF(1)
IF Col% = 5 THEN
INPUT #1, A#, B#, c, d, e
IF c <> -1 AND d <> -1 THEN WRITE #2, A#, B#, c, d, e
ELSEIF Col% = 4 THEN
INPUT #1, A#, B#, c, d
IF c <> -1 AND d <> -1 THEN WRITE #2, A#, B#, c, d
END IF
WEND
PRINT RENUM
CLOSE #1: CLOSE #2

EndShort:
IF UCASE$(F$) = "Q" THEN FO$ = ""
END SUB

'*****************************************
SUB VAXConvert

ReEnter8:
CLS
LOCATE 5, 10
PRINT "C O N V E R S I O NF O R S U R F A C EII": PRINT
PRINT
PRINT "VAXCONV: prepares dyke data for plotting on the VAX"
PRINT "using SURFACE II plot pkg - run REFORM on VAX"
PRINT "to finish preparation for SURFACE II"
PRINT
PRINT "Will produce x1,y1,x2,y2 for both Az/Dip & strike case"
PRINT "Input: X,Y,Az.,Dip";
PRINT "Output: X1,Y1,X2,Y2,Symbol. 29-4-90 D.A.v.E."
'
rad = 3.1415926534# / 180
TryAgain5:
PRINT
INPUT "Compute x1,y1,x2,y2 for (S)trike or (A)z/dip @
@or (B)oth: ", Comp$
Comp$ = UCASE$(Comp$)
IF Comp$ <> "S" AND Comp$ <> "A" AND Comp$ <>@
@ "B" THEN GOTO TryAgain5:
PRINT : INPUT "Enter data file name (Q=quit): ", F$
IF UCASE$(F$) = "Q" THEN GOTO EndVAX:
OPEN F$ FOR INPUT AS #1
'----If file not found
IF Nerr% = 53 THEN
Nerr% = 0
GOTO ReEnter8:
END IF
PRINT "Output will be to: "
IF Comp$ = "A" OR Comp$ = "B" THEN
FO$ = MID$(F$, 1, LEN(F$) - 3) + "AZD"
PRINT "Az/Dip X1,Y1,X2,Y2: "; FO$
OPEN FO$ FOR OUTPUT AS #2
END IF
IF Comp$ = "S" OR Comp$ = "B" THEN
FO$ = MID$(F$, 1, LEN(F$) - 3) + "STR"
PRINT "Strike X1,Y1,X2,Y2: "; FO$
OPEN FO$ FOR OUTPUT AS #3
END IF
'
LINE INPUT #1, Data$
PRINT "Example record from "; F$: PRINT ""; Data$
CLOSE #1: OPEN F$ FOR INPUT AS #1
Column:
INPUT "Enter # of columns in data file (4 or 5): ", Col%
IF Col% < 4 OR Col% > 5 THEN GOTO Column:
'
X = CSRLIN: I = 0
PRINT "Reading, computing and writing record #";
'----Initialize the max and min variables
xmin = 10000000: ymin = xmin
xmax = -10000000: ymax = xmax
WHILE NOT EOF(1)
I = I + 1
IF Col% = 4 THEN
INPUT #1, x1, y1, Az, Dip
ELSEIF Col% = 5 THEN
INPUT #1, x1, y1, Az, Dip, Dummy
END IF
IF I MOD 10 = 0 THEN LOCATE X, 40: PRINT I;
'----Convert the azimuth and dip angle to x,y coordinates for
'----later plotting and convert azimuth to strike x,y coords.
IF Comp$ = "S" OR Comp$ = "B" THEN
Azz = Az - 90
IF Azz < 0 THEN Azz = Azz + 180
IF Azz > 180 THEN Azz = Azz - 180
Azz = Azz * rad
XS1 = x1 - SIN(Azz) * 250
YS1 = y1 - COS(Azz) * 250
XS2 = x1 + SIN(Azz) * 250
```

```
YS2 = y! + COS(Azz) * 250
END IF
IF Comp$ = "A" OR Comp$ = "B" THEN
Az = Az * rad: Dip = Dip * rad
x2 = SIN(Az) * COS(Dip) * 500 + x1
y2 = COS(Az) * COS(Dip) * 500 + y1
END IF
'---If no dip was given (dip=0) then set symbol to 1 else 0
IF Dip = 0 THEN
symbol = 1
ELSE
symbol = 0
END IF
IF Comp$ = "A" OR Comp$ = "B" THEN
WRITE #2, x1, y1, x2, y2, symbol
END IF
IF Comp$ = "S" OR Comp$ = "B" THEN
WRITE #3, XS1, YS1, XS2, YS2
END IF
WEND
'
CLOSE #1: CLOSE #2: CLOSE #3
PRINT : PRINT "Finished.": PRINT
PRINT : PRINT "Press any key to continue": DO: LOOP UNTIL
INKEY$ <> ""
'
EndVAX:
IF UCASE$(F$) = "Q" THEN FC$ = ""
END SUB
```

```
'----MINTSTAT.BAS
'----program to sum trace lengths by mineral filling
'----dimension arrays
DIM M$(10), T(10, 10), S(10, 4), LT(10, 10), LS(10, 2)
M$(1) = "e": M$(2) = "z": M$(3) = "k": M$(4) = "c": M$(5)
= "h"
M$(6) = "m": M$(7) = "p": M$(8) = "x": M$(9) = "j": M$(10)
= "n"
CLS
'----print title
PRINT "Mineral Filling Versus Trace Length Statistics": PRINT
'----get input batch file name
'----names are dom?.aut where ?=2,3,4,5,6 (in C:\DATA)
FOR K = 2 TO 6
  BF$ = "DOM" + LTRIM$(RTRIM$(STR$(K))) + ".AUT"

PRINT "Enter batch file name: ", BF$
OF$ = MID$(BF$, 1, LEN(BF$) - 3) + "OUT"
CLOSE #1: CLOSE #3
OPEN BF$ FOR INPUT AS #1
OPEN OF$ FOR OUTPUT AS #3
PRINT "Output will be to: "; OF$
INPUT #1, Dir$
Dir$ = Dir$ + "\"
PRINT "Input directory: "; Dir$
'----first pass to get the mean
FOR I = 1 TO 10
  S(I, 1) = 0: S(I, 2) = 0: S(I, 3) = 0: S(I, 4) = 1000
  LS(I, 1) = 0: LS(I, 2) = 0
NEXT I
WHILE NOT EOF(1)
  INPUT #1, F$
  CLOSE #2
  OPEN Dir$ + F$ FOR INPUT AS #2
  PRINT "Reading: "; F$
  WHILE NOT EOF(2)
    INPUT #2, D$
    IF MID$(D$, 1, 1) = "1" THEN
      FOR I = 1 TO 10
        IF MID$(D$, 33, 1) = M$(I) OR MID$(D$, 36, 1) =
M$(I) OR MID$(D$, 39, 1) = M$(I) THEN
          IF VAL(MID$(D$, 27, 4)) < > 0 THEN
            V = VAL(MID$(D$, 27, 4))
            IF S(I, 3) < V THEN S(I, 3) = V
            IF S(I, 4) > V THEN S(I, 4) = V
            LV = LOG(V)
            S(I, 1) = S(I, 1) + V
            S(I, 2) = S(I, 2) + 1
            LS(I, 1) = LS(I, 1) + LV
          END IF
        END IF
      NEXT I
    END IF
  WEND
WEND
'----calculate the mean trace length for each mineral
'----LS refers to the log transformed values
FOR I = 1 TO 10
  IF S(I, 2) < > 0 THEN
    S(I, 1) = S(I, 1) / S(I, 2)
    LS(I, 1) = LS(I, 1) / S(I, 2)
  ELSE
    S(I, 1) = 0
    LS(I, 1) = 0
  END IF
NEXT I
'----second pass to get other stats
'----to get first (absolute), second, third, and fourth
'----moments of the deviation form the mean
'----T(I,1)=average deviation
'----T(I,2)=variance
'----T(I,3)=skewness
'----T(I,4)=kurtosis
'----LT(I,?)=the log transformed version of T
FOR I = 1 TO 10: FOR J = 1 TO 10: T(I, J) = 0: LT(I, J) = 0:
NEXT J: NEXT I
CLS
PRINT "Mineral Filling Versus Trace Length Statistics": PRINT
PRINT "Second pass to get four moments of deviation"
PRINT "Input directory: "; Dir$
CLOSE #1
OPEN BF$ FOR INPUT AS #1
INPUT #1, Dir$
Dir$ = Dir$ + "\"
WHILE NOT EOF(1)
  INPUT #1, F$
  PRINT "Reading: "; F$
  CLOSE #2
  OPEN Dir$ + F$ FOR INPUT AS #2
  WHILE NOT EOF(2)
    INPUT #2, D$
    IF MID$(D$, 1, 1) = "1" THEN
      FOR I = 1 TO 10
        IF S(I, 1) < > 0 THEN
          IF MID$(D$, 33, 1) = M$(I) OR MID$(D$, 36, 1) =
M$(I) OR MID$(D$, 39, 1) = M$(I) THEN
            IF VAL(MID$(D$, 27, 4)) < > 0 THEN
              V = VAL(MID$(D$, 27, 4))
              LV = LOG(V)
              T(I, 5) = V - S(I, 1)
              T(I, 1) = T(I, 1) + ABS(V)
              T(I, 6) = T(I, 5) * T(I, 5)
              T(I, 2) = T(I, 2) + T(I, 6)
              T(I, 6) = T(I, 6) * T(I, 5)
              T(I, 3) = T(I, 3) + T(I, 6)
              T(I, 6) = T(I, 6) * T(I, 5)
              T(I, 4) = T(I, 4) + T(I, 6)
              T(I, 7) = T(I, 7) + 1
'----now do the same for the log transformed values
              LT(I, 5) = LV - LS(I, 1)
              LT(I, 1) = LT(I, 1) + ABS(LV)
              LT(I, 6) = LT(I, 5) * LT(I, 5)
              LT(I, 2) = LT(I, 2) + LT(I, 6)
              LT(I, 6) = LT(I, 6) * LT(I, 5)
              LT(I, 3) = LT(I, 3) + LT(I, 6)
              LT(I, 6) = LT(I, 6) * LT(I, 5)
              LT(I, 4) = LT(I, 4) + LT(I, 6)
            END IF
          END IF
        END IF
      NEXT I
    END IF
  WEND
WEND
FOR I = 1 TO 10
  IF T(I, 7) > 1 THEN
    T(I, 1) = T(I, 1) / T(I, 7)  'average deviation
    T(I, 2) = T(I, 2) / (T(I, 7) - 1)
    var = T(I, 2)                'variation
    T(I, 2) = SQR(var)           'standard deviation
```

```
    IF var < > 0 THEN
      T(I, 3) = T(I, 3) / (T(I, 7) * T(I, 2) * T(I, 2) * T(I, 2))
'skewness
      T(I, 4) = T(I, 4) / (T(I, 7) * var * var) - 3
'kurtosis
    END IF
'----now do the same for the log transformed values
    LT(I, 1) = LT(I, 1) / T(I, 7)  'average deviation
    LT(I, 2) = LT(I, 2) / (T(I, 7) - 1)
    Lvar = LT(I, 2)            'variation
    LT(I, 2) = SQR(Lvar)       'standard deviation
    IF Lvar < > 0 THEN
      LT(I, 3) = LT(I, 3) / (T(I, 7) * LT(I, 2) * LT(I, 2) * LT(I,
2))  'skewness
      LT(I, 4) = LT(I, 4) / (T(I, 7) * Lvar * Lvar) - 3
'kurtosis
    END IF
  ELSE
    FOR J = 1 TO 10: T(I, J) = 0: LT(I, J) = 0: NEXT J
  END IF
NEXT I
PRINT "Min  #  Mean  Average  Standard  Skewness
Kurtosis  Max  Min"
PRINT "                Deviation  Deviation"
FOR I = 1 TO 10
  PRINT M$(I); "  ";
  PRINT USING "####"; T(I, 7);
  PRINT USING "######.##"; S(I, 1);
  FOR J = 1 TO 4
    PRINT USING "######.##"; T(I, J);
  NEXT J
  PRINT USING "######.##"; S(I, 3); S(I, 4)
  PRINT
NEXT I
PRINT "The following are the stats of the log transformed trace
lengths"
PRINT "  The results are given as arithmetic values": PRINT
PRINT "Min  #  Mean  Average  Standard  Skewness
Kurtosis"
PRINT "                Deviation  Deviation"
FOR I = 1 TO 10
  PRINT M$(I); "  ";
  PRINT USING "####"; T(I, 7);
  PRINT USING "######.##"; EXP(LS(I, 1));
  FOR J = 1 TO 4
    PRINT USING "######.##"; EXP(LT(I, J));
  NEXT J
  PRINT
NEXT I
'----Output to the file
PRINT #3, "Min  #  Mean  Average  Standard  Skewness
Kurtosis  Max  Min"
PRINT #3, "                Deviation  Deviation"
FOR I = 1 TO 10
  PRINT #3, M$(I); "  ";
  PRINT #3, USING "####"; T(I, 7);
  PRINT #3, USING "######.##"; S(I, 1);
  FOR J = 1 TO 4
    PRINT #3, USING "######.##"; T(I, J);
  NEXT J
  PRINT #3, USING "######.##"; S(I, 3); S(I, 4)
  PRINT #3,
NEXT I
PRINT #3, "The following are the stats of the log transformed
trace lengths"
PRINT #3, "  The results are given as arithmetic values": PRINT
PRINT #3, "Min  #  Mean  Average  Standard  Skewness
Kurtosis"
PRINT #3, "                Deviation  Deviation"
FOR I = 1 TO 10
  PRINT #3, M$(I); "  ";
  PRINT #3, USING "####"; T(I, 7);
  PRINT #3, USING "######.##"; EXP(LS(I, 1));
  FOR J = 1 TO 4
    PRINT #3, USING "######.##"; EXP(LT(I, J));
  NEXT J
  PRINT #3,
NEXT I
CLOSE

NEXT K
END
```

```
'---ORS.BAS
'---program ORS to convert Cyprus data files to FRACMAN
'---ORS format using input data of the following format
'---11001s0800300101.50cn251581.702-nurdf001
'---first line of batch file contains the directory path name
'--- to the data files the remaining lines contain the file names
'---initialize
Num = 0: BatFlg = 0: CLS
'---header
PRINT : PRINT "CONVERSION CYPRUS FORMAT TO
FRACMAN FORMAT": PRINT
'---get file or batch file name
INPUT "Enter file name for conversion (or BATCH): ", F$
F$ = UCASE$(F$)
'---batch mode
IF F$ = "BATCH" THEN
INPUT "Enter batch file name: ", BatF$
OPEN BatF$ FOR INPUT AS #10
INPUT #10, Dir$
PRINT "I/O directory is: "; Dir$
Dir$ = UCASE$(Dir$) + "\"
INPUT "Enter name for survey file (no extension): ", OF1$
OF1$ = OF1$ + ".SVY"
BatFlg = 1
'---single file mode
ELSE
INPUT "Enter I/O directory name (<CR> for current):", Dir$
Dir$ = Dir$ + "\"
OPEN Dir$ + F$ FOR INPUT AS #1
OF1$ = MID$(F$, 1, LEN(F$) - 3) + "SVY"
END IF
OPEN Dir$ + OF1$ FOR OUTPUT AS #3
PRINT #3, "File contains data from: "; F$
PRINT #3, "Standard Survey File"
PRINT #3, "B/S/AScanScan @
@TransvTransv ScanTransv"
PRINT #3, "Code Xo Yo ZoTrendPlunge @
@Trend PlungeLengthLength"
PRINT #3, "ID |Name (m)(m)(m)(deg) (deg) @
@(deg) (deg)(m)(m)"
IF BatFlg = 0 THEN GOTO SingleFile:
'---start reading batch file names
WHILE NOT EOF(10)
Num = Num + 1
INPUT #10, F$
SingleFile:
CLOSE #1
OPEN Dir$ + F$ FOR INPUT AS #1
OF$ = MID$(F$, 1, LEN(F$) - 3) + "ORS"
PRINT "Output: "; OF$
CLOSE #2
OPEN Dir$ + OF$ FOR OUTPUT AS #2
PRINT #2, "-5,"; Num; ","; OF1$
NewTot = 0: OldLength = 0: Length = 0: Flg = 0
'---read individual files
WHILE NOT EOF(1)
INPUT #1, D$
IF MID$(D$, 1, 1) = "1" AND LEN(D$) > 45 THEN
IF Flg = 0 THEN
Flg = 1
PRINT #3, USING "##"; Num;
PRINT #3, " S ";
PRINT #3, TAB(6); MID$(F$, 1, 4); TAB(15); "0.0. 0.";
```

```
ts# = VAL(MID$(D$, 7, 3)): sp# = VAL(MID$(D$, 10, 2))
PRINT #3, USING "###.#"; TAB(41); ts#; TAB(50); sp#;
ts# = ts# + 180: tp# = 90 - sp#
WHILE ts# > 360: ts# = ts# - 360: WEND
PRINT #3, USING "####.#"; TAB(58); ts#; TAB(67); tp#;
END IF
PRINT #2, USING "####.##"; VAL(MID$(D$, 22, 3));
PRINT #2, " ";
PRINT #2, USING "####.##"; VAL(MID$(D$, 25, 2));
PRINT #2, "1";
PRINT #2, USING "####.##"; VAL(MID$(D$, 27, 4))
Length = VAL(MID$(D$, 15, 5))
IF Length - OldLength < -3 THEN
NewTot = NewTot + OldLength
END IF
OldLength = Length
END IF
WEND
NewTot = NewTot + Length
PRINT #3, USING "######.#"; TAB(73); NewTot; TAB(82); !0!
IF BatFlg = 0 THEN GOTO SingleFile1:
WEND
SingleFile1:
CLOSE
END
```

```
'----PARAPLAT.BAS
'----Program to calculate permeability by the Norton and Knapp
'----(1977) planar, parallel fracture model used by Nehlig and
'----Juteau (1988). The formula used is K=nd^3/12, n is the
'----number of fractures per distance and d is the fracture
'----aperture. 15-2-91 D.A.v.E.
'----Method: use only the dyke parallel fractures with
'----mineral filling within 20 degrees of the mean dyke
'----orientation
DECLARE SUB AzDipToDirCos (Az, Dip, X, Y, Z)
DECLARE SUB DirCosToAzDip (Z1!, Z2!, z3!, Az!, Dip!)
DIM Tr(5), TMax(5), TMin(5)
CLS
PRINT "Permeabiliy calculations on Cyprus scanline data"
PRINT "(Using the Norton and Knapp (1977) method)": PRINT
INPUT "Enter batch file name: ", bf$
OPEN bf$ FOR INPUT AS #1
of$ = "NEHLIG.OUT"
PRINT "Results are output to "; of$: PRINT
OPEN of$ FOR OUTPUT AS #3
OPEN "NEHLIG.TRL" FOR OUTPUT AS #4
INPUT #1, Dir$
WHILE NOT EOF(1)
INPUT #1, f$
filename$ = Dir$ + "\" + f$
OPEN filename$ FOR INPUT AS #2
PRINT "Reading "; f$; " for dyke data."
'----read through data file once to get the dyke margin orientations
XT = 0: YT = 0: ZT = 0
WHILE NOT EOF(2)
INPUT #2, d$
IF MID$(d$, 1, 1) = "1" THEN
IF MID$(d$, 20, 2) = "cn" THEN
Az = VAL(MID$(d$, 22, 3))
Dip = VAL(MID$(d$, 25, 2))
'----convert Az and Dip to direction cosines sum and convert back
AzDipToDirCos Az, Dip, X, Y, Z
XT = XT + X
YT = YT + Y
ZT = ZT + Z
DirCosToAzDip XT, YT, ZT, DykeAz, DykeDip
END IF
END IF
WEND
CLOSE #2
OPEN filename$ FOR INPUT AS #2
'----determine which fractures are subparallel to the dyke margins
'----count these (if they have same mineral filling). Orientations
'----are taken as parallel if they are within 20 degrees of mean
'----dyke orientation.
EFrac = 0: ZFrac = 0: CFrac = 0: AFrac = 0
NFrac = 0: NumFrac = 0
EAperture = 0: ZAperture = 0: CAperture = 0
AAperture = 0: NAperture = 0
PRINT "Reading "; f$; " for aperture and spacing data."
MaxDist = 0
FOR i = 1 TO 5
TMax(i) = 0: TMin(i) = 1000: Tr(i) = 0
NEXT i
WHILE NOT EOF(2)
INPUT #2, d$
IF MID$(d$, 1, 1) = "1" THEN
NumFrac = NumFrac + 1
```

```
IF MaxDist < VAL(MID$(d$, 15, 5)) THEN MaxDist =
VAL(MID$(d$, 15, 5))
FracAz = VAL(MID$(d$, 22, 3))
FracDip = VAL(MID$(d$, 25, 2))
IF ABS(FracAz - DykeAz) <= 20 AND ABS(FracDip -
DykeDip) <= 20 THEN
Trlen = VAL(MID$(d$, 27, 4))
IF MID$(d$, 33, 1) = "e" OR MID$(d$, 36, 1) = "e" OR@
@MID$(d$, 36, 1) = "e" THEN
EFrac = EFrac + 1
EAperture = EAperture + VAL(MID$(d$, 47, 3))
IF Trlen < TMin(1) THEN TMin(1) = Trlen
IF Trlen > TMax(1) THEN TMax(1) = Trlen
Tr(1) = Tr(1) + Trlen
END IF
IF MID$(d$, 33, 1) = "z" OR MID$(d$, 36, 1) = "z" OR@
@MID$(d$, 36, 1) = "z" THEN
ZFrac = ZFrac + 1
ZAperture = ZAperture + VAL(MID$(d$, 47, 3))
IF Trlen < TMin(2) THEN TMin(2) = Trlen
IF Trlen > TMax(2) THEN TMax(2) = Trlen
Tr(2) = Tr(2) + Trlen
END IF
IF MID$(d$, 33, 1) = "c" OR MID$(d$, 36, 1) = "c" OR@
@ MID$(d$, 36, 1) = "c" THEN
CFrac = CFrac + 1
CAperture = CAperture + VAL(MID$(d$, 47, 3))
IF Trlen < TMin(3) THEN TMin(3) = Trlen
IF Trlen > TMax(3) THEN TMax(3) = Trlen
Tr(3) = Tr(3) + Trlen
END IF
IF MID$(d$, 33, 1) <> "n" THEN
AFrac = AFrac + 1
AAperture = AAperture + VAL(MID$(d$, 47, 3))
IF Trlen < TMin(4) THEN TMin(4) = Trlen
IF Trlen > TMax(4) THEN TMax(4) = Trlen
Tr(4) = Tr(4) + Trlen
END IF
IF MID$(d$, 33, 1) = "n" THEN
NFrac = NFrac + 1
NAperture = NAperture + VAL(MID$(d$, 47, 3))
IF Trlen < TMin(5) THEN TMin(5) = Trlen
IF Trlen > TMax(5) THEN TMax(5) = Trlen
Tr(5) = Tr(5) + Trlen
END IF: END IF: END IF
WEND
'----calculate the average trace length
IF EFrac <> 0 THEN Tr(1) = Tr(1) / EFrac
IF ZFrac <> 0 THEN Tr(2) = Tr(2) / ZFrac
IF CFrac <> 0 THEN Tr(3) = Tr(3) / CFrac
IF AFrac <> 0 THEN Tr(4) = Tr(4) / AFrac
IF NFrac <> 0 THEN Tr(5) = Tr(5) / NFrac
CLOSE #2
'----calculate the average aperture for the scanline for each
'----of the classes
PRINT "calculating average aperture, spacing and permeability"
IF EFrac <> 0 THEN EApAv = EAperture / EFrac
IF ZFrac <> 0 THEN ZApAv = ZAperture / ZFrac
IF CFrac <> 0 THEN CApAv = CAperture / CFrac
IF AFrac <> 0 THEN AApAv = AAperture / AFrac
IF NFrac <> 0 THEN NApAv = NAperture / NFrac
'----calculate the average fracture spacing for each class
ESpace = EFrac / MaxDist
ZSpace = ZFrac / MaxDist
CSpace = CFrac / MaxDist
ASpace = AFrac / MaxDist
NSpace = NFrac / MaxDist
'----calculate the permeability for each case (convert the aperture
'----in millimetres to metres (/1000)
IF EFrac <>0 THEN EK=(ESpace) * ((EApAv / 1000) ^ 3) / 12
IF ZFrac <>0 THEN ZK=(ZSpace) * ((ZApAv / 1000) ^ 3) / 12
IF CFrac <>0 THEN CK=(CSpace) * ((CApAv / 1000) ^ 3) / 12
IF AFrac <>0 THEN AK=(ASpace) * ((AApAv / 1000) ^ 3) / 12
IF NFrac <>0 THEN NK=(NSpace) * ((NApAv / 1000) ^ 3)/ 12
'----output the results
PRINT "printing results to: "; of$
PRINT #3, "Permeability results using Norton and Knapp method"
PRINT #3,
PRINT #3, "ScanlineScanline-LengthMean-DykeAz/DykeDip@
@Number-Fractures"
PRINT #3, " NumberAperture (mm)Spacing (1/m)@
@Permeability (m^2)"
PRINT #3,
PRINT #3, MID$(f$, 1, LEN(f$) - 4); "("; MaxDist; ;
PRINT #3, USING "####"; DykeAz; : PRINT #3, "/";
PRINT #3, USING "##"; DykeDip;
PRINT #3, USING "####"; NumFrac; : PRINT #3, ")"
IF EFrac <> 0 THEN
PRINT #3, " epidote: ";
PRINT #3, USING "####"; EFrac;
PRINT #3, USING "#####.#"; EApAv; ZSpace;
PRINT #3, USING "##.#^^^^"; EK
END IF
IF ZFrac <> 0 THEN
PRINT #3, " zeolite: ";
PRINT #3, USING "####"; ZFrac;
PRINT #3, USING "#####.#"; ZApAv; ZSpace;
PRINT #3, USING "##.#^^^^"; ZK
END IF
IF CFrac <> 0 THEN
PRINT #3, " calcite: ";
PRINT #3, USING "####"; CFrac;
PRINT #3, USING "#####.#"; CApAv; CSpace;
PRINT #3, USING "##.#^^^^"; CK
END IF
IF AFrac <> 0 THEN
PRINT #3, " all : ";
PRINT #3, USING "####"; AFrac;
PRINT #3, USING "#####.#"; AApAv; ASpace;
PRINT #3, USING "##.#^^^^"; AK
END IF
IF NFrac <> 0 THEN
PRINT #3, " none: ";
PRINT #3, USING "####"; NFrac;
PRINT #3, USING "#####.#"; NApAv; NSpace;
PRINT #3, USING "##.#^^^^"; NK
END IF
PRINT #3,
PRINT #4, MID$(f$, 1, LEN(f$) - 4);
FOR i = 1 TO 5
PRINT #4, USING "#####.#"; Tr(i); TMax(i); TMin(i);
NEXT i
PRINT #4,
WEND
PRINT : PRINT "Output is in :"; of$
CLOSE #1: CLOSE #3: CLOSE #4

REM $DYNAMIC
'*****************************************
SUB AzDipToDirCos (A, d, X, Y, Z)
```

```
Grad = 3.1415926544# / 180
'----If the dip is 90 then make it 89.9 to preserve the azimuth
IF d = 90 THEN d = 89.9
'----Calculate direction cosines from azimuth and dip
azimuth = A * Grad
Dip = d * Grad
Z = SIN(Dip)
Y = COS(Dip) * COS(azimuth)
X = COS(Dip) * SIN(azimuth)

END SUB

'*****************************************
SUB DirCosToAzDip (Z1, Z2, z3, Az, Dip)

Grad = 3.1415926544# / 180
'----convert direction cosines to azimuth dip
'----to avoid division by 0 if z2=0, set az=90
IF Z2 = 0 THEN
Az = 90
ELSE
Az = ATN(ABS(Z1 / Z2)) / Grad
END IF
IF Z1 < 0 AND Z2 > 0 THEN
Az = 360 - Az
ELSEIF Z1 < 0 AND Z2 < 0 THEN
Az = Az + 180
ELSEIF Z1 > 0 AND Z2 < 0 THEN
Az = 180 - Az
END IF
hyp = SQR(Z1 * Z1 + Z2 * Z2)
'----if z1,z2=0 then the direction is vertical so to avoid division
'----by 0 set dip=90
IF hyp = 0 THEN
Dip = 90
ELSE
Dip = ATN(z3 / hyp) / Grad
END IF
'----Just a safety precaution
IF z3 = 0 THEN Dip = 0

END SUB
```

```
'----PREPROC.BAS
'----Program to pre-process the cyprus data for the permeability
'----calculation 22.5.92D.A.v.E.
'----Subroutine declarations
DECLARE SUB MakeDataLine (AP$, C!, Data$(), Az$, Dip$,
d$, Dist$, @
@MaxLen!, FillAp$)
DECLARE SUB DirCosToAzDip (Z1!, Z2!, z3!, Az!, Dip!)
DECLARE SUB AzDipToDirCos (A!, d!, X!, Y!, Z!)
'----dimension arrays and set constant
DIM Data$(500)
Grad = 3.1415926544# / 180
CLS
PRINT "Pre-processor for the permeability calculations"
PRINT
BatchFlg% = 0
'----get input file name and directory
INPUT "Enter directory name: ", Dir$
PRINT "Data directory: "; Dir$
INPUT "Enter input data file name (Cyprus format or type
BATCH): ", F$
IF UCASE$(F$) <> "BATCH" THEN
OPEN Dir$ + "\" + F$ FOR INPUT AS #1
ELSEIF UCASE$(F$) = "BATCH" THEN
BatchFlg% = 1
INPUT "Enter batch file name: ", BF$
OPEN BF$ FOR INPUT AS #10
INPUT #10, Dir$
END IF
'----decide what data parameters to use
PRINT
PRINT "Enter the number corresponding to your choice below:"
PRINT "(1) All fractures"
PRINT "(2) Unfilled fractures"
PRINT "(3) Filled fractures"
PRINT "(4) Epidote filled fractures"
PRINT "(5) Zeolite filled fractures"
PRINT "(6) Calcite filled fractures"
PRINT ">> "; : Choice$ = UCASE$(INPUT$(1)): PRINT
Choice$
IF Choice$ = "1" OR Choice$ = "A" THEN
EXT$ = "SA": Choice% = 1
ELSEIF Choice$ = "2" OR Choice$ = "U" THEN
EXT$ = "SU": Choice% = 2
ELSEIF Choice$ = "3" OR Choice$ = "F" THEN
EXT$ = "SF": Choice% = 3
ELSEIF Choice$ = "4" OR Choice$ = "E" THEN
EXT$ = "SE": Choice% = 4
ELSEIF Choice$ = "5" OR Choice$ = "Z" THEN
EXT$ = "SZ": Choice% = 5
ELSEIF Choice$ = "6" OR Choice$ = "C" THEN
EXT$ = "SC": Choice% = 6
END IF
'----Check if only near dyke orientation fractures are to be used
Dyke$ = "N"
PRINT "Use only fractures within 20 degrees of dykes [N]: ";
Dyke$ = UCASE$(INPUT$(1))
IF Dyke$ = CHR$(13) THEN Dyke$ = "N"
PRINT Dyke$
IF Dyke$ = "N" THEN EXT2$ = "A" ELSE EXT2$ = "D"
'----check to fill in fractures with no aperture as = 0.1 mm
PRINT
PRINT "If fracture has no associated aperture, assume
```

```
Ap=0.01mm ? [N] ";
FillAp$ = UCASE$(INPUT$(1))
IF FillAp$ = CHR$(13) THEN FillAp$ = "N"
PRINT FillAp$
'----open output file
BatchRun:
IF BatchFlg% = 1 AND NOT EOF(10) THEN
INPUT #10, F$
CLOSE #1: CLOSE #2
OPEN Dir$ + "\" + F$ FOR INPUT AS #1
PRINT "Reading "; F$
ELSEIF BatchFlg% = 1 AND EOF(10) THEN
CLOSE : END
END IF
OF$ = "C:\SCRATCH\" + LTRIM$(MID$(F$, 1, LEN(F$) - 3)
+ EXT$ + EXT2$)
PRINT "Output to: "; OF$
OPEN OF$ FOR OUTPUT AS #2
PRINT #2, "File: "; F$; ". ";
'----put info line in data output file
IF Choice% = 1 THEN
PRINT #2, "All fractures. ";
ELSEIF Choice% = 2 THEN
PRINT #2, "Unfilled fractures. ";
ELSEIF Choice% = 3 THEN
PRINT #2, "Filled fractures. ";
ELSEIF Choice% = 4 THEN
PRINT #2, "Epidote filled fractures. ";
ELSEIF Choice% = 5 THEN
PRINT #2, "Zeolite filled fractures. ";
ELSEIF Choice% = 6 THEN
PRINT #2, "Calcite filled fractures. ";
END IF
IF FillAp$ = "Y" THEN PRINT #2, " If Ap=blank then
Ap=0.1.";
'----read the data file first to get the mean dyke orientation
IF Dyke$ = "Y" THEN
WHILE NOT EOF(1)
INPUT #1, d$
IF MID$(d$, 1, 1) = "1" THEN
IF MID$(d$, 20, 2) = "cn" THEN
Az = VAL(MID$(d$, 22, 3))
Dip = VAL(MID$(d$, 25, 2))
'----convert Az and Dip to direction cosines sum and convert back
'----If the dip is 90 then make it 89.9 to preserve the azimuth
IF Dip = 90 THEN Dip = 89.9
'----Calculate direction cosines from azimuth and dip
azimuth = Az * Grad: Dp = Dip * Grad
Z = SIN(Dp)
Y = COS(Dp) * COS(azimuth)
X = COS(Dp) * SIN(azimuth)
XT = XT + X
YT = YT + Y
ZT = ZT + Z
'----convert direction cosines to azimuth dip
'----to avoid division by 0 if z2=0, set az=90
IF YT = 0 THEN
DykeAz = 90
ELSE
DykeAz = ATN(ABS(XT / YT)) / Grad
END IF
IF XT < 0 AND YT > 0 THEN
DykeAz = 360 - DykeAz
ELSEIF XT < 0 AND YT < 0 THEN
DykeAz = DykeAz + 180
ELSEIF XT > 0 AND YT < 0 THEN
DykeAz = 180 - DykeAz
END IF
hyp = SQR(XT * XT + YT * YT)
'----if z1,z2=0 then the direction is vertical so to avoid division
'----by 0 set dip=90
IF hyp = 0 THEN
DykeDip = 90
ELSE
DykeDip = ATN(ZT / hyp) / Grad
END IF
'----Just a safety precaution
IF ZT = 0 THEN DykeDip = 0
END IF
END IF
WEND
PRINT #2, " Dyke: Az="; DykeAz; " Dip="; DykeDip
CLOSE #1: OPEN Dir$ + "\" + F$ FOR INPUT AS #1
END IF
IF Dyke$ = "N" THEN PRINT #2,
'----read the data file and using the above choices output results
C = 0: Prev = 1
WHILE NOT EOF(1)
INPUT #1, d$
'----if a fracture data line is encountered
IF MID$(d$, 1, 1) = "1" THEN
SELECT CASE Choice%
CASE 1'----All fractures
Az$ = MID$(d$, 22, 3): Dip$ = MID$(d$, 25, 2)
AP$ = MID$(d$, 47, 3)
FracAz = VAL(Az$): FracDip = VAL(Dip$)
IF Dyke$ = "Y" THEN
IF ABS(FracAz - DykeAz) <= 20 AND ABS(FracDip -
DykeDip)@
@ <= 20 THEN
CALL MakeDataLine(AP$, C, Data$(), Az$, Dip$, d$, Dist$@
@, MaxLen, FillAp$)
END IF
ELSEIF Dyke$ = "N" THEN
CALL MakeDataLine(AP$, C, Data$(), Az$, Dip$, d$, Dist$@
@, MaxLen, FillAp$)
END IF
CASE 2'----None filled fractures
IF MID$(d$, 33, 1) = "n" THEN
Az$ = MID$(d$, 22, 3): Dip$ = MID$(d$, 25, 2)
AP$ = MID$(d$, 47, 3)
FracAz = VAL(Az$): FracDip = VAL(Dip$)
IF Dyke$ = "Y" THEN
IF ABS(FracAz - DykeAz) <= 20 AND ABS(FracDip -@
@ DykeDip) <= 20 THEN
CALL MakeDataLine(AP$, C, Data$(), Az$, Dip$, d$@
@, Dist$, MaxLen, FillAp$)
END IF
ELSEIF Dyke$ = "N" THEN
CALL MakeDataLine(AP$, C, Data$(), Az$, Dip$, d$, Dist$@
@, MaxLen, FillAp$)
END IF
END IF
CASE 3'----Filled fractures
IF MID$(d$, 33, 1) <> "n" THEN
Az$ = MID$(d$, 22, 3): Dip$ = MID$(d$, 25, 2)
AP$ = MID$(d$, 47, 3)
FracAz = VAL(Az$): FracDip = VAL(Dip$)
IF Dyke$ = "Y" THEN
IF ABS(FracAz - DykeAz) <= 20 AND ABS(FracDip -@
```

```
@ DykeDip) <= 20 THEN
CALL MakeDataLine(AP$, C, Data$(), Az$, Dip$, d$@
@, Dist$, MaxLen, FillAp$)
END IF
ELSEIF Dyke$ = "N" THEN
CALL MakeDataLine(AP$, C, Data$(), Az$, Dip$, d$, Dist$@
@, MaxLen, FillAp$)
END IF
END IF
CASE 4'----Epidote filled fractures
IF MID$(d$, 33, 1) = "e" OR MID$(d$, 36, 1) = "e" OR@
@MID$(d$, 39, 1) = "e" THEN
Az$ = MID$(d$, 22, 3): Dip$ = MID$(d$, 25, 2)
AP$ = MID$(d$, 47, 3)
FracAz = VAL(Az$): FracDip = VAL(Dip$)
IF Dyke$ = "Y" THEN
IF ABS(FracAz - DykeAz) <= 20 AND ABS(FracDip -
DykeDip)@
@ <= 20 THEN
CALL MakeDataLine(AP$, C, Data$(), Az$, Dip$, d$@
@, Dist$, MaxLen, FillAp$)
END IF
ELSEIF Dyke$ = "N" THEN
CALL MakeDataLine(AP$, C, Data$(), Az$, Dip$, d$, Dist$@
@, MaxLen, FillAp$)
END IF
END IF
CASE 5'----Zeolite filled fractures
IF MID$(d$, 33, 1) = "z" OR MID$(d$, 36, 1) = "z" OR@
@ MID$(d$, 39, 1) = "z" THEN
Az$ = MID$(d$, 22, 3): Dip$ = MID$(d$, 25, 2)
AP$ = MID$(d$, 47, 3)
FracAz = VAL(Az$): FracDip = VAL(Dip$)
IF Dyke$ = "Y" THEN
IF ABS(FracAz - DykeAz) <= 20 AND ABS(FracDip -
DykeDip)@
@ <= 20 THEN
CALL MakeDataLine(AP$, C, Data$(), Az$, Dip$, d$@
@ , Dist$, MaxLen, FillAp$)
END IF
ELSEIF Dyke$ = "N" THEN
CALL MakeDataLine(AP$, C, Data$(), Az$, Dip$, d$, Dist$@
@ , MaxLen, FillAp$)
END IF
END IF
CASE 6'----Calcite filled fractures
IF MID$(d$, 33, 1) = "c" OR MID$(d$, 36, 1) = "c" OR@
@MID$(d$, 39, 1) = "c" THEN
Az$ = MID$(d$, 22, 3): Dip$ = MID$(d$, 25, 2)
AP$ = MID$(d$, 47, 3)
FracAz = VAL(Az$): FracDip = VAL(Dip$)
IF Dyke$ = "Y" THEN
IF ABS(FracAz - DykeAz) <= 20 AND ABS(FracDip -
DykeDip)@
@<= 20 THEN
CALL MakeDataLine(AP$, C, Data$(), Az$, Dip$, d$@
@, Dist$, MaxLen, FillAp$)
END IF
ELSEIF Dyke$ = "N" THEN
CALL MakeDataLine(AP$, C, Data$(), Az$, Dip$, d$, @
@Dist$, MaxLen, FillAp$)
END IF
END IF
CASE ELSE
END SELECT

'----if a scanline information line (2) is encountered
ELSEIF MID$(d$, 1, 1) = "2" THEN
C = C + 1
IF C > 1 THEN
Data$(Prev) = "S: " + STR$(MaxLen) + " " + Data$(Prev)
END IF
MaxLen = 0
Trnd$ = MID$(d$, 7, 3): Plng$ = MID$(d$, 10, 2)
Data$(C) = Trnd$ + " " + Plng$
Prev = C
END IF
IF EOF(1) THEN Data$(Prev) = "S: " + STR$(MaxLen) + " "@
@ + Data$(Prev)
WEND
'----output the resulting data array to a file
FOR I = 1 TO C: PRINT #2, Data$(I): NEXT I
'----
IF BatchFlg% = 1 THEN GOTO BatchRun:
CLOSE
END

'****************************************
SUB MakeDataLine (AP$, C, Data$(), Az$, Dip$, d$, Dist$,@
@ MaxLen, FillAp$)
'----Subroutine to compile the data array for azimuth, dip and
aperture
'----also calulates the length of the scanline

'----if fracture aperture = blank or 0 then ignore data
IF FillAp$ = "N" THEN
'----ignore data if either the azimuth or the dip are blank
IF Az$ <> "" AND Az$ <> "" AND Dip$ <> "" AND@
@ Dip$ <> "" THEN
IF AP$ <> "" AND AP$ <> "" AND AP$ <> "0" THEN
C = C + 1
Data$(C) = "F: " + Az$ + " " + Dip$ + " " + AP$
END IF
Dist = VAL(MID$(d$, 15, 5))
IF Dist > MaxLen THEN MaxLen = Dist
END IF
'----the Aperture is set to 0.1 (mm) if FillAp$="Y" if it
'----is non-zero but blank
ELSEIF FillAp$ = "Y" THEN
IF Az$ <> "" AND Az$ <> "" AND Dip$ <> "" AND@
@Dip$ <> "" AND AP$ <> "0" THEN
C = C + 1
IF AP$ = "" OR AP$ = "" THEN AP$ = "0.1"
Data$(C) = "F: " + Az$ + " " + Dip$ + " " + AP$
Dist = VAL(MID$(d$, 15, 5))
IF Dist > MaxLen THEN MaxLen = Dist
END IF
END IF
END SUB
```

'-----QUICKPLOT.BAS

Quickplot is published in:

van Everdingen, D.A., van Gool, J.A.M., and Vissers, R.L.M.; 1992; QuickPlot: A Microcomputer-Based Program For Processing of Orientation Data; Computers and Geosciences v18 n2/3 p183-287.

```
'----QPSEP.BAS
'----Program to make visual separation of orientation data
'----and to tabulate the totals of the various fracture characteristics
'----separated data can be written to a file
'----as well as the tabulated results. Required input
'----is a Cyprus format (fracture characteristics) data file
'----Created: 31/1/91 By: D.A.v.E.

'----File units used are #1: Data input (Cyprus format)
'----#2: Table output
'----#3: Result record output
'----#4: Result orientation data
'----#5: Result PIC file output
'
'----Declare subs
DECLARE SUB Tabulate (Chosen%())
DECLARE SUB PFsize (Picture$, X%, Y%)
DECLARE SUB PMove (Picture$, X%, Y%)
DECLARE SUB PText (Picture$, D1%, P%, Msg$)
DECLARE SUB PDraw (Picture$, X%, Y%)
DECLARE SUB PDrawSym (Picture$, X%, Y%, isym%)
DECLARE SUB GetHex (ival%, hi$, lo$)
DECLARE SUB POpen (Picture$)
DECLARE SUB RePLot ()
DECLARE SUB SaveFile ()
DECLARE SUB CalcBound (Bound#(), C%, Chosen%())
DECLARE SUB ReadData ()
DECLARE SUB InputData ()
DECLARE SUB GraphicsCard ()
DECLARE SUB Plotting ()
'----Set screen/monitor type variable
TYPE Display'Display type characteristics
MX AS INTEGER'max X limit of screen
MY AS INTEGER'max Y limit of screen
CX AS INTEGER'X size of character
CY AS INTEGER'Y size of character
ML AS INTEGER'# of lines of screen
MD AS INTEGER'default diamter of circle
ASP AS SINGLE'default aspect ratio for screen
SCR AS INTEGER'screen type (Herc, CGA, EGA or VGA)
END TYPE
'----Dimension arrays
DIM ThetR(300), AzR(300), XC(300)
DIM YC(300), XCP(300), YCP(300)
DIM DL$(300), Bound#(50, 2), Chosen%(300), NotChosen%(300)
'----Set common variables and arrays
COMMON SHARED /Display/ D AS Display
COMMON SHARED Nerr%, YRatio, DL$(), ThetR(), AzR()
COMMON SHARED Numb%, Grad, XX%, YY%
COMMON SHARED XC(), YC(), Bound#(), F$, Chosen%()
COMMON SHARED BNum%, SaveFlg%, PicFlg%
COMMON SHARED NotChosen%(), Picture$, XCP(), YCP()
COMMON SHARED X%, Y%, Dir$
'----Set the screen aspect ratio and constants
PI = 3.1415926544: Grad = PI / 180
'----Set error trapping
ON ERROR GOTO Generr:
'----Determine the type of graphics card
GraphicsCard
YRatio = D.ASP
'----Input the data
Dir$ = ""
InputData
'----Plot the data
Plotting
'----Start the main program and cursor routine
LOCATE 1, 1: PRINT SPACE$(78);
DIM Cross(4000), SampFind$(100), East#(100), North#(100),
D1$(100)
LINE (1, 4)-(7, 4): LINE (4, 1)-(4, 7)
GET (1, 1)-(7, 7), Cross
LOCATE 1, 1: PRINT "SEPARATE DATA ON BASIS OF
ORIENTATION"
CFlg% = 1: LFlg% = 1
X# = XX%: Y# = YY%
NMax# = D.CY * 24 + 8: NMin# = D.CY * 3 + 6
EMax# = D.CX * 77 + 6: EMin# = D.CX * 30
Dist% = 10
LINE (1, D.CY * 2 + 3)-(D.CX * 79 + 7, D.CY * 2 + 3)
'----Display screen message
LOCATE 2, 1: PRINT SPACE$(79);
LOCATE 2, 1
PRINT "Outline data points with cursor and [SPACE]. [H]elp
[Q]uit"
DO: DO
Move$ = INKEY$
LOOP UNTIL Move$ <> ""
CursMovFlg% = 0
IF CFlg% = 0 THEN PUT (X# - 3, Y# - 3), Cross, XOR
CFlg% = 0
Move$ = UCASE$(Move$)
SELECT CASE Move$
'----PgUp
CASE CHR$(0) + CHR$(73)
Dist% = Dist% + 5
'----PgDn
CASE CHR$(0) + CHR$(81)
IF Dist% <= 0 THEN
Dist% = 1
ELSE
Dist% = Dist% - 5
END IF
'----Up
CASE CHR$(0) + CHR$(72)
IF Y# < NMin# THEN
Y# = NMax#
ELSE
Y# = Y# - Dist%
END IF
CursMovFlg% = 1
'----Left
CASE CHR$(0) + CHR$(75)
IF X# < EMin# THEN
X# = EMax#
ELSE
X# = X# - Dist%
END IF
CursMovFlg% = 1
'----Right
CASE CHR$(0) + CHR$(77)
IF X# > EMax# THEN
X# = EMin#
ELSE
X# = X# + Dist%
END IF
CursMovFlg% = 1
'----Down
CASE CHR$(0) + CHR$(80)
```

```
IF Y# > NMax# THEN
Y# = NMin#
ELSE
Y# = Y# + Dist%
END IF
CursMovFlg% = 1
'----Esc
CASE CHR$(27)
'----Erase line and put cross at previous point
IF C% > 1 THEN
LINE (Bound#(C%, 1), Bound#(C%, 2))-(Bound#(C% - 1, 1),@
@ Bound#(C% - 1, 2)), 0
oldX# = Bound#(C% - 1, 1): oldY# = Bound#(C% - 1, 2)
C% = C% - 1
X# = Bound#(C%, 1): Y# = Bound#(C%, 2)
END IF
'----Spacebar=draw line
CASE CHR$(32)
IF LFlg% = 1 THEN
oldX# = X#: oldY# = Y#
FirstX# = X#: FirstY# = Y#
LFlg% = 0
C% = 1
Bound#(1, 1) = X#: Bound#(1, 2) = Y#
ELSE
LINE (oldX#, oldY#)-(X#, Y#)
oldX# = X#: oldY# = Y#
C% = C% + 1
Bound#(C%, 1) = X#: Bound#(C%, 2) = Y#
END IF
CASE "C", "c"
IF LFlg% = 0 THEN
C% = C% + 1
Bound#(C%, 1) = FirstX#: Bound#(C%, 2) = FirstY#
LINE (oldX#, oldY#)-(FirstX#, FirstY#)
LFlg% = 1
IF SaveFlg% = 0 THEN
LOCATE 2, 1: PRINT SPACE$(79);
LOCATE 2, 1: PRINT " Save Results [Y/N]"
Q$ = UCASE$(INPUT$(1))
IF Q$ = "Y" THEN SaveFile
END IF
CalcBound Bound#(), C%, Chosen%()
'----Erase boundary
FOR I = 2 TO C%
LINE (Bound#(I - 1, 1), Bound#(I - 1, 2))-(Bound#(I, 1),@
@Bound#(I, 2)), 0
NEXT I
'----Redraw chosen points
RePLot
'----Pic file output of data
IF SaveFlg% = 1 OR PicFlg% = 1 THEN
POpen (Picture$)
END IF
'----Tabulate results
Tabulate Chosen%()
END IF
CASE "D"
'----Set directory
LOCATE 2, 1: PRINT SPACE$(79)
LOCATE 2, 1: INPUT "Enter directory name (e.g. C:\DATA): ";
Dir$
Dir$ = UCASE$(Dir$)
LOCATE 2, 1: PRINT SPACE$(79)
CASE "H"
'----Display message on screen
LOCATE 1, 1: PRINT SPACE$(79); : LOCATE 2, 1: PRINT
SPACE$(79);
Msg1$ = "Use cursor to move cross,[PgUp] speeds,[PgDn] slows
cursor,@
@[Q]uit to DOS"
Msg2$ = "[S]ave data,[SPACEBAR] starts line,[C]lose
polygon,[Esc] to @
@remove line"
LOCATE 1, 1: PRINT Msg1$;
LOCATE 2, 1: PRINT Msg2$;
CASE "Q"
GOTO EndPrgm1:
CASE "S"
'----Set up files for saving data
SaveFile
CASE ELSE
END SELECT
IF LFlg% = 0 AND CursMovFlg% = 1 THEN
LINE (oldX#, oldY#)-(lastX#, lastY#), 0
LINE (oldX#, oldY#)-(X#, Y#)
CursMovFlg% = 0
END IF
lastX# = X#: lastY# = Y#
PUT (X# - 3, Y# - 3), Cross, XOR
LOOP
EndPrgm1:

EndProgram:
SCREEN 0
CLOSE
END
'----Error trapping
Generr:
Nerr% = ERR
RESUME NEXT

'****************************************
SUB CalcBound (Bound#(), BNum%, Chosen%())
'----Program to determine if a point lies within an
'----enclosed irregular polygon

K = 0: L = 0
LOCATE 1, 1: PRINT SPACE$(79);
LOCATE 2, 1: PRINT SPACE$(79);
LOCATE 1, 1: PRINT "Calculating bounding area";
'----Set # of data points
DNum% = Numb%
'----Start looking for the nearest points to the boundary
FOR I = 1 TO DNum%
West = 0: East = 0
LOCATE 2, 1: PRINT "Checking point #"; I;
FOR J = 1 TO BNum%
IF J > 1 THEN
BMinus1# = Bound#(J - 1, 2)
BMinusE# = Bound#(J - 1, 1)
ELSE
BMinus1# = Bound#(BNum%, 2)
BMinusE# = Bound#(BNum%, 1)
END IF
'----Find pairs of boundary pts that cross east-west line containing
'----the data point. First case: boundary point lies on line
IF Bound#(J, 2) = YC(I) THEN
'-----Now check if the next two points on the boundary straddle it
'-----or lie to one side
```

```
IF (BMinus1# > YC(I) AND Bound#(J + 1, 2) > YC(I)) OR@
@ (BMinus1# < YC(I) AND Bound#(J + 1, 2) < YC(I)) THEN
IF Bound#(J, 1) < XC(I) THEN
West = West + 2
ELSE
East = East + 2
END IF
ELSE
IF Bound#(J, 1) < XC(I) THEN
West = West + 1
ELSE
East = East + 1
END IF
END IF
'----Two boundary points straddle line
ELSEIF (Bound#(J, 2) > YC(I) AND BMinus1# < YC(I)) OR
(Bound#(J, 2)@
@< YC(I) AND BMinus1# > YC(I)) THEN
IF BMinusE# < > Bound#(J, 1) THEN
slope# = (BMinus1# - Bound#(J, 2)) / (BMinusE# - Bound#(J, 1))
inter# = Bound#(J, 2) - (slope# * Bound#(J, 1))
Pt# = (YC(I) - inter#) / slope#
ELSEIF BMinusE# = Bound#(J, 1) THEN
Pt# = Bound#(J, 1): slope# = 0: inter# = 0
END IF
IF Pt# < XC(I) THEN
West = West + 1
ELSE
East = East + 1
END IF
END IF
NEXT J
IF East MOD 2 = 0 AND West MOD 2 = 0 THEN
Choose$ = "no" ELSE Choose$ = "yes"
END IF
'----Write the data record within the boundary to a file
IF Choose$ = "yes" THEN
IF SaveFlg% = 1 THEN
PRINT #3, DLS(I)
PRINT #4, MID$(DLS(I), 22, 3); " "; MID$(DLS(I), 25, 2)
END IF
K = K + 1
Chosen%(K) = I
ELSEIF Choose$ = "no" THEN
L = L + 1
NotChosen%(L) = I
END IF
NEXT I
'---- The first element contains number of elements for chosen
data points
Chosen%(0) = K: NotChosen%(0) = L
CLOSE #3: CLOSE #4
EndDomain:
END SUB

REM $DYNAMIC
'*****************************************
SUB GetHex (ival%, hi$, lo$)
'----convert numbers to hexadecimal format hi byte first
tmp$ = HEX$(ival%)
SELECT CASE LEN(tmp$)
CASE 0
hi$ = "&H00"
lo$ = "&H00"
CASE 1
hi$ = "&H00"
lo$ = "&H0" + tmp$
CASE 2
hi$ = "&H00"
lo$ = "&H" + tmp$
CASE 3
hi$ = "&H0" + LEFT$(tmp$, 1)
lo$ = "&H" + RIGHT$(tmp$, 2)
CASE 4
hi$ = "&H" + LEFT$(tmp$, 2)
lo$ = "&H" + RIGHT$(tmp$, 2)
CASE ELSE
END SELECT
END SUB

'*****************************************
SUB GraphicsCard
'----Determine type of graphics card
SCREEN 12'VGA
IF Nerr% = 5 THEN
Nerr% = 0: SCREEN 0
ELSEIF Nerr% = 0 THEN
D.MX = 639: D.MY = 479: D.CX = 8: D.CY = 16
D.ML = 30: SCR = 12
NoG$ = " ": D.MD = 12: D.ASP = 1!: D.SCR = 12
GOTO EndDisplay:
END IF
SCREEN 9'EGA
IF Nerr% = 5 THEN
Nerr% = 0: SCREEN 0
ELSEIF Nerr% = 0 THEN
D.MX = 639: D.MY = 349: D.CX = 8: D.CY = 14
D.ML = 25: SCR = 9
NoG$ = " ": D.MD = 12: D.ASP = .729: D.SCR = 9
GOTO EndDisplay:
END IF
SCREEN 2'CGA
IF Nerr% = 5 THEN
Nerr% = 0: SCREEN 0
ELSEIF Nerr% = 0 THEN
D.MX = 639: D.MY = 199: D.CX = 8: D.CY = 8
D.ML = 25: SCR = 2
NoG$ = " ": D.MD = 10: D.ASP = .42: D.SCR = 2
GOTO EndDisplay:
END IF
SCREEN 3'Herc
IF Nerr% = 5 THEN
SCREEN 0: CLS
ELSEIF Nerr% = 0 THEN
D.MX = 719: D.MY = 347: D.CX = 9: D.CY = 14
D.ML = 25: SCR = 3
NoG$ = " ": D.MD = 13: D.ASP = .7291667: D.SCR = 3
GOTO EndDisplay:
END IF
CLS : SCREEN 0: END
EndDisplay:

END SUB

'*****************************************
SUB InputData
'----Input data files
'----Read in Data From Disk
LINE (1, D.CY * 2 + 3)-(D.CX * 79 + 7, D.CY * 2 + 3)
InputFile:
```

```
LOCATE 1, 1
PRINT "SEPARATE DATA ON BASIS OF ORIENTATION"
LOCATE 2, 5
INPUT ; "Enter file name (Cyprus format, [D]ir): ", F$
IF UCASE$(F$) = "D" THEN
'----Set directory
LOCATE 2, 1: PRINT SPACE$(79)
LOCATE 2, 1
INPUT "Enter directory name (e.g. C:\DATA): ", Dir$
LOCATE 2, 1: PRINT SPACE$(79)
GOTO InputFile:
END IF
IF Nerr% = 52 THEN Nerr% = 0: GOTO InputFile:
IF Dir$ <> "" THEN
FF$ = Dir$ + "\" + F$
ELSE
FF$ = F$
END IF
OPEN FF$ FOR INPUT AS #1
'---- start reading in data
LOCATE 2, 1: PRINT SPACE$(79)
LOCATE 2, 1: PRINT "Loading datafile... "; UCASE$(F$)
K% = 1
'----Cyprus format data
WHILE NOT EOF(1)
INPUT #1, DL$(K%)
IF MID$(DL$(K%), 1, 1) = "1" AND MID$(DL$(K%), 22, 5)@
@ <> "" THEN
Azimuth = (VAL(MID$(DL$(K%), 22, 3)) + 180) MOD 360
AzR(K%) = Azimuth * Grad
Dip = VAL(MID$(DL$(K%), 25, 2))
ThetR(K%) = Dip * Grad
K% = K% + 1
END IF
WEND
CLOSE #1
Numb% = K%
LINE (0, (D.ML - 1) * D.CY)-(9 * D.CX, (D.ML - 2) * @
D.CY - 3), , B
LOCATE D.ML - 1, 2
PRINT "N = "; : PRINT USING "###"; Numb%;
END SUB

'*****************************************
SUB PDraw (Picture$, X%, Y%)
REM $DYNAMIC
'----sub that outputs draw command to PIC file
tmp$ = CHR$(162)
Picture$ = Picture$ + tmp$
GetHex X%, hi$, lo$
tmp$ = CHR$(VAL(hi$)) + CHR$(VAL(lo$))
Picture$ = Picture$ + tmp$
GetHex Y%, hi$, lo$
tmp$ = CHR$(VAL(hi$)) + CHR$(VAL(lo$))
Picture$ = Picture$ + tmp$
EXIT SUB
END SUB

'*****************************************
SUB PDrawSym (Picture$, X%, Y%, isym%)
REM $STATIC
DIM xvert%(10), yvert%(10)
'----sub to draw symbol in PIC file
'----X% , Y% = Hercules coords; X3%, Y3% = PIC coords
'-----------------------------------------
X3% = CINT(X% * 4.444444444#)
Y3% = CINT(2100 - (Y% * 4.444444444#))
SELECT CASE isym%
CASE 1 'Small square
PMove Picture$, X3%, Y3%
PDraw Picture$, X3%, Y3% + 2
PDraw Picture$, X3% - 2, Y3% + 2
PDraw Picture$, X3% - 2, Y3%
PDraw Picture$, X3%, Y3%
CASE 2 'circle open
PMove Picture$, X3% - 7, Y3% + 2
PDraw Picture$, X3% - 3, Y3% + 7
PDraw Picture$, X3% + 3, Y3% + 7
PDraw Picture$, X3% + 7, Y3% + 2
PDraw Picture$, X3% + 7, Y3% - 2
PDraw Picture$, X3% + 3, Y3% - 7
PDraw Picture$, X3% - 3, Y3% - 7
PDraw Picture$, X3% - 7, Y3% - 2
PDraw Picture$, X3% - 7, Y3% + 2
CASE 3 'Cross for stereonet centre
PMove Picture$, X3% - 20, Y3%
PDraw Picture$, X3% + 20, Y3%
PMove Picture$, X3%, Y3% + 20
PDraw Picture$, X3%, Y3% - 20
CASE ELSE
END SELECT
END SUB

'*****************************************
SUB PFsize (Picture$, X%, Y%)
REM $DYNAMIC
'----sub to output font size command to PIC file
tmp$ = CHR$(172)
Picture$ = Picture$ + tmp$
GetHex X%, hi$, lo$
tmp$ = CHR$(VAL(hi$)) + CHR$(VAL(lo$))
Picture$ = Picture$ + tmp$
GetHex Y%, hi$, lo$
tmp$ = CHR$(VAL(hi$)) + CHR$(VAL(lo$))
Picture$ = Picture$ + tmp$
EXIT SUB
END SUB

'*****************************************
SUB Plotting
REM $STATIC
'----Set Net diameter
Diameter = 13.9082
R% = CINT(D.MX * Diameter / 50)
'----Subroutine to plot the data on the stereo net
XX% = 2 * D.MX / 3: YY% = 5 * D.MY / 9
X% = 479: Y% = 193
Pt$ = "U1L1D2R2U2G2" 'small square
'----PlotCircle
CIRCLE (XX%, YY%), R%, , , , YRatio
LINE (XX%, YY% + YRatio * R% + 3)-(XX%, YY% +@
@ YRatio * R%)
LINE (XX%, YY% - YRatio * R% - 4)-(XX%, YY% - @
@YRatio * R% - 1)
'----N symbol
IF North% = 0 THEN PSET (XX% - 4, YY% - YRatio * R% -@
@ 6): DRAW "U8F8U8"
LINE (XX% - R% - 6, YY%)-(XX% - R%, YY%)
LINE (XX% + R%, YY%)-(XX% + R% + 6, YY%)
'----draw cross in centre
```

```
PSET (XX%, YY%): DRAW "BU3D6BU3BR4L8"
'----Draw 10 degree interval tick marks around circumference
FOR I = 0 TO 35
Th = I * 10 * Grad
XB = XX% + R% * COS(Th)
YB = YY% + R% * SIN(Th) * YRatio
XE = XX% + (R% - R% / 20) * COS(Th)
YE = YY% + (R% - R% / 20) * SIN(Th) * YRatio
LINE (XB, YB)-(XE, YE)
NEXT I
'----Plot data
LOCATE 2, 1: PRINT SPACE$(79);
LOCATE 2, 1: PRINT "Plotting data ...."
Points% = 0
FOR I = 1 TO Numb%
RSQ = R% * SQR(2)
DD = RSQ * SIN(ThetR(I) / 2): DDN = DD * YRatio
XPT = DD * SIN(AzR(I)): YPT = DDN * COS(AzR(I))
PSET (XX% + XPT, YY% - YPT): DRAW Pt$
XC(I) = XX% + XPT: YC(I) = YY% - YPT
XCP(I) = X% + XPT: YCP(I) = Y% - YPT / YRatio
NEXT I
EndPlotData:
END SUB

'*****************************************
SUB PMove (Picture$, X%, Y%)
REM $DYNAMIC
'----sub that output move command to PIC file
tmp$ = CHR$(160)
Picture$ = Picture$ + tmp$
GetHex X%, hi$, lo$
tmp$ = CHR$(VAL(hi$)) + CHR$(VAL(lo$))
Picture$ = Picture$ + tmp$
GetHex Y%, hi$, lo$
tmp$ = CHR$(VAL(hi$)) + CHR$(VAL(lo$))
Picture$ = Picture$ + tmp$
END SUB

'*****************************************
SUB POpen (Picture$)
'----routine to initialize Picture$ array so data can later be saved
'----to a .PIC file for plotting with Lotus PGRAPH (R)
REM $STATIC
DEFINT I-K
'----put header to PIC string
tmp$ = CHR$(1) + CHR$(0) + CHR$(0) + CHR$(0)
tmp$ = tmp$ + CHR$(1) + CHR$(0)
tmp$ = tmp$ + CHR$(8) + CHR$(0) + CHR$(&H44)
tmp$ = tmp$ + CHR$(0) + CHR$(0)
tmp$ = tmp$ + CHR$(0) + CHR$(0) + CHR$(&HC)
tmp$ = tmp$ + CHR$(&H7F) + CHR$(9)
tmp$ = tmp$ + CHR$(6)
Picture$ = Picture$ + tmp$
PFsize Picture$, 100, 100
'----Put file name into PIC file
F$ = UCASE$(F$)
Msg$ = MID$(F$, 1, LEN(F$) - 4) + "(N=" + STR$(Numb%)
+ ")"
PMove Picture$, 100, 2150
PText Picture$, 0, 1, Msg$
Msg$ = "Selected points"
PMove Picture$, 150, 300
PText Picture$, 0, 1, Msg$
Msg$ = "Non-selected points"
PMove Picture$, 150, 200
PText Picture$, 0, 1, Msg$
PDrawSym Picture$, 27, 405, 2
PDrawSym Picture$, 27, 428, 1
'----Draw a circle of radius Rad%, and center X2%,Y2%, with a
'----a cross at the centre
'----X,Y= Hercules circle centre coords
'----X2%,Y2% = PIC circle centre coords
'----X3%,Y3% = PIC circle and symbol coords
'-----------------------------------
X2% = CINT(X% * 4.444444444!)
Y2% = CINT(2100 - (Y% * 4.444444444!))
Rad% = 200 * 4.444444444!
'----move to circle centre
PMove Picture$, X2%, Y2%
'----draw cross at circle centre
PDrawSym Picture$, CINT(X%), CINT(Y%), 3
LOCATE 2, 1
PRINT "Creating circle for Lotus (R) Picfile. Please wait..."
X3% = X2% + Rad%
Y3% = Y2%
'----move to circle edge (90 deg.)
PMove Circle$, X3%, Y3%
PMove Picture$, X3%, Y3%
'----draw circle over 2 degree increments
FOR I = 1 TO 180
THETA = 2 * I * Grad
X3% = X2% + Rad% * COS(THETA)
Y3% = Y2% + Rad% * SIN(THETA)
PDraw Picture$, X3%, Y3%
NEXT I
'----Tick mark (90 deg.)
X3% = X2% + Rad%: Y3% = Y2%
PDraw Picture$, X3% + 25, Y3%
'----Tick mark (270 deg.)
X3% = X2% - Rad%
PMove Picture$, X3%, Y2%
PDraw Picture$, X3% - 25, Y3%
'----Tick mark (0 deg.)
Y3% = Y2% + Rad%
PMove Picture$, X2%, Y3%
PDraw Picture$, X2%, Y3% + 25
'----Draw N symbol
PMove Picture$, X2% - 20, Y3% + 45
PDraw Picture$, X2% - 20, Y3% + 95
PDraw Picture$, X2% + 20, Y3% + 45
PDraw Picture$, X2% + 20, Y3% + 95
'----Draw 10 degree interval tick marks around circumference
FOR I = 0 TO 35
Th = I * 10 * Grad
XB% = X2% + Rad% * COS(Th)
YB% = Y2% + Rad% * SIN(Th)
XE% = X2% + (Rad% - Rad% / 20) * COS(Th)
YE% = Y2% + (Rad% - Rad% / 20) * SIN(Th)
PMove Picture$, XB%, YB%
PDraw Picture$, XE%, YE%
NEXT I
'----Tick mark (180 deg.)
Y3% = Y2% - Rad%
PMove Picture$, X2%, Y3%
PDraw Picture$, X2%, Y3% - 25
'----dump circle into file
PUT #5, , Picture$
Picture$ = ""
'----plot points
```

```
FOR I = 1 TO Chosen%(0)
AX% = XC(Chosen%(I)): AY% = YCP(Chosen%(I))
PDrawSym Picture$, AX%, AY%, 2
NEXT
'----dump data to file
PUT #5, , Picture$
Picture$ = ""
'----Plot non-chosen points
LOCATE 2, 1
PRINT "Plotting chosen points to the picfile. Please wait..."
FOR I = 1 TO NotChosen%(0)
AX% = XC(NotChosen%(I)): AY% = YCP(NotChosen%(I))
PDrawSym Picture$, AX%, AY%, 1
NEXT
'----dump data to file
LOCATE 2, 1
PRINT "Plotting remaining points to picfile. Please wait..."
PUT #5, , Picture$
Picture$ = ""
'----The PIC file will be finished off in TABULATE subroutine
END SUB

'*****************************************
SUB PText (Picture$, D1%, P%, Msg$)
'----sub to send text to PIC file
REM $DYNAMIC
DEFSNG I-K
'----d% is orientation : 0 - hor l to r : 0
'---- 1 - ver b to t : 90
'----2 - hor r to l : 180
'----3 - ver t to b : 270
'----p% is position : see lotus file guide
tmp$ = CHR$(168) '&HA8
Picture$ = Picture$ + tmp$
tmp$ = "&H" + HEX$(D1%) + HEX$(P%)
tmp$ = CHR$(VAL(tmp$))
Picture$ = Picture$ + tmp$
tmp$ = Msg$ + CHR$(0)
Picture$ = Picture$ + tmp$
END SUB

'*****************************************
SUB RePLot
REM $STATIC
Pt$ = "U1L1D2R2U2G2" 'small square
Pt2$ = "BD2L1H1U2E1R2F1D2G1L1U1C0U1" 'open circle
PSET (XX%, YY%): DRAW "BU3D6BU3BR4L8"
'----Plot data
LOCATE 2, 1: PRINT SPACE$(79);
LOCATE 2, 1: PRINT "Plotting chosen points ...."
Points% = 0
FOR I = 1 TO Chosen%(0)
PSET (XC(Chosen%(I)), YC(Chosen%(I))): DRAW "C0" + Pt$
PSET (XC(Chosen%(I)), YC(Chosen%(I))): DRAW Pt2$
NEXT I
END SUB

'*****************************************
SUB SaveFile
'----Open output files for plot points and data record
DataF$ = UCASE$(MID$(F$, 1, LEN(F$) - 3) + "SEP")
PlotF$ = UCASE$(MID$(F$, 1, LEN(F$) - 3) + "PLT")
TabF$ = UCASE$(MID$(F$, 1, LEN(F$) - 3) + "TAB")
PicF$ = UCASE$(MID$(F$, 1, LEN(F$) - 3) + "PIC")
'
Q$ = "P"
WHILE INSTR("FfPp", Q$) = 0
LOCATE 1, 1: PRINT SPACE$(79);
LOCATE 2, 1: PRINT SPACE$(79);
IF SaveFlg% = 0 THEN
DM$ = "Don't save results. "
ELSE
DM$ = "Save Results. "
END IF
IF PicFlg% = 1 THEN DM$ = "Save only Pic."
LOCATE 1, 1: PRINT "Change
name:(1)Data(2)Az/Dip(3)Table(4)Pic(5)Toggle@
@save[F]inish [P]ic only.";
LOCATE 2, 1: PRINT "File setting: "; DM$; " (Data/Plot/Table@
@/Pic: "; Dir$; ")"
Q$ = UCASE$(INPUT$(1))
SELECT CASE Q$
CASE "1"
LOCATE 1, 1: PRINT SPACE$(79);
LOCATE 2, 1: PRINT SPACE$(79);
LOCATE 1, 1
INPUT "Enter new data record output file name: "; DataF$
CASE "2"
LOCATE 1, 1: PRINT SPACE$(79);
LOCATE 2, 1: PRINT SPACE$(79);
LOCATE 1, 1
INPUT "Enter new plot data output file name: "; DataF$
CASE "3"
LOCATE 1, 1: PRINT SPACE$(79); : LOCATE 2, 1: PRINT
SPACE$(79);
LOCATE 1, 1
INPUT "Enter new tabulated result output file name: "; DataF$
CASE "4"
LOCATE 1, 1
PRINT SPACE$(79); : LOCATE 2, 1: PRINT SPACE$(79);
LOCATE 1, 1: INPUT "Enter new PIC file name: "; PicF$
CASE "5"
IF SaveFlg% = 0 THEN
SaveFlg% = 1
ELSE
SaveFlg% = 0
END IF
CASE "P"
SaveFlg% = 0: PicFlg% = 1
CASE ELSE
END SELECT
WEND
IF SaveFlg% = 1 THEN
IF Dir$ <> "" THEN DF$ = Dir$ + "\" + DataF$ ELSE@
@ DF$ = DataF$
IF Dir$ <> "" THEN SF$ = Dir$ + "\" + PltF$ ELSE@
@ SF$ = PlotF$
IF Dir$ <> "" THEN TF$ = Dir$ + "\" + TabF$ ELSE TF$@
@ = TabF$
IF Dir$ <> "" THEN PF$ = Dir$ + "\" + PicF$ ELSE PF$@
@ = PicF$
OPEN TF$ FOR OUTPUT AS #2
OPEN DF$ FOR OUTPUT AS #3
OPEN SF$ FOR OUTPUT AS #4
OPEN PF$ FOR BINARY AS #5
ELSEIF SaveFlg% = 0 AND PicFlg% = 1 THEN
IF Dir$ <> "" THEN PF$ = Dir$ + "\" + PicF$ ELSE PF$@
@ = PicF$
OPEN PF$ FOR BINARY AS #5
END IF
```

```
LOCATE 1, 1: PRINT SPACE$(79);
LOCATE 2, 1: PRINT SPACE$(79);
LOCATE 1, 1
PRINT "SEPARATE DATA ON BASIS OF ORIENTATION"
LOCATE 2, 1
PRINT "Outline data points to be separated with cursor and@
@[SPACE]. [H]elp [Q]uit"

END SUB

'••••••••••••••••••••••••••••••••••••••••
SUB Tabulate (Chosen%())

LOCATE 1, 1: PRINT SPACE$(79); : LOCATE 2, 1: PRINT
SPACE$(79);
LOCATE 1, 1: PRINT "SEPARATE DATA ON BASIS OF
ORIENTATION"
LOCATE 2, 1: PRINT "Tabulating results. # chosen ="
ii = 0
FOR I = 1 TO Chosen%(0)
ii = ii + 1: LOCATE 2, 32: PRINT ii
LINE (1, D.CY * 2 + 3)-(D.CX * 79 + 7, D.CY * 2 + 3)
'----Parse the data line
Type$ = MID$(DLS(Chosen%(I)), 20, 2)
Length = VAL(MID$(DLS(Chosen%(I)), 27, 4))
Term$ = MID$(DLS(Chosen%(I)), 32, 1)
Min1$ = MID$(DLS(Chosen%(I)), 33, 1)
Min2$ = MID$(DLS(Chosen%(I)), 36, 1)
Min3$ = MID$(DLS(Chosen%(I)), 39, 1)
Rough$ = MID$(DLS(Chosen%(I)), 43, 1)
Rock$ = MID$(DLS(Chosen%(I)), 44, 1)
'----Tabulate results
IF Type$ = "cn" THEN cn1 = cn1 + 1
IF Type$ = "fr" THEN fr1 = fr1 + 1
IF Type$ = "jt" THEN jt1 = jt1 + 1
IF Length <= 2 THEN l01 = l01 + 1
IF Length > 2 THEN l21 = l21 + 1
SumLC = SumLC + Length
SumLSC = SumLSC + Length * Length
IF Term$ = "0" THEN t01 = t01 + 1
IF Term$ = "1" THEN t11 = t11 + 1
IF Term$ = "2" THEN t21 = t21 + 1
IF Term$ = "3" THEN t31 = t31 + 1
IF Min1$ = "a" THEN a1 = a1 + 1
IF Min1$ = "e" THEN e1 = e1 + 1
IF Min1$ = "c" THEN c1 = c1 + 1
IF Min1$ = "z" THEN z1 = z1 + 1
IF Min1$ = "p" THEN p1 = p1 + 1
IF Min1$ = "k" THEN k1 = k1 + 1
IF Min1$ = "l" THEN l1 = l1 + 1
IF Min1$ = "h" THEN h1 = h1 + 1
IF Min1$ = "m" THEN m1 = m1 + 1
IF Min1$ = "q" THEN q1 = q1 + 1
IF Min1$ = "x" THEN x1 = x1 + 1
IF Min2$ = "a" THEN a1 = a1 + 1
IF Min2$ = "e" THEN e1 = e1 + 1
IF Min2$ = "c" THEN c1 = c1 + 1
IF Min2$ = "z" THEN z1 = z1 + 1
IF Min2$ = "p" THEN p1 = p1 + 1
IF Min2$ = "k" THEN k1 = k1 + 1
IF Min2$ = "l" THEN l1 = l1 + 1
IF Min2$ = "h" THEN h1 = h1 + 1
IF Min2$ = "m" THEN m1 = m1 + 1
IF Min2$ = "q" THEN q1 = q1 + 1
IF Min2$ = "x" THEN x1 = x1 + 1
IF Min3$ = "a" THEN a1 = a1 + 1
IF Min3$ = "e" THEN e1 = e1 + 1
IF Min3$ = "c" THEN c1 = c1 + 1
IF Min3$ = "z" THEN z1 = z1 + 1
IF Min3$ = "p" THEN p1 = p1 + 1
IF Min3$ = "k" THEN k1 = k1 + 1
IF Min3$ = "l" THEN l1 = l1 + 1
IF Min3$ = "h" THEN h1 = h1 + 1
IF Min3$ = "m" THEN m1 = m1 + 1
IF Min3$ = "q" THEN q1 = q1 + 1
IF Min3$ = "x" THEN x1 = x1 + 1
IF Rough$ = "p" THEN rp1 = rp1 + 1
IF Rough$ = "u" THEN ru1 = ru1 + 1
IF Rough$ = "c" THEN rc1 = rc1 + 1
IF Rough$ = "s" THEN rs1 = rs1 + 1
IF Rough$ = "i" THEN ri1 = ri1 + 1
NEXT I
'----Now do the same for the not picked fractures
LOCATE 2, 40: PRINT "/ # not chosen ="
ii = 0
FOR I = 1 TO NotChosen%(0)
ii = ii + 1: LOCATE 2, 58: PRINT ii
LINE (1, D.CY * 2 + 3)-(D.CX * 79 + 7, D.CY * 2 + 3)
'----Parse the data line
Type$ = MID$(DLS(NotChosen%(I)), 20, 2)
Length = VAL(MID$(DLS(Chosen%(I)), 27, 4))
Term$ = MID$(DLS(NotChosen%(I)), 32, 1)
Min1$ = MID$(DLS(NotChosen%(I)), 33, 1)
Min2$ = MID$(DLS(NotChosen%(I)), 36, 1)
Min3$ = MID$(DLS(NotChosen%(I)), 39, 1)
Rough$ = MID$(DLS(NotChosen%(I)), 43, 1)
Rock$ = MID$(DLS(NotChosen%(I)), 44, 1)
'----Tabulate results
IF Type$ = "cn" THEN cn2 = cn2 + 1
IF Type$ = "fr" THEN fr2 = fr2 + 1
IF Type$ = "jt" THEN jt2 = jt2 + 1
IF Length <= 2 THEN l02 = l02 + 1
IF Length > 2 THEN l22 = l22 + 1
SumLNC = SumLNC + Length
SumLSNC = SumLSNC + Length * Length
IF Term$ = "0" THEN t02 = t02 + 1
IF Term$ = "1" THEN t12 = t12 + 1
IF Term$ = "2" THEN t22 = t22 + 1
IF Term$ = "3" THEN t32 = t32 + 1
IF Min1$ = "a" THEN a2 = a2 + 1
IF Min1$ = "e" THEN e2 = e2 + 1
IF Min1$ = "c" THEN c2 = c2 + 1
IF Min1$ = "z" THEN z2 = z2 + 1
IF Min1$ = "p" THEN p2 = p2 + 1
IF Min1$ = "k" THEN k2 = k2 + 1
IF Min1$ = "l" THEN l2 = l2 + 1
IF Min1$ = "h" THEN h2 = h2 + 1
IF Min1$ = "m" THEN m2 = m2 + 1
IF Min1$ = "q" THEN q2 = q2 + 1
IF Min1$ = "x" THEN X2 = X2 + 1
IF Min2$ = "a" THEN a2 = a2 + 1
IF Min2$ = "e" THEN e2 = e2 + 1
IF Min2$ = "c" THEN c2 = c2 + 1
IF Min2$ = "z" THEN z2 = z2 + 1
IF Min2$ = "p" THEN p2 = p2 + 1
IF Min2$ = "k" THEN k2 = k2 + 1
IF Min2$ = "l" THEN l2 = l2 + 1
IF Min2$ = "h" THEN h2 = h2 + 1
IF Min2$ = "m" THEN m2 = m2 + 1
IF Min2$ = "q" THEN q2 = q2 + 1
```

```
IF Min2$ = "x" THEN X2 = X2 + 1
IF Min3$ = "n" THEN n2 = n2 + 1
IF Min3$ = "e" THEN e2 = e2 + 1
IF Min3$ = "c" THEN c2 = c2 + 1
IF Min3$ = "z" THEN z2 = z2 + 1
IF Min3$ = "p" THEN p2 = p2 + 1
IF Min3$ = "k" THEN k2 = k2 + 1
IF Min3$ = "l" THEN l2 = l2 + 1
IF Min3$ = "h" THEN h2 = h2 + 1
IF Min3$ = "m" THEN m2 = m2 + 1
IF Min3$ = "q" THEN q2 = q2 + 1
IF Min3$ = "x" THEN X2 = X2 + 1
IF Rough$ = "p" THEN rp2 = rp2 + 1
IF Rough$ = "u" THEN ru2 = ru2 + 1
IF Rough$ = "c" THEN rc2 = rc2 + 1
IF Rough$ = "s" THEN rs2 = rs2 + 1
IF Rough$ = "i" THEN ri2 = ri2 + 1
NEXT I

'-----Display to screen
FOR I = 4 TO 19
LOCATE I, 1: PRINT SPACE$(30)
NEXT I
LINE (1, D.CY * 2 + 10)-(D.CX * 29 + 7, D.CY * 20 + @
@3), , B
LINE (3, D.CY * 2 + 12)-(D.CX * 29 + 5, D.CY * 20 + 1)@
@, , B
LOCATE 4, 2: PRINT "TABLE OF SELECTED DATA"
LOCATE 5, 2
PRINT "TOTAL #";
PRINT USING "### "; Chosen%(0); NotChosen%(0)
LOCATE 6, 2: PRINT "FRACTURE TYPE"
LOCATE 7, 2: PRINT " cntct";
PRINT USING " ###"; cn1; cn2
LOCATE 8, 2: PRINT " fract";
PRINT USING " ###"; fr1; fr2
LOCATE 9, 2: PRINT " joint";
PRINT USING " ###"; jt1; jt2
LOCATE 10, 2: PRINT "TRACE LENGTH"
LOCATE 11, 2: PRINT " <=2M";
PRINT USING " ###"; t01; t02
LOCATE 12, 2: PRINT " > 2M";
PRINT USING " ###"; t21; t22
LOCATE 13, 2: PRINT "TERM. MODE"
LOCATE 14, 2: PRINT " free ";
PRINT USING " ###"; t01; t02
LOCATE 15, 2: PRINT " 'T'";
PRINT USING " ###"; t11; t12
LOCATE 16, 2: PRINT " 'H'";
PRINT USING " ###"; t21; t22
LOCATE 17, 2: PRINT " splay";
PRINT USING " ###"; t31; t32
LOCATE 18, 2: PRINT "MIN. FILL"
LOCATE 19, 2: PRINT " none ";
PRINT USING " ###"; n1; n2
LOCATE 20, 2: PRINT " ep";
PRINT USING " ###"; e1; e2
LOCATE 6, 16: PRINT " calc ";
PRINT USING " ###"; c1; c2
LOCATE 7, 16: PRINT " zeo";
PRINT USING " ###"; z1; z2
LOCATE 8, 16: PRINT " pyr";
PRINT USING " ###"; p1; p2
LOCATE 9, 16: PRINT " chl";
PRINT USING " ###"; k1; k2
LOCATE 10, 16: PRINT " cela ";
PRINT USING " ###"; l1; l2
LOCATE 11, 16: PRINT " hem";
PRINT USING " ###"; h1; h2
LOCATE 12, 16: PRINT " mag";
PRINT USING " ###"; m1; m2
LOCATE 13, 16: PRINT " qtz";
PRINT USING " ###"; q1; q2
LOCATE 14, 16: PRINT " clay ";
PRINT USING " ###"; x1; X2
LOCATE 15, 16: PRINT "ROUGHNESS"
LOCATE 16, 1: PRINT " plane";
PRINT USING " ###"; rp1; rp2
LOCATE 17, 16: PRINT " undul";
PRINT USING " ###"; ru1; ru2
LOCATE 18, 16: PRINT " curve";
PRINT USING " ###"; rc1; rc2
LOCATE 19, 16: PRINT " step ";
PRINT USING " ###"; rs1; rs2
LOCATE 20, 16: PRINT " irreg";
PRINT USING " ###"; ri1; ri2
LOCATE 24, 1
PRINT "Mean Chosen Length= "; SumLC / Chosen%(0);
PRINT "Mean Not Chosen Length= "; SumLNC /@
@ NotChosen%(0);
StdC = SQR(SumLSC / Chosen%(0) - (SumLC /@
@ Chosen%(0)) * (SumLC / Chosen%(0)))
StdNC = SQR(SumLSNC / NotChosen%(0) - (SumLNC /@
@ NotChosen%(0)) * (SumLNC / NotChosen%(0)))
LOCATE 25, 1: PRINT "Std.Dev.Chosen Length= "; StdC;
PRINT "Std.Dev.Not Chosen Length= "; StdNC;
'-----Save results to file
IF SaveFlg% = 1 THEN
PRINT #2, "Tabulated fracture Characteristics for: "; @
@UCASE$(MID$(F$, 1, LEN(F$) - 4))
PRINT #2,
PRINT #2, "Total # of fractures: "; ii
PRINT #2, : PRINT #2, "# of fractures"; TAB(20); i1: PRINT #2,
PRINT #2, "Fracture type": PRINT #2,
PRINT #2, "contact "; TAB(20);
PRINT #2, USING "####"; cn1; cn2
PRINT #2, "fracture "; TAB(20);
PRINT #2, USING "####"; fr1; fr2
PRINT #2, "joint "; TAB(20);
PRINT #2, USING "####"; jt1; jt2
PRINT #2, : PRINT #2, "Trace Length": PRINT #2,
PRINT #2, " <=2M"; TAB(20);
PRINT #2, USING "####"; t01; t02
PRINT #2, " > 2M"; TAB(20);
PRINT #2, USING "####"; t21; t22
PRINT #2, : PRINT #2, "Termination mode": PRINT #2,
PRINT #2, "term 0 "; TAB(20);
PRINT #2, USING "####"; t01; t02
PRINT #2, "term 1 "; TAB(20);
PRINT #2, USING "####"; t11; t12
PRINT #2, "term 2 "; TAB(20);
PRINT #2, USING "####"; t21; t22
PRINT #2, "term 3 "; TAB(20);
PRINT #2, USING "####"; t31; t32
PRINT #2, : PRINT #2, "Mineral filling": PRINT #2,
PRINT #2, "none "; TAB(20);
PRINT #2, USING "####"; n1; n2
PRINT #2, "epidote "; TAB(20);
PRINT #2, USING "####"; e1; e2
PRINT #2, "calcite "; TAB(20);
```

```
PRINT #2, USING "####"; c1; c2
PRINT #2, "zeolite "; TAB(20);
PRINT #2, USING "####"; z1; z2
PRINT #2, "pyrite "; TAB(20);
PRINT #2, USING "####"; p1; p2
PRINT #2, "chlorite "; TAB(20);
PRINT #2, USING "####"; k1; k2
PRINT #2, "celadonite "; TAB(20);
PRINT #2, USING "####"; l1; l2
PRINT #2, "hematite "; TAB(20);
PRINT #2, USING "####"; h1; h2
PRINT #2, "magnetite "; TAB(20);
PRINT #2, USING "####"; m1; m2
PRINT #2, "quartz "; TAB(20);
PRINT #2, USING "####"; q1; q2
PRINT #2, "clay "; TAB(20);
PRINT #2, USING "####"; x1; X2
PRINT #2,
PRINT #2, "Fracture large scale roughness": PRINT #2,
PRINT #2, "planar "; TAB(20);
PRINT #2, USING "####"; rp1; rp2
PRINT #2, "undulating "; TAB(20);
PRINT #2, USING "####"; ru1; ru2
PRINT #2, "curved "; TAB(20);
PRINT #2, USING "####"; rc1; rc2
PRINT #2, "stepped "; TAB(20);
PRINT #2, USING "####"; rs1; rs2
PRINT #2, "irregular "; TAB(20);
PRINT #2, USING "####"; ri1; ri2
PRINT #2,
PRINT #2, "Mean Chosen Length= "; SumLC / Chosen%(0);
PRINT #2, "Mean Not Chosen Length= "; SumLNC /
NotChosen%(0);
PRINT #2, "Std.Dev.Chosen Length= "; StdC;
PRINT #2, "Std.Dev.Not Chosen Length= "; StdNC;
CLOSE #2
END IF
IF SaveFig% = 1 OR PicFig% = 1 THEN
'----Now start saving to PIC file
'----Draw box around results
PMove Picture$, 1, 195
PDraw Picture$, 1, 550
PDraw Picture$, 1191, 550: PDraw Picture$, 1191, 1955
PDraw Picture$, 1, 1955: PMove Picture$, 6, 1947
PDraw Picture$, 6, 556: PDraw Picture$, 1182, 556
PDraw Picture$, 1182, 1947: PDraw Picture$, 6, 1947
'----Start writing text
PMove Picture$, 1, 1900
PText Picture$, 0, 1, "TABLE OF FRACTURE DATA"
PFsize Picture$, 75, 75
Msg$ = "sel. not."
PMove Picture$, 600, 1825: PText Picture$, 0, 3, Msg$
PMove Picture$, 1150, 1825: PText Picture$, 0, 3, Msg$
Msg$ = "Total #
PMove Picture$, 25, 1750: PText Picture$, 0, 1, Msg$
Msg$ = STR$(Chosen%(0))
PMove Picture$, 450, 1750: PText Picture$, 0, 3, Msg$
Msg$ = STR$(NotChosen%(0))
PMove Picture$, 600, 1750: PText Picture$, 0, 3, Msg$
PMove Picture$, 25, 167
PText Picture$, 0, 1, "FRACT. TYPE"
Msg$ = " cntct
PMove Picture$, 50, 1600: PText Picture$, 0, 1, Msg$
Msg$ = STR$(cn1)
PMove Picture$, 450, 1600: PText Picture$, 0, 3, Msg$
Msg$ = STR$(cn2)
PMove Picture$, 600, 1600: PText Picture$, 0, 3, Msg$
Msg$ = " fract
PMove Picture$, 50, 1525: PText Picture$, 0, 1, Msg$
Msg$ = STR$(fr1)
PMove Picture$, 450, 1525: PText Picture$, 0, 3, Msg$
Msg$ = STR$(fr2)
PMove Picture$, 600, 1525: PText Picture$, 0, 3, Msg$
Msg$ = " joint
PMove Picture$, 50, 1450: PText Picture$, 0, 1, Msg$
Msg$ = STR$(jt1)
PMove Picture$, 450, 1450: PText Picture$, 0, 3, Msg$
Msg$ = STR$(jt2)
PMove Picture$, 600, 1450: PText Picture$, 0, 3, Msg$
PMove Picture$, 25, 1375: PText Picture$, 0, 1, "TRACE LEN."
Msg$ = " <=2M
PMove Picture$, 50, 1300: PText Picture$, 0, 1, Msg$
Msg$ = STR$(t01)
PMove Picture$, 450, 1300: PText Picture$, 0, 3, Msg$
Msg$ = STR$(t02)
PMove Picture$, 600, 1300: PText Picture$, 0, 3, Msg$
Msg$ = " > 2M
PMove Picture$, 50, 1225: PText Picture$, 0, 1, Msg$
Msg$ = STR$(t21)
PMove Picture$, 450, 1225: PText Picture$, 0, 3, Msg$
Msg$ = STR$(t22)
PMove Picture$, 600, 1225: PText Picture$, 0, 3, Msg$
PMove Picture$, 25, 115
PText Picture$, 0, 1, "TERM. MODE"
Msg$ = " free
PMove Picture$, 50, 1075: PText Picture$, 0, 1, Msg$
Msg$ = STR$(t01)
PMove Picture$, 450, 1075: PText Picture$, 0, 3, Msg$
Msg$ = STR$(t02)
PMove Picture$, 600, 1075: PText Picture$, 0, 3, Msg$
Msg$ = " 'T'
PMove Picture$, 50, 1000: PText Picture$, 0, 1, Msg$
Msg$ = STR$(t11)
PMove Picture$, 450, 1000: PText Picture$, 0, 3, Msg$
Msg$ = STR$(t12)
PMove Picture$, 600, 1000: PText Picture$, 0, 3, Msg$
Msg$ = " 'H'
PMove Picture$, 50, 925: PText Picture$, 0, 1, Msg$
Msg$ = STR$(t21)
PMove Picture$, 450, 925: PText Picture$, 0, 3, Msg$
Msg$ = STR$(t22)
PMove Picture$, 600, 925: PText Picture$, 0, 3, Msg$
Msg$ = " splay
PMove Picture$, 50, 850: PText Picture$, 0, 1, Msg$
Msg$ = STR$(t31)
PMove Picture$, 450, 850: PText Picture$, 0, 3, Msg$
Msg$ = STR$(t32)
PMove Picture$, 600, 850: PText Picture$, 0, 3, Msg$
PMove Picture$, 25, 775: PText Picture$, 0, 1, "MIN. FILL"
Msg$ = " none
PMove Picture$, 50, 700: PText Picture$, 0, 1, Msg$
Msg$ = STR$(n1)
PMove Picture$, 450, 700: PText Picture$, 0, 3, Msg$
Msg$ = STR$(n2)
PMove Picture$, 600, 700: PText Picture$, 0, 3, Msg$
Msg$ = " ep
PMove Picture$, 50, 625: PText Picture$, 0, 1, Msg$
Msg$ = STR$(e1)
PMove Picture$, 450, 625: PText Picture$, 0, 3, Msg$
Msg$ = STR$(e2)
```

```
PMove Picture$, 600, 625: PText Picture$, 0, 3, Msg$
'----dump data to file
PUT #5, , Picture$
Picture$ = ""
'----continue
Msg$ = " calc
PMove Picture$, 650, 1675: PText Picture$, 0, 1, Msg$
Msg$ = STR$(c1)
PMove Picture$, 1000, 1675: PText Picture$, 0, 3, Msg$
Msg$ = STR$(c2)
PMove Picture$, 1150, 1675: PText Picture$, 0, 3, Msg$
Msg$ = " zeo
PMove Picture$, 650, 1600: PText Picture$, 0, 1, Msg$
Msg$ = STR$(z1)
PMove Picture$, 1000, 1600: PText Picture$, 0, 3, Msg$
Msg$ = STR$(z2)
PMove Picture$, 1150, 1600: PText Picture$, 0, 3, Msg$
Msg$ = " pyr
PMove Picture$, 650, 1525: PText Picture$, 0, 1, Msg$
Msg$ = STR$(p1)
PMove Picture$, 1000, 1525: PText Picture$, 0, 3, Msg$
Msg$ = STR$(p2)
PMove Picture$, 1150, 1525: PText Picture$, 0, 3, Msg$
Msg$ = " chl
PMove Picture$, 650, 1450: PText Picture$, 0, 1, Msg$
Msg$ = STR$(k1)
PMove Picture$, 1000, 1450: PText Picture$, 0, 3, Msg$
Msg$ = STR$(k2)
PMove Picture$, 1150, 1450: PText Picture$, 0, 3, Msg$
Msg$ = " cela
PMove Picture$, 650, 1375: PText Picture$, 0, 1, Msg$
Msg$ = STR$(l1)
PMove Picture$, 1000, 1375: PText Picture$, 0, 3, Msg$
Msg$ = STR$(l2)
PMove Picture$, 1150, 1375: PText Picture$, 0, 3, Msg$
Msg$ = " hem
PMove Picture$, 650, 1300: PText Picture$, 0, 1, Msg$
Msg$ = STR$(h1)
PMove Picture$, 1000, 1300: PText Picture$, 0, 3, Msg$
Msg$ = STR$(h2)
PMove Picture$, 1150, 1300: PText Picture$, 0, 3, Msg$
Msg$ = " mag
PMove Picture$, 650, 1225: PText Picture$, 0, 1, Msg$
Msg$ = STR$(m1)
PMove Picture$, 1000, 1225: PText Picture$, 0, 3, Msg$
Msg$ = STR$(m2)
PMove Picture$, 1150, 1225: PText Picture$, 0, 3, Msg$
Msg$ = " qtz
PMove Picture$, 650, 1150: PText Picture$, 0, 1, Msg$
Msg$ = STR$(q1)
PMove Picture$, 1000, 1150: PText Picture$, 0, 3, Msg$
Msg$ = STR$(q2)
PMove Picture$, 1150, 1150: PText Picture$, 0, 3, Msg$
Msg$ = " clay
PMove Picture$, 650, 1075: PText Picture$, 0, 1, Msg$
Msg$ = STR$(x1)
PMove Picture$, 1000, 1075: PText Picture$, 0, 3, Msg$
Msg$ = STR$(X2)
PMove Picture$, 1150, 1075: PText Picture$, 0, 3, Msg$
PMove Picture$, 650, 100
PText Picture$, 0, 1, "ROUGHNESS"
Msg$ = " plane
PMove Picture$, 650, 925: PText Picture$, 0, 1, Msg$
Msg$ = STR$(rp1)
PMove Picture$, 1000, 925: PText Picture$, 0, 3, Msg$
Msg$ = STR$(rp2)
PMove Picture$, 1150, 925: PText Picture$, 0, 3, Msg$
Msg$ = " undul
PMove Picture$, 650, 850: PText Picture$, 0, 1, Msg$
Msg$ = STR$(ru1)
PMove Picture$, 1000, 850: PText Picture$, 0, 3, Msg$
Msg$ = STR$(ru2)
PMove Picture$, 1150, 850: PText Picture$, 0, 3, Msg$
Msg$ = " curve
PMove Picture$, 650, 775: PText Picture$, 0, 1, Msg$
Msg$ = STR$(cu1)
PMove Picture$, 1000, 775: PText Picture$, 0, 3, Msg$
Msg$ = STR$(rc2)
PMove Picture$, 1150, 775: PText Picture$, 0, 3, Msg$
Msg$ = " step
PMove Picture$, 650, 700: PText Picture$, 0, 1, Msg$
Msg$ = STR$(rs1)
PMove Picture$, 1000, 700: PText Picture$, 0, 3, Msg$
Msg$ = STR$(rs2)
PMove Picture$, 1150, 700: PText Picture$, 0, 3, Msg$
Msg$ = " irreg
PMove Picture$, 650, 625: PText Picture$, 0, 1, Msg$
Msg$ = STR$(ri1)
PMove Picture$, 1000, 625: PText Picture$, 0, 3, Msg$
Msg$ = STR$(ri2)
PMove Picture$, 1150, 625: PText Picture$, 0, 3, Msg$
'----dump data to file
PUT #5, , Picture$
Picture$ = ""
'----Put file end marker in Picture$ and dump to file, then close it
tmp$ = CHR$(&H60)
Picture$ = Picture$ + tmp$
PUT #5, , Picture$
CLOSE #5
Picture$ = ""
END IF
'----Rewrite main menu
LOCATE 1, 1: PRINT SPACE$(79); : LOCATE 2, 1: PRINT
SPACE$(79);
LOCATE 1, 1: PRINT "SEPARATE DATA ON BASIS OF
ORIENTATION"
LOCATE 2, 1
PRINT "Outline data points to be separated with cursor and
[SPACE]@
@. [H]elp [Q]uit"

END SUB
```

```
'—— ROSE.BAS
DECLARE SUB PCircle (Picture$, X%, Y%, R%)
DECLARE SUB GetFileName (FileName$, PicFile$)
DECLARE SUB PFSize (Picture$, X%, Y%)
DECLARE SUB PText (Picture$, d%, P%, Msg$)
DECLARE SUB Gethex (ival%, hi$, lo$)
DECLARE SUB PDraw (Picture$, X%, Y%)
DECLARE SUB PMove (Picture$, X%, Y%)
DECLARE SUB PHead (Picture$)
DECLARE SUB PClose (Picture$, TitleMsg$, Numb%, Batch%,
Type$, F$)
DECLARE SUB PFillo (Picture$, nvert%, xvert%(), yvert%())
DECLARE SUB PicFileOpen (Picture$, PicFlg!, Tick$)
DECLARE SUB PrintScreen (SCR)

COMMON SHARED PicFlg, Picture$, DataDirOut$, Batch%
COMMON SHARED F6%
'——Program to plot rose diagrams from an input file containing
'——orientation data in one column (i.e. linear orientations with
'—— respect to north = 0)
'——By: David van EverdingenDate: 27 October 1988

DIM Hist(36), FILES$(10), Pictures(4000), length(1500)
DIM DIRECTION(1000)
DIM xvert%(10), yvert%(10), Direc(500), DirDip(500)
F6% = 1
CLS
CL$ = COMMAND$
IF UCASE$(CL$) = "BATCH" THEN Batch% = 1
'——Set error trapping
NERR% = 0
ON ERROR GOTO GENERR:
START:
PI = 3.1415926544
'——Plot box around title
LOCATE 2, 10: COLOR 15, 0
PRINT "Rose Diagram Plotting Program": COLOR 7, 0
LOCATE 3, 5: PRINT "By: D. van Everdingenv1.1 Nov 1988"
LOCATE 1, 1: PRINT CHR$(218);
FOR II = 1 TO 47: PRINT CHR$(196); : NEXT II
PRINT CHR$(191)
LOCATE 4, 1: PRINT CHR$(192);
FOR II = 1 TO 47: PRINT CHR$(196); : NEXT II
PRINT CHR$(217)
FOR II = 1 TO
LOCATE 1 + II, 1: PRINT CHR$(179); : NEXT II
FOR II = 1 TO
LOCATE 1 + II, 49: PRINT CHR$(179); : NEXT II
LOCATE 6, 1
PRINT "This program is Hercules and CGA compatible"
PRINT "(If you have a Herc card you must run QBHERC"
PRINT "before running this program)"
PRINT
PRINT "To continue type the letter of your choice:"
COLOR 8, 1: PRINT "A"; : COLOR 7, 0
PRINT "if the orientation data file contains only one column"
COLOR 8, 1: PRINT "B"; : COLOR 7, 0
PRINT "if the orientation data is in 7th col (one input file only)"
COLOR 8, 1: PRINT "C"; : COLOR 7, 0
PRINT "if orientation by lineament length is to be plotted"
PRINT " (Data format: 6th col = length, 7th col = orientation)"
COLOR 8, 1: PRINT "D"; : COLOR 7, 0
PRINT "if orientation data is from dip-azimuth dip files (2 cols)"
COLOR 8, 1: PRINT "E"; : COLOR 7, 0
PRINT "if orientation data are dips (col#2) - file in 2 cols"
COLOR 8, 1: PRINT "F"; : COLOR 7, 0
PRINT "will exit you to DOS"
PRINT
PRINT "Note: Options B, C and D are used for data files"
PRINT "by DXFPLINE (reformat of AutoCAD .DXF)"
IF Batch% = 1 THEN
LOCATE 23, 5: COLOR 8, 1
PRINT "Operation is in Batch mode"; : COLOR 7, 0
END IF
ANS$ = "Q"
WHILE INSTR("ABCDEF", ANS$) = 0
ANS$ = UCASE$(INPUT$(1))
WEND
IF UCASE$(MID$(ANS$, 1, 1)) = "F" THEN
CLS
GOTO EndPrgrm:
END IF
FOR I = 5 TO 20
LOCATE I, 1: PRINT SPACE$(80)
NEXT I
'——Case of multiple files to be processed
IF Batch% = 1 THEN
StartAgain:
LOCATE 6, 1
INPUT "Input name of batch file (? for help/Q to quit): ",
BatchFile$
IF UCASE$(BatchFile$) = "Q" THEN
GOTO EndPrgrm:
ELSEIF BatchFile$ = "?" THEN
LOCATE 8, 1: PRINT "Batch mode operation - Input batch file@
@ Specs: e.g.#1e.g.#2"
LOCATE 9, 1: PRINT " Line 1: Input path/directory@
@C:\DATA C:\DATA"
LOCATE 10, 1: PRINT " Line 2: Output directory of PIC files @
@C:\TMPC:\TMP"
LOCATE 11, 1: PRINT " Line 3: Type of data - L=linear,@
@ V=vector L V"
LOCATE 12, 1: PRINT " Line 4:if line 3=L this line must be@
@1,2 or 3,3 N"
LOCATE 13, 1: PRINT "specifying N-S, E-W, or 360 degree@
@ plots Y ROSE.DAT"
LOCATE 14, 1: PRINT "Else this line specifies whether 10%
scale@
@ROSE.DATBEAR3.PLT"
LOCATE 15, 1: PRINT "circles are plotted - use Y or N@
@BEAR3.PLT"
LOCATE 16, 1: PRINT " Remaining lines are the file names to be
used"
LOCATE 17, 1: PRINT " e.g.#1 makes 2-360 deg. plots with
scale @
@circles from linear data"
LOCATE 18, 1: PRINT " e.g.#2 makes 2-360 deg. vector plots,
no @
@scale circles"
LOCATE 19, 1: PRINT " PIC files are produced with up to six
plots@
@ to a page."
LOCATE 21, 15: PRINT "Press any key to continue"
DO: LOOP UNTIL INKEY$ <> ""
FOR I = 6 TO 21: LOCATE I, 1: PRINT SPACE$(79): NEXT I
GOTO StartAgain:
END IF
OPEN BatchFile$ FOR INPUT AS #50
```

```
I = 1
INPUT #50, DataDirIn$
INPUT #50, DataDirOut$
IF ANS$ <> "E" THEN
INPUT #50, Type$
ELSE
Type$ = "V"
END IF
IF Type$ = "L" THEN
INPUT #50, LinType$
END IF
INPUT #50, Circles$
WHILE NOT EOF(50)
INPUT #50, FILES$(I)
I = I + 1
WEND
CLOSE #50
NUM = I - 1
BIN$ = "N": Reverse$ = "N": Printer$ = "N"
INTERVAL = 1
ELSEIF Batch% = 0 THEN
NUM = 1
FINDFILE:
FILES$(1) = ""
LOCATE 6, 1
INPUT "Input data file name: ", FILES$(1)
OPEN FILES$(1) FOR INPUT AS #1
'----Error trap for file not found
IF NERR% = 53 THEN
COLOR 24, 1
LOCATE 6, 23: PRINT "File not found. "; : COLOR 7, 0
PRINT "Press any key to continue"
DO: LOOP UNTIL INKEY$ <> ""
LOCATE 6, 23: PRINT SPACE$(45)
NERR% = 0
GOTO FINDFILE:
END IF

LOCATE 8, 1
INPUT "Input the data title to appear on the plot: ", TITLE$
IF UCASE$(ANS$) = "E" THEN
Type$ = "V"
ELSE
'----Set to dummy value
Type$ = "A"
WHILE INSTR("LV", Type$) = 0
LOCATE 9, 1
PRINT "Is data lineation or vector data (L or V): "
Type$ = UCASE$(INPUT$(1))
WEND
LOCATE 9, 44: PRINT Type$
'----Determine the type of linear rose diagram wanted
IF Type$ = "L" THEN
LinType$ = "A"'Set to dummy value
WHILE INSTR("123", LinType$) = 0
LOCATE 10, 1
PRINT "Choose 1) an East-West oriented rose diagram"
PRINT " 2) a North-South oriented rose diagram"
PRINT " 3) a 360 degree rose diagram"
LinType$ = UCASE$(INPUT$(1))
WEND
END IF
LOCATE 12, 53: PRINT LinType$
END IF
BIN$ = "Q"'Set to dummy value
WHILE INSTR("YN", BIN$) = 0
LOCATE 13, 1
PRINT "Do you want the data binned at intervals other than@
@10 degrees [Y/N]: "
BIN$ = UCASE$(INPUT$(1))
WEND
LOCATE 13, 71: PRINT BIN$
IF BIN$ = "N" THEN INTERVAL = 10
IF BIN$ = "Y" THEN
INTERVAL = 3'A dummy value for the next loop
WHILE INTERVAL MOD 10 <> 0
LOCATE 14, 1: PRINT SPACE(79)
LOCATE 14, 1
INPUT "Input new bin interval (>10, in units of 10):",
INTERVAL
IF INTERVAL MOD 10 <> 0 OR INTERVAL < 10 THEN
LOCATE 14, 1: PRINT SPACE$(80)
LOCATE 14, 1: COLOR 24, 1
PRINT "Invalid number must be >10 and in units of 10. @
@Press any key to continue": COLOR 7, 0
DO: LOOP UNTIL INKEY$ <> ""
END IF
WEND
END IF
INTERVAL = INTERVAL / 10
Reverse$ = "A"'Set to dummy value
WHILE INSTR("YN", Reverse$) = 0
LOCATE 15, 1
PRINT "Do you the rose to be black on white [Y] or white on
black [N]: "
Reverse$ = UCASE$(INPUT$(1))
WEND
LOCATE 15, 65: PRINT Reverse$
Printer$ = "A"'Set to dummy value
WHILE INSTR("YN", Printer$) = 0
LOCATE 16, 1
PRINT "Do you want diagram output to the printer [Y/N]: "
Printer$ = UCASE$(INPUT$(1))
WEND
LOCATE 16, 50: PRINT Printer$
PicFileOpen Picture$, PicFlg, "NO"
LOCATE 19, 1: PRINT "10% circles on PIC plot? [N]"
Circles$ = UCASE$(INPUT$(1))
IF Circles$ = CHR$(13) THEN Circles$ = "N"
LOCATE 19, 30: PRINT Circles$
END IF
IF Batch% = 0 THEN
LOCATE 20, 1: PRINT "To leave the graph press the spacebar"
'----Display until a key is pressed
LOCATE 23, 10: PRINT "Press any key to continue"
DO: LOOP UNTIL INKEY$ <> ""
END IF
'----Assume Hercules card is installed then check if error has
occurred
SCR = 3 '----Hercules card = 3
SCREEN SCR
'----Check which graphics card is installed
IF NERR% = 5 THEN
NERR% = 0'----reset error level
SCR = 2 '----CGA card = 2
SCREEN SCR
'----If there is still and error then bad graphics mode
IF NERR% = 5 THEN
SCREEN 0
CLS : LOCATE 10, 20
```

```
COLOR 24, 1: PRINT "Unsupported graphics card is present":
COLOR 7, 0
LOCATE 12, 10
PRINT "If you have a Hercules card you may have not run
MSHERC"
LOCATE 13, 10
PRINT "When DOS prompt appears please run MSHERC
otherwise the"
LOCATE 14, 15: PRINT "QuickBASIC graphics routines will not
work"
GOTO EndPrgrm:
END IF
END IF
'----Note to other programmers:
'----If another graphics card is to be used then the values for
'----XORIGIN, YORIGIN, ASPECT and SCALE must be changed
IF SCR = 3 THEN'Herc
XORIGIN = 150: YORIGIN = 150
ASPECT = .729
SCALE = 150
ELSEIF SCR = 2 THEN'CGA
XORIGIN = 133: YORIGIN = 89
ASPECT = .45
SCALE = 133
END IF
'---- Loop for batch mode
FOR Kount = 1 TO NUM
'----If the last plot has been dumped and a new one is to be
opened
IF Batch% = 1 THEN
PicFileOpen Picture$, PicFlg, "NO"
END IF
'----Input data and bin results into intervals as specified by BIN
above
I = 1
'----check whether data type is to linear or vector
IF Type$ = "L" THEN Count = 18
IF Type$ = "V" THEN Count = 36
'----read data into the array HIST based on the orientation
intervals
'----if plotting is to be done by length then read the whole file in
'----(maximum of 1500 points) and find the min and max lengths,
then
'----ask for the length interval to plot the orientations
CNT = 1: MIN1 = 10000: MAX1 = 0
IF ANS$ = "C" THEN
OPEN DataDirIn$ + FILES$(1) FOR INPUT AS #1
LOCATE 9, 20: PRINT "Reading file: "; UCASE$(FILES$(1))
WHILE NOT EOF(1)
INPUT #1, A, B, C, d, E, length(CNT), DIRECTION(CNT)
'----Find the min and max
IF MIN1 > length(CNT) THEN MIN1 = length(CNT)
'----length of lineaments
IF MAX1 < length(CNT) THEN MAX1 = length(CNT)
CNT = CNT + 1
WEND
PickAnotherInterval:
CLS
LOCATE 10, 1
PRINT "The minimum length is: "; MIN1
PRINT "The maximum length is: "; MAX1
INPUT "Input the length range you wish to look at (Min, Max):@
@ "; MIN2, MAX2
IF MIN2 > MAX2 THEN
PRINT "Min > Max - re-enter values - Press spacebar to
continue"
DO: LOOP UNTIL INKEY$ <> ""
GOTO PickAnotherInterval:
END IF
KK = 1
FOR I = 1 TO CNT - 1
IF length(I) >= MIN2 AND length(I) <= MAX2 THEN
FOR J = 1 TO Count
IF Type$ = "L" THEN
IF DIRECTION(I) > 180 THEN DIRECTION(I) =
DIRECTION(I) - 180
END IF
IF DIRECTION(I) >= ((J - 1) * 10) AND DIRECTION(I)@
@< (J * 10) THEN
Hist(J) = Hist(J) + 1
LOCATE 15, 10: PRINT "Number of Orientations matched: ";
KK
KK = KK + 1
END IF
NEXT J
END IF
NEXT I
NUMOBS = KK - 1
CLOSE #1
'----if only orientations are to be looked at
ELSE
IF Batch% = 1 THEN OPEN DataDirIn$ + "\" +
FILES$(Kount) FOR INPUT AS #1
LOCATE 9, 20: PRINT "Reading file "; Kount; ": ";
UCASE$(FILES$(Kount))
LOCATE 10, 20: PRINT "Number of Orientations read: "
FOR II = 1 TO 36: Hist(II) = 0: NEXT II: I = 0
IF ANS$ = "E" THEN
A$ = "": TD = 0: Mean = 0
WHILE NOT EOF(1)
I = I + 1
INPUT #1, Direc(I), DirDip(I)
LOCATE 10, 49: PRINT I
WEND
FOR J = 1 TO I: TD = TD + Direc(I): NEXT J
Mean = TD / I
IF (Mean > 44 AND Mean < 135) OR (Mean > 224 AND
Mean < 315) THEN
A$ = "N-S" 'Strike
ELSEIF (Mean > 314 AND Mean < 361) OR (Mean >= 0
AND@
@Mean < 45) OR (Mean > 134 AND Mean < 225) THEN
A$ = "E-W" 'Strike
END IF
FOR K = 1 TO I
DIR = Direc(K): DIP = DirDip(K)
IF A$ = "N-S" THEN
IF DIR > 179 AND DIR < 360 THEN
DIP = 270 - DIP
ELSE
DIP = DIP + 90
END IF
ELSEIF A$ = "E-W" THEN
IF (DIR > 270 AND DIR < 360) OR (DIR >= 0 AND DIR <
91) THEN
DIP = 270 - DIP
ELSE
DIP = DIP + 90
END IF
END IF
```

```
DIR = DIP'Convert to DIR for use by the program
FOR J = 1 TO Count
IF Type$ = "L" THEN
IF DIR > 180 THEN DIR = DIR - 180
END IF
IF DIR >= ((J - 1) * 10) AND DIR < (J * 10) THEN
Hist(J) = Hist(J) + 1
IF Type$ = "L" AND LinType$ = "3" THEN
Hist(J + 18) = Hist(J + 18) + 1
END IF
END IF
NEXT J
NEXT K
ELSE
WHILE NOT EOF(1)
I = I + 1
IF ANS$ = "B" THEN
INPUT #1, A, B, C, d, E, F, DIR
ELSEIF ANS$ = "D" THEN
INPUT #1, DIR, Junk
DIR = DIR - 90
IF DIR < 0 THEN DIR = DIR + 360'Convert to strike
ELSE
INPUT #1, DIR
END IF
FOR J = 1 TO Count
IF Type$ = "L" THEN
IF DIR > 180 THEN DIR = DIR - 180
END IF
IF DIR >= ((J - 1) * 10) AND DIR < (J * 10) THEN
Hist(J) = Hist(J) + 1
IF Type$ = "L" AND LinType$ = "3" THEN
Hist(J + 18) = Hist(J + 18) + 1
END IF
END IF
NEXT J
LOCATE 10, 49: PRINT I
WEND
END IF
CLOSE #1
NUMOBS = I
END IF
IF Type$ = "L" AND (LinType$ = "3") THEN Count = 36
CLS
'----If the bin interval is different from 10 degrees then start
'----grouping the results into the larger bins
IF INTERVAL > 1 THEN
FOR I = 1 TO Count STEP INTERVAL
FOR J = 1 TO INTERVAL
DUMMY = DUMMY + Hist(I + J - 1)
NEXT J
FOR J = 1 TO INTERVAL
Hist(I + J - 1) = DUMMY
NEXT J
DUMMY = 0
NEXT I
END IF
'----Find maximum in all the bins
MAX = 0
FOR J = 1 TO Count
IF MAX < Hist(J) THEN MAX = Hist(J)
NEXT J
'----Calculate the percentage of data that MAX represents
'----Round that to the next 10% highest frequency interval
PERC = MAX / NUMOBS * 10
PERCENT = INT(PERC + 1)
SUBPERCENT = PERCENT * 10
'----The radius of the max. percentage circle becomes SCALE
'----So calculate the number of circles in 10% intervals needed
NUMCIRCLES = 0
IF PERC > 1 THEN'----values greater then 10% exist
WHILE SUBPERCENT > 0
SUBPERCENT = SUBPERCENT - 10
IF SUBPERCENT >= 0 THEN NUMCIRCLES =
NUMCIRCLES + 1
WEND
ELSEIF PERC <= 1 THEN'----all values are less than 10%
WHILE SUBPERCENT > 0
SUBPERCENT = SUBPERCENT - 2
IF SUBPERCENT >= 0 THEN NUMCIRCLES =
NUMCIRCLES + 1
WEND
END IF
SCREEN SCR
'----PIC circle center at X=800, Y=1200 or moving if Batch job
XC% = 600: YC% = 1700
IF Batch% = 1 THEN
IF F6% = 1 THEN
XC% = 600: YC% = 1700: F6% = 2
ELSEIF F6% = 2 THEN
XC% = 1500: YC% = 1700: F6% = 3
ELSEIF F6% = 3 THEN
XC% = 2400: YC% = 1700: F6% = 4
ELSEIF F6% = 4 THEN
XC% = 600: YC% = 700: F6% = 5
ELSEIF F6% = 5 THEN
XC% = 1500: YC% = 700: F6% = 6
ELSEIF F6% = 6 THEN
XC% = 2400: YC% = 700: F6% = 1
END IF
END IF
'----Plot the rosettes
xvert%(1) = XC%: yvert%(1) = YC%
FOR J = 1 TO Count STEP INTERVAL
'----Calculate the percent value of each bin as we go along
BINPCNT = Hist(J) / NUMOBS * 100
'----From that calculate the necessary radius
RADIUS = SQR((BINPCNT / (PERCENT * 10))) * SCALE
ANGLE = J * 10
'---- Plot arc if HIST >0
IF Hist(J) > 0 THEN
A = (ANGLE + 90) * PI / 180
xvert%(2) = XC% + CINT(-COS(A + (INTERVAL - 1) * PI /@
@ 18) * RADIUS * 2.2)
yvert%(2) = YC% + CINT(SIN(A + (INTERVAL - 1) * PI /@
@ 18)' * RADIUS * 2.2)
xvert%(3) = XC% + CINT(-COS(A - PI / 18) * RADIUS * 2.2)
yvert%(3) = YC% + CINT(SIN(A - PI / 18) * RADIUS * 2.2)
PFillo Picture$, 3, xvert%(), yvert%()
ANGLE = (90 - ANGLE) * PI / 180
IF ANGLE < 0 THEN ANGLE = 2 * PI + ANGLE
IF ANGLE > 0 THEN ANGLE = -ANGLE
IF ANGLE = 0 THEN ANGLE = -.00000001#
IF Type$ = "V" OR (Type$ = "L" AND (LinType$ = "2" OR@
@LinType$ = "3")) OR NOT (Type$ = "L" AND LinType$ =@
@"1" AND J > 9) THEN
'----Hercules
CIRCLE (XORIGIN, YORIGIN), RADIUS, 1, ANGLE +@
@ (INTERVAL - 1) * PI / 18, ANGLE - PI / 18, ASPECT
END IF
```

```
'----For plotting E-W rose: need to convert the 90-180 range to
'----270-360 range
IF Type$ = "L" AND J > 9 AND LinType$ = "1" THEN
ANGLE = ANGLE - PI
IF ANGLE < -2 * PI THEN ANGLE = ANGLE + 2 * PI
IF ANGLE > 2 * PI THEN ANGLE = ANGLE - 2 * PI
CIRCLE (XORIGIN, YORIGIN), RADIUS, 1, ANGLE +
(INTERVAL - 1) *@
@PI / 18, ANGLE - PI / 18, ASPECT'Hercules
END IF
END IF
NEXT J
'----Put box around the rose diagram and fill (PAINT) the box
'----interior. Plot complete box
IF Type$ = "V" OR (Type$ = "L" AND LinType$ = "3")
THEN
IF SCR = 3 THEN '----Hercules
LINE (1, 40)-(300, 260), 1, B
PAINT (3, 43), 1
ELSEIF SCR = 2 THEN'----CGA
LINE (1, 33)-(265, 145), 1, B
PAINT (45, 45), 1
END IF
'----Plot E-W box
ELSEIF Type$ = "L" AND LinType$ = "1" THEN
IF SCR = 3 THEN'----Hercules
LINE (1, 40)-(300, 150), 1, B
PAINT (55, 55), 1
ELSEIF SCR = 2 THEN'----CGA
LINE (1, 33)-(265, 89), 1, B
PAINT (45, 45), 1
END IF
'----Plot N-S box
ELSEIF Type$ = "L" AND LinType$ = "2" THEN
IF SCR = 3 THEN'----Hercules
LINE (150, 54)-(300, 246), 1, B
PAINT (155, 55), 1
ELSEIF SCR = 2 THEN'----CGA
LINE (133, 33)-(265, 146), 1, B
PAINT (138, 35), 1
END IF
END IF
'----Calculate the radius of the scale circles and plot them
FOR J = 1 TO NUMCIRCLES
IF PERC > 1 THEN
'----If interval = 10%
Rad = SQR(J * 10) * SCALE / SQR(PERCENT * 10)
ELSEIF PERC <= 1 THEN
'----If interval = 2%
Rad = SQR(J * 2) * SCALE / SQR(PERCENT * 10)
END IF
'----PLot whole circle
CIRCLE (XORIGIN, YORIGIN), Rad, 0, , , ASPECT
IF PicFlg = 1 AND Circles$ = "Y" THEN
Rad% = CINT(Rad * 2.2)
PCircle Picture$, XC%, YC%, Rad%
END IF
'----Plot circle 0 to 90 degrees then 180 to 90 degrees
IF Type$ = "L" THEN
CIRCLE (XORIGIN, YORIGIN), Rad, 0, .00001, PI / 2,@
@ ASPECT
END IF
NEXT J
'----Put in crosshairs
IF Type$ = "V" OR (Type$ = "L" AND LinType$ = "3")@
@ THEN
COLOUR1 = 0: COLOUR2 = 0 '----For whole vector rose plot
ELSEIF Type$ = "L" AND LinType$ = "1" THEN
COLOUR1 = 1'----E-W rose
ELSEIF Type$ = "L" AND LinType$ = "2" THEN
COLOUR2 = 1'----N-S rose
END IF
IF SCR = 3 THEN
LINE (0, 150)-(300, 150), COLOUR1 '----Herc
LINE (150, 40)-(150, 260), COLOUR2
ELSEIF SCR = 2 THEN
LINE (0, 89)-(265, 89), COLOUR1'----CGA
LINE (SCALE, 33)-(SCALE, 145), COLOUR2
END IF
'----Put in N and S symbols for the vector and N-S diagram and
'----E and W symbols
LOCATE 2, 17: PRINT "N"
IF Type$ = "L" AND LinType$ = "1" THEN'----E-W rose
LOCATE 13, 1: PRINT "W"
LOCATE 13, 33: PRINT "E"
END IF
'----Plot horizontal tick marks at 2% intervals if circle interval
'----is >=10%
IF PERCENT * 10 > 10 THEN
FOR M = 1 TO PERCENT * 10 STEP 2
X = (SCALE + 4) + SQR(M) * SCALE / SQR(PERCENT * 10)
FOR MM = -2 TO 2 STEP 1
IF SCR = 3 THEN
PSET (X, 150 + MM), 0
ELSEIF SCR = 2 THEN
PSET (X, 89 + MM), 0
END IF
NEXT MM
NEXT M
END IF
'----Print title and other data
LOCATE 1, 1:PRINT TITLE$
IF PicFlg = 1 THEN
PMove Picture$, XC% - 500, YC% + 350
IF ANS$ = "E" THEN PMove Picture$, XC%, YC% + 220
IF Batch% = 0 THEN
IF ANS$ = "E" THEN
PText Picture$, 0, 4, TITLE$
ELSE
PText Picture$, 0, 1, TITLE$
END IF
ELSEIF Batch% = 1 THEN
TITLE$ = MID$(FILES$(Koun), 1, LEN(FILES$(Koun)) - 4)
IF ANS$ = "E" THEN
PText Picture$, 0, 4, TITLE$
ELSE
PText Picture$, 0, 1, TITLE$
END IF
END IF
Msg$ = "N =" + STR$(NUMOBS)
IF ANS$ = "E" THEN
PMove Picture$, XC%, YC% + 110
PText Picture$, 0, 4, Msg$
ELSE
PMove Picture$, XC% - 500, YC% - 350
PText Picture$, 0, 1, Msg$
END IF
IF ANS$ <> "E" THEN
PMove Picture$, XC%, YC% + ((SCALE + 5) * 2.2)
PDraw Picture$, XC%, YC% + ((SCALE + 50) * 2.2)
```

```
PMove Picture$, XC% - 30, YC% + ((SCALE + 65) * 2.2)
PText Picture$, 0, 1, "N"
PMove Picture$, XC%, YC% - ((SCALE + 5) * 2.2)
PDraw Picture$, XC%, YC% - ((SCALE + 50) * 2.2)
ELSE
PMove Picture$, XC% - (SCALE * 2.2), YC%
PDraw Picture$, XC% + (SCALE * 2.2), YC%
PMove Picture$, XC%, YC%
PDraw Picture$, XC%, YC% - SCALE * 2.2
PMove Picture$, XC%, YC% - ((SCALE + 50) * 2.2)
PText Picture$, 0, 4, "90"
PMove Picture$, XC% - ((SCALE + 25) * 2.2), YC%
PText Picture$, 0, 1, "0"
PMove Picture$, XC% - ((SCALE + 25) * 2.2), YC% + 100
IF A$ = "N-S" THEN Msg$ = "W" ELSE Msg$ = "N"
PText Picture$, 0, 1, Msg$
PMove Picture$, XC% + ((SCALE + 25) * 2.2), YC%
PText Picture$, 0, 1, "0"
PMove Picture$, XC% + ((SCALE + 25) * 2.2), YC% + 100
IF A$ = "N-S" THEN Msg$ = "E" ELSE Msg$ = "S"
PText Picture$, 0, 1, Msg$
END IF
END IF

IF PERC > 1 THEN
LOCATE 21, 1
PRINT "Circle interval = 10%Cross hair tick mark interval = 2 "
END IF
IF PERC <= 1 THEN LOCATE 21, 1: PRINT "Circle interval
= 2%"
LOCATE 22, 1: PRINT "Total number of values = "; NUMOBS;
PRINT " Data Type: ";
IF Type$ = "L" THEN PRINT "Lineations"
IF Type$ = "V" THEN PRINT "Vectors"
LOCATE 23, 1: PRINT "Square root distances, areas are
equal-areas";
IF ANS$ = "C" THEN PRINT "Length: Min="; MIN2; "
Max="; MAX2
'----Print the data to the right side of the graph
IF Type$ = "L" OR (Type$ = "V" AND Printer$ = "N") THEN
LOCATE 1, 38: PRINT "Int.Freq.%"
IF Count = 36 THEN LOCATE 1, 58: PRINT "Int.Freq.%"
FOR I = 1 TO Count
Col = 38: Row = I + 1
IF I > 18 THEN Col = 58: Row = I - 17
IF LinType$ = "1" AND I > 9 THEN
INTERVAL1 = (I - 1) * 10 + 180
INTERVAL2 = (I * 10) + 179
ELSE
INTERVAL1 = (I - 1) * 10
INTERVAL2 = (I * 10) - 1
END IF
LOCATE Row, Col
PRINT USING "###"; INTERVAL1;
PRINT "-";
PRINT USING "###"; INTERVAL2;
PRINT USING "#####"; Hist(I); Hist(I) / NUMOBS * 100
NEXT I
END IF
'----If the screen colours of the rose need to be reversed
IF Reverse$ = "Y" THEN
IF SCR = 3 THEN'-----Herc
IF Type$ = "V" OR (Type$ = "L" AND LinType$ = "3")@
@ THEN
X1 = 1: Y1 = 54: X2 = 300: Y2 = 246
END IF
IF Type$ = "L" AND LinType$ = "1" THEN
X1 = 1: Y1 = 54: X2 = 300: Y2 = 150
END IF
IF Type$ = "L" AND LinType$ = "2" THEN
X1 = 150: Y1 = 54: X2 = 300: Y2 = 246
END IF
ELSEIF SCR = 2 THEN'----CGA
IF Type$ = "V" OR (Type$ = "L" AND LinType$ = "3")
THEN
X1 = 1: Y1 = 33: X2 = 265: Y2 = 145
END IF
IF Type$ = "L" AND LinType$ = "1" THEN
X1 = 1: Y1 = 33: X2 = 265: Y2 = 89
END IF
IF Type$ = "L" AND LinType$ = "2" THEN
X1 = 133: Y1 = 33: X2 = 265: Y2 = 146
END IF
END IF
'----Capture the graphics image into Picture and reprint it same
location
'----in reverse
GET (X1, Y1)-(X2, Y2), Picture
PUT (X1, Y1), Picture, PRESET
'----Replot the vertical and horizontal crosshairs
IF Type$ = "V" OR (Type$ = "1" AND LinType$ = "3") THEN
Vert = 246: Horiz = 0
END IF
IF Type$ = "L" AND LinType$ = "1" THEN Vert = 150:@
@ Horiz = 0
IF Type$ = "L" AND LinType$ = "2" THEN Vert = 246:@
@ Horiz = 150
IF SCR = 3 THEN
LINE (Horiz, 150)-(300, 150), 1'----Herc
LINE (150, 54)-(150, Vert), 1
ELSEIF SCR = 2 THEN
LINE (0, 89)-(265, 89), COLOUR1'----CGA
LINE (SCALE, 33)-(SCALE, 145), COLOUR2
END IF
END IF
'----If the printout is requested then call the PrintScreen routine
IF Printer$ = "Y" THEN PrintScreen (SCR)
'----Stay in graphics mode til any key is pressed
'-----Save to a PIC file also if six plots are ready or if all files
'----have been read
IF (PicFlg = 1 AND Batch% = 0) OR (Batch% = 1 AND F6%
= 1)@
@OR (Batch% = 1 AND Kount = NUM) THEN
PClose Picture$, TitleMsg$, Numb%, Batch%, "", FILES$(Kount)
END IF
IF Batch% = 0 THEN DO: LOOP UNTIL INKEY$ <> ""
CLS
NEXT Kount
SCREEN 0
'----Does another length interval of same data set need be plotted
IF ANS$ = "C" THEN
Q1$ = "A"
WHILE INSTR("YN", Q1$) = 0
LOCATE 10, 10
PRINT "Do you wish to plot a rose for another length interval@
@ [Y/N]: "
Q1$ = UCASE$(INPUT$(1))
WEND
IF Q1$ = "Y" THEN GOTO PickAnotherInterval:
END IF
```

```
GOTO EndPrgrm:
'----Error handling - sets NERR% to the error value and resume
'----program execution
GENERR:
NERR% = ERR
RESUME NEXT
EndPrgrm:
END

'*****************************************
SUB GetFileName (FileName$, PicFile$)
'----Routine to get the letters before the period in a filename
Flagg% = 0
I = 1
FileName$ = FileName$ + "."
DO
Fchar$ = MID$(FileName$, I, 1)
IF Fchar$ <> "." AND Fchar$ <> " " THEN
PicFile$ = PicFile$ + Fchar$
ELSE
Flagg% = 1
END IF
I = I + 1
LOOP UNTIL Flagg% = 1

END SUB

'*********************************************
SUB Gethex (ival%, hi$, lo$)
'-----convert numbers to hexadecimal format hi byte first
REM $DYNAMIC

tmp$ = HEX$(ival%)
SELECT CASE LEN(tmp$)
CASE 0
hi$ = "&H00"
lo$ = "&H00"
CASE 1
hi$ = "&H00"
lo$ = "&H0" + tmp$
CASE 2
hi$ = "&H00"
lo$ = "&H" + tmp$
CASE 3
hi$ = "&H0" + LEFT$(tmp$, 1)
lo$ = "&H" + RIGHT$(tmp$, 2)
CASE 4
hi$ = "&H" + LEFT$(tmp$, 2)
lo$ = "&H" + RIGHT$(tmp$, 2)
CASE ELSE
END SELECT

END SUB

'*****************************************
SUB PCircle (Picture$, X2%, Y2%, Rad%)

'----Draw a circle of radius Rad%, and center X2%,Y2%
'----X2%,Y2% = PIC circle centre coords
'----X3%,Y3% = PIC circle edge coords
'-------------------------------------
DTOR = 3.14159265358# / 180'-----converison degrees to radians
PMove Picture$, X2%, Y2% '-----move to circle centre
X3% = X2% + Rad%
Y3% = Y2%
PMove Picture$, X3%, Y3% '----move to circle edge (90 deg.)
FOR I = 1 TO 90 '----draw circle over 2 degree increments
THETA = 4 * I * DTOR
X3% = X2% + Rad% * COS(THETA)
Y3% = Y2% + Rad% * SIN(THETA)
PDraw Picture$, X3%, Y3%
NEXT I

END SUB

'*****************************************
SUB PClose (Picture$, TitleMsg$, Numb%, Batch%, Type$, F$)
REM $STATIC
'----sub to open PIC file; dump the array Picture$ into the file and
'----then close it.
PicFile$ = ""
FileName$ = F$ + " "
I = 1
GetFileName FileName$, PicFile$
IF LEN(PicFile$) < 8 THEN
PicFile$ = UCASE$(PicFile$ + Type$ + ".PIC")
ELSEIF LEN(PicFile$) = 8 THEN
PicFile$ = UCASE$(MID$(PicFile$, 1, 7) + Type$ + ".PIC")
END IF
File$ = DataDirOut$ + "\" + PicFile$
LOCATE 25, 1: PRINT "Plot Saved To: "; UCASE$(File$);
OPEN File$ FOR BINARY AS #2
'----Put file end marker in Picture$ and dump to file
tmp$ = CHR$(&H60)
Picture$ = Picture$ + tmp$
PUT #2, , Picture$
CLOSE #2
Picture$ = ""
END SUB

'*********************************************
SUB PDraw (Picture$, X%, Y%)
REM $DYNAMIC
'----sub that outputs draw command to PIC file
tmp$ = CHR$(162)
Picture$ = Picture$ + tmp$
Gethex X%, hi$, lo$
tmp$ = CHR$(VAL(hi$)) + CHR$(VAL(lo$))
Picture$ = Picture$ + tmp$
Gethex Y%, hi$, lo$
tmp$ = CHR$(VAL(hi$)) + CHR$(VAL(lo$))
Picture$ = Picture$ + tmp$
EXIT SUB
END SUB

'*********************************************
SUB Pfill (Picture$, nvert%, xvert%(), yvert%())
REM $STATIC
'----sub to send filled poly to PIC file
tmp$ = CHR$(48) + CHR$(nvert% - 1)
Picture$ = Picture$ + tmp$
FOR I% = 1 TO nvert%
 Gethex xvert%(I%), hi$, lo$
 tmp$ = CHR$(VAL(hi$)) + CHR$(VAL(lo$))
 Picture$ = Picture$ + tmp$
 Gethex yvert%(I%), hi$, lo$
 tmp$ = CHR$(VAL(hi$)) + CHR$(VAL(lo$))
 Picture$ = Picture$ + tmp$
NEXT I%
EXIT SUB
```

```
END SUB

'•••••••••••••••••••••••••••••••••••••••••••••
SUB PFillo (Picture$, nvert%, xvert%(), yvert%())
'----sub to send outlined filled poly to PIC file
tmp$ = CHR$(208) + CHR$(nvert% - 1)
Picture$ = Picture$ + tmp$
FOR I% = 1 TO nvert%
 Gethex xvert%(I%), hi$, lo$
 tmp$ = CHR$(VAL(hi$)) + CHR$(VAL(lo$))
 Picture$ = Picture$ + tmp$
 Gethex yvert%(I%), hi$, lo$
 tmp$ = CHR$(VAL(hi$)) + CHR$(VAL(lo$))
 Picture$ = Picture$ + tmp$
NEXT I%
EXIT SUB

END SUB

'•••••••••••••••••••••••••••••••••••••••••••••
SUB PFSize (Picture$, X%, Y%)
REM $DYNAMIC
'----sub to output font size command to PIC file
tmp$ = CHR$(172)
Picture$ = Picture$ + tmp$
Gethex X%, hi$, lo$
tmp$ = CHR$(VAL(hi$)) + CHR$(VAL(lo$))
Picture$ = Picture$ + tmp$
Gethex Y%, hi$, lo$
tmp$ = CHR$(VAL(hi$)) + CHR$(VAL(lo$))
Picture$ = Picture$ + tmp$
EXIT SUB
END SUB

'•••••••••••••••••••••••••••••••••••••••••••••
DSUB PHead (Picture$)
'----sub that sends header to PIC file
tmp$ = CHR$(1) + CHR$(0) + CHR$(0) + CHR$(0)
tmp$ = tmp$ + CHR$(1) + CHR$(0)
tmp$ = tmp$ + CHR$(8) + CHR$(0) + CHR$(&H44)
tmp$ = tmp$ + CHR$(0) + CHR$(0)
tmp$ = tmp$ + CHR$(0) + CHR$(0) + CHR$(&HC)
tmp$ = tmp$ + CHR$(&H7F) + CHR$(9)
tmp$ = tmp$ + CHR$(6)
Picture$ = Picture$ + tmp$
PFSize Picture$, 100, 100
EXIT SUB
END SUB

'•••••••••••••••••••••••••••••••••••••••••••••
SUB PicFileOpen (Picture$, PicFlg, Tick$)
REM $STATIC
DEFINT I-K
'----routine to initialize Picture$ array so data can later be saved
'----to a .PIC file for plotting with Lotus PGRAPH (R)
IF Batch% = 0 THEN
IF PicFlg = 0 THEN
LOCATE 17, 1: PRINT "PIC file output? [Y]: "
Q1$ = UCASE$(INPUT$(1))
IF Q1$ = CHR$(13) THEN Q1$ = "Y"
IF Q1$ = "Y" THEN
LOCATE 18, 1
INPUT "Enter output directory for PIC file: ", DataDirOut$
CircleFlg = 0
Picture$ = ""
PicFlg = 1
'----put Header into array if .PIC file is needed
PHead Picture$
END IF
LOCATE 17, 23: PRINT Q1$
END IF
ELSEIF Batch% = 1 THEN
PicFlg = 1
IF F6% = 1 THEN
Picture$ = "": PHead Picture$
END IF
END IF
END SUB

'•••••••••••••••••••••••••••••••••••••••••••••
SUB PMove (Picture$, X%, Y%)
REM $DYNAMIC
DEFSNG I-K
'----sub that output move command to PIC file
tmp$ = CHR$(160)
Picture$ = Picture$ + tmp$
Gethex X%, hi$, lo$
tmp$ = CHR$(VAL(hi$)) + CHR$(VAL(lo$))
Picture$ = Picture$ + tmp$
Gethex Y%, hi$, lo$
tmp$ = CHR$(VAL(hi$)) + CHR$(VAL(lo$))
Picture$ = Picture$ + tmp$
END SUB

'•••••••••••••••••••••••••••••••••••••••••••••
SUB PrintScreen (GRAPHIC) STATIC
REM $STATIC
'----Printer Epson compatible output. Puts picture data from
memory into
'----a row 8 pixels deep (using the OR statement) to be directly
printed.
DIM MxRows AS INTEGER, MxCols AS INTEGER
IF GRAPHIC = 3 THEN
MxRows% = 347: MxCols% = 719'----Herc screen limits
ELSEIF GRAPHIC = 2 THEN
MxRows% = 399: MxCols% = 639'----CGA screen limits
END IF
WIDTH LPRINT 255
LPRINT
'----Set line spacing to 24/216
LPRINT CHR$(27); "3"; CHR$(24);
FOR Row% = 0 TO MxRows% STEP 8
LPRINT CHR$(9); SPC(4); '----Set tab = 4
'----Turn double density graphics mode on
LPRINT CHR$(27); "L"; CHR$(128); CHR$(2);
FOR Col% = 0 TO MxCols%
BYTE% = 0
FOR Pixel% = 0 TO 7
IF POINT(Col%, Row% + Pixel%) > 0 THEN
BYTE% = BYTE% OR 2 ^ (7 - Pixel%)
END IF
NEXT Pixel%
LPRINT CHR$(BYTE%);
NEXT Col%
LPRINT CHR$(13);'----Carriage return
NEXT Row%
LPRINT CHR$(27); "2";'----Set line spacing to 1/6" (default)
EXIT SUB
END SUB
```

```
'*****************************************
SUB PText (Picture$, d%, P%, Msg$)
REM $DYNAMIC
'----sub to send text to PIC file
'----d% is orientation : 0 - hor l to r : 0
'-----1 - ver b to t : 90
'-----2 - hor r to l : 180
'-----3 - ver t to b : 270
'-----p% is position : see lotus file guide
tmp$ = CHR$(168) '&HA8
Picture$ = Picture$ + tmp$
tmp$ = "&H" + HEX$(d%) + HEX$(P%)
tmp$ = CHR$(VAL(tmp$))
Picture$ = Picture$ + tmp$
tmp$ = Msg$ + CHR$(0)
Picture$ = Picture$ + tmp$
END SUB
```

'----SCRIPT.BAS

```
CLS
INPUT "Enter input Batch file name: ",F$
OPEN F$ FOR INPUT AS #1
I = 500
PRINT "enter 1) for data script 2) for text script 3) for both: "
C$ = UCASE$(INPUT$(1))
C% = VAL(C$)
PRINT C%
IF C% = 2 THEN GOTO 100
OF$ = MID$(F$, 1, 4) + "DATA.SCR"
OPEN OF$ FOR OUTPUT AS #2
PRINT #2, "INSERT"
WHILE NOT EOF(1)
INPUT #1, F$, X#, Y#
OPEN F$ FOR INPUT AS #3
LOCATE 5, 1: PRINT "Reading file: "; F$
WHILE NOT EOF(3)
X# = X# - I
'----Enter plane orient
PRINT #2, "DIP"
WRITE #2, X#, Y#
INPUT #3, a, d, n
j = j + 1: LOCATE 7, 1: PRINT j; " data points entered"
PRINT #2, "1": PRINT #2,
Angle = a * -1
PRINT #2, Angle
'----Now do slick orient
PRINT #2, "SLICK"
WRITE #2, X#, Y#
INPUT #3, a, d, n
PRINT #2, "1": : PRINT #2,
Angle = a * -1
PRINT #2, Angle
WEND
CLOSE #3
WEND
IF C% = 1 THEN GOTO 200
100
CLOSE #2
CLOSE #1: OPEN F$ FOR INPUT AS #1
OF$ = MID$(F$, 1, 4) + "TXT.SCR"
OPEN OF$ FOR OUTPUT AS #2
PRINT #2, "STYLE"
PRINT #2, "ROMANS"
PRINT #2, "ROMANS"
PRINT #2, "200"
PRINT #2, : PRINT #2, : PRINT #2, : PRINT #2, : PRINT #2,
LOCATE 9, 1: PRINT "Reading the files for text dips"
PRINT #2, "TEXT"
WHILE NOT EOF(1)
INPUT #1, F$, X#, Y#
Fil$ = "B:" + F$ + ".SLI"
OPEN Fil$ FOR INPUT AS #3
LOCATE 11, 1: PRINT "Reading file: "; Fil$
WHILE NOT EOF(3)
X# = X# - I
WRITE #2, X#, Y#
PRINT #2, "0"
INPUT #3, a, d, n
k = k + 1: LOCATE 13, 1: PRINT k; " data points entered"
INPUT #3, dumx, dumd, dumn
PRINT #2, d
```

```
PRINT #2,
WEND
CLOSE #3
WEND
200
CLOSE #1: CLOSE #2
END
```

```
'---SEEK.BAS
DECLARE SUB Title ()
'--- SEEK AND YE SHALL FIND
'---
'--- Program SEEK.BAS to search the raw data files
'--- pick fracture data based on various parameters:
'---
'--- By: David van Everdingen (M.U.N.)Date:12-12-89

DECLARE SUB Clustran (Name1$, Disk$)
DECLARE SUB DisplayFiles (Directory$)
DECLARE SUB DriveAndDirec (Directory$, Drive$)
DECLARE SUB Filexist (NAMEXIST$, IO$, Overwrite$)
DECLARE SUB Help (SUBROUTINE$)
DECLARE SUB InOutFileName (Disk$, NameIn$, NameOut$,@
@ Type$)
DECLARE SUB Menu (MENUS$(), NEWY%, NEWX%,@
@ OLDY%, OLDX%, CHECK$, StartR%, StartC%)
DECLARE SUB Minmatch (x$, n%)
DECLARE SUB NestBox (BoxY%, BoxX%, YLimit%, XLimit%)
DECLARE SUB PickOutputFile (NAMEP$, DISKOUT$, IO$,@
@ NOPICK$)
DECLARE SUB Position (MENUS$(), StartR%, StartC%,@
@ Chose%, Call$)
DECLARE SUB Reformat (Disk$)
DECLARE SUB SearchData (Name1$, Directory$, StartDir$,@
@ NameOut$)
DECLARE SUB Separate (Name1$, Disk$)
DECLARE SUB Slickensides (Directory$, Type$)
DECLARE SUB Sphere (Name1$, Disk$)
DECLARE SUB Stereoplot (Directory$, StartDir$, Plotdat%(),@
@ Plot$)
DECLARE SUB Subtract ()
DECLARE SUB WipeBlock (FL%, LL%, FC%, LC%)
'---
COMMON SHARED Nerr%, BatchFlg%
COMMON SHARED Disk$, Directory$, StartDir$
COMMON SHARED /Utility/ DISKOUT$, Name1$, DataFile$()
COMMON SHARED /Batch/ FilesRead%, Kounter%
'---
DIM MENUS$(36), MENUU$(36), MENUSS$(36)
DIM DataFile$(200)
'---
TYPE RegType
ax AS INTEGER
bx AS INTEGER
CX AS INTEGER
dx AS INTEGER
bp AS INTEGER
si AS INTEGER
DI AS INTEGER
flags AS INTEGER
END TYPE
DIM InRegs AS RegType, OutRegs AS RegType
CLS
'---Set error trapping and set error variable to 0
Nerr% = 0
'---ON ERROR GOTO Generr:
'---Set up main menu
DEFINT A-Z
MENUS$(1) = "Reformat a Data File"
MENUS$(2) = "Search a Data File"
MENUS$(3) = " Orientation Separation "
```

```
MENUS$(4) = ""
MENUS$(5) = " Utilities"
MENUS$(6) = "Help"
MENUS$(7) = " DOS Shell"
MENUS$(8) = "Exit to DOS "
'----Determine current directory
DEF SEG
'-----Find current drive letter
InRegs.ax = &H1900
CALL interrupt(&H21, InRegs, OutRegs)
Numb% = VAL(RIGHT$(STR$(OutRegs.ax), 1))
IF Numb% = 0 THEN Drive$ = "A:\"
IF Numb% = 1 THEN Drive$ = "B:\"
IF Numb% = 2 THEN Drive$ = "C:\"
IF Numb% = 3 THEN Drive$ = "D:\"
'----Find current subdirectory
SubDir$ = STRING$(64, " ")
InRegs.ax = &H4700
InRegs.dx = &H0
InRegs.si = SADD(SubDir$)
CALL interrupt(&H21, InRegs, OutRegs)
SubDir$ = RTRIM$(SubDir$)
SubDir$ = MID$(SubDir$, 1, LEN(SubDir$) - 1) + "\"
IF LEN(SubDir$) = 1 THEN SubDir$ = ""'----Root directory
'----Combine the results
StartDir$ = Drive$ + SubDir$
Directory$ = StartDir$
'----Start the main body of the program
WHILE Q$ <> "X"
CLS
COLOR 0, 7: LOCATE 24, 1
PRINT SPACE$(80); LOCATE 24, 1: PRINT "Directory: ";
Directory$;
LOCATE 24, 56: PRINT "D.A.v.E. (C) 12/89 v4.0";
LOCATE 1, 1: PRINT SPACE$(79)
IF BatchFlg% = 1 THEN LOCATE 1, 37: PRINT "Batch On"
LOCATE 1, 68: PRINT "Main Menu": COLOR 7, 0
NeatBox 8, 4, 8, 33
LOCATE 8, 15: PRINT " Main Menu:"
'---- Print main menu screen
Title
'---- Call up the main menu
Position MENUS$(), 9, 6, Chose%, "MAIN"
'----
SELECT CASE Chose%
CASE -1
NeatBox 11, 7, 1, 25
LOCATE 12, 8: PRINT "Exit to DOS [Y/N]? ";
SOUND 700, .5
Q1$ = UCASE$(INPUT$(1))
IF Q1$ = "Y" THEN
        GOTO ENDEND:
END IF
CASE 1
LOCATE 1, 1: COLOR 0, 7: PRINT SPACE$(79)
IF BatchFlg% = 1 THEN LOCATE 1, 37: PRINT "Batch On"
LOCATE 1, 60: PRINT "Submenu: REFORMAT": COLOR 7, 0
Reformat Directory$
CASE 3
LOCATE 1, 1: COLOR 0, 7: PRINT SPACE$(79)
IF BatchFlg% = 1 THEN LOCATE 1, 37: PRINT "Batch On"
LOCATE 1, 60:PRINT "Submenu: SEPARATE": COLOR 7, 0
Separate Name1$, Directory$
CASE 2
LOCATE 1, 1: COLOR 0, 7: PRINT SPACE$(79)
IF BatchFlg% = 1 THEN LOCATE 1, 37: PRINT "Batch On"
LOCATE 1, 60: PRINT "Submenu: SEARCH": COLOR 7, 0
'-----Input and output file names are requested
IF BatchFlg% = 1 THEN
        FileReq$ = "IN"
ELSEIF BatchFlg% = 0 THEN
        FileReq$ = "BOTH"
END IF
InOutFileName Directory$, NameIn$, NameOut$, FileReq$
IF NameOut$ = "GETOUT" THEN GOTO EndMain:
SearchData NameIn$, Directory$, StartDir$, NameOut$
CASE 5 '----File utilities and help
QF$ = " "
WHILE INSTR("Y", QF$) = 0
Title
LOCATE 1, 1: COLOR 0, 7: PRINT SPACE$(79)
IF BatchFlg% = 1 THEN LOCATE 1, 37: PRINT "Batch On"
LOCATE 1, 60: PRINT "Submenu: UTILITY": COLOR 7, 0
MENUU$(1) = "Change Current Directory"
MENUU$(2) = "File Contents Subtracted"
MENUU$(3) = " Slickensides (SubMenu) "
IF BatchFlg% = 0 THEN
MENUU$(4) = "Batch : Off"
ELSEIF BatchFlg% = 1 THEN
MENUU$(4) = "Batch :On"
END IF

MENUU$(8) = " Main Menu <ESC>"

NeatBox 8, 4, 8, 33
LOCATE 8, 15: PRINT "Utility Menu:"
Position MENUU$(), 9, 6, ChoseU%, "Main"

SELECT CASE ChoseU%
CASE -1, 8
QF$ = "Y"
CASE 1
DriveAndDirec Directory$, Drive$
CASE 2
LOCATE 1, 60: COLOR 0, 7: PRINT "Submenu: SUBTRACT":
COLOR 7, 0
Subtract
CASE 3
QS$ = " "
WHILE INSTR("Y", QS$) = 0
Title
LOCATE 1, 56: COLOR 0, 7
PRINT "Submenu: SLICKENSIDES": COLOR 7, 0
MENUSS$(1) = " Complete Data Record"
MENUSS$(2) = "Orientations Only "
MENUSS$(3) = "Both Data and Orientations"
MENUSS$(8) = "Utility Menu <ESC> "
NeatBox 8, 4, 8, 33
LOCATE 8, 15: PRINT "Slick. Menu:"
LOCATE 12, 10: PRINT "(In separate files: data"
LOCATE 13, 10: PRINT "files have '----.SLK'----, orient."
LOCATE 14, 10: PRINT "files have '----.PLT'---- extn.) "
Position MENUSS$(), 9, 6, ChoseS%, "Main"
SELECT CASE ChoseS%
CASE -1, 8
QS$ = "Y"
CASE 1
LOCATE 1, 56
COLOR 0, 7: PRINT "Submenu: SLICK. DATA"
COLOR 7, 0
```

```
Slickenside Directory$, "DATA"
CASE 2
LOCATE 1, 56
COLOR 0, 7: PRINT "Submenu: SLICK. ORIENT"
COLOR 7, 0
Slickenside Directory$, "ORIENT"
CASE 3
LOCATE 1, 56
COLOR 0, 7: PRINT "Submenu: SLICK. BOTH": COLOR 7, 0
Slickenside Directory$, "BOTH"
CASE ELSE
QS$ = "Y"
END SELECT
WEND
CASE 4
IF BatchFlg% = 0 THEN
BatchFlg% = 1
ELSEIF BatchFlg% = 1 THEN
BatchFlg% = 0
END IF
CASE ELSE
QF$ = "Y"
END SELECT
WipeBlock 2, 22, 1, 79
WEND
CASE 6
NeatBox 2, 40, 19, 38
LOCATE 2, 50: PRINT "Help: Main"
Help "MAIN"
CASE 7
CLS
LOCATE 2, 10: PRINT "Type EXIT to return to SEEK"
SHELL
CASE ELSE
Q$ = "X"
END SELECT
CLOSE #1
EndMain:
WEND
CLOSE #1
StartDir$ = MID$(StartDir$, 1, 1) + "D" + MID$(StartDir$,@
@ 3, LEN(StartDir$) - 3)
 SHELL StartDir$
'----1989 data format
DATA 1,1,2,4,6,1,7,5,12,3,15,5,20,2,22,5,27,4,31
DATA 1,32,1,33,10,43,1
DATA 44,1,45,1,46,1,47,3,80,1
DATA Flag,Photo Number,Scanline Id.,Scanline Attribute
DATA Fracture Number
DATA Scanline Distance,Fracture Type,Orientation,Trace Length
DATA Censoring,Termination,Mineral Filling
DATA Large Scale Roughness
DATA Small Scale Roughness,Rock Type,Grain Size,Aperture
DATA Set Number
 GOTO ENDEND:
Generr:
'----
 Nerr% = ERR
 RESUME NEXT

ENDEND:
CLS
END

DEFSNG A-Z

'**************************************
'----Search the datafile based on various parameters
SUB SearchData (Name1$, Disk$, StartDir$, NameOut$)
SHARED OLD$
DEFINT A-Y
DIM Flag(30), INFLAG(30), OUTFLAG(30), FORMAT(30, 2)
DIM PHOTOS(150), MENSEF$(36)
DIM ZRANGE(2), MINERALS$(3), Match(30), MENSE$(36)
DIM HEADER$(36), APRANGE(2)
DIM OARANGE(2), ODRANGE(2), FOTOCOORDS$(100)
DIM northing$(100), Easting$(100)
DIM CHECK(3)
IF BatchFlg% = 1 THEN
INPUT #2, Disk$
WHILE NOT EOF(2)
Kounter% = Kounter% + 1
INPUT #2, DataFile$(Kounter%)
WEND
END IF
'----Set all flags to 0
FOR I = 1 TO 20
Flag(I) = 0
NEXT I
INFLG = 0
'----Read over first 37 data statement values to the menu headers
RESTORE
FOR I = 1 TO 36
READ Dummy$
NEXT I
'----Read in the menu headers
FOR I = 1 TO 18
READ MENSE$(I)
NEXT I
'----Add the remaining menu items
MENSE$(19) = ""
MENSE$(20) = "Select all to quantify later"
MENSE$(21) = "End selection process"
MENSE$(22) = "Exit to main menu"
RUNONCEAGAIN:
FOR I = 1 TO 22
HEADER$(I) = MENSE$(I)
NEXT I
SECSELECTFLG% = 0
TERMINATE$ = " "
WHILE TERMINATE$ < > "EXIT"'----while not exit requested
WipeBlock 2, 22, 1, 79
NeatBox 2, 2, 18, 22
NeatBox 3, 39, 3, 29
IF INFLG = 0 THEN
LOCATE 2, 4: PRINT "Search Parameters:"
LOCATE 1, 60: COLOR 0, 7: PRINT "Submenu: SEARCH"
LOCATE 10, 30: PRINT "Search the data file using "
ELSE
WipeBlock 10, 10, 30, 61
LOCATE 2, 4: PRINT "Output Parameters"
LOCATE 10, 30: COLOR 0, 7
PRINT "Now Select the ouput parameters using"
END IF
LOCATE 11, 30: PRINT "the Criteria in the box on the left"
LOCATE 12, 30
PRINT "Use the cursor keys to select your choice."
COLOR 7, 0
IF INFLG = 0 THEN'----the parameters that are not to be picked
HEADER$(1) = ""'----in the first selection are made blank
HEADER$(3) = ""
```

```
HEADER$(4) = ""
HEADER$(5) = ""
HEADER$(6) = ""
HEADER$(13) = ""
HEADER$(16) = ""
HEADER$(14) = ""
HEADER$(20) = "" '----the SECSELECTFLG% checks if the
second
END IF'----selection is to start
IF INFLG = 1 AND SECSELECTFLG% = 0 THEN
FOR I = 1 TO 22
HEADER$(I) = MENSE$(I)
NEXT I
SECSELECTFLG% = 1
END IF

'----call the menu display routine
Position HEADER$(), 3, 3, Chose%, "SEARCH"

SELECT CASE Chose%
CASE -1
GOTO EndSearchSub:
CASE 1'----flag parameter
Flag(1) = 1
HEADER$(1) = ""
CASE 2'----photo number parameter
REDOPHOTO:
NeatBox 3, 17, 12, 30
LOCATE 3, 20: PRINT "Photo Number:"
LOCATE 4, 15: COLOR 15, 0: PRINT "<=": COLOR 7, 0
Flag(2) = 1
IF INFLG = 0 THEN
Q1$ = "S"
WHILE INSTR("YN", Q1$) = 0
LOCATE 4, 18: PRINT "Are photo numbers to be"
LOCATE 5, 18: PRINT "entered manually?[Y/N]"
LOCATE 7, 18: PRINT "(Answer Y if all photos"
LOCATE 8, 18: PRINT "are to be searched)"
Q1$ = UCASE$(INPUT$(1))
WEND
IF Q1$ = "Y" THEN
LOCATE 10, 18: PRINT "# of photos do you want"
LOCATE 11, 18: PRINT "to search (0 for all): ";
INPUT ; "", PHONUM
WipeBlock 4, 11, 18, 45
LOCATE 4, 18: PRINT "Input "; PHONUM; " photo numbers:"
IF PHONUM > 0 THEN
FOR I = 1 TO PHONUM
IF I <= 10 THEN
J = 18
LOCATE 4 + I, J
ELSEIF I > 10 THEN
J = 28
LOCATE I - 6, J
END IF
PRINT "#"; : PRINT USING "##"; I; : PRINT ":";
COLOR 15, 0: INPUT ; " ", PHOTOS(I): COLOR 7, 0
NEXT I
END IF
ELSEIF Q1$ = "N" THEN
PHOFORM$ = "S"
WHILE INSTR("Y", PHOFORM$) = 0
LOCATE 10, 18: PRINT "Photo number data file must"
LOCATE 11, 18: PRINT "contain the number of photos"
LOCATE 12, 18: PRINT "on the first line followed"
LOCATE 13, 18: PRINT "by photo numbers on the next"
LOCATE 14, 18: PRINT "lines. Is this the case? [Y]"
PHOFORM$ = UCASE$(INPUT$(1))
IF PHOFORM$ = CHR$(13) THEN PHOFORM$ = "Y"
IF PHOFORM$ = "N" THEN GOTO EndSearchSub:
WEND
IF PHOFORM$ = "Y" THEN
Q5$ = "N"
WHILE INSTR("Y", Q5$) = 0
LOCATE 15, 18: PRINT "Photo number datafile name: "
LOCATE 16, 18: INPUT ; "", PHOTOLOC$
LOCATE 17, 22: PRINT "Okay? [Y]"
Q5$ = UCASE$(INPUT$(1))
IF Q5$ = CHR$(13) THEN Q5$ = "Y"
IF Q5$ = CHR$(27) THEN GOTO REDOPHOTO:
IF Q5$ = "N" THEN WipeBlock 8, 8, 28, 80
WEND
OPEN PHOTOLOC$ FOR INPUT AS #5
INPUT #5, Dummy$
I = 1
WHILE NOT EOF(5)
INPUT #5, PHOTOS(I)
I = I + 1
WEND
PHONUM = I - 1
CLOSE #5
END IF
END IF
END IF
IF INFLG = 1 THEN
QUES$ = "N"
WipeBlock 4, 15, 18, 46
WHILE INSTR("PM", QUES$) = 0
LOCATE 4, 18: PRINT "Do you want ";
COLOR 15, 0: PRINT "P"; : COLOR 7, 0
PRINT "hoto numbers or "
LOCATE 5, 18: COLOR 15, 0: PRINT "M"; : COLOR 7, 0
PRINT "ap coordinates included"
LOCATE 6, 18: PRINT "in the output data ?"
QUES$ = UCASE$(INPUT$(1))
WEND
IF QUES$ = "M" THEN
LOCATE 8, 18: PRINT "Map UTM coordinates put"
LOCATE 9, 18: PRINT "in as the 2nd to 15th columns"
LOCATE 10, 18: PRINT "of the output file (2-8 = "
LOCATE 11, 18: PRINT "Easting ,9-15 = northing)"
LOCATE 12, 18: PRINT "Using Photo map coordinates"
LOCATE 13, 18: PRINT "from file (FOTOCOOR.MAP)"
FotoFile$ = StartDir$ + "\FOTOCOOR.MAP"
ReopenFile:
OPEN FotoFile$ POR INPUT AS #11
IF Nerr% = 53 THEN
Nerr% = 0
CLOSE #11
WipeBlock 8, 13, 18, 46
LOCATE 8, 18: PRINT "File FOTOCOOR.MAP, containing"
LOCATE 9, 18: PRINT "map coordinates of the photos"
LOCATE 10, 18: PRINT "can not be found in:"
LOCATE 11, 18: PRINT StartDir$
Q2$ = "P"
WHILE INSTR("YN", Q2$) = 0
LOCATE 13, 18: PRINT "Does this file exist [Y]"
Q2$ = UCASE$(INPUT$(1))
IF Q2$ = CHR$(13) THEN Q2$ = "Y"
WEND
```

```
IF Q2$ = "N" THEN
QUES$ = "P"
WipeBlock 8, 13, 18, 46
GOTO PhotoLabel:
ELSEIF Q2$ = "Y" THEN
WipeBlock 8, 13, 18, 46
LOCATE 8, 18: PRINT "Enter directory containing"
LOCATE 9, 18: PRINT "FOTOCOOR.MAP"
Q5$ = "P"
WHILE INSTR("YN", Q5$) = 0
LOCATE 10, 18: INPUT "", Dir$
LOCATE 11, 22: PRINT "Okay [Y/N]?"
Q5$ = UCASE$(INPUT$(1))
IF Q5$ = CHR$(13) THEN Q5$ = "Y"
IF Q5$ = "N" THEN WipeBlock 10, 11, 18, 50
WEND
FotoFile$ = Dir$ + "\FOTOCOOR.MAP"
GOTO ReopenFile:
END IF
END IF
FOR I = 1 TO 100
FOTOCOORDS$(I) = ""
NEXT I
I = 1
INPUT #11, Dummy$
WHILE NOT EOF(11)
INPUT #11, FOTOCOORDS$(I), Easting$(I), northing$(I)
I = I + 1
WEND
NUMBEROFOTOS = I - 1
END IF
PhotoLabel:
IF QUES$ = "P" THEN
LOCATE 8, 18: PRINT "Photo and scanline id'——s"
LOCATE 9, 22: PRINT "will be output."
END IF
END IF
HEADER$(2) = ""
CASE 3'——scanline identifier
Flag(3) = 1
HEADER$(3) = ""
CASE 4'——scanline orientation
Flag(4) = 1
HEADER$(4) = ""
CASE 5'——fracture number
Flag(5) = 1
HEADER$(5) = ""
CASE 6'——scanline distance
Flag(6) = 1
HEADER$(6) = ""
IF INFLG = 0 THEN
NeatBox 3, 17, 12, 30
LOCATE 3, 19: PRINT "Scanline Distance:"
LOCATE 8, 15: COLOR 15, 0: PRINT "<=": COLOR 7, 0
LOCATE 4, 18: PRINT "To calculate spacing from"
LOCATE 5, 18: PRINT "the distance values you"
LOCATE 6, 18: PRINT "must separate the data"
LOCATE 7, 18: PRINT "based on some other para-"
LOCATE 8, 18: PRINT "meters and run the result-"
LOCATE 9, 18: PRINT "ant complete datafile"
LOCATE 10, 18: PRINT "through SPACE.FOR"
LOCATE 15, 18: PRINT "Press any key to continue"
DO: LOOP UNTIL INKEY$ <> ""
END IF
CASE 7'——fracture type parameter
Flag(7) = 1
HEADER$(7) = ""
IF INFLG = 0 THEN
NeatBox 3, 17, 10, 30
LOCATE 3, 20: PRINT "Fracture Type:"
LOCATE 8, 15: COLOR 15, 0: PRINT "<=": COLOR 7, 0
LOCATE 4, 19: PRINT "Pick fracture type:"
LOCATE 5, 19: PRINT "(Press ENTER to select;"
LOCATE 6, 19: PRINT "cursor keys to move)"
FOR J = 1 TO 30
MENSEF$(J) = ""
NEXT J
MENSEF$(1) = "Contact"
MENSEF$(2) = "Vein"
MENSEF$(3) = "Fracture"
MENSEF$(4) = "Joint"
MENSEF$(5) = "Fault"
MENSEF$(6) = "Frac. Zone"
Position MENSEF$(), 8, 22, CHOSEF%, "SEARCH"
SELECT CASE CHOSEF%
CASE -1
GOTO EndSearchSub:
CASE 1
FRCTYPE$ = "cn"
CASE 2
FRCTYPE$ = "vn"
CASE 3
FRCTYPE$ = "fr"
CASE 4
FRCTYPE$ = "jt"
CASE 5
FRCTYPE$ = "ft"
CASE 6
FRCTYPE$ = "fz"
CASE ELSE
END SELECT
END IF
CASE 8'——fracture orientation parameter
FOR I = 1 TO 30'——Check if any other items have been picked
IF Flag(I) = 1 THEN OFlg = 1
NEXT I
IF NOT (INFLG = 1 AND OFlg = 1) THEN
NeatBox 3, 17, 13, 30
LOCATE 3, 20: PRINT "Fracture Orientation:"
LOCATE 10, 15: COLOR 15, 0: PRINT "<=": COLOR 7, 0
END IF
Flag(8) = 1
HEADER$(8) = ""
IF INFLG = 0 THEN
LOCATE 4, 19: PRINT " Which fracture orient-"
LOCATE 5, 19: PRINT " tation search for?:"
LOCATE 6, 19: PRINT " (Press ENTER to select;"
LOCATE 7, 19: PRINT " cursor keys to move)"
FOR J = 1 TO 30
MENSEF$(J) = ""
NEXT J
MENSEF$(1) = "Dip Azimuth Range"
MENSEF$(2) = "Dip Range"
MENSEF$(3) = "Both"
Position MENSEF$(), 9, 20, CHOSEF%, "SEARCH"
SELECT CASE CHOSEF%
CASE -1
GOTO EndSearchSub:
CASE 1
ORIENT$ = "A"
```

```
CASE 2
ORIENT$ = "D"
CASE 3
ORIENT$ = "B"
CASE ELSE
END SELECT
WipeBlock 4, 16, 18, 45
IF ORIENT$ = "A" OR ORIENT$ = "B" THEN
LOCATE 4, 18: PRINT "Input the DIP AZIMUTH range"
LOCATE 5, 18: PRINT "in degrees (0 to 359):"
OARANGE(1) = -1
OARANGE(2) = -2
WHILE OARANGE(1) > OARANGE(2) OR OARANGE(1)@
@ < 0 OR OARANGE(2) > 359
LOCATE 7, 18: INPUT ; "LOWER end of range: ",@
@ OARANGE(1)
LOCATE 8, 18: INPUT ; "UPPER end of range: ",@
@ OARANGE(2)
IF OARANGE(1) > OARANGE(2) OR OARANGE(1) < 0 OR@
@OARANGE(2) > 359 THEN
LOCATE 10, 18: PRINT "UPPER range value must >"
LOCATE 11, 18: PRINT "LOWER range value & be-"
LOCATE 12, 18: PRINT "tween 0 and 360 degrees"
SOUND 700, 1
WipeBlock 7, 8, 18, 44
END IF
WEND
END IF
IF ORIENT$ = "D" OR ORIENT$ = "B" THEN
LOCATE 4, 18: PRINT "Input DIP range (degrees:0-90):"
ODRANGE(1) = -1
ODRANGE(2) = -2
WHILE ODRANGE(1) > ODRANGE(2) OR ODRANGE(1) < 0
OR@
@ODRANGE(2) > 90
LOCATE 5, 18: INPUT ; "Input LOWER end of range :",@
@ODRANGE(1)
LOCATE 6, 18: INPUT ; "Input UPPER end of range :",@
@ODRANGE(2)
IF ODRANGE(1) > ODRANGE(2) OR ODRANGE(1) < 0 OR@
@ODRANGE(2) > 90 THEN
LOCATE 14, 18: PRINT "The UPPER range value >";
LOCATE 15, 18: PRINT "LOWER range value & be-"
LOCATE 16, 18: PRINT "tween 0 and 90 degrees"
SOUND 700, 1
WipeBlock 5, 6, 18, 29
END IF
WEND
END IF
ELSEIF INFLG = 1 AND OFlg <> 1 THEN
FOR I = 1 TO 2
MENSEF$(I) = ""
NEXT I
WipeBlock 4, 16, 18, 45
LOCATE 4, 18: PRINT "Format wanted for output:"
LOCATE 5, 18: PRINT "(Note: If you pick any of"
LOCATE 6, 18: PRINT "the other parameters with"
LOCATE 7, 18: PRINT "orientation, output will"
LOCATE 8, 18: PRINT "be in the compressed dip-"
LOCATE 9, 18: PRINT "direction dip format of the"
LOCATE 10, 18: PRINT "raw data file - that is, a"
LOCATE 11, 18: PRINT "choice here will not affect"
LOCATE 12, 18: PRINT "the output)."
FOR P = 1 TO 30: MENSEF$(P) = "": NEXT P
MENSEF$(1) = "Dip-DirectionDip"
MENSEF$(2) = "DipDip-Direction"
Position MENSEF$(), 14, 19, CHOSEF%, "SEARCH"
SELECT CASE CHOSEF%
CASE -1
GOTO EndSearchSub:
CASE 1
OROUT$ = "AD"
CASE 2
OROUT$ = "DA"
CASE ELSE
END SELECT
END IF
OFlg = 0
CASE 9'----trace length parameter
Flag(9) = 1
HEADER$(9) = ""
IF INFLG = 0 THEN
NestBox 3, 17, 7, 30
LOCATE 3, 20: PRINT "Trace Length:"
LOCATE 11, 15: COLOR 15, 0: PRINT "<=": COLOR 7, 0
ZRANGE(1) = 200
ZRANGE(2) = 100
LOCATE 4, 18: PRINT "What fracture length range"
LOCATE 5, 18: PRINT "(METRES) do you want to "
LOCATE 6, 18: PRINT "search for?"
WHILE ZRANGE(1) > ZRANGE(2)
LOCATE 7, 18: INPUT ; "Input LOWER end of range :",@
@ ZRANGE(1)
LOCATE 8, 18: INPUT ; "Input UPPER end of range :",@
@ ZRANGE(2)
IF ZRANGE(1) > ZRANGE(2) THEN
LOCATE 9, 18: PRINT "UPPER range value must >"
LOCATE 10, 18: PRINT "LOWER range value."
SOUND 700, 1
END IF
WEND
END IF
CASE 10 '----censoring style parameter
Flag(10) = 1
HEADER$(10) = ""
IF INFLG = 0 THEN
NestBox 3, 17, 8, 30
LOCATE 3, 20: PRINT "Censoring:"
LOCATE 12, 15: COLOR 15, 0: PRINT "<=": COLOR 7, 0
LOCATE 4, 18: PRINT "What style of censoring to"
LOCATE 5, 18: PRINT "search for?"
LOCATE 6, 18: PRINT "(Press ENTER key to select"
LOCATE 7, 18: PRINT "cursor keys to move)."
FOR J = 1 TO 30
MENSEF$(J) = ""
NEXT J
MENSEF$(1) = "0 = Both ends free"
MENSEF$(2) = "1 = One end covered"
MENSEF$(3) = "2 = Both ends covered"
Position MENSEF$(), 9, 19, CHOSEF%, "SEARCH"
SELECT CASE CHOSEF%
CASE -1
GOTO EndSearchSub:
CASE 1
CENS = 0
CASE 2
CENS = 1
CASE 3
CENS = 2
'----censoring of '2' means that the termination
```

```
'----style is censored ('-') so delete from list
Flag(11) = 1
HEADER$(11) = ""
CASE ELSE
END SELECT
END IF
CASE 11 '----termination style parameter
Flag(11) = 1
HEADER$(11) = ""
IF INFLG = 0 THEN
NeatBox 3, 17, 12, 30
LOCATE 3, 20: PRINT "Termination:"
LOCATE 13, 15: COLOR 15, 0: PRINT "<=": COLOR 7, 0
LOCATE 4, 18: PRINT "What style of termination"
LOCATE 5, 18: PRINT "to search for?"
LOCATE 6, 18: PRINT "(Press ENTER key to select"
LOCATE 7, 18: PRINT "cursor keys to move)."
FOR J = 1 TO 30
MENSEF$(J) = ""
NEXT J
MENSEF$(1) = "0= Both ends free"
MENSEF$(2) = "1= 'T' junction"
MENSEF$(3) = "2= 'H' junction"
MENSEF$(4) = "3= Splay at one end"
MENSEF$(5) = "4= Splay at both ends"
MENSEF$(6) = "'-' = Censored termination"
Position MENSEF$(), 9, 18, CHOSEF%, "SEARCH"
SELECT CASE CHOSEF%
CASE -1
GOTO EndSearchSub:
CASE 1
TERM$ = "0"
CASE 2
TERM$ = "1"
CASE 3
TERM$ = "2"
CASE 4
TERM$ = "3"
CASE 5
TERM$ = "4"
CASE 6
'---if a censored termination is chosen then the censoring is '2'
'----thus the censoring item is deleted from the choice list
TERM$ = "-"
Flag(10) = 1
HEADER$(10) = ""
CASE ELSE
END SELECT
END IF
CASE 12 '----mineral filling parameter
Flag(12) = 1
HEADER$(12) = ""
IF INFLG = 0 THEN
NeatBox 3, 17, 14, 30
AnotherMineral:
LOCATE 3, 20: PRINT "Mineral Filling:"
LOCATE 14, 15: COLOR 15, 0: PRINT "<=": COLOR 7, 0
Min$ = ""
LOCATE 4, 18: PRINT "Enter Search type:"
LOCATE 5, 20: COLOR 15, 0
PRINT "1"; : COLOR 7, 0: PRINT " - 1 mineral"
LOCATE 6, 2
COLOR 15, 0: PRINT "2"; : COLOR 7, 0: PRINT " - AND"
LOCATE 7, 2
COLOR 15, 0: PRINT "3"; : COLOR 7, 0: PRINT " - OR"
LOCATE 8, 2
COLOR 15, 0: PRINT "4"; : COLOR 7, 0: PRINT " - NOT"
AnotherB:
B$ = UCASE$(INPUT$(1))
IF VAL(B$) < 0 OR VAL(B$) > 4 THEN GOTO AnotherB:
SELECT CASE B$
CASE "1"
LOCATE 10, 18: PRINT "One Mineral Choice:"
LOCATE 11, 20: COLOR 15, 0
PRINT "1"; : COLOR 7, 0: PRINT " - 1 mineral"
LOCATE 12, 24: PRINT "Fracture may have >1"
LOCATE 13, 20: COLOR 15, 0: PRINT "2";
COLOR 7, 0: PRINT " - 1 mineral"
LOCATE 14, 24: PRINT "Fracture has 1 only"
AnotherBB:BB$ = UCASE$(INPUT$(1))
IF BB$ <> "1" AND BB$ <> "2" THEN GOTO AnotherBB:
IF BB$ = "1" THEN
MFlg = 11
LOCATE 16, 20: INPUT "Enter mineral: ", Min$
ELSEIF BB$ = "2" THEN
MFlg = 12
LOCATE 16, 20: INPUT "Enter mineral: ", Min$
Min$ = MID$(Min$, 1, 1) + ""
END IF
CASE "2"
MFlg = 2
LOCATE 10, 18: PRINT "AND Search:"
LOCATE 11, 20: PRINT "Put in any order, but all"
LOCATE 12, 20: PRINT "three must match in search"
LOCATE 13, 20: PRINT "Enter mineral letters (no"
LOCATE 14, 20: INPUT "spaces, max=3): ", Min$
CASE "3"
MFlg = 3
LOCATE 10, 18: PRINT "OR Search:"
LOCATE 11, 20: PRINT "Put in any order, only one"
LOCATE 12, 20: PRINT "needs to match in search"
LOCATE 13, 20: PRINT "Enter mineral letters (no"
LOCATE 14, 20: INPUT "spaces, max=3): ", Min$
CASE "4"
LOCATE 10, 18: PRINT "Exclusion search:"
LOCATE 11, 18: COLOR 15, 0
PRINT "1"; : COLOR 7, 0: PRINT " - 1 mineral 1 in fracture"
LOCATE 12, 18: COLOR 15, 0
PRINT "2"; : COLOR 7, 0: PRINT " - as 1 >1 exclusion"
LOCATE 13, 18: COLOR 15, 0
PRINT "3"; : COLOR 7, 0: PRINT " - 1 mineral >1 in fracture"
AnotherBB1:BB$ = UCASE$(INPUT$(1))
IF BB$ <> "1" AND BB$ <> "2" AND BB$ <> "3" THEN
GOTO AnotherBB1:
END IF
IF BB$ = "1" THEN
MFlg = 41
LOCATE 14, 18: PRINT "Exclude One Mineral Frac.:"
LOCATE 15, 20: INPUT "Enter mineral to exclude: ", Min$
Min$ = MID$(Min$, 1, 1) + ""
ELSEIF BB$ = "2" THEN
MFlg = 42
LOCATE 14, 18: PRINT "Exclude One Mineral Frac.:"
LOCATE 15, 20: INPUT "Enter 1st only mineral: ", Min$
Min$ = MID$(Min$, 1, 1) + ""
LOCATE 16, 20: INPUT "Enter 2nd only mineral: ", Min2$
Min2$ = MID$(Min2$, 1, 1) + ""
ELSEIF BB$ = "3" THEN
MFlg = 43
LOCATE 14, 18: PRINT "Exclude Multi Mineral Frac.:"
```

```
LOCATE 15, 20: INPUT "Enter mineral: ", Min$
END IF
CASE ELSE
END SELECT
END IF
CASE 13 '----large scale roughness parameter
Flag(13) = 1
HEADER$(13) = ""
CASE 14 '----small scale roughness
Flag(14) = 1
HEADER$(14) = ""
CASE 15 '----rock type parameter
Flag(15) = 1
HEADER$(15) = ""
FOR I = 1 TO 30
MENSEF$(I) = ""
NEXT I
IF INFLG = 0 THEN
NeatBox 9, 14, 9, 30
LOCATE 9, 20: PRINT " Rock Type:"
LOCATE 17, 12: COLOR 15, 0: PRINT "<=": COLOR 7, 0
LOCATE 10, 18: PRINT "Which rock type to"
LOCATE 11, 18: PRINT "search for?"
LOCATE 12, 18: PRINT "(Press ENTER key to select"
LOCATE 13, 18: PRINT "cursor keys to move)."
MENSEF$(1) = "P = Pillows"
MENSEF$(2) = "D = Dykes"
MENSEF$(3) = "T = Trondjhemites"
MENSEF$(4) = "G = Gabbros"
Position MENSEF$(), 15, 18, CHOSEF%, "SEARCH"
SELECT CASE CHOSEF%
CASE -1
GOTO EndSearchSub:
CASE 1
ROCKTYP$ = "p"
CASE 2
NeatBox 9, 14, 9, 30
LOCATE 9, 20: PRINT " Dyke Type:"
LOCATE 17, 12: COLOR 15, 0: PRINT "<=": COLOR 7, 0
LOCATE 10, 18: PRINT "Which dyke type to"
LOCATE 11, 18: PRINT "search for?"
LOCATE 12, 18: PRINT "(Press ENTER key to select"
LOCATE 13, 18: PRINT "cursor keys to move)."
MENSEF$(1) = "A = All dykes"
MENSEF$(2) = "D = Non-ep.Dykes"
MENSEF$(3) = "E = Epidosites"
MENSEF$(4) = "C = Crossing"
Position MENSEF$(), 15, 18, CHOSEF%, "SEARCH"
SELECT CASE CHOSEF%
CASE -1
GOTO EndSearchSub:
CASE 1
ROCKTYP$ = "doc"
CASE 2
ROCKTYP$ = "d"
CASE 3
ROCKTYP$ = "e"
CASE 4
ROCKTYP$ = "c"
CASE ELSE
END SELECT
CASE 3
ROCKTYP$ = "t"
CASE 4
ROCKTYP$ = "g"
CASE ELSE
END SELECT
END IF
CASE 16 '----grain size parameter
Flag(16) = 1
HEADER$(16) = ""
CASE 17 '----aperture parameter
Flag(17) = 1
HEADER$(17) = ""
CASE 18 '----set number parameter
Flag(18) = 1
HEADER$(18) = ""
IF INFLG = 0 THEN
NeatBox 18, 17, 2, 30
LOCATE 18, 20: PRINT "Set Number:"
LOCATE 20, 15: COLOR 15, 0: PRINT "<=": COLOR 7, 0
LOCATE 19, 18: PRINT "Input set number to"
LOCATE 20, 18: PRINT "search (Max. = 9): "
Set = VAL(INPUT$(1))
END IF
CASE 20'----select all for later quantification
IF INFLG = 1 THEN
FOR I = 1 TO 20
Flag(I) = 1
HEADER$(I) = ""
'----Don't ask for complete data set in separate file
DATOUT$ = "N"
NEXT I
END IF
CASE 21'----end select
IF INFLG = 0 THEN
INFLG = 1
FOR I = 1 TO 20
INFLAG(I) = Flag(I)
Flag(I) = 0
NEXT I
'----At this stage the input & output parameters
'----have been picked now figure out what needs to be picked
'----from the datafile and to proceed with the search
ELSEIF INFLG = 1 THEN
INFLAG = 0
FOR I = 1 TO 20
OUTFLAG(I) = Flag(I)
Flag(I) = 0
NEXT I
'---------- Output the choices ----------
'---- Read over the first set of data statements (the formats)
RESTORE
FOR I = 1 TO 36: READ Dummy$: NEXT I
'---- Now read the choices data statements
WipeBlock 2, 22, 29, 79
NeatBox 2, 35, 18, 22
COLOR 15, 7: LOCATE 2, 4: PRINT "Search Parameters:"
LOCATE 2, 38: PRINT "Output Parameters:": COLOR 7, 0
WipeBlock 3, 20, 3, 23
FOR I = 1 TO 18
'----read from the DATA statements at prgm end
READ CHOICES$
IF INFLAG(I) = 1 THEN
LOCATE (2 + I), 3
PRINT CHOICES$
END IF
IF OUTFLAG(I) = 1 THEN
LOCATE (2 + I), 36
PRINT CHOICES$
```

```
END IF
NEXT I
Q1$ = " "
WHILE INSTR("YN", Q1$) = 0
COLOR 0, 7: LOCATE 13, 58: PRINT "These were the choices"
LOCATE 14, 58: PRINT "that you picked "
LOCATE 15, 58: PRINT "Okay? [Y] ": COLOR 7, 0
Q1$ = UCASE$(INPUT$(1))
IF Q1$ = CHR$(13) THEN Q1$ = "Y"
IF Q1$ = CHR$(27) THEN GOTO EndSearchSub:
WEND
IF Q1$ = "Y" THEN
'—— Input the data format from the data statements for the
'—— Cyprus standard data format which contains for each
parameter
'—— the first position it occupies on the data line and how many
'—— positions it occupies. First reset the data statement pointer
'—— to the start of the data statements
RESTORE
FOR I = 1 TO 18
FOR J = 1 TO 2
READ FORMAT(I, J)
NEXT J
NEXT I
'——Ask if complete data record line is to be output to separate file
'——If DATOUT$ = "N" then choice all to quantify later = picked
'——and there is no need to duplicate the output.
IF DATOUT$ <> "N" THEN DATOUT$ = " "
WHILE INSTR("YN", DATOUT$) = 0
COLOR 0, 7: LOCATE 13, 58: PRINT "Do you want the com-"
LOCATE 14, 58: PRINT "plete data record out "
LOCATE 15, 58: PRINT "out put as well [N]?": COLOR 7, 0
DATOUT$ = UCASE$(INPUT$(1))
IF DATOUT$ = CHR$(13) THEN DATOUT$ = "N"
 WEND
'——An interlude while program checks if processing a batch job
RunAnotherBatchJob:
IF BatchFlg% = 1 AND FilesRead% < Kounter% THEN
CLOSE #2: CLOSE #3
FilesRead% = FilesRead% + 1
Name1$ = DataFile$(FilesRead%)
Name1A$ = Disk$ + "\" + Name1$
OPEN Name1A$ FOR INPUT AS #2
NameOut$ = Disk$ + "\" + MID$(DataFile$(FilesRead%), 1,@
@LEN(DataFile$(FilesRead%)) - 3) + "BAC"
OPEN NameOut$ FOR OUTPUT AS #3
END IF
IF DATOUT$ = "Y" THEN
'——Remove the pathname from the file name
FOR I = 1 TO LEN(NameOut$)
IF MID$(NameOut$, I, 1) = "\" THEN Flag = I
NEXT I
NAME7$ = RIGHT$(NameOut$, LEN(NameOut$) - Flag)
NAME7$ = MID$(NAME7$, 1, LEN(NAME7$) - 3) + "TOT"
PICKANOTHER1:
Overwrite$ = "Y"
PickOutputFile NAME7$, DISKOUT$, "OUT", NOPICK$
IF NOPICK$ = CHR$(27) THEN GOTO EndSearchSub:
NAME7A$ = DISKOUT$ + "\" + NAME7$
Filexist NAME7A$, "OUT", Overwrite$
IF Overwrite$ = "N" THEN
Overwrite$ = "Y"
GOTO PICKANOTHER1
ELSEIF Overwrite$ = "Y" THEN
OPEN NAME7A$ FOR OUTPUT AS #7
END IF
END IF
'——Put file header of name and date in the output file
CHKFLG = 0
FOR I = 1 TO 18
IF OUTFLAG(I) = 1 THEN CHKFLG = CHKFLG + 1
NEXT I
IF OUTFLAG(8) <> 1 AND CHKFLG <> 1 THEN
PRINT #3, USING "\\"; UCASE$(NAME6$);
PRINT #3, " produced ";
PRINT #3, USING "\\"; DATE$;
PRINT #3, " from ";
PRINT #3, USING "\\"; UCASE$(Name1$);
PRINT #3, " by SEEK "
END IF
'——If orientation is only one picked see if output to net is wanted
IF OUTFLAG(8) = 1 AND CHKFLG = 1 THEN
IF ST = 0 THEN
StPlot$ = " "
WHILE INSTR("YN", StPlot$) = 0
COLOR 0, 7: LOCATE 13, 58
PRINT "Plot data on stereo"
LOCATE 14, 58: PRINT "net [Y]? (or only to"
LOCATE 15, 58: PRINT "a file)"
COLOR 7, 0
StPlot$ = UCASE$(INPUT$(1))
IF StPlot$ = CHR$(13) THEN StPlot$ = "Y"
IF StPlot$ = "Y" THEN StPlot% = 1
WEND
END IF
IF StPlot% = 1 THEN
SCREEN 3

'——Subroutine to plot the data on the stereo net
PI = 3.1415926540#: ZGrad = PI / 180
R% = 150
XX% = 1 * 720 / 3: YY% = 5 * 348 / 9
LINE (XX% - R% - 10, YY% - R% + 25)-(XX% + R% +@
@ 10, YY% + R% - 35), , BF
'——Draw a circle
CIRCLE (XX%, YY%), R%, 0, , , .729
LINE (XX%, YY% + .729 * R% + 3)-(XX%, YY% +@
@ .729 * R%), 0
LINE (XX%, YY% - .729 * R% - 4)-(XX%, YY% - .729@
@ * R% - 1), 0
'——N symbol
PSET (XX% - 4, YY% - .729 * R% - 6): DRAW "C0U8F8U8"
LINE (XX% - R% - 6, YY%)-(XX% - R%, YY%), 0
LINE (XX% + R%, YY%)-(XX% + R% + 6, YY%), 0
'——draw cross in centre
PSET (XX%, YY%): DRAW "C0BU4D8BU4BR5L10"
END IF
END IF
'——Start the search through the data file
Counter = 0
Counter1 = 0
Counter2 = 0
Counter3 = 0
IF StPlot% = 0 THEN WipeBlock 2, 22, 1, 79
IF BatchFlg% = 0 AND StPlot% = 0 THEN
LOCATE 4, 5: PRINT "Reading and Searching Data File: ";
ELSEIF BatchFlg% = 1 THEN
LOCATE 4, 5
PRINT "Reading and Searching File #"; FilesRead%; "of @
@ "; Kounter%; ": "'——;
```

```
END IF
IF StPlot% = 0 THEN
PRINT USING "\\"; Name1$;
PRINT "..."
END IF
WHILE NOT EOF(2)
INPUT #2, DataLine$
Counter = Counter + 1
IF StPlot% = 0 THEN
LOCATE 6, 5: PRINT "Data records read: ";
PRINT USING "#####"; Counter - 1
END IF
FOR I = 1 TO 18
Match(I) = 0
NEXT I
IF LEFT$(DataLine$, 1) = "1" THEN
'----Pick the input values
'----Note that if >1 inflag value is '1' then there must be
'----a match with ALL the criteria, not just one of them
MATCHES = 1
FOR I = 1 TO 18
IF INFLAG(I) = 1 THEN
Dummy$ = MID$(DataLine$, FORMAT(I, 1), FORMAT(I, 2))
IF I = 2 THEN
Dummy = VAL(Dummy$)
IF PHONUM > 0 THEN
FOR J = 1 TO PHONUM
IF Dummy = PHOTOS(J) THEN
Match(I) = 1
END IF
NEXT J
ELSEIF PHONUM = 0 THEN
Match(I) = 1
END IF
ELSEIF I = 7 AND Dummy$ = FRCTYPE$ THEN
Match(I) = 1
ELSEIF I = 8 THEN
Az = VAL(MID$(Dummy$, 1, 3))
Dip = VAL(MID$(Dummy$, 4, 2))
IF ORIENT$ = "A" THEN
IF Az >= OARANGE(1) AND Az <= OARANGE(2) THEN
Match(I) = 1
END IF
ELSEIF ORIENT$ = "D" THEN
IF Dip >= ODRANGE(1) AND Dip <= ODRANGE(2) THEN
Match(I) = 1
END IF
ELSEIF ORIENT$ = "B" THEN
IF Az >= OARANGE(1) AND Az <= OARANGE(2) THEN
IF Dip >= ODRANGE(1) AND Dip <= ODRANGE(2)@
@THEN
Match(I) = 1
END IF
END IF
END IF
ELSEIF I = 9 THEN
ZDummy = VAL(Dummy$)
IF ZDummy >= ZRANGE(1) AND ZDummy < ZRANGE(2)
THEN
Match(I) = 1
END IF
ELSEIF I = 10 THEN
Dummy = VAL(Dummy$)
IF Dummy = CENS THEN
Match(I) = 1
END IF
ELSEIF I = 11 THEN
IF Dummy$ = TERM$ THEN
Match(I) = 1
END IF
ELSEIF I = 12 THEN '----for 1989 data
M$ = MID$(Dummy$, 1, 1) + MID$(Dummy$, 4, 1)@
@+ MID$(Dummy$, 7, 1)
'----TEST BED START
'----case of one mineral (fracture may have >1 mineral)
IF MFlg = 11 THEN
FOR II = 1 TO 3
IF MID$(Min$, 1, 1) = MID$(M$, II, 1) THEN
Match(I) = 1
END IF
NEXT II
'----case of 1 mineral only in fracture
ELSEIF MFlg = 12 THEN
IF MID$(Min$, 1, 3) = MID$(M$, 1, 3) THEN
Match(I) = 1
END IF
'----case of any three minerals but all three must be present
ELSEIF MFlg = 2 THEN
K = 3: FOR JJ = 1 TO 3: CHECK(JJ) = 0: NEXT JJ
FOR J = 1 TO LEN(Min$)
FOR JJ = 1 TO K
IF MID$(Min$, J, 1) = MID$(M$, JJ, 1)@
@ THEN
M$ = MID$(M$, 1, JJ - 1) + @
@ MID$(M$, JJ + 1, LEN(M$))
CHECK(J) = 1
EXIT FOR
END IF
NEXT JJ
IF CHECK(J) = 1 THEN K = K - 1
NEXT J
Match(I) = 1
FOR J = 1 TO LEN(Min$)
IF CHECK(J) = 0 THEN Match(I) = 0
NEXT J
'----------case of any three minerals, only one must be present
ELSEIF MFlg = 3 THEN
FOR II = 1 TO 3
FOR J = 1 TO 3
IF MID$(Min$, II, 1) = MID$(M$, J, 1)@
@THEN Match(I) = 1
NEXT J
NEXT II
'----------case of one mineral exclusion (fracture contains only one
mineral)
ELSEIF MFlg = 41 THEN
IF MID$(Min$, 1, 3) <> MID$(M$, 1, 3) @
@THEN Match(I) = 1
'----------case of >1 mineral exclusion (only 1 per fracture)
ELSEIF MFlg = 42 THEN
IF MID$(Min$, 1, 3) <> MID$(M$, 1, 3) AND@
@MID$(Min2$, 1, 3) <> MID$(M$, 1, 3) THEN@
@Match(I) = 1
IF MID$(Min$, 1, 1) = MID$(M$, 1, 1) OR@
@MID$(Min2$, 1, 1) = MID$(M$, 1, 1) THEN@
@Match(I) = 0
'----------case of one mineral exclusion (fracture contains >1
mineral)
ELSEIF MFlg = 43 THEN
FOR II = 1 TO 3
```

```
IF MID$(Min$, I, 1) < > MID$(M$, II, 1)@
@ THEN Match(I) = 1
NEXT II
END IF
'————make sure no blanks got through
IF M$ = "" THEN Match(I) = 0
ELSEIF I = 15 THEN
IF ROCKTYP$ = "dec" THEN
IF Dummy$ = "d" OR Dummy$ = "c" OR@
@Dummy$ = "c" THEN
Match(I) = 1
END IF
ELSEIF Dummy$ = ROCKTYP$ THEN
Match(I) = 1
END IF
ELSEIF I = 17 THEN
Dummy = VAL(Dummy$)
IF Dummy > APRANGE(1) AND Dummy < APRANGE(2)
THEN
Match(I) = 1
END IF
ELSEIF I = 18 AND Set = VAL(Dummy$) THEN
Match(18) = 1
END IF
END IF
NEXT I
FOR I = 1 TO 20
IF INFLAG(I) = 1 AND Match(I) < > 1 THEN
MATCHES = 0
END IF
NEXT I
'——Now output matched data records to new output file
IF MATCHES = 1 THEN
OUTEXT$ = ""
'——If only output parameter picked is orientation, output
'——will be for Stereo or SPHERE = thus output will be formatted
'——accordingly - Dip and Dipdirection or DipDirection and Dip
CHKFLG = 0
FOR I = 1 TO 18
IF OUTFLAG(I) = 1 THEN CHKFLG = CHKFLG + 1
NEXT I
IF OUTFLAG(8) = 1 AND CHKFLG = 1 THEN
IF StPlot% = 1 THEN
ZAz = VAL(MID$(DataLine$, 22, 3))
ZDip = VAL(MID$(DataLine$, 25, 2))
ZAzR = ((ZAz + 180) MOD 360) * ZGrad
ZThetR = ZDip * ZGrad
RSQ = R% * SQR(2)
DD = RSQ * SIN(ZThetR / 2)
DDN = DD * .729
XPT = DD * SIN(ZAzR)
YPT = DDN * COS(ZAzR)
PSET (XX% + XPT, YY% - YPT)
'——Open circle
DRAW "C0BD2L1H1U2E1R2F1D2G1L1U1C1U1"
LOCATE 2, 5: PRINT "File: ", Name1$
LOCATE 3, 5: PRINT "N = "; Counter2 + 1
END IF
IF OROUT$ = "DA" THEN
IF MID$(DataLine$, 25, 2) < > "" OR @
@MID$(DataLine$, 22, 3) < > "" THEN
OUTEXT$ = MID$(DataLine$, 25, 2) + " " + @
@MID$(DataLine$, 22, 3)
END IF
ELSEIF OROUT$ = "AD" THEN
IF MID$(DataLine$, 25, 2) < > "" OR@
@MID$(DataLine$, 22, 3) < > "" THEN
OUTEXT$ = MID$(DataLine$, 22, 3) + " " + @
@MID$(DataLine$, 25, 2)
END IF
END IF
ELSE
FOR I = 1 TO 18
IF OUTFLAG(I) = 1 THEN
IF I = 2 AND OUTFLAG(2) = 1 AND QUES$ = "M"@
@ THEN
FOR IJ = 1 TO NUMBEROFOTOS
IF FOTOCOORDS$(IJ) = MID$(DataLine$,@
@ FORMAT(I, 1), FORMAT(I, 2)) THEN
OUTEXT$ = OUTEXT$ + Easting$(IJ) + @
@ northing$(IJ)
GOTO EXITTHISLOOP:
END IF
NEXT IJ
ELSE
OUTEXT$ = OUTEXT$ + MID$(DataLine$, @
@FORMAT(I, 1), FORMAT(I, 2))
END IF
END IF
EXITTHISLOOP:
NEXT I
END IF
'——If the only output on the line is to be the orientation then only
print
'——the OUTEXT$ if it is non-blank
IF OUTFLAG(8) = 1 AND CHKFLG = 1 THEN
IF MID$(DataLine$, 25, 2) < > "" OR@
@MID$(DataLine$, 22, 3) < > "" THEN
IF OUTEXT$ < > " " AND OUTEXT$ < > "" THEN@
@PRINT #3, OUTEXT$
END IF
ELSE
IF OUTEXT$ < > "" THEN PRINT #3, OUTEXT$
END IF
IF DATOUT$ = "Y" THEN
PRINT #7, DataLine$
END IF
Counter2 = Counter2 + 1
IF StPlot% = 0 THEN
LOCATE 7, 5:PRINT " Matches Found: ";
PRINT USING "#####"; Counter2
IF OUTFLAG(8) = 1 AND CHKFLG = 1 THEN
IF MID$(DataLine$, 25, 2) = "" OR@
@MID$(DataLine$, 22, 3) = "" THEN
Counter3 = Counter3 + 1
LOCATE 8, 5:PRINT "Records@
@with Nulls: ";
PRINT USING "#####"; Counter3
END IF: END IF: END IF: END IF: END IF
WEND
IF StPlot% = 1 THEN
IF BatchFlg% = 0 THEN
LOCATE 23, 1: PRINT "Press any key to continue"
DO: LOOP UNTIL INKEY$ < > ""
END IF
SCREEN 0
ELSE
LOCATE 4, 53
PRINT "Finished."
SOUND 1000, .5
```

```
LOCATE 6, 5: PRINT " Last record read:"
LOCATE 9, 5: PRINT "# of Records to Ouput File: ";
PRINT USING "#####"; Counter2 - Counter3
IF DATOUT$ = "Y" THEN
LOCATE 11, 5
PRINT "The complete data record for above data is in:"
LOCATE 12, 5: PRINT SPACE$(51)
LOCATE 12, 10: PRINT UCASE$(LTRIM$(NAME7A$))
END IF
END IF
Q6$ = "D"
IF BatchFlg% = 1 AND FilesRead% < Kounter% THEN
Q6$ = "Y"
IF SkPlot% = 1 THEN ST = 1
GOTO RunAnotherBatchJob:
ELSEIF BatchFlg% = 1 AND FilesRead% = Kounter% THEN
Q6$ = "N"
LOCATE 15, 5
PRINT " The files resulting from the batch job all @
@ have the extension: ";
COLOR 15, 7: PRINT ".BAC"; : COLOR 7, 0
LOCATE 16, 5: PRINT " and are in the following directory: ";
COLOR 15, 7: PRINT Disk$: COLOR 7, 0
LOCATE 20, 5: PRINT " Press any key to continue"
DO: LOOP UNTIL INKEY$ <> ""
END IF
WHILE INSTR("YN", Q6$) = 0
LOCATE 15, 5:PRINT "Do you want to use ";
COLOR 15, 7: PRINT Name1$; : COLOR 7, 0
PRINT " for another search? [Y]"
Q6$ = UCASE$(INPUT$(1))
IF Q6$ = CHR$(13) THEN Q6$ = "Y"
WEND
IF Q6$ = "Y" THEN
CLOSE #3: CLOSE #2: CLOSE #7
INFLG = 0
SECSELECTFLG% = 0
FOR I = 1 TO 30
Flag(I) = 0
INFLAG(I) = 0
OUTFLAG(I) = 0
HEADER$(I) = MENSE$(I)
NEXT I
OPEN Disk$ + "\" + Name1$ FOR INPUT AS #2
InOutFileName Disk$, NameIn$, NameOut$, "OUT"
RESTORE
ELSE
TERMINATE$ = "EXIT"
END IF
ELSEIF Q1$ = "N" THEN
INFLG = 0
SECSELECTFLG% = 0
FOR I = 1 TO 30
Flag(I) = 0
INFLAG(I) = 0
OUTFLAG(I) = 0
HEADER$(I) = MENSE$(I)
NEXT I
RESTORE
END IF
END IF
CASE 22'----exit to main menu
GOTO EndSearchSub:
CASE ELSE
END SELECT
WEND
EndSearch:

Name1$ = NAME6$

EndSearchSub:
END SUB

'*****************************************
SUB Title
DEFSNG A-Y
'----Subroutine to print the title screen when needed
LOCATE 3, 10: COLOR 15, 0
PRINT "SEEK AND YE SHALL FIND "
LOCATE 4, 10
PRINT " Program To Search Through The Cyprus Fracture Data"
LOCATE 9, 44: COLOR 0, 7: PRINT " Press the first letter or "
LOCATE 10, 44: PRINT " use the cursor keys to "
LOCATE 11, 44: PRINT " highlight your choice, "
LOCATE 12, 44: PRINT " press Enter to select it": COLOR 7, 0

END SUB
```

```
'----SNOWPERM.BAS
'----program to calculate principal permeability magnitudes and
'----directions of fractures along a scanline of a given length
'----and orientation. The method follows that of Bianchi and
'----Snow (1969). The direction cosines of each fracture are
'----calculated. This is multiplied by the fracture aperture and
'----divided by the scanline length. The resultant matrix is
'----summed over all the fractures into a global matrix. The eigen
'----values and vectors are then calculated - these are the
'----principal permeability magnitudes and directions.
'----D.A.van Everdingen                    5/1992
'----data format requires the first line to be a comment line and
'----on the following lines the scanline info to be prefaced
'----by 'S:' and the fracture info to be prefaced by 'F:' - each
'----line contains an additional three numbers:
'----for scanlines: linelength, azimuth and dip
'----for fractures: azimuth, dip and aperture
'----e.g.File: 1001.DOC
'----S: 30.0 354 07
'----F: 250 75 1.0
'----F: 247 79 2.0
'----Note: all varibles should be double precision (not shown
'----here to reduce clutter)
DECLARE SUB Parse (Entry$, N1!, N2!, N3!, Flg%)
CLS
'----set array sizes
N = 500: M = 15
'----declare arrays and variables
DIM A(6), EVal!(3), EVec(3, 3)
DIM VectorData(3, N), AZ(N), HEL(N), AP(N), AzR(N),
ThetR(N)
DIM Factor(N), LL(N)
DIM LineLen(M), LineAz(M), LineDip(M), D1(M), D2(M),
D3(M)
DIM Theta1(3), Phi1(3)
'----set constants
PI = 3.1415926534#
Grad = PI / 180
'----open in and output files and print header
PRINT "BIANCHI AND SNOW (1969) PERMEABILITY
METHOD
PRINT: PRINT
PRINT "File format: LINE 1:Linelength LineAzimuth LineDip"
PRINT " LINE 2-N: FractureAzimuth Dip Aperture"
INPUT "Enter file name: ", F$
OPEN F$ FOR INPUT AS #1
OF$ = MID$(F$, 1, LEN(F$) - 3) + "SNO"
OPEN OF$ FOR OUTPUT AS #2
PRINT "Output will be to: "; OF$
PRINT #2, "BIANCHI AND SNOW (1969) PERMEABILITY
PRINT #2,
'----read and print comment line and file name into output file
INPUT #1, Comment$
PRINT #2, Comment$
PRINT #2, "File: "; F$;
'----read data from file
Count = 0: I = 1: FrcCnt = 0: FrcAp = 0
WHILE NOT EOF(1)
INPUT #1, Entry$
'----parse the data string into the variables
CALL Parse(Entry$, X1, X2, X3, Flg%)
'----read scanline info
IF MID$(Entry$, 1, 2) = "S:" THEN
Count = Count + 1
LineLen(Count) = X1
LineAz(Count) = X2
LineDip(Count) = X3
'----calculate direction cosines of scanline
D1(Count) = COS(X2 * Grad) * COS(X3 * Grad)
D2(Count) = SIN(X2 * Grad) * COS(X3 * Grad)
D3(Count) = SIN(X3 * Grad)
'----read fracture info
ELSEIF MID$(Entry$, 1, 2) = "F:" THEN
AZ(I) = X1: HEL(I) = X2: AP(I) = X3: LL(I) = Count
'----calculate the total aperture and number of apertures
FrcCnt = FrcCnt + 1
FrcAp = FrcAp + AP(I)
I = I + 1
END IF
WEND
P = I - 1
'----mean aperture
MeanAp = FrcAp / FrcCnt
'----determine multiplication factor (in order to decrease
roundoff
'----error) since we are dealing with a large range of magnitudes
'----the mean rather than the minimum aperture is used
MultFac = 10 ^ (INT(LOG(MeanAp / 2000 * MeanAp / 2000@
@* MeanAp / 2000) / LOG(10)) + 1)
PRINT #2, SPACE$(20); "Mult Factor "; MultFac: PRINT #2,
'----print the scanline data
FOR I = 1 TO Count
PRINT #2, "Scanline("; I; "): L="; LineLen(LL(I)); " Trend=";
PRINT #2, LineAz(LL(I)); " Plunge="; LineDip(LL(I))
PRINT #2, " Direction Cosines: "; USING "###.####";
PRINT #2, D1(LL(I)); D2(LL(I)); D3(LL(I))
NEXT I
PRINT #2,
PRINT #2, " Az. Dip.n1 n2 n32/3L*b^3/niDi"
PRINT #2,
'----calculate direction cosines
FOR I = 1 TO P
AzR(I) = ((AZ(I) + 180) MOD 360) * Grad
ThetR(I) = HEL(I) * Grad
VectorData(1, I) = SIN(ThetR(I)) * COS(AzR(I))
VectorData(2, I) = SIN(ThetR(I)) * SIN(AzR(I))
VectorData(3, I) = COS(ThetR(I))
niDi = ABS(VectorData(1, I) * D1(LL(I)) + VectorData(2, I) * @
@D2(LL(I)) + VectorData(3, I) * D3(LL(I)))
Factor(I) = 2 * (AP(I) / 2000) ^ 3 / (3 * LineLen(LL(I)) * niDi)@
@/ MultFac
PRINT #2, USING "####"; AZ(I);
PRINT #2, " "; USING "##.#"; HEL(I); TAB(13);
FOR J = 1 TO 3
PRINT #2, USING "##.####"; VectorData(J, I);
NEXT J
PRINT #2, USING "##.#####"; Factor(I);
PRINT #2, " Line("; LL(I); ")"
NEXT I
FOR I = 1 TO 6: A(I) = 0!: NEXT I
'----assemble the global permeability matrix
FOR I = 1 TO P
FOR J = 1 TO 3
FOR K = J TO 3
L = (J - 1) + K
IF J > 1 THEN L = L + 1
IF L = 1 OR L = 4 OR L = 6 THEN
'----diagonal terms
```

```
A(L) = A(L) + (1 - VectorData(J, I) * VectorData(K,@
@I)) * Factor(I)
ELSE
'----off-diagonal terms
A(L) = A(L) - VectorData(J, I) * VectorData(K, I)@
@* Factor(I)
END IF
NEXT K: NEXT J: NEXT I
PRINT #2,
PRINT #2, "Global K = [";
FOR I = 1 TO 3: PRINT #2, USING "###.####"; A(I); : NEXT I
PRINT #2, "]"
PRINT #2, ""; USING "###.####"; A(4); A(5);
PRINT #2, "] * Mult Factor"
PRINT #2, " "; USING "###.####"; A(6);
PRINT #2, "]"
PRINT #2,
'----calculate eigenvectors (EVec) and eigenvalues (EVal)
A = A(1): B = A(2): C = A(3): D1 = A(4): E = A(5): F =
A(6)
B2 = B * B: C2 = C * C: E2 = E * E
A2 = -(A + D1 + F)
A1 = (A * (D1 + F) + D1 * F) - (B2 + C2 + E2)
A0 = (A * E2 + F * B2 + D1 * C2) - (2 * B * C * E@
@+ A * D1 * F)
Q = A1 / 3! - A2 * A2 / 9!
R = (A1 * A2 - 3! * A0) / 6! - A2 * A2 * A2 / 27!
IF ABS(R) > .000001 THEN T = SQR(-(Q * Q * Q + R * R))
IF ABS(R) <= .000001 THEN T = .5 * PI
U = SQR(R * R + T * T)
Theeta = ATN(T / R)
IF Theeta < 0! THEN Theeta = Theeta + PI
Theeta = Theeta / 3!
U3 = 2! * (U ^ .33333333#)
T1 = U3 * COS(Theeta)
T2 = -U3 * SIN(Theeta)
EVal!(1) = T1 - A2 / 3!
CON1 = -.5 * T1 - A2 / 3!
CON2 = .5 * T2 * SQR(3!)
EVal!(2) = CON1 - CON2
EVal!(3) = CON1 + CON2
'----print out eigen values after multiplication by factor
'----2/3L*b^3/nlDi*MultFac and division by # of scanlines
'----in the data set
EV1 = EVal!(1) * MultFac / Count
EV2 = EVal!(2) * MultFac / Count
EV3 = EVal!(3) * MultFac / Count
PRINT #2, "(1)(2) (3)"
PRINT #2, : PRINT #2, "EVal ";
PRINT #2, EV1; EV2; EV3: PRINT #2,
FOR J = 1 TO 3
X1 = 1
EVA = EVal!(J) - A
DEN = B * E - C * (D1 - EVal!(J))
X2 = (EVA * E + B * C) / DEN
X3 = (EVA - B * X2) / C
RS = 1! / SQR(X1 * X1 + X2 * X2 + X3 * X3)
EVec(1, J) = X1 * RS
EVec(2, J) = X2 * RS
EVec(3, J) = X3 * RS
NEXT J
FOR I = 1 TO 3
'----negative dip angle
IF EVec(3, I) < 0 THEN
FOR M% = 1 TO 3
EVec(M%, I) = -EVec(M%, I)
NEXT M%
END IF
'----Calculate Theta in the range (0 to Pi) so that COS(Theta)=X
'----QuickBASIC has no arc-cosine function so use the arc-tangent
'----function
Theta1(I) = ATN(SQR(1! - EVec(3, I) * EVec(3, I)) / @
@(EVec(3, I) + 1E-30))
'----Now transform from direction cosines to polar coordinates
IF ABS(EVec(1, I)) >= .000001 THEN
Phi1(I) = ATN(EVec(2, I) / EVec(1, I))
IF EVec(1, I) < 0! THEN Phi1(I) = Phi1(I) + PI
IF EVec(1, I) >= 0! AND EVec(2, I) < 0! THEN
Phi1(I) = Phi1(I) + 6.2831853071#
END IF
ELSE
Phi1(I) = 1.5707963271#
IF EVec(2, I) < 0! THEN Phi1(I) = 4.712388981#
END IF
Theta1(I) = 90! - Theta1(I) / Grad
Phi1(I) = Phi1(I) / Grad
NEXT I
'----print out eigen vectors as direction cosines
FOR I = 1 TO 3
PRINT #2, "EVec ";
PRINT #2, USING "####.########"; EVec(I, 1); EVec(I, 2);@
@ EVec(I, 3)
NEXT I
'----print out eigen vectors as azimuth and dip
PRINT #2, : PRINT #2, "Azim";
PRINT #2, USING "##########.##"; Phi1(1); Phi1(2); Phi1(3)
PRINT #2, "Dip ";
PRINT #2, USING "##########.##"; Theta1(1); Theta1(2);
Theta1(3)
CLOSE
END
'****************************************
SUB Parse (Entry$, N1, N2, N3, Flg%)
'----Subroutine to parse a data input string into numbers
DIM N(4)
'----Initialize some variables
FOR I = 1 TO 4: N(I) = 0: NEXT I
I = 1: Flg% = 0: First$ = ""
Length = LEN(Entry$)
WHILE I <= Length + 1 AND Flg% < 5
'----Check for non-numbers
E$ = MID$(Entry$, I, 1)
IF (E$ < CHR$(48) OR E$ > CHR$(57)) AND E$ <>@
@ CHR$(46) AND I <= Length + 1 THEN
IF First$ <> "" THEN
Flg% = Flg% + 1
N(Flg%) = VAL(First$)
First$ = ""
END IF
'----Compile a number into First$
ELSEIF E$ > CHR$(47) AND E$ < CHR$(58) OR E$ =@
@CHR$(46) AND I < Length THEN
First$ = First$ + E$
END IF
I = I + 1
WEND
EndParse:
N1 = N(1): N2 = N(2): N3 = N(3)
END SUB
```

```
'—SPACE.BAS
'—program to calculate spacing between fractures of the same set
'—requires the file EIGEN.SET to be present
DECLARE FUNCTION ArcCos! (X!)
CLS
Rad = 3.14159265#/ 180

INPUT "Enter input file name", IF$
INPUT "Enter file directory name", Dir$
Dir$=Dir$ + "\"
IF$ = MID$(IF$, 1, 5) + TRUNC$(II)
PRINT "Data file name: "; IF$; "Output name: ";
CLOSE #1: CLOSE #2: CLOSE #4
OPEN Dir$ + IF$ FOR INPUT AS #1

INPUT "Enter set number: ", Set$
OF$ = Dir$ + MID$(IF$, 1, LEN(IF$) - 2) + "SP" +
LTRIM$(Set$)
PRINT OF$
OPEN OF$ FOR OUTPUT AS #4
OPEN "eigenset.nc" FOR INPUT AS #2
File$ = MID$(IF$, 1, 4)
FF$ = "": Flg = 0
WHILE Flg = 0 AND NOT EOF(2)
INPUT #2, d$
FF$ = MID$(d$, 1, 4)
FSet$ = MID$(d$, 17, 1)
IF FF$ = File$ AND FSet$ = Set$ THEN
Flg = 1
END IF
WEND
IF Flg = 1 THEN
'—Read direction cosines of chosen set
PF = VAL(MID$(d$, 24, 7))
QF = VAL(MID$(d$, 32, 7))
RF = VAL(MID$(d$, 40, 7))
c = 0: d = 0: e = 0: f = 0: g = 0
WHILE NOT EOF(1)
INPUT #1, DL$
c = c + 1
NewLinnum$ = MID$(DL$, 2, 4)
Bear = VAL(MID$(DL$, 7, 3))
Ping = VAL(MID$(DL$, 10, 2))
FrcLen = VAL(MID$(DL$, 15, 5))
DSet$ = MID$(DL$, 51, 1)
IF DSet$ = Set$ THEN
d = d + 1
Ping = -Ping
PL = COS(Bear * Rad) * COS(Ping * Rad)
QL = SIN(Bear * Rad) * COS(Ping * Rad)
RL = SIN(Ping * Rad)
CosPhi = ((PF * PL) + (QF * QL) + (RF * RL))
Phi = ArcCos(ABS(CosPhi)) / Rad
IF FrcLen < > 0 THEN
e = e + 1
IF NewLinnum$ = OldLinnum$ THEN
f = f + 1
L = FrcLen - LagLen
IF L >= 0 THEN
g = g + 1
Space = L * COS(Phi * Rad)
PRINT #4, ""; DSet$; " "; NewLinnum$;
PRINT #4, USING "###.##"; L; Phi; Space
```

```
END IF
END IF
LagLen = PrcLen
OldLinnum$ = NewLinnum$
END IF
END IF
WEND
PRINT c; d; e; f; g
ELSE
PRINT "No set number match found": CLOSE : END
END IF

PRINT "Another file/set? [Y]"
Q$ = UCASE$(INPUT$(1))
IF Q$ = CHR$(13) THEN Q$ = "Y"
CLOSE
IF Q$ = "Y" THEN GOTO NextOne:
END

'*****************************************
FUNCTION ArcCos (X)

IF 1 = X THEN
ArcCos = 0
ELSEIF -1 = X THEN
ArcCos = 3.1415926549#
ELSE
ArcCos = 1.5707963268# - ATN(X / SQR(1 - X * X))
END IF

END FUNCTION
```

```
'--- TABULATE.BAS
'----Program to tabulate results from a search through a data file
'----such as raw fracture data files produced by SEEK.FOR.
'----Tabulation include the type, length, censoring, termination,
'----mineral filling, fracture surface characteristics, rock type,
'-----rock grain size and aperture

'----D. van Everdingen 27 January 1992

DIM a(6), fa(5), fl(5), rt(5), ra(5), rf(5)
DIM m1(12), m2(12), m3(12), l(12), t(9), c(4), te(7)

CLS : PRINT "Fracture Parameter Tabulation Program"
INPUT "input batch file name: ", f$
OF$ = MID$(f$, 1, LEN(f$) - 3) + "OUT"
OPEN f$ FOR INPUT AS #1
OPEN OF$ FOR OUTPUT AS #8
INPUT #1, dir$

flag = 0
INPUT "which set do you want to search (1,2,3,etc,a=all): ", set$
IF set$ = "a" THEN flag = 1
'----print the titles to the output file
IF flag = 1 THEN
PRINT #8, "ALL FRACTURES CHOSEN"
ELSE
PRINT #8, "SET NUMBER: "; set$
END IF
PRINT #8, : PRINT #8, " TABULATED PARAMETERS"
PRINT #8, " ========== ==========="
PRINT #8,
PRINT #8,"Fracture Type:@
@ Fracture Length:Censoring: Fracture Termination:@
@Fracture Mineral Filling Fracture Surface Characteristics@
@Rock Type: Rock Grain Size:Fracture Aperture (mm):"
PRINT #8, "SCAN # jt fr az cn vn sp fz ft #";
PRINT #8, "0-1  1-2  2-3  3-4  4-5  5-6  6-7  7-9  8-9@
@ 9-10  >10 # ";
PRINT #8, "0 1 2 #";
PRINT #8, "0 1 2 3 4 5 #";
PRINT #8, "z e k r u h p j x c - #";
PRINT #8, "z e k r u h p j x c - #";
PRINT #8, "z e k r u h p j x c - #";
PRINT #8, "Rgh Slk Smo #";
PRINT #8, "Stp Crv Und Pla #";
PRINT #8, "Gab Trn Dyk Pil #";
PRINT #8, "Fin Med Cru #";
PRINT #8, "0 0-5 5-10 10-100  >100 # "; : PRINT #8,
'----in Batch mode read filenames and open the input data file
WHILE NOT EOF(1)
INPUT #1, f$
CLOSE #7
if$ = dir$ + "\" + f$
OPEN if$ FOR INPUT AS #7
PRINT "Reading file: "; f$
'-----initialize all the arrays
FOR i = 1 TO 12
l(i) = 0
m1(i) = 0
m2(i) = 0
m3(i) = 0
NEXT i
FOR i = 1 TO 4
```

```
c(i) = 0
NEXT i
FOR i = 1 TO 7
te(i) = 0
NEXT i
FOR i = 1 TO 6
a(i) = 0
NEXT i
FOR i = 1 TO 5
fs(i) = 0
rf(i) = 0
fl(i) = 0
rt(i) = 0
rs(i) = 0
NEXT i
FOR i = 1 TO 9
t(i) = 0
NEXT i
number = 0
'----start the loop for reading the data file
WHILE NOT EOF(7)
INPUT #7, dat$
'----check if a data line is being read
IF MID$(dat$, 1, 1) = "1" THEN
'----check if there is a match in the set number
IF MID$(dat$, 1, 80) = set$ OR flag = 1 THEN
type$ = MID$(dat$, 20, 2)
length = VAL(MID$(dat$, 27, 4))
cens = VAL(MID$(dat$, 31, 1))
term = VAL(MID$(dat$, 32, 1))
min1$ = MID$(dat$, 33, 1)
min2$ = MID$(dat$, 36, 1)
min3$ = MID$(dat$, 39, 1)
fracl$ = MID$(dat$, 43, 1)
fracs$ = MID$(dat$, 44, 1)
rocktyp$ = MID$(dat$, 45, 1)
rockgr$ = MID$(dat$, 46, 1)
aper = VAL(MID$(dat$, 47, 3))
'----check how many of each variable there are
'----fracture type
IF type$ = "jt" THEN t(1) = t(1) + 1
IF type$ = "fr" THEN t(2) = t(2) + 1
IF type$ = "az" THEN t(3) = t(3) + 1
IF type$ = "cn" THEN t(4) = t(4) + 1
IF type$ = "vn" THEN t(5) = t(5) + 1
IF type$ = " s" THEN t(6) = t(6) + 1
IF type$ = "fz" THEN t(7) = t(7) + 1
IF type$ = "fl" THEN t(8) = t(8) + 1
'----length
IF length >= 0 AND length < 1! THEN l(1) = l(1) + 1
IF length >= 1! AND length < 2! THEN l(2) = l(2) + 1
IF length >= 2! AND length < 3! THEN l(3) = l(3) + 1
IF length >= 3! AND length < 4! THEN l(4) = l(4) + 1
IF length >= 4! AND length < 5! THEN l(5) = l(5) + 1
IF length >= 5! AND length < 6! THEN l(6) = l(6) + 1
IF length >= 6! AND length < 7! THEN l(7) = l(7) + 1
IF length >= 7! AND length < 8! THEN l(8) = l(8) + 1
IF length >= 8! AND length < 9! THEN l(9) = l(9) + 1
IF length >= 9! AND length < 10! THEN l(10) = l(10) + 1
IF length >= 10! THEN l(11) = l(11) + 1
'----censoring
IF cens = 0 THEN c(1) = c(1) + 1
IF cens = 1 THEN c(2) = c(2) + 1
IF cens = 2 THEN c(3) = c(3) + 1
'----termination
IF term = 0 THEN te(1) = te(1) + 1
IF term = 1 THEN te(2) = te(2) + 1
IF term = 2 THEN te(3) = te(3) + 1
IF term = 3 THEN te(4) = te(4) + 1
IF term = 4 THEN te(5) = te(5) + 1
IF term = 5 THEN te(6) = te(6) + 1
'----mineral filling
IF min1$ = "z" THEN m1(1) = m1(1) + 1
IF min1$ = "e" THEN m1(2) = m1(2) + 1
IF min1$ = "k" THEN m1(3) = m1(3) + 1
IF min1$ = "r" THEN m1(4) = m1(4) + 1
IF min1$ = "u" THEN m1(5) = m1(5) + 1
IF min1$ = "h" THEN m1(6) = m1(6) + 1
IF min1$ = "p" THEN m1(7) = m1(7) + 1
IF min1$ = "j" THEN m1(8) = m1(8) + 1
IF min1$ = "x" THEN m1(9) = m1(9) + 1
IF min1$ = "c" THEN m1(10) = m1(10) + 1
IF min1$ = "n" THEN m1(11) = m1(11) + 1
IF min2$ = "z" THEN m2(1) = m2(1) + 1
IF min2$ = "e" THEN m2(2) = m2(2) + 1
IF min2$ = "k" THEN m2(3) = m2(3) + 1
IF min2$ = "r" THEN m2(4) = m2(4) + 1
IF min2$ = "u" THEN m2(5) = m2(5) + 1
IF min2$ = "h" THEN m2(6) = m2(6) + 1
IF min2$ = "p" THEN m2(7) = m2(7) + 1
IF min2$ = "j" THEN m2(8) = m2(8) + 1
IF min2$ = "x" THEN m2(9) = m2(9) + 1
IF min2$ = "c" THEN m2(10) = m2(10) + 1
IF min2$ = "-" THEN m2(11) = m2(11) + 1
IF min3$ = "z" THEN m3(1) = m3(1) + 1
IF min3$ = "e" THEN m3(2) = m3(2) + 1
IF min3$ = "k" THEN m3(3) = m3(3) + 1
IF min3$ = "r" THEN m3(4) = m3(4) + 1
IF min3$ = "u" THEN m3(5) = m3(5) + 1
IF min3$ = "h" THEN m3(6) = m3(6) + 1
IF min3$ = "p" THEN m3(7) = m3(7) + 1
IF min3$ = "j" THEN m3(8) = m3(8) + 1
IF min3$ = "x" THEN m3(9) = m3(9) + 1
IF min3$ = "c" THEN m3(10) = m3(10) + 1
IF min3$ = "-" THEN m3(11) = m3(11) + 1
'----fracture surface type small scale
IF fracs$ = "r" THEN fs(1) = fs(1) + 1
IF fracs$ = "k" THEN fs(2) = fs(2) + 1
IF fracs$ = "s" THEN fs(3) = fs(3) + 1
'----fracture surface type large scale
IF fracl$ = "s" THEN fl(1) = fl(1) + 1
IF fracl$ = "c" THEN fl(2) = fl(2) + 1
IF fracl$ = "u" THEN fl(3) = fl(3) + 1
IF fracl$ = "p" THEN fl(4) = fl(4) + 1
'----rock type
IF rocktyp$ = "g" THEN rt(1) = rt(1) + 1
IF rocktyp$ = "t" THEN rt(2) = rt(2) + 1
IF rocktyp$ = "d" THEN rt(3) = rt(3) + 1
IF rocktyp$ = "p" THEN rt(4) = rt(4) + 1
'----rock grain size
IF rockgr$ = "f" THEN rf(1) = rf(1) + 1
IF rockgr$ = "m" THEN rf(2) = rf(2) + 1
IF rockgr$ = "c" THEN rf(3) = rf(3) + 1
'----aperture
IF aper = 0! THEN a(1) = a(1) + 1
IF aper = 0! AND aper <= 5! THEN a(2) = a(2) + 1
IF aper >= 5! AND aper <= 10! THEN a(3) = a(3) + 1
IF aper >= 10! AND aper <= 100! THEN a(4) = a(4) + 1
IF aper >= 100! THEN a(5) = a(5) + 1
number = number + 1
```

```
END IF
END IF
WEND
'----total the results
FOR i = 1 TO 5
a(6) = a(6) + a(i)
NEXT i
FOR i = 1 TO 6
te(7) = te(7) + te(i)
NEXT i
FOR i = 1 TO 3
fs(4) = fs(4) + fs(i)
c(4) = c(4) + c(i)
rf(4) = rf(4) + rf(i)
NEXT i
FOR i = 1 TO 11
l(12) = l(12) + l(i)
m1(12) = m1(12) + m1(i)
m2(12) = m2(12) + m2(i)
m3(12) = m3(12) + m3(i)
NEXT i
FOR i = 1 TO 8
t(9) = t(9) + t(i)
NEXT i
FOR i = 1 TO 4
fl(5) = fl(5) + fl(i)
rt(5) = rt(5) + rt(i)
NEXT i
'----output table of results
PRINT #8, MID$(f$, 1, LEN(f$) - 4); "  ";
PRINT #8, USING "####"; number;
FOR i = 1 TO 9: PRINT #8, USING "####"; t(i); : NEXT i
FOR i = 1 TO 12: PRINT #8, USING "####"; l(i); : NEXT i
FOR i = 1 TO 4: PRINT #8, USING "####"; c(i); : NEXT i
FOR i = 1 TO 7: PRINT #8, USING "####"; te(i); : NEXT i
FOR i = 1 TO 12: PRINT #8, USING "####"; m1(i); : NEXT i
FOR i = 1 TO 12: PRINT #8, USING "####"; m2(i); : NEXT i
FOR i = 1 TO 12: PRINT #8, USING "####"; m3(i); : NEXT i
FOR i = 1 TO 4: PRINT #8, USING "####"; fs(i); : NEXT i
FOR i = 1 TO 5: PRINT #8, USING "####"; fl(i); : NEXT i
FOR i = 1 TO 5: PRINT #8, USING "####"; rt(i); : NEXT i
FOR i = 1 TO 4: PRINT #8, USING "####"; rf(i); : NEXT i
FOR i = 1 TO 6: PRINT #8, USING "######"; a(i); : NEXT i:
PRINT #8,
WEND

CLOSE #7
CLOSE #8

END
```

```
'----TERZAGHI.BAS
'----program designed to apply Terzaghi correction to a data set of
'----orientation planes (Terzaghi, 1965)
'----it outputs corrected numbers of orientation values (az, dip)
DECLARE SUB CalcAngle (A1!, A2!, D1!, D2!, Theta!)
CLS
PRINT : PRINT "TERZAGHI CORRECTION TO
ORIENTATION DATA": PRINT
F$ = "1305.doc"
'INPUT "Enter scanline name (e.g. 1137.DOC): ", F$
F$ = "C:\DATA\FRACTURE\" + F$
OPEN F$ FOR INPUT AS #1
OF$ = MID$(F$, 1, LEN(F$) - 3) + "TZG"
OPEN OF$ FOR OUTPUT AS #2
OF$ = MID$(F$, 1, LEN(F$) - 3) + "OUT"
OPEN OF$ FOR OUTPUT AS #3
WHILE NOT EOF(1)
INPUT #1, d$
IF MID$(d$, 1, 1) = "1" AND MID$(d$, 22, 5) < > ""@
@AND MID$(d$, 22, 5) < > "" THEN
az = VAL(MID$(d$, 22, 3))
dp = VAL(MID$(d$, 25, 2))
PRINT #3, az; dp
CalcAngle az, tr, dp, pl, Theta
IF Theta = 0 THEN
N = 1
ELSE
N = 1 / SIN(Theta)
END IF
FOR i = 1 TO N
PRINT #2, az; dp
NEXT i
ELSEIF MID$(d$, 1, 1) = "2" THEN
tr = VAL(MID$(d$, 7, 3))
pl = VAL(MID$(d$, 10, 2))
PRINT "Scanline trend and plunge: "; tr; "/"; pl
END IF
WEND
CLOSE
END

'••••••••••••••••••••••••••••••••••••••••
SUB CalcAngle (A1, A2, D1, D2, Theta)

REM $DYNAMIC
Grad = 3.1415926654# / 180
IF D1 = 90 THEN D1 = 89.9
IF D2 = 90 THEN D2 = 89.9
AA1 = A1 * Grad
AA2 = A2 * Grad
DD1 = D1 * Grad
DD2 = D2 * Grad
x1 = COS(DD1) * SIN(AA1)
x2 = COS(DD2) * SIN(AA2)
y1 = COS(DD1) * COS(AA1)
y2 = COS(DD2) * COS(AA2)
Z1 = SIN(DD1)
Z2 = SIN(DD2)
T1 = x1 * x2
T2 = y1 * y2
T3 = Z1 * Z2
Theta = T1 + T2 + T3
IF (1 - Theta * Theta) < 0 THEN Theta = 1
```

```
Theta = ABS(ATN(SQR(1 - Theta * Theta) / Theta))
END SUB
```

Example macro file for use by FracMan (Dershowitz et al., 1991) to generate a fracture network. The macro uses bootstrap sampling of two input data files (in this case 0108CLU.ORS and 0108RES.ORS) which contain the fracture orientation and trace length data.

```
<FWn>
 EXIT
6
 Re-init
1
(any 5-digit #):
00455
 UTILS
1
 Change View
3
<<<title>>>  VIEWING REGION
< 4.T>
< 4.N>
< 4.S>
< 10 3 0>  Center (x,y,z)
          0,0,0
< 10 2 0>  Direction(tr,pl)
          345,30
< 11 1 0>  Scale
          0.01
<-12 0 0>       GO!
 GENERATE
2
 Fracture Set
1
<<<title>>>  FRACTURE OPTIONS
< 4.T>
<1111.L>
<6411.P>
< 8.N>
< 8.S>
<-11 0-1>  BART Baecher (Rev. Term.)
<-11 0 0>  Intens: Area/Vol
<-11 0 0>  Region: BOX
<-11 0 0>  Orientations: Dip
< 10 3 0>  Region Min (x,y,z)
          -13,-13,-13
< 10 3 0>  Region Max (x,y,z)
          13,13,13
< 1 1 0>  # of Sides
          6
<-12 0 0>       GO!
<<<title>>>  GENERATE FRACTURES
<16.T>
<1111111111111111.L>
<1611511111101311.P>
<16.N>
<16.S>
< 10 2 0>  Dip Directn (tr,pl)
          0,0
<-11 0 0>  Bootstrap
< 10 1 0>  Dispersion
          20
< 10 1 0>  Size (eqv. radius)
          3.1
<-11 0 0>  TLogNormal
< 10 1 0>  Standard deviation
          0.1
< 10 2 0>  Dir of Elong(tr,pl)
          0,0
<-11 0 0>  [constant]
<-10 0 0>
< 10 1 0>  Aspect Ratio
          1
<-11 0 0>  [constant]
<-10 0 0>
< 10 1 0>  Termination %
          84
< 10 1 0>  Frac Area/Vol
          1.095
<-11 0 0>  [constant]
<-12 0 0>       GO!
bootstrap
c:\david\nd\0108clu.ors
<<<title>>>  FRACTURE RADIUS
< 0.T>
< 3.N>
< 3.S>
< 10 1 0>  Lower Bound
          1
< 10 1 0>  Upper Bound
          25
<-12 0 0>          GO!
<<<title>>>  FRACTURE PROPERTIES
<19.T>
<11111111111111111111.L>
<11141111111111111111.P>
<19.N>
<19.S>
< 10 1 0>  Transmissivity
          0.04125
<-11 0 0>  Uncorrelated
<-10 0 0>
<-11 0 0>  LogNormal
< 10 1 0>  Std. deviation
          0.01603
<-10 0 0>
< 10 1 0>  Storativity
          0.0001
<-11 0 0>  Uncorrelated
<-10 0 0>
<-11 0 0>  [constant]
<-10 0 0>
<-10 0 0>
< 10 1 0>  Frac Thickness
          0.0001
<-11 0 0>  Uncorrelated
```

```
<-10 0 0>
<-11 0 0>  [constant]
<-10 0 0>
<-10 0 0>
<-12 0 0>       GO!
GENERATE
2
Fracture Set
1
<<<title>>>  FRACTURE OPTIONS
<4.T>
<1111.L>
<6411.P>
<8.N>
<8.S>
<-11 0-1>  BART Baecher (Rev. Term.)
<-11 0 0>  Intens: Area/Vol
<-11 0 0>  Region: BOX
<-11 0 0>  Orientations: Dip
<10 3 0>  Region Min (x,y,z)
          -13,-13,-13
<10 3 0>  Region Max (x,y,z)
          13,13,13
<1 1 0>  # of Sides
          6
<-12 0 0>      GO!
<<<title>>>  GENERATE FRACTURES
<16.T>
<1111111111111111.L>
<1611511111101311.P>
<16.N>
<16.S>
<10 2 0>  Dip Directn (tr,pl)
          0,0
<-11 0 0>  Bootstrap
<10 1 0>  Dispersion
          20
<10 1 0>  Size (eqv. radius)
          3.5
<-11 0 0>  TLogNormal
<10 1 0>  Standard deviation
          0.6
<10 2 0>  Dir of Elong(tr,pl)
          0,0
<-11 0 0>  [constant]
<-10 0 0>
<10 1 0>  Aspect Ratio
          1
<-11 0 0>  [constant]
<-10 0 0>
<10 1 0>  Termination %
          84
<10 1 0>  Frac Area/Vol
          0.283
<-11 0 0>  [constant]
<-12 0 0>      GO!
bootstrap
c:\david\nd\0108res.ors
<<<title>>>  FRACTURE RADIUS
<0.T>
<3.N>
<3.S>
<10 1 0>  Lower Bound
          1
<10 1 0>  Upper Bound
          25
<-12 0 0>       GO!
<<<title>>>  FRACTURE PROPERTIES
<19.T>
<11111111111111111111.L>
<11141111111111111111.P>
<19.N>
<19.S>
<10 1 0>  Transmissivity
          0.00141
<-11 0 0>  Uncorrelated
<-10 0 0>
<-11 0 0>  LogNormal
<10 1 0>  Std. deviation
          0.05212
<-10 0 0>
<10 1 0>  Storativity
          0.0001
<-11 0 0>  Uncorrelated
<-10 0 0>
<-11 0 0>  [constant]
<-10 0 0>
<-10 0 0>
<10 1 0>  Frac Thickness
          0.0001
<-11 0 0>  Uncorrelated
<-10 0 0>
<-11 0 0>  [constant]
<-10 0 0>
<-10 0 0>
<-12 0 0>       GO!
FILES
5
Save  File
2
3D data
*
DELETE FRACTURES
0
FILES
5
Export File
4
File Option
2
3D data
*
DELETE FRACTURES
0
EXIT
6
Re-init
1
(any 5-digit #):
0455
HALT
999
```